PROCEEDINGS OF THE TWELFTH WORKSHOP

ON

GENERAL RELATIVITY AND GRAVITATION

in JAPAN

THE UNIVERSITY OF TOKYO, KOMABA, TOKYO, JAPAN

NOVEMBER 25 – 28, 2002

Edited by

Masaru Shibata, Yoshiharu Eriguchi, Keisuke Taniguchi,
Takashi Nakamura, Kenji Tomita

PREFACE

The twelfth workshop on General Relativity and Gravitation in Japan was held at a conference hall of the Department of Mathematics, the University of Tokyo, located in the Komaba campus from 25 to 28 November 2002. The main purpose of this workshop was to review the latest progress in the field of general relativity, gravitation, and general relativistic astrophysics as well as to promote interaction between researchers working in these fields.

The workshop was organized as an international conference and composed of 11 invited talks, 2 semi-invited talks, and 67 contributed short talks. Among them, 8 were presented by the researchers from overseas. All the talks were given in English. The workshop was attended by about 150 researchers. We appreciate very much all the participants for their contribution to the workshop.

We would like to thank Ms. K. Yokota and Ms. K. Hisaga, the secretaries at the Kyoto University and at the University of Tokyo, for their devoted transaction of various official works. We are also grateful to the graduate students of the theoretical astrophysics group in the Komaba campus of the University of Tokyo for their cooperation in management of the workshop. Finally we appreciate very much the Department of Mathematics of the University of Tokyo for providing a conference room without any charge. The workshop was financially supported by Monbukagakusho Grants for scientific researches, Nos. 12440063 (PI: K. Tomita) and 14047212 (PI: T. Nakamura).

M. Shibata, Y. Eriguchi & K. Taniguchi April 2003

Organizing Committees

Y. Eriguchi, M. Shibata, K. Taniguchi (Local comittees; University of Tokyo)
T. Chiba, T. Nakamura, T. Tanaka (Kyoto University)
T. Futamase (Tohoku University)
A. Hosoya, T. Shiromizu (Tokyo Institute of Technology)
H. Ishihara, K. Nakao (Osaka City University)
Y. Kojima (Hiroshima University)
K. Maeda (Waseda University)
Y. Nambu (Nagoya University)
K. Oohara (Niigata University)
M. Sasaki, J. Yokoyama (Osaka University)
N. Sugiyama (NAOJ)
K. Tomita (Ritsumeikan University)

Table of Contents

Preface iii

Invited talks

Status of TAMA
Arai, Koji 1
Post-Newtonian Theory and its Application
Blanchet, Luc 8
Black Hole Production at a TeV
Emparan, Roberto 24
Extrinsic curvature in quasiequilibrium binary black hole spacetimes
Gourgoulhon, Eric 30
Dynamical Tachyon Condensation in String Theory
– Time-dependent background in string theory? –
Hashimoto, Koji 43
Laser Interferometric Gravitational-Wave Detectors in Future
Kawamura, Seiji 55
Millisecond oscillators in accreting neutron stars and black holes
Kluźniak, Włodek 69
Quark Star ???
Possible Formation Scenario of the Quark Star of Maximum Mass around $0.7M_{\odot}$
Nakamura, Takashi 81
The First-Generation Supernovae and Extremely Metal-Poor Stars
Nomoto, Ken'ichi 87
Brane-World Cosmology
Sasaki, Misao 98
Issues on the cosmological constant
Yokoyama, Jun'ichi 113

Semi-invited talks

Self-Similar Solutions, Critical Behavior and Convergence to Attractor in Gravitational Collapse
Harada, Tomohiro 123
Re-formulating the Einstein equations for stable numerical simulations
– Formulation Problem in Numerical Relativity –
Shinkai, Hisa-aki 137

Contributed talks

Algebraic Properties to Gravitational Lenses
Asada, Hideki 152
The Cosmic Quartet
Cosmological Parameters of a Smoothed Inhomogeneous Spacetime
Buchert, Thomas 157
Non-Topological Soliton in Three-Dimensional Supergravity
Cho, Yoshinori 162
An Accelerating Universe in Space-Time-Matter Cosmology
Fukui, Takao 167

Contributed talks (continue)

Thermodynamic properties of massive dilaton black holes
Tamaki, Takashi 405
Quantum Radiation by a Moving Brane
Tanaka, Izumi 410
Application of the Separate Universe Approach to Preheating
Tanaka, Takahiro 415
Asymptotics of topologically nontrivial spacetimes
Tanimoto, Masayuki 420
Numerical simulation of gravothermal catastrophe from a viewpoint of non-extensive thermodynamics
Taruya, Atsushi 425
Gravitational waves from quintessential inflation
Tashiro, Hiroyuki 430
Scaling Law and Non-Gaussian Velocity Distribution in Self-gravitating Ring Model
Tatekawa, Takayuki 435
Topological Structure of The Upper End of Future Null Infinity
Tomizawa, Shinya 440
Cosmological constant, dilaton field and Freund-Rubin compactification
Torii, Takashi 445
Nonlinear Supersymmetric Structure of Spacetime and Matter
Tsuda, Motomu 450
Quantum Aspects of Higher Dimensional Theories
Uzawa, Kunihito 455
On the perturbations of spatially closed locally homogeneous vacuum solutions
Yasuno, Katsuhito 460
Black hole formation in high-energy particle collisions
Yoshino, Hirotaka 465

Status of TAMA

Koji Arai,[1] and the TAMA collaboration

Space-Time Astronomy Section,
National Astronomical Observatory, Mitaka, Tokyo 181-8588, Japan

Abstract

Projects to construct interferometric detectors are in progress through the world. In Japan, TAMA300 has been constructed at the National Astronomical Observatory of Japan in Mitaka, Tokyo. TAMA300 detector started its first operation in 1999. Since then eight times of data taking runs were performed. In the sixth run (DT6) in 2001, TAMA300 was continuously operated for 50 days, having accumulated observation data of 1038 hours. The acquired data in DT6 was provided to data analyses. After this observation, the sensitivity was improved by implementation of power recycling. Currently, the eighth observation run, which is the first full-time coincidence run with LIGO, is being held.

1 Introduction

Gravitational waves are ripples of space-time propagating through the universe, derived from the linearized Einstein equation in general relativity. The existence of gravitational wave was only indirectly confirmed by Hulse and Taylor with the radio observation of a binary pulsar. Gravitational radiation now plays an important role in the models of many known astronomical systems. Because of its weak interaction with matters, however, the direct detection is not yet realized.

Direct detection of gravitational waves will provide great contributions to physics and astronomy. General relativity and alternative theories of gravity will be exposed to tests under strong gravity field for the first time. Analyses of the waveforms will pioneer a new field of astronomy, which will complement astronomy by electro-magnetic radiation. The direct observation of gravitational waves would reveal information which can not be obtained by any other ways: details of the structures of neutron stars and black holes, equation of state for nuclear matters, mechanisms of supernovae, and so on.

Attempts to catch gravitational waves originated in the 1960's by using aluminum bars as resonant mass detectors, inspiring many successive inventions for the detection. The rapid progress of laser technology in recent decades allowed us to consider laser interferometers with a long baseline as gravitational wave detectors for the first detection. These interferometers utilize the nature of Michelson interferometers; Michelson interferometers are sensitive only to differential arm length deviation. Since gravitational waves cause differential arm length fluctuations, the waveform of a gravitational wave is obtained from the change in brightness of the interference fringe.

Construction of interferometric detectors is in progress by several projects. Laser Interferometer Gravitational wave Observatory (LIGO) [1] constructed three large-scale interferometers: 4km and 2km ones in Washington, and 4km one in Louisiana. All of these interferometers became available for operation in 2002. The German-British project, GEO600 [3], constructed a 600-m length interferometer in Hannover. The GEO600 detector performed a preliminary observation in 2002 with LIGO. They are currently changing their optical configuration in order to increase the sensitivity. The French-Italian project VIRGO [2] finished tests with the short interferometer and has just started commissioning works with the 3-km arms.

In Japan, the TAMA300 [4, 5] detector began its first operation in 1999, preceding the other projects' detectors. Since then, observations and developments to enhance the performance were repeated. In this paper, overview of TAMA300, status of the 50-days observation performed in 2001 Summer, and progress of the recycling experiment are described. In addition, brief report of the joint observation with LIGO which is currently on-going is presented.

[1] E-mail:koji.arai@nao.ac.jp

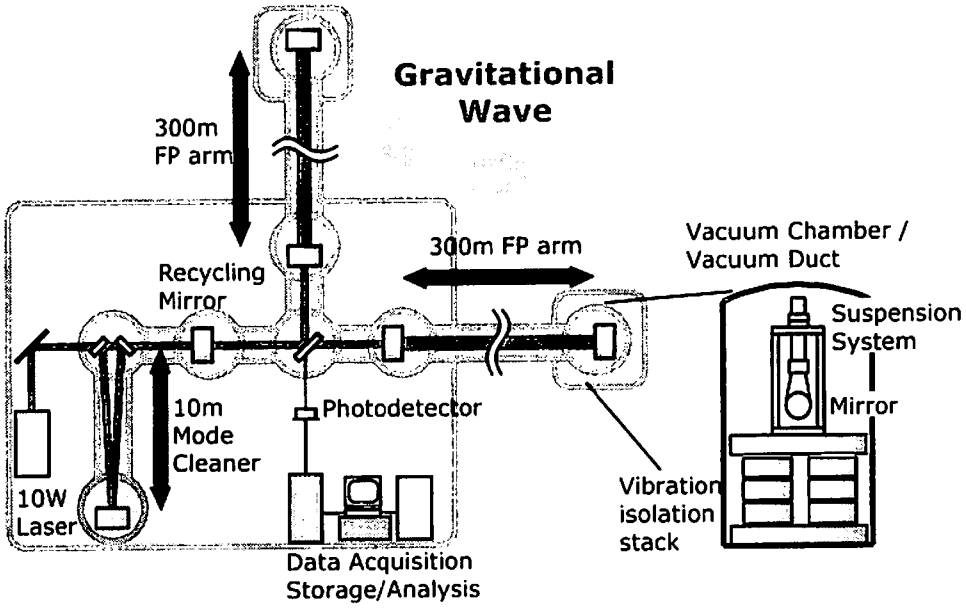


Figure 1: Schematic view of the TAMA300 detector.

2 TAMA Detector

The TAMA300 detector has been constructed on the campus of the National Astronomical Observatory of Japan in Mitaka, Tokyo. The TAMA project started in 1995. The purpose of the project is to establish the techniques that are required for the construction and operation of future km-class advanced interferometers as well as to operate the interferometer to catch possible (but rare) events from nearby galaxies. After finishing installation and shakedown of the main components of the instrument in 1999, efforts are concentrated on scientific observations and improvement of the performance. Project's initial term of seven years including two years of extension was completed in March, 2002. Currently, operation of the facility is supported by another four years' budget.

Schematic view of the detector is shown in Figure 1. When gravitational waves arrive at the detector, the proper distance between suspended mirrors in each arm varies in a differential way; one arm length shrinks while the other stretches. This differential deviation causes change of the interference condition at an optical port of the interferometer. The data acquisition system records this change as a time series data.

The light source of TAMA300 is a 10-W LD-pumped Nd:YAG laser at the wavelength of 1064 nm, developed by SONY corporation [6]. The laser beam from the light source is filtered by a 10-m mode cleaner [7]. This mode cleaner is a ring cavity with three mirrors. The function of the mode cleaner is to improve the shape of the laser beam and to stabilize the laser frequency by using the length of the mode cleaner as a reference.

The light incident on the interferometer is splitted into two beams by a beamsplitter. One beam goes into an inline arm, and the other to a perpendicular arm. These arms are Fabry-Perot optical cavity which is formed by two mirrors separated by 300 meters. The main mirrors of TAMA300 are made of fused silica (Suprasil-P10 by Shin-Etsu Quartz Products Co. Ltd.), and are 10 cm in diameter and 6 cm in thickness. This material is selected so as to realize mechanically and optically low loss. The reflecting surfaces of the mirrors are polished and covered with low-optical-loss coating.

Since any mirror motion can not be distinguished from gravitational waves, careful consideration in vibration isolation is indispensable. The main mirrors are placed on vibration isolation systems and enclosed in vacuum chambers. The vibration isolation system of TAMA300 consists of three stages. Commercial pneumatic active isolators (Alpha-2 by Tokkyo Kiki Corp.) are placed outside of the vacuum

chambers below the baseplates for four test masses. Composition of blocks of stainless steel and elastic rubber pieces, called vibration isolation stack, is installed in each vacuum chamber. Double pendulum suspensions which hang the mirrors are placed on the optical table above the stacks. The confirmed vibration isolation performance in total is better than 10^{-8} above 150Hz.

The data-acquisition system of TAMA300 records seven channels of high speed data and a timing signal from GPS system with a sampling rate of 20kHz.

Recently, power recycling mirror has been installed between the 10-m mode cleaner and the beam-splitter. Detailed descriptions about the power recycling experiment is given in the later section.

3 Data Taking 6

The TAMA project performed eight times of observation runs since 1999. Except for the eighth one which is currently on-going, the sixth one, called Data Taking 6 (DT6), was the largest one. In DT6, TAMA300 was continuously operated for 50 days. The interferometer operation was mostly stable even though the detector circumstances were not ideal for a gravitational wave detector; the site is in a noisy city area where ground motion is largely excited in the daytime by human activities, such as heavy traffic. Figure 3 shows the observation status during the 50 days' run. Each box in the figure represents continuous observation period where both the interferometer and the data acquisition system were functional. In total, observation data of 1038 hours was accumulated. This corresponds to the duty ratio of 86.5%.

The main reasons for loss of the observation time were the followings:

- Adjustment period. The interferometer operation was aborted for adjustments and measurements in the beginning week. After that period, the operation became more stationary; adjustment about 10 minutes has been performed each 3 hours. DLT tapes for data storage needed to be exchanged every four days. Each time the data acquisition system was aborted for about 30 minutes.
- Several times of human errors. Owing to mis-operation, the interferometer adjustment took long time.
- Typhoons. On August 21st and September 10th, typhoons directly stroke Tokyo area. Because of strong wind and high waves, interferometer operation was almost impossible.
- Laser trouble. Once per several days, glitches in the laser frequency appeared and disturbed stable operation. After the observation, the reason of the problem was found and fixed; the cooling system of the master laser had critical damages.

At the time of DT6, the detector had sensitivity shown in Figure 2. The floor level of the displacement noise was $1.5 \times 10^{-18}\mathrm{m}/\sqrt{\mathrm{Hz}}$. Dividing this value by the arm length 300 m, the strain sensitivity of $5 \times 10^{-21}/\sqrt{\mathrm{Hz}}$ is obtained. This sensitivity was limited by seismic noise (~20Hz), alignment noise (20~80Hz), Michelson noise (80Hz~1kHz), noise of photodetection system (1kHz~7kHz), and laser frequency noise (7kHz~). Note that the alignment noise means coupling from noise of the mirror attitude control system to the main output signal, and the Michelson noise is unidentified noise but localized in the Michelson interferometer formed by the two front mirrors.

One of the indices to evaluate the detector performance is "observable distance". It is defined by the distance at which compact binary inspiral can be detected with SNR of 10 with matched filtering analysis [5], assuming the binary has specific equal masses and present in the optimum direction for the detector. With the DT6 sensitivity, the detector had the observable distance of 17kpc, 33kpc, and 34kpc for 0.5Msolar(MACHO BH), 1.4Msolar(NS), and 10Msolar(BH) binaries, respectively. Having been monitored these observable distance during the observation, the interferometer was adjusted so as to have its best performance as far as possible.

The acquired data in DT6 was provided to data analyses. Currently the following gravitational wave search are in progress:

- Matched filtering analysis for inspirals of neutron star (1~2Msolar) binaries. (Tagoshi, et al.)
- TAMA-LISM coincidence analysis with Matched filtering for NS binary inspirals. (H. Takahashi, Tagoshi, et al.)

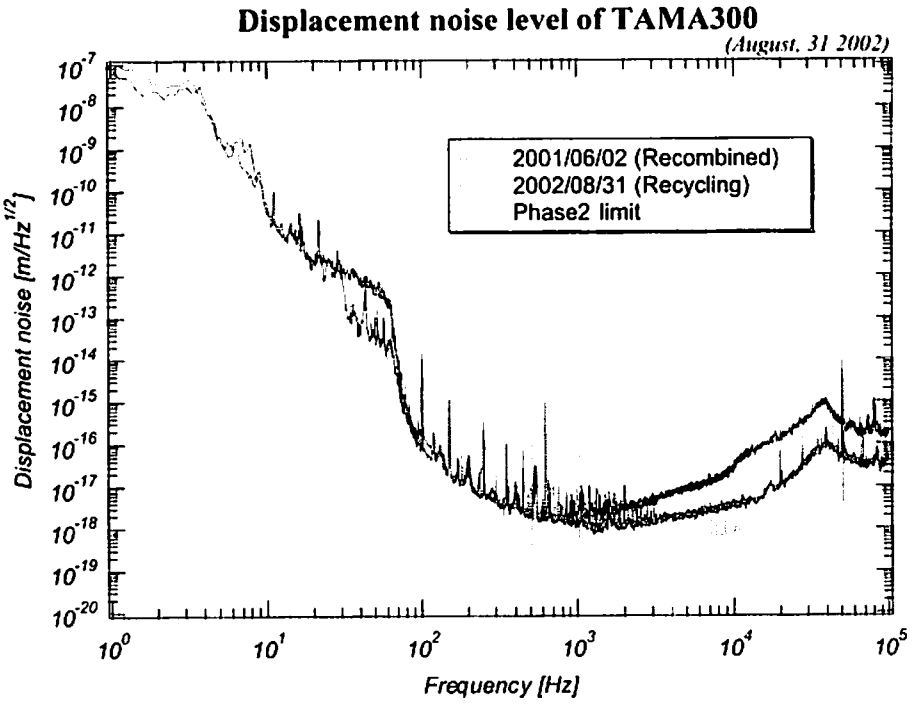


Figure 2: Displacement sensitivity of TAMA300. The curve "Recombined" shows the sensitivity without power recycling, i.e. the sensitivity at DT6. The curve "Recycling" shows the sensitivity improved with power recycling. The grey curve is the theoretical limit which can not be exceeded with the initial design of TAMA300.

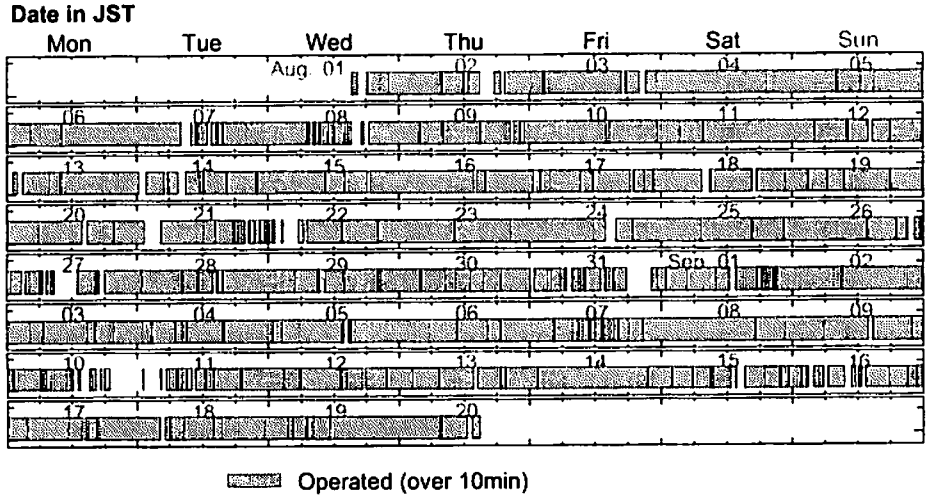


Figure 3: Observation status calendar, from August 1st, 2001 to September 20th, 2001. Each box indicates continuous observation period where both the interferometer and the data acquisition system were functional. In total, 1038 hours of observation data has been obtained. This corresponds to the duty ratio of 86.5%.

- Matched filtering analysis for inspirals of MACHO BH (~0.5Msolar) binaries. (Tatsumi, et al.)
- Matched filtering analysis for black hole ringdowns. (Tsunesada, Nakano, Kanda, et al.)
- Gravitational wave burst search using detection of nonstationarity with higher order statistics. (Ando, et al.)
- Search for possible periodic wave from SN1987a remnant. (Soida, et al.)
- Chirp signal search using wavelet analysis. (Kanda, et al.)

The details of each topic will be presented in an individual paper elsewhere.

4 Recycling experiment

After the sixth observation (DT6), an experiment to implement power recycling to TAMA300 has been started. Power recycling is a technique to enhance internal light power in the interferometer by inserting an additional partial mirror, called a recycling mirror, in front of the beamsplitter. Power recycling provides effective enhancement of input laser power. When this power enhancement factor, called recycling gain, is n, shot noise increases by a factor of $\sqrt{n}$ as well as the signal by n, resulting in the improvement of the shot-noise level by $\sqrt{n}$. In particular, the sensitivity above 1kHz at DT6 was not limited by shot noise but by noise in the photodetection system, power recycling has been considered to improve the sensitivity more than the square root of the recycling gain.

Figure 4 shows the principle of power recycling. Note that the arm cavity is omitted in this figure, for simplicity. An interferometric gravitational wave detector is designed so that most of the incident light is reflected back toward the laser source; both of the end mirrors have high reflectivity, and the optical path length is controlled so that the destructive interference fringe is realized at the dark port. Since the recycling mirror is controlled so that no light is reflected to the laser, the interferometer has no leakage field. As a result of enclosing the laser light, the internal light power increases until the total internal dissipation reaches the incident power. Thus the recycling gain is determined how much light is dissipated from the interferometer.

After a first successful lock of the recycled interferometer on December 24th, 2001, improvement of the sensitivity and the stability was pursued. The sensitivity with power recycling is shown in Figure 2. Improvement of the sensitivity above 800Hz was realized by reducing scattered light noise and by further stabilizing the laser frequency. Achieved recycling gain was 4.5. As for the stability, continuous lock of 20.5 hours was attained as a longest lock stretch since power recycling was implemented to TAMA300.

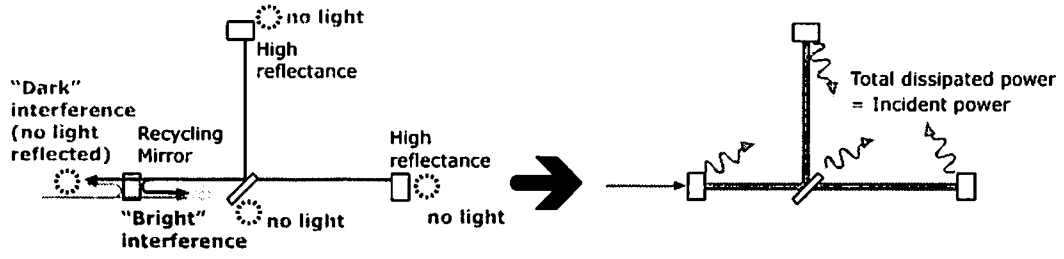


Figure 4: Principle of power recycling. In this figure, the arm cavities are omitted for simplicity. Left: The recycling mirror is controlled so that no light is reflected to the laser as well as the other optical ports are designed to have no light. Right: As a result of enclosing the laser light, the internal light power increases until the total internal dissipation reaches the incident power.

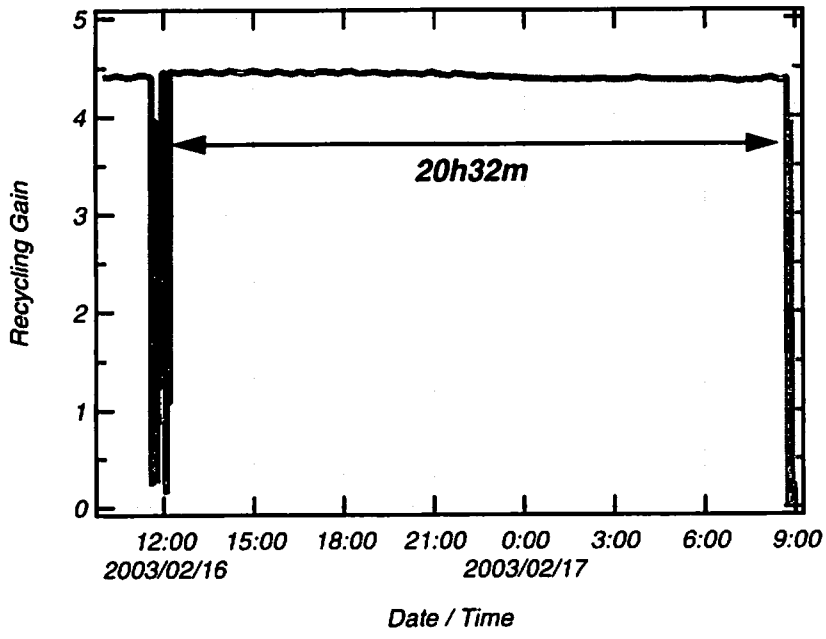


Figure 5: Longest continuous lock for 20 hours 32 minutes were attained during DT8.

5 TAMA-LIGO Joint observation

The eighth observation run of TAMA300 (DT8) from February 14th, 2003 to April 15th, 2003 is being held. This is a first long term observation after the implementation of power recycling to TAMA300. In addition, this observation is a first full-time coincident observation with LIGO's three interferometers.

For this observation, most of the interferometer operation was made automatic; only the initial alignment of the mirrors before lock acquisition should be adjusted by an operator. So far, the stable operation of TAMA300 is realized most of the time, although the operation is frequently disturbed in the daytime of weekdays by construction works around the site.

6 Summary

Projects to construct interferometric detectors are in progress through the world. In Japan, TAMA300 has been constructed on the campus of the National Astronomical Observatory of Japan in Mitaka, Tokyo. The TAMA300 detector started its first operation in 1999. Since then eight times of data taking runs were performed. In the sixth run in 2001, TAMA300 was continuously operated for 50 days. Observation data of 1038 hours was accumulated in total. This corresponds to the duty ratio of 86.5%. The acquired data in DT6 was provided to data analyses. After the sixth observation (DT6), an experiment to implement power recycling has been started. Power recycling gain of 4.5 was attained. The sensitivity improvement by power recycling has been achieved. Continuous lock of 20.5 hours was realized. Currently, the eighth observation run is being held.

7 Acknowledgment

This research is supported by a Grant-in-Aid for Creative Basic Research of the Ministry of Education, Culture, Sports, Science and Technology (09NP0801), and a Grant-in-Aid for Scientific Research on

Priority Areas (415) of the Ministry of Education, Culture, Sports, Science and Technology.

References

[1] Alex Abramovici, William. E. Althouse, Ronald W.P. Drever, Yekta Gürsel, Seiji Kawamura, Frederick J. Raab, David Shoemaker, Lisa Sievers, Robert E. Spero, Kip S. Thorne, Rochus E. Vogt, Rainer Weiss, Stanley E. Whitcomb, Michael E. Zucker, Science **256**, 325 (1992).

[2] The VIRGO Collaboration, "VIRGO Final Design Report" (1997).

[3] K. Danzmann, H. Lück, A. Rüdiger, R. Schilling, M. Schrempel, W. Winkler, J. Hough, G.P. Newton, N.A. Robertson, H. Ward, A.M. Campbell, J.E. Logan, D.I. Robertson, K.A. Strain, J.R.J. Bennett, V. Kose, M. Kühne, B.F. Schutz, D. Nicholson, J. Shuttleworth, H. Welling, P. Aufmuth, R. Rinkleff, A. Tünnermann, B. Willke, *MPQ Report* **190** (1994).

[4] Masaki Ando, et al., Phys. Rev. Lett. **86**, 3950 (2001).

[5] Hideyuki Tagoshi et al., Phys. Rev. D **63**, 062001 (2001).

[6] S. T. Yang, Y. Imai, M. Oka, N. Eguchi, and S. Kubota, Opt. Lett. **21**, 1676 (1996).

[7] Shigeo Nagano, et al., Rev. Sci. Instr. **73** 2136 (2002).

Post-Newtonian Theory and its Application

Luc BLANCHET[1]

Gravitation et Cosmologie ($\mathcal{GR}\varepsilon\mathcal{CO}$),
Institut d'Astrophysique de Paris,
98^{bis} boulevard Arago, 75014 Paris, France

Abstract

We review some recent works on the post-Newtonian theory of slowly-moving (post-Newtonian) sources, and its application to the problems of dynamics and gravitational radiation from compact binary systems. Our current knowledge is 3PN on the center-of-mass energy and 3.5PN on the gravitational-wave flux of inspiralling compact binaries. We compute the innermost circular orbit (ICO) of binary black-hole systems and find a very good agreement with the result of numerical relativity. We argue that the gravitational dynamics of two bodies of comparable masses in general relativity does not resemble that of a test particle on a Schwarzschild background. This leads us to question the validity of some "Schwarzschild-like" templates for binary inspiral which are constructed from post-Newtonian resummation techniques.

1 Introduction

Recent years have shown a tremendous revival of interest in an Old Lady: the post-Newtonian approximation (or expansion when the speed of light $c \to +\infty$), which is surely the most important technique in the arsenal of General Relativity for drawing firm predictions for the outcome of experimental facts related to gravitation. The post-Newtonian approximation is ideally suited for describing the adiabatic phase of the very interesting astrophysical systems known as inspiralling compact binaries. These systems constitute our only known-to-exist (for sure) source to hunt for in the current network of laser-interferometric detectors of gravitational waves, today composed of the large-scale interferometers VIRGO and LIGO, and the medium-scale ones GEO and TAMA.

Two compact (i.e. gravitationally-condensed) objects — neutron stars or black holes — orbit an inward spiral, with decreasing orbital radius r, decreasing orbital period P, and increasing orbital frequency $\omega = \frac{2\pi}{P}$. The inspiral is driven by the loss of energy associated with the gravitational-wave emission, or, equivalently, by the action of radiation forces. There is a long phase of *adiabatic* inspiral, with associated dimensionless adiabatic parameter

$$\frac{\dot{\omega}}{\omega^2} = \mathcal{O}\left(\frac{1}{c^5}\right) . \tag{1}$$

The order of magnitude of the right-hand-side is that of the radiation-reaction force, namely $\sim 1/c^5$ or equivalently 2.5PN order beyond the standard Newtonian acceleration (following the usual post-Newtonian jargon). The binary's dynamics being essentially "aspherical", inspiralling compact binaries are strong emitters of gravitational radiation.

The main point about the theoretical description of inspiralling compact binary is that a model made of two structureless point-particles, characterized solely by two mass parameters m_1 and m_2 (and possibly two spins), is sufficient. Most of the non-gravitational effects usually plaguing the dynamics of binary star systems: a magnetic field, an interstellar medium, etc., are dominated by gravitational forces. However, the real justification for a model of point particles is that the effects due to the finite size of the compact bodies are small. In particular, the tidal interactions between the two compact objects are expected to play a little role during most of the inspiral phase; the mass transfer (in the case of neutron stars) does not occur until very late, near the final coalescence. Thus the inspiralling compact binaries are very clean

[1]E-mail address: blanchet@iap.fr

systems, essentially dominated by gravitational forces during most of their life. This is the reason why these systems are so interesting for relativity theorists!

Our fascination for the old post-Newtonian lady is that it was recognized that *improved* waveform modelling is crucial for constructing efficient templates for searching and measuring the gravitational waves from inspiralling compact binaries in the LIGO/.../TAMA network. By *improved* we mean in fact *much* improved with respect to what is known from the "Newtonian" approximation, which corresponds in the case of the radiation field to the Einstein quadrupole formalism. And one needs much improved modelling because the orbital motion of the inspiralling compact binary — which is responsible for the gravitational-wave emission — becomes *very* relativistic when the binary reaches the so-called Innermost Circular Orbit or ICO (defined below in this article). At that point the orbital velocity is of the order of 50% of the speed of light. The price to be paid for applying the post-Newtonian approximation is that we must go to very *high* post-Newtonian order. The status of the field nowadays is the 3PN approximation (i.e. $\sim 1/c^6$) — or even better the 3.5PN one —, which is likely to be sufficient for practical purpose (at least in the case of neutron stars binaries).

After the two objects have passed the ICO they will plunge together and merge to form a single black hole, which will subsequently settle down into a stationary configuration, by emission of gravitational waves in the quasi-normal mode channel. Of course we should not expect the post-Newtonian approximation (and the description of the compact objects by point-particles) to be valid after the ICO, and we shall have to replace this model by a fully relativistic numerical computation of the phase of plunge and merger of two black holes [1]. But, up to the point of the ICO, the post-Newtonian approximation, when carried out to 3PN order, *is* physically valid, and is probably very accurate. This last point may appear to be a little surprising (it contradicts some statements in the litterature about the "failure" of the post-Newtonian approximation in the regime of the ICO), but we shall present arguments supporting it. In particular the 3PN order is probably able to locate the ICO to within an accuracy of the order of 1% or better (for binary systems with comparable masses).

2 Post-Newtonian iteration for isolated systems

Before embarking into strong statements concerning the "accuracy" of the post-Newtonian description of binary systems, it is wise to examine in a somewhat general way the well-definiteness of the approximation itself. This is especially important in view of the fact that our old lady the post-Newtonian approximation has been unjustly accused of being plagued with some apparently inherent difficulties, and furthermore which crop up around the 3PN order we are interested in. The problems arise in the general case of regular (singularity-free) matter sources. Up to the 2.5PN order the approximation can be worked out without problems, and often at the 3PN order the problems can be solved specifically for each case at hands. However, it must be admitted that these difficulties, even if appearing at higher approximations, have cast doubt in the past on the actual soundness, on the theoretical point of view, of the post-Newtonian expansion. They pose the practical question of the reliability of the approximation when comparing the theory's predictions with very precise experimental results. Here we discuss the nature of the problems – are they purely technical or linked with some fundamental drawback of the approximation? – and outline their resolution recently proposed in Ref. [2].

The first problem is that in higher approximations some *divergent* Poisson-type integrals appear. Recall that the post-Newtonian expansion replaces the resolution of an hyperbolic-like d'Alembertian equation by a perturbatively equivalent hierarchy of elliptic-like Poisson equations. Rapidly it is found during the post-Newtonian iteration that the right-hand-side of the Poisson equations acquires a non-compact support (it is distributed over all space), and that the standard Poisson integral diverges because of the bound of the integral at spatial infinity, i.e. $r \equiv |\mathbf{x}| \to +\infty$, with $t = \text{const}$. For instance some of the potentials occuring at the 2PN order in Chandrasekhar's work [3] are divergent, so the corresponding metric is formally infinite. In fact, Kerlick [4, 5] showed that the post-Newtonian computation *à la* Chandrasekhar, following the iteration scheme of Anderson and DeCanio [6], can be made well-defined up to the 2.5PN order, but that this does not solve the problem at the next 3PN order, which has been found to involve some inexorably divergent Poisson integrals.

These divergencies come from the fact that the post-Newtonian expansion is actually a singular perturbation, in the sense that the coefficients of the successive powers of $1/c$ are not uniformly valid

in space, since they typically blow up at spatial infinity like some positive powers of r. For instance, Rendall [7] has shown that the post-Newtonian expansion cannot be "asymptotically flat" starting at the 2PN or 3PN level, depending on the adopted coordinate system. The result is that the Poisson integrals are in general badly-behaving at infinity. Trying to solve the post-Newtonian equations by means of the standard Poisson integral does not *a priori* make sense. This does not mean that there are no solution to the problem, but simply that the Poisson integral does not constitute the correct solution of the Poisson equation in the context of post-Newtonian expansions. So the difficulty is purely of a technical nature, and will be solved once we succeed in finding the appropriate solution to the Poisson equation[2].

To cure the problem of divergencies we have introduced [2], at any post-Newtonian order, a generalized solution of the Poisson equation with non-compact support source, in the form of an appropriate *finite part* of the usual Poisson integral: namely we regularize the bound at infinity of the Poisson integral by means of a process of analytic continuation, analogous to the one already used to regularize the retarded integrals in Refs. [8, 12, 9, 10]. At any post-Newtonian order n we have to solve a Poisson equation with non-compact-support "source-term" $\overline{\tau}_n^{\mu\nu}$, where the overbar indicates that we are considering a (formal) post-Newtonian expansion, and pick up the coefficient of $1/c^n$ in that expansion (μ, ν are space-time indices). We multiply the source-term by a regularization factor r^B, where $r = |\mathbf{x}|$ and $B \in \mathbb{C}$, and then apply the standard Poisson integral. The result,

$$\Delta^{-1}\left[r^B \overline{\tau}_n^{\mu\nu}\right](\mathbf{x},t) = -\frac{1}{4\pi}\int_{\mathbb{R}^3} \frac{d^3\mathbf{y}}{|\mathbf{x}-\mathbf{y}|}\,|\mathbf{y}|^B\,\overline{\tau}_n^{\mu\nu}(\mathbf{y},t)\,, \tag{2}$$

is a well-defined integral (i.e. convergent at infinity, $r \to +\infty$) in some region of the B-complex plane, given by $\Re(B) < -a_{\max} - 2$, where $a_{\max}$ denotes the maximal power of r in the behaviour of the source-term $\overline{\tau}_n^{\mu\nu}$ when $r \to +\infty$, i.e. it corresponds to the maximal growth of the source-term at infinity (notice that $a_{\max}$ gets larger and larger when we increase the post-Newtonian order n). Next, we can prove that the latter function of B generates a (unique) analytic continuation down to a neighbourhood of the origin $B = 0$, except at $B = 0$ itself, around which value it admits a Laurent expansion with multiple poles up to some finite order. Then, we consider the Laurent expansion of that function when $B \to 0$ and compute the finite part ($\mathcal{FP}$), or coefficient of the zero-th power of B, of that expansion. This defines our generalized Poisson integral:

$$\widetilde{\Delta^{-1}}\left[\overline{\tau}_n^{\mu\nu}\right] = \mathcal{FP}\,\Delta^{-1}\left[r^B \overline{\tau}_n^{\mu\nu}\right]\,. \tag{3}$$

The resulting "generalized" Poisson integral constitutes an appropriate solution of the post-Newtonian equation. However this is only a *particular* solution of the Poisson equation, and the most general solution will be the sum of that particular solution and the most general solution of the corresponding homogeneous equation. At this stage, considering the post-Newtonian iteration scheme alone, we cannot do more and therefore we leave the homogeneous solution unspecified (we can see *a posteriori* that it is associated with radiation-reaction effects).

The second problem has to do with the *near-zone* limitation of the post-Newtonian approximation. Indeed the post-Newtonian expansion assumes that all retardations r/c are small, so it can be viewed as a formal *near-zone* expansion when $r \to 0$, which is valid only in the region surrounding the source that is of small extent with respect to the typical wavelength of the emitted radiation: $r \ll \lambda$ (if we locate the origin of the coordinates $r = 0$ inside the source). Therefore, the fact that the coefficients of the post-Newtonian expansion blow up at spatial infinity, when $r \to +\infty$, has nothing to do with the actual behaviour of the field at infinity. The serious consequence is that it is not possible, *a priori*, to implement within the post-Newtonian iteration the physical information that the matter system is isolated from the rest of the universe. Most importantly, the no-incoming radiation condition, imposed at past null infinity, cannot be taken into account, *a priori*, into the scheme. In a sense the post-Newtonian approximation

[2]The problem is somewhat similar to what happens in Newtonian cosmology. Here we have to solve the Poisson equation $\Delta U = -4\pi G\rho$, where the density ρ of the cosmological fluid is constant all over space: $\rho = \rho(t)$. Clearly the Poisson integral of a constant density does not make sense, as it diverges at the bound at infinity like the integral $\int r dr$. This nonsensical result has occasionally been referred to as the "paradox of Seeliger". However the problem is solved once we realize that the Poisson integral does not constitute the appropriate solution of the Poisson equation in the context of Newtonian cosmology. A well-defined solution is simply given by $U = -\frac{2}{3}\pi G\rho r^2$.

is not "self-supporting", because it necessitates some information taken from outside its own domain of validity.

The solution of the problem of the near-zone limitation of the post-Newtonian expansion resides in the *matching* of the near-zone field to the exterior field, a solution of the vacuum equations outside the source which has been developed in previous work [8] using some post-*Minkowskian* and multipolar expansions. In the case of post-Newtonian sources, the near zone, i.e. $r \ll \lambda$, covers entirely the source, because the source's radius itself is such that $a \ll \lambda$. Thus the near zone overlaps with the exterior zone where the multipole expansion is valid. What we do is to impose a matching condition resulting from the numerical equality between the multipolar and post-Newtonian fields, verified in the external part of the near-zone (say $a < r \ll \lambda$, where a is the size of the source). The matching equation reads

$$\overline{\mathcal{M}(h^{\mu\nu})} \equiv \mathcal{M}(\bar{h}^{\mu\nu}) \,, \tag{4}$$

where $\mathcal{M}$ symbolizes the multipolar (actually multipolar-post-Minkowskian) series, and as before the overbar refers to the post-Newtonian or near-zone expansion. We emphasize that the matching equation is physically justified only for post-Newtonian sources, for which the exterior near-zone exists.

The requirement of matching to the post-Newtonian solution has been shown (in a previous work [10]) to entirely determine, up to any post-Newtonian order, the multipole moments parametrizing the exterior field. In our more recent paper [2] we have proved that the still undetermined homogeneous solutions in the post-Newtonian iteration alluded to before are also fully determined by the matching equation. These homogeneous solutions are associated with radiation-reaction effects — for instance they incorporate the dominant radiation-reaction force at the 2.5PN order, as well as the tail contribution in the radiation-reaction force which is known to arise at the 4PN order [11, 12, 13]). In conclusion, the post-Newtonian expansion of the field inside an isolated system is fully determined (it can be *indefinitely* reiterated, up to any post-Newtonian order) by the matching to the exterior solution satisfying the correct boundary condition at infinity — notably the absence of incoming radiation from past null infinity.

3 Dynamics and radiation of compact binaries

By equations of motion we mean the explicit expression of the accelerations of the compact bodies in terms of the positions and velocities. In Newtonian gravity, writing the equations of motion for a system of N particles is trivial; in general relativity, even writing the equations in the case $N = 2$ is difficult. The first relativistic term, at the 1PN order, was derived by Einstein, Infeld and Hoffmann [14] by means of their famous "surface-integral" method, by which the equations of motion are deduced from the *vacuum* field equations, and so which is applicable to any compact objects (they be neutron stars, black holes, or, maybe, naked singularities).

Concerning the 2PN and 2.5PN approximations the result for the equations of binary motion in harmonic coordinates was obtained by Damour and Deruelle and collaborators [18, 15, 16, 17]. The corresponding result for the ADM-Hamiltonian of two particles at the 2PN order was given in Ref. [19]. By ADM-Hamiltonian we refer to the Fokker-type Hamiltonian, which is obtained from the matter-plus-field Arnowitt-Deser-Misner Hamiltonian by eliminating the field degrees of freedom. Kopeikin [20] derived the 2.5PN equations of motion for two extended compact objects. The 2.5PN-accurate harmonic-coordinate equations as well as the complete gravitational field (namely the metric $g_{\mu\nu}$) were computed by Blanchet, Faye and Ponsot [21], and by Pati and Will [22].

It is important to realize that the 2.5PN equations of motion are known to hold in the case of binary systems of strongly self-gravitating bodies. This is *via* an "effacing" principle for the internal structure of the bodies. As a result, the equations depend only on the "Schwarzschild" masses, m_1 and m_2, of the compact objects, as has been explicitly verified up to the 2.5PN order [20, 23]. The 2.5PN equations of motion have also been established by Itoh, Futamase and Asada [24, 25], who use a variant of the surface-integral approach [14], valid for compact bodies.

The present state of the art is the 3PN order. The equations of motion at this order have been worked out independently by two groups, by means of different methods, and with equivalent results. On one hand, Jaranowski and Schäfer [26, 27], and Damour, Jaranowski and Schäfer [28, 29, 30], employ the ADM-Hamiltonian formalism of general relativity; on the other hand, Blanchet and Faye [31, 34, 32, 33],

de Andrade, Blanchet and Faye [35], and Blanchet and Iyer [36], founding their approach on the post-Newtonian iteration initiated in Ref. [21], compute directly the equations of motion from which they infer the Lagrangian (instead of the Hamiltonian) in harmonic coordinates. The end results have been shown [29, 35] to be physically equivalent in the sense that there exists a unique "contact" transformation of the dynamical variables, that changes the harmonic-coordinates Lagrangian obtained in Ref. [35] into a new Lagrangian, whose Legendre transform coincides exactly with the Hamiltonian given in Ref. [28]. The 3PN equations of motion, however, depend on one unspecified numerical coefficient, $\omega_{\rm static}$ in the ADM-Hamiltonian formalism and λ in the harmonic-coordinates approach, which is due to some incompleteness of the Hadamard self-field regularization method. This coefficient has been fixed by means of a dimensional regularization in Ref. [30] (see Section 5).

So far the status of the post-Newtonian equations of motion is quite satisfying. There is mutual agreement between all the results obtained by means of different approaches and techniques, whenever it is possible to compare them: point-particles described by Dirac delta-functions, extended post-Newtonian fluids, surface-integrals methods, mixed post-Minkowskian and post-Newtonian expansions, direct post-Newtonian iteration and matching, harmonic coordinates versus ADM-type coordinates, different processes or variants of the regularization of the self field of point-particles.

Let us remark that the 3PN equations of motion are merely "Newtonian" as regards the radiative aspects of the problem, because with that precision they contain the radiation reaction force at only the lowest 2.5PN order. From the conservative part of the 3PN dynamics (neglecting the 2.5PN radiation reaction) we shall obtain the binary's center-of-mass energy E at the 3PN order. We now want to compute the variation of E because of the emission of gravitational radiation. For this purpose we replace the knowledge of the radiation reaction force in the local equations of motion by the computation of the total energy flux in gravitational waves, say $\mathcal{L}$, and we apply the energy balance equation

$$\frac{dE}{dt} = -\mathcal{L} \,. \tag{5}$$

Therefore in our approach the computation of the center-of-mass energy E constitutes only one "half" of the solution of the problem. The second "half', that of the computation of the energy flux $\mathcal{L}$, is to be carried out by application of a wave-generation formalism.

Following earliest computations at the 1PN level [37, 38] (at a time when the post-Newtonian corrections in $\mathcal{L}$ had a purely academic interest), the energy flux of inspiralling compact binaries was completed to the 2PN order by Blanchet, Damour and Iyer [39], using the 2PN wave-generation formalism of Ref. [9], and, independently, by Will and Wiseman [40], using their own formalism (see Refs. [41, 42] for joint reports of these calculations). The preceding approximation, 1.5PN, which represents in fact the dominant contribution of tails in the wave zone, had been obtained in Refs. [43, 44] by application of a formula for tail integrals given in Ref. [45]. Higher-order tail effects at the 2.5PN and 3.5PN orders, as well as a crucial contribution of tails generated by the tails themselves (the so-called "tails of tails") at the 3PN order, were obtained by Blanchet [46, 47]. However, unlike the 1.5PN, 2.5PN and 3.5PN orders that are entirely composed of tail terms, the 3PN approximation involves also, besides the tails of tails, many non-tail contributions coming from the relativistic corrections in the (source) multipole moments of the binary. These have been completed by Blanchet, Iyer and Joguet [48, 49], based on the expressions for the multipole moments given in Ref. [10], except for one single unknown numerical coefficient, due to the use of the Hadamard regularization, which is a combination of the parameter λ in the equations of motion, and a new parameter θ coming from the computation of the 3PN quadrupole moment.

The post-Newtonian flux $\mathcal{L}$ is in complete agreement, up to the 3.5PN order, with the result given by the very different technique of linear black-hole perturbations, valid in the "test-mass" limit where the mass of one of the bodies tends to zero (limit $\nu \to 0$, where $\nu = \mu/m$). Linear black-hole perturbations, triggered by the geodesic motion of a small mass around the black hole, have been applied to this problem [50, 51]. This technique has culminated with the beautiful analytical methods of Sasaki, Tagoshi and Tanaka [52, 53, 54], who solved the problem up to the extremely high 5.5PN order.

4 Post-Newtonian templates for compact binary inspiral

The orbital phase of the binary – i.e. the integral of the frequency $\omega(t)$:

$$\Phi(t) = \int \omega(t) dt \,, \tag{6}$$

constitutes the crucial quantity to be monitored (and therefore to be predicted) in the detectors. The templates built from the theoretical prediction for the orbital phase should be accurate enough over most of the inspiral phase, within the frequency bandwidth of the detectors, with reduced cumulative phase lags, so that the phasing errors are not significant when one attempts to extract the values of the binary's parameters (essentially the masses and spins) from the data.

The relevant model for describing the inspiral phase consists of two point-masses moving under their mutual gravitational attraction. As a simplification for the theoretical analysis, the orbit of inspiralling binaries can be considered to be circular, apart from the gradual inspiral, with a good approximation. The templates are based on the energy-balance equation (5), from which one deduces the orbital phase as

$$\Phi_c - \Phi = \int_{\omega_c}^{\omega} \frac{\omega dE}{\mathcal{L}} \,, \tag{7}$$

where Φ_c and ω_c denote the values at the instant of coalescence. The number of gravitational-wave cycles left from the current time till the coalescence instant (we consider only the dominant harmonics at twice the orbital frequency) is

$$\mathcal{N} = \frac{\Phi_c - \Phi}{\pi} \,. \tag{8}$$

It is clear because of Eq. (1) that $\mathcal{N}$ is of the order of the inverse of radiation-reaction effects, hence the formal "post-Newtonian" order is $\mathcal{N} = \mathcal{O}\left(c^{+5}\right)$.

As a matter of fact, $\mathcal{N}$ will be a large number, approximately equal to 1.6×10^4 in the case of two neutron stars between 10 and 1000 Hz (roughly the frequency bandwidth of the detector VIRGO). Data analysts have estimated that, in order not to suffer a too severe reduction of signal-to-noise ratio, one should monitor the phase evolution with an accuracy comparable to one gravitational-wave cycle (i.e. $\delta\mathcal{N} \sim 1$), over the whole detector's bandwidth. From a strict post-Newtonian point of view, we see that the consequence, since the "Newtonian" number of cycles is formally $\mathcal{O}\left(c^{+5}\right)$, is that any post-Newtonian correction therein that is larger than the order c^{-5} is expected to contribute to the phase evolution more than what is allowed by the previous estimate. Therefore, one expects that in order to construct accurate enough templates it will be necessary to compute the orbital phase up to at least the 2.5PN order at a minimum. This back-on-the-envelope estimate has been confirmed by measurement-accuracy analyses [56, 51, 57, 58] which showed that in advanced generations of detectors the 3PN approximation (or, even better, the 3.5PN one) is required in the case of inspiralling neutron star binaries.

The first ingredient in the theoretical calculation is the binding energy E (in the center-of-mass frame), defined as being the invariant energy associated with the *conservative* part of the binary's 3PN dynamics (we ignore the radiation reaction effect at the 2.5PN order). The center-of-mass energy E is deduced from the Hamiltonian in ADM-type coordinates [26, 27, 28, 29, 30], or equivalently from the Lagrangian in harmonic-coordinates [31, 32, 33, 34, 35, 36]. Restricting our consideration to circular orbits, the energy is a function or a single variable, the radial distance r between the two particles in a given coordinate system. In fact it is better to express the energy in terms of the frequency $\omega = \frac{2\pi}{P}$ of the orbital motion, or, rather, in terms of the particular frequency-related parameter

$$x \equiv \left(\frac{GM\omega}{c^3}\right)^{2/3} \,. \tag{9}$$

The individual masses of the black holes are denoted by m_1 and m_2, and the total mass is $M = m_1 + m_2$. The interest of using the parameter x, instead of some coordinate distance r, is that the energy function $E(x)$ then takes an invariant invariant (the same in different coordinate systems). The result we get consists of the Newtonian contribution, proportional to x, followed by post-Newtonian corrections up to the 3PN order:

$$E = -\frac{\mu c^2 x}{2}\left\{1+\left(-\frac{3}{4}-\frac{1}{12}\nu\right)x+\left(-\frac{27}{8}+\frac{19}{8}\nu-\frac{1}{24}\nu^2\right)x^2 + \left(-\frac{675}{64}+\left[\frac{209323}{4032}-\frac{205}{96}\pi^2-\frac{110}{9}\lambda\right]\nu-\frac{155}{96}\nu^2-\frac{35}{5184}\nu^3\right)x^3\right\}. \quad (10)$$

This expression involves the useful ratio between reduced and total masses:

$$\nu = \frac{\mu}{M} \quad \text{where} \quad \mu = \frac{m_1 m_2}{M}. \quad (11)$$

This ratio is interesting because of its range of variation: $0 < \nu \leq \frac{1}{4}$, where $\nu = \frac{1}{4}$ in the equal-mass case and $\nu \to 0$ in the test-mass limit for one of the bodies. The parameter λ denotes a point-mass regularization-constant and will be discussed in Section 5.

The second ingredient in this analysis concerns the gravitational-wave luminosity $\mathcal{L}$, calculated, in the post-Newtonian approximation, from a wave-generation formalism valid for extended "fluid" systems [9, 47, 10], and then specialized to binary systems of point-particles [39, 46, 47, 48, 49]. The calculation takes properly into account the relativistic corrections linked with the description of the source (multipole moments), as well as the non-linear effects in the propagation of the waves from the source to the far zone. The crucial input of any post-Newtonian computation of the flux is the mass quadrupole moment (because the post-Newtonian precision required for the higher multipole moments is smaller). The 3PN quadrupole moment for circular binary orbits in a harmonic coordinate system is of the form[3]

$$I_{ij} = \mu\left(A\,\hat{x}_{ij} + B\,\frac{r^2}{c^2}\,\hat{v}_{ij}\right), \quad (12)$$

and has been obtained recently by Blanchet, Iyer and Joguet [48], with result

$$A = 1+\left(-\frac{1}{42}-\frac{13}{14}\nu\right)\gamma+\left(-\frac{461}{1512}-\frac{18395}{1512}\nu-\frac{241}{1512}\nu^2\right)\gamma^2 + \left(\frac{395899}{13200}-\frac{428}{105}\ln\left(\frac{r}{r_0}\right)+\left[\frac{139675}{33264}-\frac{44}{3}\ln\left(\frac{r}{r'_0}\right)-\frac{44}{3}\xi-\frac{88}{3}\kappa\right]\nu+\frac{162539}{16632}\nu^2+\frac{2351}{33264}\nu^3\right)\gamma^3, \quad (13)$$

$$B = \frac{11}{21}-\frac{11}{7}\nu+\left(\frac{1607}{378}-\frac{1681}{378}\nu+\frac{229}{378}\nu^2\right)\gamma + \left(-\frac{357761}{19800}+\frac{428}{105}\ln\left(\frac{r}{r_0}\right)+\left[-\frac{75091}{5544}+\frac{44}{3}\zeta\right]\nu+\frac{35759}{924}\nu^2+\frac{457}{5544}\nu^3\right)\gamma^2, \quad (14)$$

where the post-Newtonian ordering parameter (defined in harmonic coordinates) reads

$$\gamma = \frac{GM}{rc^2}. \quad (15)$$

Notice the logarithms entering these formulas at the 3PN order. One type involves a constant length scale r_0 coming from the general wave-generation formalism of Refs. [9, 47, 10], and which corresponds to some "infrared" cut-off in the bound at infinity of the integrals defining the multipole moments. The constant r_0 should and will cancel out when considering the complete multipole expansion of the field exterior to the source. The other type of logarithm contains a different length scale r'_0, which should rather be viewed as an "ultra-violet" cut-off associated with the singular behaviour of the metric at the location of the point-particles; r'_0 is related to the two constants r'_1 and r'_2 — one for each particles — appearing in the 3PN equations of motion of Refs. [31, 34, 32, 33, 35, 36] by

$$\ln r'_0 = \frac{m_1}{M}\ln r'_1 + \frac{m_2}{M}\ln r'_2. \quad (16)$$

[3] We neglect a 2.5PN term and denote e.g. $\hat{x}_{ij} = x_i x_j - \frac{1}{3}\delta_{ij}r^2$, where x_i is the harmonic-coordinate separation between the two bodies and $r = |\mathbf{x}|$.

As we know that r'_1 and r'_2 are gauge constants, i.e. they can be eliminated by a gauge transformation at the 3PN order, r'_0 will necessarily disappear from our physical, gauge-invariant, result at the end. Besides the harmless constants r_0 and r'_0, there are three point-mass regularization-constants in Eqs. (13)-(14): ξ, κ and ζ (see Section 5). However, we shall see that the energy flux for circular orbits depends on one combination only of these constants: $\theta = \xi + 2\kappa + \zeta$.

Through 3.5PN order, the result is decomposed into an "instantaneous" part, i.e. generated solely by the multipole moments of the source, and a tail part. What we call here the tail part is in fact a complicated sum of "tails", "tail squares", and "tails of tails", as computed in Ref. [47]. We find, respectively,

$$\begin{aligned}
\mathcal{L}_{\rm inst} &= \frac{32c^5}{5G}\nu^2\gamma^5\left\{1+\left(-\frac{2927}{336}-\frac{5}{4}\nu\right)\gamma+\left(\frac{293383}{9072}+\frac{380}{9}\nu\right)\gamma^2\right.\\
&+ \left(\frac{53712289}{1108800}-\frac{1712}{105}\ln\left(\frac{r}{r_0}\right)\right)\\
&+ \left.\left[-\frac{332051}{720}+\frac{123}{64}\pi^2+\frac{110}{3}\ln\left(\frac{r}{r'_0}\right)+44\lambda-\frac{88}{3}\theta\right]\nu-\frac{383}{9}\nu^2\right)\gamma^3\Big\}\,, \qquad (17)\\
\mathcal{L}_{\rm tail} &= \frac{32c^5}{5G}\nu^2\gamma^5\left\{4\pi\gamma^{3/2}+\left(-\frac{25663}{672}-\frac{109}{8}\nu\right)\pi\gamma^{5/2}\right.\\
&+ \left(-\frac{116761}{3675}+\frac{16}{3}\pi^2-\frac{1712}{105}C-\frac{856}{105}\ln(16\gamma)+\frac{1712}{105}\ln\left(\frac{r}{r_0}\right)\right)\gamma^3\\
&+ \left.\left(\frac{90205}{576}+\frac{3772673}{12096}\nu+\frac{32147}{3024}\nu^2\right)\pi\gamma^{7/2}\right\}. \qquad (18)
\end{aligned}$$

The Newtonian result has been factorized out in front. Here $C = 0.577\cdots$ denotes the Euler constant. As we can see, the constant r_0 drops out from the sum of Eqs. (17) and (18). However, the gauge constant r'_0 does not seem to disappear at this stage, but that is simply due to our use of the post-Newtonian parameter γ defined by (15), and which depends *via* the equation of motion on the choice of harmonic coordinates. After substituting the frequency-related parameter x in place of γ (with the help of the 3PN equations of motion), we find that r'_0 does cancel as well – this nicely illustrates the consistency between our two computations, in harmonic-coordinates, of the equation of motion on one hand and the multipole moments on the other hand. Finally we obtain

$$\begin{aligned}
\mathcal{L} &= \frac{32c^5}{5G}\nu^2x^5\left\{1+\left(-\frac{1247}{336}-\frac{35}{12}\nu\right)x+4\pi x^{3/2}\right.\\
&+ \left(-\frac{44711}{9072}+\frac{9271}{504}\nu+\frac{65}{18}\nu^2\right)x^2+\left(-\frac{8191}{672}-\frac{535}{24}\nu\right)\pi x^{5/2}\\
&+ \left(\frac{6643739519}{69854400}+\frac{16}{3}\pi^2-\frac{1712}{105}C-\frac{856}{105}\ln(16x)\right.\\
&+ \left.\left[-\frac{11497453}{272160}+\frac{41}{48}\pi^2+\frac{176}{9}\lambda-\frac{88}{3}\theta\right]\nu-\frac{94403}{3024}\nu^2-\frac{775}{324}\nu^3\right)x^3\\
&+ \left.\left(-\frac{16285}{504}+\frac{176419}{1512}\nu+\frac{19897}{378}\nu^2\right)\pi x^{7/2}\right\}. \qquad (19)
\end{aligned}$$

The last test (but not the least) is that Eq. (19) is in perfect agreement, in the test-mass limit $\nu \to 0$, with the result of linear black-hole perturbations obtained by Tagoshi and Sasaki [53].

5 Problem of regularization ambiguities

A model of structureless point masses is expected to be sufficient to describe the inspiral phase of compact binaries. Thus we want to compute the metric (and its gradient needed in the equations of motion) at

the 3PN order for a system of two point-like particles. Applying general expressions for the metric valid in the case of continuous (smooth) matter sources, we find that most of the integrals become divergent at the location of the particles. Consequently we must supplement the calculation by a prescription for how to remove (i.e. to regularize) the infinite part of these integrals.

The "standard" Hadamard regularization yields some ambiguous results for the computation of certain integrals at the 3PN order, as Jaranowski and Schäfer [26, 27] noticed in their computation of the equations of motion within the ADM-Hamiltonian formulation of general relativity. They showed that there are *two* and *only two* types of ambiguous terms in the 3PN Hamiltonian, which were then parametrized by two unknown numerical coefficients $\omega_{\rm static}$ and $\omega_{\rm kinetic}$.

Blanchet and Faye [32, 33], motivated by the previous result, introduced their "improved" Hadamard regularization, based on a theory of pseudo-functions and generalized distributional derivatives. This new regularization is mathematically well-defined and free of ambiguities; in particular it yields unique results for the computation of any of the integrals occuring in the 3PN equations of motion. Unfortunately, this regularization turned out to be in a sense incomplete, because it was found [31, 34] that the 3PN equations of motion involve *one* and *only one* unknown numerical constant, called λ, which cannot be determined within the method. The comparison of this result with the work of Jaranowski and Schäfer [26, 27], on the basis of the computation of the invariant energy of binaries moving on circular orbits, showed [31] that

$$\omega_{\rm kinetic} = \frac{41}{24}\,, \tag{20}$$

$$\omega_{\rm static} = -\frac{11}{3}\lambda - \frac{1987}{840}\,. \tag{21}$$

Therefore, the ambiguity $\omega_{\rm kinetic}$ is fixed, while λ is equivalent to the other ambiguity $\omega_{\rm static}$. The value of $\omega_{\rm kinetic}$ given by Eq. (20) was recovered by Damour, Jaranowski and Schäfer [28], who proved that this value is the unique one for which the global Poincaré invariance of their formalism is verified. By contrast, the harmonic-coordinate conditions preserve the Poincaré invariance, and therefore the associated equations of motion should be Lorentz-invariant, as was indeed found to be the case by Blanchet and Faye [31, 34], thanks in particular to their use of a Lorentz-invariant regularization [33] (hence their determination of $\omega_{\rm kinetic}$).

The appearance of one and only one physical undeterminacy $\lambda \Leftrightarrow \omega_{\rm static}$ in the equations of motion constitutes a quite striking fact, specifically related to the use of an Hadamard-type regularization. Mathematically speaking, the presence of λ is (probably) related to the fact that it is impossible to construct a distributional derivative operator satisfying the Leibniz rule for the derivation of the product. The Einstein field equations can be written into many different forms, by operating some terms by parts with the help of the Leibniz rule. All these forms are equivalent in the case of regular sources, but they become inequivalent for point particles if the derivative operator violates the Leibniz rule.

In Ref. [60] it has been argued that the numerical value of the parameter $\omega_{\rm static}$ could be $\simeq -9$, because for such a value some different resummation techniques, *viz* Padé approximants [58] and effective-one-body (EOB) method [59], when they are implemented at the 3PN order, give approximately the same numerical result for the location of the last stable circular orbit. Even more, it was suggested [60] that $\omega_{\rm static}$ might be precisely equal to $\omega^*_{\rm static}$, with

$$\omega^*_{\rm static} = -\frac{47}{3} + \frac{41}{64}\pi^2\,. \tag{22}$$

(We have $\omega^*_{\rm static} = -9.34\cdots$.) However, the value of $\omega_{\rm static}$ in general relativity has been computed by Damour, Jaranowski and Schäfer [30] by means of a dimensional regularization, instead of an Hadamard-type one, within the ADM-Hamiltonian formalism. Their result is

$$\omega_{\rm static} = 0 \iff \lambda = -\frac{1987}{3080}\,. \tag{23}$$

As Damour *et al* [30] argue, clearing up the ambiguity is made possible by the fact that the dimensional regularization, contrary to the Hadamard regularization, respects all the basic properties of the algebraic

and differential calculus of ordinary functions[4].

Let us comment that the use of a self-field regularization in this problem, it be dimensional or based on the Hadamard partie finie, signals a somewhat unsatisfactory situation on the physical point of view, because we would like to perform, ideally, a complete calculation valid for extended bodies, taking into account the details of the internal structure of the bodies (energy density, pressure, internal velocities, etc.). By considering the limit where the radii of the objects tend to zero, one should recover the same result as obtained by means of the point-mass regularization, and determine the value of the regularization parameter λ. Because of considerable difficulties arising at the 3PN order this program has not yet been achieved.

Concerning the 3PN radiation field of two point masses – the second half of the problem, besides the 3PN equations of motion –, Blanchet, Iyer and Joguet [48] used the (standard) Hadamard regularization and found necessary to introduce three additional regularization constants ξ, κ and ζ. However the total gravitational-wave flux, in the case of circular orbits, depends only on the linear combination

$$\theta = \xi + 2\kappa + \zeta \,. \tag{24}$$

Furthermore, this θ comes in at the same level as λ, so there is in fact only one unknown constant in the flux [see Eqs. (17)-(19)]. Notice that the improved version of the Hadamard regularization proposed in Refs. [32, 33] should be able, in principle, to fix the value of the constant ζ.

6 Accuracy of the post-Newtonian approximation

In this section we discuss (some aspects of) the accuracy of the post-Newtonian approximation as regards the determination of the binary's innermost circular orbit (ICO). The ICO will be defined by the minimum, when it exists, of the energy function $E(x)$ given by Eq. (10). Notice that we do not define the ICO as an ISCO, i.e. as a point of dynamical general-relativistic unstability. See Ref. [36] for a discussion of the dynamical stability of circular binary orbits at the 3PN order.

Let us first confront the prediction of the standard (Taylor-based) post-Newtonian approximation at the 3PN order for the ICO – as given by the minimum of Eq. (10) – with a recent numerical calculation by Gourgoulhon, Grandclément and Bonazzola [61, 62]. These authors obtained numerically the energy $E(\omega)$ of binary black holes along evolutionary sequences of equilibrium configurations under the assumptions of conformal flatness for the spatial metric and of exactly circular orbits. The latter restriction is implemented by requiring the existence of an "helical" Killing vector, time-like inside the light cylinder associated with the circular motion and space-like outside. The numerical calculation [61, 62] has been performed in the case of *corotating* black holes, which are spinning with the orbital angular velocity ω. For the comparison we must therefore include within the post-Newtonian formalism yielding Eq. (10) the effects of spins appropriate to two Kerr black holes rotating at the orbital rate ω.

The Figure 1 (issued from Ref. [63]) presents the post-Newtonian results for $E_{\rm ICO}$ in the case of irrotational and corotational binaries. The points indicated by 1PN, 2PN and 3PN are defined from the obvious truncation of Eq. (10). The points $1{\rm PN}^{\rm corot}$, $2{\rm PN}^{\rm corot}$ and $3{\rm PN}^{\rm corot}$ take into account the spin effects of corotational binaries and are computed in Ref. [63]. Notice that the irrotational and corotational configurations differ only from the 2PN order. As we can see the 3PN points, and even the 2PN ones, are rather close to the numerical value (marked by an asterisk in Figure 1). As expected, the best agreement is for the 3PN approximation and in the case of corotation: i.e. the point $3{\rm PN}^{\rm corot}$. So our first conclusion is that the location of the ICO as computed by numerical relativity, under the helical-symmetry approximation [61, 62], is in good agreement with post-Newtonian predictions. This constitutes an appreciable improvement of the previous situation, because we recall that the earlier estimates of the ICO in post-Newtonian theory [64] and numerical relativity [65, 66] strongly disagree with each other, and do not match with the present 3PN results (see Ref. [62] for further discussion).

Our second conclusion comes from the fact that the 2PN and 3PN values in Figure 1 – either for irrotational or corotational binaries – are so close to each other. Indeed it seems that the 3PN points

[4]Note that the result (23) is very different from $\omega^*_{\rm static}$ given by Eq. (22): this suggests that the resummation techniques (Padé approximants and EOB method), though they are designed to "accelerate" the convergence of the post-Newtonian series, do *not* in fact converge toward the same exact solution (or, at least, not as fast as expected). See Section 7 for discussion on this point.

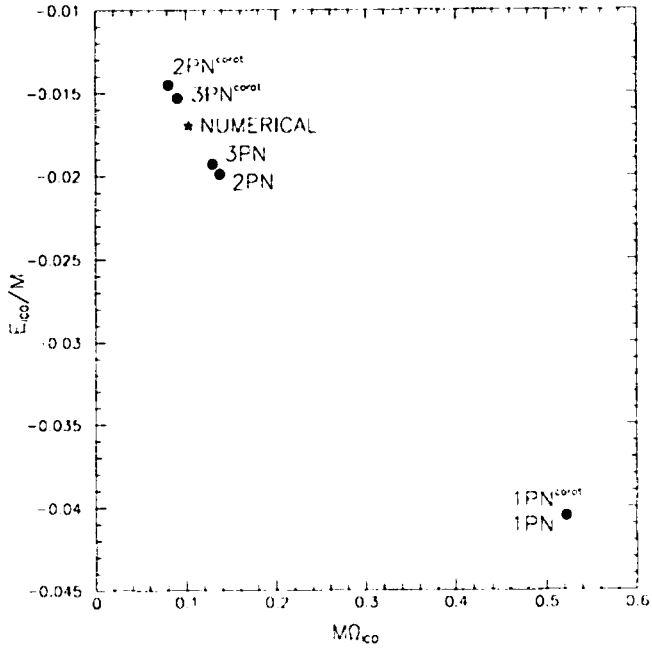


Figure 1: The center-of-mass energy $E_{\rm ICO}$ versus $\omega_{\rm ICO}$ in the equal-mass case ($\nu = \frac{1}{4}$). The asterisk marks the result calculated by numerical relativity [61, 62]. The points indicated by 1PN, 2PN and 3PN correspond to irrotational binaries, while the points denoted by $1{\rm PN}^{\rm corot}$, $2{\rm PN}^{\rm corot}$ and $3{\rm PN}^{\rm corot}$ describe corotational binaries. Both 3PN are $3{\rm PN}^{\rm corot}$ are shown for $\omega_{\rm static} = 0$.

are useful only to *confirm* the result given by the 2PN ones. This is a quite satisfying state of affairs because it indicates that the post-Newtonian approximation converges very well (in the sense of Cauchy's criterion). Figure 1 shows that the post-Newtonian approximation is well qualified to accurately locate the ICO (of course for this purpose one must go to the 3PN order — the 1PN approximation is clearly not accurate enough).

Let us elaborate more on this point. First we make a few order-of-magnitude estimates. At the location of the ICO we find (see Figure 1) that the frequency-related parameter x defined by Eq. (9) is approximately of the order of 20%. Therefore, we might *a priori* expect that the contribution of the 1PN approximation to the energy at the point of the ICO should be of the order of 20%. For the present discussion we take the pessimistic view that the order of magnitude of an approximation represents also the order of magnitude of the higher-order terms that are neglected. We see that the 1PN approximation should yield a rather poor estimate of the "exact" result, but this is quite normal at this very relativistic point where the orbital velocity is $\frac{v}{c} \sim \sqrt{x} \sim 50\%$. By the same argument we infer that the 2PN approximation should do much better, with fractional errors of the order of $x^2 \sim 5\%$, while the 3PN approximation will be even better, with the precision $x^3 \sim 1\%$.

The simple order-of-magnitude estimate suggests therefore that the 3PN order should be close to the "exact" solution for the ICO to within 1% of fractional accuracy. We think that this is very good, and we should even remember that this estimate is pessimistic, because we could reasonably expect that the neglected higher-order approximations, 4PN and so on, are in fact much smaller numerically (e.g. of the order of $x^4 \sim 0.2\%$). But let us keep for the present discussion the 1% guess for the accuracy of the 3PN approximation.

Now the previous estimates make sense only if the numerical values of the post-Newtonian coefficients in Eq. (10) are roughly of the order of one. If this is not the case, and if the coefficients increase

dangerously with the post-Newtonian order n, one sees that the post-Newtonian approximation might in fact be very bad. So let us look at the values of the coefficients of the 1PN, 2PN and 3PN approximations in Eq. (10), say

$$a_1(\nu) = -\frac{3}{4} - \frac{\nu}{12}\,, \tag{25}$$

$$a_2(\nu) = -\frac{27}{8} + \frac{19}{8}\nu - \frac{\nu^2}{24}\,, \tag{26}$$

$$a_3(\nu) = -\frac{675}{64} + \left[\frac{209323}{4032} - \frac{205}{96}\pi^2 - \frac{110}{9}\lambda\right]\nu - \frac{155}{96}\nu^2 - \frac{35}{5184}\nu^3\,. \tag{27}$$

We present in Table 1 the values of these coefficients in the test-mass limit $\nu = 0$, and in the equal-mass case $\nu = \frac{1}{4}$ when the ambiguity parameter takes the "uncorrect" value $\omega^*_{\rm static}$ [see Eq. (22)] and the correct one $\omega_{\rm static} = 0$ predicted by general relativity [30].

		Newtonian	$a_1(\nu)$	$a_2(\nu)$	$a_3(\nu)$
$\nu = 0$		1	-0.75	-3.37	-10.55
$\nu = \frac{1}{4}$	$\omega^*_{\rm static} \simeq -9.34$	1	-0.77	-2.78	-8.75
$\nu = \frac{1}{4}$	$\omega_{\rm static} = 0$	1	-0.77	-2.78	-0.97

Table 1: Sequence of coefficients of the post-Newtonian series composing the energy function (25)-(27).

Our first comment is that when $\nu = 0$ there is an *increase* of the coefficients by roughly a factor 3 at each step. This behaviour is fairly easy to understand. It comes from the existence in the Schwarzshild metric of the famous light-ring orbit: a geodesics of photon which is a circular orbit located at $R = 3M$ in Schwarzshild coordinates. As a result, the energy of the test particle in the Schwarzshild metric exhibits a singularity at $x_{\rm light-ring} = \frac{1}{3}$,

$$E^{\rm test}(x) = \mu c^2 \left(\frac{1-2x}{\sqrt{1-3x}} - 1\right)\,. \tag{28}$$

The consequence is that the radius of convergence of the post-Newtonian series is $\frac{1}{3}$, so the post-Newtonian coefficients increase by a factor ~ 3. So the post-Newtonian series is not very accurate in the case $\nu = 0$. This fact has motivated several statements in the literature (see e.g. [55, 56, 57, 58]), according to which the post-Newtonian approximation would be "poorly convergent", or that there should be a "fundamental breakdown" of its validity in the regime of the ICO. This is indeed true in the *test-mass* limit ($\nu \to 0$), where the post-Newtonian series converges slowly[5].

On the other hand, what happens in the equal-mass case ($\nu = \frac{1}{4}$)? When $\nu = \frac{1}{4}$ and we have the value $\omega^*_{\rm static}$ we notice that the coefficients increase approximately like in the test-mass case $\nu = 0$. This indicates that the gravitational interaction in the case of $\omega^*_{\rm static}$ looks like that in a one-body problem. We shall say that when the post-Newtonian coefficients rapidly increase with the order of approximation, the interaction is "Schwarzschild-like".

Now when $\nu = \frac{1}{4}$ and the ambiguity parameter takes the correct value $\omega_{\rm static} = 0$, we see that the 3PN coefficient $a_3(\frac{1}{4})$ is of the order of minus one instead of ~ -10. We think that this strongly suggests, unless 3PN happens to be quite accidental, that the post-Newtonian coefficients in general relativity do not increase very much with n, and stay rather of the order of one. This is interesting as it indicates that the actual general-relativistic two-body interaction is *not* Schwarzschild-like.

It is impossible of course to be very confident about the validity of the previous statement because we know only the coefficients up to the 3PN order. Any tentative conclusion based on the 3PN order

[5]Let us remark that this negative conclusion does not matter: indeed we shall never use the post-Newtonian approximation in the case $\nu \to 0$ simply because we know the exact result which is given by Eq. (10). The exact result for the radiation field is known as well, albeit numerically only [51, 57]. Therefore we should not worry too much about the poor convergence of the post-Newtonian series in the test-mass limit. The post-Newtonian method is useless and even one might say irrelevant when considering the motion of a test particle around a Schwarzschild black hole.

can be "falsified" when we obtain the next 4PN order. Nevertheless, we feel that the mere fact that $a_3(\frac{1}{4}) = -0.97$ in Table 1 is sufficient to motivate our (tentative) conclusion that the field of two bodies is more complicated than the Schwarzschild space-time. This conclusion is in accordance with the present author's respectfulness of the complexity of the Einstein field equations.

The nice consequence is that because the post-Newtonian coefficients when $\nu = \frac{1}{4}$ stay of the order of one, the *standard* post-Newtonian approach, based on the standard Taylor approximants, is probably very accurate. The post-Newtonian series seems to "converge well", with a "convergence radius" of the order of one[6]. A convincing support of this view is provided by Figure 1 itself. The order-of-magnitude estimates we did at the beginning of this Section are probably correct. In particular the 3PN order should be close to the "exact" solution even in the regime of the ICO.

It is also interesting to look at the numerical values of the post-Newtonian coefficients in the total flux $\mathcal{L}$ obtained in Eq. (19). For this case we do not have (like for the ICO) a clear point at which we can compare with a result of numerical relativity. Furthermore things concerning the convergence of the post-Newtonian series are less clear than with the energy function. A possible reason for that could be that the flux, in contrast to the energy, includes the contribution of tails at the 1.5PN, 2.5PN and 3.5PN orders, and even of tails-of-tails at the 3PN order.

			Newtonian	$b_1(\nu)$	$b_{3/2}(\nu)$	$b_2(\nu)$	$b_{5/2}(\nu)$	$b_3(\nu)$	$b_{7/2}(\nu)$
$\nu = 0$			1	-3.71	12.57	-4.93	-38.29	128.85	-101.51
$\nu = \frac{1}{4}$	$\lambda = -\frac{1987}{3080}$	$\theta = 0$	1	-4.44	12.57	-0.10	-55.80	115.26	0.47

Table 2: Post-Newtonian coefficients in the flux function (19). The coefficient $b_3(\nu)$ contains a log-term that we have evaluated at $x_{\rm ICO} \sim 0.2$. [The value $\theta = 0$ is taken to be indicative.]

7 On Schwarzschild-like templates for binary inspiral

Let us finally comment about a possible implication of our conclusion as regards the validity of the so-called post-Newtonian resummation techniques, i.e. Padé approximants [58, 60], which aim at "accelerating" the convergence of the post-Newtonian series in the pre-coalescence stage, and effective-one-body (EOB) methods [59, 60], which attempt at describing the late stage of the coalescence of two black holes. These techniques are based on the idea that the gravitational two-body interaction is a "deformation" – with $\nu \leq \frac{1}{4}$ being the deformation parameter — of the Schwarzschild space-time.

The Padé approximants are valuable tools for giving accurate representations of functions having some singularities. In the problem at hands they would be justified if the "exact" expression of the energy [whose 3PN expansion is given by Eqs. (25)-(27)] would admit some Schwarzschild-like features, and in particular a light-ring singularity. In the Schwarzschild case the Padé series converges rapidly toward the solution [58]: the Padé constructed only from the 2PN approximation of the energy – keeping only $a_1(0)$ and $a_2(0)$ in Eqs. (2) — already coincide with the exact result given by Eq. (8). On the other hand, the EOB method maps the post-Newtonian two-body dynamics (at the 2PN or 3PN order) on the geodesic motion on some effective metric which happens to be a ν-deformation of the Schwarzschild space-time. In the EOB method the effective metric looks like Schwarzschild *by definition*, and we might expect the two-body interaction to own some Schwarzschild-like features.

Our comment is that the validity of these resummation techniques (and the templates for binary inspiral built on them) is questionable, because as we have seen in Section 6 the value $\omega_{\rm static} = 0$ suggests that most probably the two-body interaction is not Schwarzschild-like. In particular, there does not seem to exist something like a light-ring orbit which would be a deformation of the Schwarzschild one.

To test the previous idea, let us come back to the Schwarzschild limit, where we observed that the radius of convergence of the post-Newtonian series is given by the light-ring singularity at the value $\frac{1}{3}$. Now the radius of convergence is given by d'Alembert's criterion as the limit when $n \to +\infty$ of the ratio

[6]Actually, the post-Newtonian series could be only asymptotic (hence divergent), but nevertheless it should give good results provided that the series is truncated near some optimal order of approximation. In this discussion we assume that the 3PN order is not too far from that optimum.

of successive coefficients, i.e. a_{n-1}/a_n. We might therefore *compute* the light-ring orbit by investigating the limit

$$x^{\rm test}_{\rm light-ring} = \lim_{n\to+\infty} \frac{a^{\rm test}_{n-1}}{a^{\rm test}_n} = \frac{1}{3} \,. \tag{29}$$

To test for the possible existence of a light-ring singularity in the case of comparable masses, we consider the ratio between the two highest known post-Newtonian coefficients, that are $a_2(\nu)$ and $a_3(\nu)$. This ratio will give an *estimate* of the "light-ring" singularity for non-infinitesimal mass ratios,

$$x_{\rm light-ring}(\nu) \sim \frac{a_2(\nu)}{a_3(\nu)} \,. \tag{30}$$

Using the values given in Table 1 we obtain for equal masses in the case of the "wrong" ambiguity parameter $\omega^*_{\rm static} \simeq -9.34$,

$$x_{\rm light-ring}(\tfrac{1}{4}, \omega^*_{\rm static}) \sim 0.32 \,. \tag{31}$$

As we see there seems to be in this case a (pseudo-)light-ring orbit which is a small deformation of the Schwarzschild light-ring orbit given by Eq. (29). In this Schwarzschild-like situation, we expect that Padé approximants and EOB-type methods to be appropriate.

But, in the case of general relativity ($\omega_{\rm static} = 0$), we obtain a drastically different result:

$$x_{\rm light-ring}(\tfrac{1}{4}, G.R.) \sim 2.86 \,. \tag{32}$$

If we believe the correctness of this estimate we must conclude that there is in fact no notion of a light-ring orbit in the real two-body case. Or, one might say (pictorially speaking) that the light-ring orbit gets hidden inside the horizon of the final black-hole formed by coalescence. If we consider the ratio between the 1PN and 2PN coefficients (instead of between 2PN and 3PN), we get the value ~ 0.28 instead of Eq. (32). So at the 2PN order the field seems to admit a light ring, while at the 3PN order it does not. This reinforces our idea that it is meaningless (with our present 3PN-based knowledge, and untill fuller information is available), to assume the existence of a light-ring singularity in the equal-mass case. Our expectation, therefore, is that the conditions under which the Padé and EOB methods should be legitimate might in fact not be fulfilled.

This doubt is confirmed by the finding of Ref. [60] (already alluded to above) that in the case of the "wrong" ambiguity parameter $\omega^*_{\rm static} \simeq -9.34$ the Padé approximants and the EOB method at the 3PN order give the same result for the ICO. From the previous discussion we see that this agreement is to be expected because a deformed (pseudo-)light-ring singularity seems to exist with $\omega^*_{\rm static}$. By contrast, in the case of general relativity, where $\omega_{\rm static} = 0$, the Padé and EOB methods give quite different results (*cf* the figure 2 in Ref. [60]). Another confirmation comes from the light-ring singularity which is determined from the Padé approximants at the 2PN order (see Eq. (3.22) in Ref. [58]) as $x^{\rm P-2PN}_{\rm light-ring}(\frac{1}{4}) \sim 0.44$. This value is rather close to Eq. (31) but strongly disagrees with Eq. (32). Our explanation is that the Padé series might converge toward a theory having $\omega_{\rm static} = \omega^*_{\rm static}$ and therefore which is different from general relativity.

References

[1] See the contributions of E. Gourgoulhon, M. Shibata and H. Shinkai in this volume.

[2] O. Poujade and L. Blanchet, Phys. Rev. **D65**, 124020 (2002).

[3] S. Chandrasekhar and Y. Nutku, Astrophys. J. 158, 55 (1969).

[4] G.D. Kerlick, Gen. Rel. Grav. 12, 467 (1980).

[5] G.D. Kerlick, Gen. Rel. Grav. 12, 521 (1980).

[6] J.L. Anderson and T.C. DeCanio, Gen. Relat. Grav. 6, 197 (1975).

[7] A.D. Rendall, Proc. R. Soc. London **A438**, 341 (1992).

[8] L. Blanchet and T. Damour, Philos. Trans. R. Soc. London A **320**, 379 (1986).

[9] L. Blanchet, Phys. Rev. D **51**, 2559 (1995).

[10] L. Blanchet, Class. Quantum. Grav. **15**, 1971 (1998).

[11] L. Blanchet and T. Damour, Phys. Rev. **D37**, 1411 (1988).

[12] L. Blanchet, Phys. Rev. **D47**, 4392 (1993).

[13] L. Blanchet, Phys. Rev. **D55**, 714 (1997).

[14] A. Einstein, L. Infeld and B. Hoffmann, Ann. Math. **39**, 65 (1938).

[15] T. Damour and N. Deruelle, Phys. Lett. **87A**, 81 (1981).

[16] T. Damour and N. Deruelle, C. R. Acad. Sc. Paris **293**, 537 (1981).

[17] T. Damour, C. R. Acad. Sc. Paris **294**, 1355 (1982).

[18] L. Bel, T. Damour, N. Deruelle, J. Ibañez and J. Martin, Gen. Relativ. Gravit. **13**, 963 (1981).

[19] T. Damour and G. Schäfer, Gen. Rel. Grav. **17**, 879 (1985).

[20] S.M. Kopejkin, Astron. Zh. **62**, 889 (1985).

[21] L. Blanchet, G. Faye and B. Ponsot, Phys. Rev. **D58**, 124002 (1998).

[22] M.E. Pati and C.M. Will, gr-qc 0201001.

[23] L.P. Grishchuk and S.M. Kopejkin, in *Relativity in Celestial Mechanics and Astrometry*, J. Kovalevsky and V.A. Brumberg (eds.), Reidel, Dordrecht (1986).

[24] Y. Itoh, T. Futamase and H. Asada, Phys. Rev. **D62**, 064002 (2000).

[25] Y. Itoh, T. Futamase and H. Asada, Phys. Rev. **D63**, 064038 (2001).

[26] P. Jaranowski and G. Schäfer, Phys. Rev. **D57**, 7274 (1998).

[27] P. Jaranowski and G. Schäfer, Phys. Rev. **D60**, 124003 (1999).

[28] T. Damour, P. Jaranowski and G. Schäfer, Phys. Rev. **D62**, 021501R (2000).

[29] T. Damour, P. Jaranowski and G. Schäfer, Phys. Rev. **D63**, 044021 (2001).

[30] T. Damour, P. Jaranowski and G. Schäfer, Phys. Lett. **B513**, 147 (2001).

[31] L. Blanchet and G. Faye, Phys. Lett. A **271**, 58 (2000).

[32] L. Blanchet and G. Faye, J. Math. Phys. **41**, 7675 (2000).

[33] L. Blanchet and G. Faye, J. Math. Phys. **42**, 4391 (2001).

[34] L. Blanchet and G. Faye, Phys. Rev. **D63**, 062005 (2001).

[35] V. de Andrade, L. Blanchet and G. Faye, Class. Quantum Grav. **18**, 753 (2001).

[36] L. Blanchet and B. Iyer, Class. Quantum Grav. **20**, 755 (2003).

[37] R.V. Wagoner and C.M. Will, Astrophys. J. **210**, 764 (1976).

[38] L. Blanchet and G. Schäfer, Mon. Not. R. Astr. Soc. **239**, 845 (1989).

[39] L. Blanchet, T. Damour and B.R. Iyer, Phys. Rev. D **51**, 5360 (1995).

[40] C.M. Will and A.G. Wiseman, Phys. Rev. D **54**, 4813 (1996).

[41] L. Blanchet, T. Damour, B.R. Iyer, C.M. Will and A.G. Wiseman, Phys. Rev. Lett. **74**, 3515 (1995).

[42] L. Blanchet, B.R. Iyer, C.M. Will and A.G. Wiseman, Class. Quantum Grav. **13**, 575 (1996).

[43] A. G. Wiseman, Phys. Rev. D **48**, 4757 (1993).

[44] L. Blanchet and G. Schäfer, Class. Quantum Grav. **10**, 2699 (1993).

[45] L. Blanchet and T. Damour, Phys. Rev. D **46**, 4304 (1992).

[46] L. Blanchet, Phys. Rev. D **54**, 1417 (1996).

[47] L. Blanchet, Class. Quantum. Grav. **15**, 113 (1998).

[48] L. Blanchet, B.R. Iyer and B. Joguet, Phys. Rev. D **65**, 064005 (2002).

[49] L. Blanchet, G. Faye, B.R. Iyer and B. Joguet, Phys. Rev. D **65**, 061501R (2002).

[50] E. Poisson, Phys. Rev. D **47**, 1497 (1993).

[51] H. Tagoshi and T. Nakamura, Phys. Rev. D**49**, 4016 (1994).

[52] M. Sasaki, Prog. Theor. Phys. **92**, 17 (1994).

[53] H. Tagoshi and M. Sasaki, Prog. Theor. Phys. **92**, 745 (1994).

[54] T. Tanaka, H. Tagoshi and M. Sasaki, Prog. Theor. Phys. **96**, 1087 (1996).

[55] C. Cutler, T.A. Apostolatos, L. Bildsten, L.S. Finn, E.E. Flanagan, D. Kennefick, D.M. Markovic, A. Ori, E. Poisson, G.J. Sussman and K.S. Thorne, Phys. Rev. Lett. **70**, 2984 (1993).

[56] C. Cutler, L.S. Finn, E. Poisson and G.J. Sussman, Phys. Rev. D**47**, 1511 (1993).

[57] E. Poisson, Phys. Rev. D**52**, 5719 (1995); Phys. Rev. D**55**, 7980 (1997).

[58] T. Damour, B.R. Iyer and B.S. Sathyaprakash, Phys. Rev. D**57**, 885 (1998).

[59] A. Buonanno and T. Damour, Phys. Rev. D**59**, 084006 (2001).

[60] T. Damour, P. Jaranowski and G. Schäfer, Phys. Rev. D**62**, 084011 (2000).

[61] E. Gourgoulhon, P. Grandclément and S. Bonazzola, Phys. Rev. D**65**, 044020 (2002).

[62] P. Grandclément, E. Gourgoulhon and S. Bonazzola, Phys. Rev. D**65**, 044021 (2002).

[63] L. Blanchet, Phys. Rev. D **65**, 124009 (2002).

[64] L.E. Kidder, C.M. Will and A.G. Wiseman, Phys. Rev. D**47**, 3281 (1993).

[65] H.P. Pfeiffer, S.A. Teukolsky and G.B. Cook, Phys. Rev. D**62**, 104018 (2000).

[66] T.W. Baumgarte, Phys. Rev. D**62**, 024018 (2000).

Black Hole Production at a TeV

Roberto Emparan[1]

Theory Division, CERN, CH-1211 Geneva 23, Switzerland
and
ICREA and Departament de Física Fonamental,
Universitat de Barcelona, Diagonal 647, E-08028 Barcelona, Spain

Abstract

In this talk I briefly discuss some features of a striking signature of TeV quantum gravity/strings and large dimensions: the production of exotic objects such as black holes, and their stringy precursors, the string resonances at large masses which can be dubbed 'string balls'. The focus is on aspects less frequently discussed in other reviews of this subject.

1 Introduction

Let us start by asking one of the most basic questions in theoretical physics: What is the fundamental scale for Quantum Gravity? Answer: *We don't know.* It is only quite recently that we have become fully aware of this. The reason for our ignorance is quite simple: we do not know how to formulate the correct theory of quantum gravity. What we do know is the following: the fundamental energy scale M_* has to be larger than a TeV, for otherwise we should have seen effects of quantum gravity at LEP and the Tevatron[2]. We also know that M_* can be as large as, but not larger than, the familiar Planck scale $M_{(4)} \sim 10^{19}$ GeV, since at this energy four-dimensional gravity becomes strongly coupled and quantum effects surely must become important. The phrase *four-dimensional* in the last statement betrays already the mechanism that allows M_* to be smaller than $M_{(4)}$ [1]. The introduction of large extra dimensions dilutes gravity in an internal n-dimensional volume $V_n = L^n$, and $M_{(4)}$ is revealed as an effective coupling

$$M_{(4)}^2 = M_*^{n+2} L^n \,, \tag{1}$$

describing the strength of gravity only at distances larger than the length scale of the additional dimensions.

The scenario is completed by a mechanism that prevents all particles and interactions, other than gravity, to spread out into these large extra dimensions: they are confined inside a brane, of thickness $\lesssim$ TeV^{-1}, localized in the internal space. By making L^n sufficiently large to allow M_* to be near the TeV scale, one achieves a reformulation of the hierarchy problem.

The great interest in these models has been prompted by the fact that with M_* as low as a TeV one obtains spectacular new physics in future colliders such as the LHC. The signatures due to graviton production and exchange have been thoroughly studied (see e.g. [3]). In this talk I will briefly review some aspects of a more striking signature of TeV quantum gravity/strings and large dimensions: the production of exotic objects such as black holes [4, 5, 6, 7, 8], and their stringy precursors, the string resonances at large masses which can be dubbed 'string balls' [9]. Both these objects have in common their large mass (larger than fundamental mass scale), and the fact that they have a large degeneracy of internal states. The latter is crucial to their large production cross section.

There are already a number of reviews on this subject [10] to which the reader is referred to for other details, for discussion of topics that I mentioned in my talk but are not included here such as black hole production in cosmic rays [11], and for extensive lists of references. Instead, I will mostly focus on aspects that have been less prominent in former discussions in the literature.

[1] E-mail: emparan@ffn.ub.es

[2] There are ways of sidestepping even this lower bound [2], but I will not discuss these scenarios here.

2 Black holes on branes

Finding the exact description of a black hole localized on a three-brane, whether the bulk spacetime is compact (as in ADD scenarios) or non-compact (as in the RS2 model), is an outstanding problem in General Relativity. However, the problem can be sidestepped for a black hole formed at a typical collider energy in the range of $O(10)$ TeV. Such a black hole has a size $\sim 10^{-15}$ mm, which is several orders of magnitude smaller than the size that the extra dimensions can presumably have (e.g., for $n = 7$ and $M_* \sim O(\text{TeV})$ we would have $L \sim$ fermi). Therefore, at distances smaller than L we can neglect all finite-size effects from the compact dimensions, and approximate the metric for a neutral, non-rotating black hole by the Tangherlini-Schwarzschild solution in $4 + n$ dimensions. We want this black hole to be stuck to the brane, in such a manner that, at distances $r \ll L$ the metric induced on the brane is

$$ds^2_{brane} \simeq -\left(1 - \frac{\mu}{r^{1+n}}\right) dt^2 + \frac{dr^2}{\left(1 - \frac{\mu}{r^{1+n}}\right)} + r^2 d\Omega^2_{(2)} \,. \tag{2}$$

All the interesting physics (the formation and evaporation of the black hole) happens in a region within a few horizon radii, so this approximate geometry will be enough for our purposes. Note that this is not a solution of the Einstein equations in four dimensions: the additional modes of gravity in the bulk (Kaluza-Klein modes) are not zero in the region near the black hole horizon. It can also be argued that the mass of the black hole as measured from the $4 + n$ dimensional point of view is the same as the one that a four-dimensional observer, probing distances $r \gg L$, would measure [6].

3 Scattering at $E > M_*$ and Black Hole Formation

Given our ignorance about the correct theory of quantum gravity, one might think that we cannot say anything at all about scattering at energies beyond the fundamental Planck scale M_*. This is not quite correct.[3] While there is certainly a gap in our ability to perform calculations at energies near the fundamental scale of quantum gravity, $E \sim M_*$, a number of generic arguments based on a crucial property of General Relativity, namely the appearance of horizons, allow us to argue for a description of some features of scattering in the transplanckian energy regime. There are certainly effects that, at present, we do not even have a proper theory to calculate, but in many instances an asymptotic observer will be causally cut off from them. The crucial point is cosmic censorship, which can be taken to say, quite liberally, that the extreme high energy regime will be shrouded by a horizon. Two particles scattering at transplanckian center-of-mass energy, $\sqrt{s}$, and small impact parameter b, will produce a large concentration of energy in a small volume, and therefore will induce a large spacetime curvature, larger than the fundamental scale. To a low-energy observer, this will be equivalent to a curvature singularity. Then, if cosmic censorship holds, a horizon will appear, hiding these higher-energy effects from us.

This generic argument assumes that in the collision of two transplanckian particles their energy actually gets concentrated in a small volume. One may worry that the emission of a large fraction of energy into initial state radiation might prevent this. However, this does not seem to be the case. The analyses of [16] show that trapped surfaces do form in the collision of classical transplanckian particles. Quite generically, these trapped surfaces appear before the colliding particles are at a distance where quantum gravity corrections (e.g. higher-dimension operators in the low energy effective action) must be taken into account. Once the trapped surfaces arise, a singularity will inevitably develop, and a horizon is expected to censor it out. The area of the apparent horizon (the outer envelope of the trapped surfaces), which cannot be larger than the area of the event horizon, is found to be smaller than, but still close to the area of a black hole of mass equal to $\sqrt{s}$. Hence follows a (dimension-dependent) upper bound on the fraction of gravitational radiation that is classically produced.[4]

Low energy effective field theory predicts the failure of General Relativity at energies near or above the Planck scale by the effect of higher-dimension operators in the low energy effective action becoming

[3] Ideas similar or related to those in this section have been discussed previously in, e.g., [12, 13, 5, 14, 7, 15].

[4] Still, the question remains of whether the radiation of quantum origin is also small. I thank Riccardo Rattazzi for discussions on this issue.

as important as the Einstein-Hilbert term. What the argument above says is that the effects of these operators will be largely confined inside a black hole horizon. An alternative view, using a spacetime description, would be the following: a region of large curvature can be enclosed by a surface where all curvatures are moderate; say, below a given cutoff curvature radius. This region can be cutoff and then replaced by boundary conditions at its surface. The main assumption, analogous to the locality of counterterms in the low energy effective action, is that the specification of these boundary conditions is sufficient to encode all the effects that the physics at higher curvatures would have on the lower curvature regions. The situation changes if a horizon appears, since it not only excises the large curvature region, but the horizon itself also provides a set of boundary conditions (i.e., thermal) that is largely independent of the details of the large curvatures inside the horizon[5].

These considerations reveal an essential property of quantum gravity: its softness at high energies. The higher the energy of the collision, the larger the horizon that forms, and therefore the less important that the quantum gravity corrections will be for an observer outside the horizon. So gravitational scattering at very high energies becomes softer and softer. Ultimately, the outcome of the scattering will be the Hawking radiation emitted in the decay of the black hole, whose wavelength is comparable to the black hole size, and therefore larger for higher energy collisions. This softness is also a property that can be observed in the eikonalized gravitational scattering amplitudes, in which one can have a large momentum transfer, but built out of a very large number of small momentum transfers, so at the end one does not probe the very shortest distances [12, 13]. It is also strongly reminiscent of the softness of strings in the regime of deep inelastic scattering. The reasons for it are at first sight quite different. One can see the parallels both in the Regge regime and in the deep inelastic scattering regime, and in fact the black hole/string correspondence principle suggest such a connection, which to our knowledge has not been discussed in detail in the literature. The correspondence principle also allows us to use string theory to perform a simple calculation that leads to the correct estimate for the black hole production cross section. This will be discussed in Sec. 5 below.

At transplanckian energies one must go beyond perturbation theory, but it is the *classical* gravitational dynamics that dominates the evolution of the system[6]. This is apparent both in the case where a black hole forms, and also in the eikonal analysis of the scattering. It can be interpreted as saying that one must consider diagrams with an arbitrary number of vertex insertions, but where graviton loops are absent; matter lines in the diagrams are taken to be on-shell.

A full calculation of the production cross section, using classical General Relativity, is a very complicated task. A simple estimate can be obtained by taking into account the above-mentioned bounds on initial state radiation, and other factors, such as the fact that the capture cross section of a black hole is actually larger than its area, which may raise the cross section. For practical purposes, it seems reasonable to estimate the black hole production cross section as the geometric cross section

$$\sigma \simeq \pi R_H^2 \sim \frac{1}{M_*}\left(\frac{\sqrt{s}}{M_*}\right)^{\frac{2}{n+1}} . \tag{3}$$

Since this cross section does not contain any small numbers that might suppress it, at energies above $M_* \sim$ TeV it leads to enormous cross sections, on the order of $\mathrm{TeV}^{-2} \sim O(100)$ pb. More careful estimates result in production rates at the LHC as large as a black hole per second [8, 7].

4 Black hole decay

Once the black hole forms, it will decay very rapidly due to Hawking evaporation. But, where is this radiation emitted? This is a crucial point, since if the radiation were emitted into the KK modes of the bulk graviton it would escape our detectors and we would not be able to distinguish black hole formation from other missing energy events. In fact, a simple argument appears to lead precisely to this conclusion: Since the extra dimensions are assumed to be much larger than the black hole, from the point of view of a four-dimensional observer there is an enormous number of light KK modes, of mass

[5]The extent to which the properties of the horizon are so universal and independent of the physics at short distances is closely related to the black hole no-hair conjecture, and to the problem of information loss.

[6]Semiclassical, if one also includes the decay via Hawking radiation.

smaller than the Hawking temperature. Emission into these modes would then overwhelm the radiation of the Standard Model particles that are emitted along the brane. Viewed another way, the phase space available for emission into the bulk is much larger than for emission along the brane, making virtually zero the fraction of energy that could possibly be detected.

Even if it was clear from early on that TeV-gravity scenarios greatly enhance black hole production [4, 5], these arguments prevented further discussion of their possible detection at colliders. However, in [6] a number of counterarguments were given to conclude that the outcome of the evaporation is emitted mostly along the brane and therefore can actually be detected. This opened the door to the studies of the actual phenomenology of the process [7, 8].

Instead of repeating the arguments of [6], here I will present an ellaboration of an equivalent but slightly different argument, originally due to L. Susskind.

The (erroneous) argument based on the fact that the number of KK modes is much larger than the number of brane modes assumes that Hawking radiation is emitted with roughly the same probability into all these KK modes and into the brane modes. Let us revisit this line of reasoning, but instead of labelling the KK modes by the momentum in the extra dimensions, in a plane-wave basis decomposition, we will decompose the modes in a basis of spherical harmonics. Then we classify the modes according to their partial-wave number ℓ. Viewed this way, the fact that there are many more modes coming from the $4+n$-dimensional bulk than from the four-dimensional brane is reflected in the fact that, for large ℓ, the degeneracy of a mode of given ℓ grows in the former case as $\propto \ell^{n+1}$, much faster than the degeneracy on the four-dimensional brane, which is well-known to be $2\ell+1$, i.e., $\propto \ell$. Imagine now a hot object of characteristic size R, which is radiating thermally at a typical wavelength $\lambda \ll R$. There will be radiation into modes of partial-wave number up to the large value $\ell_{max} \sim R/\lambda$. Since there are many more of these modes in higher dimensions, much more radiation will go into the bulk than into the brane.

However, a black hole is not this sort of object. The typical wavelength of Hawking radiation is actually on the order of, or a little larger than, the black hole size, $\lambda_H \gtrsim R_{bh}$. So the black hole emits predominantly into s-wave modes with $\ell = 0$. The black hole does not make use of the large number of highly degenerate ℓ-angular modes that the higher-dimensional bulk provides. Since s-waves are non-degenerate, their number of modes is the same whether the field propagates in four or $4+n$ dimensions, so each brane mode is emitted at roughly the same rate as a bulk mode. In other words, the black hole does not see the angular directions, only the radial direction, which is common to modes propagating in any number of dimensions. In typical brane-world scenarios there are ~ 60 Standard Model modes propagating along the brane, versus a single graviton propagating in the bulk. Then the black hole will radiate mainly on the brane.

The evaporation time for one of these black holes will be extremely short. The black hole will typically be only a factor $\sim O(10)$ larger than the TeV scale, so its lifetime will be $\tau \sim O(10)$ TeV$^{-1} \sim 10^{-27}$ s, much shorter-lived than a typical hadronic resonance. The collider signatures for this Hawking radiation were analyzed in [7, 8]. One should look for events with high multiplicity, due to the large number of quanta emitted during the evaporation. Events could be tagged by the presence of promt leptons and photons, of energy $\sim O(100)$ GeV, and of similarly very energetic jets.

5 String balls

The semiclassical description of a black hole must break down when its mass is close to the fundamental mass scale of gravity M_*. But in string theory, if the string coupling g_s is weak, this description breaks down even at higher masses. When the black hole radius R_H gets smaller than the string length ℓ_s (and the black hole temperature gets higher than the Hagedorn temperature), the string corrections to the low energy effective action cannot be argued, as we did before, to be hidden inside the horizon, so one must resort to a stringy description. The critical mass where this happens, i.e., the minimum mass for which a semiclassical description of the black hole is reliable, is

$$M_{min} \sim M_s/g_s^2\,, \tag{4}$$

and, for small g_s, this can be quite larger than $M_* \sim g_s^{-2/n+2} M_s$. In particular, this means that if $g_s \lesssim 0.3$, the LHC may not be able to probe the regime of black holes.

In this case, what one would be producing, instead of a black hole, is a highly excited configuration, a long, jagged, very massive string resonance: a *string ball*[7]. Over the years, a concept of correspondence between black holes and strings has been developed [17], according to which a black hole that evaporates down to the mass (4) makes a transition into a string ball. Subsequently, the string ball evaporates by emitting massless string modes at the Hagedorn temperature.

The production cross section for a string ball can be computed using string perturbation theory, by factorizing the four-point amplitude for forward, elastic string scattering in the resonant s-channel – one of the earliest calculations in string theory. This yields

$$\sigma \sim g_s^2 s / M_s^4 \,. \tag{5}$$

When viewed in the t channel, this four-point amplitude is dominated by graviton exchange. The latter indeed determines both the factor g_s^2, from tree-level exchange of a closed-string state, and the energy dependence $\propto s$, from the graviton pole. Therefore the result is universal for all string theories, since they all contain a graviton. So, besides factors that depend on the polarization of the ingoing particles, the result is independent of the initial states, as long as they are much lighter than $\sqrt{s}$.

This perturbative calculation will receive corrections at energies where the unitarity bounds are saturated, $g_s^2 s/M_s^2 \sim 1$. Above these energies, it seems reasonable to assume that the cross section saturates and remains constant at $\sigma \sim l_s^2 \sim M_s^{-2}$. This cross section then extends up to the energies (4) where the black holes form, and interpolates between all these regimes in a parametrically smooth manner. This simple argument provides evidence in favor of the geometric cross section (3).

It is clear that in scenarios with string scale near the TeV, string balls will be produced at rates as large as the black hole production rates discussed above. In fact, it may happen that only the string ball regime is accesible to the LHC. The decay modes and properties of string balls are also quite similar to those of black holes. A main difference is that the temperature of the radiation emitted (the average energy of the decay products) is fixed at the Hagedorn temperature, and is essentially independent of the mass of the string ball, whereas for black holes the temperature is smaller for larger black holes. This may help distinguish between both kinds of objects, and may also allow for a determination of parameters such as the string mass M_s.

Acknowledgements

I would like to thank the organizers of the XIIth Japanese General Relativity and Gravitation Meeting, and in particular Tetsuya Shiromizu, for the invitation to such a delightful conference.

References

[1] N. Arkani-Hamed, S. Dimopoulos and G. R. Dvali, Phys. Lett. B **429** (1998) 263 [arXiv:hep-ph/9803315]. I. Antoniadis, N. Arkani-Hamed, S. Dimopoulos and G. R. Dvali, Phys. Lett. B **436** (1998) 257 [arXiv:hep-ph/9804398].

[2] G. R. Dvali, G. Gabadadze, M. Kolanovic and F. Nitti, Phys. Rev. D **65** (2002) 024031 [arXiv:hep-th/0106058].

[3] J. Hewett and J. March-Russell, "Extra Dimensions (New),". in K. Hagiwara *et al.* [Particle Data Group Collaboration], Phys. Rev. D **66** (2002) 010001.

[4] P. C. Argyres, S. Dimopoulos and J. March-Russell, Phys. Lett. B **441** (1998) 96 [arXiv:hep-th/9808138].

[5] T. Banks and W. Fischler, arXiv:hep-th/9906038.

[6] R. Emparan, G. T. Horowitz and R. C. Myers, Phys. Rev. Lett. **85** (2000) 499 [arXiv:hep-th/0003118]. See also the discussion near the end in JHEP **0001** (2000) 007 [arXiv:hep-th/9911043].

[7] S. B. Giddings and S. Thomas, Phys. Rev. D **65** (2002) 056010 [arXiv:hep-ph/0106219].

[7] The phrase "ball of string" had been used before in a slightly different context in [18].

[8] S. Dimopoulos and G. Landsberg, Phys. Rev. Lett. **87** (2001) 161602 [arXiv:hep-ph/0106295].

[9] S. Dimopoulos and R. Emparan, Phys. Lett. B **526** (2002) 393 [arXiv:hep-ph/0108060].

[10] S. B. Giddings, in *Proc. of the APS/DPF/DPB Summer Study on the Future of Particle Physics (Snowmass 2001)* ed. N. Graf, eConf **C010630** (2001) P328 [arXiv:hep-ph/0110127]. H. Tu, arXiv:hep-ph/0205024. M. Cavaglia, arXiv:hep-ph/0210296. G. Landsberg, arXiv:hep-ph/0211043. A. Ringwald, arXiv:hep-ph/0212342.

[11] J. L. Feng and A. D. Shapere, Phys. Rev. Lett. **88** (2002) 021303 [arXiv:hep-ph/0109106]. L. Anchordoqui and H. Goldberg, Phys. Rev. D **65** (2002) 047502 [arXiv:hep-ph/0109242]. R. Emparan, M. Masip and R. Rattazzi, Phys. Rev. D **65** (2002) 064023 [arXiv:hep-ph/0109287].

[12] G. 't Hooft, Phys. Lett. B **198** (1987) 61.

[13] D. Amati, M. Ciafaloni and G. Veneziano, Phys. Lett. B **197** (1987) 81. Phys. Lett. B **216** (1989) 41. D. Amati, M. Ciafaloni and G. Veneziano, Nucl. Phys. B **347** (1990) 550. D. Amati, M. Ciafaloni and G. Veneziano, Phys. Lett. B **289** (1992) 87.

[14] R. Emparan, Phys. Rev. D **64** (2001) 024025 [arXiv:hep-th/0104009].

[15] G. F. Giudice, R. Rattazzi and J. D. Wells, Nucl. Phys. B **630** (2002) 293 [arXiv:hep-ph/0112161].

[16] R. Penrose, unpublished. P. D. D'Eath and P. N. Payne, Phys. Rev. D **46** (1992) 658. D. M. Eardley and S. B. Giddings, Phys. Rev. D **66** (2002) 044011 [arXiv:gr-qc/0201034]. E. Kohlprath and G. Veneziano, JHEP **0206** (2002) 057 [arXiv:gr-qc/0203093]. H. Yoshino and Y. Nambu, Phys. Rev. D **67** (2003) 024009 [arXiv:gr-qc/0209003].

[17] M. J. Bowick, L. Smolin and L. C. Wijewardhana, Phys. Rev. Lett. **56** (1986) 424. L. Susskind, arXiv:hep-th/9309145. G. T. Horowitz and J. Polchinski, Phys. Rev. D **55**, 6189 (1997) [arXiv:hep-th/9612146]. T. Damour and G. Veneziano, Nucl. Phys. B **568**, 93 (2000) [arXiv:hep-th/9907030].

[18] M. J. Bowick and S. B. Giddings, Nucl. Phys. B **325** (1989) 631.

Extrinsic curvature in quasiequilibrium binary black hole spacetimes

Eric Gourgoulhon,[1]

Laboratoire de l'Univers et de ses Théories, UMR 8102 du C.N.R.S., Observatoire de Paris F-92195 Meudon Cedex, France

Abstract

Two different numerical approaches to the problem of binary black holes in the pre-coalescence stage (i.e. when the notion of orbit has still a meaning) are analyzed: (i) the Effective-Potential with Bowen-York extrinsic curvature method (EPBY) and (ii) the Helical Killing Vector method (HKV). These two approaches yield different results, in particular with respect to the location of the innermost stable circular orbit, the HKV one being in good agreement with third order post-Newtonian calculations. The major difference between EPBY and HKV arises from the difference between the extrinsic curvatures that each method prescribes for the constant time hypersurfaces.

1 Introduction

1.1 Binary black holes in the Universe

The binary black holes inspiral and coalescence is according to some studies [1] the most promising source of gravitational waves for the detectors LIGO, VIRGO, GEO600 and TAMA, as well as for the space interferometer LISA. From the theoretical point of view these events constitute the two body problem per excellence in general relativity and allow to probe this theory in the strong field regime. From the astrophysical point of view, the rate of binary black hole coalescences constrains the theories of massive star evolution. Moreover the inspiral gravitational wave signal will allow a precise measure of the Hubble constant H_0 and gravitational wave observations of supermassive BH at high z give some hints for the formation of large structures.

We can distinguish two types of binary black hole coalescence:

- Coalescence of stellar black holes: $3M_\odot \lesssim M \lesssim 50M_\odot$: the event rate deduced from massive star evolution is up to ~ 20/Myr per galaxy [2] or 1.6×10^{-7} yr^{-1}Mpc^{-3} from binary black formation in globular clusters [3].
- Coalescence of massive black holes ($M \sim 10^6 - 10^9\, M_\odot$) resulting from galaxy encounters; the event rate is possibly large.

From the theoretical point of view, both types of event correspond to the same physics (scaling with M).

Note that there have been some recent observational evidences for the existence of binary black holes: (i) the Chandra X-ray satellite observations of the galaxy NGC 6240 have revealed a double nucleus [4]; (ii) in the active galactic nucleus NGC 326, the shape of the jets suggests that the central black holes result from a binary merger [5].

1.2 Evolution of binary black holes

The evolution of binary black holes is driven by the loss of energy and angular momentum via gravitational radiation. The resulting shrinking of the orbits constitutes the *inspiral phase*. The corresponding gravitational wave signal is the so-called *chirp signal* [6]. In the case of two very different masses, $M_1 \ll M_2$, the spacetime is a small deviation from Schwarzschild or Kerr spacetime and the inspiral ends by the *innermost stable circular orbit (ISCO)*:

$$R_{\rm ISCO}^{\rm Schw} = 6M, \qquad \Omega_{\rm ISCO}^{\rm Schw} = 6^{-3/2} M^{-1} \simeq 0.068\, M^{-1}. \tag{1}$$

[1] E-mail:Eric.Gourgoulhon@obspm.fr

In the comparable mass case, $M_1 \sim M_2$, the gravitational radiation dissipation implies that strictly circular orbits do not exist. The ISCO is then defined in terms of the conservative part in the equation of motions, which gives rise to circular orbits (adiabatic approximation). Considering a sequence of circular orbits of smaller and smaller radius, mimicking the inspiral, the ISCO is defined as the turning point in the binding energy of this sequence [7].

1.3 Computing quasiequilibrium configurations of close binary black holes

Various groups have tried to compute close configurations of binary black holes on circular orbits (see [8] for a review). The initial motivation was to provide initial data for numerical computation of the plunge and merger. But these configurations have interest from their own: they can lead to the (adiabatic) ISCO, which may be observed in gravitational waveforms. Basically two different method have been developed: the Effective Potential with Bowen-York extrinsic curvature method (EPBY) and the Helical Killing Vector (HKV) method. We are going to discuss successively these two methods before comparing them.

2 The Effective Potential + Bowen-York (EPBY) approach

2.1 Description

This procedure has been introduced by Cook in 1994 [9]. To get a quasiequilibrium configuration of binary black hole in circular orbit:

- Solve only for the 4 constraint equations of vacuum general relativity on a spacelike 3-dimensional surface Σ with a non-trivial topology (for instance the Misner-Lindquist topology or the Brill-Lindquist topology).
- Define the binding energy by $E = M_{\rm ADM} - M_1 - M_2$.
- Define a circular orbit as an extremum of E with respect to proper separation l at fixed angular momentum and BH individual mass:

$$\left.\frac{\partial E}{\partial l}\right|_{M_1,M_2,J} = 0. \tag{2}$$

- Compute the orbital angular velocity as

$$\Omega = \left.\frac{\partial E}{\partial J}\right|_{M_1,M_2,l}. \tag{3}$$

2.2 Ambiguities of the effective potential approach

Contrary to the ADM mass, the individual masses M_1 and M_2 are ill-defined quantities in general relativity. The Cook ansatz amounts to define the individual mass M_i from the apparent horizon area $\mathcal{A}_i$ and individual spin S_i, via the Christodoulou formula:

$$M_i^2 := \frac{\mathcal{A}_i}{16\pi} + \frac{4\pi S_i^2}{\mathcal{A}_i}. \tag{4}$$

But there are a few caveats with this prescription:

1. Christodoulou formula is only established for a single stationary black hole (Kerr spacetime);
2. moreover $\mathcal{A}_i$ must be the area of the *event* horizon, not the apparent one;
3. the individual spin S_i suffers from the same lack of unambiguous definition as the individual mass.

2.3 Solving for the constraint equations

The spatial hypersurface Σ mentioned above is geometrically described by its metric (first fundamental form) γ_{ij} induced by the spacetime metric $g_{\mu\nu}$ and its extrinsic curvature (second fundamental form) K_{ij}. The Einstein equations imply that (γ_{ij}, K_{ij}) must obey to the constraint equations:

$$R + K^2 - K_{ij}K^{ij} = 0 \qquad \text{(Hamiltonian constraint)}, \tag{5}$$

$$D_j K^{ij} - D^i K = 0 \qquad \text{(momentum constraint)}, \tag{6}$$

where K is the trace of K_{ij} and R and D_i are respectively the curvature scalar and the covariant derivative, both associated with γ_{ij}.

The constraint equations can be solved thanks to the *York-Lichnerowicz conformal decomposition* [10, 8]: first split K_{ij} into a traceless part A_{ij} and a trace part :

$$K_{ij} =: A_{ij} + \frac{K}{3}\gamma_{ij}. \tag{7}$$

Then introduce a conformal metric :

$$\gamma_{ij} =: \Psi^4 \tilde{\gamma}_{ij} \tag{8}$$

and note the identity

$$D_j A^{ij} = \Psi^{-10} \tilde{D}_j (\Psi^{10} A^{ij}), \tag{9}$$

where $\tilde{D}_i$ denotes the covariant derivative associated with $\tilde{\gamma}_{ij}$. This motivates the introduction of the conformal traceless extrinsic curvature:

$$\tilde{A}^{ij} := \Psi^{10} A^{ij}. \tag{10}$$

$\tilde{A}^{ij}$ is then split into a longitudinal part and a transverse one, according to

$$\tilde{A}^{ij} = (\tilde{L}X)^{ij} + \tilde{A}^{ij}_{\rm TT}, \tag{11}$$

with

$$(\tilde{L}X)^{ij} := \tilde{D}^j X^i + \tilde{D}^i X^j - \frac{2}{3}\tilde{D}_k X^k \tilde{\gamma}^{ij} \tag{12}$$

and

$$\tilde{D}_j \tilde{A}^{ij}_{\rm TT} = 0. \tag{13}$$

Finally the full decomposition of K^{ij} is

$$K^{ij} = \Psi^{-10}\left[(\tilde{L}X)^{ij} + \tilde{A}^{ij}_{\rm TT}\right] + \frac{K}{3}\gamma^{ij}. \tag{14}$$

The Hamiltonian constraint (5) then becomes

$$8\tilde{D}_k\tilde{D}^k\Psi - \tilde{R}\Psi - \frac{2}{3}K^2\Psi^5 + \tilde{A}_{ij}\tilde{A}^{ij}\,\Psi^7 = 0, \tag{15}$$

whereas the momentum constraint writes

$$\tilde{D}_k\tilde{D}^k X^i + \frac{1}{3}\tilde{D}^i\tilde{D}_k X^k + \tilde{R}^i{}_j X^j = \frac{2}{3}\Psi^6\tilde{D}^i K. \tag{16}$$

Note that the momentum constraint involves only the longitudinal part X^i of $\tilde{A}^{ij}$, not the TT part $\tilde{A}^{ij}_{\rm TT}$, which can thus be freely chosen.

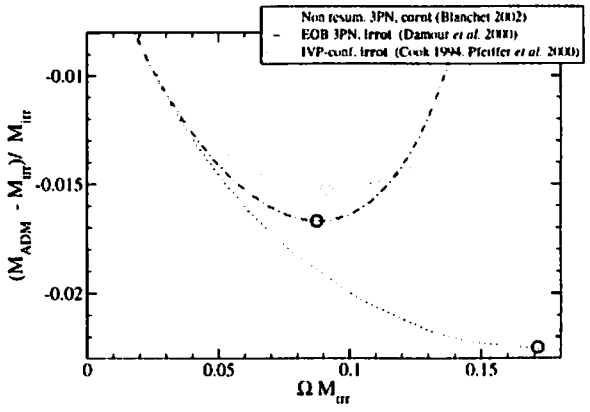


Figure 1: Binding energy along an evolutionary sequence of an equal-mass binary black hole, computed by means of the EPBY method (denoted IVP-conf on the graph) and by means of 3PN analytical treatments.

2.4 The Bowen-York solution

Let us choose

- a maximal slicing : $K = 0$ (then the momentum constraint (16) becomes independent of Ψ);
- a conformally flat 3-metric : $\tilde{\gamma}_{ij} = f_{ij}$ (flat metric);
- a vanishing TT part of $\tilde{A}^{ij}$: $\tilde{A}^{ij}_{\rm TT} = 0$.

Then the Hamiltonian constraint (15) and momentum constraint (16) become respectively

$$\underline{\Delta}\Psi = -\frac{\Psi^7}{8}\tilde{A}_{ij}\tilde{A}^{ij} \tag{17}$$

and

$$\underline{\Delta}X^i + \frac{1}{3}\bar{\nabla}^i\bar{\nabla}_k X^k = 0, \tag{18}$$

where $\underline{\Delta}$ (resp. $\bar{\nabla}_i$) denotes the Laplacian operator (resp. covariant derivative) associated with the flat metric f_{ij}.

Bowen & York [11] gave in 1980 an analytical solution of (18), representing a single black hole :

$$X^i_{\rm BY0} = -\frac{1}{4r}\left(7P^i + P_j\frac{x^j x^i}{r^2}\right) - \frac{1}{r^3}\epsilon^i{}_{jk}S^j x^k, \tag{19}$$

with $x^i = (x, y, z)$ (Cartesian coordinates) and $r^2 := x^2 + y^2 + z^2$. This solution depends on two constant vector parameters : P^i and S^i representing respectively the linear momentum and angular momentum of the black hole. For instance, choose S^i perpendicular to P^i and the Cartesian coordinate system (x, y, z) such that $P^i = (0, P, 0)$ and $S^i = (0, 0, S)$. Then

$$X^x_{\rm BY0} = -\frac{P}{4}\frac{xy}{r^3} + S\frac{y}{r^3} \tag{20}$$

$$X^y_{\rm BY0} = -\frac{P}{4r}\left(7 + \frac{y^2}{r^2}\right) - S\frac{x}{r^3} \tag{21}$$

$$X^z_{\rm BY0} = -\frac{P}{4}\frac{xz}{r^3}. \tag{22}$$

The Bowen-York extrinsic curvature is deduced from the vector $X^i_{\rm BY0}$ by Eq. (11) with $\tilde{A}^{ij}_{\rm TT} = 0$:

$$\tilde{A}^{ij}_{\rm BY0} = \frac{3}{2r^3}\left[P^i x^j + P^j x^i - \left(\delta^{ij} - \frac{x^i x^j}{r^2}\right)P^k x_k\right] + \frac{3}{r^5}\left(\epsilon^i{}_{kl}S^k x^l x^j + \epsilon^j{}_{kl}S^k x^l x^i\right). \tag{23}$$

For the binary black hole problem, one can take advantage of the linearity of Eq. (18) to define

$$X^i = X^i_{\rm BY} := X^i_{\rm BY_0}(\boldsymbol{P}_1, \boldsymbol{S}_1, x^i \to x^i_1) + X^i_{\rm BY_0}(\boldsymbol{P}_2, \boldsymbol{S}_2, x^i \to x^i_2). \tag{24}$$

Accordingly

$$K^{ij} = \Psi^{-10}\left[\tilde{A}^{ij}_{\rm BY_0}(\boldsymbol{P}_1, \boldsymbol{S}_1, x^i \to x^i_1) + \tilde{A}^{ij}_{\rm BY_0}(\boldsymbol{P}_2, \boldsymbol{S}_2, x^i \to x^i_2)\right]. \tag{25}$$

There remains to solve (numerically) the non-linear elliptic equation (17) to get Ψ. This has been done by various groups:

- Cook in 1994 [9] on hypersurfaces with the Misner-Lindquist topology ;
- Pfeiffer, Teukolsky & Cook in 2000 [12] on hypersurfaces with the Misner-Lindquist topology ;
- Baumgarte in 2000 [13] on hypersurfaces with the Brill-Lindquist topology.

2.5 Discrepancy between EPBY and post-Newtonian results

The binding energy along an evolutionary sequence of equal-mass binary black holes is represented in Fig. 1 for the EPBY calculation [9] and compared with two third order post-Newtonian (3PN) calculations by Damour, Jaranowski & Schäfer [14], using the Effective One Body approach (EOB) and Blanchet [15], using non-resumed Taylor expansions. One can notice a great discrepancy, in particular about the ISCO (minimum of the curve), between EPBY and 3PN results.

3 The Helical Killing vector (HKV) approach

3.1 Helical symmetry

We have recently proposed another approach of the binary black hole problem [16, 17], based on a four-dimensional, albeit approximate, treatment. When the black holes are far enough so that the radiation reaction timescale is large as compared to the dynamical timescale, the orbits can be approximated as closed ones. Moreover, due to the accumulated effects of the reaction to gravitational radiation, these orbits can be considered as circular. In such a case (closed circular orbits), the spacetime possesses a one-parameter symmetry group, whose integral curves are helices. The associated Killing vector $\boldsymbol{\ell}$ is called the *helical Killing vector*. It is such that far from the system, in asymptotically inertial coordinates $(t_0, r_0, \theta_0, \varphi_0)$,

$$\boldsymbol{\ell} \to \frac{\partial}{\partial t_0} + \Omega \frac{\partial}{\partial \varphi_0}. \tag{26}$$

In full general relativity, requiring the helical symmetry for a binary system implies equal amounts of outgoing and incoming gravitational radiation [18]. The spacetime cannot therefore be asymptotically flat [19]. However, there are two interesting cases where helical symmetry and asymptotic flatness are compatible: (i) in the post-Newtonian (PN) approximation, up to the second order and (ii) the Isenberg-Wilson-Mathews (IWM) approximation of general relativity [20] (see also Sec. IV.C of Ref. [21]), which assumes that the spacetime can be foliated by a family of conformally flat spacelike hypersurfaces and reduces the Einstein equations to five elliptic equations. Both approximations (i) and (ii) do not allow for gravitational radiation, which explains why they permit asymptotically flat spacetimes. They are valid approximations to general relativity when the gravitational radiation content of spacetime does not play any important dynamical role. Note that the IWM formulation contains the first order PN one.

In our first study of the binary black hole problem [16, 17], we have used the helical symmetry along with the IWM approximation.

3.2 Spacetime manifold

We have chosen the spacetime manifold to have the topology of $\boldsymbol{R} \times$ Misner-Lindquist, with an isometry I between the two sheets of the Misner-Lindquist manifold. There are two possible choice for this isometry. We have selected that for which the lapse N is an antisymmetric function $I.N = -N$. This implies $N = 0$ on the two throats $\mathcal{H}_1$ and $\mathcal{H}_2$.

3.3 Rigid rotation

Regarding the rotation state of the black holes, we have chosen each black hole to be corotating (synchronized binary), so that the whole system is in rigid rotation. There are several motivations for this: (i) It has been recently argued [22] that when the black holes are close together, tidal forces may lead to an efficient transfer of spin angular momentum to orbital angular, which might lead to synchronization. However this not clear yet. (ii) As discussed by Friedman et al. [21], corotating black holes are the only state compatible with the helical symmetry in full general relativity (basically, any other rotation state would result in shear and increase of the horizon area, which is not allowed by the helical symmetry). Detweiler [18] has already pointed this by noticing that gravitational radiation going down in the hole from the distant past piles up near the distant horizon, resulting in a divergence of the metric, except for the corotating state. (iii) For the IWM spacetimes we are considering, other rotation states are permitted [23], but the corotating one has a very simple geometrical interpretation: the black holes horizons are in this case Killing horizons, i.e. the helical Killing vector is tangent to the black hole horizons [16]:

$$\boldsymbol{\ell}\cdot\boldsymbol{\ell}|_{\mathcal{H}_1} = 0 \qquad \text{and} \qquad \boldsymbol{\ell}\cdot\boldsymbol{\ell}|_{\mathcal{H}_2} = 0\ . \tag{27}$$

[cf. the rigidity theorem for a Kerr black hole]. Since

$$\boldsymbol{\ell}\cdot\boldsymbol{\ell} = -N^2 + \boldsymbol{\beta}\cdot\boldsymbol{\beta}, \tag{28}$$

where $\boldsymbol{\beta}$ is the shift vector of corotating coordinates, and $N = 0$ on the throats, Eq. (27) leads to

$$\boldsymbol{\beta}|_{\mathcal{H}_1} = 0 \qquad \text{and} \qquad \boldsymbol{\beta}|_{\mathcal{H}_2} = 0\ . \tag{29}$$

3.4 Einstein equations

Our framework is that of the 3+1 formalism with maximal slicing: $K = 0$. Moreover, following the IWM approximation, we consider a conformally flat spatial metric:

$$\gamma_{ij} = \Psi^4 f_{ij}. \tag{30}$$

The spacetime metric then writes

$$ds^2 = -N^2dt^2 + \Psi^4 f_{ij}(dx^i + \beta^i dt)(dx^j + \beta^j dt). \tag{31}$$

This approach amounts to solve 5 of the 10 Einstein equations, which is one more than in EPBY:

$$\underline{\Delta}\Psi = -\frac{\Psi^5}{8}\hat{A}_{ij}\hat{A}^{ij} \tag{32}$$

$$\underline{\Delta}\beta^i + \frac{1}{3}\bar{\nabla}^i\bar{\nabla}_j\beta^j = 2\hat{A}^{ij}\left(\bar{\nabla}_j N - 6N\bar{\nabla}_j \ln\Psi\right) \tag{33}$$

$$\underline{\Delta}N = N\Psi^4\hat{A}_{ij}\hat{A}^{ij} - 2\bar{\nabla}_j \ln\Psi\,\bar{\nabla}^j N \tag{34}$$

with $\hat{A}_{ij} := \Psi^{-4}K_{ij}$ and $\hat{A}^{ij} := \Psi^4 K^{ij}$. The helical symmetry implies the following relation between the extrinsic curvature and the shift vector:

$$K_{ij} = D_i\beta_j + D_j\beta_i, \tag{35}$$

from which

$$\hat{A}^{ij} = \frac{1}{2N}(\bar{L}\beta)^{ij} \tag{36}$$

with

$$(\bar{L}\beta)^{ij} := \bar{\nabla}^i\beta^j + \bar{\nabla}^j\beta^i - \frac{2}{3}\bar{\nabla}_k\beta^k f^{ij}, \tag{37}$$

$$\bar{\nabla}_i\beta^i = -6\beta^i\bar{\nabla}_i \ln\Psi. \tag{38}$$

The PDE system (32)-(34) is subject to the following boundary conditions

isometry condition on γ_{rr}:		asymptotic flatness:
$\left(\frac{\partial\Psi}{\partial r_1}+\frac{\Psi}{2r_1}\right)\Big\|_{\mathcal{H}_1}=0$	$\left(\frac{\partial\Psi}{\partial r_2}+\frac{\Psi}{2r_2}\right)\Big\|_{\mathcal{H}_2}=0$	$\Psi\to 1$ when $r\to\infty$
corotating black holes:		definition of ℓ:
$\beta\|_{\mathcal{H}_1}=0$	$\beta\|_{\mathcal{H}_2}=0$	$\beta\to\Omega\frac{\partial}{\partial\varphi_0}$ when $r\to\infty$
isometry condition on N:		asymptotic flatness:
$N\|_{\mathcal{H}_1}=0$	$N\|_{\mathcal{H}_2}=0$	$N\to 1$ when $r\to\infty$

3.5 Regularity on the horizons

The throats $\mathcal{H}_1$ and $\mathcal{H}_2$ of the Misner-Lindquist slices of our spacetime are apparent horizons. In Eq. (36) the lapse function N, which vanishes at $\mathcal{H}_1$ and $\mathcal{H}_2$, appears at the denominator. In order for the extrinsic curvature to be regular on $\mathcal{H}_1$ and $\mathcal{H}_2$, one must therefore have

$$L\beta|_{\mathcal{H}}=0. \tag{39}$$

Now one has

$$\beta|_{\mathcal{H}}=0 \quad \text{(rigid rotation)} \tag{40}$$

$$l_*\beta=\beta \quad \text{(isometry)} \tag{41}$$

$$\bar{D}_i\beta^i=-6\beta^i\bar{D}_i\ln\Psi \quad (K=0) \tag{42}$$

These three conditions imply (39) (cf. [17] for details). However only (40) and the part of (41) implied by (40) are really imposed when solving the vector Poisson-like equation (33) for β. In the study [17], we have adopted the following solution for this problem. At each step of the iterative procedure, we set

$$\beta_{\rm new}=\beta_{\rm old}+\beta_{\rm cor}, \tag{43}$$

where $\beta_{\rm old}$ is the actual solution of the Poisson-like equation (33) at the given step and the "corrective" term $\beta_{\rm cor}$ is chosen so that (41) and (42) are fulfilled on the throats. When the iteration has converged, $\beta_{\rm cor}$ must be zero (to get an exact solution) or small (to get an approximate solution). In practice, we found the former case for a single rotating black hole, and the latter for binary black holes, with $|\beta_{\rm cor}|$ at most equal to $10^{-3}|\beta|$.

3.6 Determination of the orbital angular velocity

In the IWM framework, the field equations reduce to the five elliptic equations (32)-(34) and the orbital angular velocity Ω appears only in the boundary condition at infinity for the corotating shift vector. This contrasts with the fluid case, where Ω shows up in the equation governing the equilibrium of the fluid. We have determined Ω by demanding that the ADM mass $M_{\rm ADM}$ be equal to the Komar-like one $M_{\rm K}$ [16]. These two masses are given by the asymptotic expansions of the conformal factor and the lapse function:

$$\Psi\sim 1+\frac{M_{\rm ADM}}{2r} \qquad \text{and} \qquad N\sim 1-\frac{M_{\rm K}}{r} \tag{44}$$

and are different a priori. The requirement

$$M_{\rm ADM}=M_{\rm K} \tag{45}$$

is imposed by varying Ω during the numerical iteration, so that it selects a unique value for Ω. Note that with (45), the $O(r^{-1})$ part of the metric when $r\to\infty$ is the same as in Schwarzschild spacetime. Moreover, we have shown in [16] that the requirement (45) reduces to the classical virial theorem $2E_{\rm kin}+3P+E_{\rm grav}=0$ for fluid bodies at the Newtonian limit. We have also verified that when the holes are far apart, this procedure leads to Kepler's third law (cf. Fig. 3).

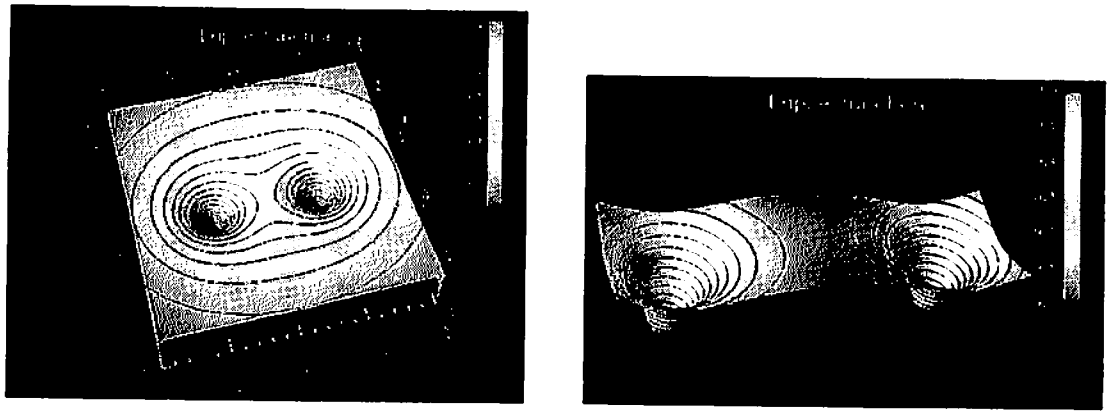


Figure 2: Lapse function in the equatorial plane for the ISCO configuration obtained by means of the HKV procedure (the right figure is an enlargement of the left one).

3.7 Defining an evolutionary sequence

An evolutionary sequence is defined by

$$\left.\frac{dM_{\rm ADM}}{dJ}\right|_{\rm sequence} = \Omega. \tag{46}$$

This is equivalent to requiring the constancy of the horizon area of each black hole, by virtue of the First law of thermodynamics for binary black holes :

$$dM_{\rm ADM} = \Omega\, dJ + \frac{1}{8\pi}\left(\kappa_1\, dA_1 + \kappa_2\, dA_2\right) \tag{47}$$

recently established by Friedman, Uryu & Shibata [21].

Within the helical symmetry framework, a minimum in $M_{\rm ADM}$ along a sequence at fixed horizon area locates a change of orbital stability and therefore locates the ISCO [21].

3.8 Numerical solution

The five non-linear elliptic equations (32)-(34) describing corotating binary black holes in the IWM approximation have been solved by means of a multi-domain spectral method [24, 25, 26]. We use spherical coordinate systems centered on each black hole, which allow for an easy implementation of the boundary conditions on the horizons. Moreover the computational domain extends to spacelike infinity, thanks to some suitable compactification of the external domain. This permits a rigorous implementation of the boundary condition at infinity (flat spacetime). The numerical implementation has been performed by means of an object-oriented code based on the LORENE library [27]. An illustration of the obtained numerical solution is presented in Fig. 2.

Numerous tests of the code have been presented in Ref [17]. Here we give only the convergence toward Kepler's third law when the two holes are far apart. This is shown in Fig. 3 by plotting a quantity which must be one for a Newtonian point-mass binary system obeying to Kepler's third law.

3.9 Comparison with post-Newtonian results

We have presented a detailed comparison of the HKV results with the post-Newtonian Effective One Body ones in Ref. [28]. The results are summarized in Fig. 4. Note that ΩM is geometrized units corresponds to the following value of the gravitational wave frequency:

$$f = 320\, \frac{\Omega M_{\rm ir}}{0.1}\, \frac{20\, M_\odot}{M_{\rm ir}}\ {\rm Hz}. \tag{48}$$

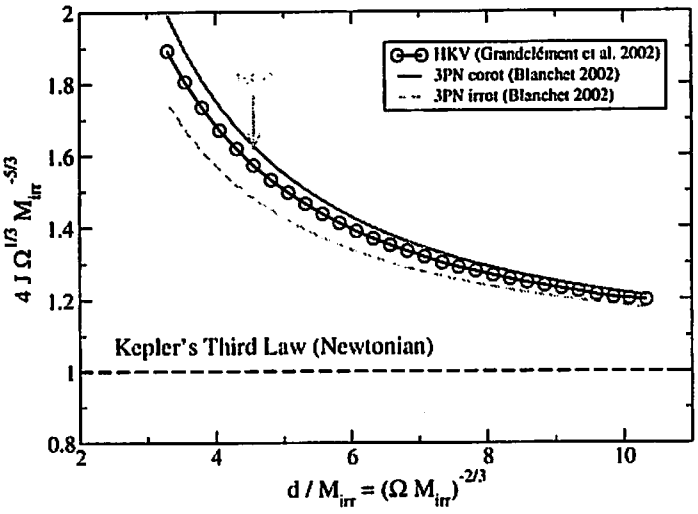


Figure 3: Comparison between the value of Ω given by the HKV procedure and that computed at the 3PN level by Blanchet [15], as a function of the separation d between the two black holes.

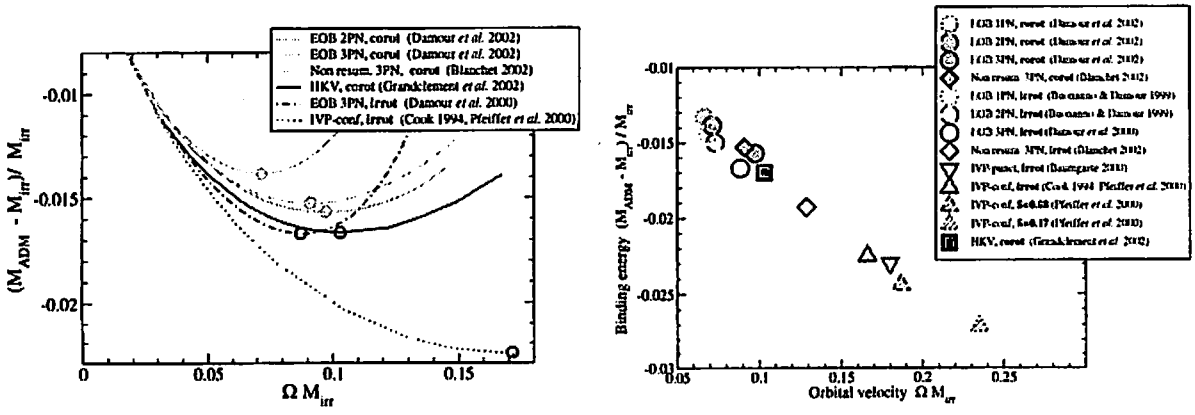


Figure 4: Comparison between numerical results and post-Newtonian ones: *left:* binding energy along a constant area sequence of binary black holes. IVP denotes the numerical results obtained from the EPBY approach. *right:* Values of the binding energy and orbital frequency at the ISCO for the EPBY approach [9, 12, 13], the HKV one [17], and post-Newtonian [28, 15, 29, 14] methods.

Note also that the values of Ω at the ISCO may be compared by the value (1) for a test particle in Schwarzschild spacetime.

It is clear on Fig. 4 that the orbital frequency at the ISCO differs by a factor of two between EPBY results on one side and HKV and 3PN results on the other side.

4 Role of the extrinsic curvature

4.1 Source of the discrepancy between EPBY and HKV

Recall that both EPBY and HKV method employ a conformally flat 3-metric, so this cannot be the reason why EPBY is far from post-Newtonian results. The two main differences between EPBY and HKV approaches are:

- the criterion for a circular orbit and determination of the orbital angular velocity Ω;
- the extrinsic curvature K_{ij} of the $t = \text{const}$ hypersurface.

Let us investigate first whether the discrepancy could be due to the determination of circular orbits. We have already mentioned that EPBY definition of circular orbit and Ω lacks of rigor, due to the ad hoc definition of the binding energy. This is unavoidable, in view of the intrinsic *3-dimensional* character of EPBY : the absence of time in EPBY forbids any well-defined velocity. On the contrary HKV is intrinsically *4-dimensional*, and its definition Ω is unambiguous (cf. § 3.6).

However, despite these differences, it turns out that the two ways of determining Ω for circular orbits yield the same result

- for irrotational black holes with the Bowen-York extrinsic curvature [30];
- for a simple analytical model of a spherical shell of collisionless particles [31].

Therefore we conclude that the main source of discrepancy between EPBY and HKV lies in the extrinsic curvature.

4.2 Analysis of the extrinsic curvature

For EPBY [cf. Eqs. (25) and (11)]:

$$K^{ij}_{\rm EPBY} = \Psi^{-10} (\tilde{L} X_{\rm BY})^{ij}, \tag{49}$$

whereas for HKV [cf. Eq. (36)]:

$$K^{ij}_{\rm HKV} = \frac{\Psi^{-4}}{2N} (\tilde{L}\beta)^{ij}, \tag{50}$$

where

$$(\tilde{L}V)^{ij} := \tilde{D}^j V^i + \tilde{D}^i V^j - \frac{2}{3} \tilde{D}_k V^k \tilde{\gamma}^{ij}, \tag{51}$$

with for both cases $\tilde{\gamma}^{ij} = f^{ij}$.

Therefore one has

$$K^{ij}_{\rm HKV} = K^{ij}_{\rm EPBY} \iff (\tilde{L}\beta)^{ij} = \frac{2N}{\Psi^6} (\tilde{L} X_{\rm BY})^{ij}, \tag{52}$$

which means that $K^{ij}_{\rm HKV}$ could be of Bowen-York type if $N = \Psi^{-6}$ and $\beta^i = 2X^i_{\rm BY}$. But β^i is determined so that the spatial coordinate lines follow the integral lines of the Killing vector; it is not freely choosable. So we have in fact

$$K^{ij}_{\rm EPBY} = K^{ij}_{\rm HKV} + B^{ij}_{\rm TT}, \tag{53}$$

where $B^{ij}_{\rm TT}$ is a transverse-traceless quantity which can be seen as the amount of spurious gravitational waves in the EPBY data (see § IV.D of Ref. [28] for a discussion of this point).

4.3 Analysis within the conformal thin-sandwich framework

The Conformal thin-sandwich (CTS) formulation of the initial value problem of general relativity has been devised by York in 1999 [32] as an alternative to the classical York-Lichnerowicz conformal decomposition presented in § 2.3 (see [8] for a discussion). The CTS extrinsic curvature is decomposed as

$$\begin{aligned} K^{ij}_{\rm CTS} &= \frac{1}{2N}\left[(L\beta)^{ij} - u^{ij}\right] + \frac{1}{3}K\,\gamma^{ij} \\ &= \frac{\Psi^{-4}}{2N}\left[(\tilde{L}\beta)^{ij} - \tilde{u}^{ij}\right] + \frac{1}{3}K\,\gamma^{ij} \end{aligned}$$

where u^{ij} and $\tilde{u}^{ij}$ represent the evolution of the conformal 3-metric between two neighboring slices:

$$u_{ij} := \gamma^{1/3}\partial_t(\gamma^{-1/3}\gamma_{ij}) = \partial_t\gamma_{ij} - \frac{1}{3}\gamma^{kl}\partial_t\gamma_{kl}\,\gamma_{ij} \tag{54}$$

and

$$\tilde{u}_{ij} := \partial_t\tilde{\gamma}_{ij} = \Psi^{-4}u_{ij}. \tag{55}$$

$\tilde{u}^{ij}$ represents the freely specifiable (i.e. not determined by the momentum constraint equation) part of K^{ij}, instead of $\tilde{A}^{ij}_{\rm TT}$ in the classical York-Lichnerowicz formulation. The key point is that $\tilde{u}^{ij}$ has much more physical meaning than $\tilde{A}^{ij}_{\rm TT}$. In particular, for a stationary spacetime : $\tilde{u}^{ij} = 0$ and for maximal slices ($K = 0$) :

$$K^{ij}_{\rm CTS} = K^{ij}_{\rm HKV}. \tag{56}$$

Thus the HKV extrinsic curvature is of the conformal thin-sandwich type, and not of the Bowen-York type.

4.4 Asymptotic behavior of the extrinsic curvature

In the HKV framework, when $r \to \infty$, $N \sim 1 - \frac{M_{\rm ADM}}{r}$, $\Psi \sim 1 + \frac{M_{\rm ADM}}{2r}$ and $K^{ij} = O\left(r^{-3}\right)$, so that the HKV momentum constraint equation (33) reduces to

$$\underline{\Delta}\beta^i + \frac{1}{3}\bar{\nabla}^i\bar{\nabla}_j\beta^j = O\left(r^{-5}\right). \tag{57}$$

Comparing with the EPBY momentum constraint (18) (see [33] for a discussion of the eigenvectors of the operator $\underline{\Delta} + 1/3\,\bar{\nabla}^i\bar{\nabla}_j$), we conclude that

$$\beta^i \sim \beta^i_{\rm kin} + 2X^i_{\rm BY} \qquad \text{when} \quad r \to \infty, \tag{58}$$

with the pure kinematical shift (corotating coordinates)

$$\beta^i_{\rm kin} := (-\Omega y, \Omega x, 0). \tag{59}$$

Hence, since $(\tilde{L}\beta_{\rm kin})^{ij} = 0$,

$$K^{ij}_{\rm HKV} \sim K^{ij}_{\rm EPBY} \qquad \text{when} \quad r \to \infty. \tag{60}$$

Therefore HKV and EPBY extrinsic curvatures agrees asymptotically; they differ only in the strong field region.

5 Conclusions

We may draw the following conclusions from the above discussions:

- The classical Bowen-York extrinsic curvature does not represent well binary black holes in quasiequilibrium orbital motion.
- This explains why the effective potential method employed by Cook and subsequent authors fails: it amounts to minimize the binding energy among a set of non-steady solutions.

- The conformal thin sandwich formalism recently introduced by York [32] seems a much better physical treatment of the initial value problem.
- The helical Killing vector approach can be described in this formalism and results in very good agreement with post-Newtonian computations.

The next computational step is relaxing the conformal flatness hypothesis, while keeping the helical symmetry.

Acknowledgments

The HKV part of this work has been performed in collaboration with Silvano Bonazzola and Philippe Grandclément, and the comparison with EOB results has been performed in collaboration with Thibault Damour. Besides, it is a pleasure to thank Luc Blanchet, Brandon Carter, David Hobill, Jérôme Novak, Masaru Shibata, Keisuke Taniguchi and Koji Uryu for very fruitful discussions. I also thank the organizers of the JGRG12 meeting for their exceptional hospitality.

References

[1] V.M. Lipunov, K.A. Postnov, and M.E. Prokhorov, New Astron. **2**, 43 (1997).

[2] K. Belczynski, V. Kalogera, and T. Bulik, Astrophys. J. **572**, 407 (2002)

[3] S.F. Portegies Zwart and S.L.W. McMillan, Astrophys. J. **528**, L17 (2000).

[4] S. Komossa, V. Burwitz, G. Hasinger, P. Predehl, J. S. Kaastra, and Y. Ikebe, Astrophys. J. **582**, L15 (2003).

[5] D. Merrit and R.D. Eckers, Science **297**, 1310 (2002).

[6] L. Blanchet, these proceedings.

[7] A. Buonanno and T. Damour, Phys. Rev. D **62**, 064015 (2000).

[8] T.W. Baumgarte and S.L. Shapiro, Phys. Rep. **376**, 41 (2003).

[9] G.B. Cook, Phys. Rev. D **50**, 5025 (1994).

[10] J.W. York, in *Sources of Gravitational Radiation*, ed. L.L. Smarr (Cambridge University Press, Cambridge, 1979), p. 83.

[11] J.M. Bowen and J.W. York, Phys. Rev. D **21**, 2047 (1980).

[12] H.P. Pfeiffer, S.A. Teukolsky, and G.B. Cook, Phys. Rev. D **62**, 104018 (2000).

[13] T.W. Baumgarte, Phys. Rev. D **62**, 024018 (2000).

[14] T. Damour, P. Jaranowski, and G. Schäfer, Phys. Rev. D **62**, 084011 (2000).

[15] L. Blanchet, Phys. Rev. D **65**, 124009 (2002).

[16] E. Gourgoulhon, P. Grandclément, and S. Bonazzola, Phys. Rev. D **65**, 044020 (2002).

[17] P. Grandclément, E. Gourgoulhon, and S. Bonazzola, Phys. Rev. D **65**, 044021 (2002).

[18] S. Detweiler, in *Frontiers in Numerical Relativity*, ed. C.R. Evans, L.S. Finn, and D.W. Hobill (Cambridge University Press, Cambridge, 1989), p. 43.

[19] G.W. Gibbons and J.M. Stewart, in *Classical General Relativity*, ed. W.B. Bonnor, J.N. Islam and M.A.H. MacCallum (Cambridge University Press, Cambridge, 1983), p. 77.

[20] J.A. Isenberg : *Waveless approximation theories of gravity*, preprint University of Maryland, unpublished (1978).

[21] J.L. Friedman, K.Uryu, and M. Shibata, Phys. Rev. D **65**, 064035 (2002).

[22] R.H. Price and J.T. Whelan, Phys. Rev. Lett. **87**, 231101 (2001).

[23] G.B. Cook, Phys. Rev. D **65**, 084003 (2002).

[24] S. Bonazzola, E. Gourgoulhon, and J.-A. Marck, Phys. Rev. D **58**, 104020 (1998).

[25] S. Bonazzola, E. Gourgoulhon, and J.-A. Marck, J. Comput. Appl. Math. **109**, 433 (1999).

[26] P. Grandclément, S. Bonazzola, E. Gourgoulhon, and J.-A. Marck, J. Comp. Phys. **170**, 231 (2001).

[27] `http://www.lorene.obspm.fr`

[28] T. Damour, E. Gourgoulhon, and P. Grandclément, Phys. Rev. D **66**, 024007 (2002).

[29] A. Buonanno and T. Damour, Phys. Rev. D **59**, 084006 (1999).

[30] M. Shibata, private communication (2002).

[31] M.L. Skoge and T.W. Baumgarte, Phys. Rev. D **66**, 107501 (2002).

[32] J.W. York, Phys. Rev. Lett. **82**, 1350 (1999).

[33] N. Ó Murchadha, in *Approaches to Numerical Relativity*, ed. R. d'Inverno (Cambridge University Press, Cambridge, 1992), p. 83.

Dynamical Tachyon Condensation in String Theory
— Time-dependent background in string theory? —

Koji Hashimoto[1]

Institute of Physics, Graduate School of Arts and Sciences,
University of Tokyo, Komaba, Meguro, Tokyo 153-8902, Japan

Abstract

In this talk I would like to review the recent development on (dynamical) tachyon condensation in string theory. The time-dependent tachyon condensation has attracted much attention in this field in the last year. Here I describe how the open string modes living on the unstable brane cease to propagate as the tachyon condensates dynamically, supporting Sen's conjecture stating that the tachyon condensation is equivalent to the disappearance of the original branes [Gibbons-Yi-K.H. hep-th/0209034].

1 Tachyon in string theory

1.1 Historical perspective

Historically, tachyon fields appearing in various string theories have been considered to be the illness of the theories. For example, usual closed or open bosonic string theories contain tachyon modes as their lowest excitation of strings, and this is the reason why these string theories have been regarded as unsatisfactory theories to describe the realistic world. This motivated researchers to consider various supersymmetric generalization of string theories, generically called superstring theories which have many varieties if we include various ways of compactifications. They are free of tachyons and thus stable at least perturbatively.

However, infinitely many perturbatively stable vacua of superstring theories have been found, and thus a non-perturbative formulation of string theories has been desired. This requires intrinsically an off-shell formulation of string theories. After the great progress of these 7 years in string theory, now some of the off-shell formulations are at our hand, although the use of them are limited. At this stage, the tachyon fields which was discarded has revived, since the tachyon condensation can be considered to be a nice test of the off-shell formulations.

Let us remind of the standard model of particle physics for example. In the model we have Higgs fields which have tachyonic mass terms. However we know the physics of the Higgs fields, that simply leads us to the other stable vacua by the field condensation. So in string theory, the idea here is that off-shell formulation of tachyon fields should give the other stable vacua defining some perturbative string theory. This is very interesting possibility : we may describe stable (possibly new) vacua of string theories by completely different degrees of freedom which sit at the top of the tachyon potential. This is a new kind of string dualities.

However, because of the lack of our knowledge on the vacuum structure of string theories, we need some guiding principles which may help us to figure out what kind of physical properties at the bottom of the tachyon potential we should examine. This role has been supplemented by so-called "Sen's conjecture on tachyon condensation" which we will review in detail in section 2. With the conjectures as a guiding principle, there have been very fruitful developments in off-shell string theories such as string field theories. We trace some of the developments in section 2. Recent development along this direction during the last year has been to investigate time-dependent tachyon condensation named "rolling tachyon," i.e. dynamical decay of unstable branes. This opened up new possibilities to describe time-dependent background in string theories. In section 3 we review some of the results found there, in particular fate of the open string modes living on the decaying brane.

[1] E-mail:koji@hep1.c.u-tokyo.ac.jp

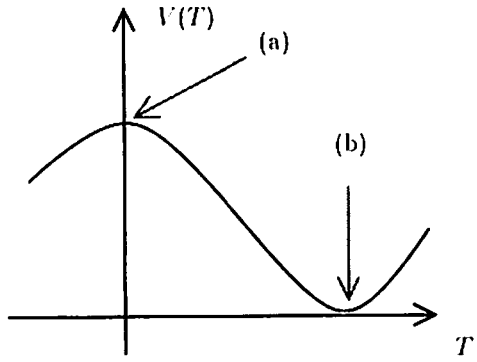


Figure 1: A schematic picture of the tachyon potential in string theory. (a) Perturbative vacuum where the tachyon exists. (b) Non-perturbative vacuum which is stable.

1.2 What is D-brane?

Before going to the tachyon condensation, here we shall give a brief summary of the definition and the properties of D-branes in string theory. Let us consider Type IIB superstring theory for simplicity. The massless fields living in the bulk 1+9 dimensional spacetime are graviton $g_{\mu\nu}$, NS-NS 2-form $B_{\mu\nu}$, dilaton ϕ, and RR $2p$-forms A, $C_{\mu\nu}$, $C^{(+)}_{\mu\nu\rho\sigma}$. In the low energy effective actions governing the dynamics of these fields, it was found that there is a nontrivial Z_2 symmetry which exchanges $B_{\mu\nu}$ and $C_{\mu\nu}$, accompanied with some transformation on ϕ and A. This is known as the S-duality symmetry of type IIB supergravity. We may assume that this symmetry can be extended to the whole type IIB superstring theory, which is a conjectural S-duality. This S-duality changes basically ϕ to $-\phi$, hence this duality is strong $\leftrightarrow$ weak coupling duality since the string coupling constant is $g_s \sim e^{\phi}$. A nontrivial outcome of this duality statement is that the strong coupling limit of this theory should be described by another string-like object. This is due to the fact that fundamental strings in the type IIB theory is charged under the gauge field $B_{\mu\nu}$, while there seems to be no fundamental object charged under $C_{\mu\nu}$ to which the NS-NS $B_{\mu\nu}$ will be transformed under the S-duality. Therefore this duality predicts existence of another string-like object charged under the RR two-form, named a D-string.

This kind of extended object has been observed as classical solutions of the type IIB supergravity, and those were called black p-branes where p denotes the spatial dimensions which the extended object has. These black p branes with supersymmetries have the RR charges. Polchinski noticed in 1995 that hypersurfaces on which open strings can end have the same RR charges. The open string boundary condition becomes Dirichlet-type, and so the black p-brane which is identified with this hypersurface is now called D(irichlet) p-branes. Basic properties of the D-branes are:

- Gravitational description of the D-branes is just the BPS black p-branes.
- Parallel D-branes are stable and leaving some of the bulk supersymmetries unbroken.
- Excitations of the open strings attached on the D-branes give massless gauge fields A_μ and transverse scalar fields Φ.
- IIB (IIA) includes D(2p+1)-branes (D(2p)-branes), which is obvious from their massless matter content. p-branes can couple to $(p+1)$-form gauge potential in the bulk spacetime.

1.3 Tachyons in string theories

We have plenty of situations where initially stationary background can have unstable excitations in string theories. Here we give some simple examples of such situations.

- Closed string tachyons.
  This is the most popular tachyon mode which appear for example in the bosonic closed string theory. However, so far the closed tachyon modes are found to be difficult to be treated, especially

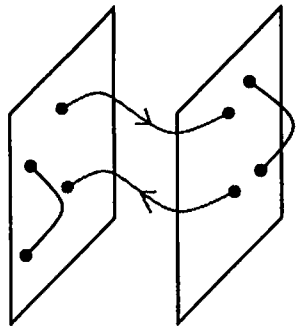


Figure 2: A pair of parallel brane and antibrane which gives a complex tachyon and two massless gauge fields.

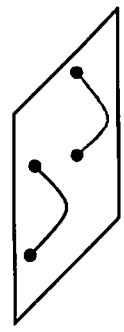


Figure 3: A non-BPS brane which gives a real tachyon and a single $U(1)$ gauge field.

in the sense that generically they are not localized. The whole target space may collapse and we may have no physically sensible endpoint of the tachyon condensation. Thus the study of this so far has been only localized closed tachyon modes.

- Open string tachyons.
  - D-branes in bosonic string theory.
    In bosonic string theory, there is no notion of BPS and thus the stability of the brane is not protected by any charge. There appears open string tachyon mode on the brane.
  - Parallel brane-antibrane in superstring theory.
    Parallelly placed D-brane antiD-brane pair is analogous to a pair of black holes which have opposite RR charges. Hence naively they are unstable. In fact, in type II superstring theories, this configuration gives rise to a complex tachyon field coming from the excitation of strings connecting two branes. Massless fields on the brane antibrane pair are — $U(1) \times U(1)$ gauge fields and transverse scalar fields.
  - Non-BPS branes in superstring theory.
    For example in type IIA theory BPS D-branes are allowed to have odd worldvolume dimensions (p: even), but we may consider D-branes with even worldvolume dimensions. These break all of the bulk supersymmetries, and thus are non-BPS. A real tachyon mode exists as the lowest excitation of the string attached to the D-brane. The massless fields on a non-BPS branes are — $U(1)$ gauge fields and several transverse scalars.

In this review, we concentrate on the tachyon on a non-BPS brane and a bosonic D-brane for simplicity. Since the fields on a non-BPS branes can be consistently embedded into the field content on a brane antibrane, we may expect similar analysis on the brane antibrane.

2 Sen's conjectures

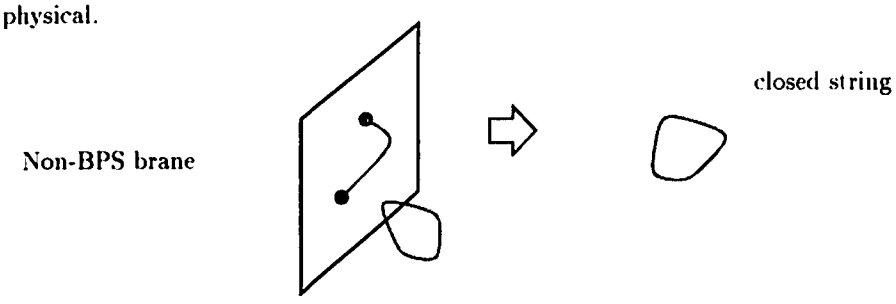
2.1 Statement

In this section we explain what are "Sen's conjectures" and explain how they contributed to the recent developments in string theories.

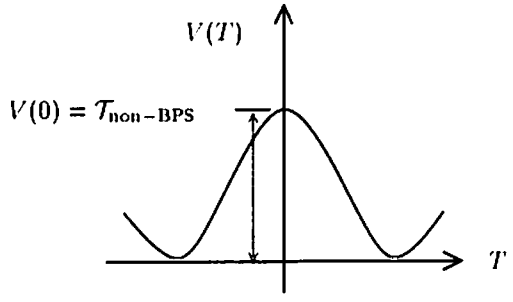
Sen's conjectures were established in his papers [9805170, 9902105, 9904207][2]. His statements are summarized into the following three conjectures. There are several version of these conjectures, depending on the brane systems to be treated. Here for simplicity we concentrate on the tachyon field on a non-BPS D-brane in type II string theory.

[2] In this note we omit writing "hep-th" in the reference.

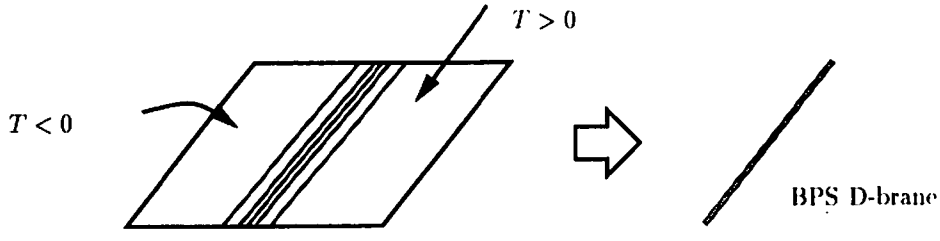
1. *When the tachyon on a non-BPS brane condenses, the original brane disappears.* The bottom of the tachyon potential is called "closed string vacuum," where only bulk closed string modes are physical.



2. *The height of the tachyon potential is exactly the tension of the original unstable brane.*



3. *If the tachyon vacuum has nontrivial topology, the topological defects corresponds to lower-dimensional D-branes.* For example, let us consider a non-BPS D($2p+1$)-brane in type IIB theory. The tachyon living on it has the potential with Z_2 symmetry $T \leftrightarrow -T$, and thus the vacua are disjoint two points. Hence there should exist a domain wall solution in the tachyon effective field theory, with co-dimension one. This domain wall which is topologically stable can be identified with a BPS Dp-brane.



2.2 History on tachyon condensation

The table is a brief summary of the development of understanding of the tachyon condensation in string theory and related research fields. Please note that this table is written based on my personal standpoint and there should be other streams which flow into this table or flow out from this.

It would be possible to say that Sen's conjectures were established around '98 ~ '99. Of course, before the appearance of the conjectures we had experienced the "second" revolution of string theory which was mainly based on the discovery of the roles of the D-branes in string theories. We understood there a portion of non-perturbative physics appearing in string theory, due to the identification of D-branes which are defined perturbatively as boundaries of open strings and black branes which are defined as solutions of classical supergravities.

However before this second revolution of string theory, there have been preceding developments on tachyons in string theory. For example, in the left column, the effective field theory approach is described. The discovery of string dualities was partially due to the discrete symmetries in these low energy effective

field theory actions. So it was natural to extend those analysis to the one including tachyons and massive modes. As for the tachyon condensation itself, there has been interesting observations around 1990 by Kostelecky and Samuel who considered application of string field theories which are off-shell formulation of string theories. However at that time the precise interpretation of the tachyon condensation was incomplete in a sense.

	Effective Actions	Boundary SFT	Cubic SFT	Noncommutative Solitons
80's	SUGRA, DBI	—	Witten, HIKKO	NCG (Connes)
'92	↓ ↓	Witten's definition	Tachyon condensation	↓ ↓
94 -96	D-branes, String dualities (BPS = supersymmetric = stable)			
98	**Sen's conjectures** on tachyons			
99	MZ model	Verification	Level truncation	Seiberg-Witten, GMS soliton
00	↓ Effective analysis		↓ VSFT	↓ NC tachyon
02	↓ Rolling Tachyon ↓		↓ ↓	↓

After the appearance of Sen's conjectures, various attempts have been made to verify some of the statements. In the following we summarize the status of whether each conjecture has been verified or not.

conjecture 1. The cubic string field theory (CSFT) which was originally defined by Witten in 1986 turned out to be a very useful tool to test Sen's conjectures. Although it includes infinite number of fields in the action since it treats all the string excitations at once, a systematic evaluation of the action by so-called "level truncation" has been developed, and it showed disappearance of open string degrees of freedom at the bottom of the tachyon potential [Hata-Teraguchi 0101162]. Another interesting variation of this CSFT is Vacuum string field theory (VSFT) which is conjectured to be a string field theory describing the bottom of the tachyon potential [Rastelli-Sen-Zwiebach 0012251]. Although we cannot say that it has been completely successful, at least it has no physical open string excitation at the bottom by its definition, and also it turned out to be possible to construct a classical solution in VSFT which describes the top of the potential, the other way around [Hata-Kawano 0108150, Okawa 0204012].

Conjecture 2. A concrete verification has been made by boundary string field theory (BSFT). This BSFT is one of the off-shell formulation of string theory though the definition allows only the appearance of the tachyon or massless degrees of freedom in the action. The definition of BSFT action was shown to be just a disk partition function of a superstring worldsheet. One turns on only the tachyon field which is constant or linear in the target space coordinates, then it can be shown that the height of the tachyon potential is exactly the tension of the original non-BPS D-brane [Ghoshal-Sen 0009191]. CSFT level truncation also provided positive evidence for this conjecture, leaving a result that the height of the potential is identical with the tension in great numerical accuracy.

Conjecture 3. Also for this conjecture the level truncation method in CSFT has been studied, and classical lumps and kinks representing D-branes were obtained. The tensions of those objects are

computed and it coincides with that of the expected lower dimensional D-branes in satisfactory numerical accuracy [Harvey-Kraus 00021 17]. More interesting results have been obtained in BSFT. BSFT provides classical solutions representing the D-branes, and the tension of these domain wall solutions were found to be identical with the tension of D-branes exactly. So BSFT was very successful in this sense [Kutasov-Marino-Moore 0009148, 0010108]. Another interesting approach to this realization of lower dimensional D-branes has been provided in non-commutative geometry. The non-commutative geometry was initiated by A. Connes in 1980's, and solitons and instantons in noncommutative spaces have been studied [Nekrasov-Schwarz 9802068]. A realization of a kind of non-commutative spacetime in string theory was noticed by [Connes-Douglas-Schwarz 9711162], and Seiberg and Witten [9908142] formulated this correspondence more concretely. When one applies the correspondence to tachyon systems in string theories, it was found that the noncommutative solitons in that system are in fact lower-dimensional D-branes whose tensions are correctly reproduced [Harvey-Kraus-Larsen-Martinec 0005031]. Although as for the tension we had much success on the reproduction, in order to show that the topological defects are D-branes, we have to reproduce all the open string modes on the defects. This is rather difficult task since here we have to incorporate all the string modes into the analysis, and this hasn't been achieved yet. There was one attempt for the reproduction of D-brane boundary state from tachyon topological defects [Asakawa-Sugimoto-Terashima 0212188], but this shows only the coupling to the closed string modes and inclusion of all the open string modes seems to be a remained issue.

In a nutshell, the present status of the verification of Sen's conjecture is that only the verification of conjecture 2 (and also the tension of conjecture 3) has been achieved and the rest seems to be incomplete. One of the main obstacles toward the verification is obviously the understanding of the bottom of the potential. It was recognized that the closed string modes which should appear there look somewhat singular, and it is difficult to see them directly. This motivates us to the following consideration: what if we start from a tachyon expectation value which is slightly away from the exact bottom of the potential? Of course if we start off from such a point then we basically will have a time-dependent classical trajectory toward to the bottom, and this is a time-dependent background in string theory which has not been studied well so far. However we might be able to see in the time-evolution process how the singularity at the bottom of the potential emerges.

There has been a big motivation to understand time-dependent backgrounds in string theory, since if we say that the string theory provides all the quantum process occurring in the universe, it should explain the expansion of the present universe and inflation etc. Hence time-dependent backgrounds in string theory are quite important in this sense. Eventually the time-dependent tachyon condensation provided an interesting approach to string cosmology recently.

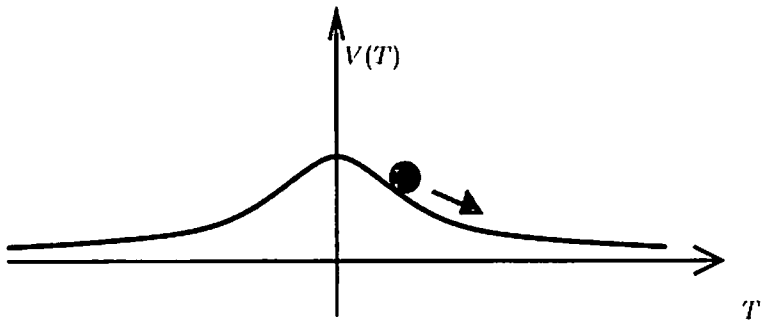
On the other hand, since due to Sen's conjecture the tachyon condensation is equivalent with the annihilation of D-branes, the time-dependent condensation means dynamical decay of branes. Therefore it opens up possibilities to describe creation and annihilation process of D-branes which is very important to find any nonperturbative formulation of string theories. The issue is — how the tachyon condensation proceeds dynamically in a non-BPS brane for example? In the next section, we review "rolling tachyon" which is a time-dependent (dynamical) tachyon condensation, and see how the physical degrees of freedom "die" as tachyon condenses.

Other recent developments along this direction of considering time-dependent backgrounds in string theory include, for example, S-branes by Gutperle and Strominger, inflationary brane worlds, and time-dependent orbifolds by Seiberg and his collaborators.

3 Rolling Tachyon

3.1 Definition

The "rolling tachyon" was named by A. Sen, which describes time-dependent tachyon condensation. Sen's papers initiating the analysis were the following three papers: "Rolling Tachyon" (0203211), "Tachyon Matter" (0203265), and "Field Theory of Tachyon Matter" (0204143). In these papers Sen studied how a non-BPS D-brane in type II superstring theory and a bosonic D-brane in bosonic string theory decay dynamically, with time-dependent tachyon condensation.



In the analysis of the dynamical decay of unstable D-branes, Sen treated only classical decay without coupling to closed strings, by using SFTs, deformed conformal field theories (CFTs) and boundary states. Here we don't review his computations but we list his main results basically coming from the deformed CFT analysis:

- There is no oscillation around the potential minimum, but everlasting evolution (rolling) toward it.
- The end product of the tachyon condensation is pressure-less non-interacting dust with finite energy density. This is named "tachyon matter," according to its properties similar to the dark matter in the universe.
- He proposed an effective field theory describing the late time properties of the tachyon condensation, i.e. the tachyon matter.

In this talk we concentrate on the third point above, and show interesting properties of the tachyon matter and related physics.

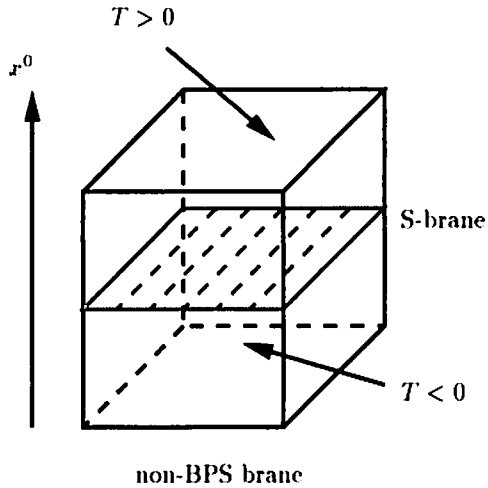


Figure 4: Definition of the S-brane.

Before going to the detailed study of the effective field theory, let us present here related notions which we will find important later. The first one is Spacelike brane, which is called S-brane in short. This S-brane can be defined through the rolling tachyon as follows. According to Sen's conjecture on a non-BPS brane, the ordinary domain wall (kink) is identified with a co-dimension one BPS D-brane. On the other hand, if we consider a time-dependent tachyon configuration which is homogeneous spatially and $T < 0$ for $x^0 < 0$ while $T > 0$ for $x^0 > 0$, then this can be regarded as a spacelike kink [Gutperle-Strominger 0202210]. If we look at the late time behavior, this is the rolling tachyon. So we can say that

a single tachyon profile which is time-dependent and spatially homogeneous provides the rolling tachyon at late time while an S-brane when the tachyon value passes $T = 0$, the top of the potential.

Another issue on the tachyon condensation is the appearance of the closed strings at the bottom of the potential. A question raised by Witten is : Where the gauge field on the brane goes in the tachyon condensation? The tachyon field on the non-BPS brane is not charged under the gauge group, so even if the tachyon acquires a VEV, there is no Higgs effect to the gauge fields. A conjectural answer by Yi to this question is interesting: The gauge fields will be confined, and the confined electric flux tube behaves like a fundamental string. So the closed strings are provided as solitonic excitation in the vacuum where the tachyon is condensed.

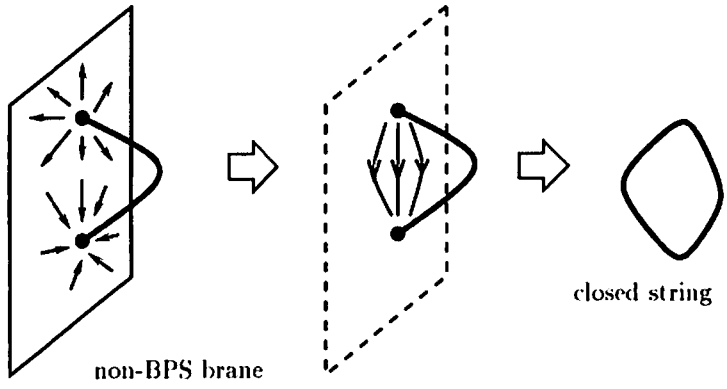


Figure 5: Confined electric flux = fundamental closed string.

3.2 Effective field theory analysis

Sen proposed that the following action describes low energy physics around the minimum of the tachyon potential :

$$S = -\int d^{p+1}x\, V(T)\sqrt{-\det(g_{\mu\nu} + \partial_\mu T \partial_\nu T)}, \tag{1}$$

where the potential $V(T)$ has a run-away behavior $\sim e^{-\sqrt{2}T/2}$ for large T. (We took the unit $\alpha' = 1$ here.) This action around $T = 0$ was originally proposed by Garousi and Bergshoeff et al., from the scattering amplitude calculation and consistency with T-dualities.

One of the features which Sen observed with use of this action is the exponential fall off of the pressure computed at late time of the classical rolling tachyon solution. Let us check this here. First, we concentrate on a spatially homogeneous solution, $\partial_i T = 0$. The conserved energy when only $\partial_0 T$ is turned on reads

$$\mathcal{E} = T_{00} = V(T)/\sqrt{1 - (\partial_0 T)^2}, \tag{2}$$

and this can be easily integrated to give the rolling tachyon solution

$$T = x^0 + \frac{1}{2\sqrt{2}\mathcal{E}^2} e^{-\sqrt{2}x^0} + \mathcal{O}(e^{-2\sqrt{2}x^0}). \tag{3}$$

From this expression, the pressure is computed to give an exponential fall off,

$$p = -\frac{1}{\mathcal{E}} e^{-\sqrt{2}x^0}. \tag{4}$$

The action allows general solutions at late time. We turn on the spatial dependence for the tachyon profile, and solve the equations of motion in the limit $V \to 0$. An interesting outcome is that we can

show the equivalence to a non-interacting dust system. The Hamiltonian is given by

$$\mathcal{H} = \int d^p x^i \sqrt{P^2 + V(T)^2}\sqrt{1 + \partial_i T \partial_i T}, \tag{5}$$

which gives the equations of motion in the limit $V(T) \to 0$

$$\partial_0 P = \partial_j \left(P \partial_j T / \sqrt{1 + \partial_i T \partial_i T} \right) \tag{6}$$

$$\partial_0 T = \sqrt{1 + \partial_i T \partial_i T} \tag{7}$$

An interesting solution is

$$T = x^0, \quad P(x) = \text{an arbitrary function of } x^i, \tag{8}$$

the meaning of which is arbitrary distribution of the tachyon matter.

One of the reasons why we have this large degeneracy is that the equations of motion possesses the scale invariance:

$$T(x) \to T(sx)/s, \quad P(x) \to s^{p+1} P(sx). \tag{9}$$

More generally, if we define $u_\mu \equiv \partial_\mu T$ and $\epsilon \equiv P/\partial_0 T$, then the equations of motion are reduced to

$$u_\mu u^\mu = -1, \quad \partial_\mu (\epsilon u^\mu) = 0. \tag{10}$$

These are the equations which dictate gradient flow of non-interacting dust (ideal fluid). This is consistent with Sen's conjectures saying that there remains no interaction at late time of the dynamical tachyon condensation.

3.3 Disappearance of the excitation?

Let us see more in detail how the physical excitations on the non-BPS branes disappear [Gibbons-Yi-K.H. 0209034]. The simplest way to see this is just to substitute a fluctuation $T = T_{\rm cl}(x^0) + t(x^0, x^i)$ into the tachyon action and take its quadratic terms, which results in the expression

$$S_{\rm f} = \frac{-\mathcal{E}}{2} \int dx^0 d^p x^i \left(\frac{-\mathcal{E}^2}{V^2} (\dot{t})^2 + (\partial_i t)^2 + M^2(x^0) t^2 \right), \tag{11}$$

where $i = 1, 2, \cdots, p$, and the time-dependent mass is

$$M^2(x^0) = \left[\frac{V''}{V} - \frac{(V')^2}{V^2} \right]_{T=T_{\rm cl}}. \tag{12}$$

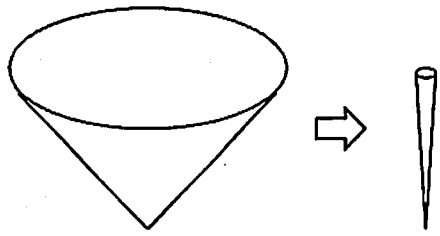
Since the time component of the kinetic term has extra factor $1/V^2$, as $x^0 \to \infty$ the effective metric governing the propagation of the fluctuation becomes very singular:

$$G_{\mu\nu} \to \text{diag}(0, 1, 1, \ldots, 1). \tag{13}$$

This singular metric is known as Carroll limit where the speed of light goes down to zero, $c \to 0$. Physically, this means that the light cone describing the propagation of the tachyon fluctuation collapses onto a timelike half line, see the figure below. In other words, the tachyon fields at different spatial points are decoupled with each other. Therefore no propagation of tachyon fluctuations can take place, and this is consistent with Sen's conjecture that physical open string modes disappear there. Although here we have used the action which Sen has proposed, it can be shown that this kind of Carrollian contraction occurs very generally, for example also in the BSFT action.

3.4 Appearance of closed string degrees of freedom?

As noted before, we have an expectation that electric flux tubes become solitonic closed strings at the bottom of the potential. Since these solitonic excitations should be able to fluctuate, we should see not all of the fluctuations cease to propagate. The flux tube is made of gauge fields, especially the electric fields, so we turn on the gauge fields in the following and continue the fluctuation analysis.



3.4.1 Gauge-Tachyon coupling

Once the tachyon action is written, it is easy to introduce the gauge coupling. It is just given by the replacement $\eta^{\mu\nu} \to (G_{\rm open}^{-1})^{\mu\nu} = (\eta + F)^{-1}_{\rm sym}$ which is the open string metric. The resultant Lagrangian is

$$\begin{aligned} \mathcal{L} &= -V(T)\sqrt{-\det(\eta+F)}\sqrt{1+(G_{\rm open}^{-1})^{\mu\nu}\partial_\mu T\partial_\nu T} \\ &= -V(T)\sqrt{-\det(g+F+\partial T\partial T)}. \end{aligned} \tag{14}$$

If we turn on only the electric field and assume the homogeneous tachyon $T(x^0)$, then the Lagrangian becomes

$$\mathcal{L} = -V(T)\sqrt{1-E^2-\dot{T}^2}. \tag{15}$$

3.4.2 Rolling tachyon solution with electric field

In the presence of the electric field, the rolling tachyon solution will be modified. It is possible to show that constant E is actually a solution. Intrinsically, the rolling tachyon solution at the late time is given by requiring that inside of $\sqrt{}$ in the action vanishes so that the total energy can remain finite while $V(T)$ goes to zero. This condition gives

$$\dot{T}^2 + E^2 = 1, \tag{16}$$

which is the rolling tachyon with the electric flux. One comment here is that critical electric field $|E| = 1$ (in the unit $2\pi\alpha' = 1$) is equivalent with infinite electric flux.

3.4.3 Effective metric for gauge fluctuation

Let us list here the result of the fluctuation analysis. Without losing generality, we turn on only E_1. Then we can show that a combination $\hat{t} \equiv \sqrt{1-E^2}\, t + E a_1$ (where a_μ is the gauge fluctuation) is governed by Carrollian metric, while a_i $(i = 2, \cdots, p)$ is governed by the following special metric

$$G_{\mu\nu} \to \lim_{\epsilon\to 0} \mathrm{diag}\left(-\epsilon, \frac{\epsilon}{E^2}, 1, \ldots, 1\right). \tag{17}$$

(Another linear combination of t and a_1 which is orthogonal to $\hat{t}$ is subject to the same effective metric.) The above metric gives interesting deformation of the light cone, shown in the following figure. Certain fluctuations can propagate only along the direction of the background electric field, and the speed of the fluctuation is given by $|E|$.

To be summarized, general vacuum with $|\vec{E}| \neq 0$ allows 1+1 dimensional propagation of small fluctuations with speed $|\vec{E}|$. Therefore, confined flux tubes can be regarded as wave guides. At the core of the confined flux tube, it is expected that the flux diverges and thus $|E| = 1$. Hence the speed of the fluctuation is the speed of light there. This means that the confined flux behaves as a closed fundamental Nambu-Goto string.

Here we adopted only the spatially homogeneous electric flux. How the electric flux can be confined inhomogeneously is described by S-brane effective actions [Ho-Wang-K.H. 0211090].

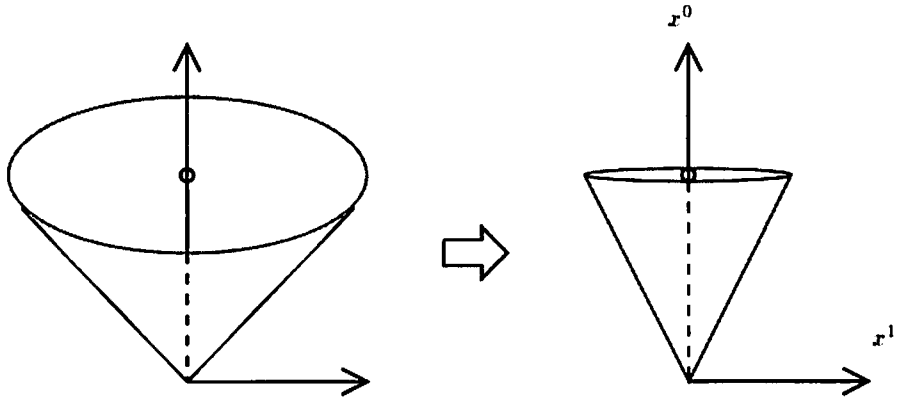


Figure 6: Deformation of the light cone by the metric (17).

3.5 Subsequent developments

Let us list the subsequent developments on this rolling tachyon.

- BSFT treatment of rolling tachyon (Sugimoto-Terashima 0205085, Minahan 0205098). The tachyon Lagrangian is give in BSFT as $\mathcal{L} = e^{-T^2/4} z 4^z \Gamma(z)/2\Gamma(2z)$, where $z \equiv (\partial_\mu T)^2$. Although the Lagrangian looks quite different, similar rolling solution exists and shows the exponential fall off of the pressure.
- Cubic string field theory / p-adic string theory (Moeller-Zwiebach 0207107, Kluson 0208028,0209255).
- Inhomogeneous rolling tachyon (Sen 0207105, Felder-Kofman-Starobinsky 0208019, Mukohyama 0208094).
- Confinement of electric flux (Ho-Wang-K.H. 0211090).
- Inclusion of / application to Gravity. Application to the brane cosmologies has been studied by many people in which they accepted naive analysis of the tachyon action + gravity in, say, 1+3 dimensions. (Gibbons 0204008 etc.) Gravitational radiation of rolling tachyon was studied in (Chen-Li-Lin 0209222), and a possible gravity solution representing the tachyon matter was provided by (K.Ohta-Yokono 0207004, Buchel-Langfelder-Walcher 0207235). Gravity solution representing S-branes were discussed by (Chen-Gal'tsov-Gutperle 0204071, Kruczenski-Myers-Peet 0204144). Another interesting direction was provided in "Time and Tachyon"(Sen 0209122), in which tachyon matter was applied to the canonical quantization of gravity.

4 Summary and Future Directions

The main message of this talk, which is based on the conjecture stating that "Tachyon condensation on unstable branes = Annihilation of the brane," is that dynamical tachyon condensation can be studied and it provides interesting physics and applications.

Motivation of study of the rolling tachyon is summarized as:

- Understanding string vacua.
- Hints for formulation of D-brane creation/annihilation.
- Describing time-dependent backgrounds in string theory for application.

And the present status of study seems to be

- Verification of Sen's conjecture has been partially achieved.

- Time-dependent analysis has just started (2002/3 -), and it is providing interesting physics such as tachyon matter.

The main problems found in the sequel are:

- An obstacle against verification of Sen's conjecture: Difficulty in dealing with SFTs which contain infinitely number of fields.
- Validity of effective field theories of tachyon (+gravity).

Future directions include applications of the rolling tachyon / tachyon matter :

- Brane cosmology (with standard model). — Is the homogeneous rolling really a good initial condition?
- Disappearance of physical open string degrees of freedom.
- Understanding of the rolling tachyon in cubic/vacuum string field theories.
- Other situations with tachyons, among which the most interesting should be the closed string tachyon.

Before ending this note, we consider here the following statement: "Is the tachyon matter really stable?" or "Is the gravitational description of rolling tachyon possible?" There are some facts showing a negative answer to these questions:

- The coupling to the massive closed string modes diverges exponentially as $\sim \exp(\sqrt{2}t)$ [Okuda-Sugimoto 0208196].
- The graviton n-point coupling in the tachyon effective field theory diverges [Gibbons-Yi-K.H. 0209034].
- A supergravity solution of the tachyon matter has diverging Hawking temperature [Ohta-Yokono 0207004].
- Too many open strings will be created [Strominger 0209090].

These arguments tell us that in the rolling tachyon or the tachyon matter the gravity description or the coupling to the gravity should be treated very carefully. They seem to suggest that for treating the decay of unstable branes, purely stringy description might be necessary.

Laser Interferometric Gravitational-Wave Detectors in Future

Seiji Kawamura,[1]

National Astronomical Observatory of Japan,
2-21-1 Osawa, Mitaka, Tokyo 1181-8588, Japan

Abstract

Several medium- to large-scale ground-based interferometric gravitational wave antennas have been constructed around the world. Although these antennas of the first generation could detect gravitational waves within a few years, it is necessary to improve the sensitivity of the detectors significantly with advanced technologies to ensure more frequent detection of gravitational waves. Development of a high power laser, use of a resonant sideband extraction interferometer, stronger seismic isolation and reduction of thermal noise especially using cryogenic mirrors are among the most important technologies that can lead us to the realization of advanced detectors. Some of the advanced technologies are already implemented in some of the existing detectors, and others are currently being investigated for the future-generation detectors such as advanced LIGO, LCGT, upgrade of GEO600, AIGO, and EURO. In parallel with these efforts on the ground-based detectors, we are also developing advanced technologies for space antennas such as LISA and DECIGO. The space antennas are very important since they aim at much lower frequency band than terrestrial detectors. We expect that these advanced detectors including the space antennas will eventually open a new window to the universe and establish a new field "gravitational wave astronomy"

1 Introduction

Several medium- to large-scale (300m to 4km) ground-based interferometric gravitational wave antennas have been constructed around the world: LIGO [1] [2] by the United States, Virgo [3] by France and Italy, GEO600 [4] by Germany and the United Kingdom, and TAMA300 [5] by Japan. In addition the Australian group (ACIGA) is preparing for AIGO [6]. It can be expected that in the near future there will be an international network of gravitational wave detectors, which can lead us to the detection of gravitational waves. However, it is necessary to improve the sensitivity of the detectors significantly with much more advanced technologies than the current ones in order to ensure more frequent detection of gravitational waves. Therefore, each project is considering, investigating, and even designing such an advanced detector as a future generation of its current detector. For example, LIGO will evolve into advanced LIGO [7], in Japan LCGT [8] will be constructed after TAMA, in Australia AIGO will be realized eventually, and in Europe EURO is under consideration as an ultimate future detector after the completion of VIRGO and the update of GEO (Fig. 1).

In this article some of the advanced technologies that are crucial to the advanced detectors will be introduced in section 2 with emphasis on a resonant sideband extraction interferometer, seismic isolation, and reduction of thermal noise especially using cryogenic mirrors. In section 3, the status and future plan for such advanced detectors are described for each project. The space antennas will be briefly explained in section 4. Finally prospects for the future detectors are summarized in section 5.

2 Advanced technologies

Among various noise sources existing in an interferometer, the shot noise, seismic noise and thermal noise are regarded as three largest fundamental noise sources, while others are considered to be practical noise sources. The sensitivity of the current detectors are ideally limited by these three kinds of noise: seismic

[1] E-mail:seiji.kawamura@nao.ac.jp

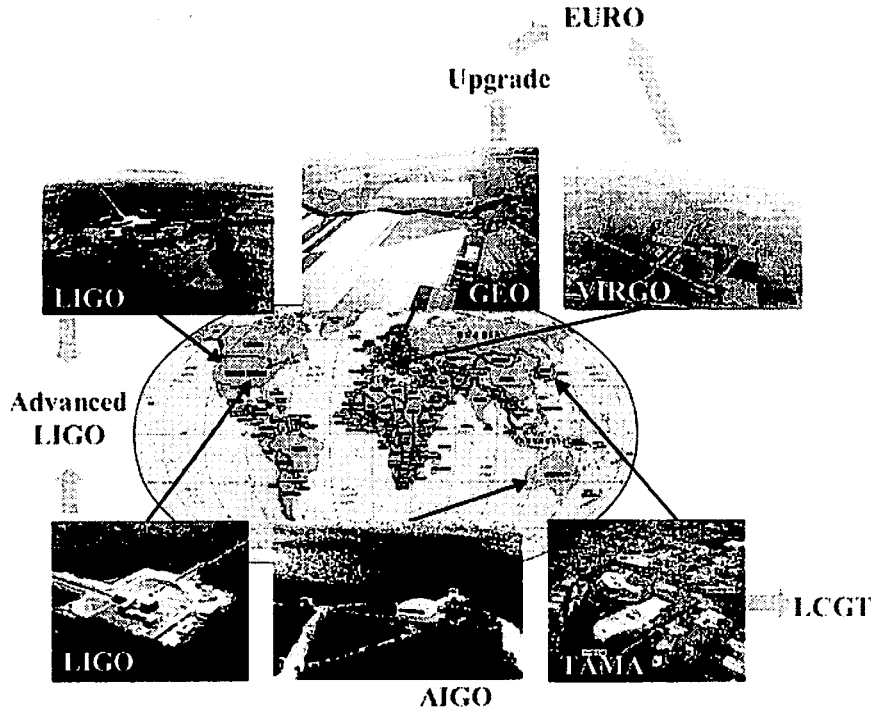


Figure 1: Current detectors and advanced detectors in the world.

noise at lower frequencies, shot noise at higher frequencies, and thermal noise at intermediate frequencies (Fig. 2). Therefore, advanced technologies required to realize the future detectors should reduce these three kinds of noise. Here such technologies for reduction of shot noise, seismic isolation, and reduction of thermal noise are discussed.

2.1 100W-class Laser

Shot noise exists because a photon has finite energy. Statistical fluctuations in the photon number in the detection process result in shot noise. In order to reduce the shot noise level, the interferometer should be operated in such a way that the intensity of the light at the detection port is dark, which gives the lowest counting fluctuations. In addition to this fringe control, it is desirable to have higher incident laser power to improve the signal-to-noise ratio for the shot noise. This is because the intensity change at the photodetector caused by gravitational waves is proportional to the incident laser power, while the intensity fluctuations caused by shot noise is proportional to the square root of the incident laser power; thus the signal to shot noise ratio is improved by the square root of the incident laser power.

Among many institutes and universities in the world, the ACIGA group is developing a 100W-class laser. They use a side-pumped, side-cooled Nd:YAG slab with zigzag mode in the plane of the pumping (Fig. 3). This zigzag configuration minimizes thermal and stress induced focusing while allowing extraction of energy from the edge of the slab where the pump density is highest. They have already attained 75 W and found that the power was limited by nonuniform pumping of the slab, causing loss of transverse mode control, and possibly by the non-optimal orientation of the crystallographic axes in the slab. These limitations are currently being investigated and corrected.

2.2 Resonant Sideband Extraction

The most critical problem associated with the use of a high power laser is that the beam quality is impaired by the thermal lensing effect of the mirrors, resulting in degradation in the mode matching of

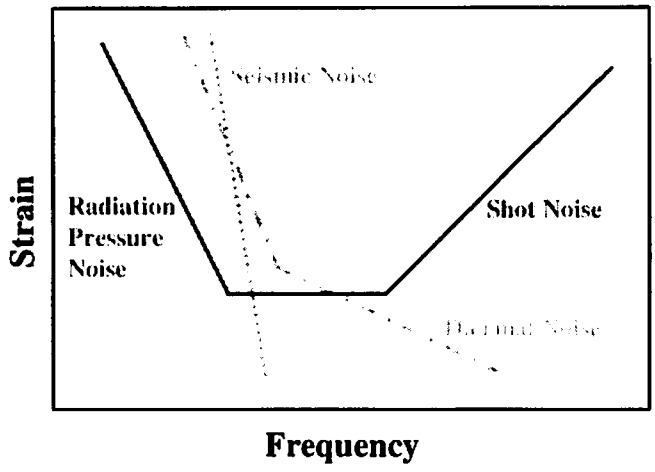


Figure 2: Three fundamental noise sources existing in an interferometric gravitational wave detector.



Figure 3: Prototype of the 100W-class laser developed by the ACIGA Group. (Provided by ACIGA).

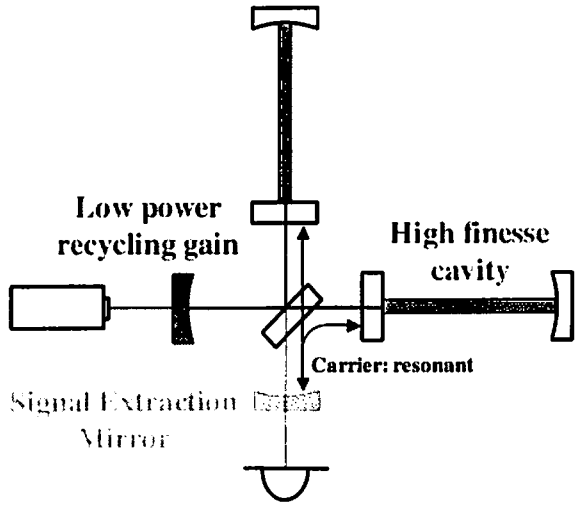


Figure 4: Optical configuration of the resonant sideband extraction interferometer.

the beam to the interferometer, thus the shot noise is increased.

Resonant sideband extraction [25] is an advanced optical configuration which has a solution to the heating problem (Fig. 4). It has a signal extraction mirror placed at the anti-symmetric port and high-finesse arm cavities. The signal extraction mirror can extract the gravitational wave signals from the arm cavities before the gravitational wave signals would be averaged out by the high-finesse arm cavity. This configuration makes it possible to reduce the circulating power inside the power recycling cavity while maintaining the optimized shot noise. This is useful to prevent the undesirable heating effect at the beamsplitter and the bulk of the input mirrors of the arm cavities. Another advantage of this interferometer is that it can detune the interferometer response to improve the shot noise within a limited frequency range. The Japanese group performed an RSE experiment with suspended mirrors for the first time in the world and demonstrated the satisfactory performance of this interferometer [12] (Fig. 5).

2.3 Seismic isolation

Seismic noise is the mirror motion caused by ground motion. It can be reduced by isolating the mirrors from the ground motion. A pendulum or a spring can work as an isolator. The isolation factor increases quadratically in frequency above the pendulum or spring resonant frequency. It should be noted that strong seismic isolation at the signal-band frequency is, of course, required to reduce seismic noise, but comparably important is seismic isolation at very low frequencies, especially between 0.1Hz and 10 Hz, which can improve the control noise, lock acquisition, and lock stability of the interferometer.

Seismic isolation can be implemented either actively or passively. Active isolation uses an accelerometer and an actuator. In order to ensure good performance of the active isolation system, the noise of the accelerometer used in the system should be very low. Passive isolation uses a spring or a pendulum. For higher isolation the resonant frequency of the resonator should be as low as possible, moreover multi-stage resonators should be used. The resonant frequency of the resonator can be lowered by adding an anti-spring to the original resonator to make the displacement dependence of its potential energy very shallow.

For example the advanced LIGO employs an active isolation system [9]. It consists of a two-stage in-vacuum active isolation platform that supports the optics table. Each stage contains relative position sensors and seismometers, which measure motion in six degrees of freedoms. Signals from these are filter/amplified and applied to coil-magnet actuators to reduce the motion of the stages. It was already demonstrated using a single-stage prototype that an isolation factor of 100 was obtained around 10 Hz. The experimental results with a full-sized two-stage active isolation platform, which has been developed at Stanford's Engineering Test Facility, will be obtained very soon.

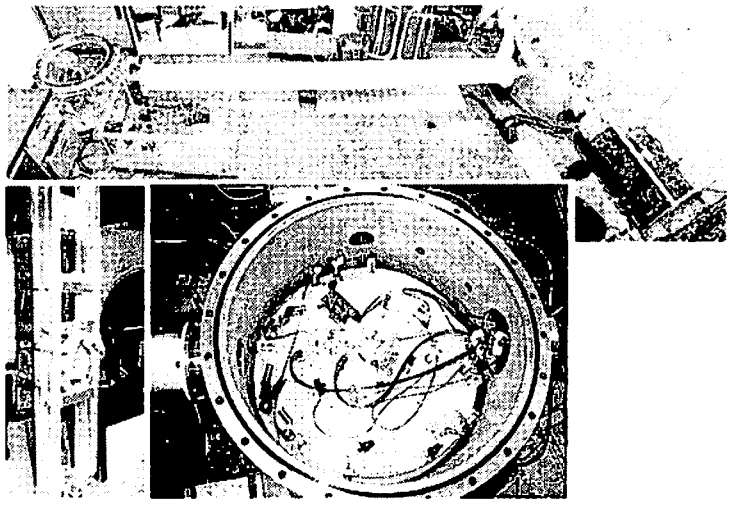


Figure 5: Experimental set-up of the RSE interferometer with suspended mirrors.

Super Attenuators [10] [11] used by the Virgo group is an example of an advanced passive isolation system. It is five cascaded 1.2-m pendulums attached at the top of an inverted pendulum (Fig. 6). The inverted pendulum has a very low resonant frequency because of the mixture of a spring and gravity potential. The vertical spring of each pendulum also gives a very low frequency resonance because of the pre-loaded blades made of Maragin steel and the anti-spring effect of the magnets. The last stage of the pendulum is a mirror and a reaction mass, both suspended from an upper mass called a marionette. The marionette is used to align the mirror. It is worth noticing that the Super Attenuator is not simply passive. The so-called "inertial damping" of the motion of the top of the inverted pendulum is an essential part of the system. A recycled short-arm Michelson interferometer with the Super Attenuators was already successfully locked. The seismic motion of the mirrors was measured to be reduced to 1×10^{-11} m/Hz$^{1/2}$ around 2 Hz and 1×10^{-13} m/Hz$^{1/2}$ around 10 Hz by this isolation system.

Another example for a passive isolator is the Seismic Attenuation System (SAS) [13] [14] developed by LIGO and TAMA in collaboration. This system is similar to the Super Attenuators except that it uses a geometrical anti-spring (Fig. 7) instead of the magnetic anti-spring for the vertical oscillator. The 3m Fabry-Perot cavity with the SAS system was successfully locked and it will be installed in TAMA300 in 2004.

It is also possible to rely on an intrinsically quiet site for reduction of seismic noise especially at low frequencies. An example for such a place is the Kamioka mine in Japan, where Super Kamiokande is located and is also where LCGT will be built in the future. The ground motion there is a factor of 100 to 1000 quieter between 1 Hz and 10Hz than Mitaka, Tokyo, where TAMA300 is located (Fig. 8). The 20m prototype called LISM [15], located in the Kamioka mine showed an extremely good stability thanks to the quiet seismic activity there; a maximum continuous locking time of 170 hours and a duty cycle of 99.8

2.4 Reduction of gravity gradient noise

Gravity gradient noise comes from fluctuations in Newtonian gravitational field caused by time-dependent distribution of matters in the vicinity of an interferometer. Moving objects that applies gravitational force to masses of the interferometer could be seismic motion of the ground, atmospheric density fluctuation, and macroscopic motion of vehicles or living creatures. The gravity gradient noise could stick out of the seismic wall after the seismic motion is isolated by the above-mentioned methods well enough. The Italian group is developing a technique to subtract the ground-originated gravity gradient noise from the interferometer data by measuring the motion of the ground surface, analyzing the geological structure of the site, and estimating the effect on the masses of the interferometer [16].

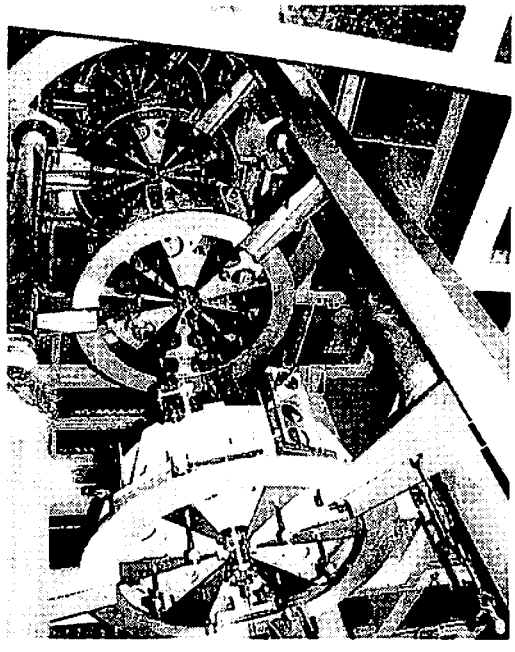


Figure 6: Super-attenuator used for the Virgo 3km gravitational wave detector (provided by the Virgo project).

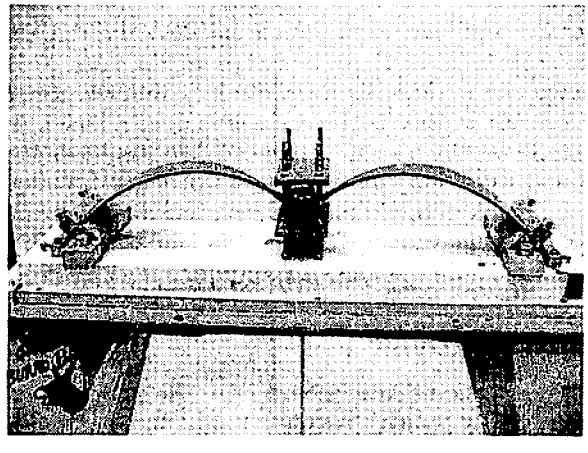


Figure 7: Vertical spring with a geometrical anti-spring used in SAS.

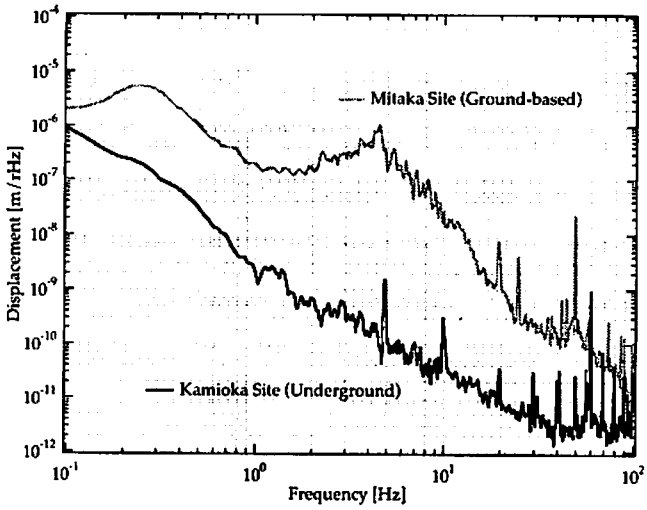


Figure 8: Ground motion in the Kamioka mine compared with that on the TAMA site.

2.5 Reduction of thermal-related noise

Thermal noise is Brownian motion of a mass as a result of the energy exchange between the mass and the outer system at a finite temperature. There are two important modes relevant to the suspended mirrors: the pendulum mode and internal mode. In both modes, a higher quality factor of the mode gives lower thermal noise at the signal-band frequencies with the expense of more energy concentrated around its resonance. The final means to reduce the thermal noise is to cool the mirrors and suspension systems because the thermal kinetic energy of the system itself is smaller at lower temperature.

In addition to the above-mentioned Brownian motion, very troublesome is thermoelastic noise [17], which can be caused either by thermodynamic fluctuations in temparature of the mirror, or by the photothermal temperature fluctuations due to the fluctuations in the photon absorption. The thermoelastic noise can be low for mirrors with small thermal expansion coefficients.

A monolithic suspension system [18] used for GEO600 is an example for the high quality suspension system. The fused silica fibers, which are found to have a much higher quality factor than metal wires, are used in their system. The fibers are welded onto specially designed ears with flat surfaces, which are attached to flats on the mass by the hydroxy-catalysis bonding (Fig. 9). This bonding technique has been shown to produce negligible additional mechanical loss in the test mass [19].

The Japanese group is developing cryogenic sapphire mirrors and suspensions for LCGT. In addition to the lower thermal energy of the mirror at cryogenic temperature, it has already been demonstrated that the quality factor of a cryogenic sapphire mirror is higher than at room temperature (Fig. 10) [20] [21]. The thermoelastic noise is also low because of the low thermal expansion coefficient of sapphire at cryogenic temperature [22]. Incidentally a thermal lensing effect, which is another problem with higher laser power, is also releaved at cryogenic temperature because of a high thermal conductivity and a low temperature dependence of refraction index of sapphire [23].

There are several issues concering cryogenic technologies: seismic isolation compatible with a cryogenic system, contamination of mirrors [24], and method of heat transfer. Since we rely on the suspension fiber for heat transfer, we have to increase the efficiency of the heat transfer as well as reduce the absorption of the light power at the mirrors. Using the resonant sideband extraction interferometer, we can reduce the light power at the beam splitter and the input mirrors, thus the heat load can be reduced.

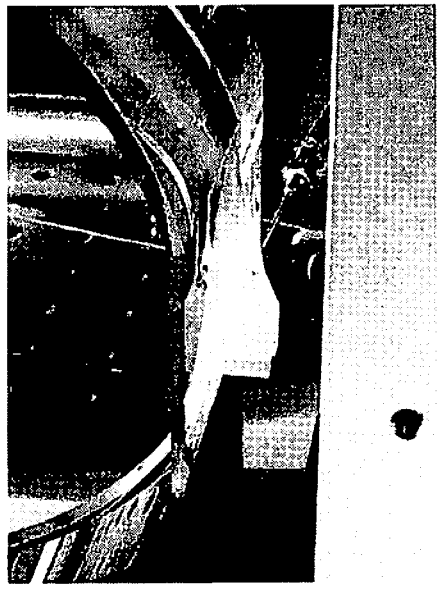


Figure 9: Monolithic suspension system used for the GEO 600m gravitational wave detector (GEO600).

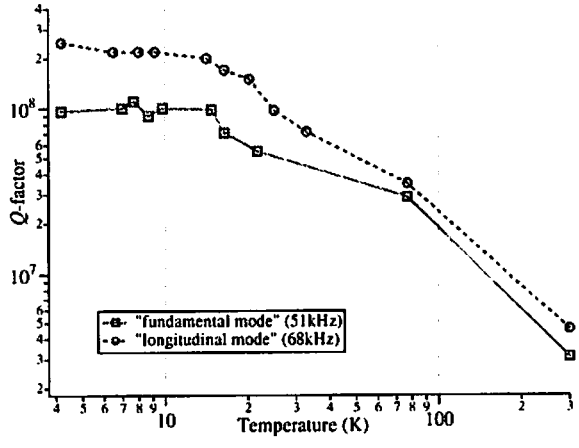


Figure 10: Temperature dependence of the quality factor of Sapphire.

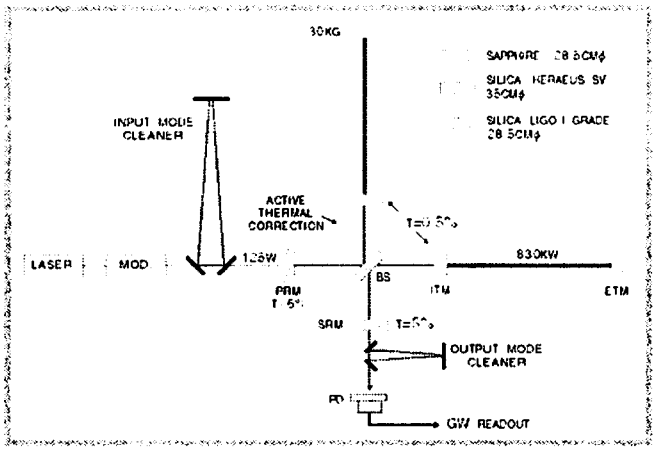


Figure 11: Conceptual design and specifications for the advanced LIGO (provided by the LIGO project).

3 Status and plans for future generations of detectors

In this section features, current status, and future plans for the advanced detectors including advanced LIGO, LCGT, AIGO, upgrade of GEO600, and EURO will be summarized.

3.1 Advanced LIGO

The advanced LIGO will use the same infrastructure as the initial LIGO with much more advanced technologies, which will give a reasonable and significant improvement from the initial LIGO on all the aspects (Fig. 11). A large number of scientists are working on research for various advanced technologies with very intensive collaboration with GEO, VIRGO, ACIGA, and TAMA. It is safe to say that it is the most mature of all the advanced detectors. The construction-funding proposal for the advanced LIGO will be ready by late 2002. It could be funded by early 2005, and installation of new detectors could start in as early as 2006.

3.2 LCGT

LCGT will use cryogenic mirrors and suspensions. The planned operating temperature is 20 K, where both Brownian and thermoelastic motions of sapphire are significantly small compared with those at room temperature. The LCGT interferometer has an arm length of 3km and will be located in the Kamioka mine. The SAS system will be used for the seismic isolation, and the resonant sideband extraction interferometer will be used for the optical configuration. The suspension point interferometer might be used to reduce vibration caused by the heat transfer system. The sensitivity goal of LCGT is limited by the radiation pressure noise and the shot noise except below 4Hz (Fig. 12). LCGT is not yet funded, but the four-year budget (2002-2005) was already approved for research and development of LCGT. Various experiments are being performed as well as design efforts for LCGT. LCGT is aiming at obtaining the budget in 2005. The advanced technologies for LCGT will be tested in various facilities. The SAS system will be installed in TAMA in collaboration with LIGO and the resonant sideband extraction interferometer will be tested at the 40m prototype at Caltech in collaboration with LIGO and GEO. The high power laser, which is currently developed by ACIGA, might be installed in TAMA. And the cryogenic technologies will be tested in CLIO (Fig. 13), which is the 100m Cryogenic prototype in Kamioka mine. Its construction will start very soon.

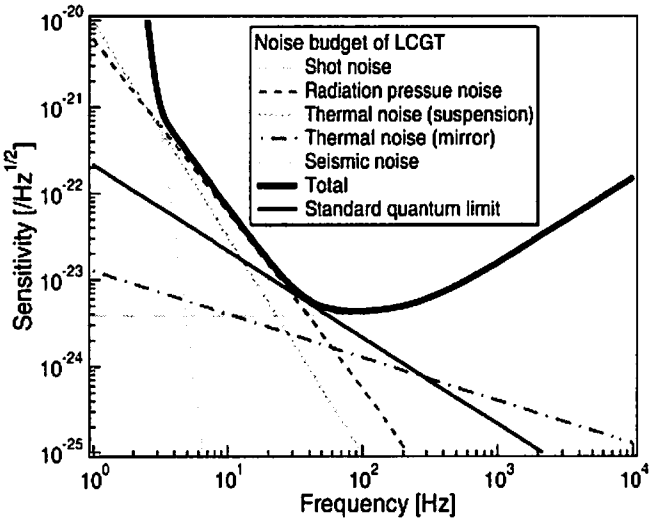


Figure 12: Sensitivity Goal for the LCGT 4km gravitational wave detector.

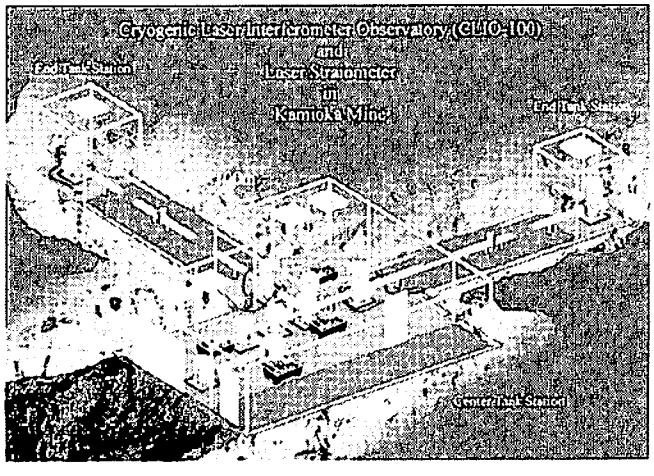


Figure 13: 100m cryogenic prototype to be constructed in the Kamioka mine.

3.3 AIGO

AIGO is currently a 80m test bed for high power laser interferometer (collaboration with LIGO) as well as a test bed for advanced suspension with Euler spring [26] and Nb flexures [27]. AIGO will be eventually extended to a km-class advanced detector.

3.4 Upgrade of GEO600

GEO600 has an upgrade plan. It will use an all reflecting configuration with Silicon optics with low-loss diffractive structure and low mechanical loss, which will be investigated very soon. The Silicon optics might be initially cooled to 120k to eliminate thermoelastic noise by operating at a temperature where Silicon has a thermal expansion coefficient of zero. It will use a high-power YAG lasers (200 W) and light sources with non-classical quantum noise properties. This upgrade will take place in 2006-2009.

3.5 EURO

EURO is the European future detector. The conceptual design is being discussed including the possibilities of being cryogenic at 4K, located underground, and SQL limited sensitivity for one tonne prefabricated, bonded, Silicon masses. The input from the results of the current-generation and the 2nd generation of detectors will be important for the design of EURO. EURO will not start before 2008.

4 Space antenna

4.1 Advantage of space antennas

An interferometric gravitational wave detector with longer arm length will be more sensitive to gravitational waves, because gravitational waves interact with the light in the interferometer for a longer time. Terrestrial detectors, however, cannot have an arm length of more than several kilo-meters mainly because of various practical reasons such as availability of lands and the construction cost of the vacuum facilities. Moreover, it is difficult to reduce seismic noise and gravity gradient noise significantly below 1Hz. Fortunately there is a solution to those difficulties; that is to build an interferometric detector in space.

4.2 LISA

NASA and ESA have been conducting a project of space antenna. It is called Laser Interferometer Space Antenna (LISA). It consists of three satellites whose distances are measured interferometrically (Fig. 14). The static distances between satellites are 5,000,000 km, and its orbit is helio-centric. LISA aims at detection of gravitational waves coming from collisions of super-massive black holes, binary white dwarfs, and the beginning of the universe in the frequency range of between 1 mHz and 30 mHz. It is planned to be launched in 2011.

4.3 DECIGO

The Japanese group has also started investigating the possibility of DECIGO, Deci-hertz Interferometer Gravitational-wave Observatory. It has a shorter arm length than LISA by a factor of 10-100, so that the aimed frequency range is between 10 mHz and 3 Hz, which is the gap frequency between the LISA band and terrestrial detectors' one (Fig. 15). DECIGO can not only detect ordinary gravitational wave sources, but also provide a method to measure the acceleration of the expansion on the universe. It can be done by measuring gravitational waves coming from binary neutron stars at a cosmological distance for ten years and comparing the data with the predicted signals [28] (Fig. 16).

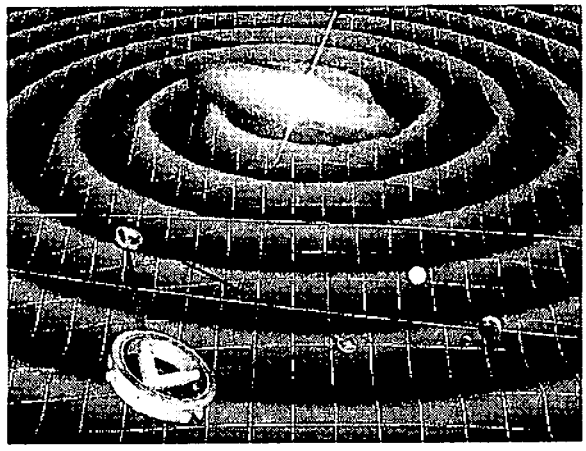


Figure 14: Laser interferometer space antenna.

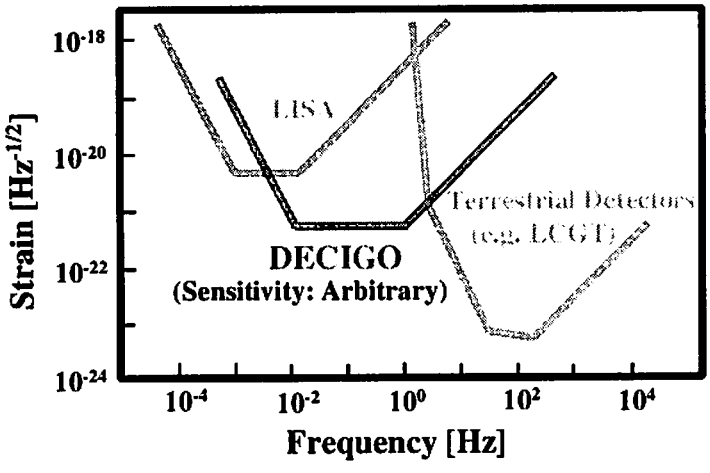


Figure 15: Deci-hertz interferometer gravitational-wave observatory.

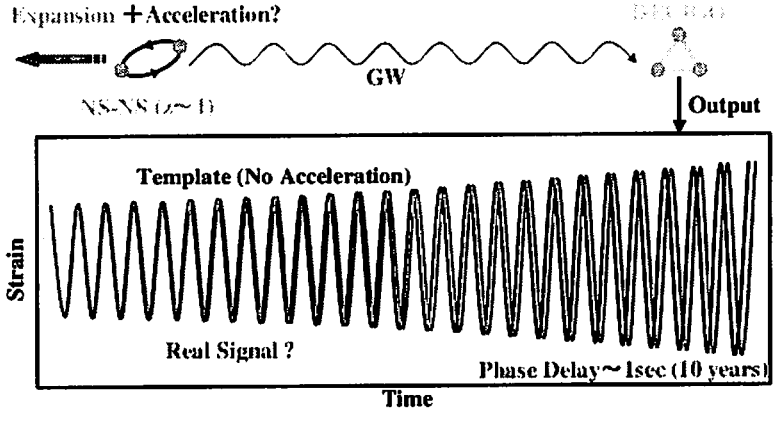


Figure 16: Method to directly measure the acceleration of the expansion of the universe using DECIGO.

5 Prospects of future detectors

Advanced detectors of various levels have been and will be studied. Various kinds of new technologies to reduce noise for such advanced detectors have been and will be developed. Intensive international collaborations are also aiming at the development of an international detector network. In parallel with the research on the ground-based detectors, we are also developing advanced technologies for space antennas such as LISA and DECIGO. We all believe that these efforts will eventually bring us to the establishment of gravitational wave astronomy in the future.

References

[1] A. Abramovici, *et al.*, Science **256**, 325 (1992).

[2] D. Sigg, Class. Quantum Grav. **19**, 1429 (2002).

[3] F. Acernese, *et al.*, Class. Quantum Grav. **19**, 1421 (2002).

[4] B. Willke, *et al.*, Class. Quantum Grav. **19**, 1377 (2002).

[5] M. Ando and the TAMA collaboration, Class. Quantum Grav. **19**, 1409 (2002).

[6] D. E. McClelland *et al.*, *Proceedings of the 3rd Edoardo Amaldi Conf., Gravitational Waves*, ed. S. Meshkov (American Institute of Physics, New York, 2000), p.140.

[7] E. Gustafson *et al.*, *LSC white paper on detector research and development*, LIGO T990080-00-D, (1999).

[8] K. Kuroda, *et al.*, Int. J. Mod. Phys. D **5**, 557 (1999).

[9] R. Abbott, *et al.*, Class. Quantum Grav. **19**, 1591 (2002).

[10] The VIRGO Collaboration (presented by S. Braccini), Class. Quantum Grav. **19**, 1623 (2002).

[11] The VIRGO Collaboration (presented by G. Losurdo), Class. Quantum Grav. **19**, 1631 (2002).

[12] O. Miyakawa, *et al.*, Class. Quantum Grav. **19**, 1555 (2002).

[13] S. Marka, *et al.*, Class. Quantum Grav. **19**, 1605 (2002).

[14] A. Takamori, *et al.*, Class. Quantum Grav. **19**, 1615 (2002).

[15] M. Ohashi *et al.*, *Proceedings of the 2nd TAMA Workshop, Gravitational Wave Detection II*, eds. S. Kawamura and N. Mio (Universal Academy Press, Tokyo, Japan, 2000), p.369.

[16] G. Cella *et al.*, *Proceedings of the 34th Rencontres de Moriond, Gravitational Waves and Experimental Gravity*, eds. J. Tran Thanh Van et al. (World Publishers, Hanoi, Vietnam, 2000), p.293.

[17] V. B. Braginsky, *et al.*, Phys. Lett. A **264**, 1 (1999).

[18] J. Hough *et al.*, *Proceedings of the 2nd TAMA Workshop, Gravitational Wave Detection II*, eds. S. Kawamura and N. Mio (Universal Academy Press, Tokyo, Japan, 2000), p.311.

[19] S. Rowan, *et al.*, Phys. Lett. A **246**, 471 (1998).

[20] T. Uchiyama, *et al.*, Phys. Lett. A **261**, 5 (1999).

[21] T. Uchiyama, *et al.*, Phys. Lett. A **273**, 310 (2000).

[22] M. Cerdonio, *et al.*, Phys. Rev. D **63**, 082003 (2001).

[23] T. Tomaru, *et al.*, Class. Quantum Grav. **19**, 2045 (2002).

[24] S. Miyoki, *et al.*, Cryogenics **41**, 415 (2001).

[25] J. Mizuno, *et al.*, Phys. Lett. A **175**, 273 (1993).

[26] J. Winterflood, *et al.*, Class. Quantum Grav. **19**, 1639 (2002).

[27] L. Ju, *et al.*, Class. Quantum Grav. **19**, 1703 (2002).

[28] N. Seto, *et al.*, Phys. Rev. Lett. **87**, 221103 (2001).

General Relativity and Gravitation
— Millisecond oscillators in accreting neutron stars and black holes —

Włodek Kluźniak,[1] Marek Abramowicz[2]

Institute of Astronomy, Zielona Góra University, ul. Lubuska 2, 65 265 Zielona Góra, Poland
CESR, 9 ave. Colonel-Roche, 31028 Toulouse, Cedex 4, France
Astrophysics Department, Chalmers University, S-41296 Göteborg, Sweden

Abstract

Millisecond variability detected in low-mass X-ray binaries (LMXBs) probably reflects motions of accreting fluid in the strong-field gravity of neutron stars or neutron stars. Parametric resonance between two oscillators with unequal eigenfrequencies provides a natural explanation for the 2:3 frequency ratio observed in some black-hole systems, and probably also in the brightest neutron stars. The two oscillators likely correspond to the meridional and radial epicyclic motions.

1 Millisecond variability in LMXBs

Frequencies as large as 1.2 kHz in the X-ray flux of LMXBs have been detected in 1996 by the first large satellite detector to have the requisite time resolution, the Rossi X-ray Timing Explorer. For a review of observations see van der Klis 2000, and for that of the previously discovered lower frequency variability, van der Klis 1989.

Millisecond variability of X-ray emission from accreting neutron stars and black holes has been expected at least from the time of Shvartsman's 1971 publication. Bath (1973) pointed out that in cataclysmic variables a natural timescale of variation is given by the Keplerian frequency and that clumps orbiting in the accretion disk could modulate the flux. For stellar-mass black holes and for neutron stars such clumps would induce millisecond variability of the X-ray flux (Sunyaev 1973). After quasi-periodic signals (QPOs) had been observed at frequencies corresponding to Keplerian motion in the inner parts of the accretion disk in a strongly magnetized accreting neutron star, the X-ray pulsar EXO 2030+375 (Angelini et al. 1989), Kluźniak, Michelson and Wagoner (1990) pointed out that scaling to the case of a moderately rotating compact neutron star of negligible magnetic field would yield a QPO at the frequency of orbital motion in the marginally stable orbit, $f_K = 2.2\,\mathrm{kHz}(1 + 0.75j)M_\odot/M$ (with j the dimensionless angular momentum of the star), and that this frequency, when observed, could be used to obtain a direct estimate of the stellar mass M.

Another line of reasoning originates with Okazaki, Kato and Fukue (1987), who pointed out that the radial epicyclic frequency in the space time metric around a black hole (or a neutron star) has a maximum, and goes to zero in the marginally stable orbit, which allows certain modes of vibration to be trapped in the inner region of the accretion disk. Diskoseismology, the theory of vibrations of accretion disks, has been developed in detail in the following years and has been recently reviewed by Wagoner (1999) and Kato (2001). In particular, it predicts the appearance of certain stable frequencies of quasi-periodic motion in black-hole accretion disks. The fundamental g-mode and c-mode, especially, have frequencies which are a function of the black-hole mass and the Kerr parameter a, alone, and which agree well with those observed in the micro-quasars.

The kHz QPOs observed in accreting neutron stars are more difficult to understand, as the observed frequencies vary considerably on a timescale of minutes or hours. Further, typically, two high frequency peaks in the power spectra are observed, where only one had at first been reported in black holes. It has been thought, initially, that the separation between the two peaks corresponds to the spin frequency of the neutron star but, in fact, this difference frequency is not constant either (e.g., van der Klis et al. 1997), whereas the spin frequency can vary only on the accretion time-scale, which is millions of years

[1] On leave of absence from the Copernicus Astronomical Center. E-mail:wlodek@camk.edu.pl
[2] E-mail:marek@fy.chalmers.se

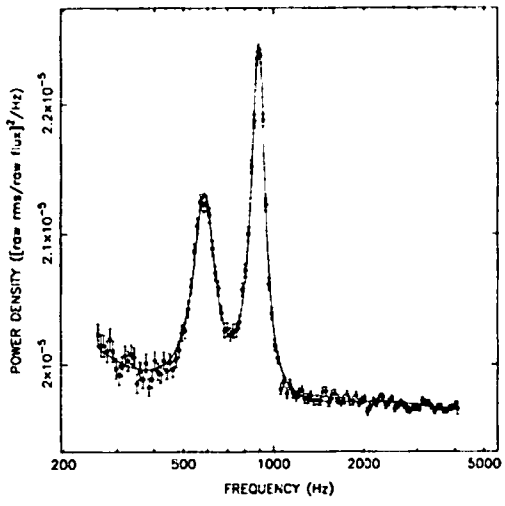


Figure 1: The two "kHz" QPOs of Sco X-1. The figure is from van der Klis et al. 1997.

in LMXBs (even in the brightest sources the accretion rate is less that $10^{-7}M_{\odot}$/y, and the neutron star mass is on the order of $1M_{\odot}$).

In spite of these differences, the power spectra of both the neutron star sources and the black hole ones are quite similar, the disparity in the characteristic frequencies being easy to explain by the higher mass of the black holes. Also, in the neutron star sources, the maximum frequency observed varies remarkably little with the accretion rate, or the type of the source. All this points to an accretion disk origin of the phenomenon.

2 The accretion disk in LMXBs

There is little doubt that mass transfer from the binary companion onto a neutron star or a black hole is responsible for the observed X-ray emission in low-mass X-ray binaries (Shklovsky 1967, Zel'dovich and Guseynov 1966). Although the central region around the compact object is too small to be resolved with current instruments (being only several tens of kilometers across, observed from a distance of kiloparsecs) it is generally agreed that the accreting fluid forms a disk around the central compact object (Prendergast and Burbidge 1968). Whether this is a geometrically thin, and hence rotation-supported, accretion disk (Shakura and Sunyaev 1973), or a sub-Keplerian, geometrically thick disk (Jaroszyński et al. 1980), is a matter of some dispute. For an artist's impression of the general appearance of the system see, e.g., the cover of the book by Kato, Fukue and Mineshige (1998).

There are two analogous types of systems in which the disk can be resolved, and in these the disk is geometrically thin. These are cataclysmic variables (binaries in which the accreting object is a non-magnetic white dwarf), and the celebrated extragalactic quasars. The correspondence between the physical processes in quasars and the Galactic X-ray novae, dubbed micro-quasars, has already been remarked upon in the literature (e.g., Mirabel and Rodriguez 1998), the main difference between the real and the "micro" quasars being in the mass of the black hole: millions or billions of solar masses as opposed to about ten $M_{\odot}$.

Water-vapour masers have been observed in some of the quasars, and radio observations allowed the mapping of the geometrical distribution of the emitters, as well as of their velocity distribution. The results leave no doubt – in NGC 4258 the masers are present in a geometrically thin and warped disk, and they orbit the central source with Keplerian velocities (Miyoshi et al. 1995). Perhaps the accretion disks in LMXBs are also Keplerian, although most of what we have to say here will apply equally well to some accretion tori.

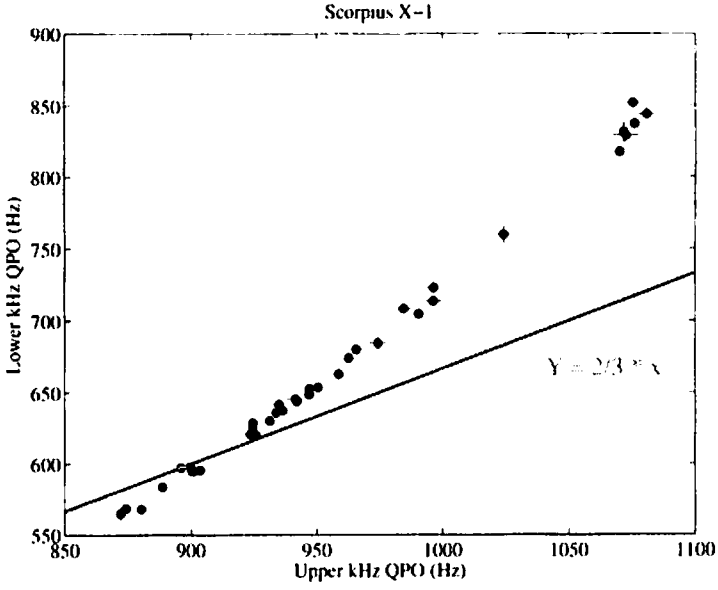


Figure 2: The frequencies of the two kHz QPOs in Sco X-1 vary with time, but remain correlated. Neither the difference, nor the ratio, of the two frequencies remains constant. The data is from van der Klis et al. 1997. Also shown is a line of constant frequency ratio (we thank an anonymous referee of Astronomy and Astrophysics for kindly plotting the data).

3 Two variable kHz frequencies: non-linear resonance?

If a common framework can be found for understanding the rapid variability of the X-ray flux in both the black hole and the neutron star sources in LMXBs, the behavior of QPOs in the latter may offer the key to unlocking the secrets of the former.

The most characteristic property of kHz QPOs in neutron stars is that there are typically two peaks in the power spectrum, located at frequencies which vary in time, but only within a limited, characteristic range (Fig. 2). A single variable frequency can be identified already in the Newtonian regime. It is also easy to find two characteristic constant frequencies. But we would like to ask what may be the origin of *two, characteristic*, but *variable* frequencies, in nearly Keplerian motion around a neutron star.

In Newtonian gravity of a spherically symmetric point mass, there is no preferred frequency (Fig. 3). Further, there is degeneracy between the orbital frequency in circular and not-quite-circular motion – this is why bound orbits are closed curves (Kepler's first law). So if neutron star exteriors were described by this theory, one would expect temporal fluctuations on all time-scales in the accretion disk, corresponding to the (huge) range of radii covered by the accreting fluid, but no characteristic frequencies.

However, characteristic frequencies can be induced in a Keplerian distribution externally – the gaps in the rings of Saturn are a well-known example. The radius of a neutron star introduces a characteristic length-scale to the problem, and a corresponding frequency, the Keplerian frequency at the surface of the star. This frequency is fixed for a given star, of course, and together with the spin frequency (which, in LMXBS, is practically constant on a human time-scale) allows two *fixed* frequencies to be identified in the Newtonian problem of accretion onto a neutron star.

If the accretion disk is terminated by the magnetosphere of the neutron star, its inner radius and the corresponding orbital frequency can vary somewhat with the accretion rate. This would lead to the appearance of a *single* characteristic, and variable, frequency, in addition to the constant stellar spin frequency. As an example take the X-ray pulsar EXO 2030+375, already mentioned in Section 1: the power spectrum of its X-ray flux exhibits prominent harmonics of the rotational frequency of the neutron star, in addition to the ~ 20 mHz QPO with frequency varying in step with the luminosity (Angelini et al. 1989).

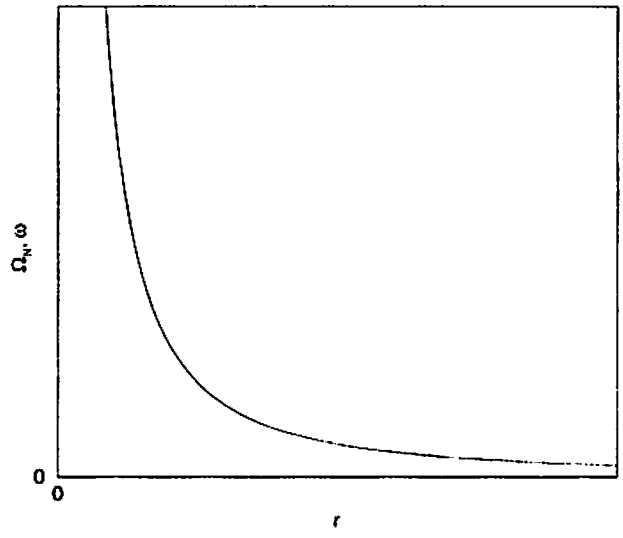


Figure 3: The orbital and epicyclic frequencies for a Newtonian $1/r$ potential. Note that there are no preferred frequencies, the problem is scale-free.

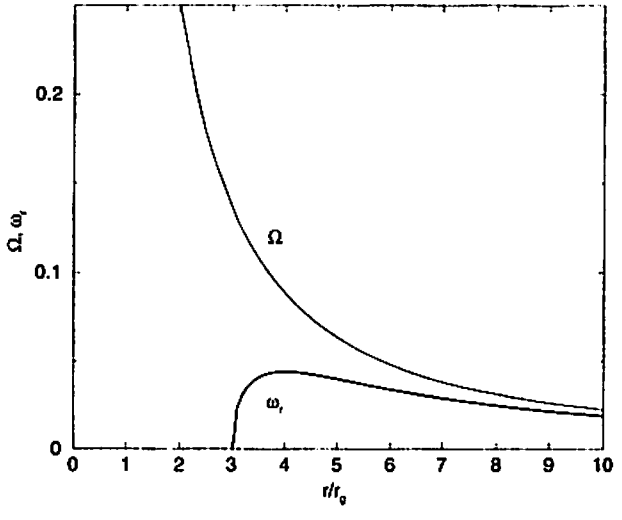


Figure 4: The orbital and the radial epicyclic frequencies in the Schwarzschild metric (after Kato et al. 1998). The Schwarzschild radius $r_g \equiv 2GM/c^2$ sets a length-scale and the corresponding characteristic frequencies.

In general relativity orbital degeneracy is broken, bound orbits are no longer closed curves ("precession of the perihelion"), the frequency of epicyclic motion induced by a radial perturbation differs from orbital frequency. There is a preferred length-scale, the gravitational radius $M(G/c^2)$, and corresponding characteristic frequencies: the radial epicyclic frequency goes to zero at the innermost (marginally) bound circular orbit, and has a maximum at a slightly larger orbit (Fig. 4). However, these are fixed frequencies.

In any sufficiently complicated system, resonances appear at characteristic frequencies. Of particular interest are resonances in non-linear systems, these occur not only when the driving frequency is close to the eigenfrequency of the oscillator, but also when the two frequencies are (nearly) in a rational ratio, $m : n$, with the strongest resonances occurring at the lowest values of the integers (Landau and Lifshitz 1976). The appearance of two, somewhat variable, frequencies in the rather complex accreting flow in LMXBs is strongly suggestive of a non-linear resonance.

4 Epicyclic resonance?

We note that there are two types of fluid perturbations in nearly circular three-dimensional flow which correspond to the two epicyclic frequencies familiar from study of test-particle orbits –the radial epicyclic frequency of planar motion, and the meridional epicyclic frequency of slightly non-planar motion. For a spherically symmetric gravitating body, the meridional epicyclic frequency is equal to the orbital frequency of the unperturbed circular orbit. For co-rotating orbits in the Kerr metric the meridional epicyclic frequency is always lower than the orbital frequency and higher than the radial epicyclic frequency (e.g., Wagoner 1999), and a similar relation obtains for rapidly rotating neutron stars. Thus, at characteristic radii, the ratio of the two epicyclic frequencies is rational, allowing the possibility of a non-linear resonance between the two types of fluid perturbations. We have suggested that this is the origin of the two kHz QPOs in neutron stars (Kluźniak and Abramowicz 2001a).

What would be the implications of this suggestion for the QPOs observed in black hole systems? When we first argued for the presence of a non-linear epicyclic resonance in LMXBs, only a single high-frequency QPOs had been observed in black hole systems. The most obvious prediction following from our hypothesis, was that a second QPO should be present also in black holes, and that the two frequencies should be in a rational ratio.

We are greatly encouraged that a second QPO has indeed been discovered in GRO J1655-40 (which reportedly has a $6M_\odot$ black hole) and that the two simultaneously observed frequencies have been reported to be 450 Hz and 300 Hz (Strohmayer 2001a), clearly in a 3:2 ratio (Abramowicz and Kluźniak 2001b). Another system, GRO J 1550-564 with a $10M_\odot$ black hole, in one of its states also shows two QPOs at the same frequency ratio, and the frequencies of 270 Hz and 180 Hz can be obtained by mass scaling from those of 1655-40, implying that the Kerr parameter of the two holes may be nearly identical (Remillard et al. 2002). Fig. 5 (reproduced from Remillard et al. 2002) illustrates how these ideas may be used to constrain the spin of the black hole, when the mass is known and the observed frequencies are identified with linear combinations of the orbital frequency and the radial epicyclic frequency (Kluźniak and Abramowicz 2001).

5 Parametric epicyclic resonance?

We have seen that the frequencies of these first twin QPOs to be discovered in black hole systems are in a 3:2 ratio. Why not 1:2 or 1:3? There is a particular type of non-linear resonance in which large-amplitude motions are easily excited by a small perturbation of the right frequency. This is parametric resonance, in which the eigenfrequency of an oscillator is varied periodically, i.e., when the eigenfrequency of a system is of the form $\omega = \omega_0(1 + h\cos\omega_1 t)$, with $h << 1$. The displacement of a harmonic oscillator with this eigenfrequency satisfies the Mathieu equation. Resonance occurs when

$$\omega_1/\omega_0 = 2/n,$$

with n integer; the amplitude grows intially exponentially to a saturation value determined by non-linearities, the fastest growing modes correspond to the lowest values of the integer n (Landau and Lifshitz 1976). For resonance to occur in the presence of dissipation, the size h of the perturbation has to exceed a certain threshold value.

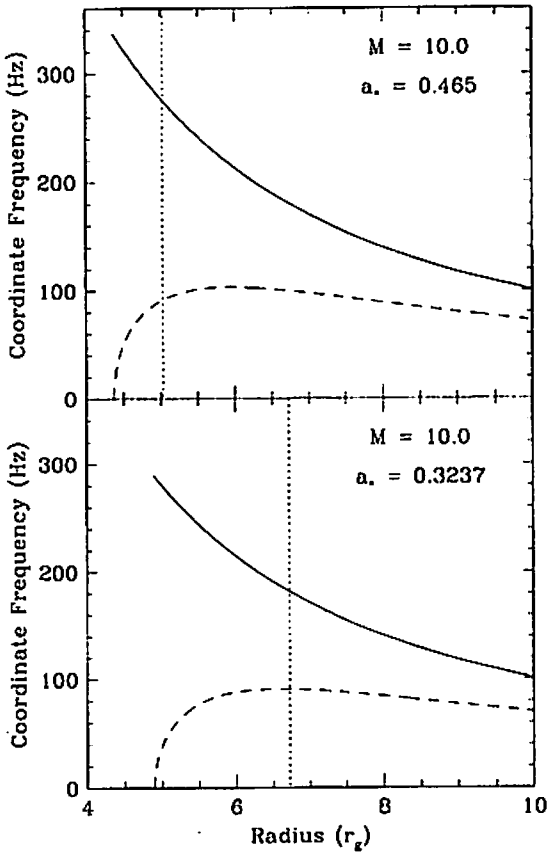


Figure 5: This figure, reproduced from Remillard et al. 2002, illustrates how the spin parameter of a black hole may be determined from the resonant condition (Kluźniak and Wagoner 2001b). The plot shows the orbital frequency Ω (continuous curve) and the radial epicyclic frequency ω_r (dashed curve), for two choices of the spin parameter for a $10M_\odot$ black hole. The most prominent of the frequencies observed in XTE J1550-564 are 270 Hz and 180 Hz. In the top panel they are identified with Ω and $\Omega-\omega_r$, in the bottom panel with $\Omega+\omega_r$ and Ω, respectively. The vertical line indicates the radial position of a 3:1 resonance between Ω and ω_r in the top panel, and a 2:1 resonance in the lower panel (the radius is in units of $r_g \equiv GM/c^2$). In this contribution, we suggest that the actual resonance is a 2:3 parametric resonance between ω_r and the meridional epicyclic frequency ω_z (not shown).

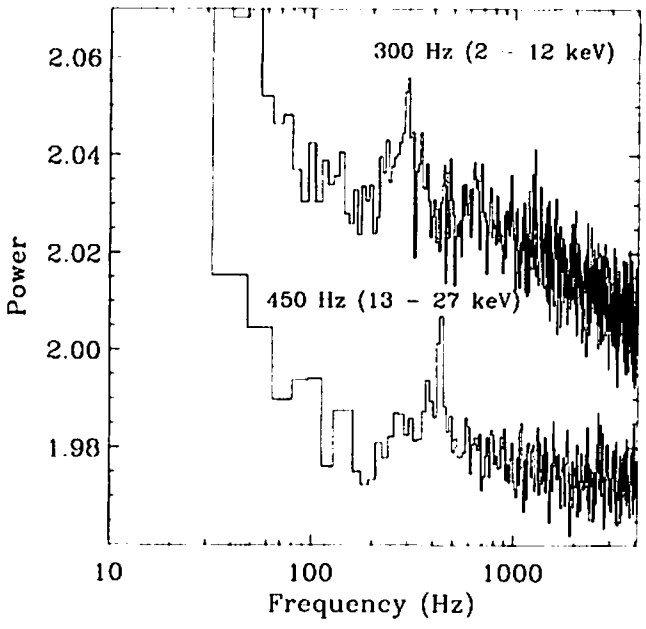


Figure 6: The two high frequency QPOs detected in GRO J1655-40. This figure is reproduced from Strohmayer 2001a.

One can write down the equations of disk perturbation in a form in which the the vertical and radial components of motion are coupled by a "pressure" term proportional to the speed of sound squared. Typically, in a linear analysis, the term can be neglected. But when a state of motion arises in which this coupling is modulated at a frequency obeying the resonant condition, this term becomes the most important one. Specifically, there are states of disk motion in which the dominant frequency is close to the radial epicyclic frequency ω_r, and other states of "vertical" motion, in which the frequency is close to the meridional epicyclic frequency ω_z. As we have seen, $\omega_r < \omega_z$ for black holes, always. Identifying ω_r with ω_1 in the Mathieu equation, and ω_z with ω_0, we see that for parametric resonance to occur in the Kerr metric, both

$$\omega_1 < \omega_0$$

and

$$\omega_1/\omega_0 = 2/n$$

must hold. The lowest value of n for which both eqs. are satisfied is $n = 3$. Hence, if 180 Hz is the value of the radial epicyclic frequency, vertical motions at a frequency of 270 Hz are easily excited in the disk.

Incidentally, it is often assumed that accretion disks in these systems have a hot corona. The observed energy dependence of the QPOs in GRO J1655-40 (Fig. 4) is easy to square with the notion that motions perpendicular to the disk plane, i.e., the ones most likely to disturb the corona, occur predominantly at the higher frequency.

6 Frequencies in the non-linear coupled system

What is the expected harmonic content of the epicyclic oscillators in resonance? First let us examine the non-linearities of the effective potential. If the unperturbed disk is symmetric with respect to reflections in the equatorial plane, in agreement with the symmetry of the black hole, the anharmonicity of the meridional oscillator is of third order in the equations of motion. In contrast, the equation of motion of the radial oscillator has second order anharmonic terms (the potential has cubic terms). This implies

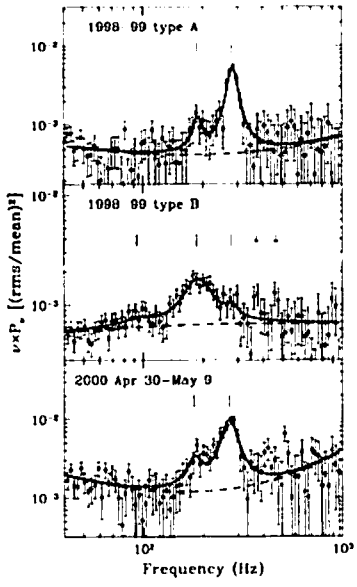


Figure 7: This figure is reproduced from Remillard et al. 2002. The panels show the power spectra in three different states of the XTE J1550-564 system. In all three, QPOs at 180 Hz and 270 Hz are clearly visible. In the state named "type B" (middle panel) a frequency of 90 Hz is also statistically significant.

that subharmonic content is possible in the motion of these oscillators (Landau and Lifshitz 1976). The meridional oscillator may have a subharmonic at $\omega = (1/3)\omega_0$ and the radial oscillator a subharmonic at $\omega = (1/2)\omega_1$. If the two oscillators are in a 2:3 resonance, $\omega_1 = (2/3)\omega_0$, and the two subharmonics coincide!

It is noteworthy, that Remillard et al. (2002) report a third QPO frequency in one of the states of XTE J1550-564. In addition to 270 Hz and 180 Hz, a weaker oscillation at 90 Hz is present (Fig. 5). The third frequency coincides with the predicted subharmonic.

7 1:2:3:5

If the two oscillators are in parametric resonance, as we have argued above, the frequency of 90 Hz in XTE J1550-564 is predicted for a more direct reason. The Mathieu equation does not admit strictly harmonic solutions. Instead, if the leading term in the solution is harmonic at frequency ω_0, additional terms must be included at "combination" frequencies, $\omega_0 + \omega_1$ and $\omega_0 - \omega_1$. For a 2:3 resonance these are at $(1/3)\omega_0$ and $(5/3)\omega_0$.

It is interesting to note that of these two combination frequencies one has been detected in XTE J1550-564, while the other may have been detected in GRS 1915+105. Why this is the case may be difficult to understand. Experience with asteroseismology shows that it is by far easier to compute the spectrum of allowed frequencies than to predict which of the frequencies will actually show up in the source at any given time. Primarily this is because energy flow in the system is very sensitive to the detailed coupling of modes in the non-linear system, and these are poorly understood. These difficulties are exacerbated in accretion disk theory, which can offer only educated guesses as to the physical state of the accreting fluid.

The state of the affairs is this. The theory of parametric resonance predicts a sequence of initial primes for the frequencies, 1:2:3:5, with 2 and 3 the most prominent. The 2:3 have been detected in two sources, GRO 1655-40 (300 Hz : 450 Hz) and XTE J1550-564 (180 Hz : 270 Hz). The "1" (90 Hz) also in XTE J1550-564, 1:2:3 really (Fig. 5). In a third system, 1915+105, the frequencies are 41.5 Hz and 69.2 Hz (Strohmayer 2001b), i.e., they are in a 3:5 ratio (Kluźniak and Abramowicz 2002).

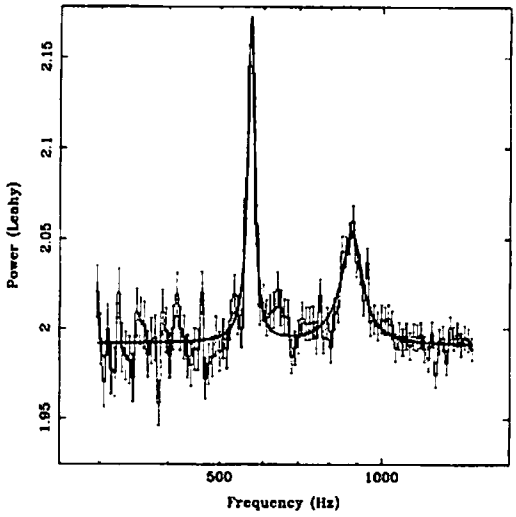


Figure 8: The kHz QPOs of 4U 1608-52. The figure is from Méndez et al. 1998. See also the review by van der Klis (2000).

8 Neutron star systems

The observed ratios of QPO frequencies in black hole systems agree very well with the theory of non-linear resonance, and parametric resonance between epicyclic oscillators in particular. We have been led to this theory by a search for the origin of two variable QPO frequencies in neutron star systems, and we view the subsequent discovery in black hole systems of double frequencies in rational ratios as confirmation of this theory. However, in neutron stars, the ratio of the two frequencies is not fixed (e.g., Fig. 2). Is the kHz QPO phenomenon in neutron stars and in black holes really a manifestation of the same physics? If so, then a 2:3 ratio should also be discernible in LMXBs containing neutron stars.

Let us begin by examining anecdotal evidence. In the van der Klis 2002 review, only two examples are shown of twin peaks in the power spectra. We have reproduced the first one, showing the kHz QPOs of Sco X-1, as Fig. 1. The second one, showing the twin QPOs of the neutron star source 4U 1608-52 (Méndez et al. 1998), is reproduced here as Fig. 8. Note that in both cases, the frequencies of the QPOs are close to 600 Hz and 900 Hz, i.e., close to a 2:3 ratio. This could be coincidental, or it could reflect the fact that certain frequencies are more likely to appear than others. Abramowicz et al. (2002b) argue that the latter is the case, at least for Sco X-1.

For Sco X-1, the two frequencies seem to be scattered over a wide range (Fig. 2), but the distribution of points along the line of correlation is not random (Abramowicz et al. 2002b). One way to demonstrate is to plot a histogram of the frequency ratios (Fig. 9). It is striking that the observations cluster about the value 2/3. We take this to be a very strong indication that a resonance is involved in the simultaneous appearance of the two frequencies. A corotation resonance has been considered (Kato 2002), but it seems to be damped (Kato 2003a). A parametric resonance may excite non-axisymmetric disk modes with variable frequencies (Kato 2003b).

Abramowicz et al. (2003) have investigated the parametric epicyclic resonance for nearly circular and nearly geodesic motion. Choosing an arbitrary, but fairly general form of coupling between the radial and vertical components of motion, they have demonstrated the presence of parametric resonance, at frequencies somewhat depending on the strength of coupling, taken to simulate pressure effects in the disk. In resonance, the ratio of the frequencies is accurately 2:3, but sizable amplitudes of motion are excited also slightly off-resonance. Quantifying with a single adjustable parameter how much off-resonance the system is, the authors have reproduced the slope of the frequency correlation found in Sco X-1 (Fig. 10).

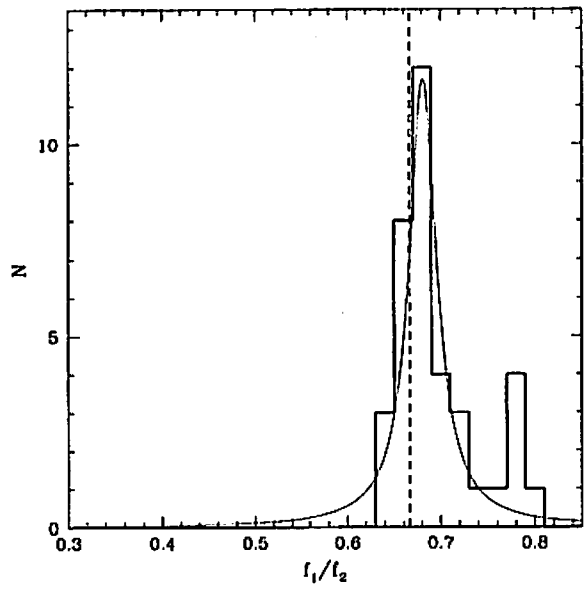


Figure 9: A histogram of the ratio of frequencies in Sco X-1. The figure is from Abramowicz et al. (2002b).

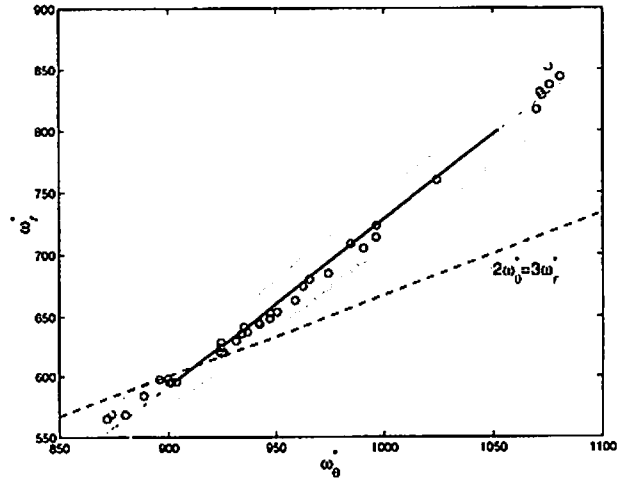


Figure 10: Frequencies slightly off-resonance from a calculation of parametric resonance in nearly-geodesic motion (thick line) superposed on the Sco X-1 data (compare Fig. 2). The figure is from Abramowicz et al. (2003).

References

[1] Abramowicz M.A., Almergren G.J.E., Kluźniak W., Thampan A.V., Wallinder F., 2002a, CQG 19, L57

[2] Abramowicz M. A., Bulik T., Bursa M., Kluźniak W., 2002b, http://xxx.lanl.gov/astro-ph/0206490

[3] Abramowicz, M.A., Karas, V., Kluźniak, W., Lee, W.H., Rebusco, P., 2003, PASJ, in press, astro-ph/0302183

[4] Abramowicz, M.A., Kluźniak, W., 2001, Astron. Astrophys. 374, L19,

[5] Angelini, L., Stella, L., Parmar A., 1989, ApJ 346, 906

[6] Jaroszyński, M., Abramowicz, M. A., Paczyński, B., 1980, Acta Astronomica, 30, 1.

[7] Bath, G. T. 1973, Nature Ph.Sc. 246, 84

[8] Kato S., 2001, PASJ 53, 1

[9] Kato S., 2002, PASJ 54, 39

[10] Kato S., 2003a, PASJ, in press

[11] Kato S., 2003b, PASJ, in preparation

[12] Kato, S., Mineshige, S., and Fukue, J. 1998, *Black Hole Accretion Disks* (Kyoto University Press, Kyoto).

[13] Kluźniak, W., Abramowicz, M.A., 2001a, astro-ph/0105057

[14] Kluźniak, W., M.A. Abramowicz 2001b, Acta Phys. Pol. B, 32, 3605, available at http://th-www.if.uj.edu.pl/acta/

[15] Kluźniak, W., Michelson, P., Wagoner, R.V. 1990, ApJ 358, 538

[16] Landau, L.D., Lifshitz, E.M., 1976, *Mechanics* (Pergamon Press, Oxford)

[17] Méndez, M., van der Klis, M., Wijnands, R., Ford, E., van Paradijs, J., Vaughan, B.A., 1998, ApJ 505, L23

[18] Mirabel, I. F.,, Rodriguez, L. F. 1998, Nature 392, 673

[19] Miyoshi, M., et al., 1995, Nature 373, 127

[20] Okazaki A. T., Kato S., Fukue J., 1987, PASJ 39, 457

[21] Prendergast, K. H., Burbidge, G. R., 1968, ApJ 151, L83

[22] Remillard R. A., Muno M.P., McClintock J.E., Orosz J.A., 2002, ApJ 580, 1030

[23] Shakura, N. I., Sunyaev, R. A., 1973, Astron. Astrophys. 24, 337

[24] Shklovskii, I.S., 1967, Astron. Zh. 44, 930

[25] Shvartsman, V.F., 1971, Soviet Astron. 15(3), 377

[26] Strohmayer, T.E. 2001a, ApJ. 552, L49

[27] Strohmayer, T.E. 2001b, ApJ. 554, L37

[28] Sunyaev, R. 1973, Soviet Astron. 16(6), 941

[29] van der Klis, M. 1989, Ann. Rev. Astron. Astrophys. 27, 517

[30] van der Klis, M. 2000, Ann. Rev. Astron. Astrophys. 8, 717

[31] van der Klis, M., Wijnands, R.A.D., Horne, K., Chen, W. 1997, ApJ 481, L97

[32] Wagoner R.W., 1999, Phys. Rev. 311, 259

[33] Zel'dovich, Ya.B., Guseynov, O.H., 1966, ApJ 144, 840

Quark Star ???
— Possible Formation Scenario of the Quark Star of Maximum Mass around 0.7 $M_\odot$ —

Takashi Nakamura

Department of Physics, Kyoto University, Kyoto 606-8502

Abstract

If there exists the quark star of maximum mass $\sim 0.7M_\odot$ as suggested by recent Chandra observations, we show that the general relativistic collapse of a neutron star of mass greater than the maximum mass of the neutron star with angular momentum parameter $q \equiv cJ/GM^2 > 1$ may lead to such a strange star. Here J and M are the angular momentum and the gravitational mass of the neutron star, respectively. Under the cosmic censorship hypothesis, such a star can not be a black hole directly. The jet formed in the soft core might explode the outer envelope and leave the quark star of mass $\sim 0.7M_\odot$. The remnant quark star has $\lesssim 10^{53}$ erg rotational energy so that the formation of the quark star may be related to the central engine of GRBs.

1 Introduction

Recently [Drake *et al.* (2002)] have made Deep Chandra LETG+HRC-S observations of the isolated neutron star candidate RXJ185635-3754 and found that the X-ray spectrum is well-represented by a $\sim$ 60eV black body. Their data contain no evidence for pulsation. The derived column density favors the distance to RXJ185635-3754 to be $D \sim$ 140pc instead of $D \sim$ 60pc [Walter(2001)]. Although [Walter & Lattimer(2002)] claim that the distance is $D \sim$ 120pc and the heavy-element atmosphere of [Pons *et al.* (2002)] should be taken, we here follow the arguments by [Drake *et al.* (2002)].

From the observed flux, the distance and the observed temperature of RXJ185635-3754, only the radiation radius defined by $R_\infty \equiv R/\sqrt{1-R_g/R}$ is determined since the observed luminosity and the observed temperature suffer from the gravitational redshift. For the given R_∞, M is given as a function of R as

$$R_g = \frac{2GM}{c^2} = R(1-(\frac{R}{R_\infty})^2). \tag{1}$$

M is positive only for $0 < R < R_\infty$ and has the maximum value $R_\infty c^2/G3\sqrt{3} = 0.7M_\odot(R_\infty/5.6km)$ at $R = R_\infty/\sqrt{3}$. If R_∞ is $\sim$ 5.6kmD_{140} as suggested by [Drake *et al.* (2002)], the maximum mass is $\sim 0.7M_\odot D_{140}$ where D_{140} is D in the unit of 140pc. Therefore R_∞ can not determine the radius of the star but gives us the upper limit of the mass as well as the upper limit of the radius of RXJ185635-3754.

X-ray luminosity of RXJ185635-3754 is $\sim 6\times10^{31}$erg/sD_{140}^2. If this is due to the accretion from a uniform medium [Bondi & Hoyle(1944)] we have the relation as

$$\pi(\frac{2GM}{V^2})^2\rho V\epsilon = 6\times10^{31}\mathrm{ergs}^{-1}D_{140}^2, \tag{2}$$

where V is the velocity of RXJ185635-3754 and ϵ is the conversion efficiency of the accreting matter to the radiation and is $\sim 0.3c^2$ for the quark star with the maximum mass $\sim 0.7M_\odot$[Witten(1984)]. From the above equation we have

$$(\frac{M}{M_\odot})^2(\frac{V}{200\mathrm{kms}^{-1}})^{-3}(\frac{n}{10^4\mathrm{cm}^{-3}})(\frac{\epsilon}{0.3c^2}) = 0.5D_{140}^2 \tag{3}$$

Since the proper motion of RXJ185635-3754 is 0.3 arc-second/y $\sim 200D_{140}$kms^{-1} [Walter(2001)] [1] the required number density of the interstellar matter is rather high even for $M \sim M_\odot$. While the column

[1] Here we assume that the optical counterpart is the same object as RXJ185635-3754 although the luminosity in the optical band can not be explained by the Rayleigh-Jeans tail of $\sim$ 60eV black body spectrum of RXJ185635-3754 [Pons *et al.* (2002), Drake *et al.* (2002), Walter & Lattimer(2002)].

density to RXJ185635-3754 is estimated as $\sim 10^{20} cm^{-2}$ [Drake *et al.* (2002)] so that the high density region should be local with the maximum size of $\sim$ 100AU. Such a local high density region of the size $<$ 100AU is observed in the interstellar medium using 21cm HI line by [Frail *et al.* (1994)] so that RXJ185635-3754 may be passing through the high density region now.

If M is $\sim 0.1 M_\odot$, the required density of the interstellar matter is so high that the column density may be in conflict with the observed one or we need very small($\sim$AU) high density region in the interstellar matter. In the latter case we expect the change of the luminosity in a time scale of 10 days or so, while only $\sim$2% change of the luminosity has been observed in the 19 months [Drake *et al.* (2002)] so that the mass is much greater than $\sim 0.1 M_\odot$. In this paper, assuming the mass and the radius of RXJ185635-3754 are $\sim 0.7 M_\odot$ and $\sim$ 3.2km, we propose a possible formation scenario of such an object.

2 Spherically Symmetric Model

First such a small radius object can not be the neutron star [Lattimer & Prakash(2000)]. Even for the softest equation of state of the high density nuclear matter, R_∞ is larger than 10km [Lattimer & Prakash(200 Except for the free neutron case [Oppenheimer & Volkoff(1939)], the maximum mass of the neutron star is greater than $0.7 M_\odot$ [Lattimer & Prakash(2000)], which is in conflict with the maximum mass of RXJ185635-3754 from the observed R_∞. The strange quark star is one of the candidate for such an object like RXJ185635-3754. In the quark star the baryon number is distributed among three quarks u, d and s so that the degenerate energy decreases by a factor of 0.89 compared with the proton and neutron nuclear matter [Witten(1984)]. In this sense the strange quark matter is stable although it contains unstable strange quarks. This reason is essentially the same as that the unstable neutron exists stably in the stable nucleus. In MIT bag model with the large bag constant $B = (245\mathrm{MeV})^4$ suggested from the finite-temperature QCD lattice data [Peshier, Kampfer & Soff(2001)] , the maximum mass of the quark star M_{MAX} is given by

$$M_{\mathrm{MAX}} = 0.7 M_\odot \left(\frac{B}{(245\mathrm{MeV})^4}\right)^{-1/2}, \tag{4}$$

$$R = 3.9 km \left(\frac{B}{(245\mathrm{MeV})^4}\right)^{-1/2}, \tag{5}$$

$$\rho_c = 1.5 \times 10^{16} \mathrm{gcm}^{-3} \left(\frac{B}{(245\mathrm{MeV})^4}\right), \tag{6}$$

where R and ρ_c are the radius and the central density of the maximum mass quark star [Witten(1984)]. Note here that the central density of the quark star with $M_{\mathrm{MAX}} \sim 0.7 M_\odot$ is much higher than the central density of the neutron star $\sim 10^{15} \mathrm{gcm}^{-3}$. Therefore to make a quark star from the neutron star we must consider how to increase the central density of the neutron star. If the bag constant is smaller, for example $B = (145\mathrm{MeV})^4$ as usual , the maximum mass and the radius are $2 M_\odot$ and 11km, respectively. However, in this case with R_∞ =5.6km , M becomes small $\sim 0.15 M_\odot$ which is in conflict with the X-ray luminosity of RXJ185635-3754 as stated in §2 so that we prefer the larger bag constant.

A naive way to increase the central density of the neutron star is to add the mass to the maximum mass neutron star by accretion from the companion star or the fall back gas in the supernova event [MacFadyen , Woosley , & Heger(2001)]. However the maximum mass of the neutron star is $1.4 M_\odot \sim 2 M_\odot$ [Lattimer & Prakash(2000)], which is at least two times larger than the putative maximum mass of the quark star relevant to RXJ185635-3754. The most plausible outcome of such a collapse is not the formation of the quark star but the black hole. In a sense the soft equation of state of the strange quark matter ($P = (\rho - 4B)/3$) is favorable to the formation of the strong shock in the supernova explosion as shown by [Takahara & Sato(1988)]. If the equation of state is soft, the large density gradient is accumulated to produce the strong shock while for the hard equation of state, the small density gradient is enough to produce the pressure gradient to support the falling gas in the collapse. However the shock is the strongest just before the formation of the black hole, that is, when the mass of the collapsing star is just a bit smaller than the maximum mass of the neutron star in the spherically symmetric model [Van Riper & Arnett(1978)]. Since in our case of the formation of the quark star, the mass of the collapsing matter is much larger than the maximum mass of the quark star so that we expect the

formation of the black hole. The detailed numerical simulations might be needed to confirm that the shock can not explode the outer envelope and the black hole is formed.

3 Rotating Model

I propose another promising scenario. First let us review the simulations of general relativistic collapse of rotating stars. [Nakamura(1981)] first performed the numerical simulations of general relativistic collapse of axially symmetric stars of mass $10M_\odot$ leading to the formation of rotating black holes. In these simulations the equation of state is hard with $\gamma = 2$ in the limit of $\rho \gg \rho_{nuc}$ and the rotation is differential with various values of initial angular momentum [Nakamura(1981)]. [Nakamura & Sato(1981a)] performed similar simulations with soft equation of state of $\gamma = 4/3$ for two kinds of rotation laws with various values of angular momentum. The results of these simulations crucially depend on one parameter q defined by

$$q = \frac{cJ}{GM^2}, \tag{7}$$

where J and M are the total angular momentum and the gravitational mass of the initial rotating star, respectively. When $q \lesssim 1$ the black hole is formed irrespective of initial rotation laws, the equation of state and the initial density distribution [Nakamura & Sato(1981b)]. If $q \gtrsim 1$, the black hole is not formed but the expanding ring, the expanding disk or the jets appear depending on initial rotation laws, equation of state and initial density distribution. This conclusion was confirmed by [Stark & Piran(1985)] and [Shibata(2000)].

Physical reason for the above result is as follows; Let us consider the collapsing star of mass M and the angular momentum J. The radius R_b when the centrifugal force balances the gravitational force is given by

$$\frac{GM}{R_b^2} \sim \frac{J^2}{M^2 R_b^3}. \tag{8}$$

Using q, we can express R_b as

$$R_b \sim \frac{GM}{c^2} q^2. \tag{9}$$

Equation (9) means that if $q \lesssim 1$, R_b is smaller than the black hole, which suggests that when the rotation becomes important, the star itself is already inside the black hole. Therefore it is natural that the black hole is formed irrespective of initial rotation laws, the equation of state and the initial density distribution.

In the sense of general relativity, the results of the simulations support the cosmic censorship hypothesis [Penrose(1973)] which says that the singularity does not exist outside the event horizon in nature. Under this hypothesis, the Kerr metric with $a/m = q < 1$ is known to be unique as the ultimate spacetime of the gravitational collapse [Robinson(1975)]. Note here that q defined in Eq. (7) and a/m in Kerr metric are the same quantity. If the whole of the collapsing star with $q \gtrsim 1$ becomes a black hole, that is the counter example of the cosmic censorship hypothesis. However numerical simulations have not yet found such a case.

In relation to the formation of the quark star, [Nakamura & Sato(1981a), Nakamura & Sato(1981b)] showed an interesting case of the jet formation. In their model of A146 which is the general relativistic collapse of the rotating star with $\gamma = 4/3$ equation of state and the initial $q = 1.46$, the jet appeared in the final phase of the collapse. This is in accord with the result of [Van Riper & Arnett(1978), Takahara & Sato(1988)]. In the rotating collapse, when the size of the star becomes $\sim R_b$ in Eq. (9), the collapse perpendicular to the rotation axis halts while the collapse along the rotation axis proceeds. When the equation of state is soft, the large density gradient accumulates to produce the jet. While if the equation of state is hard, this is not so. In reality [Nakamura, Oohara & Kojima(1987)] performed the simulations of the accreting neutron star with rotation. They used the equation of state with the maximum mass $1.4M_\odot$ and simulated the collapse of the rotating neutron star of mass $1.9M_\odot$. They found no jets. The final result was the differentially rotating neutron star.

Recently [Baumgarte, Shapiro & Shibata(2000)] computed the equilibria of differentially rotating neutron stars. They stated that some of the models exceed the Kerr limit, that is , $q > 1$. If we add certain

amount of matter to exceed the maximum mass neutron star keeping $q > 1$, the collapse will start. At R_b, the density is estimated as

$$\rho_b \sim \frac{M}{fR_b^3} = 6.7 \times 10^{16}\mathrm{gcm}^{-3} f^{-1} q^{-6} (\frac{M}{3M_\odot})^{-2}, \tag{10}$$

where $f \sim 1$ is the form factor of the rotating star. Since ρ_b can be in the quark phase for appropriate parameters, the equation of state in the central core can be soft at the centrifugal bounce. Then the matter will collapse along the rotational axis to form the jet like A146 in [Nakamura & Sato(1981a), Nakamura & Sato(1981b)]. If the jet is strong enough to explode the outer envelope and leave the central core of mass $\sim 0.7M_\odot$, the strange quark star might be formed. The important point here is that if the cosmic censorship hypothesis is correct as suggested by numerical simulations, the whole of the rotating neutron star of mass greater than the maximum mass of the neutron star with $q > 1$ can not be a black hole directly while if $q = 0$ it is possible to be a black hole directly.

The detailed numerical simulations are urgent to confirm or refute the present scenario of formation of the strange quark star of maximum mass around 0.7 $M_\odot$.

4 Discussion

[Olinto(1987)] showed that a seed of strange matter in a neutron star will convert the star into a strange star. As a seed, the quark nugget formed at the QCD phase transition in the early universe [Witten(1984)] can be considered. Then the capture cross section of the quark nugget by the neutron star is given by

$$\sigma \sim \pi R_{\mathrm{NS}} (\frac{GM_{\mathrm{NS}}}{V_{\mathrm{rel}}^2}) \sim 10^{18}\mathrm{cm}^2 (\frac{V_{\mathrm{rel}}}{100\mathrm{kms}^{-1}})^{-2}, \tag{11}$$

where R_{NS}, M_{NS} and V_{rel} are the radius of the neutrons star, the mass of the neutron star and the relative velocity, respectively. In order that at least a single quark nugget should be captured in the age of the universe (t_U) for a certain neutron star , the number density of the quark nugget (n_{nugget}) should be

$$n_{\mathrm{nugget}} > \frac{1}{\sigma V_{\mathrm{rel}} t_U} = 10^{-42}\mathrm{cm}^{-3} (\frac{V_{\mathrm{rel}}}{100\mathrm{kms}^{-1}}) (\frac{t_U}{10^{10}y})^{-1}. \tag{12}$$

Since the mass density of the quark nugget is at most the same as the dark matter density, each mass of the quark nugget m_{nugget} should be smaller than $\sim 10^{12}$g. However such a small mass quark nugget may not be formed due to the evaporation ($m_{\mathrm{nugget}} > 10^{20}$g for survival; [Bhattacharjee *et al.* (1993)]). Therefore to explain the possible strange quark star of RXJ185635-3754, the quark nugget should have been captured by chance by the progenitor neutron star.

The putative mass of $\sim 0.7M_\odot$ is just the mass of the typical white dwarf [Bragaglia Renzi & Bergeron(199 Therefore if we can compress the white dwarf of density $\sim 10^7\mathrm{gcm}^{-3}$ to $\sim 10^{16}\mathrm{gcm}^{-3}$, the strange quark star of mass $0.7M_\odot$ might be formed. A possible process is the tidal pinching proposed by [Luminet & Pichon(1989)]. If the moderate massive black hole of mass $\sim 2000M_\odot$ exists, a white dwarf passing inside the tidal radius of the black hole may be pinched and the density increases by more than a factor 50 [Luminet & Pichon(1989)]. Although the existence of such an intermediate mass black hole has been suggested [Matsumoto *et al.* (2002)], the number density of the white dwarfs is small $\sim 0.01\mathrm{pc}^{-3}$ so that the pinching number in the age of the universe for a single intermediate mass black hole is very small as

$$N_{pinch} \sim n_{WD} (\frac{6GM_{BH}}{c^2}) (\frac{GM_{BH}}{V_{\mathrm{rel}}^2}) V_{\mathrm{rel}} t_U$$
$$\sim 10^{-8} (\frac{n_{WD}}{0.01\mathrm{pc}^3}) (\frac{M_{BH}}{2000M_\odot})^2 (\frac{V_{\mathrm{rel}}}{100\mathrm{kms}^{-1}})^{-1} (\frac{t_U}{10^{10}y}).$$

Therefore to explain the possible strange quark star of RXJ185635-3754, the white dwarf should have been tidally pinched by the intermediate mass black hole by chance.

In any scenario, if the quark star of mass $M_{qs} \sim 0.7M_\odot$ is formed, the huge binding energy $\sim 4 \times 10^{53}$erg is liberated. The major part of this energy may be used to explode the outer envelope

of the progenitor neutron star. If , however, only $\sim$ 10% of this energy is deposited as the kinetic energy, it is enough to explain the luminous supernova such as SN1998bw. In the rotating model, the remnant quark star should have an initial value of $q_{qs} \lesssim 1$. Then the rotational energy is estimated as $E_{rot} \sim (GM_{qs}/Rc^2)^2 q_{qs}^2 M_{qs}c^2 \sim 10^{53}$erg. This energy is larger than or comparable to the energy needed for GRB so that the formation of the quark star may be related to the central engine of GRB.

Acknowledgments

I would like to thank Chiba, Inutsuka, Tatsumi and Tsuru for useful comments. This work was supported in part by Grant-in-Aid of Scientific Research of the Ministry of Education, Culture, and Sports, No.14047212 and No.14204024.

References

[Baumgarte, Shapiro & Shibata(2000)] Baumgarte, T. W., Shapiro, S. L. & Shibata, M. 2000, ApJl , 528 , L29

[Bhattacharjee *et al.* (1993)] Bhattacharjee , P. *et al.* 1993, Phys. Rev. D 48 , 4630

[Bragaglia Renzi & Bergeron(1995)] Bragaglia , A. , Renzi, A. , & Bergeron, P. , 1995, ApJ , 443 , 735

[Bondi & Hoyle(1944)] Bondi,H., & Hoyle, F. 1944, Mon. Not. R. astr Soc. ,104, 273

[Drake *et al.* (2002)] Drake, J. J. *et al.* 2002, astro-ph/0204159, ApJl , in press

[Frail *et al.* (1994)] Frail, D. A. *et al.* 1994, ApJ , 436 , 144

[Lattimer & Prakash(2000)] Lattimer, J., & Prakash, M. 2000, Physics Reports , 333, 121 and references therein

[Luminet & Pichon(1989)] Luminet, J. P., & Pichon, B. 1989, A and Ap, 333, 121

[MacFadyen , Woosley , & Heger(2001)] MacFadyen, A. I. , Woosley, S. E., & Heger, A., 2001, ApJ , 550, 410

[Matsumoto *et al.* (2002)] Matsumoto, H. *et al.* 2002, ApJl , 547 , L25

[Nakamura(1981)] Nakamura, T. , 1981, *Prog. Theor. Phys.*, 65 , 1876

[Nakamura & Sato(1981a)] Nakamura, T. , & Sato, H. 1981a, *Prog. Theor. Phys.*, 66 , 2038

[Nakamura & Sato(1981b)] Nakamura, T. , & Sato, H. 1981b, *Phys. Letters* , 86A , 318

[Nakamura, Oohara & Kojima(1987)] Nakamura, T., Oohara, K., & Kojima, Y., 1987. *Prog. Theor. Phys. Suppl.*, 90, 1-218, see page 54-55

[Olinto(1987)] Olinto, A.V. 1987, *Phys. Letters* , 192B , 71

[Oppenheimer & Volkoff(1939)] Oppenheimer, J. R., & Volkoff, G., *Phys. Rev.* , 56, 455

[Penrose(1973)] Penrose, R., 1973, *Ann. N. Y. Acad. Sci.* , 224, 125

[Peshier, Kampfer & Soff(2001)] Peshier, A., Kampfer, B. & Soff, G. 2001 hep-ph/0106090

[Pons *et al.* (2002)] Pons, J. A. *et al.* 2002, ApJ , 564 , 981

[Robinson(1975)] Robinson, D. C., 1975, Phys Rev Letters, 34 , 905

[Stark & Piran(1985)] Stark, R. F., & Piran, T., 1985, Phys Rev Letters, 55 , 891

[Shibata(2000)] Shibata, M., 2000, *Prog. Theor. Phys.*, 104 , 325

[Takahara & Sato(1988)] Takahara, M., & Sato, K., 1988, ApJ , 335 , 301

[Van Riper & Arnett(1978)] Van Riper, K., & Arnett, W. D., 1978, ApJl , 225 ,L129

[Walter(2001)] Walter, F. M. 2001 ApJ , 549 , 433

[Walter & Lattimer(2002)] Walter, F. M., & Lattimer, J. 2002 asro-ph/0204199

[Witten(1984)] Witten, E. 1984 , Phys. Rev D , 30 , 272

The First-Generation Supernovae and Extremely Metal-Poor Stars

Ken'ichi Nomoto[1], Keiichi Maeda[1], Hideyuki Umeda[1],
Takuya Ohkubo[1], Jinsong Deng[1], Paolo Mazzali[2]

[1] *Department of Astronomy, University of Tokyo, Tokyo 113-0033, Japan*

[2] *Osservatorio Astronomico, Via Tiepolo, 11, 34131 Trieste, Italy*

Abstract

Hypernovae are the core-collapse supernovae with very large explosion energies ($\gtrsim 10^{52}$ ergs). Nucleosynthesis in hypernovae show the following characteristics: 1) Higher energy explosions tend to produce larger [(Zn,Co,V)/Fe] and smaller [(Mn,Cr)/Fe], which can explain the trend observed in very metal-poor stars. 2) Because of enhanced α-rich freezeout, ^{44}Ca, ^{48}Ti, and ^{64}Zn are produced more abundantly than in normal supernovae. The large [(Ti, Zn)/Fe] ratios observed in very metal-poor stars strongly suggest a significant contribution of hypernovae. 3) Oxygen burning takes place in more extended regions in hypernovae, which makes the Si/O ratio larger. We thus suggest that hypernovae make important contribution to the early Galactic (and cosmic) chemical evolution. We then discuss the evolutionary origin of the recently discovered most Fe deficient star, HE0107-5240. We show that the abundance pattern of HE0107-5240 and other extremely metal-poor (EMP) stars are in good accord with those of supernovae which originate from $\sim$ 20-130 $M_\odot$ stars and form $\sim$ 3-10 $M_\odot$ black holes.

1 Introduction

Among the important developments in recent study of supernovae (SNe) is the discovery of some very energetic SNe, whose kinetic energy (KE) exceeds 10^{52} erg, about 10 times the KE of normal core-collapse SNe (hereafter $E_{51} = E/10^{51}$ erg). Because of the large KE, such a SN is called a "Hypernova". We summarize the properties of hypernovae and show that nucleosynthesis in hypernovae is quite distinct from the case of ordinary supernovae, thus making a unique contribution to galactic chemical evolution.

We then compare nucleosynthesis yields of core-collapse supernovae/hypernovae with the abundances of extremely metal-poor (EMP) stars to identify the Pop III (or first) supernovae. We show that the EMP stars, especially the C-rich class, are likely to be enriched by massive supernovae which form black holes and eject relatively small Fe.

2 Hypernova Branch and Faint Supernova Branch

Type Ic Hypernova SN 1998bw was probably linked to GRB 980425 [9], thus establishing for the first time a connection between gamma-ray bursts (GRBs) and the core-collapse SNe. However, SN 1998bw was exceptional for a SN Ic: it was as luminous at peak as a SN Ia, indicating that it synthesized ~ 0.5 $M_\odot$ of ^{56}Ni, and its KE was estimated at $E \sim 3 \times 10^{52}$ erg [17, 51].

Subsequently, other "hypernovae" have been recognized, such as SN 1997ef [18, 24], SN 1999as [21, 13], and SN 2002ap [26]. Figure 1 shows the near-maximum spectra and the absolute V-light curves of hypernovae. These hypernovae span a wide range of properties, although they all appear to be highly energetic compared to normal core-collapse SNe.

Figure 2 shows E and the mass of ^{56}Ni ejected $M(^{56}\mathrm{Ni})$ as a function of the main-sequence mass $M_{\rm ms}$ of the progenitor star obtained from fitting the optical light curves and spectra. These mass estimates place hypernovae at the high-mass end of SN progenitors.

In contrast, SNe II 1997D and 1999br were very faint SNe with very low KE [46, 11, 53]. In Figure 2, therefore, we propose that SNe from stars with $M_{\rm ms} \gtrsim$ 20-25 $M_\odot$ have different E and $M(^{56}\mathrm{Ni},)$ with

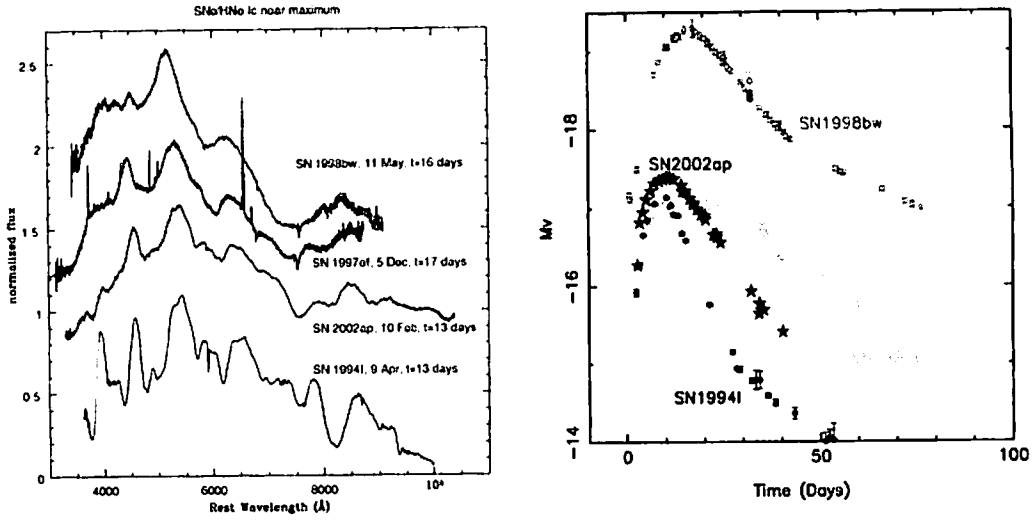


Figure 1: Left: The near-maximum spectra of Type Ic SNe and hypernovae: SNe 1998bw, 1997ef, 2002ap, and 1994I. Right: The observed V-band light curves of SNe 1998bw (*open circles*), 1997ef (*open triangles*), 2002ap (*stars*), and 1994I (*filled circles*) [26].

a bright, energetic "hypernova branch" at one extreme and a faint, low-energy SN branch at the other. For the faint SNe, the explosion energy was so small that most ^{56}Ni fell back onto the compact remnant. Thus the faint SN branch may become a "failed" SN branch at larger $M_{\rm ms}$. Between the two branches, there may be a variety of SNe [11].

This trend might be interpreted as follows. Stars with $M_{\rm ms} \lesssim 20$-$25\ M_\odot$ form a neutron star, producing $\sim 0.08 \pm 0.03\ M_\odot$ ^{56}Ni as in SNe 1993J, 1994I, and 1987A (SN 1987A may be a borderline case between the neutron star and black hole formation). Stars with $M_{\rm ms} \gtrsim 20$-$25\ M_\odot$ form a black hole; whether they become hypernovae or faint SNe may depend on the angular momentum in the collapsing core, which in turn depends on the stellar winds, metallicity, magnetic fields, and binarity. Hypernovae might have rapidly rotating cores owing possibly to the spiraling-in of a companion star in a binary system.

3 Nucleosynthesis in Hypernova Explosions

In core-collapse supernovae/hypernovae, stellar material undergoes shock heating and subsequent explosive nucleosynthesis. Iron-peak elements are produced in two distinct regions, which are characterized by the peak temperature, $T_{\rm peak}$, of the shocked material. For $T_{\rm peak} > 5 \times 10^9$K, material undergoes complete Si burning whose products include Co, Zn, V, and some Cr after radioactive decays. For 4×10^9K $< T_{\rm peak} < 5 \times 10^9$K, incomplete Si burning takes place and its after decay products include Cr and Mn [12, 45].

3.1 Supernovae vs. Hypernovae

The right panel of Figure 3 shows the composition in the ejecta of a 25 $M_\odot$ hypernova model ($E_{51} = 10$). The nucleosynthesis in a normal 25 $M_\odot$ SN model ($E_{51} = 1$) is also shown for comparison in the left panel of Figure 3.

We note the following characteristics of nucleosynthesis with very large explosion energies [30, 31, 32, 36]:

(1) Both complete and incomplete Si-burning regions shift outward in mass compared with normal supernovae, so that the mass ratio between the complete and incomplete Si-burning regions becomes larger. As a result, higher energy explosions tend to produce larger [(Zn, Co, V)/Fe] and smaller [(Mn, Cr)/Fe], which can explain the trend observed in very metal-poor stars [36].

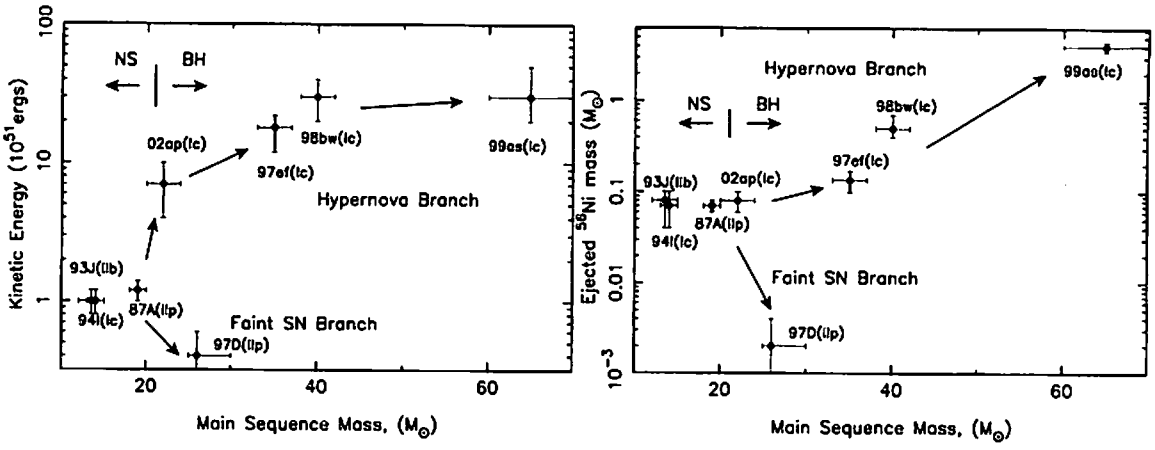


Figure 2: The explosion energy and the ejected ^{56}Ni mass as a function of the main sequence mass of the progenitors for several supernovae/hypernovae [34].

(2) In the complete Si-burning region of hypernovae, elements produced by α-rich freezeout are enhanced. Hence, elements synthesized through capturing of α-particles, such as ^{44}Ti, ^{48}Cr, and ^{64}Ge (decaying into ^{44}Ca, ^{48}Ti, and ^{64}Zn, respectively) are more abundant.

(3) Oxygen burning takes place in more extended regions for the larger KE. Then more O, C, Al are burned to produce a larger amount of burning products such as Si, S, and Ar. Therefore, hypernova nucleosynthesis is characterized by large abundance ratios of [Si,S/O], which can explain the abundance feature of M82 [49].

3.2 Hypernovae and Zn, Co, Mn, Cr

Hypernova nucleosynthesis may have made an important contribution to Galactic chemical evolution. In the early galactic epoch when the galaxy was not yet chemically well-mixed, [Fe/H] may well be determined by mostly a single SN event [3]. The formation of metal-poor stars is supposed to be driven by a supernova shock, so that [Fe/H] is determined by the ejected Fe mass and the amount of circumstellar hydrogen swept-up by the shock wave [40]. Then, hypernovae with larger E are likely to induce the formation of stars with smaller [Fe/H], because the mass of interstellar hydrogen swept up by a hypernova is roughly proportional to E [40, 43] and the ratio of the ejected iron mass to E is smaller for hypernovae than for normal supernovae.

In the observed abundances of halo stars, there are significant differences between the abundance patterns in the iron-peak elements below and above [Fe/H]~ -2.5 - -3.

(1) For [Fe/H]$\lesssim -2.5$, the mean values of [Cr/Fe] and [Mn/Fe] decrease toward smaller metallicity, while [Co/Fe] increases (Fig. 3; [27, 40]).

(2) [Zn/Fe]~ 0 for [Fe/H] $\simeq -3$ to 0 [44], while at [Fe/H] < -3.3, [Zn/Fe] increases toward smaller metallicity (Fig. 3; [39, 5]).

The larger [(Zn, Co)/Fe] and smaller [(Mn, Cr)/Fe] in the supernova ejecta can be realized if the mass ratio between the complete Si burning region and the incomplete Si burning region is larger, or equivalently if deep material from the complete Si-burning region is ejected by mixing or aspherical effects. This can be realized if (1) the mass cut between the ejecta and the compact remnant is located at smaller M_r [28], (2) E is larger to move the outer edge of the complete Si burning region to larger M_r [29], or (3) asphericity in the explosion is larger.

Among these possibilities, a large explosion energy E enhances α-rich freezeout, which results in an increase of the local mass fractions of Zn and Co, while Cr and Mn are not enhanced [47, 48, 36]. Models with $E_{51} = 1$ do not produce sufficiently large [Zn/Fe]. To be compatible with the observations of [Zn/Fe] ~ 0.5, the explosion energy must be much larger, i.e., $E_{51} \gtrsim 20$ for $M \gtrsim 20M_\odot$, i.e., hypernova-like explosions of massive stars ($M \gtrsim 25M_\odot$) with $E_{51} > 10$ are responsible for the production of Zn.

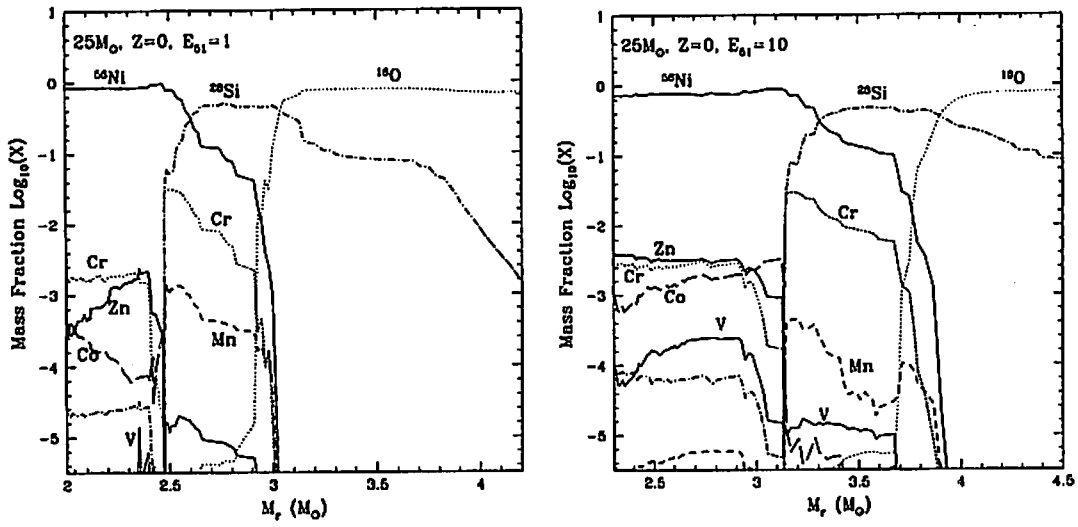


Figure 3: Abundance distribution plotted against the enclosed mass M_r after the explosion of Pop III 25 $M_\odot$ stars with $E_{51} = 1$ (left) and $E_{51} = 10$ (right) [47].

In the hypernova models, the overproduction of Ni, as found in the simple "deep" mass-cut model, can be avoided [36]. Therefore, if hypernovae made significant contributions to the early Galactic chemical evolution, it could explain the large Zn and Co abundances and the small Mn and Cr abundances observed in very metal-poor stars [48, 36]

3.3 Bipolar Explosions

If a hypernova is an explosion accompanied by formation of a black hole, the explosion is expected to be driven by bipolar jets. Several observations support, though indirectly, this hypothesis. Studies on light curves, nebular spectra, and polarization suggest the ejecta of hypernovae deviate from spherically symmetry significantly [19, 22, 24, 25, 29, 37]. The features of hydrodynamics and nucleosynthesis in jet-driven hypernova explosions are summarized in this section [23].

Figure 4 shows snapshots of one of the bipolar explosion models. The jets propagate through the stellar mantle, depositing their energies into the ambient material at the working surface. The bow shock expands laterally to push the stellar mantle sideways, which makes the accretion rate decreased. As the accretion rate decreases, the jets are turned off. Then the inflow along the r-axis turns into the weak outflow.

The outcome is a highly aspherical explosion. This is consistent with detection of polarization of some degree in SNe1998bw ([37]) and 2002ap ([19]). The accretion makes a central dence core. Densities near the center are much higher than conventional spherical models predict. The analyses of spectra and light curves of SNe1998bw ([29]) and 1997cf ([24]) indeed suggest that they should have central high density cores.

The further implications of the bipolar models are; (1) A more massive star makes a more energetic explosion in our models, because a more massive star has a stronger gravity to make the accretion rate larger. This is consistent with the relation seen in the hypernova branch (Fig. 2). (2) A more massive star leaves a more massive compact remnant. The remnant of the explosion of 40 $M_\odot$is a black hole with ~ 6 $M_\odot$in the model presented here. Our models predict explosions with black hole formations in a consistent way. Given the discovery of the evidence of a hypernova explosion accompanied by a formation of a black hole of ~ 5 $M_\odot$(X-ray Nova Sco; [16, 38]), they offer an interesting possibility.

The high temparatures along the z-axis and the low temparatures along the r-axis observed in the hydrodynamical models have large effect on nucleosynthesis, when combined with the hydrodynamical result where the matter is preferencially ejected along the z-axis.

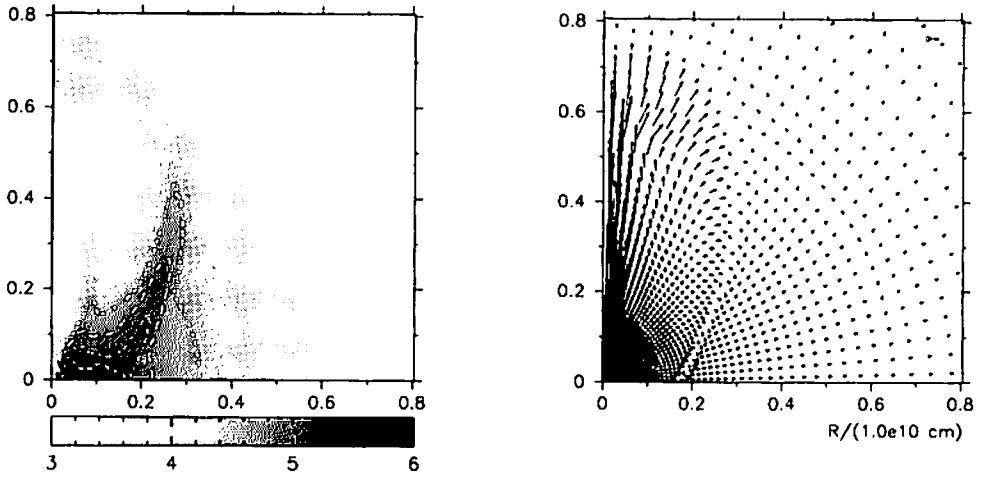


Figure 4: Density (left) and velocity (right) distribution of the bipolar explosion of a star with $M_{\rm ZAMS}$ = 40 $M_\odot$ at 1.5 second after the initiation of the jets. In the left column, densities are plotted logarithmically. In the right column, the arrow with a circle on its base shown on the right top represents 2×10^9cm s^{-1}.

First, it results in highly aspherical distribution of nucleosynthetic products. Figure 5 shows the distributions of ^{56}Ni (which decays into ^{56}Fe) and ^{16} O. The production of ^{56}Ni is elongated along the z-axis. Such configurartion, i.e., high velocity Fe and low velocity O, has been suggested to be responsible for the feature in late phase spectra of SN1998bw, where the OI] 6300 was narrower than the FeII] 5200 blend ([22, 25]).

Second, even the overall abundance patterns differ from those in spherical models. Matter which eaperiences higher entropy is preferencially ejected along the z-axis, while matter which gets lower entropy is accreated. Therefore, [Zn/Fe] and [Co/Fe] ([X/Fe] $\equiv \log 10(\rm X/Fe) - \log 10(\rm X/Fe)_\odot$) are enhanced because they are produced through a strong α-rich freezeout, though [Mn/Fe] and [Cr/Fe] produced through an incomplete Si-burning are suppressed.

The same pattern in [Zn,Co,Cr,Mn/Fe] is seen in abundances in extremely metal-poor halo stars, which contain the abundance information of supernovae in the early epochs of Galaxy ([33, 34] and references therein). As a result, the bipolar models are consistent with those observations, or even favorable compared to conventional spherical models.

4 Extremely Metal-Poor (EMP) Stars

Recently the most Fe deficient and C-rich low mass star, HE0107-5240, was discovered [7]. This star has [Fe/H] = −5.3 but its mass is as low as 0.8 $M_\odot$. This would challenge the recent theoretical arguments that the formation of low mass stars, which should survive until today, is suppressed below [Fe/H] = −4 [42].

The important clue to this problem is the observed abundance pattern of this star. This star is characterized by a very large ratios of [C/Fe] = 4.0 and [N/Fe] = 2.3, while the abundances of elements heavier than Mg are as low as Fe [7]. Interestingly, this is not the only extremely metal poor (EMP) stars that have the large C/Fe and N/Fe ratios, but several other such stars have been discovered [41]. Therefore the reasonable explanation of the abundance pattern should explain other EMP stars as well. We show that the abundance pattern of C-rich EMP stars can be reasonably explained by the nucleosynthesis of 20 - 130 $M_\odot$ supernovae with various explosion energies and the degree of mixing and fallback of the

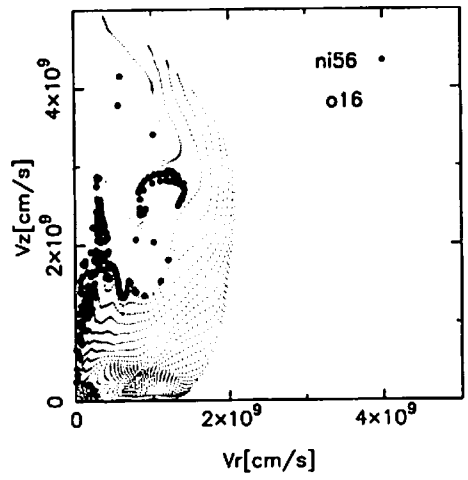


Figure 5: Distributions of ^{56}Ni and ^{16}O. The mass elements in which the mass fraction of ^{56}Ni and ^{16}O exceed 0.1 are plotted with points and dots, respectively.

ejecta.

4.1 The Most Metal-Poor Star HE0107-5240

We consider a model that C-rich EMP stars are produced in the ejecta of (almost) metal-free supernova mixed with extremely metal-poor interstellar matter. We use Pop III pre-supernova progenitor models, simulate the supernova explosion and calculate detailed nucleosynthesis [50].

In Figure 6 (right) we show that the elemental abundances of one of our models are in good agreement with HE0107-5240, where the progenitor mass is 25 $M_\odot$ and the explosion energy $E_{51} = 0.3$ [50].

In this model, explosive nucleosynthesis takes place behind the shock wave that is generated at $M_r = 1.8\ M_\odot$ and propagates outward. The resultant abundance distribution is seen in Figure 6 (left), where M_r denotes the Lagrangian mass coordinate measured from the center of the pre-supernova model [50]. The processed material is assumed to mix uniformly in the region from $M_r = 1.8\ M_\odot$ and $6.0\ M_\odot$. Such a large scale mixing was found to take place in SN1987A and various explosion models [10, 20]. Almost all materials below $M_r = 6.0\ M_\odot$ fall back to the central remnant and only a small fraction ($f = 2\times 10^{-5}$) is ejected from this region. The ejected Fe mass is $8 \times 10^{-6}\ M_\odot$.

The CNO elements in the ejecta were produced by pre-collapse He shell burning in the He-layer, which contains $0.2\ M_\odot$ ^{12}C. Mixing of H into the He shell-burning region produces $4 \times 10^{-4}\ M_\odot$ ^{14}N. On the other hand, only a small amount of heavier elements (Mg, Ca, and Fe-peak elements) are ejected and their abundance ratios are the average in the region of $M_r = 1.8$ - $6.0\ M_\odot$. The sub-solar ratios of [Ti/Fe] $= -0.4$ and [Ni/Fe] $= -0.4$ are the results of the relatively small explosion energy ($E_{51} = 0.3$). With this "mixing and fallback", the large C/Fe and C/Mg ratios observed in HE0107-5240 are well reproduced [50].

In this model, N/Fe appears to be underproduced. However, N can be produced inside the EMP stars through the C-N cycle, and brought up to the surface during the first dredge up stage while becoming a red-giant star [6].

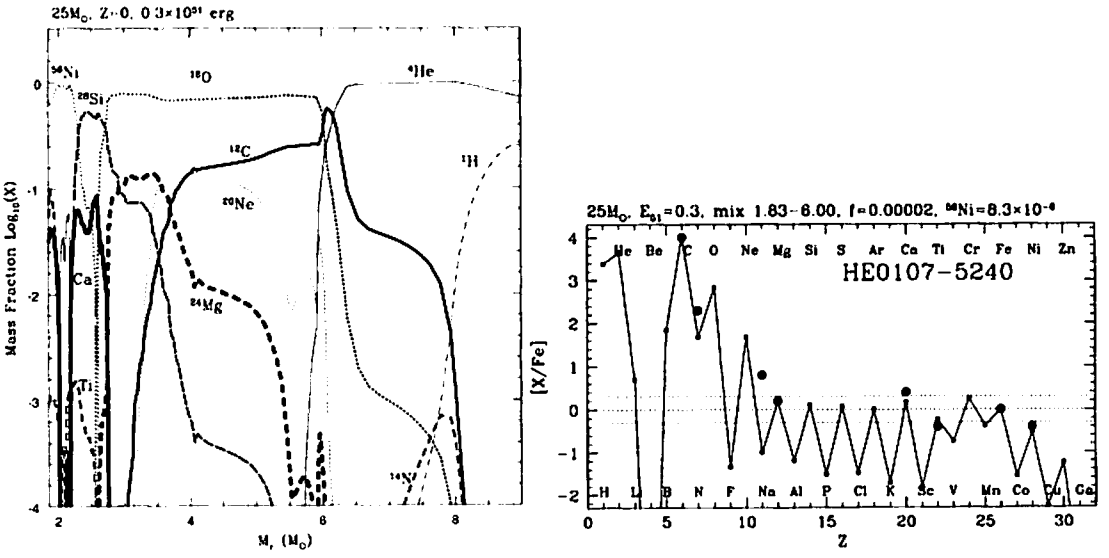


Figure 6: (left) The post-explosion abundance distributions for the 25 $M_\odot$ model with the explosion energy E_{51} = 0.3 [50]. (right) Elemental abundances of the C-rich most Fe deficient star HE0107-5240 (filled circles), compared with a theoretical supernova yield [50].

4.2 Carbon-rich EMP stars: CS 22949-037 and CS 29498-043

The "mixing and fallback" is commonly required to reproduce the abundance pattern of typical EMP stars. In Figure 7 (left) we show a model, which is in good agreement with CS22949-037 [50]. This star has [Fe/H] = −4.0 and also C, N-rich [35, 8], though C/Fe and N/Fe ratios are smaller than HE0107-5240. The model is the explosion of a 30 $M_\odot$ star with E_{51} = 20. In this model, the mixing region (M_r = 2.33 - 8.56 $M_\odot$) is chosen to be smaller than the entire He core (M_r = 13.1 $M_\odot$) in order to reproduce relatively large Mg/Fe and Si/Fe ratios. Similar degree of the mixing would also reproduce the abundances of CS29498-043 [2], which shows similar abundance pattern.

We assume a larger fraction of ejection, 2%, from the mixed region for CS22949-037 than HE0107-5240, because the C/Fe and N/Fe ratios are smaller. The ejected Fe mass is 0.003 $M_\odot$. The larger explosion energy model is favored for explaining the large Zn/Fe, Co/Fe and Ti/Fe ratios [47].

Without mixing, elements produced in the deep explosive burning regions, such as Zn, Co, and Ti, would be underproduced. Without fallback the abundance ratios of heavy elements to lighter elements, such as Fe/C, Fe/O, and Mg/C would be too large.

In this model, Ti, Co, Zn and Sc are still under-produced, however, these elements may be enhanced efficiently in the aspherical explosions [22, 23]. Almost the same effects as the "mixing and fallback mechanism" are realized if the explosion is jet-like, although the total energy can be smaller if the beaming angle of the jet is small [23].

4.3 EMP Stars with a Typical Abundance Pattern

Similarly, the "mixing and fall back" process can reproduce the abundance pattern of the typical EMP stars without enhancement of C and N. Figure 7 (right) shows that the averaged abundances of [Fe/H] = −3.7 stars in Norris et al. [35] can be fitted well with the model of 25 $M_\odot$ and E_{51} = 20 but larger fraction (∼ 10%) of the processed materials in the ejecta.

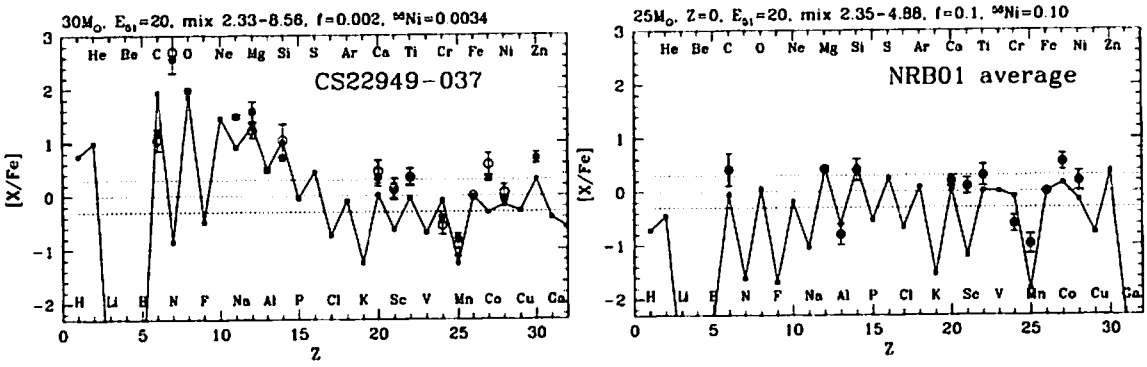


Figure 7: (left) Elemental abundances of CS 22949-037 (open circles for [35], and solid squares for [8]), compared with a theoretical supernova yield [50]. (right) Averaged elemental abundances of stars with [Fe/H] = −3.7 [35].

Table 1: The results of the stability analysis for Pop III and Pop I stars. ○ and × represent that the star is stable and unstable, respectively. The e-folding time for the fundamental mode is shown after × in units of 10^4yr [33].

mass ($M_\odot$)	80	100	120	150	180	300
Pop III	○	○	○	× (9.03)	× (4.83)	× (2.15)
Pop I	○	× (7.02)	× (2.35)	× (1.43)	× (1.21)	× (1.71)

5 The First Stars

It is of vital importance in current astronomy to identify the first generation stars in the Universe, i.e., totally metal-free, Pop III stars. The impact of the formation of Pop III stars on the evolution of the Universe depends on their typical masses. Recent numerical models have shown that, the first stars are as massive as ∼ 100 $M_\odot$ [1]. The formation of long-lived low mass Pop III stars may be inefficient because of slow cooling of metal free gas cloud, which is consistent with the failure of attempts to find Pop III stars.

If the most Fe deficient star, HE0107-5240, is a Pop III low mass star that has gained its metal from a companion star or interstellar matter [52], would it mean that the above theoretical arguments are incorrect and that such low mass Pop III stars have not been discovered only because of the difficulty in the observations?

Based on the results in the earlier section, we propose that the first generation supernovae were the explosion of ∼ 20-130 $M_\odot$ stars and some of them produced C-rich, Fe-poor ejecta. Then the low mass star with even [Fe/H] < −5 can form from the gases of mixture of such a supernova ejecta and the (almost) metal-free interstellar matter, because the gases can be efficiently cooled by enhanced C and O ([C/H] ∼ −1).

5.1 Pair-Instability Supernovae

We have shown that the ejecta of core-collapse supernova explosions of massive stars can well account for the abundances of EMP stars. We can put further constraint on the typical mass of Pop III. The abundances of all observed EMP stars including the most metal-poor one are inconsistent with the abundance pattern of pair-instability supernovae (PISNe). For typical EMP stars and CS22948-037, enrichment by PISNe cannot be consistent with the observed abundant Zn/Fe and Co/Fe ratios [47, 14]. For HE0107-5240 and other C-rich EMP stars, PISNe enrichment is difficult to account for the large C/Mg ratios. Therefore the supernova progenitors that are responsible for the formation of EMP stars

are in the range of $M \sim 20 - 130\ M_\odot$, but not more massive than 130 $M_\odot$. This upper limit depends on the stability of massive stars as will be discussed below.

5.2 Stability and Mass Loss of Massive Pop III stars

To determine the upper limit mass of the Zero Age Main Sequence (ZAMS), we analyze a linear non-adiabatic stability of massive ($80M_\odot$ - $300M_\odot$) Pop III stars using a radial pulsation code [33]. Because CNO elements are absent during the early stage of their evolution, the CNO cycle does not operate and the star contracts until temperature rises sufficiently high for the 3α reaction to produce ^{12}C. We calculate that these stars have $X_{\rm cno} \sim 1.6 - 4.0 \times 10^{-10}$, and the central temperature $T_c \sim 1.4 \times 10^8 K$ on their ZAMS. We also examine the models of Pop I stars for comparison.

Table 1 shows the results for our analysis. The critical mass of ZAMS Pop III star is $128M_\odot$ while that of Pop I star is $94M_\odot$. This difference comes from very compact structures (with high T_c) of Pop III stars.

Stars more massive than the critical mass will undergo pulsation and mass loss. We note that the e-folding time of instability is much longer for Pop III stars than Pop I stars with the same mass, and thus the mass loss rate is much lower. These results are consistent with [15] and [4]. However, the absence of the indication of PISNe may imply that these massive stars above 130 $M_\odot$ undergo significant mass loss, thus evolving into Fe core-collapse rather than PISNe.

6 Discussion

We have first shown that signatures of hypernova nucleosynthesis are seen in the abundance patterns in extremely metal-poor (EMP) stars. We suggest that hypernovae of massive stars may make important contributions to the Galactic (and cosmic) chemical evolution, especially in the early low metallicity phase. The IMF of Pop III stars might be different from that of Pop I and II stars, and that more massive stars are abundant for Pop III.

We have also shown that the most iron-poor star as well as other C-rich EMP stars is likely to be enriched by massive supernovae that are characterized by relatively small Fe ejection. Such supernovae are not just hypothetical but have been actually observed, forming a distinct class of type II supernovae ("faint supernovae" [34]). The proto-type is SN1997D, which is very under luminous and shows quite narrow spectral lines21 ([46]; also SN 1999br [53]). These features are well modeled as an explosion of the 25 $M_\odot$ star with small explosion energy $E_{51} = 0.4$. On the other hand, typical EMP stars without enhancement of C and N correspond to the abundance pattern of energetic supernovae ("hypernovae" [34]).

For both cases black holes more massive than $\sim$ 3 - 10 $M_\odot$ must be left as a results of fallback, suggesting that the copious formation of the first black holes from the first stars. These black holes may consist of some of the dark mass in the Galactic halo. In our scenario, HE0107-5240 with [Fe/H] = -5.3 was formed from C, O-enhanced gases with [C,O/H] ~ -1. With such enhanced C and O, the cooling efficiency is large enough to form small mass stars. As far as the low mass EMP stars are C-rich, therefore, their small masses are consistent with the massive Pop III star formation. Rather their C-richness implies that Pop III stars that are responsible for their formation are massive enough to form (the first) black holes.

References

[1] Abel, T., Bryan, G. L., & Norman, M. L. 2002, Science 295, 93

[2] Aoki, W., Ryan, S. G., Beers, T. C. & Ando, H. 2002, ApJ 567, 1166

[3] Audouze, J., & Silk, J. 1995, ApJ, 451, L49

[4] Baraffe, I., Heger, A., & Woosley, S. E. 2001, ApJ, 550, 890

[5] Blake, L.A.J., Ryan, S.G., Norris, J.E., Beers, T.C. 2001, Nucl. Phys. A., 688, 502

[6] Boothroyd, A.I. & Sackmann, I.-J. 1999, ApJ 510, 217

[7] Christlieb, N. et al. 2002, Nature 419, 904

[8] Depagne, E. et al. 2002, A&A 390, 187

[9] Galama, T., et al. 1998, Nature, 395, 670

[10] Hachisu, I., Matsuda, T., Nomoto, K., & Shigeyama, T. 1990, ApJ 358, L57

[11] Hamuy, M. 2002, ApJ, in press

[12] Hashimoto, M., Nomoto, K., & Shigeyama, T. 1989, A&A, 210, L5

[13] Hatano, K., Branch, D., Nomoto, K., et al. 2001, BAAS, 198, 3902

[14] Heger, A., & Woosley, S.E., 2002, ApJ, 567, 532

[15] Ibrahim, A., Boury, A., & Noels A. 1981, A&A, 103, 390

[16] Israelian, G., Rebolo, R., Basri, G. et al. 1999, Nature, 401, 142

[17] Iwamoto, K., Mazzali, P.A., Nomoto, K., et al. 1998, Nature, 395, 672

[18] Iwamoto, K., Nakamura, T., Nomoto, K., et al. 2000, ApJ, 534, 660

[19] Kawabata, K. et al. ApJ, 580, L39

[20] Kifonidis, K., Plewa, T., Janka, H.-Th., & Muller, E. 2000, ApJ 531, L123

[21] Knop, R., Aldering, G., Deustua, S., et al., 1999, IAU Circ., 7128

[22] Maeda, K., Nakamura, T., Nomoto, K., Mazzali, P., Patat, F., Hachisu, I., 2002, ApJ, 565, 405

[23] Maeda, K. & Nomoto, K. 2003, Nucl. Phys. A., in press

[24] Mazzali, P., Iwamoto, K., Nomoto, K. 2000, ApJ, 545, 407

[25] Mazzali, P., Nomoto, K., Patat, F., Maeda, K. 2001, ApJ, 559, 1047

[26] Mazzali, P.A., Deng, J., Maeda, K., Nomoto, K., et al., 2002, ApJ, 572, L61

[27] McWilliam, A., Preston, G.W., Sneden, C., Searle, L. 1995, AJ, 109, 2757

[28] Nakamura, T., Umeda, H., Nomoto, K., Thielemann, F.-K., & Burrows, A. 1999, ApJ, 517, 193

[29] Nakamura, T., Mazzali, P., Nomoto, K., Iwamoto, K. 2001a, ApJ, 550, 991

[30] Nakamura, T., Umeda, H., Iwamoto, K., Nomoto, K., Hashimoto, M., Hix, R.W., Thielemann, F.-K. 2001, ApJ, 555, 880

[31] Nomoto, K., Mazzali, P., Nakamura, T., et al. 2001a, in *Supernovae and Gamma Ray Bursts*, eds. M. Livio, et al. (Cambridge Univ. Press) 144 (astro-ph/0003077)

[32] Nomoto, K., Maeda, K., Umeda, H., & Nakamura, T. 2001b, in *The Influence of Binaries on Stellar Populations Studies*, ed. D. Vanbeveren (Kluwer) 507 (astro-ph/0105127)

[33] Nomoto, K., Maeda, K., Umeda, H., & Shirouzu, M. 2002a, in *New Trends in Theoretical and Observational Cosmology*, eds. K. Sato & T. Shiromizu (Tokyo: Univ. Academy Press) 245

[34] Nomoto, K. Maeda, K.. Umeda, H., Ohkubo, T., Deng, J., & Mazzali, P. 2002b, in *IAU Symp 212, A massive Star Odyssey, from Main Sequence to Supernova*, eds. V.D. Hucht, A. Herrero, & C. Esteban (San Francisco: ASP), in press (astro-ph/0209064)

[35] Norris, J. E., Ryan, S. G. & Beers, T. C. 2001, ApJ 561, 1034

[36] Ohkubo, T., Umeda, H., & Nomoto, K. 2003, Nucl. Phys. A., in press

[37] Patat, F. et al. 2001, ApJ, 555, 900

[38] Podsiadlowski, Ph., Nomoto, K., Maeda, K., Nakamura, T., Mazzali, P., Schmidt, B. 2002, ApJ, 567, 491

[39] Primas, F., Brugamyer, E., Sneden, C. et al. 2000, in *The First Stars*, eds. A. Weiss, et al. (Springer), 51

[40] Ryan, S.G., Norris, J.E., & Beers, T.C. 1996, ApJ, 471, 254

[41] Ryan, S. G. in *CNO in the Universe* eds. C. Charbonnel, D. Schaerer, & G. Meynet, in press (astro-ph/0211608)

[42] Schneider, R., Ferrara, A., Natarajan, P., & Omukai, K. 2002, ApJ 571, 30

[43] Shigeyama. T., & Tsujimoto, T. 1998, ApJ, 507, L135

[44] Sneden, C., Gratton, R.G., & Crocker, D.A. 1991, A&A, 246, 354

[45] Thielemann, F.-K., Nomoto, K., & Hashimoto, M. 1996, ApJ, 460, 408

[46] Turatto, M., Mazzali, P., Young, T., Nomoto, K. et al. 1998, ApJ, 498, L129

[47] Umeda, H., & Nomoto, K. 2002a, ApJ, 565, 385

[48] Umeda, H., & Nomoto, K. 2002b, in *Nuclear Astrophysics*, ed. W. Hillebrandt & E. MÏller (Garching: MPA), 164 (astro-ph/0205365)

[49] Umeda, H., Nomoto, K., Tsuru, T., & Matsumoto, H, 2002c, ApJ, 578, 855

[50] Umeda, H., & Nomoto, K. 2003, Nature, in press

[51] Woosley, S.E., Eastman, R.G., & Schmidt, B.P. 1999, ApJ, 516, 788

[52] Yoshii, Y. 1981, A&A 97, 280

[53] Zampieri, L., Pastorello, A., Turatto, M., et al. 2002, MNRAS, in press (astro-ph/0210171)

Brane-World Cosmology

Misao Sasaki

Department of Earth and Space Science,

Osaka University, Toyonaka 560-0043, Japan

§1. Historical Notes

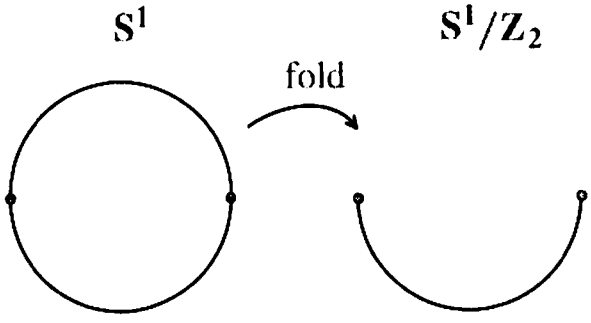
Progress in Particle Physics

$$\text{Supergravity} \quad \Rightarrow \quad \text{String theory} \quad \Rightarrow \quad \text{'M' theory}$$

• Hořava & Witten (1996) [1]

11D Supergravity with 1D compactified as $\mathbf{S^1/Z_2}$ gives a desirable string theory on the 10D boundary spacetime.

(Standard matter fields live on the boundary.)



$$\Downarrow \quad \text{Compactify extra 6D}$$

$$\partial(11D) = 10D \quad \Rightarrow \quad 6D \otimes 4D$$

Putting aside the extra 6D, we have

$$\partial(5D) = 4D \quad \cdots \quad \text{brane world!}$$

• Self-gravitating brane ≈ domain wall

⋆ $(n-1)$-brane = singular (time-like) hypersurface embedded in $(n+1)$-dim spacetime

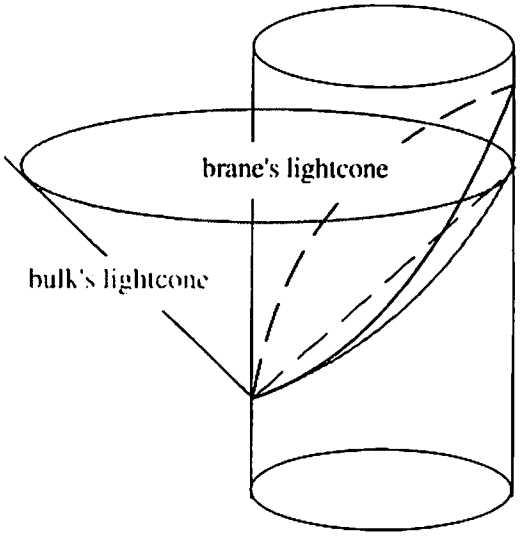
⋆ brane tension (σ) = vacuum energy ($\sigma > 0$? or $\sigma < 0$?)

vacuum energy $\neq$ cosmological constant on the brane

⋆ causality on the brane $\neq$ causality in the bulk

H. Ishihara, (2001) [2]

A new picture of the universe!



§2. Randall-Sundrum (RS) Brane World

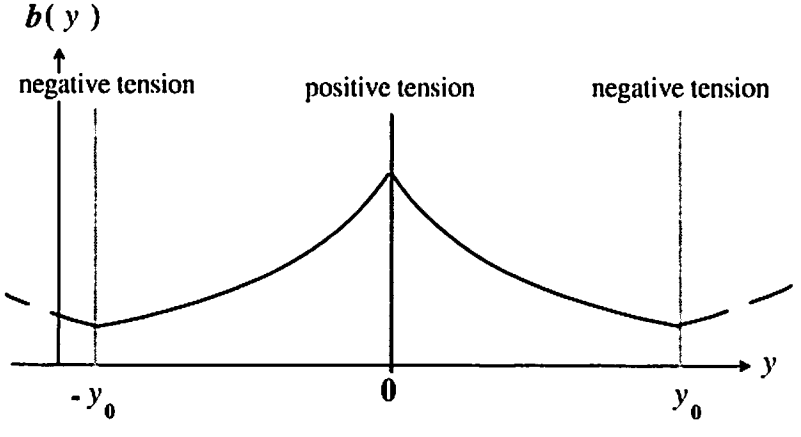
Randall & Sundrum ('99); RS1 [3], RS2[4]

• 5D-AdS bounded by 2 branes: $R^1 \times (S^1/Z_2)$

$$ds^2 = dy^2 + e^{-2|y|/\ell}\eta_{\mu\nu}dx^\mu dx^\nu \quad (-r_c \le y \le r_c)$$

$$\ell^2 = -\frac{6}{\Lambda_5}, \qquad \text{brane tension: } \sigma_\pm = \pm\frac{3}{4\pi G_5 \ell}$$

($b(y) = e^{-|y|/\ell}$ is called the warp factor)



• Possible solution to the Mass hierarchy problem in particle physics if we live on the negative tension brane [RS1: 2-brane model].

⋆ r_c is arbitrary ⇒ Existence of Radion mode

Brans-Dicke type gravity on the branes

unless [3]stabilization mechanism.

$\omega_{BD} < 0$ on the negative tension brane (Garriga & Tanaka, '99 [5])

• If we live on the positive tension brane, the negative tension brane may be absent ($r_c \to \infty$ in RS1) [RS2: 1-brane model].

⋯ 5th dimension can be non-compact

⋆ Gravity confined within $\ell \sim |\Lambda_5|^{-1/2}$ from the brane

⋆ No "radion" modes (no relative motion)

Einstein gravity is recovered on scales $\gg \ell$

$$\Phi_{\rm Newton} = -\frac{G_5 M}{r^2} \underset{r\gg\ell}{\Rightarrow} -\frac{G_5 M}{\ell r} = -\frac{G_4 M}{r}$$

The positive tension brane seems cosmologically favored.

§3. Brane Cosmology in AdS$_5$-Schwarzschild Bulk

Kraus ('99) [6], Ida ('00) [7], Mukohyama et al. ('00) [8], ⋯

• 5D AdS-Schwarzschild in Static Chart:

$$ds^2 = -A(R)dT^2 + \frac{dR^2}{A(R)} + R^2 d\Omega_K^2$$

$$A(R) = K + \frac{R^2}{\ell^2} - \frac{\alpha^2}{R^2} \quad (K = \pm 1, 0, \quad \alpha^2 = 2G_5 M)$$

⋆ For $\alpha^2 = 0$ ($K = 1$),

$$ds^2 = dr^2 + (H\ell)^2 \sinh^2(r/\ell)[-dt^2 + \cosh^2(Ht) d\Omega_{(3)}^2]$$

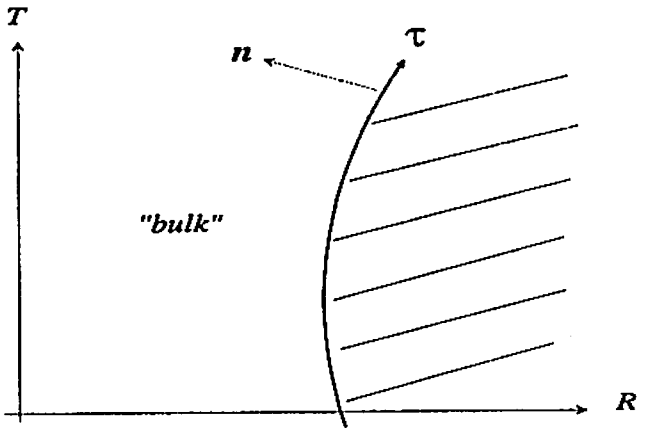
$$\begin{pmatrix} R = \ell \sinh(r/\ell)\cosh(Ht) \\ T = \ell \arctan\left((r/\ell)\sinh(Ht)\right) \end{pmatrix} \quad H \text{ is arbitrary.}$$

Any r =const. timelike hypersurface is 4D de Sitter space.

· Pure de Sitter brane at $r = r_0$ (with Z_2 symmetry): $\quad (T_{\mu\nu} = -\sigma\, g_{\mu\nu})$

$$\sigma = \frac{3}{4\pi G_5 \ell}\coth(r_0/\ell) \equiv \frac{3}{4\pi G_5 \ell_\sigma}, \qquad H^2\ell^2 = \frac{1}{\sinh^2(r_0/\ell)} = \frac{\ell^2}{\ell_\sigma^2} - 1$$

⋆ Deviates from de Sitter if $T_{\mu\nu}$ is non-trivial:



brane trajectory : $\begin{cases} R = R(\tau) \\ T = T(\tau) \end{cases}$

$$ds^2|_{\text{brane}} = \left(-A(R)\dot{T}^2 + \frac{\dot{R}^2}{A(R)}\right)d\tau^2 + R^2(\tau)d\Omega_K^2$$

· Choose τ to be Proper time on the Brane:

$$-A(R)\dot{T}^2 + \frac{\dot{R}^2}{A(R)} = -1 \quad \Rightarrow \quad \boxed{A^2(R)\dot{T}^2 = \dot{R}^2 + A(R)}$$

· Junction condition under Z_2-symmetry:

$$[K_{\mu\nu}]^+_- = 2K_{\mu\nu}(+0) = -8\pi G_5[T_{\mu\nu} - (1/3)T g_{\mu\nu}]$$

$$K_{\mu\nu} = \frac{1}{2}\mathcal{L}_n q_{\mu\nu}; \quad n_a = (\dot{R}, -\dot{T}, 0, 0, 0)$$

$q_{\mu\nu} \cdots$ induced metric on the brane

$$T^\mu{}_\nu = \text{diag}(-\rho, p, p, p) - \sigma_c\,\delta^\mu{}_\nu; \quad \sigma_c = \frac{3}{4\pi G_5 \ell}$$

$$\Rightarrow \quad \boxed{\frac{A(R)}{R}\dot{T} = \frac{4\pi G_5}{3}(\rho + \sigma_c) = \frac{4\pi G_5}{3}\rho + \frac{1}{\ell}}$$

$G_1 = G_5/\ell \cdots$ 4D Newton const.

$$\Downarrow \quad A(R) = K + R^2\ell^2 - \frac{\alpha^2}{R^2}$$

$$\left(\frac{\dot{R}}{R}\right)^2 + \frac{K}{R^2} = \frac{8\pi G_4}{3}\rho + \ell^2\left(\frac{4\pi G_4}{3}\rho\right)^2 + \frac{\alpha^2}{R^4}$$

$\cdots$ **Friedmann equation on the brane**

$\star$ presence of $\propto \rho^2$ and α^2/R^4 terms.

- ρ^2-term dominates in the early universe: $H \propto \rho$.

  For $\rho \propto R^{-4}$, $K = \alpha^2 = 0$; $R \propto \left(t + \frac{2t^2}{\ell}\right)^{1/4}$

- reduces to standard Friedmann equation for $\ell^2 G_4 \rho \ll 1$.

  $(\ell^2 G_4 \rho \ll 1 \Leftrightarrow \rho \ll \sigma_c)$

  BBN constraint: $\sigma_c \gtrsim (100\,\mathrm{MeV})^4$ $(\Leftrightarrow \ell \lesssim 10^{-13}\,\mathrm{cm})$

- α^2/R^4-term: "dark radiation" $\alpha^2 = 2G_5 M \sim$ BH mass

$$\frac{\alpha^2}{R^4} = -\frac{E_{tt}}{3}; \quad E_{\mu\nu} = C^{(5)}_{\mu a \nu b} n^a n^b \quad \text{(5D Weyl contribution)}$$

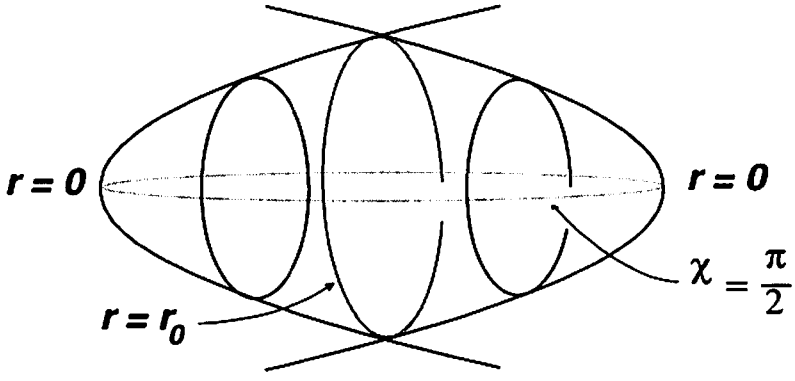
Hawking radiation from BH? $\cdots$ AdS/CFT? (T. Tanaka, gr-qc/0203082 [9])

§4. Quantum Brane Cosmology

• Euclidean AdS: H^5 $(O(5,1)$-symmetric)

$$ds^2 = dr^2 + \ell^2 \sinh^2(r/\ell)(d\chi^2 + \sin^2\chi\, d\Omega^2_{(3)})$$

$\star$ Brane at $r = r_0$ (with Z_2-symmetry) = de Sitter-brane instanton



topology $\sim S^5$

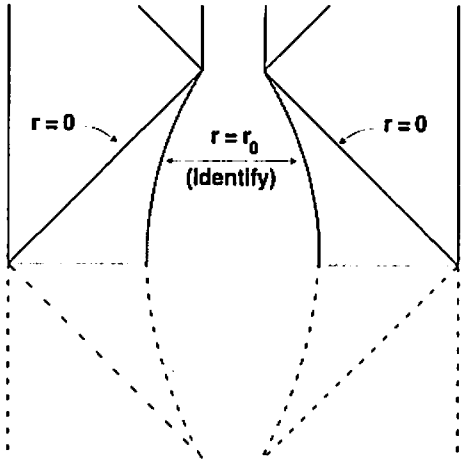
$\chi = \pi/2$: totally geodesic 4-surface

• Creation of inflating brane-world

Garriga & MS ('00) [10]; Koyama & Soda ('00) [11]

Analytic continuation: $\chi \to iHt + \pi/2$

$$ds^2 = dr^2 + (H\ell)^2 \sinh^2(r/\ell)(-dt^2 + H^{-2}\cosh^2 Ht\, d\Omega_{(3)}^2) \quad (r \le r_0)$$



Spatially Compact 5D Universe

(RS flat brane is recovered in the limit $r_0 \to \infty$)

§5. 4D Graviton and Kaluza-Klein Excitations

• Gravitational perturbation of de Sitter brane universe:

$$\begin{aligned} ds^2 &= dr^2 + (H\ell)^2 \sinh^2(r/\ell) ds_{\mathrm{dS}_4}^2 + h_{ab}dx^a dx^b \\ &= b^2(\eta)\left(d\eta^2 + H^2 ds_{\mathrm{dS}_4}^2\right) + h_{ab}dx^a dx^b \end{aligned}$$

· $dr = b(r)d\eta$ (conformal radial coordinate):

$$b(r) = \ell \sinh(r/\ell) \;\Rightarrow\; b(\eta) = \frac{\ell}{\sinh(|\eta| + \eta_0)}$$

$$\left(\sinh\eta_0 = \frac{1}{\sinh(r_0/\ell)}\,; \qquad -\infty < \eta < \infty\right)$$

· (generalized) Randall-Sundrum gauge:

$$h_{55} = h_{5\mu} = h^{\mu}{}_{\mu} = D_\mu h^{\mu\nu} = 0\,;$$

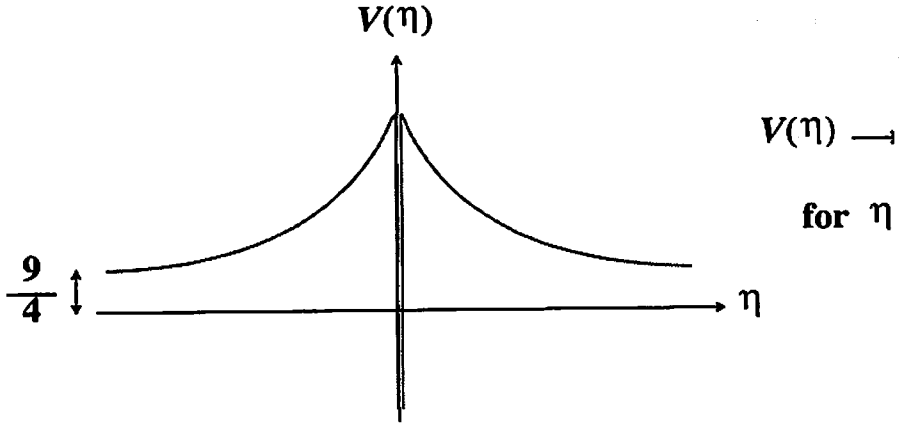
D_μ : 4D covariant derivative

• Perturbation equations: Garriga & MS ('99) [10]

$$h_{\mu\nu} = b^{1/2}\,\varphi(\eta) H_{\mu\nu}(x) \quad \Rightarrow \quad \begin{cases} -\varphi'' + \dfrac{(b^{3/2})''}{b^{3/2}}\varphi = \dfrac{m^2}{H^2}\varphi \\ (-\overset{(4)}{\Box} + 2H^2 + m^2) H_{\mu\nu} = 0 \end{cases}$$

⋆ "Volcano" potential for φ:

$$\boxed{V(\eta) \equiv \frac{(b^{3/2})''}{b^{3/2}} = \frac{15}{4\sinh^2(|\eta| + \eta_0)} + \frac{9}{4} - 3\coth\eta_0\,\delta(\eta)}$$



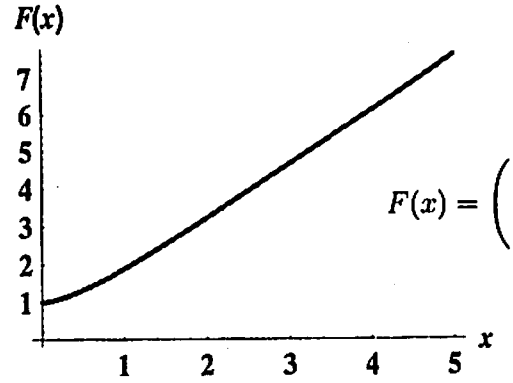
⋆ 4D graviton (zero mode $m = 0$): $\varphi \propto b^{3/2} \Rightarrow h_{\mu\nu} \propto b^2$

⋆ KK excitations ($m > 0$): $V \to (9/4) \Rightarrow m > (3/2)H$

· Zero mode is confined just like the case of the RS flat brane.

When quantized, however, the normalization (amplitude) is non-trivial:

$$\frac{P_{gw}(k)k^3}{G_4} \sim \left(\frac{H}{2\pi}\right)^2 F(H\ell) \qquad \text{(Langlois, Maartens \& Wands ('00) [12])}$$



$$F(x) = \left(\sqrt{1+x^2} - x^2 \ln\left[\frac{1+\sqrt{1+x^2}}{x}\right]\right)^{-1}$$

– large enhancement at $H\ell \gg 1$: $F \sim \dfrac{3}{2} H\ell$.

· Mass gap in KK spectrum: $\Delta m = (3/2)H$

The same is true for any bulk scalar field with $m \lesssim H$.

– No 'zero-mode' (bound state mode) for $m \gg H$.

Dubovsky, Rubakov & Tinyakov ('00) [13].

§6. Brane-world Inflation Driven by a Bulk Scalar Field

Kobayashi, Koyama & Soda ('00) [14], Himemoto et al. [15–19], ···

⋆ Randall-Sundrum's "default" parameters:

$$\text{brane tension:}\quad \sigma_c = \frac{3}{4\pi G_5 \ell}\,; \quad \ell = \left|\frac{6}{\Lambda_5}\right|^{1/2}.$$

If $|\sigma| > \sigma_c$, then inflation occurs on the brane:

$$H^2 = \frac{1}{\ell_\sigma^2} - \frac{1}{\ell^2} = \frac{1}{\ell_\sigma^2} - \frac{|\Lambda_5|}{6}\,; \quad \sigma \equiv \frac{3}{4\pi G_5 \ell_\sigma}$$

If $|\sigma| = \sigma_c$ but $|\Lambda_{5,eff}| < |\Lambda_5|$, inflation also occurs on the brane:

$$H^2 = \frac{|\Lambda_5 - \Lambda_{5,eff}|}{6}$$

$$\Downarrow$$

Brane-world inflation can be driven solely

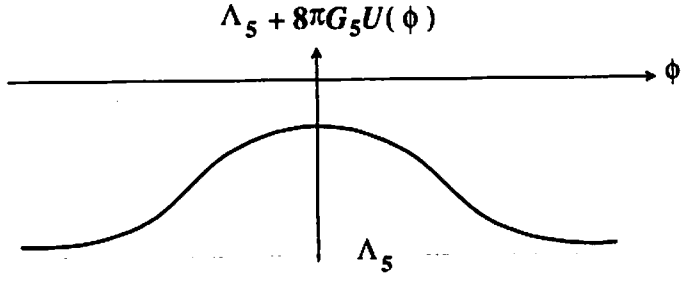
by bulk (gravitational) fields.

cf. Hawking, Hertog & Reall ('01) [20], Nojiri, Odintsov & Osetrin ('01) [21], ···

• Toy Model

$$L_5 = \frac{1}{16\pi G_5} R - \frac{1}{2} g^{ab} \partial_a \phi \partial_b \phi - U(\phi)$$

∼ a conformally transformed scalar-tensor gravity



A bulk scalar potential model.

If ϕ varies very slowly,

$$|\Lambda_{5,eff}| = |\Lambda_5 + 8\pi G_5 U(\phi)| \ < |\Lambda_5|,$$
$$H^2 = \frac{4\pi G_5 U(\phi)}{3} = \frac{8\pi G_4}{3} U_4; \quad G_5 = G_4 \ell, \quad U_4 = \frac{\ell}{2} U(\phi).$$

(ℓ is arbitrary here.)

• Friedmann equation in the presence of a bulk scalar:

$$\left(\frac{\dot{a}}{a}\right)^2 + \frac{K}{a^2} \equiv H^2 + \frac{K}{a^2} = \frac{8\pi G_4}{3} \tilde{\rho}_\phi + \frac{1}{3} E^t{}_t;$$
$$\tilde{\rho}_\phi = \ell \left(\frac{1}{4}\dot{\phi}^2 + \frac{1}{2} U(\phi)\right), \quad E^t{}_t = \overset{(5)}{C}{}^t{}_{rtr}.$$

From Bianchi Ids. on the brane and ϕ equation in the bulk,

$$E^t{}_t = -\frac{4\pi G_5}{a^4} \int^t a^4 \dot{\phi} (\partial_r^2 \phi + \frac{\dot{a}}{a} \dot{\phi})\, dt$$
$$= 2\pi G_5 \dot{\phi}^2 + \frac{C}{a^4}, \qquad \text{if} \quad \ddot{\phi} + 3H\dot{\phi} + \frac{1}{2}\partial_\phi U = 0 \text{ on the brane.}$$
$$\Rightarrow \quad \rho_{\rm eff} = \tilde{\rho}_\phi + \frac{E^t{}_t}{8\pi G_4} = \ell \left(\frac{1}{2}\dot{\phi}^2 + \frac{1}{2} U(\phi)\right) + \frac{C}{a^4}.$$

⋆ 5D scalar ϕ behaves like a 4D scalar $\Phi = \sqrt{\ell}\,\phi$ with

$$U_{\rm eff}(\Phi) = \frac{\ell}{2} U(\Phi/\sqrt{\ell})$$

When and in what situations will this be true?

• "Zero mode" and KK modes $\left(U = \frac{1}{2} M^2 \phi^2\right)$

⋆ For de Sitter brane at $r = r_0$,

$$\Phi(r, x^\mu) = u_0(r)\phi_0(x^\mu) + \int_{3/2}^{\infty} d\lambda\, u_\lambda(r)\phi_\lambda(x^\mu)$$
ϕ_0 : "zero mode" (bound state mode)

ϕ_λ : Kaluza-Klein modes $M_\lambda^2 = \lambda^2 H^2 \quad (\lambda > 3/2)$

Effective 4d mass of zero mode when $M^2 \lesssim H^2$:

$$M_0^2 = \begin{cases} M^2/2 & \text{for } H^2\ell^2 \ll 1 \\ 3M^2/5 & \text{for } H^2\ell^2 \gg 1 \end{cases}$$

$\star$ No bound state when $M^2 > H^2$.

(But there is a quasi-normal mode with $M_0 = M/\sqrt{2} - i\Gamma$)

· Zero-mode dominance $\Leftrightarrow$ consistent with the effective potential picture.

· KK modes are important when $H\ell \gg 1$

($\Leftrightarrow$ gravity zero-mode is non-trivial when $H\ell \gg 1$).

Quantum fluctuations of KK modes need be evaluated.

• Case of a scalar coupled to brane tension (Langlois & MS '03 [22])

$$S = \int d^5x\sqrt{-g}\left(\frac{1}{16\pi G_5}R - \frac{1}{2}(\nabla\phi)^2 - V_5(\phi)\right) - \int d^4x\sqrt{-q}\,\sigma(\phi)$$

$$8\pi G_5 V_5(0) = \Lambda_5 = -6\,\ell^2$$

$\star$ Friedmann equation on the brane: (Maeda & Wands '00 [23])

$$H^2 = \frac{8\pi G_5}{3}\left(\frac{1}{4}\dot{\phi}^2 + \frac{1}{2}V_5 + \frac{8\pi G_5}{12}\sigma^2 - \frac{1}{16}\left(\frac{\partial\sigma}{\partial\phi}\right)^2\right) + \frac{E^0{}_0}{3}$$

If ${}^\exists V_{\rm eff}$ s.t. $\ddot{\Phi} + 3H\dot{\Phi} + V'_{\rm eff} = -J\,, \quad \Phi \equiv \sqrt{\ell}\,\phi$

$$\Rightarrow \quad \begin{cases} H^2 = \dfrac{8\pi G_4}{3}\left[\dfrac{1}{2}\dot{\Phi}^2 + V_{\rm eff}(\Phi) + \rho_{\mathcal{E}}\right], \\ \dot{\rho}_{\mathcal{E}} + 4H\rho_{\mathcal{E}} = J\dot{\Phi}\,; \quad V_{\rm eff} = \dfrac{1}{2}V_5 + \dfrac{8\pi G_5}{12}\sigma^2 - \dfrac{1}{16}\left(\dfrac{\partial\sigma}{\partial\phi}\right)^2. \end{cases}$$

where $G_4 = G_5/\ell$ and $E^0{}_0 = 8\pi G_4\left(\rho_{\mathcal{E}} + \dfrac{1}{4}\dot{\Phi}^2\right)$.

Does this hold whenever $H^2\ell^2 \ll 1$? AdS/CFT?

§7. Cosmological Perturbations on the Brane

· General formalism $\Rightarrow$ Kodama et al. [24], Langlois [25], Mukohyama [26], ···.

· Essentially a 5-dimensional, PDE problem.

· However, some simplifications on super-horizon scales.

Langlois, Maartens, MS & Wands ('01) [27]

• Basic equations (in AdS_5 bulk background; no bulk scalar)

Shiromizu, Maeda & MS ('99) [28]

$$G_{\mu\nu} + \Lambda_4 q_{\mu\nu} = 8\pi G_4 T_{\mu\nu} + (8\pi G_5)^2 \Pi_{\mu\nu} - E_{\mu\nu}$$
$$\equiv 8\pi G_4 T^{\rm tot}_{\mu\nu} \quad (\Pi_{\mu\nu} \sim \text{quadratic in } T_{\mu\nu})$$

"$-E_{\mu\nu}$": Weyl fluid (or "dark radiation")

For $T_{\mu\nu} = \rho u_\mu u_\nu + P h_{\mu\nu} + \pi_{\mu\nu}$ ($\pi_{\mu\nu}$: anisotropic stress $= O(\epsilon)$)

$$u^\mu D^\nu E_{\mu\nu} = O(\epsilon^2)$$

Weyl fluid is decoupled on superhorizon scales.

standard 4-d theory is applicable ($E^0{}_0 = 8\pi G_4 \rho_{\mathcal{E}}$, etc.)

• Large angle CMB anisotropy

$$\left(\frac{\delta T}{T}\right)_{sw}(\vec{\gamma}, \eta_0) = (\zeta_r + \Theta)(\eta_{\rm dec}, \vec{x}(\eta_{\rm dec})) + \int_{\eta_{\rm dec}}^{\eta_0} d\eta\, \partial_\eta \Theta(\eta, \vec{x}(\eta)).$$

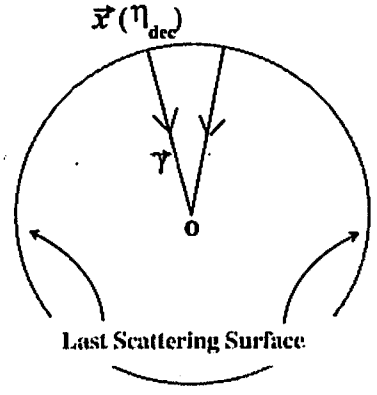
(Sachs-Wolfe) (Integrated Sachs-Wolfe)

$\zeta_r \sim$ curvature perturbation on $\rho_{\rm photon} =$ const. surfaces

$\Theta \equiv \Psi - \Phi$

$\Psi \sim$ Newton potential

$\Phi \sim$ curvature perturbation in Newton gauge



For a dust-dominated universe at decoupling,

$$\text{SW:}\quad \zeta_* + \Theta = -\frac{1}{5}\zeta_* - \frac{2}{5}S_{\rm dr} - \frac{8}{3}\frac{\rho_{\rm r}}{\rho_{\rm d}}S_{\mathcal{E}} - 8\pi G_4 a^2\,\delta\pi_{\rm tot} + \frac{16\pi G_4}{a^{5/2}}\int_0^a \delta\pi_{\rm tot}\,a^{7/2}da$$

$$\text{ISW:}\quad \partial_\eta\Theta = -\partial_\eta\left[\frac{8}{3}\frac{\rho_{\rm r}}{\rho_{\rm d}}S_{\mathcal{E}} + 8\pi G_4 a^2\,\delta\pi_{\rm tot} - \frac{16\pi G_4}{a^{5/2}}\int_0^a \delta\pi_{\rm tot}\,a^{7/2}da\right]$$

where ζ_* is the adiabatic curvature perturbation,

$$S_{\mathcal{E}} := \frac{\delta\rho_{\mathcal{E}}}{4\rho_{\rm r}} - \frac{\rho_{\mathcal{E}}\,\delta\rho}{3\rho_{\rm r}(\rho+P)} \quad \sim \text{Weyl entropy perturbation}$$

$$S_{\rm dr} := \frac{\delta\rho_{\rm d}}{\rho_{\rm d}} - \frac{3}{4}\frac{\delta\rho_{\rm r}}{\rho_{\rm r}} \quad \sim \text{standard entropy perturbation}$$

$$\delta\pi_{\rm tot} = \left(1 - \frac{\rho+3P}{2\sigma}\right)\delta\pi + \delta\pi_{\mathcal{E}} \quad \sim \text{anisotropic stress}$$

$\delta\pi_{\mathcal{E}}$: traceless part of Weyl fluid $(E^i{}_j - \frac{1}{3}\delta^i_j E^k{}_k)$

$\delta\pi_{\mathcal{E}}$ cannot be determined within this 4-d approach

§8. Summary

Brane-world gives a new picture of the universe.

Can we find cosmological evidence?

- **Quantum brane cosmology**

  ⋆ Spatially compact 5D Universe created from nothing
  - Well-posed initial value problem

  ⋆ 4D Universe created in de Sitter (inflationary) phase
  - Non-trivial quantum fluctuations if $H\ell \gg 1$
  - Effects of KK modes need to be investigated.

  ⋆ Inflation without inflaton on the brane
  - Inflation as a result of 5D gravitational dynamics

  ⋆ Mass gap ($\Delta m = (3/2)H$) in the KK spectrum
  - Isolation of the zero mode ⇔ Stability of the brane world

- **Evolution of a brane universe**

  - ⋆ Presence of ρ^2 term in Friedmann equation
    - Modified evolution when $\ell^2 G_4 \rho \gtrsim 1$
  - ⋆ Weyl fluid term (dark radiation) in Friedmann equation
    - Effect of 5D bulk gravity
  - ⋆ Large scale perturbation can be solved without 5D equations.
    - 5D effect is encoded in CMB through Weyl anisotropy.

- **Some issues on brane-world cosmology**

  - ⋆ Search for a natural brane-world inflation model
    related to cosmological constant problem ?
    cf. Kachru et al. [29], Forste et al. [30] Binetruy et al. [31]
  - ⋆ Quantitative analysis of cosmological perturbations
    5D dynamics of "$E_{\mu\nu}$" (poster by Minamitsuji [32])
  - ⋆ Analysis of two-brane cosmological models (radion dynamics)
    cf. Binetruy et al. [35], Gen & MS [36, 37], Langlois & Sorbo [34], Koyama [33], ···
    "born-again braneworld" (talk by Kanno [38])

Need a good approximation method,
e.g., Kanno-Soda's (Shiromizu-Koyama's) approach [39–41]

---

[1] P. Horava and E. Witten, Nucl. Phys. **B460**, 506 (1996); **B475**, 94 (1996).

[2] H. Ishihara, Phys. Rev. Lett. **86**, 381 (2001) [arXiv:gr-qc/0007070].

[3] L. Randall and R. Sundrum, Phys. Rev. Lett. **83**, 3370 (1999).

[4] L. Randall and R. Sundrum, Phys. Rev. Lett. **83**, 4690 (1999).

[5] J. Garriga and T. Tanaka, Phys. Rev. Lett. **84**, 2778 (1999).

[6] P. Kraus, JHEP **9912**, 011 (1999) [arXiv:hep-th/9910149].

[7] D. Ida, JHEP **0009**, 014 (2000) [arXiv:gr-qc/9912002].

[8] S. Mukohyama, T. Shiromizu and K. i. Maeda, Phys. Rev. D **62**, 024028 (2000) [Erratum-ibid. D **63**, 029901 (2001)] [arXiv:hep-th/9912287].

[9] T. Tanaka, arXiv:gr-qc/0203082, to be published in Prog. Theor. Phys. Suppl. No. 148.

[10] J. Garriga and M. Sasaki, Phys. Rev. D **62**, 043523 (2000) [arXiv:hep-th/9912118].

[11] K. Koyama and J. Soda, Phys. Lett. B **483**, 432 (2000) [arXiv:gr-qc/0001033].

[12] D. Langlois, R. Maartens and D. Wands, Phys. Lett. B **489**, 259 (2000) [arXiv:hep-th/0006007].

[13] S. L. Dubovsky, V. A. Rubakov and P. G. Tinyakov, Phys. Rev. D **62**, 105011 (2000) [arXiv:hep-th/0006046].

[14] S. Kobayashi, K. Koyama and J. Soda, Phys. Lett. B **501**, 157 (2001) [arXiv:hep-th/0009160].

[15] Y. Himemoto and M. Sasaki, Phys. Rev. D **63**, 044015 (2001) [arXiv:gr-qc/0010035].

[16] J. Yokoyama and Y. Himemoto, Phys. Rev. D **64**, 083511 (2001) [arXiv:hep-ph/0103115].

[17] N. Sago, Y. Himemoto and M. Sasaki, Phys. Rev. D **65**, 024014 (2002) [arXiv:gr-qc/0104033].

[18] Y. Himemoto, T. Tanaka and M. Sasaki, Phys. Rev. D **65**, 104020 (2002) [arXiv:gr-qc/0112027].

[19] Y. Himemoto and T. Tanaka, arXiv:gr-qc/0212114.

[20] S. W. Hawking, T. Hertog and H. S. Reall, Phys. Rev. D **62**, 043501 (2000) [arXiv:hep-th/0003052].

[21] S. Nojiri, S. D. Odintsov and K. E. Osetrin, Phys. Rev. D **63**, 084016 (2001) [arXiv:hep-th/0009059].

[22] D. Langlois and M. Sasaki, arXiv:hep-th/0302069.

[23] K. i. Maeda and D. Wands, Phys. Rev. D **62**, 124009 (2000) [arXiv:hep-th/0008188].

[24] H. Kodama, A. Ishibashi and O. Seto, Phys. Rev. D **62**, 064022 (2000) [arXiv:hep-th/0004160].

[25] D. Langlois, Phys. Rev. D **62**, 126012 (2000) [arXiv:hep-th/0005025].

[26] S. Mukohyama, Phys. Rev. D **62**, 084015 (2000) [arXiv:hep-th/0004067].

[27] D. Langlois, R. Maartens, M. Sasaki and D. Wands, Phys. Rev. D **63**, 084009 (2001) [arXiv:hep-th/0012044].

[28] T. Shiromizu, K. i. Maeda and M. Sasaki, Phys. Rev. D **62**, 024012 (2000) [arXiv:gr-qc/9910076].

[29] S. Kachru, M. B. Schulz and E. Silverstein, Phys. Rev. D **62**, 045021 (2000) [arXiv:hep-th/0001206].

[30] S. Forste, Z. Lalak, S. Lavignac and H. P. Nilles, Phys. Lett. B **481**, 360 (2000) [arXiv:hep-th/0002164].

[31] P. Binetruy, J. M. Cline and C. Grojean, Phys. Lett. B **489**, 403 (2000) [arXiv:hep-th/0007029].

[32] M. Minamitsuji, Y. Himemoto and M. Sasaki, in these proceedings.

[33] K. Koyama, Phys. Rev. D **66**, 084003 (2002) [arXiv:gr-qc/0204047].

[34] D. Langlois and L. Sorbo, Phys. Lett. B **543**, 155 (2002) [arXiv:hep-th/0203036].

[35] P. Binetruy, C. Deffayet and D. Langlois, Nucl. Phys. B **615**, 219 (2001) [arXiv:hep-th/0101234].

[36] U. Gen and M. Sasaki, Prog. Theor. Phys. **105**, 591 (2001) [arXiv:gr-qc/0011078].

[37] U. Gen and M. Sasaki, Prog. Theor. Phys. **108**, 471 (2002) [arXiv:gr-qc/0201031].

[38] S. Kanno, M. Sasaki and J. Soda, arXiv:hep-th/0210250. Prog. Theor. Phys. **109** (2003), in press.

[39] S. Kanno and J. Soda, Phys. Rev. D **66**, 043526 (2002) [arXiv:hep-th/0205188].

[40] S. Kanno and J. Soda, Phys. Rev. D **66**, 083506 (2002) [arXiv:hep-th/0207029].

[41] T. Shiromizu and K. Koyama, arXiv:hep-th/0210066.

Issues on the cosmological constant

Jun'ichi Yokoyama

Department of Earth and Space Science, Graduate School of Science, Osaka University, Toyonaka 560-0043

Abstract

Some issues of the cosmological constant or dark energy are briefly reviewed. There are an increasing number of observations that constrain the equation of state of dark energy more stringently and favor the time-independent cosmological constant. Then a plausible model of dark energy would be a theory with degenerate perturbative vacua in which its origin is explained by a nonperturbative effect so that, unlike quintessence, k-essence etc., it is separable from the perturbative problem why its amplitude is smaller than the Planckian density by a factor of $\mathcal{O}(10^{-120})$.

1 Introduction

Originally the cosmological constant Λ was introduced as an undetermined constant in the left-hand-side of the Einstein equation,

$$R_{\mu\nu} - \frac{1}{2}Rg_{\mu\nu} + \Lambda g_{\mu\nu} = 8\pi G T_{\mu\nu}, \tag{1}$$

so that this equation had a static cosmological solution, guided by the strong prejudice that our Universe is static [1]. As is well known, however, the solution thus obtained is very unstable and is not realistic. As a natural consequence, it turned out that we live in a dynamically expanding universe as theoretically pointed out by Friedmann and observationally discovered by Hubble [2].

Nowadays it is more appropriate to put Λ in the right-hand-side of the Einstein equation as a part of the energy-momentum tensor. By nature the cosmological constant is equivalent to the vacuum energy density ρ_v with the following relation.

$$\rho_v = \frac{\Lambda}{8\pi G} = \frac{M_{Pl}^2}{8\pi}\Lambda = M_G^2\Lambda, \tag{2}$$

where M_{Pl} and $M_G \equiv M_{Pl}/\sqrt{8\pi} = 2.4 \times 10^{18}$GeV are the Planck mass and the reduced Planck scale, respectively.

In the field theoretical point of view, if we add the zero-point fluctuation of a quantum field up to a cutoff k_c, we find

$$\langle\rho_v\rangle = \int_0^{k_c} \frac{d^3k}{(2\pi)^3}\frac{1}{2}\sqrt{k^2+m^2} \cong \frac{k_c^4}{16\pi^2}. \tag{3}$$

Taking the cutoff k_c at the Planck scale beyond which classical gravity may not be used, we find $\langle\rho_v\rangle = 4M_G^4$. Thus the natural scale of the vacuum energy is the Planck scale [3].

Observationally cosmic energy density today is at most of order of the critical density $\rho_{cr0} \cong 10^{-120}M_G^4$. Confronting such a huge discrepancy of 120 digits between the theoretically natural value and the observationally allowed upper bound, it was considered for a long time that there exist some mechanism to make Λ exactly vanish and its quest is the conventional cosmological constant problem to which we refer the Problem I.

Recent advance of observational cosmology, however, has revealed that our Universe is in a stage of accelerated expansion now [4]. This means that there exists a tiny magnitude of cosmological constant and/or some unknown form of matter with negative pressure driving accelerated expansion which is generically termed as dark energy. To account for the origin of this small dark energy is the new cosmological constant problem referred to the Problem II.

In this talk I first summarize the currently favored observational values of the cosmological parameters and then move on to Problems I and II and approaches to their solutions. Finally I mention the expected future of our Universe.

2 Cosmological parameters

Current trend of observational cosmology is that the values of cosmological parameters are converging to that of the so-called concordance model. Although the forthcoming data of MAP satellite will certainly provide more precise informations on them, it is still remarkable that combinations of many different means of observational determination of cosmological parameters have already terminated most of the long-standing disputes on them.

2.1 Hubble parameter

The key project of the Hubble Space Telescope has determined the value of the Hubble parameter out to about 400Mpc with various secondary indicators based on the primary cephid distance which gives $H_0 = 75 \pm 10$km/s/Mpc. The results of the secondary indicators are summarized as follows.

Type Ia Supernovae	$H_0 = 71 \pm 2(\text{stat}) \pm 6(\text{syst})$km/s/Mpc
Tully-Fisher relation	$H_0 = 71 \pm 3(\text{stat}) \pm 7(\text{syst})$km/s/Mpc
Surface brightness fluctuations	$H_0 = 70 \pm 5(\text{stat}) \pm 6(\text{syst})$km/s/Mpc
Type II Supernovae	$H_0 = 72 \pm 9(\text{stat}) \pm 7(\text{syst})$km/s/Mpc
Fundamental plane of elliptical galaxies	$H_0 = 82 \pm 6(\text{stat}) \pm 9(\text{syst})$km/s/Mpc

Combining these results Freedman et al. conclude that the final result of HST key project is $H_0 = 72 \pm 8$km/s/Mpc [5].

Sunyaev-Zel'dovich effect provides other means of determination of H_0, although it suffers from fairly large systematic errors. The current result is reported as $H_0 = 60 \pm 4^{+13}_{-18}$km/s/Mpc, which is consistent with the HST result [6].

2.2 Matter density

Nonrelativistic matter consists of baryon and cold dark matter whose identity is still unknown but two primary candidates are neutralinos and axions. Observation of light elements and standard big-bang nucleosynthesis (SBBN) gives $\Omega_{\text{b0}} = (0.019 - 0.025)h^{-2}$ with $h = H_0/100$km/s/Mpc [7].

There are a number of independent observational constraints on the matter density Ω_{m0}. To name a few, the luminosity density and average mass-to-light ratio of galaxies gives $\Omega_{\text{m0}} = 0.19 \pm 0.06$ [8], while cluster baryon fraction from X-ray emissivity supplemented by Ω_{b0} from SBBN yields $\Omega_{\text{m0}} = 0.35 \pm 0.07$ [9]. On the other hand, shape parameter of the transfer function of CDM scenario of structure formation, $\Gamma = \Omega_{\text{m0}}h$ is fit by observation for $\Gamma \simeq 0.25$ which means $\Omega_{\text{m0}} \simeq 0.35$ for $h \simeq 0.7$ [10]. Although we cannot pin down the value of Ω_{m0} yet, currently favored value is around $\Omega_{\text{m0}} \simeq 0.3$.

2.3 Spatial curvature

The angular power spectrum of cosmic microwave background radiation (CMB) provides a unique probe for the spatial geometry of the Universe. In particular, the location of the first Doppler peak reflects the angular scale subtending the sound horizon at decoupling which is sensitive to spatial curvature K. Although the data before WMAP suffer from fairly large errors around the first peak [11], they favor spatially flat universe [12]. This is a good news because it is in accordance with standard inflation models. On the other hand, it raises a question: what makes up the rest of the Universe, $1 - \Omega_{\text{m0}} \simeq 0.7$? The answer is, of course, dark energy as we see below.

2.4 Vacuum energy density

Observations of the magnitude-redshift relation of high-redshift type Ia supernovae has probed the deceleration parameter $q_0 = (\Omega_{\text{m0}} - 2\Omega_{\text{v0}})/2$ in addition to H_0 and they have found that q_0 is negative or our Universe is in a stage of accelerated expansion [4], which means that significant amount of vacuum-like energy density exists today as

$$\Omega_{\text{v0}} \simeq 1.25\Omega_{\text{m0}} + 0.5 \pm 0.5. \tag{4}$$

2.5 The concordance model

Combining all the above observational data we arrive at a model with $\Omega_{m0} \simeq 0.3$, $\Omega_{v0} \simeq 1 - \Omega_{m0} \simeq 0.7$. Then the plausible range of the cosmic age lies $t_0 = (0.9 - 1.0)H_0^{-1}$. The Hubble time corresponding to $H_0 = 72 \pm 8$km/s/Mpc reads $H_0^{-1} = 12.2 - 13.6 - 16.9$Gyr, which in turn means $t_0 = 11 - 17$Gyr with the most likely value around $t_0 \simeq 13$Gyr.

Astrophysically, age of globular clusters gives $t_0 = 11 - 14$Gyr while cosmological nuclear chronology yields $t_0 = 12 - 15$Gyr. Ever since Hubble's determination of the Hubble parameter [2], $H_0 \sim 500$km/s/Mpc, we confronted with the cosmic age problem from time to time in the history of cosmology. The above set of cosmological parameters gives consistent cosmic age with astrophysical observations and indeed deserves the name of the concordance model.

Looking back more recent history of cosmology, only one and half decades ago, theorists typically expected that we live in the Einstein-de Sitter universe with $\Omega_{m0} = 1$, $\Omega_{v0} = 0$, $K = 0$, and $H_0 \sim 50$km/s/Mpc. On the other hand, observational astronomers believed that we live in an open universe with $\Omega_{m0} \lesssim 0.2$, $\Omega_{v0} = 0$, and $H_0 = 50$ or 100km/s/Mpc depending on schools [13, 14]. Thus both parties can compromise if they admit nonvanishing vacuum energy density taking an intermediate value of the Hubble parameter. A good news with the concordance model is that it supports a theoretical prejudice that the Universe is spatially flat and so is consistent with the prediction of standard inflationary cosmology, whose another prediction, generation of almost scale-invariant adiabatic fluctuations, has also been supported by observations of CMB anisotropy. Thus we can describe evolution of the Universe in the framework of inflationary cosmology. Then the greatest mystery in cosmology is the questions, what is the origin of the vacuum energy? Why is it so small?

2.6 Note added: WMAP results

On February 12, 4AM (JST), the first-year result of the Wilkinson Microwave Anisotropy Probe was disclosed [15]. As for the values of the cosmological parameters they basically confirmed those of the concordance model with significantly smaller error bars than before with $h = 0.71^{+0.04}_{-0.03}$, $\Omega_{b0}h^2 = 0.0224 \pm 0.0009$, $\Omega_{m0}h^2 = 0.135^{+0.008}_{-0.009}$, $\Omega_{v0} = \Omega_{tot0} - \Omega_{m0}$, and $\Omega_{tot0} = 1.02 \pm 0.02$. One should note, however, that the WMAP data alone could be fit by other sets of parameters whose values are quite different from those of the concordance model. The cosmic concordance is achieved as a result of combinations of various cosmological observations.

3 Proposed solutions to the Problem I

3.1 Symmetry

Whenever we encounter an unnaturally small quantity, we usually interpret it as realized by virtue of some symmetry reason. For example, in order to stabilize the Higgs' mass in the standard particle physics model against quantum correction up to grand unification or Planck scales, we usually introduce supersymmetry (SUSY).

As is well known, global SUSY also predicts vanishing vacuum energy density at the supersymmetric ground state. The SUSY generator, Q_α, satisfies the following anti-commutation relation.

$$\left\{Q_\alpha, Q_\beta^\dagger\right\} = (\sigma_\mu)_{\alpha\beta} P^\mu, \tag{5}$$

with P^μ being the four momentum. Since the supersymmetric ground state is annihilated by this operator, we inevitably find vanishing energy density there.

$$Q_\alpha |0\rangle = Q_\alpha^\dagger |0\rangle = 0 \Rightarrow \langle 0| P^\mu |0\rangle = 0. \tag{6}$$

Unfortunately, this does not help to solve the Problem I at all, because we know that supersymmetry is broken today. On the contrary, it causes a severe disaster since breaking supersymmetry inevitably induces a positive vacuum energy density with SUSY breaking scale, $\rho_v \sim (1\text{TeV})^4 \sim 10^{29}\text{gcm}^{-3}$ or larger.

This disaster is cured by making SUSY local, namely, introducing supergravity (SUGRA). In SUGRA we do not have a relation like (6) and the vacuum energy density can be either negative or positive. Usually it is negative due to a "$-3|W|^2$" term in the scalar potential where W is the superpotential. Then we may incorporate a positive contribution from SUSY breaking to fine-tune the resultant vacuum energy density vanishing. To this end, SUGRA does not solve the conceptual Problem I either.

Thus SUSY/SUGRA does not help after all and no other symmetry is known to realize vanishing vacuum energy density even after SUSY breaking.

3.2 Adjustment mechanism

This is an attempt to dynamically cancel the cosmological constant toward zero as the passage of time. In 1982 Dolgov proposed a model with a massless scalar field nonminimally coupled to the scalar curvature [16]. He showed that in this model the effective cosmological constant decreases in the manner inversely proportional to the square of cosmic time toward zero no matter how large it may be at the outset. This evolution law is the same as that in scalar-tensor model of Fujii [17] proposed in the same year. The problem with Dolgov's model is the effective gravitational constant also decreases toward zero at the same time, so it cannot serve as the solution in the real world.

As for the impossibility of finding a successful adjustment mechanism to the Problem I, there is a no-go theorem of Weinberg [3] which states that one cannot find an equilibrium solution of the field equations with vanishing cosmological constant without fine-tuning. As a simple example, consider a model with N scalar degrees of freedom ϕ_i. Then an equilibrium or stationary configuration is determined from N equations such as $\partial_{\phi_i} V[\phi] = 0$ for each $i = 1, ..., N$ where V represents the potential of the system under consideration. In order to realize vanishing vacuum energy at the equilibrium configuration, another equation should be satisfied there to ensure $\Lambda = 0$, which requires a fine-tuning because we have already used N degrees of freedom to specify the equilibrium configuration.

3.3 Quantum Cosmological Approach

This approach was quite fashionable more than a decade ago. It is based on the wave function of the universe. In Hartle-Hawking's approach [18], the wave function with three geometry h_{ij} and matter configuration ϕ is expressed by an Euclidean path integral over all the compact manifolds C' with boundary (h_{ij}, ϕ),

$$\Psi_{HH}[h_{ij}, \phi] = \int_{C'} [dg][d\phi] e^{-I[g,\phi]}. \tag{7}$$

In this prescription, the expectation value of an operator Y is given by a path integral over all the compact Euclidean manifolds C as

$$\langle Y \rangle_{HH} = \frac{(\Psi_{HH}, Y\ \Psi_{HH})}{(\Psi_{HH}, \Psi_{HH})} = \frac{\int_C [dg][d\phi] Y e^{-I[g,\phi]}}{\int_C [dg][d\phi] e^{-I[g,\phi]}}. \tag{8}$$

If this path integral is dominated by the de Sitter instanton with the action

$$I = -\frac{1}{16\pi G} \int (R - 2\Lambda)\sqrt{g} d^4x = -\frac{3\pi}{G\Lambda}, \tag{9}$$

the wave function is peaked at $\Lambda = 0$.

$$\Psi_{HH}[h_{ij}, \phi] = \int_{C'} [dg][d\phi] e^{-I[g,\phi]} \propto \exp\left(\frac{3\pi}{G\Lambda}\right), \tag{10}$$

suggesting the vanishing cosmological constant [19].

Later on Coleman proposed to incorporate sum over topology with wormhole configurations connected to mother and baby universes. Then all the physical constants become a variable dependent on the state of baby universes α and the expectation value reads,

$$\langle Y \rangle = \frac{\int [d\alpha] e^{-\frac{\alpha^2}{2}} \langle Y \rangle_\alpha Z(\{\alpha\})}{\int [d\alpha] e^{-\frac{\alpha^2}{2}} Z(\{\alpha\})}, \quad Z(\{\alpha\}) \propto \exp\left[\exp\left(\frac{3\pi}{G\Lambda(\{\alpha\})}\right)\right]. \tag{11}$$

Thus we find an even sharper peak at $\Lambda = 0$ [20]. This mechanism may also be used to fix other physical parameters. For example, strong CP problem may be solved without introducing axions [21].

In these Euclidean approaches there is no time dependence in the expressions of expectation values and they should rather be interpreted as an average expectation value throughout the possible cosmic history which would coincide with that in the most stable ground state [3].

There are a number of serious problems in these approaches. First, the Euclidean path integral is not well-defined, because, once gravity is included, the action is not positive definite even after Wick rotation. Second, no conserved and positive-definite probability current is known in this approach, which makes its interpretation difficult. Third, in the original calculation of wormhole and baby universe system, phase of sum over spheres was miscounted and the sharper peak observed in (11) diminishes in the correct calculation [22].

For these reasons, although this approach is attractive in that it is a quantum theory, this solution is not taken seriously now.

3.4 Higher dimensional models

Higher dimensional theories may open up a new perspective to the cosmological constant problem, because lower dimensional subspace may have flat geometry even if energy-momentum tensor is nonvanishing. Hence if we could succeed in removing the gravitational effect of vacuum energy on cosmic expansion of our three-brane, this could serve as a solution to the problem. For example, if we found a modified Friedmann equation of our three-brane like

$$H^2 = f(\rho, p)(\rho + p) + ..., \tag{12}$$

after an appropriate dimensional reduction, such an equation would allow for the Minkowski solution $H = 0$ in the presence of arbitrary vacuum energy density with $\rho_v = -p_v$ on the three-brane. While many ideas have been proposed these days I do not go in detail of them because there will be many brane world talks in this workshop and I hope this issue will be covered there. It seems, however, many of them require fine-tuning, some of which are as severe as the original one, to realize such an effective equation on the brane so they could hardly evade the no-go theorem.

I would like to briefly mention, however, an exception which makes use of infinite-volume extradimensions with large-distance modification of gravity on the brane proposed by Dvali, Gabadadze, and Shifman [23]. They start with an $4 + N$ dimensional action,

$$S = M_*^{2+N} \int d^4x d^N y \sqrt{G} R_{4+N} + \int d^4x \sqrt{g} \left(M_G^2 R_4 + \mathcal{L}_{\rm SM} + \Lambda_4 \right), \tag{13}$$

where M_* is the fundamental Planck scale and M_G is the four dimensional counterpart induced by quantum correction of matter in four dimension with the Lagrangian $\mathcal{L}_{\rm SM}$. In this model the four dimensional graviton $h_{\mu\nu}$ satisfies a modified equation,

$$\left[1 + \frac{F_N}{r_c^2 \Box} \right] \Box h_{\mu\nu} = 0, \tag{14}$$

where F_N is a constant and $r_c \equiv M_G/M_*^2$ is the crossover distance beyond which gravity becomes weak. It should satisfy $r_0 \gtrsim H_0^{-1} \approx 10^{28}$cm to ensure standard cosmology. Hence we should take $M_* \lesssim 10^{-3}$eV. Since the cosmological constant problem is a far-infrared (large-scale) problem, four dimensional curvature is insensitive to it in such a modified theory of gravity. Thus we may naturally have an almost flat four dimensional spacetime no matter how large Λ_4 may be. Although this model relies on a huge hierarchy $M_*/M_G \lesssim 10^{-30}$, it is stable under the assumption of unbroken supersymmetry in the bulk.

3.5 Anthropic principle

Since the cosmological constant problem is such a difficult problem to solve, it is natural that many people are tempted to resort its solution to the anthropic consideration in which one attempts to interpret natural phenomena based on our existence [24].

Consider a proposition: We, human being, cannot live in a universe with a large cosmological constant, positive or negative. We can easily convince ourselves that this proposition is correct at least qualitatively, and more quantitative proofs can be found in the literature [25]. Now consider its contraposition: The cosmological constant in our Universe is small, because human being exists. Since a proposition and its contrapositive always have the same truth value, once we convince ourselves that the above proposition is correct, it can serve as a solution to the cosmological constant problem at least logically.

But this fact alone does not guarantee that the anthropic consideration is useful in theoretical physics. Let us consider a perhaps more illustrative question: Why does our Universe have three spatial dimensions? A possible answer based on the anthropic principle is that if the spatial dimension is not equal to three, an orbit of a planet is not closed, so that its climate would be too unstable to accommodate human life. Again this solution is logically correct answer to the original question, but it is clear that such an answer provides no insights for the compactification mechanism of extra dimensions which is one of the central issue in higher-dimensional theories. Thus in this sense this approach does not contribute to progress in theoretical physics.

I do not claim that we should not use the anthropic principle at all. On the contrary, I admit that this could be useful at some stage of investigation. As for the cosmological constant, we might use it once we have reached an ultimate theory which clarifies what physics controls it but does not predict of its value itself.

The anthropic principle resembles *sake*: if you use an appropriate amount at night, you can be happy, but if you drink it too much in the morning, you will lose your job. I think it is clear that the situation of investigation of cosmological constant problem is yet in the morning or in the premature stage and use of the anthropic principle now could be dangerous because we might well miss a chance to reach an essence of theoretical physics.

Nevertheless there is an exception. We may or even should resort the solution of what is called the coincidence problem or why-now problem, namely the question why vacuum energy is dominating only recently, to the anthropic principle, because "now" is defined by our very existence.

4 Proposed solutions to the Problem II

I now move on to various proposals to explain the origin of the tiny dark energy density observed. They are based on a common assumption that there exists some ground state with a vanishing vacuum energy density where the Problem I is solved. I would also like to note that two of the suggested solutions to the Problem I, namely the anthropic consideration [25] and Dvali et al's higher dimensional model [23], may also naturally accommodate a tiny nonvanishing dark energy density.

4.1 Decaying Λ or quintessence

This is an attempt to identify the vacuum-like energy density with a dynamical, slowly-changing and possibly spatially inhomogeneous component with negative pressure [16, 17, 26, 27]. Typical example is a scalar field Q, now called quintessence, slowly rolling down its extremely flat potential [26, 28]. By virtue of its time dependence, the Problem II, or why the observed value of the dark energy today is unnaturally small compared with, say, the Planck scale, may be relaxed. In fact, by choosing an appropriate shape of the potential $V[Q]$ it has been advocated that one can find a natural solution to the coincidence problem in which the energy density of the quintessence field decreases during radiation domination tracking evolution of the total energy density and becomes dominant some time after the equality time. Such a tracker solution is possible with a potential like $V[Q] = M^4(M_G/Q)^n$ with $n > 0$ or $V[Q] = M^4\left[\exp\left(M_G/Q\right) - 1\right]$, both with a canonical kinetic term. By nature of the tracker solution, the scalar field is still evolving today in the time scale of cosmic expansion, which means that the equation of state satisfies

$$w_Q = \frac{p_Q}{\rho_Q} = \frac{\dot{Q}^2/2 - V[Q]}{\dot{Q}^2/2 + V[Q]} \gtrsim -0.75,$$

and that its mass is comparable to the Hubble parameter today, $m_Q = \sqrt{V''[Q]} \approx H_0 = 10^{-33}\mathrm{eV}$.

As will be seen below the above characteristic of the equation of state is now confronting with observational tests. Furthermore from theoretical view point it is difficult to build a sensible particle physics model to realize such a small effective mass with a huge hierarchy $m_Q/M_w = 10^{-44} = 10^{-26}M_w/M_G$, where M_w is the weak scale. Nevertheless such a small mass might be stably realized if protected by some symmetry. One example is the model proposed by Nomura, Watari, and Yanagida [29] in which the quintessence field is identified with a pseudo Nambu-Goldstone boson. This model, unfortunately, does not lead to a tracker behavior.

4.2 Kinetically driven quintessence

It was observed by Armendáriz-Picón, Damour, and Mukhanov that a scalar field can drive inflation even if it has no potential provided that it has an appropriate non-canonical kinetic term [30]. This idea was first applied to explain the accelerated expansion observed today by Chiba, Okabe, and Yamaguchi under the name of kinetically driven quintessence [31]. Now it is abbreviated as k-essence [32, 33]. The evolution of the equation of state, w, is highly nontrivial in this class of models and may be observationally tested. An example of the scalar Lagrangian giving rise to a desired recent cosmic acceleration is given by [32]

$$L = \frac{1}{\varphi^2}\left(2\sqrt{1+X} - 2.01 + 0.03\left(10^{-5}X\right)^3 - \left(10^{-6}X\right)^4\right), X \equiv -\frac{1}{2}(\partial\varphi)^2 = \frac{1}{2}\dot{\varphi}^2. \tag{15}$$

4.3 QCD trace anomaly

The QCD trace anomaly contributes to the vacuum energy density with the amount

$$\left\langle F^a_{\mu\nu}F^{\mu\nu}_a\right\rangle = \mathcal{O}\left(\Lambda^4_{\rm QCD}\right) \approx \mathcal{O}\left((100{\rm MeV})^4\right). \tag{16}$$

Suppose that this contribution is canceled by the intrinsic cosmological constant in Minkowski vacuum state which is a part of the usual assumption that the Problem I is solved in the ground state. Then Schützhold [34] calculates the same quantity in the Friedmann vacuum under this assumption and finds a weakly time-dependent dark energy density

$$\rho_{\rm v} = \mathcal{O}\left(\Lambda^3_{\rm QCD}H\right). \tag{17}$$

Although this proposal is attractive in that it is a result of serious calculation of quantum field theory in the curved spacetime, the resultant value might be too large, $\Lambda^3_{\rm QCD}H_0 \gtrsim 30\rho_{\rm cr0}$ for $\Lambda_{\rm QCD} \gtrsim 100{\rm MeV}$.

4.4 False vacuum energy

All the proposals to the problem II discussed so far predict time-dependent dark energy. But we should also consider the possibility that we live in a false vacuum state with a finite vacuum energy density. Most people believe that such a possibility is unnatural due to the smallness of the observed vacuum energy, $\rho_{\rm v} = 10^{-120}M_G^4 = ({\rm meV})^4$. Several attempts do exist, however, to explain the existence of a false vacuum state with the desired magnitude of vacuum energy density naturally by introducing some discrete symmetry [35] or global symmetry [36] and then breaking it with some appropriate nonrenormalizable terms.

4.5 Non-perturbative explanation with degenerate vacua

Another possibility that predicts time-independent dark energy without introducing any tiny numbers is a theory with degenerate perturbative vacua. It starts with the observation that the cosmological constant Problem I is a perturbative problem, that is, why we observe vanishingly small vacuum energy even after perturbative quantum correction, (3), and we assume that this problem is solved by a yet unknown mechanism as assumed in all the other proposals above. If there exist two or more degenerate perturbative vacua, say, $|+\rangle$ and $|-\rangle$ whose vacuum energy is vanishing under the assumption that the perturbative Problem I is solved there, and if quantum tunneling between perturbative vacua is possible, these states are no longer the real ground state. Including the effect of quantum tunneling, which we

assume is described by an instanton with the Euclidean action S_0, the energy eigen states are given by superposition of perturbative vacua,

$$|S\rangle = \frac{1}{\sqrt{2}}(|+\rangle + |-\rangle), \quad |A\rangle = \frac{1}{\sqrt{2}}(|-\rangle + |-\rangle), \tag{18}$$

where $|S\rangle$ is the real ground state with $\rho_v = -m^4 e^{-S_0}$ and the first excited state is $|A\rangle$ with $\rho_v = m^4 e^{-S_0}$, with m being the energy scale associated with the quantum transition. Thus each perturbative vacua is expressed by the superposition of energy eigenstates with exponentially small energy gap, and if we still live in one of the perturbative vacua we observe a finite magnitude of dark energy density $\rho_v = m^4 e^{-S_0}$ with the probability of 50% in this case. In order to match the predicted value with the observed value, we should take $S_0 = 120 \ln 10 + 4 \ln(m/M_G)$, and the longevity of the perturbative vacua requires $m \gtrsim M_G$ [37].

This solution is attractive in two aspects: one is that the Problems I and II are properly separated and the other is that, as mentioned above, it involves no small numbers and the smallness of the observed dark energy is the largeness of the instanton action. The former feature may particularly be important because in other proposals no explanations have been given why *only* the contribution of quintessence or k-essence fields to the vacuum energy density remains finite after solving the Problem I.

5 Observational constraints on dark energy

In order to examine which, if any, of the above proposals is the right one, it is important to observationally constrain the equation of state, $w = p/\rho$, of dark energy. An increasing number of observational analysis have been done these days.

For example, Corasaniti and Copeland used SNIa data and the location of the three peaks of CMB anisotropy and obtained an ambitious constraint $-1 \leq w \leq -0.93$ [38].

Melchiorri, on the other hand, performed a joint analysis of CMB, SNIa, HST, and the large-scale structures and concluded $w \leq -0.85$ at 1σ and $w \leq -0.72$ at 2σ [39]. His result is perfectly consistent with the cosmological constant $w = -1$.

Percival et al. finds from 2dF data combined with CMB anisotropy $w \leq -0.51$ at 2σ and the probability distribution of w is peaked around $w = -1$, namely, they favor the cosmological constant [40].

From REFLEX sample of the redshift distribution of X-ray clusters combined with SNIa data, Schuecker et al. find $w = -0.95^{+0.30}_{-0.35}$ under the assumption of spatially flat Universe [41] and claims that the most natural interpretation of the data is the cosmological constant.

Thus we may conclude that the tracker solution of the quintessence scenario is already in a difficult situation and that currently available data seem to favor the cosmological constant. Note that CMB data used above are pre-WMAP ones. The new constraint obtained with WMAP is $w < -0.78$ at 2σ [15].

6 The future of the Universe dominated by Λ

If our Universe is dominated by time-independent vacuum energy density as suggested by numerous observations and if it is stable against phase transitions, we can draw some interesting conclusions about the future of our Universe [42, 43].

The existence of a positive cosmological constant means that our Universe is in a stage of asymptotically de Sitter expansion. So there will be an event horizon at the distance ≈ 5.1 Gpc and we cannot go to any galaxies with $z > 1.8$ not only in practice but also in principle. We can observe a galaxy at $z = 5$ only for 6.4 Gyr from now.

Future evolution of nearby large-scale structure in our Universe dominated by a cosmological constant has been studied by Nagamine and Loeb using an N-body simulation [44]. They find:

- Evolution of large-scale structure continues for 28 Gyrs.
- Our local group will not be bound to the Virgo cluster.
- Our galaxy is likely to merge with Andromeda galaxy within the Hubble time.

- This will be the only galaxy within the horizon 100 Gyr later.

This means that extragalactic astronomy and cosmology must be solved within 100 Gyr. So we should hurry up!

References

[1] A. Einstein, Preuss. Akad. Wiss. Berlin Sitzer. (1917) 142.

[2] E.P. Hubble, Proc. Nat. Acad. Sci. **15** (1929) 168.

[3] S. Weinberg, Rev. Mod. Phys. **61** (1989) 1.

[4] S. Perlmutter et al., ApJ, **517** (1999) 565; A.G. Riess et al., AJ, **116** (1998) 1009.

[5] W. L. Freedman et al., ApJ. **553** (2001) 47.

[6] E. D. Reese, J. E. Carlstrom, M. Joy, J. J. Mohr, L. Grego and W. L. Holzapfel, ApJ **581** (2002) 53.

[7] R.H. Cyburt, B.D. Fields, and K.A. Olive, arxiv:astro-ph/0302431.

[8] R.G. Carlberg, H.K.C. Yee, and E. Ellingson, ApJ **478** (1997) 462.

[9] D.A. White, A.C. Fabian, MNRAS **273** (1995) 73.

[10] J.A. Peacock and S.J. Dodds, MNRAS **267** (1994) 1020

[11] P. de Bernardis et al., Nature **404**(2000) 955; S. Hanany et al., ApJ **545** (2000) L5.

[12] A. H. Jaffe et al. [Boomerang Collaboration], Phys. Rev. Lett. **86** (2001) 3475.

[13] A. Sandage and G.A. Tammann, ApJ **256** (1982) 339.

[14] G. de Vaucouleurs and H.G. Corwin jr., ApJ **297** (1985) 23.

[15] C.L. Bennett et al., arXiv:astro-ph/0302207; D.N. Spergel et al., arXiv:astro-ph/0302209.

[16] A.D. Dolgov, In "Very Early Universe" Eds. G.W. Gibbons, S.W. Hawking, and S.T. Siklos, (Cambridge 1982) 449.

[17] Y. Fujii, Phys. Rev. **D26** (1982) 2580.

[18] J.B. Hartle and S.W. Hawking, Phys. Rev. D **28** (1983) 2960.

[19] E. Baum, Phys. Lett. B **133** (1983) 185; S.W. Hawking, Phys. Lett. B **134** (1984) 403.

[20] S. R. Coleman, Nucl. Phys. B **310** (1988) 643.

[21] H. B. Nielsen and M. Ninomiya, Phys. Rev. Lett. **62** (1989) 1429.

[22] J. Polchinski, Phys. Lett. B **219** (1989) 251.

[23] G. Dvali, G. Gabadadze and M. Shifman, arXiv:hep-th/0208096.

[24] For a review, see *e.g.* J.D. Barrow and F.J. Tipler, "The Anthropic Cosmological Principle" (Oxford 1986).

[25] S. Weinberg, Phys. Rev. Lett. **59** (1987) 2607; G. Efstathiou, MNRAS **274** (1995) L73;J. Garriga and A. Vilenkin, Phys. Rev. D **61** (2000) 083502.

[26] B. Ratra and P. J. Peebles, Phys. Rev. D **37** (1988) 3406.

[27] K. Sato, N. Terasawa, and J. Yokoyama, in "The Quest for the Fundamental Constants in Cosmology" Eds. J. Audouze and J. Tran Thanh Van (Editors Frontieres, 1989) 193.

[28] I. Zlatev, L. Wang, and P.J. Steinhardt, Phys. Rev. Lett. **82** (1999) 896; P.J. Steinhardt, L. Wang, and I. Zlatev, Phys. Rev. **D59** (1999) 23504.

[29] Y. Nomura, T. Watari and T. Yanagida, Phys. Lett. B **484** (2000) 103.

[30] C. Armendariz-Picon, T. Damour and V. Mukhanov, Phys. Lett. B **458** (1999) 209.

[31] T. Chiba, T. Okabe and M. Yamaguchi, Phys. Rev. D **62** (2000) 023511.

[32] C. Armendariz-Picon, V. Mukhanov and P. J. Steinhardt, Phys. Rev. Lett. **85** (2000) 4438.

[33] C. Armendariz-Picon, V. Mukhanov and P. J. Steinhardt, Phys. Rev. D **63** (2001) 103510.

[34] R. Schutzhold, Phys. Rev. Lett. **89** (2002) 081302.

[35] W. D. Garretson and E. D. Carlson, Phys. Lett. B **315** (1993) 232.

[36] S. M. Barr and D. Seckel, Phys. Rev. D **64** (2001) 123513.

[37] J. Yokoyama, Phys. Rev. Lett. **88** (2002) 151302; Int. J. Mod. Phys. D **11** (2002) 1603.

[38] P. S. Corasaniti and E. J. Copeland, Phys. Rev. D **65** (2002) 043004.

[39] A. Melchiorri, arXiv:astro-ph/0204262.

[40] W.J. Percival et al. MNRAS, **337** (2002) 1068.

[41] P. Schuecker, R. R. Caldwell, H. Bohringer, C. A. Collins and L. Guzzo, arXiv:astro-ph/0211480.

[42] A. A. Starobinsky, Grav. Cosmol. **6** (2000) 157.

[43] A. Loeb, Phys. Rev. D **65** (2002) 047301.

[44] K. Nagamine and A. Loeb, arXiv:astro-ph/0204249.

Self-Similar Solutions, Critical Behavior and Convergence to Attractor in Gravitational Collapse

Tomohiro Harada,[1]

Department of Physics, Waseda University
Shinjuku, Tokyo 169-8555, Japan

Abstract

General relativity as well as Newtonian gravity admits self-similar solutions due to its scale-invariance. This article is a review paper on these self-similar solutions and their relevance to gravitational collapse. In particular, our attention is mainly paid on the crucial role of self-similar solutions in the critical behavior and attraction in gravitational collapse.

1 Introduction

The basic equation of general relativity is the Einstein equations. Since the Einstein equations are simultaneous second-order partially differential equations (PDEs), it is not easy to obtain solutions. It is useful to assume symmetry such as spherical symmetry and staticity in obtaining solutions. However, it is often difficult to obtain inhomogeneous and dynamical solutions. In this context, it is quite useful to assume *self-similarity*. For example, in spherical symmetry, this assumption reduces the PDEs to a set of ordinarily differential equations (ODEs). Therefore, the assumption of self-similarity is very powerful in finding exact and/or numerical dynamical and inhomogeneous solutions. The application of self-similar solutions is very large including cosmological perturbations, star formation, gravitational collapse, primordial black holes, cosmological voids and cosmic censorship. Among them, the most widely researched model is the spherically symmetric self-similar system with perfect fluids, which was pioneered by by Cahill and Taub (1971) in general relativity and by Penston (1969) and Larson (1969) in Newtonian gravity.

In recent progress in general relativity, self-similar solutions have called attention not only because they are easy to obtain but also because they may play important roles in cosmological situations and/or gravitational collapse. One of the important roles of self-similar solutions is to describe asymptotic behaviors of more general non-self-similar solutions. This role has been shown explicitly in several models such as homogeneous cosmological models. In cosmological context, the suggestion that spherically symmetric fluctuations might naturally evolve from complex initial conditions via the Einstein equations to a self-similar form has been termed the 'similarity hypothesis' (Carr 1993, Carr and Coley 1999). The hypothesis has been also suggested to hold in more general situations, including gravitational collapse.

In the present article, we pay attention to a spherically symmetric system with a perfect fluid. For this system, recent numerical simulations of PDEs have revealed two interesting behaviors in gravitational collapse, one is the critical behavior and the other is the convergence to attractor. The critical behavior was observed around the threshold of black hole formation. There is a self-similar solution that sits at the threshold, which is called a critical solution. For near-critical collapse, the solution first approach the critical solution but diverges away from this solution after that. There is observed the scaling law for the formed black hole for supercritical collapse. This is observed only as a result of fine-tuning the parameter which parametrizes initial data. On the other hand, the convergence to attractor is observed without fine-tuning. The density and velocity fields around the center approach those of another self-similar solution in an approach to the formation of singularity at the center, which is called an attractor solution.

The main claim of this review article is that the critical behavior and convergence to attractor in gravitational collapse are both well understood in the context of self-similarity hypothesis and stability analysis in gravitational collapse. The difference between these two behaviors is in the stability of the

[1] E-mail:harada@gravity.phys.waseda.ac.jp

pertinent self-similar solution. We also briefly review the recent work on how these two behaviors are in Newtonian gravity.

2 Self-similarity

In general relativity, self-similarity or *homothety* is covariantly defined in terms of the homothetic vector ξ which satisfies the homothetic Killing equation

$$\mathcal{L}_\xi g_{\mu\nu} = 2g_{\mu\nu}. \tag{1}$$

We consider a perfect fluid as matter field, the stress-energy tensor of which is given by

$$T^{\mu\nu} = (\rho + P)u^\mu u^\nu + Pg^{\mu\nu}. \tag{2}$$

In a spherically symmetric spacetime with self-similarity, where the homothetic vector is neither parallel nor orthogonal to the four velocity of the fluid element, the line element is written in terms of the comoving coordinate r as (Cahill and Taub 1971)

$$ds^2 = -e^{\sigma(\xi)}dt^2 + e^{\omega(\xi)}dr^2 + r^2S^2(\xi)(d\theta^2 + \sin^2\theta d\phi^2), \tag{3}$$

where $\xi = t/r$. In this coordinate system, the dimensionless quantity h such as e^σ, e^ω and S has scale-invariance in the following sense:

$$h(t,r) = h(at,ar) = h(\xi), \tag{4}$$

where $a > 0$ is an arbitrary constant. For a self-similar spacetime, the density field ρ is given via the Einstein equations by

$$\rho(t,r) = a^2\rho(at,ar). \tag{5}$$

It implies that the density field is written as

$$\rho(t,r) = \frac{1}{8\pi r^2}\eta(\xi). \tag{6}$$

Therefore, the time evolution is equivalent with the scale transformation. An example of the time evolution of the density field is displayed in Fig. 1.

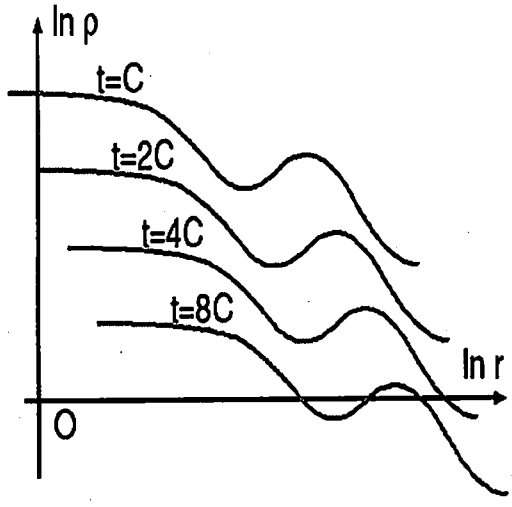


Figure 1: Schematic picture for the self-similar evolution of the density field.

The above definition of self-similarity can be generalized. One possibility is to discretize the above definition: the dimensionless quantity h satisfies

$$h(t,r) = h(at,ar), \quad a = e^{n\Delta}, \tag{7}$$

where $n = 0, \pm 1, \pm 2, \cdots$. This kind of self-similarity is referred to as *discrete self-similarity*. The discrete self-similar solution has been found to be important in the critical behavior observed in the gravitational collapse of a massless scalar field (Choptuik 1993) and gravitational waves (Abrahams and Evans 1993). In this context, the originally defined self-similarity is referred to as *continuous self-similarity*.

Another possible generalization is to allow the dimensionless quantity h to be a function of r/t^a. The generalization along this direction was done by Carter and Henriksen (1989,1991) and is referred to as *kinematic self-similarity*. The kinematic self-similarity is covariantly defined by the existence of kinematic self-similarity vector, which satisfies

$$\mathcal{L}_\xi g_{\mu\nu} = 2\delta g_{\mu\nu}, \quad \mathcal{L}_\xi u_\mu = \alpha u_\mu, \tag{8}$$

where δ and α are arbitrary constants. See Coley (1997), Benoit and Coley (1998) and Maeda et al. (2002a, 2002b, 2003) for more details of kinematic self-similarity and kinematic self-similar solutions. In this context, the originally defined self-similarity is referred to as *first-kind self-similarity*.

3 Self-similar solutions

Hereafter we mainly concentrate on the originally defined self-similarity and refer to it simply as self-similarity unless it is confusing. For a perfect fluid, the Einstein equation requires that the equation of state be given by the following form:

$$P = k\rho, \tag{9}$$

where k is constant (Cahill and Taub 1971). The fluid is referred to as a dust fluid for $k = 0$, a radiation fluid for $k = 1/3$ and a stiff matter for $k = 1$. There are infinitely many self-similar solutions. These solutions are obtained by solving ODEs. The classification of self-similar solutions of this system has been done in the homothetic approach by Goliath, Nilsen and Uggla (1998a, 1998b) and in the comoving approach by Carr and Coley (2000a, 2000b). For the complementarity of these two approaches, see Carr et al. (2001). For a brief review of self-similar solutions and, in particular, the classifications of them, see Carr and Coley (1999).

In obtaining physical solutions, it will be required that the solution be obtained from regular initial conditions. In particular, the physical solution must have the initial data with regular center. For $0 < k < 1$, the central density parameter D_0, which is defined by

$$D_0 \equiv 4\pi\rho(t,0)t^2, \tag{10}$$

well parametrizes the regular center of self-similar solutions, where t is chosen to be negative. For the regular center of self-similar solutions, the D_0 is finite and does not depend on t because

$$D_0 = \lim_{r\to 0+} 4\pi\rho(t,r)t^2 = \lim_{\xi\to-\infty} \frac{1}{2}\xi^2\eta(\xi). \tag{11}$$

For $0 < k < 1$, the ODEs have a singular point which is called a sonic point, at which the relative speed $|V|$ of the fluid element to the curve $\xi = \text{const}$ is equal to the sound speed $\sqrt{k}$. The matching condition beyond the sonic point results in nontrivial reduction of self-similar solutions. The reduction of the self-similar solutions was demonstrated by Ori and Piran (1990). If we require regularity, by which we mean the continuity of first derivatives, the possible solutions make a band structure in the space of all solutions. The D_0 axis is divided into allowed ranges and forbidden ranges (for which the solution terminates at the sonic point). If we further require analyticity (Taylor-series expandability), the possible solutions are discretized. The regular center is also analytic, where it should be noted that the analyticity at the center is defined with respect to the local Cartesian coordinates. However, only a discrete set of values for D_0 is allowed for the analyticity of the sonic point.

This complicated structure of physical solutions is due to the character of the sonic point as a critical point of the autonomous system, which was studied by Bicknell and Henriksen (1978). The sonic point regarded as a critical point of the autonomous system of ODEs after an appropriate transformation and is considered in the two-dimensional subspace of the whole state space. As a result, sonic points are classified into nondegenerate nodes, degenerate nodes, saddles and foci, among which the foci are unphysical. For every physical sonic point, there are two possible directions along which solutions can cross the sonic point, and there are two analytic solutions corresponding to these two directions. For a nondegenerate node, the two directions are called primary and secondary ones. For the former, there are one-parameter family of regular solutions including one of the analytic solutions, while for the latter, another analytic solution alone is possible. For a degenerate node, the two directions are degenerate and there are one-parameter family of regular solutions including the one analytic solution. For a saddle one, all that are regular at the sonic point are the two analytic solutions alone.

The numerical solutions with analytic initial data were investigated by Ori and Piran (1987, 1990) and Foglizzo and Henriksen (1993). This discrete set of solutions includes the flat Friedmann solution, general relativistic counterpart of the Larson-Penston solution, and that of the Hunter family of solutions. However, it is noted that the whole set of self-similar solutions with analytic initial data is still uncertain because of the numerical difficulty. Hereafter we refer to the general relativistic Larson-Penston solution and Hunter (a) solution as the Ori-Piran solution and Evans-Coleman solution for convenience. The most researched nontrivial self-similar solutions are the Ori-Piran and Evans-Coleman solutions. For the character of the sonic point, the Ori-Piran solution crosses a degenerate node along the secondary direction for $0 < k \lesssim 0.036$, a degenerate node for $k \simeq 0.036$ and a nondegenerate node along the primary direction for $0.036 \lesssim k < 1/3$ (Ori and Piran 1990, Harada 2001). Carr et al. (2001) investigated the detailed nature of the Evans-Coleman solution for $0 < k < 1$. The Evans-Coleman solution exists for $0 < k \leq 1$ (Brady et al. for $k = 1$). It crosses a saddle for $0 < k \lesssim 0.41$, a nondegenerate node along the secondary direction for $0.41 \lesssim k \lesssim 0.89$, a degenerate node for $k \simeq 0.89$ and a nondegenerate node along the primary direction for $0.89 \lesssim k < 1$. The Ori-Piran solution describes coherent collapse, while the Hunter family of solutions some oscillative collapse. The Hunter family of solutions are well labelled by the number of zeroes in their velocity fields. Ori and Piran (1987, 1990) also pointed out that a naked singularity forms in the Ori-Piran solution for $0 < k \lesssim 0.0105$, which may have some implication to cosmic censorship proposed by Penrose (1969, 1979). (See Harada, Iguchi and Nakao (2002) for recent works in naked singularity physics.) Actually, the general relativistic counterpart of the Hunter family of solutions with more than one oscillation can also have a naked singularity (Ori and Piran 1990, Foglizzo and Henriksen 1993). It is not clear whether nontrivial solutions other than the Evans-Coleman solution exist for every value of $k \in (0, 1]$, although numerical studies suggest that the structure of the solutions is common at least for $0 < k \leq 9/16$ (Ori and Piran 1990, Foglizzo and Henriksen 1993). The density profiles for these solutions are shown in Fig. 2.

For $k = 0$, i.e., a dust fluid, things are somewhat different. Ori and Piran (1990) studied self-similar dust solutions with regular center. There is one-parameter family of solutions. The regularity at the center requires that the central density parameter D_0 be $2/3$. The solutions are parametrized not by the central density parameter but by the central third-order derivative of the density field. However, this regular center is not analytic except for the flat Friedmann solution because the third-order derivative of the density field is not zero. Therefore, if we require that a physical solution has analytic initial data, the only allowed solution is the flat Friedmann solution. There is no sonic point for the dust case. See Carr (2000) for more general class of self-similar dust solutions.

4 Critical behavior

The critical behavior in gravitational collapse was numerically discovered by Choptuik (1993) in the spherical system of a massless scalar field. For a one-parameter family of initial data sets for this system, a critical value is found beyond which the evolution results in black hole formation (see Fig. 3(a)). For near-critical values, the critical behavior is observed. The solution first tends to a discrete self-similar solution, which is called a critical solution, and diverges away after that. For near-critical and supercritical

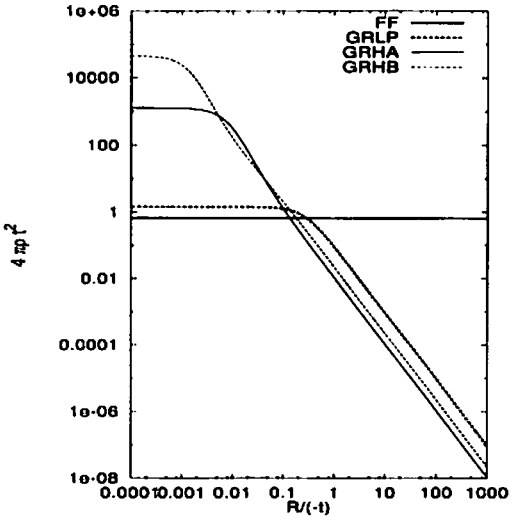


Figure 2: Density profiles for self-similar solutions with analyticity for $k = 0.01$. 'FF', 'GRLP' and 'GRHA' denote the flat Friedmann solution, general relativistic Larson-Penston solution or Ori-Piran solution and general relativistic Hunter (a) solution or Evans-Coleman solution, respectively.

collapse, the mass of the formed black hole follows a power law as

$$M_{BH} \propto |p - p^*|^\gamma, \tag{12}$$

where the constant γ is called a critical exponent (see Fig. 3(b)). The critical exponent for this system was estimated to be ≈ 0.37. After this discovery, a similar behavior was observed in various systems, such as gravitational waves (Abrahams and Evans 1993), a radiation fluid (Evans and Coleman 1994), a perfect fluid, a stiff matter (Neilsen and Choptuik 2000) and so on. Then, it has been found that the critical solution can be a discrete self-similar solution or continuous self-similar solution, depending on the system. For the fluid system including the radiation fluid system, the critical solution has continuous self-similarity. For the system of a radiation fluid, Evans and Coleman (1994) estimated the critical exponent to be ≈ 0.36 and also found that the critical solution obtained as a result of numerical simulations of the PDEs agrees very well with one of the continuous self-similar solutions which are obtained by integrating the ODEs. (That is why we refer to this self-similar solution as the Evans-Coleman solution in this article. We shall avoid the term 'critical solution' to refer to this solution because whether this solution is a critical solution may depend on the system, for example, whether we allow nonspherical perturbations or not, as we will mention later.) It has been subsequently found that the value of the critical exponent is not universal but depends on the parameter k which parametrizes the equation of state $P = k\rho$.

Koike, Hara and Adachi (1995) gave a clear picture for the critical behavior, which is called a renormalization group approach. According to this picture, the critical solution is assumed to be a self-similar solution with analytic initial data with a single unstable mode. We consider the time evolution of the solution with respect to the self-similarity coordinates $\tau \equiv -\ln|t|$ and $x \equiv -\ln|\xi|$. Then, the time evolution is regarded as a flow in the space of functions of x. The self-similar solution with a single unstable mode, which is a fixed point in the space of functions of x, has a stable manifold of codimension one. This implies that a one-parameter family of initial data generically has intersection with the stable manifold. The collapse which develops from the initial data set which is the intersection corresponds to the critical collapse, while near-critical collapse develops from the initial data set near the intersection. After a long time, the deviation of the near critical collapse from the critical solution is dominated by the single unstable mode, i.e.,

$$h(\tau, x) \approx H_{ss}(x) + (p - p^*)e^{\kappa\tau}F_{rel}(x), \tag{13}$$

where H_{ss} is the critical solution and κ and F_{rel} are the eigenvalue and eigenfunction of the single unstable

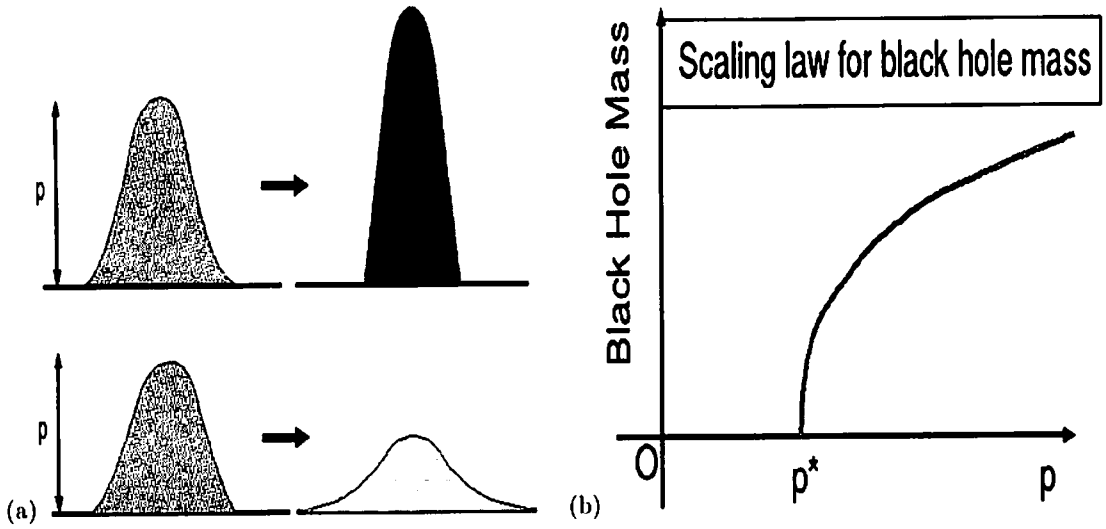


Figure 3: Schematic pictures for the critical behavior in gravitational collapse. (a) indicates that the gravitational collapse has critical nature in general. In (b), the scaling law for the formed black hole is schematically displayed.

mode. Since the apparent horizon appears when the deviation becomes $O(1)$, the mass of the black hole is estimated as

$$M = O(r) = O(e^{-\tau}) \propto |p - p^*|^\gamma \tag{14}$$

where $\gamma = \kappa^{-1}$. The eigenvalue and eigenfunction of the unstable mode are determined by the linearized Einstein equation with the regularity condition both at the center and at the sonic point. Koike, Hara and Adachi calculated the critical exponent to be ≈ 0.3558019 by the eigenvalue analysis, which agrees very well with the estimated value ≈ 0.36 from the numerical simulation.

Critical phenomena in gravitational collapse have been observed and widely researched in a great variety of systems. The implication to the formation of primordial black holes was also discussed.

One of the interesting systems is the spherical system of a stiff matter. Neilsen and Choptuik (2000) observed the critical behavior in the stiff-matter system and found that the critical solution is a continuous self-similar solution. They also estimated the critical exponent to be 0.96 ± 0.02. Brady et al. (2002) confirmed that the Evans-Coleman solution for $k = 1$ has a single unstable mode and that the critical exponent derived from the eigenvalue analysis agrees well with that estimated from the result of numerical simulations of the PDEs. This critical behavior for the stiff-matter system seems to be totally different from that for the scalar-field system. On the other hand, a massless scalar field is equivalent with a stiff matter under certain circumstances (Madsen 1988, Brady et al. 2002). Brady et al. (2002) pointed out that the critical solution, which is discrete self-similar, for the system of a massless scalar field cannot be constructed from the stiff matter because the equivalence is broken.

See Gundlach (1998, 1999) for a recent review of critical phenomena in gravitational collapse.

5 Stability

The stability of self-similar solutions against spherically symmetric perturbations has called much attention in the context of the critical behavior in gravitational collapse since Koike, Hara and Adachi (1995) showed that the critical behavior is understood in terms of the behavior of the unstable mode of the critical solution.

There are two types of spherically symmetric perturbations, analytic modes and kink modes. First we consider the analytic modes. The perturbation for a dimensionless quantity h is written as

$$h(\tau, x) = h_0(x) + \delta h(\tau, x). \tag{15}$$

After the linearization with respect to the perturbation, the perturbation δh is separated in two factors as

$$\delta h(\tau, x) = \epsilon e^{\kappa \tau} F(x). \tag{16}$$

For $0 < k \leq 1$, when the regularity condition is imposed both at the center and at the sonic point, the κ must take a discrete set of values. In other words, the allowed values for κ are determined as eigenvalues. If $\kappa > 0$, the mode is growing and referred to as an unstable mode. The stability of the Evans-Coleman solution has been investigated by Koike, Hara and Adachi (1995) for $k = 1/3$ and by Maison (1996), Koike, Hara and Adachi (1999), Harada and Maeda (2001) for more general value of $k \in (0, 1)$, and Brady et al. (2002) for $k = 1$. All these works have shown that the Evans-Coleman solution has a single analytic unstable mode for $0 < k \leq 1$. For the Evans-Coleman solution, which has a single unstable mode, the inverse of the eigenvalue of the unstable mode is interpreted as the value of the critical exponent, as we have seen in Sec. 4. The results are summarized in Fig. 4. The critical exponents directly estimated from the mass-scaling law obtained after the numerical simulations of the PDEs are also plotted.

The stability of other self-similar solutions with analytic initial data were investigated by Koike, Hara and Adachi (1999) and Harada and Maeda (2001). Then, it has been found that the Ori-Piran solution have no unstable mode, while the general relativistic counterpart of the Hunter-family solutions have unstable modes, the number of which agrees with the number of zeroes in the velocity field at least for the solutions examined there. Since the nonuniqueness of unstable modes implies that the codimension of the stable manifold is greater than one, it is expected that the approach to the self-similar solution is realized only as a result of fine-tuning more than one parameters simultaneously. This is the reason why the numerical simulations of the PDEs do not hit the self-similar solution with more than one unstable modes. On the other hand, since the Ori-Piran solution has no unstable mode, it is expected that generic evolution go towards this solution without any fine-tuning. In the next section, we will see that actually this is the case.

Next, for the kink modes, the existence in general relativity was expected by Ori and Piran (1990) and demonstrated by Harada (2001). For the analysis, we consider the initial perturbations which satisfy the following conditions: (For a while, we assume $t < 0$ and later will mention the case for $t > 0$.) (1) The initial perturbations vanish inside the sonic point. (2) The density field is continuous. (3) The density gradient field is discontinuous at the sonic point, although it has definite one-sided values inside and outside. See Fig. 5(a) for the initial setting of perturbations. The evolution of the density gradient at the sonic point turns out to be local, which simplifies the analysis. The analysis of the kink mode is possible in full order. Then, it is found that the stability against the kink mode is closely related to the classification of the sonic point, where the instability is defined by the blow up of the density gradient in a finite interval in terms of the time coordinate τ.

The result is as follows. All primary-direction nodal-point solutions, degenerate-nodal-point solutions, and saddle-point anti-transsonic solutions are unstable against the kink mode, while all secondary-direction nodal-point solutions, and saddle-point transsonic solutions are stable against the kink mode. The situation is reversed for $t > 0$ except for the case of degenerate-nodal-point solutions, which are unstable against the kink mode both for $t > 0$ and $t < 0$. Figure 5(b) shows the nonlinear evolution of the kink mode for a sonic point which is a nondegenerate node, as a typical example.

When we apply this criterion to the known solutions, we obtain the following results for the stability against the kink mode. The flat Friedmann (collapsing) solution is unstable for $0 < k < 1/3$ while stable for $1/3 \leq k < 1$. The Ori-Piran solution is stable for $0 < k \lesssim 0.036$ while unstable for $0.036 \lesssim k < 1/3$. The Evans-Coleman solution is stable for $0 < k \lesssim 0.89$ while unstable for $0.89 \lesssim k < 1$. Moreover, all regular but nonanalytic (collapsing) solutions are unstable.

The kink instability of the Evans-Coleman solution for $0.89 \lesssim k < 1$ will affect the critical behavior of a perfect fluid. However, Neilsen and Choptuik (2000) observed the critical behavior even for $0.89 \lesssim k \leq 1$ which is considered to be continuous extrapolation of that for $0 < k \lesssim 0.89$. It has not been explicitly shown but is suggested that the Evans-Coleman solution has a single analytic unstable mode even for $0.89 \lesssim k < 1$ from their result. Moreover, it was also reported that the Evans-Coleman solution has a single analytic unstable mode for $k = 1$ (Brady et al. 2002). About the reason why the kink instability did not affect the PDE calculations by Neilsen and Choptuik (2000), Harada (2001) speculated several possibilities.

The stability of the Evans-Coleman solution against nonspherical perturbations was investigated by

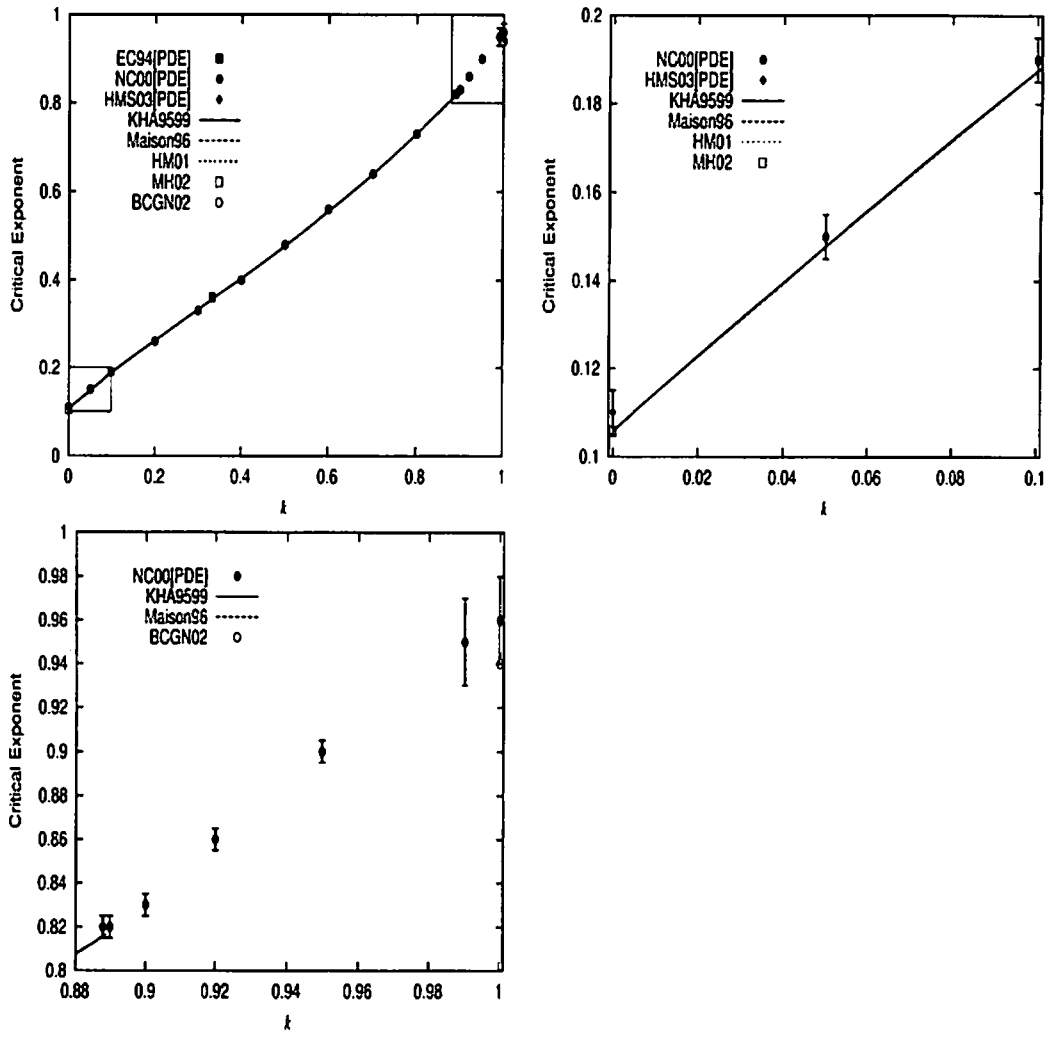


Figure 4: Critical exponents for various value of k. The plots with the label "[PDE]" were obtained as a result of numerical simulations of PDEs. All other plots were obtained by the eigenvalue analyses. The references are the following: EC94 = Evans and Coleman (1994), NC00 = Neilsen and Choptuik (2000), HMS03 = Harada, Maeda and Semelin (2003), KHA9599 = Koike, Hara and Adachi (1995, 1999), Maison96 = Maison (1996), HM01 = Harada and Maeda (2001), MH02 = Maeda and Harada (2002), BCGN02 = Brady et al. (2002). The error bars attached with the plots obtained from numerical simulations are determined from the significant digits when the numerical errors are not explicitly given in the reference. For KHA9599, Maison96 and HM01, the plots are replaced by curves because there are many plots and numerical errors are considered to be very small. Actually, these curves are hard to discriminate from each other. The plots for Newtonian case are plotted at $k = 0$ because the Newtonian system is regarded as the $k \to 0$ limit of general relativity.

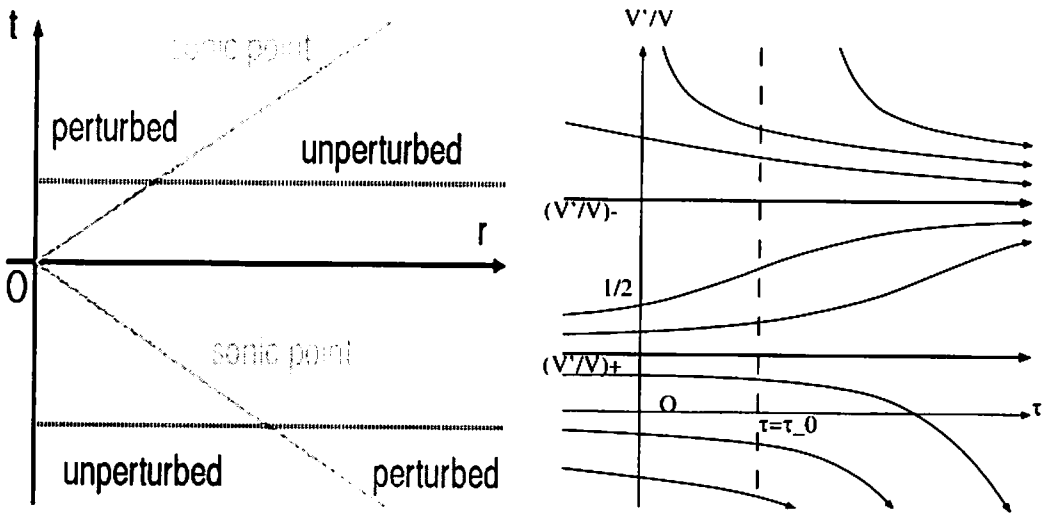


Figure 5: (a) Initial setting of kink-mode perturbations. For $t < 0$, the initial perturbation is put only outside the sonic point. (b) The nonlinear evolution of the perturbation is depicted. + and − denote the primary and secondary directions, respectively. The density gradient is proportional to the velocity gradient V'/V, where the prime denotes the partial derivative with respect to $x = -\ln|\xi|$. See Harada (2001) for details.

Gundlach (2002). The result is that the Evans-Coleman solution is stable against nonspherical perturbations for $1/9 < k \lesssim 0.49$ while is unstable for $0 < k < 1/9$ or $0.49 \lesssim k < 1$. For the stability of other self-similar solutions with analytic initial data against nonspherical perturbations, little has been known until now.

6 Attractor

As seen in the previous section, we have at least one self-similar solution which has no unstable mode. The solution is the Ori-Piran solution for $0 < k \lesssim 0.036$. From the discussion based on the renormalization group, which we have seen in Sec. 4, this solution seems to be an attractor which generic solution approach in the vicinity of the singularity formation. The numerical result obtained by Harada and Maeda (2001) strongly suggests that this is the case. In their numerical simulation of the PDEs, the collapse ended in singularity formation at the center for a certain subset of initial data sets, where the initial data sets were prepared without fine-tuning parameters. Thus obtained numerical solutions were compared with the self-similar solutions obtained by integrating the ODEs. Then, for the numerical solutions obtained by numerical simulations of the PDEs, the good continuous self-similarity is found and the profile of the density field agrees very well with the Ori-Piran solution, as seen in Fig. 6. It was confirmed that this convergence to the self-similar attractor does not depend on the choice of the initial density profile. The above is the results of numerical simulations for $0 < k \leq 0.03$.

However, it is noted that we can consider initial data sets, from which the solution does not approach the Ori-Piran solution. For example, it is clear that the initial data set for the self-similar solutions other than the Ori-Piran solution does not show the approach to the Ori-Piran solution. Furthermore, if the central region is initially homogeneous and sufficiently compact, it can be shown that the solution approach the flat Friedmann solution around the center as the collapse goes towards the singularity formation. It is suggestive that the final fate of all these counterexamples is also described by self-similar solutions. Anyway, the result of numerical simulations strongly suggests that the set of the counterexamples to the convergence to the attractor is zero-measure in the space of initial data sets. These numerical results are well incorporated in the picture of renormalization flow; the critical solution as a saddle and the attractor solution as a sink in the renormalization flow of the function space.

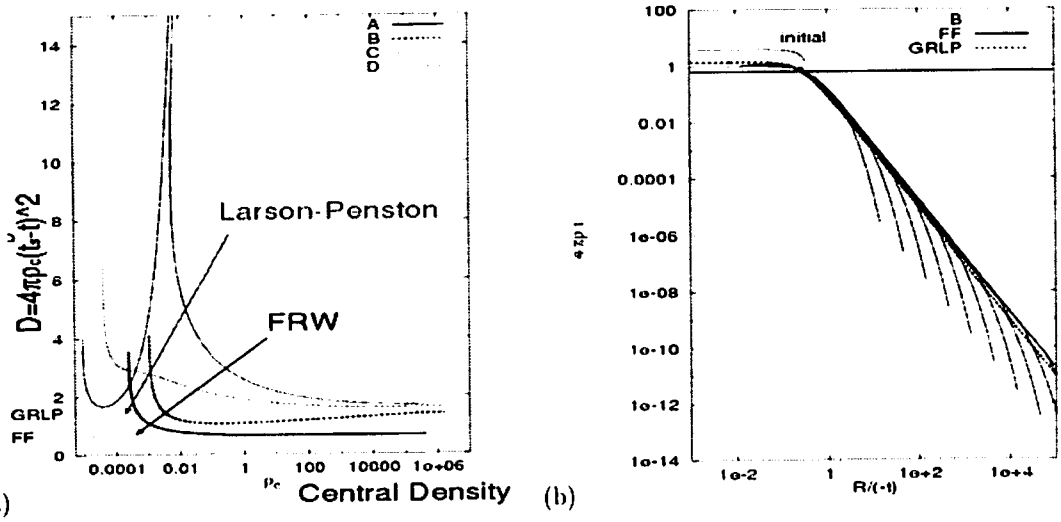


Figure 6: In (a), the time evolution of the central density parameter D_0 is depicted as the collapse proceeds and the central density increases. In (b), the snapshots of density profiles is compared with the density profile of self-similar solutions. These are obtained by the numerical simulations of the PDEs for $k = 0.01$.

This is one realization of the self-similarity hypothesis in the spherically symmetric gravitational collapse. Moreover, since a naked singularity develops from the analytic initial data in the Ori-Piran solution for $0 < k \lesssim 0.0105$, this numerical study strongly suggests that the violation of cosmic censorship is generic in spherically symmetric spacetime. It should be noted that the numerical study based on the null formulation also obtained qualitatively the same result (Harada 1998).

From these considerations, it is expected that one of self-similar solutions may describe the asymptotic behavior of generic and/or special solutions in more general situations. Actually, several other examples are known to exhibit that a self-similar solution describes the asymptotic behaviors of more general solutions (Carr and Coley 1999). If the self-similarity hypothesis is true in a large variety of systems, not only will the analysis of the singularity and/or the asymptotic behavior of the spacetime be much simplified, but also should this be argued in the context of the structure of generic singularity (cf. Belinsky, Khalatnikov and Lifshitz 1970).

7 Newtonian case

Newtonian self-similar solutions have been investigated mainly in an effort to obtain realistic solutions of gravitational collapse leading to the star formation. Penston (1969) and Larson (1969) independently found a self-similar solution, which describes a gravitationally collapsing isothermal gas sphere. Here we call this solution the Larson-Penston solution. Thereafter, Hunter (1977) found a new series of self-similar solutions with analytic initial data and that the set of such solutions is infinite and discrete. Since he named the solutions (a), (b), (c), (d) and so on, here we call these solutions the Hunter (a), (b), (c) and (d) solutions and so on. Shu (1977) found other solution and discussed its astrophysical application. Whitworth and Summers (1985) pointed out the existence of a new family of self-similar solutions with loss of analyticity and found that these solutions make a band structure in the space of all solutions. When Ori and Piran (1990) extended these Newtonian self-similar solutions to general relativity, they showed that these Newtonian self-similar solutions are obtained as the limit of $k \to 0$ of general relativistic self-similar solutions. Even for a spherical gas system with the polytropic equation of state, it is possible to extend the definition of self-similar solutions and these solutions were studied by Goldreich and Weber (1980), Yahil (1983) and Suto and Silk (1988). However, here we concentrate on the case of isothermal gas.

There are two kinds of perturbation modes, the one is the analytic modes and the other is the kink modes, as we have seen in general relativistic case. For the former, the stability of self-similar solutions were studied by Hanawa and Nakayama (1997), Hanawa and Matsumoto (2000a, 2000b) and Maeda and Harada (2001) against spherically symmetric and nonspherical perturbations. For spherically symmetric perturbations, it is found that the homogeneous collapse solution and the Larson-Penston solution have no unstable mode, while the Hunter (a), (b), (c), (d) solutions have one, two, three and four unstable modes, respectively. It is expected all Hunter-family solutions have more than one unstable modes except for the Hunter (a) solution.

For the kink-mode perturbation, Ori and Piran (1988) showed that for $t < 0$ all primary-direction nodal-point solutions, degenerate-nodal-point solutions, and saddle-point anti-transsonic solutions are unstable against the kink mode, while all secondary-direction nodal-point solutions, and saddle-point transsonic solutions are stable against the kink mode. The situation is reversed for $t > 0$ except for the case of degenerate-nodal-point solutions, which are unstable against the kink mode both for $t > 0$ and $t < 0$. Actually, the above result is completely the same as in general relativity. Applying this criterion against the kink mode, it is found that the homogeneous (collapsing) solution is unstable while the Larson-Penston solution and the Hunter (a) solution are stable.

Since the above analysis indicates that the Hunter (a) solution has a single unstable mode, Maeda and Harada (2001) identified that the Hunter (a) solution is a critical solution in Newtonian collapse. The critical exponent calculated from the eigenvalue analysis is ≈ 0.10567, which is appropriate value as the $k \to 0$ limit of the critical exponent in general relativity. Moreover, the character of the Hunter (a) solution is very similar to that of the Evans-Coleman solution. For example, for both solutions, the central region contracts, the surrounding region expanding. From these observations, Harada and Maeda (2001) and Maeda and Harada (2001) identified that the Evans-Coleman solution is the general relativistic counterpart of the Hunter (a) solution.

Moreover, since the Larson-Penston solution has no unstable mode, it is regarded as an attractor solution. Actually, it has been considered and demonstrated that the Larson-Penston solution describes the generic collapse of an isothermal gas near the center since the discovery of this solution (Penston 1969, Larson 1969, Foster and Chevalier 1993, Tsuribe and Inutsuka 1999).

To find the critical behavior in Newtonian collapse and see the relation between the attractor and critical solutions, Harada, Maeda and Semelin (2003) performed the numerical simulations of the PDEs which govern the spherical system of an isothermal gas. The result is as follows: When a one-parameter of initial data sets is prepared, there is a critical value of the parameter. For the critical value the collapse tends to the Hunter (a) solution. For near-critical subcritical case, the collapse first approaches the Hunter (a) solution, thereafter diverges from that and finally disperses away. For near-critical supercritical case, the collapse first approaches the Hunter (a) solution, thereafter diverges from that and finally approaches the Larson-Penston solution. For the solution to approach the Larson-Penston solution, the parameter fine-tuning is not necessary but the parameter only has to be supercritical. The scaling law appears for the mass of the collapsed core for the near-critical supercritical case, while for the maximum density for the near-critical subcritical case. The critical exponents for these laws were estimated to be ≈ 0.11 and ≈ -0.22, which agree very well with the expected values, ≈ 0.10567 and ≈ -0.21134, respectively. Figure 7 shows the trajectory of solutions and the obtained scaling law for the collapsed core mass.

8 Summary

The general theory of relativity as well as Newtonian gravity admits self-similar solutions. This is due to the scale-invariance of gravity. The self-similar solutions are important not only because they are dynamical and inhomogeneous solutions easy to obtain but also because they may play important roles in the asymptotic behavior of more general solutions. We have seen that the stability analysis of self-similar solutions gives a unified picture of the critical behavior and convergence to attractor in gravitational collapse, which have been both observed in recent numerical simulations of the PDEs. Since both the critical behavior and convergence to attractor are not only in general relativity but also in Newtonian gravity, these two are considered to be common characters of gravitational collapse physics. In the above sense, gravitational collapse singles out self-similar solutions even if the initial condition given is complicated. Finally, this article is concluded by the schematic picture for gravitational collapse in Fig. 8.

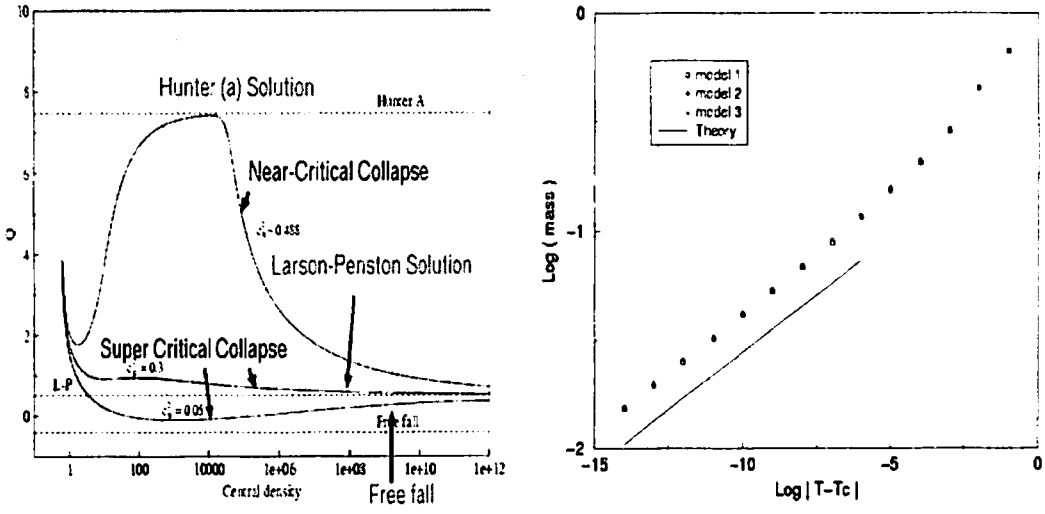


Figure 7: In (a), the time evolution of the central density parameter $Q = \ln D_0 = \ln[4\pi\rho(t,0)t^2]$ is depicted as a function of the central density. In (b), the scaling law for the collapsed core is depicted. In these simulations, the parameter of the one-parameter family of initial data sets is chosen to be the temperature of the system, the density profile fixed. For the details for definitions of quantities in this figure, see Harada, Maeda and Semelin (2003).

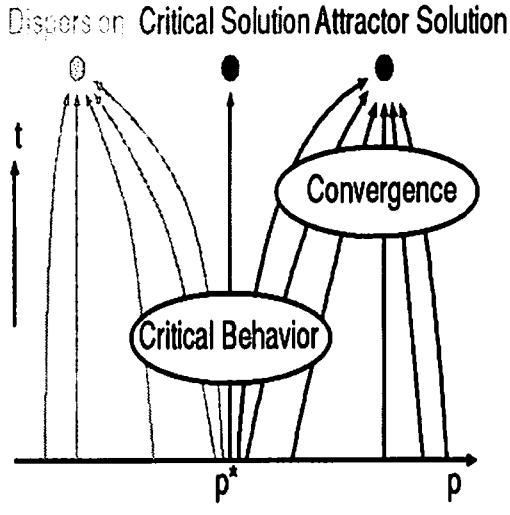


Figure 8: Schematic picture for the fate of gravitational collapse. This picture applies at least to the spherically symmetric perfect-fluid system with $0 < k \leq 0.03$ and to the Newtonian isothermal gas system.

References

[1] A.M. Abrahams and C.R. Evans, Phys. Rev. Lett. **70**, 2980 (1993).

[2] V.A. Belinsky, I.M. Khalatnikov and E.M. Lifshitz, Usp. Fiz. Nauk. **102**, 463 (1970). [English translation in Advances in Physics **19**, 525 (1970)].

[3] P.M. Benoit and A.A. Coley, Class. Quantum Grav. **15**, 2397 (1998).

[4] G.V. Bicknell and R.N. Henriksen, Astrophys. J. **225**, 237 (1978).

[5] P.R. Brady, M.W. Choptuik, C. Gundlach and D.W. Neilsen, Class. Quantum Grav. **19**, 6359 (2002).

[6] M.E. Cahill and A.H. Taub, Commun. Math. Phys. **21**, 1 (1971).

[7] B.J. Carr, unpublished (1993).

[8] B.J. Carr, Phys. Rev. D **62**, 044022 (2000).

[9] B.J. Carr and A.A. Coley, Class. Quantum Grav **16**, R31 (1999).

[10] B.J. Carr and A.A. Coley, Phys. Rev. D **62**, 044023 (2000a).

[11] B.J. Carr and A.A. Coley, Class. Quantum Grav. **17**, 4339 (2000b).

[12] B.J. Carr, A.A. Coley, M. Goliath, U. Nilsson and C. Uggla, Phys. Rev. D **61**, 081502 (2000).

[13] B.J. Carr, A.A. Coley, M. Goliath, U. Nilsson and C. Uggla, Class. Quantum Grav. **18**, 303 (2001).

[14] B. Carter and R.N. Henriksen, Ann. Physique Supp. **14**, 47 (1989).

[15] B. Carter and R.N. Henriksen, J. Math. Phys. **32**, 2580 (1991).

[16] M.W. Choptuik, Phys. Rev. Lett. **70**, 9 (1993).

[17] A.A. Coley, Class. Quantum Grav. **14**, 87 (1997).

[18] C.R. Evans and J.S. Coleman, Phys. Rev. Lett. **72**, 1782 (1994).

[19] T. Foglizzo and R.N. Henriksen, Phys. Rev. D **48**, 4645 (1993).

[20] P.N. Foster and R.A. Chevalier, Astrophys. J. **416**, 303 (1993).

[21] P. Goldreich and S.V. Weber, Astrophys. J. **238**, 991 (1980).

[22] M. Goliath, U. Nilsson and C. Uggla, Class. Quantum Grav. **15**, 167 (1998a).

[23] M. Goliath, U. Nilsson and C. Uggla, Class. Quantum Grav. **15**, 2841 (1998b).

[24] C. Gundlach, Adv. Theor. Math. Phys. **2**, 1 (1998).

[25] C. Gundlach, Living Rev. Rel. **2**, 4 (1999).

[26] C. Gundlach, Phys. Rev. D **65**, 084021 (2002).

[27] T. Hanawa and T. Matsumoto, Publ. Astron. Soc. Jpn. **52**, 241 (2000a).

[28] T. Hanawa and T. Matsumoto, Astrophys. J. **521**, 703 (2000b).

[29] T. Hanawa and K. Nakayama, Astrophys. J. **484**, 238 (1997).

[30] T. Harada, Phys. Rev. D **58**, 104015 (1998).

[31] T. Harada, Class. Quantum Grav. **18**, 4549 (2001).

[32] T. Harada, H. Iguchi and K. Nakao, Prog. Theor. Phys. **107**, 449 (2002).

[33] T. Harada and H. Maeda, Phys. Rev. D **63**, 084022 (2001).

[34] T. Harada, H. Maeda and B. Semelin, submitted to Phys. Rev. D, gr-qc/0210027 (2003).

[35] C. Hunter, Astrophys. J. **218**, 834 (1977).

[36] T. Koike, T. Hara and S. Adachi, Phys. Rev. Lett. **74**, 5170 (1995).

[37] T. Koike, T. Hara and S. Adachi, Phys. Rev. D **59**, 104008 (1999).

[38] R.B. Larson, Mon. Not. R. Astr. Soc. **145**, 271 (1969).

[39] M.S. Madsen, Class. Quantum Grav. **5**, 627 (1988).

[40] H. Maeda and T. Harada, Phys. Rev. D **64**, 124024 (2001).

[41] H. Maeda, T. Harada, H. Iguchi and N. Okuyama, Phys. Rev. D **66**, 027501 (2002a).

[42] H. Maeda, T. Harada, H. Iguchi and N. Okuyama, Prog. Theor. Phys. **108**, 819 (2002b).

[43] H. Maeda, T. Harada, H. Iguchi and N. Okuyama, in preparation (2003).

[44] D. Maison, Phys. Lett. B **366**, 82 (1996).

[45] D.W. Neilsen and M.W. Choptuik, Class. Quantum Grav. **17**, 761 (2000).

[46] A. Ori and T. Piran, Phys. Rev. Lett. **59**, 2137 (1987).

[47] A. Ori and T. Piran, Mon. Not. R. Astron. Soc. **234**, 821 (1988).

[48] A. Ori and T. Piran, Phys. Rev. D **42**, 1068 (1990).

[49] R. Penrose, Riv. Nuovo Cim. **1**, 252 (1969).

[50] R. Penrose, in *General Relativity, an Einstein Centenary Survey*, edited by S.W. Hawking and W. Israel (Cambridge University Press, Cambridge, England, 1979), p.581.

[51] M.V. Penston, Mon. Not. R. Astron. Soc. **144**, 425 (1969).

[52] F.H. Shu, Astrophys. J. **214**, 488 (1977).

[53] Y. Suto and J. Silk, Astrophys. J. **326**, 527 (1988).

[54] T. Tsuribe and S. Inutsuka, Astrophys. J. **526**, 307 (1999).

[55] A. Whitworth and D. Summers, Mon. Not. R. Astron. Soc. **214**, 1 (1985).

[56] A. Yahil, Astrophys. J. **265**, 1047 (1983).

Re-formulating the Einstein equations for stable numerical simulations

-- Formulation Problem in Numerical Relativity

Hisa-aki Shinkai [1]

Computational Science Division,
The Institute of Physical and Chemical Research (RIKEN),
Wako, Saitama, 351-0198 Japan

Abstract

We review recent efforts to re-formulate the Einstein equations for fully relativistic numerical simulations. The so-called numerical relativity (computational simulations in general relativity) is a promising research field matching with ongoing astrophysical observations such as gravitational wave astronomy. Many trials for longterm stable and accurate simulations of binary compact objects have revealed that mathematically equivalent sets of evolution equations show different numerical stability in free evolution schemes. In this article, we first review the efforts of the community, categorizing them into the following three directions: (1) modifications of the standard Arnowitt-Deser-Misner equations initiated by the Kyoto group, (2) rewriting of the evolution equations in hyperbolic form, and (3) construction of an "asymptotically constrained" system. We next introduce our idea for explaining these evolution behaviors in a unified way using eigenvalue analysis of the constraint propagation equations. The modifications of (or adjustments to) the evolution equations change the character of constraint propagation, and several particular adjustments using constraints are expected to diminish the constraint-violating modes. We propose several new adjusted evolution equations, and include some numerical demonstrations. We conclude by discussing some directions for future research. [a]

[a] More detail review is available as [42].

1 Introduction

The theory of general relativity describes the nature of the strong gravitational field. The Einstein equation predicts quite unexpected phenomena such as gravitational collapse, gravitational waves, the expanding universe and so on, which are all attractive not only for researchers but also for the public. The Einstein equation consists of 10 partial differential equations (elliptic and hyperbolic) for 10 metric components, and it is not easy to solve them for any particular situation. Over the decades, people have tried to study the general-relativistic world by finding its exact solutions, by developing approximation methods, or by simplifying the situations. Among these approaches, direct numerical integration of the Einstein equations can be said to be the most robust way to study the strong gravitational field. This research field is often called "numerical relativity".

Numerical relativity is now an essential field in gravity research. The current mainstream in numerical relativity is to analyze the final phase of compact binary objects (black holes and/or neutron stars) related to gravitational wave observations (see e.g. the conference proceedings [33]). Over the past decades, many groups have developed their numerical simulations by trial and error. Simulations require large-scale computational facilities, and long-time stable and accurate calculations. So far, we have achieved certain successes in simulating the coalescence of binary neutron stars (see e.g. [38]) and binary black holes (see e.g.[5]). However, people have still been faced with unreasonable numerical blow-ups at the end of simulations.

Difficulties in accurate/stable long-term evolution were supposed to be overcome by choosing proper gauge conditions and boundary conditions. However, recent several numerical experiments show that the

[1] E-mail:hshinkai@postman.riken.go.jp

(standard) Arnowitt-Deser-Misner (ADM) approach [9, 44, 53] is not the best formulation for numerics, and finding a better formulation has become one of the main research topics. A majority of workers in the field now believe in the existence of constraint-violating modes in most of the formulations. Thus, the stability problem is now shedding light on the mathematical structure of the Einstein equations.

The purpose of this article is to review the formulation problem in numerical relativity. Generally speaking, there are many open issues in numerical relativity, both theoretical (mathematical or physical) and numerical. We list major topics in Box 1.2 in [42].

There are several different approaches to simulating the Einstein equations. Among them the most robust way is to apply 3+1 (space + time) decomposition of space-time, as was first formulated by Arnowitt, Deser and Misner (ADM) [9] (we call this the "original ADM" system). If we divide the space-time into 3+1 dimensions, the Einstein equations form a constrained system: constraint equations and evolution equations. The system is quite similar to that of the Maxwell equations, where people solve constraint equations on the initial data, and use evolution equations to follow the dynamical behaviors.

In numerical relativity, this free-evolution approach is also the standard. This is because solving the constraints (non-linear elliptic equations) is numerically expensive, and because free evolution allows us to monitor the accuracy of numerical evolution. In black-hole treatments, recent "excision" techniques do not require one to impose explicit boundary conditions on the horizon, which is also a reason to apply free evolution scheme. As we will show in the next section, the standard ADM approach has two constraint equations; the Hamiltonian (or energy) and momentum constraints.

Up to a couple of years ago, the "standard ADM" decomposition [44, 53] of the Einstein equation was taken as the standard formulation for numerical relativists. However, numerical simulations were often interrupted by unexplained blow-ups. This was thought due to the lack of resolution, or inappropriate gauge choice, or the particular numerical scheme which was applied. However, after the accumulation of much experience, people have noticed the importance of the formulation of the evolution equations, since there are apparent differences in numerical stability although the equations are mathematically equivalent [2].

At this moment, there are three major ways to obtain longer time evolutions. Of course, the ideas, procedures, and problems are mingled with each other. The purpose of this article is to review all three approaches and to introduce our idea to view them in a unified way. Figure 1 is a chronological map of the researches.

(1) The first direction is to use a modification of the ADM system developed by the Kyoto group [30, 31] (often cited as Shibata and Nakamura [37]) and later re-introduced by Baumgarte and Shapiro [11]. (see §2.1).

(2) The second direction is to re-formulate the Einstein equations in a first-order hyperbolic form. In constructing hyperbolic systems, the essential procedures are to adjust equations using constraints and to introduce new variables, normally the spatially derivatived metric (see §2.2).

(3) The third is to construct a system which is robust against the violation of constraints, such that the constraint surface is an attractor. The idea was first proposed as a "λ-system" by Brodbeck et al [16] in which they introduce artificial flow to the constraint surface using a new variable based on the symmetric hyperbolic system (see §2.3).

The third idea has been generalized by us as an asymptotically constrained system. The main procedure is to adjust the evolution equations using the constraint equations [49, 50, 41]. The method is also applied

[2]The word *stability* is used quite different ways in the community.

- We mean by *numerical stability* a numerical simulation which continues without any blow-ups and in which data remains on the constrained surface.
- *Mathematical stability* is defined in terms of the well-posedness in the theory of partial differential equations, such that the norm of the variables is bounded by the initial data. See eq. (2.24) and around.
- For numerical treatments, there is also another notion of *stability*, the stability of finite differencing schemes. This means that numerical errors (truncation, round-off, etc) are not growing by evolution, and the evaluation is obtained by von Neumann's analysis. Lax's equivalence theorem says that if a numerical scheme is consistent (converging to the original equations in its continuum limit) and stable (no error growing), then the simulation represents the right (converging) solution. See [18] for the Einstein equations.

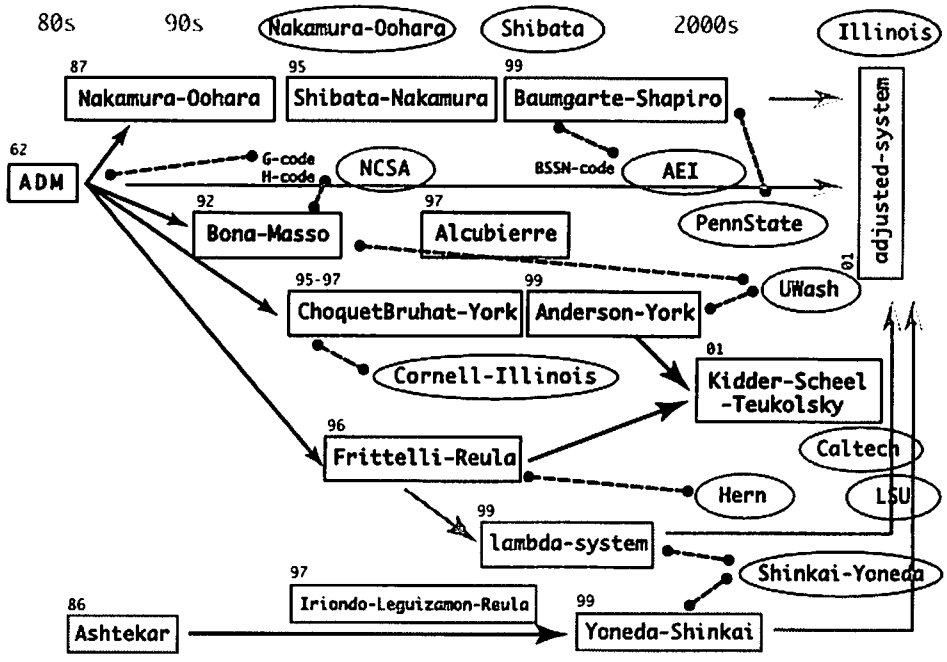


Figure 1: Chronological table of formulations and their numerical tests. Boxed ones are of proposals of formulation, circled ones are related numerical experiments. Please refer Table 1 in [42] for each references.

to explain why the above approach (1) works, and also to propose alternative systems based on the ADM [50, 41] and BSSN [51] equations. Section 3 is devoted to explain this idea with an analytical tool of the eigenvalue analysis of the constraint propagation.

We follow the notations of that of MTW[28]. We use $\mu, \nu = 0, \cdots, 3$ and $i, j = 1, \cdots, 3$ as space-time indices. The unit $c = 1$ is applied. The discussion is mostly to the vacuum space-time, but the inclusion of matter is straightforward.

2 The standard way and the three other roads

2.0 Strategy 0: The ADM formulation

2.0.1 The original ADM formulation

The idea of space-time evolution was first formulated by Arnowitt, Deser, and Misner (ADM) [9]. The formulation was first motivated by a desire to construct a canonical framework in general relativity, but it also gave the community to the fundamental idea of time evolution of space and time: such as foliations of 3-dimensional hypersurface (Figure 2). This *original* ADM formulation was translated to numerical relativists by Smarr [44] and York [53] in late 70s, with slightly different notations. We refer to the latter as the *standard* ADM formulation since this version is the starting point of the discussion.

The story begins by decomposing 4-dimensional space-time into 3 plus 1. The metric is expressed by

$$ds^2 = g_{\mu\nu}dx^\mu dx^\nu = -\alpha^2 dt^2 + \gamma_{ij}(dx^i + \beta^i dt)(dx^j + \beta^j dt), \tag{2.1}$$

where α and β_j are defined as $\alpha \equiv 1/\sqrt{-g^{00}}$ and $\beta_j \equiv g_{0j}$, and called the lapse function and shift vector, respectively. The projection operator or the intrinsic 3-metric g_{ij} is defined as $\gamma_{\mu\nu} = g_{\mu\nu} + n_\mu n_\nu$, where $n_\mu = (-\alpha, 0, 0, 0)$ [and $n^\mu = g^{\mu\nu}n_\nu = (1/\alpha, -\beta^i/\alpha)$] is the unit normal vector of the spacelike hypersurface, Σ (see Figure 2). By introducing the extrinsic curvature,

$$K_{ij} = -\frac{1}{2}\pounds_n \gamma_{ij}, \tag{2.2}$$

and using the Gauss-Codacci relation, the Hamiltonian density of the Einstein equations can be written

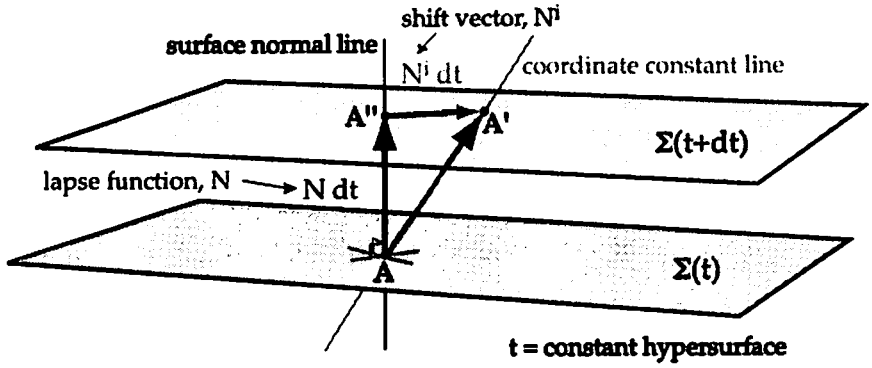


Figure 2: Concept of time evolution of space-time: foliations of 3-dimensional hypersurface. The lapse and shift functions are often denoted α or N, and β^i or N^i, respectively.

as

$$\mathcal{H}_{GR} = \pi^{ij}\dot{\gamma}_{ij} - \mathcal{L}, \quad \text{where} \quad \mathcal{L} = \sqrt{-g}R = \alpha\sqrt{\gamma}[{}^{(3)}R - K^2 + K_{ij}K^{ij}], \tag{2.3}$$

where π^{ij} is the canonically conjugate momentum to γ_{ij},

$$\pi^{ij} = \frac{\partial \mathcal{L}}{\partial \dot{\gamma}_{ij}} = -\sqrt{\gamma}(K^{ij} - K\gamma^{ij}), \tag{2.4}$$

omitting the boundary terms. The variation of $\mathcal{H}_{GR}$ with respect to α and β_i yields the constraints, and the dynamical equations are given by $\dot{\gamma}_{ij} = \frac{\delta \mathcal{H}_{GR}}{\delta \pi^{ij}}$ and $\dot{\pi}^{ij} = -\frac{\delta \mathcal{H}_{GR}}{\delta h_{ij}}$.

2.0.2 The standard ADM formulation

In the version of Smarr and York, K_{ij} was used as a fundamental variable instead of the conjugate momentum π^{ij}. (We remark that there is one replacement in (2.6) using (2.7) in the process of conversion from the original ADM to the standard ADM equations.)

The Standard ADM formulation [44, 53]: **Box 2.1**
The fundamental dynamical variables are (γ_{ij}, K_{ij}), the three-metric and extrinsic curvature. The three-hypersurface Σ is foliated with gauge functions, (α, β^i), the lapse and shift vector.

- The evolution equations:

$$\partial_t \gamma_{ij} = -2\alpha K_{ij} + D_i\beta_j + D_j\beta_i, \tag{2.5}$$

$$\partial_t K_{ij} = \alpha\, {}^{(3)}R_{ij} + \alpha K K_{ij} - 2\alpha K_{ik}K^k{}_j - D_iD_j\alpha + (D_i\beta^k)K_{kj} + (D_j\beta^k)K_{ki} + \beta^k D_k K_{ij} \tag{2.6}$$

  where $K = K^i{}_i$, and ${}^{(3)}R_{ij}$ and D_i denote three-dimensional Ricci curvature, and a covariant derivative on the three-surface, respectively.

- Constraint equations:

$$\mathcal{H}^{ADM} := {}^{(3)}R + K^2 - K_{ij}K^{ij} \approx 0, \tag{2.7}$$

$$\mathcal{M}_i^{ADM} := D_jK^j{}_i - D_iK \approx 0, \tag{2.8}$$

  where ${}^{(3)}R = {}^{(3)}R^i{}_i$: these are called the Hamiltonian (or energy) and momentum constraint equations, respectively.

The formulation has 12 free first-order dynamical variables (γ_{ij}, K_{ij}), with 4 freedom of gauge choice (α, β_i) and with 4 constraint equations, (2.7) and (2.8). The rest freedom expresses 2 modes of gravitational waves.

The constraint propagation equations [22], which are the time evolution equations of the Hamiltonian constraint (2.7) and the momentum constraints (2.8), can be written as

The Constraint Propagations of the Standard ADM: **Box 2.2**

$$\partial_t \mathcal{H} = \beta^j(\partial_j \mathcal{H}) + 2\alpha K\mathcal{H} - 2\alpha\gamma^{ij}(\partial_i \mathcal{M}_j) + \alpha(\partial_l \gamma_{mk})(2\gamma^{ml}\gamma^{kj} - \gamma^{mk}\gamma^{lj})\mathcal{M}_j - 4\gamma^{ij}(\partial_j \alpha)\mathcal{M}_i, \quad (2.9)$$

$$\partial_t \mathcal{M}_i = -(1/2)\alpha(\partial_i \mathcal{H}) - (\partial_i \alpha)\mathcal{H} + \beta^j(\partial_j \mathcal{M}_i) + \alpha K\mathcal{M}_i - \beta^k\gamma^{jl}(\partial_i \gamma_{lk})\mathcal{M}_j + (\partial_i \beta_k)\gamma^{kj}\mathcal{M}_j. \quad (2.10)$$

From these equations, we know that *if the constraints are satisfied on the initial slice* Σ, *then the constraints are satisfied throughout evolution.* The normal numerical scheme is to solve the elliptic constraints for preparing the initial data, and to apply the free evolution (solving only the evolution equations). The constraints are used to monitor the accuracy of simulations.

The ADM formulation was the standard formulation for numerical relativity up to the middle 90s. Numerous successful simulations were obtained for the problems of gravitational collapse, critical behavior, cosmology, and so on. However, stability problems have arisen for the simulations such as the gravitational radiation from compact binary coalescence, because the models require quite a long-term time evolution.

The origin of the problem was that the above statement in *Italics* is true in principle, but is not always true in numerical applications. A long history of trial and error began in the early 90s. We showed that the standard ADM equations *has* a constraint violating mode in its constraint propagation equations even for a single black-hole (Schwarzschild) spacetime [41].

2.1 Strategy 1: Modified ADM formulation by Nakamura et al

Up to now, the most widely used formulation for large scale numerical simulations is a modified ADM system, which is now often cited as the Baumgarte-Shapiro-Shibata-Nakamura (BSSN) formulation. This reformulation was first introduced by Nakamura *et al.* [30, 31, 37]. The usefulness of this reformulation was re-introduced by Baumgarte and Shapiro [11], then was confirmed by other groups to show a long-term stable numerical evolution [4, 6].

2.1.1 Basic variables and equations

The widely used notation[11] introduces the variables $(\varphi, \tilde{\gamma}_{ij}, K, \tilde{A}_{ij}, \tilde{\Gamma}^i)$ instead of (γ_{ij}, K_{ij}), where

$$\varphi = (1/12)\log(\det\gamma_{ij}), \qquad \tilde{\gamma}_{ij} = e^{-4\varphi}\gamma_{ij}, \qquad K = \gamma^{ij}K_{ij}, \quad (2.11)$$

$$\tilde{A}_{ij} = e^{-4\varphi}(K_{ij} - (1/3)\gamma_{ij}K), \qquad \tilde{\Gamma}^i = \tilde{\Gamma}^i_{jk}\tilde{\gamma}^{jk}. \quad (2.12)$$

The new variable $\tilde{\Gamma}^i$ was introduced in order to calculate Ricci curvature more accurately. In BSSN formulation, Ricci curvature is not calculated as $R^{ADM}_{ij} = \partial_k\Gamma^k_{ij} - \partial_i\Gamma^k_{kj} + \Gamma^l_{ij}\Gamma^k_{lk} - \Gamma^l_{kj}\Gamma^k_{li}$, but as $R^{BSSN}_{ij} = R^{\varphi}_{ij} + \tilde{R}_{ij}$, where the first term includes the conformal factor φ while the second term does not. These are approximately equivalent, but R^{BSSN}_{ij} does have wave operator apparently in the flat background limit, so that we can expect more natural wave propagation behavior.

Additionally, the BSSN requires us to impose the conformal factor as $\tilde{\gamma}(:= \det\tilde{\gamma}_{ij}) = 1$, during evolution. This is a kind of definition, but can also be treated as a constraint.

The BSSN formulation [30, 31, 37, 11]: **Box 2.3**
The fundamental dynamical variables are $(\varphi, \tilde{\gamma}_{ij}, K, \tilde{A}_{ij}, \tilde{\Gamma}^i)$.
The three-hypersurface Σ is foliated with gauge functions, (α, β^i), the lapse and shift vector.

- The evolution equations:

$$\partial_t^B \varphi = -(1/6)\alpha K + (1/6)\beta^i(\partial_i\varphi) + (\partial_i\beta^i), \quad (2.13)$$

$$\partial_t^B \tilde{\gamma}_{ij} = -2\alpha\tilde{A}_{ij} + \tilde{\gamma}_{ik}(\partial_j\beta^k) + \tilde{\gamma}_{jk}(\partial_i\beta^k) - (2/3)\tilde{\gamma}_{ij}(\partial_k\beta^k) + \beta^k(\partial_k\tilde{\gamma}_{ij}) \quad (2.14)$$

$$\partial_t^B K = -D^iD_i\alpha + \alpha\tilde{A}_{ij}\tilde{A}^{ij} + (1/3)\alpha K^2 + \beta^i(\partial_i K), \quad (2.15)$$

$$\partial_t^B \tilde{A}_{ij} = -e^{-4\varphi}(D_iD_j\alpha)^{TF} + e^{-4\varphi}\alpha(R_{ij}^{BSSN})^{TF} + \alpha K\tilde{A}_{ij} - 2\alpha\tilde{A}_{ik}\tilde{A}^k{}_j + (\partial_i\beta^k)\tilde{A}_{kj} + (\partial_j\beta^k)\tilde{A}_{ki} - (2/3)(\partial_k\beta^k)\tilde{A}_{ij} + \beta^k(\partial_k\tilde{A}_{ij}). \quad (2.16)$$

$$\partial_t^B \tilde{\Gamma}^i = -2(\partial_j\alpha)\tilde{A}^{ij} + 2\alpha\big(\tilde{\Gamma}^i_{jk}\tilde{A}^{kj} - (2/3)\tilde{\gamma}^{ij}(\partial_j K) + 6\tilde{A}^{ij}(\partial_j\varphi)\big) - \partial_j\big(\beta^k(\partial_k\tilde{\gamma}^{ij}) - \tilde{\gamma}^{kj}(\partial_k\beta^i) - \tilde{\gamma}^{ki}(\partial_k\beta^j) + (2/3)\tilde{\gamma}^{ij}(\partial_k\beta^k)\big). \quad (2.17)$$

- Constraint equations:

$$\mathcal{H}^{BSSN} = R^{BSSN} + K^2 - K_{ij}K^{ij}, \quad (2.18)$$

$$\mathcal{M}_i^{BSSN} = \mathcal{M}_i^{ADM}, \quad (2.19)$$

$$\mathcal{G}^i = \tilde{\Gamma}^i - \tilde{\gamma}^{jk}\tilde{\Gamma}^i_{jk}, \quad (2.20)$$

$$\mathcal{A} = \tilde{A}_{ij}\tilde{\gamma}^{ij}, \quad (2.21)$$

$$\mathcal{S} = \tilde{\gamma} - 1. \quad (2.22)$$

(2.18) and (2.19) are the Hamiltonian and momentum constraints (the "kinematic" constraints), while the latter three are "algebraic" constraints due to the requirements of BSSN formulation.

2.1.2 Remarks

Why BSSN is better than the standard ADM? Together with numerical comparisons with the standard ADM case[6], this question has been studied by many groups using different approaches. Using numerical test evolution, Alcubierre et al [4] found that the essential improvement is in the process of replacing terms by the momentum constraints. They also pointed out that the eigenvalues of BSSN *evolution equations* have fewer "zero eigenvalues" than those of ADM, and they conjectured that the instability might be caused by these "zero eigenvalues". An effort was made to understand the advantage of BSSN from the point of hyperbolization of the equations in its linearized limit [4, 34]. These studies provide some support regarding the advantage of BSSN, while it is also shown an example of an ill-posed solution in BSSN (as well in ADM) by Frittelli and Gomez [23].

As we discussed in [51], the stability of the BSSN formulation is due not only to the introductions of new variables, but also to the replacement of terms in the evolution equations using the constraints. Further, we will show several additional adjustments to the BSSN equations which are expected to give us more stable numerical simulations.

2.2 Strategy 2: Hyperbolic reformulations

2.2.1 Definitions, properties, mathematical backgrounds

The second effort to re-formulate the Einstein equations is to make the evolution equations reveal a first-order hyperbolic form explicitly. This is motivated by the expectation that the symmetric hyperbolic system has well-posed properties in its Cauchy treatment in many systems and also that the boundary treatment can be improved if we know the characteristic speed of the system.

Hyperbolic formulations **Box 2.5**

We say that the system is *a first-order (quasi-linear) partial differential equation system*, if a certain set of (complex-valued) variables u_α $(\alpha = 1, \cdots, n)$ forms

$$\partial_t u_\alpha = \mathcal{M}^{t\beta}{}_\alpha(u)\,\partial_t u_\beta + \mathcal{N}_\alpha(u), \tag{2.23}$$

where $\mathcal{M}$ (the characteristic matrix) and $\mathcal{N}$ are functions of u but do not include any derivatives of u. Further we say the system is

- *a weakly hyperbolic system*, if all the eigenvalues of the characteristic matrix are real.
- *a strongly hyperbolic system* (or a diagonalizable / symmetrizable hyperbolic system), if the characteristic matrix is diagonalizable (has a complete set of eigenvectors) and has all real eigenvalues.
- *a symmetric hyperbolic system*, if the characteristic matrix is a Hermitian matrix.

Writing the system in a hyperbolic form is a quite useful step in proving that the system is *well-posed*. The mathematical well-posedness of the system means (1°) local existence (of at least one solution u), (2°) uniqueness (i.e., at most solutions), and (3°) stability (or continuous dependence of solutions $\{u\}$ on the Cauchy data) of the solutions. The resultant statement expresses the existence of the energy inequality on its norm,

$$||u(t)|| \leq e^{\alpha\tau}||u(t=0)||, \qquad \text{where } 0 < \tau < t, \quad \alpha = const. \tag{2.24}$$

This indicates that the norm of $u(t)$ is bounded by a certain function and the initial norm. Remark that this mathematical boundness does not mean that the norm $u(t)$ decreases along the time evolution.

The inclusion relation of the hyperbolicities is,

$$\text{symmetric hyperbolic} \subset \text{strongly hyperbolic} \subset \text{weakly hyperbolic}. \tag{2.25}$$

The Cauchy problem under weak hyperbolicity is not, in general, C^∞ well-posed. At the strongly hyperbolic level, we can prove the finiteness of the energy norm if the characteristic matrix is independent of u (cf [45]), that is one step definitely advanced over a weakly hyperbolic form. Similarly, the well-posedness of the symmetric hyperbolic is guaranteed if the characteristic matrix is independent of u, while if it depends on u we have only limited proofs for the well-posedness.

From the point of numerical applications, to hyperbolize the evolution equations is quite attractive, not only for its mathematically well-posed features. The expected additional advantages are the following.

(a) It is well known that a certain flux conservative hyperbolic system is taken as an essential formulation in the computational Newtonian hydrodynamics when we control shock wave formations due to matter.

(b) The characteristic speed (eigenvalues of the principal matrix) is supposed to be the propagation speed of the information in that system. Therefore it is naturally imagined that these magnitudes are equivalent to the physical information speed of the model to be simulated.

(c) The existence of the characteristic speed of the system is expected to give us an improved treatment of the numerical boundary, and/or to give us a new well-defined Cauchy problem within a finite region (the so-called initial boundary value problem, IBVP).

These statements sound reasonable, but have not yet been generally confirmed in actual numerical simulations. But we are safe in saying that the formulations are not yet well developed to test these issues. For example, IBVP studies are preliminary yet, and most works are based on a particular symmetric hyperbolic and in a limited space-time symmetry. We will come back to this issue in §2.2.3, but meanwhile let us view the hyperbolic formulations from the comparisons of pure evolution equations.

2.2.2 Hyperbolic formulations of the Einstein equations

Most physical systems can be expressed as symmetric hyperbolic systems. In order to prove that the Einstein's theory is a well-posed system, to hyperbolize the Einstein equations is a long-standing research area in mathematical relativity.

The standard ADM system does not form a first order hyperbolic system. This can be seen immediately from the fact that the ADM evolution equation (2.6) has Ricci curvature in RHS. So far, several first order hyperbolic systems of the Einstein equation have been proposed. In constructing hyperbolic systems, the essential procedures are (1°) to introduce new variables, normally the spatially derivatived metric, (2°) to adjust equations using constraints. Occasionally, (3°) to restrict the gauge conditions, and/or (4°) to rescale some variables. Due to process (1°), the number of fundamental dynamical variables is always larger than that of ADM.

Due to the limitation of space, we can only list several hyperbolic systems of the Einstein equations.

- The Bona-Massó formulation [13, 14]
- The Einstein-Ricci system [19, 1] / Einstein-Bianchi system [7]
- The Einstein-Christoffel system [8]
- The Ashtekar formulation [10]
- The Frittelli-Reula formulation [24, 45]
- The Conformal Field equations [21]
- The Kidder-Scheel-Teukolsky (KST) formulation [26]

Please refer [42] for each brief introductions.

2.2.3 Remarks

When we discuss hyperbolic systems in the context of numerical stability, the following questions should be considered:

> Q From the point of the set of evolution equations, does hyperbolization actually contribute to numerical accuracy and stability? Under what conditions/situations will the advantages of hyperbolic formulation be observed?

Unfortunately, we do not have conclusive answers to these questions, but many experiences are being accumulated. Several earlier numerical comparisons reported the stability of hyperbolic formulations [14, 15, 35, 36]. But we have to remember that this statement went against the standard ADM formulation, which has a constraint-violating mode for Schwarzschild spacetime as has been shown recently[41].

These partial numerical successes encouraged the community to formulate various hyperbolic systems. Recently, Calabrese et al [17] reported there is a certain differences in the long-term convergence features between weakly and strongly hyperbolic systems on the Minkowskii background space-time. However, several numerical experiments also indicate that this direction is not a complete success.

Objections from numerical experiments

- Above earlier numerical successes were also terminated with blow-ups.
- If the gauge functions are evolved according to the hyperbolic equations, then their finite propagation speeds may cause pathological shock formations in simulations [2, 3].
- There are no drastic differences in the evolution properties *between* hyperbolic systems (weakly, strongly and symmetric hyperbolicity) by systematic numerical studies by Hern [25] based on Frittelli-Reula formulation [24], and by the authors [40] based on Ashtekar's formulation [10, 48].
- Proposed symmetric hyperbolic systems were not always the best ones for numerical evolution. People are normally still required to reformulate them for suitable evolution. Such efforts are seen in the applications of the Einstein-Ricci system [36], the Einstein-Christoffel system [12], and so on.

Of course, these statements only casted on a particular formulation, and therefore we have to be careful not to over-emphasize the results. In order to figure out the reasons for the above objections, it is worth stating the following cautions:

Remarks on hyperbolic formulations

(a) Rigorous mathematical proofs of well-posedness of PDE are mostly for simple symmetric or strongly hyperbolic systems. If the matrix components or coefficients depend on dynamical variables (as in all any versions of hyperbolized Einstein equations), almost nothing was proved in more general situations.

(b) The statement of "stability" in the discussion of well-posedness refers to the bounded growth of the norm, and does not indicate a decay of the norm in time evolution.

(c) The discussion of hyperbolicity only uses the characteristic part of the evolution equations, and ignores the rest.

We think the origin of confusion in the community results from over-expectation on the above issues. Mostly, point (c) is the biggest problem. The above numerical claims from Ashtekar and Frittelli-Reula formulations were mostly due to the contribution (or interposition) of non-principal parts in evolution. Regarding this issue, the recent KST formulation finally opens the door. KST's "kinematic" parameters enable us to reduce the non-principal part, so that numerical experiments are hopefully expected to represent predicted evolution features from PDE theories. At this moment, the agreement between numerical behavior and theoretical prediction is not yet perfect but close [27].

If further studies reveal the direct correspondences between theories and numerical results, then the direction of hyperbolization will remain as the essential approach in numerical relativity, and the related IBVP researches will become a main research subject in the future. Meanwhile, it will be useful if we have an alternative procedure to predict stability including the effects of the non-principal parts of the equations. Our proposal of adjusted system in the next subsection may be one of them.

2.3 Strategy 3: Asymptotically constrained systems

The third strategy is to construct a robust system against the violation of constraints, such that the constraint surface is an attractor. The idea was first proposed as "λ-system" by Brodbeck et al [16], and then developed in more general situations as "adjusted system" by the authors [49].

2.3.1 The "λ-system"

Brodbeck et al [16] proposed a system which has additional variables λ that obey artificial dissipative equations. The variable λs are supposed to indicate the violation of constraints and the target of the system is to get $\lambda = 0$ as its attractor.

The "λ-system" (Brodbeck-Frittelli-Hübner-Reula) [16]: **Box 2.7**
For a symmetric hyperbolic system, add additional variables λ and artificial force to reduce the violation of constraints.
The procedure:

1.	Prepare a symmetric hyperbolic evolution system	$\partial_t u = M\partial_i u + N$
2.	Introduce λ as an indicator of violation of constraint which obeys dissipative eqs. of motion	$\partial_t \lambda = \alpha C - \beta\lambda$ $(\alpha \neq 0, \beta > 0)$
3.	Take a set of (u, λ) as dynamical variables	$\partial_t \begin{pmatrix} u \\ \lambda \end{pmatrix} \simeq \begin{pmatrix} A & 0 \\ F & 0 \end{pmatrix} \partial_i \begin{pmatrix} u \\ \lambda \end{pmatrix}$
4.	Modify evolution eqs so as to form a symmetric hyperbolic system	$\partial_t \begin{pmatrix} u \\ \lambda \end{pmatrix} = \begin{pmatrix} A & \tilde{F} \\ F & 0 \end{pmatrix} \partial_i \begin{pmatrix} u \\ \lambda \end{pmatrix}$

Since the total system is designed to have symmetric hyperbolicity, the evolution is supposed to be unique. Brodbeck et al showed analytically that such a decay of λs can be seen for sufficiently small $\lambda(>0)$ with a choice of appropriate combinations of αs and βs.

Brodbeck et al presented a set of equations based on Frittelli-Reula's symmetric hyperbolic formulation [24]. The version of Ashtekar's variables was presented by the authors [39] for controlling the constraints or reality conditions or both. The numerical tests of both the Maxwell-λ-system and the Ashtekar-λ-system were performed [49], and confirmed to work as expected. Although it is questionable whether the recovered solution is true evolution or not [43], we think the idea is quite attractive. To enforce the decay of errors in its initial perturbative stage seems the key to the next improvements, which are also developed in the next section on "adjusted systems".

However, there is a high price to pay for constructing a λ-system. The λ-system can not be introduced generally, because (i) the construction of λ-system requires the original evolution equations to have a symmetric hyperbolic form, which is quite restrictive for the Einstein equations, (ii) the final system requires many additional variables and we also need to evaluate all the constraint equations at every time step, which is a hard task in computation. Moreover, (iii) it is not clear that the λ-system is robust enough for non-linear violation of constraints, or that λ-system can control constraints which do not have any spatial differential terms.

2.3.2 The "adjusted system"

Next, we propose an alternative system which also tries to control the violation of constraint equations actively, which we named "adjusted system". We think that this system is more practical and robust than the previous λ-system.

The Adjusted system (procedures): **Box 2.9**

1.	Prepare a set of evolution eqs.	$\partial_t u = J\partial_i u + K$
2.	Add constraints in RHS	$\partial_t u = J\partial_i u + K \underbrace{+\kappa C}$
3.	Choose the coeff. κ so as to make the eigenvalues of the homogenized adjusted $\partial_t C$ eqs negative reals or pure imaginary.	$\partial_t C = D\partial_i C + EC$ $\partial_t C = D\partial_i C + EC \underbrace{+F\partial_t C + GC}$

The process of adjusting equations is a common technique in other re-formulating efforts as we reviewed. However, we try to employ the evaluation process of constraint amplification factors as an alternative guideline to hyperbolization of the system. We will explain these issues in the next section.

3 A unified treatment: Adjusted System

This section is devoted to present our idea of "asymptotically constrained system". Original references can be found in [49, 50, 41, 51].

3.1 Procedures : Constraint propagation equations and Proposals

Suppose we have a set of dynamical variables $u^a(x^i, t)$, and their evolution equations,

$$\partial_t u^a = f(u^a, \partial_i u^a, \cdots), \tag{3.1}$$

and the (first class) constraints,

$$C^\alpha(u^a, \partial_i u^a, \cdots) \approx 0. \tag{3.2}$$

Note that we do not require (3.1) forms a first order hyperbolic form. We propose to investigate the evolution equation of C^α (constraint propagation),

$$\partial_t C^\alpha = g(C^\alpha, \partial_i C^\alpha, \cdots), \tag{3.3}$$

for predicting the violation behavior of constraints in time evolution. We do not mean to integrate (3.3) numerically together with the original evolution equations (3.1), but mean to evaluate them analytically in advance in order to reformulate the equations (3.1).

There may be two major analyses of (3.3); (a) the hyperbolicity of (3.3) when (3.3) is a first order system, and (b) the eigenvalue analysis of the whole RHS in (3.3) after a suitable homogenization. However, as we critically viewed the hyperbolization road in the previous section, we prefer to proceed the road (b).

Amplification Factors of Constraint Propagation equations: **Box 3.1**

We propose to homogenize (3.3) by a Fourier transformation, e.g.

$$\partial_t \hat{C}^a = \hat{g}(\hat{C}^a) = M^a{}_\beta \hat{C}^\beta,$$
$$\text{where } C(x,t)^\rho = \int \hat{C}(k,t)^\rho \exp(ik\cdot x) d^3k, \tag{3.4}$$

then to analyze the set of eigenvalues, say As, of the coefficient matrix, $M^a{}_\beta$, in (3.4). We call As the constraint amplification factors (CAFs) of (3.3).

The CAFs predict the evolution of constraint violations. We therefore can discuss the "distance" to the constraint surface using the "norm" or "compactness" of the constraint violations (although we do not have exact definitions of these "$\cdots$" words).

The next conjecture seems to be quite useful to predict the evolution feature of constraints:

Conjecture on Constraint Amplification Factors (CAFs): **Box 3.2**

(A) If CAF has a *negative real-part* (the constraints are forced to be diminished), then we see more stable evolution than a system which has positive CAF.

(B) If CAF has a *non-zero imaginary-part* (the constraints are propagating away), then we see more stable evolution than a system which has zero CAF.

We found that the system becomes more stable when more As satisfy the above criteria. A general feature of the constraint propagation is reported in [52].

The above features of the constraint propagation, (3.3), will differ when we modify the original evolution equations. Suppose we add (adjust) the evolution equations using constraints

$$\partial_t u^a = f(u^a, \partial_i u^a, \cdots) + F(C^a, \partial_i C^a, \cdots), \tag{3.5}$$

then (3.3) will also be modified as

$$\partial_t C^a = g(C^a, \partial_i C^a, \cdots) + G(C^a, \partial_i C^a, \cdots). \tag{3.6}$$

Therefore, the problem is how to adjust the evolution equations so that their constraint propagations satisfy the above criteria as much as possible.

3.2 Applications

For the Maxwell equation and the Ashtekar version of the Einstein equations, we numerically found that this idea works to reduce the violation of constraints, and that the effects are much better than by constructing its symmetric hyperbolic versions [40, 49].

Applications to ADM The idea was applied to the standard ADM formulation which is not hyperbolic and several attractive adjustments were proposed [50, 41]. We made various predictions how additional adjusted terms will change the constraint propagation. Systematic numerical comparisons are also progressing, and we show two sample plots here.

Figure 3 (a) is a test numerical evolution of Detweiler-type adjustment [20] on the Minkowskii background. We see the adjusted version gives convergence on to the constraint surface by arranging the magnitude of the adjusting parameter, κ. Figure 3 (b) is obtained by a 3-dimensional numerical evolution of weak gravitational wave, the so-called Teukolsky wave [46]. The lines are of the original/standard ADM evolution equations, Detweiler-type adjustment, and a part of Detweiler-type adjustment. For a particular choice of κ, we observe again the L2 norm of constraint (violation of constraints) is reduced than the standard ADM case, and can evolve longer than that.

Notion of Time Reversal Symmetry During the comparisons of adjustments, we found that it is necessary to create time asymmetric structure of evolution equations in order to force the evolution on to the constraint surface. There are infinite ways of adjusting equations, but we found that if we follow the guideline Box 3.5, then such an adjustment will give us time asymmetric evolution.

Trick to obtain asymptotically constrained system: **Box 3.5**
= Break the time reversal symmetry (TRS) of the evolution equation.

1. Evaluate the parity of the evolution equation.
   By reversing the time ($\partial_t \to -\partial_t$), there are variables which change their signatures (parity $(-)$) [e.g. $K_{ij}, \partial_t \gamma_{ij}, \mathcal{M}_i, \cdots$], while not (parity $(+)$) [e.g. $g_{ij}, \partial_t K_{ij}, \mathcal{H}, \cdots$].
2. Add adjustments which have different parity of that equation.
   For example, for the parity $(-)$ equation $\partial_t \gamma_{ij}$, add a parity $(+)$ adjustment $\kappa \mathcal{H}$.

One of our criteria, the negative real CAFs, requires breaking the time-symmetric features of the original evolution equations. Such CAFs are obtained by adjusting the terms which break the TRS of the evolution equations, and this is available even at the standard ADM system.

Applications to BSSN This analysis was also applied to explain the advantages of the BSSN formulation, and again several alternative adjustments to BSSN equations were proposed [51]. Recently Yo *et al*[47] reported their simulations of stationary rotating black hole, and mentioned that one of our proposal was contributed to maintain their evolution of Kerr black hole (J/M up to $0.9M$) for long time ($t \sim 6000M$). Their results also indicates that the evolved solution is closed to the exact one, that is, the constrained surface.

4 Outlook

4.1 What we have achieved

We reviewed recent efforts on this problem by categorizing them into (0) The standard ADM formulation (§2.0, Box 2.1), (1) The modified ADM (so-called BSSN) formulation (§2.1, Box 2.3), (2) Hyperbolic formulations (§2.2, Box 2.5), and (3) Asymptotically constrained formulations (§2.3). Among them, the approach (2) is perhaps best justified on mathematical grounds. However, as we critically reviewed in §2.2.3, the practical advantages may not be available unless we kill the lower-order terms in its hyperbolized equation, as in KST's formulation.

We therefore proceeded in the direction (3). Our approach, which we term *adjusted system*, is to construct a system that has its constraint surface as an attractor. Our unified view is to understand the evolution system by evaluating its constraint propagation. Especially we proposed to analyze the

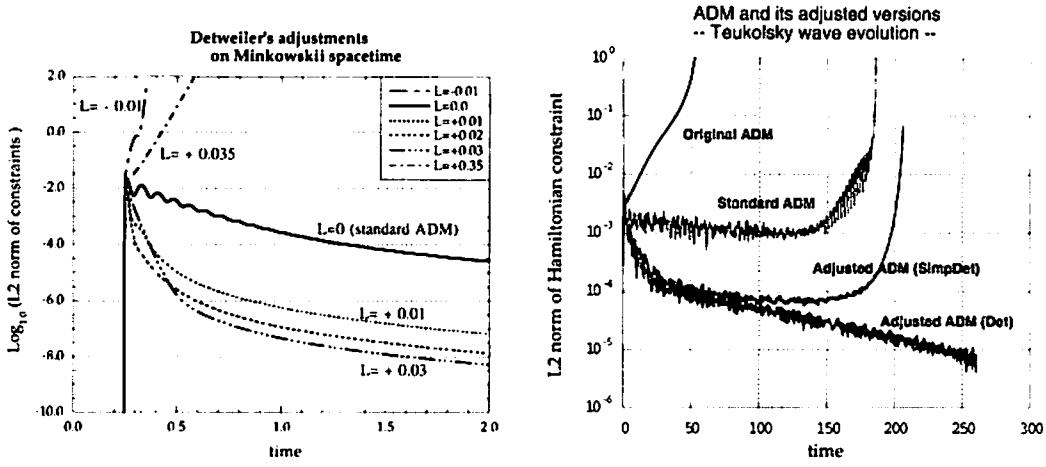


Figure 3: Comparisons of numerical evolution between adjusted ADM systems. (a) Demonstration of the Detweiler's modified ADM system on Minkowskii background spacetime, 1-dimensional simulation. The L2 norm of the constraints $\mathcal{H}^{ADM}$ and $\mathcal{M}^{ADM}$ is plotted in the function of time. Artificial error was added at $t = 0.25$. L is the parameter in Detweiler's adjustment. We see the evolution is asymptotically constrained for small $\kappa > 0$. (b) L2 norm of the Hamiltonian constraint $\mathcal{H}^{ADM}$ of evolution using ADM/adjusted ADM formulations for the case of Teukolsky wave, 3-dimensional simulation.

constraint amplification factors (Box 3.1) which are the eigenvalues of the homogenized constraint propagation equations. We analyzed the system based on our conjecture (Box 3.2) whether the constraint amplification factors suggest the constraint to decay/propagate or not. We concluded that

- The constraint propagation features become different by simply adding constraint terms to the original evolution equations (we call this the *adjustment* of the evolution equations).
- There *is* a constraint-violating mode in the standard ADM evolution system when we apply it to a single non-rotating black hole space-time, and its growth rate is larger near the black-hole horizon.
- Such a constraint-violating mode can be killed if we adjust the evolution equations with a particular modification using constraint terms (Box 2.7). An effective guideline is to adjust terms as they break the time-reversal symmetry of the equations (Box 3.5).
- Our expectations are borne out in simple numerical experiments using the Maxwell, Ashtekar, and ADM systems. However the modifications are not yet perfect to prevent non-linear growth of the constraint violation.
- We understand why the BSSN formulation works better than the ADM one in the limited case (perturbative analysis in the flat background), and further we proposed modified evolution equations along the lines of our previous procedure.

The common key to the problem is how to adjust the evolution equations with constraints. Any adjusted systems are mathematically equivalent if the constraints are completely satisfied, but this is not the case for numerical simulations. Replacing terms with constraints is one of the normal steps when people hyperbolize equations. Our approach is to employ the evaluation process of constraint amplification factors for an alternative guideline to hyperbolization of the system.

4.2 Final remarks

If we say the final goal of this project is to find a robust algorithm to obtain long-term accurate and stable time-evolution method, then the recipe should be a combination of (a) formulations of the evolution equations, (b) choice of gauge conditions, (c) treatment of boundary conditions, and (d) numerical integration methods. We are in the stages of solving this mixed puzzle. The ideal almighty algorithm

may not exit, but we believe our accumulating experience will make the ones we do have more robust and automatic.

We have written this review from the viewpoint that the general relativity is a constrained dynamical system. This is not only a proper problem in general relativity, but also in many physical systems such as electrodynamics, magnetohydrodynamics, molecular dynamics, mechanical dynamics, and so on. Therefore sharing the thoughts between different field will definitely accelerate the progress.

When we discuss asymptotically constrained manifolds, we implicitly assume that the dynamics could be expressed on a wider manifold. Recently we found that such a proposal is quite similar with techniques in e.g. molecular dynamics. For example, people assume an extended environment when simulating molecular dynamics under constant pressure (with a potential piston) or a constant temperature (with a potential thermostat) (see e.g. [32]). We have also noticed that a dynamical adjusting method of Lagrange multipliers has been developed in multi-body mechanical dynamics (see e.g. [29]). We are now trying to apply these ideas back into numerical relativity.

In such a way, communication and interaction between different fields is encouraged. Cooperation between numerical and mathematical scientists is necessary. By interchanging ideas, we hope we will reach our goal in next few years, and obtain interesting physical results and predictions. It is our personal view that exciting revolutions in numerical relativity are coming soon.

Acknowledgment

This review is based on the series of works with Gen Yoneda. HS is supported by the special postdoctoral researchers program at RIKEN, and this work was supported partially by the Grant-in-Aid for Scientific Research Fund of Japan Society of the Promotion of Science, No. 14740179.

References

[1] A. Abrahams, A. Anderson, Y. Choquet-Bruhat, and J.W. York, Jr., Phys. Rev. Lett. **75**, 3377 (1995); Class. Quant. Grav. **14**, A9 (1997).

[2] M. Alcubierre, Phys. Rev. D **55**, 5981 (1997).

[3] M. Alcubierre and J. Massó, Phys. Rev. D **57**, R4511 (1998).

[4] M. Alcubierre, G. Allen, B. Brügmann, E. Seidel and W-M. Suen, Phys. Rev. D **62**, 124011 (2000).

[5] M. Alcubierre, W. Benger, B. Brügmann, G. Lanfermann, L. Nerger, E. Seidel, and R. Takahashi, Phys. Rev. Lett. **87** 271103 (2001).

[6] M. Alcubierre, B. Brügmann, T. Dramlitsch, J.A. Font, P. Papadopoulos, E. Seidel, N. Stergioulas, and R. Takahashi, Phys. Rev. D **62**, 044034 (2000).

[7] A. Anderson, Y. Choquet-Bruhat, J.W. York, Jr., Topol. Methods in Nonlinear Analysis, **10**, 353 (1997).

[8] A. Anderson and J. W. York, Jr, Phys. Rev. Lett. **82**, 4384 (1999).

[9] R. Arnowitt, S. Deser and C.W. Misner, in *Gravitation: An Introduction to Current Research*, ed. by L.Witten, (Wiley, New York, 1962).

[10] A. Ashtekar, Phys. Rev. Lett. **57**, 2244 (1986); Phys. Rev. **D36**, 1587 (1987).

[11] T.W. Baumgarte and S.L. Shapiro, Phys. Rev. D **59**, 024007 (1999).

[12] J.M. Bardeen, L.T. Buchman, Phys. Rev. D. **65**, 064037 (2002).

[13] C. Bona, J. Massó, Phys. Rev. D **40**, 1022 (1989); Phys. Rev. Lett. **68**, 1097 (1992).

[14] C. Bona, J. Massó, E. Seidel and J. Stela, Phys. Rev. Lett. **75**, 600 (1995); Phys. Rev. D **56**, 3405 (1997).

[15] C. Bona, J. Massó, E. Seidel, and P. Walker, gr-qc/9804052.

[16] O. Brodbeck, S. Frittelli, P. Hübner, and O.A. Reula, J. Math. Phys. **40**, 909 (1999).

[17] G. Calabrese, J. Pullin, O. Sarbach, and M. Tiglio, Phys. Rev. D **66**, 041501 (2002).

[18] M.W. Choptuik, Phys. Rev. D **44**, 3124 (1991).

[19] Y. Choquet-Bruhat and J.W. York, Jr., C.R. Acad. Sc. Paris **321**, Série I, 1089, (1995).

[20] S. Detweiler, Phys. Rev. D **35**, 1095 (1987).

[21] H. Friedrich, Proc. Roy. Soc. **A375**, 169 (1981); *ibid.* **A378**, 401 (1981).

[22] S. Frittelli, Phys. Rev. D **55**, 5992 (1997).

[23] S. Frittelli and R. Gomez, J. Math. Phys. **41**, 5535 (2000).

[24] S. Frittelli and O.A. Reula, Phys. Rev. Lett. **76**, 4667 (1996).

[25] S. D. Hern, PhD thesis, gr-qc/0004036.

[26] L.E. Kidder, M.A. Scheel, S.A. Teukolsky, Phys. Rev. D **64**, 064017 (2001).

[27] L. Lindblom and M. Scheel, gr-qc/0206035

[28] C.W. Misner, K.S. Thorne, J.A. Wheeler, *Gravitation*, (Freeman, N.Y., 1973).

[29] T. Nagata, in Proceedings of the first Asian Conference on Multibody Dynamics 2002 (ACMD02), held at Fukushima, Japan.

[30] T. Nakamura, K. Oohara and Y. Kojima, Prog. Theor. Phys. Suppl. **90**, 1 (1987).

[31] T. Nakamura and K. Oohara, in *Frontiers in Numerical Relativity* edited by C.R. Evans, L.S. Finn, and D.W. Hobill (Cambridge Univ. Press, Cambridge, England, 1989).

[32] S. Nosé, Prog. Theor. Phys. **103**, 1 (1991).

[33] Proceedings of *Black Holes and Gravitational Waves* ed. by T. Nakamura and H. Kodama, as the issue of Prog. Theor. Phys. Suppl. **136** (1999).

[34] O. Sarbach, G. Calabrese, J. Pullin, and M. Tiglio, Phys. Rev. D **66**, 064002 (2002).

[35] M.A. Scheel, T.W. Baumgarte, G.B.Cook, S.L. Shapiro, S.A. Teukolsky, Phys. Rev. D **56**, 6320 (1997).

[36] M.A. Scheel, T.W. Baumgarte, G.B. Cook, S.L. Shapiro, S.A. Teukolsky, Phys. Rev. D **58**, 044020 (1998).

[37] M. Shibata and T. Nakamura, Phys. Rev. **D52**, 5428 (1995).

[38] M. Shibata and K. Uryu, Prog. Theor. Phys. **107**, 265 (2002).

[39] H. Shinkai and G. Yoneda, Phys. Rev. D **60**, 101502 (1999).

[40] H. Shinkai and G. Yoneda, Class. Quant. Grav. **17**, 4799 (2000).

[41] H. Shinkai and G. Yoneda, Class. Quant. Grav. **19**, 1027 (2002).

[42] H. Shinkai and G. Yoneda, in *Progress in Astronomy and Astrophysics* (Nova Science Publ) to be published. The manuscript is available as gr-qc/0209111.

[43] F. Siebel and P. Hübner, Phys. Rev. D **64**, 024021 (2001).

[44] L. Smarr, J.W. York, Jr., Phys. Rev. D **17**, 2529 (1978).

[45] J.M. Stewart, Class. Quant. Grav. **15**, 2865 (1998).

[46] S.A. Teukolsky, Phys. Rev. D **26**, 745 (1982).

[47] H-J. Yo, T.W. Baumgarte and S.L. Shapiro, gr-qc/0209066.

[48] G. Yoneda and H. Shinkai, Phys. Rev. Lett. **82**, 263 (1999); Int. J. Mod. Phys. D. **9**, 13 (2000).

[49] G. Yoneda and H. Shinkai, Class. Quant. Grav. **18**, 441 (2001).

[50] G. Yoneda and H. Shinkai, Phys. Rev. D **63**, 124019 (2001).

[51] G. Yoneda and H. Shinkai, Phys. Rev. D **66**, 124003 (2002).

[52] G. Yoneda and H. Shinkai, gr-qc/0209106.

[53] J.W. York, Jr., in *Sources of Gravitational Radiation*, ed. by L.Smarr, (Cambridge, 1979).

Algebraic Properties to Gravitational Lenses

Hideki Asada,[1]

Faculty of Science and Technology,
Hirosaki University, Hirosaki 036-8561, Japan

Abstract

Algebra offers powerful tools for studying the gravitational lensing. For illustrations, we study two cases: First, we show that the lens equation for a binary gravitational lens being a set of two coupled real fifth-order algebraic equations (equivalent to a single complex equation of the same order) can be reduced to a single real fifth-order algebraic equation. We find that the number of images on each side of the separation axis is independent of the mass ratio and separation unless the source crosses the caustics. Furthermore, the discriminant of the quintic equation enables us to study changes in the number of solutions, namely in the number of images. Next, we consider galaxy lenses which are frequently modeled as isothermal ellipsoids. We present explicit expressions for the lens equation for a cored isothermal ellipsoidal gravitational lens as a a single real sixth-order algebraic equation. Furthermore, we derive simple analytic expressions for the caustics and critical curves for a singular isothermal ellipsoid.

1 Introduction

Gravitational lensing is now one of the most important fields in astrophysics [1]: We can detect MACHOs by microlensing, put constraints on cosmological parameters through observation of galactic lenses, and discuss the evolution of large scale structure by measuring the cosmic shear. A study of gravitational lensing starts with the lens equation, which is a mapping of 2 dimensional vectors corresponding to the source and image. As a result, the equations are coupled non-linearly, so that we need numerical implementations. We have recently revealed that for some models, the apparently coupled lens equations are reduced to a single real equation. One case is a binary lens [2], and the other an isothermal ellipsoidal lens [3].

Gravitational lensing by binary objects has attracted a great deal of interest [1] since the pioneering work [4]. It offers an important tool in the search for extrasolar planets [5, 6], which is independent of the Doppler method, which suffers from uncertainties in inclination angles [7]. However, it is not easy to study binary lensing in detail: The lens equation adopted until now consists of a set of two coupled real fifth-order (quintic) equations, or, equivalently, a complex quintic equation [8]. As a result, it seems quite difficult to solve these equations, since there are no well-established method for solving coupled nonlinear equations numerically with sufficient accuracy [9].

The lens equation for a binary is reduced to a single master equation that is fifth-order in a real variable with real coefficients [2]. In addition, the discriminant of the quintic equation is shown to be factorizable into two parts [10]: One represents the condition that the lens equation can be reduced to a single quintic equation, while the other corresponds to the caustics. Here, the caustics are curves on which the Jacobian of the lens mapping vanishes on a source plane. The number of images has been classified in terms of caustics.

Gravitational lensing due to a galaxy is also important for probing mass distributions and determining cosmological parameters. Galaxy lenses are often modeled as cored isothermal ellipsoids. Until now, the lens equation for the cored isothermal ellipsoid has been solved numerically as a *nonlinearly coupled* system. For a singular isothermal ellipsoidal lens, the apparently coupled lens equations can be reduced to a single equation [1], though explicit expressions were not given there. Along this course, we reexamine the coupled lens equations for the cored isothermal ellipsoid, and show that they are reduced to a single equation with a condition for physical solutions and to give analytic criteria for determining the number of images for isothermal ellipsoidal lenses [3].

[1] E-mail:asada@phys.hirosaki-u.ac.jp

2 Gravitational Lenses

This section is devoted to a brief summary of a basic theory of gravitational lensing. We assume the thin lens approximation, since the typical dimension of the lens is much shorter than the distances among the observer, lens and source. We denote the angular position vector for the source and image by $\boldsymbol{\beta}$ and $\boldsymbol{\theta}$, respectively. The deflection angle is denoted by $\boldsymbol{\alpha}$. In this case, the trajectory of the light ray is written as

$$\boldsymbol{\beta} = \boldsymbol{\theta} - \frac{D_{LS}}{D_S}\boldsymbol{\alpha}(D_L\boldsymbol{\theta}), \tag{1}$$

where D_S is the distance from the observer to the source, D_L is from the observer to the lens, and D_{LS} is from the lens to the source, respectively. The vectors $\boldsymbol{\alpha}$, $\boldsymbol{\beta}$ and $\boldsymbol{\theta}$ are 2-dimensional vectors. In a cosmological situation, the unlensed position $\boldsymbol{\beta}$ is not an observable, because we cannot remove the lens from the observed position.

For a point mass lens, the deflection angle takes a simple form, so that the lens equation becomes a quadratic equation, which is solved immediately. In a general case, the lens equation is considered as a set of coupled equations.

Now, we consider a lens mapping. The amplification is a Jacobian between the mapping, which is defined as $|\partial\boldsymbol{\theta}/\partial\boldsymbol{\beta}|$. *Critical curves* on a lens plane are defined as

$$\left|\frac{\partial\boldsymbol{\theta}}{\partial\boldsymbol{\beta}}\right| = \infty, \tag{2}$$

which is considered as an equation for $\boldsymbol{\theta}$. By using the lens mapping, we can obtain the *caustics*, which are curves on a source plane.

3 Binary Lenses

We consider a binary system of two bodies with mass M_1 and M_2 and separation vector $\boldsymbol{L}$ from the object 1 to 2. For a later convenience, let us define the Einstein ring radius angle as

$$\theta_{\rm E} = \sqrt{\frac{4GMD_{LS}}{c^2 D_L D_S}}, \tag{3}$$

where G is the gravitational constant, M is the total mass $M_1 + M_2$. We choose the position of the object 1 as the coordinate center.

In the unit of the Einstein ring radius angle, the lens equation reads

$$\boldsymbol{\beta} = \boldsymbol{\theta} - \left((1-\nu)\frac{\boldsymbol{\theta}}{|\boldsymbol{\theta}|^2} + \nu\frac{\boldsymbol{\theta}-\boldsymbol{\ell}}{|\boldsymbol{\theta}-\boldsymbol{\ell}|^2}\right), \tag{4}$$

where we defined the mass ratio and the angular separation vector as

$$\nu = \frac{M_2}{M_1 + M_2}, \tag{5}$$

$$\boldsymbol{\ell} = \frac{\boldsymbol{L}}{D_{\rm L}\theta_{\rm E}}. \tag{6}$$

It is convenient to use the Cartesian coordinates $(\theta_x, \theta_y) = (r\cos\phi, r\sin\phi)$ and $(\beta_x, \beta_y) = (\rho C, \rho S)$ for $\rho = |\boldsymbol{\beta}|$.

3.1 Sources on the symmetry axis

Let us consider the case of sources on the symmetry axis, for which analytic solutions can be obtained: For a binary with two equal masses, explicit solutions were found by Schneider and Weiß (1986), while no explicit solutions have been given for an arbitrary mass ratio until now [2].

We consider a source at $(\beta_x, \beta_y) = (\rho C, 0) \equiv (\bar{\rho}, 0)$ for $\bar{\rho} \in (-\infty, \infty)$. First, we find on-axis solutions as

$$\theta_x = 2\sqrt{-p}\cos\sigma + \frac{\ell + \bar{\rho}}{3}, \tag{7}$$

with $\sigma = \sigma_0$, for $\sigma_0 = \frac{1}{3}\cos^{-1}(\frac{q}{2p\sqrt{-p}})$, $p = -\frac{1}{9}(\ell+\bar{\rho})^2 + \frac{1}{3}(\ell\bar{\rho}-1)$, $q = -\frac{2}{27}(\ell+\bar{\rho})^3 + \frac{1}{3}(\ell+\bar{\rho})(\ell\bar{\rho}-1) + \ell(1-\nu)$. Actually, we can show that $p < 0$ and $q^2 + 4p^3 < 0$, which mean these three solutions exist for any source position. They are on-axis solutions, while the remaining two solutions are off-axis solutions, which are present only for sources within the caustics: If and only if $\ell > \bar{\rho}$,

$$r = \sqrt{\frac{\ell(1-\nu)}{\ell - \bar{\rho}}}, \tag{8}$$

$$\cos\phi = \frac{1}{2}\sqrt{\frac{\ell - \bar{\rho}}{\ell(1-\nu)}}\left(\ell + \frac{\bar{\rho} - \nu\ell}{\bar{\rho}(\ell - \bar{\rho})}\right). \tag{9}$$

3.2 Off-axis sources

Here, we consider the case of off-axis sources. It has been shown [2] that Eq. (4) reduces to a fifth-order equation for $\cot\phi$,

$$\sum_{i=0}^{5} a_i (\cot\phi)^{5-i} = 0. \tag{10}$$

Here, none of these coefficients $a_0, \cdots a_5$ are singular, because they are polynomials in ℓ, ρ, ν, C and S all of which are finite.

As seen from Eq. (10), $\cot\phi$ remains finite, because a_0 never vanishes for off-axis sources. Hence, any solution of Eq. (10) is finite. As a consequence, we can derive the following theorem: When the source moves around off the symmetry axis ($\beta_y = 0$, i.e., $S = 0$), images never cross the separation axis ($\theta_y = 0$, i.e., $\cot\phi = \pm\infty$). This implies that the number of images on each side of the separation axis is invariant, unless the source crosses the caustics. This property holds for arbitrary ℓ and ν, because the number of images is an integer. An analytic study of a symmetric binary ($\nu = 1/2$) [4, 2] is sufficient to determine the invariant number. In this case, only a single image appears on the source side of the axis, while two images appear on the side opposite to the source outside the caustics or four images appear on the side opposite to the source inside the caustics.

We factorized the discriminant [11] D_5 of the quintic equation Eq. (10) using Mathematica [12] into the form

$$D_5 = -4S^2\ell^2\nu^2\rho^2 W^2 K, \tag{11}$$

where we defined $K = \sum_{i=0}^{16} k_i \rho^{16-i}$, for $k_0 = \ell^8$, $k_1 = 8C\ell^7(1 - \ell^2 - 2\nu)$, $\cdots$. Here, $k_2, \cdots, k_{16}$ have rather lengthy forms.

Changes in the number of images are usually studied in terms of the caustics ($J = 0$). In our approach for a *real* algebraic equation, changes in the number of solutions for the lens equation Eq. (10) correspond directly to those in the signature of the discriminant D_5. Actually, we can show that $K = 0$ is a condition for the caustics [10, 13, 14].

4 Isothermal Lenses

4.1 Lens Equation for a Singular Isothermal Ellipsoid

First, let us consider the singular isothermal ellipsoidal lens with ellipticity $0 \leq \epsilon < 1/5$. A condition that the surface mass density projected onto the lens plane must be non-negative everywhere puts a constraint on the ellipticity as $\epsilon < 1$. A tighter constraint $\epsilon < 1/5$ comes from that the density contours must be convex, which is reasonable for an isolated relaxed system.

For simplicity, we introduce variables as $x \equiv \sqrt{1-\epsilon}\theta_1$, $y \equiv \sqrt{1+\epsilon}\theta_2$, $a \equiv \sqrt{1-\epsilon}\beta_1$ and $b \equiv \sqrt{1+\epsilon}\beta_2$, so that the lens equation can be written as

$$a = x\left(1 - \frac{1-\epsilon}{\sqrt{x^2+y^2}}\right). \tag{12}$$

$$b = y\left(1 - \frac{1+\epsilon}{\sqrt{x^2+y^2}}\right). \tag{13}$$

4.2 Sources on the symmetry axes

For $a = 0$, we obtain explicit solutions:

$$x = 0, \tag{14}$$

$$y = \begin{cases} b - (1+\epsilon) & \text{for } b < -(1+\epsilon)\,, \\ b \pm (1+\epsilon) & \text{for } -(1+\epsilon) \le b \le 1+\epsilon\,, \\ b + (1+\epsilon) & \text{for } 1+\epsilon < b\,, \end{cases} \tag{15}$$

and

$$x = \pm\frac{1-\epsilon}{2\epsilon}\sqrt{4\epsilon^2 - b^2}, \tag{16}$$

$$y = -\frac{(1-\epsilon)b}{2\epsilon}. \tag{17}$$

4.3 Off-axis sources

Here, we consider off-axis sources ($a \neq 0$ and $b \neq 0$). In this case, Eqs. (12) and (13) show $x \neq 0$ and $y \neq 0$. Eliminating $\sqrt{x^2+y^2}$ from Eqs. (12) and (13), we obtain

$$y = \frac{(1-\epsilon)bx}{(1+\epsilon)a - 2\epsilon x}, \tag{18}$$

which determines y uniquely for any given x. Substituting Eq. (18) into Eq. (12), we obtain the fourth-order polynomial for x as

$$\begin{aligned} D(x) &\equiv [(a-x)^2 - (1-\epsilon)^2][(1+\epsilon)a - 2\epsilon x]^2 \\ &\quad + (1-\epsilon)^2 b^2 (a-x)^2 \\ &= 0, \end{aligned} \tag{19}$$

where we used $x \neq 0$.

The number of real roots for a fourth-order equation is discussed by the discriminant D_4 [11], which becomes for Eq. (19)

$$\begin{aligned} D_4 &= -64a^2b^2\epsilon^2(1-\epsilon)^{12} \\ &\quad \times[(a^2+b^2-4\epsilon^2)^3 + 108a^2b^2\epsilon^2]. \end{aligned} \tag{20}$$

Furthermore, the lens equation implies

$$\frac{a-x}{x} < 0. \tag{21}$$

We find

$$D(a) = -a^2(1-\epsilon)^4 < 0, \tag{22}$$

$$D(0) = a^2(1-\epsilon^2)^2\left(\frac{a^2}{(1-\epsilon)^2} + \frac{b^2}{(1+\epsilon)^2} - 1\right). \tag{23}$$

Hence, the signature of $D(0)$ plays a crucial role in the number of images.

Analytic expressions for caustics are found: The outer caustic is an ellipse which is given by

$$\frac{a^2}{(1-\epsilon)^2} + \frac{b^2}{(1+\epsilon)^2} = 1. \tag{24}$$

The inner caustic is an asteroid which is parametrized as

$$a = 2\epsilon \cos^3 t, \tag{25}$$

$$b = 2\epsilon \sin^3 t, \tag{26}$$

where $t \in [0, 2\pi)$.

4.4 Lens Equation for a Cored Isothermal Ellipsoid

Let us consider a cored isothermal ellipsoidal lens with the angular core radius c. Similarly, we obtain a sixth-order lens equation

$$\sum_{i=0}^{6} C_i x^i = 0. \tag{27}$$

The discriminant at the sixth order is not sufficient for determining the exact number of solutions, so that further investigations must be done.

5 Conclusion

Algebra offers powerful tools for studying the gravitational lensing: For a binary lens and an isothermal ellipsoidal lens, we derived the discriminant for a real algebraic lens equation to obtain analytic expressions for caustics. It might be interesting to apply algebraic theorems to lensing study.

References

[1] P. Schneider, J. Ehlers, and E. E. Falco, *Gravitational Lenses* (Springer-Verlag, Berlin, 1992).

[2] H. Asada, Astron. Astrophys. **390** (2002), L11.

[3] H. Asada, T. Hamana and M. Kasai, Astron. Astrophys. *in press* (2002), astro-ph/0211389.

[4] P. Schneider and A. Weiß, Astron. Astrophys. **164** (1886), 237.

[5] S. Mao and B. Paczynski, Astrophys. J. **374** (1991) 37L.

[6] A. Gould and A. Loeb, Astrophys. J. **396** (1992) 104.

[7] G. W. Marcy and R. P. Butler, Ann. Rev. Astron. Astrophys. **36** (1998) 57.

[8] H. J. Witt, Astron. Astrophys. **236** (1990), 311.

[9] W. H. Press, B. P. Flannery, S. A. Teukolsy and W. T. Vetterling, *Numerical Recipes in C* (Cambridge University Press, Cambridge, 1988).

[10] H. Asada, T. Kasai and M. Kasai, Prog. Theor. Phys. *in press* (2002), astro-ph/0211390.

[11] B. L. van der Waerden, *Algebra I* (Springer, 1966).

[12] S. Wolfram, *The Mathematica Book, 4th ed.* (Cambridge University Press, Cambridge, 2000).

[13] H. J. Witt and A. Petters, J. Math. Phys. **34** (1993), 4093.

[14] H. J. Witt, Astrophys. J. **403** (1993), 530.

The Cosmic Quartet
Cosmological Parameters of a Smoothed Inhomogeneous Spacetime

Thomas Buchert[a,1] and Mauro Carfora[b,2]

[a] *Theoretische Physik, Ludwig Maximilians-Universität, Theresienstr. 37, D-80333 München, Germany and Department of Physics and Research Center for the Early Universe (RESCEU) School of Science, The University of Tokyo, Tokyo 113-0033, Japan*

[b] *Dipartimento di Fisica Nucleare e Teorica, Università degli Studi di Pavia and Istituto Nazionale di Fisica Nucleare, Sezione di Pavia, via A. Bassi 6, I-27100 Pavia, Italy*

Abstract

We discuss the relation between 'bare' cosmological parameters as the true spatial average characteristics that determine the cosmological model, and the parameters interpreted by observers with a "Friedmannian bias", i.e., within a homogeneous space geometry. We may say that the latter are 'dressed' by the smoothed-out geometrical inhomogeneities of the surveyed spatial region. We identify two effects that quantify the difference between 'bare' and 'dressed' parameters: 'curvature backreaction' and 'volume effect'. An estimate of the latter is given in terms of a simple geometrical example.

1 Introduction

Contemporary cosmology is heading, as is the generally held believe, towards a theoretical home stretch marked by the determination of three cosmological parameters that characterize the standard model of cosmology and with it the whole global history of our Universe. This standard model looks back on a long period of challenges that were mastered by its apparent robustness. Essentially, it is based on solutions of Einstein's equations for a homogeneous and isotropic distribution of matter in the Universe. So, it is indeed a simple model that was iconed by Neta Bahcall et al. [1] in terms of a 'cosmic triangle'. The final phase of combat, in which we are in at present and as a large body of cosmologists would put it, consists of a phase of high-precision cosmology which, through a plethora of orthogonal observations, will soon exclaim highly accurate numbers for those three cosmological parameters. But, should we really believe this enormously simplified pledge of the standard model en-chaining predictions throughout all space and time?

A more level-headed approach immediately reminds us of the foundations of the standard model: it ignores structure in the Universe. Of course, nobody is as naive as ignoring the existence of structure, which in the recent past was celebrated by a number of observational successes: the discovery of large-scale structure, essentially blowing up the picture of a homogeneous Universe and replacing it by a strongly proncounced honeycomb structure of the distribution of galaxies. Those structures are extending as deep as hundred millions of lightyears and are still continuing at the borders of our maps of the Universe such as that currently drawn by the Sloan Digital Sky Survey group. The "excuse" is a conjecture: to maintain the standard model we have to assume that *on average* the cosmic evolution follows the Friedmannian equations whose solutions are fixed by the cosmic triangle.

Guided by the idea that a universe model should remain simple, while respecting the inhomogeneities that are present in the matter distribution as well as in the geometry of spacetime, we have worked out a cosmology that can still be characterized by 'cosmological parameters', but there are essentially three important colors that have to be added to the standard picture: firstly, replacing the parameters of the homogeneous universe model by corresponding spatial averages entails a scale-dependence, i.e., the values of the parameters must depend on the spatial scale over which we average the distribution. Secondly, in addition to the standard model parameters, there is a fourth player which encodes the

[1] E-mail:buchert@theorie.physik.uni-muenchen.de
[2] E-mail:mauro.carfora@pv.infn.it

fluctuations of matter inhomogeneities [3]. If averaged on sufficiently large scales this new parameter may be a small quantity, but it adds a substantial qualitative impact: cosmological parameters are now allowed to communicate, they evolve freely governed by the evolution of structure and they are not fixed each individually by initial conditions as in the standard model [6]; we may say that the 'cosmic triangle' is transformed into a 'cosmic terzet'. Thirdly, and this turns out to be a more deeply rooted insight: cosmological parameters that we would measure and interprete with a "Friedmannian bias" (i.e. in a homogeneous spacetime geometry) are 'dressed' [8], i.e., they acquire correction factors stemming from the geometrical inhomogeneities.

Understanding this latter fact took a long and rather challenging route of employing a number of results that were obtained by mathematicians who work on Riemannian geometry [7], reinforcing the Ricci flow as a natural candidate for the smoothing of geometry [12],[10]. We shall demonstrate in this note that 'the emperor's new clothes' can be seen, and the effect of 'dressing' can be calculated. Possibly, the values interpreted with a Friedmannian bias are appreciably different from the true averages that govern the dynamics of spacetime. Further work must be devoted to quantifying this effect: could we eventually dismiss the cosmological constant, which now seems to be an unavoidable thigh of the cosmic triangle? It will be exciting to follow this new route of understanding the influence of structure of the fluctuating geometry of spacetime itself on the evolution of our Universe.

2 Bare and Dressed Cosmological Parameters

To begin with let us concentrate on the density parameter which measures the actual matter content in a spatial slice of the Universe on some spatial scale of observation. We assume that we are given a suitable split into space and time, i.e., a foliation of spacetime. Since the determination of the *total mass on a regional domain* in relativistic cosmology is a subject of controversy (see, e.g., [2]), we only make use of the well-defined concepts of a local energy density ϱ (here, we only refer to the restmass density for the matter model 'dust'), and its spatial Riemannian volume average evaluated on a compact domain, e.g., a geodesic ball $\mathcal{B}_0$, $\langle\varrho\rangle_{\mathcal{B}_0} := \int_{\mathcal{B}_0}\varrho d\mu_g/V_{\mathcal{B}_0}$ with the Riemannian volume element $d\mu_g$ associated with the 3-metric of the hypersurface, and the ball's volume $V_{\mathcal{B}_0} = \int_{\mathcal{B}_0} d\mu_g$. Using this averager for all scalar variables in a $3+1$ ADM setting, we can investigate regional averages of all relevant spatial variables such as the density and, e.g., the expansion rate $\langle\theta\rangle_{\mathcal{B}_0} =: 3H_{\mathcal{B}_0}$, defining an effective "Hubble-constant" on the domain of averaging. Hence, the cosmological density parameter that determines the true ('bare') source of the effective dynamics can be unambiguously defined.

The averaged Hamiltonian constraint may be cast into a relation among a set of *regional cosmological parameters* as the following scale-dependent functionals [3]:

$$\Omega^M_{\mathcal{B}_0} := \frac{8\pi G M_{\mathcal{B}_0}}{3V_{\mathcal{B}_0}H^2_{\mathcal{B}_0}} \;;\; \Omega^\Lambda_{\mathcal{B}_0} := \frac{\Lambda}{3H^2_{\mathcal{B}_0}} \;;\; \Omega^R_{\mathcal{B}_0} := -\frac{\langle\mathcal{R}\rangle_{\mathcal{B}_0}}{6H^2_{\mathcal{B}_0}} \;;\; \Omega^{\mathcal{Q}^K}_{\mathcal{B}_0} := -\frac{\mathcal{Q}^K_{\mathcal{B}_0}}{6H^2_{\mathcal{B}_0}} \;,$$

$$\text{obeying by construction the Hamiltonian constraint } \Omega^M_{\mathcal{B}_0} + \Omega^\Lambda_{\mathcal{B}_0} + \Omega^R_{\mathcal{B}_0} + \Omega^{\mathcal{Q}^K}_{\mathcal{B}_0} = 1 \;, \qquad (1)$$

with the ball's material mass content $M_{\mathcal{B}_0}$, the scalar curvature $\mathcal{R}$, and the cosmological constant Λ. In contrast to the standard FLRW cosmological parameters there are four players. In the FLRW case there is by definition no fluctuating source (condensed into the "kinematical backreaction" $\mathcal{Q}^K_{\mathcal{B}_0}$ that is composed of positive-definite expansion and shear fluctuation terms (see [3]). Hence, the *effective cosmology* as the spatially averaged model can be determined by a scale-dependent and regional 'cosmic quartet' [4] rather than by a global 'cosmic triangle' [1].

Eq. (1) forms the basis of a discussion of cosmological parameters as they determine the theoretical model. They may not be, however, directly accessible to observations. Unlike in Newtonian cosmology, where the corresponding averages have a similar form [5], it is not straightforward to compare the above relativistic average model parameters to observational data. The reason is that the volume-averages contain information on the actually present *geometrical inhomogeneities* within the averaging domain. In contrast, the "observer's Universe" is described in terms of a Euclidean or constant curvature model. Consequently, the common interpretation of observations within the set of the standard model parameters, if extended by the backreaction parameter or not, neglects the geometrical inhomogeneities that (through the Riemannian volume-average) are hidden in the average characteristics of the theoretical cosmology.

We have suggested an answer to this problem in [7] (see also [9] for a preliminary attempt). Let us highlight some results.

According to [7], the picture discussed above strictly depends on the ratio between two density profiles defined on the averaging domain: one is naturally associated with the actual matter content of the gravitational sources, whereas the other is the mass density corresponding to the matter content in the given region, but now thought of as averaged over a geometrically smoothed out domain $\overline{\mathcal{B}}$ with homogeneous geometry:

$$\langle \varrho \rangle_{\mathcal{B}_0} = M_{\mathcal{B}_0}/V_{\mathcal{B}_0} \quad ; \quad \langle \varrho \rangle_{\overline{\mathcal{B}}} = M_{\overline{\mathcal{B}}}/V_{\overline{\mathcal{B}}} \ . \tag{2}$$

We have implemented a regional smoothing procedure for the geometry of the hypersurface under the assumption of preservation of the ball's material content. We can infer already from (2) that the average density measured with a "Friedmannian bias" is dressed by a *volume effect* due to the difference between the volume of a smoothed region and the actual volume of the bumpy region.

A further result that explicitly involves the geometrical smoothing flows (e.g., the Ricci flow for the metric) is furnished by a relation between the constant regional curvature in the smoothed model (e.g., a FLRW domain) and the actual regional average curvature in the theoretical cosmology:

$$\overline{\mathcal{R}}_{\overline{\mathcal{B}}} = \langle \mathcal{R} \rangle_{\mathcal{B}_0} (V_{\overline{\mathcal{B}}}/V_{\mathcal{B}_0})^{-2/3} - \mathcal{Q}^R_{\mathcal{B}_0} \ , \tag{3}$$

where we have introduced a novel measure for the "backreaction" of geometrical inhomogeneities capturing the deviations from the standard FLRW space section, the *regional curvature backreaction*:

$$\mathcal{Q}^R_{\mathcal{B}_0} := \int_0^\infty d\beta \, \frac{V_{\mathcal{B}_\beta}(\beta)}{V_{\overline{\mathcal{B}}}} \left[\frac{1}{3} \langle \left(\mathcal{R}(\beta) - \langle \mathcal{R}(\beta) \rangle_{\mathcal{B}_\beta} \right)^2 \rangle_{\mathcal{B}_\beta} - 2 \langle \tilde{\mathcal{R}}^{ab}(\beta) \tilde{\mathcal{R}}_{ab}(\beta) \rangle_{\mathcal{B}_\beta} \right] \ , \tag{4}$$

with $\tilde{\mathcal{R}}_{ab} := \mathcal{R}_{ab} - \frac{1}{3} g_{ab} \mathcal{R}$ being the trace–free part of the Ricci tensor $\mathcal{R}_{ab}$ in the hypersurface. $\mathcal{Q}^R_{\mathcal{B}_0}$, built from scalar invariants of the intrinsic curvature, appears to have a similar form as the "kinematical backreaction" term (that was built from invariants of the extrinsic curvature). It features two positive–definite parts, the *scalar curvature amplitude fluctuations* and *fluctuations in metrical anisotropies*. Depending on which part dominates we obtain an under– or overestimate of the actual averaged scalar curvature, respectively. β parametrizes integral curves of the smoothing flow for the metric, so that the expression above indeed refers to the explicit form of this flow. Notwithstanding, this term may be estimated by the actual curvature fluctuations, since the Ricci flow acts in a controllable way such that the maxima of the curvature inhomogeneities are monotonically decreasing during the deformation.

From Eq. (3) we can understand the physical content of geometrical averaging. It makes transparent that, in the smoothed model, the averaged scalar curvature is 'dressed' both by the *volume effect* mentioned above, and by the *curvature backreaction effect* itself. The volume effect is expected precisely in the form occurring in (3), if we think of comparing two regions of distinct volumes, but with the same matter content, in a constant curvature space. Whereas the backreaction term encodes the deviation of the averaged scalar curvature from a constant curvature model, e.g., a FLRW space section.

Correspondingly, an observer with a "Friedmannian bias" would interprete his measurements in terms of the 'dressed' cosmological parameters:

$$\overline{\Omega}^M_{\overline{\mathcal{B}}} := \frac{8\pi G M_{\overline{\mathcal{B}}}}{3 V_{\overline{\mathcal{B}}} \overline{H}^2_{\overline{\mathcal{B}}}} \ ; \ \overline{\Omega}^\Lambda_{\overline{\mathcal{B}}} := \frac{\Lambda}{3\overline{H}^2_{\overline{\mathcal{B}}}} \ ; \ \overline{\Omega}^R_{\overline{\mathcal{B}}} := -\frac{\overline{\mathcal{R}}_{\overline{\mathcal{B}}}}{6\overline{H}^2_{\overline{\mathcal{B}}}} \ ; \ \overline{\Omega}^{\mathcal{Q}^\kappa}_{\overline{\mathcal{B}}} := -\frac{\overline{\mathcal{Q}}^\kappa_{\overline{\mathcal{B}}}}{6\overline{H}^2_{\overline{\mathcal{B}}}} \ , \text{ obeying } \ \overline{\Omega}^M_{\overline{\mathcal{B}}} + \overline{\Omega}^\Lambda_{\overline{\mathcal{B}}} + \overline{\Omega}^R_{\overline{\mathcal{B}}} + \overline{\Omega}^{\mathcal{Q}^\kappa}_{\overline{\mathcal{B}}} = 1 \ . \tag{5}$$

The latter equation follows from our assumption that the smoothing procedure requires to respect the Hamiltonian constraint of Einstein's equations. (For a more detailed discussion see [8].)

3 The Volume Effect: a Geometrical Example

Comparing and using the relations (1) and (5), we conclude that the problem has been condensed into a recipee–type rule of applying results that were obtained on theoretically quite involved grounds. Notwithstanding, the formulation appears simple and therefore immediately suggests questions of practical importance. Concrete numbers are needed in order to persuade workers in observational cosmology of

the actual quantitative importance of the outlined effects. However, to give concrete numbers needs a substantial effort beyond the currently available methods. One of the obstacles to provide immediate estimates is the dependence of the proposed effects on generic dynamical models, which are not well-developed in relativistic cosmology. To employ (non-generic) spherically symmetric models is one way to go, and we are currently conducting research in this direction.

Hellaby [13] used spherically symmetric models of clusters and voids to obtain the error made by estimating average characteristics in comparison with parameters of a corresponding FLRW cosmology. The notion 'corresponding' is defined in the sense of *volume matching* proposed earlier by Ellis and Stoeger [11]. To compare Hellaby's approach with our framework is difficult in detail. The volume fraction which would have to be estimated in our framework is 1 by definition, the 'curvature backreaction' being the only geometrical effect. But, since Hellaby compares scalar average characteristics that involve the averaged curvatures and the averaged densities on a given scale of interest by keeping the volumes the same, the calculated effect still can be used as an indication for the deviations of the averages due to geometrical differences of the two models. It must be emphasized, however, that a detailed comparison has to follow from an explicit investigation of our effects, and therefore Hellaby's quoted numbers (amounting to 10-30% for typical clusters and voids) can at best be used as an indication. Moreoever, as Hellaby pointed out himself, the effect depends on details of the dynamical model which, in the cases he investigated, are still simple solutions that can be done analytically. Also, as he mentioned, the effect would strongly depend on the topology of the domain which he chooses to be the simplest.

A complementary aspect of the problem is that we need to analyze realistic models of hypersurfaces in order to learn about the global effect on very large scales; note that, even if we have realistically modelled clusters and voids, we would still need to arrange those patterns according to knowledge of the distribution of large-scale structure. In this sense the effect calculated by Hellaby (loc.cit.) is plausible, but it will not provide the answer on cosmological scales. Let us illustrate this comment: researches employing rough-surface models to realistically model e.g. the moon's surface for the purpose of better estimates on reflection intensity of light from the surface, would work with factors of 40 for the fraction of the moon's modelled inhomogeneous surface to the surface of a sphere (Karl Vogler, priv. comm.). For cosmological volumes the situation is more subtle, since different patterns may increase, but they may also decrease the volume of the spatial domain. Concerning this problem we are currently investigating a generic relativistic model based on a relativistic generalization of Zel'dovich's approximation, which is a well-known approximate tool in Newtonian cosmology to model generic structure formation [6].

For the sake of illustration of the effect of the volume scaling on the mass density, let us consider the following explicit example. Its construction requires the following steps:

(i) Take a large Euclidean manifold, say a flat 3-torus T^3 of *typical* size $R \times R \times R$.

(ii) Remove from such a manifold, k Euclidean balls $B_E(\frac{\pi}{2}r)$ of radius $\frac{\pi}{2}r$ with $\frac{r}{R}$ small, (the $\frac{\pi}{2}$ is for computational convenience).

(iii) Glue, in place of the removed Euclidean balls $\{B_E(\frac{\pi}{2}r)\}$, a corresponding number k of 3-spherical balls $\{B_{S^3}(\frac{\pi}{2}r)\}$, (*i.e.*, balls cut out of the surface of a 3-sphere S^3_r, if the 3-sphere has radius r then the ball $B_{S^3}(\frac{\pi}{2}r)$ is one hemisphere of S^3_r).

(iv) Note that such a glueing requires a *small* amount of negative curvature along the boundary 2-spheres of $B_E(\frac{\pi}{2}r)$ in order to have a smooth interface between the flat geometry of the torus T^3 and the positive curvature geometry of the 3-spherical balls $\{B_{S^3}(\frac{\pi}{2}r)\}$.

(v) Denote by T^3_{inh} the resulting curved torus, where the $B_{S^3}(\frac{\pi}{2}r)$'s correspond to the local geometric inhomogeneity over a region of radius $\frac{\pi}{2}r$ in a space section of the *observed* universe, (a sort of naive Swiss-cheese model).

Under such assumptions (typically, if r/R is suitably small) it is reasonable to conjecture that the geometry of T^3_{inh} will Ricci flow towards the geometry of a flat torus $\overline{T^3}$ (with $\text{Vol}(\overline{T^3}) = \text{Vol}(T^3_{\text{inh}})$), and we can estimate the relative density fraction $\frac{\langle\varrho\rangle_{B_{\text{inh}}}}{\langle\varrho\rangle_{B_E}}$ in such a setting. Note that the generic region $B_{S^3}(\frac{\pi}{2}r)$ supporting the local inhomogeneity in T^3_{inh} corresponds to a Euclidean ball $B_E(\frac{\pi}{2}r)$ in the flat smoothed-out $\overline{T^3}$.

Under the local mass preservation constraint, the actual $\langle\varrho\rangle_{B_{S^3}}$ and the smoothed-out $\langle\varrho\rangle_{B_E}$ mass densities are related to each other by (2):

$$\frac{\langle\varrho\rangle_{B_{S^3}}}{\langle\varrho\rangle_{B_E}} = \frac{\mathrm{Vol}\left(B_E(\frac{\pi}{2}r)\right)}{\mathrm{Vol}\left(B_{S^3}(\frac{\pi}{2}r)\right)}. \tag{6}$$

Recall that

$$\mathrm{Vol}\left(B_{S^3}(\frac{\pi}{2}r)\right) = \mathrm{Vol}\left(S^2(r)\right)\int_0^{\frac{\pi}{2}r}\sin^2\left(\frac{t}{r}\right)dt = \pi^2 r^3\,, \tag{7}$$

where $\mathrm{Vol}\left(S^2(r)\right)$ is the area of the 2-sphere of radius r. Since

$$\mathrm{Vol}\left(B_E(\frac{\pi}{2}r)\right) = \frac{4}{3}\pi\left(\frac{\pi}{2}r\right)^3 = \frac{\pi^4}{6}r^3\,, \tag{8}$$

we get

$$\frac{\langle\varrho\rangle_{B_{S^3}}}{\langle\varrho\rangle_{B_E}} = \frac{\mathrm{Vol}\left(B_E(\frac{\pi}{2}r)\right)}{\mathrm{Vol}\left(B_{S^3}(\frac{\pi}{2}r)\right)} = \frac{\pi^2}{6} \simeq 1.6449\,. \tag{9}$$

This shows that indeed one can have a significant mismatch between the actual average mass density and the smoothed-out mass density owing only to the volume effect (the curvature backreaction effect was not considered in this rather qualitative example).

Acknowledgments

TB acknowledges hospitality by the University of Tokyo and financial support by the Research Center for the Early Universe (RESCEU, Tokyo), COE Monkasho Grant. This work is also partially supported by the Sonderforschungsbereich SFB 375 'Astroparticle physics' by the German science foundation DFG, and by the Ministero dell' Universita' e della Ricerca Scientifica under the PRIN project 'The Geometry of Integrable Systems'.

References

[1] N. A. Bahcall, J. P. Ostriker, S. Perlmutter and P. J. Steinhardt, Science **284**, 1481 (1999).

[2] H. L. Bray, Notices of the AMS **49**, 1372 (2002).

[3] T. Buchert, G.R.G. **32**, 105 (2000).

[4] T. Buchert, in: *9th JGRG Meeting, Hiroshima 1999*, Y. Eriguchi et al. (eds.), pp. 306-321 (2000).

[5] T. Buchert and J. Ehlers, A.& A. **320**, 1 (1997).

[6] T. Buchert, M. Kerscher and C. Sicka, P.R.D. **62**, 043525 (2000).

[7] T. Buchert and M. Carfora, C.Q.G. **19**, 6109 (2002).

[8] T. Buchert and M. Carfora, P.R.L. **90**, 31101 (2003).

[9] M. Carfora and K. Piotrkowska, P.R.D. **52**, 4393 (1995).

[10] B. Chow, Preprint: math.DG/0211266 (2002).

[11] G. F. R. Ellis and W. Stoeger, C.Q.G. **4**, 1697 (1987).

[12] R. S. Hamilton, in *Surveys in Differential Geometry Vol 2*, International Press, pp.7-136 (1995).

[13] C. Hellaby, G.R.G. **20**, 1203 (1988).

Non-Topological Soliton in Three-Dimensional Supergarvity

Yoshinori Cho,[1] Kenji Sakamoto,[2] and Kiyoshi Shiraishi[3]

Graduate School of Science and Engineering, Yamaguchi University, Yoshida, Yamaguchi-shi, Yamaguchi 753-8512, Japan

Abstract

We construct non-topological solitons in three-dimensional $U(1)$-gauged $\mathcal{N} = 2$ supergravity. The metric approaches asymptotically the BTZ solution when the scalar field runs into a vacuum of the negative value at radial infinity.

1 Introduction

As is well known, three-dimensional pure Einstein gravity sector is topological theory and has no-propagating degrees of freedom. The solutions are locally flat apart from conical singularities at the location of matter sources in no cosmological constant case [1, 2]. Moreover, cosmological gravity and supergravity are solvable in many cases [3, 4, 5, 6, 7, 8, 9].

Recently, supergravity in three dimensions has been investigated in various situations intensively. The non-linear sigma models coupled to $D = 3$, $\mathcal{N}$-extended supergravity were studied [10]. The geometry of the target manifolds parametrized by scalar fields were classified completely: the target space is Riemanian, Kähler, and quaternionic for $\mathcal{N} = 1$, 2 and $\mathcal{N} = 3$ respectively. For $\mathcal{N} = 4$ it generally decomposes into two separate quaternionic spaces, associated with inequivalent supermultiplets. For $\mathcal{N} = 5, 6, 8$ there is a symmetry space for any given number of supermultiplets. For $\mathcal{N} = 9, 10, 12$ and 16 there are only theories based on a single supermultiplet associated with coset spaces with the exceptional isometry groups F_4, E_6, E_7, and E_8 respectively.

The maximal gauged $\mathcal{N} = 16$ supergravity in three dimensions were constructed [11, 12]. The duality relation between the gauge fields and the scalar fields plays an important role in the derivation of the ungauged $\mathcal{N} = 16$ supergravity: in order to expose its global $E_{8(8)}$ symmetry, all vector fields obtained by dimensional reduction of $D = 11$ supergravity on an 8-torus must be dualized into scalar fields. Moreover, in order for the $\mathcal{N} = 16$ supergravity to gauge, Chern-Simons term (rather than the Yang-Mills term) must be required in the Lagrangian, which does not carry physical degrees of freedom.

Recently, the supersymmetric vortex solutions in $U(1)$-gauged $D = 3$, $\mathcal{N} = 2$ supergravity whose scalar sector is an arbitrary Kähler manifold with $U(1)$ isometry were studied [17]. It has been found that the Einstein equations and the matter field equations of the model can be recast into a set of self-duality equations for a specific eighth-order choice of the Higgs potential which reduces to the sixth-order potential of the flat space model when the Newton gravitational coupling constant is set to zero. The Abelian Chern-Simon Higgs model in three-dimensional Minkowski space and its vortex solution were studied by [13, 14, 15]. It was shown that the model with a specific sixth-order Higgs potential admits topologically stable vortex solutions which satisfy the Bogomol'nyi-type or the first order self-duality equations [16].

We restrict ourselves to the simple case of the Kähelr manifold, and a circularly symmetric ansatz for the metric which approaches asymptotically the BTZ solution [19], which is asymptotically anti-de Sitter space (rather than asymptotically flat) and has no curvature singularity at the origin. In this setting, we construct the non-topological solitons from the eighth-order potential in three-dimensional $U(1)$-gauged $\mathcal{N} = 2$ supergravity rather than the self-coupling constant given by the rotating boson stars, which were obtained numerically by [18].

[1]E-mail:b2669@sty.cc.yamaguchi-u.ac.jp
[2]E-mail:b1795@sty.cc.yamaguchi-u.ac.jp
[3]E-mail:shiraish@sci.yamaguchi-u.ac.jp

2 $U(1)$-gauged $D = 3$, $\mathcal{N} = 2$ supergarvity

In this section we review the construction of $U(1)$-gauged $D = 3$, $\mathcal{N} = 2$ supergarvity by applying the usual Noether method to the non-linear sigma model coupled to $D = 3$, $\mathcal{N} = 2$ supergravity whose target space is assumed to be an arbitrary Kähler manifold with $U(1)$ isometry [10, 11, 12, 17].

The gravity multiplet of the ungauged $D = 3$, $\mathcal{N} = 2$ supergravity contains a dreibein $e_\mu{}^a$ and a complex spinor ψ_μ. On the other hand, the matter sector is given by p copies of the $\mathcal{N} = 2$ scalar multiplet, each consisting of two real scalars and fermions. The scalar fields parametrize a Kähler manifolds of real dimension $2p$, characterized by its Kähler potential $K(\phi^\alpha, \bar{\phi}^{\bar{\alpha}})$.

The ungauged $\mathcal{N} = 2$ supergravity part $\mathcal{L}^S$ is given by:

$$\mathcal{L}^S = \frac{1}{4}eR + \epsilon^{\mu\nu\rho}\bar{\psi}_\mu D_\nu \psi_\rho - eG_{\alpha\bar{\alpha}}(\partial_\mu \phi^\alpha \partial^\mu \bar{\phi}^{\bar{\alpha}} + \bar{\lambda}^{\bar{\alpha}}\gamma^\mu D_\mu \lambda^\alpha) + eG_{\alpha\bar{\alpha}}\bar{\lambda}^{\bar{\alpha}}\gamma^\mu\gamma^\nu\psi_\mu\partial_\nu\phi^\alpha + eG_{\alpha\bar{\alpha}}\bar{\psi}_\mu\gamma^\nu\gamma^\mu\lambda^\alpha\partial_\nu\bar{\phi}^{\bar{\alpha}}, \tag{1}$$

up to terms quartic in the fermions. Here, $G_{\alpha\bar{\alpha}} \equiv G_{\alpha\bar{\alpha}}(\phi, \bar{\phi})$ denotes the Kähler metric $G_{\alpha\bar{\alpha}}(\phi, \bar{\phi}) = \partial_\alpha \partial_{\bar{\alpha}} K(\phi, \bar{\phi})$. We use 2×2 matrices γ^a for the $SO(2,1)$ Dirac algebra, with $\gamma^a\gamma^b = \eta^{ab} - \epsilon^{abc}\gamma_c$; the charge conjugation matric is γ^0. Our metric signature $(-,+,+)$, and $\epsilon^{012} = 1$. The sign of the Newton constant, which in three dimensions is not physically fixed, is taken to be positive.

The property of the non-linear sigma model geometry is invariant under the Kähler transformations

$$K(\phi, \bar{\phi}) \to K(\phi, \bar{\phi}) + F(\phi) + \bar{F}(\bar{\phi}). \tag{2}$$

It is assumed that the Kähler potential possesses an $U(1)$ isometry generated by the vector field

$$\xi = i(\phi^\alpha \partial_\alpha - \bar{\phi}^{\bar{\alpha}}\partial_{\bar{\alpha}}), \tag{3}$$

i.e., ξ generates a Kähler transformation

$$\mathcal{L}_\xi K = i(\phi^\alpha \partial_\alpha - \bar{\phi}^{\bar{\alpha}}\partial_{\bar{\alpha}})K = f(\phi) + \bar{f}(\bar{\phi}), \tag{4}$$

where $F(\phi), f(\phi)$ are the holomorphic function. Then, the Lagrangian $\mathcal{L}^S$ is invariant under the global $U(1)$ isometry.

As in the maximally gauged supergravity theories [11, 12], the following Chern-Simons term $\mathcal{L}^{CS}$ is required, in order to gauge the $U(1)$ Kähler isometry:

$$\mathcal{L}^{CS} = -\frac{1}{8}ge^{\mu\nu\rho}A_\mu F_{\nu\rho}, \tag{5}$$

where $F_{\mu\nu}$ is Abelian field strength and g is a gauge coupling constant. Note that this term is topological and hence does not introduce new propagating degrees of freedom in the gauged theory.

As usual, extra terms in supersymmetry transformations of Eq. (1), due to the g-dependent terms introduced above, are

$$[\mathcal{D}_\mu, \mathcal{D}_\nu]\psi_\rho = \frac{1}{4}R_{\mu\nu}{}^{ab}\gamma_{ab}\psi_\rho + 2G_{\alpha\bar{\alpha}}\mathcal{D}_{[\mu}\phi^\alpha \mathcal{D}_{\nu]}\bar{\phi}^{\bar{\alpha}}\psi_\rho + igCF_{\mu\nu}\psi_\rho, \tag{6}$$

where C is a real Kähler invariant function. In order to compensate these terms, the following extra Yukawa-type bilinear fermionic terms and a scalar potential terms must be added in the Lagrangian:

$$\mathcal{L}^Y = -eg\bar{\psi}_\mu\gamma^{\mu\nu}\psi_\nu B - eg\bar{\lambda}^\alpha\lambda^\alpha S_{\alpha\bar{\alpha}} + egC(\bar{\psi}\gamma^\mu\lambda^\alpha S_\alpha - \bar{\lambda}^\alpha\gamma^\mu\psi_\mu S_{\bar{\alpha}}), \tag{7}$$

$$\mathcal{L}^V = eg^2 V, \tag{8}$$

where the functionals $B(\phi, \bar{\phi})$ and $V(\phi, \bar{\phi})$ are real scalars, while the vector functionals $S_\alpha(\phi, \bar{\phi}) = \overline{S_{\bar{\alpha}}(\phi, \bar{\phi})}$ are complex.

The full Lagrangian of the supersymmetric transformations modified by g-dependent contributions is therefore obtained by:

$$\mathcal{L} = \mathcal{L}^S + \mathcal{L}^{CS} + \mathcal{L}^Y + \mathcal{L}^V. \tag{9}$$

Then the supersymmetric variations are:

$$\delta e_\mu{}^a = \bar{\epsilon}\gamma^a\psi_\mu - \bar{\psi}_\mu\gamma^a\epsilon, \quad \delta\psi_\mu = \mathcal{D}_\mu\epsilon - gB\gamma_\mu\epsilon, \quad \delta\phi^\alpha = \bar{\epsilon}\lambda^\alpha, \tag{10}$$

$$\delta\lambda^\alpha = \mathcal{D}_\mu\phi^\alpha\gamma^\mu\epsilon - gG^{\alpha\bar{\alpha}}CS_{\bar{\alpha}}\epsilon, \quad \delta A_\mu = -2i(\bar{\epsilon}\psi_\mu - \bar{\psi}_\mu\epsilon)C + 2iG_{\alpha\bar{\alpha}}(\phi^\alpha\bar{\lambda}^{\bar{\alpha}}\gamma_\mu\epsilon + \bar{\phi}^{\bar{\alpha}}\bar{\epsilon}\gamma_\mu\lambda^\alpha), \tag{11}$$

and the functionals $B, S_\alpha, S_{\alpha\bar{\alpha}}$ satisfy the following set of the consistency relations:

$$\partial_\alpha B = -CS_\alpha, \quad S_\alpha = 2G_{\alpha\bar{\alpha}}\bar{\phi}^{\bar{\alpha}}, \tag{12}$$

$$\partial_\beta S_\alpha - \Gamma^\gamma_{\alpha\beta}S_\gamma = 0, \quad S_{\alpha\bar{\beta}} = BG_{\alpha\bar{\beta}} - S_\alpha S_{\bar{\beta}} + C\partial_{\bar{\beta}}S_\alpha, \tag{13}$$

while the potential is obtained by

$$V = 2B^2 - G^{\alpha\bar{\alpha}}\partial_\alpha B\partial_{\bar{\alpha}}B. \tag{14}$$

The general solution to these equations takes the form

$$B = C^2 + b, \quad S_\alpha = -2\partial_\alpha C = 2G_{\alpha\bar{\alpha}}\bar{\phi}^{\bar{\alpha}}, \tag{15}$$

$$S_{\alpha\bar{\beta}} = BG_{\alpha\bar{\beta}} - S_\alpha S_{\bar{\beta}} - 2C\partial_\alpha\partial_{\bar{\beta}}C, \tag{16}$$

where b is an arbitrary constant real parameter. In the limit $g \to 0$, one recovers the ungauged theory.

3 Non-topological soliton

We restrict ourselves to the simple case of the full Lagrangian constructed in the preceding section. We adopt a single complex scalar field case, that is $p = 1$. Moreover, we assume that the Kähler manifolds for which f as defined in Eq. (4) is an imaginary constant $f = iC_0$, i.e. K is a function of $R = |\phi|$ only and Kähler potential is $K(R) = R^2$ in order to obtain the canonical kinetic term for the scalar fields. And $G \equiv G_{11}$ is set to be unity.

The bosonic parts of the full Lagrangian Eq. (9) then is given by:

$$\mathcal{L}^{BP} = \frac{1}{4}eR - e\mathcal{D}_\mu\phi\mathcal{D}^\mu\bar{\phi} - \frac{1}{8}g\epsilon^{\mu\nu\rho}A_\mu F_{\nu\rho} - eg^2V, \tag{17}$$

where $D_\mu\phi = (\partial_\mu + igA_\mu)\phi$, and the eighth-order scalar potential (shown in Fig.1 (a)) is given by:

$$V = -2g^2[\phi^8 - 2(2c+1)\phi^6 + 2(3c^2+2c+b)\phi^4 - 2c(2c^2+c+2b)\phi^2 + c^4 + b^2 + 2bc^2]. \tag{18}$$

where b and c are arbitrary real constant parameters.

We assume the three-dimensional metric for a circularly symmetric spacetimes as

$$ds^2 = -e^{-2\delta(r)}\Delta(r)dt^2 + \Delta^{-1}(r)dr^2 + r^2(d\theta^2 - \Omega(r)dt)^2, \tag{19}$$

where δ, Δ, and Ω are functions of the radial coordinate r only.

For the single complex scalar field, we also assume the following dependence on the coordinates:

$$\phi = R(r)e^{-in\theta}. \tag{20}$$

where $R(r)$ is a function of the radial coordinate r only and n is a constant. For the boundary condition in order to obtain the non-topological soliton, we adopt that $\phi(r)$ approaches zero when the radial coordinate r is taken to infinity.

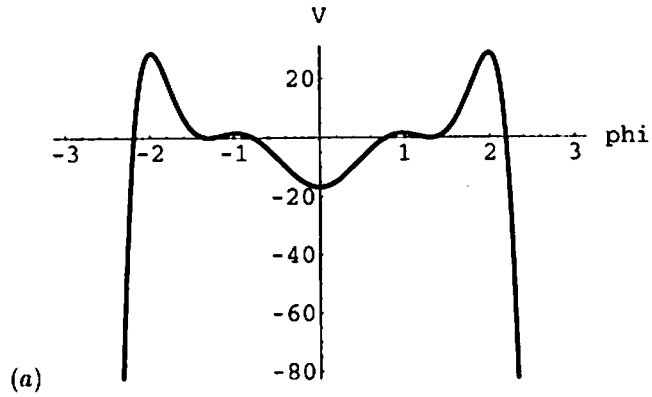
For the vector field A_μ we choose the gauge in which

$$A_r = 0, \quad A_\theta = P(r) + \frac{n}{g}, \quad A_t = W(r). \tag{21}$$

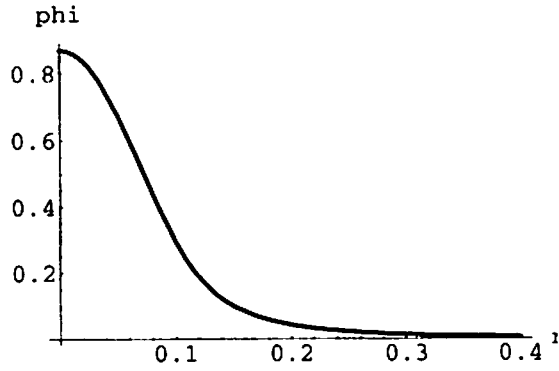
Here $P(r)$ and $W(r)$ are a function of the radial coordinate r only.

Varying the Lagrangian with respect to the gauge field, the scalar field and the metric yields equations of motion. The equation of motion for Chern-Simons term induces the first order equations

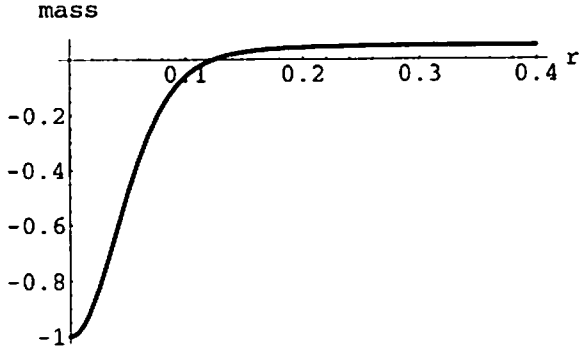
$$\epsilon^{\mu\nu\rho}F_{\nu\rho} = 8ire^{-\delta}(\bar{\phi}\mathcal{D}^\mu\phi - \phi\mathcal{D}^\mu\bar{\phi}), \tag{22}$$



(a)



(b)



(c)

Figure 1: eighth-order scalar potential (a), ϕ as a function of the radial coordinate r (b) and mass as the function of the radial coordinate r (c)

two of these equations take the form:

$$\partial_r W = -4gr\Delta^{-1}e^{\delta}R^2\Omega(W+\Omega P)+4gR^2Pr^{-1}e^{-\delta}, \tag{23}$$

$$\partial_r P = 4gr\Delta^{-1}R^2e^{\delta}(W+\Omega P), \tag{24}$$

and $r=\mu$ is automatically satisfied.

The scalar field equation is reduced to the form:

$$R''+\left(\frac{\Delta'}{\Delta}+\frac{1}{r}-\delta'\right)R'+\frac{g^2e^{2\delta}R}{\Delta^2}(W+\Omega P)^2-\frac{g^2P^2R}{r^2\Delta}=\frac{1}{2\Delta}\frac{\partial V}{\partial R}. \tag{25}$$

And also Einstien equation is reduced to:

$$\frac{1}{2}\frac{\Delta'}{r}+\frac{1}{4}r^2e^{2\delta}(\Omega')^2 = -\kappa^2\left[\frac{e^{2\delta}}{\Delta}g^2R^2(W+\Omega P)^2+\Delta(R')^2+\frac{(gPR)^2}{r^2}+V\right], \tag{26}$$

$$\frac{\Delta}{r}\delta' = -2\kappa^2\left[\frac{e^{2\delta}}{\Delta}g^2R^2(W+\Omega P)^2+\Delta(R')^2\right], \tag{27}$$

$$\frac{\Delta}{2r^2}(r^3e^{\delta}\Omega')' = 2\kappa^2g^2R^2Pe^{\delta}\frac{W+\Omega P}{r}. \tag{28}$$

If we require that there be no singularity in the central vacuum region, the spacetime must be the anti-de Sitter spacetime. We set the metric which approaches asymptotically the BTZ solution. These equations unfortunately cannot be solved analytically. Then we will find the numerical solution. We have shown that Fig. 1 (b) is the soliton ϕ as the function of the radial coordinate r and Fig. 1 (c) is the mass as the function of the radial coordinate r.

4 Conclusion

We have constructed numerically the non-topological solitions, which has a positive mass, in three-dimensional $U(1)$-gauged $\mathcal{N} = 2$ supergravity. It is shown that the metric approaches asymptotically the BTZ solution when the scalar field runs into a vacuum of the negative value at radial infinity. The soliton does not preserve the supersymmetry, because the metric is described by the BTZ solution at radial infinity. So far, we have treated the soliton with zero-winding number case, i.e. $n = 0$ only. We will further investigate the binding energy, the stability of the soliton.

References

[1] S. Desr, R. Jackiw, and G. 't Hooft, Ann. Phys. (N. Y.) **152,** 220 (1984).

[2] S. Giddings, J. Abbott, and K. Kuchar, Gen. Relativ. Gravit. **16,** 751 (1984).

[3] E. Witten, Nucl. Phys. **B311,** 46 (1988).

[4] I. Bengtsson, Phys. Lett. B **220,** 51 (1989).

[5] S. Carlip and J. E. Nelson, Phys. Lett. B **324,** 299(1994).

[6] H.-J. Matschull, Class. Quantum Grav. **16,** 2599 (1999).

[7] S. Deser, R. Jackiw, and G. 't Hooft, Ann. Phys. (N.Y.) **153,** 405 (198).

[8] S. Deser and J. H. Key, Phys. Lett. **120B,** 97 (1983).

[9] A. Achúcarro and P. K. Townsend, Phys. Lett. **180B,** 89 (1986).

[10] B. de Wit, A. K. Tollsén, and H. Nicolai, Nucl. Phys. **B392,** 3 (1993).

[11] H. Niclai and H. Samtleben, Phys. Rev. Lett. **86,** 1686 (2001).

[12] H. Niclai and H. Samtleben, J. High Energy Phys. **04,** 022 (2001).

[13] J. Hong, Y. Kim, and P. Y. Pac, Phys. Rev. Lett. **64,** 2230 (1990).

[14] R. Jackiw and E. J. Weinberg, Phys. Rev. Lett. **64,** 2234 (1990).

[15] R. Jackiw, K.-Y. Lee, and E. J. Weinberg, Phys. Rev. D **42,** 3488 (1990).

[16] E. B. Bogomol'nyi, Sol. J. Nucl. Phys. **4,** 449 (1976).

[17] M. Abou-Zeid and H. Samtleben, Phys. Rev. D **65,** 085016 (2002).

[18] K. Sakamoto and K. Shiraishi, Phys. Rev. D **62,** 124014 (2000).

[19] M. Bañados, C. Teitelboim, and J. Zanelli, Phys. Rev. Lett. **69,** 1849 (1992); M. Bañados, M. Henneaux, C. Teitelboim, and J. Zanelli, Phys. Rev. D **48,** 1506 (1993). For a review of BTZ black holes, S. Carlip, Class. Quantum Grav. **12,** 2853 (1995).

An Accelerating Universe in Space-Time-Matter Cosmology

Takao Fukui[1]

Department of Language and Culture,
Dokkyo University, Gakuencho, Soka, Saitama 340-0042, Japan

Abstract

Parameters appeared in a 5D Space-Time-Matter cosmology are explored by taking account of an accelerating universe in the present era. A favourable combination of the domains for the parameters leads the universe to avoid singularity at the beginning of the universe.

1 Introduction

5D Space-Time-Matter (hereafter abbreviated to 5D STM) theory of gravity is defined as a thoery that the fifth (Matter) coordinate $l \equiv Gm/c^2$ is introduced to the 4D Sapce-Time theory of gravity. m is the rest mass of matter. The procedure is just along the same line as that taken by Minkowski in fusing space and time to form a unified four-dimensional spacetime continuum. The 5D STM theory, called an induced matter theory, was proposed by Wesson first [1]. It has the advantage of interpreting most physical properties of matter in the 4D spacetime as the result of 5D Riemannian geometry. For example, a solution obtained by Fukui in a vacuum 5D STM cosmology gives the state of the radiation era in the 4D universe [2]. The other states of the universe are shown by Fukui and Overduin through studying the relation of the 5D STM theory to the scalar-tensor theory [3]. The 5D STM theory enables Wesson and Seahra to study the shape of universe, i.e. accurate pictures of the Big Bang [4]. Wesson elaborates the whole works on the 5D STM theory of gravity in his book [5].

Recently a new solution was found by Fukui et al. by applying the theory to the Robertson-Walker like uiverse [6]. The solution contains three major parameters which concern the evolution of the universe. It means that an accelerating universe inferred from the observational data on type Ia supernovae might play a role in narrowing the domains for the parameters to take. In the present work, we place some constraints on these parameters and choose a favourable combination of the domains for the parameters.

2 Solution

The following 5D metric is assumed in the present work, by adding the fifth coordinate l defined above, to the 4D Robertson-Walker (RW) metric,

$$dS^2 = \sigma\left\{dt^2 - a^2\left[\frac{dr^2}{1-kr^2} + r^2 d\Omega^2\right]\right\} + \epsilon b^2 dl^2, \tag{1}$$

where a conformal factor $\sigma = \sigma(l)$ is taken for generality of the 4D universe. The scale factors of 4D and 5D manifolds, a and b are functions of time and matter coordinates, $a = a(t,l)$, $b = b(t,l)$. $\epsilon = \pm 1$ describes the nature of the extra dimension. We employ $c = G = 1$ unit systemCi.e. L=M=T=1.

The 5D field equations in vacuum are obtained from an extended 5D Einstein tensor being equal to zero, $G_{AB} = 0$. A, B run over $0 - 3, 5$. The 5D STM universe should be in vacuum in order to derive 4D physical properties from 5D Riemannian geometry. In the case of $\sigma = const. \equiv \sigma_0$, a simple class of solutions are obtained by Fukui et al. [6], and are cited below for covenience,

1) Extra-dimensional scale factor;

The solution of the fifth dimensional scale factor $b(t,l)$ gives us a clue to non-variability of mass in the 4D universe. The solution is given as follows,

$$b(t,l) = -\frac{4\epsilon\sigma_0 f f' F^2 t^2 - 2g' F^2 t + gg' F - \epsilon\sigma_0 f f'(g^2+\kappa)}{4af F^2}, \tag{2}$$

[1]E-mail:tfukui@dokkyo.ac.jp

where $(') \equiv \partial/\partial l$, $F = F(l) \equiv \epsilon\sigma_0 f^2 + k$, $f = f(l)$, $g = g(l)$, and κ is an integration constant with respect to the fifth coordinate. In the case of $f' = g' = 0$, i.e. $b = 0$, the metric reduces to the 4D RW metric by a scale transformation $\tilde{g}_{\mu\nu} = \sqrt{\sigma_0} g_{\mu\nu}$. Therefore the 4D universe migt be embedded where f and g attain their extrema in the 5D STM universe. There the value of l should be fixed on the conditions of $f' = g' = 0$, and thus the rest mass in the 4D universe does not vary. More speculatively, if we could assume that in the 5D STM universe, there are wave-like irregularities, ripples, expressed as follows ,

$$f(l) = sin(\alpha_f l + \beta_f) \tag{3}$$

and

$$g(l) = sin(\alpha_g l + \beta_g), \tag{4}$$

then our 4D universe would appear where $cos(\alpha l + \beta) = 0$, i.e. $\alpha l + \beta = \pi/2 + n\pi$. α and β are constants. The situation fixes the value of l, and thus the rest mass in the 4D universe results in being non-variable. By taking different values of n, we might explain the characteristic mass of matter, e.g. of an elementary particle [7].

2) 3-dimensional scale factor;

The 3D scale factor $a(t, l)$ which is concerned with the evolution of the 4D universe, is given as follows,

$$a^2(t, l) = -\frac{(2Ft - g)^2 + \kappa}{4F}. \tag{5}$$

The evolutionary path of the 4D universe depends on the three parameters F, κ and g. Among the sensible combinations of the domains for the parameters to take according to a conventional evolution of the 4D universe, the followings are probable. The other combinations give strange evolution, e.g. an imaginary 3D scale factor or a contracting universe at the beginning of the universe.

F	κ	g	Comments
+	−	+	$g^2 + \kappa < 0$, no singularity→ expansion→ contraction $g^2 + \kappa = 0$, singularity→ expansion→contraction
0	−	+	$a = \sqrt{gl}$
−	+	+, 0	no singularity→ expansion
	0	+	no singularity→ expansion
		0	singularity→expansion
	−	+	$g^2 + \kappa > 0$, no singularity→ expansion $g^2 + \kappa = 0$, singularity→ expansion

Table 1: Probable Combinations of the Domains for F, κ and g

3 Deceleration Parameter

To study the acceleration of the universe, here we derive the deceleration parameter proper to the present model of the universe. According to the definition of the deceleration parameter, the parameter for the present solution Eq.(5) is obtained as follows,

$$q \equiv -\frac{\ddot{a}a}{\dot{a}^2} = -\frac{\kappa}{(2Ft - g)^2}. \tag{6}$$

Then $\kappa > 0$ is demanded from an acceleration of the universe. Among the probable combinations above, only $F < 0$, $\kappa > 0$ and $g \geq 0$ is the case. From Eq.(5), $a \neq 0$ at $t = 0$, because $g^2 + \kappa \neq 0$. That is, the favourable combination implies that the universe starts without a singularity and bounces at $t = g/2F \leq 0$ from contraction to expansion. The avoidance of the singularity is mainly caused by κ which is introduced with respect to the fifth coordinate. Therefore in the present scenario, an accelerating universe spontaneously leads to no initial singularity. This might be one of the advantages of the 5D STM theory. However the combination forces the universe to accelerate throughout its history neither with the decelerating period nor with the exponential expansion at the very beginning of the universe. It might change drastically the conventional evolution of the universe.

4 Comments

According to Misner et al. [8], the m-z relation is given as follows,

$$m = 5log_{10}[(1+z)R_c] - 2.5log_{10}L + const., \tag{7}$$

where L is intrinsic luminosity of a celestial body. R_c is the "radius of curvature" of the 2-sphere surrounding the emitter and passing through the receiver at the time of reception of the light from the celestial body, and is given as follows,

$$R_c = \begin{cases} a_R sinh(\chi_R - \chi_E) & \text{if } k = -1, \\ a_R(\chi_R - \chi_E) & \text{if } k = 0, \\ a_R sin(\chi_R - \chi_E) & \text{if } k = 1. \end{cases} \tag{8}$$

The Schwarzschild radial coordinate r in Eq.(1) is transformed into χ by the following relations,

$$r = \begin{cases} sinh\chi & \text{if } k = -1, \\ \chi & \text{if } k = 0, \\ sin\chi & \text{if } k = 1. \end{cases} \tag{9}$$

Subscripts R and E denote receiving and emitting respectively. The "radial comoving distance" for the photon propagation $\chi_R - \chi_E$ is obtained by using Eq.(5), the 3D scale factor a, in the favourable combination $F < 0$, $\kappa > 0$ and $g \geq 0$ as follows,

$$\chi_R - \chi_E = \int_{t_E}^{t_R} \frac{1}{a} dt = \frac{1}{\sqrt{-F}} log \frac{\tau_R + \sqrt{\tau_R{}^2 + \kappa}}{\tau_E + \sqrt{\tau_E{}^2 + \kappa}}, \tag{10}$$

where $\tau \equiv -2Ft + g$. In the case that κ is negligibly small as compared to τ, Eq.(10) is approximated to

$$\chi_R - \chi_E \sim \frac{1}{a_R H_R} log(1+z), \tag{11}$$

where H is the Hubble parameter. Eq.(11) reduces to the conventional equation for small z. Numerical calculations however are needed to evaluate Eq.(10), or Eq.(11) for higher z.

Before the favourable combination might be justified, the m-z relation and other effectes on the evolution of the universe have to be further explored .

References

[1] P.S. Wesson, Astron. Astrophys. **119**, 145 (1983).

[2] T. Fukui, Gen. Rel. Grav. **19**, 43 (1987).

[3] T. Fukui and J.M. Overduin, Int. J. Mod. Phys. **D11**, 669 (2002).

[4] P.S. Wesson and S.S. Seahra, Ap. J. Letters, **558**, L75 (2001).

[5] P.S. Wesson, *Space-Time-Matter* (World Scientific, Singapore, 1999).

[6] T.Fukui, S.S. Seahra and P.S. Wesson, J. Math. Phys. **42**, 5195 (2001).

[7] T. Fukui, Gen. Rel. Grav. **20**, 1037 (1988).
T. Fukui, in *Abstracts of 12th International Conference on General Relativity and Gravitation* (University of Colorado at Boulder, 1989), p.372.

[8] C.W. Misner, K.S. Thorne and J.A. Wheeler, *Gravitation* (W.H. Freeman and Company, San Francisco, 1970), p.784.

Recent progress in wormhole dynamics

Sean A. Hayward[1]

Department of Science Education, Ewha Womans University, Seoul 120-750, Korea

Abstract

Space-time wormholes were introduced in Wheeler's idea of space-time foam. Traversible wormholes as defined by Morris & Thorne became popular as potential short cuts across the universe and even time machines. More recently, the author proposed a general theory of wormhole dynamics, unified with black-hole dynamics. This article gives a brief review of the above ideas and summarizes progress on wormhole dynamics in the last year. Firstly, a numerical study of dynamical perturbations of the first Morris-Thorne wormhole showed it to be unstable, either collapsing to a black hole or exploding to an inflationary universe. This provides a mechanism for inflating a wormhole from space-time foam to usable size. Intriguing critical behaviour was also discovered. Secondly, a wormhole solution supported by pure radiation was discovered and used to find analytic examples of dynamic wormhole processes which were also recently found in a two-dimensional dilaton gravity model: the construction of a traversible wormhole from a Schwarzschild black hole and vice versa, and the enlargement or reduction of the wormhole.

1 Introduction

Space-time wormholes were first described as such by Wheeler [1], who envisaged the still-popular space-time foam: the smooth space-time of General Relativity suffering quantum-gravitational fluctuations in topology at the Planck scale, becoming a continual foam of transient interconnections. Curiously, all the standard black-hole solutions have a wormhole spatial topology, with a minimal surface connecting two asymptotically flat regions, our universe and a mirrored universe. For the simplest Schwarzschild black hole, this Einstein-Rosen bridge was properly understood only much later, also by Wheeler, as a non-traversible wormhole: the two universes are not in causal contact, with any attempted crossing leading only into the black hole. (See last year's proceedings [2] for space-time diagrams and explanations mostly not repeated here). Later still, Morris & Thorne [3] proposed traversible wormholes, which have similar spatial geometry, with a minimal surface connecting two asymptotically flat regions, but such that the minimal surface (the wormhole throat) is preserved in time. Thus a traveller can cross between the two universes at will. Such wormholes became popular both in science fiction and as a research topic [4], apparently also allowing time-machine construction. However, most research has concerned static or cut-and-paste wormholes, or lacked an independently defined exotic matter model. In contrast, the dynamical behaviour of wormholes has received little attention until recently, and it is only in the last year or two that exact solutions describing wormhole construction and enlargement have been found.

2 Static and dynamic wormholes

Morris & Thorne's unusually accessible article gave a list of criteria for traversible wormholes which is still worth consulting. Paraphrasing briefly, the basic wormhole criteria were: (1) a static, spherically symmetric space-time; (2) the Einstein equation; (3) a throat (minimal surface) connecting two asymptotically flat regions; and (4) no (Killing) horizon, so that the wormhole allows two-way travel. The usability criteria were (5) small tidal gravitational forces and (6) small proper time for crossing, by human scales. Finally, the criteria which were mentioned but largely left open were: (7) physically reasonable matter; (8) perturbative stability, e.g. due to a spaceship; and (9) that it should be possible to assemble the wormhole. These are, of course, the more interesting issues.

[1]E-mail: hayward@mm.ewha.ac.kr

Recent work can be summarized by a corresponding list. (1) One needs to generalize to any space-time, without symmetry, in particular to non-static space-times. (2) Although Einstein gravity will be assumed in this article, many alternative gravitational theories allow traversible wormhole solutions, including scalar-tensor theories and brane-world models. The most fundamental point is that one needs to (3) generalize and localize the definition of the throat and (4) impose local two-way traversibility. Such a definition was given by the author [5] in terms of trapping horizons, which are hypersurfaces foliated by marginal surfaces, which are extremal surfaces in a null (light-like) hypersurface [6]–[8]. They can be locally classified as future or past and outer or inner. Examples include the outer and possible inner horizons of black and white holes. For a Morris-Thorne wormhole, the throat is a double outer trapping horizon; double since the minimal surfaces are extremal in both null directions, and outer since the extremal surface should be minimal rather then maximal, encoding the so-called flare-out condition. The doubled nature of the throat indicates that a non-static wormhole will generally have two mouths, defined by outer trapping horizons, connected by a tunnel of trapped surfaces. In the static case, the tunnel shrinks away and the mouths coincide as the throat. A similar understanding was reached contemporaneously by Hochberg & Visser [9], though their flare-out condition can generically select maximal rather than minimal surfaces in a time-symmetric hypersurface.

The author proposed that a black hole can be locally characterized by an achronal (spatial or null) future outer trapping horizon, and a traversible wormhole by two temporal (time-like) outer trapping horizons in mutual causal contact [5]. Note that the main difference is the causal nature of the horizon, which is respectively one-way or two-way traversible, as expected in each case. The Einstein equation then shows that they occur respectively under positive and negative energy density, specifically referring to the null energy condition [5]. This means that they are supported respectively by normal matter or vacuum, and what was dubbed exotic matter [3]. This explains why black holes are common astrophysically, while wormholes have not been observed. However, the recently discovered acceleration of the universe implies that cosmic evolution is dominated by unknown dark energy, which violates at least the strong energy condition. Also, it is well known that negative energy densities are endemic in quantum field theory. Whatever the identity of the exotic matter, there is a unified framework for traversible wormholes, black holes and white holes [5]–[8]. Since the causal nature of the horizons depends on the sign of the energy density, which may change with time, black holes and wormholes should theoretically be interconvertible. A famous example is a Schwarzschild black hole evaporating by Hawking radiation, which semi-classically is a traversible wormhole by any reasonable definition [2, 5].

Returning to the Morris-Thorne criteria, the usability criteria (5)–(6) are already sufficiently general. However, any concrete study of wormhole dynamics requires (7) a specific exotic matter model, so that there are field equations to determine the evolution. Most early studies ignored the identity of the exotic matter [3, 4], but authors increasingly address this issue. Much work has concentrated on alternative gravitational theories such as scalar-tensor theories, where static wormhole solutions are found to be common. Other work draws the exotic matter from quantum field theory in a semi-classical approximation. The author has proposed using simple exotic matter models, in order to study issues of principle which were hardly understood. This has led to concrete examples which show conclusively that (8) wormhole stability depends on the exotic matter model. Although there have been various studies of linearization stability, dynamic stability has been investigated in only two cases: the HKL wormhole was found analytically to be dynamically stable [10], while the first Morris-Thorne wormhole was found numerically to be dynamically unstable [11]. Finally, concerning (9) how to assemble or construct a wormhole: irradiating a CGHS black hole with negative energy converts it to an HKL wormhole [10, 12], and similarly a wormhole discovered recently by the author [13] can be constructed from a Schwarzschild black hole [14]. The main results of these recent studies are summarized in the following.

3 Analytical results

The first concrete results were found using an exactly soluble model, CGHS two-dimensional dilaton gravity, generalized to include a massless ghost (negative-energy) Klein-Gordon field, which supports the existence of static wormhole solutions [10]. One can then set initial data corresponding to dynamical perturbations of a CGHS black hole or an HKL wormhole, then analytically find the evolved space-time. As described in last year's proceedings [2], solutions were found describing wormhole collapse to a black

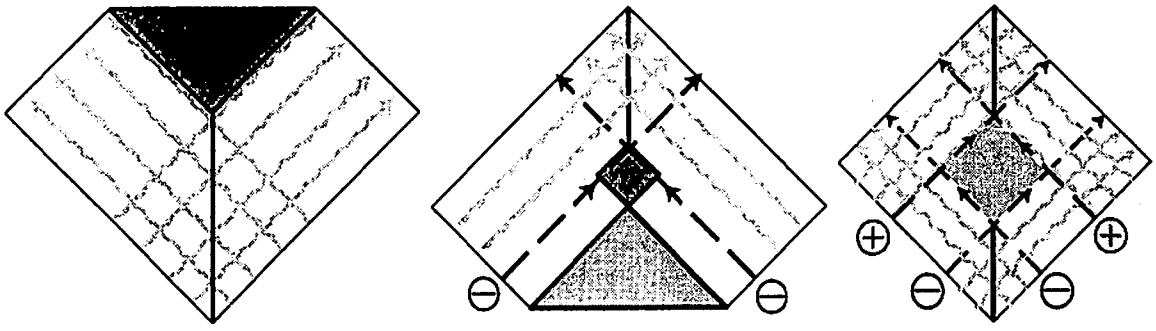


Figure 1: Penrose space-time diagrams. (i) A wormhole collapses to a black hole if the supporting ghost radiation, represented by wavy lines, is switched off. (ii) A wormhole is constructed from a black hole by irradiating with impulsive ghost radiation, represented by dashed lines, followed by constant non-impulsive radiation to support the resulting wormhole. (iii) A wormhole is enlarged by beaming in impulsive ghost radiation, switching off the non-impulsive radiation, then beaming in compensating impulsive normal radiation. The bold lines represent the trapping horizons, light shading indicates past trapped regions and darker shading indicates future trapped regions. The impulses discontinuously shift the trapping horizons constituting the black-hole horizons or the wormhole throat. In the dilaton gravity model, this refers to the CGHS black hole and the HKL wormhole, and in full Einstein gravity to the Schwarzschild black hole and a recently discovered wormhole.

hole, wormhole construction from a black hole, wormhole operation for transport, including the back-reaction of the transported matter on the wormhole, and wormhole maintenance, i.e. maintaining a static state under transportation [10].

In order to study similar dynamic processes in full Einstein gravity, the author proposed a simple exotic matter model, pure ghost radiation, i.e. pure radiation with negative energy density [2]. Wormhole solutions of the Morris-Thorne type were found [13], supported by equal left-moving and right-moving radiation. Since the radiation propagates without interaction or backscattering, it is easy to see what happens if it is suddenly switched off from both sides of the wormhole: the wormhole collapses to a black hole, as in Fig.1(i). The radiation escapes in Vaidya regions, leaving a vacuum Schwarzschild region, with continuity determining that the wormhole throat bifurcates to form the black-hole horizons.

For other dynamic processes, a useful idealization is impulsive radiation, where the radiation is concentrated so as to deliver finite energy and momentum in an instant. In the two-dimensional model, further examples were given of wormhole construction and operation, plus how to stably enlarge a wormhole [12]. Corresponding versions of some of these processes can be found analytically in full Einstein gravity by matching Schwarzschild, Vaidya and static-wormhole regions [14]. In particular, irradiating a Schwarzschild black hole with impulsive then constant ghost radiation can convert it to a wormhole of the above type, as in Fig.1(ii). Also, the wormhole can be enlarged by adding additional impulsive ghost radiation followed by balancing normal impulsive radiation, as in Fig.1(iii). The ghost radiation is switched off between the impulses, so that the middle region is found analytically as part of a Schwarzschild white hole, therefore expanding and increasing the wormhole size. The opposite ordering of the impulses would reduce the wormhole size. These will be the first analytic solutions describing wormhole construction or enlargement in full Einstein gravity.

4 Numerical results

The first numerical study of wormhole dynamics was also performed recently [11]. The starting point was a static wormhole which is best known as Morris & Thorne's opening example, though it is actually a solution for a massless ghost Klein-Gordon field, as was shown earlier by various authors. The idea was to study dynamical perturbations of this static wormhole, using the spherically symmetric Einstein system with the above exotic matter model, and also a normal massless Klein-Gordon field, to see the effect on the wormhole of normal matter, like an astronaut or spaceship traversing the wormhole.

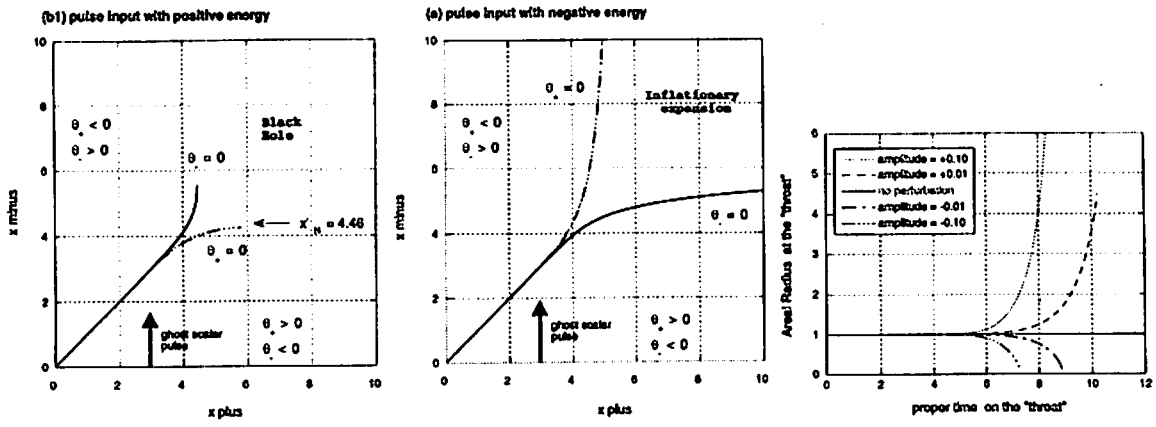


Figure 2: Location of the trapping horizons $\theta_{\pm} = 0$ when the static wormhole is perturbed by Gaussian pulses with (i) positive energy and (ii) negative energy. The axes are the dual-null coordinates $x^{\pm}$, so that a 45° counterclockwise rotation of the figure is a partial Penrose diagram. (iii) Areal radius of the throat $x^{+} = x^{-}$, plotted as a function of proper time. Additional negative energy causes inflationary expansion, while reduced negative energy causes collapse to a black hole and central singularity. For smaller initial energy, the collapse or explosion occurs more slowly.

A numerical code was developed based on a dual-null coordinate system, in order to follow the horizon dynamics and radiation propagation accurately. After testing the code by evolving the static wormhole, the numerical experiments added or subtracted Gaussian pulses in the ghost field or the normal field, parametrized by amplitude, width and position. The space-time evolution was followed by tracking the trapping horizons and quantities such as area and energy. The local gravitational energy [7] is a key indicator: for the static wormhole it is positive, maximal at the throat and tends to zero at infinity, so that the total (Bondi or ADM) mass of the static wormhole vanishes. For dynamic perturbations, the sign and size of the initial Bondi energy E_0 was found to be the main factor affecting the outcome.

Fig.2(i) shows what happens for a positive-energy pulse, $E_0 > 0$: when the pulse hits the wormhole throat, the double trapping horizon bifurcates to form a tunnel of future trapped surfaces, with the two mouths accelerating away from each other and approaching the speed of light, forming the horizons of a black hole. The final mass M of the black hole can be easily extracted due to rapid convergence in the dual-null system. In summary, the wormhole has collapsed to a black hole.

Fig.2(ii) shows what happens for a negative-energy pulse, $E_0 < 0$: when the pulse hits the wormhole throat, the double trapping horizon bifurcates to form a tunnel of past trapped surfaces, with the two mouths accelerating away from each other and approaching the speed of light, forming the cosmological horizons of an inflationary universe. The Hubble constant H can be found by fitting the exponential curve of area against proper time, Fig.2(iii). In summary, the wormhole has exploded into an inflationary universe. This provides the first concrete mechanism for inflating wormholes from space-time foam to macroscopic size.

For Gaussian pulses in the normal field, the results are similar, except that the total energy E_0 is necessarily positive and so the wormhole always collapses to a black hole. Thus a traveller successfully crossing the wormhole would nevertheless look back to discover that the passage has caused the wormhole to collapse, thereby ironically sealing off the causal connection to the home universe.

By varying mainly the amplitude of the pulse, perturbations as small as $E_0 \approx \pm 10^{-4} a/2$ can be reliably evolved, where a is the initial throat radius. In all cases, positive or negative initial energy respectively causes collapse or explosion. Clearly the wormhole is dynamically unstable, though it had been previously found to be linearization stable, indicating a non-linear instability. For smaller perturbations, the collapse or explosion occurs more slowly and the final mass or Hubble constant is smaller. Unexpected critical behaviour was also discovered: the initial energy determines the collapse time $x - x_0 = -0.60 \ln E_0$ and there appears to be a minimal black-hole mass $M = 0.30a$ or Hubble constant $H = 1.1/a$ as perturbations tend to zero, for both exotic and normal field perturbations. All this is unexplained.

5 Conclusions

The largely new area of wormhole dynamics has been substantially developed recently, based on a local, dynamical theory of traversible wormholes [5], with mouths defined by temporal outer trapping horizons, unified with a local, dynamical theory of black holes [6]–[8]. Concrete examples [10]–[14] have supported the following conclusions.

- Traversible wormholes can be constructed from black holes by absorbing exotic matter.
- Traversible wormholes can collapse to black holes, by losing exotic matter or gaining normal matter, such as a traveller or spaceship.
- Traversible wormholes can explode to inflationary universes, by gaining exotic matter. This provides a mechanism for inflating wormholes from space-time foam to usable size.
- An exotic matter model must be specified for a given problem. Apart from semi-classical quantum field theory, dark energy models and alternative gravitational theories, simple models have theoretical merit in understanding basic principles.
- Traversible wormholes can be dynamically stable or unstable, depending on the exotic matter model. Linearization stability is not conclusive.
- Stable wormholes can be operated and maintained by balance of positive and negative energy, and enlarged or reduced by ordering of positive and negative energy.
- Numerically discovered critical behaviour suggests critical black-hole and inflationary-universe solutions.
- Wormhole dynamics with a specific exotic matter model need not be plagued by naked singularities or causal loops. Time-machine construction [3, 4], often described as ridiculously easy from (cut-and-paste) wormholes, is still an open question if given field equations are to be satisfied everywhere. Cosmic Censorship and Chronology Protection may yet survive physically reasonable exotic matter.

Research partially supported by Korea Research Foundation grant KRF-2001-015-DP0095. Thanks to the conference organizers for support and Hiroko Koyama and Hisa-aki Shinkai for supplying figures.

References

[1] J A Wheeler, Ann. Phys. **2**, 604 (1957).

[2] S A Hayward, in *Proceedings of the eleventh workshop on general relativity and gravitation*, eds. J Koga *et al.* (Waseda University 2002), p.233.

[3] M S Morris & K S Thorne, Am. J. Phys. **56**, 395 (1988).

[4] M Visser, *Lorentzian Wormholes: from Einstein to Hawking*, (AIP Press 1995).

[5] S A Hayward, Int. J. Mod. Phys. **D8**, 373 (1999).

[6] S A Hayward, Phys. Rev. **D49**, 6467 (1994).

[7] S A Hayward, Class. Quantum Grav. **15**, 3147 (1998).

[8] S A Hayward, in *Proceedings of the Ninth Marcel Grossmann Meeting on General Relativity*, eds. V G Gurzadyan *et al.* (World Scientific 2002).

[9] D Hochberg & M Visser, Phys. Rev. Lett. **81**, 746 (1998).

[10] S A Hayward, S-W Kim & H Lee, Phys. Rev. **D65**, 064003 (2002).

[11] H Shinkai and S A Hayward, Phys. Rev. **D66**, 044005 (2002).

[12] H Koyama, S A Hayward and S-W Kim, *Construction and enlargement of dilatonic wormholes by impulsive radiation*, Phys. Rev. **D** (to appear).

[13] S A Hayward, Phys. Rev. **D65**, 124016 (2002).

[14] H Koyama, S A Hayward and S-W Kim, in preparation.

[15] Many important references have been omitted here due to size and format restrictions.

An Investigation of the Tomimatsu-Sato Spacetime

Wataru Hikida[1] and Hideo Kodama[2]

Yukawa Institute for Thoretical Physics, Kyoto University, Kyoto 606-8502,Japan

Abstract

We investigate the structure of the $\delta = 2$ Tomimatsu-Sato spacetime. We show that this spacetime has degenerate horizons with two components, in contrast to the general belief that the Tomimatsu-Sato solutions with even δ do not have horizons.

1 Introduction

One of the most important problems in the relativistic astrophysics and gravitation theory is the final state of a massive star. In general relativity, such a collapse is usually assumed to end up with the formation of a regular black hole, but the possibility of the formation of a naked singularity is not ruled out. Concerning to this problem, Penrose [1] proposed the conjecture that the latter possibility will not be realized under physically realistic conditions, which is called the *cosmic censorship hypothesis*. This conjecture, however, still remains to be proved and there are many counterexamples in the spherically symmetrical cases.

The best known example of naked singularities is the shell-focusing singularities in the spherically symmetric dust collapse, so called the Tolman-Bondi model [2, 3]. Another important example is the critical phenomena in gravitational collapse, which was first found for spherically symmetric collapse of a massless scalar field by Choptuik [4]. In this example, although the naked singularity formation is not generic, a naked singularity solution and a self-similar structure appears as a critical point for a generic continuous initial data. Hence, there exist a generic set of regular solutions in any small neighborhood of the singular solutions in the initial data space. Due to this, the structure of the singular solutions play a crucial role in determining the behavior of solutions near the critical point, and the fate of the gravitational collapse.

Although these examples show that the formation of naked singularities is rather generic and solutions with naked singularities may play a key rule for the spherically symmetric gravitational collapse, the assumption of the spherically symmetry is too restrictive to say anything on the cosmic censorship hypothesis in realistic systems. We must investigate systems with less symmetry. In such investigations, it is expected that the analysis of naked singular solutions provides useful information on the final fate of gravitational collapse, as the above example of the critical phenomena indicates. From this point of view, the Tomimatsu-Sato solutions are the best system to analyze as the starting point, because they are the simplest extension of the Kerr black hole solution.

Although it has been a long time since the Tomimatsu-Sato solutions were found, little is known about these solutions yet and sometimes wrong statements were made in the literature. For example, although it has been shown that the Tomimatsu-Sato solutions with odd δ have a Killing horizon at the segment $\rho = 0, |z| < \sigma$ in the Weyl coordinate, it has been believed that the solutions with even δ have no horizon because the corresponding segment for these solutions is not Killing horizon [7]. In the present paper, we will show that this belief is false and the two points $\rho = 0, z = \pm\sigma$ are actually degenerate horizons for $\delta = 2$.

2 Tomimatsu-Sato Spacetime

In canonical form of the stationary axisymmetric metric [5]

$$ds^2 = -f(dt - \omega d\phi)^2 + f^{-1}[e^{2\gamma}(d\rho^2 + dz^2) + \rho^2 d\phi^2], \tag{1}$$

[1]E-mail:hikida@yukawa.kyoto-u.ac.jp
[2]E-mail:kodama@yukawa.kyoto-u.ac.jp

the Kerr-TS family is expressed as [6]

$$f = \frac{A}{B}, \quad \omega = \frac{2mq}{A}(1-y^2)C, \quad e^{2\gamma} = \frac{A}{p^{2\delta}(x^2-y^2)^{\delta^2}}, \tag{2}$$

where the functions A, B and C are polynomials with the degrees of $2\delta^2, 2\delta^2$ and $2\delta^2 - 1$, respectively, in the prolate spheroidal coordinates x and y defined by

$$\rho = \sigma\sqrt{(x^2-1)(1-y^2)}, \quad z = \sigma xy, \tag{3}$$

and σ, p and q are related with mass m and angular momentum J as

$$p^2 + q^2 = 1, \quad \sigma = \frac{mp}{\delta}, \quad J = m^2 q. \tag{4}$$

In the Kerr ($\delta = 1$) and the $\delta = 2$ Tomimatsu-Sato case, A, B and C are given by

$$\delta = 1 \ : \quad A = p^2(x^2-1) - q^2(1-y^2), \quad B = (px+1)^2 + q^2y^2, \quad C = -px - 1, \tag{5}$$

$$\begin{aligned}
\delta = 2 \ : \quad A &= p^4(x^2-1)^4 + q^4(1-y^2)^4 \\
&\quad -2p^2q^2(x^2-1)(1-y^2)\{2(x^2-1)^2 + 2(1-y^2)^2 + 3(x^2-1)(1-y^2)\} \\
B &= \{p^2(x^2+1)(x^2-1) - q^2(y^2+1)(1-y^2) + 2px(x^2-1)\}^2 \\
&\quad +4q^2y^2\{px(x^2-1) + (px+1)(1-y^2)\}^2 \\
C &= -p^3x(x^2-1)\{2(x^2+1)(x^2-1) + (x^2+3)(1-y^2)\} \\
&\quad -p^2(x^2-1)\{4x^2(x^2-1) + (3x^2+1)(1-y^2)\} + q^2(px+1)(1-y^2)^3.
\end{aligned} \tag{6}$$

In this paper, we focus on the $\delta = 2$ Tomimatsu-Sato metric. The properties of the corresponding spacetime that have been found so far are summarized as follows [6, 7].

Ring singularity: This spacetime has a ring singularity at the root of $B(x, y = 0) = 0$. (The cross in Figure 1)

Ergosphere: The timelike Killing vector becomes null at the roots of A. There are two single roots for $x \geq 1$ (The dotted lines in Figure 1), the smaller of which coincides with the ring singularity.

Causality violation region: Since ϕ is the periodic angular coordinate, this spacetime has closed timelike loops in the region with negative $g_{\phi\phi}$. (The shaded portion in Figure 1)

Directional singularity: This metric has directional singularities at the points $(\rho, z) = (0, \pm\sigma)$, where the value of a curvature invariant has different limits when the point is approached from different directions. (The two filled circles in Figure 1)

The nature of the surface $x = 1$: In the Kerr case, $x = 1 (\rho = 0, |z| \leq \sigma)$ surface is an event horizon. However, in the $\delta = 2$ Tomimatsu-Sato case, this is not the case. Because the induced metric is Lorentzian and two Killing vectors ∂_t and ∂_ϕ become parallel there, $x = 1$ surface cannot be a null surface.

3 Extension of Tomimatsu-Sato spacetime

Ernst [8] pointed out that the quasi-regular directional singularities at $\rho = 0, z = \pm\sigma$ are hypersurfaces in reality, by introducing a polar coordinate system around each point. He further studied the behavior of geodesics crossing these surfaces, and concluded that they are timelike surfaces. Now, we show that his conclusion is false and these surfaces are horizons, by introducing an appropriate coordinate system.

First, we rewrite the metric in the former

$$ds^2 = -e^{2\nu}dt^2 + e^{2\psi}(d\phi - \Omega dt)^2 + e^{2\mu}\left(\frac{dx^2}{x^2-1} + \frac{dy^2}{1-y^2}\right), \tag{7}$$

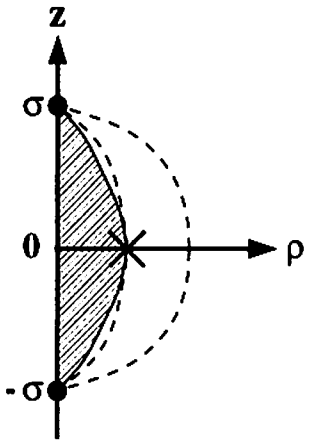


Figure 1: The structure of the spacetime. The crossed sign, dotted lines and the two filled circles denote the ring singularity, the infinite redshift surfaces and the directional singularities respectively. In the shaded portion, the closed timelike loops exist.

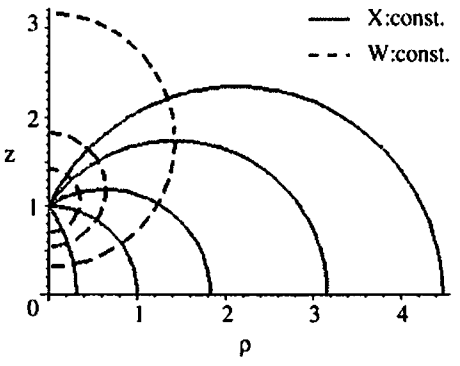


Figure 2: The relation between (ρ, z) and (X, W) coordinate system. The solid lines and the dotted lines are X =constant and W =constant lines respectively.

where

$$e^{2\nu} = \frac{p^2(x^2-1)B}{D}\,,\ \Omega = -\frac{4pqC}{D}\,,\ e^{2\psi} = \frac{(1-y^2)D}{p^2B}\,,\ e^{2\mu} = \frac{B}{p^4(x^2-y^2)^3}, \tag{8}$$

and D is a polynomial determined by the equation

$$D = \frac{p^2(x^2-1)B^2 - 4\delta^2q^2(1-y^2)C^2}{A}. \tag{9}$$

In the $\delta = 2$ Tomimatsu-Sato case, the explicit expression for D is given by

$$\begin{aligned} D &= p^6(x^2-1)(x^8+28x^6+70x^4+28x^2+1) - 16q^6(1-y^2)^3 \\ &+ p^4q^2[(x^2-1)\{32x^2(x^4+4x^2+1) - 4(1-y^2)(x^2-1)^3 + (-6x^4+12x^2+10)(1-y^2)^3\} \\ &- 4(1-y^2)^3(x^4+6x^2+1)] + p^2q^4[(x^2-1)\{64x^4+(1-y^2)^2(y^4+14y^2+1)\} \\ &- 16(1-y^2)^3(x^2+2)] + 8p^5x(x^4-1)(x^4+6x^2+1) - 32pq^4x(1-y^2)^3 \\ &+ 8p^3q^2x[(x^2-1)\{8x^2(x^2+1)+(1-y^2)^2(2y^2-x^2+1)\} - 4(1-y^2)^3]. \end{aligned} \tag{10}$$

Here, we have renormalized σ as $\sigma = 1$.

Next, we introduce the new coordinates X and W by

$$x^2 = \frac{1+X}{1+X-W}, \qquad y^2 = \frac{(1+X)(1-W)}{1+X-W} \tag{11}$$

Figure 2 shows the relation between the (ρ, z) and the (X, W) coordinate system. In this (X, W) coordinate system, the metric is written

$$ds^2 = -e^{2\nu}dt^2 + e^{2\psi}(d\phi - \Omega dt)^2 + e^{2\mu}\frac{(1+X)W}{4(1+X-W)}\left[\frac{dX^2}{(1+X)^2X} + \frac{dW^2}{(1-W)W^2}\right]. \tag{12}$$

In the region near $W = 0$, A, B, C and D behave as

$$\begin{aligned}
A &= \left(\frac{W}{1+X-W}\right)^4 (p^4 + X^4q^4 - 4p^2q^2X - 4p^2q^2X^3 - 6p^2q^2X^2), \\
B &\sim 8(p+1)(p^2+q^2X^2)\left(\frac{W}{1+X-W}\right)^2 + 8(p+1)(p^2-q^2X^3)\left(\frac{W}{1+X-W}\right)^3, \\
C &\sim -4p^2(1+X)(p+1)\left(\frac{W}{1+X-W}\right)^2, \\
D &\sim 64p^2(p+1)^2\left(\frac{W}{1+X-W}\right) + 128p^2(p+1)^2\left(\frac{W}{1+X-W}\right)^2.
\end{aligned} \tag{13}$$

From this, it follows that at $W \sim 0$, $e^{2\nu}, e^{\psi}, \Omega$ and e^{μ} are expressed as

$$\begin{aligned}
e^{2\nu} &\sim \frac{p^2+q^2X^2}{8(p+1)}\left(\frac{W}{1+X}\right)^2 + \frac{-q^2X^3+p^2}{8(p+1)}\left(\frac{W}{1+X}\right)^3, \\
\Omega &\sim \frac{pq(1+X)}{4(p+1)}\left(\frac{W}{1+X-W}\right), \\
e^{2\psi} &\sim \frac{8(p+1)X}{(p^2+q^2X^2)}, \\
e^{2\mu} &\sim \frac{8(p+1)(p^2+q^2X^2)}{p^4W(1+X)^2} + \frac{8(p+1)(-q^2X^2-q^2X^3)}{p^4(1+X)^3}.
\end{aligned} \tag{14}$$

This asymptotic behavior suggests that the $\delta = 2$ Tomimatsu-Sato spacetime can be extended regularly across the surface $W = 0$ in terms of the advanced coordinate v and the ϕ_+ coordinate defined by

$$dv = dt + \frac{4(p+1)dW}{p^2W^2\sqrt{1-W}}, \quad d\phi_+ = d\phi + \frac{qdW}{pW\sqrt{1-W}}. \tag{15}$$

Actually, in the (v, W, X, ϕ_+) coordinate system, the metric is expressed as

$$\begin{aligned}
ds^2 &= -e^{2\nu}\left(dv - \frac{4(p+1)dW}{p^2W^2\sqrt{1-W}}\right)^2 + e^{2\psi}\left\{\left(d\phi_+ - \frac{qdW}{pW\sqrt{1-W}}\right) - \Omega\left(dv - \frac{4(p+1)dW}{p^2W^2\sqrt{1-W}}\right)\right\}^2 \\
&\quad + e^{2\mu}\frac{(1+X)W}{4(1+X-W)}\left[\frac{dX^2}{(1+X)^2X} + \frac{dW^2}{(1-W)W^2}\right] \\
&= -\frac{p^2+q^2X^2}{8(p+1)}\left(\frac{W}{1+X}\right)^2[1+O(W)]dv^2 + \frac{p^2+q^2X^2}{p^2(p+1)}\frac{1+O(W)}{(1+X)^2}dvdW \\
&\quad + \frac{8(p+1)X}{(p^2+q^2X^2)}[1+O(W)]\left(d\phi_+ - \frac{pqW}{4(p+1)}dv + O(W^2)dv + O(1)dW\right)^2 \\
&\quad + O(1)dW^2 + \frac{2(p+1)(p^2+q^2X^2)}{p^4(1+X)^2}[1+O(W)]\frac{dX^2}{(1+X)^2X},
\end{aligned} \tag{16}$$

which is regular at $W = 0$. This expression also shows that $W = 0$ surface is a null hypersurface, whose normal vector is a Killing vector. Hence, the $W = 0$ surface is a Killing horizon. Because $W = 0$ is the double root of $e^{2\nu}$, the horizon is degenerate, i.e., the surface gravity vanishes.

Finally, we examine the shape of horizon. The Tomimatsu-Sato spacetime has a Killing vector ∂_ϕ. So the radius R is given by

$$g_{\phi\phi}|_{(X_0,W_0)} = R^2|_{(X_0,W_0)}. \tag{17}$$

Figure 3 shows the relation between $g_{\phi\phi}$ and X at horizon ($W = 0$). There p^2 parameterizes the angular momentum as is seen from eq.(4): $p^2 = 1$ corresponds to the non-rotating case, and p^2 decreases as the angular momentum increases. Figure 4 expresses the shape of horizon for $p^2 = 0.5$. From this figure we see that the horizons of $\delta = 2$ Tomimatsu-Sato spacetime consist of two spheres.

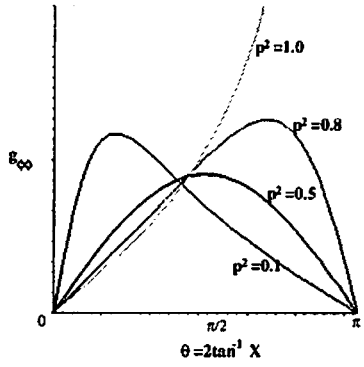


Figure 3: The relation between $g_{\phi\phi}$ and X at horizon ($W = 0$).

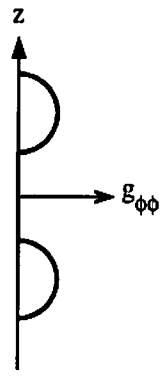


Figure 4: The shape of horizon in the $p^2 = 0.5$ case.

4 Conclusion

We have investigated the structure of the $\delta = 2$ Tomimatsu-Sato spacetime. By introducing an appropriate coordinate system, we have shown that the two points in the Weyl coordinates, which have been recognized as the directional singularities, are really two-dimensional surfaces and that these surfaces are horizons. We have also shown that each of the two horizons has the topology of a sphere. This result is rather surprising because the $\delta = 2$ Tomimatsu-Sato solution is obtained from the Neugebauer-Kramer solution representing a superposition of two Kerr solutions, as the limit that the centers of two black holes coincide [9]. This may indicates a new possibility for the final states of gravitational collapse.

References

[1] R.Penrose Riv. Nuovo. Cimento. **1**, 252 (1969)

[2] R.C.Tolman Proc. Nat. Acad. Sci. **20**, 169 (1934)

[3] H.Bondi Mon. Not. R. Astron. Soc. **107**, 410 (1947)

[4] M.W.Choptuik Phys. Rev. Lett. **70**, 9 (1993)

[5] D. Kramer, H. Stephani, M. MacCallum and E. Herlt eds.: *Exact Solutions of Einstein's Field Equations*(Cambridge Univ. Press, Cambridge, 1980)

[6] Akira Tomimatsu and Humitaka Sato Prog. Theor. Phys. **50**, 95 (1973)

[7] G.W.Gibbons and R.A.Russell-Clark. Phys. Rev. Lett. **30**, 398 (1973)

[8] F.J.Ernst. J. Math. Phys. **17**, 1091 (1976)

[9] Ken-ichi Oohara and Humitaka Sato. Prog. Theor. Phys. **65**, 1891 (1981)

Braneworld reheating in bulk inflaton model

Yoshiaki Himemoto,[1] Takahiro Tanaka [2]

Yukawa Institute for Theoretical Physics Kyoto University, Kyoto 606-8502, Japan

Abstract

In the context of the braneworld inflation driven by a bulk scalar field, we study the energy dissipation from the bulk scalar field into the matter on the brane in order to understand the reheating after inflation. Deriving the late-time behavior of the bulk field with dissipation by using the Green function method, we give a rigorous justification of the statement that the standard reheating process is reproduced in this bulk inflaton model as long as the Hubble parameter on the brane and the mass of the bulk scalar field are much smaller than the 5-dimensional inverse curvature scale. Our result supports that the brane inflation model caused by a bulk scalar field is expected to be a viable alternative scenario of the early universe.

1 Introduction

An alternative scenario of the inflationary universe in the context of the second Randall-Sundrum model (RS2) [1] was proposed by Himemoto and Sasaki [2]. In this scenario, inspired by the higher dimensional gravitational theory including a dilatonic scalar field or higher curvature terms, 5-dimensional Einstein-scalar system was studied. Investigating the dynamics of a minimally coupled massive scalar field ϕ for a 5-dimensional bulk scalar field in the braneworld scenario of RS2 type, it was shown that a bulk scalar field can play the role of inflaton field. We refer to such a model as the bulk inflaton model. In this short paper, in order to give the viability of the bulk inflaton model, investigating the late-time behavior of the evolution of a bulk scalar field with an arbitrary, regular initial data using the Green function method, we show that the braneworld reheating also mimics the 4-dimensional standard process [3].

The organization of this paper is as follows. In Sec. 2, we review the basic picture of the reheating scenario after the braneworld inflation driven by a bulk scalar field proposed in [4]. In Sec. 3, we consider the late-time behavior of the bulk scalar field on the brane by using the property of the retarded Green function. Then we explain how to construct the Green function for a scalar field with dissipation. Subsequently we discuss the effective description of the dynamics from the 4-dimensional point of view and show that the conventional reheating process is effectively reproduced in the braneworld. Section 4 is devoted to summary and discussion.

2 Model of reheating after braneworld inflation

We introduce the model for the reheating process after braneworld inflation driven by a bulk scalar field. We consider the 5-dimensional Einstein-scalar system in the braneworld scenario of the RS2 type. The bulk geometry satisfies the 5-dimensional Einstein equations

$$R_{ab} - \frac{1}{2}g_{ab}R + \Lambda_5 g_{ab} = \kappa_5^2 \left(T_{ab} + S_{ab}\delta(r - r_0)\right) , \tag{1}$$

where r is the coordinate normal to the brane and the brane is assumed to be located at $r = r_0$ at the fixed point of Z_2 symmetry. S_{ab} represents the energy-momentum tensor composed of the brane tension σ and the contribution of matter fields confined on the brane τ_{ab}:

$$S_{ab} = -\sigma q_{ab} + \tau_{ab} , \tag{2}$$

[1] E-mail:himemoto@vega.ess.sci.osaka-u.ac.jp
[2] E-mail:tanaka@yukawa.kyoto-u.ac.jp

where q_{ab} is the induced metric on the brane. T_{ab} is the energy momentum tensor of a bulk scalar field. For simplicity, we assume a minimally coupled massive scalar field with the interaction on the brane. We set $\Lambda_5 = -\kappa_5^4\sigma^2/6$ so as to recover the Randall-Sundrum flat braneworld when T_{ab} and τ_{ab} vanish.

In order to represent the energy dissipation from the bulk scalar field ϕ to the matter fields on the brane, the equation for ϕ is modified as

$$(\Box_5 - m^2)\phi = \Gamma_d\,\ell\,\delta\,(r - r_0)\,\dot{\phi}\,, \tag{3}$$

where $\ell = 6/(\kappa_5^2\sigma)$ is the AdS_5 curvature radius, and m is the mass of the bulk scalar field. An overdot is differentiation with respect to the cosmological proper time. Γ_d represents the decay constant. Integrating Eq. (3) together with Z_2 symmetry, we obtain the boundary condition

$$\partial_r\phi|_{r=r_0} = \frac{\Gamma_d\ell}{2}\dot{\phi}(t, r_0). \tag{4}$$

In the analyses below, we neglect the terms quadratic in Γ_d. Here, we do not consider the energy release to the bulk space for simplicity. Such a dissipation process in the bulk is investigated in Ref .[5].

3 Bulk scalar dynamics with dissipation

We consider solutions of Eq. (3) under the conditions

$$m\ell\,,\, H\ell \text{ and } \Gamma_d\ell \ll 1\,, \tag{5}$$

where m and H are, respectively, mass of the bulk scalar field and the expansion rate of the 4-dimensional metric induced on the brane. Then we investigate the late-time behavior of solutions by extending the Green function method used in Ref. [6].

3.1 Initial value problem

We consider the field equation

$$\mathcal{L}_X\,\Psi(X) \equiv \left[-\partial_t^2 + \partial_y^2 - W(y) - U(y)\partial_t\right]\Psi(X) = 0\,, \tag{6}$$

where X denotes $\{t, y\}$. We assume $W(y)$ and $U(y)$ are functions whose asymptotic value at $|y| \to \infty$ is supposed to be a constant. We solve this field equation imposing Z_2 symmetry at $y = 0$.

Let us consider the retarded Green function which satisfies

$$\mathcal{L}_X G(X, X') = -\delta(t - t')\delta(y - y'), \tag{7}$$

with the causal condition that $G(X, X') = 0$ for X' not in the causal past of X. Note that this Green function satisfies the reciprocity for time reversal operation $t \to -t$, namely, $G(t, y, t', y') = G(-t', y', -t, y)$. Using the reciprocity, the evolution of Ψ for any given initial data can be described as

$$\Psi \;=\; \int_{t'=t_i}\left[G(X, X')\frac{\partial\Psi(X')}{\partial t'} - \frac{\partial G(X, X')}{\partial t'}\Psi(X') + U(y')G(X, X')\Psi(X')\right]dy', \tag{8}$$

where t_i is the initial time. This representation of Ψ implies that the asymptotic behavior of Ψ can be understood by the late-time behavior of $G(X, X')$.

Let us now construct the Green function which satisfies Eq. (7). Due to the time translation invariance, we can express the Green function in terms of Fourier transformation as

$$G(X, X') = \frac{1}{2\pi}\int_{\mathcal{C}} dp\, G_p(y, y')e^{-ip(t-t')}\,, \tag{9}$$

where we choose the path $\mathcal{C}$ so that the retarded condition is satisfied. Namely, $\mathcal{C}$ runs from $p = -\infty$ to $p = +\infty$ on the complex plane for the integrand G_p to contain neither pole nor the branch cut above $\mathcal{C}$.

We make use of the fact that the late-time behavior is determined by the singularities in G_p. From the out-going boundary condition at the infinity and Z_2 symmetric condition at the brane, the equation that determines the location of the poles is given by

$$\mathcal{D}[u_p^{(\mathrm{out})}(y)] \equiv [\partial_y - \hat{W} + ip\hat{U}]u_p^{(\mathrm{out})}(y)|_{y=0+} = 0\,, \tag{10}$$

where $\hat{W}$ and $\hat{U}$ are the coefficients in front of $\delta(y)$ contained in $W(y)/2$ and $U(y)/2$, respectively. Here $u_p^{(\mathrm{out})}(y)$ descibes the mode function which behaves asymptotically as $e^{ik|y|}$ at $|y| \to \infty$, where we defined $k^2 = \lim_{|y|\to\infty} p^2 - W(y) + ipU(y)$.

3.2 Application to Braneworld

Using the formulas developed in the previous section, we consider the evolution of a massive bulk scalar field with dissipation, which will well approximate the situation that ϕ oscillates at the bottom of the potential. We assume that the background spacetime is 5-dimensional anti-de Sitter space with boundary de-Sitter brane given by $ds^2 = dr^2 + \{H\ell\sinh(r/\ell)\}^2(-dt^2 + H^{-2}e^{2Ht}d\mathbf{x}_{(3)}^2)$ [7]. In order to use the formulas presented in the preceding subsection, we introduce the conformal coordinates $\{\tau, y\}$ defined by $\tau \equiv Ht$ and $R(y) \equiv \ell\sinh^{-1}(|y|+y_0) = \ell\sinh(r/\ell)$, where y_0 is specified by $\sinh(y_0) = \sinh^{-1}(r_0/\ell) = H\ell$. Then, the metric becomes

$$ds^2 = R(y)^2\left(dy^2 - d\tau^2 + e^{2\tau}\,d\boldsymbol{x}_{(3)}^2\right)\,. \tag{11}$$

Setting $\phi = R^{-3/2}e^{-3\tau/2}\Psi(y,\tau)$, Eq. (3) reduces to Eq. (6) with

$$W(y) = \frac{15+4m^2\ell^2}{4\sinh^2(|y|+y_0)} - \left(\frac{3\sqrt{1+H^2\ell^2}}{H\ell} + \frac{3}{2}\Gamma_d\ell\right)\delta(y), \tag{12}$$

$$U(y) = \Gamma_d\ell\,\delta\,(y)\,. \tag{13}$$

We note that both $W(y)$ and $U(y)$ vanish for $|y| \to \infty$, and hence the conditions that they asymptotically become constant are satisfied. Although $U(y)$ is localized on the brane in the present model, dissipation in the bulk can be also discussed by using the same technique as long as $U(y)$ satisfies this property.

The mode solution satisfying the out-going asymptotic behavior is

$$u_p^{(\mathrm{out})}(y) = \Gamma(1-ip)P_{\nu-1/2}^{ip}[\coth(|y|+y_0)]\,, \tag{14}$$

where $\nu = \sqrt{m^2\ell^2+4}$. In the present case, the operator is defined in Eq.(10) reduces to

$$\mathcal{D} = \partial_y + \frac{3}{2}\frac{\sqrt{1+H^2\ell^2}}{H\ell} + \left(ip + \frac{3}{2}\right)\frac{\Gamma_d\ell}{2}\,. \tag{15}$$

Then, from Eqs. (10) and (14) under the condition (5), we obtain the location of the poles with the largest imaginary part in the complex p plane as

$$p_\pm \approx \frac{1}{H}\left[-i\frac{\Gamma_d}{2} \pm \sqrt{m_{\mathrm{eff}}^2 - \frac{(3H+\Gamma_d)^2}{4}}\right]\,, \tag{16}$$

where

$$m_{\mathrm{eff}}^2 = \frac{m^2}{2}. \tag{17}$$

Here the terms neglected are quadratic or higher order in ℓ. Besides these two poles, there are an infinite sequence of poles. However, they do not give a dominant contribution to the late-time behavior since they have smaller imaginary part. (See Ref. [6].) Therefore the asymptotic behavior of the field ϕ is dominated by the poles $p_\pm$, and hence we have

$$\phi \propto e^{-\frac{3}{2}\tau}G(X,X') \propto e^{-(\frac{3}{2}+ip_\pm)Ht}. \tag{18}$$

3.3 Effective 4-dimensional description

In the preceding section, we confirmed that the late-time behavior of a bulk scalar field on the brane can be effectively described by a 4-dimensional scalar field Φ which satisfies

$$\ddot{\Phi} + (3H + \Gamma_d)\dot{\Phi} + m_{\rm eff}^2\Phi = 0. \tag{19}$$

Our main interest here is to compare the law of cosmic expansion on the brane to that expected in the usual 4-dimensional model with the scalar field Φ. First we present a rather general framework to discuss the cosmic expansion of homogeneous universe realized on the brane without specifying the explicit form of the energy momentum tensor in the bulk.

We introduce a unit vector in the time direction u^a parallel to the brane. Toward the outside of the brane u^a is extended so as to satisfy $u^a{}_{;b}n^b = 0$, where n_b is the out-going unit normal vector of the brane. Then, considering the integration of the 5-dimensional conservation law

$$0 = \int \sqrt{-g}\, d^5x\, (S_a{}^b\delta(r - r_0) + T_a{}^b)_{;b}u^a, \tag{20}$$

for a thin region surrounding the brane, we obtain

$$\dot{\rho} + 4H\rho + H\tau^\mu_{\ \mu} = 2T_{ab}u^a n^b, \tag{21}$$

where $\rho := u^\mu u^\nu \tau_{\mu\nu}$, and Latin indices run over 4-dimensional coordinates on the brane.

The conservation law for the matter field localized on the brane $\tau^{\mu\nu}{}_{;\nu} = 0$ is violated because there is energy transfer between brane and bulk fields. However, from the Bianchi identity the 4-dimensional conservation law is guaranteed to be preserved in total. The 4-dimensional effective Einstein equation is derived from (1) as[8]

$${}^{(4)}G_{\mu\nu} = \kappa_4^2(\tau_{\mu\nu} + \tau^{(\pi)}_{\mu\nu} + \tau^{(s)}_{\mu\nu} + \tau^{(E)}_{\mu\nu}), \tag{22}$$

where $\kappa_4^2 = \kappa_5^2/\ell$ and

$$\begin{aligned}
\tau^{(\pi)}_{\mu\nu} &= -\frac{\kappa_5^2\ell}{24}(6\tau_{\mu\alpha}\tau_\nu{}^\alpha - 2\tau\tau_{\mu\nu} - q_{\mu\nu}(3\tau_{\alpha\beta}\tau^{\alpha\beta} - \tau^2)), \\
\tau^{(s)}_{\mu\nu} &= \frac{2\ell}{3}\left[T_{ab}q^a{}_\mu q^b{}_\nu + q_{\mu\nu}\left(T_{ab}n^a n^b - \frac{1}{4}T^a{}_a\right)\right], \\
\tau^{(E)}_{\mu\nu} &= -\frac{\ell}{\kappa_5^2}{}^{(5)}C_{rbrd}\, q^b_\mu\, q^d_\nu .
\end{aligned} \tag{23}$$

Here ${}^{(5)}C_{rbrd}$ is the 5-dimensional Weyl tensor with its two indices projected in the normal direction. Then we have

$$\tau^{({\rm tot})\mu\nu}{}_{|\nu} = 0, \tag{24}$$

with

$$\tau^{({\rm tot})}_{\mu\nu} := \tau_{\mu\nu} + \tau^{(\pi)}_{\mu\nu} + \tau^{(s)}_{\mu\nu} + \tau^{(E)}_{\mu\nu}. \tag{25}$$

Here a vertical line represents covariant differentiation with respect to the 4-dimensional induced metric $q_{\mu\nu}$. In the homogeneous universe, the temporal component of the conservation law reduces to

$$\dot{\rho}^{({\rm tot})} + 4H\rho^{({\rm tot})} + H\tau^{({\rm tot})\mu}{}_\mu = 0, \tag{26}$$

where $\rho^{({\rm tot})} := u^\mu u^\nu \tau^{({\rm tot})}_{\mu\nu}$. Similarly we define the energy density for each component by $\rho^{(i)} := u^\mu u^\nu \tau^{(i)}_{\mu\nu}$. Then, using the facts that $\rho^{(\pi)} = \rho^2/2\sigma$, $\tau^{(\pi)\mu}{}_\mu = (\rho/\sigma)(\tau^\mu{}_\mu + 2\rho)$, [8] and $\tau^{(s)\mu}{}_\mu = 2\ell T_{ab}n^a n^b$, we find that the effective energy density of the bulk field $\rho_{\rm eff} := \rho^{(E)} + \rho^{(s)}$ satisfies

$$\dot{\rho}_{\rm eff} + 4H\rho_{\rm eff} = -2\left(1 + \frac{\rho}{\sigma}\right)T_{ab}u^a n^b - 2H\ell T_{ab}n^a n^b. \tag{27}$$

Now let's return to our specific model, in which the bulk energy-momentum tensor is given by

$$T_{ab} = \phi_{,a}\phi_{,b} - g_{ab}\left(\frac{1}{2}g^{cd}\phi_{,c}\phi_{,d} + \frac{1}{2}m^2\phi^2\right). \tag{28}$$

Then we find,

$$T_{ab}u^a n^b = \frac{\Gamma_d \ell}{2}\dot{\phi}^2 \quad \text{and} \quad T_{ab}n^a n^b = \frac{1}{2}\dot{\phi}^2 - \frac{1}{2}m^2\phi^2, \tag{29}$$

where the terms quadratic in $\Gamma_d \ell$ were neglected. If we set the identification [6]

$$\Phi = \sqrt{\ell}\,\phi, \tag{30}$$

from Eqs. (21) and (27), we obtain the formulas for the cosmic expansion valid in the law energy regime (5) as

$$\begin{aligned} H^2 &= \frac{\kappa_4^2}{3}(\rho_{\rm eff} + \rho), \\ \dot{\rho}_{\rm eff} + 4H\rho_{\rm eff} &= -H\left(\dot{\Phi}^2 - 4V_{\rm eff}\right) - \Gamma_d \dot{\Phi}^2, \\ \dot{\rho} + 4H\rho + H\tau^{\mu}_{\mu} &= \Gamma_d \dot{\Phi}^2, \end{aligned} \tag{31}$$

where $V_{\rm eff}(\Phi) = \frac{1}{2}m_{\rm eff}^2\Phi^2 = (\ell/4)m^2\phi^2$. This set of equations is the same that is satisfied by a 4-dimensional model having a scalar field Φ with mass-squared $m_{\rm eff}^2 = m^2/2$ and the decay width $\Gamma_d/2$. To conclude, provided that the conditions (5) are satisfied, the effective dynamics of the Einstein-scalar system on the brane is indistinguishable from a 4-dimensional theory even if we consider the energy dissipation from the bulk scalar field to the matter fields on the brane.

4 Summary and Discussion

We have investigated the late-time behavior of a bulk scalar field with dissipation to the matter fields on the brane. We have shown that a bulk scalar field observed on the brane effectively behaves as a 4-dimensional scalar field. Furthermore, we have shown that the set of equations to determine the cosmic expansion is also indistinguishable from that of a corresponding standard 4-dimensional model. Though we have just analyzed perturbatively the dynamics of a bulk scalar field on a fixed 5-dimensional anti-de Sitter background with a boundary de Sitter brane, our result suggests that 4-dimensional inflaton dynamics including reheating era is effectively reproduced by the dynamics of a 5-dimensional scalar field. Thus the brane inflation model caused by a bulk scalar field is expected to be a viable alternative scenario of the early universe.

Genuine braneworld effects which can be used to test the scenario is, however, in the deviations from the standard. Our analysis shows that the corrections are suppressed by a factor $H^2\ell^2$ or $|m^2|\ell^2$. We did not go into detail about this correction in this paper. Here we just mention that we have to consider the dynamics of a bulk scalar field with a general FRW brane boundary when we discuss the corrections of this order, because the expected suppression of the correction due to the variation of the expansion rate is of the same order: $\dot{H}\ell^2 \sim H^2\ell^2$. We plan to attack this issue in order to clalify the braneworld signature in a future publication.

References

[1] L. Randall and R. Sundrum, Phys. Rev. Lett. **83**, 4690 (1999) [hep-th/9906064].

[2] Y. Himemoto and M. Sasaki, Phys. Rev. D **63**, 044015 (2001) [gr-qc/0010035].

[3] Y. Himemoto and T. Tanaka, [gr-qc/0212114].

[4] J. Yokoyama and Y. Himemoto, Phys. Rev. D **64**, 083511 (2001) [hep-ph/0103115].

[5] T. Tanaka and Y. Himemoto, [gr-qc/0301010].

[6] Y. Himemoto, T. Tanaka and M. Sasaki, Phys. Rev. D **65**, 104020 (2002) [gr-qc/0112027].

[7] J. Garriga and M. Sasaki, Phys. Rev. D **62**, 043523 (2000) [hep-th/9912118].

[8] T. Shiromizu, K. Maeda and M. Sasaki, Phys. Rev. D **62**, 024012 (2000) [gr-qc/9910076].

Higher Dimensional Gravitational Instanton with Cosmological Constant

Mitsuo Hiragane,[1]

Department of Physics, Graduate School of Science,
Osaka City University, Sugimoto, Sumiyosi, Osaka 558-8585, Japan

Abstract

We investigate the Einstein equation for Sp(2)-invariant metrics on a cohomogeneity one manifold $\hat{M} \simeq$R $\times$ Sp(2)/Sp(1).Using numerical techniques,we establish the existence of a compact inhomogeneous Einstein space of this form with positive Ricci curvature.

1 Introduction

Recently,developments in higher-dimensional theories have led to an interest in Remannian Eisntein manifolds.Though there are many examples of homogeneous spaces,only few inhomogeneous spaces are known. So,we consider the cohomogeneity one manifolds in order to find new inhomogeneous examples at the beginning.Concretely,we consider the Sp(2)-invariant metrics on $\mathbf{R} \times$ Sp(2)/Sp(1).

2 Einstein equation

The metric anzatz is

$$\begin{aligned}\hat{g} = dt^2 \quad & +a^2(t)\sigma_1^2 + b^2(t)\sigma_2^2 + c^2(t)\sigma_3^2 \\ & +f^2(t)(\Sigma_1^2 + \Sigma_2^2 + \Sigma_3^2 + \Sigma_4^2),\end{aligned}$$

where σ's and Σ's are the Sp(2) left invariant 1-forms[1]. The Einstein equation $\widehat{\mathrm{Ric}}(\hat{g})=\lambda\,\hat{g}$ becomes

$$\dot{L} = -(\mathrm{tr}L)L + \mathrm{Ric} - \lambda 1_7, \tag{1}$$

$$\mathrm{tr}(\dot{L}) = -\mathrm{tr}(L^2) - \lambda, \tag{2}$$

where 1_7 is 7-dimensional unit matrix, the extrinsic curvature L on the surface t=const is

$$L = \mathrm{diag}\left(\frac{\dot{a}}{a}, \frac{\dot{b}}{b}, \frac{\dot{c}}{c}, \frac{\dot{f}}{f}, \frac{\dot{f}}{f}, \frac{\dot{f}}{f}, \frac{\dot{f}}{f}\right), \tag{3}$$

and Ric is

$$\begin{cases} \mathrm{Ric}_{11} = \dfrac{a^4 - (b^2-c^2)^2}{2a^2b^2c^2} + \dfrac{a^2}{f^4}, \\ \mathrm{Ric}_{22} = \dfrac{b^4 - (c^2-a^2)^2}{2a^2b^2c^2} + \dfrac{b^2}{f^4}, \\ \mathrm{Ric}_{33} = \dfrac{c^4 - (a^2-b^2)^2}{2a^2b^2c^2} + \dfrac{c^2}{f^4}, \\ \mathrm{Ric}_{\alpha\beta} = -\dfrac{a^2+b^2+c^2}{2f^4} + \dfrac{3}{f^2}, \alpha,\beta = 4 \sim 7. \end{cases}$$

[1]E-mail:hiragane@sci.osaka-cu.ac.jp

3 Boundary Condition

All Einstein spaces with positive λ are necessarily compact.Then

$$t \in [t_0, t_1] \subset \mathbf{R}.$$

At t=t_0 and t_1,at least one of a,b,c,and f become zero. Generally,such points become the singular points,but the singularities must become the apparent singularity. So,there are only three possibilities for curvature-regular boundary conditions:

1. nut

$$\begin{cases} a = t + \cdots, \\ b = t + \cdots, \\ c = t + \cdots, \\ f = t + \cdots. \end{cases}$$

2. S^4-bolt

$$\begin{cases} a = t + \cdots, \\ b = t + \cdots, \\ c = t + \cdots, \\ f = f_0 + \cdots, (f_0 : \text{constant}). \end{cases}$$

3. CP(3)-bolt

$$\begin{cases} a = kt + \cdots, (k = \text{integer or } l^{-1} : l = \text{integer}) \\ b = b_0 + \cdots, (b_0 : \text{constant}), \\ c = c_0 + \cdots, (c_0 : \text{constant}), \\ f = f_0 + \cdots, (f_0 : \text{constant}). \end{cases}$$

4 Solutions

1. b=c=f[2]
   analytic solutions

$$\begin{cases} S^{4n+4}, \mathbf{C}P(2n+2) \\ \mathbf{C}P(2n+2) \sharp \overline{\mathbf{C}P(2n+2)} \end{cases}$$

2. a=b=c[3]

$$\begin{cases} S^{4n+4}, \mathbf{H}P(n+1) : \textit{analytic} \\ \mathbf{H}P(n+1) \sharp \overline{\mathbf{H}P(n+1)} : \textit{numerical} \end{cases}$$

3. b=c

We find a new numerical solution.The boundarys of the solution are S^4-bolt and CP(3)-bolt.

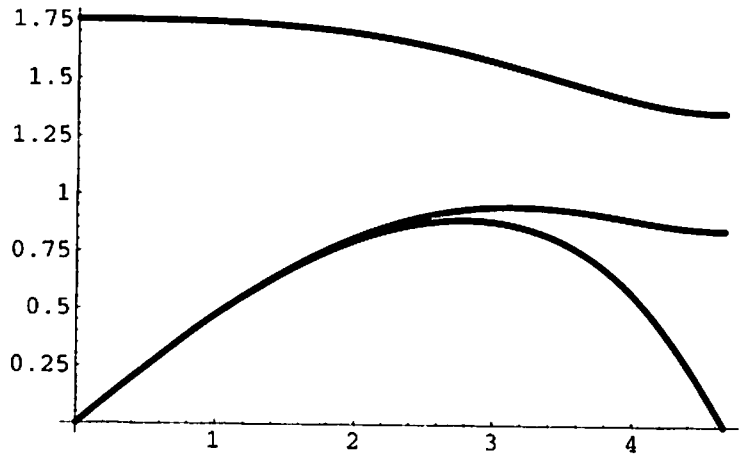


Figure1:graph of new numerical solution.The left side bounadary is S^4-bolt,and the right side boundary is CP(3)-bolt.

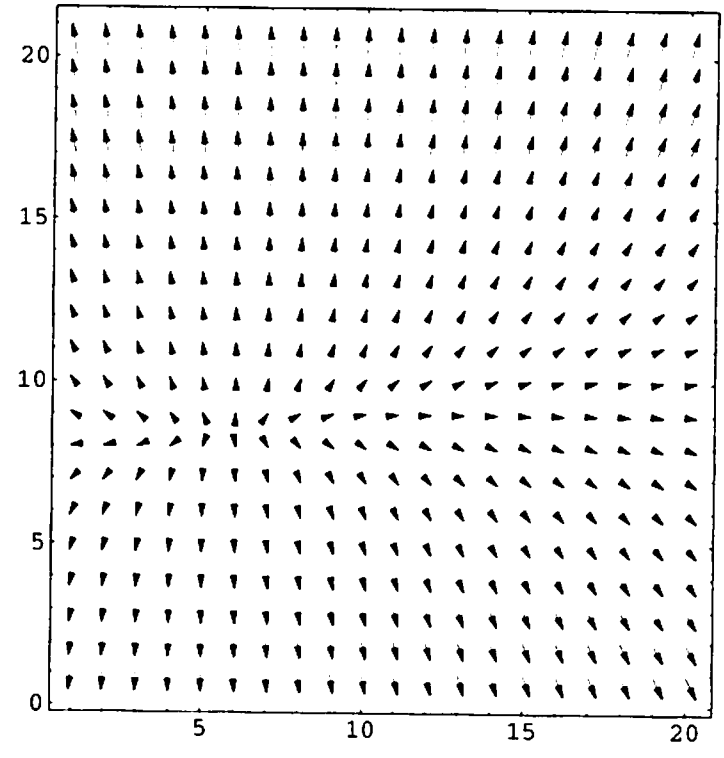


Figure2:existence proof of the new solution.The parameter space consists of $(f_0, a_3 - b_3)$ at S^4-bolt,and the vectors consist of $(\dot{a}+2, \dot{b})$ at CP(3)-bolt.There is one source of vectors,the vector at the point is zero vector,and the point is the solution point.

5 Conclusion

We find a new compact inhomogeneous Riemannian Einstein spaces.This model is easily generalised to a (4n+4)-dimensional model.Concretely,Sp(2)/Sp(1) is generalized to a principal SU(2) bundle over quaternionic Kähler manifolds with positive Ricci curvature.Then,Einstein equation is also a system of ordinary differential equations in spite that it includes a dimension parameter n, and there will be the solutions like our new numerical solution.

References

[1] Y.Konishi,and M.Naka,hep-th/0104208

[2] D.N.Page, and C.N.Pope, Class. Quantum. Grav. 4, (1987) 213-225

[3] D.N.Page, and C.N.Pope, Class. Quantum. Grav. 3, (1986) 249-259

Holographic Charge Excitation on the BTZ Black Hole
— Falling Matter Effect —

Masahiro Hotta,[1]

Department of Physics, Faculty of Science,
Tohoku University, Sendai 980-8578, Japan

Abstract

This report is based on the paper [1]. We argue that the falling matter effect does not break the integrability condition of the horizontal charges of the BTZ black hole. It is possible to trace the proccesses in which the matter imprints the information on the horizon by use of the charged states. It is naturally expected that in the thermal equilibrium with the Hawking radiation the black hole wanders ergodically through different horizontal states due to thermal fluctuation of incoming matter. This fact strengthens plausibility of the basic part of Carlip's idea [2].

1 Introduction

For long years the black hole entropy problem [3] has been attacked by many people and the effort yields significant progresses. Recently the state counting on BPS branes has been achieved in the string theory and the precise entropy form of the corresponding black branes, $\mathcal{A}/4G$, is obtained, using the stability of the BPS states against the strong coupling of the gravitational interaction [4]. This is quite an interesting result because the analysis really proves that the origin of the black hole entropy is entirely statistical. Even though such a cruicial success has been performed, it should be stressed that there still a lot of questions remain. For example, we do not know where the states contributing to the entropy live in the macroscopical black-hole spacetimes. In addition, we must explain explicitly how the no-hair theorem is reconciled with the hairy black hole with large entropy. In the string argument the BPS states are counted just in the weak coupling region, that is, in the flat spacetime. Hence no real curved spacetime with horizon appears in the step and we cannot find any resolution in the argument to answer the above questions.

From the view point that the black hole horizon is essential to resolve the questions, Carlip [2] proposed a quite stimulating scenario. He pointed out a possibility that a part of gauge freedom of the general covariance becomes dynamical on the horizon and generates physical states contributing to the entropy. The idea itself does not depend on the spacetime dimensions and the gravity theories (general relativity, dilatonic gravity and so on) as long as the theories possess the general covariance in the action. In his idea the reconcilation between the no-hair theorem and the tremendous amount of the entropy becomes fairy evident. The point is that the charges mentioned in the no-hair theorem, mass M, angular momentum J and gauge charges Q, characterize just the geometrical property of the black-hole spacetimes. In fact the charges appear in geometrical quantities like curvature in any coordinate system. Hence the change of the charges means generation of different geometry which cannot be yielded by any coordinate transformation. On the other hand the horizontal charges are proposed to be generators of a part of general coordinate transformation. Therefore the transformation generated by the horizontal charges does not make a different geometry at all. The situation may be easily understood by recalling that momentum P of a black hole is a significant physical charge, but translation generated by P does not change the geometry itself. Clearly two quantum states with different P values are orthogonal to each other, thus the two states are physically different and, for example, will contribute independently to the partitional function and the entropy of a black-hole many-body system. The similar mechanism will

[1] E-mail:hotta@tuhep.phys.tohoku.ac.jp

happen near horizon of a black hole and the horizontal charges are expected to generate many different states without deformation of the geometry, respecting the no-hair theorem.

As a path to reach the universal realization of his basic idea in arbitrary dimensions, a lot of people including himself [5] tried to find a Virasoro symmetry with classically nonvanishing central charge on the horizon in order to get the entropy via Cardy's CFT formula [6]. Unfortunately, various difficulties prevent the scenario from succeeding so far[7]. For example, some models need to pick up a circle S^1 without any convincing reason in higher-dimensional geometries, some have ill-defined boundary charge or no classical central extension for Cardy's formula and some suffer from ghost states with negative norm. Hence fully-satisfactory resolution based on the Virasoro-algebra scenario has not been achieved yet to explain the entropy.

In order to reach the realization of essential part of the Carlip's idea, another way may be still open. It has been pointed out [8] that the Schwarzschild black hole admits local time translation and angular diffeomorphism on the horizon to be a well-defined asymptotic symmetry and that nontrivial representation with nonvanishing canonical charge can be really constructed. In four dimensions the charges are labeled by the spherical harmonic indices (lm) like Q_{lm}. The symmetry appears naturally in arbitrary dimensions (higher than two dimensions) and does not request any selection of a circle S^1 near the horizon. Though the algebra does not have any classical central extension, the regular symmetry on the horizon is the first example, as far as we know, which possesses a nonsinglet representation even in the classical theory. The number of the charges, which is classically infinite, looks so large as to incorporate huge degeneracy of the black hole states into the representational space. Available values of the charges distinguish a tremendous number of different physical states and might generate the exact black hole entropy.

We argue in this report that falling matter into the horizon does not break the integrability condition of the charges in the pertubation level. Consequently it is argued that the states with the nontrivial charges of BTZ black hole are actually excited by ordinary falling matter including Hawking radiation. From this observation it is naturally expected that, in the thermal equilibrium with the Hawking radiation, the black hole wanders ergodically through different horizontal states due to thermal fluctuation of incoming matter. This fact strengthens plausibility of the basic part of the Carlip's idea. See the detailed analysis in the paper [1].

2 Horizontal Charge and Boundary Condition

Let us consider the three-diemsional Einstein gravity with negative cosmological constant. The action reads

$$S = \frac{1}{16\pi G}\int d^3x\sqrt{-g}(R + 2\mu^2), \tag{1}$$

where the constant $\mu(> 0)$ fixes the cosmological constant scale. In the system it is well known that the black hole solution exists, so called the BTZ black hole. The asymptotic form of the metric near horizon is given as follows.

$$d\bar{s}^2 = \Delta(-dt^2 + d\rho^2) + (r_+^2 + O(\Delta))d\phi^2 + O(\Delta^2). \tag{2}$$

Here r_+ is the horizontal radius and Δ has been defined as

$$\Delta = e^{-\frac{\rho}{\epsilon}} \sim 0. \tag{3}$$

Then we propose asymptotic metrices to the BTZ background in eqn(2) in the same spirit of [8] as follows.

$$\begin{bmatrix} g_{tt} & g_{t\rho} & g_{t\phi} \\ g_{\rho t} & g_{\rho\rho} & g_{\rho\phi} \\ g_{\phi t} & g_{\phi\rho} & g_{\phi\phi} \end{bmatrix} = \begin{bmatrix} -\Delta + O(\Delta^2) & O(\Delta^2) & O(\Delta) \\ O(\Delta^2) & \Delta + O(\Delta^2) & O(\Delta) \\ O(\Delta) & O(\Delta) & O(1) \end{bmatrix}, \tag{4}$$

where $O(\Delta^k)$ implies that

$$\left| \lim_{\rho \to \infty} \frac{O(\Delta^k)}{\Delta^k} \right| = |f(t, \phi)| < \infty. \tag{5}$$

Note that the boundary congruence defined by

$$\rho = \infty, \tag{6}$$

$$\phi = const. \tag{7}$$

is always null in regular spacetimes with the metric in eqn(4). This implies that the boundary is just analogous concept to the Rindler horizon in the flat spacetime, that is, any physical matter across the boundary cannot come back to the outside. Taking account of the gravitational backreaction, falling matter from the thermal bath may temporarily shift the physical position of the boundary at $\rho = \infty$ apart from the global event horizon. (Here the shift should be measured by appropriate geometrical length $d\tilde{l}$ between the congruence and the horizon without gauge ambiguity.) However the deviation is not expected to become so large because the black hole swallows both positive energy flux (associated with on-shell incoming matter) and negative energy flux (associated with quanta pair-created with positive-energy particles of the Hawking radiation). The average magnitudes of the both fluxes take the same value because of the thermal equilibrium. Hence the average shift of the boundary position will be suppressed.

It is rather straightfoward to prove that infinitesimal coordinate transformations which preserve the asymptotic condition in eqn(4) take the following form.

$$\xi^t = U(\phi) + O(\Delta), \tag{8}$$

$$\xi^\rho = O(\Delta), \tag{9}$$

$$\xi^\phi = V(\phi) + O(\Delta), \tag{10}$$

where $U(\phi)$ and $V(\phi)$ are arbitrary periodic functions of ϕ. It can be proven that the generator of the transformations is integrable in the canonical sense [1].

For the discussion of falling matter effect, it is convienient to to change the variables as follows.

$$u = t - \rho, \tag{11}$$

$$\rho = \rho, \tag{12}$$

$$\phi = \phi. \tag{13}$$

The asymptotic condition in eqn(4) is now rewritten as

$$\begin{bmatrix} g_{uu} & g_{u\rho} & g_{u\phi} \\ g_{\rho u} & g_{\rho\rho} & g_{\rho\phi} \\ g_{\phi u} & g_{\phi\rho} & g_{\phi\phi} \end{bmatrix} = \begin{bmatrix} -\Delta + O(\Delta^2) & -\Delta + O(\Delta^2) & O(\Delta) \\ -\Delta + O(\Delta^2) & O(\Delta^2) & O(\Delta) \\ O(\Delta) & O(\Delta) & O(1) \end{bmatrix}, . \tag{14}$$

It is checked that the integrability of the symmetric charges via the covariant phase-space formulation in the paper [9] is satisfied. Actually the form of the local time translation charge, for example, is given as

$$Q_m^{(T)} = \frac{1}{16\pi G\epsilon} \oint_{\rho=\infty} d\phi e^{im\phi} [1 - 2\epsilon\partial_u] \sqrt{g_{\phi\phi}}. \tag{15}$$

3 Excitations with the Horizontal Charge

In this section we argue that falling matter does not break the asymptotic boundary condition in eqn(14) at least in the perturbative level. The horizontal states with nontrivial charges are actually excited by the matter.

Let us consider the following spinless BTZ black hole solution with horizon radius r_+ as the background for the perturbation.

$$d\bar{s}^2 = -\frac{1}{\sinh^2(\mu\rho)}\left(du^2 + 2dud\rho\right) + r_+^2\coth^2(\mu\rho)d\phi^2. \tag{16}$$

In the background the action of free massive scalar field reads

$$S_{matter} = \int d^3x\sqrt{-\bar{g}}\left[-\frac{1}{2}(\bar{\nabla}\varphi)^2 - \frac{M^2}{2}\varphi^2\right], \tag{17}$$

where M is the mass of the field. Solving the equation of motion of the field, the general in-coming-wave solution can be explicitly written down as

$$\begin{aligned}\varphi \;=\; & \sum_{L=-\infty}^{\infty}\int_0^{\infty} dE A_L^{in}(E)\left[2\sinh(\mu\rho)\right]^{-i\frac{E}{\mu}}\left[\coth(\mu\rho)\right]^{-i\frac{L}{\mu r_+}} e^{iE(u+\rho)+iL\phi} \\ & \times F\left(a(E,L), b(E,L), c(E,L); -\sinh^{-2}(\mu\rho)\right) \\ & + c.c,\end{aligned} \tag{18}$$

where

$$a = \frac{1}{2}\left(1+\sqrt{1+\frac{M^2}{\mu^2}}\right) + \frac{i}{2}\left(\frac{E}{\mu} - \frac{L}{\mu r_+}\right), \tag{19}$$

$$b = \frac{1}{2}\left(1-\sqrt{1+\frac{M^2}{\mu^2}}\right) + \frac{i}{2}\left(\frac{E}{\mu} - \frac{L}{\mu r_+}\right), \tag{20}$$

$$c = 1 + i\frac{E}{\mu}. \tag{21}$$

Near the horizon ($\rho \sim \infty$), the solution behaves as

$$\varphi = \sum_L \int_0^{\infty} dE\left(A_L^{in}(E)e^{iEu+iL\phi} + A_L^{in}(E)^* e^{-iEu-iL\phi}\right) + O\left(e^{-\frac{\rho}{\mu}}\right). \tag{22}$$

In order to solve the Einstein equation, let us introduce the Chern-Simons variables:

$$A_\mu^a = \omega_\mu^a + \mu e_\mu^a, \tag{23}$$

$$\bar{A}_\mu^a = \omega_\mu^a - \mu e_\mu^a. \tag{24}$$

Taking variation of the equation, we get the first-order perturbative equation of motion. Here let us choose the gauge fixing as

$$\delta A_u^c = \delta\bar{A}_u^c = 0. \tag{25}$$

The perturbative equation corresponding can be integrated out formally. Then it is proven that the asymptotic metric condition in eqn(14) still holds because the perturbative correction induced by the matter field is given as

$$\begin{bmatrix} \delta g_{uu} & \delta g_{u\rho} & \delta g_{u\phi} \\ \delta g_{\rho u} & \delta g_{\rho\rho} & \delta g_{\rho\phi} \\ \delta g_{\phi u} & \delta g_{\phi\rho} & \delta g_{\phi\phi} \end{bmatrix} = \begin{bmatrix} 0 & O(\Delta^2) & O(\Delta) \\ O(\Delta^2) & O(\Delta^2) & O(\Delta) \\ O(\Delta) & O(\Delta) & O(1) \end{bmatrix}. \tag{26}$$

Initially the horizontal charges $Q_m^{(T)}$ vanish for the background metric in eqn(16) except $m = 0$. After the matter falls into the black hole, they get the following corrections, which are generally nonzero.

$$\delta Q_m^{(T)} = r_+ \oint d\phi e^{im\phi}\left[\int_{-\infty}^{u}\left(\partial_u\varphi(u',\infty,\phi)\right)^2 du'\right]. \tag{27}$$

Therefore it is concluded that the matter certainly excites the states with $Q^{(T)}_{m\neq 0}$ nonvanishing. As a simple example, let us consider a shock-wave solution of the matter field near the horizon:

$$(\partial_u \varphi)^2 = \kappa(\phi)\delta(u) + O(\Delta), \tag{28}$$

where $\kappa(\phi)$ is arbitrary periodic positive function of ϕ. Passing across the boundary, the wave imprints the nonzero value on the charges $Q^{(T)}_m$ as

$$\delta Q^{(T)}_m(u>0) = r_+ \oint e^{im\phi}\kappa(\phi)d\phi. \tag{29}$$

Interestingly note that if one observes the charges $\delta Q^{(T)}_m$ after the matter falling, the functional form of $\kappa(\phi)$ is reproduced completely as follows.

$$\kappa(\phi) = \frac{1}{2\pi r_+}\sum_m \delta Q^{(T)}_m e^{-im\phi}. \tag{30}$$

Thus the horizontal charge plays a role of recorder on the horizon.

If the black hole completely evapolates swallowing negative quantum flux, the information registered in the horizontal charges will be released into the space via the black hole radiation because of the conservation law of the charges. (Note that the black hole radiation does not always look isotropic in the coordinate system in which the asymptotic condition in eqn(14) is satisfied at each time.)

References

[1] M.Hotta, *Holographic Charge Excitation on a Horizontal Boundary*, hep-th/0206222, to appear in PRD.

[2] S.Carlip, Phys.Rev.**D51**,632,(1995).

[3] J.D.Bekenstein, Phys.Rev.**D7**,2333,(1973).
S.W.Hawking, S.W.Hawking, Commun.Math.Phys.**43**,199,(1975).

[4] A.Strominger and C.Vafa, Phys.Lett.**B379**,99,(1996).

[5] S.Carlip, Phys.Rev.Lett.**82**,2828,(1999).

[6] S.N.Solodukhin, Phys.Lett.**B454**,213,(1999).
F.-L.Lin and Y.-S.Wu, Phys.Lett.**B453**,222,(1999).
D.Navarro, J.Navarro-Salas, P.Navarro, Nucl.Phys.**B580**,311,(2000).
R.Brustein, Phys.Rev.Lett.**86**,576,(2001).
S.Das, A.Chosh and P.Mitra, Phys.Rev.**D63**,024023,(2001).
J.Jing and M.-L. Yan, Phys.Rev.**D64**,064015,(2001).

[7] M.-I.Park and J.Ho, Phys.Rev.Lett.**83**,5595,(1999).
S.Carlip, Phys.Rev.Lett.bf 83,5596,(1999).
M.-I. Park and J.H.Yee, Phys.Rev.**D61**,088501,(2000).
O.Dreyer, A.Ghosh and J.Wisniewski,
Class.Quant.Grav.**18**,1929,(2001).
J.Koga, Phys.Rev.**D64**,124012,(2001).

[8] M.Hotta, K.Sasaki and T.Sasaki, Class.Quant.Grav.**18**,1823,(2001).

[9] J.Lee and R.M.Wald, J.Math.Phys.**31**,725,(1990).
V.Iyer and R.M.Wald, Phys.Rev.**D50**,846,(1994);
Phys.Rev.**D52**,4430,(1995).

[10] R.M.Wald and A.Zoupas, Phys.Rev.**D61**,084027,(2000).

Disappearing Dark Matter in Brane World Cosmology

K. Ichiki,[1a] P.M.Garnavich,[b] T. Kajino,[a] G.J.Mathews,[b] M. Yahiro[c]

[a] *National Astronomical Observatory, 2-21-1, Osawa, Mitaka, Tokyo 181-8588, Japan*

[b] *Center for Astrophysics, University of Notre Dame, Notre Dame, IN 46556*

[c] *Department of Physics and Earth Sciences, University of the Ryukyus, Nishihara-chou, Okinawa 903-0213, Japan*

Abstract

We explore cosmological consequences of dark matter as massive particles trapped on a brane embedded in a Randall-Sundrum noncompact higher dimension AdS_5 space. In this picture, massive particles are metastable and can disappear into the bulk dimension. Here, we examine cosmological constraints on the new possibility that dark matter decays into the extra dimension. We show that disappearing dark matter is consistent (at the 95% confidence level) with both present observations of Type Ia supernovae at the highest redshift and trends in the mass-to-light ratios of galactic clusters with redshift

1 Introduction

There is currently considerable interest in the possibility that our universe could be a submanifold embedded in a higher-dimensional spacetime. This brane-world paradigm is motivated by the D-brane solution found in ten-dimensional superstring theory. Technically, in type IIB superstrings, an $AdS_5 \times S^5$ geometry is formed near the stacked D3-branes [1]. In simple terms this means that a model can be proposed [2] whereby our universe is represented as a thin three-brane embedded in an infinite five-dimensional anti-de Sitter space (AdS_5). In such Randall-Sundrum II (hereafter referred to as simply RS) models, physical particles are trapped on a three-dimensional brane, while gravitons can reside as a fluctuation in the background gravitational field living in the noncompact extra dimension (the bulk). This representation of extra dimensions is an alternative to the standard Kaluza-Klein compactification.

Although massive particles can indeed be trapped on the brane, they are also expected to be metastable [4]. That is, for both scalar and fermion fields, the quasi-normal modes are metastable states that can decay into continuum states in the higher dimension. From the viewpoint of an observer in the 4-dimensional space time, these massive particles can appear to propagate for some time in three spatial dimensions and then literally disappear into the fifth dimension.

The mathematical realization of this decay is that the eigenvalues for the mass modes of the field theory are complex when one imposes radiation (outgoing-wave) boundary conditions. The four-dimensional mass eigenvalues are thus of the form, $m = m_0 - i\Gamma$, where, the the quasi-discrete four-dimensional masses are given by $m_0^2 = \mu^2/2$, with μ being the bulk mass term in the AdS_5 field equation. For a massive scalar boson, the width Γ is given by $\Gamma/m_0 = (\pi/16)(m_0/L)^2$, where $L \approx \sqrt{-\Lambda_5/6} \approx \tau/6M_5^3$ [3] where Λ_5 is the negative bulk cosmological constant, τ is the brane tension and M_5 the five dimensional Planck mass. A construction of the propagator for particles on the brane then has a pole at complex p^2 which corresponds to an unstable particle with mass m_0 and width Γ. Thus, the comoving density of massive scalar particles can be expected to decay over time with a rate, $(\rho a^3)\exp[-\Gamma t]$ (using natural units $\hbar = c = 1$).

In this paper, we consider the possibility that cold dark matter can decay in this way into the extra dimension. In principle, normal fermionic matter (e.g. baryons) could decay in this way as well. This would have many far reaching consequences in astrophysics and cosmology. However, it is likely that the decay of normal fermionic fields is suppressed relative to that of a dark-matter scalar particle [4]. For the remaining discussion we shall assume that fermionic decay can be ignored.

[1] E-mail:ichiki@th.nao.ac.jp

2 DDM cosmology

Cosmological constraints on decaying matter have been considered in many papers, particularly with regard to the effects of such decays on big bang nucleosynthesis (cf. [5] and Refs. therein). The present discussion differs from the previous considerations in that the decaying particles do not produce photons, hadronic showers, or residual annihilations in our four-dimensional spacetime.

In the present application, particles disappear into a noncompact extra dimension. There are, however, two complications. One is that, in general, an energy flow to the bulk induces a back reaction from the background gravitational field [6]. This can enhance the electric part of the bulk Weyl tensor (dark radiation), as analyzed below. The other is that particles which enter the bulk dimension can still interact gravitationally with particles on the brane. The strength of this interactions, however, is greatly diminished [7] by a factor of $(R/z)^2$, where z is the distance into the bulk, and R is the "radius" of the bulk dimension $R = 1/L$. Hence, particles literally disappear in the bulk.

To distinguish the disappearance of dark matter in the present application, from the previous decay applications, we shall refer to it here as *disappearing dark matter.*

The five-dimensional Einstein equation for the present braneworld is reduced to an effective four-dimensional equation on the brane [8], in which the right-hand side has the energy-momentum tensor of dark matter, the corresponding term $t_{\mu\nu}$ of ordinary matter, a term quadratic in $t_{\mu\nu}$ and a term with bulk Weyl tensor. The (0,0) component of the 4d Einstein equation reduces to a new generalized Friedmann equation [9] for the observed Hubble expansion in the three brane,

$$\left(\frac{\dot{a}}{a}\right)^2 = \frac{8\pi G_{\rm N}}{3}(\rho + E) - \frac{k}{a^2} + \frac{\Lambda_4}{3} + \frac{\kappa_5^4}{36}\rho^2. \tag{1}$$

Here, $a(t)$ is the scale factor at cosmic time t, and $\rho = \rho_B + \rho_\gamma + \rho_{DM}$ where ρ_B and ρ_γ represent the usual contributions from nonrelativistic (mostly baryons) and relativistic particles, respectively. In the present application we presume that only the dark matter can decay into the extra dimension. Hence, we write $\rho_{DM} = Ce^{-\Gamma t}/a^3$, where Γ is the decay width into the extra dimension.

In equation (1), several identifications of cosmological parameters were required in order to recover standard big-bang cosmology. For one, the first term on the right hand side is obtained by relating the four-dimensional gravitational constant $G_{\rm N}$ to the five-dimensional gravitational constant, κ_5. Specifically, $G_{\rm N} = M_4^{-2} = \kappa_5^4\tau/48\pi$, where τ is the intrinsic tension of the brane and $\kappa_5^2 = M_5^{-3}$, where M_5 is the five dimensional Planck mass. Secondly, the four-dimensional cosmological constant Λ_4 is related to its five-dimensional counterpart Λ_5, $\Lambda_4 = \kappa_5^4\tau^2/36 + \Lambda_5/6$. A negative Λ_5 is required for Λ_4 to obtain its observed small value [3].

The term E shows an effective energy density derived from electric part of bulk Weyl tensor. The Bianchi identity for the effective 4d Einstein equation yields $\dot{E} + 4HE + \dot{\rho}_{DM} + 3H\rho_{DM} = 0$, leading to

$$\dot{E} + 4HE = \Gamma\rho_{DM} \tag{2}$$

for $H = \dot{a}/a$ and $\rho_{DM} = Ce^{-\Gamma t}/a^3$. When $\Gamma = 0$, E scales as μ/a^4, just like normal radiation with a constant comoving energy density μ. Hence, it is called 'dark radiation'. Upper and lower limits of μ at big-bang nucleosynthesis (BBN) epoch have been determined from observations [10]. Figure 1 illustrates the evolution of dark radiation in a disappearing dark matter cosmology. As a simple case, consider a flat $\Lambda_4 = k = 0$, cosmology with negligible ρ^2 term. This cosmology separates into four characteristic regimes identified on Figure 1.

Early on the contribution from the dark radiation component evolves (from eq.(2)) as $E \propto a^{-1}$ and $E \propto a^{-3/2}$, during regimes I and II, respectively, and can be neglected. Thus dark radiation does not contribute during the epochs of nucleosynthesis ($z \sim 10^{10}$) or CMB photon decoupling ($z \sim 10^3$). On the other hand, the dark radiation can become comparable to and even in excess of the dark matter contribution in epoch III. The interesting region is during the transition from epoch II to epoch III. This occurs at intermediate times $t \sim 2\Gamma^{-1}$ and redshifts of $0 < z < 2$ on Figure 1. Here, the fact that there is both more dark matter and more dark energy at higher redshifts means that the universe decellerates faster during in the redshift regime $1 < z < 2$ than during the more recent epoch $0 < z < 1$. This can have an important effect on the luminosity-redshift relation and may be constrainable by the observations of supernovae at high redshift and galaxy mass-to-light ratios as we now show.

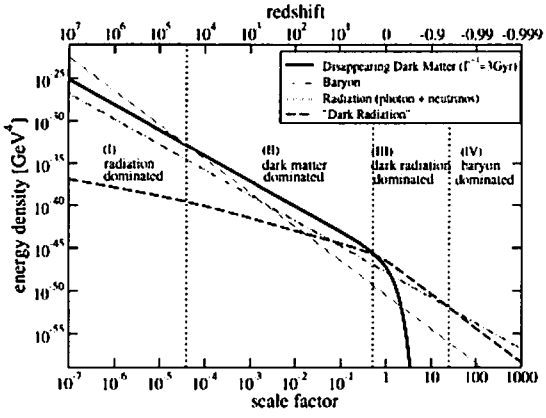


Figure 1: Illustration of the energy densities with scale factor in models with dark-matter decay into the extra dimension.

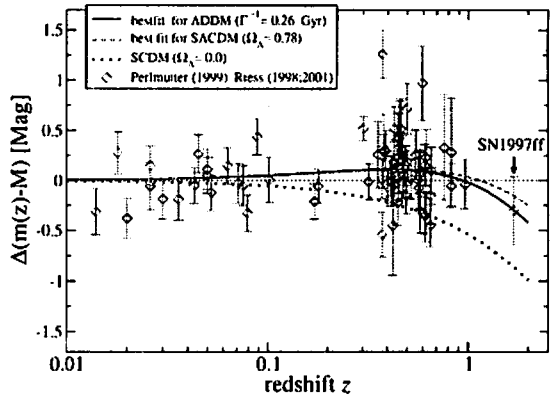


Figure 2: Illustration of the supernova magnitude redshift relation for various cosmological models with and without disappearing dark matter.

3 Supernova Constraint

The apparent brightness of the Type Ia supernova standard candle with redshift is given by a simple relation in a standard Friedmann cosmology which we slightly modify to include the dark-energy term.

$$D_L = \frac{c(1+z)}{H_0\sqrt{\Omega_k}} sinn\left\{\sqrt{\Omega_k}\int_0^z [\Omega_\gamma(1+z')^4 + (\Omega_{DM}(t)+\Omega_B)(1+z')^3 + \Omega_k(1+z')^2 + \Omega_\Lambda + \Omega_E(t)\Big]^{-1/2} dz'\right\} , \quad (3)$$

where H_0 is the present value of the Hubble constant, and $sinn(x) = \sinh x$ for $\Omega_k > 0$, $sinn(x) = x$, for $\Omega_k = 0$ and $sinn(x) = \sin x$ for $\Omega_k < 0$. The Ω_i are the usual closure quantities, i.e. the contribution from all relativistic particles is $\Omega_\gamma = 8\pi G\rho_\gamma/3H_0^2$, the baryonic contribution is $\Omega_B = 8\pi G\rho_B/3H_0^2$, with $\Omega_k = k/a_0^2H_0^2$, and $\Omega_\Lambda = \Lambda/3H_0^2$.

In the present context, we have added a redshift-dependent contribution from the dark radiation, $\Omega_E = 8\pi GE(z)/3H_0^2$. The dark matter contribution Ω_{DM} becomes a function of redshift through, $\Omega_{DM} \longmapsto \Omega_{DM}^0 \exp\{\Gamma(t_0 - t)\}$, where $\Omega_{DM}^0 = 8\pi G\rho_{DM}^0/3H_0^2$ is the present dark-matter content, and the look-back time $t_0 - t$ is a function of redshift,

$$t_0 - t = H_0^{-1}\left\{\int_0^z (1+z')^{-1}\Big[\Omega_R(1+z')^4 + (\Omega_B+\Omega_{DM})(1+z')^3 + \Omega_k(1+z')^2 + \Omega_\Lambda + \Omega_E\Big]^{-1/2} dz'\right\} . \quad (4)$$

Figure 2 compares recent data from the combined data of the High-Z Supernova Search Team and the Supernova Cosmology Project [11]. Shown are the K-corrected magnitudes $m = M + 5\log D_L + 25$ vs. redshift. Curves are plotted relative to an $\Omega_M = 0.0$, $\Omega_\Lambda = 0$ open cosmology. Of particular interest is the point for SN1997ff [12] at $z = 1.7$. At present this is the only existing constraint on the redshift evolution during the matter dominated decelerating phase relevant to this paper. It is of particular interest that an optimum standard flat $\Omega_\Lambda = 0.7$ ($S\Lambda CDM$) cosmology passes somewhat above this point. This is even more relevant in view of the fact that dust around the supernova would cause the inferred data point to be even lower on this plot. This datum is therefore in reality only an upper limit [12]. Nevertheless, even in the conservative assumption that this point is not an upper limit, we find that this point implies at least a marginal preference for a finite disappearance rate for dark matter.

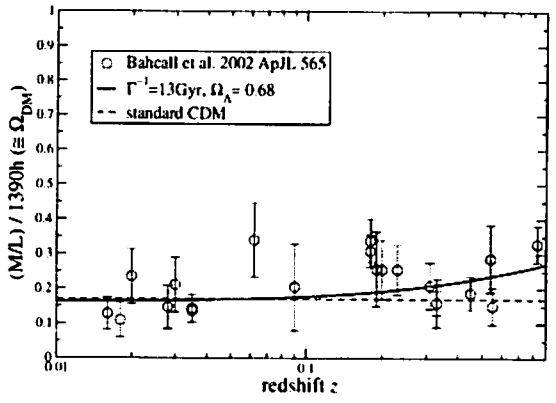


Figure 3: Illustration of the mass-to-light ratio redshift relation for cosmological models with and without disappearing dark matter.

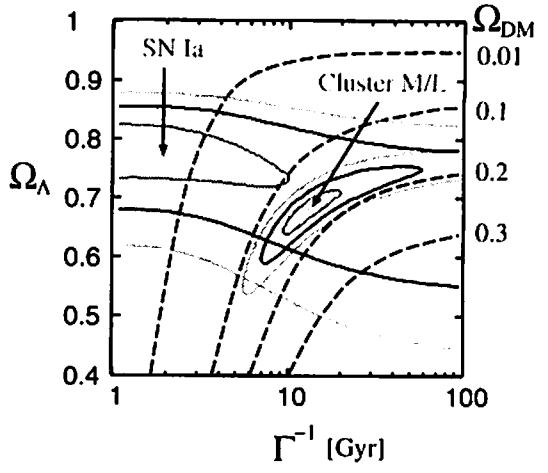


Figure 4: Contours of constant χ^2 in the Ω_Λ vs. Γ^{-1} plane. The dashed lines indicate those of constant Ω_{DM} as labeled.

4 M/L ratio constraint

As shown in Figure 4, the optimum decay lifetime from SNIa corresponds to a relatively small contribution from dark matter at the present time. Moreover, the SNIa data available so far, however, do not constrain the decay lifetime at the 2σ level even though a finite lifetime is probably favored by the non-trivial expansion history of disappearing dark matter and the dark radiation. On the other hand, another interesting cosmological probe comes from the classical technique to obtain the universal mass density from galaxy cluster mass-to-light ratios. A most recent value of $\Omega_M = 0.17 \pm 0.05$ is given in [13] based upon 21 galactic clusters out to $z \approx 1$ corrected for their color evolution with redshift. In that paper it was demonstrated that there exists a mild, but robust increase in the mass to light ratio M/L with temperature. This was anticipated in cosmological simulations which showed that higher density (high temperature) clusters collapse at earlier times. This means that their luminous matter has had more time to evolve and dim so that a larger M/L is expected for higher temperature clusters.

On the other hand, these data suggest an important test of this disappearing dark matter paradigm. If one observes clusters at high redshift, one should expect in standard CDM models that they have had less time to evolve and dim. Hence, their M/L ratios should decline with increasing redshift. In the present disappearing dark matter paradigm, however, the dark matter can diminish with time, while the normal baryonic luminous matter remains mostly confined to the brane. Hence, in the context of the present work, the M/L ratio should actually increase rather than decrease with look-back time, i.e. $M/L \propto \Omega_{DM} \exp[(t_0 - t)/\Gamma]/\Omega_B$ assuming that the decay rate is much greater than the luminosity evolution time scale. In our disappearing dark-matter models (cf. Figure 1) a redshift of $z \approx 1$ corresponds to a look back time of $t_0 - t \approx 7$ Gyr. Thus, the dark matter and associated M/L ratio should have increased by a factor of $\approx \exp(7\Gamma)$ over that interval.

We have analyzed the color-corrected cluster data in [13] and find marginal evidence for an increase in M/L with redshift (Figure 3). Based upon a standard χ^2 goodness of fit analysis, we obtain limits from the galaxy cluster data of 7 Gyr $\leq \Gamma^{-1} \leq$ 62 Gyr at the 95% confidence level for our flat Λ plus disappearing CDM models.

5 Discussion and Conclusion

In this paper we explore the cosmological consequences from disappearing dark matter scenario and examine constraints on this new possibility from Type Ia SN and mass-to-light ratios in galactic clusters.

Based upon these two constraints we conclude that a likely concordance region corresponds to a decay lifetime which starts from less than the present cosmological age, i.e. 7 Gyr $\leq \Gamma^{-1} \leq 62$ Gyr. Clearly, more work is needed to unambiguously identify evidence for a finite decay width. Obviously, there is great need for more Type Ia supernova data in the $z > 1$ regime as well as more galactic cluster mass-to-light ratios at high redshifts. Such data could definitively answer the interesting question as to whether or not dark matter decays into the higher dimension.

Although the evidence for disappearing dark matter is of marginal statistical significance at the present time, the purpose of this letter is to emphasize the potential importance of future studies aimed at unambiguously determining the decay width. If such a finite value of Γ were to be established, it would constitute the first observational indication for noncompact extra dimensions. It would also provide valuable insight into the physical parameters of the higher-dimensional space.

Rewriting the equation for the decay width, along with the relations between various quantities in the modified Friedmann equation, i.e. κ_5, G_N, M_4, M_5, Λ_4, and Λ_5, leads to the following relation between the five-dimensional Planck mass M_5 and quantities which can be measured in the four dimensional space time, $M_5^6 = (M_4^4/64\pi^2)(\pi/16\Gamma)m_0^3 + \Lambda_4)$. Other fundamental parameters in five dimensions, e.g. Λ_5 and the brane tension τ, are derivable from M_5 via equations given previously. This implies that, should the dark-matter mass m_0 ever be known, all of the five-dimensional parameters could be determined. For example, a dark matter mass of $m_0 = 10^{-4}$ GeVand our putative decay lifetime of $\Gamma^{-1} = 7$ Gyr, would imply $(M_5/M_4) = 3.6 \times 10^{-7}(m_0/10^{-4}\text{eV})^{1/2}(\Gamma^{-1}/7\text{ Gyr})^{1/6}$.

6 Acknowledgments

One of the authors (MY) would like to thank K. Ghoroku for helpful discussions. We acknowledge T. Tanaka and Y. Himemoto for discussions which improve early works of our paper.

References

[1] J. Maldacena, Adv. Theor. Math. Phys. **2** (1998) 231; S.S. Gubser, I.R. Klebanov, and A.M. Polyakov Phys. Lett. **B 428** (1998) 105; E. Witten, Adv. Theor. Math. Phys. **2** (1998) 253; A.M. Polyakov, Int. J. Mod. Phys. **A14** (1999) 645.

[2] L. Randall and R. Sundrum, Phys. Rev. Lett. **83**, 3370 (1999); **83**, 4690 (1999).

[3] K. Ghoroku and M. Yahiro, hep-th/0206128.

[4] S. L. Dubovsky, V. A. Rubakov and P. G. Tinyakov, Phys. Rev. D 62, 105011 (2000).

[5] R. A. Malaney and G. J. Mathews, Phys. Rep., **229**, 145 (1993); M. Kawasaki, K. Kohri and T. Moroi, Phys. Rev., **D63**, 103502 (2001).

[6] R. Gregory, V. Rubakov and S. Sibiryakov, Class. Quant. Grav., **17**, 4437 (2000); D. Langlois, L. Sorbo, and M. Rodriguez-Martinez, Phys. Rev. Lett. **D89**, 171301-1(2002); T. Tanaka and Y. Himemoto, (gr-qc/0301010) (2003).

[7] S. B. Giddings, E. Katz, and L. Randall, J. High Energy Phys. **3**, 23 (2000).

[8] T. Shiromizu, K.I. Maeda, and M. Sasaki, Phys. Rev. **D62**, 024012(2000).

[9] P. Binétruy, C. Deffayet, U. Ellwanger, and D. Langlois, Phys. Lett. **B477**, 285 (2000); P. Binétruy, C. Deffayet, and D. Langlois, Nucl. Phys. **B565**, 269 (2000).

[10] K. Ichiki, M. Yahiro, T. Kajino, M. Orito and G. J. Mathews, Phys. Rev. **D66**, 043521 (2002).

[11] P. M. Garnavich, et al., Astrophys. J., **509**, 74 (1998); S. Perlmutter, et al. Nature, **391**, 51 (1998).

[12] A. G. Riess, et al., Astrophys. J., **536**, 62 (2000).

[13] N. Bahcall and J. M. Comerford, Astrophys. J. Lett., **565**, L5 (2002).

Scalar perturbation of the five-dimensional Kerr black hole

Daisuke Ida, [1]

Department of Physics, Tokyo Institute of Technology, Tokyo 152-8550, Japan

Abstract

The scalar perturbation of the higher-dimensional Kerr black hole has been investigated. The field equation turns out to be separable in arbitrary dimensions. The quasi-normal modes of the scalar field have been searched in five dimensions using the continued fraction method. The numerical result shows the evidence for the stability of the scalar perturbation of the five-dimensional Kerr black holes. The time scale of the resonant oscillation in the rapidly rotating black hole, in which case the horizon radius becomes small, is characterized by (black hole mass)$^{1/2}$(Planck mass)$^{-3/2}$ rather than the light-crossing time of the horizon.

Recently, it has been suggested that the evidence of the existence of the extra dimensions might be proved in the future high-energy experiments, if the fundamental scale is of order TeV. This argument follows from the brane-world scenario [1]. In such a model, the Standard Model particles are confined to the three-brane, which means that the Kaluza-Klein modes of the SM particles are not excited, and only gravitons can propagate in the bulk, hence there are rather mild constraints on the size of the extra dimensions, so that the fundamental (higher-dimensional) Planck scale can reduce to TeV scale. This is a possible solution to the hierarchy problem. Another type of the brane-world models has been proposed by Randall and Sundrum, which utilize the warped metric of the AdS space.

If the fundamental scale is given by TeV, the black holes will be produced at the future colliders such as the CERN Large Hadron Collider (LHC), of which center of mass energy is 14TeV [2, 3]. Though the classical approximation might be marginal for hypothetical black holes to be produced at LHC, we shall here discuss the higher-dimensional classical black holes, which is relevant for future colliders beyond the LHC. Recent studies show that the higher-dimensional black holes might be qualitatively rather different from usual four-dimensional ones.

Significantly, the stationary black hole solutions are shown to be nonunique, while the uniqueness of static black hole has been established [4]. There are five-dimensional Kerr solution, while Emparan and Reall [6] have recently found the rotating black ring solution with $S^1 \times S^2$ horizon, and there exists a parameter ranges where Kerr black hole and black ring have the common mass M and the angular momentum J. The dimensionless Kerr parameter $a_* := a/r_H$, where $a = 3J/2M$ is the Kerr parameter and r_H the horizon radius, are characteristic quantity determining the property of the five-dimensional Kerr black hole, which are equivalent to the another dimensionless quantity J^2/GM^3 via

$$\frac{J^2}{GM^3} = \frac{32}{27\pi}\frac{a_*^2}{a_*^2+1}. \tag{1}$$

The five-dimensional Kerr black hole can have arbitrary $a_* > 0$ for fixed total mass. Consider a sequence of the solution with the mass being fixed. Starting with $a_* = 0$ (Schwarzschild black hole), spin up the black hole. At $a_* = 2.3$, there emerge two branches of black ring solutions with same J, both have less horizon area than the Kerr black hole. However, for $a_* > 2.8$, the horizon area of the larger black ring exceeds that of the Kerr black hole with same J. Since the horizon area is just the black hole entropy, it means that the five-dimensional Kerr black hole are entropically unfavourable in microcanonical ensemble. Though this is a purely thermodynamical argument, one might wonder the stability of the rapidly rotating black holes, and this is the subject of the present paper.

As a simplest case, we here investigate the massless scalar field in the five-dimensional Kerr background.

[1] E-mail:d.ida@th.phys.titech.ac.jp

The metric of the $(4+n)$-dimensional Kerr metric with only one non-zero angular momentum is given in Boyer-Lindquist-type coordinates by [5]

$$\begin{aligned} g &= -\frac{\Delta - a^2\sin^2\vartheta}{\Sigma}dt^2 - \frac{2a(r^2+a^2-\Delta)}{\Sigma}dtd\varphi + \frac{(r^2+a^2)^2 - \Delta a^2\sin^2\vartheta}{\Sigma}\sin^2\vartheta d\varphi^2 \\ &\quad + \frac{\Sigma}{\Delta}dr^2 + \Sigma d\vartheta^2 + r^2\cos^2\vartheta d\Omega_n^2, \end{aligned} \tag{2}$$

where

$$\Sigma = r^2 + a^2\cos^2\vartheta, \tag{3}$$

$$\Delta = r^2 + a^2 - \mu r^{1-n}, \tag{4}$$

and $d\Omega_n^2$ denotes the standard metric of the unit n-sphere. This metric describes a rotating black hole in asymptotically flat, empty space-time with mass and angular momentum proportional to μ and μa, respectively. Hereafter, $\mu, a > 0$ are assumed.

The event horizon is located at $r = r_H$, such that $\Delta|_{r=r_H} = 0$, which is homeomorphic to S^{2+n}. When $n = 1$, an event horizon exists only when $a < \sqrt{\mu}$, and the event horizon shrinks to zero-area in the extreme limit $a \to \sqrt{\mu}$. On the other hand, when $n \geq 2$, $\Delta = 0$ has exactly one positive root for arbitrary $a > 0$. Thus, there are no extreme Kerr black holes in higher dimensions.

Here we consider the scalar perturbation on the background metric (2). We put $\phi = e^{i\omega t - im\varphi}R(r)S(\vartheta)Y(\Omega)$ into the massless scalar field equation $\nabla^2\phi = 0$, where $Y(\Omega)$ is the hyperspherical harmonics on n-sphere, of which eigenvalues given by $-j(j+n-1)$ $(j = 0, 1, 2, \cdots)$. Then we obtain the separated equations

$$\frac{1}{\sin\vartheta\cos^n\vartheta}\left(\frac{d}{d\vartheta}\sin\vartheta\cos^n\vartheta\frac{dS}{d\vartheta}\right) + \left[\omega^2a^2\cos^2\vartheta - m^2\csc^2\vartheta - j(j+n-1)\sec^2\vartheta + A\right]S = 0 \tag{5}$$

and

$$r^{-n}\frac{d}{dr}\left(r^n\Delta\frac{dR}{dr}\right) + \left\{\frac{\left[\omega(r^2+a^2) - ma\right]^2}{\Delta} - \frac{j(j+n-1)a^2}{r^2} + 2m\omega - \omega^2a^2 - A\right\}R = 0. \tag{6}$$

The eigenvalues of the angular equation (5) are given by

$$\begin{aligned} A &= (2\ell + j + |m|)(2\ell + j + |m| + n + 1) + O(\omega_*a_*), \\ &\quad (\ell = 0, 1, 2, \cdots) \end{aligned} \tag{7}$$

and the 0th-order eigenfunctions are given in terms of the Jacobi polynomials:

$$P_{\ell jm} = (\sin\vartheta)^{|m|}(\cos\vartheta)^j F\left(-\ell, \ell + j + |m| + \frac{n+1}{2}, j + \frac{n+1}{2}; \cos^2\vartheta\right). \tag{8}$$

Hence, each resonant mode turns to have the wave number ℓ.

In what follows, we concentrate on the five-dimensional case $(n = 1)$. In the case of non-rotating black hole, the first eight quasi-normal modes with several values of angular momentum obtained in our computation are plotted in Fig. 1. Typical examples of quasi-normal modes of the five-dimensional Kerr black holes are plotted in Figs. 2-4, where the Kerr parameter a_* is continuously varied. Here the resonant frequencies are normalized by $\sqrt{\mu}$ rather than r_H, *i.e.*, we work on $\sqrt{1+a_*^2}\omega_*$-plane, where we have defined the dimensionless parameters $(a_*, \omega_*) = (a/r_H, \omega r_H)$. Though the Kerr parameter a_* is taken to be sufficiently large values, each mode does not seem to pass through the real axis of the frequency plane in any cases. The $m > 0$ branches seem to approach to some points on the real axis, which is a similar behaviour to the four-dimensional case [7, 8, 9, 10]. Though we have searched for unstable modes up to $|m|, j \leq 5$, they are not found.

We have investigated the massless scalar field equation in the higher-dimensional Kerr black hole background. The field equation is separable in arbitrary dimensions. Under the quasi-normal boundary

condition, we have searched for the resonant frequencies in the complex ω_*-plane in the case of the five dimensions.

In the Schwarzschild case ($a_* = 0$), the resonant frequencies are characterized by ℓ and the excitation number N. For nonzero Kerr parameter, these resonant frequencies split for different sets of m and j. Continuously varying the Kerr parameter a_*, we keep track of resonant modes, of which trajectories are characterized by the set of wave numbers: (ℓ, m, j, N). Each trajectory does not pass through the real axis of the complex frequency plane. For $m > 0$, however, these trajectories seem to approach to points on the real axis of the frequency plane. The corresponding time scale of the resonant oscillation in the limit $a_* \to 0$, in which case the horizon radius shrinks to zero, is characterized by the mass scale $\sim \mu^{1/2}$ rather than the light-crossing time $\sim r_H$.

These results show the evidence of the stability of the scalar perturbation of the five-dimensional Kerr black holes.

Acknowledgments

The author was supported by JSPS Research, and this research was supported in part by the Grant-in-Aid for Scientific Research Fund (No. 6499).

References

[1] N. Arkani-Hamed, S. Dimopoulos and G.R. Dvali, Phys. Lett. **B429**, 263 (1998); I. Antoniadis *et al.*, Phys. Lett. **B436**, 257 (1998); L. Randall and R. Sundrum, Phys. Rev. Lett. **83**, 3370 (1999).

[2] P.C. Argyres, S. Dimopoulos and J. March-Russell, Phys. Lett. **B441**, 96 (1998).

[3] S.B. Giddings and S. Thomas, hep-ph/0106219.

[4] G.W. Gibbons, D. Ida and T. Shiromizu, gr-qc/0203004; G.W. Gibbons, D. Ida and T. Shiromizu, Phys. Rev. Lett. **89**, 041101 (2002); G.W. Gibbons, D. Ida and T. Shiromizu, Phys. Rev. D **66**, 044010 (2002); M. Rogatko, Class. Quantum Grav. **19**, L151 (2002).

[5] R.C. Myers and M.J. Perry, Ann. Phys. **172**, 304 (1986).

[6] R. Emparan and H.S. Reall, Phys. Rev. Lett. **88**, 101101 (2002).

[7] E.W. Leaver , Proc. R. Soc. London. **A402**, 285 (1985)

[8] S.L. Detweiler and S. Chandrasekhar , Proc. R. Soc. London. **A352**, 381 (1977)

[9] H. Onozawa , Phys. Rev. D **55**, 3593 (1997)

[10] E. Seidel and S. Iyer , Phys. Rev. D **41**, 374 (1990)

[11] D. Ida, Y. Uchida and Y. Morisawa, gr-qc/0212035

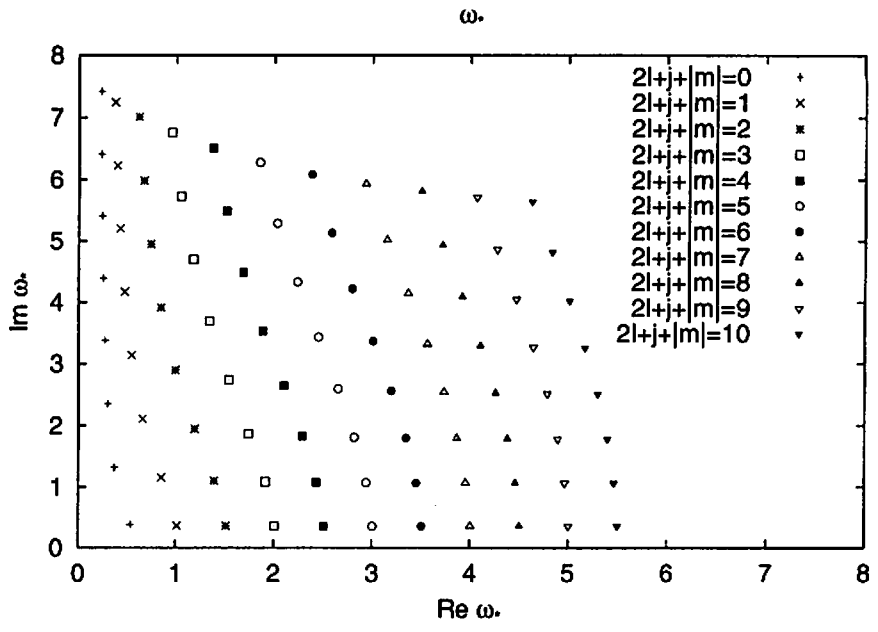


Figure 1: For non-rotating black hole, first eight quasi-normal frequencies for $2\ell + j + |m| = 0, \cdots, 10$ are plotted in the complex ω_* plane.

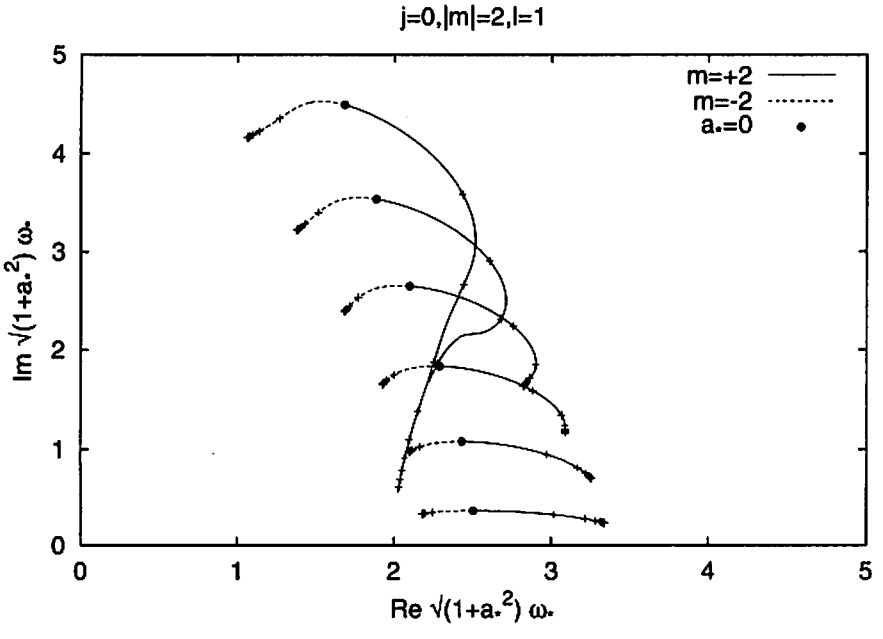


Figure 2: The first six quasi-normal modes of Kerr black hole for $j = 0$, $m = \pm 2$, $\ell = 1$ are plotted in the $\sqrt{1 + a_*^2}\omega_*$ plane. The bullets are the quasi-normal modes of Schwarzschild black hole ($a_* = 0$). The right part starting from the Schwarzschild mode is the branch of the $m = +2$ modes. The left part is the branch of the $m = -2$ modes. The crosses are the modes with integer values of a_*.

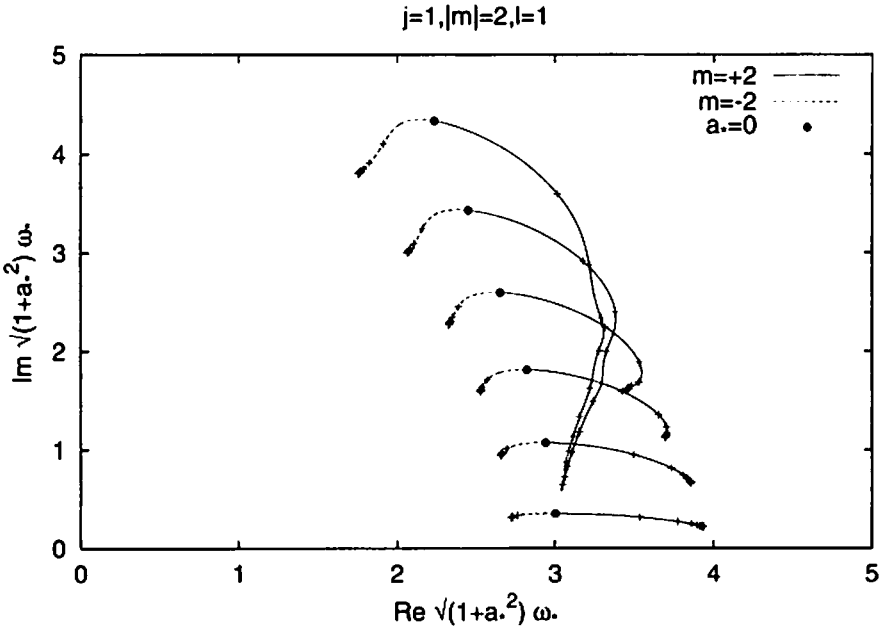


Figure 3: The first six quasi-normal modes of Kerr black hole for $j = 1$, $m = \pm 2$, $\ell = 1$ are plotted in the $\sqrt{1 + a_*^2}\omega_*$ plane. The bullets are the quasi-normal modes of Schwarzschild black hole ($a_* = 0$). The right part starting from the Schwarzschild mode is the branch of the $m = +2$ modes. The left part is the branch of the $m = -2$ modes. The crosses are the modes with integer values of a_*.

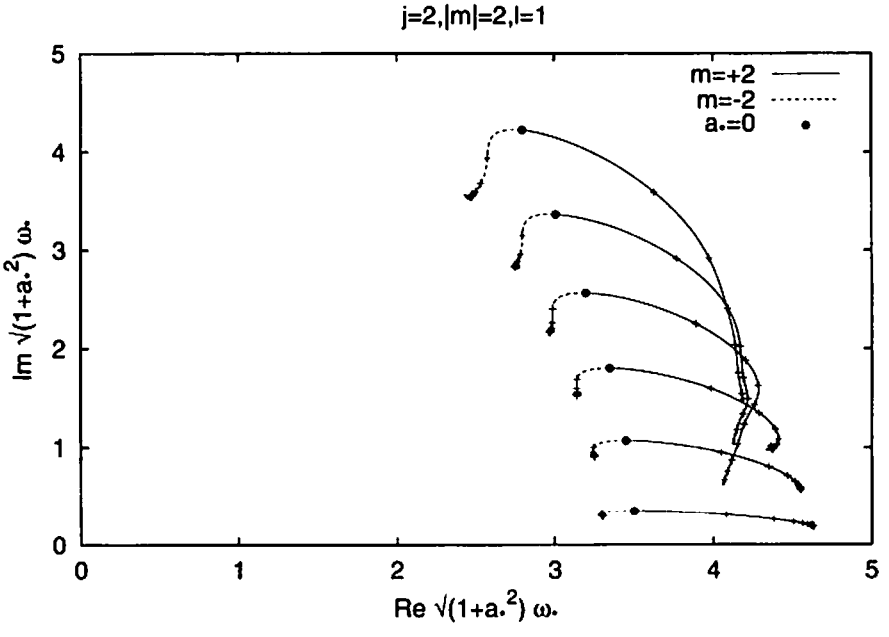


Figure 4: The first six quasi-normal modes of Kerr black hole for $j = 2$, $m = \pm 2$, $\ell = 1$ are plotted in the $\sqrt{1 + a_*^2}\omega_*$ plane. The bullets are the quasi-normal modes of Schwarzschild black hole ($a_* = 0$). The right part starting from the Schwarzschild mode is the branch of the $m = +2$ modes. The left part is the branch of the $m = -2$ modes. The crosses are the modes with integer values of a_*.

Multi-graviton theory, a latticized dimension, and the cosmological constant [1]

Nahomi Kan[2], Kiyoshi Shiraishi[3]

Graduate School of Science and Engineering, Yamaguchi University, Yoshida, Yamaguchi-shi, Yamaguchi 753-8512, Japan

Abstract

Beginning with the Pauli-Fierz theory, we construct a model for multi-graviton theory. Couplings between gravitons belonging to nearest-neighbor "theory spaces" lead to a discrete mass spectrum. Our model coincides with the Kaluza-Klein theory whose fifth dimension is latticized. We evaluate one-loop vacuum energy in models with a circular latticized extra dimensions as well as with compact continuous dimensions. We find that the vacuum energy can take a positive value, if the dimension of the continuous space time is $6, 10, \ldots$. Moreover, since the amount of the vacuum energy can be an arbitrary small value according to the choice of parameters in the model, our models is useful to explain the small positive dark energy in the present universe.

1 INTRODUCTION AND SUMMARY

It is well known that the weak-field limit of the Einstein gravity reduces to the theory of a single massless spin-two field [1]. We call the second-order symmetric tensor field $h_{\mu\nu}$, which represents deviation from a flat space ($g_{\mu\nu} = \eta_{\mu\nu} + h_{\mu\nu}$), as a "graviton". Multi-graviton theories have been studied be Boulanger *et al.* [2, 3]. They have shown that there is no consistent interaction of gravitons and the possible action is a sum of replicated Pauli-Fierz actions [4].

We consider a model for a multi-graviton theory with nearest-neighbor coupling in the theory space. To be precise, the gravitons are not interacting each other in our model, but they have a discrete mass spectrum. The simplest model is explained in Sec. 2. In the limit of a large number of gravitons, the mass spectrum of gravitons resembles that of the Kaluza-Klein (KK) theory. Therefore our model is equivalent to the KK theory with a discretized dimension.

The emergence mechanisms of a space dimension have been suggested in refs. [5, 6, 7], which is in the stream of dimensional deconstruction [8, 9]. Recently the authors have been informed of ref. [10], in which the gravity with the theory space is also argued. Although our model for the gravitation theory with a discretized dimension is very simple, it may be a toy model adequate for studying qualitative features of more complicated theory and mechanisms included in it.

For example, we evaluate the vaccum energy in our model in Sec. 3. We also consider a model in the continuous $(4+\delta)$ dimensional space-time with a discretized dimension. We show that an arbitrary small amount of positive vacuum energy can be obtained if $(4+\delta) = 6, 10, \ldots$.

2 MULTI-GRAVITON THEORY AND A LATTICIZED DIMENSION

We consider a multi-graviton (N-graviton) theory [2, 3] given by the lagrangian

$$\bar{\mathcal{L}}_0 = \sum_{k=1}^{N} \left[-\frac{1}{2}\partial_\lambda h^k_{\mu\nu}\partial^\lambda h^{k\,\mu\nu} + \partial_\lambda h^{k\,\lambda}{}_{\mu}\partial_\nu h^{k\,\nu\mu} - \partial_\mu h^{k\,\mu\nu}\partial_\nu h^k + \frac{1}{2}\partial_\lambda h^k \partial^\lambda h^k \right] , \tag{1}$$

[1] This work is based on gr-qc/0212113.

[2] E-mail:b1834@sty.cc.yamaguchi-u.ac.jp

[3] E-mail:shiraish@sci.yamaguchi-u.ac.jp

where $h \equiv h^{\mu}_{\mu}$. It can be said that a massless graviton lives in each "theory space", which is labeled by k.

Instead of adding the mere mass term to the lagrangian (1), we put the term including couplings of other gravitons with the nearest-neighbor suffix:

$$\begin{aligned}\bar{\mathcal{L}}_m &= \bar{\mathcal{L}}_0 - \frac{m^2}{2}\sum_{k=1}^{N}\left[(h^k_{\mu\nu} - h^{k+1}_{\mu\nu})^2 - (h^k - h^{k+1})^2\right] \\ &\quad -2\sum_{k=1}^{N}\left[m(A^{k\,\mu} - A^{k-1\,\mu}) + \partial^{\mu}\varphi^k\right](\partial^{\nu}h^k_{\mu\nu} - \partial_{\mu}h^k) - \frac{1}{2}\sum_{k=1}^{N}(\partial_{\mu}A^k_{\nu} - \partial_{\nu}A^k_{\mu})^2 \ , \end{aligned} \tag{2}$$

where a constant m corresponds to the mass of graviton. We have omitted here the gauge fixing term as well as the ghost term. In this notation, one should read as $h^{k+N} = h^k$, $h^0 = h^N$, $h^{N+1} = h^1$, and so on. The multi-graviton lagrangian (2) is invariant under the following transformations:

$$\begin{aligned} h^k_{\mu\nu} &\to h^k_{\mu\nu} + \partial_{\mu}\xi^k_{\nu} + \partial_{\nu}\xi^k_{\mu} \ , \\ A^k_{\mu} &\to A^k_{\mu} + m\xi^k_{\mu} - m\xi^{k+1}_{\mu} - \partial_{\mu}\zeta^k \ , \\ \varphi^k &\to \varphi^k + m\zeta^k - m\zeta^{k-1} \ . \end{aligned} \tag{3}$$

As in the case with 5D QED studied by Hill and Leibovich [11], $N-1$ massive gravitons and one massless graviton are described by the lagrangian. The eigenvalues for the mass matrix are

$$M_p^2 = 4m^2\sin^2\left(\frac{\pi p}{N}\right) \qquad (p = 1, \ldots, N) \ . \tag{4}$$

Massive vector and scalar field are absorbed by the massive graviton fields by means of the transformations (3) and then they have correct spin-degree of freedom, five.

3 VACUUM ENERGY

In this section, we evaluate the one-loop vacuum energy density in the model of the previous section. We will also offer an extension of the model, which includes both latticized and continuous extra dimensions, and the vacuum energy is estimated in the model.

Recently, the scenarios explaining the small positive cosmological constant in the present universe (10^{-47} GeV^4, according to [12]) are discussed through the study of the Casimir-like energy in the higher-dimensional theories [13, 14]. Because the latticized model would have different UV behavior from that of continuum model, we expect a novel expression of the cosmological constant.

First, we consider one scalar degree of freedom which has the mass spectrum discussed in the previous section. Then the vacuum energy density in the one-loop calculation is written by the zeta-function technique [15] as

$$\frac{1}{2}\ln\det[-\nabla^2 + M_p^2] = -\frac{1}{2}\frac{d\zeta(s)}{ds}\bigg|_{s=0} \ , \tag{5}$$

where

$$\zeta(s) = \frac{\mu^{2s}}{16\pi^2\Gamma(s)}\sum_p\int_0^{\infty} dt\, t^{s-3}\exp(-M_p^2 t) \ , \tag{6}$$

with

$$M_p^2 = 4m^2\sin^2\left(\frac{\pi p}{N}\right) \ . \tag{7}$$

Here the constant μ has the dimension of mass.

The calculation of the zeta function can be done by the similar method used in refs. [16, 17]. Therefore the zeta function is written as

$$\zeta(s) = \frac{Nm^4}{\pi^2}\left(\frac{\mu^2}{4m^2}\right)^s\frac{\Gamma(\frac{5}{2}-s)}{\sqrt{\pi}}\left[\frac{1}{(s-1)(s-2)\Gamma(3-s)} + \frac{2}{\Gamma(s)}\sum_{q=1}^{\infty}\frac{\Gamma(qN-2+s)}{\Gamma(qN+3-s)}\right] \ . \tag{8}$$

Now we obtain

$$-\left.\frac{d\zeta(s)}{ds}\right|_{s=0} = -\frac{3Nm^4}{16\pi^2}\ln\left(\frac{\bar{\mu}^2}{4m^2}\right) - \frac{3m^4}{2\pi^2}\sum_{q=1}^{\infty}\frac{1}{q(q^2N^2-1)(q^2N^2-4)}\,, \tag{9}$$

where

$$\ln\left(\frac{\bar{\mu}^2}{4m^2}\right) = \ln\left(\frac{\mu^2}{4m^2}\right) + \psi(3) - \psi(5/2) + \frac{3}{2}\,. \tag{10}$$

Because there are five states in each mass level, the vacuum energy in the multi-graviton model in the previous section is

$$V = V_R - \frac{15Nm^4}{32\pi^2}\ln\left(\frac{\bar{\mu}^2}{4m^2}\right) - \frac{15m^4}{4\pi^2}\sum_{q=1}^{\infty}\frac{1}{q(q^2N^2-1)(q^2N^2-4)}\,, \tag{11}$$

where $V_R(\bar{\mu})$ is the renormalized vacuum energy.

According to ref. [18], We require the invariance of V with respect to the scale $\bar{\mu}$ and we choose $V_R(\bar{\mu}_R) = 0$ for a normalization point $\bar{\mu}_R$. Then we find

$$V = -\frac{15Nm^4}{32\pi^2}\ln\left(\frac{\bar{\mu}_R^2}{4m^2}\right) - \frac{15m^4}{4\pi^2}\sum_{q=1}^{\infty}\frac{1}{q(q^2N^2-1)(q^2N^2-4)}\,. \tag{12}$$

Unfortunately, this vacuum energy density is negative, for $\bar{\mu}_R$ is considered as a cutoff due to a scale of a new physics, $\bar{\mu}_R > m$. The boundary condition $V_R(\bar{\mu}_R) = 0$ can be interpreted as the expectation that the new physics forces the vacuum energy or cosmological constant to vanish at such a high-energy scale.

Let us consider the extension of our model to the one with $4+\delta$ dimensional continuous spacetime. Here the extra δ dimensional space is taken as $(S^1)^\delta$ with a common radius b. One can regard the new model as the theory with a latticized circle and δ continuous circle. In this model the mass spectrum of the gravitons is expressed as

$$M^2_{p,\{\mathbf{n}\}} = 4m^2\sin^2\left(\frac{\pi p}{N}\right) + \frac{\mathbf{n}^2}{b^2}\,, \tag{13}$$

where $\mathbf{n} = (n_1, n_2, \ldots, n_\delta)$ and the components take integer values.

Using the Poisson resummation formula, we can express the zeta function as

$$\begin{aligned}\zeta(s) &= \frac{\mu^{2s}N(2\pi b)^\delta}{(4\pi)^{2+\delta/2}\Gamma(s)}\sum_{\mathbf{n}}\left[\int_0^\infty dt\, t^{s-\delta/2-3}\exp\left(-2m^2t - \pi^2b^2\mathbf{n}^2/t\right) I_0(2m^2t)\right.\\ &\left. +2\sum_{q=1}^{\infty}\int_0^\infty dt\, t^{s-\delta/2-3}\exp\left(-2m^2t - \pi^2b^2\mathbf{n}^2/t\right) I_{qN}(2m^2t)\right]\,.\end{aligned} \tag{14}$$

If δ is odd, all the term in the parentheses are finite and lead to no logarithm term in the vacuum energy. The vacuum energy can be found to be finite and negative in this case, as in the case of the KK theory with torus compactification. Thus we assume that δ is even.

For even δ, in the limit $s \to 0$, only the first term with $\mathbf{n} = \mathbf{0}$ is divergent in the parentheses on the right hand side of (14) if N is larger than $2 + \delta/2$. Thus, after taking account of the degrees of freedom, the vacuum energy density in our extended model takes the form

$$V = V_R - (-1)^{\delta/2}\frac{(5+\delta)(2+\delta)Nm^4}{4\pi^2}(4\pi m^2b^2)^{\delta/2}\frac{\Gamma\left(\frac{5+\delta}{2}\right)}{\sqrt{\pi}\Gamma\left(3+\frac{\delta}{2}\right)^2}\ln\left(\frac{\bar{\mu}^2}{4m^2}\right) - \cdots\,, \tag{15}$$

where

$$\ln\left(\frac{\bar{\mu}^2}{4m^2}\right) = \ln\left(\frac{\mu^2}{4m^2}\right) + 2\psi(3+\delta/2) - \psi(5/2+\delta/2) + \gamma\,, \tag{16}$$

(γ is the Euler's constant) and ... means the positive finite terms.

As seen from the sign of logarithmic term, we can obtain the positive vacuum energy after taking account of the renormalization discussed above; in other words, we have the positive cosmological constant when $\delta = 4k + 2$ ($k = 0, 1, 2, \ldots$), such as $\delta = 2$ ($D = 4 + \delta = 6$), $\delta = 6$ ($D = 10$) , and so on.

We will further investigate the possibility of the arbitrarily small cosmological constant. Since the contribution from the finite q terms in the zeta function can be estimated as at most $O(N^{-4})$, it can be neglected if a large N is assumed. Futher if $mb \ll 1$, we find

$$\begin{aligned} V &\approx \frac{(5+\delta)(2+\delta)Nm^4}{4\pi^2}(4\pi m^2 b^2)^{\delta/2}\frac{\Gamma\left(\frac{5+\delta}{2}\right)}{\sqrt{\pi}\Gamma\left(3+\frac{\delta}{2}\right)}\ln\left(\frac{\bar{\mu}_R^2}{4m^2}\right) \\ &\quad - \frac{(5+\delta)(2+\delta)N}{4\pi^{(4+\delta)/2}(2\pi b)^4}\Gamma\left(\frac{4+\delta}{2}\right)\sum_{\mathbf{n}\neq 0}\frac{1}{(\mathbf{n}^2)^{(4+\delta)/2}} \qquad (mb \ll 1)\ . \end{aligned} \tag{17}$$

Therefore when $(2\pi mb)^{4+\delta}\ln(\bar{\mu}_R/m) \approx O(1)$, an arbitrary small vacuum energy can be obtained. Note that the condition does not include N in this approximation.

The difficulty of the present model in this section is the problem of tunning the scale of the extra dimensions. The model does not provide a mechanism to determine the value of b, because there is no minimum value of V as a function of b. We should consider either the value of b is due to the other mechanism or b takes an appropriate value only in the present universe. For the latter case, the motion of b may play a role of quintessence or dark energy, as similar to the suggestion in ref. [19]. This possibility will be considered elsewhere.

We only considered the vacuum energy at the one-loop level. Even at the same level, the correction to the Newton constant may also be induced in general. This would be related with the restriction or determination of the scale of the extra dimensions as well as the scale of m.

We should investigate the nature of coupling to the matter fields and back reaction problem in the case with a small cosmological constant. Through such studies, the case with strong gravity will also be revealed.

Finally, we remember that we have not treated the hierarchy problem in this paper. It will be clarified by the further study whether incorporating supersymmetry (and its break-down) into the model is necessary or not.

References

[1] B. Hatfield (ed.), *"Feynman Lectures on Gravitation"* (1995, Addison-Wesley, Reading, Mass.).

[2] N. Boulanger, hep-th/0111216.

[3] N. Boulanger, T. Damour, L. Gualtieri and M. Henneaux, *Nucl. Phys.* **B597** (2001) 127.

[4] M. Fierz and W. Pauli, *Proc. Roy. Soc. Lond.* **A173** (1939) 211.

[5] A. Sugamoto, *Prog. Theor. Phys.* **107** (2002) 793; hep-ph/0210235.

[6] M. Bander, *Phys. Rev.* **D64** (2001) 105021.

[7] V. Jejjala, R. G. Leigh and D. Minic, hep-th/0212057.

[8] N. Arkani-Hamed, A. G. Cohen and H. Georgi, *Phys. Rev. Lett.* **86** (2001) 4757; *Phys. Lett.* **B513** (2001) 232.

[9] C. T. Hill, S. Pokorski and J. Wang, *Phys. Rev.* **D64** (2001) 105005.

[10] N. Arkani-Hamed, H. Georgi and M. D. Schwartz, hep-th/0210184.

[11] C. T. Hill and A. K. Leibovich, *Phys. Rev.* **D66** (2002) 016006, hep-ph/0205057.

[12] V. Sahni, *Class. Quant. Grav.* **19** (2002) 3435.

[13] A. Gupta, hep-th/0210069.

[14] K. A. Milton, hep-ph/0210170 and hep-th/0107241; K. A. Milton, R. Kantowski, C. Kao and Y. Wang, *Mod. Phys. Lett.* **A16** (2001) 2281, hep-ph/0105250.

[15] S. W. Hawking, *Commun. Math. Phys.* **55** (1977) 133.

[16] K. Shiraishi, K. Sakamoto and N. Kan, *"Shape of Deconstruction"*, hep-ph/0209126, *J. Phys.* **G** to appear.

[17] N. Kan, K. Sakamoto and K. Shiraishi, *"Deconstructing Scalar QED at Zero and Finite Temperature"*, hep-th/0209096.

[18] I. O. Cherednikov, *Acta Phys. Pol.* **33** (2002) 1973, astro-ph/011287; gr-qc/0205017.

[19] I. K. Wehus and F. Ravndal, hep-ph/0210292.

Black Hole Entropy from Near-Horizon Conformal Symmetry

Gungwon Kang[a,1], Jun-ichirou Koga[b,2]

[a] *School of Physics, Korea Institute for Advanced Study, 207-43 Cheongryangri-dong, Dongdaemun-gu, Seoul 130-012, Korea*

[b] *Advanced Research Institute for Science and Engineering, Waseda University, Shinjuku-ku, Tokyo 169-8555, Japan*

Abstract

We show that, in the vacuum Einstein gravity with cosmological constant in any dimensions higher than two, the near-horizon conformal symmetry produces a nonvanishing central charge in the Virasoro algebra for its corresponding generators. The application of the Cardy's formula reproduces the Bekenstein-Hawking entropy when the periodicity of the base functions is chosen suitably. Some implications of our results are also discussed in the connection to the two-dimensional case studied by Carlip.

1 Introduction

It is a very interesting idea that the black hole entropy could be derived from some symmetry inherited in general relativity classically, without knowing the details of quantum gravity. Brown and Henneaux [1] found that the algebra of diffeomorphisms at spatial infinity for configurations of asymptotically three dimensional anti-de Sitter space (AdS_3) induces a pair of Virasoro algebras with nonvanishing central charge. Based on it, Strominger [2] showed that the application of the Cardy formula for an AdS_3 black hole exactly yields the Bekenstein-Hawking entropy. Carlip proposed a generalization of such idea based on the algebra of surface deformations at a black hole horizon in arbitrary dimensions [3, 4]. Various work in this direction have appeared subsequently. However, none of them is as yet fully satisfactory (see Ref. [5] and refs. therein). It is mainly because the problem of imposing right boundary conditions for the presence of a horizon is not understood well. In addition, the expression for the central term obtained in the Virasoro algebra is not in the desirable form. Namely, it does not include the integration over the time parameter along the horizon. In particular, the prescription for this problem used in Ref. [4] does not work in the two-dimensional case simply because there is no additional angular direction in two spacetime dimensions.

Recently, Carlip [5] suggested several new ingredients that might lead to an improved description of the near-horizon symmetries and possibly overcome those problems mentioned above. He points out that, in the presence of a black hole with a momentarily stationary region near its horizon, the general relativity acquires a new conformal symmetry, which is different from the diffeomorphism symmetry to which corresponding Virasoro algebra has been sought in the approach above. Moreover, a new contribution from the horizon is added to the canonical symplectic form of general relativity so that the central term naturally includes an integration along the horizon. With these new ingredients Carlip considered the two-dimensional dilaton gravity and claimed that the Virasoro algebra for generators corresponding to the infinitesimal near-horizon conformal symmetry acquires a nonvanishing central charge, and that the Cardy formula yields the Bekenstein-Hawking entropy.

It will be of great interest to see if this new approach works in the four-dimensional case. In this letter we apply Carlip's new ingredients to the case of pure gravity with cosmological constant in any spacetime dimensions higher than two dimensions. It turns out that the new approach with slight modifications from Ref. [5] reproduces the Bekenstein-Hawking entropy provided that the period in the base functions is chosen appropriately. Implications of our results are also discussed.

[1] E-mail address: gwkang@kias.re.kr

[2] E-mail address: koga@gravity.phys.waseda.ac.jp

2 Black hole entropy

We consider the pure Einstein gravity with cosmological constant in an arbitrary dimension given by

$$I = \frac{1}{16\pi G}\int d^D x\sqrt{-g}\,(R - 2\Lambda). \tag{1}$$

As shown in Ref. [5], this action is invariant under following conformal transformations near the horizon

$$g_{ab} \to g_{ab} + \nabla_c(f\chi^c)g_{ab}. \tag{2}$$

Here the presence of a stationary black hole is assumed. More generally, we assume that the manifold contains a momentarily stationary horizon. That is, if Δ is a segment of such horizon, the neighborhood $\mathcal{N}$ of it admits a Killing vector field χ^a for which Δ is a Killing horizon. The function f in the above conformal transformations is assumed to be smooth and have non-vanishing support only in $\mathcal{N}$.

Now the variation of the "Hamiltonian" generator associated with such asymptotic symmetry near the horizon is given by

$$\delta L[f] = \hat{\Omega}[\delta, \delta_f] = \int_C \omega[\phi; \delta\phi, \delta_f\phi] + \int_{\tilde{\Delta}} \omega[\phi; \delta\phi, \delta_f\phi]. \tag{3}$$

Here the first term is the usual one integrated over a spacelike Cauchy hypersurface C, and the additional term newly introduced in Ref. [5] is the second one integrated over $\tilde{\Delta}$, the stretched horizon which will be taken to be the horizon at the end of the calculation, i.e., $\tilde{\Delta} \to \Delta$. The symplectic potential $(D-1)$-form is defined as

$$\omega[\phi; \delta_1\phi, \delta_2\phi] = \delta_2\Theta(\phi; \delta_1\phi) - \delta_1\Theta(\phi; \delta_2\phi), \tag{4}$$

where $\Theta_{bcd\cdots} = \epsilon_{abcd\cdots}\Theta^a$ with

$$\Theta^a = \frac{1}{16\pi G}(g_{bc}\nabla^a\delta g^{bc} - \nabla_b\delta g^{ab}) \tag{5}$$

for the theory in Eq. (1). Let l^a be the null normal vector of the stretched horizon $\tilde{\Delta}$. Thus, $l^a l_a = 0$ always and we choose $l^a \to \chi^a$ as $\tilde{\Delta} \to \Delta$. Since the conformal transformations have their support only in a small neighborhood $\mathcal{N}$ of the stretched horizon $\tilde{\Delta}$, the main contribution in Eq. (3) comes from the integral along $\tilde{\Delta}$ as argued in Ref. [5]. For variations $\delta g_{ab} = \nabla_c(fl^c)g_{ab}$, therefore, we have

$$\delta L[f] = \frac{(D-1)(D-2)}{16\pi GD}\int_{\tilde{\Delta}} g^{ab}\delta g_{ab}\, l^c\nabla_c(l^d\nabla_d f + kf)\tilde{\epsilon}, \tag{6}$$

where $\tilde{\epsilon}$ is the induced volume element on $\tilde{\Delta}$ and $k = \nabla_c l^c$.

One can check that the variational form of the Hamiltonian L in Eq. (6) is actually integrable. Namely, when the variation δ is thought of a derivative on the space of metric fields, an explicit calculation shows $\delta_1(\delta_2 L) - \delta_2(\delta_1 L) = 0$. Thus, one does not require any further condition on f in order to have the integrability condition being satisfied. Since the Virasoro algebra will be in the form given by

$$\{L[f_m], L[f_n]\} = \delta_{f_m} L[f_n] = -i(m-n)L[f_{m+n}] - i\frac{c}{12}m(m^2-1)\delta_{m+n,0}, \tag{7}$$

one can use Eq. (6) to extract out the central charge c and the eigenvalue of the L_0 operator. A basis for the functions f is chosen as follows. Let v be a non-affine parameter describing the null trajectory on $\tilde{\Delta}$, e.g., $l^a\nabla_a v = 1$. We choose

$$f_n = \frac{P}{\pi D}z^n, \qquad z = e^{2\pi i v/P}, \tag{8}$$

where the normalization is chosen such that the base function f_n satisfies the standard Diff(S^1) commutation relations:

$$\{f_m, f_n\} = \frac{D}{2}(l^c\nabla_c f_m f_n - l^c\nabla_c f_n f_m) = i(m-n)f_{m+n}. \tag{9}$$

Here the periodicity P in Eq. (8) is assumed to be arbitrary for the moment.

Now Eq. (6) gives

$$\begin{aligned}\delta_{f_m} L[f_n] &= \frac{(D-1)(D-2)}{16\pi G}\int_{\tilde{\Delta}} (l^c\nabla_c f_m + k f_m)\, l^c\nabla_c (l^d\nabla_d f_n + k f_n)\tilde{\epsilon} \qquad (10)\\ &= \frac{(D-1)(D-2)}{4\pi G D^2}\int_{\tilde{\Delta}} \Bigg\{ -n[mn + (\frac{Pk}{2\pi})^2] + i\frac{Pk}{2\pi}n(m+n) \\ &\qquad + (m - i\frac{Pk}{2\pi})\frac{P^2 l^c\nabla_c k}{4\pi^2}\Bigg\} z^{m+n}\frac{dz}{z}d\Sigma. \qquad (11)\end{aligned}$$

Here $d\Sigma$ is the infinitesimal volume element of the spatial cross section of the stretched horizon $\tilde{\Delta}$, and $dv = Pdz/2\pi iz$. The integrand above is not constant in general. As the stretched horizon approaches the horizon (i.e., $\tilde{\Delta} \to \Delta$), however, one can see that the quantity $k = \nabla^c l_c$ becomes the surface gravity κ. Let the null vector n^a be $n^c l_c = -1$. Then

$$\begin{aligned} k &= (h^{ab} - l^a n^b - l^b n^a)\nabla_a l_b \qquad (12)\\ &= \theta - n^b l^c \nabla_c l_b \qquad (13)\\ &\to \kappa. \end{aligned}$$

Here we used that $l^b n^a \nabla_a l_b = n^a \nabla_a (l^b l_b)/2 = 0$, that the expansion of the congruence of null geodesics $\theta = h^{ab}\nabla_a l_b$ vanishes at the horizon, and that $l^a \to \chi^a$ as $\tilde{\Delta} \to \Delta$. The surface gravity of a stationary event horizon may be defined as $\chi^c\nabla_c\chi_b = \kappa\chi_b$, which is constant along the horizon. One can also check that $l^c\nabla_c k \to 0$ as $\tilde{\Delta} \to \Delta$. Thus, the integrand becomes constant as the stretched horizon approaches the event horizon. Finally, we have at the horizon

$$\delta_{f_m} L[f_n] = \frac{2(D-1)(D-2)}{D^2}\frac{A}{4G}\Bigg\{ -i(m-n)\frac{1}{2}\left[1 + (\frac{P\kappa}{2\pi})^2\right]\delta_{m+n,0} - im(m^2-1)\delta_{m+n,0}\Bigg\}, \tag{14}$$

where $A = \oint d\Sigma$ is the surface area of the $(D-2)$-dimensional horizon cross section.

By comparing it with Eq. (7), therefore, we obtain the nonvanishing central charge given by

$$\frac{c}{12} = \frac{2(D-1)(D-2)}{D^2}\frac{A}{4G}, \tag{15}$$

and the eigenvalue of the L_0 operator given by

$$\Delta = \frac{1}{2}\left[1 + (\frac{P\kappa}{2\pi})^2\right]\frac{2(D-1)(D-2)}{D^2}\frac{A}{4G} = \frac{1}{2}\left[1 + (\frac{P\kappa}{2\pi})^2\right]\frac{c}{12}. \tag{16}$$

By applying the Cardy formula for the density of states

$$\rho(\Delta) \sim \exp\left[2\pi\sqrt{(\frac{c}{12} - 2\Delta_0)(2\Delta - \frac{c}{12})}\right] \tag{17}$$

with $\Delta_0 = 0$, the entropy becomes

$$S = \ln \rho = \frac{2(D-1)(D-2)P\kappa}{D^2} \frac{A}{4G}. \tag{18}$$

This exactly yields the Bekenstein-Hawking entropy if the periodicity is chosen to be

$$P = \frac{D^2}{2(D-1)(D-2)} \kappa^{-1}. \tag{19}$$

3 Discussion

To conclude, for the pure Einstein gravity with cosmological constant in any spacetime dimensions higher than two dimensions we have shown that a subset of the near-horizon conformal symmetries in the form of Eq. (2) could yield a Virasoro algebra with nonvanishing central charge. It also shows that Cardy formula with the suitable choice of periodicity P in the base functions as in Eq. (19) exactly reproduces the Bekenstein-Hawking entropy. Although our result is essentially the simple extension of Carlip's idea for the two dimensional case in Ref. [5], we would like to point out some interesting aspects of our results.

First of all, our choice of the base functions f_n in Eq. (8) is different from that in Carlip's. One can easily see that Carlip's choice of the base functions is singular as the event horizon is being approached. Consequently, this results in the divergence of the conformal transformations at the horizon. It is not easy to understand why such singular fluctuations in the horizon area are responsible for the black hole entropy. On the other hand, the base functions we chose are regular and oscillatory even at the event horizon.

Secondly, although the Virasoro algebra associated with the near horizon conformal symmetry in Carlip's [5] yields the nonvanishing central charge, the correct application of the Cardy formula actually gives vanishing entropy [6]. However, it turns out that our choice of the base functions produce nonvanishing entropy for the dilaton gravity Carlip considered in two dimensions.

Finally, notice that the central charge Eq. (15) and the entropy Eq. (17) obtained in our method depend on the spacetime dimensionality explicitly. The entropy vanishes when the spacetime dimension is two. Although the suitable choice of the periodicity as in Eq. (19) gives the correct Bekenstein-Hawking entropy, we do not have a physical explanation for why such specific dimension dependent value should be chosen for the periodicity. Further work is required for this question. Other details and interesting aspects of our current work will appear soon in Ref. [6].

Acknowledgments

GK would like to thank Makoto Natsuume and Mu-In Park for useful discussions. This work was in part supported by JSPS (Japanese Society for Promotion of Sciences).

References

[1] J. D. Brown and M. Henneaux, Commun. Math. Phys. **104**, 207 (1986).

[2] A. Strominger, JHEP **9802**, 009 (1998) [arXiv:hep-th/9712251].

[3] S. Carlip, Phys. Rev. Lett. **82**, 2828 (1999) [arXiv:hep-th/9812013].

[4] S. Carlip, Class. Quant. Grav. **16**, 3327 (1999) [arXiv:gr-qc/9906126].

[5] S. Carlip, Phys. Rev. Lett. **88**, 241301 (2002) [arXiv:gr-qc/0203001].

[6] G. Kang, J. Koga, and M. Park;"Black Hole Entropy from Near Horizon Conformal Symmetry in Any Dimension," in preparation.

Born-Again Braneworld

Sugumi Kanno,[1] Misao Sasaki,[2] and Jiro Soda[3]

[1] *Graduate School of Human and Environmental Studies, Kyoto University, Kyoto 606-8501, Japan*
[2] *Department of Earth and Space Science, Graduate School of Science, Osaka University, Toyonaka 560-0043, Japan*
[3] *Department of Fundamental Sciences, FIHS, Kyoto University, Kyoto 606-8501, Japan*

Abstract

We propose a cosmological braneworld scenario in which two branes collide and emerge as reborn branes with signs of tensions opposite to the original tensions of respective branes. In this scenario, the branes are assumed to be inflating. However, the whole dynamics is different from the usual inflation due to the non-trivial dynamics of the radion field. Transforming the conformal frame to the Einstein frame, this born-again scenario resembles the pre-big-bang scenario. Thus our scenario has features of both inflation and pre-big-bang scenarios. In particular, the gravitational waves produced from vacuum fluctuations will have a very blue spectrum, while the inflaton field will give rise to a standard scale-invariant spectrum.

1 Introduction

The inflationary universe scenario is a natural solution to fundamental problems of the big-bang model such as horizon problem. However, it is not a unique choice. A universe with an era of contraction is also a possibility. The pre-big-bang scenario is a realization of such a case in the superstring context[1]. Unfortunately, however, the pre-big-bang scenario suffers from a singularity problem which cannot be solved without understanding the stringy non-perturbative effects.

One of the remarkable features of superstring theory is the existence of extra dimensions. Conventionally, the extra dimensions are considered to be compactified to a small compact space of the Planck scale. However, recent revolutionary progress in string theory has lead to the brane-world picture [2]. In this talk, we consider a system of two branes having tensions of opposite signs, with the intermediate spacetime (bulk) described by an anti-de Sitter space (AdS_5) [3]. One of the branes is assumed to be our universe, and there exists an inflaton field which leads to inflation. The other brane is assumed to be vacuum but with a non-zero cosmological constant.

Assuming slow roll of the inflaton field, we may regard both branes as vacuum (de Sitter) branes. So far, mostly the static de-Sitter two-brane system is considered in the cosmological context. However, it is now well-known that a static de-Sitter two-brane system is unstable. We therefore investigate the non-trivial radion dynamics and dwell on its cosmological consequences [4].

2 Radion Dynamics

Most inflationary models are based on slow-roll inflation which have a sufficiently flat potential. In this section, we consider dynamics of branes with vacuum energy as a first order approximation of a slow-roll inflation model. Qualitative features of the brane cosmology can be understood by this simplified vacuum brane model.

We take the matter Lagrangeans to be $\mathcal{L}^{\oplus} = -\delta\sigma^{\oplus}$ and $\mathcal{L}^{\ominus} = -\delta\sigma^{\ominus}$. The effective action on the positive ($\oplus$) tension brane for this setup reads [5] (see also [6, 7, 8])

$$S_{\oplus} = \frac{\ell}{2\kappa^2}\int d^4x\sqrt{-h}\left[\Psi R - \frac{3}{2(1-\Psi)}\Psi^{|\alpha}\Psi_{|\alpha}\right] - \delta\sigma^{\oplus}\int d^4x\sqrt{-h} - \delta\sigma^{\ominus}\int d^4x\sqrt{-h}\,(1-\Psi)^2\,. \qquad (1)$$

[1] E-mail:kanno@phys.h.kyoto-u.ac.jp
[2] E-mail:misao@vega.ess.sci.osaka-u.ac.jp
[3] E-mail:jiro@phys.h.kyoto-u.ac.jp

Since our theory is a scalar-tensor type theory, we call this original action the Jordan-frame effective action. In order to discuss the dynamics of radion, it is convenient to move to the Einstein frame in which the action takes the canonical Einstein-scalar form. Applying a conformal transformation $h_{\mu\nu} = \frac{1}{\Psi} g_{\mu\nu}$ and introducing a new field $\eta = -\log\left|\frac{\sqrt{1-\Psi}-1}{\sqrt{1-\Psi}+1}\right|$, we obtain the Einstein-frame effective action

$$S_{\oplus} = \frac{\ell}{2\kappa^2}\int d^4x\sqrt{-g}\left[R(g) - \frac{3}{2}\nabla^\alpha\eta\nabla_\alpha\eta\right] - \int d^4x\sqrt{-g}\,V(\eta)\,, \tag{2}$$

where ∇ denotes the covariant derivative with respect to the metric $g_{\mu\nu}$ and the radion potential now takes the form,

$$V(\eta) = \delta\sigma^{\oplus}\left[\cosh^4\frac{\eta}{2} + \beta\sinh^4\frac{\eta}{2}\right], \quad \beta = \frac{\delta\sigma^{\ominus}}{\delta\sigma^{\oplus}}\,. \tag{3}$$

We can also start from the effective action on the negative ($\ominus$) tension brane to obtain the same Einstein-frame effective action. By a conformal transformation $f_{\mu\nu} = \frac{1}{\Phi} g_{\mu\nu}$ and introducing a new field $\eta = -\log\left|\frac{\sqrt{\Phi+1}-1}{\sqrt{\Phi+1}+1}\right|$, we also arrive at Eq. (2).

We note that the two branes are infinitely separated when $\eta = 0$ ($\Psi = 1$) and they collide when $\eta = \infty$ ($\Psi = 0$). For definiteness, let us assume $\delta\sigma^{\oplus} > 0$. If $\delta\sigma^{\oplus} + \delta\sigma^{\ominus} > 0$, Ψ will move towards unity, i.e., the branes will move away from each other. While, if $\delta\sigma^{\oplus} + \delta\sigma^{\ominus} < 0$, the potential has a maximum at $\Psi_c = 1 + 1/\beta$, and the behavior depends on whether $\Psi > \Psi_c$ or $\Psi < \Psi_c$. If $\Psi > \Psi_c$, the branes will become infinitely separated. If $\Psi < \Psi_c$, the branes will approach to each other and eventually collide. From the 5-dimensional point of view, this is surely a singularity where the spacetime degenerates to 4-dimensions. However, as far as observers on the branes are concerned, nothing seems to go wrong. In fact, the action (1) is well-defined even in the limit $\Psi \to 0$. Let us assume that Ψ smoothly become negative after collision. Then replacing Ψ as $\Psi \to -\tilde{\Psi}$ in the action (1), we find

$$\begin{aligned} -S_{\oplus} &= \frac{\ell}{2\kappa^2}\int d^4x\sqrt{-h}\left[\tilde{\Psi}R(h) + \frac{3}{2}\frac{1}{1+\tilde{\Psi}}\tilde{\Psi}^{|\alpha}\tilde{\Psi}_{|\alpha}\right] + \int d^4x\sqrt{-h}(-\mathcal{L}^{\oplus}) \\ &\quad + \int d^4x\sqrt{-h}\left(1+\tilde{\Psi}\right)^2(-\mathcal{L}^{\ominus})\,. \end{aligned} \tag{4}$$

This is the same as the effective action on the negative tension brane

$$\begin{aligned} S_{\ominus} &= \frac{\ell}{2\kappa^2}\int d^4x\sqrt{-f}\left[\Phi R(f) + \frac{3}{2(1+\Phi)}\Phi^{;\alpha}\Phi_{;\alpha}\right] \\ &\quad + \int d^4x\sqrt{-f}\mathcal{L}^{\ominus} + \int d^4x\sqrt{-f}\mathcal{L}^{\oplus}(1+\Phi)^2\,. \end{aligned} \tag{5}$$

except for the overall change of sign and the associated change of signs in front of the matter Lagrangeans. One can interpret this fact as follows. After collision, the positive tension brane turns into a negative tension brane together with the sign change of the matter Lagrangean, and vice versa for the initially negative tension brane. This implies that, if we live on either of the branes, our world transmutes into quite a different world and so does ourselves without much damage to the world. That is, we are born again!

3 Born-Again Braneworld

If our world had been initially a positive tension brane, we would be now on the negative tension brane. However, this case contradicts with observation. Therefore we take the position that we were initially on the negative tension brane before the collision.

Let us first investigate the cosmological evolution of the negative tension brane in the original Jordan frame. We consider the spatially isotropic and homogeneous metric on the brane,

$$ds^2 = -dt^2 + a^2(t)\gamma_{ij}dx^i dx^j\,, \tag{6}$$

where $a(t)$ is the scale factor and γ_{ij} is the metric of a maximally symmetric 3-space with comoving curvature $K = 0, \pm 1$. The field equations on the negative tension brane give

$$\dot{H} - \frac{K}{a^2} = -2\left(H^2 + \frac{K}{a^2}\right) - \frac{2\kappa^2}{3\ell}\delta\sigma^{\odot} . \tag{7}$$

Integrating this equation, we obtain the Friedmann equation with a dark radiation,

$$H^2 + \frac{K}{a^2} = -\frac{\kappa^2}{3\ell}\delta\sigma^{\odot} + \frac{C}{a^4} . \tag{8}$$

We also find the relation between the radion and the dark radiation,

$$\frac{\kappa^2\delta\sigma^{\odot}}{3\ell}\frac{1+\Phi}{\Phi}\left[1 + \frac{(1+\Phi)}{\beta}\right] - H\frac{\dot{\Phi}}{\Phi} - \frac{1}{4}\frac{1}{1+\Phi}\frac{\dot{\Phi}^2}{\Phi} = \frac{C}{a^4} . \tag{9}$$

This gives, in particular, the relation between the initial conditions of the radion and the sign of the dark radiation.

To realize the born-again braneworld scenario, we consider a case of colliding branes. For simplicity, we assume $K = 0$. We can see numerically that Φ passes through zero smoothly and approaches -1, i.e., the reborn branes will be eventually infinitely separated.

Let us analyze this collision. We denote the Hubble constant at the time of collision $t = t_c$ by H_c. Applying Eq. (9) to the vicinity of the time of collision, we find

$$\Phi = -2(1 - \sqrt{\gamma})H_c(t - t_c); \quad \gamma = 1 - \frac{H_*^2}{H_c^2}\left(1 + \frac{1}{\beta}\right) , \tag{10}$$

where $H_*^2 = (\kappa^2/3\ell)(-\delta\sigma^{\odot})$. As expected, Φ behaves perfectly smoothly around the time of collision. The brane geometry is, of course, perfectly regular as well. In fact, the Friedmann equation (8) continues to hold without a hint of collision.

Now we transform these quantities into the Einstein frame. Since $\Phi \to -1$ eventually, we may regard our present universe to be described by the Einstein frame. The relation between the Einstein frame and the Jordan frame is

$$\begin{aligned} ds_E^2 &= -dt_E^2 + b^2(t_E)\delta_{ij}dx^i dx^j \\ &= |\Phi|\left[-dt_J^2 + a(t_J)^2\delta_{ij}dx^i dx^j\right] , \end{aligned} \tag{11}$$

where we attached the subscripts E and J to the time coordinates to denote the cosmic time in the Einstein frame and the Jordan frame, respectively. Thus we have $b = \sqrt{|\Phi|}\,a$, $dt_E = \sqrt{|\Phi|}\,dt_J$. Therefore, the Hubble parameter in the Einstein frame behaves in the vicinity of collision as

$$\frac{\dot{b}(t_E)}{b(t_E)} = \frac{1}{3t_E} + \frac{H_c}{\left(3(1-\sqrt{\gamma})H_c|t_E|\right)^{1/3}} , \tag{12}$$

where the collision time in the Einstein frame is set to be $t_E = 0$.

We note that in the Einstein frame, the universe is contracting rapidly just before the collision and the Hubble parameter diverges to minus infinitely at collision. Then the universe is reborn with an infinitely large Hubble parameter, which looks like a big-bang singularity. Thus, since there exists no singularity in the Jordan frame, the pre-big-bang phase and the post-big-bang phase in the Einstein frame is successfully connected. That is, our scenario is indeed a successful realization of the pre-big-bang scenario in the context of the braneworld.

4 Observational Implication

As we can see from Eq. (8), the universe will rapidly converge to the quasi-de-Sitter regime, while the radion can vary as far as the relation (9) is satisfied. In the Jordan frame, as the metric couples with the radion, the non-trivial evolution of the radion field affects the perturbations. This possibility discriminate our model from the usual inflationary scenario. On the other hand, the inflaton does not couple directly with the radion field. Hence, the inflaton fluctuations are expected to give adiabatic fluctuations with a flat spectrum. This feature is an advantage compared with the pre-big-bang model.

4.1 Radion fluctuation

To study the behavior of the radion fluctuations, it is convenient to work in the Einstein frame. The action for the curvature perturbation $\mathcal{R}$ on the $\delta\eta = 0$ (i.e., radion-comoving) slice reads

$$S = \frac{1}{2}\int d\eta\, d^3x\, z^2 \left[\mathcal{R}_c'^2 - \mathcal{R}_c^{|i}\mathcal{R}_{c|i}\right], \tag{13}$$

where $\mathcal{H} = b'/b$ and

$$\mathcal{R}_c = \mathcal{R} - \mathcal{H}\frac{\delta\eta}{\eta'}, \quad z = \sqrt{\frac{3\ell}{2\kappa^2}}\frac{b\eta'}{\mathcal{H}}. \tag{14}$$

As the background behaves as $b \sim (-\tau)^{1/2}$, $\mathcal{H} \sim (2\tau)^{-1}$ and $\eta' \sim (-\tau)^{-1}$, we have $z \propto b$, and the positive frequency modes for the adiabatic vacuum is given by

$$\mathcal{R}_{c,k} \sim \sqrt{\frac{\pi\kappa^2}{6H_*\ell}}\, H_0^{(1)}(-k\tau), \tag{15}$$

where we have normalized b as $b = |H_*\tau|^{1/2}$. Then we have

$$\langle\mathcal{R}_c^2\rangle_k \equiv \frac{k^3}{2\pi^2}P(k) = \frac{k^3}{2\pi^2}|\mathcal{R}_{c,k}|^2 \sim \frac{k^3}{H_* M_{pl}^2}, \tag{16}$$

where $M_{pl}^2 = \kappa^2/\ell$. Thus the spectrum is very blue. If we define the spectral index by $P(k) \propto k^{n-4}$, this implies $n = 4$.

4.2 Gravitational waves

Next, consider the tensor perturbations:

$$ds^2 = b^2(\tau)\left[-d\tau^2 + (\delta_{ij} + h_{ij})dx^i dx^j\right] \tag{17}$$

where h_{ij} satisfy the transverse-traceless conditions, $h_{ij}{}^{,j} = h^i{}_i = 0$. As for the gravitational tensor perturbations, we have

$$h_k'' + 2\mathcal{H}h_k' + k^2 h_k = 0, \tag{18}$$

where h_k is the amplitude of h_{ij}. Since $\mathcal{H} \sim (2\tau)^{-1}$, h_k has approximately the same spectrum as that for $\mathcal{R}_c$, including the magnitude. In particular, the spectral index for the gravitational waves is also $n = 4$ (with the spectral index defined by $P_h(k) \propto k^{n-4}$ as in the case of scalar curvature perturbation; for the tensor perturbation, the conventional definition is $n_T = n - 1$). Provided that inflation ends right after collision, this gives a sufficiently blue spectrum that can amplify Ω_g by several order of magnitudes or more on small scales as compared to conventional inflation models. Thus, there arises a possibility that it may be detected by a space laser interferometer for low frequency gravitational waves such as LISA [9].

4.3 Inflaton perturbation

To investigate the inflaton perturbation rigorously, one needs to introduce an inflaton field explicitly and consider a system of equations fully coupled with the radion and the metric perturbation. The estimation shows that the effect of the metric perturbation induced by radion fluctuations on the inflaton perturbation is small. Hence, the inflaton fluctuations will have a standard scale-invariant spectrum.

5 Conclusion

In this paper, we proposed a scenario in which two branes collide and are reborn as new branes, called the born-again braneworld scenario. Our model has the features of both inflationary and pre-big-bang

scenarios. In the original frame, which we call the Jordan frame since gravity on the brane is described by a scalar-tensor type theory, the brane universe is assumed to be inflating due to an inflaton potential. While, the radion, which represents the distance between the branes and which acts as a gravitational scalar on the branes, has non-trivial dynamics and theses vacuum branes can collide and pass through smoothly. After collision, it is found that the positive tension and the negative tension branes exchange their role. Then, they move away from each other, and the radion becomes trivial after a sufficient lapse of time. The gravity on the originally negative tension brane (whose tension becomes positive after collision) will then approach the conventional Einstein theory except for tiny Kaluza-Klein corrections.

One can also consider the cosmological evolution of the branes in the Einstein frame. Note that the two frames are indistinguishable at present if our universe is on the positive tension brane after collision. In the Einstein frame, the brane universe is contracting before the collision and one encounters a singularity at the collision point. This resembles the pre-big-bang scenario. Thus our scenario may be regarded as a non-singular realization of the pre-big-bang scenario in the braneworld context.

As our braneworld is inflating and the inflaton has essentially no coupling with the radion field, the adiabatic density perturbation with a flat spectrum is naturally realized. While, as the collision of branes mimics the pre-big-bang scenario, the primordial background gravitational waves with a very blue spectrum may be produced. This brings up the possibility that we may be able to see the collision epoch by a future gravitational wave detector such as LISA.

References

[1] M. Gasperini and G. Veneziano, Astropart. Phys. **1**, 317 (1993) [arXiv:hep-th/9211021].

[2] I. Antoniadis, N. Arkani-Hamed, S. Dimopoulos and G. R. Dvali, Phys. Lett. B **436**, 257 (1998) [arXiv:hep-ph/9804398];
P. Horava and E. Witten, Nucl. Phys. B **460**, 506 (1996) [arXiv:hep-th/9510209];
P. Horava and E. Witten, Nucl. Phys. B **475**, 94 (1996) [arXiv:hep-th/9603142].

[3] L. Randall and R. Sundrum, Phys. Rev. Lett. **83**, 3370 (1999) [arXiv:hep-ph/9905221].

[4] S. Kanno, M. Sasaki and J. Soda, "Born-again braneworld," to appear in Prog. Teor. Phys., arXiv:hep-th/0210250.

[5] S. Kanno and J. Soda, Phys. Rev. D **66**, 083506 (2002) [arXiv:hep-th/0207029].

[6] T. Wiseman, Class. Quant. Grav. **19**, 3083 (2002) [arXiv:hep-th/0201127].

[7] S. Kanno and J. Soda, Phys. Rev. D **66**, 043526 (2002) [arXiv:hep-th/0205188].

[8] S. Kanno and J. Soda, "Braneworld effective action at low energies," arXiv:gr-qc/0209087;
J. Soda and S. Kanno, "Holographic view of cosmological perturbations," arXiv:gr-qc/0209086;
T. Shiromizu and K. Koyama, "Low energy effective theory for two brane systems: Covariant curvature formulation," arXiv:hep-th/0210066.

[9] P. Bender et. al, LISA. Pre-Phase A Report, second edition, July 1998. A choice of reference texts on the LISA project can be found at http://www.lisa.uni-hannover.de/lisapub.html.

Dynamical Instability in Rapidly and Differentially Rotating Polytrope

Shigeyuki Karino,[1] Yoshiharu Eriguchi[2]

Department of Earth Science and Astronomy, Graduate School of Arts and Sciences, University of Tokyo, Komaba, Meguro, Tokyo 153-8902, Japan

Abstract

We have studied the f-mode oscillations of differentially rotating polytropes by using linear stability analysis method. We found that the critical rotation rates where the dynamical instability against the $m = 2$ f-mode oscillations sets in decrease significantly as the degree of differential rotation becomes higher. Here m is an azimuthal quantum number and T and W are the rotational energy and the gravitational potential energy, respectively. This tendency is almost independent from the polytropic index.

1 Introduction

It is well known that rapidly rotating stars suffer from dynamical instability against nonaxisymmetric oscillations. In particular, the growth rate for the $m = 2$ or bar-type f-mode instability has been considered to be largest. Classically, it is known that uniformly rotating incompressible fluids become dynamically unstable when the ratio of the rotational energy, T, to the absolute value of the gravitational potential energy, W, exceeds 0.27, i.e. $\beta \equiv T/|W| \geq 0.27$.

In this three decades, a lot of works about dynamical instability of bar-mode have been done [1] [2] [3] [4]. Their main result about the $m = 2$ dynamical instabilities of compressible stars was that rapidly rotating configurations become unstable also when the condition $\beta \geq 0.27$ is satisfied irrespective of the compressibilities and the rotation laws as far as they investigated.

However, the situation has been changing because there appear many recent results of hydrodynamical simulations which show that configurations with lower values of β suffer from dynamical instabilities (see e.g. [5] [6] [7] [8]). Some of them shows the dynamical instability even if $\beta < 0.20$. These results seem to imply that the critical value of β for the occurrence of the $m = 2$ bar-type dynamical instability cannot be considered to be universal any more. In order to see the unstable nature of rotating stars, we need to investigate sequences of rotating configurations systematically. For that purpose, the best method would be the linear stability analysis rather than hydrodynamical simulations. Thus, in this paper, we will study systematically the dynamical stability of rapidly and differentially rotating polytropic stars by using the linear stability analysis. It should be noted that the linear stability analysis of differentially rotating polytropes in this paper will give exact values of $\beta_{\rm critical}$ for the onset of $m = 2$ f-mode dynamical instabilities for the first time.

2 Numerical Method

The method to investigate stability by solving linearized basic equations is the same as that used in Karino et al.[9] [10]. Therefore, we will summarize the essence of the method briefly.

2.1 Equilibrium states

Axisymmetric equilibrium configurations of rotating Newtonian stars are obtained by solving the following equations in the spherical polar coordinates (r, θ, φ):

$$\frac{1}{\rho}\nabla p = -\nabla\phi + r\sin\theta\Omega^2\vec{e}_R \ , \tag{1}$$

[1] E-mail:karino@provence.c.u-tokyo.ac.jp
[2] E-mail:eriguchi@valis.c.u-tokyo.ac.jp

$$\triangle \varphi = 4\pi G \rho \ . \tag{2}$$

where p, ρ, φ, Ω, $\vec{e}_R$, and G are the pressure, the density, the gravitational potential, the angular velocity, a unit vector in the R direction of the cylindrical coordinates (R, φ, z), and the gravitational constant, respectively. As for the equation of state, we assume the polytropic relation, $p = K\rho^{1+\frac{1}{N}}$, where K and N are the polytropic constant and the polytropic index, respectively. The rotation law is assumed as follows:

$$\Omega = \frac{\Omega_c A^2}{(r\sin\theta)^2 + A^2} \ , \tag{3}$$

where Ω_c is the central angular velocity. The quantity A is a parameter which represents the degree of differential rotation. The rotation becomes more differential as A becomes smaller. We call this rotation law as the j-constant rotation law.

One equilibrium state can be characterized by specifying three parameters as follows: the polytropic index N, the parameter A and the parameter describing the amount of rotation which can be represented by the axis ratio, $q \equiv r_p/r_e$, where r_p and r_e are the polar and equatorial radii, respectively. These equations are solved by applying the proper boundary conditions and using the SFNR method of Eriguchi and Müller [11].

2.2 Perturbed States

As mentioned before, the linearized equations are solved by the scheme developed by Karino et al.[9] [10]. The perturbed quantities are expanded as follows:

$$\delta f(r, \theta, \varphi, t) = \sum_m \exp(i(\sigma t - m\varphi)) f_m(r, \theta), \tag{4}$$

where δf means the Euler perturbation of the corresponding quantity. Here, m is the azimuthal quantum number and σ is the eigenfrequency of the oscillation mode. As for the density and the pressure perturbations, we assume the adiabatic changes. Since we want to study the bar-type oscillations, we will consider only the oscillation modes with $m = 2$ in this paper.

3 Numerical Results

By fixing the values of A and N and by changing the value of q, we can obtain eigenvalues of $m = 2$ f-mode oscillations along an equilibrium sequence. After that by changing the values of A and/or N and following the same procedure, we can obtain eigenstates for many equilibrium sequences. In this paper, we have examined sequences with $N = 1.0$ and 1.5, and mainly $1.0 \leq A^{-1}$. It may be noted that for models with large values of A, mass shedding will start before the dynamical instability sets in. Hence it is not necessary to consider lager values of A.

In Figure 1, the real part (left panel) and the positive imaginary part (right panel) of eigenfrequencies of the $N = 1.0$ sequences with $A = 1.0$ is plotted against the value of β. In this plane, the bar-mode has two branches for lower values of β while these two real branches merge into two complex conjugate branches for higher values of β. For this sequence, i.e. $N = 1.0$ and $A = 1.0$ sequence, the critical value where the dynamical instability for $m = 2$ f-mode sets in is $\beta \simeq 0.266$.

The dependency of the critical points of dynamical instability on the degree of differential rotation and the compressibility can clearly seen from Figure 2. In this figure, the values of β at the critical points for $N = 0.0, 1.0$ and 1.5 polytropes are plotted against the parameter A^{-1}. The critical values of β for the $m = 2$ f-mode dynamical instability depend significantly on the values of A but depend only slightly on the values of N for the high degree of differntial rotation. Note that, as it should be, the critical value of $\beta_{\rm critical}$ approaches to $\beta_{\rm critical} = 0.27$ when the rotation law tends to the rigid rotation ($A^{-1} \to 0$) and the unperturbed configuration becomes the Maclaurin spheriod.

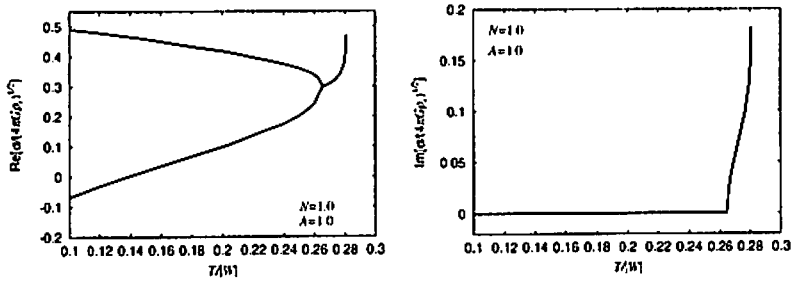


Figure 1: In the left panel, the real part of the eigenvalue of the bar-mode is plotted against the ratio $T/|W|$ for polytropes with $N = 1.0$ and $A = 1.0$. Here ρ_c denotes the central density. In slowly rotating regions, the f-mode has two real branches, but when the stellar rotation exceeds a certain critical point, these two branches merge into one branch. At the same point of $T/|W|$, the absolute value of imaginary part of the eigenvalue plotted in right panel appears and grows rapidly. This corresponds to the critical point where the $m = 2$ f-mode dynamical instability sets in.

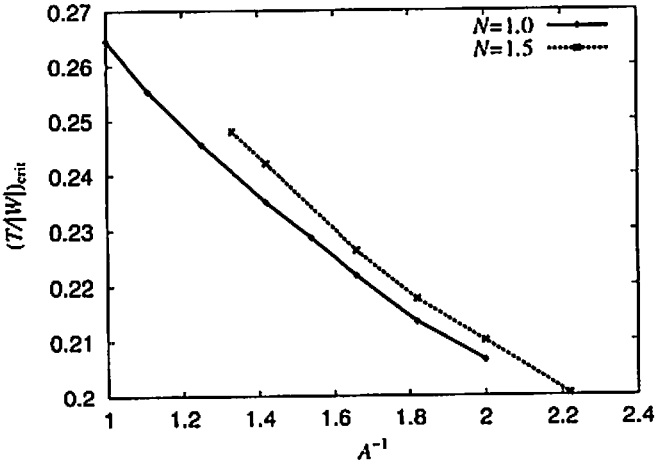


Figure 2: Values of $T/|W|$ at the critical points where the $m = 2$ f-mode dynamical instability sets in are plotted against the degree of differential rotation, A^{-1}. The stellar models are polytropes with $N = 1.0$ and 1.5. As the degree of differential rotation becomes higher, the critical value of $T/|W|$ tends to decrease.

4 Discussions and Concluding Remarks

By making use of the linear stability analysis, we have shown that, for $m = 2$ f-mode oscillations, higher degree of differential rotation makes the stars more unstable than the previous knowledges. Although results of recent dynamical simulations have shown the same tendency, it should be noted that our present results have been obtained by the systematic analysis of the oscillations and that we can understand the occurrence of this type of instability from the higher standpoint.

Since the parameter regions for the existence of dynamically unstable configurations are widened, we need to reconsider some astrophysical situations under the light of the present results. There are several situations where highly differential rotation would be realized. One example can be outcomes of collapsing stars, i.e. core collapse stages of massive stars or accretion induced collapse processes of stars. Other example may be outcomes of collision or merging of two stars, i.e. merging of two neutron stars in a binary neutron star system. A typical example is related to newly born neutron stars. There are several ways for neutron stars to be formed. One is the formation via core collapse of massive stars followed by Type II supernovae. In recent simulations, it is shown that the compact object formed from an iron core collapse is rotating rapidly and differentially with $\beta \sim 0.2$ [12] [13]. Another is a merging of two neutron stars in a binary neutron star system. In the merging process in a binary neutron star system, there appears a rapidly rotating massive neutron star with high degree of differential rotation (see e.g. [14]). Neutron stars are also considered to be formed by accretion onto massive white dwarfs. In this accretion induced scenario, the outcome would be a rapidly and differentially rotating massive neutron star (see e.g. [8]). Therefore, for these differentially rotating neutron stars, it would be very likely that the dynamical instability would set in easily and lead the systems to nonaxisymmetric configurations just depending on the degree of differential rotation and irrespective of the compressibility. Those deformed and rapidly rotating compact objects would emit a large amount of gravitational waves. Hence, such young neutron stars could be important targets of ground-based laser interferometric detectors of gravitational waves (see e.g. [15]).

This study is partially supported by the Research Fellowship of the Japan Society for the Promotion of Science for Young Scientists and by the Grant-in-Aid for Scientific Research (C) of the JSPS (14540244).

References

[1] S. Chandrasekhar, *Ellipsoidal Figures of Equilibrium* (Yale University Press, New Haven, 1969).

[2] J. L. Tassoul and J. P. Ostriker, ApJ, **154**, 613 (1968).

[3] J. P. Ostriker and J. L. Tassoul, ApJ, **155**, 987 (1969).

[4] J. P. Ostriker and P. Bodenheimer, ApJ, **180**, 171 (1973).

[5] J. E. Tohline and I. Hachisu, ApJ, **361**, 394 (1990).

[6] B. Pickett, R. Durisen, and G. Davis, ApJ, **458**, 714 (1996).

[7] J. Centrella, K. New, L. Lowe, and D. Brown, ApJ, **550**, L193 (2001).

[8] Y. T. Liu and L. Lindblom, MNRAS, **324**, 1063 (2000).

[9] S. Karino, S'i. Yoshida, S'j. Yoshida, and Y. Eriguchi, Phys. Rev. D,**62**, 084012 (2000).

[10] S. Karino, S'i. Yoshida, and Y. Eriguchi, Phys. Rev. D,**64**, 024003 (2001).

[11] Y. Eriguchi and E. Müller, A&A, **146**, 260 (1985).

[12] T. Zwerger and E. Müller, A&A, **320**, 209 (1997).

[13] H. Dimmelmeier, J. A. Font, and E. Müller, A&A, **393**, 523 (2002).

[14] M. Shibata, and K. Uryu, Phys. Rev. D,**61**, 064001 (2000).

[15] M. Shibata, S. Karino, and Y. Eriguchi, MNRAS, **334**, L27 (2002).

Exact Solutions and Stability of General Wormholes

Sung-Won Kim[1]

Department of Science Education, Ewha Womans University, Seoul 120-750, Korea

Abstract

We examined the general solution of Lorentzian traversable wormhole with charge or angular momentum. It is found that the wormhole shape function is modified by the charge term similar to Reissner-Nordstrom black hole. It is also shown that the throat radius is reduced by the charge effect, which generally supports the recent results that the instability of the wormhole can be caused by the addition of the sufficient normal nonexotic matter. We also investigated the perturbation problem for dynamic wormholes.

1 Introduction

The traversable wormhole consists of two asymptotically flat regions and the throat connecting two regions.[1] Recently the general solutions of wormhole with charge[2] and angular momentum[3] are obtained like the RN(Reissner-Nordström) and Kerr black holes. This means that the wormhole also satisfy the no hair theorem like the black hole.

However, the instability can be caused from the addition of the matter according to the magnitude of the quantity. Thus, in this paper, we examined the stability problem for two kind of ways: the addition of matter and the perturbation of dynamic wormholes.

2 General Solution

2.1 Classical Scalar field

Before dealing with the charged wormhole, consider the wormhole with scalar field.[4] The addition of the scalar field $T^{(1)}_{\mu\nu}$ to the existing wormhole matter $T^{(0)}_{\mu\nu}$ gives the general solution with backreaction by the additional matter. If we add $G^{(1)}_{\mu\nu}$ as an additional geometry to $G^{(0)}_{\mu\nu}$, the Einstein equation becomes

$$\frac{b'}{8\pi r^2} + \frac{1}{8\pi}\frac{\alpha}{r^4} = \rho^{(0)} + \frac{1}{2}\varphi'^2\left(1-\frac{b}{r}\right), \tag{1}$$

$$\frac{b}{8\pi r^3} - \frac{1}{8\pi}\frac{\alpha}{r^4} = \tau^{(0)} - \frac{1}{2}\varphi'^2\left(1-\frac{b}{r}\right), \tag{2}$$

$$\frac{b-b'r}{8\pi r^3} - \frac{1}{8\pi}\frac{\alpha}{r^4} = P^{(0)} - \frac{1}{2}\varphi'^2\left(1-\frac{b}{r}\right). \tag{3}$$

The interaction term is neglected here and $\alpha > 0$. The additional geometry $G^{(1)}_{\mu\nu}$, α/r^4 is added to the field equation, since $\varphi'^2\left(1-\frac{b}{r}\right) \propto r^{-4}$. If we set $b_{\rm eff} = b - \alpha/r$ instead of b, then the Einstein equation is satisfied self-consistently. Thus the effect by the scalar field on the wormhole is only by changing the wormhole function b into $(b-\alpha/r)$ without any interaction term in the left hand side.

For the power law of the shape function as $b = b_0^{2\beta/(2\beta+1)} r^{1/(2\beta+1)}$, it can be analyzed easily. When $-1 < \beta < -\frac{1}{2}$, the power of $b(r)$ is less than -1, the power of the second term, so $b(r)$ vanishes more quickly in the far region. Thus it gives the negative region for $b_{\rm eff}$ at large r, even though it has the positive regions near throat when $b_0 > \alpha$. The region of the positive $b_{\rm eff}$ is $b_0 < r < r_0$, where

[1] E-mail: sungwon@ewha.ac.kr

$r_0 = \alpha^{(1+2\beta)/(2+2\beta)}/b_0^{\beta/(1+2\beta)}$. If $b_0 < \alpha$, $b_{\rm eff}$ is negative at all r, which is not suitable for wormhole formation.

When $\beta \leq -1$ and $b_0 > \alpha$, the wormhole is safe, because $b_{\rm eff}$ is positive at all r. Otherwise, the scalar field effect will change the wormhole structure into others, since the scalar field dominates the exotic matter. Thus the addition of the minimally-coupled, massless scalar field does not guarantee the structure of wormhole.

For example, $\beta = -1$, $b = b_0^2/r$,

$$\varphi = \varphi_0 \left[1 - \cos^{-1}\left(\frac{b_0}{r}\right)\right], \tag{4}$$

$$\alpha = \varphi_0^2 b_0^2, \tag{5}$$

where b_0 is the minimum size of the wormhole and φ_0 is the value of $\varphi(r)$ at $r = b_0$. Therefore, $\varphi_0 < b_0^{-1/2}$ is the condition that is required for maintaining the wormhole under the addition of the scalar field. In this choice of $\beta = -1$, there is no r_0 at which $b_{\rm eff}$ changes from positive value to negative one.

2.2 Charged Wormhole

Consider the metric[2]

$$ds^2 = -\left(1 + \frac{Q^2}{r^2}\right)dt^2 + \left(1 - \frac{b(r)}{r} + \frac{Q^2}{r^2}\right)^{-1} dr^2 + r^2(d\theta^2 + \sin^2\theta d\phi^2). \tag{6}$$

This satisfy the Einstein field equation. When $Q = 0$, the equation becomes MT(Morris-Thorne)[1] wormhole. Shape function $b = 0$ means the R-N black hole with zero mass. If we see the Einstein-Maxwell Equation,

$$\frac{b'}{r^2} + \frac{Q^2}{r^4} = 8\pi(\rho + \rho^{(1)}), \tag{7}$$

$$\frac{b}{r^3} - \frac{Q^2}{r^4} - 2\left(1 - \frac{b}{r} + \frac{Q^2}{r^2}\right)\left(-\frac{Q^2}{r^2(r^2+Q^2)}\right) = 8\pi(\tau + \tau^{(1)}), \tag{8}$$

$$\left(1 - \frac{b}{r} + \frac{Q^2}{r^2}\right)\left[\frac{Q^2(3r^2+Q^2)}{r^2(r^2+Q^2)^2} - \left(\frac{b'r - b + \frac{2Q^2}{r}}{2(r^2 - br + Q^2)}\right)\left(-\frac{Q^2}{r(r^2+Q^2)^2}\right),\right.$$

$$\left. + \left(-\frac{Q^2}{r(r^2+Q^2)^2}\right)^2 - \frac{Q^2}{r^2(r^2+Q^2)^2} - \frac{b'r - b + \frac{2Q^2}{r}}{2r(r^2 - br + Q^2)}\right] = 8\pi(P + P^{(1)}). \tag{9}$$

$$\rho^{(1)} = \tau^{(1)} = P^{(1)} = \frac{Q^2}{8\pi r^4} \tag{10}$$

There is the interaction term in geometry, even though no interaction term in matter. If $b \to b_{\rm eff} = b - \frac{Q^2}{r}$, it self-consistently satisfies the field equations without Q. It is the same as the case of scalar field.

For example, if $\beta = -1$, $b = b_0^2/r$, $Q^2 < b_0^2$ is the condition that is required for maintaining the wormhole under the addition of the charge. In this choice of $\beta = -1$, there is no r_0 at which $b_{\rm eff}$ changes from positive value to negative one.

Table 1. The sign of the effective wormhole function $b_{\rm eff}(r)$.

Value of β	$b_0^2 > Q^2$ or $\alpha^\dagger$	$b_0^2 < Q^2$ or $\alpha^\dagger$
$\beta < -1$	+	$-+^\ddagger$
$\beta = -1$	+	−
$-1 < \beta < -\frac{1}{2}$	$+-^\ddagger$	−

$^\dagger Q^2$ in case of electric charge and α in case of scalar field.
‡The signs change at r_0.

2.3 Rotating Wormhole

There is also a solution for rotating wormhole that resembles the Kerr black hole.[3] He obtained the stationary and axisymmetric metric element for the rotating wormhole as

$$ds^2 = -N^2dt^2 + \left(1 - \frac{b}{r}\right)^{-1} dr^2 + r^2K^2[d\theta^2 + \sin^2\theta(d\phi - \omega dt)^2], \tag{11}$$

where N, b, K, ω depends on (r, θ). This is the symptotic solution of Kerr type wormhole.[5] If $K = 1$ and $a = 0$, this is just the MT wormhole.

For example,

$$N = K = 1 + \frac{1 + (4a\cos\theta)^2}{r}, \qquad b = 1, \qquad \omega = \frac{2a}{r^3} \tag{12}$$

which is the embedded surface for the equatorial plane

$$z(r) = \pm 2\sqrt{r - 1}. \tag{13}$$

The proper radius of throat is $R = 1 + (4a\cos\theta)^2$ at $r = 1$. The ergoregion similar to ergosphere of the Kerr geometry exists, when $r^2 = |2a\sin\theta| > 1$, or $|a| > 1/2$.

3 Stabilities

We can consider the stability problem along the following two ways. At first we think of the stability problem by the addition of matter for the case of charged wormhole[2] and (1+1)-dimensional wormhole.[7, 8] Next we think about the perturbation problem for the case of dynamic Visser type wormhole[9] and it with cosmological constant.[10]

3.1 Addition of Matter

3.1.1 Charged Case

As we see the solution of the charged wormhole, the simple substitution of the modified shape function that is added by the charge term satisfy the Einstein's field equation. For the special case of $b = \frac{b_0^2}{r}$,

$$ds^2 = -\left(1 + \frac{Q^2}{r^2}\right)dt^2 + \left(1 - \frac{b_0^2}{r^2} + \frac{Q^2}{r^2}\right)^{-1} dr^2 + r^2(d\theta^2 + \sin^2\theta d\phi^2). \tag{14}$$

and

$$b_{0\text{eff}} = b_0 - Q. \tag{15}$$

The size of the throat is reduced by the effect of the charge addition.[6] This fact generally supports the recent result that the instability of the wormhole can be caused by the addition of the sufficient normal nonexotic matter. As we mentioned, the limit for the stability is $Q^2 < b_0^2$. Meanwhile, the size of throat in the case of rotating wormhole is larger than that of non-rotating case except $\cos\theta = 0$.

3.1.2 (1+1)-dimensional model

For the case of (1+1) dimensional CGHS(Callan-Giddings-Harvey-Strominger) model[11], we set the Lagrangian as

$$\int d^2x \left[e^{-2\phi}(R + 4(\nabla\phi)^2 + 4\lambda^2) - \frac{1}{2}(\nabla f)^2 + \frac{1}{2}(\nabla g)^2\right], \tag{16}$$

where ϕ is a scalar dilaton field, λ is a cosmological constant, f is a scalar matter field and g is a ghost field with negative gravitational coupling.[8] By controlling the addition of two fields, the stability can be discussed. The line element in this model may be written as

$$ds^2 = -2e^{2\rho}dx^+dx^- \tag{17}$$

in null coordinates (x^+, x^-). With appropriate gauge condition $\rho = \phi$ and convenient transformation $r = 2e^{-2\phi}$, we can get the constraint

$$\partial_\pm \partial_\pm r = (\partial_\pm g)^2 - (\partial_\pm f)^2 \tag{18}$$

added to the field equations. These may be reduced to $\partial_\pm \partial_\pm r_\pm = G_\pm^2 - F_\pm^2$, where $F_\pm = \partial_\pm f_\pm$ and $G_\pm = \partial_\pm g_\pm$. Here $r_\pm, f_\pm, g_\pm$ are defined by

$$f(x^+, x^-) = f_+(x^+) + f_-(x^-), \tag{19}$$

$$g(x^+, x^-) = g_+(x^+) + g_-(x^-), \tag{20}$$

$$r(x^+, x^-) = r_+(x^+) + r_-(x^-) - 4\lambda^2 x^+ x^-. \tag{21}$$

If we consider the case that a step pulse of positive-energy radiation is beamed through the wormhole as

$$F_+ = \begin{cases} 0, & x^+ < 0, \\ \Delta, & 0 \le x^+ < x_0, \\ 0, & x_0 \le x^+, \end{cases} \tag{22}$$

$$F_- = 0, \tag{23}$$

with $G_\pm = \pm 2\lambda$, then the wormhole becomes non-static but, for small-energy pulse, remains traversable for a long time.

The wormhole may be maintained by beaming in additional negative-energy radiation before the positive energy pulse. Thus if we take the same step pulse in F_+ and precede it with a compensating pulse in G_+:

$$G_+ = \begin{cases} 2\lambda, & x^+ < -x_0, \\ \sqrt{4\lambda^2 + \Delta^2}, & -x_0 \le x^+ < 0, \\ 2\lambda, & 0 \le x^+, \end{cases} \tag{24}$$

$$G_- = -2\lambda, \tag{25}$$

the wormhole returns to its original static state.

In this model, we can conclude that the wormhole is "neutrally" stable under the backreaction of the transported matter and it can be maintained indefinitely for transport of signaling by balance of positive and negative energy.

3.2 Perturbation of dynamic wormhole

Matt Visser tried to make wormhole by using minimal exotic matter.[9] He took two copies of the Schwarzschild manifold and remove from them the four-dimensional regions described by $\Omega_{1,2} = \{r_{1,2} < a \mid a > r_H\}$. One is left with two geodesically incomplete manifolds with boundaries $\partial\Omega_{1,2} = \{r_{1,2} = a \mid a > r_H\}$. By identifying these two hypersurfaces, we get the spacetime possessing two asymptotically Schwarzschild regions connected by a wormhole. Since there is the delta function type stress-energy tensor at the throat, the Ricci tensor at the junction is calculated in terms of the discontinuity in the second fundamental forms, $\mathcal{K}_{\mu\nu}$, Across the boundary, there are jumps,

$$\mathcal{K}_{ij} = \mathcal{K}_{ij}^+ - \mathcal{K}_{ij}^-. \tag{26}$$

For dynamic case, the jump are given by

$$\mathcal{K}_\theta^\theta = \mathcal{K}_\phi^\phi = \frac{\sqrt{1 - 2M/a + \dot{a}^2}}{a}, \tag{27}$$

$$\mathcal{K}_\tau^\tau = \frac{\dot{a} + M/a^2}{\sqrt{1 - 2M/a + \dot{a}^2}}. \tag{28}$$

Then the Einstein's equations become

$$\sigma = -\frac{\sqrt{1 - 2M/a + \dot{a}^2}}{2\pi a}, \tag{29}$$

$$\Theta = -\frac{1}{4\pi a} \frac{1 - M/a + \dot{a}^2}{\sqrt{1 - 2M/a + \dot{a}^2}}, \tag{30}$$

where σ is the surface energy density and Θ is the surface tension. The conservation law is

$$\dot{\sigma} = -2(\sigma - \Theta)\frac{\dot{a}}{a}. \tag{31}$$

The dynamical equation becomes

$$\dot{a}^2 - \frac{2M}{a} - (2\pi\sigma)^2 a^2 = -1. \tag{32}$$

In case of σ = constant, the wormhole can blow up to infinity or to collapse to zero. When $\sigma \propto a^{-1}$, it is bounded, but can collapse.

For the case of Schwarzschild-de Sitter type wormhole,[10] we can get the dynamical equation,

$$\dot{a}^2 - \frac{2M}{a} - \frac{a^2}{R_0^2} - (2\pi\sigma)^2 a^2 = -1. \tag{33}$$

In case of σ = constant, the dynamics of the wormhole is the same as the Schwarzschild case.[9] However, if you depict the potential for negative cosmological constant Λ, you can see that Λ provide a chance to prevent the wormhole from blowing up, and that it has a stable state when $M < 0$ only, whereas it may collapse to zero in other cases. By comparing with the Schwarzschild case, the wormhole is confined when $\sigma \propto a^{-2}$, which means that Λ allows the possibility of blowing up to infinity.

4 Summary and Discussion

Here we studied the general solutions of wormhole with hair. The scalar field and charge may break the wormhole structure when the field and the variation of the field is large. Similar consequences are obtained in other field case.

It is natural that the addition of the nonexotic matter will break wormhole if the "auxiliary effect" is large. In this paper, the interaction between the extra field and the original matter is neglected. If the interaction exists and it is large, it can change the whole geometry drastically. If it is very small, it does not change the main structure of the wormhole.

In the dynamic case of Visser type, the stability depends on the surface energy density and the wormhole can collapse to zero in most cases.

References

[1] M. Morris and K. S. Thorne, Am. J. Phys. **56**, 395 (1988).

[2] S.-W. Kim and H. Lee, Phys. Rev. D**63**, 064014 (2001).

[3] E. Teo, Phys. Rev. D **58**, 024014 (1998).

[4] S.-W. Kim, Grav. & Cosmology **6**, 337 (2000).

[5] S.-W. Kim, in preparation.

[6] S.-W. Kim, Grav. & Cosmology **9**, 4909 (2002).

[7] S.-W. Kim and H. Lee, Phys. Lett. B**458**, 245 (1999).

[8] S. A. Hayward, S.-W. Kim, and H. Lee, Phys. Rev. D **65**, 064003 (2002).

[9] M. Visser, Nucl. Phys. B**328**, 203 (1989).

[10] S.-W. Kim, S. K. Kim, and J. Yang, J. Kor. Phys. Soc. **25**, S267 (1992).

[11] C. Callan, S. Giddings, J. Harvey, and A. Strominger, Phys. Rev. D**45**, R1005 (1992).

Radion and Bulk Scalar in Two Branes System

Shinpei Kobayashi,[1] Kazuya Koyama[2]

Graduate School of Human and Environment Studies, Kyoto University, Kyoto 606-8501, Japan
Department of Physics, The University of Tokyo, Tokyo 113-0033, Japan

Abstract

We investigate cosmological evolutions of the bulk scalar field $\phi(t)$ and the radion $d(t)$ in five-dimensional dilatonic two branes model. This model includes Randall-Sundrum model and five-dimensional Hořava-Witten theory. We consider matter on both branes and arbitrary potentials on the branes and in the bulk. These matter and potentials induce the cosmological expansion of the brane as well as the time evolution of the bulk scalar field and the radion. Starting with full five-dimensional equations, we derive four-dimensional effective equations which govern the low-energy dynamics of brane worlds. Note that this proceeding is the extract of [1] and detailed analysis is performed in [1].

1 Introduction

Of all compactification mechanisms of the extra dimensions, Hořava-Witten (HW) theory is a fascinating one[2][3]. Hořava and Witten showed that the eleven-dimensional limit of M-theory compactified on $S^1/\mathbf{Z}_2$ orbifold can be identified as the strongly coupled ten-dimensional $E_8 \times E_8$ heterotic string theory with two orbifold fixed planes. Witten also showed that there exists a consistent compactification of this theory where the universe appears as a five-dimensional spacetime with two boundary branes [4]. Then the five dimensional effective action for this theory was derived [5] and the cosmological evolution of the branes has been studied [6]-[9]. In this model, the bulk scalar field is necessarily associated with the compactification. As well as the bulk scalar field, there is another important scalar degree of freedom in two branes model, that is, a radion which describes the inter-brane distance. The radion plays a crucial role in gravitational interactions on the brane. For example, in RS model [10],[11], the radion acts as a Brans-Dicke (BD) field and the observational constraints on BD parameter gives strong constraint on the model.

The purpose of this paper is to investigate the cosmological consequences of the bulk scalar field and the radion. We consider a model where the bulk potential for the bulk scalar field ϕ is given by an exponential function $V_{bulk} \propto \exp(-2\sqrt{2}b\phi)$. This model includes HW theory (with $b = 1$) and RS model (with $b = 0$). We will consider matter on both branes and arbitrary potentials on the branes and in the bulk. These matter and potentials induce the cosmological expansion of the brane as well as the time evolution of the bulk scalar field and the radion.

Here we will derive four-dimensional effective equations for the radion and the bulk scalar field starting with full five-dimensional equations. In order to do so, we use the low-energy expansion scheme. The low-energy means that the energy density of the matter on the brane is much lower than the tension of the brane. This relation holds at late times in cosmological evolution. Under such an approximation, we can derive the effective four-dimensional equations for scale factor, radion and bulk scalar field. We can also determine the correspondent five-dimensional geometry.

The organization of this paper as follows. In Sec. II, we review the setup of our model and introduce the low-energy approximation. Using this approximation, we give the background solutions. In Sec. III, we will give effective equations which govern the low energy dynamics of the two branes system are presented. Sec. IV is devoted to conclusions[3] .

[1] E-mail:shinpei@phys.h.kyoto-u.ac.jp
[2] E-mail:kazuya@utap.phys.s.u-tokyo.ac.jp
[3] This proceeding is the extract of [1] and detailed analysis is performed in [1]

2 Setup

2.1 Action and Equations of Motion

We consider the bulk action of the form

$$S_{bulk} = \frac{1}{2\kappa^2}\int_{M_5} d^5x\sqrt{-g_5}\left(R - \partial_M\phi\partial^M\phi + V_{bulk}(\phi)\right), \tag{1}$$

where κ^2 denotes the five-dimensional gravitational constant and σ denotes the tension of the 3-brane. The bulk potential is taken as

$$V_{bulk}(\phi) = -\left(b^2 - \frac{2}{3}\right)e^{-2\sqrt{2}b\phi}\sigma^2 + V(\phi). \tag{2}$$

Here we split V_{bulk} into an explicit, exponential potential for ϕ and an arbitrary potential $V(\phi)$ according to Ref.[12]. The parameter b is determined by the theory. If we choose $b = 0$ and $V(\phi) = 0$, we retrieve the action for the Randall-Sundrum model and if $b = 1$ and $V(\phi) = 0$, we retrieve the action for Hořava-Witten model, which were derived in [5].

We consider a five-dimensional spacetime with structure $M_5 = S^1/\mathbf{Z}_2 \times M_4$ where $S^1/\mathbf{Z}_2$ is an orbifold and M_4 is a smooth manifold. We use the coordinate y to parameterize the orbifold and the range of y is chosen as $-r \le y \le r$. Because this spacetime has $\mathbf{Z}_2$-symmetry (i.e. we identify y with $-y$), there are two endpoints in this spacetime. These two endpoints are called orbifold fixed planes, which are 3-branes. A positive tension brane is set at $y = 0$ and a negative tension brane is set at $y = r$. We take the actions for them as

$$\begin{aligned} S_{brane} &= S_+ + S_- \\ S_+ &= \int_{M_4^{(1)}} d^4x\sqrt{-g_4}U_{brane} + \int_{M_4^{(1)}} d^4x\sqrt{-g_4}\mathcal{L}_m, \\ S_- &= \int_{M_4^{(2)}} d^4x\sqrt{-g_4}\tilde{U}_{brane} + \int_{M_4^{(2)}} d^4x\sqrt{-g_4}\tilde{\mathcal{L}}_m, \end{aligned} \tag{3}$$

where the potentials are given by

$$\begin{aligned} U_{brane} &= -\frac{\sqrt{2}}{\kappa^2}e^{-\sqrt{2}b\phi}\sigma - U(\phi), \\ \tilde{U}_{brane} &= \frac{\sqrt{2}}{\kappa^2}e^{-\sqrt{2}b\phi}\sigma - \tilde{U}(\phi). \end{aligned} \tag{4}$$

The action for the positive tension brane and the negative tension brane is denoted by S_+ and S_-, respectively. $U(\phi)$ and $\tilde{U}(\phi)$ are arbitrary potentials. $\mathcal{L}_m$ and $\tilde{\mathcal{L}}_m$ are the Lagrangian density of the matter on each brane. We assume that they do not couple to the bulk scalar, that is, $\delta\mathcal{L}_m/\delta\phi = \delta\tilde{\mathcal{L}}_m/\delta\phi = 0$. It is true that in HW model, there are field strengths of E_8 and E_6 gauge field which couple to the bulk scalar field, but in this paper, we replace them with the energy density of perfect fluids.

Now we take the five-dimensional metric as

$$ds^2 = e^{2\gamma(y,t)}dy^2 - e^{2\beta(y,t)}dt^2 + e^{2\alpha(y,t)}\delta_{ij}dx^idx^j. \tag{5}$$

Using the action and the metric, we derive the Einstein equation and the equation of motion for the scalar field.

2.2 Low Energy Expansion Scheme

In this subsection, we formulate the low energy expansion scheme to solve the equations [4] . At late times, the energy density and the pressure of the perfect fluid is much smaller than the tension of the brane. Hence we can impose the following conditions,

$$\sigma \gg \kappa^2\rho,\ \kappa^2 p,\ \sigma^{-1}V,\ \kappa^2 U,\ \kappa^2\tilde{U}. \tag{6}$$

[4] Generalizations to covariant form of this iteration scheme are performed in [13], [14]

Then, we can define a small parameter of the system as follows,

$$\varepsilon \equiv \frac{\kappa^2 \rho}{\sigma}. \tag{7}$$

Thus for $\varepsilon \ll 1$, we can solve five-dimensional Einstein equations perturbatively by expanding a metric and scalar field as

$$\alpha(y,t) = \alpha_{(0)}(y,t) + \alpha_{(1)}(y,t) + \alpha_{(2)}(y,t) + \cdots, \tag{8}$$

where $\alpha_{(i)}$ is the function of the order $\mathcal{O}(\varepsilon^i)$. We expand $\beta(y,t)$, $\gamma(y,t)$, and $\phi(y,t)$ in a similar way. The important point is that t-derivative of the lower order solution is the same order as y-derivative of the higher order solution;

$$\ddot{\alpha}_{(i-1)} \sim \alpha''_{(i)}. \tag{9}$$

This is because the derivative with respect to y is of the order $\alpha' \sim \sigma$ for $\varepsilon \ll 1$ from the junction conditions. On the other hand, from the Friedmann equation, we expect that the derivative with respect to t is of the order $\dot{\alpha}^2 \sim \kappa^2 \sigma \rho$. Then the derivative with respect to t is suppressed by the factor $\varepsilon^{1/2}$ compared with the derivative with respect to y;

$$\left(\frac{\dot{\alpha}}{\alpha'}\right)^2 \sim \varepsilon. \tag{10}$$

Hence, the leading order equation of the order $\mathcal{O}(\epsilon^0)$ contains only the y-derivative of the 0-th order solution (i.e., $\alpha''_{(0)}$, $\beta''_{(0)}, \cdots$), and 1st order equations are consisted of t-derivatives of 0-th order functions and y-derivatives of 1st order functions (i.e., $\ddot{\alpha}_{(0)}$, $\ddot{\beta}_{(0)}, \cdots$, $\alpha''_{(1)}$, $\beta''_{(1)}, \cdots$). At each order, Einstein equations give ordinary differential equations for $(\alpha_{(i)}, \beta_{(i)}, \cdots)$ with respect to y. Then it is possible to solve the equations analytically.

3 4D Effective equations

3.1 Friedmann equation, equations of motion for radion and scalar field

Using the low energy expansion scheme, we can explicitly write down four-dimensional effective equations as the equations of motion of the order $\mathcal{O}(\epsilon^1)$[5] . First, the evolution equations for scale factor are given by

$$\ddot{\tilde{\alpha}} + 2\dot{\tilde{\alpha}}^2 + \frac{1}{6}\dot{\phi}^2 = \frac{\sqrt{2}}{36}\kappa^2\sigma((1-3w)\rho + 4U + 3\sqrt{2}bU')e^{-\sqrt{2}b\phi} - \frac{1}{6}V(\phi^{(0)}), \tag{11}$$

$$\begin{aligned}\ddot{\tilde{\alpha}} + 2\dot{\tilde{\alpha}}^2 + \frac{1}{6}\dot{\phi}^2 = &-\frac{\sqrt{2}}{36}\kappa^2\sigma((1-3\tilde{w})\tilde{\rho} + 4\tilde{U} + 3\sqrt{2}b\tilde{U}')e^{-\sqrt{2}b\phi}\tilde{H}^{-\frac{3\Delta+4}{3\Delta+8}} \\ &- \frac{1}{6}\tilde{H}^{\frac{4}{8+3\Delta}}V(\tilde{\phi}^{(0)}) + \frac{2}{3\Delta+8}\left(\ddot{d} + 3\dot{d}\dot{\tilde{\alpha}} + \sqrt{2}b\dot{d}\dot{\phi}\right)\tilde{H}^{-1} + \frac{3\Delta+4}{(3\Delta+8)^2}\dot{d}^2\tilde{H}^{-2},\end{aligned} \tag{12}$$

$$\begin{aligned}\dot{\tilde{\alpha}}^2 + \sqrt{2}b\dot{\tilde{\alpha}}\dot{\phi} - \frac{1}{6}\dot{\phi}^2 = &\frac{\sqrt{2}(\Delta+4)}{24(1-\tilde{H}\zeta)}\kappa^2\sigma\left[\rho + U + (\tilde{\rho}+\tilde{U})\tilde{H}^{\frac{8}{3\Delta+8}}\right]e^{-\sqrt{2}b\phi} \\ &- \frac{\sqrt{2}}{24}(\Delta+4)\sigma d\frac{1}{1-\tilde{H}\zeta}\int_0^r dy H^{\frac{8}{8+3\Delta}}V + \frac{3\tilde{H}\zeta(\Delta+4)}{1-\tilde{H}\zeta}\left[-\frac{1}{3\Delta+8}\dot{d}\dot{\tilde{\alpha}}\tilde{H}^{-1} + \frac{1}{(3\Delta+8)^2}\dot{d}^2\tilde{H}^{-2}\right].\end{aligned} \tag{13}$$

[5]The readers who are interested in the detailed derivation, see [1].

The equation for $\hat{\phi}$ is given by

$$\ddot{\hat{\phi}}+3\dot{\hat{\alpha}}\dot{\hat{\phi}}+\sqrt{2}b\dot{\hat{\phi}}^2 = \frac{b\kappa^2\sigma}{6(1-\tilde{H}^{\zeta})}\left[(1-3w)\rho+4U-\sqrt{2}b^{-1}U'+((1-3\tilde{w})\tilde{\rho}+4\tilde{U}-\sqrt{2}b^{-1}\tilde{U}')\tilde{H}^{\frac{8}{3\Delta+8}}\right]e^{-\sqrt{2}b\hat{\phi}}$$
$$+\frac{\sqrt{2}}{8}(\Delta+4)\sigma d\frac{1}{1-\tilde{H}^{\zeta}}\int_0^r dy H^{\frac{8}{8+3\Delta}}\left(V'+\sqrt{2}bV\right)-\frac{1}{1-\tilde{H}^{\zeta}}\frac{\sqrt{2}b}{2}V(\phi^{(0)})\left(1-\tilde{H}^{\frac{3\Delta+16}{3\Delta+8}}\frac{V(\tilde{\phi}^{(0)})}{V(\phi^{(0)})}\right)$$
$$+\frac{\tilde{H}^{\zeta}}{1-\tilde{H}^{\zeta}}\left[-\frac{6\sqrt{2}b}{3\Delta+8}(\ddot{d}+3\dot{d}\dot{\hat{\alpha}})\tilde{H}^{-1}-\frac{6\Delta+20}{3\Delta+8}\dot{d}\dot{\hat{\phi}}\tilde{H}^{-1}+\frac{24\sqrt{2}b}{(3\Delta+8)^2}\dot{d}^2\tilde{H}^{-2}\right]. \quad (14)$$

Finally the equation for $d(t)$ is given by

$$\ddot{d}+3\dot{d}\dot{\hat{\alpha}}+\sqrt{2}b\dot{d}\dot{\hat{\phi}}+\frac{3\Delta+4}{2(3\Delta+8)}\dot{d}^2\tilde{H}^{-1}$$
$$=\frac{\sqrt{2}(3\Delta+8)}{72}\tilde{H}\kappa^2\sigma\left[(1-3w)\rho+4U+3\sqrt{2}bU'+((1-3\tilde{w})\tilde{\rho}+4\tilde{U}+3\sqrt{2}b\tilde{U}')\tilde{H}^{-\frac{3\Delta+4}{3\Delta+8}}\right]e^{-\sqrt{2}b\hat{\phi}}$$
$$-\frac{8+3\Delta}{12}\tilde{H}V(\phi^{(0)})\left(1-\tilde{H}^{\frac{4}{8+3\Delta}}\frac{V(\tilde{\phi}^{(0)})}{V(\phi^{(0)})}\right), \quad (15)$$

where we defined

$$\tilde{H}\equiv H(r,t)=1-d(t), \qquad \zeta\equiv\frac{3(\Delta+4)}{3\Delta+8}. \quad (16)$$

To make the spacetime non-singular, we set the negative tension brane at $r=1/(\sqrt{2}b^2\sigma)$ and assume $d<1$. We can also get the energy conservation law as follows,

$$\dot{\rho}+3(1+w)\rho\dot{\hat{\alpha}} = 0, \quad (17)$$

$$\dot{\tilde{\rho}}+3(1+\tilde{w})\tilde{\rho}\left(\dot{\hat{\alpha}}-\frac{\sqrt{2}}{3\Delta+8}\dot{d}\tilde{H}^{-1}\right) = 0, \quad (18)$$

which can be derived from above equations. Because we have five equations for five unknown functions $(\hat{\alpha},\hat{\phi},d,\rho,\tilde{\rho})$ we can consistently solve these equations.

4 Conclusions and Future Works

Here we considered two branes model with bulk scalar field, which is a generalization of both Randall-Sundrum model and Hořava-Witten model. The bulk potential of the scalar field has a exponential functions $V_{bulk}=\exp(-2\sqrt{2}b\phi)$. We considered matter on both branes and arbitrary potentials in the bulk and on the brane. These matter and potentials induce the cosmological expansion of the brane as well as the time evolution of the bulk scalar field and radion. Because it is expected that the tension of the brane is much larger than the energy density of matter at late time cosmology, we have used the low-energy approximation to derive the equations which describe the cosmological evolution on the brane.

The main results of this paper are the four-dimensional effective equations (11)-(15) which govern the low energy dynamics of the two branes system. The important point is that once the four dimensional dynamics is determined by these effective equations, we can construct a correspondent full five-dimensional geometry. This correspondence would be useful to investigate the effect of the bulk geometry on four dimensional brane dynamics.

In [1], we also investigated observational constraints imposed on the model. We assume we are living on positive tension brane. First, we studied the case where the radion $d(t)$ is stabilized. In such a case, we can regard this model as Brans-Dicke theory with a Brans-Dicke parameter $1/2b^2$. From the observational constraint, we concluded b^2 must be smaller than 1.6×10^{-4}. Second, we consider the case where $\dot{\hat{\phi}}=const.$ We found that this model can be identified with the scalar-tensor theory where the

Brans-Dicke parameter is given by $(3/2(3b^2+1))(\varphi/1-\varphi)$, where φ is the BD field which is defined by $d(t)$. For RS model with $b=0$, this agrees with the result obtained in [13],[14],[15]. The observational constraint implies the negative tension brane should be sufficiently away from the positive tension brane. In general cases where there in no stabilization mechanism, the effective theory becomes bi-scalar tensor theory.

Using the effective equations, we also constructed several simple models for inflation in [1]. The inflation can be driven by potentials on the brane and bulk. We can construct various models for boundary inflation. It is very interesting to know we can distinguish these models from conventional four-dimensional model. The detailed analysis of these inflation models including the primordial fluctuations will be given in the near future.

Note added

After almost completing this work, we found [16]. In [16], the equations for the radion and the bulk scalar are derived using a moduli approximation and qualitatively the same result is obtained.

Acknowledgements

The work of K.K. was supported by JSPS.

References

[1] S. Kobayashi and K. Koyama, JHEP **02** (2002) 056.

[2] P. Hořava and E. Witten, Nucl. Phys. **B460** (1996) 506.

[3] P. Hořava and E. Witten, Nucl. Phys. **B475** (1996) 94.

[4] E. Witten, Nucl. Phys. **B471** (1996) 135.

[5] A. Lukas, B. A. Ovrut, K. S. Stelle and D. Waldram, Nucl. Phys. **B552** (1999) 246.

[6] A. Lukas, B. A. Ovrut, K. S. Stelle and D. Waldram, Phys. Rev. **D59** (1999) 086001.

[7] A. Lukas, B. A. Ovrut, K. S. Stelle and D. Waldram, Phys. Rev. **D60** (1999) 086001.

[8] U. Ellwanger, hep-th/0001126.

[9] H. S. Reall, Phys. Rev. **D59** (1999) 103506.

[10] L. Randall and R. Sundrum, Phys. Rev. Lett. **83.** (1999) 3370.

[11] L. Randall and R. Sundrum, Phys. Rev. Lett. **83.** (1999) 4690.

[12] A. Lukas, B. A. Ovrut and D. Waldram, Phys. Rev. **D61** (1999) 023506.

[13] S. Kanno and J. Soda, Phys. Rev **D66** (2002) 043526.

[14] S. Kanno and J. Soda, Phys. Rev. **D66** (2002) 083506.
(2001) 086004.

[15] J. Garriga and T. Tanaka, Phys. Rev. Lett. **84** (2000) 2778.

[16] Ph. Brax, C. van de Bruck, A.-C. Davis and C. S. Rhodes, hep-th/0209158.

Cosmological Gravitational Waves in Braneworld

Tsutomu Kobayashi,*[1] Takahiro Tanaka,†[2] Hideaki Kudoh*[3]

* *Department of Physics, Kyoto University, Kitashirakawa, Sakyo-ku, Kyoto 606-8502, Japan*

† *Yukawa Institute for Theoretical Physics, Kyoto University, Kitashirakawa, Sakyo-ku, Kyoto 606-8502, Japan*

Abstract

We discuss generation of primordial gravitational waves during inflationary stage in Randall-Sundrum braneworld model. We consider a situation in which the Hubble parameter slightly changes during the inflationary phase, and evaluate the production of gravitational waves from vacuum fluctuations in zero-mode and Kaluza-Klein modes. The power spectrum of gravitational waves is derived and is compared with the four-dimensional one. It is shown that the five-dimensional spectrum coincides with the four-dimensional one at low energies of the inflation, but they are different at high energies. However, we find that it is possible to approximately reconstruct the five-dimensional power spectrum at high energies from the four-dimensional one only by a linear transformation.

1 Introduction

Recent development of the braneworld scenarios that our four-dimensional Universe is embedded as a three dimensional brane in a higher dimensional spacetime brought interesting possibilities to the scenario of very early universe. A lot of efforts have been devoted to the search for the new and characteristic features of the braneworld cosmology [1]. The investigation of the cosmological perturbations is important and is a useful tool since the brane inflation might leave their characteristic imprints on the primordial spectrum of perturbations. We might be able to observe them by the observations of the CMB anisotropies and the stochastic background of gravitational waves.

Although there are many works on this topic [2], the presence of the extra dimension prevents us from fully evaluating the evolution of the cosmological perturbations. Without taking into account the non-trivial evolution of perturbations in the five-dimensional bulk, the primordial spectra of density perturbations and of gravitational wave perturbations were studied in a model of inflation brought by a slowly-rolling scalar field confined on the brane [3, 1]. There are a few works in which the dynamics of the perturbations in the bulk have been partly taken into account under some assumptions (see the second Ref. of [2]). Another approach is made on gravitational wave perturbations by Gorbunov et. al. [4]. To solve the perturbations in the bulk, they considered a simplified inflation model; de Sitter stage of inflation is instantaneously connected to Minkowski space. They further focus on perturbations at super-Hubble scale at the end of the inflation for simplicity.

In this article, we discuss generation of gravitational waves during inflation on the brane [6]. If the Hubble parameter is exactly constant, the power spectrum becomes flat. However, even in the inflationary stage, the Hubble parameter changes its value in general and therefore we focus our attention to this effect to investigate characteristic features of braneworld inflation.

2 Model of changing Hubble parameter

We first consider gravitational wave (tensor-type) perturbations in AdS_5 spacetime bounded by a de Sitter brane. It is convenient to describe the perturbations in coordinates where the position of the de

[1] E-mail:tsutomu@tap.scphys.kyoto-u.ac.jp
[2] E-mail:tanaka@yuakwa.kyoto-u.ac.jp
[3] E-mail:kudoh@yuakwa.kyoto-u.ac.jp

Sitter brane is fixed. Such coordinates are given by

$$ds^2 = \frac{\ell^2}{\sinh^2\xi}\left\{\frac{1}{\eta^2}\left[-d\eta^2 + (\delta_{ij} + h_{ij}^{\rm TT})dx^i dx^j\right] + d\xi^2\right\}, \tag{1}$$

where $h_{ij}^{\rm TT}$ are transverse-traceless perturbations and ℓ is the bulk curvature radius. In this coordinate system, the de Sitter brane is placed at $\xi = \text{const.} = \xi_B$. Indeed, the Hubble parameter on the $\xi = \xi_B$ plane is $H = \ell^{-1}\sinh\xi_B = \text{const.} \equiv H_1$.

Spatial Fourier modes of $h_{ij}^{\rm TT}$,

$$h_{ij}^{\rm TT}(\eta, \boldsymbol{x}, \xi) = \frac{\sqrt{2}}{(M_5)^{3/2}} \cdot \frac{1}{(2\pi)^{3/2}} \int d^3p \phi(\eta, \xi; p) e^{i\boldsymbol{p}\cdot\boldsymbol{x}} e_{ij}^{\rm TT}, \tag{2}$$

obey the Klein-Gordon equation for a massless scalar field in AdS_5,

$$\left[\eta^2\frac{\partial^2}{\partial\eta^2} - 2\eta\frac{\partial}{\partial\eta} + p^2\eta^2 - \frac{\partial^2}{\partial\xi^2} + 3\coth\xi\frac{\partial}{\partial\xi}\right]\phi = 0. \tag{3}$$

Here M_5 represents the five-dimensional Planck mass, and is related to the four-dimensional Planck mass $M_{\rm Pl}$ as $\ell M_5^3 = M_{\rm Pl}^2$. The boundary condition for ϕ is obtained from the junction condition, $\partial_\xi\phi|_{\xi=\xi_B} = 0$. Equation (3) has separable solutions. The zero-mode is independent of ξ:

$$\phi_0^{(\pm)} = \ell^{-1/2} C(H_1) \frac{H_1}{\sqrt{2p}} e^{\pm ip\eta}\left(\eta \pm \frac{i}{p}\right), \tag{4}$$

where the normalization factor $C(H_1)$ is the same as that given in, for example, Ref. [5]. This factor behaves like $C^2 \sim 1$ for low energy inflation ($\ell H_1 \ll 1$) and $C^2 \sim 3\ell H_1/2$ for high energy inflation ($\ell H_1 \gg 1$). The massive Kaluza-Klein (KK) modes, labeled by $\kappa(\geq 0)$, have the form $\phi_\kappa = \psi_\kappa(\eta)\cdot\chi_\kappa(\xi)$ where $\psi_\kappa^{(\pm)}(\eta)$ and $\chi_\kappa(\xi)$ are written by the Hankel functions and the Legendre functions, respectively. (The explicit form of the KK modes is given in Ref. [4].) Note that the mode labeled by $\kappa = 0$ does not correspond to the zero-mode.

We consider a model which allows the Hubble parameter to change during inflation. As we explained, the constant Hubble parameter means that the de Sitter brane is placed at a fixed coordinate point. Therefore to describe the change of the Hubble parameter, we move the position of the brane. For simplicity, we consider the case in which the Hubble parameter changes its value discontinuously at $\eta = \eta_0$ from H_1 to $H_2 = H_1 - \delta H$. Here $\delta H/H_1$ is assumed to be small. In order to describe the de Sitter brane after the transition, we introduce new coordinate system $(\tilde\eta, \tilde\xi)$ by $\eta\cosh\xi - \eta_0\cosh\xi_B = \tilde\eta\cosh\tilde\xi - \tilde\eta_0\cosh\tilde\xi_B$ and $\eta\sinh\xi = \tilde\eta\sinh\tilde\xi$. In the new coordinates, the brane whose Hubble parameter is H_2 is placed at $\tilde\xi_B = \text{const.}$ Mode functions for tensor-type perturbations in this coordinate system are easily obtained by replacing ξ, η, and H_1 in the above expressions for ϕ_0 and ϕ_κ with $\tilde\xi$, $\tilde\eta$, and H_2, respectively. We denote these modes as $\tilde\phi_0$ and $\tilde\phi_\kappa$.

3 Generation of primordial gravitational waves and its amplitude

Let us consider generation of primordial gravitational waves during inflation. This is described by particle creations due to a change of vacuum state, and is given by calculating the Bogoliubov coefficients between in-vacuum state and out-vacuum state. Because we consider the effect from the transition of the Hubble parameter, we refer to the vacuum before the transition as in-vacuum, and that after the transition as out-vacuum.

To calculate the Bogoliubov coefficients, we develop the same method used in Ref. [4]. First, we consider the wave function that becomes the zero-mode $\tilde\phi_0^{(-)}$ at the infinite future $\tilde\eta = 0$. Then, by making use of the advanced Green's function, we solve evolution equation (3) backward in time under the Neumann boundary condition on the brane, and obtain a solution at the infinite past $\eta = -\infty$. The

solution is expressed as a linear combination of the modes $\phi_0^{(\pm)}$ and $\phi_\kappa^{(\pm)}$, and therefore one can simply read off the Bogoliubov coefficients from the expression.

The Bogoliubov coefficients are given by

$$\beta_{0\kappa} = 2i\ell^3 \int_{-\infty}^{\eta_0} \frac{d\eta}{(\sinh\xi_B)^3\eta^4} \phi_\kappa^{(-)}(\eta,\xi_B) \left[\partial_\xi \tilde{\phi}_0^{(-)}(\eta,\xi)\right]_{\xi=\xi_B}, \tag{5}$$

$$\alpha_{0\kappa} = \left(\tilde{\phi}_0^{(-)} \cdot \phi_\kappa^{(-)}\right) - 2i\ell^3 \int_{-\infty}^{\eta_0} \frac{d\eta}{(\sinh\xi_B)^3\eta^4} \phi_\kappa^{(+)}(\eta,\xi_B) \left[\partial_\xi \tilde{\phi}_0^{(-)}(\eta,\xi)\right]_{\xi=\xi_B}, \tag{6}$$

where $(\ \cdot\ )$ represents the Klein-Gordon inner product. Hereafter, we assume $p|\eta_0|\delta H/H_1 \ll 1$ in addition to the assumption of $\delta H/H_1 \ll 1$. This additional assumption simplifies the calculation of the inner product. We investigate these coefficients in two limiting cases: $\ell H_1 \ll 1$ and $\ell H_1 \gg 1$. At low energies ($\ell H_1 \ll 1$), the Bogoliubov coefficients relating the initial zero-mode to the final one become

$$\beta_{00} \approx \frac{i}{2p\eta_0}\frac{\delta H}{H_1} e^{-2ip\eta_0 - ip\eta_0\delta H/H_2}, \quad \alpha_{00} \approx \left[1 + \frac{i}{2p\eta_0}\frac{\delta H}{H_1}\right] e^{-ip\eta_0\delta H/H_2}. \tag{7}$$

Note that these expressions are correct including the second order in $\delta H/H_1$. Equation (7) coincides with the result of the four-dimensional calculation $\beta^{(4D)}$ and $\alpha^{(4D)}$. The Bogoliubov coefficients relating the initial KK modes to the final zero-mode have a form of

$$|\beta_{0\kappa}|^2,\ |\alpha_{0\kappa}|^2 \approx (p\text{ - dependent part}) \times (\ell H_1)^2 \left(\frac{\delta H}{H_1}\right)^2. \tag{8}$$

These coefficients are suppressed by the factors of ℓH_1 and $\delta H/H_1$. At high energies ($\ell H_1 \gg 1$), the Bogoliubov coefficients β_{00} and α_{00} are reduced to

$$\beta_{00} \approx \frac{3}{2}\frac{i}{2p\eta_0}\frac{\delta H}{H_1} e^{-2ip\eta_0 - ip\eta_0\delta H/H_1}, \quad \alpha_{00} \approx \left[1 - \frac{ip\eta_0}{2}\frac{\delta H}{H_1} - \frac{(p\eta_0)^2}{2}\left(\frac{\delta H}{H_1}\right)^2 + \cdots\right] e^{-ip\eta_0\delta H/H_1}, \tag{9}$$

where "$\cdots$" represents omitted terms of order $\delta H/H_1$ and $(\delta H/H_1)^2$ that are not enhanced for large p. The Bogoliubov coefficients $\beta_{0\kappa}$ and $\alpha_{0\kappa}$ are

$$|\beta_{0\kappa}|^2,\ |\alpha_{0\kappa}|^2 \approx (p\text{ - dependent part}) \times \left(\frac{\delta H}{H_1}\right)^2. \tag{10}$$

In contrast to the low energy case (8) in which a suppression factor $(\ell H_1)^2$ appears, this high energy behavior is not associated with such suppression.

Figure 1 displays the total number of zero-mode gravitons created from vacuum fluctuations in the initial KK modes. Since the coefficients behave as $\beta_{0\kappa} \approx -\alpha_{0\kappa}^* \propto (p|\eta_0|)^{1/2}$ at $p|\eta_0| \ll 1$, the number of created gravitons is proportional to p well outside the Hubble horizon. It has a peak around the horizon scale and then decreases to zero inside the horizon. Note that the quantity $|\alpha_{0\kappa}|$ increases as $|\alpha_{0\kappa}|^2 \sim |(\tilde{\phi}_0^{(-)} \cdot \phi_\kappa^{(-)})|^2 \propto (p\eta_0)^2$ inside the horizon.

So far, we have discussed the Bogoliubov coefficients to observe the number of created gravitons. However, we are interested in the power spectrum of gravitational waves because it is a quantity of physical and observational importance. Gravitational waves generated from pure de Sitter inflation on a brane have a scale free spectrum $\mathcal{P}_{5D} = (2C^2(H)/\ell M_5^3)(H/2\pi)^2$. Since $C^2 \approx 1$ at $\ell H \ll 1$, this power spectrum coincides with the standard four-dimensional result $\mathcal{P}_{4D} = (2/M_{Pl}^2)(H/2\pi)^2$ [5]. Time variation of the Hubble parameter during inflation brings a small modification to the spectrum. The modified spectrum is given in terms of the Bogoliubov coefficients as $\mathcal{P}_{5D}(p) = \mathcal{P}_{5D}^{(zero)}(p) + \mathcal{P}_{5D}^{(KK)}(p)$ where

$$\mathcal{P}_{5D}^{(zero)}(p) \equiv \frac{2C^2(H_2)}{\ell M_5^3}\left(\frac{H_2}{2\pi}\right)^2 |\alpha_{00} + \beta_{00}^*|^2, \quad \mathcal{P}_{5D}^{(KK)}(p) \equiv \frac{2C^2(H_2)}{\ell M_5^3}\left(\frac{H_2}{2\pi}\right)^2 \int_0^\infty d\kappa |\alpha_{0\kappa} + \beta_{0\kappa}^*|^2. \tag{11}$$

The former represents the contribution from the initial zero-mode and the latter from the initial KK modes. Since corresponding spectrum in the four-dimensional theory is

$$\mathcal{P}_{4D}(p) = \frac{2}{M_{Pl}^2}\left(\frac{H_2}{2\pi}\right)^2 \left|\alpha^{(4D)} + \beta^{*(4D)}\right|^2, \tag{12}$$

there are two apparent differences between $\mathcal{P}_{5D}$ and $\mathcal{P}_{4D}$; the normalization factor C and the contribution from KK modes $\mathcal{P}_{5D}^{(KK)}$. In the low energy case $\ell H_1 \ll 1$, $\mathcal{P}_{5D}$ coincides with $\mathcal{P}_{4D}$. This is because the zero-mode contribution $\mathcal{P}_{5D}^{(zero)}$ is exactly the same as $\mathcal{P}_{4D}$ (up to the normalization factor, as noted above), and the KK mode contribution is suppressed (see Eq. (8)). On the other hand, when ℓH_1 is large, the amplitude of gravitational waves deviates from the four-dimensional result owing to the amplification factor C^2.

To compare the two spectra, we apply a linear transformation to $\mathcal{P}_{4D}$:

$$\mathcal{P}_{4D}(p) \longmapsto A\mathcal{P}_{4D}(p) + B = \mathcal{P}_{res}(p) \to \begin{cases} \frac{2C^2(H_1)}{\ell(M_5)^3}\left(\frac{H_1}{2\pi}\right)^2 & (p|\eta_0| \to 0) \\ \frac{2C^2(H_2)}{\ell(M_5)^3}\left(\frac{H_2}{2\pi}\right)^2 & (p|\eta_0| \to \infty) \end{cases} . \tag{13}$$

In this linear transformation, H_1 and H_2 correspond to $C(H_1)H_1$ and $C(H_2)H_2$, respectively. Thus, we obtain a rescaled spectrum $\mathcal{P}_{res}$ to be compared with $\mathcal{P}_{5D}$. We analyze the differences between these two quantities by expanding them with respect to $\delta H/H_1$:

$$\mathcal{P}_{5D}(p) = \frac{2C^2(H_1)}{\ell(M_5)^3}\left(\frac{H_1}{2\pi}\right)^2\left\{1 + \left[\frac{\sin(2p\eta_0)}{p\eta_0} - 2\right]\frac{C^2(H_1)}{\sqrt{1+(\ell H_1)^2}}\frac{\delta H}{H_1}\right\} + \mathcal{P}_{5D}^{(2)} + \cdots + \mathcal{P}_{5D}^{(KK)}, \tag{14}$$

$$\mathcal{P}_{res}(p) = \frac{2C^2(H_1)}{\ell(M_5)^3}\left(\frac{H_1}{2\pi}\right)^2\left\{1 + \left[\frac{\sin(2p\eta_0)}{p\eta_0} - 2\right]\frac{C^2(H_1)}{\sqrt{1+(\ell H_1)^2}}\frac{\delta H}{H_1}\right\} + \mathcal{P}_{res}^{(2)} + \cdots . \tag{15}$$

Here $\mathcal{P}_{5D}^{(2)}$ and $\mathcal{P}_{res}^{(2)}$ represent terms of order $(\delta H/H_1)^2$. Note that all the terms in the right hand side of Eq. (14) except the last one come from the initial zero-mode contribution. Note that $\mathcal{P}_{5D}^{(KK)}$ is also of order $(\delta H/H_1)^2$.

It is clear from Eqs. (14) and (15) that they coincide exactly with each other up to order $\delta H/H_1$. Moreover, the coincidence is approximately achieved up to the second order in $\delta H/H_1$, namely, $\mathcal{P}_{5D}^{(2)} + \mathcal{P}_{5D}^{(KK)} \approx \mathcal{P}_{res}^{(2)}$, as shown in Figure 2. This is confirmed by the following observations. At $p|\eta_0| \ll 1$, one can show $\mathcal{P}_{5D}^{(2)} \sim (p\eta_0)^2$, $\mathcal{P}_{res}^{(2)} \sim (p\eta_0)^2$, and $\mathcal{P}_{5D}^{(KK)} \sim (p\eta_0)^3$, so the difference is suppressed as $|\mathcal{P}_{5D} - \mathcal{P}_{res}| \lesssim O\left((p\eta_0)^2\right) \times (\delta H/H_1)^2$ outside the horizon. At large $p|\eta_0|$, the zero-mode contribution $\mathcal{P}_{5D}^{(2)}$ reduces the fluctuation amplitude like $\mathcal{P}_{5D}^{(2)} - \mathcal{P}_{res}^{(2)} \propto -(p\eta_0)^2$. On the other hand, for such large $p|\eta_0|$, $\mathcal{P}_{5D}^{(KK)}$ is dominated by $\alpha_{0\kappa}$ coefficients and increases in proportion to $(p\eta_0)^2$, i.e., $\mathcal{P}_{5D}^{(KK)} \propto \int d\kappa|\alpha_{0\kappa} + \beta_{0\kappa}^*|^2 \sim \int d\kappa|\alpha_{0\kappa}|^2 \propto +(p\eta_0)^2$. This contribution could be overwhelmingly large for sufficiently large $p|\eta_0|$. However, carrying out the integration with respect to κ, we find that these increasing and decreasing effects cancel out: $(\mathcal{P}_{5D}^{(2)} - \mathcal{P}_{res}^{(2)}) + \mathcal{P}_{5D}^{(KK)} = -(3/4)(p\eta_0)^2 + (3/4)(p\eta_0)^2 = 0$. As a result, $\mathcal{P}_{5D}$ coincides with $\mathcal{P}_{res}$ up to order $(\delta H/H_1)^2$ in the high energy case.

4 Discussion

We have discussed the generation of primordial gravitational waves and its power spectrum in the inflationary braneworld model. The gravitons are generated during the inflation from the in-vacuum of zero-mode and that of Kaluza-Klein modes. We have assumed in this paper a discontinuous change of the Hubble parameter, and we investigated the effect on the power spectrum $\mathcal{P}_{5D}(p)$ of the generated gravitons due to the slight change of the Hubble parameter.

The power spectrum has been compared with the four-dimensional counterpart. At low energies ($\ell H_1 \ll 1$), the five-dimensional spectrum coincides with the standard four-dimensional spectrum because no zero-mode graviton is produced from KK in-vacuum states. However at high energies ($\ell H_1 \gg 1$), the power spectrum of gravitational waves are amplified, and it is significantly different from the four-dimensional results.

This amplification effect was found in Ref. [5] in the context of pure de Sitter inflation (H = const.), and is attributed to the unconventional normalization factor of the zero-mode $C(H)$. What we found in this paper is a similar amplification rule which generalizes the previous result. Namely, the spectrum $\mathcal{P}_{5D}(p)$ can be well estimated from the four-dimensional counter part $\mathcal{P}_{4D}(p)$ by a simple mapping of

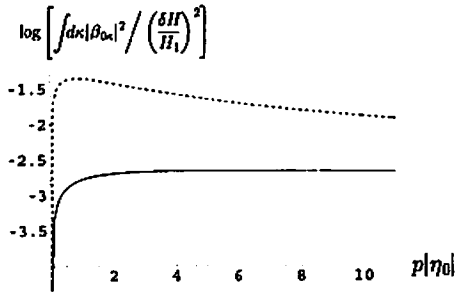


Figure 1: Total number of zero-mode gravitons created from vacuum fluctuations in the initial KK modes. Solid line represents the low energy case with $\ell H_1 = 0.1$, while dashed line shows the high energy case.

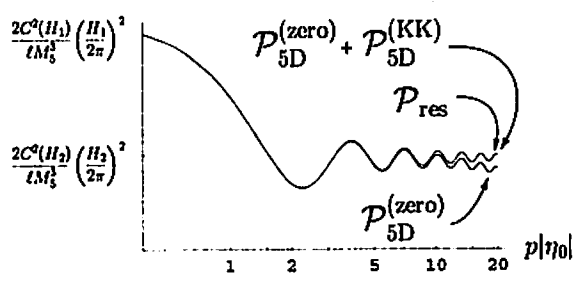


Figure 2: Power spectra of gravitational waves at $\ell H_1 \gg 1$. The deviation between $\mathcal{P}_{5D}^{(zero)}$ and $\mathcal{P}_{res}$ appeared inside the horizon is canceled out by adding $\mathcal{P}_{5D}^{(KK)}$.

the amplitude, $H \mapsto HC(H)$. A nontrivial point which we might need to stress is that a non-negligible fraction of $\mathcal{P}_{5D}(p)$ comes from the vacuum fluctuations of initial KK modes $\mathcal{P}_{5D}^{(KK)}(p)$ (except for the limiting case of $\ell H_1 \ll 1$).

However, we have confirmed this correspondence relation only in our present setup. Therefore, although our result is suggestive, it is not clear whether the correspondence is a general feature and in particular whether a smooth variation of $H = H(\eta)$ permits the correspondence. Further investigations are need to answer this question.

References

[1] See, for example, D. Langlois, "Brane cosmology: an introduction" [hep-th/0209261], and references therein.

[2] See, for example, H. Kodama, A. Ishibashi and O. Seto, Phys. Rev. D **62**, 064022 (2000), K. Koyama and J. Soda, Phys. Rev. D **62**, 123502 (2000), D. Langlois, Phys. Rev. D **62**, 126012 (2000).

[3] R. Maartens, D. Wands, B. A. Bassett and I. P. C. Heard, Phys. Rev. D **62**, 041301 (2000).

[4] D. S. Gorbunov, V. A. Rubakov and S. M. Sibiryakov, JHEP **0110**, 015 (2001).

[5] D. Langlois, R. Maartens and D. Wands, Phys. Lett. B **489**, 259 (2000).

[6] T. Kobayashi, T. Tanaka and H. Kudoh, in preparation.

Degeneracy of Killing horizon

Jun-ichirou Koga[1]

Advanced Research Institute for Science and Engineering, Waseda University, Okubo, Shinjuku, Tokyo 169-8555, Japan

Abstract

We focus on the local features of a Killing horizon, and analyze degeneracy of a Killing horizon. We first show that a Killing horizon is generally regarded as degenerate in the sense that there exist infinitely many horizons with the same local geometric structures as a Killing horizon, which we call asymptotic Killing horizons. It is also argued that the degeneracy will be removed by quantum effects. We then consider Kerr-Newman black holes and incorporate the electromagnetic field into the notion of asymptotic Killing horizons. Consequently, we find that the entropy of an extreme black hole can either be zero or be the same as a non-extreme one, which is consistent with both string theory and the Euclidean approach to black hole thermodynamics. These results provide evidences that the degeneracy of a Killing horizon is responsible for black hole entropy.

1 Introduction

By following the success to derive the entropy of B.T.Z. black holes in a microscopic manner[1], Carlip[2] applied to a black hole horizon the same framework of asymptotic symmetries. This idea seems reasonable, because a structure of a group of asymptotic symmetries is generally related closely to the local geometry near a hypersurface where they are defined. Since black hole entropy is expressed as a local quantity on the horizon, this is a plausible feature of asymptotic symmetries on a black hole horizon. In addition, because of their nature as symmetries associated with the gravitational field, it is expected that they describe somehow relationship between "equivalent states" of classical geometry, which is regarded as classical degeneracy. If we can show that this degeneracy is removed by quantum effects, we will have a desired picture that there exist quantum statistical degrees of freedom on a black hole horizon that are not distinguished classically, but should be distinguished quantum theoretically. Such a picture is indeed necessary for a black hole to carry entropy whose statistical origin is not found in the classical theory of gravity.

Then, some efforts have been made[2, 3, 4, 5] to formulate asymptotic symmetries on a black hole horizon and obtain the same structure of the algebra associated with asymptotic symmetries as that in the case of anti-de Sitter space, the so-called Virasoro algebra with the desired form of a central charge. Although even an extended idea is proposed recently[6], this subject is still controversial[7, 8]. While some of them are focusing on developing mathematical tools that mimic the asymptotic symmetries in anti-de Sitter space, it is more important to understand physical and geometric aspects of asymptotic symmetries on a black hole horizon.

Thus, in this talk, we start with a geometrical analysis of asymptotic symmetries. We follow the previous work[8] on neutral and spherically symmetric Killing horizons, and extend it so that asymptotic symmetries are universally defined on arbitrary Killing horizons. This is necessary for asymptotic symmetries to describe black hole thermodynamics, since the thermodynamic laws of black hole are universal. It is also interesting to see whether the framework of asymptotic symmetries provides consistent results with other methods. In particular, we pay attention to the entropy of an extreme black hole, which is shown to be proportional to its area as a non-extreme black hole in string theory, but calculated to vanish in the Euclidean approach to black hole thermodynamics. Thus, we particularly consider Kerr Newman black holes and incorporate the electromagnetic field. We then analyze behavior of asymptotic symmetries and its implication for the entropy of an extreme black hole.

[1]E-mail:koga@gravity.phys.waseda.ac.jp

2 Universality of Asymptotic Killing horizon

We begin with recalling the definition of a Killing horizon. A Killing horizon is defined as a null hypersurface where a Killing vector becomes null and tangent to the hypersurface. This definition involves the global information of the spacetime geometry, since the Killing equation should hold globally. In contrast, the idea introduced in Ref.[8] is to focus only on the Killing horizon, and consider the asymptotic Killing equation that states the Lie derivative of the metric vanishes only on the horizon, but need not off the horizon.

Based on this idea, the notion of an asymptotic Killing horizon, which is a local version of the notion of a Killing horizon, is defined as follows.

Definition 1 *Let H be a portion of a null hypersurface in a spacetime $(\mathcal{M}, g_{\mu\nu})$ and let $\xi^\mu_{(h)}$ be a vector that is not identically zero in any neighborhood of H. Then, H with the horizon generating vector $\xi^\mu_{(h)}$ is defined to be an asymptotic Killing horizon, provided the following conditions are satisfied;*

1. *there exists a regular scalar u such that $u = 0$ and $\nabla_\mu u \neq 0$ on H,*
2. $\mathcal{L}_{\xi_{(h)}} g_{\mu\nu} = \mathcal{O}(u)$,
3. $g_{\mu\nu}\xi^\mu_{(h)}\xi^\nu_{(h)} = \mathcal{O}(u)$,
4. $\xi^\mu_{(h)}\nabla_\mu u = \mathcal{O}(u)$.

Here, any background spacetime is not involved to define an asymptotic Killing horizon. Thus, the above definition is a generalization of the one presented in Ref.[8]. Correspondingly, a regular scalar u is introduced so that we can specify the null hypersurface by $u = 0$ with its non-vanishing normal vector $\nabla_\mu u$. It is not difficult to find such a scalar in the usual circumstances, since a regular null coordinate satisfies these conditions on u. (When we use u as a coordinate, $\nabla_\mu u$ is its coordinate basis, and hence it does not vanish if the coordinate is regular.)

We can show that there exist infinitely many horizon generating vectors $\xi^\mu_{(h)}$ for a fixed metric $g_{\mu\nu}$, and hence that there exist infinitely many asymptotic Killing horizons on the same null hypersurface. As it is analyzed in Ref.[8], these asymptotic Killing horizons are transformed to each other by the asymptotic symmetries. (We called these transformations the horizon deformations in Ref.[8].) Indeed, if $\xi^\mu_{(h)}$ is a horizon generating vector of an asymptotic Killing horizon with a metric $g_{\mu\nu}$, the vectors that are infinitesimally transformed from $\xi^\mu_{(h)}$ by the asymptotic symmetries, given by

$$\widetilde{\xi}^\mu_{(h)} = \xi^\mu_{(h)} + \omega\xi^\mu_{(h)} - \lambda\nabla^\mu\omega + \mathcal{O}(u^2), \tag{1}$$

are also horizon generating vectors of asymptotic Killing horizons with the same metric $g_{\mu\nu}$, where ω is an infinitesimal but arbitrary function and $\lambda = \mathcal{O}(u)$ is defined based on proportionality of $\xi^\mu_{(h)}$ and $\nabla^\mu u$ on the horizon as

$$\xi^\mu_{(h)} = -n\nabla^\mu u + \mathcal{O}(u) \equiv \nabla^\mu\lambda + \mathcal{O}(u), \tag{2}$$

by using the regular scalar n. (They are horizon generating vectors even for metrics of the form $g_{\mu\nu}+\mathcal{O}(u)$ actually, but we will not consider this issue here.) Thus, we see that once there exists one asymptotic Killing horizon, it is accompanied with infinitely many equivalent asymptotic Killing horizons. In particular, an exact Killing horizon is an asymptotic Killing horizon, and there exist infinitely many asymptotic Killing horizons on the same null hypersurface. From the local point of view, there are no reasons to distinguish the Killing horizon from other asymptotic Killing horizons. All of them should be considered on an equal footing. Therefore, these asymptotic Killing horizons degenerate into a single local geometric structures, and then we consider it as degeneracy of a Killing horizon.

However, it is necessary to analyze whether this degeneracy is physically meaningful. In order to show an evidence, we use the fact that when $\xi^\mu_{(h)}$ is the exact Killing vector of an exact Killing horizon, the orbits of $\widetilde{\xi}^\mu_{(h)}$ given by Eq.(1) are timelike "outside" the horizon. Then, we can consider the accelerations of these orbits. If the surface gravity κ_0 of the Killing horizon is non-vanishing, the magnitude a of the acceleration of the four-velocity $\widetilde{\xi}^\mu_{(h)}/\sqrt{-\widetilde{\xi}_{(h)}\cdot\widetilde{\xi}_{(h)}}$ is given by

$$a = \frac{1}{\sqrt{-\xi_{(h)}\cdot\xi_{(h)}}}\left[\kappa_0 + \frac{1}{2}\xi^\mu_{(h)}\nabla_\mu\omega - \frac{1}{2\kappa_0}\xi^\mu_{(h)}\nabla_\mu\xi^\nu_{(h)}\nabla_\nu\omega + \mathcal{O}(u)\right], \tag{3}$$

near the horizon. Eq.(3) shows that the acceleration of each orbit differs depending on $\xi^{\mu}_{(h)}\nabla_{\mu}\omega$ and its derivative, and hence that particle detectors that run along these orbits respond differently from each other under the same quantum vacuum. It indicates that asymptotic Killing horizons will exhibit different quantum behavior, while they are regarded as equivalent from the classical and local point of view. Therefore, it is expected that classical degeneracy of a Killing horizon will be removed by quantum effects, which is the desired feature for a black hole to carry the entropy.

3 Kerr–Newman horizon

Although the analysis of asymptotic Killing horizons so far is universal, it is based only on the behavior of the metric. However, a black hole generally possesses matter fields in addition to the gravitational field. Then, here we incorporate matter fields into the notion of asymptotic Killing horizons. As an example, we consider a Kerr–Newman black hole and its electromagnetic field.

Similarly to the metric, we require that the electromagnetic field to behave along horizon generating vectors in the same manner as it does along the Killing vector, in order that all asymptotic Killing horizons are regarded as equivalent even when we incorporate the electromagnetic field. While the electromagnetic field has a gauge degree of freedom, it is natural to choose a gauge that is constant along the Killing horizon of a black hole, so that each point on the Killing horizon is treated on the same footing. We then write for the Killing vector $\xi^{\mu}_{(h)}$ as

$$\mathcal{L}_{\xi_{(h)}}A_{\mu} = \nabla_{\mu}\chi + \mathcal{O}(u). \tag{4}$$

Here we impose the condition that the gauge function χ should be constant on the horizon, so that we can set $\chi = \mathcal{O}(u)$ without loss of generality. This condition is required naturally when the transformations generated by the asymptotic symmetries are well-defined in the phase space. It is also emphasized that we work in a regular gauge, since otherwise the field variables and their derivatives are not well defined on the horizon. We then obtain, by using Eq.(1),

$$\mathcal{L}_{\tilde{\xi}_{(h)}}A_{\mu} = \xi^{\alpha}_{(h)}A_{\alpha}\nabla_{\mu}\omega + \nabla_{\mu}\tilde{\chi} + \mathcal{O}(u), \tag{5}$$

where $\tilde{\chi} = \mathcal{O}(u)$. We see that the condition

$$\xi^{\alpha}_{(h)}A_{\alpha}\nabla_{\mu}\omega = \mathcal{O}(u) \tag{6}$$

should be satisfied for horizon generating vectors $\tilde{\xi}^{\mu}_{(h)}$ to behave in the same manner as the Killing vector $\xi^{\mu}_{(h)}$.

Fortunately, however, the condition Eq.(6) is automatically satisfied on the horizon of a non-extreme black hole. This is because the horizon of a non-extreme black hole is bifurcate and the Killing vector $\xi^{\mu}_{(h)}$ vanishes on the bifurcation surface. Furthermore, we can show that $\xi^{\alpha}_{(h)}A_{\alpha}$ is constant along the horizon as $\mathcal{L}_{\xi_{(h)}}\xi^{\alpha}_{(h)}A_{\alpha} = \mathcal{O}(u)$. Thus, we see that

$$\xi^{\alpha}_{(h)}A_{\alpha} = \mathcal{O}(u), \tag{7}$$

holds on the horizon of a non-extreme black hole, and so does Eq.(6). In contrast, Eq.(7) is not necessarily satisfied on the horizon of an extreme black hole, since an extreme black hole does not possess a bifurcation surface. While it is possible to impose a boundary condition that imitates a non-extreme black hole as

$$\xi^{\mu}_{(h)}A^{I}_{\mu} = \mathcal{O}(u)\ , \tag{8}$$

we have in general

$$\xi^{\mu}_{(h)}A^{II}_{\mu} = \mathcal{O}(1)\ , \tag{9}$$

for a regular gauge. Notice that the gauge A^{II}_{μ} respects the particular geometric feature of an extreme black hole, i.e., the generators of the horizon are complete and hence there does not exist a bifurcation surface.

If we choose the gauge A^{I}_{μ}, Eq.(6) is satisfied and the function ω is allowed to be arbitrary, as in the non-extreme case. On the other hand, when the gauge A^{II}_{μ} is chosen and then $\xi^{\mu}_{(h)}A^{II}_{\mu}$ does not necessarily

vanish, we need to require $\nabla_\mu \omega = 0$ on the horizon for Eq.(6) to be satisfied. In the latter case, the function ω must be constant on the horizon, and hence only the exact Killing vector $\xi^\mu_{(h)}$ is allowed as horizon generating vectors. Other vectors that could be horizon generating vectors if ω were arbitrary are not allowed to be horizon generating vectors when we choose the gauge A^{II}_μ. Consequently, the only possible asymptotic Killing horizon is the exact Killing horizon, which indicates that the horizon is not degenerate when the gauge A^{II}_μ is chosen. In contrast, when we choose the gauge A^{I}_μ, the horizon of an extreme black hole is degenerate to the same amount as a non-extreme black hole, since all asymptotic Killing horizons allowed in the non-extreme case are asymptotic Killing horizons also in the extreme case.

Although we have not proven that the degeneracy of a Killing horizon is responsible for black hole entropy, it is interesting to speculate that it is true. Since an extreme black hole is degenerate to the same extent as a non-extreme black hole when the gauge A^{I}_μ is chosen, we see that an extreme black hole will carry the same amount of entropy as a non-extreme black hole does. On the other hand, if we choose the gauge A^{II}_μ, the entropy of an extreme black hole will vanish because there is no degeneracy. Therefore, two different results on the entropy of an extreme black hole are possible, depending on how we set the behavior of the electromagnetic field on the horizon. It is the same as that of a non-extreme black hole if we require the electromagnetic field to behave similarly to a non-extreme black hole, while it vanishes when we respect the particular geometric feature of an extreme black hole. Recall here that the analysis in string theory shows that the entropy of an extreme black hole is proportional to its area as non-extreme black holes[9], while it is shown to vanish based on the Euclidean approach due to the particular geometry of an extreme black hole[10]. We thus see that the speculation that the degeneracy of a Killing horizon is responsible for black hole entropy is consistent both with string theory and the Euclidean approach. Since the discrepancy between string theory and the Euclidean approach, both of which seem reliable, should be resolved by quantum theory of gravity in a unified manner, it is remarkable that the degeneracy of a Killing horizon can describe both of them at a single stroke. Then, this provides another evidence that the degeneracy of a Killing horizon is responsible for black hole entropy.

4 Summary and Discussion

By focusing only on the local geometric features of a Killing horizon, where we simply replaced the Killing equation by the asymptotic Killing equation, we have shown that a Killing horizon is degenerate in general. There exist infinitely many asymptotic Killing horizons, which have the same local geometric properties as a Killing horizon. We also discussed that this degeneracy will be removed by quantum effects, and hence it will describe quantum statistical degrees of freedom of a black hole. This result holds universally on an arbitrary Killing horizon. We then focused on Kerr-Newman black holes and analyzed how the electromagnetic field is incorporated into the notion of asymptotic Killing horizons. As a result, we found that the entropy of an extreme black hole can either be zero or be the same as a non-extreme black hole, when we speculate that the degeneracy of a Killing horizons is responsible for black hole entropy. This result is consistent with both string theory and the Euclidean approach to black hole thermodynamics. Thus, we expect that the degeneracy of a Killing horizons is responsible for black hole entropy. Quantum theoretical analyses in the future are necessary in order to prove that this is indeed the case.

The behavior of the degeneracy of an extreme black hole has been derived by choosing a gauge of the electromagnetic field that is "constant" on the horizon, as given by Eq.(4). If we did not impose this condition on the electromagnetic field and allowed arbitrary gauges, any asymptotic Killing horizons were possible even in the extreme case. However, Eq.(4) is naturally required when we demand that transformations between asymptotic Killing horizons, which are generated by the asymptotic symmetries in the spacetime, are well defined also in the phase space. These transformations in the phase space are generated by conserved charges through the Poisson brackets. On the other hand, these conserved charges are defined as derivatives in the phase space, and hence we need to impose a boundary condition on the field variables for the conserved charges to be integrable. By analyzing the integrability condition[11], we can show that the most natural boundary condition is $\delta g_{\mu\nu} = \mathcal{O}(u)$ and $\delta A_\mu = \nabla_\mu \chi + \mathcal{O}(u)$, where δ denotes derivatives of the field variables in the phase space, to which $\mathcal{L}_{\xi_{(h)}}$ belongs. Thus, the behavior of the degeneracy of an extreme black hole presented here is indeed based on the requirement that the well-defined phase space associated with the asymptotic symmetries exists.

Once the phase space is well defined, we can analyze the Poisson brackets algebra between the conserved charges. By following the method in Ref.[8], it is proven that the Poisson brackets algebra includes the Virasoro sub-algebra, which generates position-dependent translations along the null direction on the horizon. However, it turns out that the central charge of the algebra vanishes, as in Ref.[8]. Then, the direct application of Cardy's formula similar to Ref.[1] would give the vanishing entropy of a black hole. However, we emphasize that use of Cardy's formula is just one of methods and that it has not even been justified completely. Physical aspects of Cardy's formula in the present case has not been clarified yet, either. It is important to understand physical processes that give rise to a non-vanishing central charge and identify the Hilbert space associated with those physical processes. In particular, it will not be inevitable to analyze effects relevant to quantum and thermal fluctuations of the horizon. It is worth pointing out that the integrability condition of the conserved charges in the phase space is not compatible with a flux of the charge across the horizon. This is the case even when we consider a dynamically evolving horizon. Thus, we cannot incorporate Hawking radiation into the present framework, which is crucial for the thermal aspect of a black hole. In the case of a Killing horizon (stationary horizon), this fact will imply that possible fluctuations of the horizon resulting from charge fluxes across the horizon due to quantum and thermal processes are not included in the phase space of the present framework. Then, from the point of view of obtaining the Virasoro algebra with the desirable form of the central charge compatibly with string theory, it will be also important to investigate quantum and thermal fluctuations of asymptotic Killing horizons.

References

[1] A. Strominger, JHEP **02**, 009 (1998).

[2] S. Carlip, Phys. Rev. Lett. **82**, 2828 (1999).

[3] S. Carlip, Class. Quantum Grav. **16**, 3327 (1999).

[4] M.-I. Park, Nucl. Phys. **B634**, 339 (2002).

[5] S. Silva, Class. Quantum Grav. **19**, 3947 (2002).

[6] S. Carlip, Phys. Rev. Lett. **88**.

[7] O. Dreyer, A. Ghosh and J. Wisniewski, Class. Quantum. Grav. **18**, 1929 (2001).

[8] J. Koga, Phys. Rev. D **64**, 124012 (2001).

[9] A. Strominger and C. Vafa, Phys. Lett. **B379**, 99 (1996); see, for review, G. T. Horowitz, preprint gr-qc/9604051.

[10] S. W. Hawking, G. T. Horowitz and S. F. Ross, Phys. Rev. D **51**, 4302 (1995); C. Teitelboim, Phys. Rev. D **51**, 4315 (1995).

[11] R. M. Wald and A. Zoupas, Phys. Rev. D **61**, 084027 (2000).

Toward determining the primordial spectrum from WMAP data

Noriyuki Kogo,[1] Makoto Matsumiya,[2] Misao Sasaki,[3] and Jun'ichi Yokoyama[4]

Department of Earth and Space Sience, Graduate School of Science, Osaka University, Toyonaka 560-0043, Japan

Abstract

Highly precise data of the CMB temperature fluctuations were released by the WMAP team in February, 2003. Using their data, the recently developed "cosmic inversion" method makes it possible to reconstruct the primordial spectrum without any assumption on its functional form. In this talk, we report the result of testing the cosmic inversion method for data that contain observational errors at the level of WMAP. We performed a Monte Carlo simulation, and resulting errors in the reconstructed primordial spectra were about $20 \sim 30\%$.

1 Introduction

The cosmic microwave background (CMB) gives us wealth information about the early universe. The Wilkinson Microwave Anisotropy Probe (WMAP) satellite [1] has made a map of the temperature fluctuations of the CMB radiation with much higher resolution, sensitivity, and accuracy than COBE. The first data by WMAP were released in February, 2003. On the analysis of the CMB anisotropy, most of the past analyses of observational data assumed a power-law primordial spectrum as predicted by a standard inflation model. However, the primordial spectrum should be determined by observations, that is, we should reconstruct the primordial spectrum as an arbitrary function from the CMB anisotropy.

We investigate how accurately the primordial spectrum can be determined by the "cosmic inversion" method proposed by [5], [6], taking accout of the observational errors of WMAP, under the assumption of a spatially flat universe with an adiabatic initial condition.

2 Inversion method

The CMB anisotropy is quantified by the angular correlation function defined as

$$C(\theta) \equiv \left\langle \frac{\delta T}{T}(\hat{\mathbf{n}}_1)\frac{\delta T}{T}(\hat{\mathbf{n}}_2) \right\rangle = \sum_{\ell=0}^{\infty} \frac{2\ell+1}{4\pi} C_\ell P_\ell(\cos\theta), \quad \cos\theta = \hat{\mathbf{n}}_1 \cdot \hat{\mathbf{n}}_2 , \tag{1}$$

where $(\delta T/T)(\hat{\mathbf{n}})$ is the temperature fluctuation in the direction $\hat{\mathbf{n}}$ and C_ℓ is the angular power spectrum. The angular scale and the multipole are related by $\theta \approx \pi/\ell$.

The Boltzmann equation for the temperature fluctuations in Fourier space, $\Theta(\eta, k)$ can be transformed into the following integral form under the tight coupling approximation [3].

$$(\Theta + \Psi)(\eta_0, k, \mu) = \int_0^{\eta_0} d\eta \left\{ [\Theta_0 + \Psi - i\mu\Theta_1]\mathcal{V}(\eta) + (\dot{\Psi} - \dot{\Phi})e^{-\tau(\eta)} \right\} e^{ik\mu(\eta-\eta_0)}, \tag{2}$$

where $\mu = \hat{\mathbf{k}} \cdot \hat{\mathbf{n}}$, k is the comoving wavenumber, overdots denote derivatives with respect to the conformal time η, its present value is η_0, Ψ and Φ are the Newton potential and the spatial curvature perturbation respectively, and

$$\mathcal{V}(\eta) \equiv \dot{\tau} e^{-\tau(\eta)}, \quad \tau(\eta) \equiv \int_\eta^{\eta_0} \dot{\tau} d\eta, \tag{3}$$

[1] E-mail:kogo@vega.ess.sci.osaka-u.ac.jp
[2] E-mail:matumiya@vega.ess.sci.osaka-u.ac.jp
[3] E-mail:misao@vega.ess.sci.osaka-u.ac.jp
[4] E-mail:yokoyama@vega.ess.sci.osaka-u.ac.jp

are the visibility and the optical depth for Thomson scattering, respectively. If we assume that the recombination occurs instantaneously,

$$\mathcal{V}(\eta) \approx \delta(\eta - \eta_*), \quad e^{-\tau(\eta)} \approx \theta(\eta - \eta_*), \tag{4}$$

where η_* is the recombination time when the visibility is maximum.

Actually, recombination continues for a finite period. Therefore, in order to include this effect, we approximate Eq. (2) as

$$(\Theta + \Psi)(\eta_0, k, \mu) \approx \int_{\eta_{*\rm start}}^{\eta_{*\rm end}} d\eta \left\{ [\Theta_0 + \Psi - i\mu\Theta_1]\mathcal{V}(\eta) + (\dot{\Psi} - \dot{\Phi})e^{-\tau(\eta)} \right\} e^{-ik\mu d}, \tag{5}$$

where $\eta_{*\rm start}$ and $\eta_{*\rm end}$ are the time when the recombination starts and ends respectively. Here, we introduce the transfer functions $f(k)$ and $g(k)$ defined by

$$\int_{\eta_{*\rm start}}^{\eta_{*\rm end}} d\eta \left[(\Theta_0 + \Psi)(\eta, k)\mathcal{V}(\eta) + (\dot{\Psi} - \dot{\Phi})(\eta, k)e^{-\tau(\eta)} \right] \equiv f(k)\Phi(0, \mathbf{k}), \tag{6}$$

$$\int_{\eta_{*\rm start}}^{\eta_{*\rm end}} d\eta\, \Theta_1(\eta, k)\mathcal{V}(\eta) \equiv g(k)\Phi(0, \mathbf{k}). \tag{7}$$

The transfer functions are obtained numerically from the evolution equations for the perturbation. We decompose the temperature fluctuations into multipole moments,

$$\Theta(\eta, k, \mu) = \sum_{\ell=0}^{\infty} (-i)^\ell \Theta_\ell(\eta, k) P_\ell(\mu). \tag{8}$$

Then, we find

$$\Theta_\ell^{\rm app}(\eta_0, k) = (2\ell + 1)\left[f(k) j_\ell(kd) + g(k) j_\ell'(kd) \right] \Phi(0, \mathbf{k}). \tag{9}$$

The angular power spectrum is expressed as

$$\frac{2\ell + 1}{4\pi} C_\ell = \frac{1}{2\pi^2} \int_0^\infty \frac{dk}{k} \frac{k^3 \langle |\Theta_\ell(\eta_0, k)|^2 \rangle}{2\ell + 1}. \tag{10}$$

Putting Eq. (9) into Eq. (10), we obtain the approximated angular power spectrum.

Here, we define r by

$$r = 2d \sin\frac{\theta}{2}. \tag{11}$$

Then, our approximation gives rise to a one-to-one correspondence between the CMB anisotropy and the perturbation variables on the last scattering surface. Using Eq. (1) and the relation

$$\sum_{\ell=0}^{\infty} (2\ell + 1) P_\ell(\cos\theta) {j_\ell}^2(kd) = \frac{\sin kr}{kr}, \tag{12}$$

the angular correlation function is given by

$$\begin{aligned} C^{\rm app}(r) &= \frac{1}{2\pi^2} \int_0^\infty dk\, k^2 P(k) \left[f^2(k) + f(k)g(k) \frac{r}{kd} \frac{\partial}{\partial r} \right. \\ &\quad \left. + \frac{g^2(k)}{k^2} \left\{ \left(-\frac{1}{r} + \frac{r}{4d^2} \right) \frac{\partial}{\partial r} + \left(\frac{r}{2d} \right)^2 \frac{\partial^2}{\partial r^2} \right\} \right] \frac{\sin kr}{kr} \\ &= \frac{1}{2\pi^2} \int_0^\infty dk\, k^2 P(k) \left[f^2(k) \frac{\sin kr}{kr} + \frac{g^2(k)}{k^2 r^2} \left(\frac{\sin kr}{kr} - \cos kr \right) \right. \\ &\quad \left. + \frac{f(k)g(k)}{kd} \left(-\frac{\sin kr}{kr} + \cos kr \right) + \frac{g^2(k)}{4k^2 d^2} \left(\frac{\sin kr}{kr} - \cos kr - kr \sin kr \right) \right], \end{aligned} \tag{13}$$

where the primordial spectrum $P(k)$ is defined for Φ,

$$P(k) \equiv \langle |\Phi(0,\mathbf{k})|^2 \rangle . \tag{14}$$

In the small scale limit $r \ll d$,

$$\begin{aligned} r^3 C^{\rm app}(r) &= \frac{1}{2\pi^2}\int_0^\infty dk\, P(k)\left[f^2(k)kr^2\sin kr - g^2(k)r\cos kr + \frac{g^2(k)}{k}\sin kr\right] \\ &= \frac{1}{2\pi^2}\int_0^\infty dk\left[-\frac{\partial^2}{\partial k^2}\{kf^2(k)P(k)\} + \frac{\partial}{\partial k}\{g^2(k)P(k)\} + \frac{g^2(k)}{k}P(k)\right]\sin kr. \end{aligned} \tag{15}$$

Defining

$$\tilde{C}(r) \equiv \frac{1}{r}\frac{\partial}{\partial r}\{r^3 C(r)\}, \tag{16}$$

and using the Fourier sine transformation formula, we obtain a first order differential equation in which the source term contains the information of the angular correlation function [5],

$$-k^2 f^2(k)P'(k) + \left[-2k^2 f(k)f'(k) + kg^2(k)\right]P(k) = 4\pi\int_0^\infty dr\,\tilde{C}^{\rm app}(r)\sin kr \equiv S(k). \tag{17}$$

Because $f(k)$ and $g(k)$ are oscillatory functions, the equation has singularities which are zero points of $f(k)$. These singularities cause difficulties in solving it numerically. However, if we assume that $P'(k)$ is finite, we can determine the value of $P(k)$ at these points as

$$P(k_s) = \frac{S(k_s)}{k_s\, g^2(k_s)}, \quad \text{for} \quad f(k_s) = 0. \tag{18}$$

Using these values as boundary conditions, we can solve the differential equation.

But the approximated angular power spectrum, $C_\ell^{\rm app}$, is different from the exact one, $C_\ell^{\rm ex}$, obtained by a full numerical calculation such as CMBFAST [2]. The errors caused by the approximation are as large as about 30%. Fortunately, however, we empirically find that the ratio

$$b_\ell \equiv \frac{C_\ell^{\rm ex}}{C_\ell^{\rm app}}, \tag{19}$$

is almost independent of $P(k)$. Therefore, assuming the cosmological parameters are known, we can calculate this ratio for a fiducial (power-law) $P(k)$, and use $C_\ell^{\rm obs}/b_\ell^{\rm fid} \approx C_\ell^{\rm app}$ instead of $C_\ell^{\rm obs}$ as the source of the differential equation. Then, we can reconstruct a $P(k)$ with much higher accuracy by iteration [6], provided that the observational errors are sufficiently small.

Observational errors in the angular power spectrum are analytically estimated as [4]

$$\Delta C_\ell = \sqrt{\frac{2}{(2\ell+1)f_{\rm sky}}}\left(C_\ell^{\rm real} + 4\pi\frac{\sigma_{\rm pix}^2}{N_{\rm pix}}e^{\ell^2\sigma_{\rm beam}^2}\right), \tag{20}$$

where $f_{\rm sky}$ is the sky coverage, $N_{\rm pix}$ is the number of pixels, $\sigma_{\rm pix}$ is the error per pixel, $\sigma_{\rm beam}$ is the beam size, and $C_\ell^{\rm real}$ is the real power spectrum. The error is mainly duo to "cosmic variance" at small ℓ, and due to the detecter noise at large ℓ. We assume that the number of data points is 18 ($\ell_{\rm min} = 52$, $\ell_{\rm max} = 902$, $\Delta\ell = 50$) and the errors are given by Eq. (20) with the parameters of WMAP ($f_{\rm sky} = 1$, $N_{\rm pix} = 1.4 \times 10^6$, $\sigma_{\rm pix} = 35\,\mu$K, $\sigma_{\rm beam} = 0.23^\circ$) at each ℓ. These errors are about $5 \sim 10\%$.

With these parameters, we perform a Monte Carlo simulation to reconstruct $P(k)$ from $C_\ell^{\rm obs}$. We generate random numbers with the Gaussian distribution at each data point ℓ and interpolate between them. Then, solving the differential equation (17), we reconstruct $P(k)$'s from 100 realizations. Finally, we estimate the mean and the variance of the reconstructed $P(k)$ at each k.

We must mention that the present analysis is not based on the iterative method [6]. If the observational errors were sufficiently small, it would be possible to iterate the procedure to make $P(k)$ for each realization more accurate. However, in the present case, because of relatively large errors at each data point of ℓ, the iteration did not converge. Hence, we decided not to apply the iterative method. Thus the final result contains not only the effect of observational errors but also that due to our approximation. This is a shortcoming of the present method that needs to be improved.

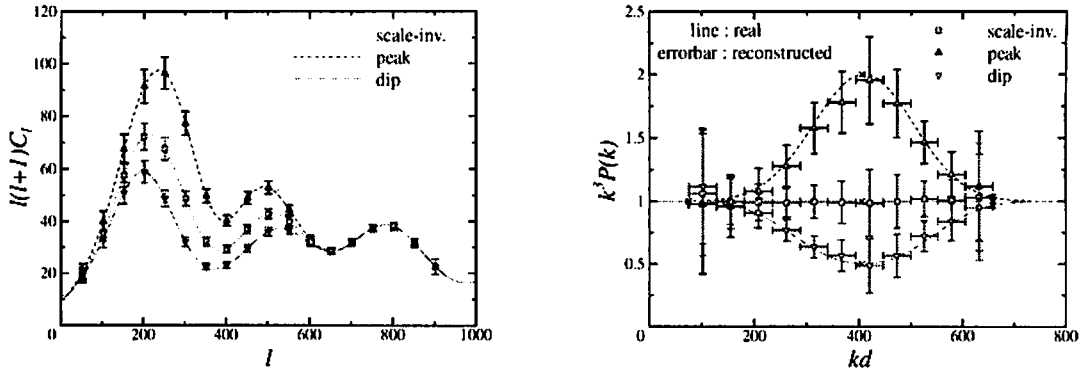


Figure 1: Left panel shows the angular power spectra and assumed data points with error bars for scale-invariant (dotted line and squares), peaked (dashed line and triangles), and dipped (dash dotted line and reverse triangles) primordial specta. Right panel shows the assumed (each line) and reconstructed (each points with error bars) primordial spectra, assuming the cosmological parameters are known. The horizontal axes are related by $\ell \approx kd$.

3 Results

We investigated the cases of scale-invariant, peaked, and dipped primordial spectra. We set the cosmological parameters $H_0 = 70$, $\Omega_b = 0.03$, $\Omega_\Lambda = 0.7$ and assumed a flat universe. We assumed these parameters are known. The resulting errors in the reconstructed $P(k)$ were about $20 \sim 30\%$ in all cases. Interestingly, although our calculation contains systematic errors due to the approximation we made as pointed out in the above, the mean of all the reconstructed $P(k)$ turns out to agree very well with the actual $P(k)$. As a result, we find it easy to discriminate the spectra for these three cases from each other.

We also investigated the effect of varying the cosmological parameters from assumed values when the spectrum is scale-invariant. We can see that the reconstructed $P(k)$ becomes negative in some cases, such as the case $H_0 = 60$, $\Omega_b = 0.05$, $\Omega_\Lambda = 0.8$. Thus, with our method, the cosmological parameters can be constrained severely under the condition that $P(k)$ must be positive.

4 Summary

We have tested our inversion method in the case when there are observational errors at the level of WMAP. For 18 data points in ℓ-space with $\Delta\ell = 50$, we find our method is capable of reproducing the primordial spectrum with about $20 \sim 30\%$ dispersion, while the errors in the mean of the reconstructed spectra are found to be order of magnitude smaller. This indicates that using every data point of ℓ, the errors in the final result can be reduced substantially. Also, we showed the possibility that the cosmological parameters can be constrained severely by our method.

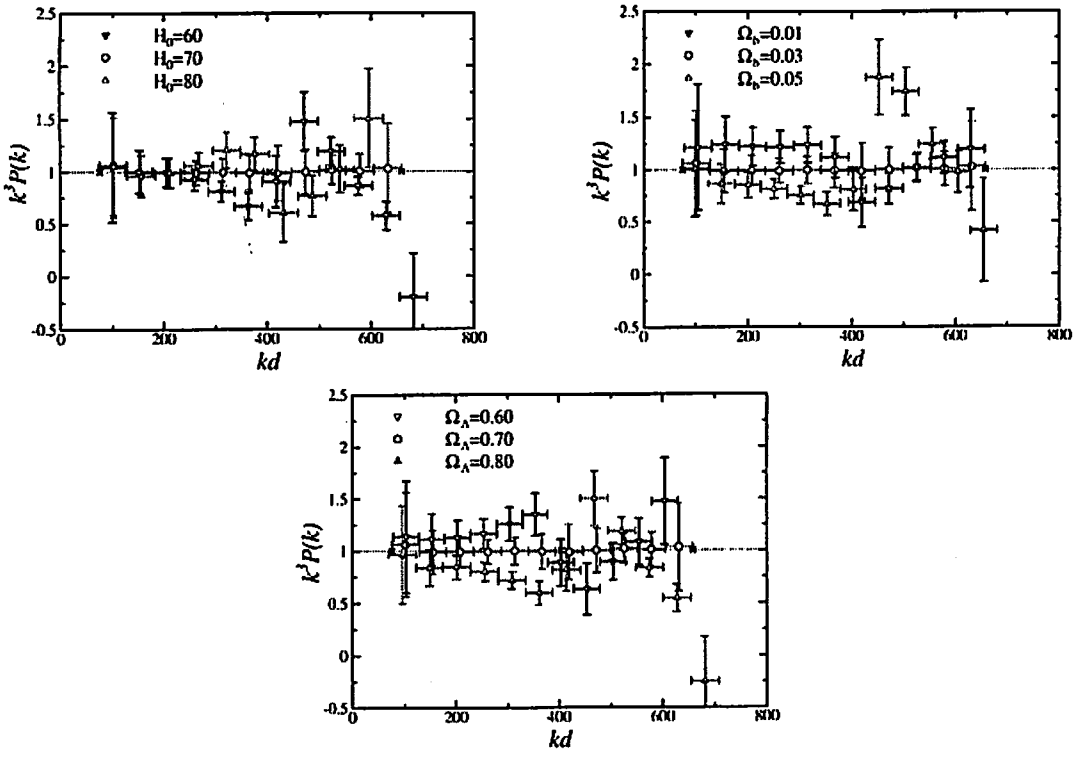


Figure 2: These panels show the variations of the reconstructed primordial spectra when the cosmological parameters are varied from the assumed values. The assumed cosmological parameters are $H_0 = 70$, $\Omega_b = 0.03$, $\Omega_\Lambda = 0.7$ for a flat universe with a scale-invariant spectrum.

References

[1] http://map.gsfc.nasa.gov/

[2] http://www.physics.nyu.edu/matiasz/CMBFAST/cmbfast.html

[3] W. Hu and N. Sugiyama, Astrophys. J. 444, 489 (1995)

[4] L. Knox, Phys. Rev. D 52, 4307 (1995)

[5] M. Matsumiya, M. Sasaki, and J. Yokoyama, Phys. Rev. D 65, 083007 (2002)

[6] M. Matsumiya, M. Sasaki, and J. Yokoyama, astro-ph/0210365 (2002)

Quark star RX J1856.5-3754 and its mass

Kazunori Kohri[1]

Research Center for the Early Universe (RESCEU), School of Science, University of Tokyo. Tokyo 113-0033, Japan

Abstract

The possibility that RX J1856.5-3754 is a compact star whose radiation radius is 3.8-8.2 km was suggested by recent deep Chandra LETG+HRC-S observations. If we assume that RX J1856.5-3754 is a pure quark star, we obtain an upper limit on its mass for various sets of the bag-model parameters. [1]

1 Introduction

These days Drake et al.[2] reported that the deep Chandra LETG+HRC-S observations of a soft X-ray source RX J1856.5-3754 provide the X-ray spectrum well represented by a blackbody of temperature $T = 61.2 \pm 1.0$ eV, and the data contain neither evidence for spectral features nor pulsation. They argued that the derived interstellar medium neutral hydrogen column density is $N_H = (0.8\text{-}1.1) \times 10^{20}$ cm^{-2}, which, together with the recent HST parallax analyses, allows them to estimate the distance, D, to RX J1856.5-3754 to be 111-170 pc. Combining this range of D with the blackbody fit leads to the radiation radius $R_\infty = 3.8\text{-}8.2$ km, which is smaller than typical neutron star radii and thus suggests that the X-ray source may be a quark star.

Earlier workers[3, 4] calculated the mass-radius relations of pure quark stars from several kinds of the equation of state (EOS) of quark matter, and compared the results with the constraints on the mass and radius of RX J1856.5-3754 derived from the inferred radiation radius. In this framework, the relation between the mass of RX J1856.5-3754 and the EOS remains to be clarified in detail. Further systematic investigations allowing for uncertainties in the EOS are needed

In this talk we consider the EOS of quark matter in the space of the parameters characterizing the bag model, and investigate the question of how massive the possible quark star can be given the inferred radiation radius. We use natural units in which $\hbar = c = k_B = 1$.

2 Upper limit on the mass of the possible quark star

We can straightforwardly compute the mass-radius relations of quark stars in the bag model [1]. The results for $B^{1/4} = 145, 200$ MeV, $m_s = 0, 150, 300$ MeV, and $\alpha_c = 0.6$ are plotted in Figs. 1 and 2.

According to the analysis of the deep Chandra LETG+HRC-S observation of RX J1856.5-3754 by Drake et al.,[2] the X-ray spectrum is well represented by a blackbody of the temperature $T = 61.2 \pm 1.0$ eV, and the X-ray luminosity is $L_X \simeq 6 \times 10^{31} (D/140 \text{ pc})^2$ erg s^{-1}.[2] Then, one has a relation between the luminosity and the temperature, $L_X = 4\pi R_\infty^2 \left(\pi^2/60 T^4\right)$, with the radiation radius R_∞ given by

$$R_\infty = \frac{R}{\sqrt{1 - \dfrac{2GM}{R}}}. \tag{1}$$

The factor $1/\sqrt{1 - 2GM/R}$ represents the redshift effect in the strong gravitational field. Namely from the observational data of R_∞ we can obtain informations about the radius and the mass of the star.

We plot the contours of the mass upper limit $M_{\rm up}$ in the space of the parameters $B^{1/4}$ and m_s in Fig. 3, calculated for $\alpha_c = 0, 0.3, 0.6, 0.9$. From this figure, we find that the contours are peaked around $B^{1/4} \sim 200$ MeV.

[1] E-mail: kohri@resceu.s.u-tokyo.ac.jp

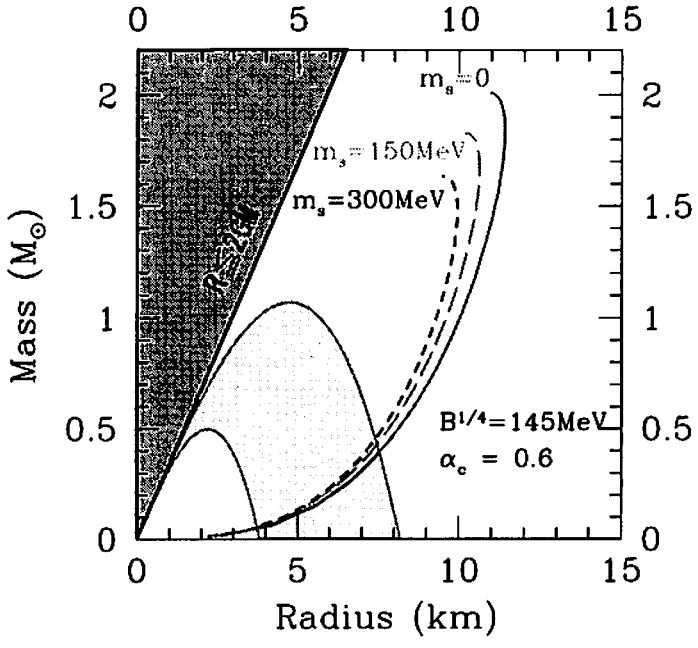


Figure 1: Mass-radius relations of pure quark stars, calculated for $\alpha_c = 0.6$ and $B^{1/4} = 145$ MeV. The dashed, long dashed, and solid lines are the results for $m_s = 300, 150, 0$ MeV, respectively. The light shadowed region is allowed by the inferred radiation radius, $R_\infty = 3.8$–8.2 km, of RX J1856.5−3754. The dark shadowed region is excluded by the fact that R should be larger than $2GM$.

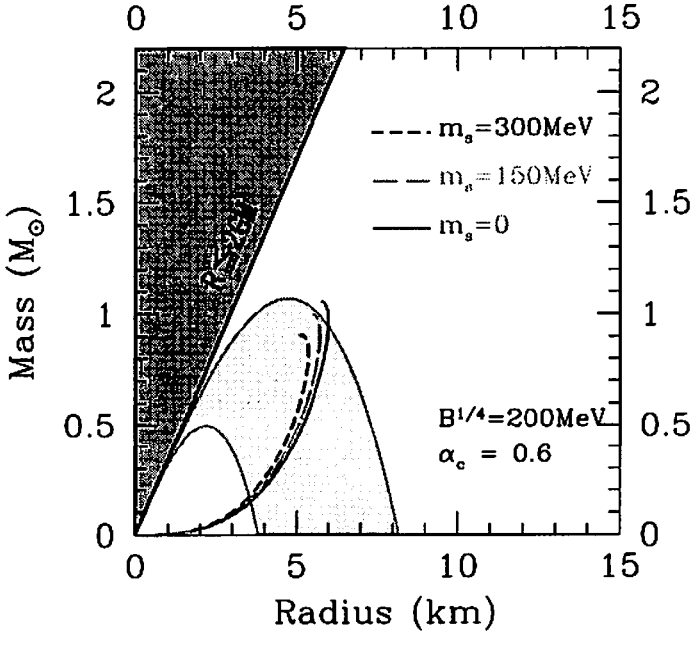


Figure 2: Same as Fig. 1 except for $B^{1/4} = 200$ MeV.

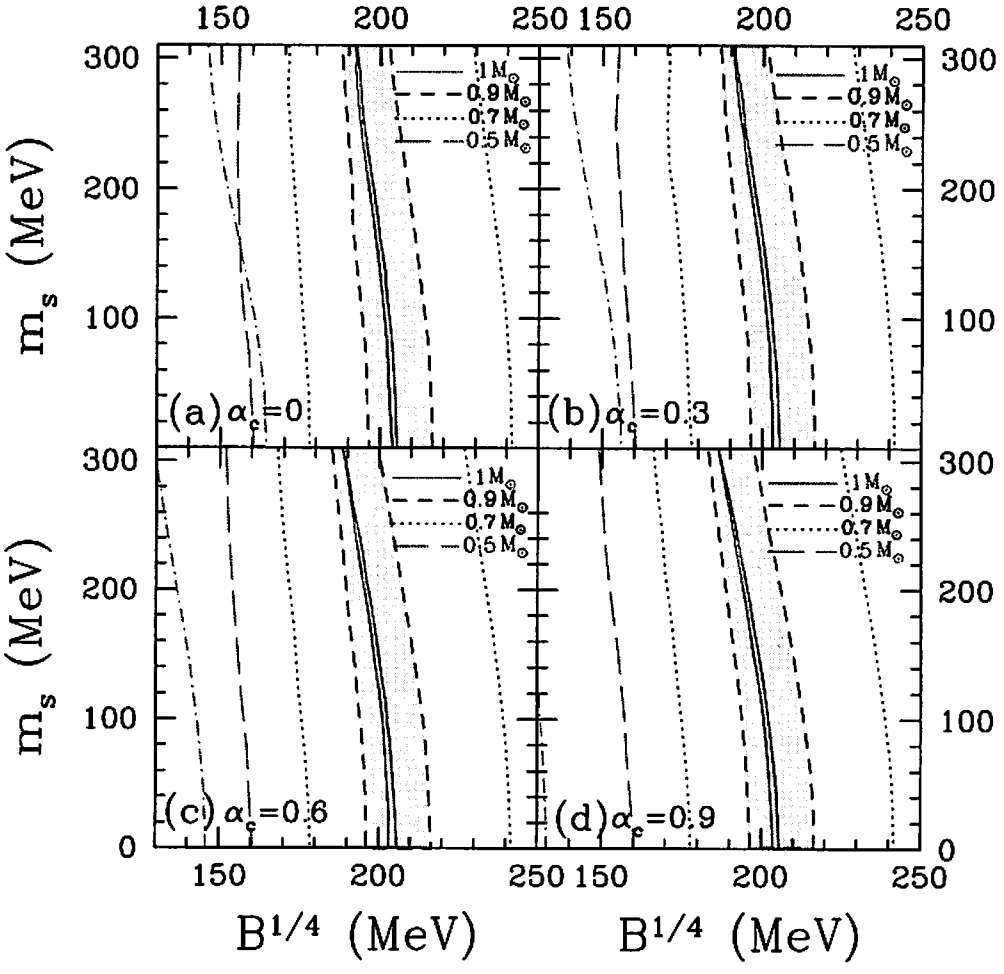


Figure 3: Contours of the mass upper limit, $M_{\rm up}$, allowed by the inferred radiation radius of the soft X-ray source RX J1856.5-3754 on the $B^{1/4}$ versus m_s plane, calculated for (a) α_c= 0, (b) 0.3, (c) 0.6, and (d) 0.9. In each panel the contours of $M_{\rm up} = 1M_\odot$ (solid lines), $M_{\rm up} = 0.9M_\odot$ (dashed lines), $M_{\rm up} = 0.7M_\odot$ (dotted lines), and $M_{\rm up} = 0.5M_\odot$ (long dashed lines) are included. For reference, we denote by dot-dashed lines the boundary below which strange matter is absolutely stable at zero pressure (for details, see Fig. 1 in Farhi and Jaffe [5]).

3 Conclusions

In this talk we have discussed the mass-radius relations of pure quark stars for various sets of the bag-model parameters, and by assuming that RX J1856.5−3754 is a pure quark star, we have obtained an upper limit on its mass, which is of order 0.5–$1M_{\odot}$. The present systematic analysis essentially covers the previous analyses utilizing the EOS models based on perturbation theory[6, 7] and finite-temperature lattice data.[8]

On the other hand, formation of quark stars is another important problem. If quark stars of masses smaller than $\sim 1M_{\odot}$ are converted from neutron stars having canonical masses of order $1.4M_{\odot}$, material in a neutron star should be partly ejected out of the star and partly changed into quark matter. Thus, possible scenarios of formation of low-mass quark stars (some of which were discussed in Refs. [9] and [10]) depend inevitably on the initial and final configuration of the star.

References

[1] K. Kohri, K. Iida, and K. Sato, astro-ph/0210259.

[2] J.J. Drake et al., Astrophys. J. **572** (2002), 996.

[3] A.R. Prasanna and S. Ray, astro-ph/0205343.

[4] D. Gondek-Rosinska, W. Kluzniak and N. Stergioulas, astro-ph/0206470.

[5] E. Farhi and R.L. Jaffe, Phys. Rev. D **30** (1984), 2379.

[6] E.S. Fraga, R.D. Pisarski and J. Schaffner-Bielich, Phys. Rev. D **63** (2001), 121702(R).

[7] J.O. Andersen and M. Strickland, Phys. Rev. D **66** (2002), 105001.

[8] A. Peshier, B. Kämpfer and G. Soff, hep-ph/0106090.

[9] R. Ouyed, J. Dey and M. Dey, Astron. Astrophys. **390** (2002), L39.

[10] T. Nakamura, astro-ph/0205526.

wormhole construction and enlargement by impulsive radiation

Hiroko Koyama,[1]

National Astronomical Observatory of Japan, Mitaka, Tokyo 153-8902, Japan

Sean A. Hayward[2] Sung-Won Kim[3]

Department of Science Education, Ewha Womans University, Seoul 120-750, Korea

Abstract

The dynamical behavior of traversable wormholes and black holes under impulsive radiation is studied in an exactly soluble dilaton gravity model. Simple solutions are presented where a traversable wormhole is constructed from a black hole, or the throat of a wormhole is stably enlarged or reduced. These solutions illustrate the basic operating principles needed to construct similar analytic solutions in full Einstein gravity.

1 Introduction

Wormholes are tunnels through space-time, linking otherwise separated regions of a single universe, or bridges joining two different universes. Since traversable wormholes were introduced by Morris and Thorne [1] as theoretically allowable geometries in Einstein gravity, wormholes have been pursued as an attractive research topic involving the possibility of rapid interstellar travel and even time machines [2]. The properties of Morris-Thorne wormholes in static cases have been studied in detail [1, 2] and it is known more generally that a negative-energy source is necessary for traversable wormholes to exist [3, 4, 5, 6]. Assuming such a source, there are interesting and practical problems of clarifying the dynamical nature of wormholes, such as how to construct a traversable wormhole and how to enlarge the throat enough to enable human beings to pass through it.

Not long ago, a unified framework for black holes and traversable wormholes was proposed [5], indicating that they are dynamically interconvertible when the trapping horizons locally characterizing them [5, 6, 8, 7] bifurcate or merge. This theory was first concretely confirmed in an exactly soluble model, CGHS two-dimensional dilaton gravity [9, 10] with an additional negative-energy scalar field to support wormholes [11], then in standard Einstein gravity numerically [12]. In seeking analytic solutions in full Einstein gravity, we have found that exact solutions seem to be difficult except in the idealization of impulsive radiation, where the radiation is concentrated so as to deliver finite energy and momentum in an instant. In this paper we construct some of the simplest models of dynamic wormhole processes by employing impulsive radiation in a generalized dilaton gravity model, specifically wormhole construction from a black hole, wormhole operation by energy balance and wormhole enlargement or reduction. Although self-inflating wormholes were recently discovered numerically [12], to date there have been no concrete examples of stable wormhole enlargement.

In this paper we consider the generalized CGHS two-dimensional dilaton gravity [9, 11] to construct the model of dynamical wormhole. We construct solutions describing the construction of a wormhole from a black hole in Sec. 2. In 3, we study processes to change the throat radius of the wormhole by controlling impulsive radiation. The final section is devoted to summary.

[1]E-mail:hiroko.koyama@nao.ac.jp
[2]E-mail:hayward@mm.ewha.ac.kr
[3]E-mail:sungwon@mm.ewha.ac.kr

2 construction of a wormhole from a black hole

We study how to construct a traversable wormhole from a black hole by irradiating it with negative energy. The CGHS two-dimensional dilaton gravity [9] is generalized by the action [11]

$$\int_S \mu \left[e^{-2\phi} \left(R + 4(\nabla\phi)^2 + 4\lambda^2 \right) - \frac{1}{2}(\nabla f)^2 + \frac{1}{2}(\nabla g)^2 \right] \tag{1}$$

where S is a 2-manifold, μ, R and ∇ are the area form, Ricci scalar and covariant derivative of a Lorentz 2-metric on S, λ represents a negative cosmological constant, ϕ is a scalar dilaton field, f is a Klein-Gordon field representing matter and g is a ghost Klein-Gordon field. The last term is added to the CGHS action in order that g provides the negative energy densities needed to support a wormhole [1, 2, 5, 3, 4, 6].

Although a similar idea has been studied in [11], now we present a simpler solution involving impulsive radiation, which is a preliminary to construct an analytic solution in four-dimensional Einstein gravity. We consider a CGHS black hole subjected to impulsive ghost radiation at some positive value x_0 of the Kruskal-like coordinates $x^\pm$, with energy density chosen in order to close up the future trapped region by merging its trapping horizons, followed by the constant irradiation needed to maintain the static wormhole:

$$\rho_\pm = -4\lambda^2 x_0 \delta(x^\pm - x_0) - 4\lambda^2 \Theta(x^\pm - x_0) \tag{2}$$

where Θ is the unit Heaviside step function and δ the Dirac (delta-function) distribution. Assuming a black hole of mass m in the initial region, we obtain the solution

$$\begin{aligned} r &= 2m - 4\lambda^2 x^+ x^- + 2\lambda^2 (x^{+2} - x_0{}^2)\Theta(x^+ - x_0) \\ &\quad + 2\lambda^2 (x^{-2} - x_0{}^2)\Theta(x^- - x_0). \end{aligned} \tag{3}$$

The solution in the final region $x^\pm > x_0$ can be recognized as an HKL wormhole [11]. In more detail, the trapping horizons

$$0 = \partial_\pm r = 4\lambda^2 \left(x^\pm \Theta(x^\pm - x_0) - x^\mp \right) \tag{4}$$

are located at

$$\begin{cases} x^\mp = 0, & x^\pm < x_0 \\ x^+ = x^-, & x^\pm > x_0. \end{cases} \tag{5}$$

and their radii are

$$r_0 = \begin{cases} 2m, & x^\pm < x_0 \\ 2m - 4\lambda^2 x_0^2, & x^\pm > x_0. \end{cases} \tag{6}$$

as depicted in Fig.1. In this solution the throat radius $a = 2m - 4\lambda^2 x_0^2$ of the wormhole is smaller than the horizon radius $2m$ of the initial black hole. Thus we require $2\lambda^2 x_0^2 < m$ in order that a wormhole is constructed. The results are similar to the previous solution [11], except that here the trapping horizons move discontinuously rather than continuously, a well-known feature under infinitesimally thin mass shells [13]. This is a general feature of the solutions presented in this article, basically stemming from the fact that the field equations or Einstein equations relate $\partial_\pm \partial_\pm r$ to the energy densities $\rho_\pm$, delta-function $\rho_\pm$ causing discontinuous $\partial_\pm r$.

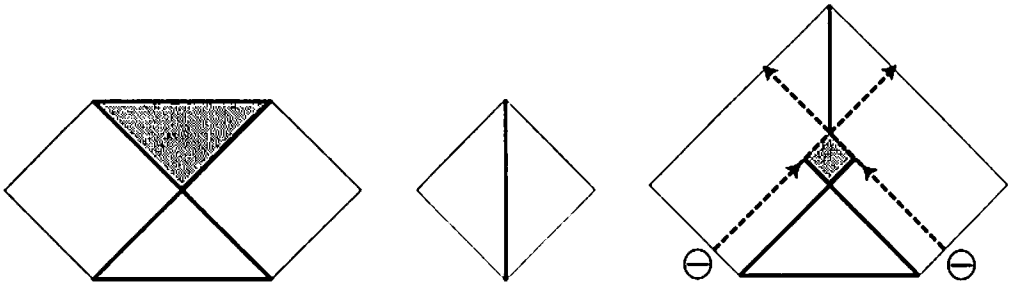


Figure 1: Penrose diagrams of (i) a CGHS black hole and (ii) an HKL traversable wormhole. The bold lines represent the trapping horizons. (iii) An HKL wormhole is constructed from a CGHS black hole by irradiating with impulsive negative-energy radiation, represented by dashed lines. The bold lines represent the trapping horizons and the shaded region consists of future trapped surfaces.

A recently discovered four-dimensional wormhole solution [14] can be similarly constructed from a Schwarzschild black hole in full Einstein gravity [16]. By the time reverse, we can also obtain a picture where a wormhole collapses into a black hole by beaming in impulsive radiation at the moment of switching off the supporting ghost radiation. In this case, the horizon radius of the black hole is larger than the throat radius of the initial wormhole. We obtain the sudden collapse case [11] again without the impulsive radiation and $x_0 = 0$.

3 wormhole enlargement and reduction

Now we construct solutions to enlarge the throat by beaming in impulsive radiation symmetrically from both universes. We give two solutions, a simple one which is difficult to generalize to full Einstein gravity, and a more complex one which can be so generalized. The first example is a symmetrized version of that of the previous section:

$$\rho_\pm = -4\lambda^2 - \beta^2\delta(x^\pm - x_0) + \beta^2\delta(x^\pm - x_1). \tag{7}$$

Assuming a wormhole with initial throat radius a, we obtain the solution

$$\begin{aligned} r = {} & a + 2\lambda^2(x^+ - x^-)^2 + \beta^2(x^+ - x_0)\Theta(x^+ - x_0) \\ & + \beta^2(x^- - x_0)\Theta(x^- - x_0) - \beta^2(x^+ - x_1)\Theta(x^+ - x_1) \\ & - \beta^2(x^- - x_1)\Theta(x^- - x_1). \end{aligned} \tag{8}$$

This also describes an HKL wormhole in the final region $x^\pm > x_1$. The initial and final wormhole regions have throats $\partial_+ r = \partial_- r = 0$ at $x^+ = x^-$, with radii

$$r_0 = \begin{cases} a & x^\pm < x_0 \\ a + 2\beta^2(x_1 - x_0) & x^\pm > x_1 \end{cases} \tag{9}$$

respectively. Then the wormhole is enlarged if $x_1 > x_0$, so that the negative-energy radiation precedes the positive-energy radiation. Again, the final formation of a static wormhole is dependent on the additional radiation having equal and opposite energies $\pm\beta^2$. For a slow burst of duration $x_1 - x_0 > \beta^2/4\lambda^2$, the wormhole mouths $\partial_\pm r = 0$ are shifted so that the oppositely moving positive-energy impulses intersect them, while for a rapid burst of duration $x_1 - x_0 < \beta^2/4\lambda^2$, the mouths enclose the entire middle region $x_0 < x^\pm < x_1$ between the impulses, Fig. 2.

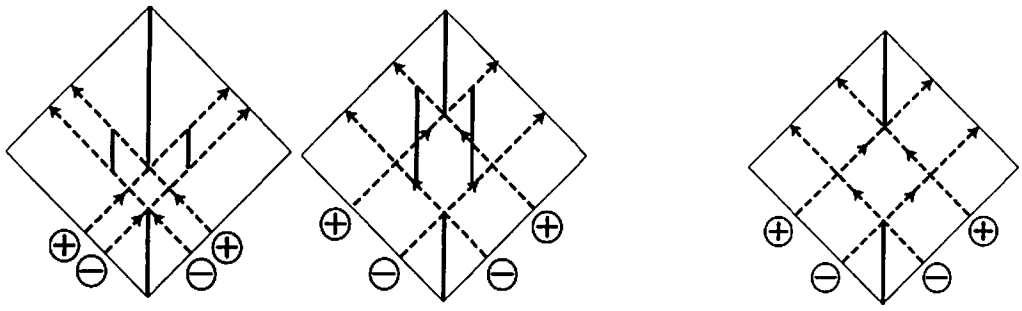


Figure 2: wormhole enlargement process by symmetric operation of impulsive radiation, keeping the non-impulsive radiation constant. Both wormhole mouths are shifted out, then back again, opening and closing a region of past trapped surfaces, shaded for a rapid burst (i) and a slow burst (ii). wormhole enlargement process by symmetric operation of impulsive radiation, with negative energy followed by positive energy. The non-impulsive radiation is switched off between the impulses. Then the middle shaded region is vacuum and consists of past trapped surfaces under the conditions given in the text.

In full Einstein gravity, we wish to patch together Schwarzschild, static-wormhole and Vaidya regions. However, the four-dimensional analogue of the middle region in the above example is not known analytically. So for the second example, we switch off the non-impulsive radiation between the impulses and switch it back on afterwards, so that the middle region is vacuum:

$$\begin{aligned} \rho_\pm &= -4\lambda^2\Theta(x_0 - x^\pm) - \beta^2\delta(x^\pm - x_0) + \alpha^2\delta(x^\pm - x_1) \\ &\quad -4\lambda^2\Theta(x^\pm - x_1). \end{aligned} \tag{10}$$

Now we want the initial and final regions $x^\pm < x_0$ and $x^\pm > x_1$ to be HKL wormholes and the middle region $x_0 < x^\pm < x_1$ to be part of a CGHS white hole in the usual coordinates, Fig. 2. Then by solving the field equations we find the relations

$$x_0 = -\frac{\beta^2}{4\lambda^2} \qquad x_1 = -\frac{\alpha^2}{4\lambda^2}. \tag{11}$$

Note that $x_0 < x_1 < 0$, so that $\alpha^2 < \beta^2$, meaning that the positive-energy impulsive radiation does not completely balance the negative-energy impulsive radiation, since some negative energy has already been removed. The difference $\alpha^2 - \beta^2 = -4\lambda^2(x_1 - x_0)$ equals the missing energy $\int_{x_0}^{x_1} \rho_\pm dx^\pm$. Assuming the throat radius a of the initial wormhole, we obtain the solution

$$r = \begin{cases} a + 2\lambda^2(x^+ - x^-)^2, & x^\pm < x_0 \\ a + \frac{\beta^4}{4\lambda^2} - 4\lambda^2 x^+ x^-, & x_0 < x^\pm < x_1 \\ a + 4\lambda^2(x_0^2 - x_1^2) + 2\lambda^2(x^+ - x^-)^2, & x_1 < x^\pm. \end{cases} \tag{12}$$

The wormhole throats are at $x^+ = x^-$ with radii

$$r_0 = \begin{cases} a, & x^\pm < x_0 \\ a + 4\lambda^2(x_0^2 - x_1^2), & x_1 < x^\pm \end{cases} \tag{13}$$

respectively. Thus the throat radius of the final wormhole is larger than that of the initial one, Fig. 2.

Combining with the results from the previous section, we have confirmed that the radius of the wormhole throat is enlarged when a region of past trapped surfaces is opened and closed between the initial and final static wormholes, by bifurcating and merging the wormhole mouths, defined as trapping horizons. In addition, the solution just presented is one of the simplest where the wormhole is enlarged, in the sense that each relevant region is part of either a static black hole, a static wormhole or a pure-radiation region, joined at null boundaries, which is also possible in full Einstein gravity [16].

4 summary

In this paper we have used an exactly soluble dilaton gravity model to study wormhole dynamics under impulsive radiation, finding solutions where a wormhole is created from a black hole or the throat radius of a wormhole is enlarged or reduced. Where the solutions consist of black-hole, static-wormhole and pure-radiation regions matched along null boundaries, we can succeed to construct similar analytic solutions in full Einstein gravity, though the analytical details are much more complex [16].

The recipe to enlarge the wormhole is to cause the wormhole mouths to bifurcate, opening up a region of past trapped surfaces, then merge again, by adding additional negative energy followed by compensating positive energy. The general proof involves the first and second laws of wormhole dynamics and is a future important work in the unified framework for black-hole and wormhole dynamics [5]. Basically, the second law determines whether the area increases or decreases, and the first law quantifies it in terms of the energy supplied and work done.

The results in this paper also suggest the possibility to create a traversable wormhole with a large throat in principle, if we can control negative-energy matter. Self-inflating wormholes were discovered recently [12], but the present solutions are the first to describe stable wormhole enlargement. Clarifying the dynamical behavior of wormholes is a quite attractive subject, since the cosmic short-cuts and time travel usually considered as science fiction are thereby closer to being realized.

acknowledgements HK was supported in part by grant R01-2000-00015 from KOSEF, SAH by Korea Research Foundation grant KRF-2001-015-DP0095, and SWK by Korea Research Foundation grant KRF-2000-041-D00128.

References

[1] M S Morris and K S Thorne, Am. J. Phys. **56**, 395 (1988).

[2] M Visser, Lorentzian Wormholes: from Einstein to Hawking (AIP Press 1995).

[3] D Hochberg and M Visser, Phys. Rev. **D58**, 044021 (1998).

[4] D Hochberg and M Visser, Phys. Rev. Lett. **81**, 746 (1998).

[5] S A Hayward, Int. J. Mod. Phys. **D8**, 373 (1999).

[6] D Ida and S A Hayward, Phys. Lett. **A260**, 175 (1999).

[7] S A Hayward, Phys. Rev. **D49**, 6467 (1994).

[8] S A Hayward, Class. Quantum Grav. **15**, 3147 (1998).

[9] C Callan, S Giddings, J Harvey and A Strominger, Phys. Rev. D **45**, R1005 (1992).

[10] S A Hayward, Class. Quantum Grav. **10**, 985 (1993).

[11] S A Hayward, S-W Kim and H Lee, Phys. Rev. **D65**, 064003 (2002).

[12] H Shinkai and S A Hayward, Phys. Rev. **D66**, 044005 (2002).

[13] S W Hawking & G F R Ellis, The large scale structure of space-time, Cambridge University Press (1973).

[14] S A Hayward, Phys. Rev. **D65**, 124016 (2002).

[15] H Koyama, S A Hayward and S-W Kim, gr-qc/0212106

[16] H Koyama, S A Hayward and S-W Kim, in preparation.

Low energy effective theory for a two branes system – Covariant curvature formulation –

Kazuya Koyama,[1] Tetsuya Shiromizu[2]

[1] *Department of Physics, The University of Tokyo, Tokyo 113-0033, Japan,*
[2] *Advanced Research Institute for Science and Engineering, Waseda University, Tokyo 169-8555, Japan,*
[2] *Department of Physics, Tokyo Institute of Technology, Tokyo 152-8551, Japan*

Abstract

We derive the low energy effective theory for a two brane system solving the bulk geometry formally in the covariant curvature formalism developed by Shiromizu, Maeda and Sasaki. As expected, the effective theory looks like a Einstein-scalar system. Using this theory we can discuss the cosmology and non-linear gravity at low energy scales.

1 Introduction

The recent progress in superstring theory provides us the new picture of the universe, so called brane world, where our universe is like domain wall in higher dimensional spacetimes. The matter is confined on the 3-brane. The simplest model was proposed by Randall and Sundrum[1, 2]. In their model the bulk spacetimes is 5-dimensional anti-deSitter spacetimes and the brane is four dimensional Minkowski spacetimes. Their first model(RS1) gives us the geometrical solution to the gauge hierarchy problem. The RS1 model consists of two brane, the positive and negative tension branes. For the gauge hierarchy problem, it is supposed that the visible brane where we are is the negative tension one. The linealised theory has been carefully investigated in [3, 4]. As a result, it is turned out that the gravity on the brane looks like the scalar-tensor gravity. However, we have no successful analysis on the non-linear aspect of the gravity except for the second order perturbation[5]. Recently there are impressive progress[6, 7, 8] on this issue. In Ref. [7], the effective equation is derived at the low energy scale.

Based on the paper [9], we re-derive the effective theory for a two brane system which was obtained by Kanno and Soda[7] in the metric based approach. On the other hand, our approach is based on the covariant curvature formalism[10, 11]. As seen later, our derivation is much simpler than the metric based approach and straightforward. The covariant curvature formalism gives us a gravitational equation on the branes. For RS2 models which consists of the single brane, this is powerful approach to look at the full view of the brane world. Indeed, it was easy to see that the Newton gravity is recovered at the low energy. The approach, however, is not regarded as so useful for RS1 models. We shall show this is not true. This is the main purpose in this paper. For simplicity, we will not address the stabilisation issue of two branes(radion stabilisation problems).

2 Covariant curvature formalism

We employ the following metric form[3]

$$ds^2 = e^{2\phi(y,x)}dy^2 + q_{\mu\nu}(y,x)dx^\mu dx^\nu. \tag{1}$$

In the above it is supposed that the positive and negative tension branes are located at $y = 0$ and $y = y_0$, respectively. The proper distance between two branes is given by $d_0(x) = \int_0^{y_0} dy e^{\phi(y,x)}$. $q_{\mu\nu}(y,x)$ is the induced metric of y =constant hypersurfaces.

[1] E-mail:kazuya@utap.phys.s.u-tokyo.ac.jp
[2] E-mail:shiromizu@th.phys.titech.ac.jp
[3] In Ref [7] it is assumed that $\phi(y,x)$ does not depend on y. However, as seen later, the assumption can be removed.

We follow the geometrical procedure(covariant curvature formalism) developed in Ref. [10, 11]. For simplicity, we do not include the bulk fields except for the bulk consmological constant. From the Gauss-Codacci equations, first of all, we have two key equations

$$ {}^{(4)}G^{\mu}_{\nu} = \frac{3}{\ell^2}\delta^{\mu}_{\nu} + KK^{\mu}_{\nu} - K^{\mu}_{\alpha}K^{\alpha}_{\nu} - \frac{1}{2}\delta^{\mu}_{\nu}(K^2 - K^{\alpha}_{\beta}K^{\beta}_{\alpha}) - E^{\mu}_{\nu} \tag{2} $$

and

$$ D_{\mu}K^{\mu}_{\nu} - D_{\mu}K = 0, \tag{3} $$

where D_{μ} is the covariant derivative with respect to $q_{\mu\nu}$. ℓ is the bulk curvature radius. ${}^{(4)}G_{\mu\nu}$ is the 4-dimensional Einstein tensor with respect to $q_{\mu\nu}$, $K_{\mu\nu}$ is the extrinsic curvature of y =constant hypersurfaces defined by

$$ K_{\mu\nu} = \frac{1}{2}\pounds_n q_{\mu\nu} = \nabla_{\mu}n_{\nu} + n_{\mu}D_{\nu}\phi, \tag{4} $$

where $n = e^{-\phi}\partial_y$. Here note that $a^{\mu} = n^{\nu}\nabla_{\nu}n^{\mu} = -D^{\mu}\phi(y,x)$. $E_{\mu\nu}$ is a part of the projected Weyl tensor defined by

$$ \begin{aligned} E^{\mu}_{\nu} &= {}^{(5)}C_{\mu\alpha\nu\beta}n^{\alpha}n^{\beta} \\ &= -D^{\mu}D_{\nu}\phi - D^{\mu}\phi D_{\nu}\phi - \pounds_n K^{\mu}_{\nu} - K^{\mu}_{\alpha}K^{\alpha}_{\nu} + \frac{1}{\ell^2}\delta^{\mu}_{\nu}, \end{aligned} \tag{5} $$

where ${}^{(5)}C_{\mu\nu\alpha\beta}$ is the 5-dimensional Weyl tensor.

The junction conditions on the branes are

$$ [K^{\mu}_{\nu} - \delta^{\mu}_{\nu}K]_{y=0} = -\frac{\kappa^2}{2}\left(-\sigma_1\delta^{\mu}_{\nu} + T_{1\ \nu}^{\mu}\right), \quad [K^{\mu}_{\nu} - \delta^{\mu}_{\nu}K]_{y=y_0} = \frac{\kappa^2}{2}\left(-\sigma_2\delta^{\mu}_{\nu} + T_{2\ \nu}^{\mu}\right). \tag{6} $$

$T_{1\ \nu}^{\mu}$ and $T_{2\ \nu}^{\mu}$ are the energy-momentum tensor localised on the positive and negative branes. σ_1 and σ_2 are the brane tensions. If one substitutes the above conditions to Eq (2), we might be able to derive the Einstein equation on the brane. Indeed, this was successful procedure for the single brane[10]. This is because $E_{\mu\nu}$ comes from just Kaluza-Klein modes and vanishes at the low energy[3, 10]. For the two brane systems, on the other hand, we have to carefully evaluate $E_{\mu\nu}$ due to the existence of the radion fields. Otherwise, we have a wrong prediction on the gravity on the branes. So we need the evolutional equation for $E_{\mu\nu}$ in the bulk. Even for the low energy scale, we learned from the linealised theory[3] that $E_{\mu\nu}$ is not negligible.

To evaluate $E_{\mu\nu}$ in the bulk, we derive its evolutional equation. The result is

$$ \begin{aligned} \pounds_n E_{\alpha\beta} &= D^{\mu}B_{\mu(\alpha\beta)} + K^{\mu\nu}{}^{(4)}C_{\mu\alpha\nu\beta} + 4K^{\mu}_{(\alpha}E_{\beta)\mu} - \frac{3}{2}KE_{\alpha\beta} - \frac{1}{2}q_{\alpha\beta}K^{\mu\nu}E_{\mu\nu} + 2D^{\mu}\phi B_{\mu(\alpha\beta)} \\ &\quad + 2\tilde{K}^{\mu}_{\alpha}\tilde{K}_{\mu\nu}\tilde{K}^{\nu}_{\beta} - \frac{7}{6}\tilde{K}_{\mu\nu}\tilde{K}^{\mu\nu}\tilde{K}_{\alpha\beta} - \frac{1}{2}q_{\alpha\beta}\tilde{K}_{\mu\nu}\tilde{K}^{\mu}_{\rho}\tilde{K}^{\rho\nu}, \end{aligned} \tag{7} $$

where $B_{\mu\nu\alpha} = q^{\rho}_{\mu}q^{\sigma}_{\nu}{}^{(5)}C_{\rho\sigma\alpha\beta}n^{\beta}$ and $\tilde{K}_{\mu\nu} = K_{\mu\nu} - \frac{1}{4}q_{\mu\nu}K$. Since the right-hand side contains $B_{\mu\nu\alpha}$, $K_{\mu\nu}$ and ${}^{(4)}C_{\mu\nu\alpha\beta}$, we also need their evolutional equations. After long calculation we are resulted in

$$ \begin{aligned} &\pounds_n{}^{(4)}R_{\mu\nu\alpha\beta} + 2{}^{(4)}R_{\mu\nu\rho[\alpha}K^{\rho}_{\beta]} + 2D_{[\mu}B_{|\alpha\beta|\nu]} + 2(D_{\mu}D_{[\alpha}\phi + D_{\mu}\phi D_{[\alpha}\phi)K_{\beta]\nu} \\ &\quad - 2(D_{\nu}D_{[\alpha}\phi - D_{\nu}\phi D_{[\alpha}\phi)K_{\beta]\mu} - 2B_{\alpha\beta[\mu}D_{\nu]}\phi - 2B_{\mu\nu[\alpha}D_{\beta]}\phi = 0 \end{aligned} \tag{8} $$

$$ \begin{aligned} &\pounds_n B_{\mu\nu\alpha} + 2D_{[\mu}E_{\nu]\alpha} + 2D_{[\mu}\phi E_{\nu]\alpha} - B_{\mu\nu\beta}K^{\beta}_{\alpha} + 2B_{\alpha\beta[\mu}K^{\beta}_{\nu]} \\ &\quad + ({}^{(4)}R_{\mu\nu\alpha\beta} - K_{\mu\alpha}K_{\nu\beta} + K_{\mu\beta}K_{\nu\alpha})D^{\beta}\phi = 0 \end{aligned} \tag{9} $$

and

$$ e^{-\phi}\partial_y K^{\mu}_{\nu} = -D^{\mu}D_{\nu}\phi - D^{\mu}\phi D_{\nu}\phi - K^{\mu}_{\alpha}K^{\alpha}_{\nu} + \frac{1}{\ell^2}\delta^{\mu}_{\nu} - E^{\mu}_{\nu}. \tag{10} $$

Eq (10) is just the rearrangement of Eq (5). The derivation is basically same with that in Ref [10].

The junction condition directly implies the boundary condition on the branes for $K_{\mu\nu}$ and $B_{\mu\nu\alpha}$ because of

$$ B_{\mu\nu\alpha} = 2D_{[\mu}K_{\nu]\alpha}. \tag{11} $$

3 Derivation of low energy effective theory

It is now ready to derive the low energy theory for two brane systems. To do so, as stressed in the previous section, we must know $E_{\mu\nu}$ and solve the equation for $E_{\mu\nu}$ in the bulk. By low energy we mean that the typical scale of the curvature scale(L) on the brane is much larger than the bulk curvature scale(ℓ), that is, $L \gg \ell$. The dimensionless parameter is $\epsilon = (\ell/L)^2$ which is tacitly entered into the equations below. We expand K^μ_ν and E^μ_ν as

$$K^\mu_\nu = {}^{(0)}K^\mu_\nu + {}^{(1)}K^\mu_\nu + \cdots, \quad E^\mu_\nu = {}^{(1)}E^\mu_\nu + \cdots. \tag{12}$$

3.1 0-th order

At the 0-th order, the evolutional equation which we have to solve is only one for $K_{\mu\nu}$;

$$e^{-\phi}\partial_y {}^{(0)}K^\mu_\nu = \frac{1}{\ell^2}\delta^\mu_\nu - {}^{(0)}K^\mu_\alpha {}^{(0)}K^\alpha_\nu. \tag{13}$$

And $K_{\mu\nu}$ satisfies the constraint

$$D_\mu {}^{(0)}K^\mu_\nu - D_\nu {}^{(0)}K = 0. \tag{14}$$

It is easy to see that the solution is

$${}^{(0)}K^\mu_\nu = -\frac{1}{\ell}\delta^\mu_\nu. \tag{15}$$

From the definition

$$\frac{1}{2}e^{-\phi}\partial_y {}^{(0)}q_{\mu\nu} = -\frac{1}{\ell}{}^{(0)}q_{\mu\nu}, \tag{16}$$

the metric at the 0th order becomes

$${}^{(0)}q_{\mu\nu}(y,x) = e^{-2d(y,x)/\ell}h_{\mu\nu}(x), \tag{17}$$

where $h_{\mu\nu}(x)$ is a tensor field depending on only the coordinate x on the brane and $d(y,x) = \int_0^y e^{\phi(y',x)}dy'$.

At this order the junction condition is

$$[{}^{(0)}K^\mu_\nu - \delta^\mu_\nu {}^{(0)}K]_{y=0} = \frac{\kappa^2}{2}\sigma_1\delta^\mu_\nu, \quad [{}^{(0)}K^\mu_\nu - \delta^\mu_\nu {}^{(0)}K]_{y=y_0} = -\frac{\kappa^2}{2}\sigma_2\delta^\mu_\nu. \tag{18}$$

Thus the junction condition implies the relation between the bulk curvature radius ℓ and the brane tension $\sigma_{1,2}$ as

$$\frac{1}{\ell} = \frac{1}{6}\kappa^2\sigma_1 = -\frac{1}{6}\kappa^2\sigma_2. \tag{19}$$

This is just the fine-tuning of Randall-Sundrum models[1, 2].

3.2 1st order

At the first order, the Riemann tensor does appear in the basic equations. So we can expect that the Einstein field equation will be able to described at this order. Indeed, the Gauss equation of Eq (2) becomes

$${}^{(4)}G^\mu_\nu = -\frac{2}{\ell}({}^{(1)}K^\mu_\nu - \delta^\mu_\nu {}^{(1)}K) - {}^{(1)}E^\mu_\nu. \tag{20}$$

The first term in the right-hand side will be easily written in terms of the energy-momentum tensor on the branes using the junction condition at this order. So the unknown tensor is ${}^{(1)}E^\mu_\nu$.

The evolutional equation which we must solve are

$$e^{-\phi}\partial_y {}^{(1)}E_{\mu\nu} = \frac{2}{\ell}{}^{(1)}E_{\mu\nu}. \tag{21}$$

and

$$e^{-\phi}\partial_y {}^{(1)}K^\mu_\nu = -(D^\mu D_\nu\phi + D^\mu\phi D_\nu\phi) + \frac{2}{\ell}{}^{(1)}K^\mu_\nu - {}^{(1)}E^\mu_\nu. \tag{22}$$

Eq (21) is easily solved as

$${}^{(1)}E_{\mu\nu} = e^{2d(y,x)/\ell}e_{\mu\nu}(x), \quad {}^{(1)}E^\mu_\nu = e^{4d(y,x)/\ell}\hat{e}^\mu_\nu(x), \tag{23}$$

where $\hat{e}^\mu_\nu(x) = h^{\mu\alpha}e_{\alpha\nu}(x)$.

Substituting the expression Eq (23) into Eq (22), we can obtain the solution for ${}^{(1)}K^\mu_\nu$ easily;

$$\begin{aligned} {}^{(1)}K^\mu_\nu(y,x) &= e^{2d/\ell}{}^{(1)}K^\mu_\nu(0,x) - \frac{\ell}{2}(1-e^{-2d/\ell}){}^{(1)}E^\mu_\nu(y,x) \\ &\quad - \left[D^\mu D_\nu d - \frac{1}{\ell}\left(D^\mu d D_\nu d - \frac{1}{2}\delta^\mu_\nu (Dd)^2\right)\right] \end{aligned} \tag{24}$$

For the comparison, note that $e_{\mu\nu}$ cannot be determined by the junction condition in the RS2 model[8, 10]. To do so we need the boundary condition near the Cauchy horizon.

3.3 Low energy effective theory for two brane systems

At the 1st order the junction condition on the positive and negative tension branes becomes

$${}^{(1)}K^\mu_\nu(0,x) - \delta^\mu_\nu {}^{(1)}K(0,x) = -\frac{\kappa^2}{2}T_1{}^\mu{}_\nu, \quad {}^{(1)}K^\mu_\nu(y_0,x) - \delta^\mu_\nu {}^{(1)}K(y_0,x) = \frac{\kappa^2}{2}T_2{}^\mu{}_\nu. \tag{25}$$

Using the above Eq (25), the Gauss equation on the negative tension brane becomes

$${}^{(4)}G^\mu_\nu = -\frac{2}{\ell}\left({}^{(1)}K^\mu_\nu(y_0,x) - \delta^\mu_\nu {}^{(1)}K(y_0,x)\right) - {}^{(1)}E^\mu_\nu(y_0,x) = -\frac{\kappa^2}{\ell}T_2{}^\mu{}_\nu - {}^{(1)}E^\mu_\nu(y_0,x). \tag{26}$$

Using the expression of Eq (24), the junction condition on the negative tension brane is written as

$$\begin{aligned} {}^{(1)}K^\mu_\nu(y_0,x) - \delta^\mu_\nu {}^{(1)}K(y_0,x) &= -\frac{\kappa^2}{2}e^{2d_0/\ell}T_1{}^\mu{}_\nu - \left(D^\mu D_\nu d_0 - D^\mu D_\nu d_0\right) \\ &\quad + \frac{1}{\ell}\left(D^\mu d_0 D_\nu d_0 + \frac{1}{2}\delta^\mu_\nu (Dd_0)^2\right) - \frac{\ell}{2}(1-e^{-2d_0/\ell}){}^{(1)}E^\mu_\nu(d_0,x) = \frac{\kappa^2}{2}T_2{}^\mu{}_\nu. \end{aligned} \tag{27}$$

In the right-hand side of the first line, we used the solution of Eq (24). The second line is just junction condition. From Eq (27), then, the tensor $e_{\mu\nu}$(and then ${}^{(1)}E_{\mu\nu}$) is completely fixed as

$$\begin{aligned} \frac{\ell}{2}(1-e^{-2d_0/\ell})e^{4d_0/\ell}\hat{e}^\mu_\nu(x) &= -\frac{\kappa^2}{2}(e^{2d_0/\ell}T_1{}^\mu{}_\nu + T_2{}^\mu{}_\nu) - \left(D^\mu D_\nu d_0 - \delta^\mu_\nu D^2 d_0\right) \\ &\quad + \frac{1}{\ell}\left(D^\mu d_0 D_\nu d_0 + \frac{1}{2}\delta^\mu_\nu (Dd_0)^2\right). \end{aligned} \tag{28}$$

The trace of Eq (28) gives the equation for d_0 because e^μ_ν is traceless. In general the radion field is massive. Substituting Eq (28) into the Gauss equation at the first order, we can obtain the effective equation on the branes. On the negative tension brane, we have

$$\begin{aligned} {}^{(4)}G^\mu_\nu &= \frac{\kappa^2}{\ell}\frac{1}{\Phi}T_2{}^\mu{}_\nu + \frac{\kappa^2}{\ell}\frac{(1+\Phi)^2}{\Phi}T_1{}^\mu{}_\nu + \frac{1}{\Phi}(D^\mu D_\nu\Phi - \delta^\mu_\nu D^2\Phi) \\ &\quad + \frac{\omega(\Phi)}{\Phi^2}\left(D^\mu\Phi D_\nu\Phi - \frac{1}{2}\delta^\mu_\nu (D\Phi)^2\right), \end{aligned} \tag{29}$$

where $\Phi = e^{2d_0/\ell} - 1$ and $\omega(\Phi) = -\frac{3}{2}\frac{\Phi}{1+\Phi}$. As should be so, this is exactly same result obtained by Kanno and Soda[7]. We also derive the effective equation on the positive tension brane easily:

$$
\begin{aligned}
{}^{(4)}G^{\mu}_{\nu} &= \frac{\kappa^2}{\ell}\frac{1}{\Psi}T_1{}^{\mu}{}_{\nu} + \frac{\kappa^2}{\ell}\frac{(1-\Psi)^2}{\Psi}T_2{}^{\mu}{}_{\nu} + \frac{1}{\Psi}(\hat{D}^{\mu}\hat{D}_{\nu}\Psi - \delta^{\mu}_{\nu}\hat{D}^2\Psi) \\
&\quad + \frac{\omega(\Psi)}{\Psi^2}\left(\hat{D}^{\mu}\Psi\hat{D}_{\nu}\Psi - \frac{1}{2}\delta^{\mu}_{\nu}(\hat{D}\Psi)^2\right), \qquad (30)
\end{aligned}
$$

where $\Psi = 1 - e^{-2d_0/\ell}$, $\omega(\Psi) = \frac{3}{2}\frac{\Psi}{1-\Psi}$ and $\hat{D}$ is the covariant derivative with respect to the induced metric $h_{\mu\nu}$ on the positive tension brane.

4 Summary

In this paper we derived the gravitational equation on the branes for the two brane systems at the low energy using the covariant curvature formalism[10] and low energy expansion scheme[7, 8]. The theory obtained here is presumably applicable to the cosmology and non-linear gravity at low energy scales. What we have done here is the evaluation of $E_{\mu\nu}$ at the low energy. In Ref [10], we thought that the anti-gravity appears on the negative tension brane supposing $E_{\mu\nu}$ is negligible. However, this is not correct and $E_{\mu\nu}$ is not negligible even at the low energy.

Here we shoud comment on the difference between the study in Ref [7] and the present one. In Ref [7] $E_{\mu\nu}$ appears as the "constant of integration". Thus it is difficult to proceed the discussion while keeping the physical meaning. This is just because of the metric based approach. On the other hand, $E_{\mu\nu}$ explicitly enters into the basic equations in the covariant curvature formalism and its physical meaning is manifest. Yet, the evolutional equation for $E_{\mu\nu}$ is simple at the low energy limit.

For simplicity, we focused on the two a brane system without the radion stabilisation. If one is serious about the gauge hierarchy problem, we must assume that we are living on the negative tension brane. In this case, the gravity on the negative tension brane is scalar-tensor type and the scalar coupling is not permitted from the experimental point of view[3]. So we should reconstruct our formalism in two brane systems with the radion stabilisation mechanism. This issue is left for future study.

We are also interested in the higher order effects. We can expect that the effective theory with higher order corrections is higher-derivative type due to the non-local feature of the brane world[7, 8].

References

[1] L. Randall and R. Sundrum, Phys. Rev. Lett. **83**, 3370 (1999).

[2] L. Randall and R. Sundrum, Phys. Rev. Lett. **83**, 4690 (1999).

[3] J. Garriga and T. Tanaka, Phys. Rev. Lett. **84**, 2778 (2000).

[4] C. Charmousis, R. Gregory and V. A. Rubakov, Phys. Rev. **D62**, 067505(2000).

[5] H. Kudoh and T. Tanaka, Phys. Rev. **D65**, 104034(2002).

[6] T. Wiseman, Class. Quantum Grav. **19**, 3083(2002).

[7] S. Kanno and J. Soda, Phys. Rev. **D66**, 083506 (2002).

[8] S. Kanno and J. Soda, Phys. Rev. **D66**, 043526(2002).

[9] T. Shiromizu and K. Koyama, Phys. Rev. **D**, to be appeared.

[10] T. Shiromizu, K. Maeda and M. Sasaki, Phys. Rev. **D62**, 024012 (2000); M. Sasaki, T. Shiromizu and K. Maeda, Phys. Rev. **D62**, 024008 (2000).

[11] R. Maartens, Phys. Rev. **D62**, 084023(2000).

Volume expansion of a Swiss-cheese universe

Hiroshi Kozaki,[1] Ken-ichi Nakao[2]

Department of Physics, Graduate School of Science, Osaka City University, Osaka 558-8585, Japan

Abstract

In order to investigate the effect of inhomogeneities on the volume expansion of the universe, we study modified Swiss-cheese universe model. Since this model is an exact solution of Einstein equations, we can get an insight into non-linear dynamics of inhomogeneous universe from it. If the inhomogeneities can not be treated as small perturbations, the volume expansion of the universe depends on the type of fluctuations. Although the volume expansion rate approaches to the background value asymptotically, the volume itself can be finally arbitrarily smaller than the background one and can be larger than that of the background but there is an upper bound on it.

1 INTRODUCTION

The standard Big Bang scenario is based on an assumption of the homogeneous and isotropic distribution of matter and radiation. This assumption then leads to the Robertson-Walker spacetime geometry and the Friedmann-Lemaître (FL) universe model through the Einstein equations. This model has succeeded in explaining various important observational facts.

The cosmic microwave background radiation (CMBR) gives a strong observational basis for the assumption of homogeneity and isotropy of our universe by its highly isotropic distribution together with the Copernican principle; we know that our universe was highly isotropic and homogeneous at least on the last scattering surface where CMBR comes from. Hence, in the early stage of our universe, the linear perturbation analysis in the FL universe model is a powerful tool to investigate the dynamical evolution of our universe.

In order to perform the perturbation analysis, we need an appropriate background universe model, i.e., information of the Hubble parameter, the density parameter and further the equation of state of the matter, radiation and so on, in the real universe. To fix the background universe, we use the observational data in the neighborhood of our galaxy. Especially the Hubble parameter is determined from the data about the distance-redshift relation within $100h^{-1}$Mpc except for the type Ia supernova. However, the universe in a region within $100h^{-1}$Mpc is highly inhomogeneous and hence there are non-trivial prescriptions to identify the present inhomogeneous universe to the homogeneous and isotropic FL universe model. If those procedure are not appropriate, we might miss finding the correct background universe.

It is often stated that the spatially averaged observational data in the vicinity of our galaxy are recognized as those of the background FL universe model. The Hubble parameter determined by the observed distance-redshift relation in our universe is regarded as the expansion rate of the volume of the region co-moving to matter. There are several researches for the effects of inhomogeneities on the volume expansion of the universe. Especially, Nambu applied the renormalization group method to the second order cosmological perturbation theory and claimed that the expansion of the dust filled universe is decelerated by the inhomogeneities[1].

In the real universe, this back reaction effect might be very small. However in order to get deeper insight into the dynamics of the inhomogeneous universe, we will consider the situation in which the back reaction of the inhomogeneities seems to be effective. For this purpose, we consider the Swiss-cheese (SC) universe model and investigate the volume expansion in it. The original Swiss-cheese universe model is constructed by choosing non-overlapping spherical regions in the background homogeneous and

[1]E-mail:furusaki@sci.osaka-cu.ac.jp
[2]E-mail:knakao@sci.osaka-cu.ac.jp

isotropic dust filled universe and then replacing these regions by the Schwarzschild spacetime whose mass parameter is identical with the "gravitational" mass of the dust fluid in the removed region. On the other hand, in this article, we consider a modified version; we first remove spherical regions from the homogeneous and isotropic dust filled universe and then fill these regions with spherically symmetric but inhomogeneous dust balls. A spherically symmetric inhomogeneous dust ball is described by the Lemaître-Tolman-Bondi (LTB) solution which is an exact solution of the Einstein equations, and hence by this procedure, we obtain an exact solution of Einstein equations, which represents an inhomogeneous universe. Using this solution, we can study non-linear effects of inhomogeneities on the volume expansion of the universe without use of perturbation analysis.

In the LTB solution, shell crossing singularities are generic. Since the LTB solution is no longer valid after the occurrence of the shell crossing, we need to change the treatment if it occurs. As a crude approximation to describe the dynamics after the shell crossing, we adopt a model in which the shell crossing region is replaced by a spherical dust shell.

We use the units in which $c = G = 1$ throughout the paper.

2 MODIFIED SWISS CHEESE UNIVERSE MODEL

We give a prescription to construct a modified SC (MSC) universe model. First we consider a Einstein-de Sitter (EdS) universe and then remove spherical regions from it; these removed regions should not overlap with each other. Next these regions filled with inhomogeneous dust balls with the same radii and the same gravitational mass as those of the removed homogeneous dust balls. In this MSC universe model, each inhomogeneous region is described by the Lemaître-Tolman-Bondi (LTB) solution which is an exact solution of Einstein equations.

LTB solution describes the dust filled spherically symmetric spacetime. Adopting synchronous and co-moving coordinate system, the line element is written as

$$\begin{aligned} ds^2 &= -dt^2 + \gamma_{ij}dx^i dx^j \\ &= -dt^2 + \frac{Y'^2(t,\chi)}{1-\chi^2 k(\chi)}d\chi^2 + Y^2(t,\chi)(d\theta^2 + \sin^2\theta d\varphi^2), \end{aligned} \tag{1}$$

where the prime $'$ denotes the differentiation with respect to the radial coordinate χ. $k(\chi)$ is an arbitrary function and determines the dynamics of the solution. The areal radius $Y(t,\chi)$ is determined through the Einstein equations.

For simplicity, we consider the simplest version of MSC universe models shown in fig. 1; there is only one inhomogeneous spherical region at the center in each identical cubic region Ω. We focus on only one cubic co-moving region Ω (fig. 2). We consider a following model. Assuming $0 < \chi_1 < \chi_2 < \chi_3 < \chi_{sc}$,

$$k(\chi) = \begin{cases} k_0 & \text{for } 0 \le \chi < \chi_1 \\ \dfrac{k_0}{2\chi^2}\left\{\dfrac{(\chi^2-\chi_2^2)^2}{\chi_1^2-\chi_2^2} + \chi_1^2 + \chi_2^2\right\} & \text{for } \chi_1 \le \chi < \chi_2 \\ \dfrac{k_0}{2\chi^2}(\chi_1^2+\chi_2^2) & \text{for } \chi_2 \le \chi < \chi_3 \\ \dfrac{k_0}{2\chi^2}(\chi_1^2+\chi_2^2)\left\{\left(\dfrac{\chi^2-\chi_3^2}{\chi_{sc}^2-\chi_3^2}\right)^2 - 1\right\}^2 & \text{for } \chi_3 \le \chi < \chi_{sc} \end{cases}, \tag{2}$$

where k_0 is constant.

We investigate the volume expansion rate of a cubic co-moving region Ω. The volume V is defined by

$$V(t) := \int_\Omega \sqrt{\gamma} d^3x, \tag{3}$$

where γ is the determinant of the spatial metric γ_{ij}. The volume expansion rate is defined as $\dot{V}/V$.

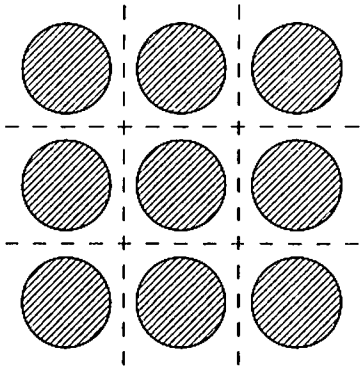


Figure 1: The MSC universe model. Each shaded region represents the inhomogeneity and is described by LTB solution.

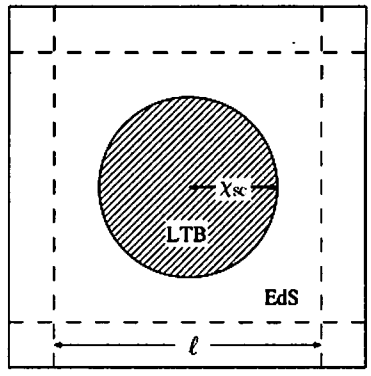


Figure 2: One cubic region Ω of the MSC universe model. ℓ and χ_{sc} are the co-moving scales of this cubic region and the inhomogeneous region respectively.

3 The Case of Non-Linear Fluctuations

In order to specify an effect due to inhomogeneity, we need a background homogeneous cubic region to be compared with an inhomogeneous one. We consider the rest mass M_R defined by

$$M_R := \int_\Omega \rho u^0 \sqrt{-g} d^3x \tag{4}$$

where g is the determinant of the metric tensor. M_R is a conserved quantity by virtue of the continuity of the rest mass density. We introduce a background as a cubic region with the same rest mass as the corresponding inhomogeneous cubic region. Note that in general, the rest mass of the dust M_R in a cubic co-moving region disagrees with that of the original EdS universe. Hence a cubic region of the original EdS universe is not background.

The rest mass density ρ_B and scale factor a_B of the background are introduced in the following manner,

$$\rho_B a_B^3 \ell^3 := M_R. \tag{5}$$

Even if we specify M_R, ρ_B and a_B are not fixed completely; we need one more condition. Here we impose a condition in which the volume $V(t)$ approaches to the volume of the background cubic region $(a_B^3(t)\ell^3)$ for $t \to 0$.

The background scale factor a_B is given by

$$a_B(t) := a\left\{1 + \frac{4\pi}{\ell^3}\int_0^{\chi_{sc}} \left(\frac{1}{\sqrt{1-\chi^2 k}} - 1\right)\chi^2 d\chi\right\}^{1/3}. \tag{6}$$

3.1 The Case of $k_0 > 0$

In this model, the volume V approaches the value much smaller than the background one, asymptotically. The volume expansion is also much different from that of the background in the intermediate stage (see fig. 3).

3.2 The Case of $k_0 < 0$

Shell crossing singularities necessarily appear in this model [2]. Before it, the volume expansion is shown in fig. 4. For $k(\chi) < 0$, background scale factor a_B cannot differ from original one very much. We plot the ratio of the volume $V(t)$ to $a^3\ell^3$ and $a_B^3\ell^3$. We find that the inhomogeneities decelerate the volume expansion before shell crossing singularity appears.

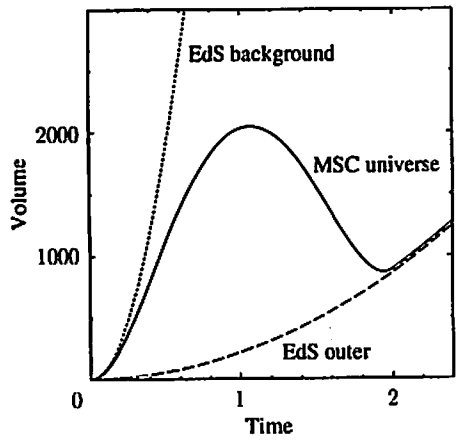


Figure 3: Volume expansion with positive $k(\chi)$. The dotted line is the temporal evolution of the co-moving volume measured by the background EdS geometry and the dashed line is that measured by the outer EdS geometry.

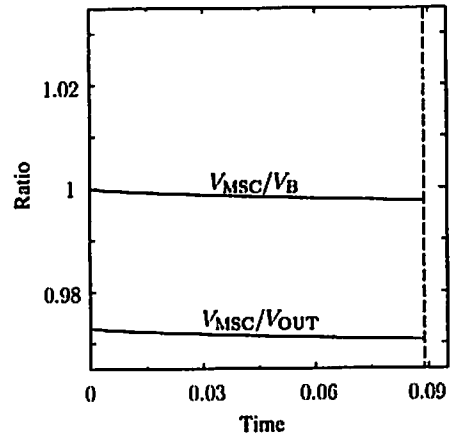


Figure 4: Temporal evolution of the ratios before shell crossing singularity appears. Dashed line corresponds to the shell crossing time. $V_{\rm MSC}$ is the volume of the co-moving cubic region Ω in modified Swiss-cheese universe. $V_{\rm B}$ is the volume of Ω measured by the background EdS geometry, i.e., $V_{\rm B} = a_{\rm B}^3 \ell^3$. $V_{\rm OUT}$ is the volume of Ω measured by the outer EdS geometry, i.e., $V_{\rm OUT} = a^3 \ell^3$.

Here, we investigate the volume expansion rate after the appearance of this shell crossing singularity. The structure formed by the shell crossing depends on what is approximated by the dust matter. In case that the dust matter is extremely cold fluid, a shock wave will form after the shell crossing. If the dust matter consists of collisionless particles, a spherical wall will form. When the width of the shock wave or of the wall is much smaller than the radius of it, we can treat the shock front or the wall as a timelike singular hypersurface. The physical property of the singular hypersurface is characterized by its surface stress-energy. We focus on the singular hypersurface generated by a trajectory of a dust shell.

In order to get an insight into the dynamics after shell crossing, we study the volume expansion of a cubic region with a spherically symmetric dust shell. The model is constructed by enclosing the interior LTB region by a spherically symmetric timelike singular hypersurface.

We consider a interior volume $\tilde{V}_{\rm in}$ normalized by the volume of the removed homogeneous dust ball in the original EdS universe,

$$\tilde{V}_{\rm in} := \frac{V_{\rm in}}{4\pi R^3/3} = \frac{3}{2}\left(\frac{t}{R}\right)^3 \left[\frac{R}{t}\sqrt{1+\left(\frac{R}{t}\right)^2} - \ln\left\{\frac{R}{t}+\sqrt{1+\left(\frac{R}{t}\right)^2}\right\}\right], \tag{7}$$

where R is the areal radius of the dust shell. $\tilde{V}_{\rm in}$ is monotonically decreasing function of R/t: it approaches to unity in the limit of $R/t \to 0$.

For sufficiently large t, the areal radius R of the dust shell becomes much smaller than the cosmological horizon scale H^{-1}. In this case, the the motion of the dust shell is well described by the Newtonian approximation. Maeda and Sato showed that for sufficiently large t, R behaves as[3]

$$R(t) \propto t^{(15+\sqrt{17})/24} \sim t^{0.797}. \tag{8}$$

Hence we find that $R/t \propto t^{-0.203} \to 0$ for $t \to \infty$. Using this result we find $\tilde{V}_{\rm in} \longrightarrow 1$ for $t \to \infty$, and hence for $t \to \infty$,

$$V \longrightarrow a^3(t)\ell^3. \tag{9}$$

This equation means that the volume expansion rate approaches to the background value asymptotically. The effect of inhomogeneities on the volume expansion rate vanishes after the dust shell becomes much

smaller than the horizon scale H^{-1}. However, as in the case of $k_0 > 0$, the volume itself is different from the background value $a_{\rm B}^3\ell^3$. By eq. (6), we find that the asymptotic value of V is larger than the background value $a_{\rm B}^3\ell^3$. However it should be noted that there is an upper limit on the asymptotic value of V. Since k can be arbitrarily small in this model, $\sqrt{1-\chi^2 k}$ can be made arbitrarily larger than unity except at $\chi = 0$ and $\chi = \chi_{\rm sc}$. Hence we obtain

$$a_{\rm B}(t) > a(t)\left(1 - \frac{4\pi}{3\ell^3}\chi_{\rm sc}^3\right)^{1/3} > a(t)\left(1 - \frac{\pi}{6}\right)^{1/3}, \tag{10}$$

where the last inequality is obtained by setting $\chi_{\rm sc} = \ell/2$. Using this inequality, we obtain

$$a_{\rm B}^3(t)\ell^3 < a^3(t)\ell^3 < \left(1 - \frac{\pi}{6}\right)^{-1} a_{\rm B}^3(t)\ell^3 \sim 2.10 \times a_{\rm B}^3(t)\ell^3. \tag{11}$$

In contrast with the case of $k_0 > 0$, the volume itself can not be so different from the background value.

4 SUMMARY AND DISCUSSION

We have investigated an effect of inhomogeneities on the volume expansion in modified Swiss-cheese universe model. We considered two cases; the inhomogeneities collapse into black holes ($k_0 > 0$), while inhomogeneities expands faster than the background volume expansion ($k_0 < 0$).

We introduced the background homogeneous universe in order to satisfy the conditions; the cubic region in the background homogeneous universe with the same rest mass have the same evolution of the volume as that of corresponding region in the modified Swiss-cheese universe in the limit of $t \to 0$.

In the case of non-linear fluctuation with $k_0 > 0$, we find that the volume expansion rate approaches to that of background universe asymptotically. Since the modified Swiss-cheese model is an exact solution of Einstein equation, we can obtain the precise behavior of the volume expansion. We set it so that for $t \to 0$, the temporal evolution agrees with background one. Then we found that for $t \to \infty$, the temporal evolution agrees with that of outer EdS universe. We can see these asymptotic behaviors analytically but we have to rely only on the numerical method to obtain the behavior of the intermediate stages. From the result of the numerical calculation (fig. 3), we found that volume expansion is decelerated by the inhomogeneities. This behavior coincides with a result obtained by Nambu. We note that his result is based on the perturbation theory but our result is not. In our highly non-linear example, the volume expansion rate becomes negative at the intermediate stage. This result may be the characteristics of the effect of non-linear fluctuations which can not be treated by the perturbation method.

In the case of $k_0 < 0$, the shell crossing singularity appears in the inhomogeneous region. In this article, we assumed that a spherical dust shell forms after the shell crossing singularity appears. We find that the inhomogeneities decelerate the volume expansion before it appears (fig. 4). This is consistent with the previous results by Nambu but the inhomogeneities cannot be treated as the perturbation of homogeneous universe. After a spherical dust shell forms, the volume expansion rate approaches to that of the background universe asymptotically. Our dust shell universe model is a crude approximation, but the asymptotic behavior ($t \to \infty$) might be free from this approximation.

We fixed the form of $k(\chi)$. Temporal evolution of the volume depends on the form of $k(\chi)$ but the asymptotic behavior may be independent of the form of $k(\chi)$.

Acknowledgements

We are grateful to colleagues in Department of Physics, Osaka City University for helpful discussions.

References

[1] Y. Nambu, Phys. Rev. **D62**, 104010 (2000).

[2] C. Hellaby and K. Lake, Astrophys. J. **290**, 381(1985),

[3] K. Maeda and H. Sato, Prog. Theor. Phys. **70**, 772 (1983).
K. Maeda and H. Sato, Prog. Theor. Phys. **70**, 1276 (1983).

Numerical Solutions of Braneworld Black Holes

Hideaki Kudoh [1]

Department of Physics, Kyoto University, Kyoto 606-8502, Japan

Abstract

We construct numerical solutions of localized black holes whose horizon radius is small compared to the bulk curvature scale, and quantitatively analyze the behavior of the black hole, focusing on the thermodynamic quantities. The shape of the small black hole exhibits a flattened geometry in the bulk, and the thermodynamic relations indicate that the localized black hole solutions show a smooth transition from five-dimensional Schwarzschild black hole, which is the solution in the limit of small horizon radius, to solutions that have thermodynamic character similar to four-dimensional Schwarzschild black hole. However, it becomes difficult to find black hole solutions as its horizon radius increases, and we could not construct large black holes whose horizon radius is greater than the bulk curvature scale.

1 Introduction

Recent developments in the scenario of large extra dimensions [1] brought us a new interest in higher dimensional black holes, since an interesting possibility of black hole production at collider was pointed out [2, 3]. There is another type of braneworld models proposed by Randall and Sundrum (RS) [4]. In these models, the geometry warped in the direction of an extra dimension is used to explain the hierarchy between TeV scale and Planck scale, and to realize four-dimensional gravity effectively on the 3-brane. Also in the context of RS models, the higher dimensional black holes may play an important roll. These so-called braneworld scenarios provide us new and interesting situations to investigate higher dimensional black holes.

For RS models, since the 3-brane has tension, it is difficult to find black hole solutions. Trivial black string solution is allowed in these models. However the black string is unstable due to Gregory-Laflamme instability. There are many discussions about black hole in this model and several authors have considered some black hole solutions. However, unfortunately, any realistic black hole solutions, which are stable and have no naked singularity, have not been known so far, and finding them is an interesting open question of nonlinear gravity in the braneworld.

Shape of black holes in the RS infinite braneworld [4] is conjectured based on the Gregory-Laflamme instability [5]. It was argued that an unstable black string will be pinched into many black holes. Besides black holes in the bulk, there will be a black hole that is localized on the 3-brane. We can imagine this as a black hole bound to a domain wall if the 3-brane is realized by a domain wall. An exact solution representing a localized black hole is known in 4D braneworld model, which we call in this paper Emparan-Horowitz-Myers (EHM) solution [6]. However the corresponding solution in the original 5D braneworld model has not been discovered. While the localization of black hole was inspired by the classical instability of black string, the anticipated dynamics of pinching off the horizon is questionable. Recently, Wiseman discovered non-uniform black string by numerical calculation [7]. The obtained solutions are likely to be unstable, but they are suggestive as a missing link between the localized black hole and the black string.

Based on Ref [9], we review and summarize the results of the paper. In the paper, the problem of black hole in the RS infinite braneworld is explored and we consider a numerical construction of black hole solution in this model. The method we use is based on a scheme developed by Wiseman [8]. Our method does not require any assumptions for the induced metric on the 3-brane, and Einstein equations can be solved numerically under the boundary conditions determined by physical requirements. We will find small black hole solutions, whose horizon radius is smaller than the AdS curvature radius, although large black hole solutions have not been discovered.

[1] E-mail:kudoh@yukawa.kyoto-u.ac.jp

2 Formulation

Let us consider the elliptic equations and constraint equations that we solve. From the five dimensional vacuum Einstein equations, we obtain nonlinear systems of equations taking "conformal gauge"

$$ds^2 = \frac{\ell^2}{z^2}\left(-T^2dt^2 + e^{2R}(dr^2+dz^2) + r^2e^{2C}d\Omega^2\right) . \tag{1}$$

Since we consider a localized black hole, polar coordinates

$$r = \rho\sin\chi, \quad z = \ell + \rho\cos\chi, \quad \xi = \chi^2, \tag{2}$$

are more convenient to impose boundary conditions. Without loss of generality, this coordinate choice allows us to set the location of the event horizon to be at $\rho = \text{const.} = \rho_h$ [8, 9]. The derived equations are reduced to the set of elliptic equations;

$$\Delta X_i = S_{X_i}(T, R, C) . \tag{3}$$

Here S_{X_i} shows the source term, and X_i means T, R, or C. Constraint equations, $\Theta_1 = 0$ and $\Theta_2 = 0$, are also obtained from remaing Einstein equations.

We perform numerical calculations for the elliptic equations using a relaxation method. The constraint equations are not explicitly solved but they are used as a check of accuracy. Before proceeding further, we discuss an important property of the constraint equations. The constraint equations multiplied some functions satisfy Cauchy-Riemann relations. They are obtained from the non-trivial components of the Bianchi identities. Assuming that equations for T, R, and C are satisfied, we obtain Cauchy-Riemann relations for them, and hence each of them satisfies Laplace equation. Therefore in principle, if $\Theta_1 = 0$ is satisfied on all boundaries and provided that Θ_2 vanishes at any one point, the two constraint equations must be solved in all places as long as the elliptic equations for T, R, and C are satisfied.

In order to solve the elliptic equations, we must specify the boundary conditions.

$\underline{\chi = 0}$ Let us first discuss boundary conditions on the symmetry axis of $r = 0(\chi = 0)$. The regularity at $r = 0$ requires

$$R = C \quad (\text{at } \xi = 0), \tag{4}$$

which determines the boundary condition for R. The axial symmetry requires that r derivative of the metric functions vanishes at $r = 0$. However, as long as we use ξ coordinate, finiteness of the derivative in this coordinate automatically guarantees the regularity because $T_{,r} \propto \sqrt{\xi}T_{,\xi}$. Hence, we adopt a free boundary condition for T and C. The values of T and C at $r = 0$ are evolved in the same way as the values at an ordinary grid point. The only difference is to use the one-sided differentiation to evaluate the first order derivatives with respect to ξ. The second order derivatives disappear at $\xi = 0$ from the Laplace operator.

$\underline{\rho = \rho_h}$ On the horizon, the Killing vector ∂_t must become null. Therefore we have

$$T = 0 \quad (\text{at } \rho = \rho_h) , \tag{5}$$

In the present gauge, the horizon is given by a constant radius, and thus we have $T_{,\xi}|_{\rho=\rho_h} = T_{,\xi\xi}|_{\rho=\rho_h} = 0$. Here we assume that metric functions and their derivatives are finite on the horizon. Note that the surface gravity on the horizon is given as

$$\kappa = e^{-R}T_{,\rho} \quad (\text{at } \rho = \rho_h) . \tag{6}$$

This condition can be used to impose a Dirichlet boundary condition for R on the horizon. For this purpose, we rewrite it as

$$R = C|_{\xi=0} + \log\left(\frac{T_{,\rho}}{T_{,\rho}|_{\xi=0}}\right) \quad (\text{at } \rho = \rho_h) , \tag{7}$$

using Eq. (4). From the zeroth law of black hole thermodynamics, and assuming the surface gravity is nonzero (non-extremal), we find that $T_{,\rho}$ must be nonzero on the horizon; $T_{,\rho} \neq 0$. Then, from the regularity on the horizon, a condition for $C_{,\rho}$ is derived as

$$C_{,\rho} = -\frac{\ell}{\rho_h z} \quad (\text{at } \rho = \rho_h)\,. \tag{8}$$

On the other hand, the condition that the expansion is zero on the horizon gives

$$(R + 2C)_{,\rho} + \frac{3\ell}{\rho_h z} = 0 \quad (\text{at } \rho = \rho_h)\,, \tag{9}$$

which guarantees the constraint equation on the horizon. In the numerical calculation, we basically impose these Neumann boundary conditions on the horizon for R and C. As a supplementary condition to improve the accuracy, we also use Eq. (7), but we do not use Eq. (6). Hence, in our calculation the surface gravity is not given by hand as a parameter.

$\chi = \pi/2$ The Israel's junction condition for the RS braneworld model gives the boundary conditions on the brane as

$$\frac{\partial_\xi T}{T} = \partial_\xi R = \partial_\xi C = -\frac{\rho}{2\ell\sqrt{\xi}}\left(1 - e^R\right) \quad \left(\text{at } \xi = (\pi/2)^2\right). \tag{10}$$

One of constraint equations is manifestly satisfied under these conditions.

$\rho \to \infty$ We must also specify asymptotic boundary conditions. For the asymptotic infinity, the boundary conditions to obtain asymptotically AdS spacetime are $T \to 1$ and $R, C \to 0$. The metric functions must smoothly approach these asymptotic values. In actual numerical calculations, these asymptotic boundary conditions are imposed at a finite, but sufficiently far region, and we must check that the solutions are insensitive to the position.

With these boundary conditions, we can solve the elliptic equations as a boundary value problem. Moreover, these boundary conditions guarantee the constraint equation Θ_1 to be satisfied on all boundaries and Θ_2 to be satisfied at least on the horizon. Hence the two constraint equations are automatically satisfied as long as the elliptic equations are exactly solved.

It should be noted that all elliptic equations, constraint equations and boundary conditions can be rewritten in terms of non-dimensional coordinates without any dimensionful parameters. Then this system of equations, and hence a black hole solution is characterized only by a single parameter

$$L = \ell/\rho_h. \tag{11}$$

In our numerical calculation, we take $\rho_h \equiv 1$ and change ℓ to specify this parameter, since we want to fix a coordinate region where numerical calculations are performed.

3 Thermodynamic quantities

The formulation outlined in the previous section indeed works well to solve the Einstein equations as a boundary value problem, using an iterative convergence scheme of relaxation method. Since the 5D Schwarzschild solution in isotropic coordinates

$$T(\rho) = \frac{\rho^2 - \rho_h^2}{\rho^2 + \rho_h^2}, \quad R(\rho) = C(\rho) = \log\left(1 + \frac{\rho_h^2}{\rho^2}\right), \tag{12}$$

is the solution in the flat background limit $\ell \to \infty$, we have used this solution as an initial guess configuration with which we start the relaxation. Some explicit examples of numerical solution are found in [9]. In this study, we restrict the numerical calculations only to small black holes that are characterized by $L > 1$. It becomes in general more difficult to find solutions as the nonlinear effects of differential equations grow. We could not keep sufficient accuracy to construct large black holes ($L \lesssim 1$) so that the calculation breaks down in the end. Thus we concentrate only on small black holes ($L > 1$), although

it is important to improve our scheme by identifying and removing the ultimate origin of numerical instabilities.

We are more interested in the deviations of the numerically obtained solutions from the 5D Schwarzschild solution. To quantify the deviations, we focus on thermodynamic quantities. The surface gravity (or temperature) is determined by Eq. (6), and the area (or entropy) of a black hole horizon is given by

$$A_5 = 2\rho_h^3 \int d\Omega \int_0^{(\pi/2)^2} d\xi \frac{\sin^2\sqrt{\xi}}{2\sqrt{\xi}} \left(\frac{\ell}{z}\right)^3 e^{R+2C}. \tag{13}$$

Here the factor 2 is due to Z_2 symmetry. The proper area of the intersection between the horizon and the brane is given by

$$A_4 = 4\pi\rho_h^2 e^{2C} \quad (\chi = \pi/2).$$

In Figures 1 we show the behavior of the relations between thermodynamic quantities. The figure gives a relation between the 4D area A_4 and the surface gravity κ taking an appropriate non-dimensional combination. In the figure the thermodynamic relations for the 4D and the 5D Schwarzschild solutions are also plotted for comparison. We observe that for large L, i.e., for very small black holes, the numerical solutions behave like the 5D Schwarzschild solution, and then as L becomes small they deviate from the 5D Schwarzschild black hole and show a tendency to behave like the 4D Schwarzschild black hole. A relation between the 5D area and the surface gravity also shows the same tendency (Figure 1). When the horizon is sufficiently small ($\kappa\ell \gg 1$), the result for the numerical solutions approximately coincide with the line expected by the 5D Schwarzschild-AdS solution. However, as the horizon radius increases, the plot points for the numerical solutions deviate from it, toward the opposite direction. In the end they cross the line for the black string.

We can compare the thermodynamic relation of the 5D localized black hole with the relation of the EHM solution in the 4D braneworld [6]. One can see a similar behavior of thermodynamic relation for $\ln\kappa\ell \gtrsim 0$, and it seems to give an insight toward extrapolating the thermodynamic relation to larger black hole solutions. However, there is a big difference between the 5D model and the 4D model. On one hand, in the case of the 5D model the metric induced on the brane for a large black hole is expected to mimic the 4D Schwarzschild metric with some small corrections. On the other hand, 3D black hole solution that corresponds to the 4D Schwarzschild metric in the 5D model does not exist. Thus we cannot naively apply the analogy of the EHM solution. Furthermore, the numerical errors of the solutions also grow along the flow of the solutions. We could not obtain sufficiently relaxed numerical solutions for $L \lesssim 1$. Hence, at present we cannot say anything definite for large black hole solutions.

4 Discussion

We have performed the numerical calculations and found non-trivial localized black hole solutions whose horizon radiuses ρ_h are small compared to the bulk curvature scale ℓ. However we could not succeed in finding black hole solutions with large horizon radius. The convergence of the relaxation method becomes slower for larger horizon radius, and we could not keep enough accuracy of computation in the end.

In the limit of small black hole, $\ell/\rho_h \to \infty$, the 5D Schwarzschild black hole is the solution. Then we are interested in the deviations of the small localized black holes from the 5D Schwarzschild black hole. To observe it by quantitative comparison, the thermodynamic quantities are calculated for these small black holes. We found that the numerically obtained solutions significantly deviate from the naive expectation based on the 5D Schwarzschild-AdS solution as its horizon radius increases (Figure 1). The comparison of the thermodynamic quantities also suggests that the numerical solutions approach to solutions whose induced metric on the brane behaves like the 4D Schwarzschild solution (Figure 1), although we could not obtain a clear evidence for it from the direct comparison of the induced metric. Moreover, we can observe the transition of the shape of the small localized black hole in the bulk [9]. The black hole tends to flatten as its horizon radius increases. This is expected due to the nature of the AdS geometry, and is also observed in the EHM solution of localized black hole in the 4D braneworld [6]. Although the EHM solution is the solution in the lower dimensions, it is interesting to compare our solution with it. We can compare the thermodynamic relation of the EHM solution with that of the 5D numerical solutions, and it show a similarity between them [9]. This observation might be suggestive, but since our calculations

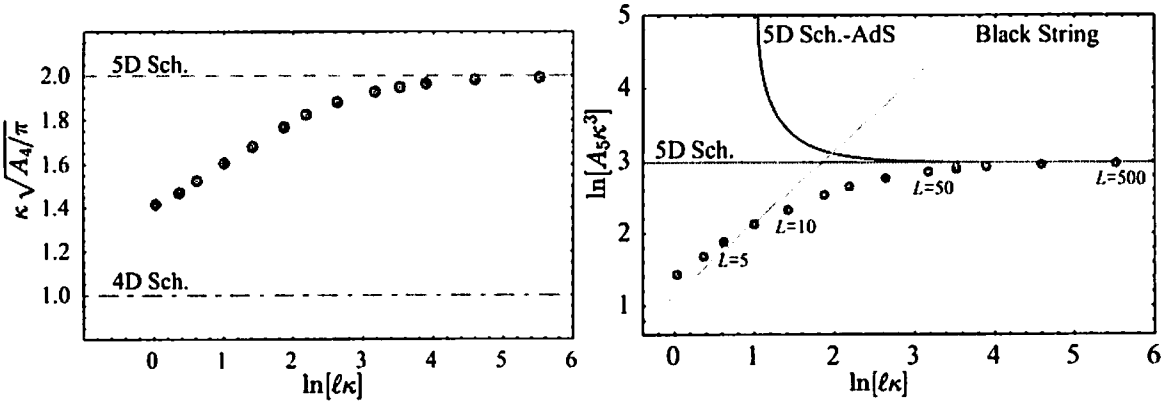


Figure 1: (a) Thermodynamic relation between the surface gravity κ and the 4D area A_4. Appropriate non-dimensional combinations are taken. The filled circles represent the numerical solutions. For reference, we plotted the same thermodynamic relations for the 4D and the 5D Schwarzschild black hole. One clearly sees that the larger the parameter $\kappa\ell$ becomes, the closer the numerical solutions lie to the line of the 5D Schwarzschild black hole. As $\kappa\ell$ decreases, the solutions deviate from the line of the 5D Schwarzschild black hole and move toward that of the 4D Schwarzschild black hole. (b) Thermodynamic relation for the surface gravity κ and the 5D area A_5 with an appropriate non-dimensional combination ($L = 3 \sim 500$). Thermodynamic relations for the 5D Schwarzschild, the 5D Schwarzschild-AdS and the black string are also plotted. As $\ell\kappa$ is decreased, the numerical solutions deviate from the curve of the 5D Schwarzschild solution, and it approaches and crosses the line of the black string.

are restricted only to small black hole solutions ($\rho_h/\ell < 1$), we could not discuss anything definite about large black hole solutions ($\rho_h/\ell \gtrsim 1$). Thus, it is an important open question to identify the character of large black hole solutions. In particular, the induced gravity and its deviation from the 4D Schwarzschild black hole at large distance are interesting. It may be worth pointing out that since we do not have any uniqueness theorem in the context of the braneworld, there is a possibility of finding another sequence of solutions than that found in this paper if we start with a completely different initial guess.

As a direction of future work, it is crucially important to find large black hole solutions if they exist, and it needs further developments of technique and investigation.

References

[1] N. Arkani-Hamed, S. Dimopoulos and G. R. Dvali, Phys. Lett. B **429**, 263 (1998); I. Antoniadis, N. Arkani-Hamed, S. Dimopoulos and G. R. Dvali, Phys. Lett. B **436**, 257 (1998)

[2] S. B. Giddings and S. Thomas, Phys. Rev. D **65**, 056010 (2002)

[3] S. Dimopoulos and G. Landsberg, Phys. Rev. Lett. **87**, 161602 (2001)

[4] L. Randall and R. Sundrum, Phys. Rev. Lett. **83**, 4690 (1999), L. Randall and R. Sundrum, Phys. Rev. Lett. **83**, 3370 (1999)

[5] A. Chamblin, S. W. Hawking and H. S. Reall, Phys. Rev. D **61**, 065007 (2000).

[6] R. Emparan, G. T. Horowitz and R. C. Myers, JHEP**0001**, 007 (2000); JHEP **0001**, 021 (2000)

[7] T. Wiseman, hep-th/0209051; T. Wiseman, hep-th/0211028.

[8] T. Wiseman, Phys. Rev. D **65**, 124007 (2002)

[9] H. Kudoh, T. Tanaka and T. Nakamura, gr-qc/0301089.

Quasinormal modes of D1/D5 black holes

Yasunari Kurita,[1] Masa-aki Sakagami[2]

Graduate School of Human and Environmental Studies, Kyoto University,Sakyo-ku, Kyoto 606-8501, Japan

Faculty of Integrated Human Studies, Kyoto University, Sakyo-ku, Kyoto 606-8501, Japan

Abstract

We consider the quasinormal modes(QNMs) of the D1/D5 black hole which is a string theoretical object. The condition for QNMs is obtained in the low energy region. As a check, we also evaluate the absorption cross section and confirm that it agrees with one from supergravity analysis.

1 Introduction

It is well known that black holes have thermodynamical properties, i.e. entropy[1, 2] and temperature[3], which can be understood in the framework of general relativity[4] and quantum theory of matter in curved spacetime[5]. In these formalisms, the entropy for a black hole is given by a quarter of its horizon area and Hawking radiation can be explained as a particle creation caused by existence of the horizon. In the final stage of Hawking radiation or evaporation, the size of such black holes is so small as compared with the planck scale, implying it is needed to consider quantum gravitational effects.

Some years ago, in the string theory, which seems to be most promising candidate for a quantum theory of gravity, it was found that the D-brane can also describe black hole spacetime and its thermodynamical properties[6]. In this prescription, the entropy for a black hole is derived by counting the number of microscopic states on the D-brane[7], and Hawking radiation can be recognized as emission process of closed strings from the D-brane[8, 9].

QNMs of black holes characterize the emission of a gravitational wave which represents a response to a perturbation affected to a black hole spacetime[10, 11]. As briefly reviewed in appendix A, it is obtained by solving the wave equation on the background with the suitable boundary conditions that the flux at the horizon is ingoing and outgoing at spatial infinity. QNMs is characterized by a complex frequency whose imaginary part represents the time scale in which the perturbation to the black hole spacetime decays. Since black holes are interpreted as thermal objects that are characterized by thermal quantities such as the temperature and entropy, the imaginary part of the QNMs frequency can be recognized as the relaxation time within which black holes approach to the thermal equilibrium.

As was well known, the relationship between D-branes and black holes in string theory is an important precursor to the AdS/CFT correspondence. And connection between QNMs and the decay of perturbations in the dual CFT was first suggested in the work of [12] based on the numerical computation of QNMs for AdS-Schwarzschild black holes in several dimensions. QNMs of AdS black holes and BTZ black holes are investigated in [13, 14, 15, 16, 17, 18, 19, 20, 21, 22, 23] and those of near extremal black branes are found in [24]. Furthermore in [25], it was shown that the frequencies of QNMs for BTZ black holes are in exact agreement with the location of the poles of the retarded correlation function describing the linear response on the CFT side.

The frequencies of QNMs for BPS D3-brane are evaluated in [26]. That frequencies are qualitatively agree with those of corresponding extremal black 3-brane that is type IIB supergravity solution.

In this paper, we consider the D1/D5 system as one of the candidates for the final state of the black hole evaporation. The condition for the low energy QNMs of this black hole is obtained. We perturbatively solve the equation derived from the low energy effective action for the D1/D5 system, i.e. the Dirac-Born-Infeld action. And we apply a general condition for QNMs to the scattering problem of this D1/D5 black hole.

[1] E-mail:kurita@phys.h.kyoto-u.ac.jp

[2] E-mail:sakagami@phys.h.kyoto-u.ac.jp

A brief outline of this paper is following. In the next section, we obtain the QNMs condition of the D1/D5 system. In the section 3, we compare the absorption cross section evaluated by our method with one from supergravity. We discuss the remained problem in the section 4.

2 The condition for QNMs of D1/D5 system

The D1/D5 system is the composite system of D1-brane, D5-brane and open string gas[8]. Now, D5-branes are in the 5,6,7,8,9 direction and D1-brane is in the 9th direction. Q_5 D5-brane are wrapped around T^5 and Q_1 D1-brane are wrapped around S^1. We set the radius of S^1 in the 9th direction to R. Open string thermal gas moving along D1-brane is both left and right direction in the 9th direction and their temperatures are T_L, T_R. Their distributions are the Bose distribution. At low energy, fermionic modes of open string give much less contribution as discussed in [9], so we neglect it. We consider a graviton h_{67} as a test particle as in [9] and its scattering by D1/D5 system. The low energy effective theory of this system is the Dirac-Born-Infeld theory, in which a interaction including graviton h_{67} is $L_{int} = \sqrt{2}\kappa_5 h_{67}\partial_\alpha X^6 \partial^\alpha X^7$, where $\kappa_5 = \kappa_{10}/V5$ and κ_{10} is the ten dimensional gravitational coupling. X^6, X^7 are open string fluctuations of D1-brane on the D5-brane each along to 6 and 7 direction. We throw the graviton h_{67} into the D1/D5 system and evaluate the reflective amplitudes or incident amplitudes, then the general condition for QNMs frequency that is vanishing incident amplitude can be evaluated. For this purpose, we must take the free bulk propagation also into account, so the equations of motion are,

$$\partial^\mu \partial_\mu h_{67} = \delta^{(4)}(X) \int dX^9 \sqrt{2}\kappa_5 h_{67} \partial_\alpha X^6 \partial^\alpha X^7 \tag{1}$$

$$\partial_\alpha \partial^\alpha X^{6,7} = -\sqrt{2}\kappa_5 \partial_\alpha \left(h_{67} \partial^\alpha X^{7,6} \right) \tag{2}$$

$\mu = 0,1,2,3,4$ and $\alpha = 0,9$. We solve these equations by the spacetime approach [27]-[30]. The concrete calculation for this system is much similar to that for the D3-brane case [26]. Please refer [26] for detail calculation. The fields can be expanded in terms of the coupling constant κ_5 as follows,

$$h_{67} = h_{67}^{(0)} + \kappa_5 h_{67}^{(1)} + \kappa_5^2 h_{67}^{(2)} + \cdots \tag{3}$$

$$X^{6,7} = X_{(0)}^{6,7} + \kappa_5 X_{(1)}^{6,7} + \kappa_5^2 X_{(2)}^{6,7} + \cdots \tag{4}$$

The perturbative solution of eq.(1),(2) with frequency ω is

$$h_{67} = Ce^{-i\omega t}\left[e^{-i\omega r} + e^{i\omega r}\left(1 - \frac{\kappa_5^2 \omega^4 R Q_1 Q_5}{16}(1 + \rho_L(\omega/2) + \rho_R(\omega/2)) - \frac{2i}{\pi\omega} G(\omega) \right) \right] + \mathcal{O}(\omega^6 \kappa_5^4) \tag{5}$$

$$\rho_{L,R}(\epsilon) = \frac{1}{e^{\epsilon/T_{L,R}} - 1} \tag{6}$$

$$G(\omega) = \int_0^\infty dp (1 + \rho_L(p) + \rho_R(p)) p \frac{P.V}{p - \omega/2}, \tag{7}$$

where $P.V$ means principle value. In this calculation, detailed balance between the Hawking emission and absorption of test particle must be taken into account.

$$(1 + \rho_L)(1 + \rho_R) - \rho_L \rho_R = 1 + \rho_L + \rho_R \tag{8}$$

We take this factor as the distribution function of reflective waves. The reflective amplitude is given by,

$$\frac{\mathcal{R}}{\mathcal{I}} = 1 - \frac{\kappa_5^2 \omega^4 R Q_1 Q_5}{16}(1 + \rho_L(\omega/2) + \rho_R(\omega/2)) - \frac{2i}{\pi\omega} G(\omega) + \mathcal{O}(\omega^6 \kappa_5^4) \tag{9}$$

So, the condition of QNMs frequencies is

$$0 = \frac{\mathcal{I}}{\mathcal{R}} = 1 + \frac{\kappa_5^2 \omega^4 R Q_1 Q_5}{16}(1 + \rho_L(\omega/2) + \rho_R(\omega/2)) - \frac{2i}{\pi\omega} G(\omega) + \mathcal{O}(\omega^6 \kappa_5^4) \tag{10}$$

The ω satisfying this equation is the QNMs frequencies.

3 The absorption cross section

As a check for this calculation, we compare the absorption cross section of the D1/D5 system with one from supergravity[32]. In the low energy limit, D1/D5 system becomes five dimensional black hole solution of type IIB classical supergravity. The metric is given by,

$$ds^2 = -\left(1-\frac{r_0^2}{r^2}\right)f(r)^{-2/3}dt^2 + f(r)^{1/3}\left[\frac{dr^2}{1-r_0^2/r^2}+r^2d\Omega_3^2\right], \tag{11}$$

$$f(r) = \left(1+\frac{r_1^2}{r^2}\right)\left(1+\frac{r_5^2}{r^2}\right)\left(1+\frac{r_n^2}{r^2}\right), \tag{12}$$

where four parameters r_1, r_5, r_n, r_0 are related by,

$$r_1^2 = \frac{4G_5R}{\pi g l_s^2}Q_1, \quad r_5^2 = g l_s^2 Q_5, \quad r_0^2 = \frac{8G_5}{\pi R}\sqrt{N_L N_R}, \quad r_n^2 = \frac{4G_5}{\pi R}\left(\sqrt{N_L}-\sqrt{N_R}\right)^2. \tag{13}$$

In eq.(13), N_L, N_R are the total left or right moving momentum of open string gas around D1-brane. g is a string coupling and l_s is a string length. The horizon of black hole is $r = r_0$. In this backgroud, massless scalar fields with frequency ω obey the wave equation,

$$\left[\frac{1-r_0^2/r^2}{r^3}\frac{d}{dr}\left(1-\frac{r_0^2}{r^2}\right)r^3\frac{d}{dr}+\omega^3 f(r)\right]\phi(r) = 0. \tag{14}$$

In the outer region ($r \gg r_1, r_5$), the solution can be described with Mathieu function,

$$\phi = \frac{\sqrt{r_1 r_5}}{r}\left(\alpha J\left(\nu, \ln\frac{\sqrt{r_1 r_5}}{r}\right)+\beta N(\nu, \ln\frac{\sqrt{r_1 r_5}}{r})\right), \tag{15}$$

where the notation of Mathieu function is the same as in [31]. The coefficients α, β are determined by matching the near horizon solution satisfying the ingoing boundary condition at the horizon. In the near horizon region ($r \ll r_1, r_5$), the solution which is ingoing at the horizon is hypergeometric function,

$$\phi = A\left(1-\frac{r_0^2}{r^2}\right)^{-i(a+b)/2} F\left(-ia, -ib, 1-ia-ib; 1-\frac{r_0^2}{r^2}\right), \tag{16}$$

$$a := \frac{\omega r_1 r_5\sqrt{N_L}}{2r_0} = \frac{\omega}{4\pi T_R}, \quad b := \frac{\omega r_1 r_5\sqrt{N_R}}{2r_0} = \frac{\omega}{4\pi T_L}. \tag{17}$$

The matching region is $r_0 \approx \omega r_i^2 \ll r \ll \omega^{-1}, i = 1, 5$. We can determine the coefficient α, β as follows,

$$\alpha = -\frac{\omega\sqrt{r_1 r_5}}{A}\left[\frac{\Gamma(1-ia-ib)}{\Gamma(1-ia)\Gamma(1-ib)}\left(2\gamma-1+\psi(1-ia)+\psi(1-ib)\right)\right], \tag{18}$$

$$\beta = -\frac{\pi\omega\sqrt{r_1 r_5}}{2}A\frac{\Gamma(1-ia-ib)}{\Gamma(1-ia)\Gamma(1-ib)}. \tag{19}$$

Then we obtain the absorption cross section as in [26],[31],[32]. The result is

$$\sigma_{abs} = 2\pi^2 r_1^2 r_5^2\frac{\pi\omega}{2}\frac{e^{\omega/T_H}-1}{(e^{\omega/2T_L}-1)(e^{\omega/2T_R}-1)}, \qquad \frac{1}{T_H} := \frac{1}{2}\left(\frac{1}{T_L}+\frac{1}{T_R}\right). \tag{20}$$

This is also obtained from Eq.(9) in previous section by,

$$\sigma_{abs} = \frac{4\pi}{\omega^3}\left(1-|\frac{\mathcal{R}}{\mathcal{I}}|^2\right). \tag{21}$$

So, the unusual evaluation method in the previous section is consistent with AdS/CFT correspondence.

4 Discussion

In this paper we present the evaluation method for the condition for the QNMs frequency of D1/D5 black holes as in D3-brane case. The absorption cross section of D1/D5 brane evaluated by this method are compared with that of the corresponding black hole solution in supergravity. We can see the two cross sections are in agreement perturbatively. So, our evaluation method is the reliable method in perturbative analysis for the scattering problems.

But, we have a problem. Usually, the dominant scale of QNMs is the typical scale of the system. Our perturbative methods is not effective for such typical scale beyond the perturbation. We must take another evaluation methods for the dominant QNMs frequencies.

The typical scale of D1/D5 black holes are the planck or string scale, on the other hands, our observable scale is much lower than the plank scale. So, if we can observe the QNMs of D1/D5 black holes, they are low energy QNMs of D1/D5 black holes where our evaluation methods are effective. But the signal of such QNMs maybe much small and difficult to detect it. This methods may have only a little meaning in the observational points of view.

In the theoretical points of view, we should compare the obtained condition for QNMs frequencies with the supergravity counterpart as in the absorption cross section. We expect these two conditions will be in agreement qualitatively as in D3-brane case.[26] But supergravity analysis are difficult to evaluate it. This is a remained problem.

References

[1] J.D.Bekenstein, Phys.Rev.D **5** 1239, (1972)

[2] S.W.Hawking Phys.Rev.Lett. **26**, 1344 (1971)

[3] S.W.Hawking Commun.Math.Phys. **43** 199, (1975)

[4] e.g. R.M.Wald "*General Relativity*" (The University of Chicago Press, Chicago and London, 1984)

[5] e.g. N.D.Birrell and P.C.W.Davies "*Quantum Fields in Curved Space*" (Cambridge University Press, Cambridge, 1982)

[6] See e.g, G.Horowitz gr-qc/9604051.

[7] A.Strominger and C.Vafa Phys. Lett. B **379**, 99 (1996).

[8] C.G.Callan and J.M.Maldacena Nucl.Phys.**B472**,591 (1996).

[9] S.R.Das and S.D.Mathur Nucl.Phys.**B 478**, 561 (1996).

[10] S.Chandrasekhar and S.Detweiler Proc. R. Soc. London, **A 344** 441 (1975).

[11] See e.g. S. Chandrasekhar, *The Mathematical Theory of Black Holes* (Clarendon, Oxford, 1983)

[12] G.T.Horowitz and V.E.Hubeny Phys.Rev.D **62** (2000) 024027

[13] J.S.F. Chan, R.B. Mann Phys.Rev.D **55** (1997) 7546

[14] J.S.F. Chan, R.B. Mann Phys.Rev.D **59** (1999) 064025

[15] B.Wang, C.Lin, E.Abdalla Phys.Lett.B **481** (2000) 79-88

[16] T.R.Govindarajan, V.Suneeta Class.Quant.Grav.**18** (2001) 265-276

[17] Jiong-Ming Zhu, Bin Wang, Elcio Abdalla Phys.Rev. D **63** (2001) 124004

[18] Danny Birmingham Phys.Rev. D **64** (2001) 064024

[19] Vitor Cardoso, Jose' P. S. Lemos Phys.Rev. D **64** (2001) 084017

[20] Vitor Cardoso, Jose' P. S. Lemos Class.Quant.Grav.**18** (2001) 5257-5267

[21] Ian G Moss, James P Norman Class.Quant.Grav. **19** (2002) 2323-2332

[22] B. Wang, E. Abdalla, R.B. Mann Phys.Rev.D **65** (2002) 084006

[23] R.A.Konoplya hep-th/0205142, gr-qc/0207028

[24] Andrei O. Starinets hep-th/0207133

[25] D.Birmingham, I.Sachs and S.N.Solodukhin Phys.Rev.Lett **88**, 151301 (2002).

[26] Y.Kurita and M.Sakagami hep-th/0208063

[27] R. P. Feynman Rev. Mod. Phys. **21**, 425 (1949).

[28] R. P. Feynman Rev. Mod. Phys. **20**, 367 (1948).

[29] R. P. Feynman Phys. Rev. **76**, 749 (1949).

[30] J. J. Sakurai "Advanced Quantum Mechanics" Addison Wesley Publishing Company **Chapter 4-5**

[31] S. S. Gubser and A. Hashimoto hep-th/9805140

[32] J. Maldacena and A. Strominger Phys.Rev.D **55**, 861 (1997)

Criticality and convergence in Newtonian collapse

Hideki Maeda,[a,1] Tomohiro Harada,[b,2] Benoit Semelin,[c,3]

[a] *Advanced Research Institute for Science and Engineering, Waseda University, Tokyo 169-8555, Japan*
[a,b] *Department of Physics, Waseda University, Tokyo 169-8555, Japan*
[c] *LERMA, Observatoire de Paris, Paris 75014, France*

Abstract

We study through numerical simulation the spherical collapse of isothermal gas in Newtonian gravity. We observe a critical behavior which occurs at the threshold of gravitational instability leading to core formation. For a given initial density profile, we find a critical temperature T_c, which is of the same order as the virial temperature of the initial configuration. For the exact critical temperature, the collapse converges to a self-similar form, the first member in Hunter's family of self-similar solutions. For a temperature close to T_c, the collapse first approaches this critical solution. Later on, in the supercritical case ($T < T_c$), the collapse converges to another self-similar solution, which is called the Larson-Penston solution. In the subcritical case ($T > T_c$), the gas bounces and disperses to infinity. We find two scaling laws with respect to $|T - T_c|$: one for the collapsed mass in the supercritical case and the other, which was not predicted before, for the maximum density reached before dispersal in the subcritical case. The value of the critical exponent is measured to be $\simeq 0.11$ in the supercritical case, which agrees well with the predicted value $\simeq 0.10567$.

1 Introduction

The Newtonian isothermal gas is indeed a good description for cold molecular clouds found in the galactic interstellar medium. Since they are the prime location for star formation, their physics determines the whole star formation history in the galaxy. A detailed understanding of the physics of these systems will lead to predictions for the properties of star formation. The basic behavior of a clump of isothermal gas is the following. In a sufficiently dense and/or cold configuration, the gas will collapse due to its self-gravity, while in a diffuse and/or hot one it will expand due to its internal pressure forces. A critical behavior appears at the transition between these two regimes.

In 1993, Choptuik [1] showed the existence of a so-called critical phenomenon in the spherical collapse of a massless scalar field by general relativistic numerical simulations. The simulations were performed for a one-parameter family of initial data sets. He found a self-similar solution with critical properties at the threshold of black hole formation. In this first case, the self-similarity holds for a discrete set of transformations only (periodicity in logarithmic time). He showed that the mass of the formed black hole follows a scaling law, and that the phenomenon is universal in the sense that it does not depend on the one-parameter family of initial data sets. Soon after that, similar critical phenomena were observed in the spherical collapse of radiation fluid by Evans and Coleman [2]. In this second case, self-similarity holds for a continuous set of transformations. Koike, Hara and Adachi [3] gave a clear picture of these phenomena by using the renormalization group approach. Recently, critical phenomena have been found in perfect fluids with more general equation of state [4]. The solution with critical properties is only one of several known self-similar solutions. It was conjectured by Carr [5] that a generic solution gradually evolves toward a self-similar form, which suggest that one of the self-similar solutions may be an attractor solution. This is called the self-similarity hypothesis. In Newtonian gravity, a self-similar solution, the so-called Larson-Penston solution [6] is known to be an attractor solution in the spherical collapse of isothermal gas [7].

The present paper shows that critical phenomena exist in Newtonian gravity also. We concentrate on a spherically symmetric system of isothermal gas in Newtonian gravity. The existence of a critical

[1] E-mail:hideki@gravity.phys.waseda.ac.jp
[2] E-mail:harada@gravity.phys.waseda.ac.jp
[3] E-mail:benoit.semelin@obspm.fr

phenomenon was predicted by Harada and Maeda [8] and Maeda and Harada [9]. In these papers, based on the renormalization group analysis, it was predicted that a critical phenomenon is associated with the first member of Hunter's family of continuous self-similar solutions [10]. The criticality appears in the scaling law for the collapsed mass, which is satisfied for continuous values of the mass. The value of the critical exponent was predicted to be $\simeq 0.10567$.

2 Basic equations

The dynamics of a spherically symmetric isothermal gas system is described in the following set of equations:

$$\frac{\partial \rho}{\partial t} + \frac{1}{r^2}\frac{\partial}{\partial r}(r^2 \rho v) = 0, \tag{1}$$

$$\frac{\partial}{\partial t}(\rho v) + \frac{1}{r^2}\frac{\partial}{\partial r}(r^2 \rho v^2) = -c_s^2 \frac{\partial \rho}{\partial r} - \rho \frac{Gm}{r^2}, \tag{2}$$

$$\frac{\partial m}{\partial t} + v\frac{\partial m}{\partial r} = 0, \tag{3}$$

$$\frac{\partial m}{\partial r} = 4\pi r^2 \rho, \tag{4}$$

where $\rho = \rho(t,r)$, $v = v(t,r)$, $m = m(t,r)$, $c_s \equiv (kT/m_B)^{1/2}$ and G, denote the density, radial velocity, total mass inside the radial coordinate r, sound speed, and gravitational constant, respectively.

In fact, for Eqs. (1)–(4), there is a discrete set of self-similar solutions with analyticity at the center and at a sonic point, such as the homogeneous free-fall, Larson-Penston, Hunter (a), (b), (c) and (d) solutions, and so on. The properties of these solutions are written in [9]. Maeda and Harada [9] found a unique relevant (unstable) mode for the Hunter (a) solution but no relevant mode for the Larson-Penston solution. It was concluded that the former is a critical solution while the latter is an attractor solution. In the former case, the eigenvalue κ of the unique relevant mode was evaluated to $\kappa \simeq 9.4637$ by solving the eigenvalue problem. Other members of Hunter's family have more than one relevant modes, which implies that these solutions are not critical solutions. The homogeneous free-fall solution suffers from kink instability [11].

If we assume the existence of the critical solution and use renormalization group analysis, we obtain the scaling law for the collapsed mass or the 'core' mass for the supercritical collapse,

$$m_{\rm core} \propto (p - p^*)^{\gamma}, \tag{5}$$

while for the maximum density for the subcritical case,

$$\rho_{\rm max} \propto (p - p^*)^{-2\gamma}, \tag{6}$$

with the critical exponent $\gamma = 1/\kappa \simeq 0.10567$. The initial conditions of the collapse are characterised only by one parameter p. p^* is the critical value between collapse and dispersion. See [12] for more detail. In our simurations, the parameter p is identified with the temparature T since the parameter for the family of initial data sets is given by T. It should be noted that the parameter is not necessarily the temperature but may be the mass or the radius of the cloud if we fix the temperature.

3 Numerical simulations

We have performed numerical simulations of the spherical collapse of an isothermal Newtonian gas. The basic equations for the evolution of the system are given by Eqs. (1)–(4). The code is based on the Lagrangian description of hydrodynamics and a finite difference scheme. We have chosen Lagrangian (comoving) radial coordinates, attached to spherical shells with infinitesimal thickness. The mass inside coordinate r_i is consequently constant throughout the simulation. We call such coordinates mass coordinates. Shells are initially positioned at constant intershell distance and their mass is computed from the desired density profile (we do not use equal mass shells). With these choices, we achieve high accuracy for

the dynamics in the dense central region where the shells collapse during the simulations. The number of shells used in the simulation is 10^4. One simulation with 10^5 shells has been run to check the influence of numerical resolution. No effect has been detected. This is proof of the accuracy of the code. In this section, we adopt units in which $G = k/m_B = 1$ and the total mass m_{tot} and initial radius $r_{s,i}$ of the cloud are unity.

We have computed the evolution of four types of initial density profiles. Details of the models for the initial density profiles are summarized in Table 1. The initial velocity profile is always set to be identically zero. This assumption seems the most relevant for astrophysical applications, but the same dynamics should develop for different initial velocity profiles. Model 2 is our reference model, in which the initial density profile is given by a quartic polynomial and both the density and the density gradient (i.e., pressure forces) are continuous at the cloud surface. We have computed collapse simulations for various values of the temperature.

Table 1: Models of initial density profiles

Model	Density Profile ρ_i	Critical Temperature T_c
1	$\propto (1-r^2)$	0.488260887209925
2	$\propto (1-r^2)^2$	0.535188638440868
3	$\propto \cos^2(\pi r/2)$	0.547073928440245
4	$\propto \theta(1-r)$	0.275256858581273

For each model, we find a critical temperature T_c, which is of the same order of magnitude as the virial temperature estimated from the initial gravitational energy of the system. For temperatures just below T_c, the cloud collapses and the central density goes to infinity in a finite time, producing a singularity. We call this collapse a supercritical collapse. For temperatures just above the critical temperature, the cloud begins to collapse but bounces afterward, and the density finally goes to zero everywhere. We call this incomplete 'collapse' a subcritical collapse.

In the critical and supercritical cases, we can estimate the time t_s of the singularity at the center in different ways. First we can just define it as the instant when the numerical density reaches a very high threshold (e.g., $\rho \sim 10^{15}$ while initially of the order of one). Or we can assume the convergence to a self-similar behavior and use the relation $\rho_c \propto (t_s - t)^{-2}$ for the central density ρ_c. Both approaches have been tried and give the same results. The origin of time is then set to t_s. When the temperature is fine-tuned to the critical one, a case that we call the critical case for convenience, the simulations show that the collapse approaches the Hunter (a) solution for a while before it diverges. (See Fig. 1 in [12].) The finer the tuning of the temperature, the closer the approach and the later the divergence.

In the supercritical case, the collapse first approaches the critical solution. We find that the curve of the critical collapse approaches the value of the Hunter (a) (critical) solution. However, it afterward diverges and approaches the value of the Larson-Penston solution. (See Fig. 2 in [12] for more detail.) This happens because the tuning of the temperature to the critical temperature is not perfect, and because the critical solution is unstable against such fluctuations. During and after the approach to the critical solution, the surrounding region expands away and leaves a finite-mass 'core' in the central region. The density field in the central collapsed core at late times is well described by the Larson-Penston solution. This is the case early on for a supercritical collapse also, where the temperature is not fine-tuned to the critical temperature. This type of collapse also produce a finite (more massive) core and an expanding shell. We identify the Larson-Penston solution as an attractor solution. (See Fig. 3 in [12].)

We can see in the velocity profile around the center for a supercritical collapse that the physical radius of the collapsing core is almost constant. (See Fig. 4 in [12].) We can see that at all supercritical temperature, the collapsing mass tends rapidly to a constant and therefore the 'core' mass is well defined irrespective of time. (See Fig. 5 in [12].) Figure 1 shows the relation between the core mass and the temperature fluctuation $|T - T_c|$. The numerical results reproduce the scaling law derived by the renormalization group analysis in the previous section. The numerical value of the critical exponent is $\simeq 0.11$, which agrees well with the theoretical value $\simeq 0.10567$ determined from the eigenvalue problem of the linear mode analysis. It should be noted that the power-law relation holds approximately for

$|\delta T|/T_c \lesssim 0.01$.

For the subcritical collapse, the central density reaches a maximum and then bounces away. Figure 2 shows the relation between the maximum density and the temperature excess $T - T_c$. It shows that the maximum density also follows a scaling law, as is expected from the renormalization group analysis. The measured value $\simeq -0.22$ of the critical exponent agrees with the theoretical value $\simeq -0.21134$. Again, it should be noted that the power-law relation holds approximately for $\delta T/T_c \lesssim 0.01$.

Although we have concentrated on Model 2, the above features have been checked for Models 1 and 3. They are identical in all three models except for the specific value of the critical temperature. Model 4, the top-hat model, is special because the cloud is initially homogeneous. In this case, the central region of the cloud remains homogeneous and freely falls to a singularity if the condition $m_{\rm tot}/r_{\rm s,i} > \pi^2 c_{\rm s}^2/2$ is satisfied. If the condition is not satisfied, the collapse converges to Larson-Penston (attractor) solution.

4 Summary

We have analyzed the critical behavior in the collapse of a Newtonian isothermal gas by the renormalization group approach and in numerical simulations. The renormalization group analysis in the Newtonian case is similar to the general relativity case. We have observed the critical phenomenon in the numerical simulation, which can be compared to those observed during black hole formation in the collapse of radiation fluid in general relativity. The scaling law for the formed black hole mass with critical exponent $\simeq 0.36$ in general relativity is replaced by a scaling law for the collapsed core mass with critical exponent $\simeq 0.11$. The critical solution is a continuous self-similar solution, specifically the first member of Hunter's family of solutions.

For the supercritical collapse, the collapse near the center converges (early for low temperature, late for almost critical temperature) to another continuous self-similar solution, the Larson-Penston solution. Generic collapse converges to this attractor solution, which suggests the universality of self-similarity in gravitational collapse. This phenomenon is an example for the validity of the self-similarity hypothesis in gravitational collapse.

We have also studied the response of the system to temperature fluctuation and discuss astrophysical implications for the insterstellar medium structure and for the star formation process [12].

References

[1] M.W. Choptuik, Phys. Rev. Lett. **70**, 9 (1993).

[2] C.R. Evans and J.S. Coleman, Phys. Rev. Lett. **72**, 1782 (1994).

[3] T. Koike, T. Hara and S. Adachi, Phys. Rev. Lett. **74**, 5170 (1995).

[4] D. Maison, Phys. Lett. B **366**, 82 (1996); T. Koike, T. Hara and S. Adachi, Phys. Rev. D **59**, 104008 (1999); D.W. Neilsen and M.W. Choptuik, Class. Quantum Grav. **17**, 733 (2000); D.W. Neilsen and M.W. Choptuik, Class. Quantum Grav. **17**, 761 (2000).

[5] B.J. Carr, gr-qc/0003009 (2000).

[6] M.V. Penston, Mon. Not. R. Astron. Soc. **144**, 425 (1969); R.B. Larson, Mon. Not. R. Astron. Soc. **145**, 271 (1969).

[7] T. Hanawa and K. Nakayama, Astrophys. J. **484**, 238 (1997); T. Hanawa and T. Matsumoto, Publ. Astron. Soc. Jpn. **52**, 241 (2000); T. Hanawa and T. Matsumoto, Astrophys. J. **521**, 703 (2000); T. Tsuribe and S. Inutsuka, Astrophys. J. **526**, 307 (1999).

[8] T. Harada and H. Maeda, Phys. Rev. D **63**, 084022 (2001).

[9] H. Maeda and T. Harada, Phys. Rev. D **64**, 124024 (2001).

[10] C. Hunter, Astrophys. J. **218**, 834 (1977).

[11] A. Ori and T. Piran, Mon. Not. R. Astron. Soc. **234**, 821 (1988).

[12] T. Harada, H. Maeda and B. Semelin, submitted to Phys. Rev. D, gr-qc/0210027.

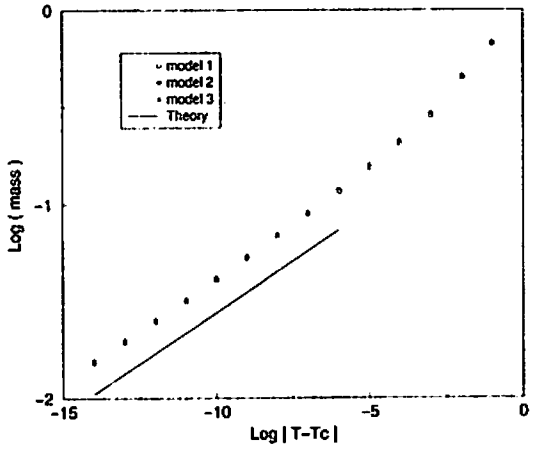


Figure 1: Scaling law for the mass of the collapsed core in supercritical collapses. The masses of the collapsed core formed in supercritical collapses in each model are plotted for different temperatures just below the critical temperature. The theoretical slope determined by the renormalization group analysis is also depicted.

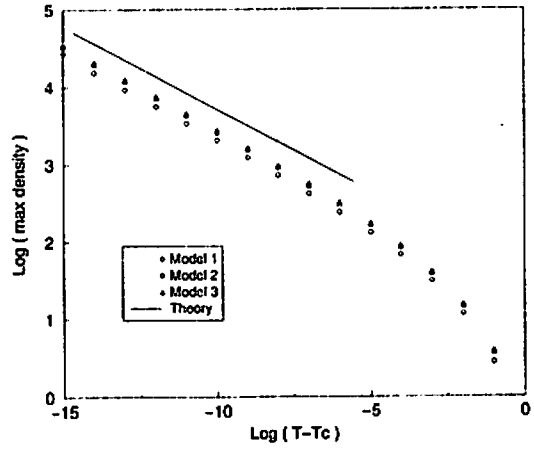


Figure 2: Scaling law for the maximum density reached in subcritical collapses. The maximum densities reached in subcritical collapses in each model are plotted for different temperatures just above the critical one. The theoretical slope determined by the renormalization group analysis is also depicted.

An iterative method for reproducing the primordial spectrum from the CMB data

Makoto Matsumiya,[1] Misao Sasaki[2] and Jun'ichi Yokoyama[3]

Department of Earth and Space Science, Graduate School of Science, Osaka University, Toyonaka 560-0043, Japan

Abstract

We present a method to determine the shape of the initial curvature perturbation spectrum $P(k)$ from the CMB data. The thickness of the last scattering surface (LSS) and the integrated Sachs-Wolfe (ISW) effect, which we neglect in the previous paper, are taken into account and an iterative method is newly developed. The new method can reproduce the primordial power spectra with a high accuracy, given the correct values of the cosmological parameters. Conversely, there appear spurious peaks and dips in the reconstructed power spectrum if we use the cosmological parameters slightly different from the true values, while there appear regions of negative $P(k)$ in some cases if we use substantially different values. In other words, our reconstruction method provides a new tool to constrain the cosmological parameters without recourse to models of the primordial power spectra.

1 Introduction

Cosmic microwave background (CMB) is now playing a central role in the precision cosmology and enables us to extract wealth of information on the cosmological parameters and the primordial universe. The past CMB experiments suggest that our universe is consistent with spatially flat ΛCDM universe with scale-invariant initial spectrum, which is predicted by conventional slow-roll inflation models. Nevertheless these results are not too restrictive and other cosmological models are still possible under the present accuracy of the observational data. In the near future, we will attain unprecedentedly precise data by MAP [1] and PLANK [2] experiments. Then, we will be able to discuss the results much more quantitatively than we can now.

In particular, on the analysis of the CMB anisotropy, it is more desirable to deal with the initial spectrum of perturbation as an arbitrary function, although most of the past analyses of observational data assumed a power-law spectrum. On the theoretical side, a variety of generation mechanisms of broken scale-invariant spectra have been proposed, even in the context of inflationary cosmology [3]. In our previous paper (hereafter Paper I) [4], we built up a basic framework to reconstruct the primordial spectrum of curvature perturbations, $P(k)$, out of CMB anisotropy data by solving a differential equation for $P(k)$, in which not only the SW effect but also the Doppler effect are taken into account.

In this paper, we improve the method to a more accurate one which can be applied to real data. The width of the LSS and Integrated Sachs-Wolfe term are newly included. We also investigate the dependence on the cosmological parameters.

This paper is organized as follows. In Sec. II, we describe our inversion method in some detail, which is an improved version of the one presented in Paper I. In Sec. III, we apply our method to some model spectra, assuming the true cosmological parameters are known. We find that the new method can reproduce the primordial spectrum to quite accurately. In Sec. IV, we investigate the dependence of the reconstructed spectrum on the cosmological parameters. We find the cosmological parameters can be constrained severely without any assumption on the primordial spectrum. We discuss the implications of our method in Sec. V

[1] E-mail:matumiya@vega.ess.sci.osaka-u.ac.jp
[2] E-mail:misao@vega.ess.sci.osaka-u.ac.jp
[3] E-mail:yokoyama@vega.ess.sci.osaka-u.ac.jp

2 Inversion Formula

First we write down basic equations. We use the same notation as Paper I. Working in the Fourier space and denoting the direction cosine between the wavenumber vector $\boldsymbol{k}$ and the momentum vector of the photon by μ, an integral form of the Boltzmann equation for the temperature anisotropy, $\Theta(\eta, \mu, k)$, is given in the Newton gauge by [5]

$$\Theta(\eta_0, k, \mu) + \Psi(\eta_0, k) = \int_0^{\eta_0} \left\{ (\Theta_0 + \Psi - i\mu V_b)\, \mathcal{V}(\eta) + (\dot{\Psi} - \dot{\Phi}) e^{-\tau(\eta)} \right\} e^{ik\mu(\eta - \eta_0)} d\eta. \tag{1}$$

Here, an overdot denotes a derivative with respect to the conformal time η, and η_0 is its present value, Ψ and Φ are the Newtonian potential and spatial curvature perturbation on the Newton slices, respectively [6], and Θ_0 is the monopole component of the multipole expansion,

$$\Theta(\eta, k, \mu) = \sum_\ell (-i)^\ell \Theta_\ell(\eta, k) P_\ell(\mu). \tag{2}$$

The function $\mathcal{V}(\eta)$ is called the visibility function and $\tau(\eta)$ is the opacity, which are given by

$$\mathcal{V}(\eta) = \dot{\tau}(\eta) e^{-\tau(\eta)}, \quad \tau(\eta) = \int_\eta^{\eta_0} \dot{\tau}(\eta') d\eta', \quad \dot{\tau} = a x_e n_e \sigma_T, \tag{3}$$

where a is the cosmic scale factor, $x_e n_e$ is the free electron density, and σ_T is the Thomson cross section.

Now, we improve the transfer functions by including the effect of the thickness of the LSS. For this purpose, we use the following approximate expression.

$$\begin{aligned} \Theta_\ell^{\rm app}(\eta_0, k) &= (2\ell+1) \left[\int_0^{\eta_0} (\Theta_0 + \Psi)(\eta, k) \mathcal{V}(\eta) d\eta \right] j_\ell(kd) \\ &\quad + (2\ell+1) \left[\int_0^{\eta_0} \Theta_1(\eta, k) \mathcal{V}(\eta) d\eta \right] j_\ell'(kd) \\ &\quad + (2\ell+1) \left[\int_0^{\eta_0} \left(\dot{\Psi}(\eta, k) - \dot{\Phi}(\eta, k) \right) e^{-\tau(\eta)} d\eta \right] j_\ell(kd), \end{aligned} \tag{4}$$

The first two terms of the above formula partially take account of the thickness of the LSS, which would be exact if the spherical Bessel functions would not oscillate but remain constant over the thickness of the LSS, which is the case for low wavenumber modes. Note that the ISW term, which was ignored in Paper I, is now included in the third term. It takes account of the early ISW effect, since the matter-radiation equality time is fairly close to the decoupling epoch. Although the width of the time interval during which the integrand of the third term is non-negligible is somewhat larger than the width of the LSS, the early ISW effect happens to be described by this approximation fairly accurately.

Defining new transfer functions $\overline{f}(k)$ and $\overline{g}(k)$ to express (4) as

$$\Theta_\ell^{\rm app}(\eta_0, k) = (2\ell+1) \overline{f}(k) \Phi(0, k) j_\ell(kd) + (2\ell+1) \overline{g}(k) \Phi(0, k) j_\ell'(kd), \tag{5}$$

and repeating the same procedure as in Paper I, we arrive at the following differential equation.

$$-\overline{f}^2(k) k^2 P'(k) + \left[-2\overline{f}(k) \overline{f}'(k) k + \overline{g}^2(k) \right] k P(k) = 4\pi \int_0^\infty \tilde{C}^{\rm app}(r) \sin kr dr, \tag{6}$$

where the right-hand-side should now be calculated using (4).

The above differential equation can be solved when $\tilde{C}^{app}(r)$ is given. However, if we used the observed correlation function obtained by, say, MAP satellite [1] in the right-hand-side of (6), we would reach an incorrect primordial spectrum $P(k)$, because, although the approximate formula (4) reproduces the locations of peaks and troughs of the true spectrum quite well, the amplitude still deviates from the one obtained by full numerical calculation [7] which is to be compared with the observed one.

Fortunately, there exists a remedy for errors caused by the formula (4). To show this, let us consider the ratio of the exact to the approximated angular power spectrum, which we define as

$$b_\ell \equiv \frac{C_\ell^{\rm exact}}{C_\ell^{\rm app}}. \tag{7}$$

Of course, this depends on the shape of the initial spectrum. However, the dependence turns out to be relatively weak as is illustrated in Fig. 1. That is, for a fixed set of the cosmological parameters, b_ℓ is found to be rather insensitive to the variation of the initial spectrum. This suggests the following procedure of reconstruction. Consider we are given the observational data ($\equiv C_\ell^{\rm obs}$). Assuming the cosmological parameters are known, we calculate the correction factor b_ℓ for a fiducial initial spectrum $P^{(0)}(k)$. Namely, we calculate the exact angular spectrum $C_\ell^{(0)}$ and the approximate one $C_\ell^{\rm app(0)}$ using Eq. (4) from $P^{(0)}(k)$ and take their ratio which we denote by $b_\ell^{(0)}$. Then dividing $C_\ell^{\rm obs}$ by $b_\ell^{(0)}$, we estimate $C_\ell^{\rm app}$. Let us denote this estimated approximate angular spectrum by $C_\ell^{\rm app(0)}$. Then, we can insert it into Eq. (6) to reconstruct the initial spectrum. If b_ℓ were rigorously invariant, this procedure would recover the true initial spectrum. Due to small errors caused by the non-invariance of b_ℓ, however, the reconstructed spectrum, denoted by $P^{(1)}(k)$, will not be exactly equal to the true primordial spectrum $P(k)$. Nonetheless, we can expect $P^{(1)}(k)$ to be fairly close to the true $P(k)$, or at least better than the fiducial spectrum $P^{(0)}(k)$ which is a blind guess. Then, we can iterate this procedure to improve the accuracy.

Schematically, this iterative procedure is described as

$$P^{(n)}(k) \quad \rightarrow \quad b_\ell^{(n)} = \frac{C_\ell^{(n)}}{C_\ell^{\rm app(n)}} \quad \rightarrow \quad C_\ell^{\rm app(n+1)} = \frac{C_\ell^{\rm obs}}{b_\ell^{(n)}} \quad \underset{\text{Eq. (6)}}{\longrightarrow} \quad P^{(n+1)}(k)\,, \tag{8}$$

where the last step is the inversion procedure, and $C_\ell^{\rm app(n)}$ is the approximate angular spectrum for $P^{(n)}(k)$ using the formula (4). We repeat this procedure until we obtain a given degree of convergence.

The invariance of b_ℓ, of course, will not hold between entirely different initial spectra. Recent observations, however, suggest that the initial spectrum is almost scale-invariant on very large scales. We therefore assume that the scale-invariant spectrum is a good guess, apart from possible features like peaks and dips and/or some smooth variations of the power-law index over a range of one or two orders of k.

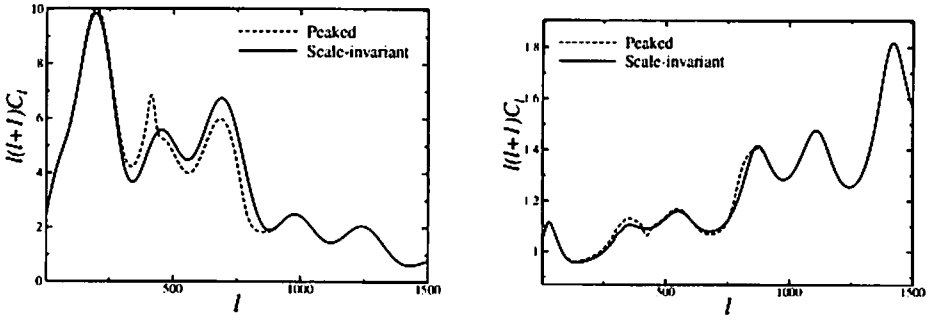


Figure 1: The right panel shows the angular power spectra C_ℓ for scale-invariant (solid line) and peaked (dashed line) initial spectra. The left panel shows the ratio $b_l = C_\ell^{\rm exact}/C_\ell^{\rm app}$ for the two initial spectra.

3 Results

In order to test the validity of our method, we apply it to several shapes of initial spectra in flat CDM models. For initial spectra having distinct features, a spectrum obtained at the first round of inversion sometimes contains regions of negative values or has extraordinary sharp peaks or dips (with height or depth of more than a factor of ten relative to the continuum) due to errors in the estimation of b_ℓ. Since a real spectrum must be positive definite, we make it a rule to cut off the negative part from the spectrum and smooth out sharp peaks and dips to mild ones, and use it for the next round of the inversion procedure. Although there is no justification for this prescription, we find that these peculiar features

disappear from the spectrum at the next round when they are spurious, while they show up again when they are real.

We first assume the correct cosmological parameters are known. Then the iteration converges by a few times, although the rate of convergence depends on a spectrum. We find the converged spectrum agrees well with the original spectrum. In actual applications, we need to calculate the corresponding angular spectrum again to compare it with an observed spectrum $C_\ell^{\rm obs}$. We plot the result for a spectrum with a peak and a dip in Fig. 2.

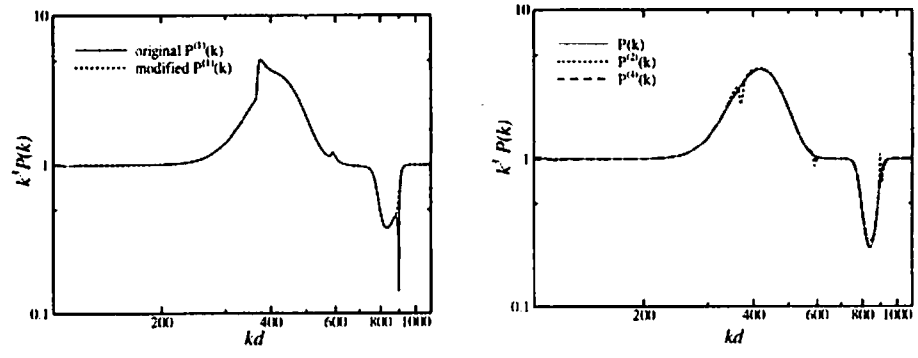


Figure 2: Test of our inversion method for a primordial spectrum with a peak and a dip superposed on a scale-invariant spectrum. The left panel shows $P^{(1)}(k)$ which is obtained from the first round of iteration. The solid curve is the original $P^{(1)}(k)$ which happens to have a very spiky dip at $kd \simeq 900$. We assume such a feature is spurious and remove it by simply cutting that part off and interpolating from the both sides, which is plotted by the dotted curve. The right panel shows $P^{(2)}(k)$ and $P^{(4)}(k)$ together with the original (true) spectrum $P(k)$.

4 Constraining cosmological parameters

In the previous section, we showed that the initial spectrum can be determined with a high precision. However we had to assume that the cosmological parameters, which are usually estimated from the CMB data, are exactly known by some other observations from the beginning. Here we examine consequences of the use of incorrect cosmological parameters in our procedure.

As an example, Fig. 3 shows the reconstructed spectra for several values of h and Ω_b when $C_\ell^{\rm obs}$ is given by a scale-invariant spectrum with $h = 0.7$ and $\Omega_b = 0.03$ in the flat CDM universe. As for the h dependence, spiky peaks appear at the singularities for larger values of h, while spiky dips appear for smaller values of h and the dips become too deep to render the spectrum negative for $h \lesssim 0.65$. Therefore, the positivity condition of the spectrum severely constrains models with smaller values of h and larger values of Ω_b, while models with larger values of h and smaller values of Ω_b can be also constrained unless there is a good reason to believe that locations of the spikes and the singularities should coincide.

5 Conclusion

We have presented a method to solve the inversion problem of reconstructing the primordial curvature perturbation spectrum $P(k)$ solely from the CMB angular power spectrum C_ℓ. In this paper, we improved the method presented in Paper I significantly by fully incorporating both the thickness of the LSS and the early ISW effect. We have found the new method can recover the original spectrum accurately, to within relative errors of 4%, even in cases when there are distinct features like peaks and dips in the spectrum.

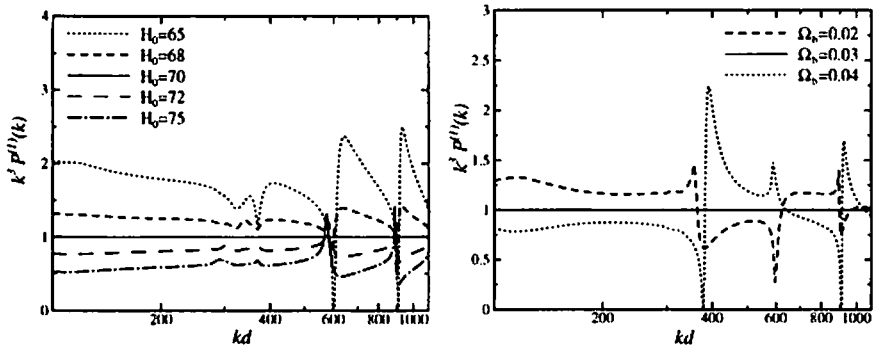


Figure 3: The cosmological parameter dependence of the reconstructed spectrum. The real spectrum is scale-invariant with $h = 0.7$ and $\Omega_b = 0.03$ in the flat CDM universe. We plot the reconstructed spectra for $h = 0.65$, 0.68, 0.7, 0.72 and 0.75, and Ω_b=0.02, 0.03 and 0.04.

We have also studied the effect of using the cosmological parameters that are different from their true values. We found that a small deviation from the true value results in the appearance of peaks and dips at the locations of singularities of the differential equation for $P(k)$, which can be easily judged as spurious. In particular, depending on the direction and the size of deviations, the spurious dips can become so deep that the positivity condition of $P(k)$ is violated there. Thus, contrary to our concern about the inversion method mentioned above, it may be regarded as an advantage in the sense that the cosmological parameters can be constrained severely with no regard to the shape of the initial spectrum. This is in accordance with a widely accepted assertion that the cosmological parameters can be determined from the heights and locations of peaks in the observed CMB spectrum. What is new is that we have not only justified this assertion qualitatively but also provided a means to quantify the level of its validity or limitations without any assumptions on the form of the primordial spectrum.

References

[1] http://map.gsfc.nasa.gov/

[2] http://astro.estec.esa.nl/SA-general/Projects/Planck/

[3] A. D. Linde, Phys. Lett. B **158**, 375 (1985). L. A. Kofman and A. D. Linde, Nucl. Phys. B **282**, 555 (1987). J. Silk and M. S. Turner, Phys. Rev. D **35**, 419 (1987). H. M. Hodges and G. R. Blumenthal, Phys. Rev. D **42**, 3329 (1990). J. Yokoyama and Y. Suto, Astrophys. J. **379**, 427 (1991); M. Sasaki and J. Yokoyama, Phys. Rev. D **44**, 970 (1991). A. A. Starobinsky, JETP Lett. **55**, 489 (1992); [Pisma Zh. Eksp. Teor. Fiz. **55** (1992) 477]; J. Yokoyama, Astron. Astrophys. **318**, 673 (1997); J. Yokoyama, Phys. Rev. D **58**, 083510 (1998);**59**, 107303 (1999); S. M. Leach and A. R. Liddle, Phys. Rev. D **63**, 043508 (2001) [arXiv:astro-ph/0010082]; S. M. Leach, M. Sasaki, D. Wands and A. R. Liddle, Phys. Rev. D **64**, 023512 (2001) [arXiv:astro-ph/0101406].

[4] M. Matsumiya, M. Sasaki and J. Yokoyama, Phys. Rev. D **65**, 083007 (2002) [arXiv:astro-ph/0111549].

[5] W. Hu and N. Sugiyama, Astrophys. J. **444**, 489 (1995).

[6] H. Kodama and M. Sasaki, Prog. Theor. Phys. Suppl **78**, 1 (1984)

[7] cmbfast; http://physics.nyu.edu/matiasz/CMBFAST/cmbfast.html

Bulk Effects onto the Brane due to a Bulk Scalar Field

Masato Minamitsuji,[1] Yoshiaki Himemoto [2] and Misao Sasaki, [3]

Department of Earth and Space Science, Graduate School of Science Osaka University, Toyonaka OSAKA 560-0043, Japan

Abstract

Based on the 2nd Randall-Sundrum brane world scenario (the RS2 scenario), we consider the braneworld inflation model driven by the dynamics of a gravitational scalar field living in the 5-dimensional bulk, the so-called "bulk inflaton model". We need to estimate the bulk effects specific to the brane universe on this model, before disccusing the cosmological perturbation theory on the brane. Bulk gravitational effects onto the brane appear in the effective Einstein equations on the brane. The bulk gravitational effects cannot be evaluated only by the dynamics on the brane, and we have to solve the evolution equations in the bulk. We derived the equations, and applied them to the spatially homogeneous case, for a consistency check.

1 Introduction

It is widely accepted that our universe is not 4 dimensional but higher dimensional, from the view point of the unified theory/M-theory. Hořava and Witten (HW) showed the possibility that desirable gauge fields may consistently appear on the 10-dimensional brane-boundary of the $\mathbf{Z_2}$ symmetric 11-dimensional space-time. Randall and Sundrum(RS) proposed the interesting braneworld scenarios [1] which inherited the spirits of the HW scenario. Especially their 2nd scenario has attracted much attention of relativity and cosmology communities, because of the attractive feature that the Newton gravity is recovered on the 4-dimensional brane-boundary in the low energy limit without compactifying the extra 5th dimension. In recent years, the braneworld cosmology based on the RS2 scenario has been studied extensively.

The inflationary cosmology is also widely accepted because of its success in explaining the cosmological observations. It is therefore very interesting to consider the inflationary cosmology from the point of view of the braneworld scenario. We consider a braneworld inflation model driven by the dynamics of the gravitational scalar field, proposed by Himemoto and Sasaki [2]. The exsistence of such a scalar field is supported from the point of view of the unified theory, as the 5-dimensional reduction of the higher dimensional gravitational theory. Braneworld inflation can occur on the brane in an appropriate parameter region, and the standard slow-roll inflation can be realized at the low energy limit [2, 3, 4].

As a next step, we need to verify if the bulk inflaton model can reproduce the observational results, and can predict effects specific to the brane universe. For this purpose, we consider the cosmological perturbation theory on the brane in terms of the perturbed effective Einstein equations

$$\delta^{(4)}G_{\mu\nu} = \kappa_4^2 \delta T^{(b)}_{\mu\nu} - \delta E_{\mu\nu}. \tag{1}$$

The gravitational effects in the 5-dimensional bulk to the brane $\delta E_{\mu\nu}$ cannot be elavuated only by the dynamics on the brane, and we need to solve the equations in the bulk

$$\mathcal{L}\,\delta E_{\mu\nu} = S_{\mu\nu}[\delta T_{ab}]. \tag{2}$$

This talk is organized as follows. In Sec. 2, we review the bulk inflaton model. In Sec. 3, we derive the evolution equations of the gravitational effects in the bulk. In Sec. 4, we applied them to the spatially homogeneous case, for a consistency check. In Sec. 5, we summarize the results.

[1] E-mail:masato@vega.ess.sci.osaka-u.ac.jp
[2] E-mail:himemoto@vega.ess.sci.osaka-u.ac.jp
[3] E-mail:misao@vega.ess.sci.osaka-u.ac.jp

2 Review of the Bulk Inflaton Model

First, we shall review the bulk inflaton model [2]. We choose the metric nearby the brane in Gaussian normal coordinates

$$ds^2 = (n_a n_b + q_{ab})dx^a dx^b = dr^2 + q_{\mu\nu}dx^\mu dx^\nu. \tag{3}$$

Keeping the spirit of RS2 scenario in mind, we assume that the brane is located at $r = r_0$ which is the reflection point of the $\mathbf{Z_2}$ symmetry.

By minimizing the action of the 5-dimensional Einstein-scalar system with a RS brane, the Einstein equations in the bulk take the form

$${}^{(5)}G_{ab} + \Lambda_5 g_{ab} = \kappa_5^2 T_{ab}[\phi] + S_{ab}\delta(r - r_0), \tag{4}$$

where κ_5^2 and Λ_5 are the 5-dimensional gravitational and cosmological constants, respectively, and $T_{ab}[\phi]$ is the energy momentum tensor of the minimally coupled bulk scalar field whose form is

$$T_{ab}[\phi] = \partial_a\phi\partial_b\phi - g_{ab}\Big(\frac{1}{2}g^{cd}\partial_c\phi\partial_d\phi + V[\phi]\Big). \tag{5}$$

Here we impose the Neumann boudary condition

$$\partial_r\phi|_{r=r_0} = 0 \tag{6}$$

on the scalar field, which implies that the scalar field does not couple to the surface energy momentum on the brane, given by

$$S_{ab} = -\sigma q_{ab}, \tag{7}$$

where σ is the brane tension.

From Israel's junction condition on the brane

$$\Big[K_{\mu\nu}\Big] = -\kappa_5^2\Big(S_{\mu\nu} - \frac{1}{3}q_{\mu\nu}S\Big) = -\frac{1}{3}\kappa_5^2\sigma q_{\mu\nu}\,, \tag{8}$$

and the $\mathbf{Z_2}$ symmetry, we obtain the 4-dimensional effective Einstein equations on the brane [5]

$${}^{(4)}G_{\mu\nu} = \kappa_4^2 T^{(b)}_{\mu\nu} - E_{\mu\nu}, \tag{9}$$

where

$$\kappa_4^2 = \frac{1}{6}\kappa_5^4\sigma\,, \tag{10}$$

$$T^{(b)}_{\mu\nu} = \frac{4}{\sigma\kappa_5^2}\Big[T_{cd}q^c_a q^d_b + \Big(T_{cd}n^c n^d - \frac{1}{4}T\Big)q_{ab}\Big]\,, \tag{11}$$

$$E_{\mu\nu} \equiv {}^{(5)}C_{abcd}q^a_\mu q^c_\nu n^b n^d. \tag{12}$$

Here we choose the brane tension such that the 4-dimensional, cosmological constant Λ_4 vanishes for $T^{(b)}_{\mu\nu} = 0$.

Considering the FRW metric on the brane with the cosmological scale factor $a(t)$, $E_{\mu\nu}$ is evaluated by Eq. (9) and the 4-dimensional Bianchi identities as

$$E_{tt} = \frac{\kappa_5^2}{2a^4(t)}\int^t dt' a^4(t')\Big(\partial_r^2\phi + \frac{\dot{a}}{a}\dot{\phi}\Big), \quad E_{it} = E_{ij} = 0\,(i \neq j), \tag{13}$$

where we have neglected the contribution of the dark radiation term originated from the integration constant.

Furthermore, we assume that the potential takes the form

$$V[\phi] = V_0 + \frac{1}{2}m^2\phi^2, \tag{14}$$

and consider the region $|m|^2\phi^2/2 \ll V_0$. Under this assumption, we take the perturbation analysis with respect to the amplitude of the scalar field.

In the 0th order, the background metric is determined as [6]

$$ds^2 = b^2(z)(dz^2 - dt^2 + a(t)^2\delta_{ij}dx^i dx^j), \tag{15}$$
$$b(z) = \frac{Hl}{\sinh[H(|z| + z_0)]}, \quad a(t) = \frac{e^{Ht}}{H}.$$

Here $dr = b(z)\,dz$ and the brane is located at $z = 0$. $l = \sqrt{-6/|\Lambda_5 + \kappa_5^2 V_0|}$ is the effective AdS_5 radius. The braneworld inflates with the Hubble rate H described as

$$H^2 = \kappa_5^2 \frac{V_0}{6}. \tag{16}$$

In the 1st order, the evolution of the scalar field on the background metric is determined. Assuming the separable solution form, we obtain the effective 4-dimensional mass as

$$m_{\rm eff}^2 \approx \frac{m^2}{2}, \tag{17}$$

for $H^2 l^2 \ll 1$ and $|m^2|l^2 \ll 1$. The slow-roll condition becomes $|m^2|/H^2 \ll 1$.[4] In this limit, E_{tt} is evaluated as

$$E_{tt} = -\frac{\kappa_5^2}{2a^4}\int^t dt\, a^4\dot{\phi}(\ddot{\phi} + 2H\dot{\phi}) = -\frac{\kappa_5^2}{4}\dot{\phi}^2. \tag{18}$$

Thus, in the 2nd order, the effective Friedmann equations are obtained as

$$3\left(\frac{\dot{a}}{a}\right)^2 = \kappa_4^2\rho_{\rm eff}, \quad -\left[2\frac{\ddot{a}}{a} + \left(\frac{\dot{a}}{a}\right)^2\right] = \kappa_4^2 p_{\rm eff}, \tag{19}$$

where

$$\rho_{\rm eff} = \frac{1}{2}\dot{\Phi}^2 + U_{\rm eff}[\Phi], \tag{20}$$
$$p_{\rm eff} = \frac{1}{2}\dot{\Phi}^2 - U_{\rm eff}[\Phi],$$

and Φ is defined as

$$\Phi = \sqrt{l_0}\phi, \quad l_0 = \frac{6}{\kappa_5^2\sigma}, \tag{21}$$
$$U[\Phi] = \frac{l_0}{2}V(\phi/\sqrt{l_0}).$$

The effective 4-dimensional field Φ behaves as a conventional inflaton on the brane. Thus the standard slow-roll inflation can be realized on the brane at the low-energy limit.

3 Evolution Equations of the Bulk Gravitational Effects

For the spatially homogeneous scalar field, the bulk gravitational effects can be evaluates as Eq. (13). But for considering the comological perturbation theory on the brane, the fluctuation of the effects $\delta E_{\mu\nu}$ must be evatuated by the solving the evolution equations in the 5-dimensional bulk.

First of all, we derive the equations [5, 7]. From the 5-dimensional Bianchi identities and Einstein equations, we find

$$\pounds_n E_{ab} = D^c B_{c(ab)} + K^{cd(4)}C_{acbd} + 4K^c_{(a}E_{b)c} - \frac{3}{2}KE_{ab} - \frac{1}{2}q_{ab}K^{cd}E_{cd} \tag{22}$$
$$+2\tilde{K}_{ac}\tilde{K}^{cd}\tilde{K}_{bd} - \frac{7}{6}\tilde{K}_{ab}\tilde{K}^{cd}\tilde{K}_{cd} + P_{ab}[T^{(2)}_{ab}]$$

[4] It was shown that KK-corrections are negligible for a wide class of initial conditions.

where

$$P_{ab}[T^{(2)}_{ab}] \equiv -\frac{1}{3}\kappa_5^2 T^{(2)}_{de} n^d n^e q_{ab} K + \frac{1}{3}\kappa_5^2 T^{(2)} K_{ab} - \frac{2}{3}\kappa_5^2 K^d_{(a} q^e_{b)} T^{(2)}_{de} + \frac{1}{3}\kappa_5^2 K^{de} T^{(2)}_{de} q_{ab} \tag{23}$$
$$+\frac{2}{3}\kappa_5^2 \pounds_n F^{(2)}_{ab} - \frac{2}{3}\kappa_5^2 D^c \left(T^{(2)}_{de} n^e q^d_{[c} q_{(a]b)} \right) - \kappa_5^2 D_{(a} \left[q^d_{b)} T^{(2)}_{de} n^e \right],$$
$$F^{(2)}_{ab} = T^{(2)}_{fg} q^f_a q^g_b - (T^{(2)}_{fg} n^f n^g - \frac{1}{4} T^{(2)}) q_{ab} - \frac{1}{2} T^{(2)}_{fg} q^{fg} q_{ab}, \quad \tilde{K}_{ab} = K_{ab} - \frac{1}{4} K q_{ab},$$

and

$$\pounds_n B_{abc} = -2 D_{[a} E_{b]c} + K^g_c B_{abg} - 2 B_{cg[a} K^g_{b]} + Q_{abc}[T^{(2)}_{ab}], \tag{24}$$

with

$$Q_{abc}[T^{(2)}_{ab}] \equiv -\frac{2}{3}\kappa_5^2 T^{(2)}_{de} n^e \left(q^d_{[a} K_{b]c} - K^d_{[a} q_{b]c} \right) + \frac{2}{3}\kappa_5^2 \pounds_n \left[T^{(2)}_{de} n^e q^d_{[a} q_{b]c} \right] \tag{25}$$
$$-\frac{2}{3}\kappa_5^2 D_{[a} \left[q_{b]c} (T^{(2)}_{de} n^d n^e - \frac{T^{(2)}}{2}) \right] - \frac{2}{3}\kappa_5^2 D_{[a} \left[q^d_{b]} q^e_c T^{(2)}_{de} \right].$$

B_{abc} is another projection tensor of the 5-dimensional Weyl tensor

$$B_{abc} \equiv q^d_a q^e_b {}^{(5)}C_{decf} n^f, \tag{26}$$

and T_{ab} is the 2nd order part of the energy momentum tensor of the bulk scalar field with respect to the amplitude of the scalar field.

Choosing the conformal coordinate Eq. (15) and eliminating the $B_{\mu\nu\alpha}$ term from the above equations, we obtain the evolution equations of $E_{\mu\nu}$ in the bulk

$$\mathcal{L} E_{\mu\nu} = S_{\mu\nu}[T^{(2)}_{ab}], \tag{27}$$

where

$$\mathcal{L} \equiv b(z) \frac{\partial}{\partial z} \frac{1}{b(z)} \frac{\partial}{\partial z} + \Box_4 - 4H^2, \tag{28}$$
$$S_{\mu\nu}[T^{(2)}_{ab}] \equiv b(z)^4 \left[D^\alpha Q_{\alpha(\mu\nu)}[T^{(2)}_{ab}] + \pounds_n \left(P_{\mu\nu}[T^{(2)}_{ab}] \right) + 2 \left(\frac{b'(z)}{b(z)^2} \right) P_{\mu\nu}[T^{(2)}_{ab}] + D_{(\mu} \Sigma_{\nu)}[T^{(2)}_{ab}] \right],$$
$$\Sigma_\nu[T^{(2)}_{ab}] \equiv \kappa_4^2 D^\alpha T^{(b.2)}_{\nu\alpha} + 2\kappa_5^2 \frac{b'(z)}{b(z)^2} \left(q^\beta_\nu T^{(2)}_{\beta\gamma} n^\gamma \right),$$

to the 2nd order in ϕ. The constraint conditions are

$$D^\mu E_{\mu\nu} = \Sigma_\nu[T^{(2)}_{ab}], \tag{29}$$

which are obtained from the contracted Bianchi identities on the z =constant hypersurface.

The boudary condition on the brane is

$$\frac{\partial}{\partial z} \left(\hat{E}_{\mu\nu} \right) \Big|_b = P_{\mu\nu}[T^{(2)}_{ab}]|_b, \tag{30}$$

which is obtained from Eq. (22) and Israel's junction conditions Eq. (8).

4 Application to the Homogenous Case

For a consistency check of the equations derived in the previous section, we applied them to the spatially homogeneous case.

The (t,t)-component of Eq. (27) is

$$\left[b(z)\partial_z\left(\frac{1}{b(z)}\partial_z\right) - \partial_t^2 - 7H\partial_t - 12H^2\right]E(t,z) = \tilde{S}_{tt}\left[T^{(2)}_{ab}\right], \tag{31}$$

$$\tilde{S}_{tt}\left[T^{(2)}_{ab}\right] = b(z)^4\left[D^\alpha Q_{\alpha tt} + \frac{1}{b(z)^3}\partial_z\left(b(z)^2 P_{tt}\right) + (\partial_t + 4H)\Sigma_t\right].$$

Defining $f(t,z) \equiv a(t)^4 b(z)^3 \tilde{P}_{tt}(t,z)$ and $g(t,z) \equiv -a(t)^4 b(z)^4 \Sigma_t(t,z)$, the relation

$$\partial_t f(t,z) = \partial_z g(t,z) \tag{32}$$

is satisfied in the bulk. This fact implies the existence of a function $M(t,z)$ satisfying

$$f(t,z) = \partial_z M(t,z)\ ,\ g(t,z) = \partial_t M(t,z). \tag{33}$$

Introducing a rescaled function of $M(t,z)$ as

$$\tilde{M}(t,z) \equiv a(t)^{-4} M(t,z), \tag{34}$$

the source function $\tilde{S}_{tt}$ is described as

$$\tilde{S}_{tt}(t,z) = \left[b(z)\partial_z\left(\frac{1}{b(z)}\partial_z\right) - \partial_t^2 - 7H\partial_t - 12H^2\right]\tilde{M}(t,z). \tag{35}$$

The operator acting on $\tilde{M}(t,z)$ is the same as that acting on $\tilde{E}_{tt}$ in Eq.(31). Thus, the solution is

$$\tilde{E}_{tt}(t,z) = \tilde{M}(t,z) \tag{36}$$

in the bulk, neglecting the dark radiation term. Also, we can obtain $\tilde{E}_{it} = \tilde{E}_{ij} = 0 (i \neq j)$ because of $\tilde{S}_{it} = \tilde{S}_{ij} = 0 (i \neq j)$ in the bulk.

Thus, E_{tt} in the bulk can be obtained either by integrating $f(t,z)$ with respect to z or by integrating $g(t,z)$ with respect to t. In particular, the result agrees with Eq. (13) on the brane, which verifies the consistency of Eq. (27).

5 Conclusion

The aim of our study is to verify if the bulk inflaton model can reproduce the observational results and can predict new effects specific to the braneworld scenario. The spatially homegeneous background solution has been shown to reproduce the standard picture at the low energy limit [2, 3, 4]. The perturbed bulk gravitational effects onto the brane is described by $\delta E_{\mu\nu}$, and it must be evaluated by solving the evolution equation (2) in the bulk.

In this talk, we derived the evolution equations for $E_{\mu\nu}$, and solved them in the case of the homogeneous background. The result is in complete agreement with the previous result obtained on the brane [2, 4]. Our next step is to solve $\delta E_{\mu\nu}$ using the equations derived in the above. This is currently in progress.

References

[1] L. Randall and R. Sundrum, Phys. Rev. Lett. **83**, 4690 (1999).

[2] Y. Himemoto and M. Sasaki, Phys. Rev. D **63**, 044015 (2001).

[3] N. Sago, Y. Himemoto and M. Sasaki, Phys. Rev. D **65**, 024014 (2002).

[4] Y. Himemoto, T. Tanaka and M. Sasaki, Phys. Rev. D **65**, 104020 (2002).

[5] T. Shiromizu, K. i. Maeda and M. Sasaki, Phys. Rev. D **62**, 024012 (2000).

[6] J. Garriga and M. Sasaki, Phys. Rev. D **62**, 043523 (2000).

[7] M. Sasaki, T. Shiromizu and K. i. Maeda, Phys. Rev. D **62**, 024008 (2000).

Particle velocity in noncommutative space-time

Umpei Miyamoto,[1] Takashi Tamaki,[2] and Tomohiro Harada[3]

Department of Physics, Waseda University, Ohkubo, Shinjuku, Tokyo 169-8555, Japan

Takashi Torii,[4]

Advanced Research Institute for Science and Engineering, Waseda University, Ohkubo, Shinjuku, Tokyo 169-8555, Japan

Abstract

We investigate a particle velocity in the κ-Minkowski space-time, which is one of the realization of a noncommutative space-time. We emphasize that arrival time analyses by high-energy γ-rays or neutrinos, which have been considered as powerful tools to restrict the violation of Lorentz invariance, are not effective to detect space-time noncommutativity. In contrast with these examples, we point out a possibility that *low-energy massive particles* play an important role to detect it.

1 Introduction

Several attempts have been made to extract information and effects of the microscopic space-time structure. Among them, the simplest way is modifying the dispersion relation that leads to the violation of Lorentz invariance. We call the theories obtained by this method modified dispersion relation (MDR) models.

Remarkably enough, it was discussed that the anomalous detection of the ultra-high energy cosmic rays beyond the Greisen-Zatsepin-Kuzmin cutoff may be observational evidence for the violation of Lorentz invariance[1].

It has been discussed that there is a severe constraint on the energy scale where the Lorentz invariance might be violated, i.e., the scale of quantum gravity as $E_{QG} \gtrsim 7.2 \times 10^{16}$ GeV by the detection of γ-rays from Markarian (Mk) 421 as pointed out in Ref. [2]. They examined the energy dependence of the arrival time of photons and compared it with the observations of Mk 421 to obtain this constraint.

In general, however, it is plausible that not only a dispersion relation but also other relations such as energy-momentum conservation laws might be altered in a Planck scale physics. A particle velocity in such models may have qualitative difference from that in the MDR models. To investigate these features, we employ a model called κ-Minkowski space-time, where noncommutativity is introduced as $[x^i, t] = i\lambda x^i$ [3], and compare a group velocity in the κ-Minkowski space-time evaluated in our previous paper[1] with that in the MDR models.

We also discuss a possibility that the space-time noncommutativity might be detected by using low-energy massive particles. See [4] for details. We use the signature $(-,+,+,+)$ and units in which $c = \hbar = 1$ below.

2 Modified Dispersion Relation Models

Although there are various ways to modify the dispersion relation, we consider here the form in Ref. [2] as $p^2 + m^2 = E^2[1 + f(E/E_{QG})]$, where f is a model-dependent function and E_{QG} is the effective energy

[1] E-mail:umpei@gravity.phys.waseda.ac.jp
[2] E-mail:tamaki@gravity.phys.waseda.ac.jp
[3] E-mail:harada@gravity.phys.waseda.ac.jp
[4] E-mail:torii@gravity.phys.waseda.ac.jp

scale of quantum gravity. In the low-energy limit, $E \ll E_{QG}$, the above dispersion relation becomes

$$p^2 + m^2 = E^2 + \frac{\xi E^n}{E_{QG}^{n-2}}, \tag{1}$$

up to the lowest correction. We have chosen $\xi = \pm 1$ and $n \geq 3$ is the integer, which is determined by the form of the function f.

The velocity v_{MDR} in this model is obtained by differentiating the dispersion relation (1) with respect to p,

$$v_{MDR} := \frac{dE}{dp} = \frac{2\sqrt{E^2 - m^2 + \xi E^n / E_{QG}^{n-2}}}{2E + n\xi E^{n-1}/E_{QG}^{n-2}}. \tag{2}$$

Let us consider a γ-ray from the distant source. We approximate the velocity of the γ-ray by expanding Eq. (2) by E/E_{QG} to

$$v_{MDR} \approx 1 - \frac{\xi(n-1)}{2}\left(\frac{E}{E_{QG}}\right)^{n-2}. \tag{3}$$

The time delay is evaluated as

$$\begin{aligned} \delta t &= \frac{L}{v_{MDR}(E_1)} - \frac{L}{v_{MDR}(E_2)} \\ &\approx \frac{(n-1)\xi L}{2{E_{QG}}^{n-2}}({E_1}^{n-2} - {E_2}^{n-2}), \end{aligned} \tag{4}$$

where L, E_1 and E_2 are the distance from the source to the Earth, amounts of the energy of particles 1 and 2, respectively.

One of the examples of this kind of analyses is the arrival time analysis by γ-rays from Mk 421 ($\sim$ 150 Mpc from the Earth). It was reported that γ-rays in the energy range between 1 and 2 TeV arrived at the Earth within the time difference $\sim$ 200 seconds[5]. Then, E_{QG} is constrained to $E_{QG} \gtrsim \left[3.6 \times (n-1)(n-2) \times 10^{13}\right]^{1/(n-2)} \times 10^3$ GeV. Since the value of n has been assumed to be 3 in most of the previous works, it has been concluded that $E_{QG} \gtrsim 7.2 \times 10^{16}$ GeV. We should note, however, that n may be 4 or larger. In this case, the constraint becomes $E_{QG} \gtrsim 1.5 \times 10^{10}$ GeV for $n = 4$ and $E_{QG} \gtrsim 7.6 \times 10^7$ GeV for $n = 5$. Hence the constraint may become quite loose compared with the previous reports.

3 κ-Poincarè algebra and κ-Minkowski space-time

Here, we review the κ-Poincarè algebra[6], which has the structure of a Hopf algebra (quantum group). The generators of the κ-Poincarè algebra $\mathcal{P}_\kappa$ satisfy the following commutation relations:

$$[M_{\mu\nu}, M_{\rho\sigma}] = i\left(\eta_{\mu\sigma}M_{\nu\rho} - \eta_{\mu\rho}M_{\nu\sigma} + \eta_{\nu\rho}M_{\mu\sigma} - \eta_{\nu\sigma}M_{\mu\rho}\right), \tag{5}$$

$$[M_i, p_0] = 0, \tag{6}$$

$$[M_i, p_j] = i\epsilon_{ijk}p_k, \tag{7}$$

$$[N_i, p_0] = ip_i, \tag{8}$$

$$[N_i, p_j] = -i\delta_{ij}\left[\frac{1}{2\lambda}\left(1 - e^{2p_0\lambda}\right) + \frac{\lambda}{2}\mathbf{p}^2\right] + i\lambda p_i p_j, \tag{9}$$

$$[p_\mu, p_\nu] = 0, \tag{10}$$

where $M_i \equiv \frac{1}{2}\epsilon_{ijk}M_{jk}, N_i \equiv M_{0i}$ and p_μ are generators of rotation, boost and translation, respectively. We can recover the ordinary commutation relations of the Poincarè algebra in the limit $\lambda \to 0$. The

dispersion relation is determined by the eigenvalue of the Casimir operator that commutes with all elements in $\mathcal{P}_\kappa$:

$$\frac{2\cosh(\lambda p_0)}{\lambda^2} - \boldsymbol{p}^2 e^{-\lambda p_0} = \frac{2\cosh(\lambda m)}{\lambda^2}, \tag{11}$$

where the rest mass m is defined as the energy with $p_i = 0$. The coproducts $\Delta : \mathcal{P}_\kappa \to \mathcal{P}_\kappa \otimes \mathcal{P}_\kappa$ of the basic generators are

$$\begin{aligned}
\Delta(M_i) &= M_i \otimes 1 + 1 \otimes M_i, & (12)\\
\Delta(N_i) &= N_i \otimes 1 + e^{p_0\lambda} \otimes N_i - \lambda \epsilon_{ijk} p_j \otimes M_k, & (13)\\
\Delta(p_0) &= p_0 \otimes 1 + 1 \otimes p_0, & (14)\\
\Delta(p_i) &= p_i \otimes 1 + e^{p_0\lambda} \otimes p_i. & (15)
\end{aligned}$$

The above coproducts of p_μ, (14) and (15), are interpreted as the non-Abelian addition law of energy-momenta for particles 1 and 2 as

$$(E_1, \boldsymbol{p}_1) \hat{+} (E_2, \boldsymbol{p}_2) := \left(E_1 + E_2, \boldsymbol{p}_1 + e^{\lambda E_1} \boldsymbol{p}_2\right), \tag{16}$$

where we identify p_0 with energy E.

The asymmetry of the coproducts for the permutation of particles is called noncocommutativity. The noncocommutativity of the coproducts for the translation sector $T \subset \mathcal{P}_\kappa$ has two important meanings. One is that the noncommutativity of the κ-Minkowski space-time is a direct consequence of the noncocommutativity. Elements in the κ-Minkowski space-time are defined as linear functionals on the translation sector, $T^* : T \to \mathbf{C}$. The products in T^* is defined in terms of coproducts in T, i.e., $\forall x, y \in T^*$ and $\forall p \in T$,

$$\begin{aligned}
\langle xy, p\rangle :=& \quad \langle x \otimes y, \Delta p\rangle & (17)\\
=& \quad \sum_a \langle x, p_{a(1)}\rangle \langle y, p_{a(2)}\rangle, & (18)
\end{aligned}$$

where we write the coproducts as $\Delta(p) = \sum_a p_{a(1)} \otimes p_{a(2)}$. With the duality relations $\langle x^\mu, p_\nu\rangle = -i\delta^\mu_\nu$, this leads to the following commutation relations[3]:

$$\begin{aligned}
\left[x^i, x^0\right] &= i\lambda x^i, & (19)\\
\left[x^0, x^0\right] &= 0, & (20)\\
\left[x^i, x^j\right] &= 0. & (21)
\end{aligned}$$

The other is that the noncocommutativity leads to a deformed group velocity formula[1], which is different from the usual velocity formula $dE/d\boldsymbol{p}$ as will be shown in the next section.

The plane wave $\psi_{(E,\boldsymbol{p})} = e^{i\boldsymbol{p}\cdot\boldsymbol{x}} e^{iEt}$ in the κ-Minkowski space-time introduced in [7] respects the non-Abelian addition law of energy-momenta in the sense

$$\begin{aligned}
\psi_{(E_1,\boldsymbol{p}_1)}\psi_{(E_2,\boldsymbol{p}_2)} &= e^{i\boldsymbol{p}_1\cdot\boldsymbol{x}} e^{iE_1 t} e^{i\boldsymbol{p}_2\cdot\boldsymbol{x}} e^{iE_2 t} & (22)\\
&= \psi_{(E_1+E_2,\boldsymbol{p}_1+e^{\lambda E_1}\boldsymbol{p}_2)}. & (23)
\end{aligned}$$

4 Velocity formula

From the properties in the κ-Minkowski space-time in Sec 3, we can establish group velocity formulae. For this purpose, we consider infinitesimal changes ΔE and $\Delta\boldsymbol{p}$ in E and $\boldsymbol{p}$, respectively, as a result of adding $(\Delta E', \Delta\boldsymbol{p}')$ as

$$(E, \boldsymbol{p}) \hat{+} (\Delta E', \Delta\boldsymbol{p}') = (E + \Delta E, \boldsymbol{p} + \Delta\boldsymbol{p}). \tag{24}$$

By the addition law (16), we have

$$(\Delta E', \Delta\boldsymbol{p}') = (\Delta E, \frac{\Delta\boldsymbol{p}}{e^{\lambda E}}). \tag{25}$$

Next, we construct a wave packet by superposing plane waves. Here we only consider two waves for simplicity, whose momenta and amounts of energy are different infinitesimally from each other.

$$\begin{aligned} I &= \psi_{(E-\Delta E,\boldsymbol{p}-\Delta\boldsymbol{p})} + \psi_{(E+\Delta E,\boldsymbol{p}+\Delta\boldsymbol{p})} \\ &\cong 2e^{i\boldsymbol{p}\cdot\boldsymbol{x}}e^{iEt}\cos\left[\frac{\Delta\boldsymbol{p}}{e^{\lambda E}}\cdot\left(\boldsymbol{x}+\frac{e^{\lambda E}\Delta E t}{\Delta\boldsymbol{p}}\right)\right], \end{aligned} \tag{26}$$

where we neglected the terms that vanish in the limit $\Delta\boldsymbol{p}\to 0$. The group velocity v_λ of this wave packet can be written as

$$v_\lambda := e^{\lambda E}\frac{dE}{d\boldsymbol{p}}. \tag{27}$$

This velocity can be expressed explicitly in terms of the functions of E and m by using the dispersion relation. By the definitions of v_λ, we find

$$v_\lambda = \frac{e^{\lambda E/2}\sqrt{2[\cosh(\lambda E)-\cosh(\lambda m)]}}{|e^{\lambda E}-\cosh(\lambda m)|}\boldsymbol{e}, \tag{28}$$

where $\boldsymbol{e} := \boldsymbol{p}/|\boldsymbol{p}|$.

5 Measurements of the effective scale of "Quantum Gravity" by massive particles

In this section, we compare v_λ with v_{MDR} and discuss the possibility of detection of effective scale of quantum gravity by observations and experiments. The behavior of the velocities is quite different depending on the mass and energy of the particle. Hence, we consider two limiting cases: (i) the "relativistic" case ($m \ll E$) and (ii) "non-relativistic" case ($m \approx E$).

In the relativistic case, $m \ll E$, and under the assumptions, $E \ll E_{QG}$ and $E \ll |\lambda^{-1}|$, v_{MDR} and v_l are

$$v_{MDR} \approx 1-\frac{1}{2}\left(\frac{m}{E}\right)^2-\frac{\xi(n-1)}{2}\left(\frac{E}{E_{QG}}\right)^{n-2}, \tag{29}$$

$$v_l \approx 1-\frac{1}{2}\left(\frac{m}{E}\right)^2+\frac{\lambda m^2}{2E}, \tag{30}$$

at the lowest order of m/E and E/E_{QG} in the MDR models and λE in the κ-Minkowski space-time, respectively. When $m=0$ in the MDR models, E_{QG} can be constrained by the γ-rays from the Mk 421 as mentioned in Sec. 2. However, since $v_\lambda = 1$ for massless particles, (we can confirm this is also true for all order of λm and λE), λ is not constrained by massless particles. The situation changes for massive particles since the lowest order correction appears in the coupled form with the mass of the particle in the κ-Minkowski space-time, while that of the MDR models does not depend on the mass of the particle.

Next, we examine the non-relativistic case, $m \sim E \ll E_{QG}$ (or $|\lambda^{-1}|$). The velocity in each model are

$$\begin{aligned} v_{MDR} &\approx \sqrt{1-\left(\frac{m}{E}\right)^2}\times \\ &\quad\left[1+\frac{\xi}{2}\frac{E^2(1-n)+nm^2}{E^2-m^2}\left(\frac{E}{E_{QG}}\right)^{n-2}\right], \end{aligned} \tag{31}$$

$$v_\lambda \approx \sqrt{1-\left(\frac{m}{E}\right)^2}\left(1+\frac{\lambda m^2}{2E}\right). \tag{32}$$

Note that the absolute value of the correction for the velocity in the κ-Minkowski space-time decreases with the energy, while that in the MDR model increases. Although, in the low-energy limit, the dispersion

relation in the κ-Minkowski space-time has the same form as that in the MDR models, the correction for the velocity is quite different.

Because of the above difference in the correction terms, there is a possibility that the evidence for space-time noncommutativity can be detected in use of the low-energy massive particles. Here, we consider the ultra-cold neutrons with energy $E_n - m_n \sim 10^{-2}$ eV[8]. Since the mass of a neutron m_n is measured with high accuracy, we can estimate the time interval in which the neutron travels the interval L in the Minkowski space-time. If a time lag is obtained in an experiment, it can be interpreted as the effect of space-time noncommutativity. This time lag is calculated in the κ-Minkowski space-time as

$$\delta t = \frac{L}{v_l} - \frac{L}{v_M} \approx \frac{L}{v_M} \frac{\lambda m_n^2}{2E_n}. \tag{33}$$

By substituting the value of the apparatus[9], $L \sim 100$ m, we have

$$\delta t \sim 10^{-1} \lambda m_n. \tag{34}$$

If the resolution for the measurement of the time lag is $\sim 10^{-10}$ s and $|\lambda| \gtrsim 10^{-18}$ eV^{-1}, we can detect space-time noncommutativity.

6 Conclusion

We have investigated what are the qualitative differences of the velocity formula in the κ-Minkowski space-time from that in the MDR models.

We have found that since massless particles move in a constant speed in the κ-Minkowski space-time, the arrival time analyses by γ-rays are not capable to detect the difference from the Minkowski space-time. This example shows that it is difficult to constrain all kinds of Lorentz invariance by a single experiment. Therefore, we need to investigate specific models individually. We have also considered the possibility to detect space-time noncommutativity by low-energy massive particles. In our model, if the resolution for the measurement of the time lag is given by $\sim 10^{-10}$ s, it *is* possible to constrain λ to $|\lambda| \gtrsim 10^{-18}$ eV^{-1}. Although these features had not been investigated so far, it may be important.

References

[1] G. Amelino-Camelia and T. Piran, Phys. Rev. D **64**, 036005 (2001); T. Tamaki, T. Harada, U. Miyamoto, and T. Torii, Phys. Rev. D **65**, 083003 (2002).

[2] G. Amelino-Camelia et al., Nature **393**, 763 (1998).

[3] S. Majid and H. Ruegg, Phys. Lett. B **334**, 348 (1994).

[4] T. Tamaki, T. Harada, U. Miyamoto, and T. Torii, Phys. Rev. D **66**, 105003 (2002).

[5] Biller et al., Phys. Rev. Lett. **83**, 2108 (1999).

[6] J. Lukierski, A. Nowicki, H. Ruegg and V. N. Tolstoy, Phys. Lett. B **264**, 331 (1991).

[7] P. Kosiński, J. Lukierski, P. Maślanka and A. Sitarz, Czech. Journal of Phys. **48**, 1407 (1998); P. Kosiński, J. Lukierski and P. Maślanka, *Proc. of XXII Int. Colloquium on Group-Theor. Methods in Physics, p.423*, (International Press, Boston, 1999); P. Kosiński, J. Lukierski and P. Maślanka, Phys. Rev. D **62**, 025004 (2000); G. Amelino-Camelia and S. Majid, Int. J. Mod. Phys. A **15**, 4301 (2000).

[8] D. Dubbers, Prog. in Part. and Nucl. Phys. A **26**, 173 (1991).

[9] D. R. Rich et al., physics/9908050.

Cosmology based on the Brane-induced gravity theory with higher curvature terms

Shuntaro Mizuno[a1] , Kei-ichi Maeda[a,b,c2] , Takashi Torii[b3]

[a] *Department of Physics, Waseda University, Okubo 3-4-1, Shinjuku, Tokyo 169-8555, Japan*
[b] *Advanced Research Institute for Science and Engineering, Waseda University, Shinjuku, Tokyo 169-8555, Japan*
[c] *Waseda Institute for Astrophysics. WasedaUniversity, Shinjuku, Tokyo 169-8555, Japan*

Abstract

We study the cosmology based on the brane-induced gravity theory, in which gravitational action on the brane is induced via quantum effects of matter fields. At first, we present the effective equations to describe the four-dimensional gravity of a brane world, assuming that a five-dimensional bulk spacetime satisfies the Einstein equations and gravity is confined on the Z_2 symmetric brane. Applying this formalism, we study the effects of the higher-curvature terms to the cosmological scenario.

1 Introduction

Recent several observations suggest that the universe is dominated by a cosmological constant, or a kind of dark energy, whose value is almost comparable to the present mass density of the universe. From the viewpoint of particle physics, however, it is quite difficult to explain such a tiny value by 14 orders of magnitude smaller than the electroweak scale. The failure of theoretical explanations for the present value of the cosmological constant is known as the so-called "Cosmological Constant Problem."

Recently, in order to explain this, brane-induced gravity model proposed by Dvali Gabadadze, and Porrati are explored, [1]. This model is interesting because the gravity induced by the interaction between the bulk gravity and brane matter leads four-dimensional Newtonian gravity on a 3-brane at high energy scale, [2]. In Sec.2, we derive the covariant effective gravitational field equations on a brane, [3].

Even though the original brane-induced gravity model did not include other than Einstein-Hilbert term, in principle, our approach can treat higher curvature terms. Among the correction terms, the terms related to trace-anomaly naturally arise in the context of the quantum field theory in curved space, [4]. Actually, the inflation model driven by the trace-anomaly of massless, conformally coupled matter field are extensively studied within the framework of the four-dimensional theory, [5]. (For the relation between this model and AdS/CFT correspondence see[6].) In sec. 3, we study the cosmological scenario with higher terms of brane-induced gravith and evaluate the possibility of building a model, in which early inflation and present acceleration of the universe without any scalar field, [7].

2 Model

We consider the following model;

$$S = \frac{1}{2\kappa_5{}^2}\int d^5x\sqrt{-g}\left[{}^{(5)}R - 2^{(5)}\Lambda\right] + \int d^4x\sqrt{-q}\left[\frac{\mu^2}{2}R + L_{correction}(q_{\mu\nu}) - \lambda + L_m\right]. \tag{1}$$

where κ_5 is related to the five-dimensional gravitational constant as $\kappa_5^2 = 8\pi G_5$, and μ is the four-dimensional Planck mass on the brane; as they stand in (1), κ_5 and μ are independent.${}^{(5)}R$ is the scalar curvature with respect to the five-dimensional metric $g_{\mu\nu}$ and R is that to the four-dimensional induced metric $q_{\mu\nu}$ on the brane. These metrics are related with $q_{\mu\nu} = g_{\mu\nu} - n_\mu n_\nu$, where n^μ is the vector

[1] E-mail:shuntaro@gravity.phys.waseda.ac.jp
[2] E-mail:maeda@gravity.phys.waseda.ac.jp
[3] E-mail:torii@gravity.phys.waseda.ac.jp

unit normal to the brane. In this talk, since we do not persist in Minkowski bulk, we generalize Dvali, Gabadadze and Porrati model by including the five-dimensional cosmological constant ${}^{(5)}\Lambda$ and the bane tension λ. In the following, we will consider the case only for the case $\lambda > 0$. $L_{correction}(q_{\mu\nu})$ is the correction term related with the gravity on the brane and L_m is the matter Lagrangian on the brane.

In such situations, the gravitational field equations on the brane are obtained [8], by use of Israel's thin shell formalism and assuming Z_2 symmetry, by

$$G_{\mu\nu} = -\Lambda q_{\mu\nu} + \frac{\kappa_5^4}{6}\lambda\tau_{\mu\nu} + \kappa_5{}^4\pi_{\mu\nu} - E_{\mu\nu}, \tag{2}$$

where $G_{\mu\nu}$ is the Einstein tensor with respect to the intrinsic metric $q_{\mu\nu}$ and Λ is the four-dimensional cosmological constant given by

$$\Lambda = \frac{1}{2}\left[{}^{(5)}\Lambda + \frac{1}{6}\kappa_5{}^4\lambda^2\right]. \tag{3}$$

$E_{\mu\nu}$ is a part of the five-dimensional Weyl tensor and carries some information about bulk geometry. For "energy momentum tensor" $\tau_{\mu\nu}$, in addition to the ordinal matter energy-momentum tensor, the contributions from the brane-induced gravity is added, and it takes the following form as

$$\begin{aligned}\tau_{\mu\nu} : &= -\frac{2}{\sqrt{-q}}\frac{\delta}{\delta q^{\mu\nu}}\left[\sqrt{-q}\left(\frac{\mu^2}{2}R + L_{matter} + L_{correction}(q_{\mu\nu})\right)\right] \\ &= T_{\mu\nu} - \mu^2 G_{\mu\nu} - F_{\mu\nu},\end{aligned} \tag{4}$$

where $F_{\mu\nu}$ expresses the effects of the higher curvature. $\pi_{\mu\nu}$ is quadratic in this $\tau_{\mu\nu}$,

$$\pi_{\mu\nu} = -\frac{1}{4}\tau_{\mu\alpha}\tau_\nu{}^\alpha + \frac{1}{12}\tau\tau_{\mu\nu} + \frac{1}{8}q_{\mu\nu}\tau_{\alpha\beta}\tau^{\alpha\beta} - \frac{1}{24}q_{\mu\nu}\tau^2. \tag{5}$$

Next, in order to discuss the cosmology, we derive the Friedmann equation on the brane. If we assume the Friedmann-Robertson-Walker metric and the perfect fluid matter with the equation of state $p = (\gamma - 1)\rho$ on the brane, $\tau_{\mu\nu}$ is calculated as

$$\tau_{tt} = \rho - 3\mu^2 X - F_{tt}, \quad \tau_{ij} = \left\{p + \mu^2(3X + 2Z) - F_{kk}\right\}q_{ij}, \tag{6}$$

where we have used the new variables X and Z related to the Hubble parameter $H = \dot{a}/a$ and its derivative, defined by $X \equiv H^2 + (k/a^2)$ and $Z \equiv \dot{H} - (k/a^2)$.

Substituting these relations into (5), we obtain

$$\pi_{tt} = \frac{1}{12}\tau_{tt}^2, \quad \pi_{ij} = \frac{1}{12}\tau_{tt}(\tau_{tt}q_{ij} + 2\tau_{ij}). \tag{7}$$

Then the Friedmann equation becomes

$$X - \frac{\rho}{3\mu^2} + \frac{1}{3\mu^2}F_{tt} = \frac{\lambda}{3\mu^2} + \epsilon\frac{2}{\kappa_5^2\mu^2}\sqrt{X + \frac{\kappa_5^4\lambda^2}{36} + \frac{E_{tt}}{3} - \frac{1}{3}\Lambda}, \tag{8}$$

where $\epsilon = \pm 1$, and we will use this in the following in this order. (l.h.s.)$= 0$ is the usual 4-dimensional Friedmann equation with higher curvature corrections, and the r.h.s is the effect of the brane-induced gravity.

For the time evolution of the energy density of the matter, since it can be shown that the local energy conservation holds on the brane, $(\nabla^\mu T_{\mu\nu} = 0)$, $\rho \propto a^{-3\gamma}$ holds. For the contribution from the Weyl tensor $E_{\mu\nu}$, because in the Friedmann-Robertson-Walker spacetime, it can be shown that the following constraint equation, $(\nabla^\mu E_{\mu\nu} = 0)$ holds even with the brane-induced gravity model, $E_{\mu\nu}$ behaves like the radiation, that is $E_{tt} \propto a^{-4}$. With these relations, and some initial conditions, this system can be closed.

3 Cosmology with higher curvature terms

Based on the Friedmann equation derived in the previous section, we propose a new cosmological scenario. As for the induced gravity on the brane, in addition to Einstein-Hilbert action, we consider the term originated from the trace-anomaly. (For four-dimensional trace-anomaly driven inflation, see [5].)

3.1 Trace-anomaly

It is known that in a curved space-time, even in the absence of matter, quantum fluctuations of matter fields give nontrivial contributions to $< T_{\mu\nu} >$. In the case of free, massless, conformally invariant fields, these quantum corrections take the following form, [4].

$$F_{\mu\nu} = - < T_{\mu\nu} > = F^{(1)}_{\mu\nu} + F^{(3)}_{\mu\nu}, \tag{9}$$

$$F^{(1)}_{\mu\nu} = -k_1\Big(2RR_{\mu\nu} - \frac{1}{2}g_{\mu\nu}R^2 - 2\nabla_\mu\nabla_\nu R + 2g_{\mu\nu}\nabla_\alpha\nabla^\alpha R\Big), \tag{10}$$

$$F^{(3)}_{\mu\nu} = k_3\Big(-R^\sigma_\mu R_{\nu\sigma} + \frac{2}{3}RR_{\mu\nu} + \frac{1}{2}g_{\mu\nu}R^{\sigma\tau}R_{\sigma\tau} - \frac{1}{4}g_{\mu\nu}R^2\Big). \tag{11}$$

$F^{(1)}_{\mu\nu}$ can be derived by the variation of $\sqrt{-g}R^2$. Since in the quantum field theory, an arbitrary finite counter-term of this form can be added, the coefficient k_1 can take any value and can be determined by experiment. Here, as in [5], in order to end the first inflation, we will take k_1 not to be 0. The tensor $F^{(3)}_{\mu\nu}$, on the other hand, is conserved only in conformally flat spacetime and cannot be obtained by varying a local action and its coefficient k_3 is uniquely determined as,

$$k_3 = \frac{1}{1440\pi^2}\Big(N_0 + \frac{11}{2}N_{1/2} + 31N_1\Big), \tag{12}$$

where N_0, $N_{1/2}$, and N_1 are the numbers of quantum fields with spin 0, 1/2, and 1, respectively.

3.2 Basic equation

Substituting this form into (8) , we obtain the Friedmann equation,

$$X - \frac{\rho}{3\mu^2} - \frac{k_1}{3\mu^2}\Big[-18Z(2X+Z) - 36H(2\dot{X}+\dot{Z}) + \frac{k_3}{k_1}X^2\Big] = \frac{\lambda}{3\mu^2} + \epsilon\frac{2}{\kappa_5^2\mu^2}\sqrt{X + \frac{\kappa_5^4\lambda^2}{36} + \frac{E_{tt}}{3} - \frac{1}{3}\Lambda}. \tag{13}$$

Furthermore, for simplicity, we assume only the flat universe brane, ($k = 0$) and zero cosmological constant on the brane. In this case, the variable X and Z in Eq.(13) can be written as $X = H^2$ and $Z = \dot{H}$. In addition to this, in order to investigate the role of the correction terms, we concentrate on the vacuum solution which can be applied in the early stage before particle production and late stage after matter energy density has been diluted. Then, the Friedmann equation (13) becomes

$$\ddot{H} + \Big(3H - \frac{\dot{H}}{2H}\Big)\dot{H} + \frac{\mu^2}{12k_1}\Big[-\frac{k_3}{\mu^2}H^3 + H - \frac{\lambda}{3\mu^2 H} - \epsilon\frac{2}{\kappa_5^2\mu^2}\sqrt{1 + \frac{\kappa_5^4\lambda^2}{36H^2}}\Big] = 0, \tag{14}$$

where we have neglected $E_{\mu\nu}$ tensor, because it behaves like radiation ($E_{tt} \propto a^{-4}$) and it can be expected this term is dilluted sufficiently during the inflationary stage.

This equation can be analyzed as follows: If we assume the second term of Eq.(14) as the friction term, this can be understood as the motion of the test particle in the presence of the effective potential $V(H)$, that is given as

$$V(H) = -\frac{k_3}{48k_1}H^4 + \frac{\mu^2}{24k_1}H^2 - \frac{\lambda}{36k_1}\left[\ln H + \epsilon\left(\sqrt{1 + \frac{36H^2}{\kappa_5^4\lambda^2}} + \ln\left(\frac{6H}{\kappa_5^2\lambda + \sqrt{\kappa_5^4\lambda^2 + 36H^2}}\right)\right)\right], \tag{15}$$

where we have assumed the expanding universe, that is $H \geq 0$. If we choose the parameters satisfying $\mu/\sqrt{k_3} \gg (\sqrt{2}/\mu)\sqrt{(\lambda/3) + (2/\kappa_5^4\mu^2)}$, the schematical shape of this potential takes as Fig.1 for $\epsilon = 1$.

3.3 Inflationary phase

Then, we will analyze the time evolution at the early stage of this model. Initially, according to [6], H is near the top of the potential $H \sim \mu/\sqrt{k_3}$ and $|\dot{H}|$ is small, $|\dot{H}| \ll \mu^2/k_3$. In this situation, Eq.(14) can be rewritten as

$$\ddot{H} + \Big(3H - \frac{\dot{H}}{2H}\Big)\dot{H} - \frac{k_3}{12k_1}H^3 + \frac{\mu^2}{12k_1}H = 0. \tag{16}$$

This is nothing but the equation of the conventional four-dimensional trace-anomaly driven inflation. [5] Therefore, the analysis for finding the unstable inflationary solution is the same as that case. We will first solve Eq.(16) assuming $H(t)$ to be slowly varying, ($|\dot{H}| \ll H^2$, $|\ddot{H}| \ll |H\dot{H}|$.) Then, in this stage, the solution of this equation is

$$H(t) = \frac{\mu}{\sqrt{k_3}}\tanh\Big[\gamma - \frac{\sqrt{k_3}\mu}{36k_1}t\Big], \qquad \gamma = \frac{1}{2}\ln\Big(\frac{1}{1-(k_3/\mu)H(0)}\Big), \tag{17}$$

where $H(0)$ is the hubble parameter at initial, $t = 0$.

From this equation, we see that $H(t)$ changes on a time scale $\sim 36k_1/(\mu\sqrt{k_3})$.Therefore, long inflation is obtained if $36k_1 \gg k_3$. To estimate the limits of validity of this approximation, we substitute it in Eq.(16) and find when the neglected terms become compatible to those we have kept. This happens at $t = 36\gamma k_1/(\mu\sqrt{k_3})$ and $H \sim \mu/(\sqrt{6k_1})$. Therefore, in this stage, in the course of inflation, the habble parameter gradually changes from $H \sim \mu/\sqrt{k_3}$ to $H \sim \mu/\sqrt{6k_1}$.

3.4 Oscillating phase

After H becomes smaller than $\mu/\sqrt{6k_1}$, since $H \ll \mu/\sqrt{k_3}$, the last term of Eq.(16) can be neglected, and as long as the condition $H \gg (\sqrt{2}/\mu)\sqrt{(\lambda/3) + (2/\kappa_5^4\mu^2)}$ satisfies, the following equation holds:

$$2H\ddot{H} + 6H^2\dot{H} - \dot{H}^2 + \frac{\mu^2}{6k_1}H^2 = 0. \tag{18}$$

An approximate solution of Eq.(18) is

$$H = \frac{4}{3t}\cos^2\Big[\frac{\mu t}{2\sqrt{6k_1}t}\Big]\Big[1 - \frac{\sin\frac{\mu t}{2\sqrt{6k_1}t}}{\frac{\mu t}{2\sqrt{6k_1}t}}\Big] + O(t^{-3}) \tag{19}$$

$$a(t) = \text{const} \times t^{2/3}\big[1 + (2\sqrt{6k_1}/3\mu t)\sin(\mu t/\sqrt{6k_1}) + O(t^{-2})\big]. \tag{20}$$

This stage corresponding to the "oscillating phase" in the ordinary scalar field driven inflation model and the particle production is expected to be occurred at this stage. After this, radiation dominant universe is realized.

3.5 Late-time behavior

After this, as H decreases to the same order as $(\sqrt{2}/\mu)\sqrt{(\lambda/3) + (2/\kappa_5^4\mu^2)}$, the effect of the brane induced gravity becomes clearer, and depending on the sign of ϵ, the late time cosmology is classified. For the $\epsilon = 1$ branch, as can be seen from the shape of the potential $V(H)$, the inflationary solution with $H = \sqrt{\frac{2}{\mu^2}(\frac{\lambda}{3} + \frac{2}{\kappa_5^4\mu^2})}$ is the late-time attractor. On the other hand, $\epsilon = -1$ branch, the $H = 0$ Minkowski spacetime is the late-time attractor and around the scale $H \sim \sqrt{\frac{2}{\mu^2}(\frac{\lambda}{3} + \frac{2}{\kappa_5^4\mu^2})}$ the expansion law is changed from the four-dimensional one to the five-dimensional one, unless we consider the nonzero Λ.

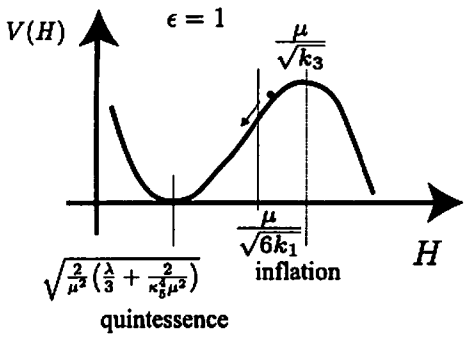


Figure 1: The shape of the effective potential for H. In the case for $\epsilon = -1$, the minimum shifts to $H = 0$.

3.6 Constraints for the parameters

As the above, if the parameters are set to be well and $\epsilon = 1$ branch are selected, this model serves as "scalar field free quintessential inflation model." For this scenario works well, we discuss the constraints for parameters $k_1, k_3, \mu, \kappa_5, \lambda$ here. At first, k_3 is fixed by the theory as Eq.(12), and as long as the condition $k_1 \gg k_3$ satisfies, it is not constrained by observations directly. k_1 is constrained by the tensor perturbation produced during the inflationary stage, $k_1 \geq 10^9$. In order to explain the present acceleration of the universe, we need to choose Max $[1/(\kappa_5^4\mu^2), \lambda] \sim 10^{-16}(\mathrm{eV})^4$, If we choose $\lambda = 0$, this gives $\kappa_5 \sim (100\mathrm{MeV})^{-3/2}$, like Dvali et al's model.

4 Summary

In this paper, we present the effective equations to describe the four-dimensional gravity of a brane world, in which the brane action can include a gravitational contribution which may arise via quantum effects of matter fields confined on the brane. Applying this formalism, we study the brane-induced gravity model by Dvali, Gabadadze, and Porrati and model higher curvature terms included. As a result, we obtain a "scalar field free quintessential inflation model", in which both accelerations at early stage of the universe and present time driven by the curvature term. However, to obtain this scenario, we need to explain our brane to be in $\epsilon = 1$ branch and five-dimensional planck mass to be as low as 100 MeV.

References

[1] C. Deffayet, S. J. Landau, J. Raux, M. Zaldarriaga, and P. Astier, Phys. Rev. D **66**, 024019 (2002).

[2] G. Dvali, G. Gabadadze, and M. Porrati, Phys. Lett. B **485**, 255 (2000); G. Dvali, and G. Gabadadze, Phys. Rev. D **63**, 065007 (2001).

[3] K. Maeda, S. Mizuno, and T. Torii, in preparation.

[4] N. D. Birrell, and P. C. W. Davies, *Quantum Fields in CurvedSpace* (Cambridge University Press, Cambridge, England,1982).

[5] A. A. Starobinsky, Phys. Lett. **91B**, 99 (1980), A. Vilenkin, Phys. Rev. D **32**, 2511 (1985).

[6] S. W. Hawking, T. Hertog, and H. S. Reall, Phys. Rev. D **62**, 043501 (2000); S. W. Hawking, T. Hertog, and H. S. Reall, *ibid.* **63**, 083504 (2001); S. W. Hawking, and T. Hertog, *ibid.* **65**, 103515 (2002); S. W. Hawking, and T. Hertog, *ibid.* **66**, 123509 (2002).

[7] S. Mizuno, K. Maeda, and T. Torii, in preparation.

[8] T. Shiromizu, K. Maeda, and M. Sasaki, Phys. Rev. D **62**, 024012 (2000).

Balance of forces in wall-BH system

Yoshiyuki Morisawa, Daisuke Ida, Akihiro Ishibashi, and Ken-ichi Nakao

[1,4] *Department of Physics, Osaka City University, Osaka 558-8585, Japan,*

[2] *Department of Physics, Tokyo Institute of Technology, Tokyo 152-8551, Japan,*

[3] *Yukawa Institute for Theoretical Physics, Kyoto University, Kyoto 606-8502, Japan*
and
Enrico Fermi Institute, University of Chicago, Chicago, IL 60637, USA

Abstract

We discuss the gravitationally interacting system of a thick domain wall and a black hole. We numerically solve the scalar field equation in the Schwarzschild spacetime and obtain a sequence of static axi-symmetric solutions representing thick domain walls. We find that, for the walls near the horizon, the Nambu-Goto approximation is no longer valid. Introducing the point of view of the balance of forces, this deviation from Nambu-Goto membrane can be interpreted as the effect of the pressure gradient force.

1 Introduction

Topological defects are relics of cosmological phase transitions and their evolution is considered to have played an important role in cosmology (see *e.g.*, [1]). They have so far attracted attention as, for example, a potential source of the cosmic structures. Recently renewed interests especially in domain walls have been raised by considering them as a candidate for some kind of dark matter [2], or as a brane universe in higher dimensional theories (see *e.g.*, [3]). The topological defects have therefore been an important subject of recent study.

Domain walls are of special interests in general relativity because they are extended objects with large tension and hence cause non-trivial gravitational effects [4, 5]. Then, it is intriguing to study how such extended relativistic objects interact with a gravitational source like a black hole. In particular, domain walls around a black hole may have experienced large deformation and be a possible source of gravitational waves. Such an expectation prompts us to study the gravitationally interacting system of topological defects.

In this work, we study the thick domain wall configuration in black hole spacetime. We numerically solve the scalar field equation in the Schwarzschild spacetime and obtain a sequence of static axi-symmetric solutions representing thick domain walls. We find that, for the walls near the horizon, the Nambu-Goto approximation is no longer valid. Introducing the point of view of the balance of forces, this deviation from Nambu-Goto membrane can be interpreted as the effect of the pressure gradient force.

2 Basic equation and boundary conditions

We shall consider a static thick domain wall constructed by a scalar field with self-interaction in the Schwarzschild black hole spacetime. The metric of the background Schwarzschild black hole is written in terms of the isotropic coordinates $\{t, r, \vartheta, \varphi\}$ as

$$g = -\left(\frac{2r-M}{2r+M}\right)^2 \mathrm{d}t^2 + \left(1+\frac{M}{2r}\right)^4 \left[\mathrm{d}r^2 + r^2(\mathrm{d}\vartheta^2 + \sin^2\vartheta \mathrm{d}\varphi^2)\right]. \tag{1}$$

We are concerned with the region outside the event horizon, where $r \geq M/2$.

Let us consider a real scalar field ϕ with ϕ^4 potential $V[\phi] = \frac{\lambda}{4}(\phi^2 - \eta^2)^2$, of which Lagrangian is given by

$$\mathcal{L} = -\frac{1}{2}(\nabla^\mu\phi)(\nabla_\mu\phi) - V[\phi]. \tag{2}$$

The equation of motion for ϕ is

$$\nabla^2\phi - \frac{\partial V}{\partial\phi} = 0. \tag{3}$$

We will search the static and axi-symmetric solutions $\phi = \phi(r, \vartheta)$ which represent domain walls in the Schwarzschild background. Since the equation (3) is elliptic, the relaxation method is useful to solve the discretized version of Eq. (3).

We now consider the boundary conditions suitable for our purpose.

- The regularity of the scalar field at the symmetry axis:

$$\left.\frac{\partial\phi}{\partial\vartheta}\right|_{\vartheta=0} = \left.\frac{\partial\phi}{\partial\vartheta}\right|_{\vartheta=\pi} = 0. \tag{4}$$

- The regularity of the scalar field at the event horizon:

$$\left.\frac{\partial\phi}{\partial r}\right|_{r=M/2} = 0. \tag{5}$$

- The asymptotic condition as adiabatic capture process (details are in [6]).

3 Numerical results

We show the core surfaces (where $\phi = 0$) of the obtained wall solutions are plotted as solid lines in Fig. 1 for the following three typical cases:

(a) the wall far away from the black hole,

(b) the wall which is away from the black hole at the distance comparable to the wall thickness,

(c) the wall whose core surface is located near the black hole but does not intersect the horizon.

Here, thickness of the wall is about 10×(BH radius).

It is non-trivial whether or not the core surfaces of the wall configurations are actually well described by the Nambu-Goto membranes. If it is the case, one might be able to understand the qualitative behavior of domain walls even in the thick wall case by means of Nambu-Goto membranes, which are much easier to analyze than scalar field configurations.

To compare the configuration of the core surfaces with the Nambu-Goto membranes, for each core surface, the Nambu-Goto membrane tangent to the core surface at the point on the symmetry axis is also plotted as dashed line in Fig. 1. We see that the membranes well approximate the core surfaces for the walls (a) and (b), but does not for (c). This shows that, when thick domain walls in a black hole spacetime are concerned, the approximate description of the core surface by means of a Nambu-Goto membrane breaks down near the horizon.

4 Balance of forces

Now we shall briefly discuss the reason why the Nambu-Goto approximation breaks down, examining the structure of the energy-momentum tensor for the scalar field. The energy-momentum tensor obtained from the Lagrangian (2) is

$$T_{\mu\nu} = (\nabla_\mu\phi)(\nabla_\nu\phi) - g_{\mu\nu}\left[\frac{1}{2}(\nabla_\sigma\phi)(\nabla^\sigma\phi) + V\right]. \tag{6}$$

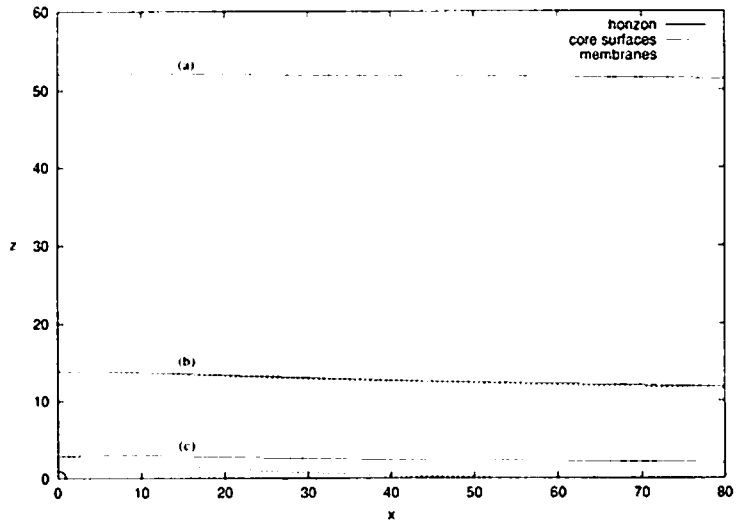


Figure 1: We plot the core surfaces (where $\phi = 0$) of the three thick wall solutions (a), (b) and (c). For each core surface, a Nambu–Goto membrane tangent to the core surface at the point on the symmetry axis is plotted. We see that the membranes well approximate the core surfaces for the walls (a) and (b), but does not for (c). The Nambu–Goto approximation in a black hole spacetime breaks down near the horizon. Here the coordinates (x, z) are isotropic coordinates and normalized as BH radius= 1.

Let us consider the following quantities defined by

$$\lambda\eta^4 P_\perp \equiv T_{\mu\nu}n^\mu n^\nu = \frac{1}{2}(\nabla_\sigma\phi)(\nabla^\sigma\phi) - V, \tag{7}$$

$$\lambda\eta^4 E \equiv \frac{1}{2}(\nabla_\sigma\phi)(\nabla^\sigma\phi) + V, \tag{8}$$

where n^μ denotes the unit normal vector to the core surface, given by $n^\mu = N\nabla^\mu\phi$ with $N^{-2} = (\nabla_\mu\phi)(\nabla^\mu\phi)$. Then, the energy-momentum tensor $T_{\mu\nu}$ can be diagonalized as

$$T_{\mu\nu} = -\lambda\eta^4 E(g_{\mu\nu} - n_\mu n_\nu) + \lambda\eta^4 P_\perp n_\mu n_\nu. \tag{9}$$

The first term of Eq. (9) looks just like the energy-momentum tensor for a Nambu–Goto membrane, once $\lambda\eta^4 E$ and $g_{\mu\nu} - n_\mu n_\nu$ are identified with the tension and the induced metric, respectively. The second term can be interpreted to describe the pressure perpendicular to the wall and thus the deviation from the Nambu–Goto membrane. Non-vanishing $P_\perp$ means that the gradient term and the potential term do not have the same contribution to the energy density E, *i.e.*, $\lambda\eta^4 E \neq 2V$.

Next, let us derive the equation to decide the configuration of the core surface. The energy-momentum tensor (9) satisfies the usual conservation law $\nabla_\nu T_\mu{}^\nu = 0$. Then, noticing that the trace of the extrinsic curvature $K_{\mu\nu}$ of the core surface is given by

$$\mathrm{tr}K = \nabla_\nu n^\nu, \tag{10}$$

(in this convention, $\mathrm{tr}K$ is positive for outward normal n of a sphere), we can find that the normal component of the conservation law,

$$n^\mu\nabla_\nu T_\mu{}^\nu = 0, \tag{11}$$

reduces to the equation,

$$\mathrm{tr}K = -\frac{n^\mu\partial_\mu P_\perp}{E + P_\perp}. \tag{12}$$

The core surface obeys Eq. (12) while the Nambu–Goto membrane obeys $\mathrm{tr}K = 0$ as is well-known.

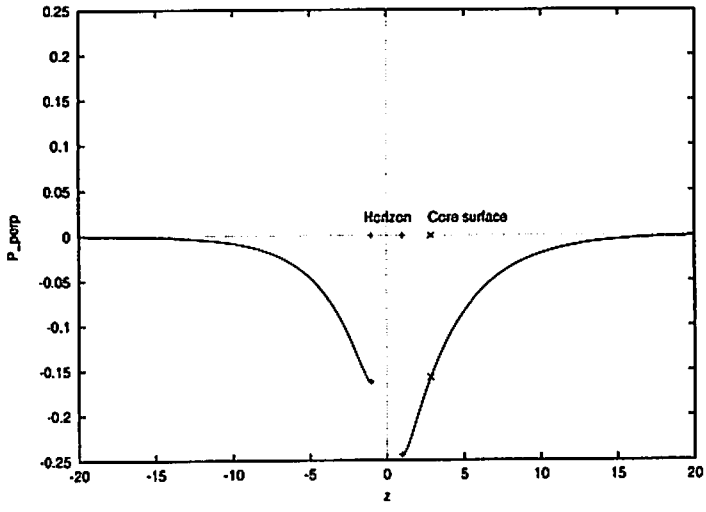


Figure 2: The value of $P_\perp$ on the symmetry axis for the wall (c) is plotted. Two lines are split by the event horizon. The position of the core surface is also shown. The $P_\perp$ has negative value near the horizon and asymptotes to zero.

In order to make the meaning of the balance equation (12), the spatial configuration of the domain wall is more useful. Thus we rewrite Eq. (12) by using the extrinsic curvature κ_{ij} which specifies how the core surface is embedded in the constant time hypersurface, not in the whole spacetime. The trace $\mathrm{tr}\kappa$ of the extrinsic curvature κ_{ij} is related to $\mathrm{tr}K$ as

$$\mathrm{tr}K = \mathrm{tr}\kappa + n^\mu \partial_\mu \ln \sqrt{-g_{tt}}. \tag{13}$$

The second term of Eq. (13) can be rewritten by the gradient of the Newton potential Φ_N in the weak field limit. From Eqs. (12) and (13), we obtain the following equation:

$$\mathrm{tr}\kappa = -n^\mu \partial_\mu \Phi_N - \frac{n^\mu \partial_\mu P_\perp}{E + P_\perp}. \tag{14}$$

The equation (14) requires the balance of the three forces: the tension, the gravitational force, and the pressure gradient.

The $P_\perp$ for the wall (c) has negative value near the horizon and asymptotes to zero as in Fig. 2. Then, Eq. (14) implies that the configuration of the core surface of (c) is more convex in the direction of the horizon than that of the corresponding Nambu-Goto membrane as in Fig. 1.

5 Summary and Discussion

We have numerically solved the equation of motion for a real scalar field with ϕ^4 potential which have a discrete set of degenerate minima, in the Schwarzschild black hole background. We showed that there exist the static axi-symmetric field configurations which represent domain walls ten times as thick as the horizon radius located around the black hole. There are two types of the wall configurations; ones are far away from the black hole and the others are not. As naturally expected from asymptotic flatness of the background spacetime, the wall configurations in the former family are similar to the walls in the flat spacetime and are well approximated by the Nambu-Goto membranes. For the wall solutions in the latter family, we have obtained the wall solution whose core surface shows different behavior from the Nambu-Goto membrane. Then, we have shown the existence of the pressure gradient $\partial_n P_\perp$ along the transverse direction to the core surface of that solution. The pressure $P_\perp$ never has a place in the walls in the flat spacetime and Nambu-Goto membranes.

If the black hole is absent (*i.e.*, for the hyperbolic tangent walls in the flat spacetime), the gradient term and the potential term in the expression of $P_\perp$ cancel each other. On the other hand, we impose the Neumann boundary condition on the symmetry axis and the horizon of the Schwarzschild black hole, and then the gradient term for static configurations vanishes at the north pole and the south pole of the horizon. Thus we may say that the gradient term cannot become large enough to balance the potential term caused by the wall near these points, and then the $P_\perp$ is negative there. When the $P_\perp$ is negative near the horizon and asymptotes to zero, Eq. (14) shows that the configuration of the core surface in the constant time hypersurface is more convex in the direction of the horizon than that of the corresponding Nambu–Goto membrane.

One way of thinking about domain wall configurations we obtained here is in terms of gravitational scattering and capture of thick domain walls by a black hole. One might be able to think that a series of the wall solutions represents adiabatic capture process with infinitesimal velocity, with the wall lying in the equatorial plane [7] being a possible final state. This picture should be examined by a fully dynamical computation.

In this work, we have considered the Schwarzschild black hole as the background spacetime. One might expect that the scalar field would behave qualitatively in the same way as that in the Schwarzschild case, as far as static spherically symmetric black holes are considered as the background. However, the behavior of the scalar field near the event horizon indeed depends on what kind of a black hole one considers. It is amusing to note that a contrastive case to our present result is the case of extremal black holes. As is well-known, the behavior of gravity around an extremal black hole is quite different from the Schwarzschild black hole; an extremal black hole has a vanishing surface gravity hence the static observers along the extremal horizon are not accelerated. Emparan, Gregory, and Santos [8] and Rogatko [9] investigated domain walls intersecting charged and dilaton extremal black holes and showed that there are domain wall solutions whose contour lines wrap the event horizon with the scalar field remaining in the symmetric phase on the horizon. One can say in other words that extremal black holes expel the domain wall.

In this work, we ignored the effect of the gravity of the wall on the black hole spacetime. As mentioned in [7], this test wall assumption is valid as far as concerning very light domain walls with the symmetry breaking scale being much lower than the Planck scale. It has been shown [10] that gravitating domain walls change the global geometry drastically; they makes spatial section compact. The equation of motion of a self gravitating thick domain wall is perturbatively evaluated in [11]. It is fair to say that our solutions should be regarded to describe the local behavior of thick domain walls around a non-extremal black hole.

References

[1] A. Vilenkin and E.P.S. Shellard, *Cosmic Strings and other Topological Defects* (Cambridge University Press, New York, 1994).

[2] R.A. Battye, M. Bucher and D. Spergel, [astro-ph/9908047].

[3] L. Randall and R. Sundrum, Phys. Rev. Lett. **83** 3370 (1999); Phys. Rev. Lett. **83** 4690 (1999).

[4] A. Vilenkin, Phys. Lett. **B133**, 177 (1983).

[5] J. Ipser and P. Sikivie, Phys. Rev. **D30**, 712 (1984).

[6] Y. Morisawa, D. Ida, A. Ishibashi and K. i. Nakao, accepted for publication in Phys. Rev. D [arXiv:gr-qc/0209070].

[7] Y. Morisawa, R. Yamazaki, D. Ida, A. Ishibashi and K. Nakao, Phys. Rev. **D62**, 084022 (2000).

[8] R. Emparan, R. Gregory and C. Santos, Phys. Rev. D **63**, 104022 (2001).

[9] M. Rogatko, Phys. Rev. D **64**, 064014 (2001).

[10] F. Bonjour, C. Charmousis and R. Gregory, Class. Quant. Grav. **16**, 2427 (1999).

[11] F. Bonjour, C. Charmousis and R. Gregory, Phys. Rev. D **62**, 083504 (2000).

Oscillatory behaviors of gravitating Nambu-Goto membranes
— General relativistic gauge invariant perturbation on the flat spacetime background —

Kouji Nakamura[1]

Division of Theoretical Astrophysics, National Astronomical Observatory, Tokyo, Mitaka 181-8588, Japan

Abstract

Oscillatory behaviors of an infinite gravitating Nambu-Goto string are considered using the general relativistic gauge invariant perturbation with the flat background spacetime. We have seen that the conclusions in Refs.[1] does not contradict to the test string motion due to the existence of the pp-wave exact solution.

1 Introduction

Nambu-Goto membranes are the simplest models of the extended objects which appear in the various physical context. Particularly, the gravitational field of the extended objects are interesting and important topics in the recent physics: the dynamics of topological or non-topological defects (domain walls, cosmic strings[2]) and gravitational waves from them; the simplest type of brane world (vacuum brane[3]).

In this article, we consider the oscillatory behaviors of the gravitating Nambu-Goto membrane. If the self-gravity of membranes is ignored, the equation of motion derived from the Nambu-Goto action admits oscillatory solutions and membranes can oscillate freely. However, recent investigations using exactly soluble models in Refs.[4, 5, 6] have pointed out that the oscillatory behaviors of gravitating Nambu-goto walls are different from the test walls in which their self-gravity is ignored, i.e., gravitating walls cannot oscillate freely. The points of these works are essentially separated into two parts: First, they showed that *the dynamical degree of freedom of the perturbative oscillations of the wall is completely determined by that of gravitational waves.* Second, considering the gravitational wave scattering by the wall, they showed that *there is no resonance pole in this scattering except for the damping mode.*

Similar analysis was extended to the perturbative oscillations of an infinite Nambu-Goto string case[1]. Results in Refs[1] are summarized as follows: *the dynamical degree of freedom of string oscillations is that of gravitational waves* (as the wall cases) and *an infinite string can oscillate but these oscillations are just the propagation of gravitational waves along the string*, which corresponds to the pp-wave exact solution to the Einstein equation, called cosmic string traveling waves. We note that the existence of the pp-wave solution closely related to the spacetime symmetry. Then, it is natural to expect that existence of the continuous oscillations in Refs.[1] is due to the special symmetry of the model and the traveling wave solutions will not exist in more generic situations, though it is a mere speculation, here.

In any case, it is true that "the dynamical degree of freedom of string oscillations is that of gravitational waves". Since background spacetime in Refs.[1, 4, 5, 6] is exact solutions, this statement also implies that *oscillatory behaviors of gravitating membranes might be different from those of test membranes even if their energy density are very small.* On the other hand, if we regard the Nambu-Goto string as the idealization of GUT scale cosmic strings, their deficit angle is about 10^{-6}. Then, the following expectation also seems natural: *If the energy density of membranes are very small, their gravitational field will be described by the perturbation with the Minkowski spacetime background and their dynamics is well-described by those of test membranes.* These statements seems contradict to each other.

In this article, we reconsider the dynamics of an infinite Nambu-Goto string in Refs.[1] using the perturbation theory on the Minkowski background spacetime as one of the attempts to clarify the oscillatory behaviors of Nambu-Goto membranes. The organization of this article is as follows: First, we develop the two parameter gauge invariant perturbation theory on the Minkowski spacetime background. We denote one of the parameters for the perturbation by ϵ, which corresponds to the string oscillation

[1]E-mail:kouchan@th.nao.ac.jp

amplitude, and another by λ, which corresponds to the string energy density. To determine the motion of the string, we solve the Einstein equation order by order: In $O(\epsilon)$ order, oscillations of the test string are described; In $O(\lambda)$ order, the static gravitational field of the straight string is derived; In $O(\epsilon\lambda)$ order, the oscillations of a gravitating string are described. Then, we show that the $O(\epsilon\lambda)$ order Einstein equations leads almost the same conclusion as in Refs.[1] and it does not contradict to the motion of the test string.

2 Self-gravitating Nambu-Goto string

To consider the dynamics of gravitating extended objects with codimension two, we should care the delicate problem in general relativity. It is well-known that there is no simple prescription of an arbitrary line source where a metric becomes singular[7]. Although it seems plausible to expect that the string dynamics is well-approximated by the dynamics of conical singularities, it is shown that the worldsheet of conical singularities must be totally geodesic[8], which called Israel's paradox. This implies that it is impossible to regard that the generic Nambu-Goto strings are idealized by conical singularities.

One of the simplest procedures to avoid this delicate problem is to introduce the string thickness[9]. As discussed in Refs.[1], we first consider the thick Nambu-Goto string, in which the singularity is regularized. Using this regularized string, we consider the perturbative dynamics of the thick string by solving the Einstein equations. After that, we consider the thin string situation as in Refs.[1].

The energy momentum tensor for the regularized Nambu-Goto string is given by

$$T_a{}^b = -\rho q_a{}^b, \tag{1}$$

where q_{ab} is the four dimensional extension of the intrinsic metric on the string worldsheet and ρ is the energy density of the string. The string thickness is characterized by the support of the energy density ρ. The divergence of this energy momentum tensor $\nabla_b T_a{}^b = 0$ is given by

$$q^{ab}\nabla_b\rho + \rho\gamma^{bc}\nabla_b q_c{}^a = 0, \tag{2}$$

$$\rho q^{bc}\nabla_b q_c{}^a =: \rho K^a = 0, \tag{3}$$

where $\gamma^{ab} := g^{ab} - q^{ab}$. The equation (2) is the continuity equation, and the equation (3) is just the equation of motion derived from the Nambu-Goto action. Hence, to discuss the dynamics of gravitating Nambu-Goto string, we may concentrate on the Einstein equation with the energy momentum tensor (1).

3 Two parameter perturbation in general relativity

We consider the perturbative oscillations of an infinite Nambu-Goto string using the Einstein equation with the above energy momentum tensor. We choose so that the background for the perturbation is the Minkowski spacetime and we have two infinitesimal parameters (the string oscillation amplitude ϵ and the string energy density λ) for the perturbation. Hence we develop the perturbation theory with two parameters in general relativity.

In this two-parameter perturbation theory, the perturbative gravitational field of the static infinite string, which does not oscillate, is described in $O(\lambda^n)$ orders. On the other hand, the oscillating string without gravitational field, which corresponds to the oscillations of a test string, is described in $O(\epsilon^n)$ orders. The others describe the oscillations of the gravitating string. In this article, we only consider the lowest order of perturbations: the $O(\lambda)$ order for the static gravitational field of the string; the $O(\epsilon)$ order for the oscillations of the test string; and the $O(\epsilon\lambda)$ order for the oscillations of the gravitating string.

3.1 Perturbative variables

The energy momentum tensor for the Nambu-Goto string is expanded as

$$T_{ab} = -\lambda\rho q_{ab} - \epsilon\lambda\left(\delta\rho q_{ab} + \rho\delta q_{ab}\right). \tag{4}$$

$O(\epsilon)$ order perturbation δq_{ab} of the intrinsic metric q_{ab} in Eq.(4) is given by

$$\delta q_a{}^b = \gamma_{ac} q_d{}^b h^{cd} - \gamma_{\alpha\beta} g^{db} (\zeta^\alpha)_d q_a{}^c \nabla_c \xi_1^\beta - \gamma_{\alpha\beta} (\zeta^\alpha)_a q_c{}^b \nabla^c \xi_1^\beta, \tag{5}$$

where $(\zeta^\alpha)_a := \nabla_a \xi^\alpha$ is the coordinate basis normal to the string world sheet ($\xi^\alpha = const.$) of order $O(\lambda)$ and $\gamma_{\alpha\beta}$ is the inverse matrix of $\gamma^{\alpha\beta} := g^{ab} \nabla_a \xi^\alpha \nabla_b \xi^\beta$. In $O(\epsilon\lambda)$ order, the string world sheet is given by the surface on which $\xi^\alpha + \epsilon \xi_1^\alpha = const.$. On the other hand, the spacetime metric g_{ab} is expanded as

$$g_{ab} = \eta_{ab} + \epsilon h_{ab} + \lambda l_{ab} + \epsilon\lambda k_{ab}. \tag{6}$$

Using these expansions, we calculate the perturbative Einstein equations order by order. To discuss the oscillation of the string and compare with the result in Refs.[1], we must pay attention to the gauge freedom of the perturbations. Then we develop the perturbation theory with two infinitesimal parameter in a gauge invariant manner.

3.2 Gauge transformations

Here, we develop the two-parameter gauge invariant perturbation theory. To do this, it is necessary to clarify the mathematical meaning of the "gauge freedom" of the perturbations.

Let us consider the spacetime $(\mathcal{M}_0, \eta_{ab})$, which is the background spacetime for the perturbations, and a physical spacetime $(\mathcal{M}, g_{ab})$, which we attempt to describe as a perturbation of the background $(\mathcal{M}_0, \eta_{ab})$. In relativistic perturbation theory, we are used to the expression of the forms (4) and (6) relating a perturbed tensor field such as the metric with the background value of the same field and with the perturbation. Let us denote these expressions by

$$Q(x) = Q_0(x) + \delta Q(x), \tag{7}$$

symbolically. In this expression, we are implicitly assigning a correspondence between points of the perturbed and the background spacetime. Moreover, the perturbed and unperturbed variables at the "same" point "x" are also defined, implicitly. In the expression (7), we are implicitly considering the map $\mathcal{M} \to \mathcal{M}_0 : p \in \mathcal{M}_0 \mapsto q \in \mathcal{M}_0$. This correspondence associated with the map $\mathcal{M} \to \mathcal{M}_0$ is what is usually called a gauge choice in the context of perturbation theory. Clearly, this is more than the usual assignment of coordinate labels to points of a single spacetime. Furthermore, the correspondence established by relations such as (7) is not *per se* unique, but rather (7) involves the degree of freedom of the choice of the map $\mathcal{M} \to \mathcal{M}_0$. This is called gauge freedom which always arise unless certain specific restrictions are satisfied by the fields involved (e.g., some metric components vanish).

Recently, this idea has been applied to the specific case of two parameter perturbation theory and derived the gauge transformation upto fourth order[10]. Here, we show their $O(\epsilon)$, $O(\lambda)$, and $O(\lambda\epsilon)$ order results. In two parameter perturbation of $O(\epsilon\lambda)$, we must consider three kind of gauge transformation for the perturbation of an physical variable Q on the physical manifold $\mathcal{M}$. We denote $O(\epsilon)$, $O(\lambda)$, and $O(\epsilon\lambda)$ order perturbations under the gauge $\mathcal{X} : \mathcal{M} \to \mathcal{M}_0$ by ${}^{\mathcal{X}}\delta^{(\epsilon)}Q$, ${}^{\mathcal{X}}\delta^{(\lambda)}Q$, and ${}^{\mathcal{X}}\delta^{(\epsilon\lambda)}Q$, respectively. We consider the gauge transformation $\Phi := \mathcal{Y} \circ \mathcal{X}^{-1} : \mathcal{M}_0 \to \mathcal{M}_0$ (the gauge transformation from $\mathcal{X}$ to $\mathcal{Y}$). Under this gauge transformation, the perturbative variables are transformed as follows:

$$\begin{aligned}
&{}^{\mathcal{Y}}\delta^{(\epsilon)}Q - {}^{\mathcal{X}}\delta^{(\epsilon)}Q = \mathcal{L}_{(\epsilon)\xi} Q_0, \\
&{}^{\mathcal{Y}}\delta^{(\lambda)}Q - {}^{\mathcal{X}}\delta^{(\lambda)}Q = \mathcal{L}_{(\lambda)\xi} Q_0, \\
&{}^{\mathcal{Y}}\delta^{(\epsilon\lambda)}Q - {}^{\mathcal{X}}\delta^{(\epsilon\lambda)}Q = \mathcal{L}_{(\epsilon)\xi}\, {}^{\mathcal{X}}\delta^{(\lambda)}Q + \mathcal{L}_{(\lambda)\xi}\, {}^{\mathcal{X}}\delta^{(\epsilon)}Q + \left\{ \mathcal{L}_{(\epsilon\lambda)\xi} + \frac{1}{2}\mathcal{L}_{(\epsilon)\xi}\mathcal{L}_{(\lambda)\xi} + \frac{1}{2}\mathcal{L}_{(\lambda)\xi}\mathcal{L}_{(\epsilon)\xi} \right\} Q_0,
\end{aligned} \tag{8}$$

where ${}^{(\epsilon)}\xi$, ${}^{(\lambda)}\xi$, and ${}^{(\epsilon\lambda)}\xi$ are the $O(\epsilon)$, $O(\lambda)$, and $O(\epsilon\lambda)$ order generators of Φ, respectively. Though the results in Ref.[10] includes excess parameters in $O(\lambda\epsilon)$ order, it is easily to check that these parameters can be fixed by the replacement of the $O(\lambda\epsilon)$ order generator ${}^{(\epsilon\lambda)}\xi$ of Φ and obtained the above transformation rules (8). Inspecting these transformation rules (8), we develop the gauge invariant perturbation theory on the Minkowski spacetime.

4 Perturbed Einstein Equations

Here, we evaluate the perturbative Einstein equations order by order. First, we consider the $O(\epsilon)$ order solutions to the Einstein equation. In this order, the infinite string may oscillate but does not produce the gravitational field. Physically, the linearized Einstein equations describe the free propagation of gravitational waves which have nothing to do with the string oscillations. We impose that there is no such gravitational wave. Hence, as the $O(\epsilon)$ order solution, we obtain the pure gauge solution :

$$h_{ab} = 2\nabla_{(a}{}^{(\epsilon)}X_{b)}, \tag{9}$$

where ${}^{(\epsilon)}X_a$ is transformed as ${}^{\mathcal{Y}(\epsilon)}X_a - {}^{\mathcal{X}(\epsilon)}X_a = {}^{(\epsilon)}\xi_a$ under the gauge transformation $\Phi = \mathcal{Y} \circ \mathcal{X}^{-1}$.

Next, we consider the $O(\lambda)$ order solutions to the Einstein equation. In this order, the infinite string stays static without their oscillations and it produces the static gravitational potential. Besides this static gravitational potential, the linearized Einstein equations also describe the free propagation of gravitational waves which have nothing to do with the string oscillations. We again impose that there is no such gravitational wave. Then, we easily see that $O(\lambda)$ order solution has the form

$$l_{ab} = \frac{1}{2}\gamma_{ab}\Xi + 2\nabla_{(a}{}^{(\lambda)}X_{b)}, \tag{10}$$

where Ξ is the gauge invariant scalar potential and the vector field ${}^{(\lambda)}X_a$ is transformed as ${}^{\mathcal{Y}(\lambda)}X_a - {}^{\mathcal{X}(\lambda)}X_a = {}^{(\lambda)}\xi_a$ under the gauge transformation Φ. The $O(\lambda)$ order Einstein equations are reduced to the single equation for the scalar potential Ξ:

$$\Delta\Xi = -32\pi G\rho, \tag{11}$$

where $\Delta := D^a D_a$ and D_a is the covariant derivative associated with the metric γ_{ab}.

Finally, we consider the $O(\epsilon\lambda)$ order perturbations. For the metric perturbation, we can define the $O(\epsilon\lambda)$ order gauge invariant variable $\hat{\mathcal{K}}_{ab}$ for the metric perturbation as follows:

$$k_{ab} =: \hat{\mathcal{K}}_{ab} + 2\nabla_{(a}{}^{(\epsilon\lambda)}X_{b)} + \pounds_{(\epsilon)X}l_{ab} + \pounds_{(\lambda)X}h_{ab} - \frac{1}{2}\left\{\pounds_{(\epsilon)X}\pounds_{(\lambda)X} + \pounds_{(\epsilon)X}\pounds_{(\lambda)X}g_{ab},\right\}. \tag{12}$$

Under the gauge transformation $\Phi = \mathcal{Y} \circ \mathcal{X}^{-1}$, $\hat{\mathcal{K}}_{ab}$ and ${}^{(\epsilon\lambda)}X_a$ are transformed as

$${}^{\mathcal{Y}}\hat{\mathcal{K}}_{\mu\nu} - {}^{\mathcal{X}}\hat{\mathcal{K}}_{\mu\nu} = 0, \quad {}^{\mathcal{Y}(\epsilon\lambda)}X^a - {}^{\mathcal{X}(\epsilon\lambda)}X^a = {}^{(\epsilon\lambda)}\xi^a + \frac{1}{2}[{}^{(\lambda)}\xi, {}^{(\epsilon)}X]^a + \frac{1}{2}[{}^{(\epsilon)}\xi, {}^{(\lambda)}X]^a. \tag{13}$$

The perturbative variables of the Nambu-Goto string are also defined by

$$\hat{\Sigma} := \delta\rho - {}^{(\epsilon)}X^a\nabla_a\rho, \qquad \hat{V}_a := \gamma_{\alpha\beta}(\zeta^\alpha)_a\xi_1^\beta - \gamma_{ab}{}^{(\epsilon)}X^b, \tag{14}$$

where $\hat{\Sigma}$ and $\hat{V}_\mu$ are the gauge invariant variables corresponding to the energy density perturbation and the string displacement of the string. Then the $O(\epsilon\lambda)$ order Einstein equation $\frac{\partial^2}{\partial\lambda\partial\epsilon}\left(G_a{}^b - 8\pi G T_a{}^b\right) = 0$ is given by

$$-2\left(\nabla_{[a}\hat{\mathcal{K}}_{c]b}{}^c - \frac{1}{2}\eta_{ab}\nabla_{[c}\hat{\mathcal{K}}_{d]}{}^{cd}\right) = 8\pi G\left(-q_{ab}\hat{\Sigma} + 2\rho q_{c(a}\nabla^c\hat{V}_{b)}\right), \qquad \hat{\mathcal{K}}_{ab}{}^c := \nabla_{(a}\hat{\mathcal{K}}_{b)}{}^c - \frac{1}{2}\nabla^c\hat{\mathcal{K}}_{ab}. \tag{15}$$

This Einstein equations are almost same as those in Refs.[1] except that the covariant derivative appears in (15) is associated with the metric η_{ab} but that in Refs.[1] is not.

5 Comparison with the curved space background analyses

Here we consider the comparison with the results in Refs.[1]. To solve the Einstein equation (15), we use the mode expansion developed in Refs.[1]. We skip the introduction of the mode functions in this article. Details can be seen in Refs.[1]. As in Refs.[1], we treat the dynamical mode which propagate along the

string ($\kappa = 0$ mode) and others ($\kappa \neq 0$ mode), separately. In this article, we only show the result for $\kappa = 0$ mode perturbations.

For $\kappa = 0$ mode perturbation, the $O(\lambda\epsilon)$ order Einstein equation is given by

$$\Delta H_{ab} = 2\left(D_{(a}V_{b)} - \frac{1}{2}\gamma_{ab}D_cV^c\right), \quad H_c{}^c = 0, \quad D^cH_c{}^a + 2\omega^2H^a = V^a,$$
$$D_aV^a + \frac{1}{2}\Sigma = 0, \quad D^cH_c + 2\omega^2H = 0, \quad \Delta H^a = 0, \quad \Delta H = 0. \tag{16}$$

These equations are same as those in Ref.[1] except for the background curvature term in the first equation of (16). This difference is not essential to obtain the same conclusion as in Refs.[1]. Hence, we reach to the conclusion : *"the dynamical degree of freedom of the string oscillations is that of gravitational waves and the string oscillations are just the propagation of the gravitational waves along the string."*

6 Summary

In this article, we have considered the perturbative Einstein equation of order $O(\epsilon\lambda)$. They almost coincide with the perturbative equations with the curved spacetime background which is an exact solution to the Einstein equation. The same conclusion as in Refs.[1] is maintained i.e., *the dynamical degree of freedom of string oscillations is that of gravitational waves* (as the wall cases) and *an infinite string can oscillate but these oscillations are just the propagation of the gravitational waves along the string*, which corresponds to cosmic string traveling waves (the exact solution).

Further, we must point out that the equation of motion of order $O(\epsilon)$ is given by

$$\frac{\partial}{\partial\epsilon}K^a = -\mathcal{D}^b\mathcal{D}_b\widehat{V}^a = 0, \tag{17}$$

where $\mathcal{D}_a$ is the covariant derivative associated with the metric q_{ab}. This is nothing but the equation of motion for the test string in the first order of the string oscillation amplitude. We note that the model discussed here includes traveling waves and the string can continue to oscillate. There is no contradiction to the equation of motion of a test string. This is just due to the existence of the pp-wave exact solution. So, it is interesting to consider the other models in which the perturbation theory on the Minkowski spacetime is well-defined and there is no traveling waves solution along the membrane.

References

[1] K. Nakamura, A. Ishibashi and H. Ishihara, Phys. Rev. **D62**, 101502(R) (2002); K. Nakamura and H. Ishihara, *ibid*, **D63**, 127501 (2001).

[2] A. Vilenkin and E.P.S Shellard, *"Cosmic Strings and Other Topological Defects"*, (Cambridge University Press, Cambridge, England, 1994) and the references therein. A. Vilenkin, and A.E. Everett Phys. Rev. Lett. **48**, 1867, (1982). T. Vachaspati, A.E. Everett and A. Vilenkin, Phys. Rev. **D30**, 2046 (1984).

[3] L. Randall and R. Sundrum, Phys. Rev. Lett. **83**, 4690 (1990).

[4] H. Kodama, H. Ishihara and Y. Fujiwara, Phys. Rev. **D50**, 7292 (1994); A. Ishibashi and H. Ishihara, *ibid*, **D56** 3446 (1997).

[5] K. Nakamura, Phys. Rev. **D66**, 084005 (2002).

[6] A. Ishibashi and T. Tanaka, "Can a brane fluctuate freely?", preprint, gr-qc/0208006 (2002).

[7] R. Geroch and J. Traschen, Phys. Rev. **D36**, 1017 (1987).

[8] W.G. Unruh, G. Hayward, W. Israel and D. McManus, Phys. Rev. Lett. **62**, 2897 (1989).

[9] K. Nakamura, Class. Quantum Grav. **19**, 783 (2002).

[10] M. Bruni, L. Gualtieri and C.F. Sopuerta, Class. Quantum Grav. **20**, 535, (2003).

Gauge Problem in the Gravitational Self-Force
— Under Regge-Wheeler Gauge —

Hiroyuki Nakano[a 1], Norichika Sago[a,b 2], Misao Sasaki[a 3]

[a] *Department of Earth and Space Science, Graduate School of Science, Osaka University, Toyonaka, Osaka 560-0043, Japan*
[b] *Department of Physics, Graduate School of Science, Kyoto University, Kyoto 606-8502, Japan*

Abstract

In this paper, we discuss the gravitational self-force on a particle in a black hole spacetime. When the point particle is treated, its self-force diverges. In the previous works, the metric perturbation which arises from the particle, is devided into two parts, i.e., the direct (S) part and the tail (R) part. It has been known that the gravitational self-force on a particle is derived from the R part. When we calculate the R part of the metric perturbation, we face to the two problems, "subtraction problem" and "gauge problem". For the subtraction problem, that is how to subtruct the singular part, the method of 'mode decomposition regularization' is used. We solve the gauge problem, that arises in the substraction, by using the 'intermediate gauge' which is considered as the Regge-Wheeler gauge for the R part of the metric perturbation.

1 Introduction

Due to the recent advances in technology, the gravitational wave detectors are under construction or have entered the observing phase. The observation of gravitational waves is a new window to observe our universe. We also expect that the detection of gravitational waves provides a direct experimental test of general relativity.

The gravitational radiation from an inspiralling compact binary in the black hole perturbation approach, is considered as the gravitational wave emitted by a point particle orbiting a black hole, assuming the mass of the particle (μ) is much less than the mass of the black hole (M). The gravintational wave from the above situation is detected by the space-based detectors, LIGO and DECIGO.

In the lowest order in the mass ratio (μ/M), its motion can be represented the geodesic of the black hole geometry. Already in this lowest order, this approach has been proved to be very powerful for evaluating general relativistic corrections to the gravitational wave forms from a compact binary, even for neutron star-neutron star (NS-NS) binaries.[1] If we take acount of the next order effect, however, the orbit deviate from it because the spacetime is perturbed by the particle. We can interpret this deviation as the effect by the self-force of the particle itself. To obtain the accurate orbit in the order of (μ/M), we have to derive the equation of motion in consideration of the self-force.

Now, we consider the linearized metric perturbation defined by

$$h_{\mu\nu} = g_{\mu\nu} - g^{(\mathrm{b})}_{\mu\nu}\,, \tag{1}$$

where $g^{(\mathrm{b})}_{\mu\nu}$ and $g_{\mu\nu}$ are the background and the perturbed metric, respectively. Here we can define the force by the metric perturbation as the deviation from the geodesic of the background:

$$\frac{d^2 z^\alpha}{d\tau^2} + \Gamma^\alpha_{\mu\nu}\frac{dz^\mu}{d\tau}\frac{dz^\nu}{d\tau} = F^\alpha[h]\,, \tag{2}$$

[1] E-mail:denden@vega.ess.sci.osaka-u.ac.jp
[2] E-mail:sago@tap.scphys.kyoto-u.ac.jp
[3] E-mail:misao@vega.ess.sci.osaka-u.ac.jp

where $z^\alpha(\tau)$ represents the orbit of the particle parametrized by the proper time in $g^{(\mathrm{b})}_{\mu\nu}$, and $\Gamma^\alpha_{\mu\nu}$ is the connection of the background metric. From the geodesic equation associated with $g_{\mu\nu}$, we obtain

$$F^\alpha[h] = -\mu P^\alpha_\beta(\bar{h}_{\beta\gamma;\delta} - \frac{1}{2}g_{\beta\gamma}\bar{h}^\epsilon{}_{\epsilon;\delta} - \frac{1}{2}\bar{h}_{\gamma\delta;\beta} + \frac{1}{4}g_{\gamma\delta}\bar{h}^\epsilon{}_{\epsilon;\beta})u^\gamma u^\delta\,, \tag{3}$$

where $P_\alpha{}^\beta = \delta_\alpha{}^\beta + u_\alpha u^\beta$, $\bar{h}_{\alpha\beta} = h_{\alpha\beta} - \frac{1}{2}g^{(\mathrm{b})}_{\alpha\beta}h_\mu{}^\mu$ and the four-velocity of a particle $u^\alpha = dz^\alpha/d\tau$. So we can calculate the force from the metric perturbation.

In the case that the perturbation is produced by the point particle, however, we face the problem that $h_{\mu\nu}$ diverges at the location of the particle and so does the force. Therefore, we can not naively apply the above formula to obtain the self-force on a particle. Mino, Sasaki and Tanaka [2] and Quinn and Wald [3] gave the prescription to obtain the self-force under the harmonic (H) gauge condition. According to them, the metric perturbation in the vicinity of the orbit can be divided into two parts, the direct part and the tail part. The direct part has support only on the past null cones of the field point x^μ and diverges at the limit $x^\mu \to z^\mu(\tau)$. The tail part has support inside the past null cones and gives the physical self-force which is regular at the location of the particle. But it is so difficult to calculate the tail part of the metric perturbation directly, because the tail part depend on the global structure of the space-time and the history of the particle motion. From the fact that F^α is a linear differential operator, we can calculate the self-force by subtracting the direct part from the full force under H gauge as

$$\lim_{x\to z(\tau)} F_\alpha[h^{\mathrm{tail,H}}(x)] = \lim_{x\to z(\tau)} \left(F_\alpha[h^{\mathrm{full,H}}(x)] - F_\alpha[h^{\mathrm{dir,H}}(x)]\right)\,. \tag{4}$$

When we perform this subtraction, the full metric perturbation $h^{\mathrm{full,H}}$ and the direct part $h^{\mathrm{dir,H}}$ must be evaluated under H gauge condition because this division is meaningful only in H gauge.

The direct part can be evaluated by the local analysis around the particle location. But it is difficult that we directly obtain the full metric perturbation in H gauge. In order to overcome this difficulty, we consider the gauge transformation to H gauge from the gauge in which the full metric perturbation can be calculated by using the Regge-Wheeler-Zerilli or Teukolsky formalism [4, 5, 6, 7]. In our previous paper [8], we worked on this problem for the Schwarzschild case, i.e., considered the gauge transformation from the Regge-Wheeler (RW) gauge to H gauge. We wrote down the gauge equation in the Fourier-harmonic expanded form and derived a set of the decoupled equations for the coefficients. And then we found that these equations can be formally solved by using the Green function method, although it involves products of the Green functions with double integrals. The application of this method is studying now [9].

Recently, Detweiler and Whiting added the slight modification to the above division of the metric perturbation [10]. Their new singular part, called the S part $h^{\mathrm{S,H}}_{\mu\nu}$, is an inhomogeneous solution of the linearized Einstein equation under H gauge as

$$\bar{h}^{\mathrm{full/S,H};\alpha}_{\mu\nu;\alpha} + 2R_\mu{}^\alpha{}_\nu{}^\beta\bar{h}^{\mathrm{full/S,H}}_{\alpha\beta} = -16\pi T_{\mu\nu}\,. \tag{5}$$

And their new regular part, called the R part $h^{\mathrm{R,H}}_{\mu\nu}$, is a homogeneous solution of this equation. Since the S and R part is the solution of the Einstein equation, we can define the S and R part under the other gauge condition by performing the gauge transformation. Therefore, we can consider the subtraction procedure under the other appropriate gauge condition by transforming the S part from H gauge. Our aim is that we calculate the S part in RW or radiation gauge, where we have the formalism to evaluate the full metric perturbation, and we obtain the self-force in this gauge by performing the subtraction. In this paper, we consider RW gauge and the the 'mode decomposition regularization' [11, 12, 13, 14] is used for the subtraction.

2 Gauge Transformation and Intermediate Gauge

We consider the metric perturbation which arises from a particle around the Schwarzschild black hole. The Schwarzschild metric is given as

$$g^{(\mathrm{b})}_{\mu\nu}dx^\mu dx^\nu = -f(r)dt^2 + f(r)^{-1}dr^2 + r^2(d\theta^2 + \sin^2\theta d\phi^2)\,, \qquad f(r) = 1 - \frac{2M}{r}\,, \tag{6}$$

by the Boyer-Lindquist coordinates. The location of the particle at its proper time $\tau = \tau_0$ is shown as

$$\{z_0^\alpha\} = \{z^\alpha(\tau_0)\} = \{t_0, r_0, \theta_0, \phi_0\}\,. \tag{7}$$

Formally, we have known the gravitational self-force of $O(\mu/M)$ acting on the particle, i.e., the deviation from the geodsic motion on the background spacetime $F_{\rm H}^\mu$, is given by [2, 3] under H gauge condition. We note that the equation (4) is rewritten by the full metric perturbation $h_{\mu\nu}^{\rm full,H}$ and the S part of the metric perturbation $h_{\mu\nu}^{\rm S,H}$ under H gauge condition by [10] as

$$\begin{aligned} F_\alpha^{\rm H}(\tau) &= \lim_{x\to z(\tau)} F_\alpha\left[h_{\mu\nu}^{\rm R,H}\right](x) \\ &= \lim_{x\to z(\tau)} F_\alpha\left[h_{\mu\nu}^{\rm full,H} - h_{\mu\nu}^{\rm S,H}\right](x) \\ &= \lim_{x\to z(\tau)} \left(F_\alpha\left[h_{\mu\nu}^{\rm full,H}\right](x) - F_\alpha\left[h_{\mu\nu}^{\rm S,H}\right](x)\right)\,. \end{aligned} \tag{8}$$

Here $h_{\mu\nu}^{\rm S,H}$ can be calculated by the local coordinate expansion [12] and the derivation of $h_{\mu\nu}^{\rm full,H}$ is discussed in [8]. But the derivation of the full metric perturbation under H gauge is so complicated that we discuss the regularized self-force under an "intermediate gauge" in the remaining paper.

Now, we consider the gauge transformation from H gauge to RW gauge defined by

$$x_\mu^{\rm H} \;\to\; x_\mu^{\rm RW} = x_\mu^{\rm H} - \xi_\mu^{\rm H\to RW}\,, \tag{9}$$

$$h_{\mu\nu}^{\rm H} \;\to\; h_{\mu\nu}^{\rm RW} = h_{\mu\nu}^{\rm H} + 2\,\xi_{(\mu;\nu)}^{\rm H\to RW}\,, \tag{10}$$

where $\xi_\mu^{\rm H\to RW}$ is the generator of the gauge transformation. Let's consider the gauge transformation of the gravitational reaction force. For the Eq. (8), a finite gauge trasformation which connects the R part under H gauge with that under RW gauge, is considered.

$$\begin{aligned} \lim_{x\to z(\tau)} F_\alpha\left[h_{\mu\nu}^{\rm R,H} + 2\,\xi_{(\mu;\nu)}^{\rm H\to RW}\left[h_{\mu\nu}^{\rm R,H}\right]\right](x) &= \lim_{x\to z(\tau)} F_\alpha\left[h_{\mu\nu}^{\rm full,H} - h_{\mu\nu}^{\rm S,H} + 2\,\xi_{(\mu;\nu)}^{\rm H\to RW}\left[h_{\mu\nu}^{\rm full,H} - h_{\mu\nu}^{\rm S,H}\right]\right](x) \\ &= \lim_{x\to z(\tau)} F_\alpha\Big[h_{\mu\nu}^{\rm full,H} + 2\,\xi_{(\mu;\nu)}^{\rm H\to RW}\left[h_{\mu\nu}^{\rm full,H}\right] \\ &\qquad - h_{\mu\nu}^{\rm S,H} - 2\,\xi_{(\mu;\nu)}^{\rm H\to RW}\left[h_{\mu\nu}^{\rm S,H}\right]\Big](x) \\ &= \lim_{x\to z(\tau)} F_\alpha\left[h_{\mu\nu}^{\rm full,RW} - h_{\mu\nu}^{\rm S,RW}\right](x) \\ &= \lim_{x\to z(\tau)} \left(F_\alpha\left[h_{\mu\nu}^{\rm full,RW}\right](x) - F_\alpha\left[h_{\mu\nu}^{\rm S,RW}\right](x)\right) \\ &= F_\alpha^{\rm RW}(\tau)\,. \end{aligned} \tag{11}$$

The self-force defined by the above gauge transformation is called as the RW self-force.

When we consider the self-force under the intermediate gauge condition which is satisfied with RW gauge for the R part of the metric perturbation, i.e., the RW self-force [4], there is some problem for RW gauge. In the following, we discuss this problem formally.

3 Discussion

The RW gauge condition is defined for the $\ell \geq 2$ modes in terms of the spherical harmonics. When we consider the $\ell = 0$ and 1 modes, the other treatment is needed.

Here, these are considered formally under H gauge. According to Detweiler and Whiting [10], the R part of the metric perturbation is the homogeneous solution of the Einstein equation. So, the nonradiative $\ell = 0$ and 1 modes do not appear in the R part and do not contribute to the regularized self-force, i.e.,

[4] The RW self-force on a particle moving on circular orbit is discussed now [15].

we may consider the regularization for $\ell \geq 2$.

$$\begin{aligned} F^{\mathrm{R,H}} &= \sum_{\ell \geq 2} \left(F_\ell^{\mathrm{full,H}} - F_\ell^{\mathrm{S,H}} \right) \\ &= \sum_{\ell \geq 0} \left(F_\ell^{\mathrm{full,H}} - F_\ell^{\mathrm{S,H}} \right) \\ &= \sum_{\ell \geq 0} \left(F_\ell^{\mathrm{full,H}} - F_\ell^{\mathrm{S,H,Ap}} \right) - D_{\ell \geq 0} \\ &= \sum_{\ell \geq 2} \left(F_\ell^{\mathrm{full,H}} - F_\ell^{\mathrm{S,H,Ap}} \right) + \sum_{\ell = 0,1} \left(F_\ell^{\mathrm{full,H}} - F_\ell^{\mathrm{S,H,Ap}} \right) - D_{\ell \geq 0} \,. \end{aligned} \tag{12}$$

where $F^{\mathrm{R,H}}$, $F_\ell^{\mathrm{full,H}}$ and $F_\ell^{\mathrm{S,H}}$ denote the R part of the self-force, the ℓ mode of the full force and that of the S force under H gauge, respectively. But the S part is defined only in the neighborhood of the particle location, and when we consider the harmonic decomposition, we have some ambiguity in the S part. So, we calculate the approximate S part $F_\ell^{\mathrm{S,H,Ap}}$ which corresponds to the quadratic divergent terms A and the linearly divergent terms B of the self-force defined by the mode decomposition regularization in [11, 12, 13, 14], and use the fact that the remaining term $D_{\ell \geq 0}$ vanishes at the particle location after summing over $\ell \geq 0$. It is noted that $D_{\ell \geq 2}$ does not vanish in the concidence limit to the particle location. Here the remaining term $D_{\ell \geq 0}$ is $O(y)$ and we note that the $\ell = 0$ and 1 contribution of the self-force

$$\begin{aligned} \delta F_{\ell=0,1} &= \sum_{\ell=0,1} \left(F_\ell^{\mathrm{full,H}} - F_\ell^{\mathrm{S,H,Ap}} \right) \\ &= D_{\ell=0,1} \,, \end{aligned} \tag{13}$$

because

$$\sum_{\ell=0,1} \left(F_\ell^{\mathrm{full,H}} - F_\ell^{\mathrm{S,H}} \right) = 0 \,. \tag{14}$$

When we consider the mode decomposition of a local quantity, each ℓ mode is not important due to some ambiguity. Only the quantity after ℓ-summation is meaningful. This ambiguity is used in the following discussion and the gauge transformation from H gauge to RW gauge.

A new quantity $\delta \tilde{F}_{\ell=0,1}$ is defined by

$$\begin{aligned} \delta \tilde{F}_{\ell=0,1} &= \delta F_{\ell=0,1} - \delta F_{\ell=2} \\ &= O(y) \,, \end{aligned} \tag{15}$$

where we set $\delta F_{\ell=2}$ as the above by using the ambiguity. Using the ambiguousness discussed above, we calculate the mode decomposition again to be able to ignore the contribution from $\ell = 0$ and 1 modes, and convert these modes to the $\ell = 2$ mode. This is correspond to the coordinate transformation. That is to say,

$$\begin{aligned} \delta F_{\ell=2} &= \delta F_{\ell=0,1} + O(y) \\ &= \sum_{\ell=0,1} \left(F_\ell^{\mathrm{full,H}} - F_\ell^{\mathrm{S,H,Ap}} \right) \,. \end{aligned} \tag{16}$$

Here, if we can calculate $F_\ell^{H,F}$ and $F_\ell^{\mathrm{S,H,Ap}}$ for $\ell = 0, 1$, $\delta F_{\ell=2}$ is derived. In fact, we consider this calculation under RW gauge, because we can treat the gauge transformation for $\ell = 2$ mode. The regularized self-force is calculated as

$$F^{H,R} = \sum_{\ell \geq 2} \left(F_\ell^{\mathrm{full,H}} - F_\ell^{\mathrm{S,H,Ap}} \right) + \delta F_{\ell=2} - D_{\ell \geq 0} \,. \tag{17}$$

The above equation is rewritten as

$$F^{H.R} = \sum_{\ell \geq 2} \left(F_\ell^{\rm full.H} - \tilde{F}_\ell^{\rm S.H.Ap} \right) - D_{\ell \geq 0} , \tag{18}$$

$$\tilde{F}_{\ell=2}^{\rm S.H.Ap} = F_{\ell=2}^{\rm S.H.Ap} - \delta F_{\ell=2} , \tag{19}$$

$$\tilde{F}_{\ell \geq 3}^{\rm S.H.Ap} = F_{\ell \geq 3}^{\rm S.H.Ap} . \tag{20}$$

We summarize the treatment of the $\ell = 0$ and 1 modes. First, we consider the $\ell = 0$ and 1 modes under the harmonic gauge, and then these modes is transfered to $\ell = 2$ mode. By using the ambiguity of the mode decomposition as discussed above, we may consider the new $\ell = 2$ mode as usual $\ell = 2$ mode. So the gauge transformation from H gauge to RW gauge is derive as usual way. We conclude that the $\ell = 0$ and 1 modes are needed.

4 Acknowledgements

We would like to thank T. Tanaka, Y. Mino and S. Jhingan for useful discussions. HN and MS would like to thank all the participants at the Radiation Reaction Focus Session and the 5th Capra Ranch Meeting, PSU, State College in U.S.A., for invaluable discussions. This work was supported in part by Monbukagaku-sho Grant-in-Aid for Scientific Research Nos. 1047214 and 12640269, and by the Center for Gravitational Wave Physics, which is funded by the National Science Foundation under Cooperative Agreement PHY 0114375.

References

[1] For a review, see e.g., Y. Mino, M. Sasaki, M. Shibata, T. Tagoshi and T. Tanaka, Prog. Theor. Phys. Suppl. **128**, 1 (1997).

[2] Y. Mino, M. Sasaki and T. Tanaka, Phys. Rev. D **55**, 3457 (1997) [arXiv:gr-qc/9606018].

[3] T. C. Quinn and R. M. Wald, Phys. Rev. **D 56**, 3381 (1997); Phys. Rev. **D 60**, 064009 (1999).

[4] T. Regge and J. A. Wheeler, Phys. Rev. **108**, 1063 (1957).

[5] F. Zerilli, Phys. Rev. **D2**, 2141 (1970).

[6] S. A. Teukolsky, Astrophys. J. **185**, 635 (1973).

[7] S. Jhingan and T. Tanaka, arXiv:gr-qc/0211060.

[8] N. Sago, H. Nakano and M. Sasaki, arXiv:gr-qc/0208060.

[9] N. Sago, H. Nakano and M. Sasaki, in preparation.

[10] S. Detweiler and B. F. Whiting, arXiv:gr-qc/0202086.

[11] L. Barack, Y. Mino, H. Nakano, A. Ori and M. Sasaki, Phys. Rev. Lett. **88**, 091101 (2002) [arXiv:gr-qc/0111001].

[12] Y. Mino, H. Nakano and M. Sasaki, Prog. Theor. Phys. **108**, 1039 (2002) [arXiv:gr-qc/0111074].

[13] L. Barack and A. Ori, Phys. Rev. **D 66**, 084022 (2002) [arXiv:gr-qc/0204093].

[14] L. Barack and A. Ori, arXiv:gr-qc/0209072.

[15] H. Nakano, N. Sago and M. Sasaki, in preparation.

The Gravitational Radiation from Cylindrical Naked Singularity

Kei-ichi Nakao,[1] and Yoshiyuki Morisawa[2]

Department of Physics, Graduate School of Science,
Osaka City University, Osaka 558-8585, Japan

Abstract

We study the asymptotic behavior of the cylindrically symmetric dust collapse. As well known, the resultant spacetime singularity is naked, i.e., observable in principle. Assuming that the speeds of fluid elements are almost equal to the speed of light, we perform a linear perturbation analysis; the background solution describes the gravitational collapse of a cylindrical null dust. We find that when the background null dust constitutes an infinitesimally thin cylindrical shell, infinite amounts of gravitational radiation are emitted by its gravitational collapse. On the other hand, if the background null dust constitutes a thick cylindrical shell, the energy of the gravitational waves generated by its gravitational collapse is finite. These results imply that the smaller "time scale" of the singularity formation leads to larger amounts of the gravitational radiation.

1 Introduction

The gravitational collapse and spacetime singularity formation are important issues in general relativity. In the research for this problem, the spherically symmetric system has been mainly studied in detail since it is rather simple due to the lack of gravitational radiation. On the other hand, the gravitational collapse in the cylindrically symmetric system has not been studied in so detail. This is because there is a degree of freedom of the gravitational radiation in this system; in general, it is difficult to study analytically the physical processes accompanied by the generation of gravitational waves.

Other remarkable feature of the cylindrically symmetric system is that assuming the energy condition, there is no black hole[1]. This means that singularities formed in the cylindrical system are necessarily naked. Nakamura, Shibata and one of the present authors have conjectured that the large curvature in the neighborhood of a naked singularity can propagate away to infinity in the form of the gravitational radiation by virtue of the lack of the event horizon and therefore the mass of the naked singularity dries up by large amounts of the gravitational emission[2]. If this conjecture is true, the process of the naked singularity formation is a strong source of the gravitational radiation.

There are a few investigations of the gravitational wave generation by the cylindrical singularity formation. Echeverria numerically investigated the gravitational collapse of a cylindrical dust shell and showed that large amounts of the gravitational radiation are really generated by it[3]. On the other hand, Chiba investigated the gravitational collapse of the dust fluid and showed that the gravitational radiation generated by it is negligibly small amounts.[4] In this article, in order to understand the reason of the difference between the results by Echeverria and Chiba, we would like to analytically construct an asymptotic solution of the gravitational collapse of the cylindrical dust fluid. For this purpose, we assume that the speeds of the dust fluid elements are almost equal to the speed of light due to the large gravitational acceleration near the spacetime singularity. Then we perform a linear perturbation analysis.

In this article, we adopt $c = 1$ unit and basically follow the convention and notation in Wald[5].

2 The Gravitational Collapse of Almost Null Dust

The line element of the spacetime with whole-cylinder symmetry is written in the form[6],

$$ds^2 = e^{2(\gamma-\psi)}\left(-dt^2 + dr^2\right) + e^{2\psi}dz^2 + e^{-2\psi}R^2 d\varphi^2. \tag{1}$$

[1] E-mail:knakao@sci.osaka-cu.ac.jp
[2] E-mail: morisawa@sci.osaka-cu.ac.jp

We consider a timelike dust fluid as a matter field. The stress-energy tensor is

$$T_{\mu\nu} = \rho u_\mu u_\nu, \tag{2}$$

where ρ is rest mass density and u^μ is a 4-velocity of the fluid element. Due to the assumption of the whole-cylinder symmetry, the components of the 4-velocity u^μ are written as

$$u^\mu = u^t\,(1, -1 + V,\ 0,\ 0)\,. \tag{3}$$

By the normalization $u^\mu u_\mu = -1$, u^t is expressed as

$$u^t = \frac{e^{-\gamma+\psi}}{\sqrt{V\,(2-V)}}. \tag{4}$$

Here we introduce a new variable D defined by

$$D := \frac{\sqrt{-g}\rho u^t}{\sqrt{V\,(2-V)}} = \frac{Re^{\gamma-\psi}\rho}{V\,(2-V)}. \tag{5}$$

Then the stress-energy tensor is written as

$$T_{ab} = \frac{e^{\gamma-\psi}}{R} D k_a k_b, \tag{6}$$

where

$$k^\mu = (1, -1 + V,\ 0,\ 0). \tag{7}$$

At the final stage of the gravitational collapse, the speed of the dust fluid element might be almost equal to the speed of light. In the limit of $V \to 0_+$, k^μ becomes a null vector and hence the stress-energy tensor is almost equal to that of the collapsing null dust when $0 < V \ll 1$.

First we consider the case of the complete null dust $V = 0$; the solution is easily obtained as[7]

$$\psi = 0, \quad \gamma = \gamma_B(v), \quad R = r \quad \text{and} \quad 8\pi G D e^{\gamma_B} = \frac{d\gamma_B}{dv}, \tag{8}$$

where $v = t + r$ and $\gamma_B(v)$ is an arbitrary function of the advanced time v. This solution was studied recently by Nolan in detail[8]. In the region of non-vanishing $d\gamma_B/dv$ on $r = 0$, the naked singularity forms, which is non-scalar polynomial singularity[9]. We will regard this solution as a background spacetime and perform a linear perturbation analysis.

We introduce a small parameter ϵ and assume the order of the variables as $V = O(\epsilon)$ and $\psi = O(\epsilon)$. Further we rewrite the variables γ, R and D as

$$e^\gamma = e^{\gamma_B}(1 + \delta_\gamma), \quad R = r(1 + \delta_R) \quad \text{and} \quad D = \frac{1}{8\pi G e^{\gamma_B}} \frac{d\gamma_B}{dv}(1 + \delta_D), \tag{9}$$

and assume that δ_γ, δ_R and δ_D are $O(\epsilon)$.

The 1st order equations with respect to ϵ are given as follows; the Euler equation becomes as

$$\partial_u V = 0; \tag{10}$$

the mass conservation law leads to

$$\partial_u \delta_D + \frac{V}{2}\frac{d}{dv}\ln\left|\frac{de^{-\gamma_B}}{dv}\right| + \frac{1}{2}\left\{2\partial_u(\delta_\gamma - \psi) - V\dot{\gamma}_B + V'\right\} = 0, \tag{11}$$

where we have used Euler equation; the Einstein equations become

$$\delta_\gamma{}' = \frac{d\gamma_B}{dv}\left\{\delta_\gamma + \delta_D - 2\partial_u(r\delta_R) - 2(r\delta_R)'\right\} + (r\delta_R)'', \tag{12}$$

$$\dot{\delta}_\gamma = \frac{d\gamma_B}{dv}\left\{\delta_\gamma + \delta_D - 2\partial_u(r\delta_R) - 2(r\delta_R)' - V\right\} + (r\dot{\delta}_R)'. \tag{13}$$

$$\ddot{\delta}_\gamma - \delta_\gamma{}'' = 0, \tag{14}$$

$$r\ddot{\delta}_R - (r\delta_R)'' = 2V\frac{d\gamma_B}{dv}, \tag{15}$$

$$\ddot{\psi} - \psi'' - \frac{1}{r}\psi' = \frac{V}{r}\frac{d\gamma_B}{dv}. \tag{16}$$

Eq.(10) implies that V is an arbitrary function of the advanced time v and hence V does not vanish even in the limit to the spacetime singularity; the speed of the dust fluid does not become that of the light even at the spacetime singularity.

The lowest order of the C-energy flux vector in the vacuum region is given by

$$\sqrt{-g}P^t = \frac{r}{8\pi G}\left(\dot{\psi}^2 + \psi'^2\right), \tag{17}$$

$$\sqrt{-g}P^r = -\frac{r}{4\pi G}\dot{\psi}\psi'. \tag{18}$$

Hence we need to know the solution for only ψ to see the C-energy flux. Giving initial conditions on $\psi(r,t)$ and $\partial_t\psi(r,t)$ at some moment $t = t_i$, the solution of Eq.(16) is easily obtained by using the Green's function of the (2+1)-dimensional Minkowski spacetime.

2.1 Thin Dust Shell

As an example, we consider an infinitesimally thin shell;

$$D_B e^{\gamma_B} = \mu\delta(v), \tag{19}$$

where μ is a positive constant. The spacetime singularity forms first at $(t,r) = (0,0)$. Because of the restriction on the length of the manuscript, we omit the detailed calculations which will be given elsewhere[10]. Setting the metric function γ_B to be zero inside the shell so that the origin $r = 0$ is regular at the initial moment $t = t_i < 0$, we obtain $\gamma_B = 8\pi G\mu$ outside the shell by the above equation and Eq.(9). From Eqs.(9) and (19), we obtain

$$\psi(t,r) = \frac{8\sqrt{2|t_i|}G\mu V(0)}{\sqrt{r}} I(t,r;t_i) + \text{initial data dependent part}, \tag{20}$$

where

$$I(t,r;t_i) = \int_{\Omega(t,r;t_i)}^{1} \frac{dz}{z + t/r}\sqrt{\frac{z - \Omega(t,r;t_i)}{1 - z^2}}, \tag{21}$$

and

$$\Omega(t,r;x) := \frac{t^2 - r^2 - 2tx}{2rx}. \tag{22}$$

It should be noted that we set $t_i < 0$.

From Eq.(20), we find that the asymptotic behavior in the limit to approach the Cauchy horizon $t = r$ is

$$\psi_s(t,r) \longrightarrow -\frac{8G\mu V(0)\sqrt{|t_i|}}{\sqrt{r}} \ln|t - r|. \tag{23}$$

Hence the C-energy flux behaves as

$$\sqrt{-g}P^r \longrightarrow \frac{16G\mu^2V^2(0)|t_i|}{\pi(t - r)^2}. \tag{24}$$

The C-energy ΔE radiated from the neighborhood of the naked singularity is then given by

$$\Delta E = 2\pi\int^t \sqrt{-g}P^r dt \longrightarrow \frac{16G\mu^2V^2(0)|t_i|}{\pi|t - r|}. \tag{25}$$

Hence the C-energy diverges on the Cauchy horizon. This result does not agree with the conclusion obtained by Echeverria[3]. However this does not imply that Echeverria's results are incorrect, but merely means that our linear approximation breaks down.

2.2 Thick Dust Shell

We consider the case

$$D_B c^{\gamma m} = \mathcal{D}_B(v) = \int_{-\infty}^{+\infty} \mathcal{D}_B(v_s)\delta(v - v_s)dv_s, \tag{26}$$

where $\mathcal{D}_B$ is an arbitrary but non-negative function of the advanced time v. Then by superposing the solutions of the thin dust shell (20), we obtain the solution of ψ as

$$\begin{aligned} \psi(t,r) &= \frac{8\sqrt{2|t_i|}G}{\sqrt{r}} \int_{-\infty}^{+\infty} dv_s \mathcal{D}_B(v_s) V(v_s) I(t - v_s, r; t_i) \\ &+ \text{initial data dependent part.} \end{aligned} \tag{27}$$

In order to estimate Eq.(27), here we assume

$$\mathcal{D}_B(v)V(v) = Q\vartheta(v)\vartheta(v_o - v), \tag{28}$$

where v_o and Q are positive constant. Also in this case, the Cauchy horizon is located on $t = r$. If ψ diverges in the limit to approach the Cauchy horizon, the origin of this divergence comes from the integral in the neighborhood of $v_s = 0$ in Eq.(27). Hence in order to see the effect of the naked singularity formation on ψ, it is sufficient to consider the case that v_o/r does not vanish but is much smaller than unity. Then in the limit to the Cauchy horizon, Eq.(27) becomes

$$\psi(t,r) \longrightarrow -\frac{8GQ\sqrt{|t_i|}}{\sqrt{r}} (v_o \ln v_o - v_o) + \text{initial data dependent part.} \tag{29}$$

Thus ψ does not diverge even on the Cauchy horizon. However, the C-energy flux does;

$$\sqrt{-g}P^r \longrightarrow \frac{16GQ^2|t_i|}{\pi} (\ln|t - r|)^2 . \tag{30}$$

Using the above result, we can easily see that the radiated energy is finite. The energy ΔE radiated from the neighborhood of the naked singularity is estimated as

$$\begin{aligned} \Delta E &= \int^t 2\pi\sqrt{-g}P^r dt \sim 32GQ^2|t_i| \int^t (\ln|t - r|)^2 dt \\ &= 32GQ^2|t_i|(t - r)\left\{(\ln|t - r|)^2 - 2\ln|t - r| + 2\right\} + \text{constant}. \end{aligned} \tag{31}$$

Clearly, the first term in the final equality vanishes in the limit to the Cauchy horizon $t = r$. Thus in this case, the linear approximation does not break down. Our solution can be regarded as an asymptotic solution describing the final stage of the cylindrical dust collapse to the spacetime singularity.

3 Discussion

We performed the linear perturbation analysis for the gravitational collapse of a cylindrically symmetric dust fluid by assuming that the speeds of the dust fluid elements are almost equal to the speed of light.

In the case that the dust fluid constitutes an infinitesimally thin shell, the C-energy carried by the gravitational radiation diverges in the limit to the Cauchy horizon. This means that the perturbation analysis breaks down and hence we need to treat the original non-linear equations. This is just the matter studied by Echeverria; he showed that the gravitational collapse of the cylindrical dust shell generates large amounts of the gravitational radiation and the dust shell itself is accelerated to the speed of light.

On the other hand, the thick dust shell emits finite amounts of the C-energy of the gravitational radiation even in the limit to the Cauchy horizon. Hence our linear perturbation analysis does not break down for appropriate initial conditions. We find that in the limit to the Cauchy horizon, the speed of the fluid elements in the thick shell does not approach the speed of light. The thin shell limit is obtained by $v_o \to 0$ with Qv_o fixed and then from Eq.(29), we find that in this limit, the gravitational wave ψ on the Cauchy horizon diverges. The thin shell case corresponds to the simultaneous collapse while the thick shell case represents the run away collapse. Hence *the smaller "time scale" of the singularity formation leads to larger amounts of the gravitational radiation.*

Acknowledgements

We are grateful to colleagues in the astrophysics and gravity group of Osaka City University for helpful discussion and criticism.

References

[1] K.S. Thorne, in *Magic Without Magic; John Archibald Wheeler*, edited by J. Klauder (Frieman, San Francisco, 1972), p231.

[2] T. Nakamura, M. Shibata and K. Nakao Prog. of Theor. Phys. **89** 821 (1993).

[3] F. Echeverria, Phys. Rev. **D47** 2271 (1993).

[4] T. Chiba, Prog. Theor. Phys. **95**, 321 (1996).

[5] R.M. Wald, *General Relativity*, (The University of Chicago Press, Chicago 1984).

[6] K.S. Thorne, Phys. Rev. **138** B251 (1965).

[7] T. A. Morgan, GRG 4 273 (1973).

[8] B. C. Nolan, Phys. Rev. **D65** 104006 (2002).

[9] P. S. Letelier and A. Wang, Phys. Rev. **D49** 5105 (1994).

[10] K. Nakao and Y. Morisawa, in preparation.

Fermion Casimir energy for a de Sitter brane in AdS_5

Ian G. Moss [1], Wenceslao Santiago-Germàn [2]

Department of Mathematics, University of Newcastle Upon Tyne,
Newcastle Upon Tyne, NE1 7RU, UK

Wade Naylor [3], Misao Sasaki [4]

Department of Earth and Space Science, Graduate School of Science, Osaka University,
Toyonaka 560-0043, Japan

Abstract

Based on some recent work of the authors, we focus on the relationship between the Casimir energy of a Majorana spinor field for a Euclidean Einstein universe $S^4 \times R$ and for a Euclidean de Sitter brane (S^4) embedded in AdS_5. This is for a conformally coupled massless field. Interestingly, the one brane effective potential is zero and the results are equivalent, as for the scalar case, when evaluated in the conformal (cylindrical) frame. However, in the original frame this equivalence no longer holds because a non-trivial contribution from the path integral measure (known as the cocycle function) must also be evaluated.

1 Introduction

This short talk is based on a small part of some recent (and continuing) work [1, 2, 3, 4] relating to possible quantum effects in brane world cosmology (BWC) models. The ideas relate to the one brane Randall-Sundrum model [5] and its generalisation to include a curved brane [6, 7]. An interesting BWC scenario has been developed in [8], known as the bulk inflaton model, where it is possible to obtain inflation on a single positive tension brane solely due to the effect of a bulk gravitational scalar field. In this regard, the vacuum energy of the bulk scalar field could have some affect on the cosmological evolution of the brane, (depending on the size and sign of this quantity) and is an interesting subject in its own right.

Employing ζ-function methods we evaluate the one-loop effective potential for a de Sitter brane embedded in a bulk 5-dimensional anti-de Sitter spacetime. In fact, for this case, in the conformal frame, the effective potential reduces to the Casimir energy on S^4, see [1]. Thus, first we also evaluate the vacuum (Casimir) energy on the Euclidean Einstein universe $S^4 \times R$. We focus on massless conformally coupled Majorana spinor fields and compare with the scalar field results. This is based on results from [4] which continues from previous work [2], for scalar fields. For references relating to flat brane calculations see those cited in [2].

In what follows we mention that there are no zero modes to deal with. This is because for fermion fields the relevant boundary conditions are mixed, meaning half the field components satisfy Neumann and the other half satisfy Dirichlet boundary conditions. This cancels any zero modes (by zero modes, we mean $n = 0$ modes in our mode sum and not null eigenvectors).

[1] E-mail: ian.moss@ncl.ac.uk
[2] E-mail: g.w.santiago- german@ncl.ac.uk
[3] E-mail: wnaylor@vega.ess.sci.osaka-u.ac.jp
[4] E-mail: misao@vega.ess.sci.osaka-u.ac.jp

2 Casimir energy

Before evaluating the vacuum energy, we must find the eigenvalues to be employed in the ζ-function. We start with the Euclidean metric suitable for de Sitter branes [9]

$$ds^2 = dr^2 + \ell^2 \sinh^2(r/\ell) d\Omega_4^2, \tag{1}$$

where $\ell = (-6/\Lambda_5)^{1/2}$ is the anti-de Sitter radius and $d\Omega_4^2$ is the metric on the unit 4-sphere. At the classical level, boundary or junction conditions relate the location of the single positive tension brane (located at r_0) to the brane tension σ according to [9]

$$\sigma = \frac{3}{4\pi G_5 \ell} \coth(r_0/\ell). \tag{2}$$

The quantum corrections will introduce other sources of stress-energy on the brane which modify these relations. The metric can be written in conformal form

$$ds^2 = a^2(z)(dz^2 + d\Omega_4^2) \qquad a(z) = \frac{\ell}{\sinh(z_0 + |z|)}, \tag{3}$$

where the coordinates are chosen to have the positive tension brane at $z = 0$. The above form of the metric is conformal to a cylinder $I \times S^4$. However, as in the bulk inflaton model, it may also be of interest to consider the compact space $S^1 \times S^4$ [9]. If two branes are present then the other brane is placed at $|z| = L$, with the one brane limit given by $L \to \infty$.

For spin-1/2 fermion fields, ψ, the massless Dirac equation is automatically conformally covariant. We shall concentrate on Majorana spinors, see [4]. Taking the square of the Dirac operator to evaluate the effective action gives

$$W^M = -\frac{1}{4} \log \det \Delta \tag{4}$$

for Majorana fermions, where

$$\Delta = -\nabla^2 + \frac{1}{4} R^{(5)} \tag{5}$$

The squared operator is not conformally invariant, but it is nevertheless still possible to relate the effective actions of fermions with conformally related metrics [10].

On the cylinder and noting that for conformal coupling all delta function contributions cancel,

$$\Delta = \left(-\partial_z{}^2 - \Delta_f^{(4)} + 3 \right), \tag{6}$$

where on S^4, $R^{(4)} = 12$. The eigenvalues of the spinor Laplacian, $\Delta_f^{(4)}$, on the 4-sphere are well known (e.g., see [11]) and are given by $(m+2)^2 - 3$. Half of the field components satisfy Dirichlet boundary conditions and half satisfy Neumann boundary conditions, commonly known as mixed boundary conditions. The eigenvalues of Δ are

$$\lambda_{n,m}^M = \left(\frac{\pi n}{L} \right)^2 + (m+2)^2 . \tag{7}$$

The degeneracy for the 8 component Majorana spinors is given by [11]

$$d^M(m) = 8 \times \frac{1}{6}(m+1)(m+2)(m+3) \tag{8}$$

where we take $n \in Z$. Then, the ζ-function method can be employed to find the contribution to the effective action from the cylinder. The generalised zeta function is given by

$$\zeta^M(s) = \sum_{m,n=0}^{\infty} d(m) \lambda_{m,n}^{-s}. \tag{9}$$

with the one-loop effective action related to $\zeta(s)$ by (e.g., see [11, 14])

$$W^M = \frac{1}{4} \zeta^{M\prime}(0) + \frac{1}{4} \zeta(0) \log \mu^2 \tag{10}$$

for Majorana fermions, where μ is the renormalisation scale. The effective potential is then obtained by dividing by the total volume.

As in [2] we first begin with the simpler case of the vacuum energy for the Einstein universe $S^4 \times R$. The evaluation of such quantities on $S^3 \times R$ using an exponential cut off in the mode sum was performed by Ford [12, 13], for scalar and spinor fields respectively. This is equivalent to finding the zero point energy of the equation

$$\partial_t^2 \psi - \Delta_f^{(4)} \psi + \frac{1}{4} R^{(4)} \psi = 0. \tag{11}$$

The eigenvalues and degeneracy are given by Eq. (7,8), with $n = 0$. From our definition of W^M (Eq. (10)) the vacuum energy for a Majorana field is defined as

$$E_0^M = -\frac{1}{4}\zeta^M(-1/2) = -\frac{1}{3}\left(\zeta(2s-3,2) - \zeta(2s-1,2)\right)_{s\to -1/2} = 0, \tag{12}$$

where $\zeta(a,b)$ is the generalised (or Hurwitz) ζ-function. This result is expected because in an odd number of dimensions there is no conformal anomaly [14], i.e. as in the case of $S^2 \times R$.

Now, we come to evaluate the effective potential for a one brane configuration on the cylinder, where the discrete n modes become continuous. It is then possible to show that

$$\zeta^M(s) = \frac{2L}{\pi}\int_0^\infty dk \sum_{m=0}^\infty d^M(m)\left(k^2 + (m+2)^2\right)^{-s}, \tag{13}$$

where the factor of 2 is because we choose to undo the Z_2 symmetry as in [9]. For large s we can interchange the order of the sum and the integral and perform the k integration,

$$\begin{aligned}\zeta^M(s) &= \frac{2L}{\pi}\frac{\sqrt{\pi}}{2}\sum_{m=0}^\infty \frac{\Gamma(s-1/2)}{\Gamma(s)} d^M(m)(m+2)^{1-2s}, \\ &= \frac{L}{\pi}\frac{4}{3}\sqrt{\pi}\frac{\Gamma(s-1/2)}{\Gamma(s)}\left(\zeta(2s-4,2) - \zeta(2s-2,2)\right),\end{aligned} \tag{14}$$

where in the second step we have used simple algebra to rewrite the equation in terms of generalised (Hurwitz) ζ-functions. The analytic continuation to $s = 0$ is contained naturally in the definition of the ζ-function, in this case. For $s = 0$ it is clear that $\zeta^M(0) = 0$ because $\frac{1}{\Gamma(s)} = s + \gamma s^2 + O(s^3)$, where γ is Euler's constant. Thus,

$$\zeta^{M\prime}(0) = \frac{L}{\pi}\frac{4}{3}\sqrt{\pi}\,\Gamma(-1/2)\left(\zeta(-4,2) - \zeta(-2,2)\right) = 0. \tag{15}$$

Therefore, as for scalar fields [1, 2], the one loop effective potential on the cylinder is zero in the one brane case. Just to see the relationship between the vacuum energy Eq. (12) and the effective potential, let us note that

$$W = -\frac{2}{3}L\left(\zeta(-4,2) - \zeta(-2,2)\right) = 0. \tag{16}$$

Thus, apart from the extra factor of 2 due to our mode doubling, the effective potential agrees with the vacuum energy density on $S^4 \times R$.

3 Summary

In this talk we have evaluated, in the conformal frame, the effective potential for a de Sitter brane embedded in a bulk AdS_5 spacetime. We also evaluated the vacuum energy on the Euclidean Einstein universe $S^4 \times R$ and found the two results to agree. However, there is a slight subtlety concerning our calculation, because when boundaries are present, conformal transformations induce a non-trivial Jacobian in the path integral measure. This is taken care of by evaluating an extra term, known as the cocycle function, [4]. Using the conformal frame, defined by Eq. (3), the cocycle function is found to vanish because the conformal volume is infinite, as first argued in [1]. However, working in the original frame, defined by Eq. (1), the cocycle function does not vanish because the volume is finite, see [4].

As the original frame is the one of physicality we conclude that the cocycle function must be included. However, there is still a close relationship between the vacuum energy density on $S^4 \times R$ and the effective potential for a single S^4 brane in AdS_5.

Aside from the cocycle function, the fact that the vacuum energy on $S^4 \times R$ with a mass or non-conformal curvature coupling will be non-zero, we then can infer that this will also be true of the de Sitter brane case. This considerably simplifies our analysis for the one brane case, which in the conformal frame is the evaluation of the Casimir energy on $S^4 \times R$. When applying the conformal transformation technique to the most general case, i.e. any mass or curvature coupling, the potential is non-homogenous on the cylinder.

4 Acknowledgements

W.N. acknowledges support from JSPS for Postdoctoral Fellowship for Foreign Researchers No. P01773. W.S. is grateful to CONACYT of Mexico, Grant Number 116020, for financial support. The work of M.S. is supported by Monbukagaku-sho Grant-in-Aid for Scientific Research (S) No. 14102004.

References

[1] S. Nojiri, S. D. Odintsov and S. Zerbini, Class. Quant. Grav. **17** (2000) 4855.

[2] W. Naylor and M. Sasaki, Phys. Lett. B **542** (2002) 289.

[3] E. Elizalde, S. Nojiri, S. D. Odintsov and S. Ogushi, hep-th/0209242.

[4] I. G. Moss, W. Naylor, W. Santiago-Germàn and M. Sasaki, paper in preparation.

[5] L. Randall and R. Sundrum, Phys. Rev. Lett. **83** (1999) 4690.

[6] T. Shiromizu, K. I. Maeda and M. Sasaki, Phys. Rev. D **62** (2000) 024012.

[7] J. Garriga and T. Tanaka, Phys. Rev. Lett. **84** (2000) 2778.

[8] Y. Himemoto and M. Sasaki,
Phys. Rev. D **63** (2001) 044015.

[9] J. Garriga and M. Sasaki, Phys. Rev. D **62** (2000) 043523.

[10] I. G. Moss, in *The Future of Theoretical Physics*, essays in honour of S. W. Hawking's 60th birthday (Cambridge University Press).

[11] I. G. Moss, *Quantum Theory, Black Holes and Inflation* (Wiley, 1996).

[12] L. H. Ford, Phys. Rev. D **11** (1975) 3370.

[13] L. H. Ford, Phys. Rev. D **14** (1976) 3304.

[14] N. D. Birrel and P. C. .W. Davies, *Quantum Fields in Curved Space* (Cambridge University Press, 1981).

Alternative to Higgs and Unification

Miyuki Nishikawa[1]

Department of Physics, Graduate School of Science,
University of Tokyo, Hongo, Bunkyo, Tokyo 113-0033, Japan

Abstract

In this paper, we discuss the self-consistency condition for the spherical-symmetric Klein-Gordon equation, and then discuss a natural possibility that gravity and weak coupling constants g_G and g_W may be defined after g_{EM}. In this point of view, gravity and the weak force are subsidiary derived from electricity. Particularly, $SU(2)_L \times U(1)$-unification is derived without assuming a phase transition. A possible origin of the Higgs mechanism is proposed. Each particle pair of the standard model is associated with the corresponding asymptotic expansion of an eigen function.

1 Introduction

In usual dimensional counting, a momentum has dimension one. But a function $f(x)$, when differentiated n times, does not always behave like one with its power smaller by n. For example, this can occur in the neighborhood of $x = 0$ if the function $f(x)$ has an essential singularity at $x = 0, f(0) \to 0 (x \to 0)$. Thus the dimension of a momentum is such an *operator* that cannot be fixed unless the operand of the differential operator is explicit. This inevitable uncertainty may be essential in general theory of renormalization, including quantum gravity[1].

In this paper, the settings to deal with this problem are as follws. We assume the spherical-symmetric part of the Klein-Gordon equation

$$\Delta R(r) = \left[\frac{1}{r^2}\frac{d}{dr}(r^2\frac{d}{dr}) - \frac{l(l+1)}{r^2}\right] R(r) = -\frac{(E - e\phi(r))^2 - m^2c^4}{\hbar^2c^2}R(r) =: V(r)R(r) \tag{1}$$

with a time-independent spherical-symmetric $U(1)$ potential $A^\mu := (\phi(r), 0, 0, 0)$. Let us neglect spins for a while and require the following self-consistent conditions for a realistic gauge field:

1. There exists at least one C^2-class eigen function $R(r)$ satisfying (1) with $l = 0$.
2. The free field part of lagrangian is finite for the $R(r)$.
3. This $R(r)$ in turn creates another potential $\phi'(r) \propto R$ and the corresponding force $\propto -\text{grad } R$.

We can classify most possible powers of the potentials by assuming $R(r)$ to be a 'generalized Taylor expansion' defined in the next section.

2 Construction of the generalized Taylor expansion

In fact there are various kinds of singularities. For example, we can replace the power of any term of a Taylor series of a complex variable z with an arbitrary real number n, or $\log z$. An infinite power is called an essential singularity, and we can make more and more complex singularities by finite times of operations including summations, subtractions, multiplications, divisions (by $\neq 0$), and compositions (with the shape of $f(g(z))$, where $g(z)$ converges monotonically to $+0$ as $z \to +0$, or othrwise $f(z) = \exp z$ and $g(z)$ diverges monotonically to $\pm\infty$ as $z \to +0$). The most general shape of a singularity that is closed in these operations is the whole sum

$$(1)_i + (2)_j + \cdots + (m)_k\,, \qquad \text{where} \tag{2}$$

[1] E-mail:nisikawa@hep-th.phys.s.u-tokyo.ac.jp

$$
\begin{aligned}
(1)_i &:= \Bigg(\sum_{n\in\{n\}_i}^{\infty} \sum_{m_{i1},\cdots,m_{id_i}=-\infty}^{m_{i1},\cdots,m_{id_i}} a_{inm_1\cdots m_{d_i}} z^n (-\log z)^{m_1} (-\log(-z/\log z))^{m_2} \\
&\qquad\qquad \cdots (-\log(-z/(-\log(-z/\log\cdots z))))^{m_{d_i}} \Bigg)_i, \\
(2)_{\pm j} &:= \sum_{i\in\{i\}_j} (\pm) e^{\pm(1)_i}, \\
(3)_{\pm k} &:= \sum_{j\in\{j\}_k} (\pm) e^{\pm(2)_j}, \\
&\vdots
\end{aligned} \tag{3}
$$

Here the $(\pm)$ in front of e takes each of the signatures depending on each i (or $j, k, \cdots$), while the $\pm$ on the shoulder of e and in front of $j, k, \cdots$ takes the signature such that the coefficient of the first term in $\sum$ is of the same signature as j after choosing the signatures. Each term is ordered in partially ascending powers with regards for any sums. The sum with index n is performed according to the monotonically non-decreasing sequence of real numbers $\{n_i\}$ $(-\infty < n_i)$ depending on i. In the same manner, the sum with index $i, j, \cdots$ is performed according to the finite, monotonically non-decreasing sequence $\{i_j\}$, $\{j_k\}\cdots$ of natural numbers. $m_{i_1}, \cdots, m_{i_{d_i}}$ take finite values, but they increase in correspondence with n and grows $\to \infty$ as $n \to \infty$, and depend on i. d_i is the maximal 'depth' of the composition of logs, or the number of logs, depending on i and of finite value. [2] The more precise construction and the meaning of this expansion are in my preprint[1]. Notice that this has several number of infinite series in one expansion but is valid under the special rule that we must not decompose an exponential until the end of the calculation. Then we can rewrite (3) for the condition 1. i.e., a C^2-class $R(z)$;

$$
R(z) = a + bz + \sum_{n=2}^{\infty} a_n z^n \sim + \sum_{i<0} (\pm) e^{-b_i z^i \sim \cdots} + \sum_{j<0} (\pm) e^{-e^{c_j z^j} \sim \cdots} + \sum_{k<0} (\pm) e^{-e^{e^{d_k z^k} \sim \cdots} \sim \cdots} \cdots, \tag{4}
$$

where a, b, a_n are real constants; $i, j, k, \cdots < 0$; $b_i, c_j, d_k, \cdots > 0$; $\sim$ represents the abbreviation of $\log z \sim$, and $\cdots$ the higher order terms.

3 Classification of powers

We assume $l = 0$ and extend (1) to a higher spatial dimension N with the inverse variable $z := r^{-1}e^{i\theta}$. Then, we can classify the possible powers for the form (4) of $R(r)$ as follows[3].

$$
\begin{aligned}
\frac{\Delta R(r)}{R(r)} &= \frac{1}{R(z)} \left\{ \frac{dz}{dr}\frac{d}{dz}\left(\frac{dz}{dr}\frac{dR(z)}{dz}\right) + (N-1)z\frac{dz}{dr}\frac{dR(z)}{dz} \right\} \\
&= z^4 \frac{R''(z)}{R(z)} - z^3(N-3)\frac{R'(z)}{R(z)}
\end{aligned}
$$

[2] The power is smaller when $m_1 + m_2 + \cdots + m_{i_1}$ is greater for the same n, and when it is also the same and m_1 is smaller, and when it is also the same and m_2 is smaller, ..., and so on.

[3] The line 2 in the big { includes the case $a \neq 0$ and $b = 0$ and ${}^3a_n \neq 0$ and $N = n + 2 \neq 3$, when $\frac{\Delta R(r)}{R(r)} \to (m - N + 2)m\frac{a_m}{a} z^{m+2}$ or the like, where a_m is the term next to $a_n z^n$.

In addition, line 2, 4, 7, 8 include the Yukawa potential case, when $\phi(r) \sim z^l e^{-\frac{b_i}{z^i}}$, the only finite solutions are

$$
\frac{\Delta R(z)}{R(z)} \to \frac{d}{a}(b_i i)^2 z^l e^{-\frac{b_i}{z^i}} \quad \left(R(z) = \begin{cases} a + bz^n + dz^k e^{-\frac{b_i}{z^i}} + \cdots & (b = 0 \text{ if } N \neq n+2) \text{ or} \\ az^n + dz^{k+n} e^{-\frac{b_i}{z^i}} + \cdots & (N = n+2) \end{cases} \right),
$$

where $a, d \neq 0$ and $b_i, i > 0$ and $k = 2i - l$. It is curious that there are some 'degenerate' eigen functions for the same asymptotic potential, even if not normalizable for $N < 4$.

Finally, this and line 9 allow for a single term with pure imaginary b_i, except for which an imaginary coefficient on the shoulder of the exponential leads to a non-physical oscillatory or imaginary potential. This is indeed the case for the Coulomb scattering of a photon.

$$\rightarrow \begin{cases} (3-N)\frac{b}{a}z^3 \ (a \neq 0 \text{ and } b \neq 0 \text{ and } N \neq 3) \\ (n-N+2)n\frac{a_n}{a}z^{n+2} \ \text{(or higher order)} \ (a \neq 0 \text{ and } b = 0 \text{ and } {}^{\exists}a_n \neq 0 \text{ and } N \neq 3) \\ (n-1)n\frac{a_n}{a}z^{n+2} \ (a \neq 0 \text{ and } {}^{\exists}a_n \neq 0 \text{ and } N = 3) \\ (\pm)\,0 \ (a \neq 0 \text{ and } b =^{\forall} a_n = 0 \text{ and } {}^{\exists}b_i \text{ or } c_j \text{ or } d_k \text{ or} \cdots > 0) \\ (3-N)z^2 \ (a = 0 \text{ and } b \neq 0 \text{ and } N \neq 3) \\ (n-1)n\frac{a_n}{b}z^{n+1} \ (a = 0 \text{ and } b \neq 0 \text{ and } {}^{\exists}a_n \neq 0 \text{ and } N = 3) \\ (\pm)\,0 \ (a \text{ or } b \neq 0 \text{ and } {}^{\forall}a_n = 0 \text{ and } {}^{\exists}b_i \text{ or } c_j \text{ or } d_k \text{ or} \cdots > 0 \text{ and } N = 3) \\ (n-N+2)nz^2 \ \text{(or higher order)} \ (a = b = 0 \text{ and } {}^{\exists}a_n \neq 0) \\ +(-ib_i)^2 z^{2i\pm 2\epsilon+2} \ (a = b =^{\forall} a_n = 0 \text{ and } {}^{\exists}b_i > 0) \\ +\infty \ (a = b =^{\forall} a_n =^{\forall} b_i = 0 \text{ and } {}^{\exists}c_j \text{ or } d_k \text{ or} \cdots > 0) \end{cases} \tag{5}$$

4 Theorems for the long distance limit

Now we define the following normalization conditions for later convenience.
The **Normalization Conditions for free fields in the long distance limit** are
for **Massive Boson field (NC-MB)**, $n \leq -\frac{N+1}{2}$;
for **Massless Boson field (NC-0B)**, $n \leq \frac{1-N}{2}$;
for **Massive Fermion field (NC-MF)**, $n \leq -\frac{N+1}{2}$;
for **Massless Fermion field i(NC-0F)**, $n \leq -\frac{N}{2}$,
where the field behaves like r^n and $=$ means logarithmic divergence, all of them with the
Exceptional rule for massless particles (NC-0Ex) that
an arbitrary constant can be added, with the next term $n \leq -1$ for bosons; $n \leq -3$ for fermions.

It's unclear to me whether or not previous results is valid for the Dirac equation, but for a moment we keep away the validity as a later discussion and just describe the specific results given by application for fermions by writing in a [ ]. Then, from the previous result we can verify the following theorems for the long distance limit.

Theorem 1
A massless boson [or fermion] that behaves like $\sim \frac{1}{r}$ can not feel a dominant $\frac{1}{r^2}$-like long range force.
Proof
For $N < 3$, this is proven by taking $E = m = 0$ in (1) and comparing with the line 5 of (5). The former contradicts the latter condition that $V(+\infty)$ must be positive for $N < 3$. For $3 < N$, this is proven just because a nonzero b in the line 5 breaks **NC-0B**, and for $3 < N$, that is a weaker condition than **NC-MB** and **NC-0F**. For $N = 3$, the line 6, 7 of (5) require that $V(r)$ vanishes more rapidly than r^{-2}, when $\phi(r)$ vanishes more rapidly than r^{-1} and thus can not create a $\frac{1}{r^2}$-like long range force.

Some people might suspect that we can not always take $E = 0$ because it means a virtual photon, but at least in situations a photon is bounded by the potential and another photon is not bounded, we can always take $E = 0$ and thus we dare say
Theorem 2
For $N \leq 3$, a charged static spherical symmetric black hole can not exist. For $3 < N$, the electric field decreases more rapidly than $\frac{1}{r^{N-1}}$, if such a black hole can exist.
Proof
Even a black hole has its gravitational potential $\sim \frac{1}{r}$ in the distance, for its density is finite and spherical-symmetric, and obeys Gauss' law and $\frac{1}{r^2}$-law experimentally, and gravity is always attractive. A black hole is of course such a matter that even a light can not escape, therefore a bound state exists for a photon. Taking $E = m = 0$, the only possible cases are line 5, 8 of (5). Strictly speaking, there might be exceptions for the theorem, where the black hole potential is deviated from the $\frac{1}{r}$-law because of the presence of another long range force that a photon can feel. In the standard model of particles, this is not the case, for no other long range force (gluons nor a photon) couple with a photon.

Even if we can not take $E = mc^2$, the only remaining possibility for a boson to feel a dominant $\frac{1}{r^2}$-like long range force is the line 9 of (5). Then,
Theorem 3
A gauge boson that feels a dominant $\frac{1}{r^2}$-like long range force can not create a long range force.

By the way, from the argument of footnote 3, we can also verify
Theorem 4

If a boson [or fermion] feels a dominant Yukawa-type potential, then the eigen function of the particle is not L^2. Particularly, such a boson [or fermion] must be massless for $N < 5$; can be massive for $5 \leq N$.

proof

This is because if we take $E = mc^2$ and Yukawa-type potential $\phi \sim z^l e^{-\frac{b_i}{i^i}}$, the only finite solutions are $\frac{\Delta R(z)}{R(z)} \to \frac{d}{a}(b_i i)^2 z^l e^{-\frac{b_i}{i^i}}$ $\left(R(z) = \begin{cases} a + bz^n + dz^k e^{-\frac{b_i}{i^i}} + \cdots & (b = 0 \text{ if } N \neq n+2) \text{ or} \\ az^n + dz^{k+n} e^{-\frac{b_i}{i^i}} + \cdots & (N = n+2) \end{cases} \right)$, where $a, d \neq 0$ and $b_i, i > 0$ and $k = 2i - l$, $R(r)$s vanish no more rapidly than r^{2-N}, to be compared with **NC-MB**, **NC-0B**, [**NC-MF**, **NC-0F**], and **NC-0Ex**. Notice that for $N = 3$, a logarithmic divergence inevitably appears even for a massless boson in the second case of { , and therefore this case is impossible for $3 < N$. It is surely a severe condition for realistic physics and thus

Corollary 1

A short range force must always be dominated by a longer range force, or otherwise $N < 5$ and not felt by a massive boson [and fermion], or otherwise $5 \leq N$, where the term 'longer' used to notice that any force that survives more slowly than any Yukawa potential is allowed.

From now on, we take $N = 3$ and concentrate on the two-body problem for every pair of particles in the standard model. Then, the eigen function must be common for both particles in the pair, feeling the same potential. Thus

Corollary 2

If we do not include gravity, a boson with a charge of a short range force must have another charge of a longer range force, or otherwise be massless.

Notice that here we used the reduced mass $\frac{M_X M_Y}{M_X + M_Y}$. [The theorem is almost valid for neutrinos]. Thus we can prove $SU(2)_L \times U(1)$-unification without assuming the usual Higgs mechanism or experiments.

5 Proposal for the origin of Higgs mechanism

Now, remember that massless free spin 1 and 2 bosons are always identified with a photon and a graviton respectively, and create a $\frac{1}{r^2}$-like long range force, and a graviton couples equivalently to all matter [2]. Let us consider a world where only a photon and a graviton exist. Then, from **Theorem 3** the photon can not create a $\frac{1}{r^2}$-like long range force. Suppose that a massive boson has a charge. If we do not take account of gravity as the dominant force, and if it is a charge of a short range force, then from **Corollary 2** the boson has a charge of a longer range force. Thus, we can naturally assume that the 'boson with a charge of a short range force' has a charge of a long range force, say, electric charge, and call it W^+, for a photon of course exists and creates a long range force. Then, from the CPT-theorem, its anti-particle W^- also exists. And this is the source of the short range force, therefore must be identified with the 'photon that feels a $\frac{1}{r^2}$-force and can create a Yukawa-type electric field' i.e., the line 9 of (5), for the Gauss' law is valid also for the field of the 'reshaped photon' and gives the real charge distribution. Then, the identity

$$\left(E_\gamma - \frac{b}{r}\right)^2 = \left(E_W - \frac{a_1}{r} - \frac{a_2}{r^2} - \frac{a_3}{r^3} \cdots\right)^2 - {M_W}^2 c^4 \tag{6}$$

implies that a massless photon with an energy E_γ feeling the gravitational potential $\phi_G := \frac{b}{r}$ is equivalent to $W^\pm$ bosons with an energy E_W and the (reduced) mass $M_W c^2 := \sqrt{E_W^2 - E_\gamma^2}$ feeling the gravitational plus electrical potential $\phi'_G + e\phi_{EM} := \frac{a_1}{r} + \frac{a_2}{r^2} + \frac{a_3}{r^3} \cdots$. If we take $E_\gamma = 0$, then $a_1 = 0$ and $b^2 = a_1^2 - 2M_W a_2, \cdots$. This is in good agreement with the line 9 of (5), if we take b to be pure imaginary $\pm\sqrt{-2}\hbar c$. Notice that an imaginary b is seemingly contradict to the proof of **Theorem 1**, but if we take m to be pure imaginary and $n := \frac{ib}{2}$ real in

$$\begin{aligned} \frac{\Delta R(r)}{R(r)} &= -\frac{(E_\gamma - \phi_G)^2}{\hbar^2 c^2} \sim -\frac{(E_W - \phi'_G - e\phi_{EM})^2 - {M_W}^2 c^4}{\hbar^2 c^2} \\ &\sim m^2 - 2mn\frac{1}{r} + n(n-1)\frac{1}{r^2}, \qquad R(r) \sim e^{-mr} r^n, \end{aligned} \tag{7}$$

there is no problem.

We would rather adopt the redefinition of gravity as the integral constants of a laplacian, i.e.,

$$\phi_G(r) := a + \frac{b}{r} = e^2 G(r), \qquad \Delta G(r) =: 0. \tag{8}$$

Then, the equation (7) can be solved for a photon as

$$A^0(z) := \sum_{n=2}^{\infty} a_{An} z^n \sim \cdots \quad \text{and} \quad A^{\pm}(z) := \sum_{k=1,2,3\cdots}^{\infty} \sum_{l_k=1}^{\infty} d_{Akl_k}^{\pm} e^{\pm ik\frac{\pi}{s}} z^{l_k} \quad \text{satisfy}$$

$$\frac{\Delta A(z)}{A(z)} = -\frac{(\pm E_\gamma - \phi_G)^2}{\hbar^2 c^2}, \quad E_\gamma := \begin{cases} im\hbar c \ (\text{for} A^0(z)) \\ im\hbar c + \omega \ , \text{where } \omega \text{ is any positive number } (\text{for} A^{\pm}(z)) \end{cases} \tag{9}$$

Let us infer the form of b for a general two-body problem. The fact that even a massless photon can feel gravity and the symmetry requirement imply $b \propto M_X + M_Y$ instead of $M_X M_Y$. The Newton potential can then be derived by scaling E with the unit $\frac{M_X M_Y}{M_X + M_Y} c^2$, and $\frac{b^2}{r^2}$ means the Schwarzschild correction.

6 Unification

We can also infer the form of the eigen function for each pair of the standard model particles as follows[1]:

$$Z^0(z) := (a_Z - bz)\left(\delta_{E_Z M_Z} \pm \sum_{k=1,2,3\cdots}^{\infty} \sum_{l_k=1}^{\infty} d_{Zkl_k} e^{-k\frac{m}{s}} z^{l_k} + \cdots\right) \quad \text{and}$$

$$\nu^0(z) :\approx a_\nu \left(\delta_{E_\nu M_\nu} \pm \sum_{k=1,2,3\cdots}^{\infty} \sum_{l_k=1}^{\infty} d_{\nu kl_k} e^{-k\frac{m}{s}} z^{l_k} + \cdots\right) \quad \text{and}$$

$$W^{\pm}(z) := a_W \left(\left(\pm 1 \text{ or } \sum_{n=2}^{\infty} a_{Wn} z^n \sim\right) \delta_{E_W M_W} + \sum_{k=1,2,3\cdots}^{\infty} \sum_{l_k=1}^{\infty} d_{Wkl_k} e^{-k\frac{m}{s}} z^{l_k} + \cdots\right) \quad \text{and}$$

$$Q^{\pm}(z) :\approx a_Q \left(\left(\pm 1 \text{ or } \sum_{n=2}^{\infty} a_{Qn} z^n \sim\right) \delta_{E_Q M_Q} + \sum_{k=1,2,3\cdots}^{\infty} \sum_{l_k=1}^{\infty} d_{Qkl_k} e^{-k\frac{m}{s}} z^{l_k} + \cdots\right)$$

$$\text{or} \sum_{k'=1,2,3\cdots}^{\infty} \sum_{l'_{k'}=1}^{\infty} f_{Qk'l'_{k'}} e^{-k'\frac{M}{s^2}} z^{l'_{k'}} + \cdots \tag{10}$$

Here is no space, but a pair of Z^0 bosons escapes **Corollary 2** by having an 'anti-gravity potential' itself. Furthermore, the last terms of the quark $Q^{\pm}$ correspond to a linear potential, well account for the QCD.

7 Conclusion

We classified possible singularities of a potential for the spherical-symmetric Klein-Gordon equation, assuming that a potential ϕ has at least one normalizable eigen function $R(r)$, which in turn creates another potential $\phi' \propto R$. Then we discussed a natural possibility that gravity and weak coupling constants g_G and g_W are defined after g_{EM}. In this point of view, gravity and the weak force are subsidiary derived from electricity. The iterative solution inevitably includes several infinite series of different order in one expansion and does not satisfy the Lipschitz continuity condition, which may be the origin of the gauge invariance. Thus we can prove $SU(2)_L \times U(1)$ -unification.

References

[1] M. Nishikawa, preprint hep-th/0202086; hep-th/0207063.

[2] S. Weinberg, Phys. Rev. **133**, B1318 (1964); **134**, B882 (1965); **138**, B988 (1965); **181**, 1893 (1969).

Detectability of time evolution and geometric distortion of clustering from galaxy redshift surveys

Hiroaki Nishioka[1]

Department of Physics, Hiroshima University, Higashi-Hiroshima 739-8526, Japan

Abstract

We examine the detectability of the geometric distortion and time evolution of clustering from the galaxy redshift surveys like the 2dFGRS and SDSS. We present the realistic estimator to infer the cosmological parameters and the derivative of the bias parameter $d\ln b(z)/dz$ at present, based on the method proposed by Nakamura, Matsubara and Suto (1998). In their method we can measure the anisotropy of the two-point correlation function induced by the geometric distortion and the time evolution of clustering independently of the shape and amplitude of the underlying fluctuation spectrum. We calculate the variances of the estimators to examine how accurately we can constrain the cosmological parameters and models for bias from the real galaxy redshift surveys. We find that from the SDSS galaxy sample, the time evolution of bias is not constrained while the SCDM model ($\Omega_m = 1$, Ω_Λ=0) can be ruled out for the fiducial cosmological model ($\Omega_m = 0.3$, Ω_Λ=0.7).

1 Introduction

It is well known that the anisotropy of the galaxy clustering caused by the peculiar velocity can be used to measure the redshift-distortion parameter $\beta(z) = b(z)^{-1} d\ln D_1(z)/d\ln a(z)$, where $D_1(z)$ is the liner growth rate, $b(z)$ is the linear and time-dependent bias parameter, and $a(z)$ is the scale factor. Recently, Pecock et al.[1] measured β with the quadrupole to monopole ratio of the two-point correlation function from the galaxy redshift catalog of the 2dF Galaxy Redshift Survey (2dFGRS). They reported the resulting redshift-distortion parameter $\beta = 0.43\pm0.07$. The accuracy of the measure of this parameter will be higher when the 2dFGRS and the Sloan Digital Sky Survey (SDSS) are complete.

In addition to the peculiar velocity, the geometric distortion changes the clustering pattern in the nonzero depth of the survey. The geometric distortion in such a depth of these galaxy redshift surveys is weak. However de Laix and Starkman [2] suggested the possibility of measuring the geometric distortion and constraining the cosmological parameters without the external constraints assuming the surveys of approximate depth of the SDSS. In their analysis, the quadrupole to monopole ratio of the power spectrum has been adopted. Here we adopt the method proposed by Nakamura, Matsubara and Suto [3]. Their method does not need any assumption in the shape of the underlying fluctuation spectrum although the direct fit using the two-point correlation function or power spectrum does need. Therefore, by this method we can get the clean signal from the redshift-space distortions. However, how well this method work in real galaxy redshift surveys has not been examined. In this paper, I test this method by variance calculations of the estimators. Throughout the present paper we use the unit in which $c = 1$.

2 Two-point correlation function in redshift space

For the samples from the nearby galaxy redshift surveys, radial distances of galaxies are usually determined with the Hubble law, $s = z/H_0$. Then in this paper we define the redshift-space radial coordinate to be the coordinate determined by $s = z/H_0$ from the observed redshift z. Then in redshift space, the separation R of the two points located at redshift z, and separated by $\Delta z(\ll z)$ and angle $\Delta\theta(\ll 1)$ are written as

$$R = [(\Delta z/H_0)^2 + \{(z/H_0)\Delta\theta\}^2]^{1/2}. \quad (1)$$

[1] E-mail:nishioka@theo.phys.sci.hiroshima-u.ac.jp

The cosine of the angle between the difference vector of the two points and the line of sight direction is

$$\mu = (\Delta z/H_0)/R. \tag{2}$$

In redshift space, the two-point correlation function can be expanded up to the linear order of z in terms of R and μ as [3],

$$\xi^s(R,\mu;z) \simeq \sum_{l=0}^{3} \zeta_{2l}(R;z)P_{2l}(\mu), \tag{3}$$

where $P_{2l}(\mu)$ is the Legendre polynomials and

$$\zeta_{2l}(R;z) \simeq \xi_{2l}(R) + z\eta_{2l}[R;\beta_0,q_0,\phi_0,\psi_0,\xi(R)]. \tag{4}$$

The first term of the right-hand side of equation (4) is the two-point correlation function at present and the second term describes the effect of the geometric distortion and the time evolution. $\xi_{2l}(R)$ and $\eta_{2l}(R)$ in equation (4) are expressed as

$$\xi_0(R) = \left[1 + \frac{2}{3}\beta_0 + \frac{1}{5}\beta_0^2\right]\xi(R), \tag{5}$$

$$\xi_2(R) = \left[\frac{4}{3}\beta_0 + \frac{4}{7}\beta_0^2\right]\xi_d(R), \tag{6}$$

$$\xi_4(R) = \frac{8}{35}\beta_0^2\left[\xi_d(R) + \frac{7}{2}\xi_q(R)\right], \tag{7}$$

$$\eta_0(R) = -\left[\left(1+\frac{1}{3}\beta_0\right)\phi_0 + \left(\frac{1}{3}\beta_0 + \frac{1}{5}\beta_0^2\right)\psi_0\right]\xi(R) - \frac{2}{3}\left[1 + \frac{4}{5}\beta_0 + \frac{9}{35}\beta_0^2\right]\frac{d\xi(R)}{d\ln R}(1+q_0), \tag{8}$$

$$\eta_2(R) = -\left[\frac{2}{3}\beta_0\phi_0 + \left(\frac{2}{3}\beta_0 + \frac{4}{7}\beta_0^2\right)\psi_0\right]\xi_d(R) + \left[\left(\frac{20}{7}\beta_0 + \frac{4}{3}\beta_0^2\right)\xi_d(R) - \frac{1}{3}\left(1 + \frac{26}{7}\beta_0 + \frac{11}{7}\beta_0^2\right)\frac{d\xi(R)}{d\ln R}\right](1+q_0), \tag{9}$$

$$\eta_4(R) = -\phi_0\xi_4(R) + \left[\left(\frac{8}{7}\beta_0 + \frac{24}{11}\beta_0^2\right)\xi_d(R) + \frac{32}{11}\beta_0^2\xi_q(R) - \frac{8}{35}\left(\beta_0 + \frac{13}{11}\beta_0^2\right)\frac{d\xi(R)}{d\ln R}\right](1+q_0), \tag{10}$$

$$\eta_6(R) = \frac{4}{33}\beta_0^2\left[4\xi_d(R) + 9\xi_q(R) - \frac{2}{7}\frac{d\xi(R)}{d\ln R}\right](1+q_0), \tag{11}$$

where $\xi(R)$ is the real-space two-point correlation function of galaxies at present, q_0 is the deceleration parameter at present, and β_0 is the redshift-distortion parameter at present. The parameters ϕ_0 and ψ_0 are defined as

$$\phi_0 = 2f_0 - 2b_1, \tag{12}$$

$$\psi_0 = \frac{3\Omega_m}{f_0} - 2(1-q_0), \tag{13}$$

respectively, where $f_0 = f(z=0)$, $b_1 = d\ln b(z)/dz|_{z=0}$. The functions $\xi_d(R)$ and $\xi_q(R)$ are defined in terms of $\xi(R)$ as

$$\xi_d(R) = \xi(R) - \bar{\xi}(R), \tag{14}$$

$$\xi_q(R) = \bar{\xi}(R) - \bar{\bar{\xi}}(R), \tag{15}$$

where

$$\bar{\xi}(R) = \frac{3}{R^3}\int_0^R dRR^2\xi(R), \tag{16}$$

$$\bar{\bar{\xi}}(R) = \frac{5}{R^5}\int_0^R dRR^4\xi(R). \tag{17}$$

Performing the integrations

$$I_0(R) = \left[\frac{3}{R^3}\int_0^R dR'R'^2 - \frac{5}{R^5}\int_0^R dR'R'^4\right]\eta_0(R'), \tag{18}$$

$$I_2(R) = \frac{3}{R^5}\int_0^R dR'R'^4\eta_2(R'), \tag{19}$$

$$I_4(R) = \frac{35}{4}R^2\int_R^\infty dR'R'^{-3}\eta_4(R'), \tag{20}$$

we find

$$Ax = d, \tag{21}$$

where ${}^t x = [1+q_0, \phi_0, \psi_0]$ and ${}^t d = [I_0(R), I_2(R), I_4(R)]$. The elements of the 3×3 matrix A are given by

$$A_{11} = \frac{2}{3}\left[1+\frac{4}{5}\beta_0+\frac{9}{35}\beta_0^2\right][2\xi_d(R)-5\xi_q(R)], \tag{22}$$

$$A_{12} = -\left[1+\frac{1}{3}\beta_0\right]\xi_q(R), \tag{23}$$

$$A_{13} = -\left[\frac{1}{3}\beta_0+\frac{1}{5}\beta_0^2\right]\xi_q(R), \tag{24}$$

$$A_{21} = -\left[1+\frac{26}{7}\beta_0+\frac{11}{7}\beta_0^2\right]\xi_d(R) - \left[1+8\beta_0+\frac{25}{7}\beta_0^2\right]\xi_q(R), \tag{25}$$

$$A_{22} = \beta_0\xi_q(R), \tag{26}$$

$$A_{23} = \left[\beta_0+\frac{6}{7}\beta_0^2\right]\xi_q(R), \tag{27}$$

$$A_{31} = 2\left[\beta_0+\frac{13}{11}\beta_0^2\right]\xi_d(R) + \frac{40}{11}\beta_0^2\xi_q(R), \tag{28}$$

$$A_{32} = 0, \tag{29}$$

$$A_{33} = -\beta_0^2\xi_q(R). \tag{30}$$

3 The estimator

Here we consider the following estimator of the two-point correlation function instead of binning the data:

$$\xi_z^{\rm est}(R,\mu) = \frac{DD_z^{\rm o} - DR_z^{\rm o} + RR_z^{\rm o}}{RR}. \tag{31}$$

The data-data, data-random, and random-random pair counts, $DD_z^{\rm o}$, $DR_z^{\rm o}$ and $RR_z^{\rm o}$, respectively, are calculated as

$$DD_z^{\rm o} = \frac{1}{2}\sum_{ij} w_{ij} z_{ij}^{\rm o} n_i n_j \Theta_{ij}^{R,\mu}, \tag{32}$$

$$DR_z^{\rm o} = \frac{1}{2}\sum_{ij} w_{ij} z_{ij}^{\rm o} n_i n_j^{\rm r} \Theta_{ij}^{R,\mu}, \tag{33}$$

$$RR_z^{\rm o} = \frac{1}{2}\sum_{ij} w_{ij} z_{ij}^{\rm o} n_i^{\rm r} n_j^{\rm r} \Theta_{ij}^{R,\mu}, \tag{34}$$

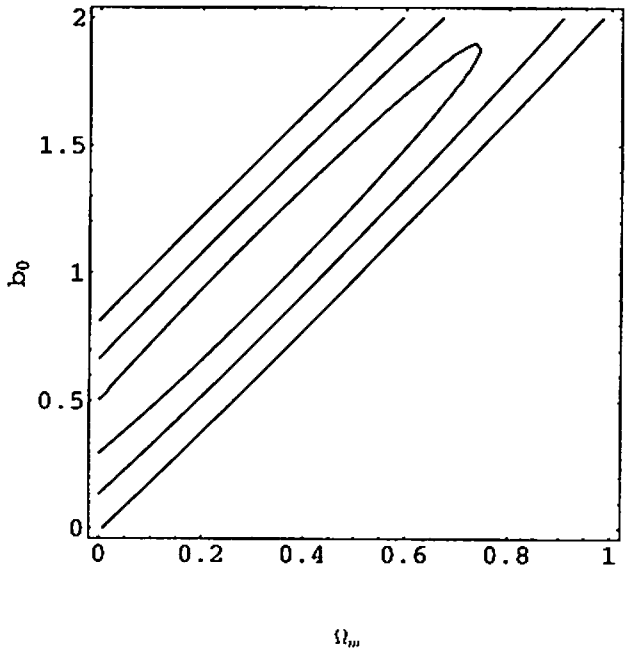


Figure 1: The 1σ, 2σ, and 3σ confidence levels for $\Omega_{\rm m}$ and b_0.

where $z_{ij} = (z_i + z_j)/2$, $\alpha = 0$ or 1, n_i is the galaxy number density and w_{ij} is the pair weighting. We introduce the observable quantity

$$\zeta_{2l}^{\alpha}(R) = \frac{4l+1}{2} \int_{-1}^{1} d\mu \xi_z^{\alpha}(R,\mu) P_{2l}(\mu). \tag{35}$$

The ensemble average of equation (35) reduces to

$$\langle \zeta_l^{\alpha}(R) \rangle \simeq c_1^{\alpha} \xi_l(R) + c_2^{\alpha} \eta_l(R). \tag{36}$$

The functions $\xi_l(R)$ and $\eta_l(R)$ are estimated with $\zeta_l^0(R)$ and $\zeta_l^1(R)$. Then the inversion of equation (21) yields the measure of q_0, ϕ_0 and ψ_0. Consequently we can estimate $\Omega_{\rm m}$, Ω_Λ, b_0 and b_1.

4 Results and Conclusions

We have performed the variance calculations adopting the estimator (31). Here we have assumed the main galaxy sample in the SDSS and the LCDM model ($\Omega_{\rm m} = 0.3$, $\Omega_\Lambda = 0.7$) for the fiducial cosmological

model. Figure 1 shows the 1σ, 2σ, and 3σ confidence levels for Ω_m and b_0. We see that the time evolution of bias (parameter b_1) is not constrained while the SCDM model ($\Omega_m = 1$, $\Omega_\Lambda = 0$) can be ruled out for the fiducial LCDM model. However more precise analyses using the mock sample from a N-body simulation are needed because our analyses presented in the present paper has been performed in the linear regime.

I would like to thank Yasufumi Kojima and Kazuhiro Yamamoto for useful comments and discussions. I also acknowledge the Japan Society for Promotion of Science (JSPS) Research Fellowship.

References

[1] J. A. Peacock et al., Nature **410**, 169 (2001)

[2] A.A. de Laix and G. D. Starkman, Astrophys. J. **510**, 427 (1998)

[3] T. T. Nakamura, T. Matsubara, and Y. Suto, Astrophys. J. **494**, 13 (1998)

Some Properties of Axisymmetric Pulsar Magnetosphere Constructed by Numerical Calculation

Jun Ogura,[1] Yasufumi Kojima[2]

Department of Physics, Hiroshima University, Higashi-Hiroshima, Hiroshima 739-8526, Japan

Abstract

We have explored the magnetosphere given by a numerical solution for axisymmetric rotating field satisfying the force-free and ideal MHD conditions everywhere. The electric current distribution is determined from the requirement of continuity and smoothness in flux-function across the light-cylinder. Overall magnetic field structure is shown using the numerical result. We also checked the drift velocity of a charged particle, which is caused by resultant electric and magnetic fields. It is found that the velocity exceeds the light speed beyond a few times light-cylinder. This fact suggests the breakdown of the underlying some assumptions.

1 Introduction

It is well known that rotating magnetized neutron stars are responsible for the radiation from pulsar, and power supply to surrounding nebula. The basic idea of pulsar was proposed more than 30 years ago[1], but the detailed consistent models are still unsolved. Almost all energy is carried out from pulsar by electromagnetic field, but will be converted to particle kinetic energy at large distances[2]. Several authors discussed the conversion mechanism such as non-ideal MHD effects[3] and magnetic reconnection[4]. Since the dissipation of electro-magnetic field is related with the accelerations of particles and hence the observed radiation, the determination of the mechanism is very important.

Global structure of magnetosphere even without the dissipation is not easily determined. The configuration is highly coupled with the plasma flow. Several authors used a simplified electromagnetic models, in order to investigate the plasma dynamics. For instance, Michel[5, 6] considered cold MHD winds for aligned pulsar, and Bogovalov[7] extended to oblique one. It is truly desirable to consider the plasma dynamics with more realistic magnetic field, e.g., dipole field near the star. We will gradually confirm the general picture, or may find incorrect aspect of the previous models, using the realistic model. Recently, Contopoulos et al.[8] obtained a numerical solution of the so-called pulsar equation, which determines axially symmetric MHD field in the force-free limit. We refer their solution as CKF solution in this paper. Their solution represents an interesting structure that the solution is smooth across the light-cylinder, and there is no evidence of singularity as for the flow and field. In this subsequent paper[9], Contopoulos and Kazanas proposed a possible conversion mechanism of pulsar power into particle energy in the wind region, using their solution.

In this way, the CKF solution is quite interesting. In particular, the non-singular property is amazingly contrary to the previous expectation that the dissipation-free flow would lead to singularity in the flow and the magnetic field, occurring a short distance beyond the light-cylinder, e.g., Ref. [3]. The drift approximation is expected to break down near the light-cylinder, e.g., Ref. [10], since the drift velocity $|\vec{v}_\perp| = c|\vec{E} \times \vec{B}|/B^2$ approaches the light speed c, due to $|E| \sim |B|$ in the wind region. These arguments sound reasonable, but strongly depend on the electro-magnetic field configuration.

The purpose of this paper is exploring the physical quantities described by the CKF solution. In particular we explicitly calculate the drift velocity of the solution. These quantities are not shown in their paper[8] and numerically calculated by differentiating the magnetic flux-function. For the numerical differentiation, we have to construct the flux-function with much larger grid points. Furthermore, the validity of the CKF solution is investigated.

[1] E-mail:ogura@theo.phys.sci.hiroshima-u.ac.jp
[2] E-mail:kojima@theo.phys.sci.hiroshima-u.ac.jp

2 Assumptions and Formalism

In this section we shall briefly summarize the equations governing the stationary axisymmetric magnetosphere. In the axisymmetric case, it is convenient to decouple the poloidal and toroidal parts of the magnetic fields in cylindrical coordinates (R, ϕ, Z). The poloidal field $\vec{B}_p = (B_R,\ B_Z)$ is written in terms of the flux-function $\Phi(R, Z)$, while toroidal field is given by another function $A(R, Z)$ as

$$(B_R,\ B_\phi,\ B_Z) = \left(-\frac{1}{R}\partial_Z\Phi,\quad \frac{1}{R}A,\quad \frac{1}{R}\partial_R\Phi\right). \tag{1}$$

From some assumptions, the function A should depend only on Φ as discussed later. The plasma is assumed to be frozen to the magnetic field everywhere. In the limit of large magnetic Reynolds number, the velocity component perpendicular to the magnetic field is described by the so-called " $E \times B$ " drift velocity,

$$\vec{v}_\perp = \frac{c\vec{E} \times \vec{B}}{B^2}. \tag{2}$$

Including the velocity along the magnetic field line, the electric and magnetic fields satisfy the relation,

$$\vec{E} + \frac{\vec{v}}{c} \times \vec{B} = 0. \tag{3}$$

This condition holds if there exists sufficient amount of charge density, whose origin in discussed in the literature[10].

As a first step to understanding overall structure without realistic dissipation mechanism, we here neglect the small gap regions, and consider the electro-magnetic structure in much larger scale of length of the regions. From the ideal MHD condition (3), the electric field can be expressed by

$$(E_R,\ E_\phi,\ E_Z) = \left(-\frac{\Omega}{c}\partial_R\Phi,\ \ 0,\quad -\frac{\Omega}{c}\partial_Z\Phi\right) = -\vec{\nabla}\left(\frac{\Omega}{c}\Phi\right), \tag{4}$$

where angular velocity of magnetic field line Ω is also a function of Φ in general, but assumed to be a constant in this paper. Therefore the magnetosphere rotates like a rigid body. The charge density ρ_e is given by the divergence of electric field (Gauss's law), and the current $\vec{j}$ by the rotation of the magnetic field (Ampere's law). They are explicitly written as

$$\rho_e = -\frac{\Omega}{4\pi c}\Delta\Phi = -\frac{\Omega}{4\pi c}\left(\frac{1}{R}\partial_R R\partial_R\Phi + \partial_Z^2\Phi\right), \tag{5}$$

$$(j_R,\ j_\phi,\ j_Z) = \frac{c}{4\pi}\left(-\frac{1}{R}\partial_Z A,\quad -\frac{1}{R}\left(\Delta\Phi - \frac{2}{R}\partial_R\Phi\right),\quad \frac{1}{R}\partial_R A\right). \tag{6}$$

We assume that the electro-magnetic force dominates. That is, we neglect the gravity, pressure and the inertial terms. The force-free condition is written as

$$\rho_e\vec{E} + \frac{\vec{j}}{c} \times \vec{B} = 0. \tag{7}$$

After some algebra, the function A is constant on the surface of Φ, i.e., $A = A(\Phi)$. The function Φ should satisfy the so-called 'pulsar equation',

$$\left(1 - \beta^2\right)\Delta\Phi - \frac{2}{R}\partial_R\Phi + AA' = 0, \tag{8}$$

where β is cylindrical radius normalized by the light-cylinder, $\beta = R\Omega/c = R/R_{LC}$. Using eq.(8), the charge density and current are rewritten as

$$\rho_e = -\frac{\Omega}{4\pi c}\frac{2B_Z - AA'}{1 - \beta^2}, \tag{9}$$

$$(j_R,\ j_\phi,\ j_Z) = \frac{c}{4\pi}\left(A'B_R,\quad -\frac{1}{R}\frac{2\beta^2 B_Z - AA'}{1 - \beta^2},\quad A'B_Z\right). \tag{10}$$

The current flow within the flux tube Φ is given by

$$J(\Phi) = \int_0^\Phi \vec{j} \cdot d\vec{S} = \int_0^\Phi \frac{1}{4\pi R} A' |\nabla\Phi| \frac{2\pi R d\Phi}{|\nabla\Phi|} = \frac{c}{2} A(\Phi), \tag{11}$$

where we have assigned as $\Phi = 0$ at the Z-axis. Therefore,

$$A(0) = 0, \tag{12}$$

is given from the regularity of toroidal magnetic field (see §3).

3 Numerical scheme to solve singular equation

At first sight, the pulsar equation (8) has a singular surface, i.e., the light-cylinder $R = R_{LC} = c/\Omega$. Both inside and outside the light-cylinder, the equation becomes partial differential equation of elliptic type, for a given function A. The procedure to construct the numerical solution of (8) is to solve the equation in each side and to match the solutions at the light-cylinder. The interior and exterior solutions are not in general continuous across the light-cylinder for the assumed function A. Therefore, the function A should be modified in an iterative way so as to converge.

We set the boundary conditions for the elliptic equation that it is almost same as CKF solution. The function Φ near the star is described by a dipole magnetic field with the magnetic dipole moment m as $\Phi = mR^2/(R^2 + Z^2)^{3/2}$. The last open field line for this dipole field corresponds to $\Phi = \Phi_{pc} \equiv m/R_{LC}$, which passes the light-cylinder on the equatorial plane. At the polar axis, Φ is given by the Dirichlet condition as $\Phi(0, Z) = 0$. The boundary conditions at the outer right, and the upper outermost are given by $\partial_R \Phi(R_{max}, Z) = 0$, $\Phi(R, Z_{max}) = 0$, respectively. The numerical domain of calculation is limited to $0 \leq R \leq R_{max}$, $0 \leq Z \leq Z_{max}$. The conditions, $R_{max} = \infty$ and $Z_{max} = \infty$, were applied to CKF solution, using a certain coordinate transformation, but we limited the spatial domain as $R_{max} = Z_{max} = 9R_{LC}$. This change is numerically checked, and we found that there is no substantial difference. Our choice is better to facilitate the numerical convergence. We also changed the outer boundary conditions, but found that they are not so sensitive to the almost same solution as CKF. The boundary condition on the equatorial plane is divided by the light-cylinder. Since particles can co-rotate with the star within the light-cylinder, we have $\partial_Z \Phi(R, 0) = 0$ $(R \leq R_{LC})$. Outside the light-cylinder, the line is extended to infinity. We therefore set it as $\Phi(R, 0) = \Phi_{open}$ $(R > R_{LC})$, where Φ_{open} is the last inner open field line, i.e., $\Phi(R_{LC}, 0)$ calculated for the interior solution.

In order to avoid the singular surface of eq.(8), we require at the light-cylinder $R = R_{LC} = c/\Omega$

$$AA' = \frac{2}{R} \partial_R \Phi = 2B_Z. \tag{13}$$

In this case, singularities of the charge density ρ_e and toroidal current j_ϕ vanish at the same time. See eqs.(9)-(10).

It is not clear a priori which functional form of $A(\Phi)$ satisfies whole boundary conditions. We should therefore follow some iterative process to obtain the solution. Contopoulos et al. [8] successfully solved the equation by searching for the suitable function A so as to match the interior and exterior solutions at the surface. We have followed the same relaxation-type technique.

4 Results

4.1 Flux function

We solved eq.(8) with the boundary conditions in the numerical domain $R_{max} = Z_{max} = 9R_{LC}$. The self-consistent solution for Φ and $A(\Phi)$ is calculated on 80×80 numerical grid-points inside and another 80×80 points outside the light-cylinder to assure the numerical accuracy. The calculation demanded more than 10^4 iterations until obtaining the smooth result. We have performed a lot of trials to search

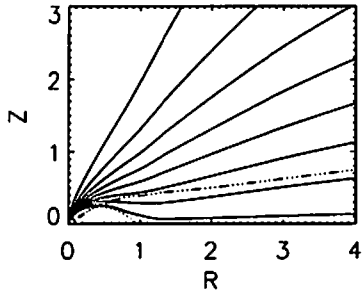
for different type of solutions, but just one, the CKF solution. This may be a unique solution satisfying the boundary conditions, although there is no proof. The overall structure of the solution is the same as the CKF solution, but the value of the last open field line is a little bit larger than theirs. Their result on 30×30 grid-points is $\Phi_{open} = 1.36\Phi_{pc}$, but our result is $\Phi_{open} = 1.66\Phi_{pc}$. The origin of this discrepancy is presumably due to the numerical resolution. The number of our grid-points is twice in each direction. We also checked their result by the calculation of 30×30 grid-points. The value Φ_{open} slightly increases with the grid number, but our numerical experiment seems to be saturated around $\Phi_{open} = 1.66\Phi_{pc}$. It is interesting to compare this value with that for constant A case [6], in which $\Phi_{open} = 1.592\Phi_{pc}$. The precise value depends on the numerical accuracy, but just scales the physical quantities. The calculated function $\Phi(R, Z)$ is shown in Fig.1. Both interior and exterior functions are smoothly connected across the light-cylinder. We only show the inner part of numerical calculation "$0 \leq R/R_{LC} \leq 4$, $0 \leq Z/R_{LC} \leq 3$". This region is almost unaffected by any choice of outermost boundary conditions at R_{max}, Z_{max}.

The function needed during the numerical iterations is not A but AA'. The conditions adopted in our numerical calculation are given as $AA' = 0$ for $\Phi = 0$ and $\Phi \geq \Phi_{open}$, where we used eq.(12) and implicit assumption that the electric circuit is closed in the whole system:

$$A(\Phi) = 0 \quad (\Phi \geq \Phi_{open}). \tag{14}$$

The function A is constructed from the numerical data for AA'. The result shows that $A(\Phi_{open}) \neq 0$. This causes big problems when applying to a physical situation. It is that the current closure is not satisfied. The total current from the upper hemisphere has a definite sign, $J < 0$. A simple way to use this model is introducing a thin current-sheet on Φ_{open}. This artificially ensures that the return current-sheet equal to $-A(\Phi_{open})$ flows along the equatorial plane($R > R_{LC}$), and the last open field line. However, in the model with the current-sheet, enormously strong force, such as pressure, would be required.

One may think that a stringent condition, such as $A = 0$ at $\Phi = 0$ and $\Psi_{open} = 0$, should be imposed, in order to construct more realistic model (without the artificial current-sheet). We used this condition for the numerical iteration, but did not have any convergent solution. Our numerical experience may not be complete, but suggest that the global solution of the pulsar equation can be obtained only under the week conditions of A, used by the previous authors[8].



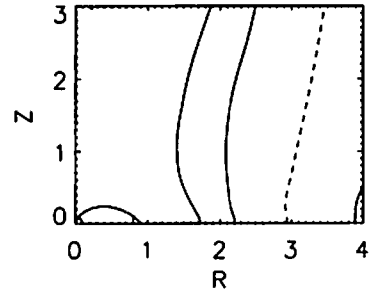


Figure 1: [Left] Flux function of the axisymmetric force-free magnetosphere. Solid lines represent flux surfaces in intervals of $0.2\Phi_{pc}$, with $\Phi = 0$ along the axis. A dotted line shows the last open field line $\Phi_{open} = 1.66\Phi_{pc}$. A numerical boundary condition near the star is imposed at the quarter circle indicated in the lower left-hand corner of the figure. A dotted dash line indicates the null-surface.

Figure 2: [Right] Contours of the drift velocity. Solid lines show $|\vec{v}_\perp| = 0.8$, 0.9, and $1.1c$ (solid), and $|\vec{v}_\perp| = 1.0c$ (dotted).

4.2 Drift velocity

The components of the drift velocity is given by (2), and the absolute magnitude is

$$v_\perp = R\Omega \frac{(B_R^2 + B_Z^2)^{1/2}}{(B_R^2 + B_\phi^2 + B_Z^2)^{1/2}} = R\Omega \frac{B_p}{(B_t^2 + B_p^2)^{1/2}}. \tag{15}$$

It is clear that the condition $v_\perp \leq c$ holds inside the light-cylinder. The condition is no longer guaranteed outside the light-cylinder, and significantly depends on the magnetic field configuration. In Fig.2, we show the drift velocity $v_\perp$ calculated from the CKF solution. Numerical result shows that $v_\perp < 0.8c$ within the light-cylinder, and that the value $v_\perp$ gradually increases with R. The drift velocity exceeds the light speed approximately beyond $R > 3R_{LC}$. It is thus seen that the applicable range of the CKF solution is limited within a few time light-cylinder.

5 Remarks

In this paper, we have explored the axially symmetric magnetosphere around an aligned rotating dipole field. The ideal MHD and force-free conditions are satisfied everywhere by assuming a sufficient charge density. The electro-magnetic structure can be determined by so-called the pulsar equation, which is a coupled equation for Φ and A. Some authors examined some special cases in the past, e.g., A is constant [11], linear of Φ [12], and quadratic of Φ [5]. These never correspond to the realistic situation. A new numerical solution presented by Contopoulos, et al. [8] seems to be promising. The solution may be useful as the starting point for more realistic pulsar magnetosphere. From this point, we have examined the flux-function and drift velocity in detail. Our result show that the global structure is required the current-sheet. Moreover, it also shows the breakdown of the drift approximation at a few times light-cylinder. This result may modify the scenario about CKF solution, proposed in Ref. [9]. They showed that the Lorents factor of the outflowing plasma increases linearly with distance from the neutron star. Therefore, at large distance $R \sim 10^3 R_{LC}$, the inertia term can not be neglected, i.e., force-free condition breaks down, whereas our numerical calculation showed that the validity of the CKF solution is much limited within a short distance $\sim 3R_{LC}$.

Acknowledgements

This work was supported in part by the Grant-in-Aid for Scientific Research (No.14047215) from the Japanese Ministry of Education, Culture, Sports, Science and Technology.

References

[1] P. Goldreich and W. H. Julian, Astrophys. J. **157** (1969), 869.

[2] M. J. Rees and J. E. Gunn, Mon. Not. Roy. Astron. Soc. **167** (1974), 1.

[3] L. Mestel and S. Shibata, Mon. Not. Roy. Astron. Soc. **271** (1994), 621.

[4] F. V. Coroniti, Astrophys. J. **349** (1990), 538.

[5] F. C. Michel, Astrophys. J. **158** (1969), 727.

[6] F. C. Michel, Astrophys. J. Lett. **180** (1973), L133.

[7] S. V. Bogovalov, Astron. Astrophys. **349** (1999), 1017.

[8] I. Contopoulos, D. Kazanas and C. Fendt, Astrophys. J. **511** (1999), 351.

[9] I. Contopoulos and D. Kazanas, Astrophys. J. **556** (2002), 336.

[10] V. S. Beskin, A. V. Gurevich and Ya. N. Istomin, *Physics of the Pulsar Magnetosphere* (Cambridge University Press, 1993).

[11] F. C. Michel, Astrophys. J. **180** (1973), 207.

[12] E. T. Scharlemann and R. V. Wagoner, Astrophys. J. **182** (1973), 951.

Accurate Determination of the Hubble Constant from Supernova Lensing

Masamune Oguri,[1]

Department of Physics, Graduate School of Science, University of Tokyo, Tokyo 113-0022, Japan

Yozo Kawano[2]

Department of Physics and Astrophysics, Nagoya University, Nagoya 464-8062, Japan

Abstract

First we review the determination of the Hubble constant, and show possible problems in the Hubble constant. Next we propose new method to determine the global Hubble constant quite accurately. This method use the strong gravitational lensing of Type Ia supernovae instead of (traditional) quasars. Since the Type Ia supernovae have quite narrow luminosity function, we can determine the magnification factor directly. Inclusion of observed magnification factor in performing χ^2 minimization breaks the degeneracy between radial mass distribution of the lens galaxy and the Hubble constant and substantially improve the precision of the determination of the Hubble constant.

1 The Hubble Constant Problem?

The Hubble constant is the most important parameter in cosmology and astronomy, because it determine all scales of distance and time. There are several ways to determine the Hubble constant observationally. In this section, we review how well the Hubble constant is determined.

The representative ways to measure the Hubble constant are following:

- Distance Ladder
  This is a traditional way to measure the Hubble constant. Cepheid distances are used to calibrate the second distance indicators such as type Ia supernovae, Tully-Fisher relation, fundamental plane, type II supernovae, and surface brightness fluctuations. This method can measure only the *local* value of the Hubble constant.

- Sunyaev-Zel'dovich Effect
  The flux of Sunyaev-Zel'dovich effect is $\propto n_e T_e$, where n_e and T_e are electron number density and temperature, while X-ray flux is $\propto n_e^2 T_e^{1/2}$. From these different dependences on n_e, we can determine the luminosity distance to the cluster. Therefore we can measure the Hubble constant without using the distance ladder. What we should notice in using this method is that at high redshift ($z \sim 1$) derived Hubble constant is sensitive to assumed cosmological model.

- Gravitational Lens Time Delay
  Gravitational lens time delays offer another way to measure the global Hubble constant because time delays are dimensional quantity (i.e., $\Delta t \propto H_0^{-1}$) while other observables (image separations, etc.) are dimensionless. The derived Hubble constant is sensitive to the assumed radial mass distribution of the lens galaxy, for which we usually assume the singular isothermal mass distribution ($\rho \propto r^{-2}$; see the next section).

[1] E-mail:oguri@utap.phys.s.u-tokyo.ac.jp
[2] E-mail:kawano@a.phys.nagoya-u.ac.jp

Method	H_0 with 1σ error	Distance	Reference
Distance Ladder (HST)	$72 \pm 3 \pm 7$ km/s/Mpc (stat.+syst.)	$z < 0.1$	[1]
Sunyaev-Zel'dovich Effect	60^{+4+13}_{-4-18} km/s/Mpc (stat.+syst.)	$0.1 < z < 0.8$	[8]
Gravitational Lens Time Delay	48 ± 2 km/s/Mpc (stat.)	$0.3 \lesssim z \lesssim 3$	[4]
CMB anisotropy	59 ± 11 km/s/Mpc (stat.)	$1 \ll z$	[10]

Table 1: Summary of the Hubble constant determinations. For the distance ladder and Sunyaev-Zel'dovich effect measurements, we show both statistical and systematic errors. For the gravitational lens time delay and CMB anisotropy measurements, only statistical errors are quoted.

- Cosmic Microwave Background anisotropy
  Now physics of CMB anisotropy is well understood, and the power spectrum of CMB anisotropy can be well predicted. The reason is that before recombination epoch fluctuations are small enough to justify linear approximations. Fluctuation patterns are very sensitive to cosmological parameters, so we can determine cosmological parameters from the comparison between theory and observations. But the Hubble constant is poorly determined by CMB data alone because of the degeneracy between parameters.

The derived values are summarized in Table 1. As easily seen, the local estimate seems to predict the larger value of the Hubble constant compared with other estimates. In particular, the Hubble constant derived from gravitational lens time delay seems too low to be reconciled with the local estimate using distance ladder. Does this mean the Hubble constant problem? For the gravitational lens time delay measurements, the value of the Hubble constant can be much larger than the value shown in Table 1 if we consider more centrally concentrated lens galaxy (see next section). But such centrally concentrated lens galaxy cannot be reproduced in the context of cold dark matter scenario. Therefore, avoidance of the Hubble constant problem by introducing concentrated mass distribution leads us to a new problem, namely the dark matter problem!

2 Degeneracy in the Hubble Constant

Gravitational lens time delays can measure the global Hubble constant independently with the local estimates. A main drawback is, however, the strong degeneracy between radial mass profiles of the lens galaxy and the Hubble constant. If we parameterize radial mass distribution by β so that the lens potential is

$$\psi \propto r^{\beta}, \tag{1}$$

then this degeneracy is expressed as (see [6])

$$H_0 \propto 2 - \beta. \tag{2}$$

Note that singular isothermal mass distribution corresponds to $\beta = 1$. In practice, currently observed lens systems are well fitted for almost all β (e.g., [2]). Therefore, unless we specified radial mass distribution β, we cannot constrain the Hubble constant. This degeneracy can be broken if the Einstein ring images of host galaxies are observed [3]. But the observation of host galaxies is often very difficult because of the large brightness contrast between quasars and host galaxies. Other way to break this degeneracy stems from the central core images (e.g., [9]). The lack of central core images, however, places only the lower limit of the mass concentration, and this corresponds to the lower limit of H_0. Information of stellar kinematics and the mass-to-light ratio also allows one to constrain the radial mass profile of the lens galaxy and to break the degeneracy in the Hubble constant, although the measurement of velocity dispersions for distant galaxies is very difficult and involves large uncertainties. Treu and Koopmans [11], for instance, concluded that the mass density profile of the lens PG1115+080 is steeper than the singular isothermal mass distribution, and obtained a value of the Hubble constant $H_0 \sim 60 \mathrm{km\,s^{-1}Mpc^{-1}}$ which is marginally consistent with the local measurement.

3 Lensing of Distant Supernovae: Break the Degeneracy

We propose supernova lensing to break the degeneracy between radial mass profiles and the Hubble constant [6]. This is possible because of the following reasons:

- The standard candle nature of type Ia supernova luminosity function allows one to measure the magnification factor directly [7].
- The magnification factor has the strong dependence on the radial mass profile, $\mu \propto (2-\beta)^{-2}$ (see [2]).

These two properties allow one to measure the Hubble constant quite accurately. To illustrate how accurately we can determine β and H_0, we show the results of our simulation. To do so, first we assume the lens galaxy is well characterized by the following lens potential [2]

$$\psi_{\rm lens}(\vec{x}) = r^{\beta}(a_0 + a_2\cos 2\theta + a_3\cos 3\theta + b_2\sin 2\theta + b_3\sin 3\theta). \tag{3}$$

We also take account of the effect of external shear as

$$\psi_{\rm shear}(\vec{x}) = \frac{1}{2}\gamma r^2\cos(2\theta - 2\theta_\gamma). \tag{4}$$

Then total lens potential is given by

$$\psi_{\rm total}(\vec{x}) = \psi_{\rm lens}(\vec{x}) + \psi_{\rm shear}(\vec{x}). \tag{5}$$

We randomly put a source, generate quadruple images, and calculate differential time delays and magnification factors, assuming following parameters: $\beta = 1.0$, $H_0 = 50\,{\rm km/s/Mpc}$, $a_0 = 0.5$, $a_2 = b_2 = 0.01$, $a_3 = b_3 = 0.001$, $\gamma_1 = \gamma\cos 2\theta_\gamma = 0.1$, and $\gamma_2 = \gamma\sin 2\theta_\gamma = -0.01$, where a_i and b_i are values when $\vec{x}$ is in units of arcsec. Source and lens are placed at $z_S = 1.5$ and $z_L = 0.5$, respectively. For the observable quantities, such as image positions and time delays, the Gaussian noise is added. We assume following dispersions:

$$\sigma_x = 0.01'', \tag{6}$$

$$\sigma_{\Delta t} = 0.05\,[{\rm day}], \tag{7}$$

$$\sigma_{\log r_{ij}} = 0.09, \tag{8}$$

$$\sigma_{\log \mu_i} = 0.12. \tag{9}$$

The dispersion of magnification ratio, which roughly corresponds to $\sim 20\%$ fractional error, is a fiducial error often assumed in χ^2 minimization (e.g., [4]). We assume that the dispersion of the magnification factor is somewhat larger than this, roughly corresponds to $\sim 30\%$ fractional error, because not only substructure in the lens galaxy [5] but also the intrinsic dispersion of SNe Ia peak magnitudes contribute to $\sigma_{\log\mu_i}$.

After the virtual "observational data" is generated, we perform χ^2 minimization using the same lens model. At that time, we fix values of β and H_0, and optimize the other parameters such as a_i, b_i, γ, and the source position. In calculating χ^2, we consider following two cases: (1) Only the magnification ratio r is measured. This case corresponds to traditional quasar lensing. (2) The magnification factor is directly measured. This is the case of SN Ia lensing we are interested in. For each case, we calculate the contour of $\Delta\chi^2 = \chi^2 - \chi^2_{\rm min}$ in the β-H_0 plane.

The results of the simulations are shown in Figure 1. This figure clearly shows that in the case of SN Ia lensing β and H_0 are well constrained separately. It is surprising that the Hubble constant is determined with $\sim 10\%$ accuracy (68% confidence) from only one lens system, and $\sim 5\%$ accuracy (68% confidence) from only several lens systems. On the other hand, we hardly determine the Hubble constant if we don't use the magnification factor as constraints. Therefore, we conclude that magnification factors which are observed in SN Ia lensing provide indeed important information to break the β-H_0 degeneracy.

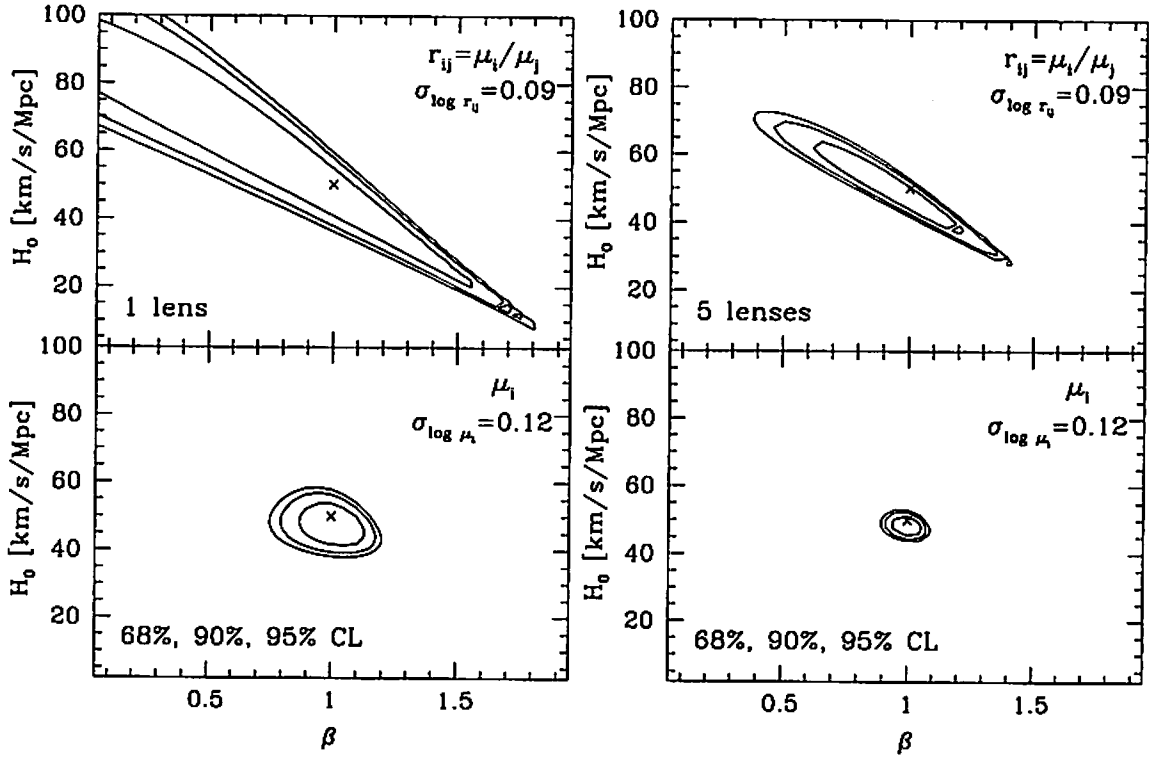


Figure 1: Constraints on the radial mass profile β and the Hubble constant. Crosses indicate the assumed value in generating observable quantities; $(\beta, h) = (1.0, 0.5)$. In the upper panels, image positions $\vec{x}_i$, differential time delays Δt_{ij}, and magnification ratios r_{ij} are used to calculate χ^2, while in the lower panels, instead of r_{ij}, magnification factors μ_i are used to calculate χ^2. *Left panel:* constraints from one lens event. *Right panel:* constraints from five lens systems.

References

[1] W. L. Freedman et al., Astrophys. J. **553**, 47 (2001).

[2] Y. Kawano, M. Oguri, T. Matsubara, and S. Ikeuchi, Astrophys. J. submitted.

[3] C. S. Kochanek, C. R. Keeton, and B. A. McLeod, Astrophys. J. **547**, 50 (2001).

[4] C. S. Kochanek, astro-ph/0204043.

[5] S. Mao and P. Schneider, Mon. Not. R. Astron. Soc. **295**, 587 (1998).

[6] M. Oguri and Y. Kawano, Mon. Not. R. Astron. Soc. **338**, L25 (2003).

[7] M. Oguri, Y. Suto, and E. L. Turner, Astrophys. J. **583**, 584 (2003).

[8] E. D. Reese, J. E. Carlstrom, M. Joy, J. J. Mohr, L. Grego, and W. L. Holzapfel, Astrophys. J. **581**, 53 (2002).

[9] D. Rusin and C.-P. Ma, Astrophys. J. **549**, L33 (2001).

[10] J. L. Sievers et al., astro-ph/0205387.

[11] T. Treu and L. V. E. Koopmans, Mon. Not. R. Astron. Soc. **337**, L6 (2002).

The Orbital Evolution of a Point Particle in the Kerr Spacetime

Norichika Sago,[1] Yasushi Mino,[2] Sanjay Jhingan,[3] Takahiro Tanaka [4]

[1]Department of Physics, Graduate School of Science, Kyoto University, Kyoto 606-8502, Japan

[1]Department of Earth and Space Science, Graduate School of Science, Osaka University, Toyonaka, Osaka 560-0043, Japan

[2]Department of Physics, Washington University, Campus Box 1105, One Brookings Dr., St.Louis, MO 63130-4899, USA

[3]Department of Theoretical Physics, University of the Basque Country, Apdo. 644, 48080 Bilbao, Spain

[4]Yukawa Institute for Theoretical Physics, Kyoto University, Kyoto 606-8502, Japan

Abstract

The geodesics in Kerr geometry are characterized by three constants of motion, energy E, azimuthal angular momentum L, and Carter constant Q. Under the adiabatic approximation, we can characterize the orbital evolution of a point particle by the time evolution of these constants. For E and L, we can evaluate their evolution by considering the conservation law for the energy and angular momentum. On the other hand, for the evolution rate of Carter constant, we need to calculate the self-force exerted on the particle because we do not have the conservation law for it. In this manuscript, by using the radiative Green's function, we introduce a scheme to evaluate the evolution of Carter constant avoiding the delicate issue of regularizing the self-force.

1 Introduction

A supermassive black hole (SMBH) accompanied by a compact object (CO) is among the most promising candidates for gravitational wave sources. Due to their nature we can get information from gravitational waves which cannot be obtained by any electromagnetic wave observations. For this purpose, however, we need to know the accurate waveforms from such sources in advance.

To investigate gravitational waves from the SMBH-CO binary system, we use the black hole perturbation method and the point particle approximation: the background geometry here is the black hole spacetime with the mass and angular momentum of the SMBH, respectively, M and aM, and the CO is regarded as a point particle with the mass μ. In the lowest order in mass ratio (μ/M), the particle moves along the background geodesic. In the next order, however, its orbit shifts from the background geodesic because system losses both the energy and the angular momentum in the form of gravitational waves.

In the Schwarzschild background, the particle's orbit can be characterized completely by energy E and azimuthal angular momentum L_z. Therefore we can evaluate the orbital evolution from the evolution rate of energy and the angular momentum, $\dot{E}$ and $\dot{L}_z$. The situation here is much simpler as we can evaluate them by considering the energy-momentum conservation law; the energy and the angular momentum that the particle loses are equal to the ones that are radiated to the infinity or across the horizon as gravitational waves. Therefore, we can determine the orbital evolution from the asymptotic behavior of the metric perturbations in the Schwarzschild case.

On the other hand, to completely specify a geodesic in the Kerr background, not only E and L_z but also Carter constant Q is necessary. Since we do not have global conservation law for Carter constant, the evolution rate of Q can't be evaluated only by the asymptotic behavior of the metric perturbations and we need to calculate the self-force on the particle [1]. Though the formal prescription to calculate the self-force is well known [2, 3], doing explicit calculation is not so straight forward.

[1]E-mail:sago@tap.scphys.kyoto-u.ac.jp
[2]E-mail:mino@wugrav.wustl.edu
[3]E-mail:sjhingan@yukawa.kyoto-u.ac.jp
[4]E-mail:tanaka@yukawa.kyoto-u.ac.jp

Gal'tsov [4] employed the *radiative* part of the metric perturbation which was introduced earlier by Dirac [5] to calculate $\dot{E}$ and $\dot{L}_z$. His results were consistent with the ones obtained from the conservation law. However, since there was no justification of using the radiative part, it was not trivial whether Gal'tsov's scheme deduces the correct result for the evolution rate of Carter constant. Recently the situation has changed. Mino has shown that this scheme gives the limit of adiabatic approximation [6]. In this manuscript, we explain the outline of this new proposal and discuss its application.

This paper is organized as follows. In Sec. 2, we introduce the constants of motion of a point particle orbiting the Kerr black hole. We investigate the property of the geodesic of the Kerr geometry in Sec. 3. We show that the geodesic is characterized by three constants of motion and is invariant under certain coordinate transformation including the time-reversal. In Sec. 4, we show the scheme to calculate the evolution rate of Carter constant without requiring any regularization procedure. We summarize and discuss the application of this scheme.

2 Background

In this section, we give a very brief review of the Kerr geometry and define some notations which we have used in this paper.

We take the Kerr geometry as the background spacetime:

$$ds^2 = -\left(1-\frac{2Mr}{\Sigma}\right)dt^2 - \frac{4Mar\sin^2\theta}{\Sigma}dtd\phi + \frac{\Sigma}{\Delta}dr^2 + \Sigma d\theta^2 + \left(r^2+a^2+\frac{2Ma^2r}{\Sigma}\sin^2\theta\right)\sin^2\theta d\phi^2, \quad (1)$$

where

$$\Sigma = r^2 + a^2\cos^2\theta, \quad \Delta = r^2 - 2Mr + a^2. \quad (2)$$

M and aM are the mass and the angular momentum of the black hole, respectively. There are two Killing vectors concerned with its stationary and axisymmetric property:

$$\xi^\mu_{(t)} = (1,0,0,0), \quad \xi^\mu_{(\phi)} = (0,0,0,1). \quad (3)$$

In addition, the Kerr spacetime possesses a Killing tensor,

$$K_{\mu\nu} = 2\Sigma l_{(\mu}n_{\nu)} + r^2 g_{\mu\nu}, \quad (4)$$

where l_μ, n_μ are the null vectors,

$$l^\mu = \left(\frac{r^2+a^2}{\Delta}, 1, 0, \frac{a}{\Delta}\right), \quad n^\mu = \left(\frac{r^2+a^2}{2\Sigma}, -\frac{\Delta}{2\Sigma}, 0, \frac{a}{2\Sigma}\right). \quad (5)$$

Next, we consider the trajectory of a point particle moving in the Kerr geometry:

$$z^\alpha(\tau) = (t_z(\tau), r_z(\tau), \theta_z(\tau), \phi_z(\tau)), \quad (6)$$

where τ is the proper time along this orbit. Then, the constants of motion can be obtained as follows:

$$E = -u^\alpha \xi^{(t)}_\alpha = \left(1-\frac{2Mr_z}{\Sigma}\right)\dot{t}_z + \frac{2Mar_z\sin^2\theta_z}{\Sigma}\dot{\phi}_z, \quad (7)$$

$$L = u^\alpha \xi^{(\phi)}_\alpha = -\frac{2Mar_z\sin^2\theta_z}{\Sigma}\dot{t}_z + \frac{(r_z^2+a^2)^2 - \Delta a^2\sin^2\theta_z}{\Sigma}\sin^2\theta_z\dot{\phi}_z, \quad (8)$$

$$Q = K_{\alpha\beta}u^\alpha u^\beta = \frac{(L-aE\sin^2\theta_z)^2}{\sin^2\theta_z} + a^2\cos^2\theta_z + \Sigma^2\dot{\theta}_z^2, \quad (9)$$

where $u^\alpha = dz^\alpha/d\tau$. In addition, we introduce an alternative notation for Carter constant:

$$C \equiv Q - (aE-L)^2, \quad (10)$$

which is defined so as to vanish for the equatorial orbit.

3 Geodesic Motion in the Kerr Spacetime

In this section, we show that the geodesic in the Kerr geometry can be specified by three constants of motion which are introduced in the previous section. We also discuss a certain symmetry property of these geodesics.

In the case of a test particle under no external force, its orbit is represented by the geodesic for the background geometry. In the Kerr geometry, the geodesic equations are

$$\frac{dt_z}{d\lambda} = -a(aE\sin^2\theta_z - L) + \frac{r_z^2+a^2}{\Delta}\left[E(r_z^2+a^2) - aL\right], \tag{11}$$

$$\left(\frac{dr_z}{d\lambda}\right)^2 = \left[E(r_z^2+a^2) - aL\right]^2 - \Delta[r_z^2 + (aE-L)^2 + C], \tag{12}$$

$$\left(\frac{d\theta_z}{d\lambda}\right)^2 = C - \cos^2\theta_z\left[a^2(1-E^2) + \frac{L^2}{\sin^2\theta_z}\right], \tag{13}$$

$$\frac{d\phi_z}{d\lambda} = -\left(aE - \frac{L}{\sin^2\theta_z}\right) + \frac{a}{\Delta}\left[E(r_z^2+a^2) - aL\right], \tag{14}$$

where we have introduced a new parameter λ so that $d\lambda = d\tau/\Sigma$. Note that with new parameter the equation for the r-component and that for the θ-component are decoupled. Therefore, now we can deal with the motion in r- and θ- directions independently.

In general, we can characterize the geodesics by the initial values of the particle's spacetime position, z^α, and its initial four-velocity, $dz^\alpha/d\lambda$:

$$z_0^\alpha = (t_0, r_0, \theta_0, \phi_0), \quad \frac{dz_0^\alpha}{d\lambda} = \left(U_0^t, U_0^r, U_0^\theta, U_0^\phi\right)\Big|_{\lambda=\lambda_0}. \tag{15}$$

Here we consider only bound orbits: $r_{\min} \le r_z \le r_{\max}$ and $\theta_{\min} \le \theta_z \le \theta_{\max}$. Assuming that λ_{r0} is one of the solutions of $r_z(\lambda_{r0}) = r_{\max}$ and that $\lambda_{\theta 0}$ is of $\theta_z(\lambda_{\theta 0}) = \theta_{\max}$, we find

$$\left.\frac{dr_z}{d\lambda}\right|_{\lambda=\lambda_{r0}+m\lambda_r} = 0, \quad \left.\frac{d^2r_z}{d\lambda^2}\right|_{\lambda=\lambda_{r0}+m\lambda_r} < 0, \tag{16}$$

$$\left.\frac{d\theta_z}{d\lambda}\right|_{\lambda=\lambda_{\theta 0}+n\lambda_\theta} = 0, \quad \left.\frac{d^2\theta_z}{d\lambda^2}\right|_{\lambda=\lambda_{\theta 0}+n\lambda_\theta} < 0, \tag{17}$$

where m and n are integers, and we denote the periods of oscillations in $r-$ and $\theta-$ directions as λ_r and λ_θ, respectively. If the ratio of λ_r to λ_θ is irrational, we can choose m and n that satisfies $\lambda_{r0} + m\lambda_r \simeq \lambda_{\theta 0} + n\lambda_\theta$. Therefore we can set

$$U_0^r = U_0^\theta = 0, \tag{18}$$

approximately by changing the origin of λ. In addition, U_0^t can be represented by U_0^ϕ due to the condition $u^\alpha u_\alpha = -1$. Furthermore, due to the stationarity and the axisymmetric property of the Kerr spacetime, we can set $t_0 = 0$ and $\phi_0 = 0$. Therefore, we have three independent initial values, r_0, θ_0 and U_0^ϕ. These values can be transformed to E, L and Q by using Eqs.(7)-(9). After all, we found that the particle's orbits in the Kerr geometry can be characterized by the three constants of motion.

Next, we investigate the property of the geodesics in the Kerr geometry. We consider the coordinate transformation,

$$(t, r, \theta, \phi) \to (\bar{t}, \bar{r}, \bar{\theta}, \bar{\phi}) = (-t, r, \theta, -\phi), \tag{19}$$

accompanied by the transformation of the proper time,

$$\tau \to \bar{\tau} = -\tau \quad (\lambda \to \bar{\lambda} = -\lambda). \tag{20}$$

This transformation was named the Geodesic Preserving Symmetry (GPS) transformation by Mino and has the following properties. First, the Kerr metric, Eq. (1), is invariant under this transformation. Therefore, the null vectors, the Killing vectors and the Killing tensor are also invariant. Furthermore, we

find that the constants of motion, E, L, Q, are invariant. This implies that $\bar{z}^\alpha(\bar{\lambda})$ also satisfies the same equations Eqs.(11)-(14). Since the geodesics in the Kerr spacetime are characterized by E, L and Q, as we have shown above, these two orbits, $z^\alpha(\lambda)$ and $\bar{z}^\alpha(\bar{\lambda})$, coincide with each other:

$$z^\alpha(\lambda) \longrightarrow \bar{z}^\alpha(\bar{\lambda}) = z^\alpha(\bar{\lambda}). \tag{21}$$

In addition, since the time direction is reversed under this transformation, the retarded (advanced) field at any points $z^\alpha(\lambda)$ is transformed to the advanced (retarded) field at $z^\alpha(-\lambda)$:

$$\phi^{(\mathrm{ret/adv})}(z(\lambda)) \longrightarrow \phi^{(\mathrm{adv/ret})}(z(-\lambda)). \tag{22}$$

4 The Time Evolution of the Carter Constant

In this section, we introduce the scheme to calculate the evolution rate of Carter constant without requiring any regularization procedure.

From the definition of Carter Constant Eq.(9), we can obtain its λ- derivative as follows:

$$\frac{DQ}{d\lambda} = \Sigma \frac{DQ}{d\tau} = 2\Sigma K_{\alpha\beta} u^\alpha \hat{f}^\beta [h^{\mathrm{ret}}_{\mu\nu}]\Big|_{x=z(\lambda)}, \tag{23}$$

where $D/d\tau$ is the covariant derivative with the proper time and $\hat{f}^\alpha$ is the differential operator,

$$f^\alpha[h_{\mu\nu}] = -\frac{1}{2}(g^{\alpha\beta} + u^\alpha u^\beta)(h_{\beta\gamma;\delta} + h_{\beta\delta;\gamma} - h_{\gamma\delta;\beta})u^\gamma u^\delta.$$

Under the adiabatic approximation, we consider the mean value of Eq.(23) over a long time period,

$$\left\langle \frac{DQ}{d\lambda} \right\rangle \equiv \frac{1}{2T}\int_{-T}^{T} d\lambda \frac{DQ}{d\lambda} = \frac{1}{T}\int_{-T}^{T} d\lambda\, \Sigma K_{\alpha\beta} u^\alpha \hat{f}^\beta [h^{\mathrm{ret}}_{\mu\nu}]\Big|_{x=z(\lambda)}. \tag{24}$$

Under the GPS transformation, both sides of Eq.(24) are transformed as

$$\left\langle \frac{DQ}{d\lambda} \right\rangle \longrightarrow \left\langle \frac{DQ}{d\bar{\lambda}} \right\rangle = -\left\langle \frac{DQ}{d\lambda} \right\rangle, \tag{25}$$

$$\frac{1}{T}\int_{-T}^{T} d\lambda\, \Sigma K_{\alpha\beta} u^\alpha \hat{f}^\beta [h^{\mathrm{ret}}_{\mu\nu}]\Big|_{x=z(\lambda)} \longrightarrow \frac{1}{T}\int_{-T}^{T} d\lambda\, \Sigma K_{\alpha\beta} u^\alpha \hat{f}^\beta [h^{\mathrm{adv}}_{\mu\nu}]\Big|_{x=z(\lambda)}. \tag{26}$$

Therefore, we obtain

$$\left\langle \frac{DQ}{d\lambda} \right\rangle = -\frac{1}{T}\int_{-T}^{T} d\lambda\, \Sigma K_{\alpha\beta} u^\alpha \hat{f}^\beta [h^{\mathrm{adv}}_{\mu\nu}]\Big|_{x=z(\lambda)}. \tag{27}$$

From Eqs.(24) and (27), we finally obtain

$$\left\langle \frac{DQ}{d\lambda} \right\rangle = \frac{1}{T}\int_{-T}^{T} d\lambda\, \Sigma K_{\alpha\beta} u^\alpha \hat{f}^\beta [h^{\mathrm{rad}}_{\mu\nu}]\Big|_{x=z(\lambda)}, \tag{28}$$

where $h^{\mathrm{rad}}_{\mu\nu}$ is the radiative part of the metric perturbation:

$$h^{\mathrm{rad}}_{\mu\nu} = \frac{h^{\mathrm{ret}}_{\mu\nu} - h^{\mathrm{adv}}_{\mu\nu}}{2}, \tag{29}$$

which is a homogeneous solution for the Einstein equations. This shows that we can obtain the evolution rate of Carter constant completely avoiding the regularization procedure which involves troublesome calculations.

5 Summary

In this paper, we have reviewed the scheme to calculate the evolution rate of Carter constant, proposed by Mino. In this scheme, since we need only the calculation for the radiative part of the metric perturbation, which is the homogeneous solution for the field equation, we can avoid the regularization procedure of the self-force.

To obtain the radiative part of the metric perturbation, we use the Teukolsky formalism [7] and the Chrzanowski's method [8]. Since the scheme to solve the Teukolsky equation is known analytically [9], we can calculate the radiative part of the Weyl scalar, which is a homogeneous solution. In the latter method, we can reconstruct the metric perturbation from the Weyl scalar in the radiation gauge as far as a homogeneous solution is concerned. Therefore, we can obtain the radiative part of the metric perturbation. Substituting it into Eq.(28), given in Sec.4, we obtain the expression for the evolution rate of the Carter constant as given by Gal'tsov in the case of E and L_z. This work is under preparation.

Acknowledgment

We would like to thank T. Nakamura, H. Nakano, M. Sasaki and H. Tagoshi for invaluable discussions. This work was supported by Monbukagaku-sho Grant-in-Aid for Scientific Reasearch of the Japanese Ministry of Education, Culture, Sports, Science and Technology, No.14047212.

References

[1] A. Ori, Phys. Lett. A 202, 347 (1995); Phys. Rev. D 55, 3444 (1997).

[2] Y. Mino, M. Sasaki, and T. Tanaka, Phys. Rev. D 55, 3457 (1997).

[3] T.C. Quinn and R.M. Wald, Phys. Rev. D 56, 3381 (1997).

[4] D.V. Gal'tsov, J.Phys. A 15, 3737 (1982).

[5] P.A.M. Dirac, Proc. R. Soc. London A167, 148 (1938).

[6] Y. Mino, in preparation.

[7] S.A. Teukolsky, Astrophys. J. 185, 635 (1973).

[8] P.L. Chrzanowski, Phys. Rev. D 11, 2042 (1975).

[9] S. Mano, H. Suzuki and E. Takasugi, Prog. Theor. Phys. 95, 1079 (1996); Prog. Theor. Phys. 96, 549 (1996).

Hawking Radiation from an Inflating Monopole

Hiromi Saida,[1] Ken-ichi Nakao,Hideki Ishihara,Yoshiyuki Morisawa,Daisuke Ida,[‡]

Department of Mathematics and Physics, Osaka City University, Sugimoto 3-3-138, Sumiyoshi-ku, Osaka 558-8585, Japan

‡ *Deptartment of Physics, Tokyo Institute of Technology, Ookayama 2-12-1, Meguro-ku, Tokyo 152-8551, Japan*

Abstract

We investigate what phenomena we will find if there are inflating monopoles around us. The inflating monopole is one of the topological defects whose inside expands inflationary due to the vacuum energy of the field forming the monopole. It has already studied that the inside geometry of the inflating monopole is given by the de-Sitter spacetime, and the outside is a black hole spacetime. The inside inflating region is behind the event horizon of the outside black hole geometry. Therefore it is impossible for the outside observer to tell an inflating monopole from a black hole using only geometrical (classical) informations. Hence quantum properties become important, and we derive the Hawking radiation from an inflating monopole received by the outside observer, and compare it with the usual Hawking radiation from a black hole. The resultant Hawking radiation has the black body spectrum, but its temperature is different from the usual Hawking temperature of the outside black hole geometry. The temperature of the inflating monopole can not be determined uniquely by the surface gravity of the outside black hole geometry, but depends on the process of producing the inflating monopole. Finally we discuss the remained problem about the derivation of our resultant spectrum.

1 Introduction

Inflating monopole is usually used for the topological inflation model [1]. In this model, it is assumed that our universe was born in a topological defect, for example a monopole, and that the inside of the monopole expands inflationary due to the vacuum energy of the field forming the monopole. By the way, there is a possibility that some monopoles exist around us. In this case, we are not in the inside of a monopole but at the outside. Then a simple question arises: *what phenomena will we find if the monopoles around us are the inflating monopoles?*

The spacetime structure of an inflating monopole with an electric charge has already been studied numerically in references [2], where spherical symmetry and asymptotic flatness are assumed. According to these references, the conformal diagram can be modeled as figure 1, where we neglect the electric charge for simplicity. This model is constructed by replacing the inside of the event horizon of a static spherical black hole spacetime by a portion of the de-Sitter spacetime as shown in figure 2. Reflecting the inflationary expansion of the inside geometry, the junction surface Σ is timelike for past region but becomes spacelike for future region. However the structure of the infinite past is unknown, which should be determined by the process of producing the inflating monopole. Throughout this paper we leave the infinite past structure be unknown. That is, what we are interested in is *how an inflating monopole looks once it has already been produced.*

Because the inside inflating region of an inflating monopole is behind the event horizon of the outside black hole geometry, it is impossible for the outside observer to tell an inflating monopole from a black hole using only geometrical (classical) informations. On the other hand for a usual black hole spacetime, it has already been well known that the black hole emits a black body radiation from the event horizon due to the quantum effects of matter fields (Hawking radiation) [3]. Generally it is believed that, under natural choice of the vacuum states, the quantum radiation in the presence of the event horizon has the black body spectrum of the Hawking temperature $T_H = \kappa/2\pi$, where κ is the surface gravity of

[1] E-mail: saida@sci.osaka-cu.ac.jp

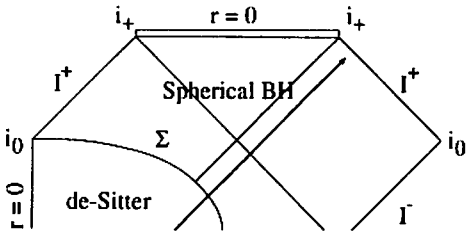


Figure 1: The conformal diagram of the inflating monopole without electric charge. The arrow denotes an out-going null geodesic which passes near the event horizon.

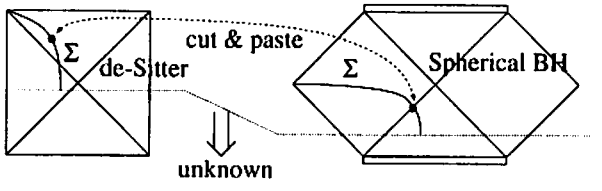


Figure 2: The construction of the background spacetime. The event horizon of outside geometry is connected into the region $r > r_0$ of the static chart of the de-Sitter geometry.

the event horizon. But this belief has not been proved. So the quantum radiation may become the key property to telling an inflating monopole from a black hole. Then our aim in this paper is *to derive the Hawking radiation from an inflating monopole received by the outside observer, and compare it with the usual Hawking radiation from a black hole.*

In section 2, the construction and properties of the background spacetime are briefly reviewed. Section 3 is devoted to the derivation of the Hawking radiation from an inflating monopole. Concluding discussion is in section 4. The unit is $c = h = 1$ and set $k_B = 1$ throughout this paper.

2 Background Spacetime

The metric for the outside of the inflating monopole is given by the static spherical black hole:

$$ds^2_{(out)} = -C(r)\,dt^2 + \frac{dr^2}{C(r)} + r^2\,d\Omega^2 = -C(r)\,du^2 - 2\,du\,dr + r^2\,d\Omega^2\,,$$

where $d\Omega = d\theta + \sin^2\theta\,d\varphi$ is the line element on a sphere and u is the out-going null coordinate defined as $u = t - r^*$, $dr^* = dr/C(r)$. The event horizon is located at $r = r_g$ ($C(r_g) = 0$), and $C(r \to \infty) = 1$ due to the asymptotic flatness. The surface gravity of the event horizon $\kappa^{(out)}$ is given by $2\,\kappa^{(out)} = dC/dr\,|_{r=r_h}$.

The metric for the inside of the inflating monopole is the de-Sitter spacetime:

$$ds^2_{(in)} = -A(r)\,d\tau^2 + \frac{dr^2}{A(r)} + r^2\,d\Omega^2 = -A(r)\,d\tilde{u}^2 - 2\,d\tilde{u}\,dr + r^2\,d\Omega^2\,,$$

where $\tilde{u}$ is the out-going null coordinate defined as $\tilde{u} = \tau - \tilde{r}$, $d\tilde{r} = dr/A(r)$, $A(r) = 1 - H^2\,r^2$, $H^2 = \Lambda/3$, and Λ is the cosmological constant. The cosmological horizon is at $r = r_0 \equiv 1/H$ ($A(r_0) = 0$), and the surface gravity of this horizon $\kappa^{(in)}$ is given by $2\,\kappa^{(in)} = dA/dr\,|_{r=r_0} = 2H$. The static chart $(\tau, r, \theta, \varphi)$ is useful for later calculations, but it does not express the inflationary expansion. The transformation to the inflationary chart $(\lambda, \rho, \theta, \varphi)$ is given by $r = e^{H\,\lambda}\,\rho$, $2\,H\,\tau = -\ln[\,e^{-2H\,\lambda} - H^2\,\rho^2\,]$, which gives

$$ds^2_{(in)} = -d\lambda^2 + e^{2H\,\lambda}\left[\,d\rho^2 + \rho^2\,d\Omega^2\,\right] = e^{2H\,\lambda}\left[\,-d\eta^2 + d\rho^2 + \rho^2\,d\Omega^2\,\right]\,,$$

where η is the conformal time defined as $d\eta = e^{-H\,\lambda}\,d\lambda$.

The junction conditions at Σ are given by the Israel condition [5]. In this paper not all of these conditions are strictly used. The useful one is the continuity of the value of metrics, $ds^2_{(out)}|_\Sigma = ds^2_{(in)}|_\Sigma$. This condition will be considered at (3). And for later use we parameterize the coordinate of the spacetime point $p \in \Sigma$ by τ: $p = (t(\tau), r(\tau), \theta, \varphi)$ seen from the outside, or $p = (\tau, r(\tau), \theta, \varphi)$ seen from the inside. Because the surface Σ is expanding in being measured with the areal coordinate r, we should set $dr(\tau)/d\tau > 0$. Further reflecting the inflationary expansion inside the monopole, Σ is timelike at past region, then it becomes spacelike at future region [2].

3 Hawking Radiation

We set the observer to stay in the rest frame (r =constant) in the asymptotically flat region in the outside of the inflating monopole. And introduce a massless scalar field Φ satisfying $\Box\Phi = 0$ as the representative of the radiation emitted from an inflating monopole. [2] Then, by quantizing Φ on the background spacetime, we can obtain the Hawking radiation from an inflating monopole. The expectation value of the number of particles $I(\omega)$ emitted as the Hawking radiation is given by

$$I(\omega) = \langle \mathrm{vac}| a_\omega^{(out)\dagger} a_\omega^{(out)} |\mathrm{vac}\rangle , \tag{1}$$

where ω is the energy (frequency) of the particle, $|\mathrm{vac}\rangle$ is the vacuum state defined with respect to the mode function of Φ defined on the inflating chart of the inside geometry of the inflating monopole, and $a_\omega^{(out)}$ is the annihilation operator which is obtained with respect to the mode function defined on the Schwarzschild chart of the outside geometry. That is, the value $I(\omega)$ is the number of particles (of field Φ) created on the vacuum state of the inflating region inside the monopole. In order to compare the Hawking radiation from an inflating monopole with the usual Hawking radiation from a black hole, it is necessary to introduce the same conditions under which the usual Hawking radiation has been derived for a black hole case [3]. They are summarized in three conditions:

- Consider only the modes propagating near the event horizon of the outside geometry.
- Ignore the curvature scattering.
- Consider only the out-going modes.

These conditions have also been introduced in deriving the well known statements that a black hole of surface gravity κ emits a black body radiation of the Hawking temperature $T_H = \kappa/2\pi$ [3].

The calculation of $I(\omega)$ can be carried out by the Bogoljubov transformation, which is the change of basis (mode functions) of Φ with which Φ is quantized. Simply by the technical reason, we consider the following two successive Bogoljubov transformations:

1st step: Transformation from the out-going mode function defined on the inflating chart of the inside geometry $f_{\tilde{\omega}}^{(in.inf.)}$ to that defined on the static chart of the inside geometry $f_{\tilde{\omega}}^{(in.stat.)}$.

2nd step: Transformation from $f_{\tilde{\omega}}^{(in.stat.)}$ to that defined on the Schwarzschild chart of the outside geometry $f_\omega^{(out)}$.

To carry out the first step, let $a_{\tilde{\omega}}^{(in.stat.)}$ denote the annihilation operator defined on the static chart. It has already been well known that the particles defined on the static chart are created on the vacuum state $|\mathrm{vac}\rangle$ defined on the inflating chart [6], which results in

$$\langle \mathrm{vac}| a_{\tilde{\omega}}^{(in.stat.)\dagger} a_{\tilde{\omega}}^{(in.stat.)} |\mathrm{vac}\rangle = \frac{1}{\exp(2\pi\tilde{\omega}/\kappa^{(in)}) - 1} . \tag{2}$$

This is the black body spectrum of temperature $\kappa^{(in)}/2\pi = 1/2\pi r_0$.

The essence of the second step is the red shift which the out-going mode $f_{\tilde{\omega}}^{(in.stat.)}$ receives during propagating from Σ to the observer. The red shift is the change of the phase of $f_{\tilde{\omega}}^{(in.stat.)}$. Since Φ is

[2] This field Φ does express just the radiation from the monopole, and has no relation with the field forming the monopole.

massless, the phase of $f_{\tilde{\omega}}^{(in\ stat.)}$ is given by the out-going null coordinate $\tilde{u}$. Therefore, the red shift can be evaluated from the junction condition of the metrics, $ds^2_{(out)}|_\Sigma = ds^2_{(in)}|_\Sigma$, which results in

$$u \simeq b\tilde{u} + c \quad \text{where} \quad b = \frac{1}{2}\left(1 + \frac{A}{\dot{r}}\right)\Big|_{r_h}, \; c = \text{const.}, \tag{3}$$

where $\dot{r} = dr(\tau)/\tau$ on Σ, and we considered the approximation up to the leading term with the expansion by the small parameter $(r - r_h)/r_h \ll 1$. [3] By tracing the mode $f_{\tilde{\omega}}^{(in\ stat.)}$ at the inside of the inflating monopole toward the observer, we can obtain the Bogoljubov coefficients $\alpha_{\omega\tilde{\omega}}$ and $\beta_{\omega\tilde{\omega}}$ as

$$f_{\tilde{\omega}}^{(in\ stat.)}(\tilde{u}) \rightarrow f_{\tilde{\omega}}^{(in\ stat)}(u/b - c/b) = \int_0^\infty d\omega \left[\alpha_{\omega\tilde{\omega}} f_\omega^{(out)}(u) + \beta_{\omega\tilde{\omega}} f_\omega^{(out)*}(u)\right],$$

where $f_\omega^{(out)}(u) = e^{-i\omega u}/\sqrt{4\pi\omega}$ and $f_{\tilde{\omega}}^{(in\ stat.)}(\tilde{u}) = e^{-i\tilde{\omega}\tilde{u}}/\sqrt{4\pi\tilde{\omega}}$, since the curvature scattering is ignored. Then we obtain $\alpha_{\omega\tilde{\omega}} = e^{-i\omega c}\delta(\omega - \tilde{\omega}/b)$, $\beta_{\omega\tilde{\omega}} = 0$. This means that there is no superposition between the positive frequency mode defined in the inside of the inflating monopole and the negative frequency mode defined in the outside. Consequently no quantum particle creation occur in passing through the junction surface Σ. But if some particles have already existed in the inside like (2), these particles should receive the classical red shift (3) after passing through Σ. Finally we obtain the Hawking radiation (1) to be

$$I(\omega) = \frac{1}{\exp(2\pi b\,\omega/\kappa^{(in)}) - 1}. \tag{4}$$

This is the black body radiation of the temperature

$$T_{IM} = \frac{\kappa^{(in)}}{2\pi b} = \frac{1}{\pi r_0}\left(1 + \frac{A}{\dot{r}}\right)^{-1}_{r=r_h}, \tag{5}$$

which depends on three unknown parameters, r_0, r_h and $\dot{r}|_{r=r_h}$.

4 Concluding Discussion

We have derived the Hawking radiation from an inflating monopole. Here we should point out two issues: unusual properties of (4) and remained problems about the validity of our derivation of (4). Let us discuss about these issues in the following.

Unusual properties of (4)

Because the inflating monopole can not be distinguished from a black hole for the outside observer using only classical informations, it is naively expected that the Hawking radiation from the inflating monopole has the same spectrum as the usual black hole. But our result says that, though the spectrum (4) is also of black body, the temperature (5) has quite different property from that of a usual black hole. For a usual black hole case, the Hawking temperature is uniquely determined by the surface gravity of the event horizon without respect to the details of the gravitational collapse. But for the inflating monopole, the temperature (5) can not be determined uniquely by the surface gravity, but depends on the process of producing the inflating monopole, which is reflected by the parameter $\dot{r}|_{r=r_h}$.

Further as denoted by figure 2, we find the relation $r_0 < r_h$. From this relation, the lower bound of T_{IM} can be obtained.

$$r_0 < r_h \Rightarrow A(r_h) < 0 \Rightarrow (0 <) b < \frac{1}{2} \Rightarrow T_{IM} > \frac{1}{\pi r_0} > \frac{1}{\pi r_h} \equiv T_{min}.$$

For a spherical black hole, it is easily checked that $T_{min} > T_H = \kappa^{(out)}/2\pi$. That is, it is concluded that the radiation flux of an inflating monopole is stronger than that of a usual black hole.

[3] For the details of calculations, see the reference [4].

As mentioned in section 1, it is generally believed that the quantum radiation in the presence of the event horizon has the black body spectrum of the Hawking temperature $T_H = \kappa^{(out)}/2\pi$. But this belief has not been proved. So it seems that our result deny this common belief. But, before accepting our result, we should be careful about the validity of our derivation of (4).

Remained problems about the validity of our derivation of (4)

In the derivation of (4), some approximations have been used due to the three conditions given at the beginning of section 3. Particularly, we have not strictly solved the Klein-Gordon equation $\Box\Phi = 0$ for obtaining the mode functions, $f_\omega^{(in\,inf)}$, $f_\omega^{(in\,stat)}$ and $f_\omega^{(out)}$. Instead we have considered a simple argument about the red shift using the junction of the null coordinates at Σ (3). Such an approximated derivation has had powerful performance to extract easily the essence of the usual Hawking radiation from a black hole, where only one step of Bogoljubov transformation was considered. However, since we have used two Bogoljubov transformations, it may be necessary to be more careful about the use of the approximations. To confirm our unusual result (4), it is the best way to solve the Klein-Gordon equation more strictly, which we are now under consideration.

References

[1] A. Vilenkin, Phys. Rev. Lett. **72**, 3137 (1994); A. Linde, Phys. Lett. **B327**, 208 (1994); A. Linde and D. Linde, Phys. Rev. **D50**, 2456 (1994).

[2] N. Sakai, H. Shinkai, T. Tachizawa and K. Nakao, Phys. Rev. **D53**, 655 (1996); N. Sakai, Phys. Rev. **D54**, 1548 (1996); N. Sakai, K. Nakao and T. Harada, Phys. Rev. **D61**, 127302 (2000).

[3] S.W. Hawking, Commun. Math. Phys. **43**, 199 (1975); W.G. Unruh, Phys. Rev. **D14**, 870 (1976).

[4] N.D. Birrell and P.C.W. Davies, *Quantum fields in curved space* (Cambridge University Press, 1982), p.255

[5] W. Israel, Nuovo Cim. **44B**, 1 (1966), and Nuovo Cim. **48B**, 463 (1967).

[6] G.W. Gibbons and S.W. Hawking, Phys. Rev. **D15**, 2738 (1977); A.S. Lapedes, J. Math. Phys. **19**, 2289 (1978); R.H. Brandenberger, Rev. Mod. Phys. **57**, 1 (1985).

One-Armed Spiral Instability in Differentially Rotating Stars

Motoyuki Saijo [1] [(a)] , Thomas W. Baumgarte [2] [(b),(c)], and Stuart L. Shapiro [3] [(c),(d),(e)]

[(a)] *Department of Physics, Kyoto University, Kyoto 606-8502, Japan*

[(b)] *Department of Physics and Astronomy, Bowdoin College, 8800 College Station Brunswick, Maine 04011-8488, USA*

[(c)] *Department of Physics, University of Illinois at Urbana-Champaign, Urbana, Illinois 61801-3080, USA*

[(d)] *Department of Astronomy, University of Illinois at Urbana-Champaign, Urbana, Illinois 61801, USA*

[(e)] *NCSA, University of Illinois at Urbana-Champaign, Urbana, Illinois 61801, USA*

Abstract

We investigate the dynamical instability of the one-armed spiral $m = 1$ mode in differentially rotating stars by means of $3+1$ hydrodynamical simulations in Newtonian gravitation. We find that both a soft equation of state and a high degree of differential rotation in the equilibrium star are necessary to excite a dynamical $m = 1$ mode as the dominant instability at small values of the ratio of rotational kinetic to potential energy, $T/|W|$. We find that this spiral mode propagates outward from its point of origin near the maximum density at the center to the surface over several central orbital periods. An unstable $m = 1$ mode triggers a secondary $m = 2$ bar mode of smaller amplitude, and the bar mode can excite gravitational waves. As the spiral mode propagates to the surface it weakens, simultaneously damping the emitted gravitational wave signal. This behavior is in contrast to waves triggered by a dynamical $m = 2$ bar instability, which persist for many rotation periods and decay only after a radiation-reaction damping timescale.

1 Introduction

Stars in nature are usually rotating and may be subject to nonaxisymmetric rotational instabilities. An exact treatment of these instabilities exists only for incompressible equilibrium fluids in Newtonian gravity [1, 2]. For these configurations, global rotational instabilities may arise from non-radial toroidal modes $e^{im\varphi}$ (where $m = \pm 1, \pm 2, \ldots$ and φ is the azimuthal angle).

For sufficiently rapid rotation, the $m = 2$ bar mode becomes either *secularly* or *dynamically* unstable. The onset of instability can typically be identified with a critical value of the non-dimensional parameter $\beta \equiv T/|W|$, where T is the rotational kinetic energy and W the gravitational potential energy. Uniformly rotating, incompressible stars in Newtonian theory are secularly unstable to bar-mode formation when $\beta \geq \beta_{\rm sec} \simeq 0.14$. This instability can grow only in the presence of some dissipative mechanism, like viscosity or gravitational radiation, and the associated growth timescale is the dissipative timescale, which is usually much longer than the dynamical timescale of the system. By contrast, a dynamical instability to bar-mode formation sets in when $\beta \geq \beta_{\rm dyn} \simeq 0.27$. This instability is independent of any dissipative mechanisms, and the growth time is the hydrodynamic timescale.

Determining the onset of the dynamical bar-mode instability, as well as the subsequent evolution of an unstable star, requires a fully nonlinear hydrodynamic simulation. Simulations performed in Newtonian gravity have shown that $\beta_{\rm dyn}$ depends only very weakly on the stiffness of the equation of state. Once a bar has developed, the formation of a two-arm spiral plays an important role in redistributing the angular momentum and forming a core-halo structure. Both $\beta_{\rm dyn}$ and $\beta_{\rm sec}$ are smaller for stars with high degree

[1] E-mail: saijo@tap.scphys.kyoto-u.ac.jp
[2] E-mail: tbaumgar@bowdoin.edu
[3] E-mail: shapiro@astro.physics.uiuc.edu

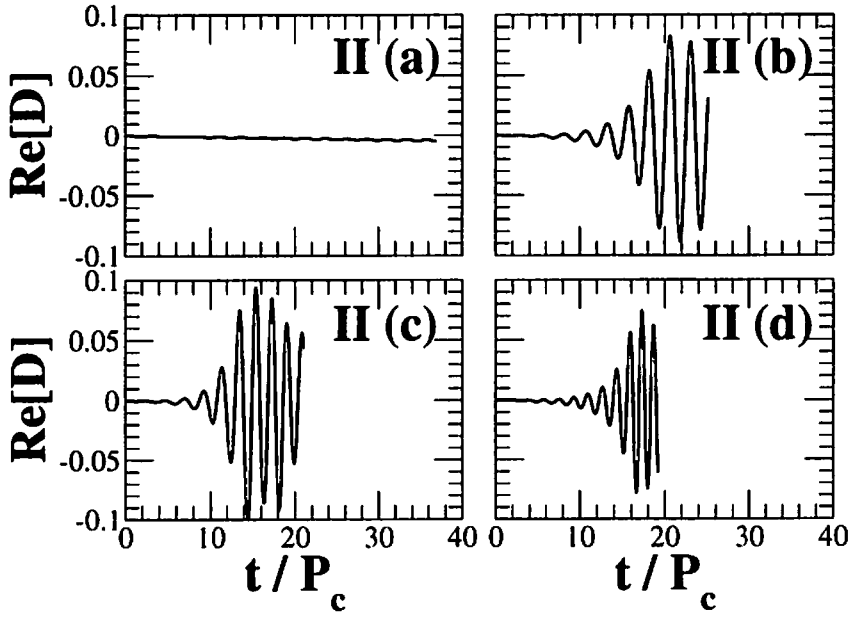


Figure 1: Diagnostic D as a function of t/P_c for Models II (see Table 3 of Ref. [5]). The stiffness of the equation of state decreases from model (a) to (d). We terminate our simulation at $t \sim 25P_c$ or when the maximum density of the star exceeds about 10 times its initial value.

of differential rotation. Simulations in relativistic gravitation have shown that $\beta_{\rm dyn}$ decreases with the compaction of the star, indicating that relativistic gravitation enhances the bar mode instability. In order to efficiently use computational resources, most of these simulations have been performed under certain symmetry assumptions (e.g. π-symmetry), which do not affect the growth of the $m = 2$ bar mode, but which suppress any $m = 1$ modes.

Recently, Centrella et al. [3] reported that such $m = 1$ "one-armed spiral" modes are dynamically unstable at surprisingly small values of $T/|W|$. Centrella et al. [3] found this instability in evolutions of highly differentially rotating equilibrium polytropes with polytropic index $n = 3.33$. Typically, these equilibria have a "toroidal" structure, so that the maximum density is not located at the geometric center but rather on a toroid rotating about the center.

The purpose of this paper is to study further the conditions under which a dynamical $m = 1$ instability is excited. We vary both the polytropic index, i.e. the stiffness of the equation of state, and the degree of differential rotation to isolate their effects on the instability. Since the onset of rotational instabilities is often characterized by β we keep this value approximately fixed in our sequences. We find that a soft equation of state and a high degree of differential rotation are both necessary to dynamically excite the $m = 1$ mode at the small value of $\beta = 0.14$ chosen in this paper. We find that a toroidal structure is not sufficient to trigger the $m = 1$ instability, but our findings suggest that a toroidal structure may be necessary.

While our goal is to gain a deeper understanding of the nature of the $m = 1$ instability as opposed to simulating realistic astrophysical scenarios, we point out that there exist evolutionary sequences that may well lead to rapidly and highly differentially rotating configurations. For example, cooling by thermal emission from a rotating star will cause the star to contract and spin up. If internal viscosity and magnetic fields are sufficiently weak, this process will lead to differential rotation even if the initial configuration is rotating uniformly. This scenario may arise in supermassive stars, where the equation of state is dominated by radiation pressure and may be modeled by a (soft) $n = 3$ polytrope. In the absence of viscosity and magnetic braking, the star will contract quasi-statically as it cools to a toroidal configuration, which may be subject to $m = 1$ or $m = 2$ instabilities [4].

This paper is organized as follows. We discuss our numerical results in § 2, and briefly summarize our

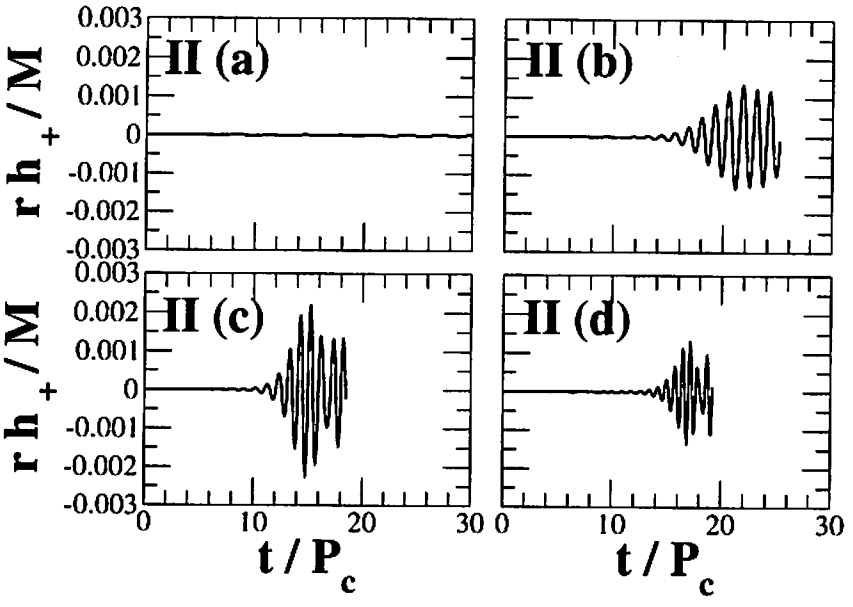


Figure 2: Gravitational waveforms as seen by a distant observer located on the z-axis for Models II.

findings in § 3. Throughout this paper we use gravitational units [4] with $G = c = 1$ and adopt Cartesian coordinates (x, y, z). A more detailed discussion is presented in Ref. [5].

2 Numerical Results

2.1 Stiffness of the equation of state

We parametrize the stiffness of the equation of state by varying the polytropic index n between $n = 3.33$ and $n = 2$. In this sequence we keep the degree of differential rotation (i.e. Ω_c/Ω_{eq}) fixed, and adjust the overall rotation rate (parametrized by the ratio of the polar to equatorial radius R_p/R_{eq}) so that the value of $T/|W|$ remains very close to 0.144 (as for Model I (a) in Table 1 of Ref. [5]). We list our four different Models II in Table 3 of Ref. [5].

Figure 1, where we plot the dipole diagnostic D as a function of time, clearly shows that an $m = 1$ instability is excited in Models II (b) and II (c) in addition to Model II (d). We find that D starts decreasing immediately after reaching a maximum. This is a consequence of the star rearranging its density profile, and of the spiral arm propagating outward to lower density regions. Model II (a), however, which has the most pronounced toroidal structure, remains stable.

In Fig. 6 of Ref. [5], we show the maximum density as a function of time. The maximum density slowly increases in all cases due to dissipation of differential rotation. Once the one-armed spiral forms in Models II (b) and II (c), however, this increase is much more rapid, which indicates again that the unstable mode rearranges the matter in the star and destroys the toroidal structure.

We show the gravitational wave signal emitted from Models II in Fig. 2. As consistent with the diagnostic D, the gravitational wave signal emitted by the one-armed spiral mode does not persist over many rotational periods, and instead decays fairly rapidly after it has been excited. This characteristic is very different from what has been found for $m = 2$ bar mode instabilities (compare § 3.2 of Ref. [5]). We also find that the maximum wave amplitude is much smaller than can be found for configurations unstable to a pure bar mode (compare Fig. 3 of Ref. [5]) as gravitational radiation requires a quadrupole

[4] Since we adopt Newtonian gravity in this paper, the speed of light only enters in the gravitational waveforms.

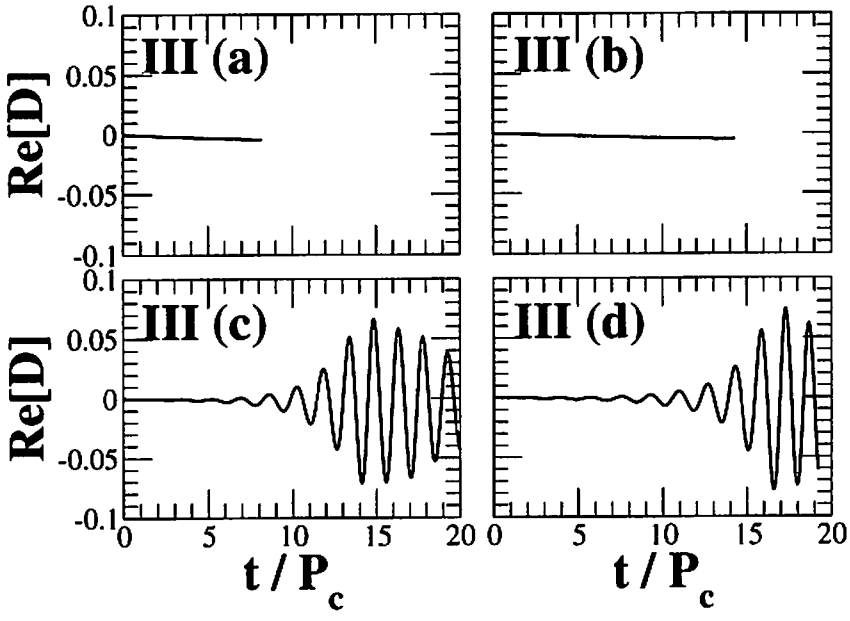


Figure 3: Diagnostic D as a function of t/P_c for Models III (see Table 4 of Ref. [5]). The degree of differential rotation increases from model (a) to (d).

distortion and the $m = 2$ perturbation in Models II is only being excited as a lower-amplitude harmonic of the $m = 1$ mode.

2.2 Degree of differential rotation

We now analyze the dependence of the one-armed spiral instability on the degree of differential rotation. Starting again with Model I (a), we now increase Ω_c/Ω_{eq} to vary the degree of differential rotations. As before, we would like to keep $\beta \sim 0.14$ in this sequence. For very soft equations of state, this value can only be achieved for very strong degrees of differential rotation. Therefore, in order to keep β approximately constant, we simultaneously have to decrease n as we decrease the degree of differential rotation. We list the details of our Models III in Table 4 of Ref. [5].

We show the dipole diagnostic D as a function of time in Fig. 3, which shows that Models III (a) and III (b) are stable against one-armed spiral formation while Models III (c) and III (d) are not. We find that the one-armed spiral results in a large increase in the central density, and an elimination of the toroidal structure.

We show gravitational waveforms from Models III in Fig. 4. We again find that the amplitude decreases after reaching a maximum. In some cases, however, this decrease is not monotonic, and the amplitude may increase again to form several distinct wave packets. Our numerical data are not sufficient to determine the generic character of the gravitational waves emitted from $m = 1$ instabilities, and we expect that this will be subject of future investigations. The problem is that the growth of central concentration during the evolution exceeds the ability of our code to resolve the innermost regions for arbitrary long times in all cases.

3 Discussion

We have studied the conditions under which Newtonian, differentially rotating stars are dynamically

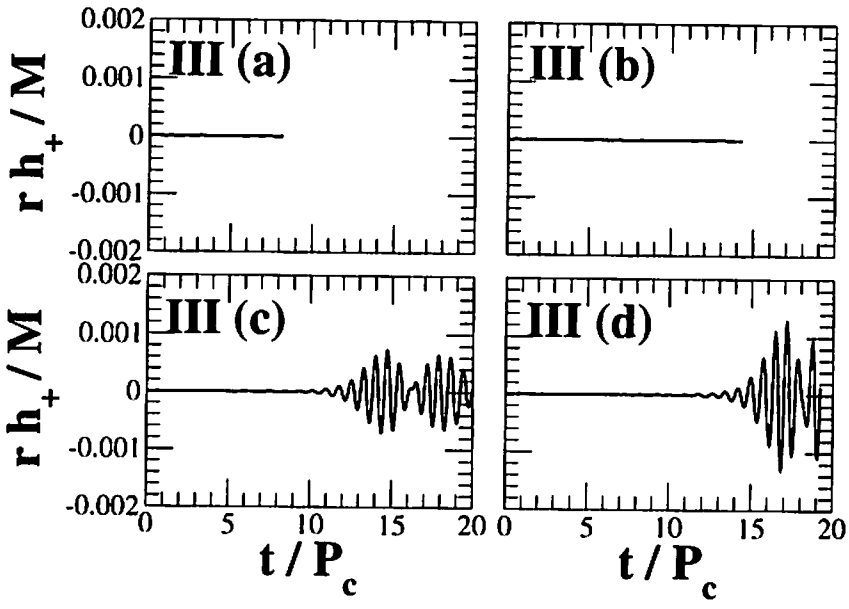


Figure 4: Gravitational waveforms as seen by a distant observer located on the z-axis for Models III.

unstable to an $m = 1$ one-armed spiral instability, and found that both soft equations of state and a high degree of differential rotation are necessary to trigger the instability. For sufficiently soft equations of state and sufficiently high degrees of differential rotation we found that stars are dynamically unstable even at the small values of $T/|W| \sim 0.14$ considered in this paper.

While we find that a toroidal structure alone is not sufficient for the $m = 1$ instability, all the models that are unstable do have a toroidal structure, suggesting that this may be a necessary condition. The growing $m = 1$ mode redistributes the matter in the unstable star and destroys the toroidal structure after a few central rotation periods.

Quasi-periodic gravitational waves emitted by stars with $m = 1$ instabilities have smaller amplitudes than those emitted by stars unstable to the $m = 2$ bar mode. For $m = 1$ modes, the gravitational radiation is emitted not by the primary mode itself, but by the $m = 2$ secondary harmonic which is simultaneously excited, albeit at a lower amplitude. Unlike the case for bar-unstable stars, the gravitational wave signal does not persist of many periods, but instead is damped fairly rapidly in most of the cases we have examined.

We have plotted typical wave forms for stars unstable to $m = 2$ bar modes in Fig. 3 of Ref. [5] and for stars unstable to one-armed spiral $m = 1$ modes in Figs. 2 and 4. Characteristic wave frequencies f_{GW} are seen to be $\sim P_c^{-1} \sim \Omega_c$, and are considerably higher than $\Omega_{eq} \sim (M/R^3)^{1/2}$ due to appreciable differential rotation. For supermassive stars ($M \gtrsim 10^5 M_\odot$) the amplitudes and frequencies of these waves fall well within the detectable range of LISA [4].

References

[1] S. Chandrasekhar, *Ellipsoidal Figures of Equilibrium* (Yale University Press, New York, 1969), p. 61.

[2] J. Tassoul, *Theory of Rotating Stars* (Princeton University Press, Princeton, 1978).

[3] J. M. Centrella, K. C. B. New, L. L. Lowe, and J. D. Brown, Astrophys. J. Lett. **550**, L193 (2001).

[4] K. C. B. New and S. L. Shapiro, Astrophys. J. **548**, 439 (2001).

[5] M. Saijo, T. W. Baumgarte, S. L. Shapiro, submitted to Astrophys. J. (2003).

Hybrid Monopole Inflation and Massive Black-Hole Formation

Nobuyuki Sakai[1]

Faculty of Education, Yamagata University, Yamagata 990-8560
and Graduate School of Science and Engineering, Yamagata University, Yamagata 990-8560

Jun'Ichi Yokoyama

Department of Earth and Space Science, Graduate School of Science,
Osaka University, Toyonaka 560-0043

Abstract

We study the dynamics of magnetic monopoles in hybrid inflation. If the vacuum expectation value is of order of the Planck mass, astronomically massive monopoles are created. Those monopoles could be the origins of MACHOs or other astronomical black holes.

1 Introduction

Topological defects are created when a scalar field σ^a with a potential,

$$V(\sigma) = \frac{\lambda}{4}(\sigma^2 - \eta^2)^2, \quad \sigma \equiv \sqrt{\sigma^a \sigma^a}, \tag{1}$$

relax to the true vacuum $\sigma = \eta$ with spatially random phase. Although they were originally regarded as solitonic objects, it was shown that they expand exponentially and even contain inflationary universes if $\eta \gtrsim 0.35 m_{Pl}$ [1, 2, 3]. In the context of unified theories magnetic monopoles are the most realistic, and their dynamics is the most interesting [3, 4]. When a monopole inflates, a Schwarzschild-like black hole (wormhole) appears around it. Unfortunately, however, it is almost impossible to observe the relics of inflating monopoles or black holes for the following reasons. First, our Universe must once experience an inflationary phase according to inflationary cosmology. Without additional inflaton field our big-bang Universe must come out of one inflating monopole. In this case the number of relic black holes is at most one in our Universe. Second, once a monopole configuration is formed ($\sigma \approx \eta$ except in the center), its gravitational mass remains unchanged even though the monopole core continues to inflate. Its mass is of order of η, which is typically 10^{19}GeV$\sim 10^{-5}$g, and hence it does not leave any observable trace.

On the other hand, hybrid Inflation [5] is described by a potential like

$$V(\sigma,\ \phi) = \frac{\lambda}{4}(\sigma^2 - \eta^2)^2 + \frac{m^2}{2}\phi^2 + \frac{g^2}{2}\phi^2\sigma^2. \tag{2}$$

In this paper we consider what happens if σ^a is a triplet scalar field with gauge coupling and if η is large enough in the model (2). One may expect that monopoles inflate similarly, as discussed by Garcia-Bellodo et al. [6]. What we shall show is that those inflating monopoles give rise to astronomical black holes if the parameters are appropriately chosen.

2 Scenario

The original scenario of hybrid inflation by Linde was as follows [5]. The effective mass squared of σ is equal to $-\lambda\eta^2 + g^2\phi^2$. In the first stage when $\phi \gg \phi_c \equiv \sqrt{\lambda}\eta/g$, one expects that σ converges to zero and ϕ rolls down slowly along $\sigma \approx 0$ just like chaotic inflation ("ϕ-inflation"). At the moment when the phase

[1]E-mail: sakai@ke-sci.kj.yamagata-u.ac.jp

transition with symmetry breaking occurs, inflation ends as σ rolls down rapidly to $\sigma = \eta$. Topological defects can form, depending on the topology of the new vacuum $\sigma = \eta$. Due to the complex evolution of the scalar fields, a variety of density perturbation spectrum can be produced.

Our scenario is, on the other hand, as follows. We assume σ^a is a triplet scalar field with gauge coupling; then magnetic monopoles appear inevitably. We also assume $\eta \sim m_{Pl}$; then following "ϕ-inflation", inflation continues after $\phi = \phi_c$ as a slow rolling in the σ-direction takes place ("σ-inflation"). Because the whole region continues to inflate until a monopole configuration forms ($\sigma \approx \eta$ except in the center), the monopole gains a huge gravitational mass. Once a monopole configuration forms, its gravitational mass is unchanged even though the monopole core continues to inflate.

Let us discuss the dynamics of σ in a simplified model. At a classical level σ converges to the potential valley, $\sigma = 0$, when $\phi > \phi_c$. However, the quantum fluctuations with wavelength H^{-1} and amplitude $\delta\sigma \approx H/2\pi$ are generated continuously, where H is the Hubble parameter and $H \approx H_0 \equiv \sqrt{(8\pi/3m_{Pl}^2)(\lambda\eta^4/4)}$. Therefore, we consider the simplified model where at the moment $\phi = \phi_c$, $\sigma = 0$ inside the horizon sphere, $r < H_0^{-1}$, and $\sigma = H/2\pi$ for $r > H_0^{-1}$.

We assume the outer region is described by Friedmann-Robertson-Walker metric. Although the outside becomes inhomogeneous gradually, this treatment gives an approximation until the inhomogeneity becomes large. The evolution equations for $\sigma(t)$ and the scale factor $a(t)$ are

$$\ddot{\sigma} + 3H\dot{\sigma} = -\lambda\sigma(\sigma^2 - \eta^2) - g^2\phi^2\sigma, \quad H^2 = \frac{8\pi}{3m_{Pl}^2}V(\sigma, \phi). \tag{3}$$

where an overdot denotes d/dt. Hereafter we suppose $\phi \ll \phi_c$. The slow-roll conditions for σ ($|\ddot{\sigma}| \ll |3H\dot{\sigma}|$, $\dot{\sigma}^2/2 \ll V$) are equivalent to

$$\epsilon \equiv \frac{m_{Pl}}{\sqrt{6\pi}\eta} \ll 1, \quad \sigma \ll \sigma_f \equiv \eta\left(1 - \frac{\epsilon}{2}\right). \tag{4}$$

We may regard the time t_f when $\sigma = \sigma_f$ as the time when inflation ends outside the sphere. When $\phi \ll \phi_c$ and (4) are satisfied, the solutions of (3) are

$$N \equiv \ln\frac{a_f}{a} = \frac{\pi}{m_{Pl}^2}\left(2\eta^2 \ln\frac{\sigma_f}{\sigma} + \sigma^2 - \sigma_f^2\right). \tag{5}$$

If we take $\sigma = H_0/2\pi$, (5) gives the total e-foldings during σ-inflation.

While the outer region undergoes inflation, the 3-space is not so curved. Hence, the gravitational mass of the monopole core is approximated by the proper mass:

$$M \sim \frac{4}{3}\pi H_0^{-3}V(0,0)e^{3N} = \frac{H_0^{-1}}{2m_{Pl}^{-2}}e^{3N} = \frac{0.75\times10^{-5}}{\sqrt{\lambda}}\left(\frac{m_{Pl}}{\eta}\right)^2 e^{3N}\ [\mathrm{g}]. \tag{6}$$

If we take $\lambda = 0.001$ and $\eta = m_{Pl}$, for example, (5) gives $N = 28$, and (6) gives $M \sim 10^{33}$g, which is of order of the solar mass. The above estimate is quite rough; we have neglected the effects of spacetime inhomogeneity and of gauge fields completely. Actually, our numerical solutions indicate much larger mass, as shown in the next section. Nevertheless the above arguments are helpful to understand intuitively why massive monopoles can form in our model.

It is instructive to consider the spacetime structure. After ϕ-inflation homonenizes the global spacetime, σ-inflation makes a number of massive black holes. The local spacetime around a single black hole is approximated by Reissner-Nordstörom spacetime. The possible conformal diagram is shown in Fig. 1.

3 Numerical Analysis

In order to demonstrate massive monopoles really form, we solve the field equations numerically. We assume a spherically symmetric spacetime and adopt the coordinate system:

$$ds^2 = -dt^2 + A(t,r)^2dr^2 + B(t,r)^2r^2(d\theta^2 + \sin^2\theta d\phi^2). \tag{7}$$

Our basic equations are the Einstein equations and the field equations for $\sigma(t,r)$, $\phi(t,r)$ and the gauge field function $w(t,r)$. Our numerical method is essentially based on [7], but we improve it in several ways. Our initial conditions are

$$\phi = \phi_c, \quad \sigma = \frac{H_0}{2\pi}\tanh(H_0 r), \quad \dot{\sigma} = \dot{\phi} = 0, \quad A = B = 1. \tag{8}$$

We show an example of the solutions in Fig. 2, where we take $\lambda = 10^{-2}$, $g = 1$, $e = 1$, $\eta = m_{Pl}$, $m = 10^{-3} m_{Pl}$. Figure 2(d) indicates that inflation continues eternally in the monopole core while inflation eventually stops in the outer region. Figure 2(e) reports that the Misner-Sharp mass M_{MS} in the far region grows for a finite time but converges to a constant both in space and in time. Then we may regard the Misner-Sharp mass at the far region as the ADM mass. In this example the final value is $M_{MS} \sim 10 M_\odot$.

Figures 2(a)-(c) show $\sigma \approx \eta$, $\phi \approx 0$, $w \approx 0$ at late time in far regions. If $\sigma = \eta$, $\phi = 0$, $w = 0$ exactly, the spacetime should be Reissner-Nordstörom. Therefore, we believe that the outer spacetime approaches Reissner-Nordstörom. Actually, in this example, we find that black-hole apparent horizons appear at later time, $t \approx 130 H_0^{-1}$.

4 Discussions

We have studied the dynamics of magnetic monopoles in hybrid inflation. If $\sigma \sim m_{Pl}$, created monopoles are astronomically massive. Their mass becomes of order of the solar mass if we choose the parameters appropriately. Therefore, those monopoles could be the origin of MACHOs or other astronomical black holes.

The formation of such massive monopoles or black holes is in principle possible even in the model of a single scalar field model with the potential (1), if we give an initial condition like $(\sigma = H_0/2\pi)\tanh(H_0 r)$. In this model, however, there is no mechanism which provides $\sigma \approx 0$. The essence of hybrid inflation is to give the "initial" condition $\sigma \approx 0$, which makes it possible to create massive black holes.

It is also important to estimate the number density of black holes taking quantum fluctuations of the scalar fields into account to discuss the reality of our model, which is under investigation now.

NS would like to thank D. Ida, K. Nakao, H. Saida and M. Sasaki for discussions, and also Yukawa Institute for Theoretical Physics, where a part of this work has been done as a visitor program. This work was partially supported by the JSPS Grant-in-aid for Scientific Research Fund (Nos. 13640285 and 13740139).

References

[1] A.D. Linde, Phys. Lett. B **327** (1994) 208; A. Vilenkin, Phys. Rev. Lett. **72** (1994) 3137.

[2] N. Sakai, H. Shinkai, T. Tachizawa & K. Maeda, Phys. Rev. **D53** (1996) 655.

[3] N. Sakai, Phys. Rev. **D54** (1996) 1548.

[4] N. Sakai, K. Nakao & T. Harada, Phys. Rev. **D61** (2000) 127302.

[5] A.D. Linde, Phys. Rev. **D49** (1994) 748.

[6] J. Garcia-Bellido, A.D. Linde & D. Wands, Phys. Rev. **D54** (1996) 6040.

[7] N. Sakai, J. Yokoyama & K. Maeda, Phys. Rev. **D59** (1999) 103504.

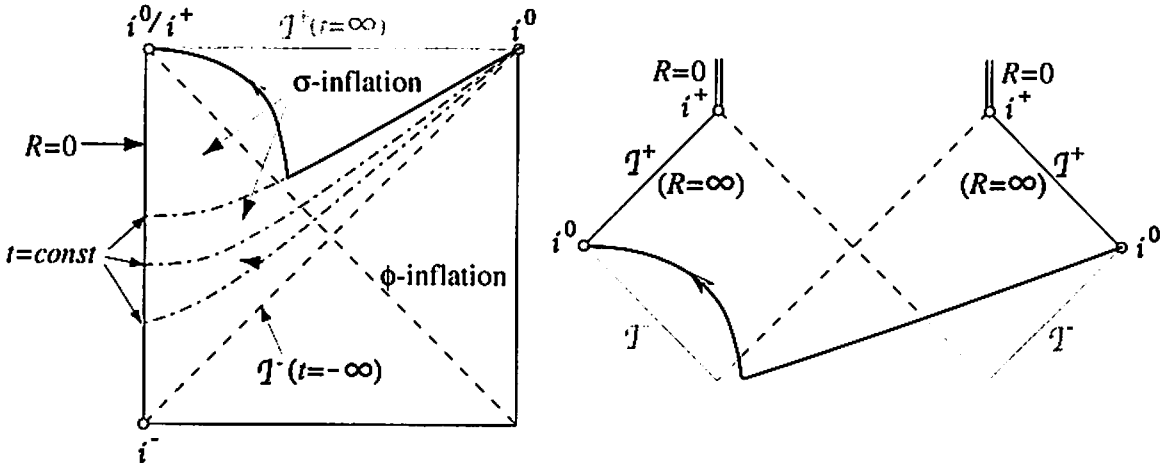
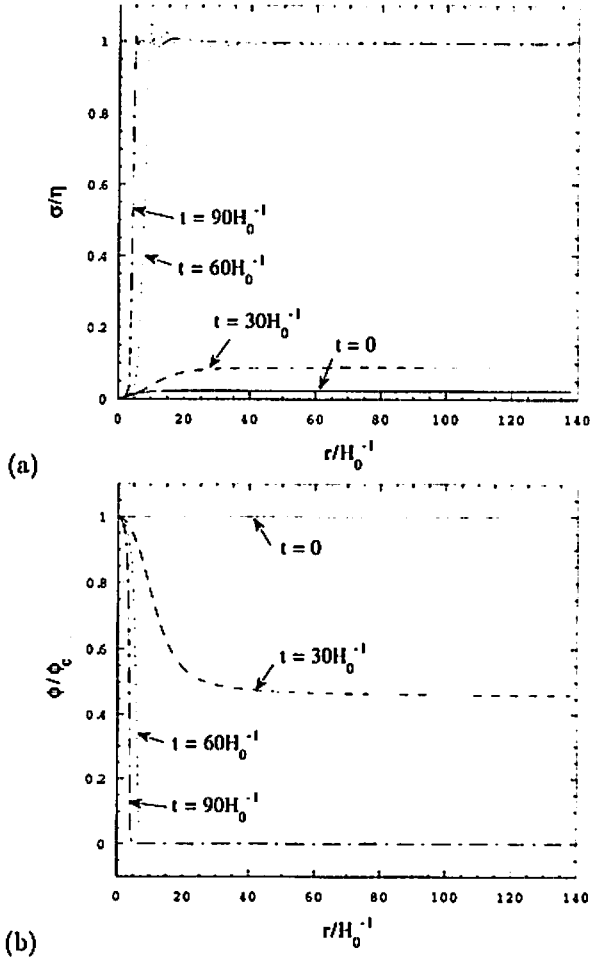
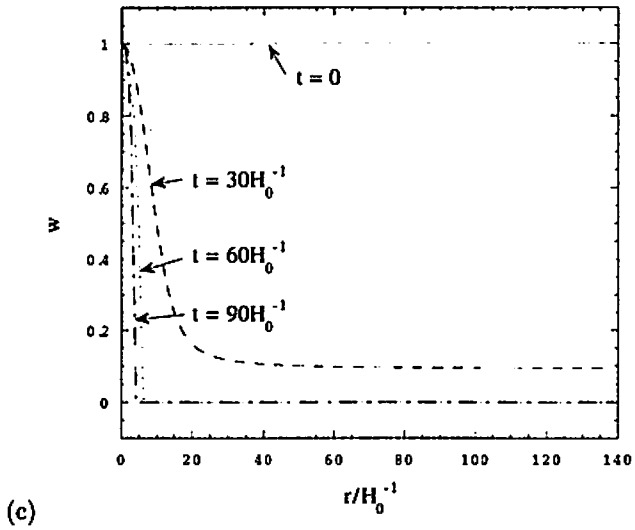
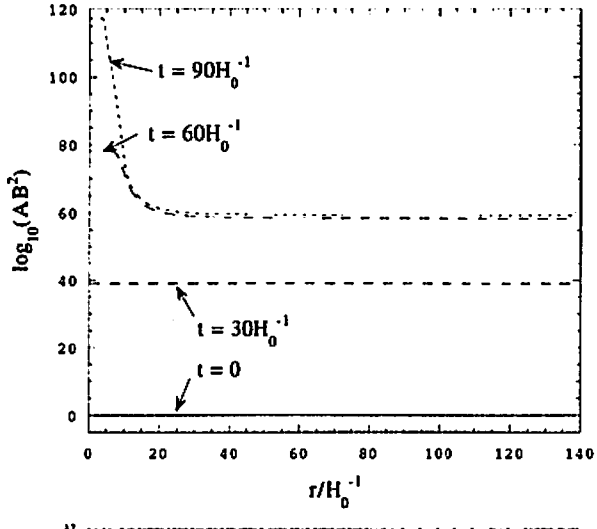


Figure 1: Possible conformal diagram for the spacetime of hybrid monopole inflation. The inflationary region is approximated to be de Sitter spacetime with spatially flat sections. The outside is approximated to be Reissner-Nordstörom spacetime.

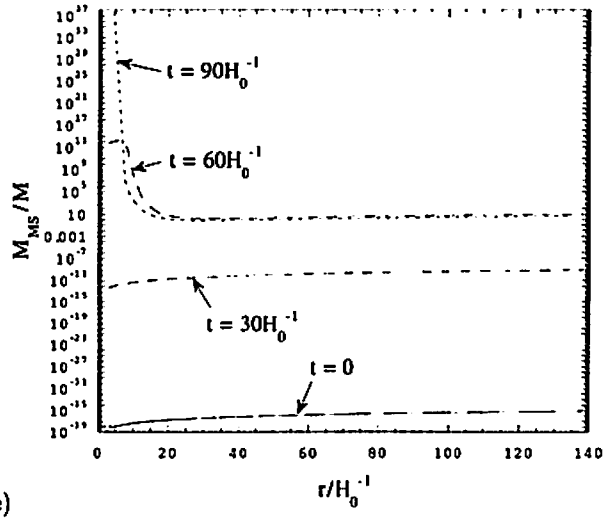




(c)



(d)



(e)

Figure 2: An example of solutions of hybrid monopole inflation. (a), (b), (c), (d) and (e) represent the evolution of the scalar fields σ and ϕ, the gauge field function w, a volume element $\log(AB^2)$ and the Misner-Sharp mass in unit of the solar mass $M_\odot$, respectively.

Discrimination of Quark Stars from Neutron Stars in Quadrupole Oscillations

Koh-ichi Sakata[1] and Yasufumi Kojima[2]

Department of Physics, Hiroshima University, Higashi-Hiroshima 739-8526, Japan

Abstract

Frequencies and decay times due to gravitational radiation are calculated for models of self-bound quark stars. The results are compared with those for models of neutron stars, and it is found that they differ markedly in less relativistic regime. The difference derived here may be relevant to future theoretical and observational studies, because the oscillation properties depend essentially on the mass and radius for an equilibrium star.

1 Introduction

Recently, *Chandra* X-ray observations have been revealed a new aspect of compact stars. The isolated neutron star candidate RX J1856.5-3754, which may be the closest to us, has a radiation radius 3.8–8.2 km [1]. This size is evidently much smaller than that of a neutron star, $\sim$ 12 km. The radiation radius R_∞ is expressed by the stellar radius R in Schwarzschild coordinates and the gravitational mass M as $R_\infty = R\sqrt{1-2GM/Rc^2}$. It is clear that $R \leq R_\infty$. After some algebra, we also find $GM/c^2 \leq R_\infty/(3\sqrt{3})$. The gravitational mass must be less than 0.49–1.05 $M_\odot$, corresponding to the observed value of R_∞. This limit of the mass is significantly less than the canonical mass of a neutron star, $\sim 1.4M_\odot$. It is thus seen that the characteristic size and mass are unusual for any models of neutron stars. However, there have been several attempts to reconcile these observations with the standard models of neutron stars. At present, there is no favorable results of such attempts.

The most simple hypothesis is that RX J1856.5-3754 is not a neutron star, but a quark star due to its high density profile. Nakamura [2] proposed a possible formation scenario of a quark star. It is difficult to produce such a light remnant in the standard scenario of the formation of a neutron star after a supernova. If the progenitor has a significantly rapid rotation, a small core may be left. In such a case, a huge amount of energy can be radiated by gravitational waves, which carry important properties from a source. In particular, we would definitely judge the state of the compact star if a different kind of information such as mass is given by gravitational waves.

Motivated by the above-mentioned observations, we study the properties of models of quark stars. Our concern is dynamical aspects, that is, non-radial oscillations resulting from small disturbance. In particular, we compute the characteristic frequency of the quadrupole f-mode oscillations, which is the most important for gravitational radiation. Extensive calculations of this kind were performed for several non-rotating neutron stars [3, 4], and slowly rotating polytropic models [5]. By extending to models of quark stars, the catalog is enlarged for future gravitational wave astromony. In addition to direct gravitational wave signals, oscillatory phenomena following some kinds of bursts or flares may appear in X-ray and/or gamma-ray observations. Non-spherical distortions efficiently decay due to gravitational wave emission with characteristic frequency and decay time. These properties, irrespective of observational bands and tools, provide useful diagnosis concerning the interior of compact stars. The model and numerical method are summarized in §2. The results are given in §3. In §4, we compare self-bound quark stars with neutron stars with respect to their oscillation frequencies and decay times. Finally in §5, concluding remarks are given.

[1] E-mail:sakata@theo.phys.sci.hiroshima-u.ac.jp
[2] E-mail:kojima@theo.phys.sci.hiroshima-u.ac.jp

2 Models and calculations

Witten [6] conjectured that three-flavor quark matter, consisting of u, d and s quarks, may actually be the ground state of the strong interaction. If this strange matter hypothesis is true, it is quite likely that pure quark stars exist. We consider its equation of state (EOS) phenomenologically, that is, the MIT bag model is used. This model includes the most important aspects of the strong interaction, i.e. asymptotic freedom and the confinement of quarks. By neglecting the mass of quarks and quark-gluon interactions, the EOS can be written as a sum of the free-quark pressure and the bag pressure $-B$ as [7]

$$p = \frac{1}{3}\rho c^2 - \frac{4}{3}\frac{B}{(\hbar c)^3} . \tag{1}$$

Using this EOS, the equilibrium properties of quark stars have been explored in Refs. [7, 8]. A self-bound star has a sharp edge at its surface, corresponding to $p = 0$, and therefore $\rho c^2 = 4B/(\hbar c)^3$. In this case, the density is sufficiently high, and the interior density distribution does not change drastically from the center to the surface. The mass-radius relation for the equilibrium sequence of quark stars has also been calculated. It is expressed by $M \propto R^3$ in the range $M \leq M_\odot$. This relation implies that the average density is constant along the sequence of self-bound quark stars. For the simple EOS (1), the equilibrium models exhibit a scaling law with the bag constant B. In terms of the radii and masses of one sequence of stars with B, those for any other choice of B' can be found from

$$R(B') = \sqrt{B/B'}\, R(B) , \quad M(B') = \sqrt{B/B'}\, M(B) . \tag{2}$$

Here we consider the spherically symmetric equilibrium models and perturbations of them. Oscillation with small amplitude are described by a perturbation of the Einstein equation. Because of the spherical symmetry of the background model, the perturbed quantities can be decomposed into spherical harmonics Y_{lm}. We consider the f-mode of the quadrupole (l=2) only, which is the most important for gravitational radiation. The eigen-frequencies are determined by solving a fourth-order system of differential equations inside the star and a second-order system of differential equations outside the star. They are subject to appropriate boundary conditions. We thus derive the normal frequency in the form of a complex number. The real part $\sigma_{\rm R}$ represents the oscillation frequency, and the imaginary part $\sigma_{\rm I}$ represents the decay rate. The equations and numerical methods are summarized in detail in Ref. [5]

3 Results

The oscillation frequency and the decay rate for the EOS (1) have already been calculated for only a few stellar models [4]. Here we extend this kind of calculation to much larger range of stellar models in order to understand general properties. The angular frequency $\sigma_{\rm R}$ is plotted as a function of the compactness GM/Rc^2 in Fig. 1. The frequency is normalized by $\Omega_{\rm K} = \sqrt{GM/R^3}$. The results for $n = 1$, 0.5 and 0.2 of polytropic EOS $p = K\rho^{1+1/n}$ are also shown in Fig. 1. The oscillation frequencies for the EOS (1) can be approximated in the same manner as stellar models with smaller $n \approx 0$. Because the case of smaller n corresponds to the uniform density model and quark star have also uniform density profile mentioned in §2. We find that the agreement in the Newtonian limit becomes better as $n \to 0$, but the overall agreement over some range of GM/Rc^2 is not realized for any value of n. Thus, models of quark stars are approximated by the polytropic model with $n \approx 0$ in less relativistic regime. The uniform density profile do not keep at large GM/Rc^2 due to the effect of gravity.

In Fig. 2, we plot the decay rate $\sigma_{\rm I}$ of the mode. The characteristic decay rate can be evaluated using the energy loss rate with the quadrupole radiation formula, $\sigma_{\rm I} = dE/dt/(2E) \propto (GM)^3/(R^4c^5)$. We use this scale as the normalization in Fig. 2. The dependence of the compactness is also very similar to that found in the model with small n. In this way, the general behavior of the frequency and the decay rate for the EOS (1) can be described by the results for stellar models with polytrope index $n \approx 0$. The general properties of oscillation depend on the density profile of the star.

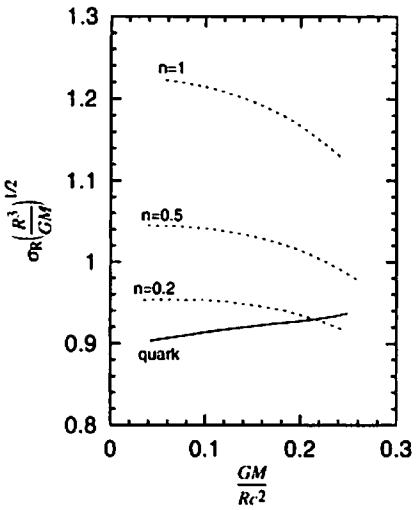


Figure 1: Angular frequencies of quadrupole f-mode oscillation as functions of star compactness. The solid and dotted curves correspond to quark and polytropic stars, respectively.

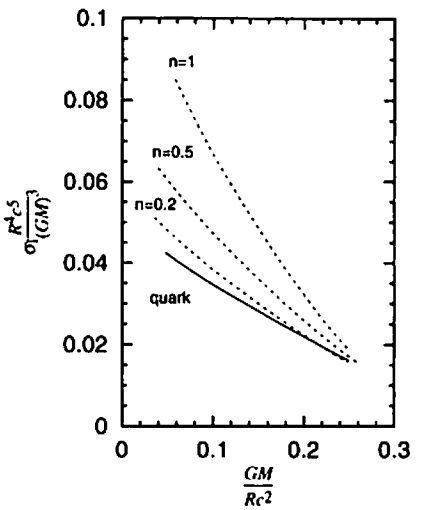


Figure 2: Decay rates of quadrupole f-mode oscillation as functions of star compactness. The solid and dotted curves correspond to quark and polytropic stars, respectively.

4 Comparison among various models

The frequency of the self-bound quark-star model also exhibits the scaling $\sigma \propto \sqrt{M/R^3} \propto \sqrt{B}$. The bag constant B has not been precisely determined, but is usually chosen as $B^{1/4} = 145$–165 MeV [7, 8]. We use $B^{1/4} = 155$ MeV, i.e. an energy density of $B/(\hbar c)^3 = 75$ MeV/fm^3, as a representative example. The energy density at the stellar surface, $4B/(\hbar c)^3$, corresponds to approximately twice the energy of normal nuclear matter, $\rho_n c^2 = 141$ MeV/fm^3 ($= 2.5 \times 10^{14}$ g/cm^3). We also give the results scaled to $B^{1/4} = 180$ MeV, i.e. $B/(\hbar c)^3 = 137$ MeV/fm^3. In Fig. 3, we display the frequency $\nu = \sigma_R/2\pi$ of quadrupole oscillations along the sequence of quark stars with a fixed value of B. We also include the results for various neutron-star models there. Many EOSs have been proposed for high-density neutron matter, but only selected EOSs are used. This set of EOSs might be out of date, but it covers the range from soft to stiff EOSs. We do not consider EOSs that are too soft, that is, those that yield a maximum mass of neutron stars below 1.4 $M_\odot$. The four models we consider are denoted by A, BJ, PPS-T and PPS-M in Fig. 3. Descriptions of these EOSs are also given elsewhere [3].

There is a large difference between the dependences on the compactness GM/Rc^2 of the frequencies for gravitationally bound and self-bound stars. In the equilibrium sequence of neutron stars, the oscillation frequency increases with GM/Rc^2, because the mass increases and the radius decreases, and hence $\nu \propto \sqrt{GM/R^3}$ increases rapidly. In order to understand this property, we labeled the average densities $3M/4\pi R^3$ along each equilibrium sequence in Fig. 3. They are normalized by the nuclear density ρ_n. Contrastingly, both the mass and radius in the sequence of self-bound quark star models increase as $M \propto R^3$, and hence the oscillation frequency is almost constant, i.e. $\nu \propto \sqrt{GM/R^3} \approx$ constant. Actually, the average density of the model of $B^{1/4} = 155$ MeV varies within the range 2.1–3.2 ρ_n, and it is almost constant in less relativistic regime. In the case of $B^{1/4} = 180$ MeV, it varies within the range 3.9–5.9 ρ_n. The frequency ν of a quark star is approximated as

$$\nu = \frac{\sigma_R}{2\pi} \approx 1.7 \times \left\{1 + 4\left(\frac{GM}{Rc^2}\right)^2\right\} \left(\frac{B^{1/4}}{155\ \text{MeV}}\right)^2 \text{kHz} . \tag{3}$$

The dependence on the bag constant B is exact, but relativistic correction in the braces is introduced so as to be fitted in the range $GM/Rc^2 \leq 0.25$. In general, the frequencies of quark stars are discriminated from those of neutron stars in a less relativistic regime. In that case, the radius of the quark star is much smaller, and the frequency is higher.

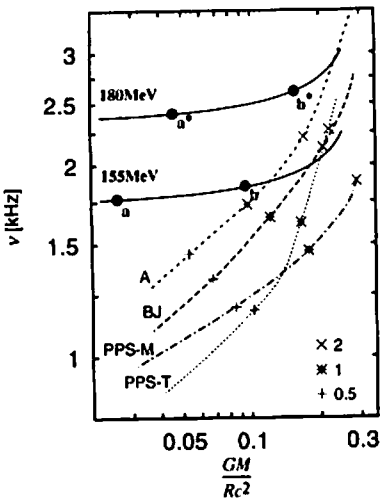


Figure 3: Frequencies in units of kHz as functions of stellar compactness. The solid curves correspond to the quark star models with two different values of the bag constant. Other curves correspond to neutron star models based on different equations of state. The symbols on the curves for neutron star models indicate the average density normalized by the nuclear density. (See the text for details.)

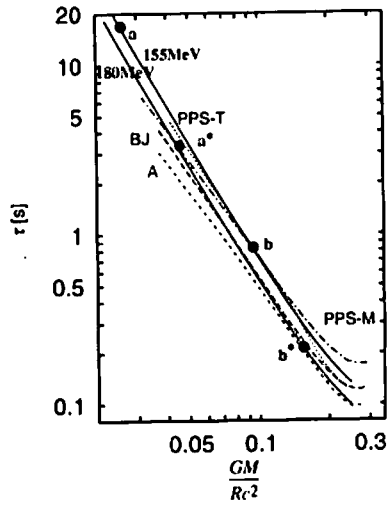


Figure 4: Decay times in units of seconds as functions of stellar compactness. The solid curves correspond to the quark star models with two different values of the bag constant. Other curves correspond to neutron star models based on different equations of state. (See the text for details.)

In Fig. 4, we plot the decay time $\tau = 1/\sigma_I$ for self-bound quark stars and neutron stars. It is seen that the decay times of both stellar models depend strongly on the compactness GM/Rc^2. We found that there is not such a clear difference unlike in the case of the oscillation frequency. The decay time τ for the EOS (1) is approximated as

$$\tau = \frac{1}{\sigma_I} \approx 1.7 \times 10^{-3} \left\{ 1 + 12 \left(\frac{GM}{Rc^2} \right)^{3/2} \right\} \left(\frac{GM}{Rc^2} \right)^{-5/2} \left(\frac{B^{1/4}}{155 \text{ MeV}} \right)^{-2} \text{s} . \tag{4}$$

This formula provides the exact dependence on the bag constant B and the value in the Newtonian limit. The expression in the braces of Eq. (4) is the relativistic correction, which fits the results in the range $GM/Rc^2 \leq 0.25$. In Figs. 3 and 4, we only show the results for two choices of B, but results can easily be obtained for the other choices using Eqs. (3) and (4).

From these figures, we can discriminate quark stars from neutron stars using the frequencies ν and the decay times τ of their oscillations. Suppose that we have such informations from a star simultaneously. In Fig. 4, we can determine the range of stellar compactness GM/Rc^2 regardless of models of a star. In Fig. 3, we can identify the stellar model in that range of GM/Rc^2, whether it is a quark star with one bag constant B or a neutron star with one EOS. Note that this method works at least in the case of less relativistic regime ; if $GM/Rc^2 \geq 0.1$, it is difficult to identify the model of a star in Fig. 3. We expect that quark stars are realized in a less relativistic regime.

We now apply our results to the parameters inferred from the quark star candidate RX J1856.5-3754. This compact star has small radiation radius, $\sim 3.8 - 8.2$ km, as mentioned in §1. This information provides one constraint on the mass M and radius R. In Table 1, we show the possible mass and radius corresponding to the observed radiation radius of RX J1856.5-3754 assumed that $B^{1/4} = 155$ MeV and 180 MeV. When the oscillation frequency and the decay time for RX J1856.5-3754 are given by observations, it is likely possible to know its model of the structure, i.e. the bag constant if it is a quark star.

$B^{1/4}$ (MeV)	R_∞ (km)	M ($M_\odot$)	R (km)	label
155	4.0	0.068	3.8	a
155	8.0	0.46	7.2	b
180	4.0	0.12	3.8	a*
180	8.0	0.70	6.6	b*

Table 1: The mass and the radius corresponding to RX J1856.5-3754 assumed that $B^{1/4} = 155\,\mathrm{MeV}$ and $180\,\mathrm{MeV}$. The last column means the labels in Figs. 3 and 4.

5 Concluding remarks

In this paper, we have presented suggestive results regarding the pulsations associated with gravitational radiation. Gravitational waves carry key information concerning their sources. We can in principle use them as probes of compact stars. The oscillation frequency scales with the average density of a star as $\nu \propto \sqrt{M/R^3}$, because the f-mode has no radial node. The decay time due to gravitational radiation depends significantly on the relativistic factor GM/Rc^2. It may be possible to utilize these properties to discriminate self-bound quark stars from gravitationally bound neutron stars. If self-bound quark stars are realized in a less relativistic regime, the oscillation frequency would be high enough due to the high density, but the decay time would be longer than that of a neutron star. In that case, the mass and size would be quite different in the equilibrium sequences of the two types of compact stars. It is clear that the present self-bound quark model is too crude. This model is used to carry out explicit calculations, but the resultant properties of the oscillations depend roughly on the macroscopic values, such as the mass and radius. We therefore believe that such properties should be included in any realistic model.

Finally, we comment on the astrophysical relevance of quadrupole f-mode oscillation. The driving mechanism like Cepheid variables is not yet known, so that persistent oscillations would not be observed. Rather, abrupt changes of the structure, like formation [2] and/or some kinds of bursts may be relevant. The origin and nature of these events are also unclear at the moment. However, it is evident that gravitational wave emission is crucial in such a dynamical process. The most efficient mode is the quadrupole ($l = 2$) f-mode, which was calculated here. We should wait for a fully relativistic numerical calculation to simulate violent events, but the oscillation frequency may be used even to check the numerical code.

References

[1] J.J. Drake et al., Astrophys. J. **572**, 996 (2002).

[2] T. Nakamura, Astro-ph/0205526 (2002).

[3] L. Lindblom and S.L. Detweiler, Astrophys. J. Suppl. **53**, 73 (1983).

[4] C. Cutler, L. Lindblom and R.J. Splinter, Astrophys. J. **363**, 603 (1990).

[5] Y. Kojima, Prog. Theor. Phys. Suppl. **128**, 251 (1997).

[6] E. Witten, Phys. Rev. D **30**, 272 (1984).

[7] N.K. Glendenning, *Compact Stars* (Springer-Verlag New York, 1996).

[8] C. Alcock, E. Farhi and A.V. Olinto, Astrophys. J. **310**, 261 (1986).

Non-linear Gravity on Branes and Effective Action

Jiro Soda,[1] Sugumi Kanno [2]

[1] *Department of Fundamental Sciences, FIHS, Kyoto University, Kyoto 606-8501, Japan*

[2] *Graduate School of Human and Environmental Studies, Kyoto University, Kyoto 606-8501, Japan*

Abstract

We develop the general formalism to study the low energy regime of the brane world. We apply our formalism to the single brane model where the AdS/CFT correspondence will take an important role. We also consider the two-brane system and show the system is described by the quasi-scalar tensor gravity. Our result provides a basis for predicting CMB fluctuations in the braneworld models.

1 Introduction

The existence of the initial singularity in the standard cosmology is a notorious problem which is expected to be solved by taking into account the quantum effects of the gravity. It is widely accepted that the superstring theory is the most promising candidate for the quantum theory of gravity. One prominent feature of the superstring theory is the existence of the extra dimensions. To fill the gap between this theoretical prediction and our 4-dimensional universe, we need to hide the extra dimensions someway. The conventional idea is the Kaluza-Klein compactification scenario where the internal dimensions are assumed to be compactified to the Planck scale. Recently, however, a new picture, the so-called braneworld, has emerged thanks to the developments of the non-perturbative aspects of the superstring theory [1, 2]. In the braneworld picture, the ordinary matter exists on the brane while the gravity can propagate in the bulk. In particular, we are on the brane! Hence, what we would like to know is how the non-linear gravity appears on the brane. In general, it would be difficult to get such a description due to the strong coupling of the bulk degrees of freedom with those of the brane. However, in the low energy regime $\frac{\rho}{\sigma} \sim \ell^2 R \ll 1$, it is possible to obtain the 4-dimensional effective theory approximately [3, 4, 5]. Indeed, this is sufficient except for the extreme situation for which we need more profound understanding of the string theory. For example, if we take the curvature scale ℓ as 10^{-16}cm, our approximation is valid at the energy scale below 10^{11}GeV or the gravitational radius greater than 10^{-21}km. In fact, this is the interesting regime for most astrophysical and cosmological phenomena. In this paper, we review our recent results on this issue [4, 5].

In the next section, we will develop the general formalism. In sec.3, we apply our formalism to the single brane model where the AdS/CFT correspondence will play an important role. In sec.4, we consider the two-brane system and show the system is described by the quasi-scalar tensor gravity. Sec.5 is devoted to the conclusion.

2 General Formalism

If there exists no matter, the ground state is the Minkowski spacetime in the 4-dimensional theory. Correspondingly, if there exists no matter on the brane, we would expect the induced metric on the brane is Minkowski and the bulk geometry is the Anti-deSitter spacetime. Indeed, we have such solution

$$ds^2 = dy^2 + \Omega^2(y)\eta_{\mu\nu}dx^\mu dx^\nu \ ,$$

where $\Omega^2 = \exp[-2y/\ell]$ is the warp factor. The brane is located at $y = 0$ in this coordinate system. To obtain the above solution we have imposed the relation $\kappa\sigma = 6/\ell$.

[1] E-mail:jiro@phys.h.kyoto-u.ac.jp

[2] E-mail:kanno@phys.h.kyoto-u.ac.jp

Let us put the small amount of matter on the brane. Then, the brane will be curved and the bulk geometry will be deformed as

$$ds^2 = dy^2 + \left(\Omega^2(y)h_{\mu\nu}(x) + \delta g_{\mu\nu}(y, x^\mu)\right) dx^\mu dx^\nu \ , \tag{1}$$

where the boundary condition $\delta g_{\mu\nu}(y = 0, x^\mu) = 0$ is imposed so that $h_{\mu\nu}$ becomes the induced metric on the brane. How the geometry will be deformed is determined by the 5-dimensional Einstein equations:

$$G^{(5)}_{AB} = \frac{6}{\ell^2} g_{AB} + \delta(y) 8\pi G_N \ell \left(-\sigma g_{\mu\nu} + T_{\mu\nu}\right) \delta^\mu_A \delta^\nu_B \ , \quad A = (y, \mu) \ , \tag{2}$$

where $T_{\mu\nu}$ is the energy-momentum tensor of the matter. As we are considering the deviation from the Anti-deSitter spacetime, it is convenient to define the variables

$$\delta K^\mu_{\ \nu} = -\frac{1}{2}\delta\left[g^{\mu\alpha} g_{\alpha\nu,y}\right] \equiv \delta\Sigma^\mu_{\ \nu} + \frac{1}{4}\delta^\mu_{\ \nu}\delta K \ , \tag{3}$$

where $\delta\Sigma^\mu_{\ \mu} = 0$. In terms of these variables, the Hamiltonian constraint equation becomes

$$\delta K = -\frac{\ell}{6}\left[\frac{3}{4}\delta K^2 - \delta\Sigma^\mu_{\ \nu}\delta\Sigma^\nu_{\ \mu} - \overset{(4)}{R}\right] \tag{4}$$

and the momentum constraint equation reads

$$\nabla_\lambda \delta\Sigma^\lambda_{\ \mu} - \frac{3}{4}\nabla_\mu \delta K = 0 \ . \tag{5}$$

The evolution equation in the direction to y is

$$\frac{1}{\Omega^4}\left[\Omega^4 \delta\Sigma^\mu_{\ \nu}\right]_{,y} = \delta K \delta\Sigma^\mu_{\ \nu} - \left[\overset{(4)}{R}{}^\mu_{\ \nu}\right]_{\text{traceless}} \ . \tag{6}$$

As we have the singular source at the brane position, we must take into account the junction condition,

$$\frac{2}{\ell}\left[\delta\Sigma^\mu_{\ \nu} - \frac{3}{4}\delta^\mu_\nu \delta K\right]\Big|_{y=0} = 8\pi G_N T^\mu_{\ \nu} \ , \tag{7}$$

where we have imposed the Z_2 symmetry on the spacetime.

After solving the bulk equations of motion, the junction condition gives the effective equations of motion for the induced metric. By integrating the evolution equation, we have

$$\begin{aligned}
\frac{2}{\ell}\left[\delta\Sigma^\mu_{\ \nu} - \frac{3}{4}\delta^\mu_\nu \delta K\right] &= -\frac{\ell^2 \chi^\mu_{\ \nu}}{\Omega^4} - \frac{2}{\ell\Omega^4}\int^y dy \Omega^4 \left[\overset{(4)}{R}{}^\mu_{\ \nu} - \frac{1}{4}\delta^\mu_\nu \overset{(4)}{R} - \delta K \delta\Sigma^\mu_{\ \nu}\right] \\
&\quad - \frac{1}{4}\delta^\mu_\nu \overset{(4)}{R} + \frac{1}{4}\delta^\mu_\nu \left[\frac{3}{4}\delta K^2 - \delta\Sigma^\mu_{\ \nu}\delta\Sigma^\nu_{\ \mu}\right] \\
&= -\frac{\ell^2 \chi^\mu_{\ \nu}(x)}{\Omega^4(y)} + \overset{(4)}{G}{}^\mu_{\ \nu}\left(\Omega^2(y) h_{\mu\nu}(x)\right) + \mathcal{O}(\ell^4 R^2) \ ,
\end{aligned}$$

where we introduced the constants of integration $\chi_{\mu\nu}$. This integration can be performed iteratively with the expansion parameter $\ell^2 R$. The resulting equations take the form

$$\overset{(4)}{G}{}^\mu_{\ \nu}\left(\Omega^2|_{y=0} h_{\mu\nu}\right) = 8\pi G_N T^\mu_{\ \nu} + \frac{\ell^2}{\Omega^4|_{y=0}}\chi^\mu_{\ \nu} + t^\mu_{\ \nu} \ , \tag{8}$$

where we have included the trivial factor $\Omega|_{y=0} = 1$ for memorizing how the warp factor comes in to the effective theory. Here we have decomposed the corrections to the conventional Einstein theory into the nonlocal part $\chi_{\mu\nu}$ and the local part $t_{\mu\nu}$.

We can expand these corrections in the order of the $\ell^2 R$:

$$\text{Nonlocal} \quad \chi_{\mu\nu} = \underbrace{\chi^{(1)}_{\mu\nu}}_{\mathcal{O}(\ell^2 R)} + \underbrace{\chi^{(2)}_{\mu\nu}}_{\mathcal{O}(\ell^4 R^2)} + \cdots \tag{9}$$

$$\text{Local} \quad t_{\mu\nu} = \underbrace{t^{(2)}_{\mu\nu}}_{\mathcal{O}(\ell^4 R^2)} + \underbrace{t^{(3)}_{\mu\nu}}_{\mathcal{O}(\ell^6 R^3)} + \cdots \tag{10}$$

where the expansion of the local tensor starts from the second order because the first order part is already included as the Einstein tensor. Notice that we have $\chi^{(1)\mu}{}_{\mu} = 0$ because of $\Sigma^{\mu}_{\ \mu} = 0$.

3 Single Brane Model (RS2): AdS/CFT correspondence

Now we shall apply the general formalism to the single brane model [4]. A natural boundary condition for the single brane model is to impose the regularity at the Cauchy horizon, namely asymptotically AdS boundary condition. Taking this boundary condition, we obtain $\chi^{(1)}_{\mu\nu} = 0$. Thus, we have recovered Einstein theory at the leading order.

At the next order $\mathcal{O}(l^4 R^2)$, the traceless part of $t^{(2)}_{\mu\nu}$ is proportional to

$$\begin{aligned} \mathcal{S}^{\mu}_{\nu} &= R^{\mu}{}_{\alpha} R^{\alpha}{}_{\nu} - \frac{1}{3} R R^{\mu}{}_{\nu} - \frac{1}{4}\delta^{\mu}_{\nu}(R^{\alpha}{}_{\beta} R^{\beta}{}_{\alpha} - \frac{1}{3}R^2) \\ &\quad - \frac{1}{2}\left(R^{\alpha\mu}{}_{|\nu\alpha} + R^{\alpha}{}_{\nu}{}^{|\mu}{}_{|\alpha} - \frac{2}{3} R^{|\mu}_{|\nu} - \Box R^{\mu}{}_{\nu} + \frac{1}{6}\delta^{\mu}_{\nu}\Box R \right) \end{aligned} \tag{11}$$

where $\mathcal{S}^{\mu}{}_{\nu|\mu}$ is transverse and traceless: $\mathcal{S}^{\mu}{}_{\nu|\mu} = 0$, $\mathcal{S}^{\mu}_{\ \mu} = 0$. The nonlocal part $\tilde{\chi}^{(2)}_{\mu\nu} = \chi^{(2)}_{\mu\nu} + 1/4 h_{\mu\nu} t^{(2)\mu}{}_{\mu}$ can not be determined by the Einstein equations, but constrained as

$$\tilde{\chi}^{(2)\mu}_{\ \ \mu} = -\frac{1}{8}\left(R^{\alpha}{}_{\beta} R^{\beta}{}_{\alpha} - \frac{1}{3} R^2 \right) .$$

Here, the AdS/CFT correspondence comes in. As the trace anomaly for some supersymmetric theories proportional to the above result, we make the following identification

$$\tilde{\chi}^{(2)}_{\mu\nu} = \frac{\kappa^2}{\ell^3} T^{\rm CFT}_{\mu\nu} . \tag{12}$$

Note that the effective number of the CFT fields $\ell^3/\kappa^2 \sim \ell^2/G \sim 10^{66}$ is so huge. This is the regime where AdS/CFT correspondence holds.

Thus, the effective equations of motion become

$$G^{(4)}_{\mu\nu} = 8\pi G_N T_{\mu\nu} + 8\pi G_N T^{\rm CFT}_{\mu\nu} + \alpha \mathcal{S}^{\mu}_{\ \nu} . \tag{13}$$

Seeing Eq.(11), one can read off the effective action

$$S_{\rm eff} = \frac{1}{16\pi G_N}\int d^4x\sqrt{-h}R + S_{\rm matter} + S_{CFT} + \frac{\alpha\ell^2}{16\pi G_N}\int d^4x\sqrt{-h}\left[R^{\mu\nu}R_{\mu\nu} - \frac{1}{3}R^2 \right] . \tag{14}$$

Now one can consider the cosmology using the above effective theory. One can obtain the renormalized action for the CFT, $S^{\rm CFT}$, then we can deduce the one point function from the formula

$$< T^{\rm CFT}_{\mu\nu} >= -\frac{2}{\sqrt{-g}}\frac{\delta S^{\rm CFT}}{\delta g^{\mu\nu}} .$$

The two point correlation function can be also calculated as

$$< T^{\rm CFT}_{\mu\nu}(x) T^{\rm CFT}_{\lambda\rho}(y) >= -\frac{2}{\sqrt{-g}}\frac{\delta < T^{\rm CFT}_{\mu\nu}(x) >}{\delta g^{\lambda\rho}(y)} .$$

Thus, we obtain the perturbed effective Einstein Equations

$$\delta G_{\mu\nu} = 8\pi G_N \delta T_{\mu\nu} - \frac{1}{2}\int d^4y\sqrt{-g(y)} < T^{\rm CFT}_{\mu\nu}(x) T^{\rm CFT\lambda\rho}(y) > \delta g_{\lambda\rho} + \alpha\delta t^{(2)}_{\mu\nu} \ . \tag{15}$$

This is nothing but the integro-differential equation. It is possible in principle to solve numerically the linearized equations of motion in the cosmological situation. We leave this for the future work.

4 Two Brane Model (RS1): Radion

In this section, we will consider the two-brane system which is more realistic from the M-theory point of view [3, 5](see also [6]). In the two-brane system, the radion field plays an important role. The radion is defined as the distance between the positive tension brane and the negative tension brane, $d(x)$. Now the warp factor $\Omega^2 = \exp[-2d(x)/\ell]$ becomes dynamical variable.

The general formula gives the equation on the positive tension brane:

$$G^{(4)\mu}{}_{\nu}(h_{\mu\nu}) = \frac{\kappa^2}{\ell} T^{\oplus\mu}{}_{\nu} + \ell^2 \chi^{(1)\mu}{}_{\nu} \tag{16}$$

where $\chi_{\mu\nu}$ represents the effect of the bulk geometry on the brane. Importantly, this equation holds irrespective of the existence of the other brane. Similarly, the equation of motion on the negative tension brane is given by

$$G^{(4)\mu}{}_{\nu}(f_{\mu\nu} = \Omega^2 h_{\mu\nu}) = -\frac{\kappa^2}{\ell} T^{\ominus\mu}{}_{\nu} + \frac{\ell^2}{\Omega^4}\chi^{(1)\mu}{}_{\nu} \tag{17}$$

where $f_{\mu\nu}$ is the induced metric on the negative tension brane. Here, the effect of the bulk geometry enhanced by the factor $1/\Omega^4$ since the bulk geometry shrinks towards to the negative tension brane. Although Eqs. (16) and (17) are non-local individually, with undetermined $\chi^{(1)}_{\mu\nu}$, one can combine both equations to reduce them to local equations for each brane. This happens to be possible since $\chi^{(1)}_{\mu\nu}$ appears only algebraically; one can easily eliminate $\chi^{(1)}_{\mu\nu}$ from Eqs. (16) and (17). Defining a new field $\Psi = 1 - \Omega^2$, we find

$$\begin{aligned}\frac{\ell^3}{2}\chi^{(1)\mu}{}_{\nu} &= -\frac{\kappa^2(1-\Psi)}{2\Psi}\left(T^{\oplus\mu}{}_{\nu} + (1-\Psi)T^{\ominus\mu}{}_{\nu}\right) \\ &\quad -\frac{l}{2\Psi}\left[\left(\Psi^{|\mu}{}_{|\nu} - \delta^{\mu}_{\nu}\Psi^{|\alpha}{}_{|\alpha}\right) + \frac{3}{2(1-\Psi)}\left(\Psi^{|\mu}\Psi_{|\nu} - \frac{1}{2}\delta^{\mu}_{\nu}\Psi^{|\alpha}\Psi_{|\alpha}\right)\right] \ .\end{aligned}$$

The condition $\chi^{(1)\mu}{}_{\mu} = 0$ gives the equations of motion for the radion field:

$$\Box\Psi = \frac{\kappa^2}{3\ell}(1-\Psi)\left\{T^{\oplus} + (1-\Psi)T^{\ominus}\right\} - \frac{1}{2(1-\Psi)}\Psi^{|\mu}\Psi_{|\mu} \ . \tag{18}$$

Interestingly, we can rearrange the above equations as

$$G^{\mu}{}_{\nu}(h) = \frac{\kappa^2}{\ell\Psi}T^{\oplus\mu}{}_{\nu} + \frac{\kappa^2(1-\Psi)^2}{l\Psi}T^{\ominus\mu}{}_{\nu} + \frac{1}{\Psi}\left(\Psi^{|\mu}{}_{|\nu} - \delta^{\mu}_{\nu}\Psi^{|\alpha}{}_{|\alpha}\right) + \frac{\omega(\Psi)}{\Psi^2}\left(\Psi^{|\mu}\Psi_{|\nu} - \frac{1}{2}\delta^{\mu}_{\nu}\Psi^{|\alpha}\Psi_{|\alpha}\right) \tag{19}$$

and

$$\Box\Psi = \frac{\kappa^2}{\ell}\frac{T^{\oplus} + (1-\Psi)T^{\ominus}}{2\omega(\Psi)+3} - \frac{1}{2\omega(\Psi)+3}\frac{d\omega(\Psi)}{d\Psi}\Psi^{|\mu}\Psi_{|\mu} \ , \tag{20}$$

where the coupling function $\omega(\Psi)$ takes the following form: $\omega(\Psi) = 3\Psi/2(1-\Psi)$. We named this system as the quasi-scalar-tensor theory. Eqs.(19) and (20) can be derived from

$$S_A = \frac{l}{2\kappa^2}\int d^4x\sqrt{-h}\left[\Psi R(h) - \frac{3}{2(1-\Psi)}\Psi^{|\alpha}\Psi_{|\alpha}\right] + \int d^4x\sqrt{-h}\mathcal{L}^{\oplus} + \int d^4x\sqrt{-h}\,(1-\Psi)^2\,\mathcal{L}^{\ominus} \ . \tag{21}$$

This is the effective action on the positive tension brane.

The effective action on the negative tension brane can be also derived in the similar way as

$$S_B = \frac{l}{2\kappa^2}\int d^4x\sqrt{-f}\left[\Phi R(f) + \frac{3}{2(1+\Phi)}\Phi^{;\alpha}\Phi_{;\alpha}\right] + \int d^4x\sqrt{-f}\mathcal{L}^{\ominus} + \int d^4x\sqrt{-f}(1+\Phi)^2\mathcal{L}^{\oplus}\ , \quad (22)$$

where $\Phi = 1/\Omega^2 - 1$.

Thus, we have derived a closed set of equations (19) and (20). By solving these equations, we can know the anisotropic stress $\chi^{(1)}_{\mu\nu}$ explicitly. Now, we can make a precise predictions on the CMB fluctuations! This will be reported somewhere else.

5 Conclusion

We have developed the general formalism to obtain the effective action in the low energy regime.

In the case of the single brane model, by imposing asymptotically AdS boundary condition, we have obtained the Einstein theory with corrections represented by CFT and higher curvature polynomial. It is suggested that the cosmological perturbation theory in the brane world can be formulated as the integro-differential equations.

In the case of the two-brane model, we have shown that the system is described by the quasi-scalar-tensor theory. Equivalently, it can be regarded as the Einstein theory with the extra energy source, $\chi^{(1)}_{\mu\nu}$ corresponding to the dark radiation in the homogeneous cosmological case. This turns out to be determined by the radion field and the energy momentum tensors on positive and negative tension branes. The next order corrections due to Kalza-Klein massive modes can be represented by the higher curvature terms. It is interesting to study the cosmological scenario based on the effective action we have derived [7].

Acknowledgements

This work was supported in part by the Monbukagakusho Grant-in-Aid for Scientific Research, Nos. 14540258.

References

[1] I. Antoniadis, N. Arkani-Hamed, S. Dimopoulos and G. R. Dvali, Phys. Lett. B **436**, 257 (1998) [arXiv:hep-ph/9804398]; P. Horava and E. Witten, Nucl. Phys. B **460**, 506 (1996) [arXiv:hep-th/9510209]; P. Horava and E. Witten, Nucl. Phys. B **475**, 94 (1996) [arXiv:hep-th/9603142].

[2] L. Randall and R. Sundrum, Phys. Rev. Lett. **83**, 3370 (1999) [arXiv:hep-ph/9905221].

[3] T. Wiseman, Class. Quant. Grav. **19**, 3083 (2002) [arXiv:hep-th/0201127].

[4] S. Kanno and J. Soda, Phys. Rev. D **66**, 043526 (2002) [arXiv:hep-th/0205188].

[5] S. Kanno and J. Soda, Phys. Rev. D **66**, 083506 (2002) [arXiv:hep-th/0207029].

[6] S. Kanno and J. Soda, "Braneworld effective action at low energies," arXiv:gr-qc/0209087; J. Soda and S. Kanno, "Holographic view of cosmological perturbations," arXiv:gr-qc/0209086; T. Shiromizu and K. Koyama, "Low energy effective theory for two brane systems: Covariant curvature formulation," arXiv:hep-th/0210066.

[7] S. Kanno, M. Sasaki and J. Soda, "Born-again braneworld," to appear in Prog. Teor. Phys., arXiv:hep-th/0210250.

Nonradial oscillations of quark stars

Hajime Sotani,[1] Tomohiro Harada[2]

Department of Physics, Waseda University, Okubo 3-4-1, Shinjuku, Tokyo 169-8555, Japan

Abstract

Recently, it has been reported that a candidate for a quark star may have been observed. In this article, we pay attention to quark stars with radiation radii in the reported range. We calculate nonradial oscillations of w-, $w_{\rm II}$- and f-modes. Then, we find that the dependence of the lowest $w_{\rm II}$-mode quasi-normal frequency on the bag constant and stellar radiation radius is very strong and different from that of the f-mode quasi-normal frequency. Therefore, the observation of gravitational waves both of the f-mode and of the lowest $w_{\rm II}$-mode would provide a powerful probe of the equation of state of quark matter and the properties of quark stars.

1 Introduction

Since the 1980s, there have been many studies about objects known as quark stars. If the true ground state of matter is not the nuclear state but a quark state as Witten conjectured [1], there may exist objects composed of quark matter. For simplicity, the bag model equation of state (EOS) has often been used for studying quark matter. Lattimer and Prakash calculated stellar properties with this EOS [2]. In reality, it is quite difficult to determine the EOS of quark matter by experiments on the ground, because quark matter will appear at extremely high density. In this respect, the observation of astrophysical compact objects may be a unique means to determine the EOS for cold high-density matter [3, 4].

Recently, the radiation radius of the compact star RXJ185635-3754 was estimated to be very small ($3.8{\rm km} \lesssim R_\infty \lesssim 8.2{\rm km}$) based on X-ray observations by *Chandra* [5]. The radiation radius is related as $R_\infty \equiv R/\sqrt{1-2M/R}$ to the areal radius R and mass M of the star. This compact star is too small to construct with normal EOS's which are currently adopted for neutron stars [2]. Therefore this star may be a candidate for a quark star. Motivated by this observation, Nakamura proposed several scenarios about the formation of quark stars [6].

If a compact object oscillates for some reason, gravitational waves are emitted from the object. The oscillations damp out because the gravitational waves carry away oscillational energy. So these oscillations are called quasi-normal modes (QNMs). If the gravitational waves from a compact object are detected, we can get information about the source object. In this context, Yip, Chu and Leung studied nonradial stellar oscillations of quark stars whose radii are around 10 km [7]. However, the reported radius of the star RXJ185635-3754 is much smaller than the radii of the stellar models examined by Yip, Chu and Leung. In this paper, we calculate nonradial oscillations of quark stars whose radiation radii are in the range of $3.8{\rm km} \lesssim R_\infty \lesssim 8.2{\rm km}$, and examine the relation between QNMs of the quark stars and the EOS of quark matter. Concerning the detection of gravitational waves, gravitational wave interferometers such as LIGO, VIRGO, GEO600 and TAMA300, are progressing steadily. For example, TAMA300, GEO600 and LIGO are now in operation.

QNMs are classified into two classes. One is fluid modes, which mainly couple with the stellar fluid, while the other is spacetime modes which are connected with spacetime oscillation, which couple mainly to metric perturbations. Non-rotating stars admit fluid modes only for polar perturbations. The most widely studied fluid modes are f-, p- and g-modes [9, 10]. The f-mode is the fundamental mode. There is only one f-mode for each l. The p-mode is the pressure mode which arises from fluid pressure. The g-mode is the gravity mode which is caused by buoyancy due to density discontinuity and/or temperature gradient of stars and other factors. The damping rates of these fluid modes are very small compared with the frequency. The spacetime modes include w- and $w_{\rm II}$- modes[11]. The damping rate of w-modes

[1] E-mail:sotani@gravity.phys.waseda.ac.jp
[2] E-mail:harada@gravity.phys.waseda.ac.jp

is comparable to the frequency. For each stellar model, there are found one or a few $w_{\rm II}$-modes, whose complex frequency is located near the imaginary axis. For simplicity, we pay attention here only to w-, $w_{\rm II}$- and f-modes. Recently, Kojima and Sakata calculated the f-mode quasi-normal frequency for quark star models, and pointed out the possibility of distinguishing between quark stars and neutron stars by detecting the f-mode frequency and damping rate [8].

2 Structure of Quark Stars

We consider a static and spherical star. For this case, the metric is described by

$$ds^2 = -e^{2\Phi}dt^2 + e^{2\Lambda}dr^2 + r^2\left(d\theta^2 + \sin^2\theta d\phi^2\right), \tag{1}$$

where Φ, Λ are metric functions of r. The mass function satisfies

$$\frac{dm}{dr} = 4\pi r^2 \rho, \tag{2}$$

where ρ is the energy density. The equilibrium stellar model is derived by solving the Tolman-Oppenheimer-Volkoff equation,

$$\frac{dP}{dr} = -\frac{(\rho + P)\left(m + 4\pi r^3 P\right)}{r\left(r - 2m\right)}, \tag{3}$$

where P is the pressure of the fluid, and the potential Φ is given by

$$\frac{d\Phi}{dr} = \frac{\left(m + 4\pi r^3 P\right)}{r\left(r - 2m\right)}. \tag{4}$$

For solving these equations, we need an additional equation, i.e., the equation of state.

Though a quark star may be either a light quark star made up of u and d quarks or a strange quark star composed of a mixture of u, d and s quarks, we construct simple models by using the bag model EOS, which neglects the masses of u and d quarks. This bag model EOS is characterized by three parameters; the strong interaction coupling constant α_c, the bag constant B and the mass m_s of the s quark. In this paper we use the bag model EOS derived for a massless strange quark,

$$P = \frac{1}{3}(\rho - 4B). \tag{5}$$

The bag constant B is a positive energy density, which corresponds to latent heat. The stellar radius R is defined as the position where the pressure is zero. At the surface, the density profile is discontinuous. Although the value of the bag constant, which is a phenomenological parameter, should be determined by the underlying strong interaction dynamics, it is difficult to determine this value from our present understanding of QCD. However, if strange quark matter is the true ground state, the energy of this true ground state per particle would not be over the nucleon mass 939 MeV at baryon density for zero pressure matter. This constraint implies a maximum value of the bag constant B as follows [12]: $B \leq B_{\rm max} = 94.92\text{MeV fm}^{-3}$.

For definiteness, we use three values of the bag constant, B = 28.9, 56.0 and 94.92 MeV fm^{-3}. Although $B_{st}^{1/4}$ = 145 MeV or B_{st} = 57.8 MeV fm^{-3} has been often used for the study of quark-gluon plasma so far, we adopt B = 56.0 MeV fm^{-3} to compare with the results in [7]. The other values of the bag constant are the maximum value and half the standard value B_{st}. We show the mass M of the quark star as a function of the central density ρ_c for these three values of the bag constant in Fig. 1(a), the relations between M and R and between M and R_∞ in Fig. 1(b), and the relation between "average density" $\bar{\rho} \equiv 3M/4\pi R^3$ and R_∞ in Fig. 1(c). These figures are plotted for $4B < \rho_c \leq 5.0 \times 10^{15}$ g/cm^{-3}. The radiation radius may be determined from X-ray observations such as [5]. We pay attention to the stars whose radiation radii are in the range of 3.8 – 8.2 km. In this range of radiation radius, we pick up three values, R_∞ = 3.8, 6.0 and 8.2 km.

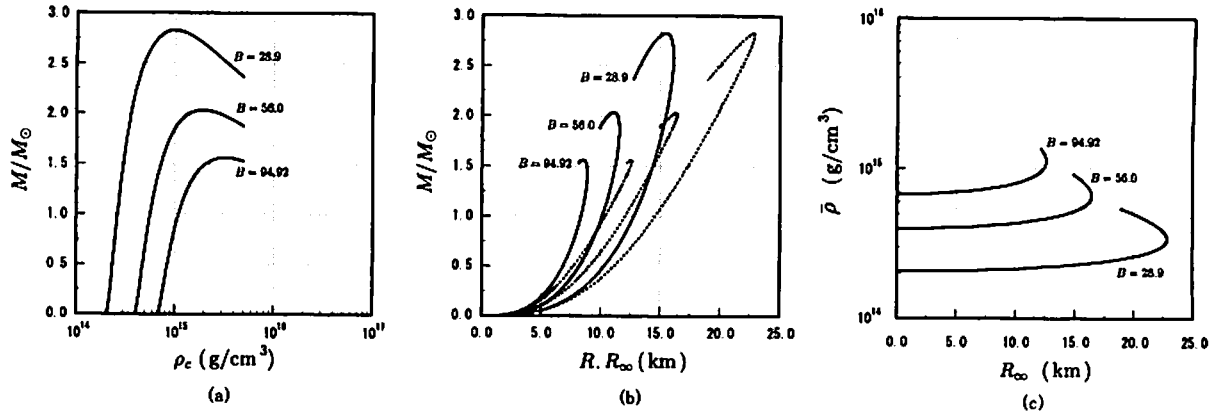


Figure 1: Relations (a) between mass M and central density ρ_c, (b) between M and radius R (solid line) and between M and radiation radius R_∞ (broken line), and (c) between "average density" $\bar{\rho} \equiv 3M/4\pi R^3$ and radiation radius R_∞ of quark stars.

3 Nonradial Oscillations of Quark Stars

3.1 Method

The QNMs are determined by solving the perturbation equations with appropriate boundary conditions. The perturbation equations inside the star, which are derived from Einstein equations, are given in [10]. The perturbation equations outside the star are described by the Zerilli equations. By imposing boundary conditions such that perturbative variables are regular at the center of the star, the Lagrangian perturbation of pressure vanishes at the stellar surface, and the gravitational wave is only outgoing one at infinity, one can reduce this to an eigenvalue problem. For the treatment of the boundary condition at infinity, we adopt the method of continued-fraction expansion proposed by Leaver [13]. The details of the determination of quasi-normal frequencies are given in [10].

3.2 Results

3.2.1 w- and $w_{\rm II}$-modes

The calculated complex frequencies of w- and $w_{\rm II}$-modes for $l = 2$ are plotted in Fig. 2. In these figures, the filled and non-filled marks correspond to w- and $w_{\rm II}$-modes, respectively. Figures 2(a), (b) and (c) correspond to $B = 28.9$, 56.0 and 94.92 MeV fm^{-3}, respectively. In each figure, the upper, middle and lower sequences correspond to the stellar models of $R_\infty = 3.8$ km ($A1$, $B1$, $C1$), $R_\infty = 6.0$ km ($A2$, $B2$, $C2$) and $R_\infty = 8.2$ km ($A3$, $B3$, $C3$), respectively.

In order to obtain the tendency of w- and $w_{\rm II}$-modes with changing compactness, we calculate the w- and $w_{\rm II}$-modes of the stellar models whose compactness is much larger than that of the stellar models depicted in Figs. 2(a), (b) and (c). From this calculation, we find two $w_{\rm II}$-modes for the stellar model of higher compactness, for example, for $\rho_c = 1.4 \times 10^{15}$ g/cm^{-3} with $B = 56.0$ MeV fm^{-3}. Furthermore, we see that as the compactness of quark star gets smaller, the complex frequencies of the $w_{\rm II}$-modes shift toward the imaginary axis, while both the frequency and damping rate of w-modes become slightly larger. If the compactness is very small, the frequencies of $w_{\rm II}$-modes can be too small to find except for the lowest $w_{\rm II}$-mode which has the largest frequency among all $w_{\rm II}$-modes. That is why Figs. 2(a), (b) and (c) are quite different from the results obtained by Yip, Chu and Leung [7] in the location of $w_{\rm II}$-modes.

We pick up the lowest $w_{\rm II}$-mode and plot in Fig. 3 for each stellar model. The frequency of the lowest $w_{\rm II}$-mode depends strongly on the bag constant. Thus, we can get information about the bag constant or the stellar radiation radius by observing the lowest $w_{\rm II}$-mode frequency. Moreover, we could obtain a more stringent restriction by using the damping rate, although it seems more difficult to determine the damping rate by observation.

On the other hand, in Fig. 2, we see that both the frequency and damping rate of w-modes have little dependence on the bag constant. Therefore it is difficult to determine the value of the bag constant by employing the observation of w-modes. In fact, the w-mode frequencies are all far beyond the frequency band for which gravitational wave interferometers such as LIGO, VIRGO, GEO600 and TAMA300 have good sensitivity [14].

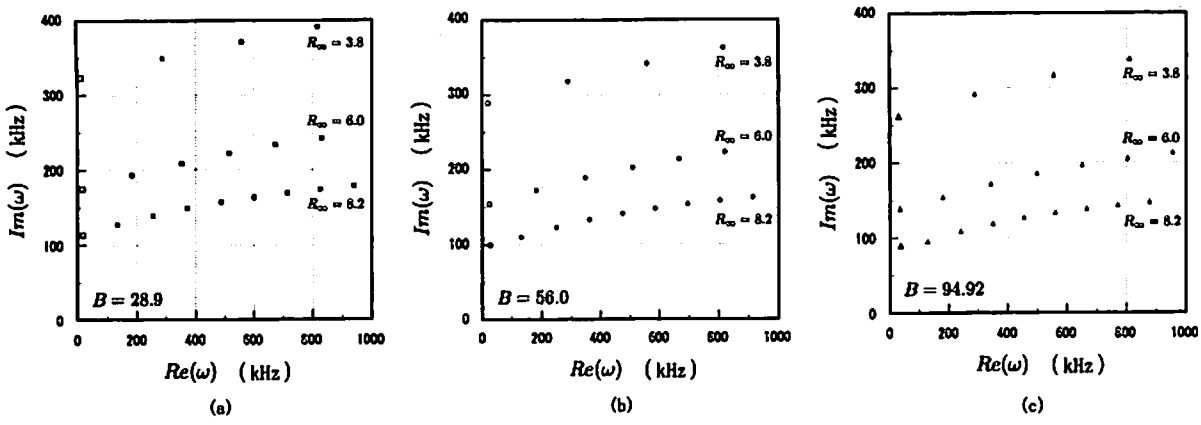


Figure 2: Complex frequencies of both w- and $w_{\rm II}$-modes (a) for $B = 28.9$ MeV fm^{-3}, (b) for $B = 56.0$ MeV fm^{-3} and (c) for $B = 94.92$ MeV fm^{-3}.

3.2.2 f-mode

We plot the complex frequencies of the f-mode for $l = 2$ in Fig. 4. In this figure, the squares, triangles and circles denote the cases $B = 28.9$ MeV fm^{-3}, $B = 56.0$ MeV fm^{-3} and $B = 94.92$ MeV fm^{-3}, respectively. On each set, the upper, middle and lower marks correspond to the stellar models of $R_\infty = 8.2$ km, $R_\infty = 6.0$ km and $R_\infty = 3.8$ km, respectively.

As can be seen in Fig. 4(a), the f-mode frequency depends strongly on the bag constant but very weakly on the stellar radiation radius. This result agrees with that of Kojima and Sakata [8]. Therefore, if the radiation radius of quark star is determined by observation, even though the value of radiation radius is somewhat uncertain, we can obtain the value of the bag constant by detecting f-mode QNMs. Furthermore, we can restrict the mass of the source star by employing the observational value of the radiation radius. The reason why the f-mode frequency depends strongly on the bag constant is understood as follows. The f-mode frequency depends strongly on average density but very weakly on the EOS [9]. In the case of quark stars with small radii, the average density is almost determined by the bag constant alone, as can be seen in Fig. 1(c). Thus, the f-mode frequency depends strongly on the bag constant.

Moreover, we can see that the damping rate of the f-mode depends on the stellar radiation radius for each bag constant, which also agrees with the result by Kojima and Sakata [8]. So, if we get data on the damping rate of the f-mode by observation, we can determine the stellar radiation radius independently of X-ray observations.

4 Conclusion

We calculate the nonradial oscillations of quark stars whose radiation radii are in the range of $3.8 \lesssim R_\infty \lesssim 8.2$ km, paying particular attention to w-, $w_{\rm II}$- and f-modes of quark stars constructed with the bag model EOS. We adopt three values of the bag constant and construct nine stellar models. We find that both the frequency and damping rate of the lowest $w_{\rm II}$-mode strongly depend on the bag constant and the stellar radius. Therefore we can get information about the properties of quark stars or the EOS governing quark matter from observations of the lowest $w_{\rm II}$-mode frequency. If the damping rate of this mode could be obtained, we would get more stringent constraints on the properties and EOS parameter.

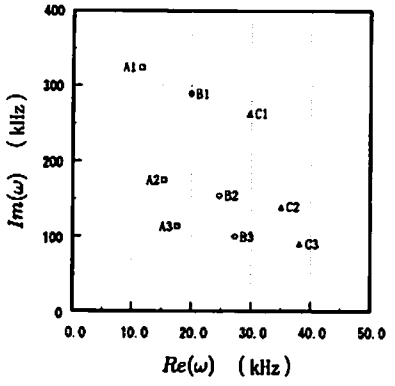


Fig.3

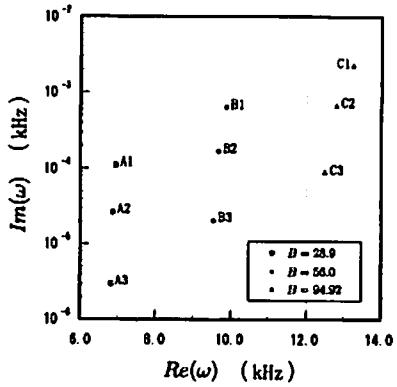


Fig.4

Figure 3: Complex frequencies of the lowest $w_{\rm II}$-mode for each stellar model is plotted.

Figure 4: Complex frequencies of f-mode for the quark stars.

On the other hand, because the frequency of the f-mode also strongly depends on the bag constant, we can restrict the bag constant by observations of the f-mode frequency. Moreover, since the damping rate of the f-mode depends on the stellar radius for each bag constant, we can restrict the stellar radius by detailed observations of the f-mode damping rate.

The dependence of the f-mode frequency on the bag constant and radiation radius is different from that of the lowest $w_{\rm II}$-mode frequency. Therefore, if it becomes possible to obtain simultaneously both the f- and $w_{\rm II}$-mode frequencies by the observation of gravitational waves, we can determine the bag constant and stellar radiation radius. In the near future, we can get information about the EOS of quark matter by detecting gravitational waves from objects composed of quark matter.

References

[1] E. Witten, Phys. Rev. D **30**, 272 (1984).

[2] J. M. Lattimer, and M. Prakash, Astrophys. J. **550**, 426 (2001).

[3] L. Lindblom, Astrophys. J. **398**, 569 (1992).

[4] T. Harada, Phys. Rev. C **64**, 048801 (2001).

[5] J. J. Drake et al., Astrophys. J. **572**, 996 (2002).

[6] T. Nakamura, astro-ph/0205526 (2002).

[7] C. W. Yip, M.-C. Chu, and P. T.Leung, Astrophys. J. **513**, 849 (1999).

[8] Y. Kojima, and K. Sakata, astro-ph/0209320 (to appear in Prog. Theor. Phys.).

[9] N. Andersson, and K. D. Kokkotas, Mon. Not. R. Astron. Soc. **299**, 1059 (1998).

[10] H. Sotani, K. Tominaga, and K. Maeda, Phys. Rev. D **65**, 024010 (2001).

[11] K. D. Kokkotas, and B. F. Schutz, Mon. Not. R. Astron. Soc. **255**, 119 (1992).

[12] M. Prakash, E. Baron, and M. Prakash, Phys. Lett. B **243**, 175 (1990)

[13] E. W. Leaver, Proc. Roy. Soc. London Ser. A **402**, 285 (1985).

[14] K. S. Thorne, in *Black Holes and Relativistic Stars*, edited by R. M. Wald (University of Chicago Press, Chicago, 1998), p. 41.

I-balls

S. Kasuya[a], M. Kawasaki[b] and Fuminobu Takahashi[b1]

[a] *Helsinki Institute of Physics, P.O. Box 64, FIN-00014, University of Helsinki, Finland*
[b] *Research Center for the Early Universe, University of Tokyo, Tokyo 113-0033, Japan*

Abstract

We find that there exists a soliton-like solution "I-ball" in theories of a real scalar field if the scalar potential satisfies appropriate conditions. Although the I-ball does not have any topological or global $U(1)$ charges, its stability is ensured by the adiabatic invariance for the oscillating field.

1 Introduction

Scalar fields play important roles in theories of the early universe. It is believed that our universe experienced quasi-exponential expansion phase (= inflation) in its very early stage, which solves the flatness and horizon problems of the standard cosmology and explains the origin of the density fluctuations of the universe such as observed by COBE and other experiments The inflationary universe scenario is realized by the vacuum energy of some scalar field (inflaton). After inflation, the inflaton starts to oscillate and decays into other particles which reheat the universe through thermalization processes.

Similar dynamics is found in the Affleck-Dine mechanism for baryogenesis [1] which is a promising candidate for explaining the matter-antimatter asymmetry of the universe. The mechanism makes use of a scalar field (AD field) corresponding to a flat direction in the scalar potential of the minimal supersymmetric standard model.

Recently, it was found that the oscillating AD field deforms into lumps of the scalar condensate called Q balls [2, 3, 4, 5]. The Q ball is a non-topological soliton and its stability comes from the global charge (=baryon number) conservation. Since the Q ball is stable owing to the charge conservation, the scalar field responsible for the Q ball must be complex. Then, a question arises whether or not a real scalar field deforms into lumps similar to the Q balls. At first glance, no stable lumps are formed because any conservation quantities like a global charge do not exist for the system of a real scalar field. However, the previous studies on the dynamics of scalar fields showed that some soliton-like objects are formed. For example, "oscillons" are formed for phase the double well potentials [9] and the axion field fragments into "axitons" [10]. In both cases the numerical simulations showed the existence of some scalar lumps inside which the scalar fields are rapidly oscillating. However, the reason why such quasi-stable scalar lumps are formed was not clear at all.

Thus, it has been seen that real scalar fields fragment into quasi-stable lumps in numerical simulations for various situations. Here, therefore, we face the important problem concerning the real scalar dynamics, that is, what makes the scalar lump quasi-stable? Because the conserved baryon number plays a crucial role for stability of the Q ball, we need similar conservation quantity to stabilize the real scalar lump. In classical mechanics it is well-known that the adiabatic invariant exists for oscillating phenomena [11]. As will be seen later, we find that the adiabatic invariant can be extended to the field theories. Then, the existence of the stable lump can be explained by the adiabatic charge I (see the next section for definition) for the oscillating scalar field. We call this scalar lump "I-ball", since the adiabatic charge I plays the same role as the global $U(1)$ charges in the case of Q balls. We obtain the condition on the form of the scalar potential for the I-ball formation and derive the equation which determines the field configuration of the I-ball. In particular, it is found that the adibaticity requires the scalar potential to be dominated by a quadratic term.

[1] E-mail:fumi@resceu.s.u-tokyo.ac.jp

2 Adiabatic Charge

In this section we derive the conservation of an adiabatic charge, which guarantees the stability of the I-ball as discussed later. First we shortly review an adiabatic invariant in a mechanical system, according to Ref.[11]. Let us suppose that a system is executing a finite motion in one dimension and characterized by some parameter $\lambda(t)$ which specifies the properties of the external field. We assume that λ varies slowly enough (*i.e.*,"adiabatically"):

$$\left|\frac{\dot{\lambda}}{\lambda}\right| \ll T^{-1}, \tag{1}$$

where an overdot represents a derivative with respect to time, and T is the period of the motion. If λ is constant, the system executes a strictly periodic motion with a constant energy E. For slowly varying λ, the energy E varies slowly, while there is a quantity which remains constant, called an adiabatic invariant. This is written as

$$I_{\rm 1dim} \equiv \frac{1}{2\pi}\oint p\, dq, \tag{2}$$

where q and p are the coordinate and momentum, and the integral is taken over the variation of the coordinate during one period. Note that the periodicity plays an essential role in the proof of the existence for the adiabatic invariant. Before we go on to the case of the field theory, it will be useful to discuss a multi-dimensional system. Let us consider a system with any number of degrees of freedom $\{q_i, p_i\}$, executing a finite motion in all the coordinates. It is assumed the variables are separable so that the action can be written as the sum of functions each depending on only one coordinate. As shown in Ref. [11], the motion of the system is in general not strictly periodic, but ***conditionally periodic*** since the system passes arbitrarily close to a given state in the corse of a sufficient time. In fact, it is periodic only if the frequencies of all degrees of freedom are commensurable for arbitrary values of $\{q_i\}$. In this case, there exists only one adiabatic invariant in the system. On the other hand, if the variables are not separable, there is no adiabatic invariant in general. However, if the Hamiltonian of the system differs only by small terms from one which allows separation of the variables, the properties of the motion are close to the periodic motion.

Thus, in order to extend the adiabatic invariant to the case of the field theory, we have to impose the following two assumptions. First, the gradient energy is always sub-dominant everywhere, since the action of a scalar field is separable except the gradient term. Second, the scalar potential is quadratic, which would ensure the strictly periodic motion if it were not for the gradient term. In the following arguments, we adopt these two assumptions.

Let us consider the system of a real scalar field ϕ, whose motion is finite and characterized by a parameter $\lambda(\mathbf{x}, t)$. We suppose that λ varies adiabatically, and that its dependence on the position $\mathbf{x}$ is weak enough as well. In the limit of constant λ, the motion of the scalar field is homogeneous and periodic with the period T. The Lagrangian is given as,

$$\mathcal{L} = \frac{1}{2}\partial_\mu\phi\partial^\mu\phi - V(\phi,\lambda), \tag{3}$$

$$V(\phi,\lambda)|_{t<0} = \frac{1}{2}m^2\phi^2, \tag{4}$$

where we assumed that the potential is quadratic with the mass equal to m before the external field $\lambda(\mathbf{x}, t)$ is turned on at $t = 0$. If λ were constant, the energy-momentum conservation law leads to

$$\partial_\mu j^\mu = 0, \tag{5}$$

$$j^\mu \equiv T^{\mu 0} = T^{0\mu} = \dot{\phi}\,\partial^\mu\phi - \eta^{\mu 0}\mathcal{L}, \tag{6}$$

where an overdot represents ∂_t, and $\eta_{\mu\nu} = \mathrm{diag}(+,-,-,-)$. With slowly varying λ for $t > 0$, the motion of the scalar field changes adiabatically. Then the energy-momentum current j^μ is no longer conserved:

$$\partial_\mu j^\mu = (\partial_\mu\lambda)\frac{\partial j^\mu}{\partial\lambda}. \tag{7}$$

If we average Eq. (7) over the period T, we have

$$\overline{\partial_\mu j^\mu} = (\partial_\mu \lambda)\frac{1}{T}\int_t^{t+T} dt\, \frac{\partial j^\mu}{\partial \lambda} = (\partial_\mu \lambda)\left(\oint \frac{d\phi}{\dot{\phi}}\right)^{-1} \oint \frac{\partial j^\mu}{\partial \lambda}\frac{d\phi}{\dot{\phi}}, \tag{8}$$

where the overline represents the average over the period of the motion. In deriving Eq. (8), we used the two assumptions, one of which states that λ varies adiabatically:

$$\left|\frac{\dot{\lambda}}{\lambda}\right| \ll T^{-1}. \tag{9}$$

Therefore, λ can be regarded as a constant, when $\oint d\phi$ is integrated over the total motion of ϕ during one period at fixed $\mathbf{x}$. The other assumption is that λ depends on the position weakly enough:

$$\left|\frac{\nabla \lambda}{\lambda}\right| \ll T^{-1}, \tag{10}$$

where T can be interpreted as a typical spatial scale of the oscillating system. This condition is necessary because otherwise the gradient term becomes too large to be negligible. Note that the large gradient term also changes the value of $\overline{\phi^2}$ significantly during one period, leading to the violation of the adiabaticity. For a small but nonzero $\nabla\lambda$, the motion is not strictly periodic, and the deviation from the orbit obtained as if λ were constant can be estimated to be of the order of $\delta\phi \sim \phi T \nabla\lambda$ after one period. We neglect such small corrections, and would like to focus attention on the leading terms in the following argument. Thus the motion of ϕ is approximated to be both periodic over T and homogeneous in the volume $V = [\mathbf{x} - T/2, \mathbf{x} + T/2]$. Hence there are four conserved quantities $J^\mu \equiv \int_V T^{\mu 0} d^3x$ along the path of the motion, and one can regard $\partial^\mu\phi$ as a function of (ϕ, J^μ, λ).

By differentiating the equation : $j^\nu(\phi, \partial_\mu\phi, \lambda) = J^\nu$ with λ, we have

$$\frac{\partial j^\mu}{\partial \lambda} = -\dot{\phi}\frac{\partial \partial^\mu \phi}{\partial \lambda}. \tag{11}$$

In deriving Eq. (11), we have used the relation $\frac{\partial j^\nu}{\partial(\partial^\mu\phi)} \simeq \dot{\phi}\,\delta^\nu{}_\mu$, where the non-diagonal components are higher order in $\dot{\lambda}$ and $\nabla\lambda$, and hence we neglect them. With the use of Eq. (11), Eq. (8) can be rewritten as

$$\oint \left(\partial_\mu\lambda \frac{\partial(\partial^\mu\phi)}{\partial\lambda} + \overline{\partial_\mu j^\nu}\frac{\partial(\partial^\mu\phi)}{\partial j^\nu}\right) d\phi = 0. \tag{12}$$

Hence we have

$$\overline{\partial_\mu\left(\oint d\phi\, \partial^\mu\phi\right)} = 0, \tag{13}$$

where the time component ($\mu = 0$) is the leading term, and has a definite physical meaning. Thus, we are led to define the adiabatic charge I as

$$I \equiv \frac{1}{2m}\int d^3x\, \overline{\dot{\phi}^2}, \tag{14}$$

where the factor $1/m$ in the definition here is introduced to make I dimensionless. Apparently I is conserved,

$$\frac{dI}{dt} = 0. \tag{15}$$

3 Conditions for existence of I-balls

With the use of the adiabatic charge derived in the previous section, let us consider the condition that I-balls are formed. We would like to focus attention on λ in the first place. It specifies the properties

of the external field, hence the energy of the system is no longer conserved for varying λ (see Eq. (7)). Alternatively, it could be argued that the role of λ is played by the self-interaction of the scalar field, which must be such that the adiabatic conditions, (9) and (10) are satisfied. Then the total energy of the system including the interaction would be conserved, although the energy of the free part varies due to the self-coupling. In other words, there are two invariants, the energy and adiabatic charge for the whole system including 'the external field'.

We assume that the scalar potential $V(\phi)$ is given as

$$V(\phi) = \frac{1}{2}m^2\phi^2 + V_1(\phi), \tag{16}$$

where the self-interaction $V_1(\phi)$ is small enough to respect the adiabatic conditions. That is to say, the adiabatic conditions are assumed to be satisfied by the dynamics of the system. First, we separate ϕ into the rapidly oscillating part ($\tilde{P}$) and slowly varying part (Φ) as

$$\phi(\mathbf{x},t) = \Phi(\mathbf{x},t)\tilde{P}(\mathbf{x},t). \tag{17}$$

For the general potentials, $\tilde{P}$ might strongly depend on $\mathbf{x}$, which leads to the large gradient energy $(\nabla\phi)^2$ and violates the adiabatic condition (10). However, we can safely adopt the ansatz that $\tilde{P}$ is homogeneous over a sufficiently large scale in which we are interested, since the periodicity of the system is guaranteed if the adiabatic conditions are satisfied. Thus,

$$\tilde{P}(\mathbf{x},t) = P(t) \tag{18}$$

where $P(t)$ oscillates between -1 and 1 with the period T. We also define O(1) constants c_n ($n = 1,2,3,\cdots$) for the later use.

$$\overline{\phi^{2n}} = c_n\Phi^{2n}, \tag{19}$$

$$\overline{\dot{\phi}^2} = c_1 m^2\Phi^2, \tag{20}$$

where we used the fact that the scalar potential is dominated by the quadratic term.

We take advantage of the method of Lagrange multipliers to look for the minimum of the energy E at fixed I, and minimize

$$\begin{aligned} E_\omega &= \overline{E} + \tilde{\omega}\left(I - \frac{1}{2m}\int d^3x\,\overline{\dot{\phi}^2}\right), \\ &= \int dr 4\pi r^2 c_1 \left(\frac{1}{2}\left(\frac{d\Phi}{dr}\right)^2 + V(\Phi) - \frac{\omega}{2m}\Omega^2\Phi^2 - \frac{\omega m}{2}\Phi^2\right) + (\omega + m)\,I\,, \end{aligned} \tag{21}$$

where $\tilde{\omega} \equiv \omega + m$, $V(\Phi) \equiv \overline{V(\phi)}/c_1$, and we assumed that the bounce solution is spherically symmetric.

In order to minimize E_ω with respect to Φ, we have to seek for the bounce solution, which is equivalent to solving the equation,

$$\frac{d^2\Phi}{dr^2} + \frac{2}{r}\frac{d\Phi}{dr} + \frac{dU}{d\Phi} = 0\,, \tag{22}$$

where

$$U(\Phi) \equiv \frac{\omega m}{2}\Phi^2 - V(\Phi)\,. \tag{23}$$

The bounce solution should satisfy the following boundary conditions:

$$\left.\frac{d\Phi}{dr}\right|_{r=0} = 0\,, \tag{24}$$

$$\Phi(\infty) = 0\,. \tag{25}$$

Hence, the bounce solution (I-ball solution) exists if the following inequalities are satisfied.

$$\min\left[\frac{2V(\Phi)}{\Phi^2}\right] < \omega m < m^2. \tag{26}$$

Now we investigate the constraint on the interaction V_1. For the field configuration to satisfy the adiabatic condition (10), we require $|(d\Phi/dr)/\Phi| \ll m$. Since the spatial scale of the I-ball solution is determined by the mass scale of $U(\Phi)$, this requirement is equivalent to

$$\left|\frac{d^2U(\Phi)}{d\,\Phi^2}\right| \sim \left|\frac{d^2V_1(\Phi)}{d\,\Phi^2}\right| \ll m^2 \tag{27}$$

where we used the inequality (26). If the interaction satisfies this constraint, the periodicity of the system is maintained, and the I-ball configuration which minimizes the total energy of the system is also gently-sloping enough.

4 Conclusion

We have studied the system of a real scalar field and found the solution of the quasi-stable scalar lump, I-ball. The stability of the I-ball can be explained by the adiabatic invariant charge I, which does stem from the dynamics of the system, not any symmetries. For the I-ball solution to exist, the scalar potential should be dominated by the quadratic term ($m^2\phi^2$) and satisfy the condition (26) which is almost same as that for the Q-ball.

Furthermore, we have performed numerical simulations (see Ref. [12]) and have found that the quasi-stable I-balls are really produced and their properties are in agreement with the theoretical predictions. Since scalar fields prevail in theories of the early universe, the I-balls may be formed and play important roles in various cosmological processes.

References

[1] I. Affleck and M. Dine, Nucl. Phys. **B249**, 361 (1985).

[2] A. Kusenko and M. Shaposhnikov, Phys. Lett. B **418**, 46 (1998).

[3] K. Enqvist and J. McDonald, Nucl. Phys. **B538**, 321 (1999).

[4] S. Kasuya and M. Kawasaki, Phys. Rev. D **61**, 041301 (2000).

[5] S. Kasuya and M. Kawasaki, Phys. Rev. Lett. **85**, 2677 (2000).

[6] S. Kasuya and M. Kawasaki, Phys. Rev. D **64**, 123515 (2001).

[7] J. McDonald, hep-ph/0105235 (2001).

[8] E.J. Copeland, S. Pascoli, A. Rajantie, Phys. Rev. D **65**, 103517 (2002).

[9] E. J. Copeland, M. Gleiser and H. -R. Muller, Phys. Rev. D **52**, 1920 (1995).

[10] E. W. Kolb and Igor I. Tkachev, Phys. Rev. D **49**, 5040 (1994).

[11] L. D. Landau and E. M. Lifshitz, *Mechanics* (Pergamon, 1976).

[12] S. Kasuya, M. Kawasaki and F. Takahashi, hep-ph/0209358.

The coincident event search using TAMA300 and LISM data

Hirotaka Takahashi[a,b,1], Hideyuki Tagoshi[a] and The TAMA Collaboration

[a] *Department of Earth and Space Science , Osaka University, Toyonaka, Osaka 560-0043, Japan*

[b] *Graduate School of Science and Technology, Niigata University, Niigata, Niigata 950-2181, Japan*

Abstract

The TAMA300 and LISM detectors performed long data taking in the summer of 2001. We performed TAMA-LISM coincidence analysis based on matched filtering for inspiral compact binaries. The mass range is from $1M_{\odot}$ to $2M_{\odot}$. The results of the coincidence analysis are reported.

1 Introduction

Several laser interferometric gravitational wave detectors are now under the construction. These include LIGO [1],VIRGO [2], GEO600 [3],and TAMA300 [4].

In Japan, there are two laser interferometric gravitational wave detectors. One is the TAMA300 detector. The TAMA300 is an interferometric gravitational wave detector with $300m$ baseline length located at Mitaka campus of the National Astronomical Observatory in Tokyo $(35.68°N, 139.54°E)$. The other is the LISM detector which is operated mainly by people in ICRR (Univ. of Tokyo). It is an interferometric gravitational wave detector with $20m$ baseline length located at Kamioka mine,Gifu $(36.25°N, 137.18°E)$.

The TAMA300 and LISM observed during August 1st and September 20th,2001(JST). We call this observation Data taking 6. The best sensitivity of the TAMA300 was about $5 \times 10^{-21}/\sqrt{Hz}$ around $800Hz$. About 1100 hours of data was taken during Data Taking 6. The best sensitivity of the LISM was about $6.5 \times 10^{-20}/\sqrt{Hz}$ around $800Hz$. About 780 hours of data was taken during that period.

In the past, very little work has devoted to develop the coincident analysis using real data of two or more laser interferometers. A coincident analysis of bursts events in a pair of laser interferometers has been performed by D. Nicholson et al. [5]. They do not use the matched filtering techniques. we perform a coincident analysis based on matched filter using real TAMA300 and LISM data. In this paper, we report results of coincidence analysis for inspiral compact binaries.

2 Inspiral compact binaries

Gravitational waves from inspiral compact binaries, consisting of neutron stars with mass $\sim 1.4M_{\odot}$ or black hole, have been considered to be the most promising target for laser interferometers. These compact binaries can be produced as a consequence of normal stellar evolution of binaries. It has been also suggested that MACHOs in our Galactic halo may be primordial black holes with mass $\sim 0.5M_{\odot}$ .If so, it is reasonable to expect that some of them are in binaries which coalesce due to gravitational radiation reaction [6].

3 Onestep Search

We assume that the time-sequential data of the detector outputs $s(t)$ consists of a signal plus noise $n(t)$. We also assume that the waveform of the signal is predicted theoretically with sufficiently good accuracy.

[1] E-mail:hirotaka@vega.ess.sci.osaka-u.ac.jp

We call this waveform *templates*. Hence the signal is supposed to be identical to one of the templates except for the normalization of it's amplitude.

To characterize the detector noise, we define one-sided power spectrum density $S_n(f)$ by $S_n(f) = 2\int_{-\infty}^{\infty} < n(t)n(t+\tau) > e^{2\pi i f\tau} d\tau$ where $< >$ represents the operation of taking the statical average.

We adopt the templates calculated by using the post-Newtonian approximation of general relativity[7]. We use a simplified version of the post-Newtonian templates in which the phase evolution is calculated 2.5 post-Newtonian order, but the amplitude evolution contains only the lowest Newtonian quadrupole contribution. We also use the stationary phase approximation.

The parameters consist of the coalescing time t_c,the total mass $M(\equiv m_1 + m_2)$,the mass ratio $\eta(\equiv m_1 m_2/M^2)$,and the spin parameters. In this analysis, we did not take account of the effect of spin angular momentum. The templates corresponding to a given set of the parameters are represented in Fourier space two independent templates $\tilde{h}_c$ and $\tilde{h}_s$[8] as $\tilde{h}(f) = \tilde{h}_c(f)\cos\phi_c + \tilde{h}_s(f)\sin\phi_c$ where ϕ_c is the phase of wave.

Here we define outputs of matched filter as

$$\rho(m_1, m_2, t_c, \cdots) \equiv 2\int_{-\infty}^{\infty} \frac{\tilde{s}(f)\tilde{h}^*(f)}{S_h(f)} df = (s|h) \tag{1}$$

where $*$ means the operation of taking the complex conjugate. In equation (1), we can analytically take the maximization over ϕ_c.

$$\rho = \sqrt{(s|h_c)^2 + (s|h_s)^2} \tag{2}$$

This ρ has an expectation value $\sqrt{2}$ in the presence of Gaussian noise. Thus, the Signal-to-Noise Ratio (SNR) is given by $SNR = \rho/\sqrt{2}$

Analyzing the real data, we found that the noise contained a large amount of non-stationary and non-Gaussian noise whose statistical properties have not been understood well yet. In order to remove the influence of such noise, we introduce a χ^2 test [9]. In this paper,we do not explain a χ^2 test in detail which was explained by the Tanaka and Tagoshi [8].

We searched the parameter space of $1.0M_\odot \leq m_1, m_2 \leq 2.0M_\odot$. In this parameter spaces,we prepared a mesh. The mesh points define templates used for search. The mesh separation is determined so that maximum loss of SNR becomes less than 3%. We use the Tanaka-Tagoshi coordinates. Using geometrical arguments, Tanaka and Tagoshi[8] introduced a new parameterization of masses that simplifies algorithm to determine the mesh points. The parameter space defined by using the Tanaka-Tagoshi coordinates turned out to contain about 200 to 1000 templates for the TAMA300 data, and about 200 to 600 templates for the LISM data.

We independently performed onestep search using TAMA300 and LISM data. As a results of onestep search, we obtain ρ and χ^2 as functions of masses and coalescing time t_c. In each small interval of coalescing time Δt_c, we looked for an event which had the maximum ρ. In this search, we choose $\Delta t_c \sim 3.2sec$. If the events which had the maximum ρ were $\rho > 7$, we recorded the events on event lists.

4 Coincident event search

As a result of the one step matched filtering search, we obtain the independent TAMA300 and LISM events lists. In order to perform the coincident event search, we extracted the TAMA300 and LISM events lists for common lock parts.

We compared candidate event list by requiring consistency condition as real gravitational wave events. This produces a list of coincidence events. We examine whether events in the coincident list are consistent with accidental event rate and examine candidate events further by another analysis method. We also evaluated an upper limit to the event rate.

In this search, the parameters on which the waveforms depend are $\theta^i = (\mathcal{A}, t_c, \phi_c, \mathcal{M}, \eta)$ where $\mathcal{M} \equiv M\eta^{3/5}$ is the chirp mass. If the events are *true* gravitational waves, they should have the same intrinsic parameters in the both detectors. However, we may observe real events with different parameters by the effects of detector noise and other effects. Therefore we have to determine the allowed parameter windows which take into account of these effects.

Time selection: The distance between TAMA300 and LISM is about $220km$. Therefore, the maximum delay of gravitational wave signal arrival time is $\Delta t_{dis} = 0.73msec$. Moreover, the parameter-estimation errors of t_c due to noise $\Delta t_{cTAMA(LISM)}$ were determined by using Fisher Information Matrix[10]. We allowed $\Delta t_{noise} = 3.29\Delta t_c$ ($\Delta t_c = \sqrt{\Delta t^2_{cTAMA} + \Delta t^2_{cLISM}}$) for the difference of parameters of each events. This corresponds to 0.1% for loss of events. If the parameters t_c^{tama}, t_c^{lism} observed in both detectors satisfied $|t_c^{tama} - t_c^{lism}| < \Delta t_{dis} + \Delta t_{noise}$, we recorded the candidate gravitational wave events on coincident event lists.

Mass selection: Over the candidate events survived time selection, we performed mass selection.

Similarly, the parameter-estimation errors of mass parameters due to noise $\Delta\mathcal{M}_{noise}$, $\Delta\eta_{noise}$ were determined by using Fisher Information Matrix. But we explain them in details here, we also determined the mesh size effects $\Delta\mathcal{M}_{mesh}$, $\Delta\eta_{mesh}$. If the parameters $\mathcal{M}^{tama}$, $\mathcal{M}^{lism}$, η^{tama}, η^{lism} observed in both detectors satisfy $|\mathcal{M}^{tama} - \mathcal{M}^{lism}| < Max(\Delta\mathcal{M}_{noise}, \Delta\mathcal{M}_{mesh})$, $|\eta^{tama} - \eta^{lism}| < Max(\Delta\eta_{noise}, \Delta\eta_{mesh})$, we recorded the candidate gravitational wave events on coincident event lists.

Amplitude selection: Over the candidate events survived time and mass selection, we performed amplitude selection.

There is a difference of arm direction of TAMA300 and LISM. LISM rotate from TAMA300 at $60deg$. Sensitivity of TAMA300 is typically 15 times better than that of LISM. So real events will be detected with different SNR by each detector depending on its incident direction and polarization. But we still want a window for amplitude to reduce the number of fake events. We perform a Galactic event simulation to determine the parameter window, but we explain them in details here. If the parameters ρ_{tama}, ρ_{lism} observed in both detectors satisfy $\delta_{sens} - \delta_{simu} \leq \log\left(\frac{\rho_{tama}}{\rho_{lism}}\right) \leq \delta_{sens} + \delta_{simu}$, where δ_{sens} is log ratio of detector sensitivity and δ_{simu} is allowed difference derived from Galactic simulation so that 99.9% of Galactic events will be detected, we recorded the candidate gravitational wave events on coincident event lists.

5 Accidental coincidence

It is possible to measure the number of coincidence experimentally by the usual procedure of shifting one of two sets of data by a time δt (called time delay) and determining the number of coincidences $n_c(\delta t)$ [11] [12]. Repeating for m different values of time delay, the expected number of coincidences is simply the sample mean of the $m-1$ values of $n_c(\delta t)$ at delays other than $\delta t = 0$,

$$\bar{n}_{acc} = \frac{1}{m-1}\sum_{i=1}^{m-1} n_c(\delta t_i). \tag{3}$$

The corresponding experimental standard deviation is given by

$$\bar{\sigma}_{acc} = \sqrt{\sum_{i=1}^{m-1}\left(n_c(\delta t_i) - \bar{n}_{acc}\right)^2/(m-1)}. \tag{4}$$

Since there is no signal at delays other than $\delta t = 0$, the number of coincidences at these delays can be considered an experimental estimation of the parent distribution from which the accidental coincidences are drawn. For detectors with stationary events rates the parent distribution is Poisson with mean given by above equation. The number of coincidences at zero time delay can then compared to the experimental distribution. If enough gravitational waves are present in the data, $n_c(0)$ will lie outside of the distribution.

6 Results and Discussion

Our analysis was done with 9 Compaq Alpha machines and also with 16 Intel Pentium4 machines in our laboratory at Osaka University. The matched filtering and coincidence analysis codes are written in C language and are MPI paralleled.

We independently performed onestep search using TAMA300 and LISM data. Among the TAMA300 DT6 data, we analysed 1039 hours of data. For the LISM data, we have only analysed the data from last two weeks. The length analysed is 322 hours. Other portion of data are unlocked or some adjustment.

The portion of data for TAMA300 and LISM commonly lock is 244 hours. As a result of independent one step matched filtering search for common lock parts, there are the 158437 for TAMA300 and 142465 for LISM candidate gravitational wave events (Table 1) .

	TAMA300	LISM
One step search results (Δt_c = 3.2 sec)	158437	142465

Table 1: Result of one step matched filtering search for common lock parts.

Over these candidate gravitational wave events, we performed the time, mass and amplitude selection.

In Table 2, we show the coincident event search results. In Fig.1, we also show an experimental estimation of the parent distribution from which the accidental coincidences are drawn. And we show the $\rho_{tama}/\sqrt{\chi^2_{tama}}$-$\rho_{lism}/\sqrt{\chi^2_{lism}}$ scatter plots in Fig.2 .

	n_{obs}	$\bar{n}_{acc} \pm \bar{\sigma}_{acc}$
after time selection	70	70.45 ± 8.53
after time and mass selection	18	17.55 ± 4.08
after time, mass and amplitude selection	13	12.76 ± 3.35

Table 2: Coincident event search results. $\bar{n}_{acc}$, $\bar{\sigma}_{acc}$ are the experimental average number of coincidence estimated by the method of Sec.5.

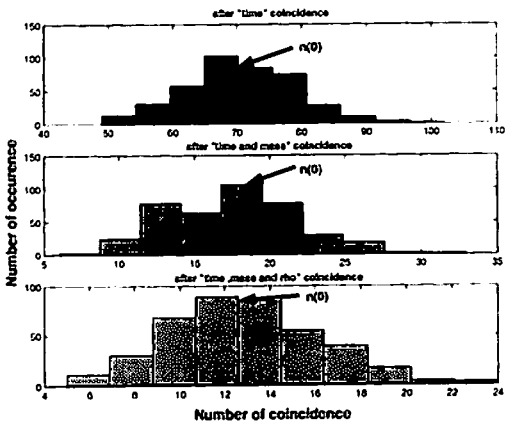


Figure 1: An experimental estimation of the parent distribution from which the accidental coincidences are drawn. From top to bottom, after time selection, after time and mass selection and after time, mass and amplitude selection.

As can be seen in Table 2, our coincident event search results can be explained as the accidental coincidences. These results are consistent with accidental coincidence. So we concluded that no significant coincident excess were observed.

These method to perform coincidence analysis are easily applicable to other multiple detector case.

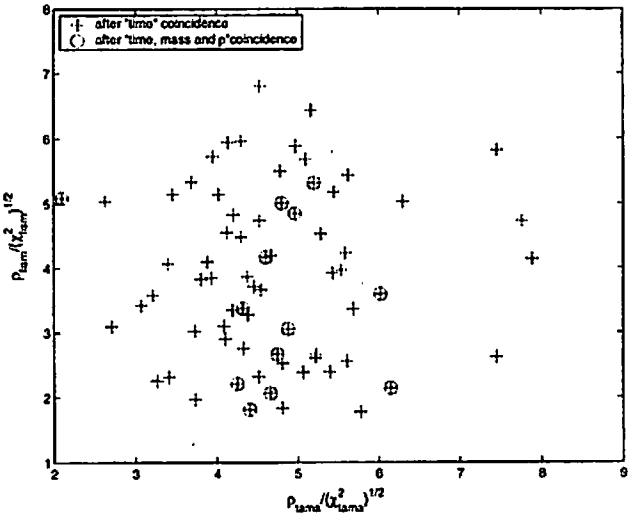


Figure 2: $\rho_{tama}/\sqrt{\chi^2_{tama}}$ -$\rho_{tism}/\sqrt{\chi^2_{tism}}$ scatter plots. + marks shows the events survived time selection and circle marks shows the events survived time, mass and amplitude selection.

References

[1] A. Abramovici et al., sience **256**,325 (1992).

[2] B. Caron et al., in *Gravitaional Wave Experiments*, edited by E. Coccia, G. Pizzella, and F. Ronga,(World Scientific, Singapore,1995).

[3] K. Danzmann et al., in *Gravitaional Wave Experiments*, edited by E. Coccia, G. Pizzella, and F. Ronga,(World Scientific, Singapore,1995).

[4] K. Tsubono, in *Gravitational Wave Experiments*, edited by E. Coccia, G. Pizzella, and F. Ronga,(World Scientific, Singapore,1995).

[5] D. Nicholson et al.,Phys.Lett.A,218 (1996).

[6] T. Nakamura, M. Sasaki, T. Tanaka, and K.S. Thorne, Astrophys. J. Lett. **487**, L139 (1997)

[7] L. Blanchet et al., Phys. Rev. Lett. **74**,3515 (1995).

[8] T. Tanaka and H. Tagoshi, Phys.Rev.D **62**,082001.(2000)

[9] B. Allen et al., Phys.Rev.Lett. **62**,1489 .(1999)

[10] C. Cutler and É. E. Flanagan, Phys.Rev.D **49**,082001.(1994)

[11] E. Amaldi et al. ,Astron. Astrophys. **216**,325 (1989).

[12] P. Astone et al. , Phys.Rev.D **59**,122001.(1999)

Primordial fluctuations in bulk inflaton model

Keitaro Takahashi,[1] Kazuya Koyama [2]

Department of Physics, University of Tokyo
7-3-1 Hongo, Bunkyo, Tokyo 113-0033, Japan

Abstract

An inflationary brane model driven by a bulk inflaton with exponential potential is proposed. We find a family of exact solutions that describe power-law inflation on the brane. These solutions enable us to derive exact solutions for metric perturbations analytically. By calculating scalar and tensor perturbations, we obtain a spectrum of primordial fluctuations at the end of the inflation.

1 Introduction

Higher dimensional formulation is necessary for theories such as superstring and M theory. All these theories are confronted with a problem that our universe seems to be four-dimensional, which is conventionally coped with compactifications of the extra dimensions. Braneworld model where our universe is a four-dimensional subspace in a higher dimensional spacetime, is an epoch-making scenario because it broke the conventional idea that the extra dimensions must be compact and small. In this scenario, ordinary matter fields are confined on the brane, while graviton can propagate through the extra dimensions. Thus higher-dimensional feature of spacetime must emerge in the nature of gravity.

In the early universe, inflation can amplify vacuum fluctuation of Kalzua Klein modes as well as a massless mode. Thus inflation is a powerful tool to probe the extra dimensions. Inflation can occur by the dynamics of inflaton either on the brane or in the bulk. In this contribution we propose a new model where dynamics of inflaton can be exactly solved including the back-reaction to the bulk spacetime even at high-energies. We deal with a bulk scalar field with exponential potential. We will point out that an inflationary model can be easily realized by increasing the potential energy of the scalar field in the bulk. A remarkable thing is that the metric perturbations in this background spacetime can be exactly solved. Then we can consistently calculate the primordial fluctuations and examine a feature of bulk inflaton model which should be compared with conventional 4D models or inflation models driven by inflaton on the brane. For details of this study, see [1].

2 Background spacetime

We start from the five-dimensional Einstein-Hilbert action with a bulk scalar field,

$$S = \int d^5x\sqrt{-g_5}\left(\frac{1}{2\kappa^2}R - \frac{1}{2}\partial_\mu\phi\partial^\mu\phi - \Lambda(\phi)\right) - \int d^4x\sqrt{-g_4}\lambda(\phi), \tag{1}$$

where κ^2 is five-dimensional gravitational constant. The potential of the scalar field in the bulk and on the brane are taken to be exponential:

$$\kappa^2\Lambda(\phi) = \left(\frac{\Delta}{8} + \delta\right)\lambda_0^2 e^{-2\sqrt{2}b\kappa\phi}, \quad \kappa^2\lambda(\phi) = \sqrt{2}\lambda_0 e^{-\sqrt{2}b\kappa\phi}. \tag{2}$$

Here λ_0 is the energy scale of the potential, b is the dilaton coupling and we defined $\Delta = 4b^2 - 8/3$.

We assume a solution of the form;

$$\begin{aligned} ds^2 &= e^{2W(z)}\left(-dt^2 + e^{2a(t)}\delta_{ij}dx^i dx^j + e^{2\sqrt{2}b\kappa\phi(t)}dz^2\right), \\ \phi(t,z) &= \phi(t) + \Xi(z). \end{aligned} \tag{3}$$

[1]E-mail:ktaro@utap.phys.s.u-tokyo.ac.jp
[2]E-mail:kazuya@utap.phys.s.u-tokyo.ac.jp

From the five-dimensional Einstein equations and the equation of motion for the scalar field, the solution is obtained as follows:

$$e^{W(z)} = \mathcal{H}(z)^{\frac{2}{3(\Delta+2)}}, \quad e^{\kappa\Xi(z)} = \mathcal{H}(z)^{2\frac{\sqrt{2}b}{(\Delta+2)}}, \tag{4}$$

$$\mathcal{H}(z) = \sqrt{-1-\frac{\Delta}{8\delta}}\sinh Hz, \quad H = -(\Delta+2)\sqrt{-\frac{\delta}{\Delta}}\lambda_0, \tag{5}$$

$$e^{\alpha(t)} = (H_0 t)^{\frac{2}{3\Delta+8}} = (-H\eta)^{\frac{2}{3(\Delta+2)}}, \tag{6}$$

$$e^{\sqrt{2b}\kappa\phi(t)} = H_0 t = (-H\eta)^{\frac{3\Delta+8}{3(\Delta+2)}}, \tag{7}$$

$$H_0 \equiv -(3\Delta+8)H/(3(\Delta+2)) \tag{8}$$

where we assumed $\frac{\Delta}{8}+\delta<0$ (for other cases, see [1] and a conformal time η is defined as

$$\eta = \int e^{-\alpha}dt = \frac{3\Delta+8}{3(\Delta+2)}H_0^{\frac{2}{3\Delta+8}}t^{\frac{3(\Delta+2)}{3\Delta+8}}. \tag{9}$$

We should notice that power-law inflation occurs on the brane for $-8/3 \le \Delta \le -2$. The location of the brane $z=z_0$is determined by $e^{W(z_0)}=1$. Above solutions properly satisfy junction conditions at $z=z_0$;

$$\partial_z W(z)|_{z=z_0} = -\frac{\sqrt{2}}{6}\lambda_0, \quad \partial_z \Phi(z)|_{z=z_0} = -\lambda_0. \tag{10}$$

3 Cosmological perturbations

In this section we consider perturbations in this background. The perturbations can be decomposed into scalar, vector and tensor perturbations in terms of their properties on the 3-space at fixed t and y coordinate. Here we don't consider vector perturbations. Taking an appropriate gauge fixing conditions, the perturbed metric and scalar field is give by

$$\begin{aligned} ds^2 &= e^{2W(z)}\left[e^{2\sqrt{2}\kappa\phi(t)}(1+2N)dz^2 + 2Adtdz - (1+2\Phi)dt^2 + e^{2\alpha(t)}(1-2\Psi)\delta_{ij}dx^i dx^j\right], \\ \phi &= \phi(t)+\Xi(z)+\delta\phi, \end{aligned} \tag{11}$$

for scalar perturbations and

$$ds^2 = e^{2W(z)}\left[e^{2\sqrt{2b}\kappa\phi}dz^2 - dt^2 + e^{2\alpha(t)}\left(\delta_{ij}+h_{ij}(t,x,z)\right)dx^i dx^j\right], \tag{12}$$

for tensor perturbations. Here $h_{ij}(t,x,z)$ is transverse and traceless tensor($h^i_i=0, \nabla^i h_{ij}=0$). Although 5D Einstein equations for these perturbations are rather complicated, the solutions for these perturbations can be analytically obtained. Because the derivation is very long, the detailed analysis will be presented in an accompanied paper and we only present important results here.

Introducing canonical variable for scalar perturbations

$$\delta\phi_f \equiv \delta\phi + \frac{\dot{\phi}}{\dot{\alpha}}\Psi = \delta\phi + 3\sqrt{2b}\Psi, \tag{13}$$

the second-order perturbed 5D action for gravity plus scalar field for scalar perturbations can be written as

$$\delta S^{(S)} = \frac{1}{2}\int dzdtdx^3 e^{3W(z)}e^{2\sqrt{2b}\kappa\phi}e^{3\alpha}(e^{-2\sqrt{2b}\kappa\phi}\delta\phi_f'^2 - \delta\dot{\phi}_f{}^2 + e^{-2\alpha}(\nabla\delta\phi_f)^2). \tag{14}$$

The junction condition for canonical variable $\delta\phi_f$ is given by $\partial_z\delta\phi_f|_{z=z_0}=0$. In a similar way, the canonical variables for tensor perturbation is given by $\varphi_{ij}=h_{ij}/2\kappa$. Then the second-order perturbed 5D action for tensor perturbations is obtained as

$$\delta S^{(T)} = \frac{1}{2}\int dzdtdx^3 e^{3W(z)}e^{2\sqrt{2b}\kappa\phi}e^{3\alpha}(e^{-2\sqrt{2b}\kappa\phi}\varphi_{ij}'^2 - \dot{\varphi_{ij}}{}^2 + e^{-2\alpha}(\nabla\varphi_{ij})^2). \tag{15}$$

The junction condition is given by $\partial_z \varphi_{ij}|_{z=z_0} = 0$. These actions are nothing but the action for 5D massless scalar field where tensor perturbation has two degrees of freedom due to polarization. Hence both scalar perturbation and tensor perturbation are described by 5D massless scalar field with Neumann boundary condition at the barne. As in a conventional 4D inflationary cosmology, these perturbations are quantum mechanically generated during inflation. Then in the next section, we will investigate the quantum fluctuations of the 5D massless scalar field in this background spacetime.

4 Quantization of massless scalar field

In the previous section, the metric perturbations were shown to be described by a 5D massless scalar field. Thus, we shall investigate the quantum fluctuation of the massless scalar field in this background spacetime.

The equation of motion for massless filed $\varphi(t, x, z)$ is

$$e^{2\sqrt{2}b\kappa\phi}\left[\ddot{\varphi} + (3\dot{\alpha} + \sqrt{2}b\kappa\dot{\phi})\dot{\varphi} - \nabla_k\nabla^k\varphi\right] = \varphi'' + 3W'\varphi', \tag{16}$$

where ∇_k is the three-dimensional covariant derivative operator. We can use the separation of variables to solve this equation and expand $\varphi(t, x, z)$ as,

$$\varphi(t, x, z) = \int dm d^3p \left[a_{pm}\psi_m(z)\chi_m(t)e^{ipx}. + (\text{h.c.})\right] \tag{17}$$

Here a_{pm} is the annihilation operator and satisfies the following commutation relation,

$$\left[a_{pm}, a^\dagger_{p'm'}\right] = \delta(p - p')\delta(m - m'). \tag{18}$$

On the other hand, $\psi_m(z)$ and $\chi_m(t)$ satisfy the following equations,

$$\psi_m'' + 3W'\psi' + m^2\psi = 0, \tag{19}$$

$$\ddot{\chi}_m + (3\dot{\alpha} + \sqrt{2}b\kappa\dot{\phi})\dot{\chi}_m + (e^{-2\alpha}p^2 + e^{-2\sqrt{2}b\kappa\phi}m^2)\chi = 0, \tag{20}$$

where m corresponds to the Kaluza-Klein mass. In the following subsections, we discuss the solutions to Eq. (19) and Eq. (20) and their properties.

4.1 Mode function – z-direction –

Because of Z_2 symmetry along the z-direction, the junction condition for $\psi_m(z)$ is $\partial_z\psi_m(z)|_{z=z_0} = 0$. With this condition and the commutation relation for φ, the solution for Eq. (19) is completely determined. In order to know the behavior of the solutions, it is convenient to define

$$\psi_m(z) = e^{-3W(z)/2}f_m(z). \tag{21}$$

Then, Eq. (19) gives the Schrodinger-like equation for $f_m(z)$

$$-f_m'' + V_{eff}(z)f_m = m^2 f_m. \tag{22}$$

The effective potential is given by

$$\begin{aligned} V_{eff}(z) &= \frac{3}{2}W'' + \frac{9}{4}W'^2 \\ &= -\frac{\Delta+1}{\Delta}\left(\frac{\Delta}{8} + \delta\right)\lambda_0^2 e^{-3(\Delta+2)W(z)} - \frac{1}{\Delta}\delta\lambda_0^2 - \frac{1}{\sqrt{2}}\lambda_0\delta(z - z_0), \end{aligned} \tag{23}$$

where we used Einstein equations in the last equation. The explicit form of the potential is determined by the background spacetime but it can be seen that there is zero mode confined on the brane irrespective of the background spacetime. Again we consider the case with $\frac{\Delta}{8} + \delta < 0$.

From (5), the effective potential for graviton is obtained as

$$V_{eff}(z) = \frac{\Delta+1}{\Delta}(\sinh Hz)^{-2}\lambda_0^2 - \frac{1}{\Delta}\delta\lambda_0^2 - \frac{1}{\sqrt{2}}\lambda_0\delta(z-z_0). \tag{24}$$

The equation for $\psi_m(z)$ becomes

$$\psi_m'' + \frac{2H}{\Delta+2}\coth Hz\psi_m' + m^2\psi_m = 0. \tag{25}$$

There are zero mode and continuum massive modes with $m^2 \geq H^2/(\Delta+2)^2 = -\delta\lambda_0/\Delta$. Massive modes with $0 < m^2 < H^2/(\Delta+2)^2$ are not normalizable and are not investicated here. The solutions for zero mode and normalizable massive modes are

$$\psi_0(z) = \frac{1}{\sqrt{2}}\left(-1-\frac{\Delta}{8\delta}\right)^{-\frac{2}{\Delta+2}}\left[\int_{z_0}^{\infty}(\sinh Hz)^{\frac{2}{\Delta+2}}dz\right]^{-\frac{1}{2}}, \tag{26}$$

$$\psi_m(z) = \sqrt{\frac{H}{2}}\left(-1-\frac{\Delta}{8\delta}\right)^{-\frac{2}{\Delta+2}}(|\xi|^2+|\zeta|^2)^{-\frac{1}{2}}(\sinh Hz)^{-\mu} \times\left[P_\nu^\mu(\cosh Hz) + CQ_\nu^\mu(\cosh Hz)\right], \tag{27}$$

where P_ν^μ and Q_ν^μ are associated Legendre functions and

$$\mu = -\frac{\Delta}{2(\Delta+2)}, \quad \nu = -\frac{1}{2}+i\beta, \quad \beta = \sqrt{\frac{m^2}{H^2}-\frac{1}{(\Delta+2)^2}}, \tag{28}$$

$$\xi = \frac{\Gamma(i\beta)}{\Gamma(\frac{\Delta+1}{\Delta+2}+i\beta)}, \quad \zeta = \frac{\Gamma(-i\beta)}{\Gamma(\frac{\Delta+1}{\Delta+2}-i\beta)} + C\pi e^{\mu\pi i}\frac{\Gamma(\frac{1}{\Delta+2}+i\beta)}{\Gamma(1+i\beta)}, \tag{29}$$

$$C = -\frac{(\frac{\Delta+1}{\Delta+2}+i\beta)P_{\nu+1}^\mu(\cosh Hz_0) - (\frac{1}{\Delta+2}+i\beta)\cosh Hz_0 P_\nu^\mu(\cosh Hz_0)}{(\frac{\Delta+1}{\Delta+2}+i\beta)Q_{\nu+1}^\mu(\cosh Hz_0) - (\frac{1}{\Delta+2}+i\beta)\cosh Hz_0 Q_\nu^\mu(\cosh Hz_0)}. \tag{30}$$

4.2 Mode function – time-direction –

From Eq. (7) and Eq. (6), Eq. (20) becomes

$$\ddot{\chi}_m + \frac{3\Delta+14}{3\Delta+8}t^{-1}\dot{\chi}_m + \left[p^2(H_0t)^{-\frac{4}{3\Delta+8}} + \frac{m^2}{H_0^2}t^{-2}\right]\chi_m = 0. \tag{31}$$

We choose the Bunch-Davis vacuum, which coincides with the Minkowski vacuum at high frequencies. With this condition and the commutation relation, the solution to Eq. (20) is completely determined. The solutions for zero mode and normalizable massive modes with $m^2 \geq H^2/(\Delta+2)^2$ are

$$\chi_0(\eta) = \frac{\sqrt{\pi}}{2}H^{-\frac{1}{2}}(-H\eta)^{-\frac{1}{\Delta+2}}H^{(1)}_{-\frac{1}{\Delta+2}}(-p\eta), \tag{32}$$

$$\chi_m(\eta) = \frac{\sqrt{\pi}}{2}H^{-\frac{1}{2}}(-H\eta)^{-\frac{1}{\Delta+2}}e^{-\frac{\beta\pi}{2}}H^{(1)}_{i\beta}(-p\eta), \tag{33}$$

where $\beta = \sqrt{m^2/H^2 - 1/(\Delta+2)^2}$.

4.3 Vacuum expectation value of fluctuations

Both zero mode and massive mode contribute to the spectrum and the vacuum expectation value of massless scalar field will be,

$$\langle\varphi^2(x)\rangle = \int d^3p\left[|\psi_0|^2|\chi_0|^2 + \int_{\frac{H^2}{(\Delta+2)^2}}^{\infty} dm\,|\psi_m|^2|\chi_m|^2\right]. \tag{34}$$

But this naive formula is not correct because in the large m and p limit $|\chi_m|^2$ behaves

$$|\chi_m|^2 \sim \frac{(-H\eta)^3}{2H\sqrt{(m/H)^2+(-p\eta)^2}} \quad (m,p\to\infty), \tag{35}$$

and the m-integral diverges logarithmically. This ultra-violet divergence appears in the five-dimensional field theory even in Minkowski spacetime. Thus we have to subtract this divergence as following:

$$|\chi_m|^2 - \frac{(-H\eta)^3}{2H\sqrt{(m/H)^2+(-p\eta)^2}}. \tag{36}$$

Then the correct expectation value is,

$$\begin{aligned}\langle\varphi^2(x)\rangle &= \int d^3p\left[|\psi_0|^2\left(|\chi_0|^2-\frac{(-H\eta)^3}{2H\sqrt{(-p\eta)^2}}\right)\right. \\ &\quad \left.+\int_{\frac{H^2}{(\Delta+2)^2}}^{\infty} dm\,|\psi_m|^2\left(|\chi_m|^2-\frac{(-H\eta)^3}{2H\sqrt{(m/H)^2+(-p\eta)^2}}\right)\right] \qquad (37)\\ &\equiv \int d^3p\frac{1}{p^3}\left[\langle\varphi^2\rangle_0+\langle\varphi^2\rangle_m\right], \qquad (38)\end{aligned}$$

where $\langle\varphi^2\rangle_0$ and $\langle\varphi^2\rangle_m$ are contribution from zero mode and massive mode, respectively. In the small η limit, each contribution can be written as,

$$\langle\varphi^2\rangle_0 \longrightarrow C_0^2\lambda_0\left(\frac{H}{2\pi}\right)^2\left(\frac{p}{H}\right)^{\frac{3\Delta+8}{\Delta+2}}, \tag{39}$$

$$\langle\varphi^2\rangle_m \longrightarrow C_m^2\lambda_0\left(\frac{H}{2\pi}\right)^2\left(\frac{pe^{a(\eta)}}{H}\right)^3\Bigg|_{\rm end}, \tag{40}$$

where C_0^2 and C_m^2 comes from $|\psi_0^2|$ and $|\psi_m^2|$, respectively. Then the zero-mode contribution to the perturbations are written as

$$\begin{aligned}A_S^2 &= \langle\mathcal{R}_c^2\rangle_{0-mode}\sim\left(\frac{1}{3\sqrt{2b}}\right)^2 C_0^2\left(\frac{H}{M_p}\right)^2\left(\frac{p}{H}\right)^{3\Delta+8/\Delta+2},\\ A_T^2 &= \langle h_{ij}^2\rangle_{0-mode}\sim C_0^2\left(\frac{H}{M_p}\right)^2\left(\frac{p}{H}\right)^{3\Delta+8/\Delta+2}, \qquad (41)\end{aligned}$$

and the relative amplitude of the scalar and tensor perturbations is written as

$$\frac{A_S^2}{A_T^2}\sim M_p^2\left(\frac{V_4'}{V_4}\right)^2. \tag{42}$$

It would be interesting to compare our model with an inflation model driven by inflaton ϕ_b on the brane with potential.

5 Acknowledgements

We would like to thank Daisuke Ida, Tetsuya Shiromizu and Takashi Torii for fruitful discussions. KK'S work and KT's work are supported by Grant-in-Aid f or JSPS Fellows.

References

[1] K. Koyama and K. Takahashi, hep-th/0301165.

Standing Shock Formation for Accreting MHD Plasma

Masaaki Takahashi,[1] Junya Goto,[2]

Department of Physics and Astronomy, Aichi University of Education, Kariya, Aichi 448-8542, Japan

Abstract

Fast and slow magnetosonic shock formations are presented for stationary and axisymmetric magnetohydrodynamical (MHD) accretion onto a black hole. The shocked accretion solution must pass through the magnetosonic points at some locations of outside and inside the shock location. We analyze critical conditions at the magnetosonic points and the shock conditions. Then, we show the restrictions on the flow parameters for strong shocks, which can appear very close to the event horizon. Examples of such magnetosonic shocks are provided.

1 Introduction

To explain the activity of active galactic nuclei (AGN) and compact X-ray sources, we consider accreting plasmas onto a black hole. The observed huge energy outputs are mainly originated from the gravitational energy released by infalling matters. When a black hole is rapidly rotating in an external magnetic field, we can also expect the release of the rotational energy of the black hole by the Blandford-Znajek process [1], which is an interaction between the black hole's spin and the magnetic field. The global magnetic field around the black hole should be enhanced by infalling magnetized plasmas, and the magnetic field generated by the dynamo motion of the surrounding plasma can also interact to the spin of the black hole. The "black hole magnetosphere" system, which is considered as a central engine of black hole activities and is composed by a rotating black hole, surrounding plasmas and magnetic fields, would output energy in the forms of high-energy radiations (X-rays and γ-rays) and highly-accelerated plasma outflows (relativistic jets or winds). In both energy output cases, the study of plasma behaviors in the magnetosphere is the key to problems. This situation is very similar to the activity of the solar magnetosphere (i.e., the emission of X-ray and the generation of solar wind).

In this paper, we discuss general relativistic effects on the streaming magnetohydrodynamical (MHD) plasma in the black hole magnetosphere: (1)"trans-magnetosonic" accretion and (2) MHD shock formation. The accretion must be super-magnetosonic at the horizon, and the flow injected from the plasma source with low-velocity must pass through the magnetosonic points (the slow magnetosonic point, the

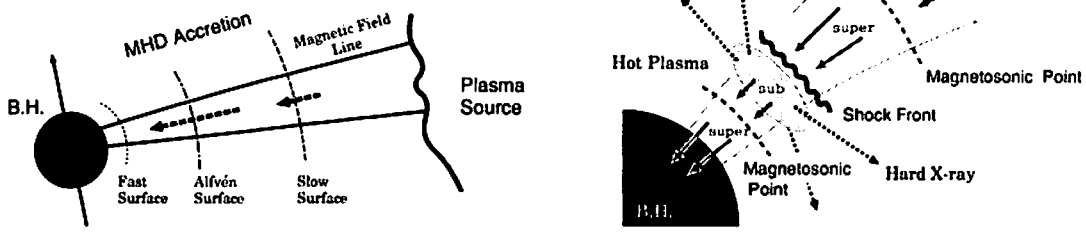


Figure 1: (a) A trans-magnetosonic accretion flow without a shock and (b) a magnetohydrodynamical shock formation. The post-shock plasma becomes hot by the entropy generation, and radiates high energy photons.

[1]E-mail:takahasi@phyas.aichi-edu.ac.jp
[2]E-mail:jgoto@hst.phyas.aichi-edu.ac.jp

Alfvén point, and fast magnetosonic point). If the magnetohydrodynamical shock is generated on the way to the event horizon, a very hot plasma region would be generated and high energy emissions from the hot plasma can carry informations of the strong gravitational field to us directly. In §2, we present the general relativistic MHD flows. The critical conditions at the magnetosonic point for MHD flows are argued in §3. The MHD shock generation is discussed in §4.

2 General Relativistic Magnetohydrodynamics

We consider stationary and axisymmetric ideal MHD accretion in Kerr geometry. The ideal MHD condition is $u^\beta F_{\alpha\beta} = 0$, the particle conservation law is $(nu^\alpha)_{;\alpha} = 0$, the equation of motion is $T^{\alpha\beta}_{\ ;\beta} = 0$, where u^α is the fluid 4-velocity, n is the number density of plasma, $F_{\mu\nu} = A_{\nu;\mu} - A_{\mu;\nu}$ is the electromagnetic tensor (A_μ is a vector potential). The energy-momentum tensor is given by $T^{\alpha\beta} = n\mu u^\alpha u^\beta - Pg^{\alpha\beta} + (1/4\pi)[F^\alpha_{\ \lambda}F^{\lambda\beta} + (1/4)g^{\alpha\beta}F^2]$, where $\mu = (\rho + P)/n = m_{\rm p} + (P/n)\Gamma/(\Gamma - 1)$ is the relativistic enthalpy, P is the gas pressure, ρ is the total energy density, Γ is the adiabatic index, $m_{\rm p}$ is the particle's mass and $F^2 \equiv F_{\mu\nu}F^{\mu\nu}$. We also assume the relativistic Polytropic relation [2] $P = K\rho_0^\Gamma$, where $\rho_0 = nm_{\rm p}$ is the rest mass density, which is related to the total energy density by $\rho = \rho_0 + P/(\Gamma - 1)$

In the stationary and Axisymmetric magnetosphere, we can define magnetic field lines as $\Psi(r,\theta) =$ constant lines, where $\Psi(= A_\phi)$ is the magnetic stream function. The plasma streams along the magnetic field line with five constants of motions: (1) the particle number flux per unit magnetic flux, $\eta(\Psi) = (nu^p)/B^p$, (2) the angular velocity of the field lines, $\Omega_F(\Psi) = -F_{tr}/F_{\phi r} = -F_{t\theta}/F_{\phi\theta}$, (3)the total energy of the magnetized flow, $E(\Psi) = \mu u_t - \Omega_F B_\phi/(4\pi\eta)$, (4) the total angular momentum, $L(\Psi) = -\mu u_\phi - B_\phi/(4\pi\eta)$, and (5) Entropy $S(\Psi)$, which is related to K. From the poloidal components of equation of motion with five field aligned parameters, we can derive the general relativistic Bernoulli equation (the poloidal equation) [3, 4, 5] and the general relativistic Grad-Shafranov equation (the trans-field equation) [6, 7].

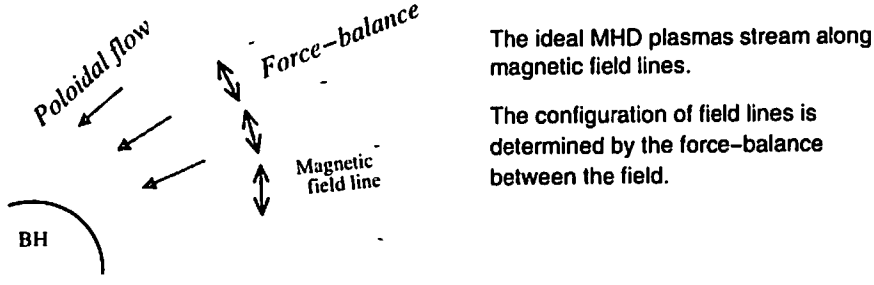


Figure 2: The structure of magnetosphere should be determined by solving the poloidal and trans-field equations self-consistently.

3 Critical Points for MHD flows

To fall into the black hole, the accreting plasma ejected from the plasma source with low-velocity must pass through the fast and slow magnetosonic points (S, F) and the Alfven point (A), which are singular points in the basic equations. The physical flow solution along a magnetic field line is restricted by the regularity conditions at these singular points. That is, the conditions restrict the possible ranges of physical flow parameters. The magnetic field configuration in the magnetosphere is affected by trans-magnetosonic flows streaming along each field lines. Even if we obtain a physical flow along a given magnetic field lines, which may be likely, the field configuration is not always consistent with the force-balance between magnetic field lines. We may obtain the modified field configuration satisfying the force-balance, but for the flow streaming along the new field lines the flow's parameter set should be also altered to satisfy the regularity conditions. We must reconsider a new parameter set for the physical trans-magnetosonic flow, and again we must regulate the field configuration. Thus, in general, it is hard to solve the magnetic structure of the magnetosphere self-consistently, so that we assume the comfiguration of the radial magnetic field line near the equatorial plane.

In the case of the black hole magnetosphere, there are two light surfaces, which are locations of $g_{tt} + g_{t\phi}\Omega_F + g_{\phi\phi}\Omega_F^2 = 0$. The plasma source must locate between these two surfaces. Although the location of the Alfvén point is determined by $\tilde{L} \equiv L/E = g^{\rm A}_{\phi\phi}(\omega_{\rm A} - \Omega_F)/(g_{tt} + g_{t\phi}\Omega_F)_{\rm A}$ [5], where label 'A' indicates quantities at the Alfven radius and $\omega \equiv -g_{t\phi}/g_{\phi\phi}$, for a slowly rotating black hole case $\omega_H < \Omega_F$ (ω_H is the angular velocity of a black hole), two locations of the Alfvén point are possible between the light surfaces. Correcponding to two locations of the Alfvén point, two distinct type accretion solutions exist [8]; (1) *magneto-like* and (2) *hydro-like* accretion solutions. The magneto-like accretion solution passes through the inner Alfvén point and is effective for the magnetically dominated flows, while the hydro-like accretion solution passes through the outer Alfvén point and becomes effective for the hydrodynamically dominated flows. For these two type solutions, the allowable parameter regions are separated, so that a discontinuous transition can be expected if the flow parameters change in a secular time-scale.

4 MHD Shock formation in curved spacetime

Now, let us consider MHD shock formations for accreting MHD flows. As mentioned the previous section, the critical conditions restrict the allowable ranges of physical flow parameters. For example, there are the maximum η and the minimum E for a magneto-like trans-fast MHD accretion. When we consider the shock formation, we must require a fast (or slow) multi-magnetosonic solution for accretion to fall into the black hole, and must apply the general relativistic MHD shock condition between two fast (or slow) magnetosonic points. The jump conditions for shocks in a relativistic MHD flow are [9, 10]

$$[nu^\alpha]n_\alpha = 0\ , \quad \text{– the particle number conservation} \tag{1}$$

$$[T^{\alpha\beta}]n_\alpha = 0\ , \quad \text{the energy momentum conservation} \tag{2}$$

$$[\mathrm{E}] \times \mathrm{n} = 0\ , \quad \text{– the continuity relations for the electric field} \tag{3}$$

$$[\mathrm{B}] \cdot \mathrm{n} = 0\ , \quad \text{– the continuity relations for the magnetic field} \tag{4}$$

where $n^\alpha = (n_0, \mathrm{n})$ is the shock normal, E and B are the electric and magnetic field in the shock rest frame, and $[\cdots] = (\cdots)_{\rm pre} - (\cdots)_{\rm post}$. From these conditions, we obtain that the four constants of motion E, L, η, Ω_F are continuous across the shock, while entropy S, which is the fifth constants of motion, is discontinuous across the shock [11]. Of course, for the physical shock the entropy must increase. When the trans-magnetosonic accretion solution, which passes though the first magnetosonic point, makes a shock on the way to the event horizon, the post-shocked sub-magnetosonic flow must pass through the second magnetosonic point (located inside the shock front) again. Such a physical accretion solution must satisfy the critical conditions at both the first and second magnetosonic points and the shock conditions. Thus, we must adjust the five parameters to the physical shocked accretion solution.

Figures 3a and 4a show the Alfvén Mach number of the fast and slow magnetosonic shock solutions, respectively. The upstream flow follows the hydro-like solution, and at the shock location the downstream flow transits to the magneto-like solution. In both demonstrated figures, the possible shock location is only one. (In Fig. 3, we can also find a location satisfying the jump condition within the second fast magnetosonic point. However, such a shocked flow cannot pass through the fast magnetosonic point to fall into the black hole, and gives an unphysical solution.) Figures 3b and 4b show the toroidal component of the magnetic field for the shocked solution; it increases at the fast magnetosonic shock, while it decrease at the slow magnetosonic shock.

The parameter search for the shocked accretion solution is very important to understand the properties of the shock formation and to guess the activities of black hole engine correctly (see [11, 12]). Figures 5a shows the relations of the total energy E and the shock location $r_{\rm s}$, and Figures 5b shows the relations of the particle number flux per the magnetic flux η and the shock location $r_{\rm s}$, for the fast magnetosonic shock. We find that $\eta_{\rm min}(\tilde{L}) < \eta(\tilde{L}) < \eta_{\rm max}(\tilde{L})$ and $E_{\rm min}(\tilde{L}) < E(\tilde{L}) < E_{\rm max}(\tilde{L})$ for the shock formation, where $\tilde{L}$, Ω_F and the hole's spin parameter a are fixed. An important point is that the maximum and minimum values (labeled by 'max' and 'min') exist; that is, the condition for the shock formation are limited by some range of the parameter value. We also see that for the range of $E(r_{\rm s} = r_{\rm A}) \lesssim E \leq E_{\rm min}$ the allowable shock locations are two. (We should discuss about the stability of MHD shock at each shock locations. However, the task is a problem beyond the scope of the present paper.) In this demonstration, we obtain

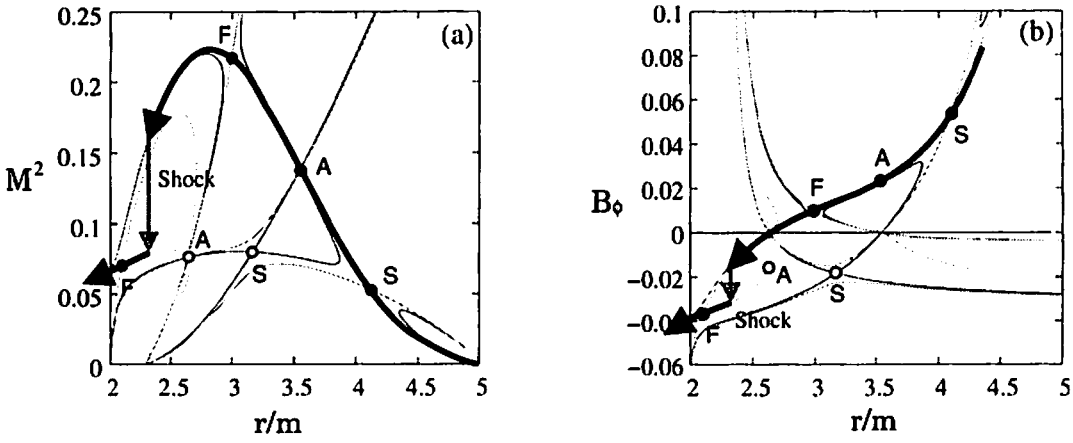


Figure 3: The fast-magnetosonic shocked accretion solution (thick curves): (a) The Mach number and (b) the toroidal magnetic field of the accretion solution ($E/m_p = 2.20$, $\tilde{L} = 4.44$, $\Omega_F = 0.154$, $4\pi\eta = 0.00461$, $a = 0$). The curves indicate constant entropy solutions, where thin curves are unphysical as shocked accretion solutions.

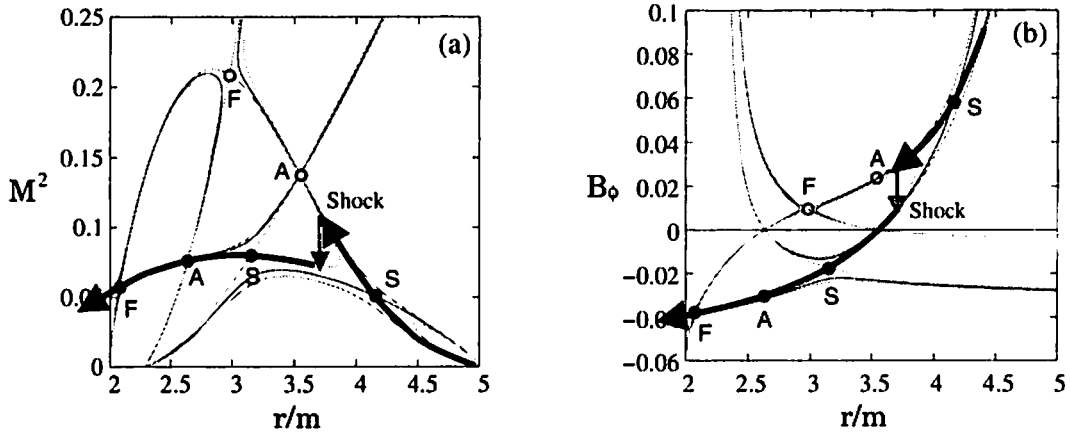


Figure 4: The slow-magnetosonic shocked accretion solution:(a) The Mach number and (b) the toroidal magnetic field of the accretion solution ($E/m_p = 2.40$, $\tilde{L} = 4.44$, $\Omega_F = 0.154$, $4\pi\eta = 0.00391$, $a = 0$).

the compression ratio to be $(nu^t)_{post}/(nu^t)_{pre} \sim 1.5 - 2$ for a distant observer and $n_{post}/n_{pre} \sim 2 - 3$ for a local observer.

5 Summary

We have discussed about MHD accretion onto a black hole with a magnetosonic shock formation, to form a hot plasma region very close to the black hole. To realize such a solution the multi-magnetosonic point solution is necessary, and then the shock formation is possible at the location satisfying the jump conditions. Although the flow parameters should be determined at the plasma injection source (the surface of an accretion disk or its corona, etc), from the restrictions of the critical conditions at the magnetosonic points and the jump conditions the shocked accretion phenomena would give us informations about plasma sources in a curved spacetime.

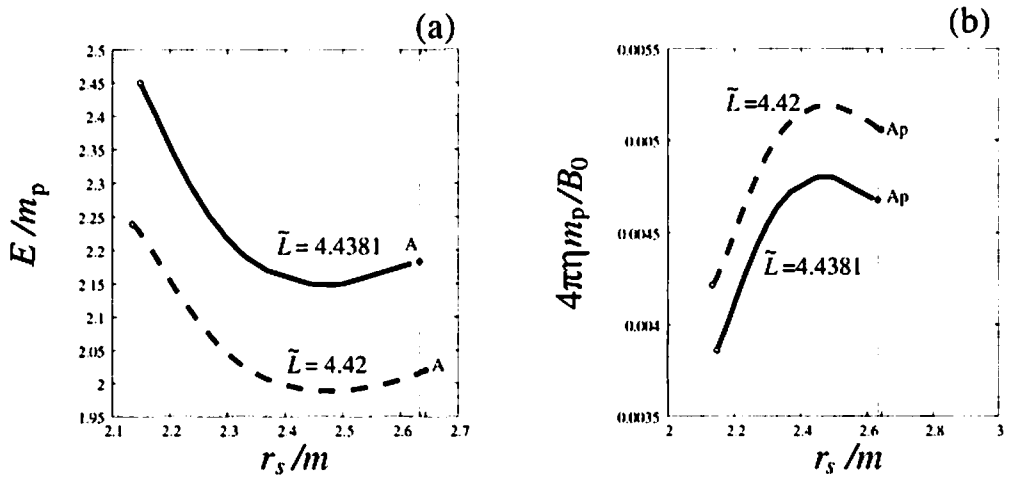


Figure 5: (a) The total energy $E(r_s)$ and (b) the particle number flux per the magnetic flux $\eta(r_s)$ for the fast magnetosonic shocked accretion at $r = r_s$. Each shocked accretion solutions passes through both the outer and inner fast magnetosonic points.

References

[1] R. D. Blandford and R. L. Znajek, Mon. Not. R. Astron. Soc. **179**, 433 (1977).

[2] R. F. Tooper, Astrophys. J. **142**, 154 (1965).

[3] M. Camenzind, Astron. Astrophys. **162**, 32 (1986).

[4] M. Camenzind, 1989, in *Accretion Disks and Magnetic Fields in Astrophysics*, ed. G. Belvedere (Kluwer, Dordrecht, 1989), p.129.

[5] M. Takahashi, S. Nitta, Y. Tatematsu, and A. Tomimatsu, Astrophys. J. **363**, 206 (1990).

[6] M. Camenzind, Astron. Astrophys. **184**, 341 (1987).

[7] S. Nitta, M. Takahashi, and A. Tomimatsu, Phys. Rev. **D44**, 2295, (1991).

[8] M. Takahashi, Astrophys. J. **570**, 264 (2002).

[9] A. Lichnerowicz, *Relativistic Hydrodynamics and Magnetohydrodynamics* (Benjamin Press, New York, 1975).

[10] S. Appl and M. Camenzind, Astron. Astrophys. **206**, 258, (1988).

[11] M. Takahashi, D. Rilett, K. Fukumura, and S. Tsuruta, Astrophys. J. **572**, 950 (2002).

[12] M. Takahashi, in *Proceedings of the 8th Asian-Pacific Regional Meeting (vol.II)*, eds. S. Ikeuchi *et al* (PASJ, Tokyo, 2002), p.359.

Multi-wavelength Astrometric Microlensing
— Detecting Microlensing Phenomena without Monitoring —

Rohta Takahashi[1]

Yukawa institute for theoretical physics, Kyoto University, Sakyo-ku, Kyoto 606-8502, Japan

Abstract

I propose multi-wavelengths observation of the astrometry to detect lensing phenomena. It is known that the astrometrical shift of the extended source depends on the size of the sources. When the objects are lensed, the positions of their centroids differ at different wavelengths, if the effective size of the emitting regions depend on the wavelengths. In such case, we can know whether or not the object is lensed by multi-wavelength observations. This method dose not require monitoring observations. Microlens events with a long crossing time (e.g. 1000 year) of Einstein-ring radius, which do not show neither the short-time photometric change nor effective positional shifts, can be detected by this method.

1 Introduction

Angular separation of multiple images formed by microlensing is generally so small that they remain unresolved by the present observational facilities. Typically these are 1 mas for microlens in our Galaxy (e.g. Paczyński 1996), and 1-100 μ as for a quasar microlensing (e.g. Schneider, Ehlers & Falco 1992). The point source approximation breaks down only when the impact parameter is comparable to the finite size of the source. Although such circumstances are rare, they carry a large scientific payoff. If there are differences beween the emitting regions at different wavelengths in a source, the separations between the centroidal positions of images at such wavelengths are expected to exist. It is because the centroidal position depends on the structure of the source. These chromatic signatures of astrometric microlens phenomena contains unique properties of microlensing and information of a source (§2). The purpose of the present study is to investigate and propose the multiwavelengths astrometrical observations as tools of detecting lensing phenomena and analysing the structure of the source. Recently, the astrometry by SIM is proposed as tools in order to investigate the structure of a quasar (Urwin 2002). In the present study, we adopt a quasar as a source. It is because some accretion disk models of quasar emittion predicts the spatial difference of the emitting region at several wavelengths and this is appropreate to the multi-wavelengths observation.

2 Chromatic signatures of quasar astrometric microlensing

I especially consider a quasar as a source object in this section. I assume a quasar as an extended source with circularlly emitting region at several wave-bands. I here consider two representative accretion flow models: the optically thick and thin disks. First, we consider the optically-thick standard disk (Shakura & Sunyaev 1973, Novikov & Thorne 1973). We set the mass of the black hole $M_{\rm BH}$ at the center of the disk to be $1.0 \times 10^9 M_\odot$. Since the disk is optically thick, we can assume blackbody radiation. As a consequence, the emitted photon energy range is rather restricted to optical-UV ranges. The next adapted solution is an optically-thin advection-dominated accretion flow (ADAF; Ichimaru 1977, Narayan & Yi 1995, Abramowicz et al. 1995). In this disk, the radiation emissivity dose not always reflect the shape of the potential well (see Kato et al. 1998 for the detailed discussion).

2.1 Astrometrical shift for multi-wavelength centroidal images

We adopt the redshift parameters of a source $z_{\rm os} = 1.675$ and a lens $z_{\rm ol} = 0.039$, which are those of Q2237+0305. z_{ls}, redshift between a source and a lens, are calculated by the relation of $1 + z_{\rm ls} =$

[1] E-mail:rohta@yukawa.kyoto-u.ac.jp

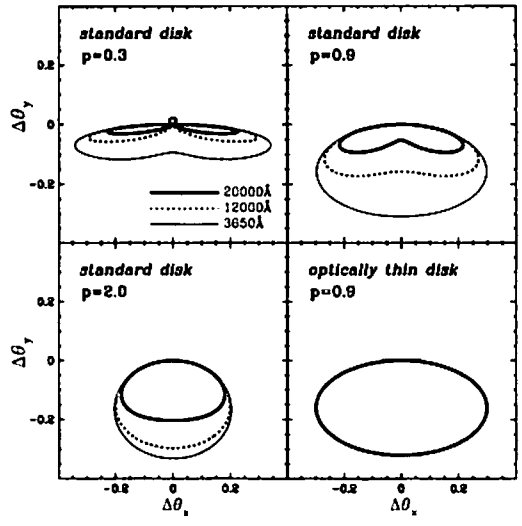


Figure 1: Astrometric trajectories of the centroids of the image for cases of a standard disk and an optically thin disk, showing effects of intensity profiles of source.

$(1+z_{os})/(1+z_{ol})$ (e.g.,Padmanabhan 1993). Note that in the case of Q2237+0305 a single point-lens approximation may be a poor approximation because the optical depths of microlensing are not low. Here we just take these redshifts as one test case and drive quite general conclusions regarding the generic properties of the multi-wavelength astrometric observations, and therefore our conclusions are independent of this particular quasar. We set a mass of a single point lens $M_{\rm lens}$ to be 0.1 $M_\odot$ and a radius of a disk to be $10^3 r_{\rm S}$, where $M_\odot$ is a solar mass and $r_{\rm S}$ is a Schwartschild radius $r_{\rm S} = 2GM_{\rm BH}/c^2$. The angular Einstein ring radius in this system is $\theta_{\rm E} = 2.3\ \mu{\rm as}\ (M_{\rm lens}/0.1M_\odot)^{1/2}(d/0.16{\rm Gpc})^{1/2}$ Here, $M_{\rm lens}$ is a mass of the lens, $d \equiv d_{\rm L}d_{\rm S}/d_{\rm LS}$, and $d_{\rm L}$,$d_{\rm S}$,$d_{\rm LS}$ are the disance to a lens, to a source and from a lens and a source, respectively. The angular Schwartzshild radius $\theta_{\rm S}$ of the radius of the accretion disk is $\theta_{\rm S} = 0.011\ \mu{\rm as}(M_{\rm BH}/10^9 M_\odot)(d_{\rm S}/1.7{\rm Gpc})^{-1}$. From these, the Einstein ring radius $\theta_{\rm E}$ and the 200 times Schwartzschild radius of the accretion disk are comparable value: $\theta_{\rm E} \sim 200\theta_{\rm S}$. The Einstein ring crossing time $t_{\rm E}$ is defined and evaluated as $t_{\rm E} = 7.8{\rm yr}(v_{\rm t}/220{\rm km}^{-1})^{-1}(d'/1.6{\rm Mpc})^{1/2}(M_{\rm lens}/0.1M_\odot)^{1/2}$. Here, $v_\perp$ is a transevese velosity in the lens plane and $d' \equiv d_{\rm LS}d_{\rm L}/d_{\rm S}$.

In figure 1, we show the astrometrical trajectories in the case of a satandard disk and an ADAF at U-band (3650Å, thin solid line), J-band (12000Å, dotted line) and K-band (20000Å, thick solid line). In the case of standaed disk, we cauculate the trajectories with impact parameters p of 0.3 (*upper-left*), 0.9 (*upper-right*) and 2.0 (*lower-right*), while in the case of ADAF with only $p = 0.9$ (*lower-left*). All the angles are normalized by the Einstein ring radius $\theta_{\rm E}(\sim 2.2\mu{\rm as})$.

For the uniform source, the maximum shift of the centroid is largest in the case that the radius of the source is nealy the Einstein ring radius. In the case of the standard disk, the maximum coodinate of x-axis of the trajectories is largest at 3650Å and smallest at 20000Å. This is because the radial profile of the emission at 3650Å concentrate much more in the central part ($< 200r_{\rm S} \sim \theta_{\rm E}$) of the disk than that of 20000Å. The smaller the impact parameter become, the more the trajectory was alongated to the x-axis direction. This property is the same as the case of the point source. In the case of the point source, trajectries of an astrometric microlensing by a single point lens are elliptics (e.g. Walker 1995, Dominik & Sahu 2000). In the case of the same impact parameter, the extended source effects are seen in the trajectories of the most extended emitting region.

The extend of the trajectories in y-direction are smaller for the smaller impact parameters. This properties are same as the case of point source and uniform source. For a point source, the shape of the trajectories are an ellipse (Dominik & Sahu 2000). The shifts of the trajectroies from an ellipse are due to the extended source size (Mao & Witt, 1998). Therefore, the shape of trajectories at 20000Å shifts from an ellipse most drastically in the case of a standard disk. We can know the impact parameters

from the shape of the trajectory and obtain the information of the radius of the emitting region from the distortion of the trajectry from the ellipse.

In the case of the ADAF, the difference of the trajectories at U-band, J-band and K-band are negligiblly small. It is because the radial distribution of emission at these wavelengths are very similar, and the discrepancies in trajectories are little.

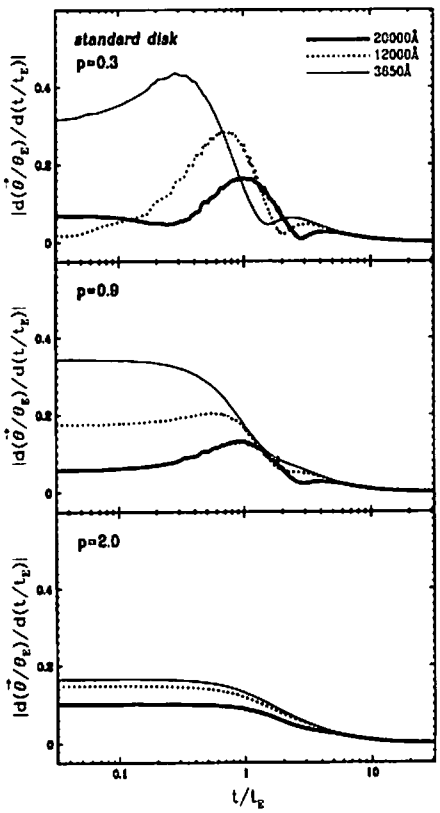


Figure 2: The time dependence of angular velosities of the centroid at 3650Å(thin solid line), 12000Å(dotted line), and 20000Å(thick solid line).

Another observational quantity is a velocity of the centroid of the image. These velocities also reflect the effect of a source and a lens. In figure 2, we show the time dependence of angular velosities of the centroid at 3650Å (thin solid line), 12000Å (dotted line), and 20000Å (thick solid line). The adapted impact parameters (p) are $p = 0.3$ (*top*), 0.9 (*middle*), and 2.0 (*bottom*), respectively. All the angles and time are normalised by the Einstein rind angular radius (θ_E) and the Einstein time t_E. The velocity and the acceleration of the centroid depends on the position of the centroid on the trajectories. Then, we can put constraints on the position of the centroid in the trajectry by the acceleration of the centroid. In the case that the shape of the trajectry is similar to an ellipse, the velocities are largest at the origin of time $t = 0$, which is seen in the cases of $p = 0.9$ at 3650Åand $p = 2.0$ at all bands. In the case of that the shape of the trajectories are shifted from an ellipse, the velocities have a peak outside the position at the origine of time , which are seen in the cases of $p = 0.9$ at 12000Å and 20000Å, and $p = 0.3$ at all bands. From the comparison of the velosity and the accelarations of the centroidal motions at different wavebands, we can catch the extended source effects and constrant on the relations between the size of the source and the impact parameters.

2.1.1 Positional difference between multi-wavelangth images

Next, we pay attention on the chromatic signatures of the trajectories. If the emission regions at several bands of the source drastically differ, the centroid positons at the corresponding bands are different each other when the source is microlensed. Therefore, we can detect the microlensing phenomena by the multi-wavelength astrometrical observations at a same time. This is a new method of detecting microlensing phenomena and this method need no monitoring of the source objects.

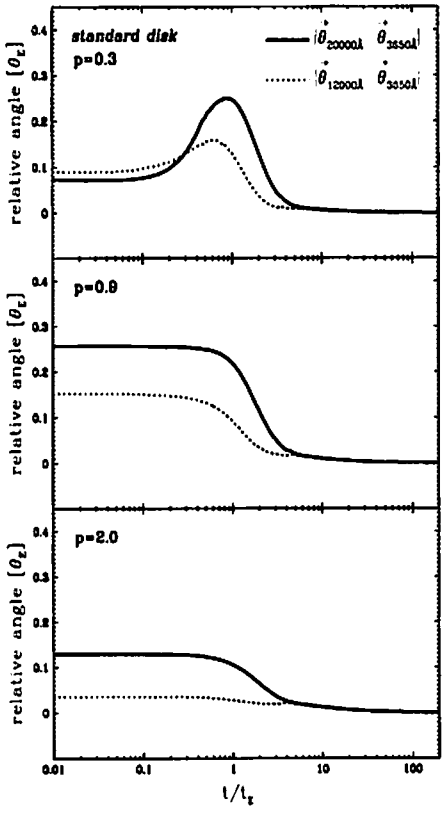


Figure 3: The time dependence of the relative angular distances between the centroids at 3650Å($\vec{\theta}_{3650A}$), 12000Å($\vec{\theta}_{12000A}$) and 20000Å($\vec{\theta}_{20000A}$) for the case of a standard disk. The relative angles of $|\vec{\theta}_{20000A} - \vec{\theta}_{3650A}|$ (solid line) and $|\vec{\theta}_{12000A} - \vec{\theta}_{3650A}|$ (dotted line) are presented. The adapted impact parameters (p) are $p = 0.3$ (*top*), 0.9 (*middle*), and 2.0 (*bottom*), respectively. All the angles and time are normalised by the Einstein rind angular radius (θ_E) and the Einstein time $t_E = \theta_E d_L/v_t$, respectively, where d_L is the distance to the lens and v_t is the transeverse velosity of the lens.

In figure 3, we shows the time dependence of the positional difference between multi-wavelengths images for the cases of $|\vec{\theta}_{43GHz} - \vec{\theta}_{3650A}|$ (solid line) and $|\vec{\theta}_{20000A} - \vec{\theta}_{3650A}|$ (dotted line). Figure 3 is the main results in the present proceeding. The adapted impact parameters (p) are $p = 0.3$ (*top*), 0.9 (*middle*), and 2.0 (*bottom*), respectively. All the angles and time are normalised by the Einstein rind angular radius (θ_E) and the Einstein time $t_E = \theta_E d_L/v_t$, respectively, where d_L is the distance to the lens and v_t is the transeverse velosity of the lens.

In the case of the $p = 0.9$ and 2.0, the leargest relative angles are achieved in time of $t \lesssim t_E$ in the both cases of $|\vec{\theta}_{20000A} - \vec{\theta}_{3650A}|$ and $|\vec{\theta}_{12000A} - \vec{\theta}_{3650A}|$. However, in the case of $p = 0.3$, the laegest relative angles at both case are around time of $t \sim t_E$. This is because in these case the trajectories suffer greatly by the effects of the extended source at $t \lesssim t_E$. As are shown in figure 1, the shapes of the trajectories exhibit clover-leaf features in the case of a standard disk with $p = 0.3$ at 20000Å, in which the distance between the positions of the centroids at 12000Å and 20000Å and that at 3650Å become shorter at

time $t \lesssim t_{\rm E}$. In our calculation, the largest relative angles are achieved at the impact parameter around $p = 0.9$. There exits the critical impact parameter which exhibits the largest relative angles between the centroids at the different wavelengths, and this impact parameter depends on the source profile at multi-wavelengths.

In the present system of a lens $= 0.1 M_{\odot}$ and a source, the anguler Einstein ring radius is $\theta_{\rm E} \sim 2.2 \mu$as. Therefore, the differences at multi-wavelenghts are not within the ability of the planned astrometry satelite. However, in the case of a more large mass $> 0.1 M_{\odot}$ of a lens and a smaller distance of a lens, the Einstein ring radius is larger than 2.2 μas. Therefore, there remains the detectabilities of a chromatic signatures of a quasar microlens phenomena by the planned astrometry missions.

3 ASTROMETRIC MICROLENSING PHENOMENA AT MULTI-WAVEBANDS

Following the past study of the the microlens events, we can count the different properties of the astrometrical observations from the photometric observations are listes up as follows: (1) We can detect the events by the shifts of images through monitoring (e.g. Walker 1995, Pczyński 1998). (2) In the case of the violent variability of the source, we can distinguish the microlensing events by the shifts of images. In this case, it is difficult to detect the microlensing events by the light curves. In the case of quasar microlens phenomena, we need the multiple images of the lensed quasar to detect the microlens phenomena by the time delay of the images because of the variability of quasar emission. The astrometrical change dose not suffer the photometric change of a source. (3) We can detect the microlensing phenomena in the case of a large impact parameter $p \sim 50 - 100\theta_{\rm E}$ using the highly advanced astrometrical technique with a positional accuracy of 10 μas (Honma & Kurayama, 2002).

The objective of this letter is to study the chromatic signatures of the astrometric microlens phenomena and we list up the unique properties of these events. Here, we mainly concentrate on the different properties between the astrometric microlensing observations at multi-wavebands and those at a single waveband.

1. We can detect the microlensing events by the shifts of positions of images at multi-wavelengths, in the case that the spacial distribution of the emission region at several wavelengths are not similar.

2. By using the technique described in the previous item, we need no monitoring to detect the microlens events.

3. In the case of the long crossing time, e.g. $t_{\rm E} \gg 1000$ year, we can detect the microlensing events by the positional difference of the multi-wavelengths images.

4. We can detect the high magnification events which dose not show the short-time photometric and positional change due to microlensing because of a large crossing time; e.g. $t_{\rm E} \gg 100$ year.

The author is grateful to S. Mineshige for continuous encouragement.

Thermodynamic properties of massive dilaton black holes

Takashi Tamaki [1]

Department of Physics, Waseda University, Ohkubo, Shinjuku, Tokyo 169-8555, Japan

Abstract

We numerically reanalyze static and spherically symmetric black hole solutions in an Einstein-Maxwell-dilaton system with a dilaton potential $m_d^2\phi^2$. We investigate thermodynamic properties for various dilaton coupling constants and find that thermodynamic properties change at a critical dilaton mass $m_{d,crit}$.

1 Introduction

The black hole solution in the Einstein-Maxwell-dilaton system (GM-GHS) has many distinctive properties from those of the conventional Reissner-Nordström (RN) black hole[1]. Hairy black holes[2, 3, 4] which have a Yang-Mills field and a Higgs field also change qualitatively when scalar hair is added[5].

However, since a massless dilaton field is excluded by experimental considerations[6], we need to investigate solutions with a massive dilaton field. Several authors have discussed this possibility and found interesting properties[7]. We concentrate here on studying the thermodynamic properties of these black holes which have not been investigated so far[8]. Throughout this paper, we use the units $G = c = \hbar = 1$.

2 Basic Equations

We take the action as follows,

$$S = \int d^4x\sqrt{-g}\left[R - 2(\nabla\phi)^2 - e^{-2\gamma\phi}F^2 - 2V(\phi)\right], \tag{1}$$

where ϕ, γ and $V(\phi)$ are a dilaton field, its coupling constant and its potential, respectively.

We consider the static and spherically symmetric metric as

$$ds^2 = -f(r)e^{-2\delta(r)}dt^2 + f(r)^{-1}dr^2 + r^2d\Omega^2, \tag{2}$$

where $f(r) := 1 - 2m(r)/r$. We choose a gauge potential $A_\mu = (A(r), 0, 0, Q_m\cos\theta)$, where Q_m is a magnetic charge. We do not consider a dyonic black hole which has both an electric and a magnetic charge here. Below, we consider a dilaton potential $V = m_d^2\phi^2$ where m_d is the dilaton mass, for simplicity. In this case, the boundary conditions at spatial infinity to satisfy asymptotic flatness are

$$m(\infty) =: M = const., \quad \delta(\infty) = 0, \quad \phi(\infty) = 0. \tag{3}$$

From the Maxwell equation, we obtain $(rK)' + K = 0$, where $' := d/dr$ and $K := A'e^{-2\gamma\phi+\delta}$. By integrating this equation, we obtain $r^2K = const. =: Q_e$. Finally, our basic equations are

$$m' = \frac{r^2}{2}\left(f\phi'^2 + B + V\right), \quad \delta' = -r\phi'^2, \quad A' = \frac{Q_e}{r^2}e^{2\gamma\phi-\delta}, \tag{4}$$

$$\phi'' + \frac{2\phi'}{r} + \frac{1}{f}\left[\phi'\left\{\frac{2m}{r^2} - r\left(B + V\right)\right\} + \gamma\left(\frac{Q_m^2}{r^4}e^{-2\gamma\phi} - \frac{Q_e^2}{r^4}e^{2\gamma\phi}\right) - \frac{1}{2}\frac{dV}{d\phi}\right] = 0, \tag{5}$$

where we use the abbreviation

$$B := \frac{Q_m^2}{r^4}e^{-2\gamma\phi} + \frac{Q_e^2}{r^4}e^{2\gamma\phi}. \tag{6}$$

[1] E-mail:tamaki@gravity.phys.waseda.ac.jp

We also assume the existence of a regular event horizon at $r = r_h$. So we have

$$m_h = \frac{r_h}{2}, \quad \delta_h < \infty, \quad \phi_h < \infty, \quad \phi_h' = \frac{r(dV_h/d\phi - 2\gamma B_h)}{2\{1 - r_h^2(B_h + V_h)\}}. \tag{7}$$

The variables with subscript h are evaluated at the horizon. We will obtain the black hole solution numerically by determining ϕ_h iteratively to satisfy these conditions.

3 The GM-GHS solution

To describe the exact solution, it is convenient to use the following spherically symmetric ansatz:

$$ds^2 = -\lambda^2 dt^2 + \frac{1}{\lambda^2} dr^2 + R^2 d\Omega^2 , \tag{8}$$

where λ and R are functions of r only. We consider the electrically charged case. Since this system has an electric-magnetic duality $F \to e^{-2\phi}\tilde{F}$, $\phi \to -\phi$, we can easily obtain the results for the magnetically charged case. With the above ansatz, we obtain

$$e^{2\phi} = \left(1 - \frac{r_-}{r}\right)^{2\gamma/(1+\gamma^2)}, \quad R = r\left(1 - \frac{r_-}{r}\right)^{\gamma^2/(1+\gamma^2)}, \quad \lambda^2 = \left(1 - \frac{r_+}{r}\right)\left(1 - \frac{r_-}{r}\right)^{(1-\gamma^2)/(1+\gamma^2)}, \tag{9}$$

where we have set the asymptotic value of the dilaton field to zero. r_+ and r_- are the event horizon and the inner horizon, respectively. Temperature T is written as

$$T = \frac{1}{4\pi r_+}\left(1 - \frac{r_-}{r_+}\right)^{\frac{1-\gamma^2}{1+\gamma^2}}. \tag{10}$$

This vanishes in the zero horizon area limit for $\gamma < 1$, whereas it has a finite value $1/(8\pi M)$ for $\gamma = 1$ and diverges for $\gamma > 1$ in the same limit. Thus, these differences are caused by the dilaton field and to examine this feature for the massive dilaton black hole is one of our basic motivations.

4 Properties of the massive dilaton black hole

If the dilaton potential V is convex[7], the dilaton is monotonically increasing (decreasing) outside the horizon for the electrically (magnetically) charged solution. When V is an even function, we also have the electric-magnetic duality mentioned above. Consider the magnetically charged solutions with $Q_m = 0.1$.

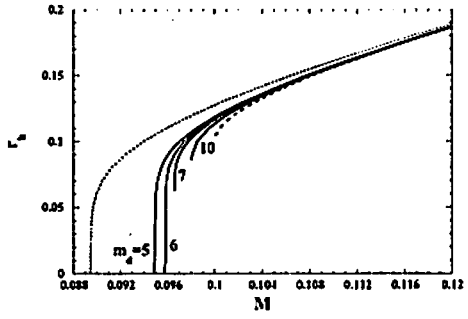
First, we consider the dilaton field in an asymptotic region. For the GM-GHS solution, the dilaton field goes as $e^{-2\phi} \sim 1 + 2\Sigma/r$ in the asymptotic region, where Σ is a dilaton charge. For the massive dilaton black hole, the dilaton field behaves as $\phi \sim \gamma Q_m^2/m_d^2 r^4$[7] since Eq. (5) can be approximated as $2\gamma Q_m^2/r^4 = dV/d\phi$, by neglecting the derivative terms of ϕ in the asymptotic region. Thus, the dilaton charge is lost because of the dilaton potential.

Next, we analyze the conditions for the existence of a degenerate horizon along the same lines as Ref. [7]. If the horizon becomes degenerate at $r = r_d$, we have $m' = 1/2$ at the horizon, which leads to

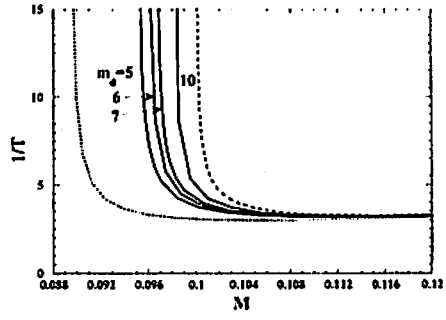
$$\frac{e^{2\gamma\phi_d}}{\phi_d(\phi_d + 1/\gamma)^2} = \gamma Q_m^2 m_d^2. \tag{11}$$

As we mentioned above, ϕ_d is restricted to $\phi_d > 0$ since the dilaton is monotonically decreasing outside the horizon for the magnetically charged case. Thus, the left-hand side of Eq. (11) reaches its minimum value $e^2\gamma^3/4$ at $\phi_d = 1/\gamma$. [e here refers to the Euler number $e = 2.71\cdots$.] Thus, the solution for $Q_m^2 m_d^2 < e^2\gamma^2/4$ does not have an extreme limit. Let us denote the dilaton mass which satisfies $Q_m^2 m_d^2 = e^2\gamma^2/4$ by $m_{d,crit}$. For $\gamma = 0.5$, 1 and $\sqrt{3}$, we find that $m_{d,crit} = 6.79\cdots$, $13.59\cdots$ and $23.54\cdots$, respectively.

r_h and $1/T$ are shown in terms of M for the case $\gamma = 0.5$, 1 and $\sqrt{3}$ (suggested by Kaluza-Klein theory) in Figs. 1, 2 and 3 (a) and (b), respectively (solid lines). We also show the GM-GHS and the RN solutions with a dotted line and a dashed line, respectively.

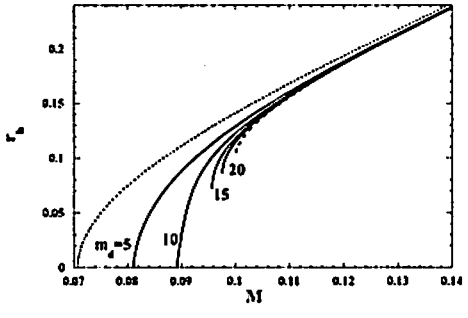


(a)

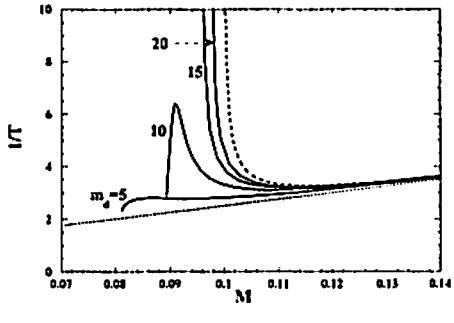


(b)

Figure 1: (a) r_h and (b) $1/T$ in terms of the mass M with $\gamma = 0.5$.

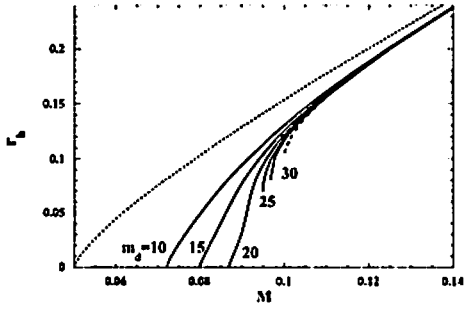


(a)

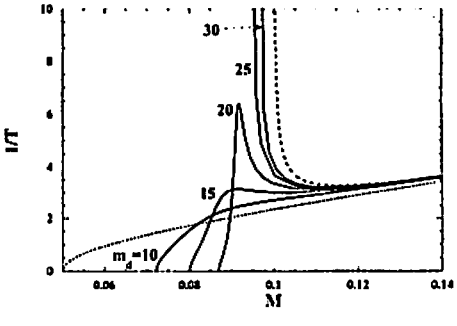


(b)

Figure 2: (a) r_h and (b) $1/T$ in terms of the mass M with $\gamma = 1$.



(a)



(b)

Figure 3: (a) r_h and (b) $1/T$ in terms of the mass M with $\gamma = \sqrt{3}$.

The relationship between the extreme solution and the zero temperature is directly connected to the first law of black hole thermodynamics. If we fix the magnetic charge, it can be expressed as

$$\frac{dr_h}{dM} = \frac{1}{2\pi r_h T} . \tag{12}$$

For the GM-GHS solutions with $\gamma = 1$, since dr_h/dM diverges as r_h approaches zero, T can remain finite. For massive dilaton black holes, there are two distinct cases. For $m_d > m_{d,crit}$, there is an extreme solution for nonzero horizon radius. For $m_d < m_{d,crit}$, the solution continues to exist in the $r_h \to 0$ limit where T remains finite nonzero value, as in the corresponding GM-GHS solution.

It is surprising that the temperature in the zero horizon limit for $m_d < m_{d,crit}$ closely resembles that of the GM-GHS solution. I.e., the temperature diverges, approaches zero or has a finite nonzero value in the zero horizon limit, according as $\gamma > 1$, $\gamma < 1$ or $\gamma = 1$, respectively. We confirmed this result for various γ. This is related to the fact that the dilaton field behaves like a massless field within its Compton wavelength. However, since the mass term of the dilaton field affects the gravitational mass even in the zero horizon limit, the solution itself is quite different from the GM-GHS solution. Thus, it is not trivial whether or not the temperature of a massive dilaton black hole in the zero horizon limit resembles that of the GM-GHS solution qualitatively.

In previous papers[7], it was shown that a necessary condition for the existence of three horizons is the violation of the strong energy condition (SEC). In our example, the violation of the SEC necessarily means that $m_d > m_{d,crit}$. So, one interesting possibility is that the final fate of the black hole depends only on the dilaton coupling for general matter fields if the SEC holds.

5 Near critical dilaton mass

Here, we show the qualitative difference caused by the dilaton mass in a more explicit way. We do this by means of a diagram for the case $\gamma = 1$. However, our discussion is general for arbitrary γ.

We plot M-r_h for $\gamma = 1$ near $m_{d,crit}$ in Fig. 4 (solid lines). We also show the "inner horizon" with dotted lines. As was shown in previous papers[7], there is no "inner horizon" for large black holes, while one does appear for small black holes. This kind of behavior is also found in charged black holes with Born-Infeld type nonlinear electrodynamics[9]. It is also worth mentioning that the inner horizon disappears in the Born-Infeld type black hole if we include a dilaton field[10].

Since we need fine-tuning of the dilaton field ϕ to satisfy regularity at the inner horizon, a curvature singularity appears there in general and is spacelike as in the GM-GHS solution. The "inner horizon" disappears below the point B in Fig. 4 where $dr_h/dM \to \infty$ and $r_h \sim 1/m_d$. The point A corresponds to the point where two horizons separate.

It is astonishing that there are solutions below points C for $14.8 \gtrsim m_d > m_{d,crit}$. Gravitational mass of the point C coincides with that of the point A. So it is supposed that uniqueness of solutions for fixed parameters holds in our system. Temperature is finite and the SEC holds in these cases.

As m_d approaches $m_{d,crit}$ for $m_d > m_{d,crit}$, the curve between A and B becomes small. For $m_d = 13.6$, A almost coincides with B and C. It is natural to suppose that A coincides with B and C for $m_d = m_{d,crit}$. This is related to the existence of a triply-degenerate horizon, as pointed out in previous papers[7].

6 Conclusion and Discussion

We have investigated static spherically symmetric solutions in the Einstein-Maxwell-dilaton system with a dilaton potential $V = m_d^2\phi^2$. We considered the magnetically charged solution for various values of the dilaton coupling. We confirmed that the properties of black holes change qualitatively at $m_{d,crit}$.

For $m_d \geq m_{d,crit}$, which means the violation of the SEC, there is an extreme solution for nonzero horizon radius. For $m_d < m_{d,crit}$, the solution continues to exist in the $r_h \to 0$ limit where the temperature remains either finite and nonzero, diverges, or approaches zero for $\gamma = 1$, $\gamma > 1$ and $\gamma < 1$, respectively.

This property may also hold when the SEC is not violated. For example, the Einstein-Yang-Mills-dilaton (EYMD) system has been considered before[2, 3, 4] and exhibits thermodynamic properties similar to those above, if the black hole has a globally magnetic (or electric) charge. To prove this for general matter fields, or to find a counterexample is a task we hope to take up in future research.

References

[1] G. W. Gibbons and K. Maeda, Nucl. Phys. B **298**, 741 (1988); D. Garfinkle, G. T. Horowitz and A. Strominger, Phys. Rev. D **43**, 3140 (1991).

[2] G. Lavrelashvili and D. Maison, Nucl. Phys. B **410**, 407 (1993); E. E. Donets and D. V. Gal'tsov, Phys. Lett. B **302**, 411 (1993); T. Torii and K. Maeda, Phys. Rev. D **48**, 1643 (1993); C. M. O'Neill, Phys. Rev. D **50**, 865 (1994).

[3] B. Kleihaus, J. Kunz and A. Sood, Phys. Lett. B **354**, 240 (1995); *ibid.*, Phys. Rev. D **54**, 5070 (1996); *ibid.*, Phys. Lett. B **372**, 204 (1996); *ibid.*, **374**, 289 (1996); *ibid.*, **418**, 284 (1998).

[4] T. Tamaki, K. Maeda and M. Inada, Phys. Rev. D **63**, 087504 (2001).

[5] T. Tamaki, K. Maeda and T. Torii, Phys. Rev. D **57**, 4870 (1998); *ibid.*, **60**, 104049 (1999).

[6] C. Will, Theory and Experiment in Gravitational Physics (Cambridge Univ. Press, Cambridge, 1981).

[7] R. Gregory and J. A. Harvey, Phys. Rev. D **47**, 2411 (1993); J. H. Horne and G. T. Horowitz, Nucl. Phys. B **399**, 169 (1993).

[8] T. Tamaki and H. Yajima, Phys. Rev. D **64**, 084002 (2001); T. Tamaki, Phys. Rev. D **66**, 104021 (2002).

[9] M. Demianski, Found. Phys. **16**, 187 (1986); H. d' Oliveira, Class. Quant. Grav. **11**, 1469 (1994).

[10] T. Tamaki and T. Torii, Phys. Rev. D **62**, 061501 (2000); *ibid.*, **64**, 024027 (2001).

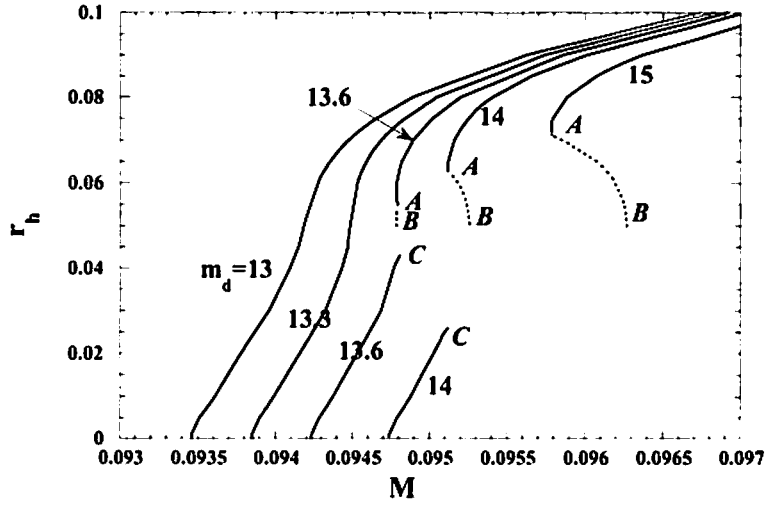


Figure 4: M-r_h with $\gamma = 1$.

Quantum Radiation by a Moving Brane

Izumi Tanaka,[1] Hideki Ishihara[2]

Department of Physics, Graduate School of Science,
Osaka City University, Sumiyoshi, Osaka 558-8585, Japan

Abstract

Embedded flat Friedmann-Robertson-Walker-brane universe in the five-dimensional anti-de Sitter spacetime is recognized as a moving boundary. The quantum effects of a minimal coupling scaler field resulting from the moving boundary is discussed.

1 Introduction

We study quantum effects resulting from the evolution of brane universe which is embedded in the five dimensional anti-de Sitter(AdS) bulk spacetime in the context of the Randall-Sundrum(RS) model with Z_2 symmetry[1]. Randall-Sandrum brane is a static vacuum solution and can be recognized as the Minkowski vacuum state against the brane containing matter.

Cosmological brane models containing matter on the brane are investigated by many authers.[2] The brane evolves on the bulk spacetime through the process of expanding phase of universe. If the universe is a sub-spacetime embedded in a higher dimensional spacetime, there may be great changes of basic properties of cosmological models[3]. On the scheme of the Z_2-symmetric brane universe[4] inspired by Horava-Witten theory[5], matter fields are confined to the brane, while gravitational fields and possible scaler fields propagate through all of spacetime. The evolving brane plays a role of moving boundary for fields living in the bulk spacetime. In this proceedings, we study a quantum effect by a evolving brane.

2 Brane Dynamics

We consider a brane universe embedded in the five-dimensional anti-de Sitter spacetime with a negative cosmological constant $-4/l^2$.

The five-dimensional anti-de Sitter spacetime has a structure of $\mathcal{N}^2 \times \mathcal{M}^3$ where $\mathcal{N}^2$ is a two-dimensional static spacetime and $\mathcal{M}^3$ is the three-dimensional flat space. The metric has the form

$$ds_5^2 = -\frac{r^2}{l^2}dt^2 + \frac{l^2}{r^2}dr^2 + \frac{r^2}{l^2}d\vec{x}^2. \tag{1}$$

Let us consider an embedding of a 4-dimensional hypersurface (three-brane), Σ, with the structure of $\mathcal{N}^1 \times \mathcal{M}^3$. We assume the position of $\mathcal{N}^1$ in $\mathcal{N}^2$ is given by

$$r = a(\tau), \quad t = T(\tau), \tag{2}$$

where a and T are functions of a parameter τ. When τ is normalized by

$$-d\tau^2 = -\frac{r^2}{l^2}dT^2 + \frac{l^2}{r^2}da^2, \tag{3}$$

the induced metric γ_{ab} on Σ has a form of the flat Robertson-Walker metric

$$ds^2 = \gamma_{ab}d\xi^a d\xi^b = -d\tau^2 + a^2(\tau)d\vec{x}^2. \tag{4}$$

If matter is confined on Σ, the surface energy-momentum tensor of the brane, S_{ab}, has a form of

$$S_{ab} = -\sigma\gamma_{ab} + T_{ab}, \quad (a, b = 0, 1, 2, 3), \tag{5}$$

[1] E-mail:itanaka@sci.osaka-cu.ac.jp
[2] E-mail:ishihara@sci.osaka-cu.ac.jp

where σ is the brane tension, and T_{ab} is the energy-momentum tensor of matter on Σ. Since the self-gravitating brane in the five-dimensional bulk should satisfy the metric junction condition[6] with Z_2 symmetry, the extrinsic curvature of Σ, K_{ab}, satisfies

$$K_{ab} = -\kappa^2 \frac{1}{2}(S_{ab} - \frac{1}{3} S\gamma_{ab}). \tag{6}$$

where κ^2 is the five-dimensional gravitational constant.

We assume, for simplicity, the energy-momentum tensor of matter takes the form of perfect fluid

$$T_{ab} = (\rho + p)u_a u_b + p\gamma_{ab}. \tag{7}$$

where $u = (\frac{\partial}{\partial \tau})$.

From the junction condition (6) with (5) and (7) we obtain the modified Friedmann equation[2]

$$\left(\frac{1}{a}\frac{da}{d\tau}\right)^2 = \frac{8\pi}{3}\frac{\kappa^4\sigma}{6}\rho + \frac{\kappa^4}{36}\rho^2, \tag{8}$$

and the conservation equation

$$\frac{d}{d\tau}(\rho a^3) + p\frac{d}{d\tau}(a^3) = 0, \tag{9}$$

where the fine tuning $1/l^2 = \kappa^4\sigma^2/36$ has been done so as to vanish the 4-dimensional effective cosmological constant on Σ.

We can rewrite (8) using (3) as

$$\left(\frac{da}{dT}\right)^2 = \frac{a^4}{l^4}\left[1 - \frac{a^2}{l^2}\left\{l^{-2}a^2 + \alpha^2 a^{2-q} + \beta^2 a^{2-2q}\right\}^{-1}\right], \tag{10}$$

where the equation of state is assumed as $p = (\frac{1}{3}q - 1)\rho$, $(q = const.)$, and α and β are constants.

When we take $q = 4$ (radiation dominant),

$$\alpha^2 = \frac{8\pi}{3}\frac{\kappa^4\sigma}{6}\rho_0 a_0^4, \qquad \beta^2 = \frac{\kappa^4}{36}\rho_0^2 a_0^8, \tag{11}$$

where ρ_0 and a_0 are the values of ρ and a at an arbitrary time t_0.

For Friedmann-Robertson-Walker(FRW) brane, asymptotic behaviour of $a(t)$ is

$$a(t) \sim \begin{cases} \dfrac{\alpha}{l}t & \text{as } t \to \infty, \\ -\dfrac{l^2}{t} & \text{as } t \to -\infty. \end{cases} \tag{12}$$

In this case, transition of the scale factor from the early behaviour to the later occurs at t_* which is determined by $a^2/l^2 \sim \alpha^2/a^2$. At this moment

$$a_* = \sqrt{\alpha l}, \qquad \rho_* = \kappa^{-2} l^{-1}. \tag{13}$$

The typical trajectory of FRW universe and Randall Sandrum model are shown together as fig.1. Viewed from the global time, Randall-Sandrum model has a trajectory of a constant acceleration in AdS. Flat FRW universe has the 3 phases of motion in AdS. In the 1st phase of early stage from the Big bang, the brane starts along null direction. In the 2nd phase, the brane universe evolves with greatly changing acceleration. This phase emerges around the value of scale factor specified by (13). In the 3rd phase, the brane can be regarded as in uniform accelerated motion.

3 Quantum Radiation by a Evolving Brane

We consider a minimally coupled real scalar field living in the 5-dimensional anti-de Sitter bulk spacetime. The lagrangian is

$$\mathcal{L} = -\frac{1}{2} g^{\mu\nu} \partial_\mu \phi \partial_\nu \phi. \tag{14}$$

The metric (1) is transformed to the conformal flat form:

$$ds^2 = \frac{l^2}{\zeta^2} \left\{ -dt^2 + d\zeta^2 + d\vec{x}^2 \right\}. \tag{15}$$

In this metric, the field equation is

$$\Box_5 \phi = \frac{l^2}{\zeta^2} \left(-\partial_t^2 + \partial_\zeta^2 - \frac{3}{\zeta} + \nabla^2 \right) \phi = 0. \tag{16}$$

The solutions are represented by

$$\phi = \int dk d\vec{p} \sqrt{\frac{k}{4(2\pi)^3 \omega l^3}} \left[A_{k,p} \psi_k + A^\dagger_{k,p} \psi^*_k \right] e^{i\vec{p}\cdot\vec{x}} \quad , \tag{17}$$

where

$$\psi_k = \exp(i\omega t) \zeta^2 H_2^{(1,2)}(k\zeta), \qquad \omega = \sqrt{p^2 + k^2}, \tag{18}$$

and $H_2^{(1,2)}$ are the Hankel functions and k is the wave number in ζ direction.

We concentrate on high frequency modes, $k\zeta >> 1$, and perpendicular to the brane modes, $p = 0$, for simplicity. In this case, the mode functions take the form of

$$\psi_k = \zeta^{3/2} \exp[-i\omega(t \pm x)]. \tag{19}$$

Next we consider the boundary conditions on the brane. Possible boundary conditions on Σ are Dirichlet Boundary condition or Neumann Boundary condition. The position of brane in the metric (15) is denoted by $\zeta = z(t) = l^2/a(t)$.

(1)Dirichlet boundary condition

Dirichlet Boundary condition is

$$\psi(t, z(t)) = 0. \tag{20}$$

We set

$$\psi_\omega = \zeta^{3/2} \left\{ e^{-i\omega v} - e^{-i\omega p(u)} \right\}, \qquad u := t - \zeta, \quad v := t + \zeta, \tag{21}$$

and $p(u)$ is a function which should be dtermined by the boundary condition.

From (20) we get

$$\psi_\omega(t, z(t)) = z^{3/2} \left\{ e^{-i\omega v(t)} - e^{-i\omega p(u(t))} \right\} = 0 \tag{22}$$

Noting that there is one to one correspondence between u and v on Σ , we obtain

$$p(u(t)) = v(t). \tag{23}$$

(2)Neumann boundary condition

Neumann Boundary condition is

$$\partial_n \psi(t, z(t)) = 0, \tag{24}$$

where ∂_n is the normal vector to Σ, i.e., $\partial_n \propto \dot{z}\partial_t + \partial_\zeta$. We set

$$\psi = \zeta^{3/2} \left\{ \cos\omega v - \cos\omega p(u) \right\}. \tag{25}$$

From (24) we get

$$\partial_n \psi(t, z(t)) = \frac{3}{2z} z^{3/2} \left\{ \cos\omega v - \cos\omega p(u) \right\} - \omega z^{3/2} \left\{ (\dot{z} + 1) \sin\omega v - (\dot{z} - 1) p' \sin\omega p(u) \right\} = 0 \tag{26}$$

In the late stage we find that

$$p(u(t)) = v(t) + \frac{2}{\omega}\theta, \qquad \tan\theta = \frac{3}{2\omega z\dot{v}}. \tag{27}$$

For calcurating the expectation value of Energy-momentum tensor,

$$T_{\mu\nu} = \partial_\mu\phi\partial_\nu\phi - \frac{1}{2}g_{\mu\nu}g^{\alpha\beta}\partial_\alpha\phi\partial_\beta\phi, \tag{28}$$

we quantize the field. The quantum scalar field in high frequency and perpendicular modes which satisfies the boundary condition is

$$\phi = \sum \left[a_\omega\psi_\omega + a_\omega^\dagger\psi_\omega^*\right], \qquad \psi_\omega = (4\pi\omega)^{-1/2}\zeta^{3/2}\left\{e^{-i\omega v} - e^{-i\omega p(u)}\right\}, \tag{29}$$

where $p(u)$ is given by (23) or (27) for Dirichlet boundary condition or Neumann boundary condition, respectively and a_ω and $a_\omega^\dagger$ are creation and annihilation operator.

We set that the vacuum is defined on Randall-Sundrum brane. For Randall-Sundrum brane $z(t) = const.$ (i.e., $p(u) = u$), we see $< T_{\mu\nu} >= 0$. The vacuum expectation value of $T_{\mu\nu}$ for FRW-brane universe is evaluated by using the point split regularization in the form[7]

$$< T_{00} > \sim z^3[p'(u)]^{1/2}\left\{[p'(u)]^{-1/2}\right\}'' \tag{30}$$

We compare $< T_{00} >$ to the radiation energy density ρ on Σ.

The Fig.2 shows that $< T_{00} > /\rho$ for Dirichlet boundary condition has a maximum. At that time, cosmological radiation density $\rho \sim \rho_*$. If we take $l \sim 1$mm then $\rho_* \sim (1\text{TeV})^4$. Except for initial stage, $< T_{00} > /\rho$ for Neumann boundary condition has a same behaviour as Dirichlet boundary condition.

If we regard the scaler fields as metric perturbation, the field can be recognized as master variable related to the perturbation of metric.[8]

We must consider effective four-dimensional Einstein equation[9]. From this viewpoint, we transform above five-dimensional energy momentum tensor to that of four-dimension by multiplying $G_5^{1/3}$, and obtain four-dimensional energy density.

To make a comparison with ref[10], let us consider an infrationary brane universe model. In the inflation era, the motion of brane is described by

$$t = \eta\cosh\xi_B, z = \eta\sinh\xi_B \propto t, \tag{31}$$

where η is a parameter and ξ_B is a constant. In this case, since $\ddot{z} = 0$ then $p'' = 0$. Therefore $< T_{\mu\nu} >= 0$ for Dirichlet boundary condition.

4 Conclusion

It is concluded that the FRW brane radiates energy toward the bulk on the stage $\rho \sim (1\text{TeV})^4$ by moving boudary effect. In the inflating phase, there is no radiation.

References

[1] L. Randall and R. Sundrum, Phys. Rev. Lett. **83,** 4690 (1999)

[2] P.Binétruy, C.Deffayet, D.Langlois, Nucl. Phys. **B 565**, 269 (2000); C. Csáki, M. Graesser, C. Kolda, J. Terning, Phys. Lett. **B462**, 34 (1999); J.M. Cline, C.Grosjean, G.Servant, Phys. Rev. Lett. **83**, 4245 (1999); P. Binétruy, C. Deffayet, U. Ellwanger and D. Langlois, Phys.Lett. **B 477**, 285 (2000); D. Ida, JHEP, **0009,** 014 (2000).

[3] H. Ishihara, Phys. Rev. Lett. **86,** 381 (2001); gr-qc/0107085

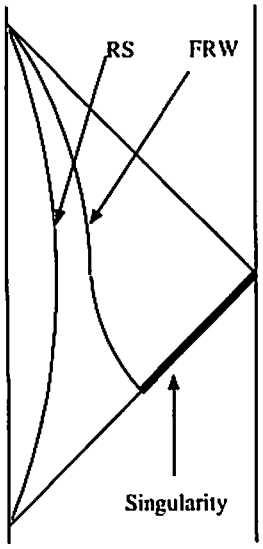


Figure 1: Fig.1:Conformal diagram of Randall-Sundrum brane and FRW brane in AdS bulk spacetime.

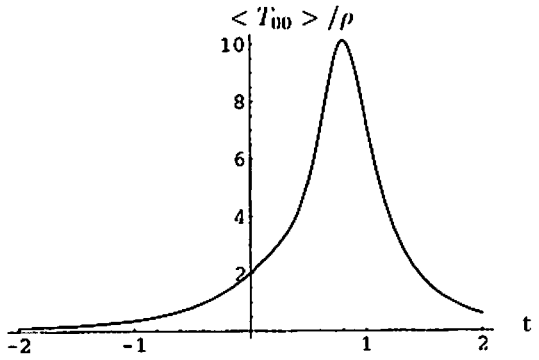


Figure 2: Fig.2: Time evolution of vacuum expectation value of energy-momentum tensor.

[4] A. Lukas, B.A. Ovrut, K.S. Stelle, and D.Waldram, Phys. Rev. **D59**, 086001 (1999); Nucl. Phys. **B552**, 246 (1999).

[5] P. Horava and E. Witten, Nucl. Phys. **B460**, 506 (1996).

[6] W. Israel, Nuovo Cimento **B44**, 1 (1966).

[7] P. C. W. Davies and S. A. Fulling, Proc. R. Soc. London **A348**, 393 (1976); **A354**, 59 (1977); N. D. Birrell and P. C. W. Davies, Quantum Fields in Curved Space (Cambridge University Press, Cambridge, 1982).

[8] H.Kodama, A.Ishibashi and O.Seto, Phys. Rev. **D62**, 064022 (2000)

[9] T.Shiromizu, K.Maeda and M.Sasaki, Phys. Rev. **D62**, 024012 (2000)

[10] D. S. Gorbunov, V. A. Rubakov, and S. M. Sibiryakov, THEP **0110**, 015 (2001); S. Alexander, Y. Ling, and L. Smolin, Phys. Rev. **D65**, 083503 (2002); C. Deffayet, G. Dvali, and G. Gabadadze, Phys. Rev. **D65**, 044023 (2002); A. Chamblin, A. Karch, and A. Nayeri, Phys. Lett. **B509**, 163 (2001).

Application of the Separate Universe Approach to Preheating

Takahiro Tanaka[a1] and Bruce Bassett[b2]

[a] *Yukawa Institute for Theoretical Physics, Kyoto University, Kyoto 606-8502, Japan*
[b] *Institute of Cosmology and Gravitation (ICG), University of Portsmouth, Mercantile House, Portsmouth, PO1 2EG, England*

Abstract

The dynamics of preheating after inflation has not been clearly understood yet.In particular, the issue of the generation of metric perturbations during preheating on super-horizon scale is still unsettled. Large scale perturbations may leave an imprint on the cosmic microwave background, or may become seeds for generation of primordial black holes. Hence, in order to make a connection between the particle physics models and cosmological observations, understanding the evolution of super-Hubble scale perturbations during preheating is important. Here, we propose an alternative treatment to handle this issue based on the so-called separate universe approach, which suggests less efficient amplification of super-Hubble modes during preheating than was expected before. We also point out an important issue which may have been overlooked in previous treatments.

1 Introduction

Rather recently, people realized that the process of reheating after inflation need not simply be described by the usual single particle decay of the inflaton field. If there are relevant scalar field degrees of freedom coupled to the inflaton field at the end of inflation, the coherent oscillation of the inflaton can excite those scalar fields by parametric resonance[1]. This process was extensively investigated, in mast cases, neglecting metric perturbations, which typically will be a good approximation as long as we are interested in processes occurring within the Hubble horizon scale. Often the energy transfer due to parametric resonance is much more efficient than that due to the usual particle decay, and sometimes it is violent. It was then suspected that there might be significant effects on the large scale perturbations beyond the Hubble scale[2] due to resonance. Some particle physics models may predict distinguishable signals in the cosmic microwave background, or formation of inconsistently large number of primordial black holes [3].

Here in this short contribution, we would like to propose another approach to discuss this issue of the generation of large scale perturbations at preheating. We make use of the separate universe approach [4]. We stress that unphysical acausal energy transfer, which may not carefully prohibited in previous treatments, does not take place in this new approach.

2 Separate universe approach

Basic Idea : We consider the system composed of many scalar fields. The discussions in this paper is based on the following statement obtained in Ref. [5, 4, 6].

> When we solve the background spatially homogeneous field equation, the e-folding number $N \equiv \log a$ until the expansion rate H reaches a given value H_r depends on the initial value of the fields Φ (and their time derivatives). Let's denote this value of N by N_{H_r}. Suppose that the initial value of Φ has spatial variation over super-Hubble scales. Then, the value of N_{H_r} becomes a function of the spatial position $\mathbf{x}$. In this case, the newly generated curvature perturbations on the constant Hubble slice $\mathcal{R}$ is simply given by ΔN_{H_r}, i.e., the fluctuations in N_{H_r}.

[1] E-mail:tanaka@yukawa.kyoto-u.ac.jp. [2] E-mail:Bruce.Bassett@port.ac.uk
This work was supported in part by Monbukagakusho Grant-in-Aid Nos. 14740165 and 14047214.

Mechanism of Generating Curvature Perturbations from Isocurvature Perturbations :

Let's consider matter fields consisting of two components. We call them ϕ and χ. They are not necessarily scalar fields here. We assume that the rates of change of the energy density of ϕ and χ due to the expansion of the universe are different. Namely,

$$\frac{d\log\rho_\phi}{dN} = -3(1+w_\phi), \quad \frac{d\log\rho_\chi}{dN} = -3(1+w_\chi), \tag{1}$$

For example, the energy density of ϕ changes like dust matter, while χ behaves as a radiation fluid. In this case, we have $w_\phi = 0$ and $w_\chi = 1/3$. Let us denote the fraction of the energy density of χ by $f := \rho_\chi/\rho$. Then, we have

$$\frac{d\log\rho}{dN} = -3(1+w_\phi) + 3(w_\phi - w_\chi)f. \tag{2}$$

From this expression, we notice that there are two factors necessary for generation of super-Hubble adiabatic perturbations. One is non-vanishing $w_\phi - w_\chi$, and the other is inhomogeneity of f.

3 Conformal two field model

Model : We consider the model whose potential is given by

$$V = \frac{\lambda}{4}\phi^4 + \frac{1}{2}g^2\phi^2\chi^2. \tag{3}$$

When $g^2 = 2\lambda$, the longest wavelength mode of χ is the fastest growing mode, and the initial spectrum of χ is scale-invariant. This appears to lead to exponential growth of pre-existing entropy perturbations even when backreaction is taken into account [7]. The equations of motion for the spatially homogeneous background are given by

$$\ddot{\Phi}^i + 3H\dot{\Phi}^i - \frac{dV}{d\Phi^i} = 0, \qquad H^2 = \frac{\kappa^2}{3}\left(\frac{1}{2}\dot{\Phi}^2 + V\right). \tag{4}$$

Here we used the vector notation to represent the two component scalar fields, ϕ and χ, simultaneously. Namely, $\Phi^1 = \phi$ and $\Phi^2 = \chi$.

Simplified Analysis with Time Averaging : We define the averaged energy in a unit comoving volume by $\mathcal{E} = \left\langle a^3\left(\frac{1}{2}\dot{\Phi}^2 + V\right)\right\rangle$, where $\langle\cdots\rangle$ represents time averaging. Let us assume that Φ^2 is bounded and is oscillating. Then, we have many zeros of $\dot{\Phi}\cdot\Phi$. If we take the average between two zeros, we have

$$0 = \left\langle \frac{d}{dN}\left(a^3\dot{\Phi}\cdot\Phi\right)\right\rangle = \left\langle \frac{a^3}{H}\left(\dot{\Phi}^2 - \lambda\phi^4 - 2g^2\chi^2\phi^2\right)\right\rangle. \tag{5}$$

Since H is slowly changing, we obtain an approximate relation: $\left\langle a^3\left(\dot{\Phi}^2 - \lambda\phi^4 - 2g^2\chi^2\phi^2\right)\right\rangle = 0$. Therefore we have

$$\frac{d\log\mathcal{E}}{dN} = 3 - 3\frac{\left\langle a^3\dot{\Phi}^2\right\rangle}{\mathcal{E}} \approx -1. \tag{6}$$

From this fact, $\mathcal{E} \approx e^{-N}$ is deduced, and hence we have $H^2 \propto \rho \approx \mathcal{E}/a^3 \propto a^{-4}$. Anyway, N_{H_*} is basically independent of the initial value of the field. Therefore it seems that additional curvature perturbations are not generated when the wavelength of a mode is longer than the horizon scale. In the language of the preceding section, $w_\phi - w_\chi$ vanishes approximately in this model. Hence, amplification of fluctuations of $O(1)$ is hardly expected. Notice that H^2 is roughly proportional to Φ^4 but the mass squared is to Φ^2. Hence, as the amplitude of Φ decays, the mass squared tends to be larger than H^2.

Detailed Analysis without Time Averaging : We solve the above set of equations numerically varying the initial value of χ. Then, we can evaluate the initial value dependence of N_{H_*}, the e-folding

number until the total energy density reaches a certain specified value. However, the original model has the following shortcoming. As there are only two degrees of freedom corresponding to the homogeneous modes of ϕ and χ-fields, the exchange of energy between them continues for ever. Then, occasionally the value of ϕ becomes exceptionally small. In this phase, the period between two neighboring zeros of $\mathbf{\Phi}\cdot\dot{\mathbf{\Phi}}$ becomes very long. If the specified target energy density is reached during this phase, ΔN becomes largely dependent on the choice of the final value of the Hubble rate H_r. Then, interpretation of the results becomes difficult. In more realistic situations, the energy density carried by these long-wavelength modes will be redistributed to a large number of other degrees of freedom (shorter wavelength modes of these or other fields) sooner or later through rescattering.

Here we assume two radiation fluids, r_ϕ and r_χ. Φ^i decays into the component r_i with decay constant Γ_i. The modified set of equations are given by

$$\ddot{\Phi}^i + (3H + \Gamma_i)\dot{\Phi}^i - \frac{dV}{d\Phi^i} = 0, \qquad \dot{\rho}_{r_i} = 4H\rho_{r_i} + \Gamma_i(\dot{\Phi}^i)^2, \qquad H^2 = \frac{\kappa^2}{3}\left(\frac{1}{2}\dot{\mathbf{\Phi}}^2 + V + \sum_{i=1}^{2}\rho_{r_i}\right), \quad (7)$$

where ρ_{r_i} is the energy density of the i-th component of radiation fluids.

We consider the case with $g^2 = 2\lambda = 0.02$ and $\Gamma_\phi = \Gamma_\chi = 10^{-5}$. We set the initial condition at $\phi = 1$ with $\dot{\phi} = \dot{\chi} = 0$. Using the convention $\kappa^2/3 = 1$, the initial Hubble rate is $H = 0.05$, where we assume a negligible contribution to the initial energy density from the χ-field. We integrate Eqs. (7) until the Hubble rate goes down to 10^{-6}, at which point the energy is almost completely transferred to the radiation fluids. In Fig. 1, we give a plot of the e-folding number N between $H = 0.05$ and $H = 10^{-6}$ varying the initial value of χ. We see small fluctuations of the e-folding number N depending on the initial value of χ. Each plot contains only 100 sampling points with equal horizontal spacing. The amplitude of fluctuation is not $O(1)$ but still it is significant compared to that observed in the cosmic microwave background. An interesting and important point is that the dependence on the initial value of χ of this fluctuation is almost random. Two panels in Fig. 1 are plots with different range of the initial value of χ. Although the scale of the horizontal axis is very different, these two plots look quite similar.

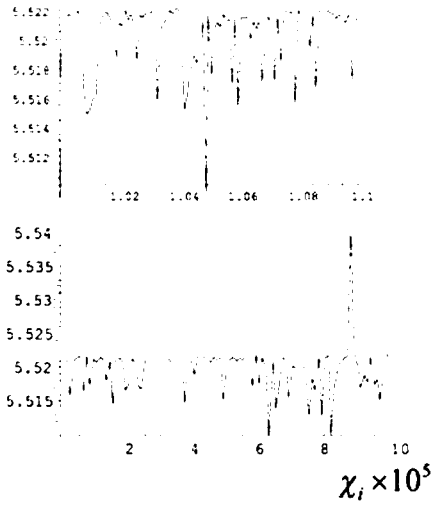


Fig.1: Plots showing the initial value dependence of the e-folding number N. In each panel 100 discrete points are plotted. The scale of the horizontal axis is different, but these two plots look quite similar. This will mean that the distribution of N is rather random.

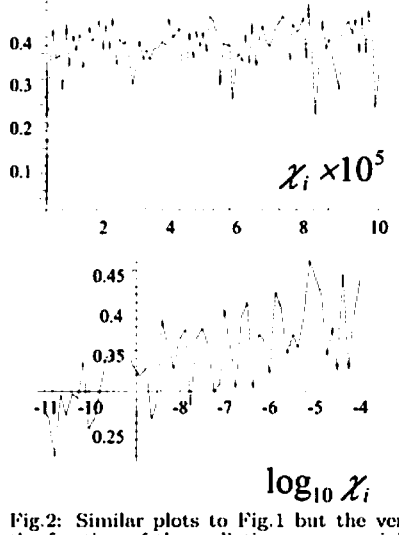


Fig.2: Similar plots to Fig.1 but the vertical axis is the fraction of the radiation energy originating from the secondary field χ. The panel (b) is a close-up view of the panel (a) for small initial value of χ. We can see a trend that the fraction increases as the initial value of χ increases.

The origin of these fluctuations can be understood as follows. If the oscillation of fields is fast compared to the change rate of H, the approximation using the time averaging must be good. The error will be exponentially suppressed. As mentioned above, however, the period of oscillation occasionally becomes very long if the motion of the scalar fields is trapped by chance in the region where the amplitude of oscillation in the direction of ϕ-field is exceptionally small. In such situation, the approximation we

made before is no longer valid. Since the motion of the two scalar fields are rather chaotic, the initially neighboring trajectories in the configuration space of ϕ and χ soon deviate. Thus, it is quite sensitive to the tiny difference in the initial condition whether this entrapment occurs or not. As a result the dependence on the initial condition is almost completely randomized.

Then, the question is whether this amplification of fluctuations can be a process that generates significant fluctuations at the super-Hubble scale during preheating? Since the amplitude of the generated curvature perturbation is so sensitive to χ_i, the variance seen in Fig. 1 will basically represent the variance of random fluctuations incoherent beyond the Hubble scale. If the fluctuations are completely random beyond a certain cutoff scale k_c^{-1}, we have $n = 4$ spectrum for $k < k_c$ in general. (Here we use the notation that $n = 1$ corresponds to the scale invariant spectrum.)

However, it is not certain whether a smoothing of $N(\chi)$, e.g., $\tilde{N}(\chi_i) := \int d\chi N(\chi) W(\chi - \chi_i)$ with an appropriate window function W is tilted or not. Hence, the averaged value on very large scale may have an additional fluctuation other than the $n = 4$ random component. The amplitude of this additional component is difficult to determine because we need to reduce the contamination of $n = 4$ component. To do so, we need to compute the average over sufficiently large volume. This means that we need to calculate the value of N for sufficiently large number of samples changing the initial value of χ, which we have not done yet. Hence, we have not completely rejected the possibility of generating fluctuation coherent beyond the Hubble scale. However, the amplitude of this coherent fluctuation should be much more suppressed than the incoherent one.

Generation of Curvature Perturbations :

If the exact conformal invariance is broken by some reason, we can expect a curvature perturbation may be generated. The easiest way will be changing the decay process of the two fields. In the above calculation, we have introduced the decay terms by hand assuming that the both scalar fields decay into a radiation fluid with the same decay constant Γ. We distinguished two components of the radiation fluids depending on which scalar field becomes the origin. Suppose, one radiation fluid is composed of massive fields, although the mass is negligible during the preheating epoch. Then, sooner or later, the mass of this radiation fluid becomes larger than the Hubble rate, and the energy density of this field starts to behave like $\propto e^{-3N}$, while the other continues to evolve as $\propto e^{-4N}$. Therefore the isocurvature perturbation imprinted as the ratio $\xi := \rho_{r_\chi}/(\rho_{r_\phi} + \rho_{r_\chi})$, is transformed into the curvature perturbation at this stage.

Now let us look at the plot of this ratio as a function of the initial value of χ. From Fig. (2a), it seems that the dependence on χ_i is just random fluctuations. However, if we close up the portion for small $|\chi_i|$ (Fig. (2b)), we can see clear dependence on χ_i, which can be explained as follows. For small χ_i, the decay to the radiation fluid becomes effective before the equi-partition between the homogeneous parts of the ϕ and χ fields is achieved by the parametric resonance. In this case, the decay to the radiation fluid is more efficiently through the ϕ field. As a result, the ratio ξ becomes small for small $|\chi_i|$. This mechanism to generate large scale fluctuations is very efficient because the fluctuation continues to be amplified until the matter radiation equality. Hence, this process will be a possible mechanism to create primordial black holes.

4 discussion

In this paper, applying the separate universe approach, we discussed generation of metric perturbations at super-Hubble scale during preheating. As an example, we considered the conformal two scalar model whose potential is given by Eq. (3). Previously, it was argued that large amplitude of fluctuations can be generated during the reheating process, but we found that the separate universe approach suggests relatively suppressed amplitude of fluctuations.

We suspect that the origin of this discrepancy is in an overlooked point in previous analyses. Usually people decompose fields as (homogeneous background)+(perturbations), using the common homogeneous background for separated universes. Let's consider two largely-separated homogeneous patches, universe A and universe B. Suppose that the preheating is efficient in the universe A but inefficient in the universe B. Then, we physically expect that the back reaction to the inflaton oscillation is also efficient in the universe A. However, as long as we use the common homogeneous background, the back reaction works in the same way both in the universe A and in the universe B. This means that artificial and acausal

energy transfer from the universe B to A easily takes place in the treatment using the homogeneous background.

However, the above criticism to the previous works does not apply to the numerical studies. For example, in Ref.[8], it was argued that super-Hubble modes are enhanced even in a single field model. They considered $\lambda\phi^4$ model. When they simulate the case that only a single mode in the resonance band is excited, there was no enhancement in super-Hubble modes. On the other hand, when all the modes in the same lowest resonance band are excited, there was enhancement in super-Hubble modes. Their explanation is as follows. The gauge invariant perturbations at super-Hubble scale are generated by the quadratic product of smaller scale perturbations in the resonance band. Namely, $\zeta_{\mathbf{k}} \propto \int d^3k\chi(\mathbf{k}')\chi(\mathbf{k}-\mathbf{k}')$. This integral becomes approximately constant for small k less than the width of the resonance band Δk. For larger k, this integral is small because, when one of the arguments of χ is in the resonance band, the other is outside of it. So this enhancement mechanism does not apply for small scale modes. In this sense, the large scale modes are selectively enhanced.

However, since $\zeta_{\mathbf{k}} \propto k^{-3/2}$ for the scale invariant spectrum, constant value of $\zeta_{\mathbf{k}}$ does not mean enhancement of larger wavelength mode. Therefore the mechanism of the enhancement of super-Hubble modes works only when the cutoff scale $a\Delta k^{-1}$ is much larger than the Hubble radius. We can easily see that this condition is not satisfied in this model. For the redefined field $\hat{\phi} = a\phi$, the field equation becomes $\hat{\phi}'' + \lambda\hat{\phi}^3 - (a''/a)\hat{\phi} = 0$. Here we used the conformal time coordinate $\eta = \int a^{-1}dt$, and a prime denotes differentiation with respect to η. Since the radiation dominant universe is a good approximation for this model, we use $a = (t/t_0)^{1/2}$. Then, $\eta = 2t_0a = 1/\mathcal{H} = 1/aH$, and therefore $H = 2t_0/\eta^2$. The amplitude of oscillation of $\hat{\phi}$ is constant. We can set the amplitude of $\lambda\hat{\phi}^2$ to unity without loss of generality. In fact, using the Friedmann equation, we have $\lambda\hat{\phi}^2 \approx (8\pi G/3a^2)\lambda\phi_i^4 = \mathcal{H}^2 = 1/(2t_0a)^2$, where we have used the fact that the initial value of ϕ, ϕ_i, is $O(m_{pl})$. Choosing t_0 appropriately, we can set $\eta_i = 1$. This also means that the comoving wave number corresponding to the initial Hubble horizon $\mathcal{H}$ is 1.

The resonance effect becomes important after $\mu\eta$ becomes $O(1)$, where μ is the growth rate of the amplitude due to parametric resonance. Hence, $\eta \approx \mu^{-1}$ when the parametric resonance becomes important. At this epoch, the comoving horizon scale is $\mathcal{H} = \eta^{-1} \approx \mu$. Then, the condition for the enhancement of the super-Hubble modes will be $\mu \gg \Delta k$. In this model $\mu < 0.267$ and $\Delta k \approx 0.2$. Therefore the condition is not satisfied.

However, the plots in Ref.[8] show steep increase of power for small k. The expected flat spectrum, which does not mean scale invariance, is not seen. This is no contradiction. When they plot the figures, they plot only discrete numbers of k modes and the plots do not have resolution less than Δk. This can be seen by looking at the shape of the resonance peak, which does not show the expected round shape. This means that the resolution is less than Δk. Since the mode $k \approx \Delta k$ is inside the Hubble scale after the resonance becomes efficient, actually only one mode outside the horizon scale is plotted in those figures. Therefore it is not strange that the expected plateau is absent in their plots. As mentioned before, this $n = 4$ spectrum is common in the situation that there are random fluctuations of a large amplitude on small scales and seems to refute the claims of [7].

References

[1] J. Traschen and R. Brandenberger, *Phys. Rev.* **D42** 2491 (1990). A. Dolgov and D. Kirilova, *Sov. J. Nucl. Phys.* **51** 172 (1990).

[2] B. Bassett, D. Kaiser and R. Maartens, *Phys. Lett.* **B455** 84 (1999).

[3] B.A. Bassett and S. Tsujikawa, *Phys. Rev. D* 63, 123503 (2001).

[4] D. Wands, K.A. Malik, D.H. Lyth and A.R. Liddle, *Phys. Rev.* **D62** 043527 (2000).

[5] M. Sasaki and T. Tanaka, *Prog. Theor. Phys.* **99** 763 (1998).

[6] H. Kodama and T. Hamazaki, *Phys. Rev.***D57** 7177 (1998); Y. Nambu and A. Taruya, *Class. Quant. Grav.***15** 2761 (1998).

[7] B. A. Bassett and F. Viniegra, Phys. Rev. D **62**, 043507 (2000) ; J. Zibin, R. Brandenberger and D. Scott, Phys. Rev. **D63**, 043511 (2001).

[8] R. Easther and M. Parry, *Phys. Rev. D* 62, 103503 (2000).

Asymptotics of topologically nontrivial spacetimes

Masayuki Tanimoto

Department of Physics, Yale University, New Haven, CT 06511-8499, USA

Abstract

An effort to carry out a linear perturbation analysis for spatially locally homogeneous solutions with nontrivial spatial topologies is reported, with a brief mention of a motivation. In particular, mode functions and their properties for a Bianchi II type solution are presented and applied to field equations on the solution.

1 Introduction

Nontrivial topology is one of the key words of the recent developments in relativity. It's been attracting more and more attention that the possible topologies of our universe are very diverse. Although the topology of the universe could affect physics in the universe in many ways, including through the pattern of the cosmic microwave background radiation, in this article we focus on the dynamical properties of the spacetime itself, especially asymptotic properties of them.

It may be surprising that there is a connection between the topology of a universe and the dynamical properties, but it is true. One of the underlying mathematical facts is Yamabe's theorem. This theorem tells us that an arbitrary metric on a closed manifold can become a metric whose scalar curvature is constant, especially, 1, 0, or -1, by a *conformal transformation*. This theorem also provides us with a simple classification of all closed manifolds, called *Yamabe types*. It is stated as follows: (1) If the manifold M admits a positive constant scalar curvature, M is called Yamabe type $+1$. In this case M also admits scalar curvatures 0 and -1. (2) If the manifold M does not admit a positive constant scalar curvature but admits zero constant curvature, M is called Yamabe type 0. In this case M also admits scalar curvature -1. (3) Otherwise, M is called Yamabe type -1. In this case M admits only negative constant scalar curvatures. These Yamabe types are a classification of manifolds (not curvatures). Yamabe's theorem tells us that, e.g., if the manifold is Yamabe type -1, then all metrics on this manifold are conformally equivalent to the metrics whose scalar curvature is -1.

This amazing fact has a substantial application in relativity. This comes from so-called the "phase space reduction scheme" by Fischer and Moncrief [3]. From now on we concentrate on Yamabe type -1 manifolds and impose so-called the Constant Mean Curvature (CMC) slicing condition on the spacetime. The CMC condition is a gauge condition where the trace of the extrinsic curvature is constant on the spatial manifold.

In this scheme one considers a conformal transformation of the gravitational data on a 3-dim manifold, where the conformal factor is determined so that it solves the Hamiltonian constraint, and the conformally transformed metric is taken to be a metric whose scalar curvature is constant, especially, -1. In this setting we can think that the true dynamical content is carried by the conformally transformed metric, and we can think of the space of metrics whose scalar curvatures are all -1 as a true configuration space, because the data in this space are not constrained anymore. This space is also called the *reduced configuration space*, and its cotangent bundle is called the *reduced phase space*.

The reduced phase space has a natural *reduced Hamiltonian*, and the time evolution caused by the reduced Hamiltonian is called the *Einstein flow*. Fischer and Moncrief showed that the reduced Hamiltonian is monotonically decreasing, and the infimum of the Hamiltonian is directly related to a topological invariant, called the *σ-constant*. So, we can say that the Einstein flow "seeks" a topological invariant.

The σ-constant has been considered one of the key elements that can play a major role to understand the topology and geometry of the manifold. There is a conjecture about Yamabe type -1 manifolds that describes how a sequence of metrics achieves the σ-constant. According to this conjecture by Anderson[1], if the manifold is Yamabe type -1 and irreducible, the manifold is decomposed into the "hyperbolic parts" and "graph manifold parts", and the σ-constant is achieved by hyperbolic metrics for the hyperbolic parts and degenerate metrics for the graph manifolds.

Combining this conjecture and the properties of the reduced Hamiltonian, we get the following picture about the dynamics in the reduced configuration space: The Einstein flow asymptotically realizes the decomposition of the manifold into the hyperbolic pieces and graph manifold pieces and the hyperbolic pieces approaches the hyperbolic manifolds, while the graph manifold pieces collapse.

But this is not a confirmed picture, in fact, (1) in many cases it is unknown what metric or sequence of metrics realizes the σ-constant, and furthermore (2) for the Einstein flow, it is unknown if the reduced Hamiltonian always asymptotically approaches its infimum under the flow. For example, a black hole formation can be an obstacle for this regular flow.

Our purpose of work lies largely in verifying and inspecting the details of this picture and considering possible applications. It may be natural to consider the hyperbolic manifolds and graph manifolds one by one, rather than a composite of them, as a first step. To deal with each of such models it is also natural to start with a perturbative approach. The hyperbolic background [4] and Bianchi III one [6, 8] have been worked out recently. In the remaining part of this article we focus our attention to Bianchi II case. (For partial results on perturbations of Bianchi class A modes, including Bianchi II, see also [2].)

2 Fields on a closed Bianchi II manifold

To study perturbations or any other field equations including the scalar field or electromagnetic field on Bianchi II spacetimes we first need to prepare a set of eigenfunctions to perform a separation of variables. Fortunately, this is possible and we can explicitly represent the eigenfunctions, thereby we can derive any necessary properties of them.

The Bianchi type II algebra can be characterized by the following vectors χ_I $(I = 1 \sim 3)$ or their dual 1-forms σ^I:

$$\chi_1 = \frac{\partial}{\partial x}, \quad \chi_2 = \frac{\partial}{\partial y} + x\frac{\partial}{\partial z}, \quad \chi_3 = \frac{\partial}{\partial z}, \tag{1}$$

$$\sigma^1 = dx, \quad \sigma^2 = dy \quad \sigma^3 = dz - xdy. \tag{2}$$

The Bianchi type II vacuum solution we consider can be expressed as

$$(M \times \mathbf{R}, g_{ab}) = (\tilde{M} \times \mathbf{R}, \tilde{g}_{ab})/\Gamma, \tag{3}$$

where M stands for the compactified spatial manifold we consider, $\tilde{M} = \mathbf{R}^3$ is the universal cover of M, $\tilde{g}_{ab}$ is the vacuum Einstein solution given below, $\Gamma \subset G_{II}$ is a discrete subgroup of the Bianchi II group G_{II} and it acts on the universal covering spacetime $(\tilde{M} \times \mathbf{R}, \tilde{g}_{ab})$ from the left in such a way that keeps the natural slicing by the homogeneous spaces, and g_{ab} is the induced metric on the spatially compactified spacetime. For definiteness, we assume that M is the "circle bundle over the torus (T^2) with Euler number $e = 1$." (See, e.g., [5].)

The exact vacuum solution we consider is

$$ds^2 = -N^2(t)dt^2 + q_1(t)(\sigma^1)^2 + q_2(t)(\sigma^2)^2 + q_3(t)(\sigma^3)^2, \tag{4}$$

where

$$N^2 = 1 + b^2 t^{4p_3}, \quad q_1 = t^{2p_1}N^2, \quad q_2 = t^{2p_2}N^2, \quad q_3 = 16p_3^2 b^2 t^{2p_3}/N^2. \tag{5}$$

$p_i (i = 1, 2, 3)$ and b are constant parameters such that $b > 0$, $p_3 \neq 0$, and

$$\Sigma p_i = \Sigma p_i^2 = 1. \tag{6}$$

When $p_1 = p_2$, therefore $q_1(t) = q_2(t)$, the solution is called *locally rotationally symmetric (LRS)*. While there seem two such cases $(p_1, p_2, p_3) = (0, 0, 1)$ and $(2/3, 2/3, -1/3)$, these two solutions represent the same one-parameter solution. When we consider a LRS solution, we take $(p_1, p_2, p_3) = (2/3, 2/3, -1/3)$, since the time coordinate t in this solution approaches the proper time at future infinity, which is more favorable.

Notice the fact that Γ is a subgroup of the Bianchi II group G_{II}. This in particular means that the invariant vector χ_I are well defined not only on the open manifold $\tilde{M}$ but also on the compactified

manifold M, because they are invariant under the action of G_{II}, and so are under $\Gamma \subset G_{II}$. We will see that because of this property the invariant one-forms χ_I play a fundamental role in developing the calculus concerning the mode expansions.

A rough procedure to construct the eigenfunctions is as follows. Remember that we are considering a compactified manifold M, not an open one. To get eigenfunctions on a compactified manifold we need two major steps. First, to make some of the eigenvalues discrete we consider a "half-open" manifold, $\bar{M} = T^2 \times \mathbf{R}$, rather than the open one $\mathbf{R}^3$. M is the direct product of the 2-dim torus and the open line, and supposed to have a standard metric of Bianchi II type. We construct eigenfunctions on it. This process is actually not so difficult. Secondly, the closed manifold we consider is obtained by introducing some identifications in this half-open manifold. As a result, the eigenfunctions on the closed manifold is obtained by taking linear combinations of the eigenfunctions on the half-open manifold.

The eigenfunctions are thus expressed as infinite sums. For example, when $m > 0$, they can be represented as below [7]. (The three cases $m > 0$, $m = 0$, and $m < 0$ should be dealt with separately. m is the eigenvalue for the χ_3 operator. See below.)

$$\phi_{l,m,n_0}(\mathbf{x}) = \sum_{k=-\infty}^{\infty} e^{i\delta(n_0 k + m\frac{k(k-1)}{2})} \bar{\phi}_{l,m,n_0+mk}(\mathbf{x}), \tag{7}$$
$$l = 0, 1, \cdots, \infty, \quad m = 1, 2, \cdots, \infty, \quad n_0 = 0, 1, \cdots, m,$$

where δ is a parameter appearing in the compactification. The functions $\bar{\phi}_{l,m,n}(\mathbf{x})$ are the eigenfunctions for the half-open manifold $\bar{M}$, for which the index n runs $-\infty$ to ∞. (As a result of the complete compactification, the index n_0 for the eigenfunction on M can take only a limited number bounded by m.)

This function has the following properties when $m > 0$. Here, the invariant vectors χ_I are regarded as (well-defined) differential operators acting on functions on M. (We omit indices n_0, for simplicity.)

$$\begin{aligned} \chi_1 \phi_{l,m} &= -\sqrt{\frac{m}{2}} \left[\phi_{l+1,m} - l\phi_{l-1,m}\right], \\ \chi_2 \phi_{l,m} &= i\sqrt{\frac{m}{2}} \left[\phi_{l+1,m} + l\phi_{l-1,m}\right], \\ \chi_3 \phi_{l,m} &= im\phi_{l,m}. \end{aligned} \tag{8}$$

As a direct application we can discuss the *scalar field equation* on our Bianchi II background. Using the mode functions, we can expand the scalar field Φ as follows:

$$\Phi(t, \mathbf{x}) = \sum_{l,m,n_0} a_{l,m,n_0}(t) \phi_{l,m,n_0}(\mathbf{x}). \tag{9}$$

Since the operators χ_I do not change m and n_0 when acting on ϕ_{l,m,n_0}, we omit these subscripts and write simply a_l and ϕ_l, as far as no confusion occurs.

The equation of motion for the scalar field on our background can be written as

$$\begin{aligned} 0 &= \mathrm{g}^{ab} \nabla_a \nabla_b \Phi \\ &= \frac{-1}{\sqrt{-g}} (\sqrt{-g} N^{-2} \dot{\Phi})\dot{} + (q_1^{-1}(\chi_1)^2 + q_2^{-1}(\chi_2)^2 + q_3^{-1}(\chi_3)^2)\Phi, \end{aligned} \tag{10}$$

where a dot stands for d/dt. Using the background spacetime solution for Bianchi II and the "χ-relations" above, we obtain the following wave equations:

$$\ddot{a}_l + \frac{1}{t}\dot{a}_l + mf(t)a_l = \frac{m}{2}(t^{-2p_1} - t^{-2p_2})[a_{l-2} + (l+2)(l+1)a_{l+2}], \tag{11}$$

where

$$f(t) \equiv \frac{2l+1}{2}(t^{-2p_1} + t^{-2p_2}) + \frac{m}{16p_3^2 b^2}(1 + b^2 t^{4p_3})^2 t^{-2p_3}. \tag{12}$$

(In Eq.(11), $a_{l<0}$ should be considered as zero.)

A notable property of these equations is that they are a set of infinitely coupled equations, unless the solution is LRS (i.e., $p_1 = p_2$). This coupling between different modes is an unavoidable feature for field equations on a non-LRS spacetime solution, because for those backgrounds the mode functions defined with respect to a standard metric are no longer eigenfunctions with respect to the Laplacian for each spatial section. That is, those eigenfunctions defined on the standard Riemannian manifold do not remain eigenfunctions in the course of the anisotropic expansion. We could define another "time-dependent" eigenfunctions to get around this difficulty, but in that case time-derivatives of the eigenfunctions come in the field equation and it makes another problem, so in any case this complexity caused by anisotropic expansion is unavoidable.

The wave equation above gives a closed equation when the background is LRS. In this case (i.e., $p_1 = p_2 = 2/3$, $p_3 = -1/3$) we find the following set of fundamental asymptotic solutions [7]:

$$a_l(t) = \left\{ t^{-\frac{2}{3}} e^{\pm i m \frac{3}{4} b^{-1} (\frac{3}{4} t^{4/3} + b^2 \log t)} (1 + o(t)) \right\}. \tag{13}$$

Like the Bianchi III case [6, 8], they decay.

Let us consider *vector fields*, next, namely, we need to make clear how we can expand an arbitrary vector on our closed Bianchi II manifold by mode vectors. In principle, this is straightforward, because we have the set of independent invariant vectors χ_I. Any vectors on the manifold can be expanded with respect to these invariant vectors and all we have to do is to expand the components using the mode functions ϕ_{l,m,n_0}. However, this straightforward expansion is found not to be useful to effectively analyze the resulting equations.

One nicer way to expand the vectors comes to our attention by considering an analogy with Regge-Wheeler's spherically symmetric case or Bianchi III hyperbolically symmetric case, where we could take advantage of the spherically or hyperbolically symmetric planes. In those cases, on the symmetric plane we were able to define so-called the 'even' vectors and 'odd' vectors, and the even and odd part equations for a linear vector field equation decoupled from each other.

For Bianchi II, although there do not exist similar symmetric planes, we can consider the "plane field" spanned by χ_1 and χ_2. This plane field is not integrable, because the commutator $[\chi_1, \chi_2] = \chi_3$ cannot be spanned by χ_1 and χ_2. Despite it, this plane field is special, because the metric can be LRS only when $q_1 = q_2$.

We define the area two-form ε of the plane field by

$$\varepsilon_{ab} = 2\sigma^1{}_{[a}\sigma^2{}_{b]}. \tag{14}$$

We can define the even vectors by

$$S_a = (\chi_1\phi_l)\sigma^1{}_a + (\chi_2\phi_l)\sigma^2{}_a, \tag{15}$$

and odd vectors by

$$V_a = i\varepsilon_a{}^b\partial_b\phi_l = i((\chi_2\phi_l)\sigma^1{}_a - (\chi_1\phi_l)\sigma^2{}_a). \tag{16}$$

We also need orthogonal vectors $S^\perp_a = (\chi_3\phi_l)\sigma^3{}_a$ and time-like vectors $S^{\mathrm{T}}_a = N^{-1}\phi_l(dt)_a$, which may be considered to belong to the even part. These four kinds of vectors may complete our set of eigenvectors.

Because of the fact that the commutator of χ_1 and χ_2 does not belong to the tangent space spanned by χ_1 and χ_2, the even and odd parts do *not* decouple from each other, even when the background is LRS. Nonetheless, the use of even and odd vectors is found useful, especially when the background is LRS, since in that case each mode is found to decouple from the others. (Do not confuse the coupling between the even and odd parts and the one between modes.) When the spacetime is not LRS, however, we will have couplings between different modes and this feature is again unavoidable, due to the anisotropic expansion.

Using these mode vectors, we can expand the *vector potential* for an electromagnetic field as follows:

$$A_a = \sum_{l,m,n_0} \alpha_0(t)S^{\mathrm{T}}_a + \alpha_1(t)S_a + \alpha_2(t)V_a + \alpha_3(t)S^\perp_a. \tag{17}$$

The four kinds of functions $a_i(t)$ $(i = 0 \sim 3)$ serve as the field variables. Let us consider the *LRS case* below, on which background, as mentioned above, couplings between different modes vanish.

The quantities we are most interested in are $(U(1)$-$)$gauge-invariant variables, which can be easily found by looking at components of the field strength $F_{ab} = \partial_a A_b - \partial_b A_a$. We obtain the following four independent gauge invariant variables:

$$Q_1 = a_1 - a_3,\ Q_2 = a_2,\ P_1 = \dot{a}_1 - a_0,\ P_2 = \dot{a}_2. \tag{18}$$

Although function $P_3 \equiv \dot{a}_3 - a_0$ is also gauge invariant, it can be obtained from the others, due to the constraint part of Maxwell's equation. The evolution equations for the LRS background are found as follows:

$$\begin{aligned}
\dot{Q}_1 &= P_1 + \frac{1}{m}\frac{q_3}{q_1}((2l+1)P_1 + P_2), \quad \dot{Q}_2 = P_2, \\
\dot{P}_1 &= \left(\frac{\dot{N}}{N} - \frac{1}{2}\frac{\dot{q}_3}{q_3}\right) P_1 - m^2\frac{N^2}{q_3}Q_1, \\
\dot{P}_2 &= \left(\frac{\dot{N}}{N} - \frac{1}{2}\frac{\dot{q}_3}{q_3}\right) P_2 - m^2\frac{N^2}{q_3}Q_2 - m\frac{N^2}{q_1}(Q_1 + (2l+1)Q_2).
\end{aligned} \tag{19}$$

Details of this set of ODEs are discussed in [7].

To tackle the gravitational perturbation equation we need to generalize our framework to be applicable to symmetric tensors. Again, thanks to the well-defined invariant vectors χ_I, separations of variable for the tensors are straightforward in principle. However, to make our analysis successful we will need to find a "well-coordinated" set of base mode tensors like the even and odd vectors used above.

3 Concluding Remarks

Although this work is motivated by the interest in the future asymptotics of vacuum spacetimes, the techniques developed in this work are also applicable to other various situations. An immediate generalization is to include matter like perfect fluid. This may have a cosmological interest, especially in the context of early universe. Also, it is possible to focus on the properties of the initial singularity. Another possible application would be this study of asymptotic behavior of spacetimes that have nontrivial topologies might be helpful to consider the so-called averaging problem, i.e., what the implication of the future asymptotic geometrization is.

The author thanks Vincent Moncrief and Katsuhito Yasuno for many helpful and enjoyable discussions. He acknowledges financial support from Japan Society for the Promotion of Science (JSPS).

References

[1] M. T. Anderson, in *Comparison Geometry*, MSRI Publications, Vol. **30**, (1997).

[2] S. Bonanos, Commun. Math. Phys. **26** (1972) 259.

[3] A. E. Fischer and V. Moncrief, in *Proc. 2nd Samos Meeting on Cosmology, Geometry and Relativity* ed S. Cotsakis and G. W. Gibbons (Springer, New York, 2000).

[4] A. E. Fischer and V. Moncrief, Class. Quantum Grav. **19** (2002) 5557.

[5] J. Hempel, *3-manifolds*, Ann. of Math. Studies 86, (Princeton University Press, Princeton, N.J., 1976); P. Scott, Bull. London Math. Soc. **15**, (1983) 401.

[6] M. Tanimoto, V. Moncrief, and K. Yasuno, preprint (2002), Perturbations of Spatially Closed Bianchi III Spacetimes. (gr-qc/0210078)

[7] M. Tanimoto, in preparation.

[8] K. Yasuno, and M. Tanimoto, in preparation.

Numerical simulation of gravothermal catastrophe from a viewpoint of non-extensive thermodynamics

Atsushi Taruya,[1] Masa-aki Sakagami[2]

[1] *Research Center for the Early Universe(RESCEU), School of Science, University of Tokyo, Tokyo 113-003, Japan*

[2] *Department of Fundamental Sciences, FIHS, Kyoto University, Kyoto 606-8501, Japan*

Abstract

With a particular attention to the recent postulate on non-extensive generalization of Boltzmann-Gibbs statistics, we study the long-term stellar dynamical evolution of self-gravitating system using a special-purpose hardware, GRAPE-6, the timescales of which are much longer than the two-body relaxation time. In a self-gravitating N-body system confined in an adiabatic wall, we show that the quasi-equilibrium sequence arising from the Tsallis entropy, so-called *stellar polytrope*, plays an important role in characterizing the transient states away from the Boltzmann-Gibbs equilibrium state.

1 Introduction

The long-term evolution of self-gravitating many-body system is an old problem with a rich history in astrophysics. The problem, in nature, involves the long-range force of attractive gravity and is fundamentally connected with statistical mechanics and thermodynamics. Historically, the important consequence from the thermodynamical arguments has arisen in 1960s, known as the *gravothermal catastrophe*, i.e., the core-collapse phenomena due to the thermodynamic instability in presence of negative specific heat[1]. Originally, the gravothermal catastrophe has been investigated in a very idealized situation, i.e., a stellar system confined in a spherical cavity[2]. Owing to the maximum entropy principle, the existence of unstable thermal state has been found from the standard analysis of statistical mechanics with a particular attention to the Boltzmann-Gibbs(BG) entropy:

$$S_{\rm BG} = -\int d^3\boldsymbol{x} d^3\boldsymbol{v}\, f(\boldsymbol{x},\boldsymbol{v}) \ln f(\boldsymbol{x},\boldsymbol{v}), \tag{1}$$

where $f(\boldsymbol{x},\boldsymbol{v})$ denotes the one-particle distribution function defined in phase-space $(\boldsymbol{x},\boldsymbol{v})$.

Since 1960s, the standard approach using the BG entropy has dramatically improved our view of the late-time phase of the globular cluster as real astronomical system[3], however, from a thermodynamic point of view, peculiarities in self-gravitating thermal state, as well as the non-equilibrium properties away from the BG state have not yet understood completely.

In this article, aiming at a better understanding of the (non-equilibrium) thermodynamic properties of stellar self-gravitating system, we present a set of long-term N-body simulations, timescale of which is much longer than the relaxation time. With a particular emphasis to the recent postulate on the non-extensive generalization of BG statistics, we focus on the early phase of the stellar dynamical evolution in an isolated star cluster before self-similar core-collapse[4]. We show that the quasi-equilibrium sequence arising from the Tsallis entropy[5] plays an important role in characterizing the non-equilibrium evolution of self-gravitating system.

2 N-body simulations

The N-body experiment considered here is the same situation as investigated in classic papers ([2], see also Ref.[6]). That is, we confine the N particles interacted via Newton gravity in a spherical adiabatic

[1] E-mail:ataruya@utap.phys.s.u-tokyo.ac.jp

[2] E-mail:sakagami@phys.h.kyoto-u.ac.jp

Table 1: Initial distributions and their evolutionary states

run #	initial distribution	parameters	# of particles	transient state	final state
A	stellar polytrope($n = 3$)	$D = 10,000$	2,048	stellar polytrope	collapse
B1	stellar polytrope($n = 6$)	$D = 110$	2,048	stellar polytrope	collapse
B2	stellar polytrope($n = 6$)	$D = 10,000$	2,048	stellar polytrope	collapse
C1	Hernquist model	$a/r_e = 0.5$	8,192	stellar polytrope	collapse(?)
C2	Hernquist model	$a/r_e = 1.0$	8,192	none	isothermal

wall, which reverses the radial components of the velocity if the particle is outside the wall. Without loss of generality, we set the units as $G = M = r_e = 1$, where G is gravitational constant, M and r_e is the total mass of the system and the radius of the adiabatic wall, respectively. Note that the typical timescales appearing in this system are the free-fall time, $T_{\rm ff} = (G\rho)^{-1/2}$, and the global relaxation time driven by the two-body encounter, $T_{\rm relax} = (0.1N/\ln N)T_{\rm ff}$ [1], which are basically scaled as $T_{\rm ff} \sim 1$ and $T_{\rm relax} \sim 0.1N/\ln N$ in our units.

To perform a expensive N-body calculation, we used a special-purpose hardware, GRAPE-6, which is especially designed to accelerate the gravitational force calculations for collisional N-body system[7]. With this implementation, the 4th-order Hermite integrator with individual time step[8] can work efficiently. We adopt the plummer softened potential with a softening length ϵ of 1/512 and 1/2048.

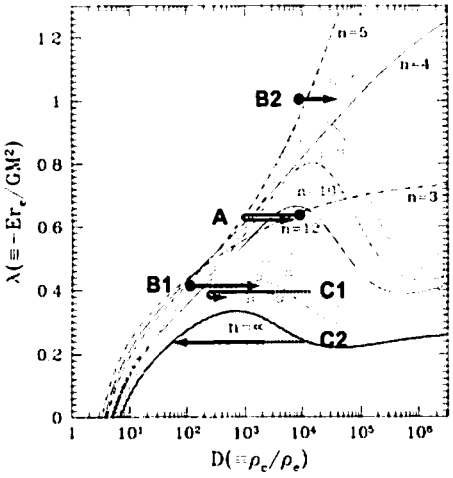


Figure 1: Equilibrium sequences of stellar polytrope and isothermal distribution ($n = \infty$) in the energy-density contrast relation, $\lambda \equiv -r_e E/(GM^2)$ v.s. $D \equiv \rho_c/\rho_e$. The thick arrows denote the evolutionary tracks in each simulation run.

In the present numerical simulation, the choice of the initial condition is important step. Here, we set the initial distribution to the stationary state of Poisson-Vlassov equation, i.e., dynamical equilibrium for spherical system with isotropic velocity distribution. According to the Jeans theorem[1], the one-particle distribution function $f(\boldsymbol{x}, \boldsymbol{v})$ can be expressed as a function of specific energy, $\varepsilon = v^2/2 + \Phi(r)$ with r and Φ being the radius and the gravitational potential. Then under keeping the energy and the mass constant, the thermal equilibrium of ordinary extensive statistics derived from the maximum entropy principle of the BG entropy (1) reduces to the exponential distribution, so-called *isothermal* distribution given by $f(\varepsilon) \propto e^{-\beta\varepsilon}$, which effectively satisfies the equation of state, $P(r) \propto \rho(r)$, where $P(r)$ is pressure and $\rho(r)$ is mass density[2].

On the other hand, as another possibility, one considers the extremum state of Tsallis' non-extensive entropy [5]:

$$S_q = -\int d^3\boldsymbol{x} d^3\boldsymbol{v}\,[\{f(\boldsymbol{x},\boldsymbol{v})\}^q - f(\boldsymbol{x},\boldsymbol{v})]/(1-q), \tag{2}$$

which might be of particularly importance in describing the meta-equilibrium state away from the BG state[9]. In this case, the maximum entropy principle leads to the power-law distribution, $f(\varepsilon) \propto (\Phi_0 - \varepsilon)^{1/(q-1)}$, referred to as the *stellar polytrope* [10, 11, 12, 13]. It satisfies the polytropic equation of state, $P(r) \propto \rho(r)^{1+1/n}$, and the polytrope index n is related to the q-parameter as $n = 1/(q-1) + 3/2$[14].

Provided the polytrope index n, the equilibrium structure can be determined by solving the Láne-Emden equation [1] and using the solution, the relationship between the dimensionless energy $\lambda \equiv -r_c E/(GM^2)$ and the density contrast $D \equiv \rho_c/\rho_e$, the core density divided by the edge density, can be drawn (see Fig.1). Note that the limit $n \to \infty$ (or $q \to 1$) corresponds to the isothermal distribution derived from the BG entropy (1).

Table 1 summarizes the list of the five simulation runs. A more systematic survey for dependence of initial condition is now in progress and the details of the results will be reported elsewhere. In Table 1, in addition to the stellar polytropic initial state, we also consider the non-stellar polytropic state of the Hernquist model[15], which was originally introduced to account for the empirical law of observed elliptical galaxies[1].

3 Results

As has been recently discussed in [11, 12, 13], the stellar polytropic distribution arising from the Tsallis entropy has consistent thermodynamic structure. As a result, the stellar polytrope confined in an adiabatic wall is shown to be thermodynamically stable when the polytrope index $n < 5$. In other words, if $n > 5$, stable equilibrium state ceases to exist for a sufficiently large density contrast $D > D_{\rm crit}$, where the critical value $D_{\rm crit}$ given by a function of n is determined from the second variation of entropy around the extremum state of Tsallis entropy, $\delta^2 S_q = 0$[11, 13]. The dotted line in Fig.1 represents the critical value $D_{\rm crit}$ for each polytrope index. Figure indicates that as long as the stellar polytrope at low density contrast $D < D_{\rm crit}$ is concerned, the system is expected to remain stable. Apart from the BG state, one might expect that the stellar polytrope acts as a role of thermal equilibrium.

Of course, this naive expectation is not correct at all. Indeed, the numerical simulations reveal that the stellar polytropic distribution gradually changes with time, on the timescale of two-body relaxation. Further, it seemed that the gravothermal instability appears at relatively smaller values of D than the predicted one, $D_{\rm crit}$, which might be partially ascribed to the non-stationarity of background stellar polytrope. Physically, the gravothermal catastrophe follows from the decoupling of the relaxation timescales between the central and the outer parts, whose behavior sensitively depends on the physical property of heat transport[16]. In a rigorous sense, thermodynamic prediction might lose the physical relevance, however, focusing on the evolutionary sequence, we found that the transient state starting from the initial stellar polytrope can be remarkably characterized by a sequence of stellar polytrope (run A, B1 and B2). This is even true in the case of the non-stellar polytropic initial distribution (run C1).

Let us show the representative results taken from run A (Fig.2). The left panel plots the snapshots of the density profile $\rho(r)$, while the middle panel represents the distribution function $f(\varepsilon)$ as a function of specific energy ε. Note that just for illustrative purpose, each output result is artificially shifted to the two-digits below. Only the final output with $T = 400$ represents the correct scales. In each panel, solid lines mean the initial stellar polytrope with $n = 3$ and the other lines indicate the fitting results to the stellar polytrope by varying the polytrope index n. Note that the number of fitting parameter just reduces to one, i.e., polytrope index, since the total energy is well-conserved in the present situation. Fig.2 shows that while the system gradually deviates from initial polytropic state, the transient state still follows a sequence of stellar polytrope. The fitting results are remarkably good until the time exceeds $T \simeq 400$, corresponding to $15T_{\rm relax}$. Afterword, the system turns to enter the gravothermally unstable regime and finally undergoes the core-collapse.

Now, focus on the evolutionary track in each simulation run summarized in energy-density contrast plane (Fig.1), where the filled circle represents the initial stellar polytrope. Interestingly, the density contrast of transient state in run A initially decreases, but it eventually turns to increase. The turning-point roughly corresponds to the stellar polytrope with index $n \sim 5 - 6$. Note, however, that the time evolution of polytrope index itself is a monotonically increasing function of time as shown in right panel of Fig.2, apart from the tiny fluctuations. This is indeed true for the other cases, indicating the Boltzmann H-theorem that any of the self-gravitating system tends to approach the BG state. The typical example is the run C2, which finally reaches at the stable BG state. However, as already shown in run A, all the systems cannot reach at the BG state. For a fixed value $\lambda > 0.335$, Fig.1 indicates that no BG state is possible and no stable stellar polytrope ceases to exist at high density contrast $D > D_{\rm crit}$. In fact, our simulations starting from the stellar polytrope finally underwent the core-collapse (run A, B1 and B2).

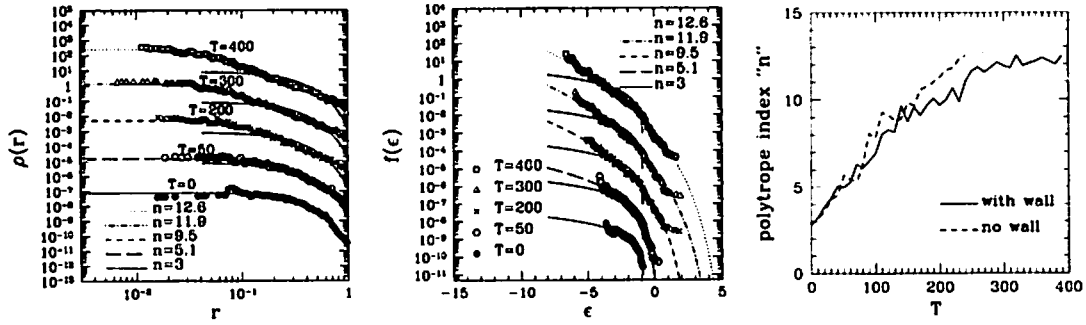


Figure 2: Results from simulation run A. *Left*: snapshots of density profile $\rho(r)$. *Middle*: snapshots of one-particle distribution function $f(\varepsilon)$. *Right*: the time evolution of polytrope index for run A with and without the boundary of adiabatic wall.

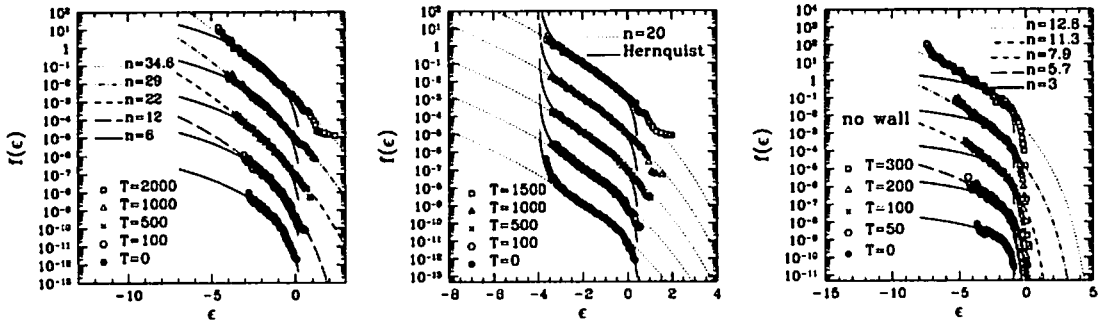


Figure 3: Evolution of one-particle distribution function in other models. *Left*: run B1; *Middle*: run C1 ; *Right*: run A removing the adiabatic wall.

Though it might not be rigorously correct, the predicted value $D_{\rm crit}$ provides a crude approximation to the boundary between the stability and the instability.

Fig.3 plots the snapshots of distribution function taken from the other runs. The initial density contrast in run B1 (*left panel*) is relatively low ($D = 110$) and thereby the system slowly evolves following a sequence of stellar polytrope. After $T = 2000 \sim 74T_{\rm relax}$, the system begins to deviate from stable equilibrium sequence, leading to the core-collapse. Another noticeable case is the run C1 (*middle panel* of Fig.3). The Hernquist model as initial distribution of run C has cuspy density profile, $\rho(r) \propto 1/r/(r+a)^3$, which behaves as $\rho \propto r^{-1}$ at inner part [15]. The resultant distribution function $f(\varepsilon)$ shows a singular behavior at negative energy region, which cannot be described by the power-law distribution. Soon after a while, however, the gravothermal expansion[6] takes place and the flatter core eventually formed. Then the system settles into a sequence of stellar polytrope and can be approximately described by the stellar polytrope with index $n = 20$ for a long time. Thus, as long as the stellar system confined in an adiabatic wall is concerned, the stellar polytrope can be regarded as a quasi-attractor and a quasi-equilibrium state.

Of course, these remarkable features could be an outcome in a very idealized situation and one suspects that quasi-equilibrium state of stellar polytrope cannot hold if we remove the boundary of the adiabatic wall. As a demonstration, right panel of Fig.3 plots the results removing the boundary, in which the initial state is the same distribution as in run A. As is expected, the high-energy particles freely escape outwards from the central region and the resultant distribution function $f(\varepsilon)$ sharply falls off at the energy region $\varepsilon \sim 0$, indicating that the density contrast D becomes effectively large. Thus, compared to the system confined in the wall, removal of the boundary makes the stellar system unstable and the core-collapse takes place earlier. Nevertheless, focusing on the inner part of the denser region, the evolution of core is not significantly affected by the escape particles at outer part and can be fitted by a sequence of stellar polytrope (see also the dashed line in right panel of Fig.2). The successful fit to the density profile $\rho(r)$ almost remains the same. Hence, the stellar polytrope characterized by the Tsallis entropy can be even realized in a realistic situation removing the boundary of the adiabatic wall.

4 Summary

We have performed a set of numerical simulation of long-term stellar dynamical evolution away from the BG state and found that the transient state of the system confined in an adiabatic wall can be remarkably fitted by a sequence of the stellar polytrope. This is even true in the case removing the outer boundary. Therefore, the stellar polytropic distribution can be a quasi-attractor and a quasi-equilibrium state of self-gravitating system.

Definitely speaking, alternative characterization of transients away from the BG state might be possible other than the q-exponential distribution of stellar polytrope. For an empirical characterization of observed structure, the one-parameter family of truncated exponential distribution, so-called King model has been used in the literature[1, 3, 17]. Also, the sequence of King model has been found to characterize the evolutionary sequence of density profile for isolated stellar system without boundary[4]. We have also tried to fit the simulation data to the King model. Similarly to the stellar polytrope, the King model accurately describes the simulated density profile $\rho(r)$ confined in an adiabatic wall, however, it fails to match the simulated distribution function $f(\varepsilon)$, especially at the cutoff energy scales. Therefore, from the quantitative description of the entire phase-space structure, the power-law distribution of stellar polytrope can be a better characterization of quasi-equilibrium state and this could yield an alternative explanation of origin of empirical King model.

References

[1] J. Binney and S. Tremaine, *Galactic Dynamics*, (Princeton Univ. Press, Princeton, 1987); L. Spitzer, *Dynamical Evolution of Globular Clusters*, (Princeton Univ. Press, Princeton, 1987).

[2] V.A. Antonov, Vest. Leningrad Gros. Univ. **7**, 135 (1962); D. Lynden-Bell and R. Wood, Mon. Rot. R. Astron. Soc. **138**, 495 (1968).

[3] G. Meylan and D.C. Heggie, Astron. Astrophys. Rev. **8**, 1 (1997).

[4] H. Cohn, Astrophys. J. **242**, 765 (1980).

[5] C. Tsallis, J. Stat. Phys. **52**, 479 (1988).

[6] H. Endoh, T. Fukushige and J. Makino, Publ. Astron. Soc. Japan **49**, 345 (1997).

[7] J. Makino, in J. Makino and P. Hut (Eds.), Proc. IAU Symp. **208**, *Astrophysical Supercomputing using Particle Simulations*, in press.

[8] J. Makino and S.J. Aarseth, Publ. Astron. Soc. Japan **44**, 141 (1992).

[9] C. Tsallis, Braz. J. Phys. **29** 1; S. Abe and Y. Okamoto (Eds.), *Nonextensive Statistical Mechanics and Its Applications* (Springer, Berlin, 2001).

[10] A.R. Plastino and A. Plastino, Phys. Lett. A **174**, 384 (1993).

[11] A. Taruya and M. Sakagami, Physica A **307**, 185 (2002).

[12] A. Taruya and M. Sakagami, Physica A (2003), in press (cond-mat/0204315).

[13] A. Taruya and M. Sakagami, Physica A (2003), in press (cond-mat/0211305).

[14] The relation between the polytrope index n and the q-parameter may change, depending on the choice of the statistical average: standard linear means[10, 11] or normalized q-values[13]. Here, we simply adopt the result using the standard linear mean.

[15] L. Hernquist, Astrophys. J. **356**, 359 (1990).

[16] J. Makino and P. Hut, Astrophys. J. **383**, 181 (1991).

[17] I.R. King, Astron. J. **71** 64 (1966).

Gravitational waves from quintessential inflation

Hiroyuki Tashiro, [1]

Department of Physics, Kyoto University,
Sakyo-ku, Kyoto, 606-8502, Japan

Abstract

Quintessential inflation explains both inflation and present accelerated expansion. These two accelerated expansion is driven by a single scalar field. We construct a model based on an exponential potential. We consider two kinds of reheating process. One is the ordinary reheating in quintessential inflation, using gravitational particle creation. The other is the instant preheating which is much more effective. We calculate the relic gravitational waves produced during inflation in our model. We find that the spectrum of the gravitational waves is quite sensitive to the reheating process. Conversely, the detection or non-detection of primordial gravitational waves at $\sim$100MHz would have profound implications for the inflationary cosmology.

1 Introduction

Recent observations of super novae Ia suggest that our universe undergoes accelerated expansion at the present [1, 2]. It is considered that this expansion is caused by cosmological constant dominating the universe in energy density. But this energy density value is fine tuned (cosmological constant problem). In order to avoid this problem it is suggested that cosmological constant is time varying, and one of the solutions based on this idea is quintessence [3]. Quintessence is a scalar field which slowly rolls down its potential. The energy of its potential is small and hardly change at present. But its potential energy has contribution to our universe as cosmological constant and brings accelerated expansion. This mechanism of expansion is similar to the idea of inflation.

Peebles and Vilenkin suggested that quintessence is identified with inflaton [4]. Both inflation and present accelerated expansion are caused by a single scalar field in this model. They called this inflation model quintessential inflation. But the potential they used is combination of chaotic inflation and quintessence potential. This potential is a toy model. In this paper we construct a smooth potential based on an exponential potential. We consider reheating process by instant preheating [5] as well as by gravitational particle production previously considered in [4].

Inflation produces primordial density perturbations and gravitational waves. The detection of the gravitational waves will be the evidence for inflation, although current and future detectors will not be able to detect them. It is known that the amplitude of gravitational waves is enhanced in quintessential inflation [4]. So, the possibility of detection of the gravitational waves is expected more than in other inflation model. We calculate the spectrum of gravitational waves in our model. We discuss the possibility of the detection and the difference of spectrum strength in our model.

2 Potential of the scalar field

We adopt as the potential form of the scalar field ϕ

$$V(\phi) = V_0 \exp(-\lambda\phi/M_{\rm pl}), \tag{1}$$

where $M_{\rm pl} = 1/\sqrt{8\pi G} = 2 \times 10^{18}$ GeV. The reason for choosing this potential form is that there are many motivation in particle physics for considering this potential form.

First, we assume that the universe is dominated by the scalar and inflation is occurred. For our potential form, the scale factor is $a \propto t^{2/\lambda^2}$ and we get the condition, $\lambda < \sqrt{2}$ for power-law inflation [6].

[1] E-mail:htashiro@tap.scphys.kyoto-u.ac.jp
This work is based on the collaboration with T. Chiba and M. Sasaki.

We can impose more severe condition of λ during the inflation. Recent observations of CMB anisotropies indicate that the spectral index of the energy density perturbation is $n_s \simeq 1.0 \pm 0.1$ [7]. Since $n_s - 1 = -\lambda^2$ under the slow-roll approximation, we get

$$\lambda \lesssim 0.3. \tag{2}$$

If we assume that at $\phi = 0$ the inflation is end by changing λ, the typical energy scale of inflation is V_0. From COBE observation, we got the energy scale, $V_0 \simeq 10^{-12} M_{\rm pl}^4$.

By changing λ, the kinetic energy dominates the universe and reheating the universe begins. This era is called as kination. We consider two kinds of reheating process, but they are mentioned later. In this era, the Friedmann equation and the equation of the field ϕ are

$$\left(\frac{\dot{a}}{a}\right)^2 = \frac{1}{3M_{\rm pl}^2}\frac{1}{2}\dot{\phi}^2,$$
$$\frac{d^2\phi}{dt^2} + 3\frac{\dot{a}}{a}\frac{d\phi}{dt} = 0. \tag{3}$$

From these equations, we obtain

$$\dot{\phi}^2 \sim V_0 (a/a_{end})^{-6}, \tag{4}$$
$$\phi \simeq \sqrt{6} M_{pl} \ln(a/a_{end}), \tag{5}$$

where $a \propto t^{1/3}$ and a_{end} is the scale factor at the end of inflation. Thus the potential energy of the field ϕ is

$$V \propto \exp(-\lambda\phi/M_{pl}) \simeq (a/a_{end})^{-\sqrt{6}\lambda}. \tag{6}$$

Therefore in order to prevent the potential energy from dominating the universe, we impose the condition,

$$\lambda > \sqrt{6}. \tag{7}$$

Because the kinetic energy density obeys Eq.(4) and the radiation energy produced by reheating is proportional to a^{-4}, the kination is end and the radiation dominant era begins.

After radiation, the potential energy eventually dominate the universe for the explanation of the present acceleration of the universe. The potential energy must dominate the kinetic energy. Therefore we require

$$\lambda < \sqrt{6}. \tag{8}$$

And the present potential energy must be $V \sim H_0^2 M_{pl}^2$.

From the requirements Eq.(2), Eq.(7) and Eq.(8), we must find λ which takes the different value at the each epoch. As an example, we consider a potential in the following form:

$$V(\phi) = V_0 \exp(-\lambda(\phi)\phi/M_{pl}), \tag{9}$$
$$\lambda(\phi) = (\tanh(\phi/M_{pl}) + A)\left(\frac{(\phi/M_{pl})^2 + u^2}{(\phi/M_{pl})^2 + v^2}\right), \tag{10}$$

where A, u and v are constants. We assume $A = 1.1$, and arrange u, v to fix $\Omega_\phi \simeq 0.7$ at the present.

3 Reheating

We consider two kinds of reheating process. One is the reheating by gravitational particle production [4], and the other is instant preheating [5].

Reheating by gravitational particle production The reheating by gravitational particle production is occurred as follows [4]. The particle creation occurred by the expansion of the universe, and the created particles thermalize among the fermions and gauge bosons. Ford investigated particle creation of the scalar field at the transition from de Sitter inflation to the radiation dominated era. This study is in the limit of nearly conformal coupling. His analysis was extended to the other coupling case [9], and to the

transition from inflation to arbitrary expansion [10]. The created energy density in their analysis is the same order as Ford's result. Therefore we use Ford's result. The created energy density from it is

$$\rho = RH_{\rm end}^4 (a/a_{\rm end})^{-4}. \tag{11}$$

where $R \sim 10^{-2} N_s$ and N_s is the number of scalar fields.

The created particles, whose typical energy is $\epsilon \sim H_{end}(a/a_{end})^{-1}$, thermalize when the rate $n\sigma$ of the interaction with gauge bosons is comparable expansion rate. Here the number density n is $n \simeq R\epsilon^3$ and the cross section σ are $\sigma \sim \alpha^2 \epsilon^{-2}$ with $\alpha \sim 10^{-2}$. Thus the thermalization occurs at $a_{th}/a_{end} \sim \alpha^{-1} R^{-1/2}$, and the temperature is $T_{th} \sim R^{3/4} \alpha H_{end}$. The kinetic energy density is proportional to a^{-6}, and the radiation energy density is proportional to a^{-4}. Therefore kinetic energy density is equal to the energy density of radiation and the radiation dominant era begins. At this beginning the temperature is

$$T_r \sim R^{3/4} V_0 M_{\rm pl}^{-3} \sim R^{3/4} \times 10^6 \text{ GeV}. \tag{12}$$

This temperature is enough for the big bang nucleosynthesis.

Instant preheating Instant preheating was suggested for the potential with no oscillation by Kofman et al. [5]. The mechanism is similar to preheating by parametric resonance. They introduce the interaction lagrangian,

$$L_{int} = -\frac{1}{2} g^2 \phi^2 \chi^2 - \frac{1}{2} \bar{\psi} \psi \chi. \tag{13}$$

The energy of the field ϕ is transferred into the energy of fermion ψ (radiation) through the scalar field χ. For simplicity, we assume that the scalar field χ does not have a bare mass. Thus, the effective mass of the field χ is $m_\chi = g|\phi|$. The particle creation of the field χ is occurred by the violation of adiabatic condition, $|\dot{m}_\chi| = m_\chi^2$. The number density of created particle is $n_\chi = (g\sqrt{V_0})^{3/2}/8\pi^3$ [11]. The field χ becomes non relativistic because of effective mass. The energy density of the field χ is $\rho_\chi = n_\chi m_\chi$, and the field χ decays into the fermion ψ with decay rate $\Gamma = h^2 g|\phi|/8$. Hence, the fermion ψ (radiation) energy ρ_r obeys the equation,

$$\dot{\rho}_\psi + 4H\rho_\psi = \Gamma \rho_\chi, \tag{14}$$

where H is determined by the kinetic energy of field ϕ Eq. (4). This reheating is more efficient than the reheating by gravitational particle production.

4 The spectrum of gravitational waves

In each reheating process, we arrange u, v to fix $\Omega_\phi \simeq 0.7$ at the present. Fig.1 is the case of reheating of gravitational particle production. In this figure the potential energy of the field ϕ is nearly constant and dominate universe at the present. At the result the present accelerated expansion is realized by a scalar field with our potential. And also in the case of instant preheating we could fix $\Omega_\phi \simeq 0.7$ at the present.

We can get the scale factors at the beginning of each epoch. By using these values, we can obtain the energy density spectrum of gravitational waves. We use the Bogliubov coefficients method to calculate gravitational waves [12, 13]. In transverse traceless gauge gravitational waves are written,

$$h_{\mu\nu} = \sum_{\lambda=(+,\times)} \int \frac{dk^3}{(2\pi)^{3/2}} \epsilon_{\mu\nu}{}^\lambda u_k(\tau) e^{i\mathbf{k}\cdot\mathbf{x}}, \tag{15}$$

where $\epsilon_{\mu\nu}$ is the polarization tensor and gravitational waves have two degree of freedom in polarization. The Einstein equations give an equation for u_k,

$$u_k'' + 2(a'/a)u_k' + k^2 u_k = 0. \tag{16}$$

where the prime denotes the derivative with respect to the conformal time. The solution of Eq.(16) at different epochs is related through Bogliubov coefficients. For example, let u_i and u_{ki} be solutions of the Eq.(16) at inflation and kination. The relation of these solutions is $u_{ki} = \alpha u_i + \beta u_i^*$ by using

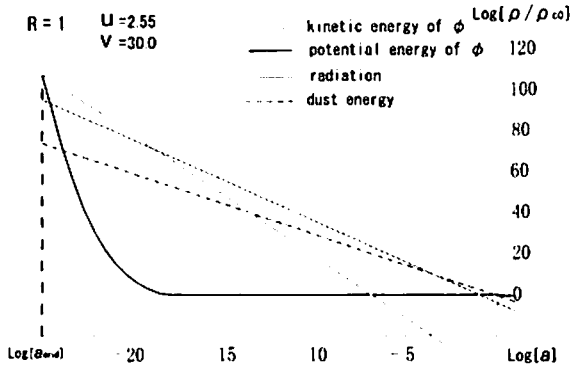


Figure 1: The energy density in the reheating by gravitational particle production. The present potential energy set $\Omega_\phi \simeq 0.7$ by arranging u, v.

Bogliubov coefficients, α, β. The number density of created particles is $|\beta|^2$. Since we want to know the number density at the present, we must obtain the Bogliubov coefficients between inflation and the present potential dominant era, α_{total}, β_{total}. From the number density we get the energy density at the present. At the frequency $f = 2\pi k/a$ the energy density is $d\rho_{\rm gw} = 2 \times 2\pi f\ |\beta_{total}|^2\ 4\pi f^2\ df$. Fig.2 is the spectrum of gravitational waves for two reheating processes. $h^2\Omega_{\rm gw}$ is the density parameter defined as $h^2\Omega_{\rm gw}(f) = (h^2/\rho_c)(d\rho_{\rm gw}/d\log f)$, where ρ_c is the present critical energy density.

The spectrum of gravitational waves has the same shape as that of ordinary inflation at the lower frequency bands. However, due to the presence of the kination the shape can be different at the higher bands. The energy density spectrum of the gravitational waves which enter into the horizon during kination is proportional to f. Therefore the gravitational waves at high frequency is amplified much more than that in ordinary inflation models. The duration of the kination depends on the efficiency of reheating, and the longer duration of the kination results in larger amplitude. But the energy density of the gravitational waves is constrained by the success of the Big Bang nucleosynthesis (It is called BBN bound) [14]. Therefore the efficiency of the reheating by gravitational particle production is restricted at the left panel in Fig.2. The sensitivity of advanced LIGO will be $h^2\Omega_{\rm gw} \simeq 10^{-11}$ at $10 \sim 100$Hz and the one of LISA will $h^2\Omega_{\rm gw} \simeq 10^{-11}$ at 1mHz [14]. Unfortunately it seems difficult to observe the gravitational waves of our inflation model by these project.

Instant preheating is more efficient than gravitational reheating so that the enhancement of the spectrum of the gravitational waves entering into horizon during kination is restricted to higher frequency. When g and h are low value the decay of the field χ is delayed. Because the energy density ρ_χ is proportional to a^{-3}, the energy density of the field χ dominates the kinetic energy density of the field ϕ, depending on these values. The universes is dominated by non-relativistic particles. In the spectrum of the gravitational waves the imprint is left distinctly. It may be possible that we know the changing of the expanding by the observation of gravitational waves at the higher bands.

5 Conclusion

We investigate the possibility of the quintessential inflation by exponential potential. We consider two kinds of reheating process: gravitational particle production and instant preheating. In both reheating processes the present accelerated expanding could be explained by the scalar field by which inflation was occurred in the past. We calculate the spectrum of gravitational waves produced during inflation. In our model the spectrum of the gravitational waves at the higher band is amplified more than that in ordinary inflation. We find that the spectrum is sensitive to reheating process and can be enhanced at ~ 100MHz. Therefore by the observation at these bands we may be able to obtain information regarding the physics of early universe. The details will be published elsewhere [15].

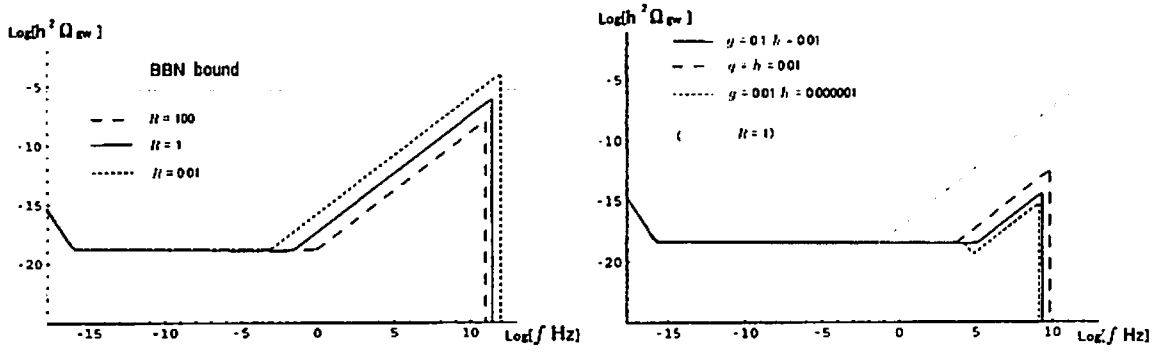


Figure 2: The spectrum of gravitational waves. The left panel is in the case of the reheating by gravitational particle production. The right one is in the case of instant preheating.

References

[1] A. G. Riess et la., ApJ **116**, 1009 (1998).

[2] S. Perlmutter et al., ApJ **517**, 565 (1999)

[3] P. J. E. Peebles and B. Ratra, Astrophys. J. **325**, L17 (1988).

[4] P. J. E. Peebles and A. Vilenkin, Phys. Rev. D **59**, 063505 (1999).

[5] G. N. Felder, L. Kofman, and A. D. Linde, Phys. Rev. D **59**, 123523 (1999).

[6] F. Lucchin and S. Matarrese, Phys. Rev. D **32**, 1316 (1985).

[7] P. de Bernardis et al., ApJ **564**, 559 (2002); R. Stomper et al., ApJ , L7 (2001); C. Pryke et al., ApJ **568**, 46 (2002); J.A. Rubino-Martin et al., astro-ph/0205367.

[8] L. H. Ford,, Phys. Rev. D **35**, 2955 (1987)

[9] T. Damour and A. Vilenkin, Phys. Rev. D **53**, 2981 (1996)

[10] M. Giovannini, Phys. Rev. D **58**, 083504 (1998)

[11] L. Kofman, A. D. Linde, and A. A. Strarobinsky, Phys. Rev. D **56**, 3258 (1999).

[12] B. Allen, Phys. Rev. D **37**, 2078 (1988)

[13] N. D. Birrell and P. C. W. Davies, *QUANTUM FIELDS IN CURVED SPACE*, Cambridge, (1982)

[14] M. Maggiore, Phys. Rept. **331**, 283 (2000).

[15] H. Tashiro, T. chiba and M. Sasaki. , in preparation.

Scaling Law and Non-Gaussian Velocity Distribution in Self-gravitating Ring Model

Takayuki Tatekawa,[1]

Department of Physics,
Waseda University, Okubo 3-4-1, Shinjuku, Tokyo 169-8555, Japan

Yasuhide Sota,[2]

Department of Physics,
Ochanomizu University, Otsuka 2-1-1, Bunkyo, Tokyo 112-8610 Japan

Abstract

Fractal structures and non-Gaussian velocity distributions are characteristic properties commonly observed in virialized self-gravitating systems such as galaxies and interstellar molecular clouds. We study the origin of these properties using a one-dimensional ring model which we proposed in previous paper. In this simple model, N particles are moving, on a circular ring fixed in three dimensional space, with mutual interaction of gravity. This model is suitable for the accurate symplectic integration method by which we argue the phase transition in this system. In this paper, we fix the total number of particles $N = 1000$. Then we analyze velocity distribution and scaling relation with one snapshot data. Especially, during relaxation process, we analyze spatial and velocity distribution of particles. When we set small initial virial ratio, the velocity distribution approaches exponential distribution for the time being. On the other hand, when we set large initial virial ratio, the velocity distribution becomes Gaussian, not appears exponential distribution.

1 Introduction

Many astrophysical objects in our universe consist of mutually interacting elements through gravity. If they are almost isolated systems, they are called self-gravitating system (SGS). For example, galaxies, clusters of galaxies, globular clusters, and molecular clouds are thought to be typical SGSs. Their statistical properties are often characterized by non-Gaussian velocity (or pair-wise velocity) distributions[1], fractal structures[2], and the scaling relation between the mass density and the system size[3]. Most of these objects are thought to be gravitationally virialized. Therefore pure gravitational force seems to play an essential role in characterizing the above statistical properties of SGS independently of initial conditions.

In our previous paper, we proposed a new model (Self Gravitating Ring: SGR) [4]. Then we show that SGR model is characterized by the phase separation and the particle state separation, and by similar recurrent motion and non-Gaussian velocity distribution of halo particles. Especially when we show scaling relation of halo particles, we superposed the snapshot data of n different times, because we fix the total number of particles $N = 100$. Although the scaling relation and peculiar behavior was appeared, someone would suspect that the result was appeared by superposition of snapshot data.

In this paper, we fix the total number of particles $N = 1000$. Then we analyze velocity distribution and scaling relation with one snapshot data. Then we analyze velocity distribution and scaling relation using ensemble average at one time. Especially, during relaxation process, we analyze spatial and velocity distribution of particles. Recently Koyama and Konishi reported when they choose the initial velocity $v = 0$ and uniformly random spacial distribution, the power-law two-point correlation function appears[5].

[1]E-mail:tatekawa@gravity.phys.waseda.ac.jp
[2]E-mail:sota@skyrose.phys.ocha.ac.jp

In SGR model, when we choose small velocity dispersion, peculiar behavior also be appeared. When we set small initial virial ratio, the velocity distribution shows quasi-equilibrium state; the distribution approaches exponential distribution at several dynamical time. On the other hand, when we set large virial ratio, the velocity distribution directly approaches Gaussian, not appears exponential distribution.

2 Self-gravitating Ring Model

We proposed a system of self-gravitating N particles with mass m, whose motions are smoothly constrained on a circular ring with a fixed radius R without friction. Each pair of particles interact with each other through a 3D gravitational force. The distance between a pair is measured by the length of the straight line combining the pair.

The Hamilonian of this system becomes

$$H_p = \frac{1}{2mR^2}\sum_{i=1}^{N} P_i^2 - \sum_{i<j}^{N} \frac{Gm^2}{\sqrt{2}R\sqrt{1-\cos(\theta_i-\theta_j)+\epsilon}}, \tag{1}$$

where ϵ means softening parameter. The position of ith particle is fully described by the angular variable $\theta ?i$ as $\mathbf{r}_i = (R\sin\theta_i, R\cos\theta_i)$. The momentum conjugate to θ_i is give by $P_i = mR^2 d\theta_i/dt$.

When the system is almost uniformly filled by moving particles, we have the longest dynamical time t_R defined by

$$t_R \equiv \sqrt{\frac{R^3}{GNm}}. \tag{2}$$

During this time t_R, a typical particle goes around the ring once. Therefore, the time scale for the whole system to attain thermodynamical equilibrium, if any, is at least larger than this time scale.

There is an another time scale. Suppose the system is stably confined in a region with a scale r, which satisfies

$$\xi \ll r \ll R, \tag{3}$$

where ξ defined as $\xi \equiv \sqrt{2\epsilon}R$. For this sclae r, the ring can be approximated as an infinite straight line and the softening effect is neglected. Under these approximation, the crossing time is defined as

$$t_E \equiv \frac{Gm^{5/2}N^{5/2}}{4\sqrt{2}|E|^{3/2}}. \tag{4}$$

This is the intrinsic time scale associated with genuine gravity independent of the softening parameter ϵ an the system size R.

For numerical simulations, we need to make all physical variables nondimensional; we use m, R, and t_R for the unit of mass, distance, and time, respectively. In these units, the physical Hamiltionian reads

$$H_p = Gm^2\frac{N}{R}H, \tag{5}$$

where

$$H = \frac{1}{2}\sum_{i=1}^{N} p_i^2 - \sum_{i<j}^{N} \frac{1}{\sqrt{2}N\sqrt{1-\cos\theta_{ij}+\epsilon}}. \tag{6}$$

The dimensionless momentum p_i is given by $p_i = d\theta_i/d\tau$ and the dimensionless time τ is introduced as $\tau \equiv t/t_R$.

2.1 Negative specific heat of SGS

First, we study the phase diagram of SGR model in the temperature-energy plane. The T-U relation is shown in Fig.1 and we observe that the region with negative specific heat, i.e. negative slope region,

apparently exists. The temperature T and the internal energy per particle U of the present system are defined respectively by

$$T \equiv \frac{2\langle K(\tau)\rangle}{N} , \tag{7}$$

$$U \equiv \frac{H}{N} . \tag{8}$$

The virial ratio is defined by

$$b \equiv \frac{2T}{U} . \tag{9}$$

The internal energy U is conserved in the present microcanonical system, while the temperature T is defined as the twice of the time-averaged (represented by angle brackets) kinetic energy per particle. The phase diagram in Fig.1 is time averaged over $500 < \tau < 1000$ where the system archives virial equilibrium. Throughout this paper, except explicitly mentioned, we fix the total number of particles $N = 1000$ for simplicity and therefore the remaining relevant parameters which characterize the quasi-equilibrium state of the system would be ϵ and U.

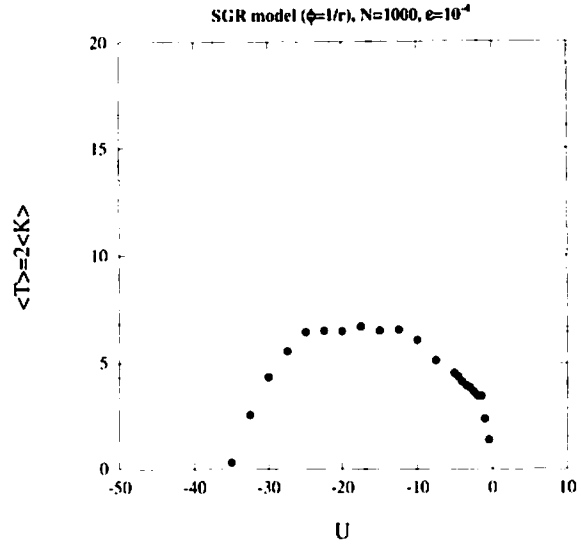


Figure 1: Diagram of temperature T vs. energy per particle U for cutoffs $\epsilon = 1.0 \times 10^{-4}$. The number of particles $N = 1000$. In T-U curve, there are two critical energy scales; $U_{\text{c-low}}(\epsilon)$ and $U_{\text{c-high}}(\epsilon)$, between which negative specific heat $\partial U/\partial T < 0$ appears.

From Fig.1, we find two characteristic energy scales where $\partial T/\partial U = 0$; $U_{\text{c-low}}(\epsilon)$ at a low energy side and $U_{\text{c-high}}(\epsilon)$ at a high energy side. The energy scale $U_{\text{c-high}}(\epsilon)$ corresponds to a mean gravitational binding energy per particle, which is estimated as $\left\langle 1/(\sqrt{2}N\sqrt{1-\cos\theta+\epsilon})\right\rangle \times (N(N-1)/2)/N \sim \mathcal{O}(1)$, while $U_{\text{c-low}}(\epsilon)$ strongly depends on the cutoff ϵ. This cutoff dependence can be estimated from the virial condition which, in our normalization, becomes

$$-\frac{1}{4\sqrt{2\epsilon}} \ll U \ll -\frac{1}{4}. \tag{10}$$

Under this condition, the negative specific heat condition in virialized state would be justified.

3 Scaling relation and non-Gaussian velocity distribution

In this section, we discuss scaling properties and non-Gaussian velocity distribution. In our previous paper, we showed that the velocity distribution of halo particles is non-Gaussian with anomalous tail and

each halo particle show intermittent recursive motion around the core without a definite time scale.

3.1 Scaling relation

We study the scaling property of the spatial distribution. At first, in order to judge whether the distribution of particles is fractal or not, we use box-counting method, which gives a fractal dimension D_F. In order to avoid effect of softening, the size of box is chosen from 10^{-4} to 10^{-2}. In G phase, i.e. when total energy U is positive, the scaling property does not appear, because the particles behave like as free particle. On the other hand, in I phase, the scaling property appears.

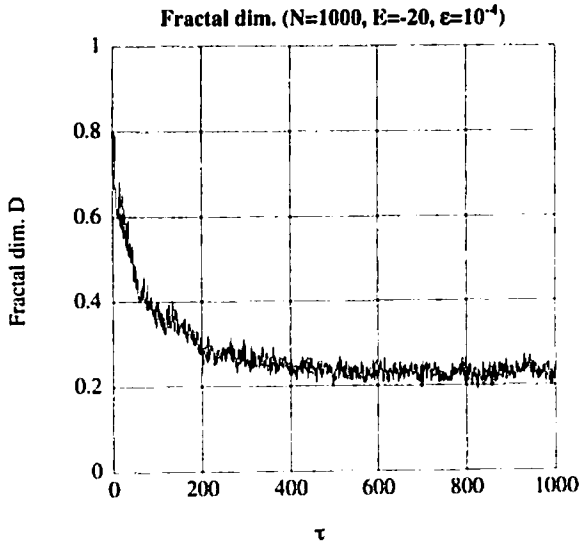


Figure 2: Fractal dimension of particle distribution ($U = -20$). The dimension decreases and converges to ~ 0.25.

Fig.2 shows the relation between time and fractal dimension D_F. During evolution, box-counting dimension seems to decrease and converge. When we increase total energy U, the definite value of fractal dimention increases.

3.2 Non-Gaussian velocity distribution

During evolution and relaxation process, velocity distribution of particles approach Gaussian. However in our analysis, transient state is appeared. If we gave spacial initial condition, i.e. the total energy stays in the negative specific heat region, and initial virial ratio is much smaller than 1, the velocity distribution approaches exponential form for a period. Fig.3 shows the velocity distribution in initial virial ratio $b = 0$ and uniformly spatial distribution $\theta \in [0, \pi/5]$ case. The total energy $U \simeq -22$. Until several dynamical times, the distribution approaches exponential distribution (Fig.3(a)). The exponential distribution seems quasi-equilibrium state, it keeps until τ 20. Then the distribution approaches Gaussian during relaxation (Fig.3(b)).

On the other hand, when we choise large initial virial ratio (b 1), the exponential velocity distribution is not appeared, directly approaches Gaussian. Special initial condition may occur peculier behavior.

4 Summary

We analyzed SGR model with 1000 particles. Especially we notice scaling law and non-Gaussian velocity distribution. In SGR model, fractal dimension of spatial distribution decreases and approaches definite value during relaxation. This character seems independent of initial condition. On the other hand, the

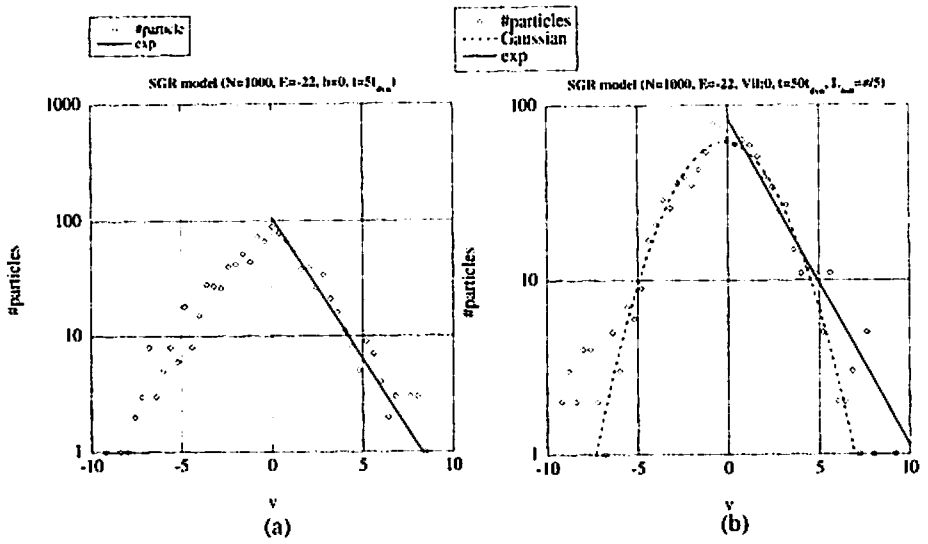


Figure 3: The velocity distribution. (a) At $\tau = 5$. The solid line means exponential distribution. (b) At $\tau = 50$. The solid line and dashed line mean exponential and Gaussian distribution respectively. The velocity distribution approaches Gaussian.

velocity distribution depends on initial virial ratio. When we set small initial virial ratio, the velocity distribution shows quasi-equilibrium state; the distribution approaches exponential distribution at several dynamical time. On the other hand, when we choice large initial virial ratio, the velocity distribution directly approaches Gaussian, not shows exponential distribution. Koyama and Konishi reported when they choose the initial velocity $v = 0$ and uniformly random spacial distribution, the power-law two-point correlation function appears[5]. However when they give small velocity dispertion, the power-law correlation does not appears. In SGR model, when we choose small initial virial ratio, peculiar behavior is appeared too. We will analyze the relation between initial virial ratio, non-Gaussian velocity distribution, and fractal structure in SGR model.

References

[1] W. H. Zurek, P. J. Quinn, J. K. Salmon, and M. S. Warren, Astrophys. J. **431** (1994) 559.

[2] F. Sylos Labini, M. Montuori, and L. Pietronero, Phys. Rep. **293** (1998) 61.

[3] G. de Vaucouleurs, Science **167** (1970) 1203.

[4] Y. Sota, O. Iguchi, M. Morikawa, T. Tatekawa, and K. Maeda, Phys. Rev. **E64**, 056133 (2001).

[5] H. Koyama and T. Konishi, Phys. Lett. A **279**, 226 (2001); Europhys. Lett. **58**, 356 (2002); Phys. Lett. A **295** 109 (2002).

Topological Structure of The Upper End of Future Null Infinity

Shinya Tomizawa[1], Masaru Siino[2]

Department of Physics, Tokyo Institute of Technology, Oh-Okayama, Tokyo 152-8550, Japan

Abstract

We propose a method to determine the topological structure of an event horizon far in the future of a spacetime from the geometrical information of its future null infinity. In the present article, we mainly consider spacetimes with two black holes. Although, in most of cases, the black holes coalesce and their event horizon is topologically a single sphere far in the future, there are several possibilities that the black holes do not coalesce eternally and such exact solutions. In our formulation, the geometrical structure of future null infinity is related to the topological structure of the upper end of the future null infinity through the Poincaré-Hopf's theorem. Since the upper end of the future null infinity determines the event horizon far in the future under the conformal embedding, the topology of event horizon far in the future will be affected by the geometrical structure of the future null infinity. Our method is not only for the case of black hole coalescence. Also we can consider more than two black holes or a black hole with non-trivial topology.

1 Introduction

We are often interested in the final state of a black hole spacetime after gravitational collapse. When matter collapses, it passes inside an event horizon and energy will be emitted to future null infinity in the form of gravitational waves. Since the amount of this energy is limited, we may expect that the spacetime will approach to a stationary state. If a black hole spacetime becomes stationary far in the future, the final state of the black holes is considerably restricted.

So far the final state of the black hole has been studied by many authors and these studies are known as uniqueness theorem of black holes. Israel showed that the only static and topologically spherical black hole is Schwartzshild solution [2] or Reissner-Nortström solution [3]. In stationary axisymmetric situations, the uniqueness theorems of a vacuum black hole and a charged black hole were shown by Carter [4] and Robinson [5],[6]. Hawking proved that a stationary black hole have to be static or axisymmetric and that the spatial topology of the horizon is the only sphere [7].

In these works, however, the existence of endpoints of event horizon generators was not considered. In dynamical situation, the endpoints of event horizon generators, where the event horizon is indifferentiable, are very important when we discuss the topology of an event horizon, because it causes the change of the spatial topology of an event horizon [8]. This is revealed by one of authors [8]. When this was discussed in [8], the topology of an event horizon far in the future is assumed to be a sphere. On the other hand, the work of Chruściel and Wald [9] implies that in a stationary spacetime, regardless of the existence of a endpoint, the spatial topologies of the connected components of black holes are only spheres under null energy condition. Therefore, if far in the future, the black hole spacetime settles down to a stationary state, we expect the spatial topology of the event horizon will consist of some connected components with spherical topology. To realize the relation of these works, it is required to determine the topology of an event horizon far in the future. There is not the simple method to know topological structure of an event horizon far in the future, that is, to determine how many black holes the final state of the black hole spacetime will consist of. We will develop such a method in the present article.

Since in an asymptotically flat spacetime [13], (to be more exact, in a strongly asymptotically predictable spacetime [13]) an event horizon is defined as the boundary of the causal past of future null infinity, we expect the topology of an event horizon will be related to the topological structure of future null infinity. Because the topology of future null infinity in an asymptotically flat spacetime is $S^2 \times \mathbf{R}$, we

[1]E-mail:tomizawa@th.phys.titech.ac.jp
[2]E-mail:msiino@th.phys.titech.ac.jp

may conclude far in the future the topology of an event horizon will always be a single S^2. Nevertheless it is well known that there are some stationary solutions including black holes which do not coalesce eternally. For example, they are Majumdar-Papapetrou solution [10], C-metric [11] and so on. The spatial topology of the event horizon of such a solution is obviously not a single sphere. In these spacetimes, is the topology of the upper end of future null infinity really S^2 ? (Of course, since the future null infinity is open at the upper end, this statement may be not well-defined.) If we regard that the topology of the upper end of future null infinity determines the topology of the event horizon far in the future, we may say that the topology of the upper end of future null infinity in such spacetimes is not one sphere but two spheres.

In the present works, we consider that in such spacetimes with the black holes which do not merge eternally, the topological structure at the upper end of future null infinity pinches. Here we emphasize that its topological structure determines the spatial topology of an event horizon far in the future.

How can we know the topology of an event horizon far in the future? As mentioned above, an event horizon is defined as the boundary of the causal past of future null infinity, whose topology is $S^2 \times \mathbf{R}$ [13]. So at first sight we think that the spatial topology of black holes is a single sphere finally. That is, all black holes coalesce and become a single far in the future. Is this real ? There are some exceptions to this. The examples of these exceptions are Majumdar-Papapetrou solution and C-metric. On the former, each black hole does not coalesce eternally by the force of electric repulsion. The latter describes two uniformly accelerated black holes connected by a string which are away from each other in the future. It is evident that in these spacetime black holes do not coalesce far in the future. It seems that these are inconsistent with the topology of future null infinity, $S^2 \times \mathbf{R}$.

Nevertheless, there is doubt that the topology of the upper end of I^+ is a sphere (FIG.1(a)). For because the definition of I^+ is $I^+ \equiv \dot{J}^+(i^0) - i^0$, it is open to the future, where $J^+(i^0)$ is the causal future of spatial infinity i^0. Therefore, there is not evidence that the topology of the upper end of I^+ is a sphere in such spacetimes. As shown in FIG.1(b), we may expect that I^+ pinches at the upper end in the spacetime where two black holes does not eternally coalesce.

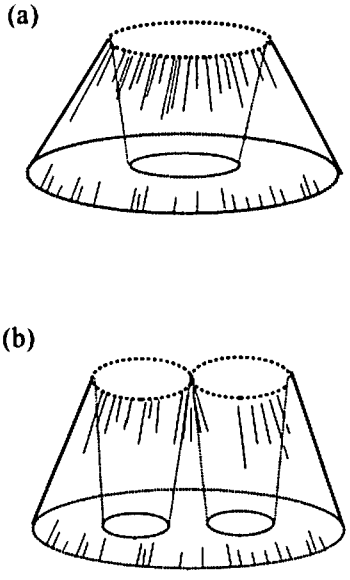


Figure 1: The topological structure of the upper end of future null infinity in the case (a) where two black holes will coalesce in the future and in the case (b) where two black holes will not collide far in the future. In (a), I^+ is a sphere at the upper end but in (b), I^+ pinches at the upper end.

2 Analysis

First of all, we must mention the method to examine the topology of the upper end of future null infinity. The following corollary [12] of the Poincaré-Hopf's theorem is useful.

Theorem 1 *Let M be a compact n-dimensional ($n > 2$ is an odd number) $C^r(r \geq 1)$ manifold with $\Sigma_1 \cup \Sigma_2 = \partial M$ and $\Sigma_1 \cap \Sigma_2 = \emptyset$. X is any C^{r-1} vector field with at most a finite number of zeros, satisfying the following two conditions: (a)The zeros of X are contained in Int M. (b)X has inward directions at Σ_1 and outward directions at Σ_2. Then the sum of the indices of X at all its zeros is related to the Euler numbers of Σ_1 and Σ_2:*

$$\chi(\Sigma_2) - \chi(\Sigma_1) = 2 \text{ index}(X), \tag{1}$$

where index(X) is given by the alternating sum of the Morse number μ_k as index $= \sum_k (-1)^k \mu_k$. The Morse number μ_k is the number of a critical point (zero of vector field X) whose index is k. The index of a critical point is given by the number of negative eigenvalue of Hesse matrix $H_{ab} = \nabla_a X_b$.

This theorem means that when the topology of slices of a manifold changes, there must be a zero of the vector field on it and equation (1) is satisfied. Because I^+ is a three-dimensional null hypersurface, we can apply this theorem to I^+. Let us consider the tangent vector field of the null generators on I^+ as the vector field in this theorem. Here, we should pay attention to the fact that, in this case, zero can exist only on the upper end of I^+, since I^+ is geodesically complete about own null generators by definition. Therefore we have to be careful to apply the theorem. Nevertheless, it would be possible to relate the theorem of index and the congruence of null generators around zero. In FIG.2 and the following, we temporarily consider small extension of future null infinity into its future directions for an explanation. From Morse's lemma, we suppose that the zero of the null generators is isolated. Since I^+ is three dimension, the behavior of the congruence around zero can be classified and their index is determined. These are illustrated in FIG.2. The left figures are three dimensional manifolds with index= ± 1 zeros, and the right represent the behavior of the null congruence on the neighborhood around their zeros. From this figure, there will be type (a) zero on upper end of I^+ with index $= +1$. Without reaching to the upper end, the asymptotic behavior of shear and expansion tells us information about the zero. Then we expect shear dominates the congruence that is approaching to the type (a) zero, and expansion to the type (b)-(c) zero with index $= -1$. If we assume that when two black holes do not coalesce, there should be a zero with index $+1$ and we can say that the ratio of the shear to the expansion will diverge near the zero.

From Newman-Penrose equations, the shear is obtained by the equation

$$n^a \tilde{\nabla}_a \lambda_{(1)} = 3\mu_{(0)}\lambda_{(1)} - \Psi_{4(1)} \tag{2}$$

in the leading order, where μ is the expansion and λ is the shear of the vector field $n^a = g^{ab}\tilde{\nabla}_b \Omega$ [1]. Integrating this, we obtain the relation

$$\lambda'_{(1)} = \exp\left(3\int \mu'_{(0)} du'\right) \int^{u'} du' \Psi'_{4(1)} \left(-3 \int \mu'_{(0)} du'\right), \tag{3}$$

where u' is the parameter of null geodesics on I^+ and is defined by $n^a \equiv (\partial/\partial u')^a$. If we transform conformal factor from affine gauge Ω into the gauge $\Omega' = \omega\Omega$ such that I^+ is compact and put $\omega = u'^{-\alpha}$, $\mu_{(0)}$ is

$$\mu'_{(0)} = \frac{\alpha}{u'}, \tag{4}$$

where variables with dashes denotes those in the gauge such that I^+ is compact. So if the behavior of Weyl curvature near the upper end of I^+ is $\Psi'_4 = \Psi'_{4(1)}\Omega' \sim \Omega'/u'^{\epsilon}$ as $u' \to \infty$, the ratio of the shear to the expansion is

$$\left|\frac{\lambda'}{\mu'}\right| \sim u'^{2-\epsilon}\Omega' + O(\Omega'^2), \tag{5}$$

where ϵ depends on ω and is a function of α. Therefore, if there is α satisfying $2 - \epsilon > 0$, this ratio can diverge, that is, the shear can be much larger than the expansion. This implies that I^+ pinches at the upper end. The point is that if Weyl curvature falls off later than some power of parameter of null generators, two black holes will not coalesce far in the future.

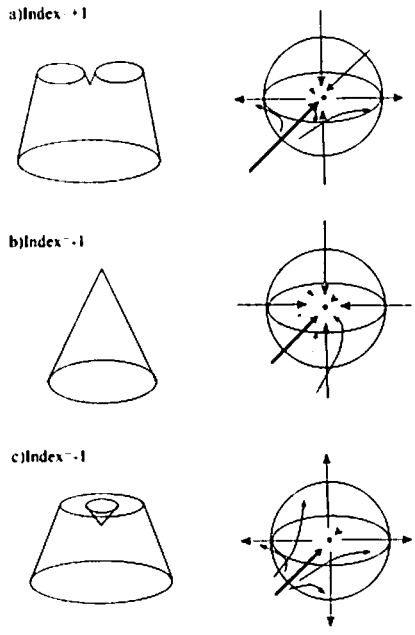


Figure 2: The behaviour of vector field around the zeros of (a) index= +1 and (b),(c)index= −1. We can expect that in (a) the shear will become larger than the expansion and that in (b),(c) the shear will smaller than the expansion.

3 Application to C-metric

We demonstrated the above condition by an example. Now we consider the vacuum C-metric as the example of the spacetime where two black holes does not eternally coalesce [15]. By a simple calculation, we confirmed that if the behavior of Weyl curvature is $\Psi_{4(1)} \sim u'^{-\epsilon}$, the ratio of the shear to the expansion of the vector field n^a diverge like the equation (5) [1].

4 Summary

We have investigated the relation between the topological structure of an event horizon far in the future and the geometrical structure of the future null infinity. A sufficient condition for topologically non-trivial final black holes is proposed and applied to C-metric as an example. If some component of Weyl curvature has a late power law tail, since future null infinity pinches off at the upper end, two black holes will not coalesce far in the future. We make sure of the validity of our method on C-metric.

While we concentrate on the gravitational radiation $\Psi_{(4)}$ of Weyl curvature as leading order contribution, there are possibilities that other component of curvature may contribute to the topological structure of future null infinity, for example, for Majumdar-Papapetrou solution. In Majumdar-Papapetrou spacetime, since gravitational field radiation $\Psi_{(4)}$ vanishes, we expect $\Psi_{(2)}$ contributes to the topological structure of the upper end of I^+ in a higher order.

In the present work, we mainly considered the case with several spherical black holes, since Wald and Chruściel proved in a stationary spacetime the black holes are spherical under null energy condition. Therefore, if we expect the final state of a black hole spacetime become stationary, our method will give the number of black hole black holes with a spherical topology far in the future.

Using the result of this article, what can we know about the collapsing stars from the observation of the gravitational radiation. The sufficient condition for topologically non-trivial black hole suggests the power of late time tail radiation will let us know about the final topology of black holes. Of course, to get rigorous statement about that, we should make clear the astrophysical meaning of the gauge choice

used in this article.

References

[1] S. Tomozawa, M. Siino, gr-qc/0209043

[2] W. Israel, Phys. Rev. **D164**, 1776 (1967)

[3] W. Israel, Commun. Math. Phys. **8**, 245 (1968)

[4] B. Carter, Phys. Rev. Lett. **26**, 331 (1971)

[5] D. C. Robinson, Phys. Rev. **D10**, 458 (1974)

[6] D. C. Robinson, Phys. Rev. Lett. **34**, 905 (1975)

[7] S. W. Hawking, Commun. Math.Phys. **25**, 152 (1972)

[8] M. Siino, Prog. Theor. Phys. **99**,1(1998)

[9] P. T. Chruściel and G. J. Galloway, gr-qc/9611032

[10] J. B. Hartle and S. W. Hawking, Commun. Math. Phys. **26**, 87 (1972)

[11] V. Pravda and A. Pravdodá, gr-qc/0003067

[12] R. D. Sorkin, Phys. Rev. **D33**.978(1985)

[13] R. M. Wald, *General Relativity* University of Chicago Press, Chicago,1984.

[14] E.Newman and R.Penrose J.Math.Phys. **3**, 566 (1962)

[15] F. H. J. Cornish and W. J. Uttley, Gen. Rel. Grav. **27**,439(1995)

[16] W. B. Bonnor, Gen. Rel. Grav. **15**,535(1981)

[17] W. B. Bonnor, Gen. Rel. Grav. **16**,269(1983)

[18] H. Bondi, M. G. J. van der Burg and A. W. K. Metzner, Proc. R. Soc. London **A269**,21 (1962)

[19] A. Tomimatsu, Phys. Rev. **D57**.2613(1998)

Cosmological constant, dilaton field and Freund-Rubin compactification

Takashi Torii,[1]

Advanced Research Institute for Science and Engineering, Waseda University, Tokyo 169-8555, Japan

Tetsuya Shiromizu,[2]

Department of Physics, Tokyo Institute of Technology, Tokyo 152-8551, Japan

Abstract

We discuss Freund-Rubin compactification with a cosmological constant and the dilaton field, and examine the stability of spacetime at low energy. Minkowski or de Sitter spacetime can be obtained if the dilation field is turned off, but only anti-de Sitter spacetime is realized in the presence of the dilaton field. The stability of spacetime depends on the dimensionality of spacetime and the compactified space, and the coupling constant of the dilaton field a. In the $a = 1$ case, which corresponds to superstring theories, the anti-de Sitter vacuum is stable at least in the linear level.

Compactification from higher dimensions to four dimensions and stabilization of the compactified space is a long-standing problem. It is well known that Freund-Rubin (FR) compactification[1] naturally introduced from supergravity gives us stable compact dimensions via a balance between the form field and the curvature at the classical level. Spacetime after compactification will becomes anti-de Sitter (adS) spacetime. Recently the realization of $M_p \times S^q$, where M_p is the p-dimensional Minkowski, de Sitter or adS spacetime, has been discussed, introducing an additional cosmological constant to the total action[2, 3]. The subject of stability has also been addressed and some parameter windows open for stable de Sitter or Minkowski as well as adS spacetimes. This is an impressive result, although the new ingredient is just the additional cosmological constant. We would like to point out, however, that a stable background with Minkowski or de Sitter spacetime is not permitted if the (NS) dilaton coupling exists. It is only adS spacetime that is permitted as the background solution. We briefly address the stability of the obtained adS vacuum in what follows.

We begin with the $D\ (= p + q)$-dimensional action in the string frame:

$$S = \frac{1}{16\pi}\int d^{p+q}x\sqrt{-\tilde{G}}\left[e^{-2a\Phi}\left(\tilde{R} - 2\Lambda + 4\partial_M\Phi\partial^M\Phi\right) - \frac{1}{2q!}F_q^2\right], \tag{1}$$

where Λ is a positive cosmological constant and F_q is the q-form field. Φ is the (NS) dilaton field and we leave its coupling constant a as a free parameter. Here we do not ask about the origin of Λ. It is convenient to transform the action to the Einstein frame by the following conformal transformation $\tilde{G}_{MN} = \Omega^2 G_{MN}$, $\Omega^2 = e^{4a\Phi/(D-2)}$. Then the action in the Einstein frame becomes

$$S = \frac{1}{16\pi}\int d^{p+q}x\sqrt{-G}\left[R - 2e^{\lambda_c\Psi}\Lambda - \frac{1}{2}\partial_M\Psi\partial^M\Psi - \frac{1}{2q!}e^{\lambda_q\Psi}F_q^2\right], \tag{2}$$

where

$$\Psi := \mu\Phi, \quad \mu := \sqrt{8\left[\frac{(D-1)a^2}{D-2} - 1\right]}, \quad \lambda_c := \frac{4a}{(D-2)\mu}, \quad \lambda_q := \frac{2a(p-q)}{(D-2)\mu}. \tag{3}$$

[1]E-mail:torii@gravity.phys.waseda.ac.jp
[2]E-mail:shiromizu@th.phys.titech.ac.jp

In superstring theories, $D = 10$ and $a = 1$ and we find $\mu = 1$, $\lambda_c = 1/2$ and $\lambda_q = (10 - 2q)/5$[4]. Note that the coupling constant of the dilaton field must satisfy $a^2 > (D-2)/(D-1)$.

We employ the following metric form

$$ds^2 = g_{\mu\nu}(x)dx^\mu dx^\nu + e^{2\phi(x)}d\Omega_q^2. \tag{4}$$

Since ϕ does not depend on the internal coordinate, this metric describes the homogeneous mode of the internal space. In this case the form field equation gives the solution $F_q = c *_q 1$, and the dilaton field equation becomes

$$\nabla_\mu\nabla^\mu\Psi + q(\nabla_\mu\phi)(\nabla^\mu\Psi) = \frac{\partial V}{\partial\Psi}, \tag{5}$$

where $*_q$ is the Hodge dual in the q-dimensional space and the potential V is

$$V = 2e^{\lambda_c\Psi}\Lambda + \frac{c^2}{2}e^{-2q\phi}e^{\lambda_q\Psi}. \tag{6}$$

The D-dimensional Einstein equations become

$$R_{\mu\nu} = \frac{1}{2}\partial_\mu\Psi\partial_\nu\Psi + \frac{2}{D-2}\left[e^{\lambda_c\Psi}\Lambda - \frac{(q-1)c^2}{4}e^{-2q\phi}e^{\lambda_q\Psi}\right]g_{\mu\nu}, \tag{7}$$

$$R_{ij} = \frac{2}{D-2}\left[e^{\lambda_c\Psi}\Lambda + \frac{(p-1)c^2}{4}e^{-2q\phi}e^{\lambda_q\Psi}\right]g_{ij}. \tag{8}$$

When $\phi \equiv 0$, which corresponds to FR compactification with the additional cosmological constant[2, 3], the Einstein equations may give $M_p \times M_q$ where M_p is de Sitter, Minkowski or adS spacetime and M_q is sphere, flat space or hyperboloid, depending on the values of Λ and c. Let us find the background solution. Before discussing the dilatonic case, we briefly summarize the non-dilatonic case for comparison.

The non-dilatonic case is realized by imposing $\Psi \equiv 0$ and $\lambda_c = \lambda_q = 0$. The Einstein equations (7) and (8) become

$${}^{(p)}R_{\mu\nu} = \frac{c^2}{2(D-2)}(f - f_p)g_{\mu\nu}, \qquad {}^{(q)}R_{ij} = \frac{c^2}{2(D-2)}(f - f_q)g_{ij}, \tag{9}$$

where ${}^{(p)}R_{\mu\nu}$ and ${}^{(q)}R_{ij}$ are p- and q-dimensional Ricci curvature, respectively, and $f = 4\Lambda/c^2$, $f_p = q - 1$ and $f_q = 1 - p$. Depending on the value of f, the p-dimensional spacetime becomes de Sitter ($f > f_p$), Minkowski ($f = f_p$) or adS ($f < f_p$) spacetime. The adS case includes $\Lambda = 0$, which corresponds to the original FR solution[1]. On the other hand, the q-dimensional space becomes S^q ($f > f_q$), R^q ($f = f_q$) and H^q ($f < f_q$). Hence the q-dimensional space is no longer compact without compactification by suitable identifications in the latter two cases. See Ref. [3] for the stability analysis.

In the dilatonic case, the parameter regions of λ_c and λ_q where stationary points of the potential function (6) exist are restricted. When $\Lambda > 0$, the constant dilaton field is realized for $\lambda_c\lambda_q < 0$, which implies that $p < q$. The value of the dilaton field is

$$\Psi \equiv \Psi_c := \frac{1}{\lambda_c - \lambda_q}\ln\left|\frac{c^2\lambda_q}{4\lambda_c\Lambda}\right| = \frac{1}{\lambda_c - \lambda_q}\ln\left|\frac{(p-q)c^2}{8\Lambda}\right|. \tag{10}$$

This point is the minimum of the potential, independent of the parameters.

When $\Lambda = 0$, $\lambda_q = 0$ (i.e. $p = q$) gives the constant dilaton field. In this case, the dilaton field is regarded as a massless scalar field with the flat potential $V \equiv c^2/2$. Hence it takes an arbitrary constant value. When $\Lambda < 0$, the solution with a constant dilaton field exists only when $\lambda_c\lambda_q > 0$, which implies that $p > q$ except for $p - q = 2$. The value of the dilaton field is also given by Eq. (10). For $p - q = 1$, the stationary point Ψ_c is the local maximum, while it is the local minimum for $p - q > 2$.

The Einstein equations (7) and (8) become

$$R_{\mu\nu} = -\frac{p-1}{\ell_p^2}g_{\mu\nu}, \qquad R_{ij} = \frac{q-1}{\ell_q^2}g_{ij}, \tag{11}$$

where the curvature radii are given by

$$\frac{p-1}{\ell_p^2} = \frac{q-1}{\ell_q^2} = \frac{1}{4}c^2 e^{\lambda_q \Psi_c} = \begin{cases} \frac{c^2}{4}\left|\frac{(p-q)c^2}{8\Lambda}\right|^{-\frac{p-q}{p-q-2}} & (p \neq q), \\ \frac{c^2}{4} & (p = q) \end{cases} \tag{12}$$

Hence the background p-dimensional spacetime is always adS and the q-dimensional space is sphere independently of the cosmological constant. It should also be noted that existence of the solution depends on the sign of the cosmological constant and dimensions p and q. These are direct effects of including the dilaton field.

Before we proceed to the stability analysis of the FR type solutions obtained above, we derive the p-dimensional effective theory to address their stability. The D-dimensional action (2) is reduced to the p-dimensional action as

$$S = \frac{1}{16\pi}\int d^p x\sqrt{-g}e^{q\phi}\Big[{}^{(p)}R + \frac{q(q-1)}{\ell_q^2}e^{-2\phi} - \frac{1}{2}D_\mu\Psi D^\mu\Psi + q(q-1)D_\mu\phi D^\mu\phi - 2e^{\lambda_c\Psi}\Lambda - \frac{c^2}{2}e^{\lambda_q\Psi}e^{-2q\phi}\Big]. \tag{13}$$

Here we have used ${}^{(q)}R = q(q-1)/\ell_q^2$, and the assumption that ϕ is the homogeneous mode. It is derived from the form field equation $d(e^{\lambda_q\Psi} * F) = 0$ that a homogeneous perturbation of the form field decouples from other fluctuations, while it couples for inhomogeneous modes[3].

We again perform the conformal translation to put the action into canonical form: $\bar{g}_{\mu\nu} = e^{2q\phi/(p-2)}g_{\mu\nu}$. Then we have the p-dimensional effective action

$$S = \frac{1}{16\pi}\int d^p x\sqrt{-\bar{g}}\Big[{}^{(p)}\bar{R} - \frac{1}{2}D_\mu\Psi D^\mu\Psi - \frac{q(D-2)}{p-2}D_\mu\phi D^\mu\phi - U(\Psi,\phi)\Big], \tag{14}$$

where the potential is

$$U(\Psi,\phi) = e^{-\frac{2q}{p-2}\phi}\Big[-\frac{q(q-1)}{\ell_q^2}e^{-2\phi} + 2e^{\lambda_c\Psi}\Lambda + \frac{c^2}{2}e^{\lambda_q\Psi}e^{-2q\phi}\Big]. \tag{15}$$

From now on we investigate the stability of the FR-type solutions. We showed that the p-dimensional background spacetime is always adS. It should be noted that the adS spacetime can be stable for some cases even in the presence of a tachyonic scalar field. We start from the positive mass theorem in adS spacetime[5, 6]. Let us begin with the derivation of Breitenlohner and Freedman's stability condition using the positive energy theorem. If the potential of the scalar fields can be written in the form

$$U = 2(p-2)^2 G^{XY}\frac{\delta W}{\delta\Phi^X}\frac{\delta W}{\delta\Phi^Y} - 2(p-1)(p-2)W^2, \tag{16}$$

the positivity of the total energy is guaranteed in the Einstein frame[5]. Indeed, the total energy can be expressed as

$$M_{\rm AD} = \int_\Sigma d^{p-1}x\Big[2|\hat{D}\epsilon|^2 + \sum_X |\delta\lambda^{(X)}|^2\Big], \tag{17}$$

where Σ is the asymptotically AdS_p space-like hypersurface, $\hat{D}_\mu := D_\mu + iW(\Phi)\gamma_\mu$ with the spinor covariant derivative D_μ, and ϵ is the spinor satisfying the Witten equation,[3] $\sum_{a=1}^{p-1}\gamma^a\hat{D}_a\epsilon = 0$. The spinor $\delta\lambda^{(X)}$ is defined by

$$\delta\lambda^{(X)} := \frac{1}{\sqrt{2}}\Big[if_Y^{(X)}\gamma^\mu\partial_\mu\Phi^Y + 2(p-2)f^{(X)Y}\frac{\delta W}{\delta\Phi^Y}\Big]\epsilon, \tag{18}$$

[3]The existence of this solution should be able to be confirmed by methods similar to those in Ref. [7]

where $f_Y^{(X)}$ is such that $G_{XY} =: \sum_Z f_X^{(Z)} f_Y^{(Z)}$ holds, which can be thought of as the orthonormal basis of the target space.

In the perturbative approach, we expand U and W as

$$U = U_0 + \frac{1}{2}\sum_X m_X^2 (\bar{\phi}^X)^2, \quad W = W_0 + \sum_X W_1^X \bar{\phi}^X + \frac{1}{2}\sum_X (W_2^X)^2 (\bar{\phi}^X)^2. \tag{19}$$

Here we have diagonalized the target space metric. From the zeroth order equation of Eq. (16), we find $W_0^2 = 1/2\ell_p^2$, $W_1^X = 0$. Here we have used $U_0 = -(p-1)(p-2)/\ell_p^2$. The second order equation gives

$$\sum_X \left[4(p-2)^2 (W_2^X)^2 - 2(p-1)(p-2) W_0 W_2^X - \frac{1}{2} m_X^2 \right] (\bar{\phi}^X)^2 = 0. \tag{20}$$

The condition that a real root of W_2^X exists is

$$(p-1)^2 (p-2)^2 W_0^2 + 2(p-2)^2 m_X^2 \geq 0, \tag{21}$$

which is rewritten in the form

$$m_X^2 \ell_p^2 \geq -\frac{(p-1)^2}{4}. \tag{22}$$

This is just the stability bound obtained by Breitenlohner and Friedmann in 4-dimensional adS spacetime[8] and extended to general dimension in [9, 10, 5].

The potential (15) is expanded around the background solution $\phi = 0$, $\Psi = \Psi_c$ as

$$U(\Psi, \bar{\phi}) = U(\Psi_c, 0) + \frac{1}{2} m_\Psi^2 (\Psi - \Psi_c)^2 + m^2 (\Psi - \Psi_c)\bar{\phi} + \frac{1}{2} m_{\bar{\phi}}^2 \bar{\phi}^2, \tag{23}$$

where

$$m_\Psi^2 = \frac{p-q-2}{2(p-q)} \lambda_q^2 c^2 e^{\lambda_q \Psi_c}, \tag{24}$$

$$m_{\bar{\phi}}^2 = \frac{1}{2(D-2)} \left[(2q-1)(p-2) + q \right] c^2 e^{\lambda_q \Psi_c}, \tag{25}$$

$$m^2 = -\sqrt{\frac{q(p-2)}{2(D-2)}} \lambda_q c^2 e^{\lambda_q \Psi_c}. \tag{26}$$

We can observe that $m_\Psi^2 = m^2 = 0$, $m_{\bar{\phi}}^2 = (p-1)c^2/2$ for $p = q$.

The linear perturbation equation is

$$D_\mu D^\mu \begin{pmatrix} \Psi \\ \bar{\phi} \end{pmatrix} = M = \begin{bmatrix} m_\Psi^2 & m^2 \\ m^2 & m_{\bar{\phi}}^2 \end{bmatrix} \begin{pmatrix} \Psi \\ \bar{\phi} \end{pmatrix}, \tag{27}$$

This equation is diagonalized as

$$D_\mu D^\mu \chi_\pm = m_\pm^2 \chi_\pm, \tag{28}$$

where

$$m_\pm^2 = \frac{e^{\lambda_q \Psi_c} c^2}{2} \left[B \pm \sqrt{B^2 + \frac{D-2}{p-q} \lambda_q^2} \right], \tag{29}$$

$$A = (2q-1)(p-2) + q > q, \quad B = \frac{1}{2} \left[\frac{p-q-2}{p-q} \lambda_q^2 + \frac{A}{(D-2)} \right]. \tag{30}$$

In the present case, the stability bound (22) is expressed as

$$F_1(p, q, a) := \frac{p-1}{2} + B - \sqrt{B^2 + \frac{D-2}{p-q} \lambda_q^2} \geq 0. \tag{31}$$

It should be empasized that this condition is independent of the cosmological constant Λ. This is in contrast with the non-dilatonic case where the criterion strongly depends on Λ[3].

Since our model has three parameter p, q and a, it is difficult to express the condition for stability explicitly in the general case. So let us focus on some specific cases.

Since the perturbation equation (28) has always one tachyonic mode for $p > q$ ($\Lambda < 0$, $\lambda_c \lambda_q > 0$), the background solution corresponds to the saddle point of the potential. On the other hand, for $p \leq q$ ($\lambda_c \lambda_q \leq 0$), B is positive semidefinite and $m_{\pm}^2 \geq 0$. Hence the adS vacuum is stable independently of the dilaton coupling constant in this case. When we consider higher-dimensional theories with $D \geq 10$, such as superstring/M theories, our result shows that Freund-Rubin compactification gives us stable 4- or 5-dimensional spacetime.

One might be interested in the case $a = 1$. In this case $\lambda_q = (p-q)/\sqrt{2(D-2)}$ and $B = (D-2)/4 > 0$. The condition for the stability becomes $2p^2 + (q-7)p + q + 3 \geq 0$. It is easy to see that this holds for $p \geq 3$. So we can conclude that the adS vacuum is stable. For general a, however, there are parameter windows for the unstable solutions. This can easily be seen for $a \simeq (D-2)/(D-1)$. In this case $\lambda_q \gg 1$ and

$$F_1 \simeq \frac{p-1}{2} - \frac{D-2}{p-q-2}. \tag{32}$$

For example, for $p - 2 = q + 1$, $F_1 \simeq -(3/2)q < 0$. Thus, this case is definitely unstable.

Let us summarize the present work. We considered the effect of the dilation field on FR compactification with a cosmological constant. As a result, Minkowski or de Sitter background spacetimes cannot be realized, while the only solution compatible with the dilaton field is adS spacetime. We also addressed the latter's stability. We know that the adS spacetime obtained from FR compactification in the non-dilatonic case is stable. On the other hand, as expected, we find an unstable background solution if the dilaton coupling exists. For the string coupling case($a = 1$), the solution is stable at low energy.

We have considered several specific cases in the low-energy limit (homogeneous perturbation). Hence it should be noted that our stability analysis is not definitive. Especially it is reported that instability does not come from the homogeneous mode but inhomogeneous modes in the non-dilatonic cases[3]. A more systematic study, possibly including non-linear stability analysis, would be a valuable subject for future study.

References

[1] P. G. O, Freund and M. A. Rubin, Phys. Lett. **B97**, 233 (1980).

[2] S. M. Carroll, J. Geddes, M. B. Hoffman and R. M. Wald, Phys. Rev. **D66**, 024036(2002).

[3] R. Bousso, O. DeWolfe and R. C. Myers, hep-th/0205080.

[4] The different type of the spontaneous compactification by the quantum effect is also discussed in type IIB superstring theory by K. Uzawa and K. Maeda. Private communications.

[5] P. K. Townsend, Phys. Lett. **B148**, 55 (1984).

[6] R. Schoen and S. T. Yau, Commun. Math. Phys. **79**, 23(1981); E. Witten, Commun. Math. Phys. **80**, 381(1981); J. M. Nester, Phys. Lett. **A83**, 241(1981).

[7] G. W. Gibbons, C. M. Hull and N. P. Warner, Nucl. Phys. **B218**, 173(1983).

[8] P. Breitenlohner and D. Z. Freedman, Phys. Lett. **B115**, 197 (1982).

[9] L. Mezincescu and P. K. Townsend, Ann. Phys. **160**, 406 (1985).

[10] P. Breitenlohner and D. Z. Freedman, Ann. Phys. **144**, 249 (1982).

Nonlinear Supersymmetric Structure of Spacetime and Matter

Kazunari Shima,[1] Motomu Tsuda[2] Manabu Sawaguchi[3]

Laboratory of Physics, Saitama Institute of Technology,
Okabe-machi, Saitama 369-0293, Japan

Abstract

Refering to the supermultiplet of the supergravity(SUGRA) the linearization of SGM action describing the nonlinear supersymmetric(NL SUSY) gravitational interaction of superon(Nambu-Goldstone(N-G) fermion) is attempted. The field contents of on-shell SUGRA supermultiplet are realized as the composites, though they have new SUSY transformations which closes on super-Poincaré algebra. Particular attentions are paid to the local Lorentz invariance.

Extending the geometrical arguments of Einstein general relativity theory(EGRT) on Riemann spacetime to new spacetime where the coset space coordinates of $\frac{superGL(4,R)}{GL(4,R)}$ turning to the N-G fermion degrees of freedom(d.o.f.) are attached at every Riemann spacetime point, we have proposed a new Einstein-Hilbert(E-H) type action[1]. The new E-H type action describes the NL SUSY[2] invariant gravitational interaction of N-G fermion *superon* in Riemann spacetime. We have shown group theoretically that the new E-H type action with global SO(10) symmetry decomposed as $\mathbf{10} = \mathbf{5} + \mathbf{5}^*$ with respect to SU(5) gives a unified description of spacetime and matter and proposed *superon(-quintet)-graviton model(SGM)*[1]. In SGM all observed elementary particles except graviton are regarded as the superon-composite eigenstates of the *linear* representation of SUSY[3] in (broken) SO(10) super-Poincaré(SP) symmetry[4] of the observed (low energy) nature.

In this letter we would like to discuss the linearization of the new E-H type action($N = 1$ SGM action) to obtain the equivalent linear SUSY theory in the low energy, which is renormalizable.
For the self-contained arguments we review SGM action briefly. SGM action is given by[1]; $L_{SGM} = -\frac{c^3}{16\pi G}|w|(\Omega + \Lambda)$. Here $|w| = \det w^a{}_\mu = \det(e^a{}_\mu + t^a{}_\mu)$, and $t^a{}_\mu = \frac{\kappa^4}{2i}\sum_{j=1}^{10}(\bar{\psi}^j\gamma^a\partial_\mu\psi^j - \partial_\mu\bar{\psi}^j\gamma^a\psi^j)$. $e^a{}_\mu$ is the vierbein of EGRT, $\psi^j (j = 1, 2, .., 10,)$ is N-G fermion(superon), $\kappa^4 = (\frac{c^3\Lambda}{16\pi G})^{-1}$ is a fundamental volume of four dimensional spacetime of V-A model[2], and Λ is a *small* cosmological constant related to the strength of the superon-vacuum coupling constant. Ω is a new scalar curvature analogous to the Ricci scalar curvature R of EGRT, whose explicit expression is obtained by just replacing $e^a{}_\mu(x)$ by $w^a{}_\mu(x)$ in Ricci scalar R. These results can be understood intuitively by observing that $w^a{}_\mu(x) = e^a{}_\mu(x) + t^a{}_\mu(x)$ defined by $\omega^a = w^a{}_\mu dx^\mu$, where ω^a is the NL SUSY invariant differential forms of V-A[2], is invertible and $s^{\mu\nu}(x) \equiv w_a{}^\mu(x)w^{a\nu}(x)$ are a unified vierbein and a unified metric tensor in SGM spacetime[1][5]. The SGM action L_{SGM} is invariant at least under the following symmetry[6]; global SO(10), ordinary GL(4R), the following new NL SUSY transformation;

$$\delta^{NL}\psi^i(x) = \frac{1}{\kappa^2}\zeta^i + i\kappa^2(\bar{\zeta}^j\gamma^\rho\psi^j(x))\partial_\rho\psi^i(x), \quad \delta^{NL}e^a{}_\mu(x) = i\kappa^2(\bar{\zeta}^j\gamma^\rho\psi^j(x))\partial_{[\rho}e^a{}_{\mu]}(x), \tag{1}$$

where $\zeta^i, (i = 1, ..10)$ is a constant spinor and $\partial_{[\rho}e^a{}_{\mu]}(x) = \partial_\rho e^a{}_\mu - \partial_\mu e^a{}_\rho$,
the following GL(4R) transformations due to (1);

$$\delta_\zeta w^a{}_\mu = \xi^\nu\partial_\nu w^a{}_\mu + \partial_\mu\xi^\nu w^a{}_\nu, \quad \delta_\zeta s_{\mu\nu} = \xi^\kappa\partial_\kappa s_{\mu\nu} + \partial_\mu\xi^\kappa s_{\kappa\nu} + \partial_\nu\xi^\kappa s_{\mu\kappa}, \tag{2}$$

where $\xi^\rho = i\kappa^2(\bar{\zeta}^j\gamma^\rho\psi^j(x))$, and the local Lorentz transformation on $w^a{}_\mu$; $\delta_L w^a{}_\mu = \epsilon^a{}_b w^b{}_\mu$ with the local parameter $\epsilon_{ab} = (1/2)\epsilon_{[ab]}(x)$ or equivalently on ψ and $e^a{}_\mu$ [6]. The local Lorentz transformation forms a

[1]E-mail:shima@sit.ac.jp
[2]E-mail:tsuda@sit.ac.jp
[3]E-mail:sawa@sit.ac.jp

closed algebra, and also the commutators of two new NL SUSY transformations (1) on $\psi(x)$ and $e^a{}_\mu(x)$ are GL(4R), i.e. new NL SUSY (1) is the square-root of GL(4R);

$$[\delta_{\zeta_1}, \delta_{\zeta_2}]\psi = \Xi^\mu \partial_\mu \psi, \quad [\delta_{\zeta_1}, \delta_{\zeta_2}]e^a{}_\mu = \Xi^\rho \partial_\rho e^a{}_\mu + e^a{}_\rho \partial_\mu \Xi^\rho, \tag{3}$$

where $\Xi^\mu = 2i(\bar{\zeta}_2 \gamma^\mu \zeta_1) - \xi_1^\rho \xi_2^\sigma e_a{}^\mu (\partial_{[\rho} e^a{}_{\sigma]})$. They show the closure of the algebra. SGM action L_{SGM} is invariant at least under[6]

$$[\text{global NL SUSY}] \otimes [\text{local GL}(4, \text{R})] \otimes [\text{local Lorentz}] \otimes [\text{global SO(N)}], \tag{4}$$

which is isomorphic to SO(10)SP whose single irreducible representation gives the group theoretical description of SGM[4].

The linearization of such a high nonlinear theory is an interesting and inevitable to obtain a renormalizable field theory which is equivalent and describes the observed low energy physics.

As a flat space exercise for SGM linerization, we have carried out the linearization of N=2 V-A model and shown that it is equivalent to the spontaneously broken N=2 linear SUSY *vector* $J^P = 1^-$ gauge supermultiplet model with SU(2) structure[7]. Interestingly SU(2) gauge structure of the electroweak standard model(SM) may be explained for the first time provided that the electroweak gauge bosons are the composite fields of this(SGM) type in the low energy. The linearization of N=1 V-A model has been carried out and proved that N=1 V-A model is equivalent to N=1 scalar supermultiplet[8] *or* N=1 axial vector gauge supermultiplet of linear SUSY[9].

In these works the linearization are carried out by using the superfield formalism and/or by the heuristic and intuitive arguments on the relations between the component fields of L SUSY and NL SUSY. The former may be applicable for $N < 9$ SUSY and gives a systematic way of the lineraization but becomes rather complicated for $N > 1$ SUSY, while the latter is intuitive and practical but needs a skilful insight in the computations in each order of the N-G field. In either case the discovery of the SUSY invariant relations which connect the supermultiplets of L and NL theories and reproduce the SUSY transformations is crucial.

In abovementioned cases of the global SUSY in flat spacetime the SUSY invariant relations are obtained straightforwardly, for the supermultiplets and the same algebraic SP structures of both L and NL theories are well understood.

The situation is rather different in SGM, for (i) the supermultiplet structure of the linearized theory of SGM is unknown except it is expected to be a broken SUSY SUGRA-like theory containing graviton and a (massive) spin 3/2 field as dynamical d.o.f. and (ii) the algebraic structure (4) is changed into SP. Especially for N=10 SGM, which is a uniquely realistic case, the linearized supermultiplet should contain fields with spin up to 3, which is beyond the naive application of the existing (superfield) formalism of SUGRA restricted to $N < 9$(i.e. spin$\leq$ 2). Therefore by the heuristic arguments and referring to SUGRA we discuss for the moment the linearization of SGM. We focus to N=1 for simplicity.

At first, we assume faithfully to SGM scenario that;

(i) the linearized theory should contain the spontaneously broken *global* (at least) SUSY

(ii) graviton is an elementary field(not composite of superons coresponding to the vacuum of the Clifford algebra) in both L and NL theories

(iii) the NL SUSY supermultiplet of SGM $(e^a{}_\mu(x), \psi(x))$ should be connected to the composite supermultiplet $(\tilde{e}^a{}_\mu(e(x), \psi(x)), \tilde{\lambda}_\mu(e(x), \psi(x)))$ for elementary graviton field and a composite (massive) spin 3/2 field of the SUGRA-like linearized theory.

From these assumptions and following the arguments performed in the flat space cases we require that the SUGRA gauge transformation with the global spinor parameter ζ should hold for the supermultiplet $(\tilde{e}^a{}_\mu(e, \psi), \tilde{\lambda}_\mu(e, \psi))$ of the (SUGRA-like) linearized theory, i.e.,

$$\delta \tilde{e}^a{}_\mu(e, \psi) = i\kappa \bar{\zeta} \gamma^a \tilde{\lambda}_\mu(e, \psi), \tag{5}$$

$$\delta \tilde{\lambda}_\mu(e, \psi) = \frac{2}{\kappa} D_\mu \zeta = -\frac{i}{\kappa} \tilde{\omega}(e, \psi)_\mu{}^{ab} \sigma_{ab} \zeta, \tag{6}$$

where $\sigma^{ab} = \frac{i}{4}[\gamma^a, \gamma^b]$, $D_\mu = \partial_\mu - \frac{i}{2}\omega_\mu{}^{ab}(e, \psi)\sigma_{ab}$, ζ is a global spinor parameter and the variations in the left-hand side are induced by NL SUSY (1).

We put the following SUSY invariant relations which connect $e^a{}_\mu$ to $\tilde{e}^a{}_\mu(e,\psi)$;

$$\tilde{e}^a{}_\mu(e,\psi) = e^a{}_\mu(x). \tag{7}$$

This relation (7) is the assumption (ii) and holds simply the metric conditions. Consequently the following covariant relation is obtained by substituting (7) into (5) and computing the variations under (1)[10];

$$\tilde{\lambda}_\mu(e,\psi) = \frac{\kappa}{4}\gamma_a\gamma^\rho\psi(x)\partial_{[\rho}e^a{}_{\mu]}. \tag{8}$$

(As discussed later these should may be considered as the leading order of the expansions in κ of SUSY invariant relations. The expansions terminate with $(\psi)^4$.) Now we show L SUSY transformation induced by (1) on the (composite) supermultiplet $(\tilde{e}^a{}_\mu(e,\psi),\ \tilde{\lambda}_\mu(e,\psi))$ form a closed algebra.
The closure of the algebra on $\tilde{e}^a{}_\mu$ can be shown as follows. The left-hand side of (5) gives

$$\delta\tilde{e}^a{}_\mu(e,\psi) = \delta^{NL}e^a{}_\mu(x) = i\kappa^2(\bar{\zeta}\gamma^\rho\psi(x))\partial_{[\rho}e^a{}_{\mu]}(x), \tag{9}$$

which is equal to the right-hand side of (5) due to (8). This shows (7) accompanying (8) is a SUSY invariant relation which reproduce (5), so far. The commutator of the two L SUSY transformations induces GL(4R) with the field dependent parameters as follows;

$$[\delta_{\zeta_1},\delta_{\zeta_2}]\tilde{e}^a{}_\mu(e,\psi) = \Xi^\rho\partial_\rho\tilde{e}^a{}_\mu(e,\psi) + \tilde{e}^a{}_\rho(e,\psi)\partial_\mu\Xi^\rho, \tag{10}$$

where $\Xi^\mu = 2i(\bar{\zeta}_2\gamma^\mu\zeta_1) - \xi_1^\rho\xi_2^\sigma e_a{}^\mu(\partial_{[\rho}e^a{}_{\sigma]})$.

On $\tilde{\lambda}_\mu(e,\psi)$, the left-hand side of (6) becomes apparently rather complicated;

$$\begin{aligned}\delta\tilde{\lambda}_\mu(e,\psi) &= \frac{\kappa}{4}\delta(\gamma_a\gamma^\rho\psi(x)\partial_{[\rho}e^a{}_{\mu]}) \\ &= \frac{\kappa}{4}\gamma_a[\delta^{NL}\gamma^\rho\psi(x)\partial_{[\rho}e^a{}_{\mu]} + \gamma^\rho\delta^{NL}\psi(x)\partial_{[\rho}e^a{}_{\mu]} + \gamma^\rho\psi(x)\partial_{[\rho}\delta^{NL}e^a{}_{\mu]}].\end{aligned} \tag{11}$$

However the commutator of the two L SUSY transformations induces the similar GL(4,R);

$$[\delta_{\zeta_1},\delta_{\zeta_2}]\tilde{\lambda}_\mu(e,\psi) = \Xi^\rho\partial_\rho\tilde{\lambda}_\mu(e,\psi) + \tilde{\lambda}_\rho(e,\psi)\partial_\mu\Xi^\rho. \tag{12}$$

These results indicate that the algebra on the linearized field closes and the initial new NL SUSY structure of SGM is maintained on the linearized supermultiplet (,i.e. disappointedly the commutators does not induce super-Poincaré symmetry) provided that the relations (7) and (8) and SUGRA transformation (5) are respected. And due to the complicated expression of L SUSY (11) which makes the physical and mathematical structures are obscure, we can hardly guess a linearized invariant action which is equivalent to SGM.

Now we attempt the linearization such that L SUSY transformation on the linearized fields induces SP transformation.

By comparing (6) with (11) we understand that the local Lorentz transformation plays a crucial role. As for the local Lorentz transformation on the linearized fields corresponding to the observed particles (in the low energy), it is natural to take the following forms

$$\delta_L\tilde{\lambda}_\mu(x) = -\frac{i}{2}\epsilon_{ab}\sigma^{ab}\tilde{\lambda}_\mu(x), \quad \delta_L\tilde{e^a}_\mu(x) = \epsilon^a{}_b\tilde{e}^b{}_\mu, \tag{13}$$

where $\epsilon_{ab} = (1/2)\epsilon_{[ab]}(x)$ is a local parameter. The ultimate Lorentz invariance encoded geometrically in SGM space-time [6], and (13), i.e. the asymptotic Lorentz invariance defined on the (composite) field in Riemann(Minkowski) space-time, is unclear. However this is particularly interesting, for in SGM the local Lorentz invariant gravitational interaction of superon are introduced by the geomtrical arguments in SGM spacetime[6] following EGRT. While in SUGRA the local Lorentz transfomation invariance (13) is realized as usual by introducing the Lorentz spin connection $\omega_\mu{}^{ab}$. And the L SUSY transformation is defined successfully by the (Lorentz) covariant derivative containing the spin connection $\tilde{\omega}_\mu{}^{ab}(e,\psi)$ as seen in (6), which causes the super-Poincaré algebra on the commutator of SUSY and is convenient for constructing the invariant action. Therefore in the linearized (SUGRA-like) theory the local Lorentz transformation

invariance is expected to be realized as usual by defining (13) and introducing the Lorentz spin connection $\omega_\mu{}^{ab}$. We investigate how the spin connection $\tilde{\omega}_\mu{}^{ab}(e,\psi)$ appears in the linearized (SUGRA-like) theory through the linearization process. This is also crucial for constructing a nontrivial(interacting) linearized action which has manifest invariances.

We discuss the Lorentz covariance of the transformation by comparing (11) with the right-hand side of (6). The direct computation of (6) by using SUSY invariant relations (7) and (8) under (1) produces complicated redundant terms as read off from (11). The local Lorentz invariance of the linearized theory may become ambiguous and lose the manifest invariance.

For a simple restoration of the manifest local Lorentz invariance we survey the possibility that such redundant terms may be adjusted by the d.o.f of the auxiliary fields in the linearized supermultiplet. As for the auxiliary fields it is necessary for the closure of the off-shell superalgebra to include the equal number of the fermionic and the bosonic d.o.f. in the linearized supermultiplet. As new NL SUSY is a global symmetry, $\tilde{\lambda}_\mu$ has 16 fermionic d.o.f.. Therefore at least 4 bosonic d.o.f. must be added to the off-shell SUGRA supermultiplet with 12 d.o.f.[11] and a vector field may be a simple candidate.

However, counting the bosonic d.o.f. present in the redundant terms corresponding to $\tilde{\omega}_\mu{}^{ab}(e,\psi)$, we may need a bigger supermultiplet e.g. $16+4\cdot 16=80$ d.o.f., to carry out the linearization, in which case a rank-3 tensor $\phi_{\mu\nu\rho}$ and a rank-2 tensor-spinor $\lambda_{\mu\nu}$ may be candidates for the auxiliary fields.

Now we consider the simple modification of SUGRA transformations(algebra) by adjusting the (composite) structure of the (auxiliary) fields. We take, in stead of (5) and (6),

$$\delta\tilde{e}^a{}_\mu(x) = i\kappa\bar{\zeta}\gamma^a\tilde{\lambda}_\mu(x) + \bar{\zeta}\tilde{\Lambda}^a{}_\mu, \tag{14}$$

$$\delta\tilde{\lambda}_\mu(x) = \frac{2}{\kappa}D_\mu\zeta + \tilde{\Phi}_\mu\zeta = -\frac{i}{\kappa}\tilde{\omega}_\mu{}^{ab}\sigma_{ab}\zeta + \tilde{\Phi}_\mu\zeta, \tag{15}$$

where (auxiliary fields) $\tilde{\Lambda}^a{}_\mu$ and $\tilde{\Phi}_\mu$ are functions of $e^a{}_\mu$ and ψ. We need $\tilde{\Lambda}^a{}_\mu$ term in (14) to alter (9), (10), (11) and (12) toward that of super-Poincaré algebra of SUGRA. We attempt the restoration of the manifest local Lorentz invariance order by order by adjusting $\tilde{\Lambda}^a{}_\mu$ and $\tilde{\Phi}_\mu$. In fact, the Lorentz spin connection $\omega_\mu{}^{ab}(e)$(i.e. the leading order terms of $\tilde{\omega}_\mu{}^{ab}(e,\psi)$) of (15) is reproduced by taking the following one

$$\tilde{\Lambda}^a{}_\mu = \frac{\kappa^2}{4}[ie_b{}^\rho\partial_{[\rho}e^b{}_{\mu]}\gamma^a\psi - \partial_{[\rho}e_{|b|\sigma]}e^b{}_\mu\gamma^a\sigma^{\rho\sigma}\psi], \tag{16}$$

which holds (10). Accordingly $\tilde{\lambda}_\mu(e,\psi)$ is determined up to the first order in ψ as follows;

$$\tilde{\lambda}_\mu(e,\psi) = \frac{1}{2i\kappa}(i\kappa^2\gamma_a\gamma^\rho\psi(x)\partial_{[\rho}e^a{}_{\mu]} - \gamma_a\tilde{\Lambda}^a{}_\mu) = -\frac{i\kappa}{2}\omega_\mu{}^{ab}(e)\sigma_{ab}\psi, \tag{17}$$

which indicates the minimal Lorentz covariant gravitational interaction of superon. Sustituting (17) into (15) we obtain the following new L SUSY transformation of $\tilde{\lambda}_\mu$(after Fiertz transformations)

$$\begin{aligned}\delta\tilde{\lambda}_\mu(e,\psi) &= -\frac{i\kappa}{2}\{\delta^{NL}\omega_\mu{}^{ab}(e)\sigma_{ab}\psi + \omega_\mu{}^{ab}(e)\sigma_{ab}\delta^{NL}\psi\} \\ &= -\frac{i}{2\kappa}\omega_\mu{}^{ab}(e)\sigma_{ab}\zeta + \frac{i\kappa}{2}\{\tilde{\epsilon}^{ab}(e,\psi)\sigma_{ab}\cdot\omega_\mu{}^{cd}(e)\sigma_{cd}\psi + \cdots\}.\end{aligned} \tag{18}$$

Remarkably the local Lorentz transformations of $\tilde{\lambda}_\mu(e,\psi)$ (,i.e. the second term) with the field dependent antisymmetric parameters $\tilde{\epsilon}^{ab}(e,\psi)$ is induced in addition to the intended ordinary global SUSY transformation. (17) is the SUSY invariant relations for $\tilde{\lambda}_\mu(e,\psi)$, for the SUSY transformation of (17) gives the right hand side of (15) with the consequent auxiliary fields. Interestingly the commutator of the two L SUSY transformations on (17) induces GL(4R);

$$[\delta_{\zeta_1},\delta_{\zeta_2}]\tilde{\lambda}_\mu(e,\psi) = \Xi^\rho\partial_\rho\tilde{\lambda}_\mu(e,\psi) + \partial_\mu\Xi^\rho\tilde{\lambda}_\rho(e,\psi), \tag{19}$$

where Ξ^ρ is the same field dependent parameter as given in (10). (10) and (19) show the closure of the algebra on (global) SUSY, (local) Lorentz and (local) GL(4R), i.e. on SP algebra provided that the SUSY invariant relations (7) and (17) are adopted, i.e. they are the composite (eigenstates) linear representations of SP algebra. These phenomena coincide with SGM scenario[1][4] from the algebraic

point of view. As for the redundant terms in (18) with $(\psi)^2$ we can adjust them by considering the modified spin connection $\tilde{\omega}_\mu{}^{ab}(e,\psi)$ particularly with the contorsion terms and (the auxiliary field) $\tilde{\Phi}_\mu(e,\psi)$. We can obtain the complete linearized (off-shell) supermultiplets of the super-Poincaré algebra by repeating the similar procedures (on the auxiliary fields) order by order which terminates with $(\psi)^4$.

Finally we mention another way of the systematic linearization by using the superfield formalism applied to the coupled system of V-A action with SUGRA[13]. We can define on such a coupled system a local spinor gauge symmetry which induces a super-Higgs mechanism[14] converting V-A field to the longitudinal component of massive spin 3/2 field. The Lagrangian obtained may be an analogue that we anticipate in above discussions but with the elementary spin 3/2 field. It is interesting if the systematic linearization by means of the NL SUSY superfield [13][15] can be extended to $N > 9$ SUSY.

The linearization of the new E-H type action L_{SGM} with the extra dimensions, which gives another unification framework describing the observed particles as elementary fields, is open. And the linearization of SGM action for spin 3/2 N-G fermion field[16] (with extra dimensions) may be in the same scope.

The authors would like to thank U. Lindström for the interest in our works and for bringing the reference to our attentions. The work of M. Sawaguchi is supported in part by the research project of High-Tech Research Center of Saitama Institute of Technology.

References

[1] K. Shima, *Phys. Lett.* **B501**, 237 (2001).

[2] D.V. Volkov and V.P. Akulov, *Phys. Lett.* **B46**, 109 (1973).

[3] J. Wess and B. Zumino, *Phys. Lett.* **B49**, 52 (1974).
Y.A. Golfand and E.S. Likhtman, *JET. Lett.* **13**, 323 (1971).

[4] K. Shima, *Z. Phys.* **C18**, 25 (1983);
K. Shima, *European. Phys. J.* **C7**, 341 (1999).

[5] K. Shima and M. Tsuda, *Class. and Quantum Grav.* **19**, 1 (2002).

[6] K. Shima and M. Tsuda, *Phys. Lett.* **B507**, 260 (2001).

[7] K. Shima, Y. Tanii and M. Tsuda, *Phys. Lett.* **B546**, 162 (2002).

[8] E.A. Ivanov and A.A. Kapustnikov, *J. Phys.* **A11**, 2375 (1978);
M. Roček, *Phys. Rev. Lett.* **41**, 451 (1978).
T. Uematsu and C.K. Zachos, *Nucl. Phys.* **B201**, 250 (1982).

[9] K. Shima, Y. Tanii and M. Tsuda, *Phys. Lett.* **B525**, 183 (2002),

[10] K. Shima, M. Tsuda and M. Sawaguchi, *Czech. J. Phys.***38**, 21 (2002). Suppl. A. Proceeding of Advanced Study Institute 2002, Praha, Czech Republic (2002), ed. by M. Finger, et.al. hep-th/0209165.

[11] K. Stelle and P. West,*Phys. Lett.* **74**, 330 (1978).
S. Ferrara and P. van Nieuwenhuisen,*Phys. Lett.* **74**, 333 (1978).

[12] D. Z. Freedman, P. van Nieuwenhuisen and S. Ferrara, *Phys. Rev.* **D13**, 3214 (1976).
S. Deser and B. Zumino, *Phys. Lett.* **B62**, 335 (1976).

[13] U. Lindström and M. Roček, *Phys. Rev.***D19**, 2300 (1979).

[14] S. Deser and B. Zumino, *Phys. Rev. Lett.* **38**, 1433 (1977).

[15] J. Wess and J. Bagger, *Supersymmetry and Supergravity*, second edittion, Princeton University Press (1992).

[16] K. Shima and M. Tsuda, *Phys. Lett.* **B521**, 67 (2001).

Quantum Aspects of Higher Dimensional Theories

Kunihito Uzawa,[1]

Graduate School of Human and Environmental Studies,
Kyoto University, Kyoto 606-8501, Japan.

Kei-ichi Maeda[2]

Department of Physics, Waseda University, Tokyo 169-8555, Japan.
Waseda Institute for Astrophysics, Waseda University, Tokyo 169-8555, Japan.
Advanced Research Institute for Science and Engineering,
Waseda University, Tokyo 169-8555, Japan.

Abstract

We investigate a stabilization of extra dimensions in a ten dimensional type IIB supergravity model. We assume $(A)dS_5 \times S^5$ compactifcation, and calculate quantum effects to find an effective potential for the radius of internal space. The effective potential has a minimum, and if the universe is created on the top of the potential hill, the universe evolves from dS_5 to $(A)dS_5$ after inflation. The radius of internal space S^5 becomes constant. Our model in IIB supergravity contains the 4-form gauge field with classically vacuum expectation value, which is role of ten dimensional cosmological constant. If the universe evolves into AdS, the five-dimensional Randall & Sundrum setup with stabilized dilaton is obtained from the type IIB supergravity model.

1 Introduction

Randall & Sundrum (RS) brane world model[1] has been investigated by many authors in the cosmological and gravitational points of view. This model shows several interesting properties. The hierarchy problem may be solved by the warp factor. Or the gravity can be confined in non-compact spacetime. However, a higher dimensional realistic model including RS setup is not so far known. The most plausible candidate is the $AdS_5 \times S^5$ compactification of the ten dimensional type IIB supergravity theory[2]. The scale of S^5, which is expected to be much smaller than that of AdS_5, is determined by the dilaton arising from a spontaneous compactification and is generally dynamical variable in the cosmological point of view. The dilaton in type IIB supergravity model has not ever been discussed as a dynamical variable but assumed to be a constant parameter. In order to discuss whether such a background is realized in the universe, we have to derive an effective potential for the dilaton, and analyze its stability. Unfortunately, in a pure gravitational system without quantum effects, there is no solution to stabilize a dilaton.

When we discuss dynamical evolution of the universe just after compactification, an inflationary expansion is required in our external spacetime. In RS setup, in which we assume the effective five-dimensional spacetime with a negative cosmological constant, the bulk spacetime may be explained naturally if we have inflation in five-dimensional external spacetime. However, it have well known that de Sitter supergravity can not arise from simple compactification of supergravity, string or M-theory[3]. It arises from nonstandard way. For example, the R symmetry group corresponding to conserved charge is not well defined and typically non-compact in de Sitter spacetime. Moreover the signature of kinetic term for RR scalar field in de Sitter spacetime is negative[3]. It is far from a realistic model in a supergravity theory. In cosmology, however, we would not need to assume a spacetime supersymmetry. Then some quantum effects will become important in the dynamics of the universe.

[1] E-mail:uzawa@phys.h.kyoto-u.ac.jp
[2] E-mail:maeda@gravity.phys.waseda.ac.jp

The purpose of our work is to investigate a stabilization mechanism of the internal space via quantum effects in the ten dimensional Kaluza-Klein theory and IIB supergravity model. We assume that the vacuum ten dimensional spacetime is compactified into the direct product of five dimensional (anti-)de Sitter spacetime and compact five dimensional sphere, i.e $(A)dS_5 \times S^5$. We consider the quantum fluctuations associated with several matter fields in order to stabilize the scale of internal space S^5. Many works suggest that quantum correction of higher dimensional matter field might provide a physical mechanism which is capable of accounting for extreme smallness of the extra dimensions.

The low energy effective action in our model is obtained by the integration of internal space, which is often called dimensional reduction. After the dimensional reduction, the dilaton couples the matter fields in external spacetime. The quantum fluctuations around a classical solution are computed in the form of quantum effective potential as a function of dilaton. Then the quantum correction of the matter field naturally contributes to the dilaton potential. Since the quantum correction is dominant effect at the small scale of internal space, this correction at nearly Planck scale is expected to be very important.

2 Dilaton dynamics in Type IIB supergravity model

Now we consider ten dimensional type IIB supergravity model. This model has been discussed by many authors from the motivation of AdS/CFT correspondence[4]. Stelle *et.al*[2] studied type IIB supergravity in $AdS_5 \times S^5$ as the candidate for the RS brane world model. However, the stability of S^5 and its dynamics in their suggestion was not shown. In order to construct a realistic RS model, we should treat the scale of S^5 as a dynamical variable and show that it stays at small value compared with that of AdS_5.

In the cosmological point of view, de Sitter spacetime is more interesting than anti-de Sitter spacetime because the de Sitter spacetime corresponds to a geometry of inflationary era in the cosmology. In fact, the brane world cosmology in dS_5 spacetime is discussed by several authors with the issues of inflation. In the following, we investigate the stabilization of S^5 in the $(A)dS_5 \times S^5$ spacetime.

Let us consider ten dimensional type IIB supergravity action [5]:

$$\begin{aligned}
S_{IIB} &= S_{NS} + S_R + S_{CS}\,, \\
S_{NS} &= \frac{1}{2\tilde{\kappa}^2}\int d^{10}X\,\sqrt{-\tilde{g}}\,e^{-2\Phi}\left(\tilde{R} + 4\tilde{g}^{MN}\partial_M\Phi\partial_N\Phi - \frac{1}{2}|H_3|^2\right), \\
S_R &= -\frac{1}{4\tilde{\kappa}^2}\int d^{10}X\,\sqrt{-\tilde{g}}\,\left(|F_1|^2 + |\tilde{F}_3|^2 + \frac{1}{2}|\tilde{F}_5|^2\right), \\
S_{CS} &= -\frac{1}{4\tilde{\kappa}^2}\int d^{10}X\,\sqrt{-\tilde{g}}\,C_4 \wedge H_3 \wedge F_3\,,
\end{aligned} \tag{1}$$

where

$$\begin{aligned}
\tilde{F}_3 &= F_3 - C_3 \wedge H_3\,, \\
\tilde{F}_5 &= F_5 - \frac{1}{2}C_2 \wedge H_3 + \frac{1}{2}B_2 \wedge F_3\,,
\end{aligned} \tag{2}$$

and $\tilde{R}$ is a Ricci scalar respect to the metric $\tilde{g}_{MN}$. Note that the subscript numbers in H_3, F_1, F_3, F_5 etc denote the rank of tensor fields. If we assume the $F_1 = F_3 = H_3 = 0$, the action is given by

$$S_{IIB} = \frac{1}{2\tilde{\kappa}^2}\int d^{10}X\sqrt{-\tilde{g}}\left\{e^{-2\Phi}\left(\tilde{R} + 4\tilde{g}^{MN}\partial_M\Phi\partial_N\Phi\right) - \frac{1}{4}|F_5|^2\right\}. \tag{3}$$

Since we consider the case when the Neveu-Schwarz(NS) scalar field Φ is time dependent, the factor $e^{2\Phi}$ before the Ricci scalar $\tilde{R}$ and the kinetic term $\tilde{g}^{MN}\partial_M\Phi\partial_N\Phi$ of the Φ is not constant. Hence the action of NS fields looks quite different from the usual massless scalar field. Then we perform the following conformal transformation

$$\tilde{g}_{MN} = e^{\Phi/2}\bar{g}_{MN}\,. \tag{4}$$

Note that we calculate the quantum effect at the local minimum of potential $V(\Phi)$(i.e. $\Phi = 0$) which arises after the compactification of S^5. Then the conformal factor becomes unity after Φ settles to $\Phi = 0$.

Consequently the change of the frame does not affect any result, provided that our results are interpreted after Φ settles to $\Phi = 0$. Using the conformal transformation (4) and rescaling Φ as $\Phi \to \Phi/(2\sqrt{17})$, the action is given by

$$S = \frac{1}{2\bar{\kappa}^2}\int d^{10}X\sqrt{-\bar{g}}\left\{(\bar{R} - \bar{g}^{MN}\partial_M\Phi\partial_N\Phi) - \frac{1}{4}|F_5|^2\right\}, \tag{5}$$

where $\bar{R}$ is a Ricci scalar of the ten dimensional metric tensor $\bar{g}_{\mu\nu}$. The background metric is expressed as [3]

$$\bar{g}_{MN}dX^M dX^N = \left(\frac{b}{b_0}\right)^{-10/3} g_{\mu\nu}dx^\mu dx^\nu + b^2\Omega^{(5)}_{ij}dy^i dy^j, \tag{6}$$

where $g_{\mu\nu}$ is the metric of a five dimensional de Sitter spacetime, b is the scale of a five dimensional sphere (i.e. a radius of S^5), a constant b_0 is an initial value of b, and $\Omega^{(5)}_{ij}dy^i dy^j$ is the line element of a unit five dimensional sphere. $g_{\mu\nu}$ and b depend only on the 5 dimensional coordinate $\{x^\mu\}(\mu = 0, 1, 2, \cdots)$. According to the ansatz (6), we truncate our model to a five dimensional effective theory, in which b is so-called "dilaton". We consider the Freund-Rubin type solution as 5-form field strength:

$$F_{M_1\cdots M_5} = \begin{cases} \left(f/\sqrt{\Omega}\right)\epsilon_{M_1\cdots M_5}, & M_1 = i, \cdots, M_5 = m, \\ 0, & \text{otherwise}, \end{cases} \tag{7}$$

where f is a constant and $\sqrt{\Omega}$ is the determinant of five dimensional sphere S^5. This field strength is wrapped around the S^5. We then set $|F_5|^2 \equiv 8\bar{\Lambda}$ and redefine the NS scalar $\varphi = \Phi/\bar{\kappa}$. The ten dimensional action (5) is now rewritten by

$$S = \int d^{10}X\sqrt{-\bar{g}}\left[\frac{1}{2\bar{\kappa}^2}(\bar{R} - 2\bar{\Lambda}) - \frac{1}{2}\bar{g}^{MN}\partial_M\varphi\partial_N\varphi\right]. \tag{8}$$

To write down the five dimensional effective action, the NS scalar φ is expanded as

$$\varphi = b_0^{-5/2}\sum_{l,m}\varphi_{lm}(x^\mu)Y^{(5)}_{lm}(y^i), \tag{9}$$

where b_0 is the initial value of b. Substituting the metric (6) and the NS scalar (9) into the action (8), we get the five dimensional effective action

$$S = \int d^5x\sqrt{-g}\left[\left(\frac{1}{2\kappa^2}R - \frac{1}{2}g^{\mu\nu}\partial_\mu\sigma\partial_\nu\sigma - U(\sigma)\right) - \sum_{l,\,m}\frac{1}{2}\left(g^{\mu\nu}\partial_\mu\varphi_{lm}\partial_\nu\varphi_{lm} + M^2_\varphi\varphi^2_{lm}\right)\right]. \tag{10}$$

where R is Ricci scalar of five dimensional metric tensor $g_{\mu\nu}$, κ is a positive constant defined by $\kappa^2 = \bar{\kappa}^2/(2^5 b_0^5\pi)$, the field σ is defined by

$$\kappa_\sigma\sigma = \ln\left(\frac{b}{b_0}\right), \qquad \kappa_\sigma = \sqrt{\frac{2}{35}}\kappa, \tag{11}$$

the mass M^2_φ of five dimensional NS scalar field φ is given by

$$M^2_\varphi = \frac{l(l+4)}{b_0^2}e^{-\frac{10}{3}\kappa_\sigma\sigma}, \tag{12}$$

and the dilaton potential $U(\sigma)$ is given by

$$U(\sigma) = \frac{\bar{\Lambda}}{\kappa^2}e^{-\frac{10}{3}\kappa_\sigma\sigma} - \frac{10K}{\kappa^2 b_0^2}e^{-\frac{10}{3}\kappa_\sigma\sigma}. \tag{13}$$

[3] Although the supersymmetry is broken in this compactification[6], there is no problem in the cosmological point of view.

Note that the classical NS scalar fields φ_{lm} in the action (10) has a potential, which vanishes at $\varphi_{lm} = 0$, unless $l = m = 0$ which does not couple to the dilaton. Furthermore, the kinetic term of φ is also approximately zero because the NS scalar is stable at $\varphi_{lm} = 0$ ($l \neq 0$). Then we expect that the massive scalar field $\varphi_{lm} = 0$ ($l \neq 0$) has a zero vacuum expectation value at least classical level, resulting in that this scalar field does not produce the energy momentum except for the massless mode. This background geometry has 3-brane which act as source for the 4-form field.

Here we consider the quantum effect of NS scalar. The NS scalar denotes the scale of eleventh dimension in eleven dimensional supergravity, which is compactified a la Kaluza-Klein. This length scale is not too far above Planck length. Even though a satisfactory quantum theory of gravity is not known so far, we expect that the quantum effect is presumably very important. As the action (10) is same form as five dimensional Einstein-Hilbert and scalar field, the 1-loop effective potential for NS scalar is given by[7]

$$\begin{aligned} V_{dS}(\sigma) &= \frac{\bar{\Lambda}}{\kappa^2} e^{-\frac{10}{3}\kappa_\sigma \sigma} - \frac{10K}{\kappa^2 b_0^2} e^{-\frac{16}{3}\kappa_\sigma \sigma} \\ &\quad + \frac{1}{b_0^5} e^{-\frac{40}{3}\kappa_\sigma \sigma} \left[-\ln(\mu a_1)^2 + \frac{25}{8192\pi} N_\phi \ln\left\{ \left(\frac{a_1}{b_0}\right)^2 e^{-\frac{16}{3}\kappa_\sigma \sigma} \right\} \right], \end{aligned} \tag{14}$$

where μ is a normalization constant with mass dimension, N_ϕ is number of scalar field, and a_1 is the scale of dS_5. The minimum of the effective potential turns out to be negative in most plausible cases. Therefore, in order to show a consistency of our results, we have to calculate the quantum correction in $AdS_5 \times S^5$ back ground and derive the effective potential. In the background is $AdS_5 \times S^5$, we obtain the effective potential for NS scalar[7]:

$$\begin{aligned} V_{AdS}(\sigma) &= \frac{\bar{\Lambda}}{\kappa^2} e^{-\frac{10}{3}\kappa_\sigma \sigma} - \frac{10K}{\kappa^2 b_0^2} e^{-\frac{16}{3}\kappa_\sigma \sigma} \\ &\quad + \frac{1}{b_0^5} e^{-\frac{40}{3}\kappa_\sigma \sigma} \left[-\ln(\mu a_2)^2 + \frac{\pi}{4320} N_\phi \ln\left\{ \left(\frac{a_2}{b_0}\right)^2 e^{-\frac{16}{3}\kappa_\sigma \sigma} \right\} \right], \end{aligned} \tag{15}$$

where a_2 is the curvature scale of AdS_5.

The above naive analysis is confirmed numerically. We survey the parameter space and find that the potential minimum is always negative when we have a stable minimum point. For example, choosing $N_\phi = 10$, and setting $\bar{\Lambda} = 1.59990 \times 10^{-3} M_\kappa^5, b_0 = 10^2 L_\kappa, \mu = b_0^{-1}$, and $a = 1.52042 \times 10^7 L_\kappa$, we find the minimum value $V_{dS}(\sigma_s) = -0.30240 M_\kappa^5$ at $\sigma_s = -5.03644 L_\kappa$ for $dS_5 \otimes S^5$ background, while we obtain the minimum value $V_{AdS}(\sigma_s) = -0.30246 M_\kappa^5$ at $\sigma_s = -5.03658 L_\kappa$ for $AdS_5 \otimes S^5$ background. The potential form is given in Figure.1. We may conclude that the stable RS model is realized from Type IIB supergravity theory.

3 Summary

We have calculated quantum effects in the $(A)dS_5 \times S^5$ compactified background of the ten dimensional type IIB supergravity and discussed its stability using the effective potential. In their pure gravity systems, a curvature term of the internal space gives a dominant contribution to the dilaton potential at small b, while a cosmological constant term becomes dominant for large b. Hence the dilaton potential is unbounded from below as $b \to 0$ and drops exponentially as $b \to \infty$. Then the extra dimension either shrinks to zero volume or is decompactified. However, if we include quantum effects, we find a stable minimum for the dilaton potential. The scale of extra dimension is stabilized by balancing the five form gauge field strength wrapped around the S^5, the curvature term of S^5 and quantum correction term induced by the NS scalar. The NS scalar is originally characterized by the direction of eleventh dimension in the eleven dimensional supergravity. Thus the quantum effect of NS scalar becomes important if the eleventh dimension is compactified near the Planck scale.

When the universe is created, the dilaton may be located near the top of the potential hill, and then the background geometry is almost dS_5 spacetime. We then have exponential expansion of the 5-dimensional

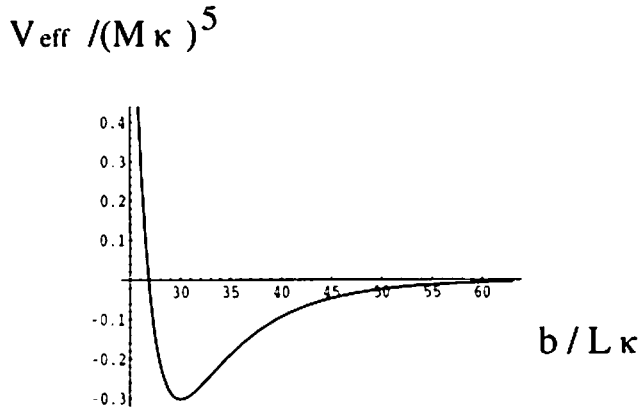


Figure 1: The dilaton effective potential given in Eq.(14) is depicted. We set $\bar{\Lambda} = 1.59990 \times 10^{-3}, b_0 = 10^2 L_\kappa, \mu = b_0^{-1}$ and $a = 1.52042 \times 10^7 L_\kappa$. The minimum of the potential is located at $\sigma_s = -5.03644 L_\kappa$ ($b_s = b_0 \exp(\kappa_\sigma \sigma_s) = 30.001 L_\kappa$) and its value is $V_{eff}(\sigma_s) = -0.30240 M_\kappa^5$. L_κ and M_κ denote the five dimensional Planck length and mass, respectively.

spacetime. As the dilaton rolls down the potential hill, the five dimensional spacetime geometry deviates from the dS_5. The dilaton potential eventually turns out to be negative, and the dilaton finds a stable minimum point. Then, the five dimensional spacetime becomes AdS_5. Hence, a five dimensional de Sitter (dS_5) spacetime evolves into a five dimensional anti-de Sitter(AdS_5) when the dilaton settles down to the potential minimum. Associated with dilaton stabilization, the change of spacetime geometry takes place.

Our solution contains a 3-brane because the background geometry has the five form gauge field strength. Hence, the ten dimensional $(A)dS_5 \times S^5$ compactification may provide a realistic model of the RS brane world[1].

However, if we have branes in our AdS_5, we may find additional contributions of quantum effect because we have new boundaries of branes. It may change some part of the present results, although we believe that AdS_5 is still stable. We leave this calculation as a future work.

References

[1] L. Randall and R. Sundrum, Phys. Rev. Lett. **83** (1999) 3370; *ibid.* **83** (1999) 4690.

[2] M. J. Duff, J. T. Liu, and K. S. Stelle, J. Math. Phys. **42** (2001) 3027.

[3] C. M. Hull, JHEP **0111** (2001) 012.

[4] J. M. Maldacena, Adv. Theor. Math. Phys. **2** (1998) 231; Int. J. Theor. Phys. **38** (1999) 1113.

[5] J. Polchinski, *String Theory I& II* (Cambridge University Press, Cambridge, England 1998).

[6] K. Pilch, P. van Nieuwenhuizen, and M. F. Sohnius, Commun. Math. Phys. **98** (1985) 105.

[7] K. Uzawa and K. Maeda, in preparation.

On the perturbations of spatially closed locally homogeneous vacuum solutions

Katsuhito Yasuno[1]

Department of Physics, Tokyo Institute of Technology,
2-12-1 Oh-Okayama Meguro-ku, Tokyo 152-8551, Japan

Abstract

We report a result of our analysis of asymptotic behavior of solutions to gauge-invariant perturbation equations about spatially closed Bianchi III vacuum solutions. We also discuss some consequences of the result concerning the stability of spatially locally homogeneous solutions.

1 Introduction

Recent work by Fischer and Moncrief (see [4] and references cited therein) on Hamiltonian reduction of Einstein's equations has led to a conjecture on what the asymptotic behavior, in the phase of unlimited expansion, of spatially compact vacuum solutions to the Einstein equations should be. The configurations of underlying spatial hypersurfaces are, in general, composed of "fundamental" building blocks of compact 3-manifolds [10]. However, a direct attack to prove this conjecture for those composite 3-manifolds seems out of reach at present. A natural first step is to obtain results for each building block. A great deal of effort has been taken to the study of spatially (locally) homogeneous solutions (see [12] for an overview). To go further than those models and to lay the groundwork for the small data analysis [3], we initiated the study of linearlized perturbations of spatially closed locally homogeneous solutions.

In a previous article [11], a basic formalism of linearized perturbations of spatially closed locally homogeneous vacuum solutions was studied, in which the Bianchi type III model with spatial topology being of a trivial circle bundle over a higher genus surface was assumed to be the background spacetime. We obtained the gauge-invariant perturbation equations for the gauge-invariant metric variables.

The immediate task is to analyze those equations into the future direction to obtain the asymptotic behavior of solutions. The result is presented in Section 2.2. It gives a new supporting evidence about the "conformal volume collapse" (see Section 3).

The stability of background solutions is a subject to be discussed. Of importance is the lack of an appropriate definition of stability among the perturbations of non-stationary background solutions. Moreover, there is the ambiguity in choosing a scale factor to eliminate the effect of the background expansion from the gauge-invariant variables because of the anisotropic expansion, in contrast to the isotropic models. We will discuss an attempt to this problem in Section 3.

The results reported here arise from a joint work with Masayuki Tanimoto and the details of this work will appear elsewhere [13].

2 Asymptotics

2.1 LRS Bianchi III vacuum solutions

We first recall a result of dynamical systems analysis of locally rotationally symmetric (LRS) Bianchi III vacuum solutions [7] to give the asymptotic expansions of solutions in the phase of unlimited expansion.

We consider a spatially closed Bianchi III vacuum spacetime $(\mathbb{R}\times M, g_{ab})$, where M is of a trivial S^1 bundle over the higher genus surface Σ_g ($g\geq 2$ the genus), $M=\Sigma_g\times S^1$, and g_{ab} is a Lorentz metric on $\mathbb{R}\times M$ of the form:

$$g_{ab} = -N^2(t)(\mathrm{d}t)_a(\mathrm{d}t)_b + q_1(t)\gamma_{ab} + q_2(t)\ell_{ab}\,, \quad q_1\,,\, q_2 > 0\,, \tag{1}$$

[1]E-mail:kyasuno@th.phys.titech.ac.jp

where $N(t)$ is the lapse function, γ_{ab} and ℓ_{ab} are the standard metrics on the base Σ_g and on the fiber circle S^1, respectively. Let π_1 and π_2 be the conjugate momenta of q_1 and q_2, respectively. The metric (1) admits the local rotational symmetry in addition to the local Bianchi III symmetry.

Let us write down the vacuum Einstein equations in the temporal gauge with $N = 3/\theta$ [12], where θ is the rate of expansion associated with the future-directed timelike unit normal to M. The corresponding time variable is denoted by τ and is set to increase into the future. The vacuum Einstein equations are

$$\theta' = -(1 + 2\Sigma_+^2)\theta\,, \tag{2}$$

$$\Sigma_+' = (1 - 2\Sigma_+)K\,, \quad s' = 6(1 - s)s\Sigma_+\,, \quad K' = 2\Sigma_+(2\Sigma_+ - 1)K\,, \tag{3}$$

where the prime denotes $\mathrm{d}/\mathrm{d}\tau$, and

$$\Sigma_+^2 + K = 1\,. \tag{4}$$

Here (Σ_+, s, K) are the scale-invariant dynamical variables defined by [9, 13]

$$\Sigma_+ := -\frac{q_1\pi_1 - 2q_2\pi_2}{q_1\pi_1 + q_2\pi_2}\,, \qquad s := \frac{q_1}{q_1 + 2q_2}\,, \qquad K := \frac{3}{\theta^2 q_1}\,,$$

and note that the Raychaudhuri equation (2) decouples from other equations.

The solutions to (3) with initial data satisfying the constraint (4) behaves as

$$\lim_{\tau\to\infty}(\Sigma_+, s, K)(\tau) = (1/2, 1, 3/4)\,. \tag{5}$$

This means that the LRS Bianchi III vacuum solutions asymptotically approach the *flat type III solution*:

$$g_{ab} = -(\mathrm{d}t)_a(\mathrm{d}t)_b + t^2\gamma_{ab} + \ell_{ab}\,. \tag{6}$$

The asymptotic expansions of solutions follow from equations (2)–(5): as $\tau \to \infty$,

$$\begin{aligned}
\Sigma_+(\tau) &= \tfrac{1}{2} + C_\sigma \mathrm{e}^{-3\tau/2}\left[1 - \tfrac{4}{3}C_\sigma \mathrm{e}^{-3\tau/2} + O(\mathrm{e}^{-3\tau})\right],\\
K(\tau) &= \tfrac{3}{4} - C_\sigma \mathrm{e}^{-3\tau/2}\left[1 - \tfrac{4}{3}C_\sigma \mathrm{e}^{-3\tau/2} + O(\mathrm{e}^{-3\tau})\right],\\
r(\tau) &= C_r^2 \mathrm{e}^{-3\tau}\left[1 + 4C_\sigma \mathrm{e}^{-3\tau/2} + O(\mathrm{e}^{-3\tau})\right],\\
\theta(\tau) &= C_\theta \mathrm{e}^{-3\tau/2}\left[1 + \tfrac{4}{3}C_\sigma \mathrm{e}^{-3\tau/2} + O(\mathrm{e}^{-3\tau})\right],
\end{aligned} \tag{7}$$

where $r := q_2/q_1 = (1 - s)/(2s)$, and $C_\sigma \in \mathbb{R}$, $C_r > 0$ and $C_\theta > 0$ are constants depending on the solution. The asymptotic forms of metric variables q_1 and q_2 in the same phase are obtained from the above results: as $\tau \to \infty$,

$$q_1(\tau) = \left(\tfrac{2}{C_\theta}\right)^2 \mathrm{e}^{3\tau}\left[1 - \tfrac{4}{3}C_\sigma \mathrm{e}^{-3\tau/2} + O(\mathrm{e}^{-3\tau})\right], \quad q_2(\tau) = \left(\tfrac{2C_r}{C_\theta}\right)^2\left[1 + \tfrac{8}{3}C_\sigma \mathrm{e}^{-3\tau/2} + O(\mathrm{e}^{-3\tau})\right]. \tag{8}$$

2.2 Solutions to gauge-invariant perturbation equations

In [11], we showed that, on the perturbations of spatially closed Bianchi III vacuum solutions, (i) sparations of variables are possible; (ii) mode couplings do not occur so that we can work in the *mode phase space* defined by each set of values (λ, m), where $-\lambda$ and $-m^2$ are the eigenvalues of the Laplacians of (Σ_g, γ_{ab}) and (S^1, ℓ_{ab}), respectively; (iii) the mode phase space is split into the *even part*, *odd part*, *harmonic part* and *TT part* (TT means the transverse-traceless with respect to γ_{ab}); (iv) by performing an appropriate canonical transformation, we can determine gauge-invariant canonical variables and then split the originally mixed mode phase space into the gauge-invariant and the pure-gauge sectors. From these, among other things, we obtained the gauge-invariant reduced sub-Hamiltonians and then the gauge-invariant perturbation equations. We are in a position to analyze the asymptotic behavior of solutions to the gauge-invariant perturbation equations. In the following, we shall distinguish quantities belonging to the even, odd, harmonic and TT parts by putting subsrcipts E, O, H and T, respectively.

Let Q_{A} (A = E, O, H, T) be the gauge-invariant configuration variables (see [11, 13]). For convenience, we introduce corresponding scale-free variables X_{A} by $X_{\mathrm{A}} := Q_{\mathrm{A}}/q_1$. The gauge-invariant perturbation equations for X_{A} are the linear second-order ordinary differential equations:

$$X_{\mathrm{A}}'' + g_{\mathrm{A}}(\tau)X_{\mathrm{A}}' + f_{\mathrm{A}}(\tau)X_{\mathrm{A}} = 0\,, \tag{9a}$$

where the coefficient functions g_A and f_A for each part are given by
Even part

$$g_E = 2(1-\Sigma_+^2) + \frac{6r}{Z}\left\{\frac{2m^2}{\lambda}(1+4\Sigma_+) + \frac{r}{1+\Sigma_+}[\lambda(2-\Sigma_+) + (1-\Sigma_+)(1+4\Sigma_+)]\right\},$$
$$f_E = 3K\left(\frac{m^2}{r} + \lambda + 2\right) \tag{9b}$$
$$+ \frac{18r}{Z}\left\{2m^2\Sigma_+(2\Sigma_+ - 1) + \frac{r}{1+\Sigma_+}[\lambda - 2\lambda(1-\Sigma_+)^2\Sigma_+ + 4\Sigma_+(1-\Sigma_+^2)]\right\},$$

where $Z := \lambda\left(\frac{2m^2}{\lambda} + r\frac{2-\Sigma_+}{1+\Sigma_+}\right)^2 + 4r\left(\frac{2m^2}{\lambda} + r\frac{2-\Sigma_+}{1+\Sigma_+}\right) - 2r^2$.
Odd part ($\lambda > 0$) and *Harmonic part* ($\lambda = 0$)

$$g_O = 2(1-\Sigma_+^2) + \frac{6r\Sigma_+}{r + m^2/(\lambda+2)}, \quad f_O = 3K\left(\frac{m^2}{r} + \lambda + 2\right). \tag{9c}$$

TT part

$$g_T = 2(1-\Sigma_+^2), \quad f_T = 3K\frac{m^2}{r}. \tag{9d}$$

Future asymptotic behavior of solutions to (9) can be analyzed by applying the standard theory of linear second-order differential equations (see, e.g. [6, Chapter XI]) with the help of (7) and (8). We shall give the result in terms of Q_A.

(a) (*Generic perturbations*: $m \neq 0$ and, for the even and odd parts, $\lambda > 0$)

$$Q_A(T) = O(T)\left[(c_1 + o(1))\cos(mT) + (c_2 + o(1))\sin(mT)\right] \qquad \text{as} \quad T \to \infty,$$

where

$$T(\tau) = C_r^{-1}e^{3\tau/2}\left[1 - 4C_\sigma\tau e^{-3\tau/2} + O(e^{-3\tau})\right],$$

and c_1 and c_2 are constants depending on the initial data.

(b) (*U(1)-symmetric perturbations*: $m = 0$ and $\lambda > 0$, $A = E, O$) As $\tau \to \infty$,

$$Q_A(\tau) = \begin{cases} O(e^{(3-k_A)\tau})\left[(c_1 + o(1))\cos(\omega\tau) + (c_2 + o(1))\sin(\omega\tau)\right] & \text{if } \lambda > 1/4, \\ O(e^{(3-k_A)\tau})\left[c_1\tau(1 + o(1)) + c_2(1 + o(1))\right] & \text{if } \lambda = 1/4, \\ O(e^{(3-k_A)\tau})\left[c_1 e^{\rho\tau}(1 + o(1)) + c_2 e^{-\rho\tau}(1 + o(1))\right] & \text{if } \lambda < 1/4, \end{cases}$$

where c_1 and c_2 are constants depending on the initial data, k_A are constants such that $k_E = 15/4$ and $k_O = 9/4$, $\omega = (3/2)(\lambda - 1/4)^{1/2}$ and $\rho = -i\omega < 3/4$.

(c) (*Zero mode perturbations*: $m = 0$ and, for the even part, $\lambda = 0$) In this case, we can express the solutions in the form:

$$Q_E(\tau) = c_1\int^\tau (3rK)^{1/2}(s)ds + c_2,$$
$$Q_H(\tau) = q_2(\tau)\left[c_1\int^\tau \left(\frac{\theta^4K^3}{3r^3}\right)^{1/2}(s)ds + c_2\right],$$
$$Q_T(\tau) = q_1(\tau)\left[c_1\int^\tau \left(\frac{\theta^4K^3}{3r}\right)^{1/2}(s)ds + c_2\right],$$

where c_1 and c_2 are constants. The asymptotic expansions are obtained by using (7) and (8):

$$Q_E(\tau) = -c_1C_re^{-3\tau/2}\left[1 + \tfrac{2}{3}C_\sigma e^{-3\tau/2} + O(e^{-3\tau})\right] + c_2,$$
$$Q_H(\tau) = c_1C_r^{-1}e^{3\tau/2}\left[1 - 8C_\sigma e^{-3\tau/2}\left(\tau - \tfrac{1}{3}\right) + O(e^{-3\tau})\right] + c_2q_2(\tau),$$
$$Q_T(\tau) = -c_1C_r^{-1}e^{3\tau/2}\left[1 - \tfrac{5}{3}C_\sigma e^{-3\tau/2} + O(e^{-3\tau})\right] + c_2q_1(\tau),$$

as $\tau \to \infty$, where $q_1(\tau)$ and $q_2(\tau)$ are given by (8).

The solutions for the generic perturbations exhibit the same asymptotic behavior among the all parts. It is oscillatory and has the increasing amplitude with the growth rate of order $\exp(3\tau/2)$ for τ large enough. On the other hand, the differences arise in the growth rate of the solutions for the U(1)-symmetric and the zero mode perturbations. As for the U(1)-symmetric perturbations, the qualitative behavior of the solutions changes according to the eigenvalue λ; it is oscillatory if $\lambda > 1/4$, while it is non-oscillatory if $\lambda \leq 1/4$,[2] in other words, for small λ the wave character of the solutions is lost.

The above results in fact imply that the solutions to the gauge-invariant perturbation equations about *non-flat* spatially closed Bianchi III vacuum solutions asymptotically approach those about *flat* type III solution (6) that is an equilibrium point in the phase space of scale-invariant variables. It is, of course, an intutively natural, expected result but it is not trivial; it can be known only after deriving the equations and checking whether the structure of the equations meets the conditions such that the asymptotic stability of solutions (in the sense of Lyapunov, see e.g. [1]) is guaranteed. Concerning the small but nonlinear perturbations, the fact indicates that the study of the nonlinearly perturbed solutions about the solutions corresponding to the future asymptotic states is important and it would yield the crucial results. (For U(1)-symmetric case, see [3].)

3 Discussions

This final section is devoted to discuss the problem of stability (see [13] for details). The next paragraph deals with the stability of the conformally rescaled, unphysical spacetimes.

Conformal stability. In connection with the work by Fischer and Moncrief, we are interested in the asymptotic behavior of conformal metrics of scalar curvature -1 on M [4]. The background conformal metric is $\bar{q}_{ab} = 2(\gamma_{ab} + r\ell_{ab})$. It follows from (7) that $\bar{q}_{ab}(\tau) \to 2\gamma_{ab}$ as $\tau \to \infty$, i.e. the conformal metric asymptotically degenerate along the fiber circle so that the volume of $\bar{q}_{ab}$ collapses asymptotically, in spite of the physical volume of q_{ab} diverges. This is the *conformal volume collapse* behavior [4, 5]. Consider perturbations of $\bar{q}_{ab}$ which do not change the value of the scalar curvature, i.e. the perturbed metric $\bar{q}_{ab} + \delta\bar{q}_{ab}$ is the metric of scalar curvature -1. The asymptotic behavior of perturbations $\delta\bar{q}_{ab}$ can be analyzed after fixing a gauge of perturbations [13]. It is found that, in the standard gauge [11], the background conformal metric is stable under the perturbations, i.e. $\delta\bar{q}_{ab}(\tau) \to 0$ as $\tau \to \infty$, if $X_{\rm A}$ asymptotically converge to zero. From the results in Section 2.2 it follows that the conformal locally homogeneous metrics are stable *up to* the zero mode solutions of the TT part which asymptotically approach non-vanishing constants. Recall that the Teichmüller parameters of M associated only with Σ_g are constants of motion on the background. The above result means that the perturbed solutions will converge to a locally homogeneous solution in which only the Teichmüller parameter differs from the original one. Moreover, since the TT part only contributes to the metric components tangent to Σ_g, the constants do not alter the qualitative picture, i.e. the asymptotic collapse of the fiber circle. The conformal volume collapse also occurs in the linearly perturbed spacetimes. We conclude that the spatially closed Bianchi III vacuum solutions are *conformally stable* under the linearized perturbations.

The following two paragraphs concern the stability of the physical spacetimes.

Averaged measure. In the cosmological models, the mean-expansion scale factor, ℓ, in our case given by $\ell = (q_1^2 q_2)^{1/6}$, is often considered to be the physical length scale since it is a natural extension of the scale factor of the Friedmann-Robertson-Walker (FRW) models [12]. Choosing this as a normalization factor to eliminate the effect of unlimited expansion of the background solutions from $Q_{\rm A}$, i.e. regarding $A_{\rm A} := \ell^{-2} Q_{\rm A}$ as the "measure" of the stability as was done in the perturbations of FRW models, we see that, since $\ell(\tau) = O(\mathrm{e}^{\tau})$ for sufficiently large τ, $A_{\rm A}(\tau) \to 0$ as $\tau \to \infty$ except the *growing* zero mode perturbations of the TT part. The amplitudes of gravitational waves, corresponding to those in the perturbations of FRW models, are $A_{\rm E}$ and $A_{\rm O}$, and they decay asymptotically. With respect to this measure, inhomogeneities disappear asymptotically but perturbed solutions go far indefinitely from the original one. The existence of growing zero mode of the TT part seems to suggest that such an "averaged" measure would not be appropriate at least for the global perturbations.

Inhomogeneity-dominance measure. From another point of view associated with the metric perturbations, one may suppose that each $Q_{\rm A}$ has its intrinsic scale factor depending on the definition of it

[2] Note that, since Σ_g is compact, there is a possibility of the existence of "small" eigenvalues with $\lambda \leq 1/4$, depending on the topology of Σ_g [2].

(cf. [8]). For example, the scale factor of $Q_{\rm T}$ might be q_1 since it is the coefficient of the basis tangent to the base manifold $(\Sigma_g, q_1\gamma_{ab})$ ($(E_9)_{ab}$ in [11]). (Note that, as for $Q_{\rm E}$, $Q_{\rm O}$ and $Q_{\rm H}$, each of which is a linear combination of components of the gauge-dependent perturbation metrics, things are not so straightforward. See [13].) On the other hand, from the result of the zero mode perturbations, we may infer that

$$Q_{\rm E}(\tau) \sim q_2(\tau)\,, \quad Q_{\rm H}(\tau) \sim (q_1 q_2)^{1/2}(\tau)\,, \quad Q_{\rm T}(\tau) \sim q_1(\tau) \qquad \text{as} \quad \tau \to \infty\,.$$

(For the odd part the zero mode perturbation is not well-defined but it may be natural, by construction [11], to apply the corresponding result of the harmonic part.) The asymptotic behavior of zero mode perturbations reflects the intrinsic scale factor of $Q_{\rm A}$. The two consistent pictures motivate us to introduce a new concept, the *inhomogeneity-dominance measure*, $M_{\rm A}$, such that

$$M_{\rm E} = Q_{\rm E}/q_2\,, \quad M_{\rm O,H} = Q_{\rm O,H}/(q_1 q_2)^{1/2}\,, \quad M_{\rm T} = Q_{\rm T}/q_1\,.$$

By inspecting $M_{\rm A}$ with the results of Section 2.2, we find that the most dominant contribution comes from the generic perturbation of the even part, $M_{\rm E}$. Thus, with respect to this measure, we conclude that the background solutions are *not* stable.

The above observations on the "stability measures" for physical spacetimes suggest that the stability of the locally homogeneous solutions is very sensitive to the choice of the measure and therefore the phase space of the Einstein equations one is working in.

Acknowledgements

I am grateful to Hideo Iguchi for discussions.

References

[1] Cesari, L., *Asymptotic Behavior and Stability Problems in Ordinary Differential Equations*, 2nd edition (Springer-Verlag, Berlin, 1963).

[2] Chavel, I., *Eigenvalues in Riemannian Geometry*, (Academic Press, Orlando, 1984).

[3] Choquet-Bruhat, Y. and Moncrief, V., Ann. Henri Poincaré **2**, 1007–1064 (2001).

[4] Fischer, A.E. and Moncrief, V., Class. Quantum Grav. **18**, 4493–4515 (2001).

[5] Fischer, A.E. and Moncrief, V., *Conformal volume collapse of spatially compact Bianchi models under the reduced Einstein flow*, to appear.

[6] Hartman, P., *Ordinary Differential Equations*, (John Wiley & Sons, New York, 1964).

[7] Hewitt, C.G. and Wainwright, J., Class. Quantum Grav. **10** 99–124 (1993).

[8] Hu, B.L., Phys. Rev. **D12**, 1551–1562 (1975).

[9] Rendall, A.D. and Uggla, C., Class. Quantum Grav. **17** 4697–4713 (2000).

[10] Scott, P., Bull. London Math. Soc. **15**, 401–487 (1983).

[11] Tanimoto, M., Moncrief, V. and Yasuno, K., *Perturbations of spatially closed Bianchi III spacetimes*, `gr-qc/0210078`, to appear in Class. Quantum Grav.

[12] Wainwright, J. and Ellis, G.F.R. (ed.), *Dynamical Systems in Cosmology*, (Cambridge University Press, Cambridge, 1997).

[13] Yasuno, K. and Tanimoto, M., *Asymptotic behavior of linearly perturbed spatially closed Bianchi III vacuum solutions*, in preparation.

Back hole formation in high-energy particle collisions

Hirotaka Yoshino,[1] Yasusada Nambu[2]

Department of Physics, Graduate School of Science,
Nagoya University, Chikusa, Nagoya, 464-8602, Japan

Abstract

We numerically investigate the formation of D-dimensional black holes in high-energy particle collision with the impact parameter and evaluate the total cross section of the black hole production. We find that the horizon formation occurs when the distance between the colliding particles is less than 1.5 times the effective gravitational radius of each particle. Our numerical result indicates that the characteristic $(D-3)$-dimensional volume (hyperhoop) of the system provide a better condition to judge the existence of the horizon compared to the one-dimensional hoop.

1 Introduction

The brane world scenario is an attractive scenario in the unified theory of elementary particles. This scenario regards our space as 3-brane in large extra-dimensions, and gauge particles and interactions are confined on the brane. If the extra-dimension is large, the Planck energy can be at O(TeV) [1]. One of the most striking consequences of lowering the Planck scale is that the properties of small black holes are totally altered. The black hole is centered on the brane but extending out into the large extra-dimensions. Thus the black hole becomes higher-dimensional, and its radius is far larger than the four-dimensional Schwarzschild radius with the same mass. This indicates that we can produce small black holes using future-planned accelerators such as the Large Hadron Collider in CERN [2].

One of the interesting quantity in the collider physics is the total cross section for the black hole production. This can be estimated by using the hoop conjecture [3]. The hoop conjecture states that the condition of black hole formation is given by

$$H_D \equiv \frac{C}{2\pi r_h(M)} \lesssim 1, \tag{1}$$

where C is the typical length which surrounds the system and $r_h(M)$ is the Schwarzschild radius corresponding to the system mass M, which is given by $r_h(M) = (16\pi G_D M/(D-2)\Omega_{D-2})^{1/(D-3)}$ with the volume of the unit $(D-2)$-sphere Ω_{D-2} and the gravitational constant G_D. This hoop conjecture is well-confirmed in four-dimensional gravity. If we assume that the hoop conjecture holds in higher-dimensional gravity, we can estimate the total cross section. At the instant of collision, the hoop is $C \sim 2b$. Using the inequality (1), the maximal impact parameter becomes $b_{\max} \sim r_h(2\mu)$ where μ is the energy of each incoming particle. Thus the total cross section is given by $\sigma_{\text{b.h.production}} \sim \pi r_h^2(2\mu)$.

To calculate the total cross section more precisely is interesting to improve the experimental predictions in collider physics. For four-dimensional spacetime, Eardley and Giddings [4] analytically investigated the value of $F(D)$ where

$$F(D) \equiv \sigma_{\text{b.h.production}}/\pi r_h^2(2\mu). \tag{2}$$

But it had not been investigated for higher-dimensional spacetime. Thus we analyze the grazing collision of particles in D-dimensional Einstein gravity. We calculated numerically the apparent horizon at the instant of collision of particles, and searched the maximal impact parameter. Note that we have neglected the structure of the extra-dimensions. This is justified when the black hole radius is much smaller than the scale of the extra-dimensions. We have also neglected the tension of the brane. This is valid when the central energy of the system is larger than few times the Planck mass.

[1] E-mail:hyoshino@allegro.phys.nagoya-u.ac.jp
[2] E-mail:nambu@allegro.phys.nagoya-u.ac.jp

We also discuss the condition for horizon formation like the hoop conjecture using our numerical results. The hoop conjecture essentially states that the mass concentration in all direction is necessary for the horizon formation. Such an understanding is important because it is useful to predict black hole formation intuitively. Although the condition for horizon formation in higher-dimensional gravity is not known, there is D. Ida and K. Nakao's hyperhoop conjecture [5]. They investigated four-dimensional conformally flat initial data of five-dimensional spacetime, and found that arbitrarily long black hole can form. This provides a counter example for the hoop conjecture. Instead of the one-dimensional hoop, they discussed that typical $(D-3)$-dimensional volume V_{D-3} (hyperhoop) gives the condition for the horizon formation in higher-dimensional gravity:

$$\mathcal{H}_D \equiv \frac{V_{D-3}}{G_D M} \lesssim 1. \tag{3}$$

We discuss the property of this conjecture for two particle systems using our results. Further discussions can be found in [6].

2 Apparent horizon in the collision of high-energy particles

Now we explain the set up of the high-energy particle collision. If we boost the Schwarzschild black hole to the speed of light, it becomes a massless particle accompanied by gravitational shock wave moving in a flat spacetime. Combining two shock waves, we set up the two particle collision. This system was originally developed by D'Eath and Payne [7]. The metric is given as

$$\begin{aligned} ds^2 &= -dudv + \left(H^{(+)}_{ik}H^{(+)}_{jk} + H^{(-)}_{ik}H^{(-)}_{jk} - \delta_{ij}\right)dx^i dx^j, \\ H^{(+)}_{ij} &= \delta_{ij} + \frac{u}{2}\theta(u)\nabla_i\nabla_j\Phi(\boldsymbol{x}-\boldsymbol{x}_+), \\ H^{(-)}_{ij} &= \delta_{ij} + \frac{v}{2}\theta(v)\nabla_i\nabla_j\Phi(\boldsymbol{x}-\boldsymbol{x}_-), \end{aligned} \tag{4}$$

where $\boldsymbol{x}$ denotes the point in the $(D-2)$-dimensional plane transverse to direction of motion. $\boldsymbol{x}_\pm$ denotes the position of each particle, which is given by

$$\boldsymbol{x}_\pm = (\pm b/2, 0, ..., 0) \tag{5}$$

where b is the impact parameter. $\Phi(\boldsymbol{x})$ is the function which characterizes the shock wave;

$$\Phi(\boldsymbol{x}) = \begin{cases} -8G_4\mu\log|\boldsymbol{x}|, & (D=4) \\ \frac{16\pi\mu G_D}{\Omega_{D-3}(D-4)}\frac{1}{|\boldsymbol{x}|^{D-4}}, & (D=5,6,...). \end{cases} \tag{6}$$

Now we explain the methods of finding the apparent horizon at the instant of collision. The apparent horizon is characterized by a $(D-3)$-dimensional surface $\mathcal{C}$ in the $(D-2)$-dimensional plane, and two functions $h_+(\boldsymbol{x})$ and $h_-(\boldsymbol{x})$. Here $\mathcal{C}$ denotes the intersection of apparent horizon and shock waves, and $h_\pm(\boldsymbol{x})$ shows the location of the apparent horizon in the direction of motion as a function on $(D-2)$-plane. $h_\pm(\boldsymbol{x})$ obeys the Laplace equation in $(D-2)$-dimensional flat space,

$$\nabla^2 h_\pm(\boldsymbol{x}) = 0, \tag{7}$$

which comes form that the surface has zero expansion. There are two boundary conditions,

$$h_\pm(\boldsymbol{x}) = \Phi(\boldsymbol{x}-\boldsymbol{x}_\pm), \tag{8}$$

$$\nabla(\Phi(\boldsymbol{x}-\boldsymbol{x}_+) - h_+(\boldsymbol{x}))\cdot\nabla(\Phi(\boldsymbol{x}-\boldsymbol{x}_-) - h_-(\boldsymbol{x})) = 4. \tag{9}$$

The condition (8) requires the continuity of the surface $\mathcal{C}$. The condition (9) comes from that the null normal vector on the apparent horizon is continuous on $\mathcal{C}$. Note that the boundary $\mathcal{C}$ is not fixed. We must search $\mathcal{C}$ as well as $h_\pm(\boldsymbol{x})$ so as to be consistent with these two boundary conditions. We numerically solved this problem.

3 Numerical results and condition for horizon formation

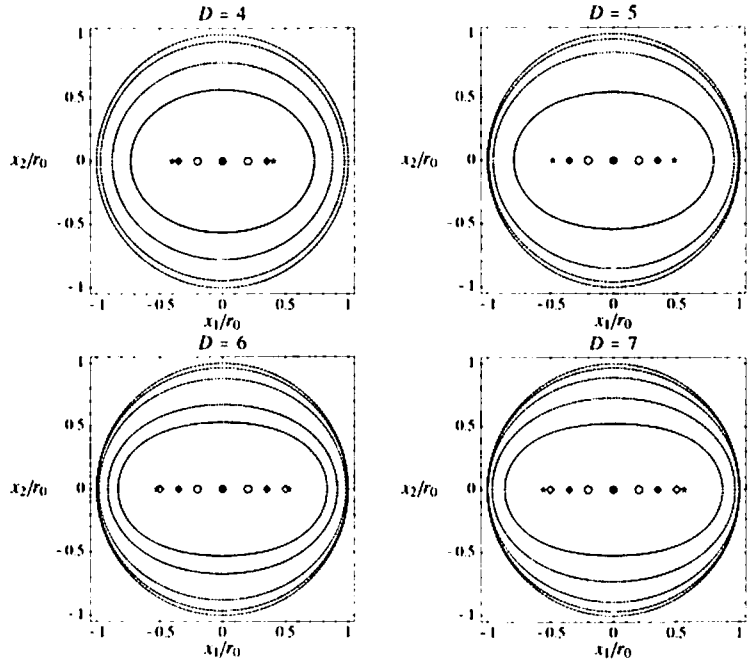


Figure 1: The shape of the apparent horizon $\mathcal{C}$ on (x_1, x_2)-plane in the collision plane $u = v = 0$ for $D = 4, ..., 7$. Incoming particles are located on the horizontal line $x_2 = 0$. Values of b/r_0 are $0(\bullet)$, $0.4(\circ)$, $0.7(\blacklozenge)$, $1.0(\Diamond$, shown only in $D = 6, 7)$, and $b_{\max}/r_0(\star)$.

Now we show the numerical results. Figure 1 shows the shape of $\mathcal{C}$ for $D = 4, ..., 7$. The points on the horizontal plane show the location of particles. The black points show the head-on collision, and the corresponding horizon is the outermost one. Its radius r_0 is given by $r_0 = (8\pi\mu G_D/\Omega_{D-3})^{1/(D-3)} \simeq r_h(2\mu)$. The stars show the collision with the maximal impact parameter, and the corresponding horizon is the innermost one. The ratio of the maximum radius and the minimum radius of $\mathcal{C}$ at the maximal impact parameter increases with D. Thus more prolate horizon can form for higher-dimensional spacetime. Figure 2 shows the relation of the impact parameter b and the minimum radius $r_{\min}$. From this figure, we can read off the maximal impact parameter. Using this value, we can calculate the total cross section. For $D \geq 5$, $F(D) \equiv \sigma_{\text{b.h.production}}/\pi r_h^2(2\mu)$ is greater than unity. Thus the black hole production rate in accelerators is larger than the previous estimation.

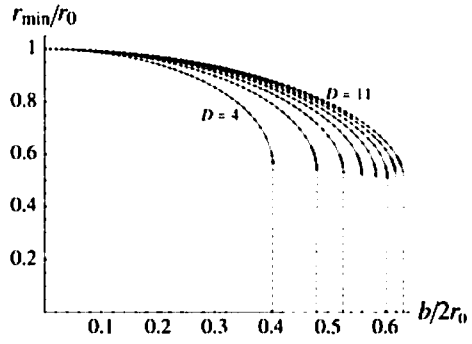


Figure 2: The relation between the impact parameter b and the minimum radius $r_{\min}$ of $\mathcal{C}$ for $D = 4, ..., 11$.

D	4	5	6	7	8	9	10	11
$b_{\max}/2r_0$	0.402	0.480	0.526	0.559	0.583	0.603	0.619	0.632
$F(D)$	0.647	1.084	1.341	1.515	1.642	1.741	1.819	1.883

Table 1: The value of $b_{\max}/2r_0$ and $F(D)$ for $D = 4, ..., 11$.

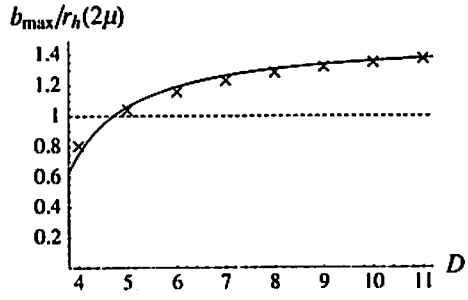


Figure 3: The value of $b_{\max}$ (crosses) as a function of the spacetime dimension D. The dashed line shows $r_h(2\mu)$ which comes from the hoop conjecture. The solid line $b_{\max} = 1.5r_h(\mu)$ gives a good fit of $b_{\max}$.

Now we turn to the condition for horizon formation. Figure 3 shows the behavior of the maximal impact parameter for each D. The crosses show the numerical results of $b_{\max}$. The dashed line shows $r_h(2\mu)$, which is predicted by the hoop conjecture. The hoop conjecture can be used for the estimation of the maximal impact parameter, but it cannot explain its increase with D. The solid line denotes $1.5r_h(\mu)$, which gives the best fit. This result leads to the following physical interpretation. $r_h(\mu)$ is the effective gravitational radius of each particle. If we consider each particle as the flat disc with effective gravitational radius, the apparent horizon forms when the two disks overlap each other and the length of overlapped region is more than one half of $r_h(\mu)$. Because the maximal impact parameter is proportional to $r_h(\mu)$, and $r_h(\mu)$ is proportional to $\mu^{1/(D-3)}$, $b_{\max}/r_h(2\mu)$ is proportional to $2^{-1/(D-3)}$. This factor can be derived by the more fundamental principle, the hyperhoop conjecture. Because the characteristic length is b in x_1-direction and $r_h(\mu)$ in other directions, characteristic $(D-3)$-dimensional volume (hyperhoop) becomes $V_{D-3} \sim br_h(\mu)^{D-4}$. If we use the condition $V_{D-3}/r_h(2\mu)^{D-3} \sim 1$, we can derive the same factor $2^{-1/(D-3)}$. Thus we consider that the $(D-3)$-dimensional hyperhoop gives a better parameter than the one-dimensional hoop for the horizon formation in higher-dimensional gravity.

4 Discussion and future direction

Now we turn to the discussion and future direction. The discussion concerns the amount of energy trapped by the produced black hole. Figure 4 shows apparent horizon mass, which is defined as

$$M_{\text{A.H.}} \equiv \frac{(D-2)\Omega_{D-2}}{16\pi G_D}\left(\frac{A_{D-2}}{\Omega_{D-2}}\right)^{(D-3)/(D-2)}, \tag{10}$$

where A_{D-2} denotes the $(D-2)$-dimensional area of the horizon. In four-dimensional gravity, this gives the irreducible mass of black hole, and coincides Hawking's quasi-local mass on the horizon. Thus the apparent horizon mass becomes an indicator of the trapped energy by the black hole. If we increase spacetime dimension or the impact parameter, the apparent horizon mass decreases. Thus only a small energy contributes to horizon formation for large D at the instant of collision.[3] This is because the energy of the shock wave is distributed to the transverse direction of motion of each particle. If the

[3]This doesn't mean that the final mass of the produced black hole is also small, because $M_{\text{A.H.}}$ gives only the lower bound of the final mass of the black hole. Part of the energy would be radiated away, but the other energy would be absorbed into the black hole or become the rotational energy. Thus the final mass of the produced black hole would be somewhat larger than $M_{\text{A.H.}}$. In the head-on collision in 4-dimensional gravity, $M_{\text{A.H.}}$ is about 71% of the total energy, but the final mass becomes about 84% [7].

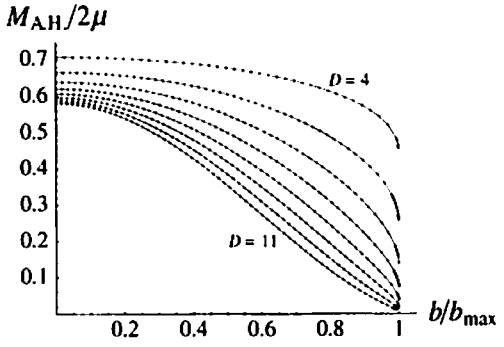


Figure 4: The relation between the horizon mass $M_{\mathrm{A.H.}}/2\mu$ and the impact parameter b for $D = 4, ..., 11$.

spacetime dimension increases, the energy distributes in the extra-dimensions. This leads to the increase of energy which does not contribute to the horizon formation. Thus we consider that our investigation of the hyperhoop conjecture is not sufficient, because we must use the quasi-local mass of the surface on which we calculate the $(D-3)$-dimensional hyperhoop of the system.

5 Conclusion

We analyzed the black hole formation in the grazing collision of high-energy particles. The total cross section for black hole production is $\sim \pi r_h^2(2\mu)$. The factor $F(D) \equiv \sigma_{\mathrm{b.h.production}}/\pi r_h^2(2\mu)$ increases with D and is greater than unity for $D \geq 5$. The effective gravitational radius of each particle determines the maximal impact parameter, $b_{\max} \sim 1.5 r_h(\mu)$. This criterion can be verified using D. Ida and K. Nakao's hyperhoop conjecture. But the trapped energy by the produced black hole decreases with D. Thus further investigation using the quasi-local mass is required for confirming the validity of the $(D-3)$-dimensional hyperhoop conjecture.

References

[1] N. Arkani-Hamed, S. Dimopoulos and G. R. Dvali, Phys. Lett. B **429**, 263 (1998); I. Antoniadis, N. Arkani-Hamed, S. Dimopoulos and G. R. Dvali, Phys. Lett. B **436**, 257 (1998).

[2] T. Banks and W. Fischler, hep-th/9906038; S. Dimopoulos and G. Landsberg, Phys. Rev. Lett. **87** 161602 (2001); S. B. Giddings and S. Thomas, Phys. Rev. D **65** 056010 (2001).

[3] K. S. Thorne, in *Magic without Magic: John Archbald Wheeler*, edited by J.Klauder (Freeman, San Francisco, 1972).

[4] D. M. Eardley and S. B. Giddings, Phys. Rev. D **66**, 044011 (2002).

[5] D. Ida and K. Nakao, Phys. Rev. D **66**, 064026 (2002).

[6] H. Yoshino and Y. Nambu, Phys. Rev. D **67**, 024009 (2003).

[7] P. D. D'Eath and P. N. Payne, Phys. Rev. D **46**, 658 (1992); **46**, 675 (1992); **46**, 694 (1992).